Gulzhian I. Dzhardimalieva
Igor E. Uflyand

Chemistry of Polymeric Metal Chelates

Springer

Springer Series in Materials Science

Volume 257

The Springer Series in Materials Science covers the complete spectrum of materials physics, including fundamental principles, physical properties, materials theory and design. Recognizing the increasing importance of materials science in future device technologies, the book titles in this series reflect the state-of-the-art in understanding and controlling the structure and properties of all important classes of materials.

More information about this series at http://www.springer.com/series/856

Gulzhian I. Dzhardimalieva
Igor E. Uflyand

Chemistry of Polymeric Metal Chelates

Gulzhian I. Dzhardimalieva
Institute of Problems of Chemical Physics
Russian Academy of Sciences
Chernogolovka, Moscow region
Russia

Igor E. Uflyand
Department of Chemistry
Southern Federal University
Rostov-on-Don
Russia

Dedicated to the memory
of Professor Anatolii D. Pomogailo—our
dear mentor and a great scientist.

Preface

This book is devoted to such interesting class of chemical compounds as polymeric metal chelates, which include polymer chain, and in various ways related metal chelate cycles. The first book on polymeric metal chelates appeared in 1991 (A.D. Pomogailo, I.E. Uflyand, Makromolekulayrnye Metallokhelaty [Macromolecular Metal Chelates] [Khimiya, Moscow, 1991]), and since then, the considerable experimental material has accumulated. However, it is difficult to generalize numerous data on polymeric metal chelates because of the need to coordinate the efforts of specialists whose interests are primarily in the specific fields of chemistry. Researchers in organic and polymer chemistry deal with the synthesis of metal chelates and metals in macromolecules, whereas specialists in physical chemistry work on problems of structure, the nature of bonds, and the properties of polymeric metal chelates. As the contents of this book show, the stage of accumulation of experimental data is almost complete. At the same time, at present many ideas are being elaborated and discussed; some of them (the development of the theory of bonds in polymeric metal chelates, the stabilization of thermodynamically unstable metal chelate structures by polymers, etc.) have still not been formulated. The present state in polymeric metal chelates area is characterized by efforts to understand the experimental materials and to find fundamental structure-properties correlations.

We are very pleased to present this book to the English-speaking readers. Any author is contented to have his book published by the world-known Springer publishing house, which has published most fundamental scholar works. It is also important for us because this book is a continuation of already published monographs in Springer Series in Materials Science from our laboratory: A.D. Pomogailo and V.N. Kestelman, Metallopolymer Nanocomposites (Springer, Berlin, Heidelberg, New York, 2005); A.D. Pomogailo, G.I. Dzhardimalieva, and V.N. Kestelman, Macromolecular Metal Carboxylates and Their Nanocomposites (Springer, Berlin, Heidelberg, 2010); and A.D. Pomogailo and G.I. Dzhardimalieva, Nanostructured Materials Preparation via Condensation Ways (Springer, Dordrecht, Heidelberg, New York, London, 2014).

Writing of this book was initiated by Prof. Anatolii D. Pomogailo (1939–2015), which was at the upstream of these studies. We only had time to discuss a plan of this work with him.

We are grateful to Dr. Svetlana Pomogailo for her invaluable assistance.

It is possible that many researchers will meet for the first time in these pages and understand that they are working on common problems of metal chelation with polymeric ligands.

We hope that this book will be useful for novices in science as well as for specialists experienced in polymeric and coordination chemistry, since it contains a great deal of references to original works in highly rated journals. In this connection, we apologize to the authors whose works are not referred to in this book, because their remarkable works are inadvertently missed in this publication for the sake of avalanche of publishing activity (predominantly in the last 10 years).

Chernogolovka, Moscow Region   Gulzhian I. Dzhardimalieva
Rostov-on-Don, Russian Federation   Igor E. Uflyand

Contents

About the Authors

Gulzhian I. Dzhardimalieva Dr. Sci. (Chem.), Ph.D. is the Head of Laboratory, Institute of Problems of Chemical Physics Russian Academy of Sciences and Professor of Department of Applied Mechanics, Moscow Aviation Institute (National Research University). She received her Ph.D. in 1987 from the Institute of Chemical Physics, RAS in Moscow, and her Doctorate in Chemistry in 2010 from Institute of Problems of Chemical Physics RAS in Chernogolovka. The scope of her scientific interest is as follows: metal-containing monomers and polymers on their base, macromolecular metal carboxylates, coordination polymers, and metallopolymer nanocomposites. Dr. Dzhardimalieva is author of about 150 articles and 4 monographs. She was an invited researcher of Auburn University, USA (2001), Warsaw Technology University, Poland (2002, 2011), Bremen University, Germany (2007), Turin University, Italy (2008), and Institute of Composite and Biomedical Materials CNR, Neapol, Italy (2011, 2013). She was an issue editor of Journal of Inorganic and Organometallic Polymers and Materials (2016, Vol. 26, 6) and a member of the Organizing Committee of the International Conference on Macromolecular Metal Complexes MMC-17 (Tokyo, Japan, August, 2017).

Prof. Igor E. Uflyand Dr. Sci. (Chem.) is the Head of Chemistry Department, Southern Federal University, Rostov-on-Don, Russia. He was born in 1956 and graduated from Rostov State University, Department of Physical and Colloid Chemistry. Professor Uflyand received his Ph.D. in 1981 and his Doctorate in Chemistry in 1996 from the Rostov State University. He received the title of Professor in 1996. The scope of his scientific interest is as follows: coordination and organometallic chemistry, metal chelate monomers and polymers on their basis, catalysis by metal complexes, and nanomaterials. Professor Uflyand is the author of over 150 scientific papers, 10 patents, and 3 books.

Acronyms

AA	Acrylic acid
AACVD	Aerosol assisted chemical vapor deposition
AAm	Acrylamide
Acac	Acetylacetonate anion
Acr	Acrylate
ADC	Acetylenedicarboxylate
AFM	Atomic force microscopy
AIBN	2,2′-azobisiso-butyronitrile
AIE	Aggregation-induced emission
AN	Acrylonitrile
ARGETATRP	Activators regenerated by electron transfer atom transfer radical polymerization
ASAP	Accelerated self-assembling procedure
ATI	N,N′-diisopropyl-aminotroponiminate
ATRP	Atom transfer radical polymerization
aza-DIPY	Azadipyromethene
-b-	*-block-*
BET	Brunauer-Emmett-Teller
BINOL	1,1′-bi-2-naphtol
BINAM	2,2′-binaphthyldiamine
BINAP	2,2′-bis(diarylphosphino)-1,1′-binaphthyl
BIP	2,6-bis(1′-methyl-benzimidazolyl)-4-hydroxypyridine
BODIPY	Pyridine-functionalized boron dipyrromethene
BP	Benzoyl peroxide
4,4′-bpe	4,4′-dipyridinethylene
BPP	2,6-bis(pyrazolyl)pyridine
bpy	2,2′-bipyridine
4,4′-bpy	4,4′-bipyridine
btp	2,6-bis(1,2,3-triazole-4-yl) pyridine
CB[n]	Cucurbit[n]uril

C3M	Coacervate core micelle
CE	Chelation efficiency
CEST	Chemical exchange saturation transfer
CD	Cyclodextrin
CDI	Carbonyldiimidazole
CIE	International Commision on Illumination
CMC	Critical concentration of micelle formation
CN	Coordinative number
-co-	Copolymer
COD	1,5-cyclooctadiene
CPL	Chelating polymer ligand
CP	Coordination polymer
CRP	Controlled radical polymerization
CuAAC	Cu(I)-catalyzed azide-alkyne cycloaddition
cyclam	1,4,8,11-tetraazacyclotetradecane
cyclen	1,4,7,10-tetraazacyclododecane
Cz	Carbazole
DAB	1,4-diaminobutane
dabco	1,4-diazabicyclo[2.2.2]octane
dansyl	1-dimethyl amino-1-naphthalene-5-sulfonyl
DB	Degree of branching
dbm	Dibenzoylmethane
DBU	1,8-diazabicyclo[5.4.0]undec-7-ene
dca	Dicyanamide
DEF	Diethylformamide
DES	Deep eutectic solvent
DFT	Density functional theory
DHP	Dihexadecyl phosphate
dien	Diethylene triamine
DLS	Dynamic light scattering
DMA	N,N-dimethylacetamide
DMF	N,N-dimethylformamide
DMSO	Dimethylsulfoxide
DNA	Deoxyribonucleic acid
DO3A	(1,4,7,10-tetraazacyclodocecane-1,4,7-triacetic acid)
DOTA	1,4,7,10-tetraazacyclododecane-1,4,7,10-tetraacetic acid
H4DO3APABn	1,4,7,10-tetraazacyclododecane-4,7,10-triacetic-1-{methyl ([4-aminophenyl] methyl) phosphinic acid}
DP	Degree-of-polymerization
Dpa	Dipicolinic acid
DPEN	1,2-diphenylethylenediamine
DPP	3,6-di(2-pyridyl)pyridazine
dppe	(Diphenylphospino)ethylene
dppp	1,3-bis(diphenylphospino)propane
DSC	Differential scanning calorimetry

DTA	Differential thermal analysis
DTG	Differential thermogravimetry
dtc	Dithiocarbamate
DTPA	Diethylenetriamine pentacetic acid
DTTA	Diethylenetriamine-tetra-t-butylacetate
DVB	Divinylbenzene
EDTA	Ethylenediaminetetraacetic acid
EDAX	Energy dispersive X-ray analysis
EI-MS	Electron ionization mass spectrometry
EL	Electroluminescence
EMIM	1-ethyl-3-methylimidazolium
En	Ethylenediamine
EOB	Extent of binding
EQE	External quantum efficiency
Fc	Ferrocene
FRET	Förster resonance energy transfer
FWHM	Full width at half maximum height
G	Dendrimer generation
GC-MS	Gas chromatography-mass spectrometry
GD	Graft degree
GL	Glycidyl methacrylate-co-ethylenedimethacrylate
GMA	Glycidyl methacrylate
GPC	Gel-penetrating chromatography
-gr-	-grafted-
HDA	Hexadecylamine
HEEDTA	Hydroxyethyl ethylenediaminetriacetic acid
H5EPTPA	Ethylenepropylenetriamine-N,N,N′,N″,N″-pentaacetic acid
HF	High-frequency
HKR	Hydrolytic kinetic resolution
HMDA	Hexamethylenediamine
HMPA	N,N,N′,N′,N″,N″-hexamethylphosphor acid triamide
HOPG	Highly oriented pyrolytic graphite
HRTEM	High-resolution transmission electron microscopy
HQ	8-hydroxyquinoline
HS	High spin
IDA	Iminodiacetic acid
IL	Ionic liquid
ITO	Indium-tin oxide
KS	Stability constants
KSV	Stern-Volmer constant
LAG	Liquid-assisted grinding
LB	Langmuir-Blodgett films
LbL	Layer-by-layer
LCP	Liquid crystal polymers
LCST	Lower critical solution temperature

LMC	Low molecular weight metal chelate
LP	Linear pyrolysis
LS	Low spin
LSCM	Laser scanning confocal microscopy
MA	Methyl acrylate
mAb	Monoclonal antibody
Mal	Maleat
MALDI-TOF-MS	Matrix-assisted laser desorption/ionization time-of-flight mass spectrometry
MAO	Methylalumoxane
MBA	N,N′-methylenebisacrylamide
MC	Merocyanine
MCD	Metal chelate dendrimer
MCM	Metal chelate monomer
Mebip	2,6-bis(1′-methyl-benzimidazolyl)pyridine
MEPE	Metallosupramolecular polyelectrolyte
MLCT	Metal-to-ligand charge transfer
MMA	Methyl methacrylate
MMPF	Metal-metalloporphyrin framework
Mn	Number-average molecular weight
MOF	Metal-organic framework
MOP	Metal-organic polyhedron
M-Pc	Metallophthalocyanine
M-Pp	Metalloporphyrin
MRI	Magnetic resonance imaging
MS	Mass spectrometry
MSP	Metallosupramolecular polymer
MSPG	Metallosupramolecular polymer gel
MXn	Metal compound
Mw	Weight-average molecular weight
MWCNT	Multi-walled carbon nanotubes
Nbd	Norbornadiene
NCF	Nitrogen-doped carbon microfibers
NIPAM	N-isopropylacrylamide
NIR	Near-infrared
NLO	Nonlinear optics
NMP	Nitroxide mediated polymerization
NTA	Nitrilotriacetic acid
OBPIMP	Oligo-2-([4-bromophenylimino]methyl) phenol
Ol	Oleate
OLED	Organic light-emitting diode
OTf	Triflate
Ox	Oxalate
PAA	Polyacrylic acid
PAAm	Polyacrylamide

PAC	Polyelectrolyte-amphiphilic complex
PAMAM	Polyamidoamines
PAN	Polyacrylonitrile
Pc	Phthalocyanine
PCD	Poly(chloromethylstyrene-co-divinylbenzene)
PCL	Poly (ε-caprolactone)
PCN	Polymer coordination network
PCS	Polychloromethylstyrene
PCT	Photoinduced charge transfer
PDA	Polydopamine
PDC	Polymer-derived ceramics
PDI	Polydispersity index
PDT	Photodynamic therapy
PE	Polyethylene
PEDOT	Poly(3,4-ethylenedioxy-thiophene)
PEG	Poly(ethylene glycol)
PEI	Polyethylene imine
PEO	Poly(ethylene oxide)
PET	Photoinduced electron transfer
PG	Polyglycerol
phen	1,10-phenanthroline
PHOX	Phosphinooxazoline
PIB	Polyisobutylene
PIC	Polyion coacervate
Pip	Piperidine
PL	Photoluminescence
PLED	Polymer light-emitting diodes
PLL	Poly-L-lysine
PLQY	Photoluminescence quantum yield
PMA	Poly(methacrylate)
PMC	Polymeric metal chelates
PMMA	Poly(methyl methacrylate)
P2MVP	Poly(2-methylvinylpyridine)
Pp	Porphyrin
PP	Polypropylene
PPD	Poly(o-phenylenediamine)
PPF	Porphyrin-paddlewheel framework
PPG	Polypropylene glycol
PPI	Polypropylene imine
PPM	Post-polymerization modification
PPr	Polymeric product
ppy	2-phenylpyridine
PS	Polystyrene
PSD	Post-synthetic deprotection
PSE	Post-synthetic exchange

PSM	Post-synthetic modification
PSME	Post-synthetic metal exchange
PSO	Poly(styrene oxide)
PSS	Poly(sodium-styrenesulfonate)
PTFE	Polytetrafluoroethylene
PTP	Proton-transfer polymerization
PVA	Poly(vinyl alcohol)
PVC	Poly(vinyl chloride)
PVp	Poly(vinylpyrolidone)
P2VP	Poly-2-vinylpyridine
P4VP	Poly-4-vinylpyridine
Py	Pyridine
pybox	Pyridine-bis(oxazoline)
pyrphos	3,4-bis(diphenylphosphino)pyrrolidine
RAFT	Reversible addition fragmentation transfer
RNA	Ribonucleic acid
ROMBP	Ring-opening multibranching polymerization
ROMP	Ring-opening metathesis polymerization
ROP	Ring-opening polymerization
SAFIN	Self-assembled fibrillar network
SALE	Solvent-assisted linker exchange
salen	N,N′-bis(salicylidene)ethylenediamine
salphen	N,N′-phenylenebis(salicylideneimine)
SAM	Self-assembled monolayer
SBB	Supramolecular building block
SBL	Supramolecular building layer
SBU	Secondary building unit
SCROP	Self-condensing ring-opening polymerization
SC-SC	Single-crystal to single-crystal transformation
SCVP	Self-condensing vinyl polymerization
SEC	Size-exclusion chromatography
SEM	Scanning electron microscopy
SGA	Self-generated atmosphere
SMASH	Shape memory assisted self-healing
SMP	Shape memory polymer
SP	Spiropyran
SPECT	Single photon emission computed tomography
SSP	«Single-source» precursors
St	Styrene
STM	Scanning thermal microscopy
TA	Thermal analysis
T_d	Decomposition temperature
TEM	Transmission electron microscopy
TEMPO	(2,2,6,6-tetramethylpiperidin-1-yl)oxyl or
	(2,2,6,6-tetramethylpiperidin-1-yl)oxidanyl

T_g	Glass-transition temperature
TGA	Thermogravimetric analysis
THF	Tetrahydrofuran
thq	Tetrahydroquinoline
Ti	Isotropization temperature
Tm	Melting point
TOP	Tri-n-octylphosphine
TOPO	Tri-n-octylphosphine oxide
tpy	2,2′:6′,2″-terpyridine
trien	Triethylenetetramine
TTA	1-(2-thenoyl)-3,3,3-trifluoroacetonate
4VP	4-vinylpyridine
Vp	Vinylpyrolidone
XPS	X-ray photoelectron spectrometer

Chapter 1
General Introduction

Abstract The polymeric metal chelates present class of chemical compounds including polymeric chain (organic, inorganic, mixed or biological nature) and metal chelate cycles. This direction of chemical science has appeared in the last decades of twentieth century at the junction of different fields of knowledge: coordination, polymer, physical, organic, colloid chemistry, biology, medicine and materials science. The need for accelerated development of this direction is confirmed by a rapid increase in the number of publications devoted to the study of polymeric metal chelates and their use as precursors of functional and nanoscale materials. Despite the variety of existing methods for synthesizing polymeric metal chelates, the main method still remains the direct interaction of metal compounds with chelating polymeric ligands. Therefore, the molecular design of chelating macroligands is an important, and in some cases, defining task both from the point of view of obtaining metal chelates with predetermined properties and structure, and their subsequent practical use. At the same time, in recent years a number of new methods have been developed for the preparation of polymeric metal chelates, primarily on the basis of metal chelate monomers, which allow one to obtain complexes in one stage with a targeted composition and structure. Progress in this field of chemistry is also associated with the emergence of new types of polymeric metal chelates, in particular, metal chelate dendrimers, star and hyperbranched polymers, as well as coordination polymers and supramolecular metal chelate polymers.

Characteristic features, allowing reliably identify the polymeric metal chelates (PMCs) as particular class of chemical compounds, is the presence of the polymeric chain (organic, inorganic, mixed or biological nature) and metal chelate cycles [1]. This area is interesting because it is located at the intersection of the boundary areas of science—polymer and coordination chemistry. The combination of metal chelates and polymers in one chemical entity represents, on one hand, a fairly complex way, where in each case we have to use their methods of synthesis and study. PMCs are highly interesting materials with properties combining typical polymeric features with the properties of metal chelates. Due to the polymer chain, PMCs behave

in many cases like ordinary macromolecular compounds, and due to the presence of metal ion in the chain, PMCs exhibit properties characteristic of a given metal ion. On the other hand, it is at the junction of polymer and coordination chemistry can expect the unexpected multidimensional spatial architectures of the polymer chains and new regularities in the formation of supramolecular structures, and hence the unusual properties of the resulting materials (catalytic, magnetic, electrical, nonlinear-optical, etc.).

These advanced metal chelate—polymeric structures can be considered from two different points of view: the only scientific knowledge or practical orientation [1–21]. In particular, PMCs allowed making significant progress in solving many theoretical problems of modern chemistry. These include the architecture of polymers, the reactivity of macromolecules, the specificity of metal chelation by polymer ligands, the synthesis of polynuclear metal chelates, competing coordination, the preparation of immobilized catalysts, and so on. Of no small importance is the fact that PMCs have multiple potential applications including catalysis, polymer light-emitting diodes (PLED), nonlinear optical (NLO) devices, sensors etc. [22–37]. In addition, it should be noted their biomedical and pharmaceutical applications as drug delivery carriers, metal-containing drugs, photodynamic therapy (PDT) agents, biosensors, and bioimaging agents [3, 5, 38–43]. PMC are ideal for building dynamic molecular systems whose movements are controlled from the outside [44, 45]. As a rule, these compounds are called «molecular machines». Self-assembly of PMC allows you to create unique spatial architectures, so they can, for example, serve as a precursor to the fabrication of the «technomimetic spoked wheels» [46, 47]. Another example of self-assembly of PMC is synthetic, in nanometer scale, «Sierpinski hexagonal gasket» [48, 49]. This nondendritic, perfectly self-similar fractal macromolecule consists of bis-terpyridine building units, which are interconnected coordination of 36 Ru and 6 Fe ions, forming a nearly flat array of ever-larger hexagons around an empty center. Finally, the self-assembling PMC on the various nanostructures and surfaces [50–53] is considered in this context.

By formal features, methods of producing PMC, representing polymer matrix in which the metal chelate units are distributed, do not differ from the most common approaches to the synthesis of metal chelates without polymer. Therefore, modern synthetic PMC chemistry is based on the general methods and principles of the synthesis of coordination compound. As in the case of low molecular weight metal chelates (LMCs), most currently known PMCs are obtained by the direct interaction of metal compounds (MX_n) with chelating polymer ligands (CPLs). Therefore, the design of CPL is an important, and in some cases, and decisive problem in terms of obtaining PMC and their future practical use. CPLs are macromolecular compounds (organic, inorganic, mixed or biological nature) with polydentate functional groups capable of forming a metallocycle by reacting MX_n. Currently there is no uniform classification of CPL. Apparently, such classification should consider the following: nature and preparation method of CPL (organic, inorganic, mixed or biopolymers); method and step number of functionalization (polymerization, polycondensation and post-polymerization modification); physical characteristics of the polymer

(homopolymers, copolymers, branched, cross-linking, grafted polymers, dendrimers, hyperbranched polymers, liquid crystalline polymers, polymeric films, etc.); structural organization of the polymer (molecular, supramolecular and topological levels); characteristic of the chelating fragments (structure, type, concentration, nature of the donor atoms, etc.).

Synthetic polymeric organic compounds containing chelating fragments represent the largest group of CPL. Their characteristic features are:

- the large number of functional (chelating) groups and comparative ease of their modification;
- a wide range of specific surface areas and pore sizes;
- controlled swelling and solubility in the reaction medium;
- adjustable mobility of chain segments (and, accordingly, chelating fragments);
- low adsorbability and stability over a wide pH range;
- weak physical adsorption capacity;
- possibility of introduction of chelating groups at the stageof the preparation and forecasting their distribution.

It should be noted that by formal features any interaction in the MX_n—CPL system can be considered as chelation reaction (multipoint metal binding with one polymer). Thus, the polydentate immobilization of a metal is often observed in the case of the polymers with monofunctional groups, for example, polyvinylpyridines, polyacids, polyvinyl alcohol, etc. And both mono- and bidentate intra- and intermolecular metal binding are observed in these systems. However, polymer ligands with monofunctional groups will not be considered in the book.

On the other hand, in recent year propagation are PMCs, in which the metal chelate units are located only on the surface of the powder, films, fibers, and PMCs may have not only three, but even two or one dimension.

Unfortunately, long time the metal chelates based on synthetic polymers belong to PMCs. However, according to the definition the metal chelates with inorganic, mixed and biopolymeric ligands are PMCs, because, for example, mostbiopolymers (DNA, RNA, enzymes, etc.) are the metal chelate macromolecular compounds. It defines the importance of PMCs in the vital functions of organisms, because the metals, for example, take place in binding of nucleic acids to proteins. The latter has a significant influence in their resistance to denaturation, the proceeding protein synthesis and the preservation of genetic information. In this connection, extensive studies were conducted to investigation of the metal chelation with biopolymer ligands and creation of their synthetic analogues. It should be noted that there are about 30 different metals used in polymeric systems for biomedical applications (Fig. 1.1) [43].

It should be noted the study of the metal chelates based on inorganic and mixed carriers, which develops in two directions: the modification of mineral carriers in order to the creation of chelating fragments on their surface followed the preparation of the metal chelates, and synthesis of the chelating macroligands based on mixed carriers.

H																	He
Li	Be											B	C	N	O	F	Ne
Na	Mg											Al	Si	P	S	Cl	Ar
K	Ca	Sc	Ti	V	Cr	Mn	Fe	Co	Ni	Cu	Zn	Ga	Ge	As	Se	Br	Kr
Rb	Sr	Y	Zr	Nb	Mo	Tc	Ru	Rh	Pd	Ag	Cd	In	Sn	Sb	Te	I	Xe
Cs	Ba	La	Hf	Ta	W	Re	Os	Ir	Pt	Au	Hg	Tl	Pb	Bi	Po	At	Rn
Fr	Ra	Ac	Rf	Db	Sg	Bh	Hs	Mt	Ds	Rg	Cn						

		Ce	Pr	Nd	Pm	Sm	Eu	Gd	Tb	Dy	Ho	Er	Tm	Yb	Lu
>>		Th	Pa	U	Np	Pu	Am	Cm	Bk	Cf	Es	Fm	Md	No	Lr

Fig. 1.1 Metals in periodic table used in polymeric systems for biomedical applications

The quantitative parameters of chelation process with the participation of the polymer ligands so far not been adequately studied in contrast to LMCs. This is due to the need to take into account a number of additional factors, mainly related to the chain nature of the polymer ligand. It is expedient to consider three levels of the spatial organization of PMCs [54]:

1. local level, which reflects the chemical and spatial structure of a single metal chelate cycle in the polymer chain (nature of the donor atoms and a center metal, cycle size, its electronic and spatial structure, etc.);
2. molecular level, defined by the spatial and chemical structure of the polymer chain (the elemental composition of monomer units, length, shape and conformation of a polymeric chain, etc.);
3. supramolecular level, reflecting the character of the intermolecular interaction of the polymer chains and the degree of their mutual ordering.

Taking these three levels of the spatial organization of the PMC into account, the free energy of the chelation involving macroligands can be represented (on the assumption that its components are additive) by the equation:

$$\Delta G = \Delta G_1 + \Delta G_2 + \Delta G_3. \tag{1.1}$$

Here ΔG_1, ΔG_2, and ΔG_3 are the free energy changes for the local, molecular, and supramolecular levels respectively. Under certain conditions, the free energy change for a particular level may be neglected, which makes it possible to analyze in detail the enthalpy (ΔH) and entropy ($T\Delta S$) contributions to ΔG for each level.

$$\Delta G = \Delta H - T\Delta S \tag{1.2}$$

In dilute solutions, chain association may be neglected; therefore $\Delta G_3 \rightarrow 0$ and (1.1) can be expressed in the form

$$\Delta G = \Delta G_1 + \Delta G_2. \tag{1.3}$$

In the case of infinitely long chains ($l \rightarrow \infty$) and low degrees of conversion[1] with respect to the chain molecule ($\alpha \rightarrow 0$), the chelation process may not exert a significant influence on the form and conformation of the macromolecule, so that $\Delta G_2 \rightarrow 0$ and hence

$$\Delta G = \Delta G_1 \tag{1.4}$$

Thus, in the case of dilute solutions with $l \rightarrow \infty$ and $\alpha \rightarrow 0$ the CPL behaves similarly to its low molecular weight analogue and the familiar Flory principle then operates: when the components of the model reaction are chosen correctly, the reactivity of the binding sites is independent of whether they belong to the polymer chain or to the low molecular weight analogue. This makes it possible to exclude from consideration the molecular and supramolecular levels and to analyze only the local chelate units.

For example, the entropy and enthalpy components of ΔG in the case of PMCs are determined mainly by the same contributions as in the case of LMCs [55–57]. Since the nature of the complex-forming metal and the chelating fragments is the same in both cases, the enthalpy of chelation changes little on passing from LMC to PMC. Therefore, for both LMC and PMC ΔG is determined by the entropy components. Formally the chelation reaction can be divided into several hypothetical elementary stages and the entropy of the entire process can be expressed as follows:

$$\Delta S_1^0 = \Delta S_{solv} + \Delta S_4^0 = \Delta S_2^0 + \Delta S_3^0 + \Delta S_5^0 + \Delta S_4^0, \tag{1.5}$$

where ΔS_1^0 is the experimental entropy of the reaction in solution, ΔS_4^0 is the calculated theoretical entropy of the reaction in the gas phase, ΔS_{solv} is the entropy of solvation of the metal ion (ΔS_2^0), of the ligand (ΔS_3^0), and of the complex formed (ΔS_5^0), which is determined as the difference between the entropies in solution and in the gas phase.

ΔS_4^0 represents in its turn the sum of the entropies of transfer (ΔS_t), internal rotation ($\Delta S_{int.rot}$), symmetry (ΔS_{sym}), isomerization (ΔS_{isom}), vibration (ΔS_{vib}), and rotation (ΔS_{rot}).

$$\Delta S_1^0 = \Delta S_{solv} + \Delta S_t + \Delta S_{int.rot} + \Delta S_{sym} + \Delta S_{isom} + \Delta S_{vib} + \Delta S_{rot} \tag{1.6}$$

It is assumed that the positive contributions to the entropy component of ΔG come from ΔS_t, ΔS_{rot}, ΔS_{sym}, and ΔS_{isom}. The contribution of ΔS_t, due to the

---

[1]The degree of conversion α is defined as the ratio of the actual number of metal ions bound to one chain and the maximum possible number.

change in the number of species on chelation, apparently changes little on passing from LMC to PMC. Consequently, the entropies of chelation are similar in the two cases, since the contribution of the transfer process is the main one. ΔS_{rot} makes a definite contribution to the entropy component. It is smaller in the case of PMC than in the reaction with monodentate ligands because the initial CPL and the PMC formed are the nonrotating species. The symmetry groups for low and high molecular weight compounds are significantly different and the number of possible isomers of PMC may be smaller, so that the contribution of isomerization is in this case reduced.

ΔS_{vib}, $\Delta S_{int.rot}$, and ΔS_{solv} make negative contributions to the entropy component. It is postulated that the contributions by the vibration and internal rotation are much lower in the case of the PMC than in the case of the LMC. If the monomeric and polymeric chelating ligands form structurally identical chelate fragments, then the contribution of solvation is approximately the same in both cases. However, as a rule such cases are rare and the polymer chain exerts a significant influence on the structure of the local chelate unit with the possibility of the formation of structures which are both less and more distorted than in the LMC.

The classification of PMCs adopted in this monograph includes four types of compounds: molecular, intracomplex, macrocyclic and polynuclear metal chelates. In the PMCs of molecular type, the metal ion chelation proceeds only through coordination bonds. Binding a metal ion by both the covalent and coordination bonds is characteristic for the PMCs of intracomplex type. Metal chelation of the CPLs contained macrocyclic groupings leads to the PMCs of macrocyclic type. Finally, polynuclear metal chelates contain two or more metal ions, and at least one of them must be part of the metallocycle. In following, PMCs are classified depending on the nature of the donor atoms (N,N–, N,O–, N,S–, O,O–, etc.).

Synthetic methodologies of PMCs in most cases consist of a series of sequential operations involving the preparation of a polymeric carrier, its functionalization towards the creation of chelating fragments, binding of MX_n, and purification of the final product. Sometimes, it is possible to achieve a reduction in the number of synthetic steps, which makes it possible to significantly simplify the entire technological chain, increase the overall yield and reduce the cost of the target product. One of the promising avenues for solving this complex problem is the one-stage synthesis of PMC, based on the (co)polymerization or polycondensation of metal chelate monomers (MCM) [1, 3, 10, 11, 14, 16, 18, 24, 30, 58–65]. Such compounds include a metal chelate ring and double bonds for (co)polymerization or functional groups for polycondensation. The undoubted advantage of this method is the possibility of purposeful production of PMCs, in which a metal ion with a predetermined spatial configuration of the chelate unit is contained in each chelating fragment.

The creation of dendrimers becomes an important landmark in the development of contemporary coordination chemistry. One of important classes of PMC is metal chelate dendrimers (MCDs) containing chelated metals in different parts of dendritic architecture, which have been obtained in the first days of dendrimer chemistry and are objects of increasing interest of researchers [66–69]. Metal chelate dendrimers are

relatively young, but rapidly developed area of PMC chemistry. Simultaneously with the metal chelate dendrimers the first examples of star and hyperbranched materials containing metal chelate units were prepared.

Extended hybrid crystalline complex compounds formed by organic ligands (also called spacers) and metal ions expanding in one, two or three dimensions due to formation of metal-ligand (M-L) coordination bond are called coordination polymers (CPs) [70–77]. CPs relate to a special class of PMCs containing metal in the main chain, whose special feature is breaking of a polymer chain after a metal is removed. First time the term «coordination polymer» was used in 1964 [78]. At the first stage of the studies, CPs were obtained using a simple mixing of components or the template method, as a result, insoluble substances were formed, whose exact structure was non-improvable. A great jump in directed design of CPs was done in 1990s by wide implementation of new techniques of synthesis of such materials, first of all, solvothermal method [79, 80], which made it possible to obtain pure substances useful for research by X-ray diffraction analysis. By controlling the process of CP molecular self-assembling, it is possible to obtain new crystalline functional materials with given practical properties. Because they contain large voids in the crystal structure, they were called porous CPs or metal-organic frameworks (MOFs). This term MOF was popularized around 1995 [81, 82] and it highlights their similarity to traditional structure of solids, in particular, zeolite framework materials, and thus characterizes reliability and porosity. MOFs differ by interesting architecture, crystalline state, capable of modifying the surface, and have potential applications in the areas of gaseous fuel storage, catalysis, magnetism and separation. Integration of MOFs become a real outbreak in science and served a powerful catalyst of intense development of CP chemistry.

Today it is absolutely clear that within relatively short time interval, with respect to historical scale, supramolecular chemistry has turned into very rapidly developed and interdisciplinary science, which includes chemical, physical, and biological aspects of studying more complicated than molecules chemical systems assembled into integral whole through intermolecular (non-covalent) interactions [83–89]. The supramolecular systems have a special niche, a level in hierarchy of matter, in which such principles of organizing and functioning of matter as molecular recognition, selective bonding, receptor-substrate interaction, trans-membrane transfer, and supramolecular catalysis are realized. Among the supramolecular systems the metallosupramolecular polymers (MSPs), which include metal-containing fragments as a basic supramolecular motif and formed as a result of spontaneous self-assembling of polytopic organic ligands and metal ions, represent of special interest [90, 91]. Concept of metallosupramolecular polymerization requires that a chelating monomer would be a telechelic system capable of continuous elongation of a chain in presence of a metal ion via well-known consecutive polycondensation mechanism. MSPs can be considered as a subset of PMCs, in which M-L interaction is dynamic by its character. These organic/inorganic hybrid systems potentially offer attractive combination of functionality of metal ions, mechanical properties and workability of polymers, as well as characteristics of self-assembling and dynamic character of supramolecular chemistry.

Among the most interesting areas of practical application of PMCs is the preparation of nanomaterials with low crystalline defects, narrow size distribution, and tunable shapes by their high-temperature thermolysis [92, 93]. From the view of the design of functional nanomaterials, solid-state thermolysis of PMCs possessing the wide diversity of the structures, compositions, and architectures is a simple and rational route to synthesize novel nanostructured materials. It should be noted the development of many important concepts such as size distribution focusing, selective adhesion shape control and branching for the description of the thermolysis process [93–96]. Thermolysis of PMC under various conditions is widely studied to obtain metal-containing nanostructures with target morphologies and sizes [2, 3, 6, 14, 15, 19, 20, 97–104]. It is important that different nanomaterials such as metals, metal oxides, metal sulfides and metal halides can be fabricated using PMC or their precursors.

The history of PMC research originates from the period of the Second World War and was stimulated, in the main, by tasks of a practical nature [1]. However, over the years, the development of PMC chemistry has been hampered by the lack of readily available synthesis techniques, difficulties in purifying the end products and convincing methods of their identification. In the early 1990s, a significant breakthrough was made in the synthesis of PMCs, which allowed the production of macromolecular soluble materials with well-defined spatial architectures. As a typical example, we note numerous synthetic methodologies of PMCs involving Schiff bases (Fig. 1.2).

These achievements allowed, in a figurative expression [105], to open a Pandora box of metal-containing polymers with new technological properties [106–114]. It

Fig. 1.2 Main directions of the synthesis of PMCs including Schiff bases

should also be noted the use of PMCs to obtain stimuli-responsive, self-healing, and shape-memory materials due to reversible metal-ligand interactions [115–119]. Extensive research of such materials began only in the last decade. Also of interest are such interesting objects as self-organizing and hierarchical architectures based on PMCs.

It should be noted the development of PMC studies as precursors of nanostructured materials, including carbon, metals, metal oxides, mixed metal oxides, etc. It is important that PMCs act not only as raw materials, but also as stabilizers of the formed nanoparticles, forming a protective shell [2, 6, 14, 15, 19, 20, 120, 121]. In recent decades, the use of PMC in nanotechnology and organic electronics, in particular in organic solar cells, nanowires, sensors, light-emitting devices, etc., has attracted considerable attention.

This book covers the major advances in the synthetic methodologies, physico-chemical properties, and spatial organization of polymeric metal chelates, and includes chapters on the synthesis and characterization of chelating polymer ligands, metal chelates based on synthetic polymers, metal chelate monomers, metal chelate dendrimers, coordination polymers containing metal chelate units, metal chelate supramolecular polymers, as well as thermolysis of metal chelate polymers. We hope that the analysis of the achievements and problems of the chemistry of polymeric metal chelates will contribute to a more accelerated development of this interesting and fascinating field of chemistry.

References

1. A.D. Pomogailo, I.E. Uflyand, *Makromolekulayrnye Metallokhelaty (Macromolecular Metal Chelates)* (Khimiya, Moscow, 1991)
2. A.D. Pomogailo, A.S. Rozenberg, I.E. Uflyand, *Metal Nanoparticles in Polymers* (Khimiya, Moscow, 2000)
3. D. Wohrle, A.D. Pomogailo, *Metal Complexes and Metals in Macromolecules* (Wiley-VCH, Weinheim, 2003)
4. I. Manners, *Synthetic Metal-containing Polymers* (Wiley VCH, Weinheim, 2004)
5. A.S. Abd-El-Aziz, C.E. Carraher, C.U. Pittman, J.E. Sheats, M. Zeldin, *Macromolecules Containing Metal and Metal-Like Elements, Biomedical Applications* (Wiley, Hoboken, New Jersey, 2004)
6. A.D. Pomogailo, V.N. Kestelman, *Metallopolymer Nanocomposites* (Springer, Berlin, Heidelberg, 2005)
7. V. Chandrasekhar, *Inorganic and Organometallic Polymers* (Springer, Berlin, Heidelberg, 2005)
8. Ch. Carraher Jr., C. Pittman Jr., A. Abd-El-Aziz, M. Zeldin, J. Sheats (eds.), *Metal and Metalloid Containing Macromolecules* (Wiley-Interscience, NY, 2006)
9. A. Abd-El-Aziz, C.E. Carraher Jr., C.U. Pittman, M. Zeldin (eds.), *Macromolecules Containing Metal and Metal-Like Elements* (J. Wiley and Sons, New Jersey, 2006)
10. J.H. Zagal, F. Bedioui, J.P. Dodelet, *N₄-Macrocyclic Metal Complexes* (Springer, NY, 2006)
11. U.S. Schubert, H. Hofmeier, G.R. Newkome, *Modern Terpyridine Chemistry* (Wiley-VCH, Weinheim, 2006)
12. A.S. Abd-El-Aziz, I. Manners, *Frontiers in Transition Metal-Containing Polymers* (Wiley, Hoboken, New Jersey, 2007)
13. A.S. Abd-El-Aziz, C.E. Carraher, C.U. Pittman, *Inorganic and Organometallic Macro-molecules: Design and Applications* (Springer, NY, 2008)

14. A.D. Pomogailo, G.I. Dzhardimalieva, *Monomer and Polymer Metal Carboxylates* (Fizmatlit, Moscow, 2009)

15. A.D. Pomogailo, G.I. Dzhardimalieva, V.N. Kestelman, *Macromolecular Metal Carboxylates and Their Nanocomposites* (Springer, Berlin, Heidelberg, 2010)

16. U.S. Schubert, A. Winter, G.R. Newkome (eds.), *Terpyridine-based Materials* (For Catalytic, Optoelectronic and Life Science Applications (Wiley-VCH, Weinheim, 2011)

17. A.S. Abd-El-Aziz, J.L. Pilfold, I. Kucukkaya, M.S. Vandel, *Metal-Containing Polymers. Encyclopedia of Polymer Science and Technology* (2012)

18. A.Z. El-Sonbati, M.A. Diab, A.A. El-Bindary, Stoichiometry of Polymer Complexes, in *Stoichiometry and Research—The Importance of Quantity in Biomedicine*, ed. by A. Innocenti (InTech, Rijeka, Croatia, 2012)

19. A.D. Pomogailo, G.I. Dzhardimalieva, *Nanostructured Materials Preparation via Condensation Ways* (Springer, Dordrecht, 2014)

20. A.D. Pomogailo, G.I. Dzhardimalieva, *Metallopolymeric Hybrid Nanocomposites* (Nauka, Moscow, 2015)

21. U.S. Schubert, A. Winter, *Supramolecular Assemblies: Polymers and Discrete Systems* (Wiley-VCH Verlag, Weinheim, 2015)

22. R.K. Khandal, M. Tyagi, G. Seshadri, *Metal Containing Polymers for Optical Applications: Metal Containing Composites with Tailor Made Optical Properties* (Lambert, 2010)

23. C.-L. Ho, W.-Y. Wong, Coord. Chem. Rev. **255**, 2469 (2011)

24. A.S. Abd-El-Aziz, P.O. Shipman, B.N. Boden, W.S. McNeil, Prog. Polym. Sci. **35**, 714 (2010)

25. S.-H. Liao, J.-R. Shiu, S.-W. Liu, S.-J. Yeh, Y.-H. Chen, C.-T. Chen, T.J. Chow, C.-I. Wu. J. Am. Chem. Soc. **131**, 763 (2009)

26. G.R. Whittell, I. Manners, Adv. Mat. **19**, 3439 (2007)

27. S.-J. Liu, Y. Chen, W.-J. Xu, Q. Zhao, W. Huang, Macromol. Rapid Commun. **33**, 461 (2012)

28. V. Marin, E. Holder, R. Hoogenboom, U.S. Schubert, Chem. Soc. Rev. **36**, 618 (2007)

29. G.R. Whittell, M.D. Hager, U.S. Schubert, I. Manners, Nat. Mat. **10**, 176 (2011)

30. A.S. Abd-El-Aziz, E.A. Strohm, Polymer **53**, 4879 (2012)

31. D.G. Kurth, Sci. Technol. Adv. Mater. **9**, 014103 (2008)

32. R.H. Staff, M. Gallei, M. Mazurowski, M. Rehahn, R. Berger, K. Landfester, D. Crespy, ACS Nano. **6**, 9042 (2012)

33. J. Elbert, M. Gallei, C. Rüttiger, A. Brunsen, H. Didzoleit, B. Stühn, M. Rehahn, Organometallics. **32**, 5873 (2013)

34. M. Gallei, Macromol. Chem. Phys. **215**, 699 (2014)

35. A.S. Abd-El-Aziz, C. Agatemor, N. Etkin, Macromol. Rapid Commun. **35**, 513 (2014)

36. J. Elbert, F. Krohm, C. Rüttiger, S. Kienle, H. Didzoleit, B.N. Balzer, T. Hugel, B. Stühn, M. Gallei, A. Brunsen, Adv. Funct. Mater. **24**, 1591 (2014)

37. A.D. Russell, R.A. Musgrave, L.K. Stoll, P. Choi, H. Qiu, I. Manners, J. Organomet. Chem. **784**, 24 (2015)

38. A. Valente, P. Zinck, Rec. Res. Devel. Polym. Sci. **11**, 99 (2012)

39. J.C. Swarts, M.J. Cook, E.N. Baker, Met. Based Drugs **2008**, 286363 (2008)

40. E.P. Ivanova, K. Bazaka, R.J. Crawford, *New Functional Biomaterials for Medicine and Healthcare* (Woodhead Publishing, Oxford, Cambridge, Philadelphia, New Delhi, 2014)

41. M.R. Roner, C.E. Carraher Jr., K. Shahi, G. Barot, Materials. **4**, 991 (2011)

42. X. Zhao, J.M. Courtney, H. Qian (eds.), *Bioactive Materials in Medicine: Design and Applications* (Woodhead Publishing, Oxford, Cambridge, Philadelphia, New Delhi, 2011)

43. Y. Yan, J. Zhang, L. Ren, C. Tang, Chem. Soc. Rev. **45**, 5232 (2016)

44. S. Bonnet, J.-P. Collin, M. Koizumi, P. Mobian, J.-P. Sauvage, Adv. Mat. **18**, 1239 (2006)

45. P. Ceroni, A. Credi, M. Venturi, Chem. Soc. Rev. **43**, 4068 (2014)

46. M. Schmittel, P. Mal, Chem. Commun. 960 (2008)

47. X. Lu, X. Li, Y. Cao, A. Schultz, J.-L. Wang, C.N. Moorefield, C. Wesdemiotis, S.Z.D. Cheng, G.R. Newkome, Angew. Chem. Int. Ed. **52**, 7728 (2013)

48. G.R. Newkome, P. Wang, C.N. Moorefield, T.J. Cho, P.P. Mohapatra, S. Li, S.-H. Hwang, O. Lukoyanova, L. Echegoyen, J.A. Palagallo, V. Iancu, S.-W. Hla, Science. **312**, 1782 (2006)

49. R. Sarkar, K. Guo, C.N. Moorefield, M.J. Saunders, C. Wesdemiotis, G.R. Newkome, Angew. Chem. Int. Ed. **126**, 12378 (2014)
50. Y. Nishimori, K. Kanaizuka, M. Murata, H. Nishihara, Chem. Asian J. **2**, 367 (2007)
51. P. Broekmann, K.-H. Dötz, C.A. Schalley (eds.), *Templates in Chemistry III* (Springer, Berlin, 2009)
52. F.C. Krebs, M. Biancardo, Sol. Energy Mater. Sol. Cells. **90**, 142 (2006)
53. P. Wang, C.N. Moorefield, S. Li, J. Manriquez, C.D. Shreiner, E. Bustos, A.L. Hartley, L.A. Godinez, G.R. Newkome, J. Mater. Chem. **17**, 3023 (2007)
54. A.D. Pomogailo, E.F. Vainshtein, I.E. Uflyand, Russ. Chem. Rev. **64**, 913 (1995)
55. M. Foscato, B.J. Houghton, G. Occhipinti, R.J. Deeth, V.R. Jensen, J. Chem. Inf. Model. **55**, 1844 (2015)
56. S. Fortuna, F. Fogolari, G. Scoles, Sci. Rep. **5**, Article number: 15633 (2015)
57. S. Di Stefano, G. Ercolani, Adv. Phys. Org. Chem. **50**, 1 (2016)
58. A.D. Pomogailo, I.E. Uflyand, J. Coord. Chem. **23**, 183 (1991)
59. I.E. Uflyand, A.D. Pomogailo, Russ. Chem. Rev. **60**, 773 (1991)
60. A.D. Pomogailo, V.V. Savostyanov, *Synthesis and Polymerization of Metal-Containing Monomers* (CRC Press, Boca Raton, London, NY, 1994)
61. I. Asselberghs, M.J. Therien, B.J. Coe, J.A. McCleverty, K. Clays, in *Metal-Containing and Metallosupra-molecular Polymers and Materials*, ACS Symposium Ser., vol. 928 (ACS, Washington, DC, 2006), p. 527
62. A.C.W. Leung, M.J. MacLachlan, J. Inorg. Organomet. Polym. **17**, 57 (2007)
63. W.K. Chan, Coord. Chem. Rev. **251**, 2104 (2007)
64. A. Wild, A. Winter, F. Schlutter, U.S. Schubert, Chem. Soc. Rev. **40**, 1459 (2011)
65. G.I. Dzhardimalieva, I.E. Uflyand, J. Inorg. Organomet. Polym. **26**, 1112 (2016)
66. S. Campagna, P. Ceroni, F. Puntoriero (eds.), *Designing Dendrimers* (Wiley, Hoboken, 2012)
67. Y. Cheng (ed.), *Dendrimer-based drug delivery systems: from theory to practice* (John Wiley & Sons, Hoboken, New Jersey, 2012)
68. D.A. Tomalia, J.B. Christensen, U. Boas, *Dendrimers, Dendrons, and Dendritic Polymers: Discovery, Applications, and the Future* (Cambridge University Press, Cambridge, 2012)
69. F. Vögtle, G. Richardt, N. Werner, *Dendrimer Chemistry: Concepts, Syntheses, Properties, Applications* (Wiley, Weinheim, 2009)
70. K.D. Karlin, D.T.D. Lili, C.L. Cahill, *Coordination Polymers of the Lanthanide Elements* (John Wiley & Sons Inc, Weinheim, 2008)
71. S.R. Batten, D.R. Turner, M.S. Neville, *Coordination Polymers: Design, Analysis and Application* (RSC, Cambridge, 2009)
72. K. Naka, Metal Organic Framework (MOF), in *Encyclopedia of Polymeric Nanomaterials*, eds. S. Kobayashi, K. Müllen (Springer, Berlin, Heidelberg, 2015)
73. M.C. Hong, L. Chen (eds.), *Design and Construction of Coordination Polymers* (Wiley, Weinheim, 2009)
74. J. Jiang (ed.), *Metal-Organic Frameworks: Materials Modeling towards Engineering Applications* (CRC, Boca Raton, 2015)
75. L.R. MacGillivray (ed.), *Metal-Organic Frameworks: Design and Application* (Wiley, Weinheim, 2010)
76. L.R. MacGillivray, C.M. Lukehart (eds.), *Metal-Organic Framework Materials* (Wiley, Weinheim, 2014)
77. O.L. Ortiz, L.D. Ramírez, *Coordination Polymers and Metal Organic Frameworks: Properties, Types, and Applications* (Nova Science Publishers, NY, 2012)
78. J.C. Bailar, Jr., in *Preparative Inorganic Reactions*, vol. 1, ed. by W.L. Jolly (Interscience, NY, 1964)
79. Y. Zhao, K. Li, J. Li, Z. Naturforsch. **65b**, 976 (2010)
80. W. Xuan, C. Zhu, Y. Liu, Y. Cui. Chem. Soc. Rev. **41**, 1677 (2012)
81. O.M. Yaghi, G. Li, H. Li, Nature **378**, 703 (1995)
82. O.M. Yaghi, H. Li, J. Am. Chem. Soc. **117**, 10401 (1995)
83. J.M. Lehn, *Supramolecular Chemistry—Concepts and Perspectives* (VCH, Weinheim, 1995)
84. J.W. Steed, J.L. Atwood, *Supramolecular Chemistry* (Wiley, Weinheim, 2005)

85. J.W. Steed, J.L. Atwood (eds.), *Encyclopedia of Supramolecular Chemistry* (Marcel Dekker, NY, 2004)
86. P.J. Cragg, *Practical Supramolecular Chemistry* (John Wiley & Sons Ltd, Chichester, UK, 2006)
87. K. Ariga, T. Kunitake, *Supramolecular Chemistry—Fundamentals and Applications* (Springer-Verlag, Heidelberg, 2006)
88. J.W. Steed, D.R. Turner, K.J. Wallace, *Core Concepts in Supramolecular Chemistry and Nanochemistry* (John Wiley & Sons Ltd., Weinheim, 2007)
89. B.M. McKenzie, S.J. Rowan, Metallosupramolecular polymers, networks, and gels, in *Molecular Recognition and Polymers: Control of Polymer Structure and Self-Assembly*, eds. by V. Rotello, S. Thayumanavan (Wiley, Weinheim, 2008)
90. B.M. McKenzie, S.J. Rowan, Metallo-Supramolecular Polymers, in *Encyclopedia of Supramolecular Chemistry*, eds. by J.L. Atwood, J.W. Steed (CRC Press, Boca Raton, 2007)
91. A. Winter, U.C. Schubert, Chem. Soc. Rev. **45**, 5311 (2016)
92. A.P. Reverberi, N.T. Kuznetsov, V.P. Meshalkin, M. Salerno, B. Fabiano, Theor. Found. Chem. Eng. **50**, 59 (2016)
93. W.L. Leong, J.J. Vittal, Chem. Rev. **111**, 688 (2010)
94. H. Liu, J. Owen, A.P. Alivisatos, J. Am. Chem. Soc. **129**, 305 (2007)
95. G.I. Dzhardimalieva, A.D. Pomogailo, Russ. Chem. Rev. **77**, 259 (2008)
96. A.D. Pomogailo, A.S. Rozenberg, G.I. Dzhardimalieva, Russ. Chem. Rev. **80**, 257 (2011)
97. M.Y. Masoomi, A. Morsali, Coord. Chem. Rev. **256**, 2921 (2012)
98. B.I. Kharisov, O.V. Kharissova, U.O. Méndez, J. Coord. Chem. **66**, 3791 (2013)
99. O. Carp, Materials obtained by solid-state thermal decomposition of coordination compounds and metal-organic coordination polymers, in *Reactions and Mechanisms in Thermal Analysis of Advanced Materials*, eds. by A. Tiwari, B. Raj (Scrivener Publishing LLC, 2015)
100. Y. Song, X. Li, L. Sun, L. Wang, RSC Adv. **5**, 7267 (2015)
101. J.-K. Sun, Q. Xu, Energy Environ. Sci. **7**, 2071 (2014)
102. M. Ramazani, A. Morsali, Ultrason. Sonochem. **18**, 1160 (2011)
103. M. Ramanathana, S.B. Darling, Polym. Int. **62**, 1123 (2013)
104. B.I. Kharisov, H.V. Rasika Dias, O.V. Kharissova, V.M. Jiménez-Pérez, B.O. Pérez, B.M. Flores, RSC Adv. **2**, 9325 (2012)
105. M. Schmittel, Chem. Commun. **51**, 14956 (2015)
106. J. Zhou, G.R. Whittell, I. Manners, Macromolecules **47**, 3529 (2014)
107. C.G. Hardy, J. Zhang, Y. Yan, L. Ren, C. Tang, Prog. Polym. Sci. **39**, 1742 (2014)
108. A.K. Yetisen, M.M. Qasim, S. Nosheen, T.D. Wilkinson, C.R. Lowe, J. Mater. Chem. C. **2**, 3569 (2014)
109. X. Wang, R. McHale, Macromol. Rapid Commun. **31**, 331 (2010)
110. Y. Nishimori, K. Kanaizuka, M. Murata, H. Nishihara, Chem. Asian J. **2**, 367 (2007)
111. V.P. Smagin, Rev. J. Chem. **3**, 163 (2013)
112. F.C. Krebs, M. Biancardo, Sol. Energy Mater. Sol. Cells. **90**, 142 (2006)
113. P. Wang, C.N. Moorefield, S. Li, J. Manriquez, C.D. Shreiner, E. Bustos, A.L. Hartley, L.A. Godinez, G.R. Newkome, J. Mater. Chem. **17**, 3023 (2007)
114. M.W. Urban (ed.), *Handbook of Stimuli-Responsive Materials* (Wiley-VCH Verlag GmbH & Co. KGaA, Weinheim, 2011)
115. B. Sandmann, S. Bode, M.D. Hager, U.S. Schubert, Adv. Polym. Sci. **262**, 239 (2013)
116. S.K. Ghosh, *Self-healing Materials: Fundamental, Design Strategies, and Applications* (Wiley-VCH, Weinheim, 2009)
117. S. Bode, D. Sandmann, M.D. Hager, U.S. Schubert, Metal-complex-based self-healing polymers, in *Self-Healing Polymers: From Principles to Applications*, ed. by W.H. Binder (Wiley, 2013)
118. C.L. Lewis, E.M. Dell, J. Polym. Sci., Part B: Polym. Phys. **54**, 1340 (2016)
119. C. Roco, C.A. Mirkin, M.C. Hersam, *Nanotechnology Research Directions for Societal Needs in 2020: Retrospective and Outlook* (Springer, Berlin, 2011)
120. M. Ramanathan, S.B. Darling, Polym. Int. **62**, 1123 (2013)
121. M. Ramanathan, Y.-C. Tseng, K. Ariga, S.B. Darling, J. Mater. Chem. C. **1**, 2080 (2013)

Chapter 2
Polymer Chelating Ligands: Classification, Synthesis, Structure, and Chemical Transformations

Abstract The past few decades were marked by significant achievements in the field of chelating polymer ligands including those of different types of polymers and various chelating fragments. The chelating polymers classification adopted in this book includes, primarily, the method of preparation and structure of the polymer backbone and then its functionality. These ligands provide broad control over the metal chelate distribution and allow to preparing polymeric materials with enhanced stability, tunable solubility in aqueous and organic media, as well as interesting optical, magnetic, and fluorescent properties. This chapter analyzes the synthetic methodologies and spatial structures such chelating polymer polymers as linear, branched, cross-linked, grafted polymers, dendrimers, star and hyperbranched polymers, as well as liquid-crystalline polymers and polymeric films. Special attention is paid to the features of chelating polymer ligand preparation methods: (co)polymerization of chelating monomers, methods of controlled radical polymerization, click chemistry methods, method of cation polymerization, chemical oxidized polymerization, electropolymerization, photo- and microwave-assisted polymerization, cyclopolymerization, asymmetrical polymerization, post-polymerization modification, polycondensation reactions, «green» synthesis, and grafted polymerization. The problems and future prospects of such chelating polymer ligands are outlined.

Chemistry of chelating polymers has reached its peak development in XXI century: keys to the synthesis of a range of new type of CPLs have been found, fine technology of fabrication of such materials as biosensors, medical implants, organic light-emitting diodes (OLED) has been developed, spatial structural organizations of interface boundaries have been basically understood. Thin films give a possibility of direct synthesis of polymers with extremely difficultly compatible functional groups. Using post-polymerization modification (PPM) in combination with click chemistry methods makes it possible to avoid limitations, which would be impossible to achieve otherwise [1]. Polymers are very convenient for fabrication of hybrid materials, because a chain gives a wide range of possibilities for integration of functional groups and active centres of different origins.

Interaction between MX_n and CPLs is the most-used method of PMC preparation [2–14]. It is important that the possibility of synthesis of PMCs, as well as their physico-chemical properties, can be engineered even at the stage of CPL design. Presently chemistry and synthesis technique of CPL are developed quite well and they continue to improve. Owing to achievements of contemporary polymer chemistry, now there are no considerable difficulties in synthesis of any chelating fragments linked by a polymer chain. Moreover, almost all types and classes of traditional polymers are involved in solutions to these problems (Fig. 2.1) [15].

All three traditional approaches of polymer chemistry are used for creation of the polymers containing chelating fragments:

- homopolymerization, co-polymerization, and grafted polymerization of monomers with chelating nodes;
- polycondensation of respective compounds, which bring to CPL formation;
- PPM of functional groups of polymers for completion of chelating fragments.

The simplest way of producing CPLs is associated with synthesis of new monomers for reactions of polymerization and polycondensation, in which necessary functionalities are included in chemical structure of their monomers. Though these precursors with chelating groups always took a special place among other methods of polymer chelation, due to their simplicity and wide range of reactions with their participation, researchers always encountered with the problems of establishment of the effect of these groups on polymerization rate and conversion, as well as introduction of sufficient number of monomer units in a polymer during copolymerization of multiactive comonomers, etc. However, a potential of this approach is limited,
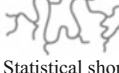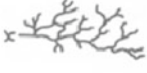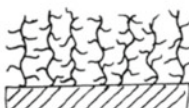
Linear	Branched	Networks	Dendritic
Flexible coil	Statistical short chain branching	Rarely cross-linked	Hyperbranched
Rigid rod	Statistical long chain branching	Densely cross-linked	Star
Cycle	Regular comb branching	Interpenetrating networks	Dendrimer
Polyrotaxane	Polymer brushes		

Fig. 2.1 Architecture of macromolecules for CPL design

since, on the one hand, a number of similar monomers is strongly limited, and on the other hand, the (co)polymerization process is accompanied by variety of chemical transformations of these monomers.

Alternative approach is PPM (post-polymerization design) of CPLs of different topology and structure from already known polymers [16, 17], especially, using commercial polymers as backbone [18, 19]. Possibilities of this way are almost infinite: from changing such simple characteristics as composition of a chelating fragment, length of linking bridges (spacers), presence of cross-linkings, etc., to subtler effects, like long-range correlations and gradient structure. Therefore, in frameworks of this approach a wide range of CPLs can be designed, almost without disturbing the main chain of initial polymer.

The developed preparation methods of CPL synthesis are widely used in laboratory practice and in industry, in particular, in production of chelating sorbents.

Increasing needs of science and engineering bring to the forefront the problems of design of principally new «functional» [20–25], «smart» [26–28], «stimuli-responsive shape memory» [29], «self-oscillating» [30], and other materials, using efficient critical technologies meeting demands of «green chemistry» [31–37]. Among them is primary choice of enzymatic catalyst [38–40], reaction medium (supercritical carbon dioxide [41–43], ionic liquids (ILs) [44], water as solvent [45–47]), design of biodegradable polymers [48], etc.

Varying of a polymer chain structure makes it possible to perform «fine tuning» of necessary parameters and properties, thus creating prerequisites for fabrication of materials with desired properties [49–53]. In this respect applying of the principles of constitutional dynamic and adaptive chemistry [54–59] is very promising, especially with usage of molecular dynamic libraries [60] or computer databases of polymers [61]. Chemical structure of macromolecules is widely variable: even a single macromolecule could be considered as a «molecular system», which can change configuration in a wide range, and abnormally low entropy makes it highly sensitive to different impacts.

2.1 Linear, Branched and Network Polymers as Chelating Macroligands

The study of the physico-chemical properties and spatial structure of polymers is one of most promising approaches to solution of the problem of design and directed synthesis of PMC with predetermined properties. In contrast to low molecular weight analogues, polymer ligand is characterized by some features, which make difficult to study its physico-chemical characteristics. This, probably, explains why many CPLs based on synthetic polymers have not been adequately studied. For them three levels of structural organization should be taken into account [62]:

– molecular, which reflects chemical structure of polymer units, their distribution in chain and stereochemical construction of the chains;

Fig. 2.2 Structure of
polymers

Linear

Branched

Networks
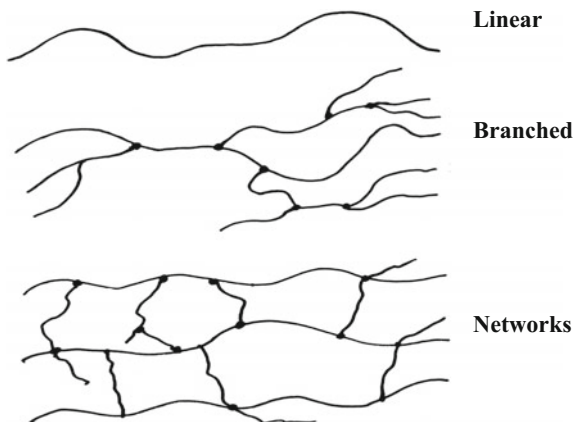
– supramolecular, which takes into account intermolecular interactions, degree of
  ordering and macromolecular packing;
– topological, which characterizes correlation between elements of the structure of
  polymers (molecular-mass distribution, parameters of 3D structure, etc.)

Among vast variety of topological structures of the polymers [2, 63], the sim-
plest are linear, branched, and network structures (Fig. 2.2).

Most widely for the CPL synthesis free radical polymerization is used, rarely
used is ionic polymerization of chelating monomers depending on character of
active particles. By a number of types of contributing monomers homopolymer-
ization (one type of monomer) and co-polymerization (two and more types of
monomers), resulting in linear or branched polymers, are distinguished. In order to
obtain spatially cross-linked polymers, polymerization is carried out in presence of
divinyl compounds, for example, divinylbenzene (DVB), N,N′-methylenebisacry-
lamide (MBA), etc., or various methods of 3D polymerization are used [64]. Wide
use of this technology is stipulated by a possibility of its application for different
vinyl monomers, soft conditions of reaction process, often by tolerance to func-
tional groups of monomers, easiness of application in industry, and low cost as
compared with other technological processes.

2.1.1 (Co)polymerization of Chelating Monomers

Polymerization begins from breaking of one chemical bonds and creation of others.
Break in double bonds leads to decrease in energy of a system and is spontaneous
exothermal process ($\Delta G < 0$, $\Delta H < 0$). However, without external impacts (ini-
tiators, catalysts, etc.) polymerization usually proceeds slowly. Thus, methacry-
loylacetone can polymerize slowly at storage at room temperature, however, its
polymerization rate is far slower than that of traditional monomers, such as methyl

methacrylate (MMA), styrene (St), etc. This is due to strong tendency to transfer of a chain by chelating fragments (for example, by enol form of β-diketonate groups) and low activity of enol radicals as compared to radicals of the chain growth [65].

To increase polymerization rates of chelating type monomers, standard methods are used: chemical action by introduction of different initiators (peroxides, azo-compounds). Thus, benzoyl peroxide (BP) was used in polymerization of monomers containing such chelating fragments as *o*-hydroxyaldehydes (ketones) [66, 67], sal-icylaldimines [68–70], 8-hydroxyquinolines (HQ) [71–74], etc.

The examples of using 2,2′-azobisiso-butyronitrile (AIBN) are polymerization of monomers with groups 1,4,8,11-tetraazacyclotetradecane (cyclam) [75], HQ [76–79], 2-acrylamidosulphadiazine [80], 2-acrolyl-quinazoline [81], 34-membered monoazacrown ether [82], and also co-polymerization of traditional monomers with chelating monomers 5-vinyl-*m*-phenylene-*m*′-phenylene-32-crown-10 [83], benzo-15-crown-5 derivative [84], acrylamidomethyl-18-crown-6 (acrylamidomethyl-15-crown-5) [85], benzo-12-crown-4 (15-crown-5, 18-crown-6)-acrylamide [86–89], Q-methacrylate [90–92], etc.

These initiators are widely used for synthesis of cross-linked co-polymers. Thus, 2-hydroxy-4-acryloyloxybenzophenone was co-polymerized with DVB in presence of AIBN [93]. Poly(vinylcatechol-*co*-DVB) resins were obtained via suspension polymerization of 3,4-dimethoxystyrene and DVB and toluene as a porogen and the following removal of protection from catechol groups (Scheme 2.1) [94].

Co-polymerization of 4-acetyl acryloyl ethyl acetate and acrylic acid (AA) was performed using AIBN as initiator and MBA as a cross-linking agent [95]. The cross-linked polymers of poly(2-hydroxy-4-acryloyloxybenzophenone) were obtained by free-radical polymerization of 2-hydroxy-4-acryloyloxybenzophenone monomer with DVB cross-linking agent [96].

It should be noted the synthesis of homo- and copolymers of poly(norbornene) containing spiropyran (SP) side groups [97]. Due to the opened merocyanine (MC) form, difficulties in the homopolymerization of SPs were observed, which resulted in low polymerization yields for homopolymers. At the same, copolymers with 10 mol% SP content were obtained in good yield. Also it is important that switching between the apolar SP form and the zwitter-ionic MC form also leads to switchable wettability.

Of considerable interest is also poly(crown ether) bearing dibenzo-24-crown-8 moieties in the polymer backbone prepared using a rotaxanation-protection proto-col, including stepwise production via the polymerization of cavity-filled [2] rotaxane and subsequent removal of the axial fragment [98].
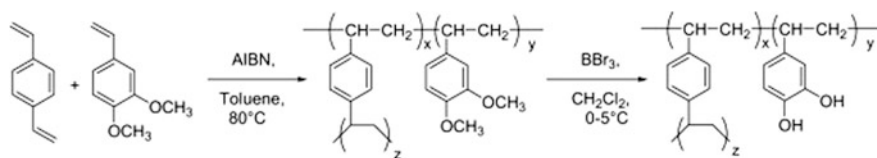
Scheme 2.1 Synthesis of porogenic catechol CPL

Values of reactivity coefficients for Q-methacrylate (r_1) and MMA (r_2) found from the Finemann-Ross dependence are 0.76 and 0.52, respectively [90]. When the values r_1 and r_2 are less than 1, azeotropic polymerization takes place, and $r_1 = 0.67$ (which corresponds to the mole fraction of Q-methacrylate in the initial monomer mixture) points to the fact that the formed co-polymer will have the same composition as the initial monomer mixture. When the molar fraction in the monomer mixture is less than 0.67, co-polymer is enriched with units of chelating monomer. The composition of the co-polymer (Table 2.1) illustrates these relationships.

The idea of a character of distribution of co-polymers of a certain molecular weight—polydispersity index (PDI = M_w/M_n), is seen from Table 2.2. The M_w and M_n values change from 13,974 to 19,996 and from 38,071 to 56,950, respectively, while PDI varies from 2.68 to 2.96. Intrinsic viscosity varies from 0.015 to 0.030 dL g^{-1}. These results show that when content of Q-methacrylate decreases in the co-polymers, average molecular weight and viscosity decrease considerably, whereas PDI varies randomly [90].

Table 2.1 Copolymer compositions data and reactivity ratios of copolymers of Q-methacrylate and MMA

Monomer feed composition		Conversion (%)	Composition of Q-methacrylate in copolymer [m_1]	Reactivity ratio	
Q-methacrylate [M_1] mol.	MMA [M_2] mol.			r_1	r_2
1.00	–	–	–	0.76	0.52
0.50	0.50	9.45	0.552		
0.40	0.60	8.86	0.425		
0.30	0.70	8.38	0.336		
0.20	0.80	9.76	0.212		
0.10	0.90	8.40	0.184		
–	1.00	–	–		

Table 2.2 Average molecular weights and viscosity data for the copolymers Q-methacrylate with MMA

Composition of Q-methacrylate in copolymer	M_n	M_w	PDI	[η], dL g^{-1}
1.00	19,219	56,950	2.96	0.030
0.552	19,966	46,153	2.72	0.023
0.425	15,210	42,356	2.78	0.020
0.336	14,539	39,626	2.73	0.019
0.212	14,210	38,071	2.68	0.016
0.184	13,974	38,102	2.73	0,015
–	14,848	40,146	2.70	0.017

Among other initiators, we shall notice 2,2′-dimethoxy-2-phenyl-acetophenone, which was used for polymerization of diethyliminodiacetate-containing monomers based on ethyl-α-bromomethacrylate and α-chloromethacryloylchloride with diethyl iminodiacetate [99]. Monomers show low homopolymerization activity, which is ascribed to steric effect of *N,N*-disubstituted methacrylamides, in presence of allylamine group they are subjected to the degradation transfer of a chain, while bulky iminodiacetate groups enclose a double bond. Monomers with diethyliminodiacetate groups are co-polymerized with acrylamide (AAm) in water under action of the 2,2′-azobis(*N,N*′-amidinopropane) dihydrochloride initiator. It should also be noted that in this system rate of polymerization and conversion of both monomers are reduced.

Among other kinetic dependencies of polymerization, we shall note that *p*-vinylbenzoylacetone polymerization follows the traditional model of radical polymerization; its rate is proportional to square root from concentration of initiator. The ratio of activities in co-polymerization is $r_1 = 2.56$ for St and $r_2 = 0.32$ for *p*-vinylbenzoylacetone in benzene [100].

Polymerization is carried out in different ways: in bulk, in solution, in suspension. For example, polyacryloylacetone is prepared by polymerization of acryloylacetone in sealed tubes [101]. Initiated polymerization of salicylic acid *O*-carboxyanhydride was performed in block at 140 °C [102]. In this case, rather pure polymer is obtained, and the main difficulty of the process is in removal of polymerization heat. Most CPLs are obtained by polymerization in solution, since it is easier to remove heat and to control composition and structure of the polymers, however, a problem of a solvent removing is raised. A scheme of radical precipitation polymerization can be represented as follows (Scheme 2.2).
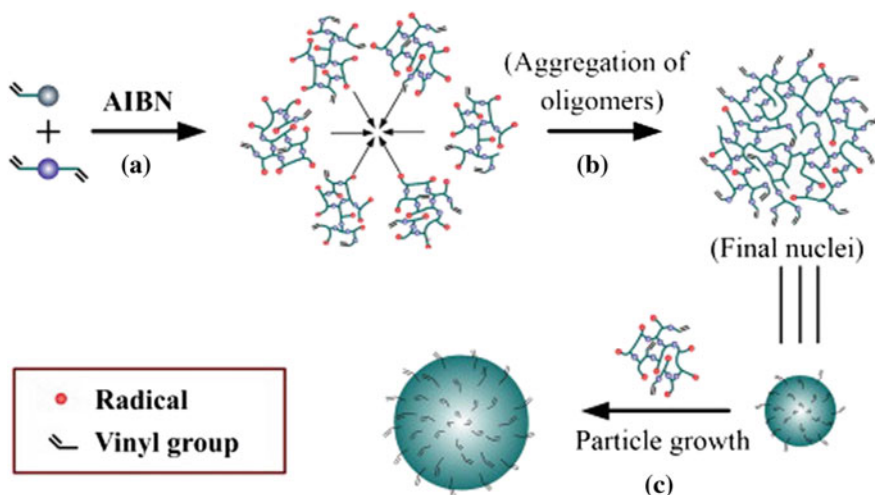
Scheme 2.2 Mechanism of particles' formation during precipitation polymerization, including particle nucleation (**a**, **b**) and particle growth (**c**)

The co-polymer PAN-*co*-poly(hexamethylene guanidine hydrochloride), where PAN is polyacrylonitrile, was also obtained by precipitation co-polymerization of acrylonitrile (AN) and modified macromonomer poly(hexamethylene guanidine hydrochloride) in water [103].

During suspension polymerization a monomer exists in form of drops dispersed in water or other liquid. As a result of the reaction, polymer beads are formed with the size from 10^{-16} to 10^{-13} m. Inversion suspension co-polymerization of hydrophilic glycidyl methacrylate (GMA) and iminodiacetic acid (IDA) [104]; suspension radical co-polymerization of 2-methacryloyl amidocysteine, and 2-hydroxyethylmethacrylate [105, 106] can be considered as examples. The traditional drawback of this method is a necessity in stabilization of suspension and washing of polymers from stabilizers.

Apart from traditional ways of initiation, polymerization of chelating monomers can also take place as a result of radiation initiation. Therefore, γ-radiation polymerization of AA is performed in presence of 2-mercaptobenzimidazole and a cross-linking agent [107]. The CPL with fragments of ethylenediaminetetraacetic acid (EDTA) is obtained via γ-radiation induced template polymerization of AA on polyacrylamide (PAAm) in presence of EDTA-Na$_2$ and MBA as a cross-linking agent [108]. Hydrogel poly(*N*-(hydroxymethyl) methacrylamide-1-allyl-2-thiourea) is synthesized under action of γ-radiation using ^{60}Co with different radiation doses to change the porosity and cross-linking density of the hydrogels [109, 110].

Control over molecular weight of macromolecules can be realized, as in the case of traditional monomers, using initiators, inhibitors, and other compounds. However, transfer and termination can take place at different stages of a chain growth, therefore macromolecules are polydisperse. A drawback of radical polymerization is a difficulty in control over molecular weight of a polymer, molecular structure, and composition of a co-polymer [111]. Therefore, there was always a necessity in improvement of the process of radical polymerization under soft conditions, so that CPLs with controlled molecular weight, required architecture of macromolecules and low PDI could be obtained.

2.1.2 Chelating Macroligands Obtained by the Methods of Controlled Radical Polymerization

A range of new chemical and biologic methods of polymerization used in large-scale and small-scale polymer production is recently developed [26]. Thus, discovery of «living» controlled radical polymerization (CRP) [112–114] was a serious step in the way of improvement of the technology, because this method provides production of high quality polymers with predetermined structure and molecular weight under conditions typical for radical polymerization. The polymers obtained by that way have narrow PDI and a specified molecular weight. Moreover, the method of CRP gives a possibility of synthesis of polymer molecules of complicated architecture

(block-*co*-polymers, star-like and grafted structures), and also a possibility of intro-duction of chelating fragments in a polymer structure. Thus, the «living» controlled radical co-polymerization is used to obtain polyfunctional block (-*b*-) St-co-MMA polymers with narrow PDI, containing units of 2,2′:6′,2″-terpyridine (tpy) in the side chain [115].

It should be noted the synthesis of «schizophrenic» copolymer (poly[1′-(2-methacryloxyethyl)-3′,3′-dimethyl-6-nitrospiro-(2H-1-benzopyran-2,2′-indoline)]-*b*-PAA) by sequential Cu(0)-mediated «living» CRP at 30 °C in an oxygen-tolerant system followed by hydrolysis of the resulting polymer [116]. The «schizophrenic» micellization behavior of as-prepared copolymer in aqueous solution regulated by light and pH stimuli was vividly demonstrated (Fig. 2.3).

In the ideal «living» polymerization reaction of irreversible chain termination does not happen, all polymer chains begin their growth almost simultaneously (at the initiation rate far higher than the growth rate of a chain). Therefore, PDI is very narrow (<1.5), and growth of polymer chains can be continued at addition of a new portion of a monomer. A decrease in contribution from the reaction of irreversible chain termination can be achieved by decrease in concentration of growing polymer radicals via introduction of mediators of polymerization, which react reversibly with growing polymer radicals, thus converting them into inactive state. Therefore, equilibrium is reached between active and inactive polymer radicals. Without going into details of quite profoundly studied mechanism, we shall notice that, depending on a way of «livening» macromolecules, the following kinds of this method are distinguished:
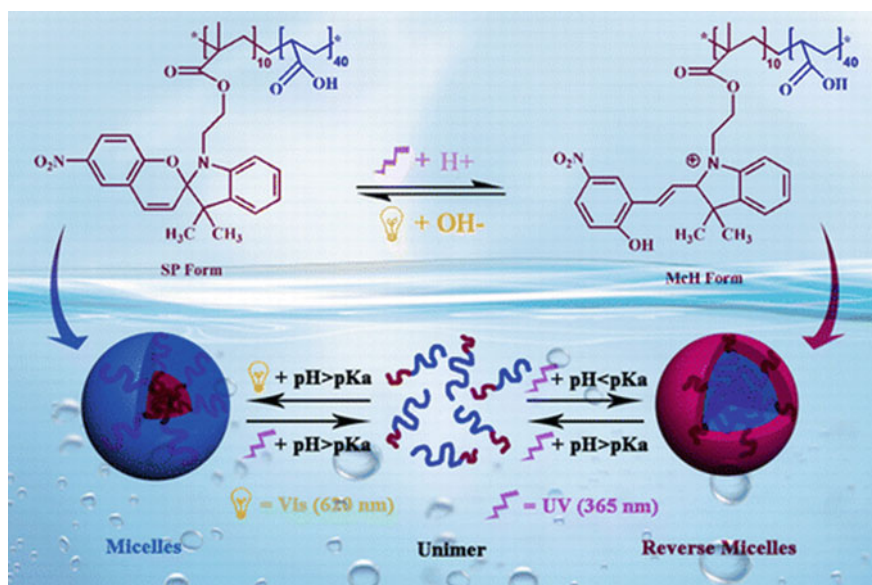

Fig. 2.3 Vividly «schizophrenic» micellization behavior in aqueous system

(1) polymerization with participation of metal complexes, so called Atom Transfer Radical Polymerization (ATRP) [117, 118];

(2) polymerization via reversible addition of a radical and fragmentation of dithioethers, in other words, Reversible Addition Fragmentation Transfer (RAFT) Polymerization [119–123];

(3) polymerization with participation of stable radicals, including nitroxyl groups, which is called Nitroxide Mediated Polymerization (NMP) [124].

In the most widely spread ATRP method «livening» of macromolecules is due to reversible atom transfer: a macroradical interacts reversibly with a special addition (catalyst, a compound of a transition metal) via redox reaction, alkyl-halide (most often bromide) is used as initiator.

The ATRP of St is performed in presence of 5-(chlorosulfonyl) salicylic acid [125, 126]. Polystyrene (PS) with end-capped HQ groups has been obtained via ATRP with 5-chloromethyl-Q acetate used as initiator. The results point to the fact that polymerization proceeds by the first order by monomer. Molecular weight of the formed polymer increases linearly with consumption of the monomer and displays very narrow molecular-weight distribution (PDI less than 1.2) [127]. Depending on molecular weight, polymers can self-assembly in hollow or solid spheres, or monolayer film with regular pores [128].

Diblock-copolymer with HQ side groups was synthesized by St polymerization using RAFT method in presence of a chain-transfer agent, which was a polymer produced by living controlled polymerization of the monomer being a product of reaction between HQ and 2-hydroxyethylmethacrylate [129]. RAFT co-polymerization of 2-((HQ-5-yl) methoxy) ethyl methacrylate with St or MMA was successfully carried in presence of 2-cyanoprop-2-yl-dithionaphthalenoate. Its kinetic behavior confirms the origin of living polymerization [130]. It is noted application the nonionic amphiphilic brush polymers such as poly(PEO methyl ether vinyl phenyl-*co*-St) trithiocarbonate and poly(PEO methyl ether vinyl phenyl-*b*-St-*b*-PEO methyl ether vinyl phenyl) trithiocarbonate as macro-RAFT agent in the emulsion RAFT polymerization of St, where PEO is poly(ethylene oxide) [131]. PS and poly(*n*-butyl acrylates) with two end tpy groups are obtained via RAFT polymerization using the symmetric bis-tpy-functionalized trithiocarbonate as the chain-transfer agent [132]. Amphiphilic polymers poly(triethyleneglycol methyl ether methacrylate)-*b*-PS with tpy groups randomly distributed along water-soluble block-copolymer have been obtained by RAFT polymerization [133]. Similarly, the PS-*b*-poly(2-hydroxy-5-vinylbenzaldehyde) copolymers are obtained from 2-hydroxy-5-vinylbenzaldehyde using the chain-transfer macroagent PS with the end trithiocarbonate groups [134].

Chelating ligand 2,2′-bipyridine (bpy) with fixed in 5,5′-positions RAFT-agents showed good controlling functions during St polymerization according to the first order kinetics and linear growth of molecular weight with conversion (Scheme 2.3) [135].

The analogous synthetic procedure is applied for synthesis of tpy with one bound RAFT-agent used for controlled co-polymerization of St and *N*-isopropylacrylamide
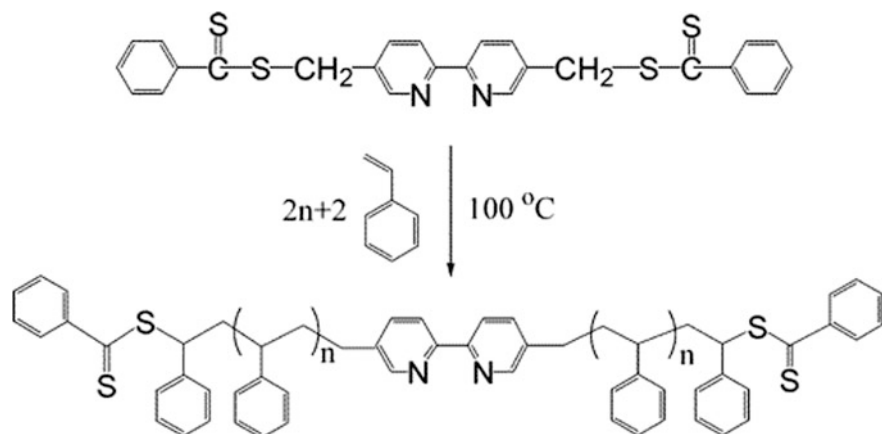
Scheme 2.3   RAFT polymerization of St using a bpy block with two cross-linked RAFT-agents

(NIPAM) resulted in formation of a polymer with the tpy-chelating end group [136]. The monomer functionalized by benzenedinitrile, 2-methyl-acrylic acid 6-(3,4-dicyano-phenoxy)-hexyl ester, was successfully polymerized via RAFT method. The polymerization has all features of the «living»/CRP: first order kinetics, linear increase of molecular weight with conversion of the monomer, narrow PDI, and successful chain-extension experiments [137]. Also RAFT polymerization was used for production of amphiphilic block-copolymers with chelating oxime group, in which hydrophobic keto-functional blocks self-assemble into micelles in water [138]. Addition of bifunctional alkoxyamine to these solutions brings to cross-linking of the micelles, forming star polymers.

Alternating RAFT copolymerization of *p*-methoxydiethylene glycol-substituted St and *N*-(2-salicylaldehyde-aminoethyl) maleimides leads to well-defined alternating copolymers with narrow polydispersity (PDI < 1.35) [139]. It is interesting that these alternating PMCs show an excellent selective fluorescence «OFF-ON» response to Zn(II) ions by inhibiting the photoinduced electron transfer (PET) effect. At the same time, the initial salicylaldimine monomer almost has no fluorescence response to Zn(II) ions due to the PET process.

RAFT polymerization was used to prepare the well-defined block copolymers based on 2-(acetoacetoxy) ethyl methacrylate (hydrophobic, metal chelating) and 9-anthryl-MMA (hydrophobic, fluorescent) with effective dual chemosensor properties (i.e., amino- and metal-ion sensors) in an organic solvent (chloroform) [140].

The controlled polymerization of commercially available 2-(acetoacetoxy) ethyl methacrylate was performed in presence of such highly efficient chain-transfer agent as 2-cyano-2-propyl dithiobenzoate and AIBN as radical initiator (Table 2.3) [141]. Under determined conditions of the reaction the quantitative conversion of the monomer is really achieved for polymerization time in the interval from 15 to 20 s. The polymerization follows the first order kinetics by the monomer, molecular

Table 2.3 Experimental conditions and molecular characteristics of (acetoacetoxy)ethyl methacrylate homopolymers obtained by RAFT radical polymerization (initiator: AIBN, solvent: ethyl acetate, temperature 60 °C)

| [Monomer]$_0$/[agent]$_0$/[AIBN]$_0$ (M)	Time (h)	x_p[a]	DP[b]	PDI
5.2/0.271/0.037	20	>0.99	30	1.16
2.6/0.132/0.020	n.d.	0.82	44	1.17
5.2/0.072/0.020	15	>0.99	106	1.16
3.7/0.052/0.007	20	0.96	145	1.15
5.2/0.026/0.005	18	0.39	177	1.13
2.6/0.021/0.004	46	0.85	176	1.13

[a]monomer conversion
[b]degree-of-polymerization

weight of the polymers increases linearly with conversion, and final products have monomodal and narrow molecular-weight distribution (apparent PDI < 1.2). These results lead to the assumption that RAFT radical polymerization provides controlled synthesis of CPLs.

A special mechanism of «living» radical polymerization is associated with using of specific initiators, so called iniferters [142]. During inifert-induced «living» radical polymerization a growing radical interacts reversibly with stable or low active radical (stable radicals, spin traps, cobalt porphyrins) with formation of adduct containing labile end group, which is able to split from the end of chain under heating or irradiation (Scheme 2.4).

The iniferter method was used, for instance, for free radical polymerization of acetone oxime acrylate [143].

In the NMP method polymerization is implemented with using of stable, including nitroxyl radicals. Thus, homo-telechelic macroligands with chelating tpy-4′-yl units at the ends of a chain are obtained by NMP of St using bis-tpy-functionalized NMP initiator [144]. The NMP method was also used to obtain amphiphilic water-soluble block-copolymer of poly(sodium-styrenesulfonate) (PSS) and 5-(4-acryloyloxyphenyl)-10,15, 20-tritolylporphyrin) [145]. Polymers with M_w higher than 60,000 containing up to 10 mol% of chelating tpy units were successfully obtained by NMP method via
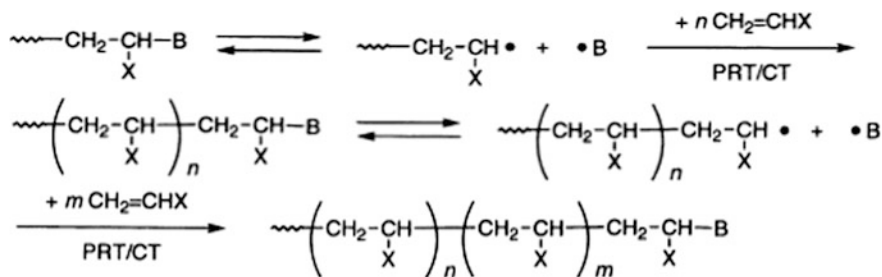
Scheme 2.4 Mechanism of iniferter-induced «living» radical polymerization

co-polymerization of MMA with a monomer containing a tpy fragment. The PDI occurred lower than 1.3, though it is well known that tpy interacts with a stationary phase during gel chromatography and broadens polydispersion [146]. Interaction between a primary produced benzylchloride-functionalized initiator with 2,6-di (2-pyridyl)-4-pyridone in presence of potassium carbonate was used to fabricate a tpy-containing initiator for NMP, which was successfully applied for controlled bulk St polymerization, resulted in production of chelating macroligand based on PS. It should be noted that the remained nitroxide groups at the end of PS can be replaced by a tpy-containing maleimide with formation of telechelic bis-tpy-functionalized PS [147].

The synthesized free-radical TEMPO-based (TEMPO is (2,2,6,6-tetramethylpiperidin-1-yl) oxyl, or (2,2,6,6-tetramethylpiperidin-1-yl) oxidanyl) initiators containing dibenzo-24-crown-8 and bis(*m*-phenylene)-32-crown-10 were used for production of PS with the end crown ether fragments and narrow PDI [148, 149].

Presently many research groups improve these methods of synthesis of polymers in order to obtain CPLs with determined beforehand molecular weight, polydispersion, topology of a chain, which also contain necessary functional groups in predetermined sites of the chain. The aforementioned methods are now essential in CRP, though many variants and combinations of them exist. We shall resume that possibilities of CRP are as follows: narrow PDI, control over the rate of polymerization, topology of macromolecules, microstructure of a chain, and composition homogeneity of copolymers, and also controlled functionality of macromolecules.

2.1.3   ROMP as a Method of Production of Chelating Polymers

An interesting method of CPL production is ring-opening metathesis polymerization (ROMP) [150]. This method, in particular, was applied to obtain chelating polymers with tpy and carbazole (Cz) groups in side chain [151, 152], porphyrin (Pp) copolymers, and long-chained alkyl norbornene using Grubbs initiator [153]. Dibenzoylmethane (dbm) initiators with one or two alcohol groups are used for creation of poly(ε-caprolactone) (PCL) macroligands with chelating fragments at the end or in the middle of a chain with low PDI ~ 1.1 (Scheme 2.5) [154].

Mono and bis(hydroxyalkyl)-bpy were used as ROMP initiators of ε-caprolactone and DL-lactide, catalyzed by tin octoate (Scheme 2.6) [155].

Hydroxypropyl-tpy macroligand was used as initiator of polymerization of ε-caprolactone with hydrogen-bound (H-bound) end groups (Scheme 2.7) [156, 157].
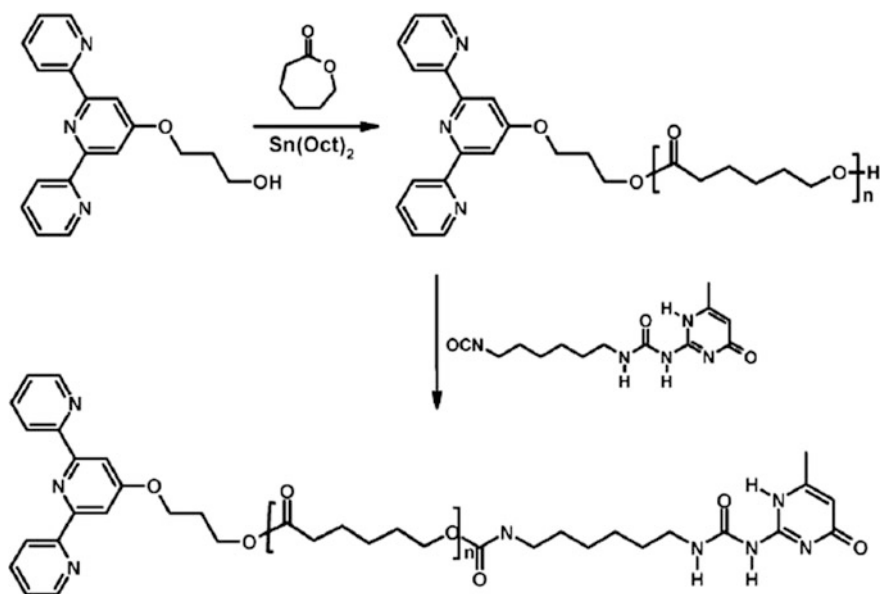
Instead of tin octoate aluminum alkoxide can be used as a catalyst of ROMP with contribution from polymer initiators (Scheme 2.8) [158].
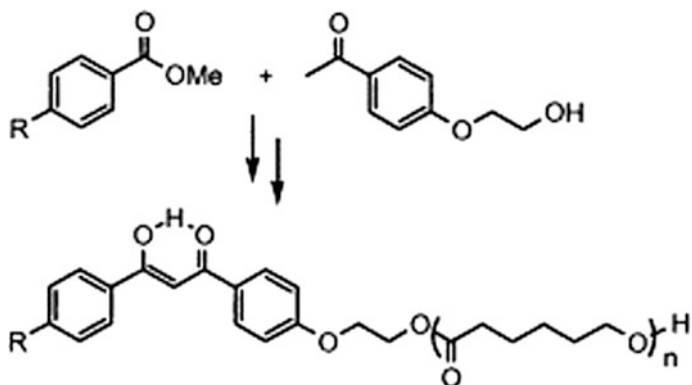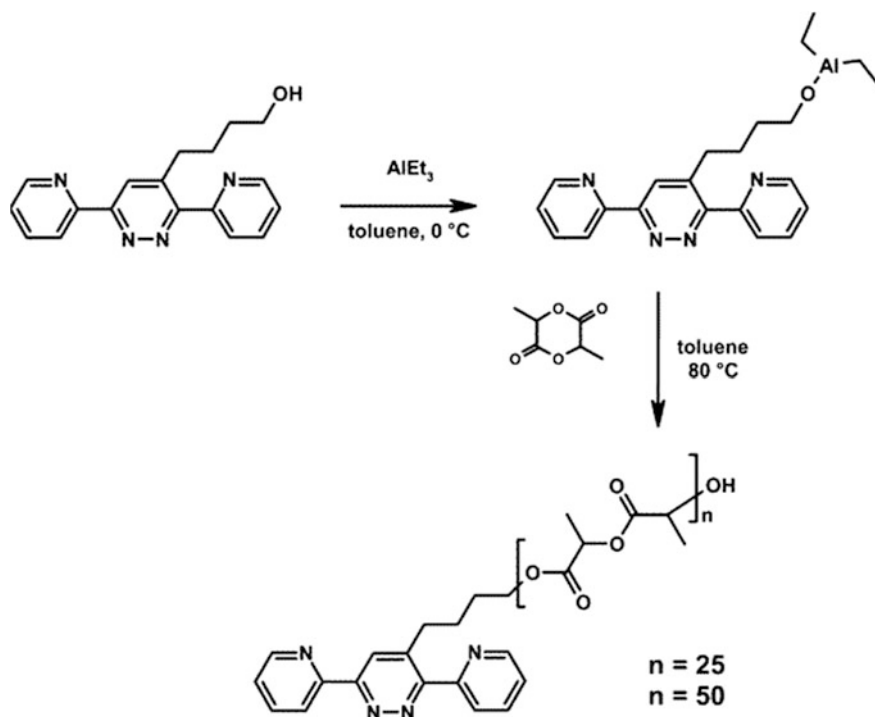
Scheme 2.5 Synthesis of CPL with dbm fragments
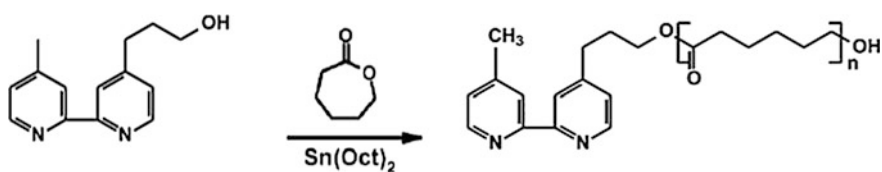
Scheme 2.6 Synthesis and chelation of bpy-containing PCL ligand using tin octoate as a catalyst

Scheme 2.7 Synthesis of PCL with tpy-chelating fragments

Scheme 2.8 Schematic representation of synthesis of poly(L-lactide)-based 3,6-di(2-pyridyl) pyridazine (DPP) chelating ligand

The cross-linked crown ether polymers with sulfur-ether group were obtained by ROMP from 3-thiopentyl glycidyl ether and diethylene glycol bisglycidyl ether with Na, NaOCH$_2$CH$_2$OCH$_2$CH$_2$OH, or BuLi as a catalyst, respectively [159].

2.1.4 Click Chemistry Methods in Synthesis of Chelating Polymers

One of the methods of control over topology of the formed CPLs is using of «click chemistry», simple in realization of reactions, which proceed stereospecifically and with high yield in easily removed solvents, with formation of easily separated side products [160, 161]. The Cu(I) catalyzed azide-alkyne cycloaddition (CuAAC) is the premier example of a click reaction [162]. The majority of studied click reaction is based on the 1,2,3-triazole as a stable linkage to connect two components. In particular, 1,4-functionalized 1,2,3-triazoles are versatile ligands with wide set of donor sites for metal chelation, including N3, N2 and C5 (Fig. 2.4).
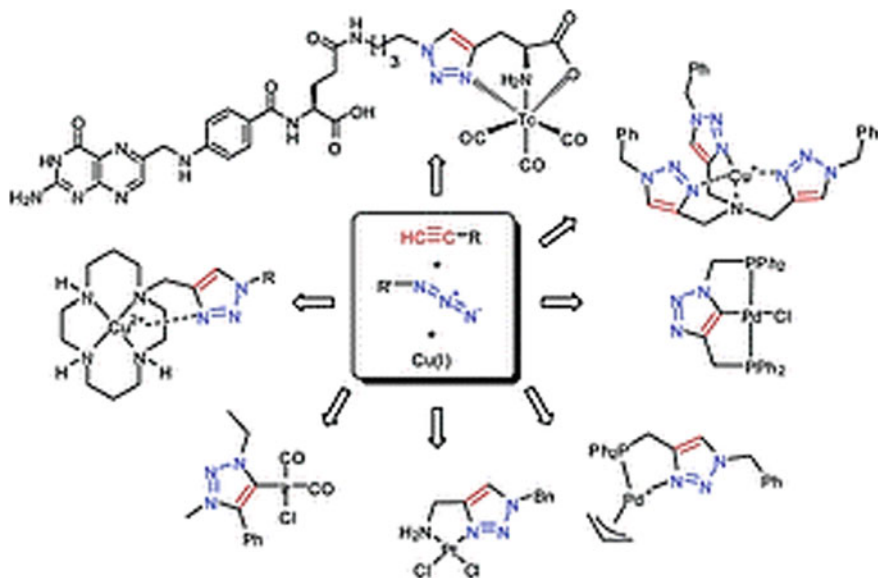
Fig. 2.4 Examples of metal coordination with participation of 1,4-functionalized 1,2,3-triazoles

Click polymerization was successfully used for synthesis of a range of Pp-containing polymers with triazole rings served as spacers. Polyaddition of Pp-containing dialkyne and 1,4-diazidobenzene is initiated either simple heating, or by Cu(I)-catalyst, bringing to polymers with relatively high molecular weight. The polymer obtained by thermally induced click polymerization has unimodal molecular-weight distribution and moderate PDI after long time of reaction up to 170 h. As compared to the metal-free click polymerization, growth rate of the molecular weight in Cu(I)-catalyzed click polymerization decreases, which results in relatively low molecular weight of the produced polymer [163].

2.1.5 Method of Cation Polymerization in Chemistry of Chelating Macroligands

Ionic polymerization proceeds via heterolytic mechanism and is initiated by ions (anions or cations). They particularly play in this case a role of active centers. Vinylcatechol monomers can be polymerized in presence of tin tetrachloride (5-vinyl-1,3-benzodioxol, 3,4-dimethoxystyrene, 6-vinyl-1,4-benzodioxane, 4-vinyl-1,3-benzodioxol) or lithium butyl (5-vinyl-1,3-benzodioxol, 2,3-dimetoxy-St, 6-vinyl-1,4-benzodioxane) with formation of polymers with molecular weights up to 95,000 [164]. N,N′-bis(vinyloxyethyl) thiuramdisulphide homopolymers are also obtained by the reaction of cation polymertization [165].

   Vinyl polymers with macrocyclic side crown ether chain are synthesized via anion polymerization of derivatives of α-(alkoxy-methyl) acrylates with 13–17 cyclic units. Counter-cation in the polymerization system predetermines a polymer yield and its stereo-regularity [166].

2.1.6   Chemical Oxidized Polymerization in the Chemistry of Chelating Polymers

Recently synthesis of PCL by chemical oxidized polymerization is widely studied [167]. Thus, linear Pp-thiophene copolymers are synthesized via polymerization of Pp bound in 5,15-positions with tetrathiophene or bithiophene fragments in presence of $FeCl_3$ as an oxidizer [168].

   Copolymers containing IDA were obtained via polymerization of MMA and chelating monomer, GMA-IDA, with potassium persulfate as initiator [169]. Oxidized copolymerization of 8-aminoquinoline and o-anisidine with using of ammonium persulfate as oxidizer brings to pure and uniform particles of the copolymer of several microns in size [170]. Polymerization yield and intrinsic viscosity of a copolymer depend strongly on the ratio of monomers (Fig. 2.5). In particular, the yield decreases in geometric progression from 64 to 16% as the content of aminoquinoline increases from zero to 100%, thus pointing that 8-aminoquinoline is inhibitor to oxidized polymerization of o-anisidine. It should be noted that 8-aminoquinoline shows higher homo-polymerization activity than two others chelating nitrogen heterocyclic amines, i.e. pyrimidylamine [171] и pyridylamine [172]. Intrinsic viscosity of 8-aminoquinoline and o-anisidine copolymers, and DP change, depending on content of 8-aminoquinoline in a complicated way.

Fig. 2.5 A change of yield of copolymerization, intrinsic viscosity, and medium degree-of-polymerization [$(DP)_n$] in polymers of 8-aminoquinoline/o-anisidine on content of 8-aminoquinoline
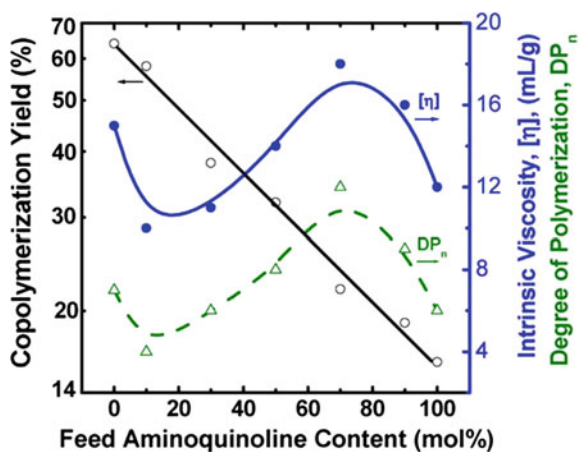
In the case of poly(*o*-phenylenediamine) (PPD) obtained using ammonium persulfate as an oxidizer, yield of a polymer depends on presence of metal ions in the reaction mixture, which can react as oxidizing reagents and/or catalysts [173]. In this case ladder polymers were obtained.

The initial rate of homogeneous polymerization of 2-methacryloyloxyethyl phosphorylcholine as betaine monomer with potassium peroxydisulfate at 40 °C corresponds to the equation $V = k[\text{activator}]^{0.98}[\text{monomer}]^{1.9}$, and the total activation energy of polymerization is 12.8 kcal mol^{-1} [174]. Copolymers of aniline and *o*-aminoacetophenone of different compositions were obtained via chemical oxidized co-polymerization using two different methods (emulsion and inverse emulsion copolymerization) with two different oxidizers (ammonium persulfate and BP) [175]. Poly(2-aminobenzoic acid) and poly(2-aminobenzoic acid-*co*-aniline) are synthesized via chemical polymerization in 1 M aqueous solution of hydrochloric acid [176, 177]. Poly(1,8-diaminonaphthalene) in form of microparticles is obtained by chemical oxidized polymerization of 1,8-diaminonaphthalene in presence of $(NH_4)_2S_2O_8$ [178]. Poly(2,6-diaminopyridine) was synthesized via interphase polymerization, in which solid $(NH_4)_2S_2O_8$ was quickly added to solution containing 2,6-diaminopyridine [179]. Morphology of thus obtained poly(2,6-diaminopyridine) is characterized by spherical microparticles with average diameter 1 μm, which is smaller than that of poly(2,6-diaminopyridine) obtained by homogeneous polymerization. Chemical interphase oxidized polymerization for synthesis of poly(1-amino-5-chloroanthraquinone) particles in nitrobenzene solution is performed with CrO_3 used as oxidizer in aqueous phase in air [180].

Copolymers of *o*-aminobenzylamine and different amounts of aniline are obtained in diluted solution of hydrochloric acid using ammonium persulfate as oxidizer [181]. Nanoparticles with properties of semiconductors are synthesized by oxidized copolymerization of 8-aminoquinoline and 2-ethylaniline [182]. Fine particles of the copolymers 8-aminoquinoline and *o*-phenetidine are synthesized via chemical oxidized polymerization in three aqueous media. Copolymer nanoparticle size decreases monotonically with increasing the content of 8-aminoquinoline from 5 to 100 mol%. A special feature of this method is fabrication of semiconductor nanoparticles without a stabilizer by incorporation of 8-aminoquinoline groups with positively charged quaternary ammonium groups adjusted to sulfone groups. Both molecular weight and bulk electric conductivity reach maximum values at content of 8-aminoquinoline 5 mol%, and yield of polymer and bulk electric conductivity are maximum at minimal temperature of polymerization 5 °C [183].

The PPD microrods are produced with iron chloride used as an oxidizer [184]. In contrast to electrochemical polymerization, which has some limitations, such as low efficiency and uniform shape of the formed film, chemical oxidized polymerization under action of $(NH_4)_2S_2O_8$ or $FeCl_3$ allows production with high yield of microparticles of poly(1,8-diaminonaphthalene) with high molecular weight [185]. Conducting nanofibrils of poly(1-amino-5-chloroanthraquinone) have been successfully synthesized by interphase chemical oxidized polymerization [186]. The nanofibrils show maximal yield 64.8%, their aspect ratio is 67 (diameter 30 nm, length 2 μm), and bulk electric conductivity 6.2×10^{-3} S cm^{-1}, when 1-amino-5-chloroanthraquinone

monomers oxidize CrO_3 in combined medium consisting nitrobenzene and 250 mmol L^{-1} of $HClO_4$ in solution.

Depending on conditions of reaction of chemical oxidation, PPD are formed as powders, colloid dispersions, thin films, or composites [187].

Polythiophenes containing oligo (ethylene glycol) spacers and crown ethers are synthesized by copolymerization of 3-methyl tetra (oxyethylene)oxy-4-methylthiophene and 3-(((2-aminobenzo-18-crown-6-ethyl) triethoxy) oxy)-4-methylthiophene in presence of $FeCl_3$ solution [188]. Thiophene monomers containing *meso*-tet raphenyl-Pp units bound via alkyl spacers, and also *meso*-3,5-*ditert*-butyl-tetra phenyl-Pp units, bound via tetra (ethylene glycol) spacers, were copolymerized in presence of 3-dodecylthiophene using $FeCl_3$ as an oxidizer [189, 190]. Studies in this field are intense.

2.1.7 Chelating Macroligands Obtained by the Methods of Photo- and Microwave-Assisted Polymerization

Series of copolymers poly(methacryloyl-2-oxy-1,2,3-propanetricarboxylic acid-*co-exo*-3,6-epoxy-1,2,3,6-tetrahydrophthalic acid), poly(methacryloyl-2-oxy-1,2,3-propanetricarboxylic acid-*co*-hydrogenethyl-*exo*-3,6-epoxy-1,2,3,6-tetrahydrophthalate), and poly(methacryloyl-2-oxy-1,2,3-propanetricarboxylic acid-*co*-α-ethoxy-*exo*-3,6-epoxy-1,2,3,6-tetrahydrophthaloyl-5-fluorouracil) were obtained from the respective monomers via photopolymerization at 25 °C for 48 h [191, 192]. M_n of the synthesized polymers was in the range from 9400 to 14,900, and PDI—1.2–1.4.

Interest in application of microwave irradiation in polymer synthesis and modifications constantly increases [193]. Especially active the method of microwave irradiation is recently applied in step-growth polymerization, open-chained polymerization, and radical polymerization [194, 195]. It is often used also in «green» synthesis of CPLs. Thus, using microwave irradiation, the CPL were obtained by condensation of thymol and guanidine with formaldehyde in 2 M hydrochloric acid with the 1:1:2 molar ratios of the reacting monomers for 15 min [196], and also dianhydride of 3,3′,4,4′-benzophenonetetracarboxylic acid, 4,4′-diaminodiphenylmethane and 4,4′-oxydianiline [197]. It is noted using of microwave irradiation for the production of phthalocyanine (Pc) polymer by the reaction of tetranitrile monomer with 4,4′-[pyridine-2,6-diylbis(methyleneoxy)] diphthalonitrile [198], different polyamidoamines (PAMAM) [199], including optically active ones containing hydantoin and thiohydantoin in the main chain [200], and also dithiabridged polymeric Pc containing a substituted thiophenylamine Schiff base [201]. Functionalization of polychloromethylstyrene (PCS) by 2-aminothiophenyl-*S*-acetic acid was performed under action of microwave irradiation [202].

Also microwave-assisted enzymatic polymerizations should be noted, which combine advantages of microwave heating and enzymatic catalysis, the field rather well studied in synthesis of CPL [203].

2.1.8 Cyclopolymerization for the Production of Chelating Macroligands

Derivatives of poly(phenyl acetylene) with crown ether units in the main chain are obtained by cyclopolymerization of the 1,14-bis(4′-ethynylphenoxy)-3,6,9,12-tetraoxatetradecane and 1,17-bis(4′-ethynylphenoxy)-3,6,9,12,15-pentaoxaheptadecane using Rh(nbd)BPh$_4$ (nbd—norbornadiene) as the catalyst [204].

Pc polymer is formed by the reaction of polytetracyclomerization of o-bis [3-(3,4-dicyanophenoxy) propyloxy] benzene synthesized via interaction of 4-nitrophthalonitrile with o-bis[(3-hydroxypropyl) oxy] benzene [205].

π-Conjugated polymers containing units of dithiafulvene and bpy are obtained by the cycloaddition polymerization of aldothioketene derivative from 5,5′-diethinyl-bpy [206]. Radical polyaddition of bis (α-trifluoromethyl-β,β-difluorovinyl) terephthalate with 18-crown-6 gives soluble fluorine-containing polymers containing crown ether units in the main chain and $M_n = 5.5 \times 10^4$ with unimodal PDI (Scheme 2.9) [207].

Stable porous organic polymers containing functional units of catechol with tunable porosities (560–1050 m^2 g^{-1}) and degrees of functionalization are synthesized using the strategy of Co-catalyzed acetylene trimerization [208].
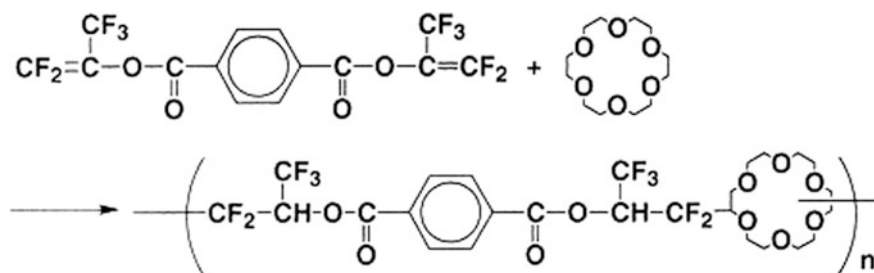
Scheme 2.9 Preparation of fluorine-containing polymers containing crown ether units in the main chain

2.1.9 Asymmetrical Polymerization in Synthesis of Chelating Polymers

Recently great attention is paid to production of chiral CPLs [209]. For example, chiral poly(L-lactides) with end tpy groups are obtained by controlled coordination polymerization [210]. Asymmetrical anion homopolymerization of *N*-4′-benzo-15-crown-5-maleimide for production of optically active polymers has been performed with chiral anion initiator consisting of metal-organic compound (*n*-butyl lithium, diethyl zinc) and chiral ligand ((−)-sparteine), (S,S)-(1-ethylpropylidene)-bis(4-benzyl-2-oxazoline) [211].

Optically active PAAm containing amino acid fragment poly [*N*-methacryloyl-L-leucine methyl ester] with controlled M_n and relatively narrow PDI (<1.3) has been obtained using initiating system methyl-2-bromopropionate/CuBr/tris(2-dimethyl-laminoethyl) amine [212]. Acetylene monomers containing salicylidene Schiff-base groups as well as Schiff base and hydroxyl groups are polymerized with the catalyst [(nbd)RhCl]$_2$/Et$_3$N with formation of polymers with high molecular weights ($M_n = 2.6$–7.2×10^5) and high yields (75–97%) [213]. The polymers form helical structures with a predominantly one-handed screw sense. The same catalyst [(nbd) RhCl]$_2$/Et$_3$N is used for polymerization of acetylene monomers, containing Schiff base and the amino group, (S)-*N*-(4-ethynylbenzylidene)-1-phenylethanamine, (R)-*N*-(4-ethynylbenzylidene)-1-phenylethanamine, *N*-(4-ethynylbenzylidene)-1-phenyl-ethanamine, (R)-*N*-(4-ethynylbenzyl)-1-phenylethanamine and (R)-*N*-(4-ethynyl-benzyl)-1-phenylethanamine with formation of polymers with lower molecular weight ($M_n = 9000$–$60{,}000$), but the same high yield (85–97%) [214]. The polymers also have helical structures with a predominantly one-handed screw sense.

Asymmetrical polymerization of 4′-isocyanatobenzo-18-crown-6 in presence of chiral initiator of lithium amide salt and (S)-(2-methoxymethyl) pyrrolidine was used to produce 4′-isocyanatobenzo-18-crown-6 with end units of (S)-(2-methoxy methyl) pyrrolidine [215]. The polymer has a positive Cotton effect (240–350 nm), and in its main chain a single-coil partial helix is formed, which does not change under action of adverse factor, chiral compound of L-phenylalanine HClO$_4$. *Cis*-transoidal 4-ethynylbenzo-15-crown-5 was polymerized with Rh(nbd)BPh$_4$ [216]. Analysis of chiral optical properties of the polymer allows it to be recommended as thermally sensitive material.

Copolymerization of monomers containing different chiral and Pp units results in formation of artificial helical polyisocyanides containing enantiopure groups [217].
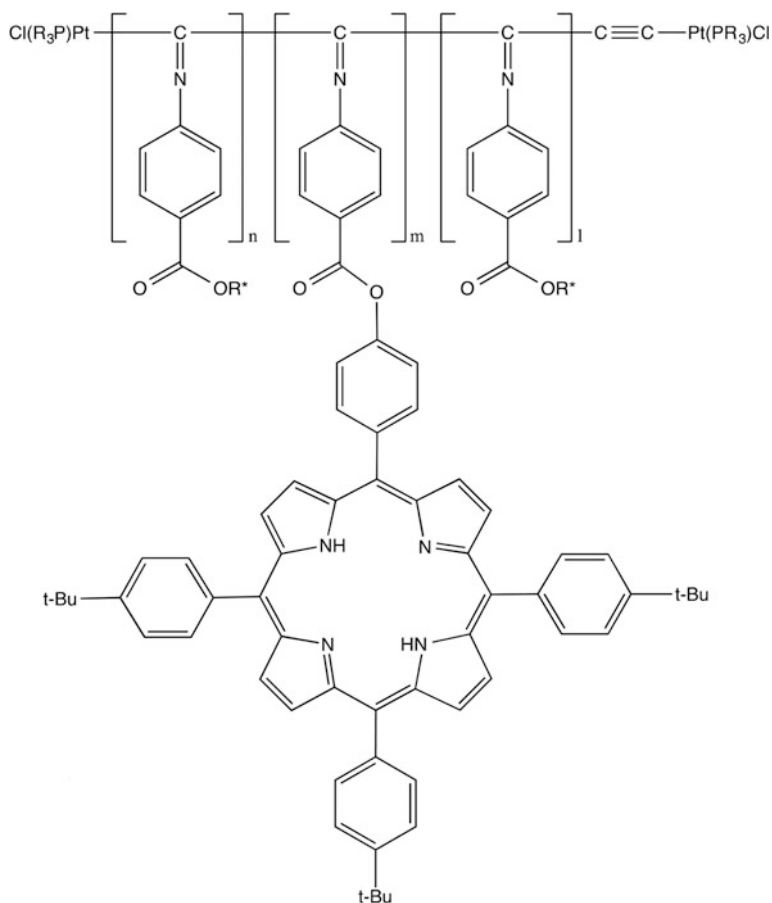
The similar approach was used in design of helical nanorods based on polymers with fixed Pp [218]. In this case, Ni(II)-catalyzed polymerization of isocyanide monomers containing chiral Pp brings to respective polymers (Scheme 2.10), Pp units of which are in four clearly defined stacks which run in parallel to the polymer axis.
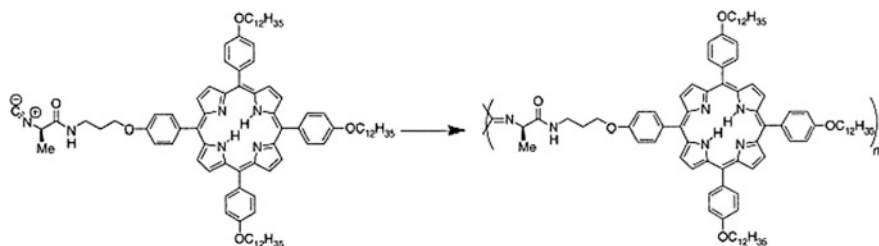
Scheme 2.10 Synthesis of Pp-containing polymers
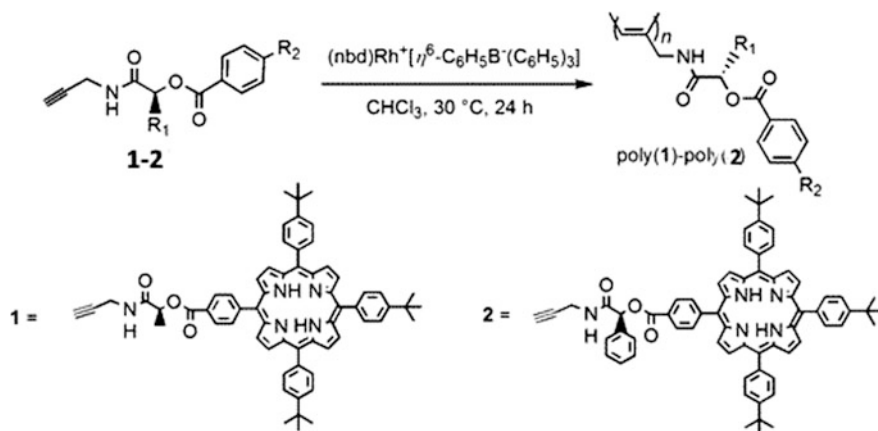
Scheme 2.11 Preparation of Pp-containing polymers based on poly(*N*-propargylamine)

Another polymer matrix was used for production of chiral poly(*N*-propargylamines) containing Pp groups (Scheme 2.11) [219]. Molecular weights of the polymers are 17,000 and 24,000 with *cis*-content 85 and 78%, respectively, displaying highly stereo-regular structures with considerable optical activity.

Cyclopolymerization of diacetylene monomers in presence of rhodium catalyst was used to produce poly(phenylacetylenes) with cavities of different sizes formed by crown ethers placed in elementary units [220]. The polymers have helical structure with single-coil macromolecules prevailing. Formation of «guest-host» complexes with achiral compounds brings to chiroptical changes based on the fluctuation in the main chain conformation. The polymers with chiral main chain cross-linked alternately with (*R,R*)-salen (where salen—*N,N*′-bis(salicylidene)ethylenediamine) and 1,4-dioctyloxybenzene, using the Pd-catalyzed C–C cross-coupling as the key stage of the reaction [221]. The polymers are soluble in standard solvents and work as

Fig. 2.6 Polymers with chiral main chain cross-linked alternately with (*R,R*)-salen and 1,4-dioctyloxybenzene, as highly selective «OFF-ON» fluorescent chemosensors on Zn(II) ion, and enantioselective recognition of (*R*)- and (*S*)-imines under action of polymer complexes

selective «OFF-ON» fluorescent chemosensors on Zn(II) ion (Fig. 2.6). The obtained Zn(II) polymeric chelates have strong chiral recognition with respect to (*R*-) and (*S*)-1-phenyl-*N*-[(pyridine-2-yl) methylene] ethanamines under ambient conditions.

2.1.10 Chelating Macroligand Preparation via Post-polymerization Modification

PPM is the most widely used method of CPL synthesis [222, 223]. The method is based on chemical interactions between reactive functional groups contained in a polymer matrix or preliminary incorporated in the polymer with respective organic compounds in direction of completion of chelating fragments. These reactions lead to a change in chemical composition of a polymer, but do not disturb its main chain. The PPM method gives a possibility to obtain different CPL structures based on polymer matrices, for example, of syndiotactic PS [16]. However, one of the main drawbacks of this method is presence of different side processes, and a necessity of removal of unlinked components.

PPM as a method of introduction of functional groups into ready reactive polymer precursors is considered as highly effective synthetic strategy for design of materials with predetermined properties [17], and also of complicated polymer topologies based on multifunctional cyclic polymers [224]. PPM of block-copolymers attracts keen attention beginning from fundamental synthesis, correlation between structure and properties, and to practical applications [225]. The formed block-copolymers with modified side chain preserve properties attributed to a parent block-copolymer, while incorporated into the side chain functionalities provide control over properties of a materials, and hence, their applications.

Thus, polyacrylic acid (PAA) was chemically modified with 1,2,4,5-tetrahydroxybenzene or benzene-1,2,4,5-tetrol via Minisci reaction. Degree of modification reached the highest value 55% under the following optimal conditions: temperature 70–80 °C, time 4 h and the ratios of the reagents 1.25 [226].

The method of nucleophilic incorporation of the lithium PS living chains to 6-position of the pyridine ring with the following termination and oxidized rearomatization was applied to perform end functionalization of the polymer. In order to prevent two living chains coupling via addition to the same bpy, or tpy unit, excess of pyridyl-containing compounds is used, which makes it possible to produce polymers consisting of 77–93% only singly end-functionalized chains [227].
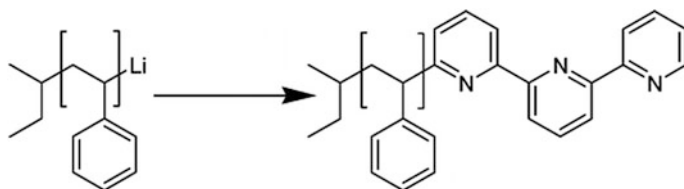
The commercial polymer Eupergit® C, which consists of epoxy-activated polymers formed from hydrophilic AAm with allyl glycidyl (epoxide) groups was modified by aminotriazole [228].
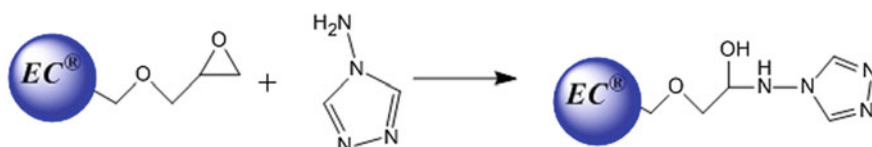
The polymer ligand having tpy as a fixed group has been obtained by Williamson etherification reaction between 4'-hydroxy-tpy and commercial PCS [229]. Interaction of monoamine-functionalized poly(ethylene glycol) (PEG) and 2-(2-aminoethoxy) ethanol with PS-*b*-poly(2-hydroxy-5-vinyl benzaldehyde) via aldehyde-amine condensation brings to amphiphilic block-copolymers containing fixed salicylidene-Schiff base with precise structure. This polymer can self-assemble in ethanol in micelles with salicylidene-Schiff base on the core-shell interface (Scheme 2.12) [134].

Interaction between *meso*-tetracarboxyporphyrin (mTCPP) and PEG-diamine brings to Pp-cross-linked hydrogel for fluorescence-guided monitoring and surgical resection (Fig. 2.7) [230].
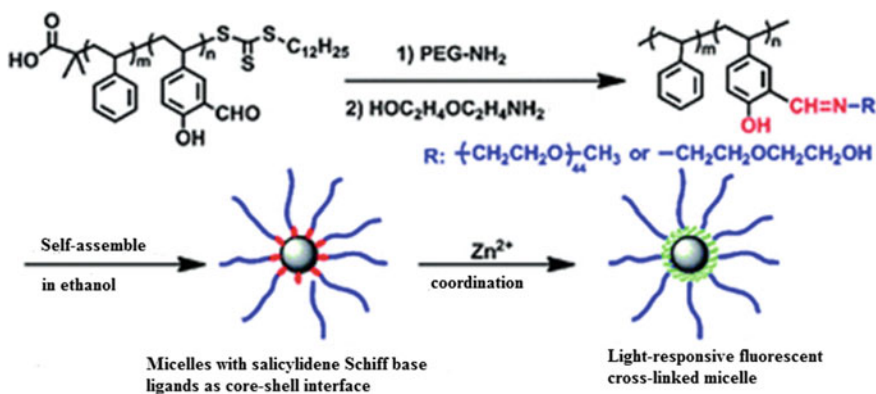
Scheme 2.12 Synthesis and self-assembly PMC based on salicylidene-Schiff base
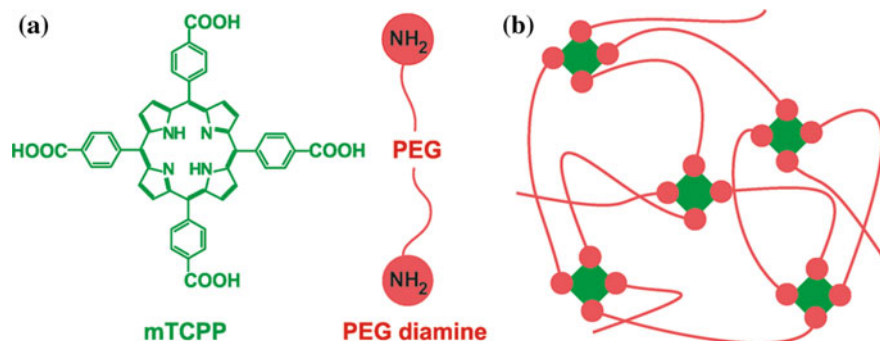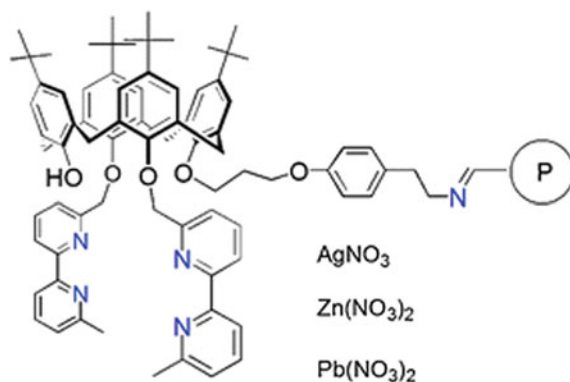
Fig. 2.7 Pp-cross-linked hydrogels. **a** mTCPP (green) structure and PEG-diamine (red); **b** schematic image of hydrogel

Benzaldehyde Wang resin was used for production of fixed calixarene-bpy ligands [231].

3D ordered macroporous cross-linked PS with 2-mercaptobenzothiazole groups incorporated in walls of pores directly or via arms of hydrophilic spacer to the polymer backbone is obtained (Scheme 2.13). Arms of the hydrophilic spacer are PEG chains with three different lengths. It is important that 3D ordered structure is well preserved after functionalization. Density of 2-mercaptobenzothiazole groups is 0.052 mmol m^{-2} [232, 233].

The reaction of condensation of sodium salt of pentane-1,3-dione and PCS in dichloromethane brings to β-diketone-functionalized resins [234]. Poly(chloromethylstyrene-*co*-divinylbenzene) (PCD) is chemically modified via alkylating by pyridylazo-α-naphthol in presence of phase transfer catalyst [235]. Poly(GMA) beads with average size 350 μm were treated by iminodiacetonitrile, and then by hydroxylamine to produce amidoxime fragments [236]. The series of amine-functionalized
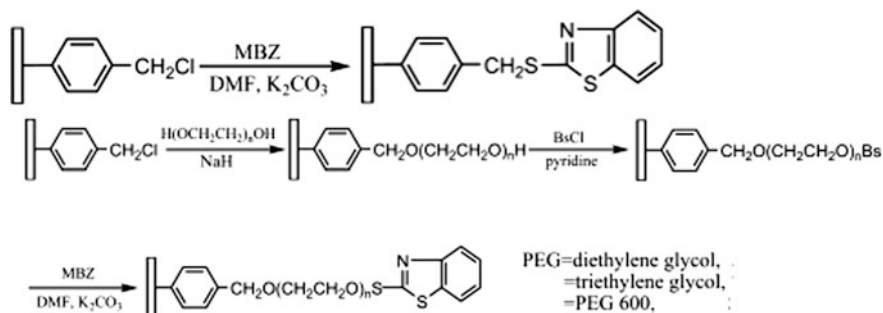
Scheme 2.13 Preparation of CPLs containing 2-mercaptobenzothiazole groups

resins with ethylenediamine (en), *N,N*-dimethylethylenediamine, *N,N*-diisopropyle-thylenediamine, 2-methoxyethylamine, diethylenetriamine (dien), tris(2-aminoethyl) amine, triethylenetetramine (trien) was obtained by chemical modification of terpolymer from glycidyl methacrylate-*co*-ethylenedimethacrylate (GL) (20 mol%), St (77 mol%) and DVB (3 mol%) [237]. The reaction of nucleophilic substitution between benzyl chloride groups of PCD microspheres and 5-amino salicylic acid brings to CPL such as PS-salicylic acid [238]. Such examples are numerous.

2.1.11 Polycondensation Reactions as a Way to Chelating Polymers

Polycondensation reaction is based on ability of phenols, amines, and other compounds to interact with aldehydes, ketones, and their derivatives in presence of alkali or acid catalysts, which results in polymer preparation, accompanied by formation of low molecular weight products. Polycondensation is carried out in melt, solution, or on interface. Depending on structure and ratio of initial components taking part in the polycondensation, CPLs of linear, branched or spatial configuration can be obtained [239, 240]. As a rule, a mixture of products of condensation forms due to synthesis. Besides, this way of CPL production has drawbacks, in particular, ambiguity of structure of produced polymers, poor reproducibility of the synthesis products, low capacity of CPL, and limited possibility of changing character of the functional groups during synthesis. Polycondensation proceeds stepwise, at that intermediates are stable, i.e. polycondensation can be stopped at any stage. The resulting low molecular weight products of reaction can be reacted with intermediates, stimulating their decomposition (hydrolysis, aminolysis, acidolysis, etc.). Therefore, low molecular weight products should be removed from the reaction medium.

Polycondensation of bifunctional compounds called linear, and polycondensation of compounds having three or more functional groups is called a three-dimensional. Thus, condensation of 2,4-dihydroxybenzophenone, oxamine and formaldehyde in various ratios in the presence of an acid catalyst led to terpolymers [241].

It should note polycondensation in melt carried out without solvents, heating monomers at the temperature by 10–20 °C higher than the melting point (softening temperature) of polymers (usually 200–400 °C). The process begins in the inert gas medium and is finished in vacuum. For example, condensation of 2,5-diformylfuran or 5,5′-oxydimethylenebis(2-furaldehyde) with carbamide at 110 °C by melting of the solid mixture gives a crystalline polymer with 90% yield (Scheme 2.14) [242].

Kinetics of synthesis of polyesters based on 1,4-naphthalene di(carboxylic acid) and hydroquinone diacetate via polycondensation in melt is studied. In particular, the polycondensation obeys the second order kinetics independently on whether it is catalyzed or not. To describe kinetics at the initial stage, a system of twelve differential equations was derived with four different rate constants [243].

For polycondensation in solution a solvent is used, which can also serve as an absorbent of low molecular weight product. Thus, method of polycondensation in solution of 2,5-bis(mercapto-acetichydrazide)-1,3,4-thiadiazole with 4,4′-biphenic, 3,3′-azodibenzoyl or 4,4′-azodibenzoyl dichlorides was used for synthesis of interesting class of poly hydrazides containing 1,3,4-thiadiazole fragment in the main chain [244].

Interphase polycondensation takes place on the interface of gases, solutions, or two immiscible liquids, and provides production of polymers with high molecular weight. We should also notice mechano-chemical synthesis of salicylic acid-formaldehyde CPLs [245].

Various polycondensation reactions are used for the synthesis of CPL, among them catalyzed cross-coupling reactions (particularly, Sonogashira [246–248], Suzuki [247, 249, 250], Heck [247], Buchwald-Hartwig [251], Wittig [252], Williamson [253], Stille [254, 255], and also Horner-Wadsworth-Emmons condensation [256]).
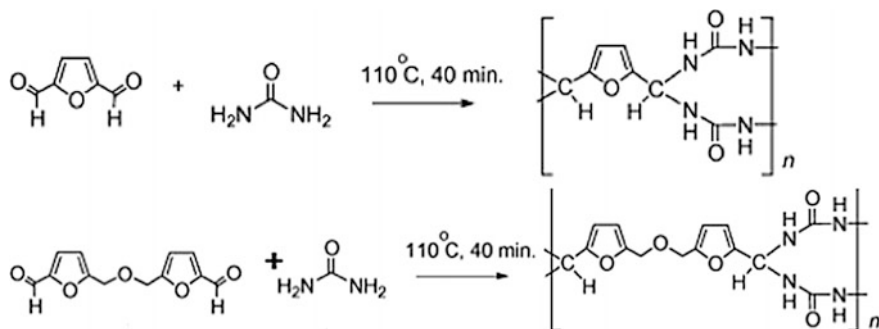
Scheme 2.14 Condensation of 2,5-diformylfuran or 5,5′-oxydimethylenebis(2-furaldehyde) with carbamide

It should be noted the use of condensation reactions for the synthesis of such interesting class of CPL as a polymeric SPs [257]. Thus, waterborne polyurethane containing SP groups is prepared by polycondensation of isophorone diisocyanate, polytetrahydrofuran glycol, dimethylol propionic acid, 1,4-butanediol, trimethylolpropane and 1-(2-hydroxyethyl)-3,3-dimethylindolino-6′-nitrobenzopyrylospiran [258]. The dispersion and film showed a very good photochromic effect.

A series of alternating copolymers of SP and flexible spacers is synthesized by Suzuki polycondensation [259]. These polymers can be transformed into the corresponding protonated form of the red alternating MC polymer in quantitative yield by direct acidification or pulsed ultrasound. At the same time deprotonation of MC polymer occurs upon the addition of a base resulting in the blue form of polymer. Suzuki polycondensation is also used for production of the main-chain conjugated copolymers based on alternating SP and 9,9-dioctylfluorene units [260]. It is important that the reaction conditions are optimized to obtain copolymers with appreciably high molecular weight up to $M_w \approx 100,000$. Ultrasound-induced isomerization of SP to the corresponding MC form yields a deep-red solution.

The combination of microwave-assisted synthesis and Suzuki-Miyaura polycondensation leads to a mechanochromic, alternating SP-based copolymer that allows the reproduction of molecular mass distributions [261]. Several parameters such as microwave power, temperature, stoichiometry, and ligand are screened, leading to molecular weights up to $M_w \sim 174,000$. Embossing films of SP-based copolymer yields the colored MC copolymer that undergoes a thermally facilitated back reaction to SP-based copolymer.

2.1.12   «Green» Synthesis of Chelating Macroligands

Recently in synthesis of CPL, like in all chemical syntheses, ecology problems receive much attention, which is realized via «green chemistry» principles, implemented by displacement of ecologically hazardous substances by more safe materials, enhancing product biodegradation cycles, using of catalysts and renewed resources for safety improvement and efficiency of polymer chemistry [34–39, 262]. Different biocatalytic syntheses can serve as examples of this approach [40]. Thus, the phenol ligand, 4-(phen-5-yliminomethyl)-phenol, was subjected to biocatalytic polymerization by Hematin [263]. Typical is increase in molecular weight with increase in conversion, though accompanied by simultaneous broadening of PDI. The drawback of this process is inability of the reaction product to recommence a living process with addition of a fresh portion of monomer. A polymer is formed exclusively due to reaction of square termination of the growth radicals.

Hemoproteins encapsulated in reversible micelles were used as catalysts of polymerization of o-phenylenediamine in presence of hydrogen peroxide. During catalysis of polymerization with hemoproteins in water, only trimers were formed. It is interesting to notice that macromolecules synthesized in presence of hemoglobin in reversible micelles are linear or trapezoid [264]. Linear PAMAM are obtained via

polymerization of ethyl acrylate and N-methyl-1,3-diaminopropane in a solvent medium in presence of lipase catalyst produced by *Candida Antarctica* [39]. Depending on conditions of reaction, lipase catalyzes polymerization of monomers or formation of Michael adduct. Lipase has high selectivity in the reaction of polymerization and provides polymer production for biomedical application. Enzymatic oxidation of o-phenylenediamine with cytochrome C as a catalyst is carried out in organic media [38]. Polyphenols with molecular weight 1000–3000 and containing 0.94–0.59 mol kg^{-1} hydroxyl groups are synthesized via reaction of phenol, catechol, and pyrogallol catalyzed by horseradish peroxidase [265]. When adding *tetra*-butyl-ammonium bromide to buffer to obtain convenient and ecologically pure system, enzymatic polymerization of phenol is more effective: the maximum conversion of phenol can reach 99.1% [266]. The catalyzed by lipase polycondensation of L-malic acid, adipic acid and 1,8-octanediol in organic media is performed using Novozym 435 as a biocatalyst [267]. M_w increases from 3200 to 16,600 as the reaction time increases from 6 to 48 h at the temperature 70 °C and remains relatively constant as the reaction time goes on increasing to 72 h.

A series of di-acids (succinic, glutaric, adipic, and sebacic acid) and diols (1,4-butanediol, 1,6-hexanediol, and 1,8-octanediol) were used for lipase-catalyzed polycondensation [268]. Synthesis of PPD is performed using a catalyst similar to oxidase in presence of cerium nanodioxide [269]. The polymer showed unique morphology, conductivity, and photoluminescence due to control over pH of the solution during synthesis (Fig. 2.8).

A combination of enzymatic polycondensation and click chemistry was used for production of grafted copolymers (Scheme 2.15) [270]. Aliphatic polyester containing fixed azide groups were obtained via enzymatic polycondensation in
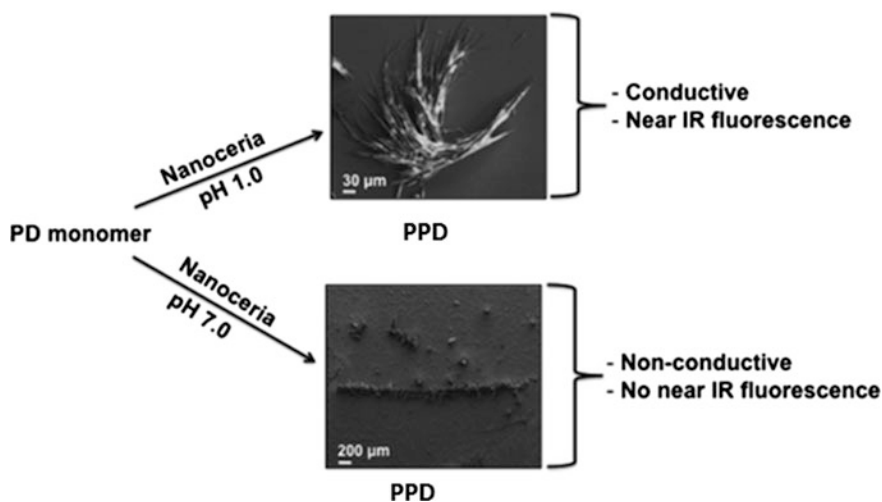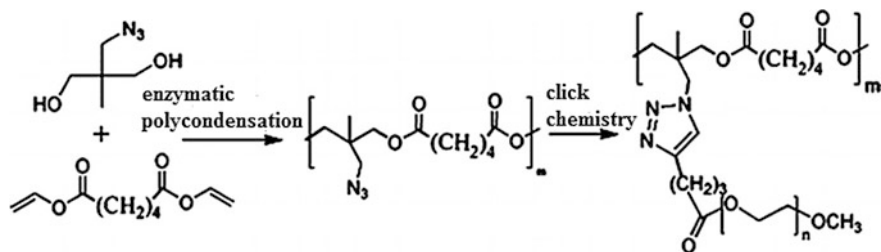

Fig. 2.8 The effect of pH synthesis on morphology, conductivity, and photoluminescence of PPD in presence of cerium nanodioxide

Scheme 2.15 An example of a combination of enzymatic polycondensation and click chemistry for production of CPLs

presence of lipase from *Candida Antarctica of B type.* Grafting to N_3-functional polyether was made quantitatively at room temperature using click reaction CuAAC with monoalkyne-functional PEO, $M_n = 750$. Moreover, both, enzymatic poly-condensation and click reaction were successfully carried out sequential in one reactor:

Enzymatic synthesis of CPL was developed with account for different types of reactions, including open-chained polymerization, polycondensation, the combination of open-chained polymerization and polycondensation, and chemoenzymatic polymerization [271].

Among demands of «green chemistry» is primary choice of reaction medium, which is safe from ecological point of view. In this regard the majority of studies were performed with water used as a solvent [45–47]. Water-soluble polymers attract a great interest due to their potential application for environment protection, for removal of polluting substances, in biomedicine, etc. Among irrefutable advantages of water-soluble polymers is the fact that their application does not cause pollution of environment, and this is not associated with using of toxic, flammable and explosive solvents [272].

The water-soluble poly(St-*co*-GMA-IDA) is formed during interaction of St with chelating vinyl monomer GMA-IDA [273].
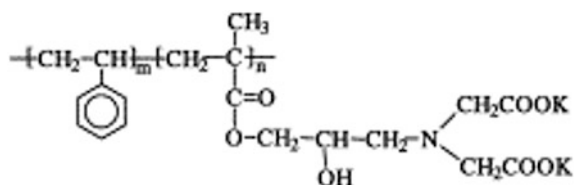
Water-soluble polyethylene imine (PEI) containing *N*-methyl hydroxamic acid chelating groups was synthesized (Scheme 2.16) [274].

Sulfonate-functionalized water-soluble conjugated polymer containing bpy units in main chain as receptors of transition metal ions was obtained by Sonogashira reaction. This polymer can be easily solved in water (5 mg mL^{-1}) and in some
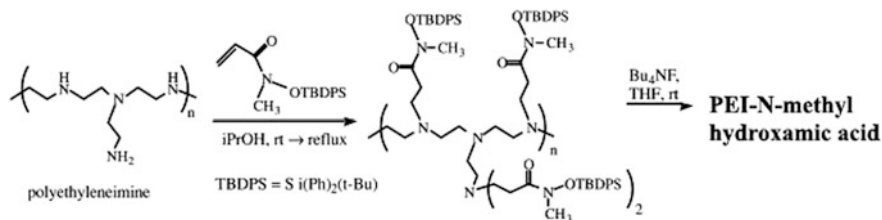
Scheme 2.16 Synthesis of water-soluble PEI containing *N*-methyl hydroxamic acid

polar organic solvents, such as methanol [275]. Anion water-soluble polyfluorene bpy-derivative polymer with side sulfonate groups in position 9 of the fluorine units is developed [276].

CPLs are obtained by one-step synthesis under soft conditions [268] via copolymerization of thiosemicarbazide and formaldehyde in water solution. Water-soluble aminosulfonate-phenol-salicylic acid-formaldehyde polymer with narrow PDI range is synthesized via reaction between phenol, sodium sulfanilate, salicylic acid and formaldehyde [277]. Dianhydride reacts with diazacrown ethers with formation of water-soluble EDTA-diazacrown ether polymers [278]. Also water-soluble polymer drug-form produced via the reaction of vinylpyrrolidone (Vp) and *N*-vinyl-*N*-glycidyl-γ-aminobutyric acid with acetylsalicylic acid is interesting [279]. Readily available and highly effective material for determination of rare earth metals based on a polymer containing amino groups for water solubility and thiourea groups for metal chelation was synthesized [280].

Using radical polymerization, the water-soluble polymers, poly-(2-acrylamidoglycolic acid) [281], and CPLs containing sulfonic acid groups [282] are obtained.

Tripyridyl-Pp monomer, 5-[4-[2-(acryloyloxy) ethoxy] phenyl]-10,15,20-tris(4-pyridyl)-Pp monomer is copolymerized with AAm to obtain hydrophobically linked water-soluble polymer [283]. Water-soluble π-conjugated polymers containing 5,5′-bpy or 6,6′-bpy units in π-conjugated main chain are obtained as scaffolds for macromolecular chelation of metal [284]. A possibility to adapt fluorescence quenching conjugated polymers under action of nitrogen oxide NO and its partial reduction with addition of Cu(II) ions in the system acetonitrile-water is considered for fluorescent detection of NO (Fig. 2.9).

Another important solvent in green chemistry of polymers is supercritical carbon dioxide [43]. Thus, following the strategy of green chemistry, gradient copolymer poly(1,1,2,2-tetrahydroperfluorodecyl acrylate-co-acetoacetoxyethyl methacrylate) successfully synthesized by RAFT in supercritical CO_2 with good control over M_n and composition [42, 285].

Ionic liquids, being a new class of solvents, which possess interesting properties, such as high ionic concentration, nonvolatility, good thermal stability and inflammability are of certain interest for green chemistry. As a typical example, we note polyhydrazides obtained by direct polycondensation of dihydrazides with benzofuro
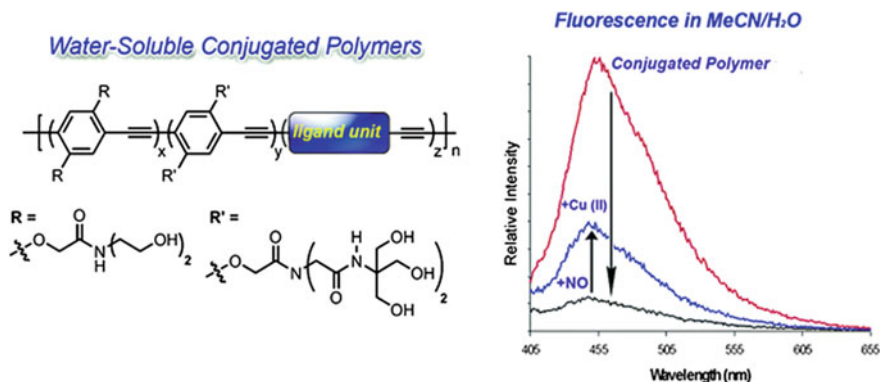
Fig. 2.9 Structure of conjugated polymers with bpy units in the main chain and change in intensity of their fluorescence at adding NO and Cu(II) ions

[2,3-b]-benzofuran-2,9-dicarboxylic acid in ILs and triphenyl phosphite (condensing agent) without any additional components (Il can act as a solvent or as a catalyst) [286].

Undoubted advantage of green chemistry is using of biodegraded polymers [48]. Thus, biodegrading poly(anhydride-ester) was synthesized by polycondensation in melt of acetylated monomer for production of a polymer prodrug [286]. The polymer consists of alkyl chains linked by ester bonds in aromatic fragments, in particular, salicylic acid, an active component of aspirin. Incorporation of this compound, having remedy properties ascribed to salicylic acid, and easiness of metabolism, into the polymer chain gives a polymer prodrug, which can have different potential applications (for example, at inflammatory bowel decease).

Hydrolytically and microbiologically degraded poly (EDTA-*co*-lactose) with linked carboxyl groups of high molar weight (132,000) was obtained via polycondensation of EDTA anhydride and lactose [287]. Also biodegraded polyamides containing α-amino acid should be noted [288].

Biodegraded poly(anhydride-esters) containing EDTA in the main chain and linked antimicrobial groups (for example, carvacrol, thymol or eugenol) are synthesized via polymerization in solution [289]. For these polymers hydrolytic degradation in vitro ends after 16 days, bringing to release of free antimicrobial drugs and EDTA. There polymers are completely decomposed in components, which are biologically relevant and provide a possibility of increasing shelf life of consumer goods in food and personal care manufacturing using antimicrobial and antioxidizing approach.

In other biodegraded poly(anhydride-esters) based on salicylic acid and diglycolic acid the bioaccessibility of salicylic acid was dependent on several factors, including solubilization rate, macroscopic erosion of the powdered polymer, and hydrolytic cleavage of the anhydride bonds [290].

Cross-linked, biodegraded cytocompatible polyesters based on salicylic acid were produced from melt condensation for localized and steady supply of salicylic acid [291].

The improved strategy of PAMAM synthesis for biomedical application is also worthy of notice: catalysis using green biocompatible salts of alkali-earth metals [292]. Outstanding results should be expected in this direction in the nearest future.

2.2 Grafted Polymerization in Chelation of Macroligands

There are many problems, to solve which it is necessary to transport a chelating fragment to the surface or near-the-surface layer of a polymer, for example, in catalysis [293]. Fixing chelating units on a polymer surface decreases considerably diffusion limits of chelation processes, and mobility of grafted chains diminishes role of spatial problems during chelation of MX_n. In many cases this purpose is achieved by the grafted polymerization techniques.

According to recommendations of IUPAC, grafted macromolecules are considered to be the macromolecules with one or more types of blocks linked to the main chain, so that these side chains have constitutional or configuration characteristics different from those of the main chain and randomly distributed. They are used as CPLs since the end of 1960s. A number of potential applications of the grafted polymers are presently substantially broadened due to development of CRP technique. Graft-copolymers containing a great number of side chains can display worm-like conformations, compact molecular packing and substantial effects of end chains due to their limited and closely fitting structures [294–298].

2.2.1 Specifics of Grafted Polymerization

The main approaches to synthesis of grafted copolymers are based on well-known methods: chemical (free-radical polymerization, ATRP, ROMP, iniferter-induced polymerization), radiation, photochemical, plasma-induction, enzymatic grafting, polycondensation reaction, etc. Grafting has noticeable advantages as compared with other methods of CPL synthesis due to several reasons, including easy and controlled incorporation of grafted chains with high density and their exact localization on the surface without changing properties of a polymer substrate. Moreover, rigid fixation of grafted chains on a polymer surface prevents them from delamination and guarantees long-term chemical stability of the integrated chain, in contrast to physically bound polymer chains [299].

The grafted polymers are most often obtained in two principal ways: «grafting-from» and «grafting-through» [300]. However, development of click chemistry has brought to appearance of the third approach «grafting-to» (Fig. 2.10) [301].
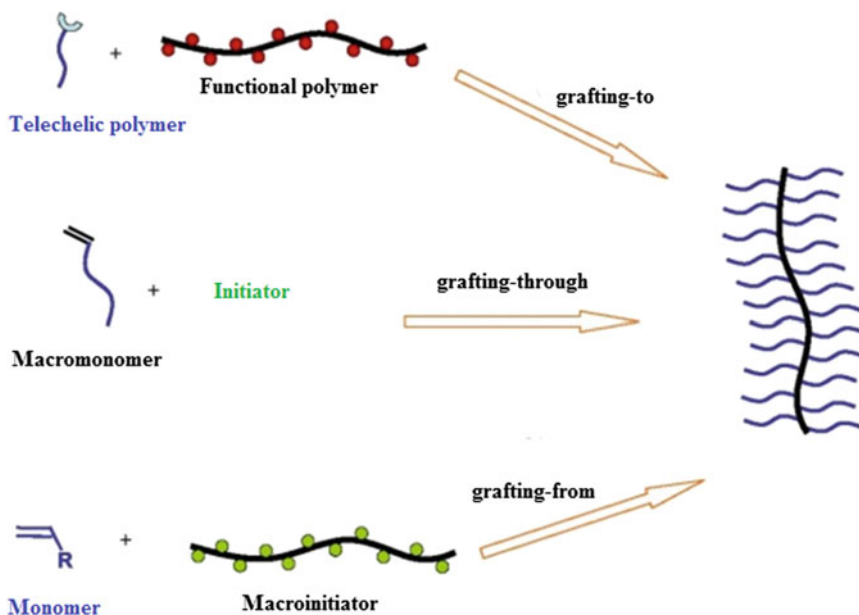
Fig. 2.10 Schematic presentation of «grafting-from», «grafting-through», and «grafting-to» processes

The main demand to successful «grafting-from» reaction is preliminary obtained macromolecule with distributed initiating active centers. In other words, in the «grafting-from» method a macromolecular matrix is modified to integrate active centers capable of initiating the grafted polymerization [21, 295, 296, 302].

Commercial polymers are widely applied as polymer carriers in the «grafting-from» polymerization processes: polyethylene (PE), polypropylene (PP), polytetrafluoroethylene (PTFE), poly(vinyl alcohol) (PVA), poly(vinyl chloride) (PVC), PCD, etc. [18, 19]. Thus, the methods of PE surface modification by grafting are compared (flame treatment, crown discharge, plasma and high energy radiation, initiators and polymer grafting, chemical and photochemical treatment, halogenation) [303], and the PE modifying methods using grafting in solution, melt, solid state grafting, other methods [304]. There is an interesting usage of grafting for surface functionalization of latexes for their following application in biotechnology [305]. Simple devices have been designed [306] for adsorption and metal ion concentration, which contain different chelating monolithic polymers, for example, poly(butyl methacrylate-*co*-ethylene dimethacrylate) monoliths with photo-grafted, en-modified GMA.
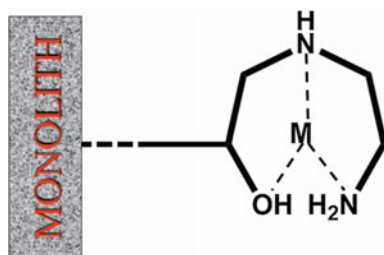
Production of polymers with grafted chelating fragments is carried out in two ways: one-stage, which includes grafted polymerization of chelating monomers to a polymer substrate, and two-stage, which supposes production of grafted multi-functional groups with their following completion up to a chelating fragment. The «grafting-from» method provides production of polymers with very different chelating fragments, for example, en, diethylenediamine, trien [307–309], 2,2′-dipyridilamine [310], thiol [311], amidoxime [312–314], sulfonic acid [315], imin-odiethanol [316, 317], di-2-propanolamine and 3-amino-1,2-propandiol [316], IDA [318–320], N-methylglucamine [316, 321], 2,3-diaminonaphthalene [322], catechol [323], β-diketones [324, 325], salicylic acid [326, 327] and acetyl salicylic acid [328], N-acylsalicylamides [329], Pp [330], crown ethers having a variety of donor-atoms (thia- and azacrown ethers, crown ethers with oxygen atoms) [331, 332], anthranilic acid [333], etc.

Surface modification of polymers is initiated by free radicals formed from an initiator and transferred to a polymer matrix for interaction with a monomer with grafted copolymers forming. Examples of directly generated free radical formation are redox reactions with participation of peroxides and persulfates. Free-radical active centers are generated by direct oxidation of a polymer matrix by ions of some transition metals (cerium, chromium, vanadium, cobalt). Thus, polymer flocculant (cross-linked copolymer PAAm-xanthate with grafted sodium gluconate) was synthesized in aqueous solution using cerium-ammonium nitrate (initiator of the reaction) and epichlorohydrin (cross-linking agent) [334]. The same initiator was used for grafting diaminomaleonitrile on PVC in nitrogen atmosphere in aqueous nitric acid [335]. The grafted copolymerization of AN to PVA microspheres was performed using cerium-ammonium sulfate as initiator. The grafted PAN was converted into poly(amidoxime) by the reaction with hydroxylamine hydrochloride [336]. Redox-potential of metal ions is an important factor, which determines efficiency of grafting. In general case metal ions with low oxidation potential are preferred as efficiency of grafting is concerned. Using metal chelates in grafting is not very suitable, but has some advantages. There are compounds, which can give free radicals upon heating, which are transferred to a polymer chain (for example, azo-compounds, peroxides, hydroperoxides, peroxide diphosphates, etc.). Apart from the aforementioned initiators, BP and AIBN are very effective in grafting reactions. Preliminary chemical treatment (for example, ozonation, diazotization,

xanthantion) of polymeric matrix can generate free radicals, which initiate the grafted polymerization process. We shall also notice formation of secondary free radicals, which initiate the grafted polymerization process, for example, CO_2^-, $C_2O_4^-$, etc. [296].

When performing grafted radical polymerization, first polymer monolayers form, as a result, catching of a double-bond on a surface is kinetically impeded at once after covering of the surface by polymer chains, due to which amount of the grafted polymer on the surface is limited and does not exceed 1.5 mg m^{-2} [337]. Polymerization on grafted self-assembled monolayers (SAM) allows controlled decoration of the surface by macromolecules [338]. Using of SAM in grafting attracted much attention due to their stability, reliability, and perfect control over orientation of functional groups.

More rarely free radical grafting in melt is used. In this case a mixture of polymer matrix, monomer and initiator is heated to high temperature, so that grafting proceeds in the melt. Thus grafted polymerization of *p*-(met) acryloyloxybenzoic acids on isotactic PP was performed [339]. Grafted polymerization of *p*-acryloyloxybenzoic acid has no effect on formation of both forms of α (monoclinic) PP, while *p*-metacryloyloxybenzoic acid brings to $α_2$ form. β-Crystalline (hexagonal) modification forms in PP-grafted(-*gr*-)-poly(acryloyloxybenzoic acid) at 185 °C; β-form was not observed in the grafted copolymers of poly(methacryloyloxybenzoic acid).

Radiation grafted polymerization is widely used as CPL synthesis technique [340]. Especially efficient is using the radiation-grafted materials (nanogels and microgels, hydrogels, fibers and monoliths, as well as membranes and brushes) for separation and purification, including environmental remediation, biotechnology, water production, chemical industry, and biomedicine categories [341]. General scheme of the grafted chelating adsorbent production can be represented as follows:

Preparation scheme of graft adsorbent
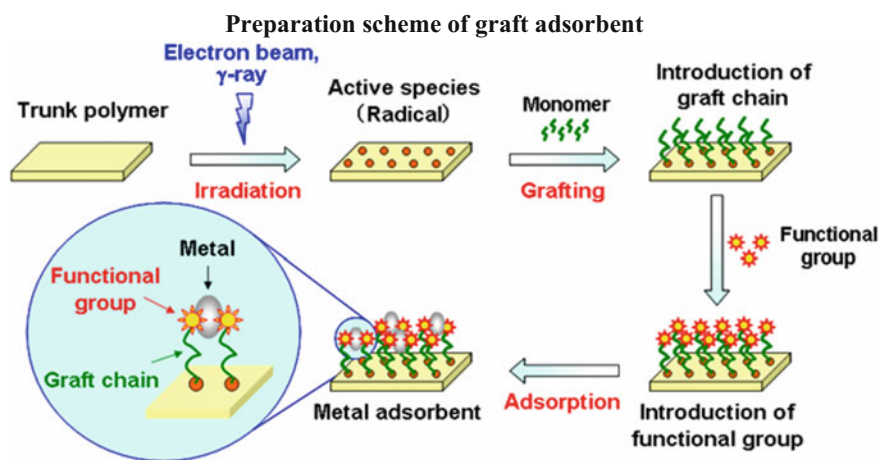
Irradiation of macromolecules can cause their homolytic splitting and, therefore, brings to formation of free radicals on a polymer surface. A medium is important in this case, for example, if irradiation is performed in air, peroxides can be formed on a polymer surface. Lifetime of free radicals depends on origin of a polymer matrix. Grafting is performed in three ways: (a) preliminary irradiation; (b) peroxidation, and (c) simultaneous irradiation technique [342, 343]. In the method of preliminary irradiation, a polymer matrix is first irradiated in vacuum or in presence of inert gas for free radical formation. The irradiated polymer matrix is then treated by a monomer in liquid or gaseous state or solution in appropriate solvent. This method, in particular, was applied to obtain chelating porous sheets for using in solid-state extraction [344]. First vinyl monomers containing epoxy-groups were radiation-grafted to PE-based porous sheets, and then the epoxy-groups were converted into IDA chelating fragments. The chelating porous sheets with density of IDA groups 2.1 mol kg^{-1} were cut into discs of 13 mm in diameter in order to fit an empty cylindrical cartridge with a capacity 6 mL. The similar procedure of preliminary irradiation of a polymer-substrate was applied for grafting GMA on preliminary irradiated PP fibers then followed by dien amination [345].

In the peroxidase grafting method, the initial polymer is subjected to irradiation with high energy in presence of air or oxygen with formation of hydroperoxides or diperoxides depending on nature of a polymer matrix and irradiation conditions. Stable peroxy products are then treated by a monomer at high temperature, at which peroxides are decomposed into radicals, which initiate the grafting process. An advantage of this method is that the intermediate peroxide products can be stored for a long time before involvement in the grafting process.

And finally, in the simultaneous irradiation method a polymer and monomers are irradiated simultaneously with formation of free radicals and the following linking. Thus, PVA aqueous solutions containing different amount of EDTA were subjected to γ-irradiation with ^{60}Co source to produce PVA-EDTA hydrogels. It occurs that content of EDTA in the hydrogel matrix is far lower than in the initial mixture [346].

The two-stage method of production of grafted siderophore-mimetic CPLs on PP surface has been developed: photo-initiated grafting poly(methacrylate) (PMA) with the following transformation into poly(hydroxamic acid) (Scheme 2.17) [1].

Photo-initiation was also used for grafting GMA on PE films followed modification at 80 °C of grafted films by disodiumimino diacetate [347]. Photo-grafting such chelating monomer as 2-acrylamidoglycolic acid, 3-sulfopropylmethacrylate, and 2-acrylamido-2-methyl-1-propanesulfonic acid on poly(ester sulfonic) membranes was performed without photoinitiator [348].

Surface modification using plasma or glow-discharge includes three possible methods: plasma treatment, plasma polymerization, and plasma-induced grafted polymerization [349, 350]. Thus was, for example, immobilized tetraphenyl-Pp on a plasma-treated PP [351]. Plasma treatment or glow discharge treatment can change properties of a surface of a polymer-substrate by integration of some polar groups, such as hydroxyl and amino groups. Thus, amino groups generated by
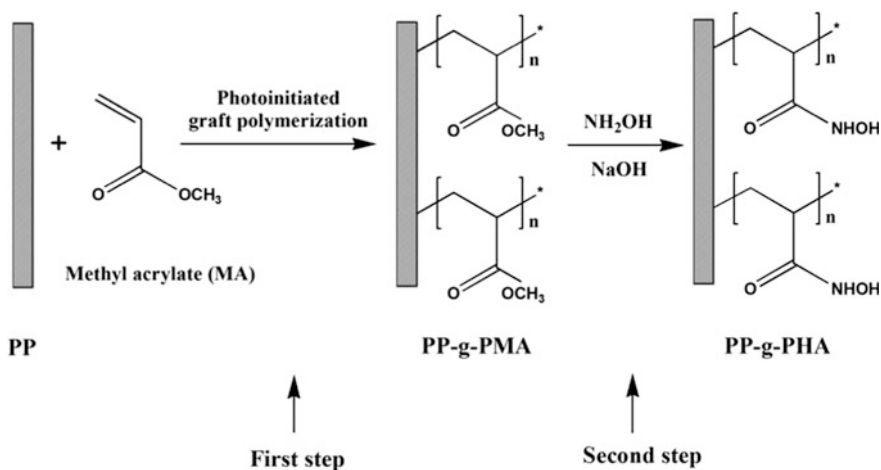
Scheme 2.17 Schematic diagram of production of PP-*gr*-poly(hydroxamic acid) using two-stage surface grafting

ammonia plasma, initiate open-chained polymerization of *N*-carboxyanhydride of γ-stearyl-L-glutamate on PP microporous membranes [352] . Also plasma-initiated grafted polymerization of benzo-18-crown-6-acrylamide should be noted [353].

2.2.2   Controlled Grafted Polymerization

The vast majority of the recent years' studies considering synthesis of grafted CPLs are focused on using CRP technologies, such as NMP, RAFT, and most often, ATRP [354–356]. Using CRP makes it possible to easily control molecular weight of the grafted chains, which, in turn, control a grafted layer thickness. Probably, the simplest way to achieve it is to control polymerization duration, experimentally this can be realized by a simple periodical removal of samples from reaction as necessary. Thus, very thin uniform layers (just several nanometers in thickness) can be obtained using slow polymerization methods and short times of growth, though thickness ∼500 nm is possible. Gradient in thickness is also formed by slow feeding of a polymerization solution (monomer and a catalyst in a solvent) in container with a substrate [357]. Control over thickness can be also achieved by addition of free (non-bound) initiator, and allows achievement of high conversion, at that molecular weight is determined by the [monomer]/[initiator] ratio.

The ATRP method has some advantages for production of well-defined grafted polymers, among which are simplicity of initiator synthesis, fair control over a polymer growth, «living» character of the grafting process and a possibility to carry out a reaction in ecologically safe solvents under fair control [296]. Many different classes of grafted polymers are obtained by ATRP method, including hydrophobic,
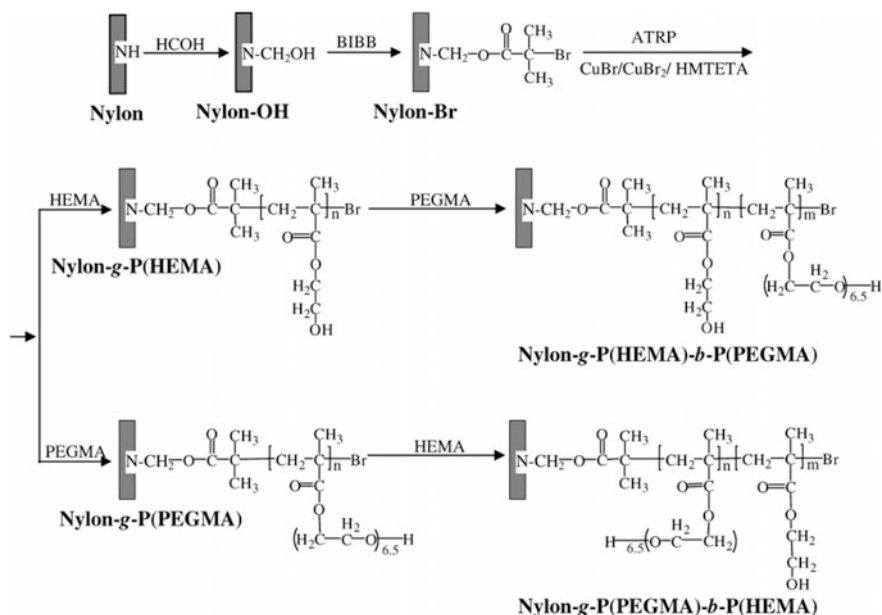
Scheme 2.18 Diagram representing activation and surface-initiated ATPRs on a nylon membrane, where HEMA is hydroxyethyl methacrylate, PEGMA is poly(ethylene glycol methacrylate), and BIBB is 2-bromoisobutyrate bromide

hydrophilic, charged (cation and anion), stimuli-responsible (pH and temperature), biocompatible, cell-adhesive, antimicrobial, and chemically active (for PPM or cross-linking) [355]. The method of surface-limited ATPR provides access to user's database of hybrid materials based on polymers for special applications [358]. CPLs are obtained by grafting poly(GMA) on bead PCD using surface-initiated ATRP, and the following reaction of epoxy groups with IDA [359]. Using ATRP method, 2-hydroxyethylmethacrylate and poly(ethylene glycol methacrylate) were grafted on a nylon-membrane surface (Scheme 2.18). Formed grafted homopolymers can interact in the following copolymerization reactions with formation of polyfunctional grafted diblock-copolymers [360].

ATRP was successfully used for the surface-initiated grafted polymerization, but it has one serious drawback, sensitivity to oxygen of Cu(I) complexes usually used for polymerization. This sensitivity requires thorough deoxygenation of solvents and polymerization containers. Therefore, a version of ATRP was developed, called Activators ReGenerated by Electron Transfer Atom Transfer Radical Polymerization (ARGETATRP), which substantially decreases sensitivity to oxygen by introduction of excess reducing agent in a reaction [361]. This approach has two important advantages as compared to conventional ATRP: it provides improved oxygen enduring and considerable decrease in concentration of a catalyst from heavy metals [362].

Electrochemically-induced ATRP (eATRP) is also developed for production of IDA-functionalized poly(GMA) grafted to carbon fibers for detection of nano-nickel from baths for chemical nickel-plating [363].

The only demand to multifunctional RAFT grafting from a macro-initiator is a possibility of radical transfer of atoms along a polymer chain. Initiating active centers can be incorporated by copolymerization [364]; they can be integral part of the first polymer [365] or can be included in PPM reactions [366]. If each active center along a polymer matrix contributes to formation of one of the branches, then a number of chains grafted to a macromolecule can be controlled by a number of active centers. Though a number of grafted chains can be regulated, there can still be a difference in lengths of each grafted chain due to kinetic and steric effects. The key feature of RAFT polymerization is a possibility of obtaining grafted polymers, for example, poly(vinyl esters) by chain extension of macroRAFT-agents containing polyfunctional fragments [367]:
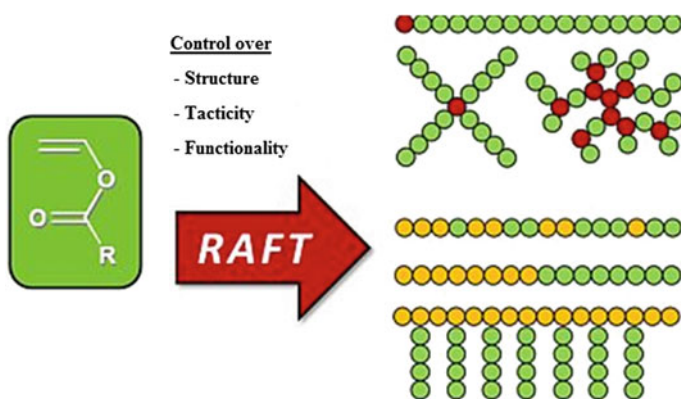
The most often used macroRAFT-agent for this purpose is *O*-ethyl xanthate-terminated PEG. An example of using a macroRAFT-agent obtained using PPM by xanthate of a polymer preliminary produced by the RAFT method is fabrication of PVA-*gr*-polyvinyl acetates using R- and Z-approaches (Scheme 2.19) [368].

Alternative approach is that, in which macroRAFT-agent (poly 2-((2-ethylxan-thatepropanoyl) oxy) ethyl methacrylate) is obtained by linking chain transfer xan-thate agents to each monomer unit of poly(2-hydroxyethyl methacrylate) obtained by ATRP method. RAFT polymerization of vinyl acetate [369], or consequent poly-merization of Vp and vinyl acetate [370] in presence of synthesized macroRAFT-agent provide production of polyfunctional polymers (Fig. 2.11).

The «grafting-from» method was successfully applied to obtain some chiral grafted polymers [371–374]. These polymers include, for example, helical poly-acetylene polymer matrix with side poly(*N,N*-dimethylamino-2-ethyl methacrylate) chains [375].

R⁻ designed xanthate   Z⁻ designed xanthate
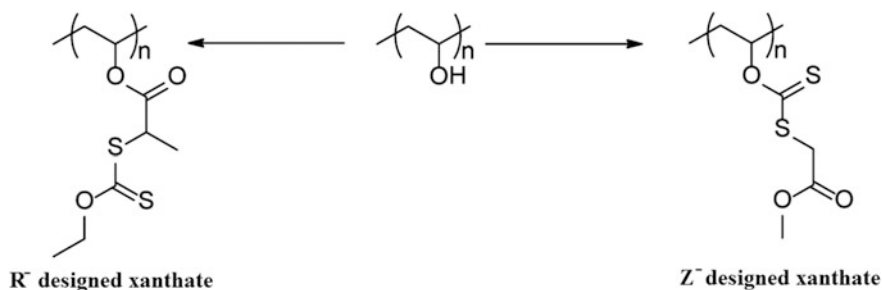
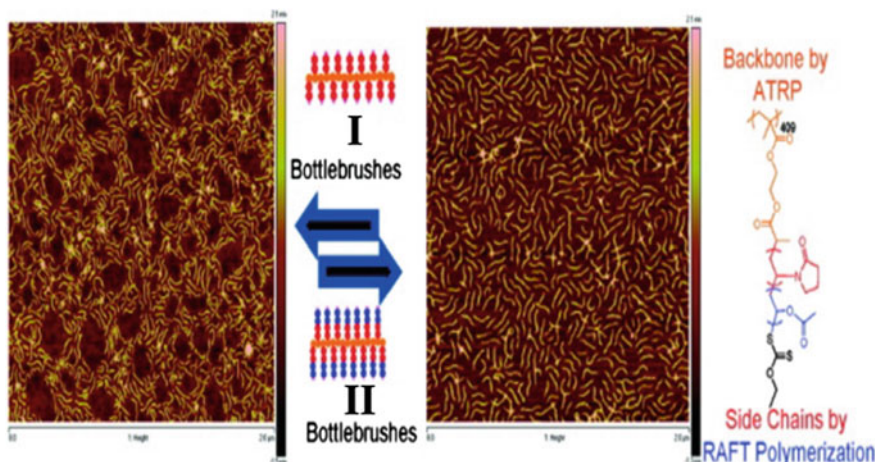**Scheme 2.19** Strategy for the R- and Z-designed PVA combs

Fig. 2.11 Grafted polymers synthesized by RAFT polymerization from ATRP-obtained macroxanthate, where **I** is poly(Vp) and **II** is poly(Vp)-*b*-poly(vinyl acetate)

Recently easily available method of grafted polymerization from a poly-dopamine (PDA) coating layer has been developed [376]. First a PDA layer is applied to virtually any surface, independently on functional groups present on the surface, which can form surface-bound radicals under sunlight. Therefore, the PDA layer can serve as a photo-inducing layer for initiation of radical grafted poly-merization of any monomer (Fig. 2.12). The special features of this method are the possibility of spatial control over architecture of the grafted polymer chains (pat-tern, gradient) and use of a vast grafting area with ultrasmall amount of a monomer solution (thin polymer layer).

Unusual strategy of creation of functionally grafted pseudo-semi-interpenetrative network structures is developed by the reaction of bifunctional linear polymers cross-linking with multifunctional dendritic cross-linking units placed in the ends of chains of linear polymers. The obtained materials have pseudo-semi-interpenetrative structure [377], in which a linear polymer is fixed by a network structure.
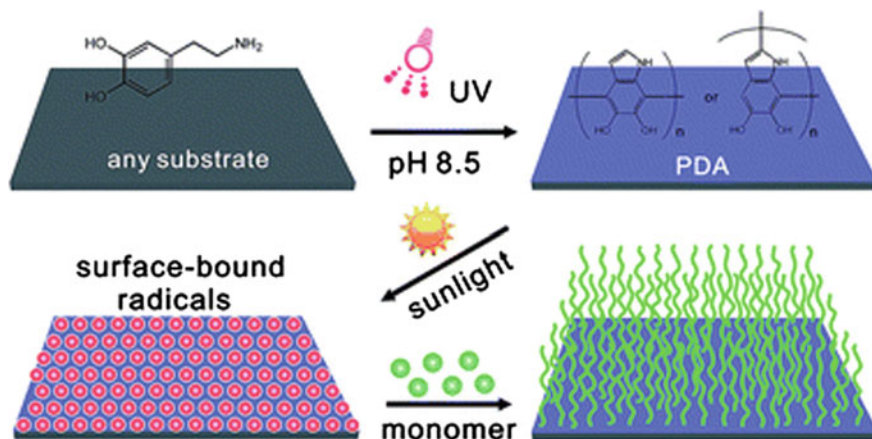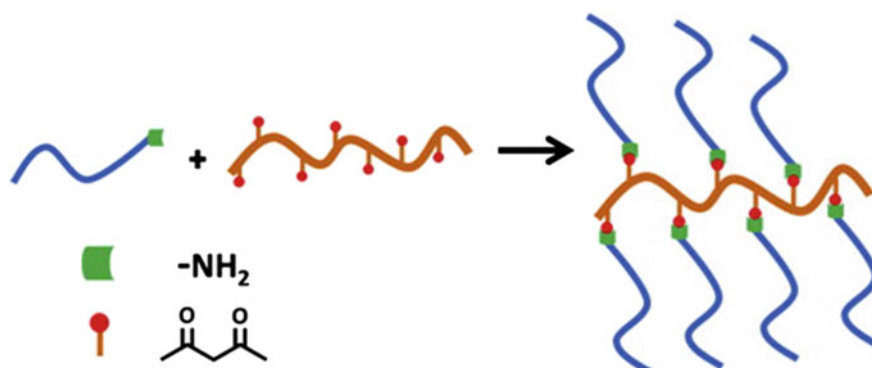
Fig. 2.12 Grafted polymerization of thin layers

Fig. 2.13 Condensation of grafted ligand

We shall notice using reaction of polycondensation for production of grafted CPLs (Fig. 2.13) [378]. In this case a polymer-substrate poly [(2-acetoacetoxy) ethyl methacrylate] with β-keto ester groups along a chain is obtained by RAFT polymerization and is introduced into reaction of polycondensation with PEG monomethyl ether with end NH_2-groups. By varying the initial molar ratio between a polymer-substrate and a polymer with end NH_2-groups, grafted polymers with varied graft density can be obtained.

The «grafting-through» (or macromonomer method) is one of the simplest ways of synthesis of grafted polymers with well-defined side chains [379, 380].

Low molecular   Polymerizable   Well defined graft copolymer
weight monomer   macromonomer
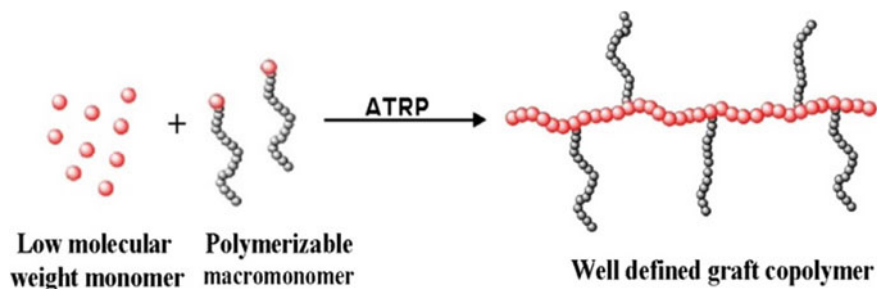
This method enables to introduce macromonomers, which are prepared by another process of controlled polymerization into matrix obtained by CRP method. Thus, for example, macroRAFT-agents of a chain transfer, α-norbornenyl-functionalized poly (t-butyl acrylates) were obtained by RAFT method and then polymerized by ROMP method using Grubbs catalyst (Fig. 2.14) [381].

Combination of controlled polymerization processes allows control over polydispersion, functionality, composition of a copolymer, a matrix length, length of grafted chains, and a distance between them by changing a molar ratio between a

**Fig. 2.14** Grafted polymerization by combination of RAFT and ROMP methods
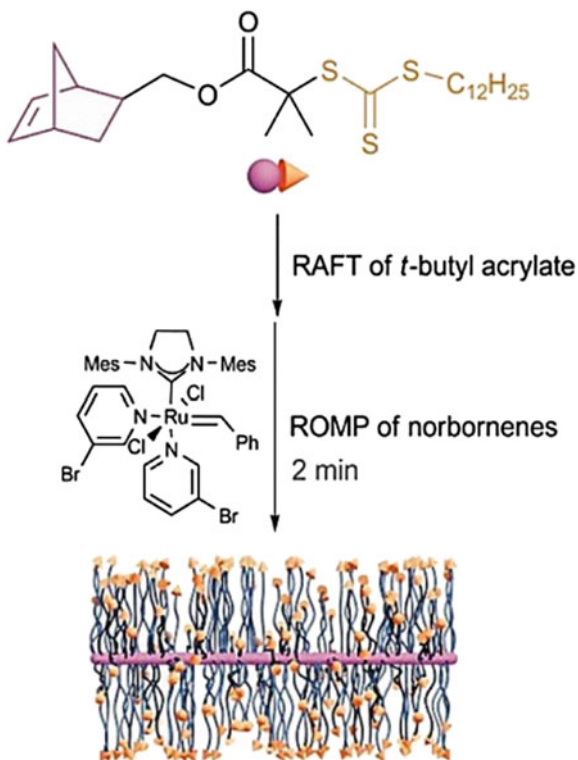
monomer and a macromonomer and relationships of reactivity values of both. The grafted chains can be homogeneously or heterogeneously distributed depending on the relations between reactivity of end functional groups on a macromonomer and a low molecular weight monomer; this has a significant effect on physical properties of materials.

Homogeneous distribution of grafts   **Heterogeneous distribution of grafts**
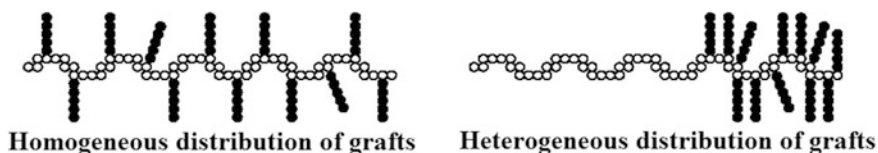
A series of segmented poly(alkyl methacrylate)-*gr*-poly(D-lactide)/poly(dimethylsiloxane) terpolymers with different topology were prepared using «grafting-through» and CRP techniques [382]. At that, two ways of synthesis were used: one-step approach, in which methacrylate monomer (MMA or butyl methacrylate) was copolymerized with the mixture of poly(D-lactide) and poly(dimethylsiloxane) macromonomers, another one was two-stage approach, in which a grafted copolymer containing one macromonomer was chain-extended by copolymerization of the second macromonomer and low molecular weight methacrylate monomer. Topology of the grafted terpolymers prepared in different combinations of two approaches can be schematically presented as:

Gradient "palm tree"   **Symmetrical gragient**   **Successive gradients**
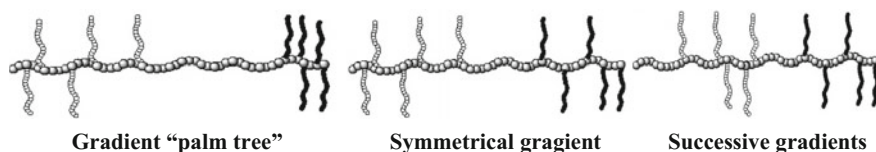
Grafting becomes more efficient way for production of grafted copolymers as different methods of click chemistry have appeared [301, 383]. This approach called «grafting-to» includes such click reactions as thiol-based additions, activated ether coupling, azide-alkyne cycloadditions, some Diels-Alder reactions, and also non-aldol carbonyl chemistry, for example, oximes, hydrazones, and amides formation [384]. Thus, a polymer-substrate with glycidyl butyrate units obtained by ATRP method is modified by sodium azide for preparation of a suitable for «grafting-to» copolymer using click chemistry (Scheme 2.20). The reaction of click-type with high yields results in the formation of a co-polymer with 1-hydroxy-2-azido functional groups with high yields, which are additionally functionalized for a second via a click reaction at room temperature. 1,3-Dipolar cycloaddition of PEO methyl ether pentynoate catalyzed by CuBr/*N,N,N',N'',N''*-pentamethyldiethylenetriamine gives grafted polyfunctional polymers with PEO hydrophilic side chains [385].
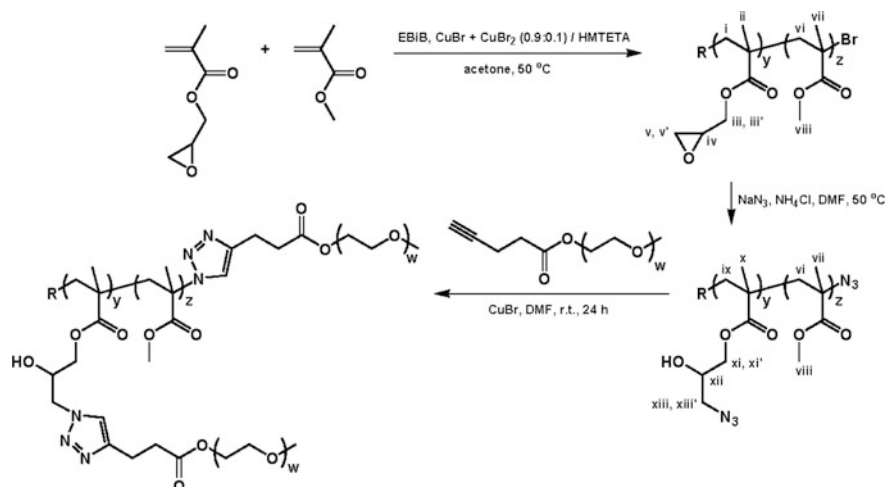
Scheme 2.20 Click reactions in grafted polymerization

«Grafting-to» approach is used for preparation of star-shaped molecules of weakly and densely grafted polymers [386]. The «grafting-to» technique assumes using a main chain with functional groups, which are randomly distributed along the chain. Formation of a grafted polymer follows the reaction of coupling between the functional matrix and end groups of the reactive grafted chains. These coupling reactions make possible chemical modification of a polymer matrix. General mechanisms of reactions used for synthesis of these copolymers include free-radical polymerization, anion polymerization, ATRP [387, 388], ring-opening polymerization (ROP) [389, 390], ROMP [391] and living polymerization technique. Copolymers prepared using the «grafting-to» method often used the technique of anion polymerization. This method including the coupling reactions of electrophilic groups of a polymer matrix and growing centers of anion living polymer would be impossible without generation of a polymer matrix having reactive groups. High yield of the chemical reaction called atom transfer nitroxide radical coupling chemistry is typical of the «grafting-to» polymerization method.

We shall focus on production of CPLs for gadolinium contrast agents using «grafting-to» strategy. For example, copolymers of activated ester monomer, pentafluorophenyl acrylate, and oligoethylene glycol methyl ether acrylate were prepared and modified with the chelating ligand 1-(5-amino-3-aza-2-oxypentyl)-4,7,10-tris (*tert*-butoxycarbonylmethyl)-1,4,7,10-tetraazacyclododecane for chelation with Gd (III) [392]. We shall notice synthesis of macrocyclic [393] and amylose-containing [394] grafted polymers by the «grafting-to» method.

Optically active grafted polymers based on helical polyacetylenes were produced using combination of ATRP, catalytic polymerization and click chemistry (Fig. 2.15) [395]. Strategy of obtaining grafted polymers consists of four main steps: (1) synthesis by ATRP method of alkynyl terminated poly(NIPAM) as one click-reagent for using as side chains in grafted polymers; (2) synthesis by catalytic polymerization of helical copolymer acting as helical polymer substrate; (3) synthesis of azido-functionalized copolymer by transformation of bromide groups into azide for production of the second click-reagent, and (4) synthesis of optically active grafted polymers by click reaction. The grafted polymers can self-assemble in aqueous solution forming core/shell structured nanoparticles having optical activity and thermal sensitivity.
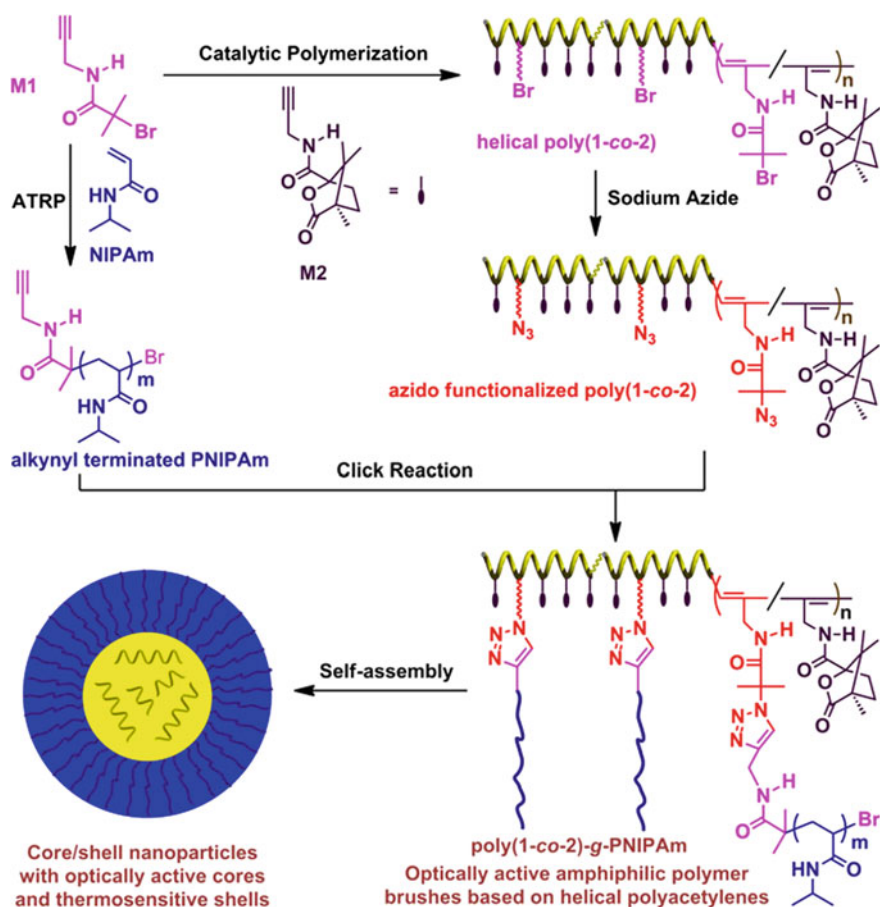
Fig. 2.15 Scheme of production and self-assembly of thermally-responsible amphiphilic polymers based on helical polyacetylenes

2.2.3 Macromolecular «Brushes»

The distinctive physical properties of grafted polymers are attributed to three interconnected parameters, such as grafting density (σ), molecular weight of the grafted chains, and quality of a solvent. The most fundamental and easily measured property of a grafted polymer is its height (H), which is determined by hydrodynamic radius (R_g) of polymer covering a particle and increasing as repulsion forces between particles increase. The main statements of theoretical and experimental approaches for description of spatial structure of grafted chains are derived from the idea that depending on density of a polymer grafting, fixed chains gain so called mushrooms or brushes configurations on the solution/substrate interface (Fig. 2.16). At that, their mutual transitions are possible, depending on different factors [396].

In a good solvent, where a surface is «inert», height of a grafted chain is determined by balance of monomer-monomer repulsion (or osmotic pressure of the monomers), which advances heightening of a grafted chain, and stretching of entropy of the chains, which promotes decrease in height. Grafting density is a number of ends of grafted chains per unit surface area of a substrate, and is expressed by equation

$$\sigma \equiv \frac{1}{(D/\alpha)^2} \tag{2.1}$$

where D is a distance between grafting points in units of monomer size. If α is very small, chains are efficiently isolated from each other and act independently: there is no additional osmotic pressure caused by the chains to stretch them away from the surface, and the chains form isolated islands or «mushrooms».

Size of isolated chains in a good solvent is determined by Flori radius:
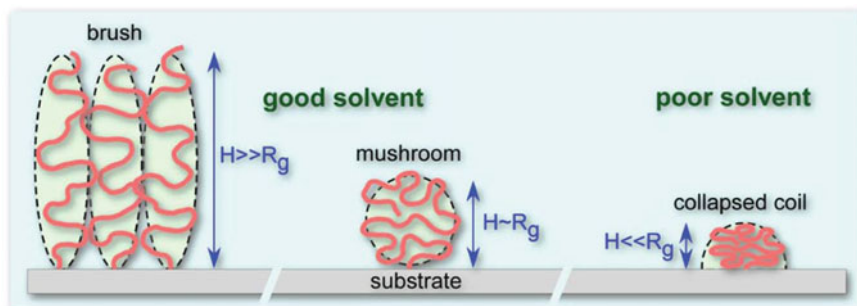
$$R_F \sim \alpha N^{3/5} \tag{2.2}$$

Fig. 2.16 Schematic representation of conformations of surface-linked polymers in the brush regime (on the left) and in the mushroom regime (on the right) in good diluter. Also conformations of surface-linked polymers in a bad solvent are shown
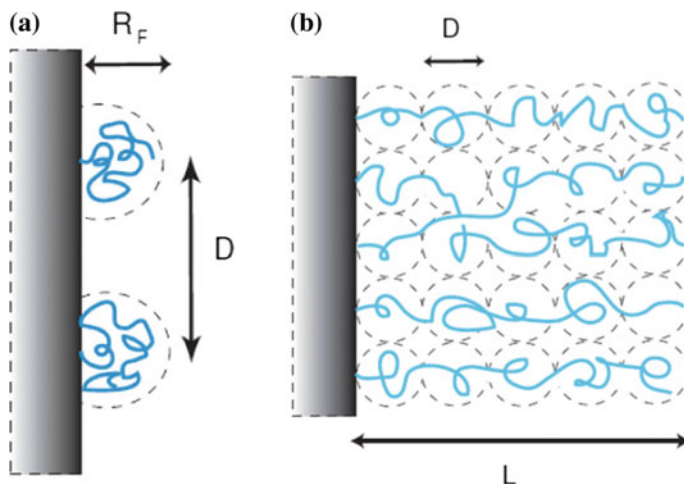
Fig. 2.17 a Scheme of chains grafted by the ends to inert substrate swelling in solvent at D distance between the grafting points. Distance between the grafting points is far more than the radius $R_F \sim aN^{3/5}$, so that these chains are isolated from each other and form mushrooms on the surface. **b** Scheme of Alexander-de-Gennes solvated brushes

so that if tethered dilutedly, size of a single-chain mushroom is R_F. Critical grafting density (σ^*), which makes a boundary between the mushroom and the brush regimes, is grafting density, at which mushrooms begin to touch each other, or if distance D between graftings is approximately equal to R_F (Fig. 2.17a).

The equations, which connect height of the grafted chains (H), polymerization degree (DP) and grafting density (σ) based on the Flori theory, are as follows:

$$H \propto DP\sigma^n$$
$$\sigma = h_d \rho N_A / M_n,$$

where h_d is thickness of a dry brush, N_A is Avogadro number, ρ is volume density of a polymer.

In a good solvent, thickness of a grafted polymer in the mushroom regime with low grafting density is $H \sim N\sigma^{1/3}$. Thus, the longer chains, the more diluted a fixing surface should be, so that the grafted chains would remain in the mushroom regime. At the early stages of polymerization, when a number of monomers in each growing chain is small, a surface is bound to isolated polymer mushrooms. But once chains become longer, each mushroom grows until they fall on each other finally forming polymer brushes.

The physical picture of Alexander-de-Gennes model is based on «blobs», as is shown in Fig. 2.17b, their size is determined by grafting distance D. The blobs works as rigid impenetrable spheres, which fill space.

Height or thickness of a brush L is equal to a number of monomers in a chain contained in a column with $(D/\alpha)^2$ area and height L/α and is estimated as:

$$\phi \sim \frac{N\alpha^3}{D^2 L} \tag{2.3}$$

Therefore, at high grafting density chains are effectively modeled by hard-core blobes, which generally spread in normal to the grafting plane direction. The Alexander-de-Gennes model determines how a blob size changes as grafting density changes. Introduction of the blob model occurs useful and simplified theoretical tool, which deals with the physical sense of the problem.

Transition from «grafted» copolymers to «brushed» happens only when density of the grafted side chains begins to affect a matrix ability to accept random coil configuration.

Macromolecular brushes belong to the general class of grafted copolymers [21, 302, 397–406]. However, in this case the grafting density can be very high, at least, in some segments of a copolymer. Really, polymers with one chain grafted on a repeated unit of a polymer matrix were obtained. This results in very tense situation along the polymer matrix, which makes a macromolecule take unusual conformations due to steric repulsion stipulated by densely packed side chains [407]. Densely grafted side chains reinforce the polymer matrix, but it retains some conformation freedoms. Dynamics of the side chains and the matrix changes as compared with respective homopolymers, and dynamics of the matrix shows that it is plastified by side chains, and the molecule becomes dynamically more uniform.

Graft copolymer   **Densely grafted brush copolymer**
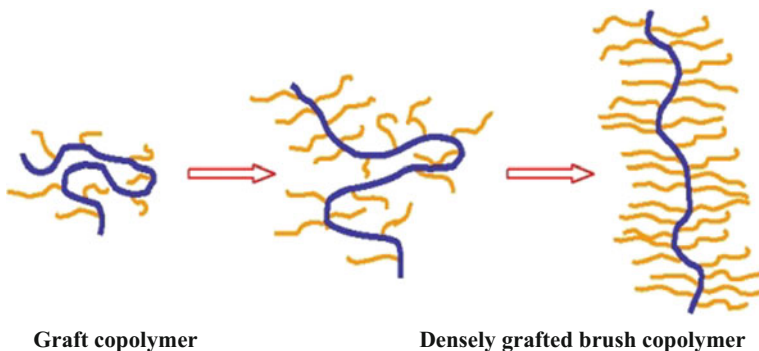
Overloaded structure of polymer brushes appears due to limited mobility of side chains. Linear brushes, also called bottle-brush copolymers, as molecular architecture are well known in biology, where they are responsible for different functions,

including mucociliary clearance of breathing ways and mechanical performance of articular cartilage.

In turn, polymer brushes are subdivided into a range of classes, among which star brush copolymers, brush block-copolymers, heterografted brush copolymers, gradient brush copolymers and molecules with double grafted side chains (brushes of brushes) are most important [385].

Thus, if a tetra-functional initiator is used for polymerization of poly(2-hydroxy ethyl methacrylate) with 2-(trimethylsilyloxy) ethyl methacrylate groups, the obtained polymer can be functionalized with formation of 4-arms macroinitiator. This product, in turn, can be used for production of 4-arms star macromolecular brushes [408].

SP-containing polymer brushes used as photoswitchable, reversible optical sensors that show selectivity for different metal ions and drastic changes in surface wettability present a special interest [409, 410].

It should be noted bifunctional polymer brushes orthogonally derivatized with oxotitanium and nitrilotriacetate-Fe(III) groups for enriching both mono- and multi-phosphorylated peptides for mass spectrometry analysis (Fig. 2.18) [411].

Topologically different materials, for example, brush macromolecules with block-copolymers of grafted side chains and «standard block-copolymers», in which one or more segments along a polymer chain are brush copolymers of different compositions, can be related to brush copolymers. The first type of grafted polymers is formed when macromolecular brushes are used as macroinitiators for polymerization of the second monomer [412].
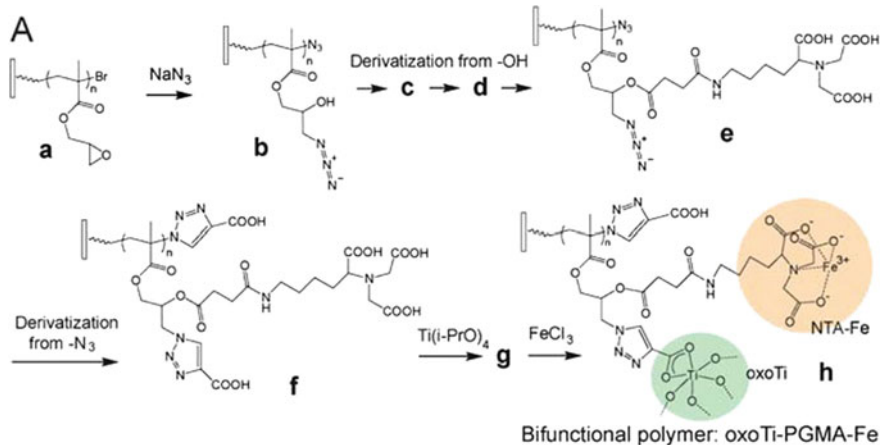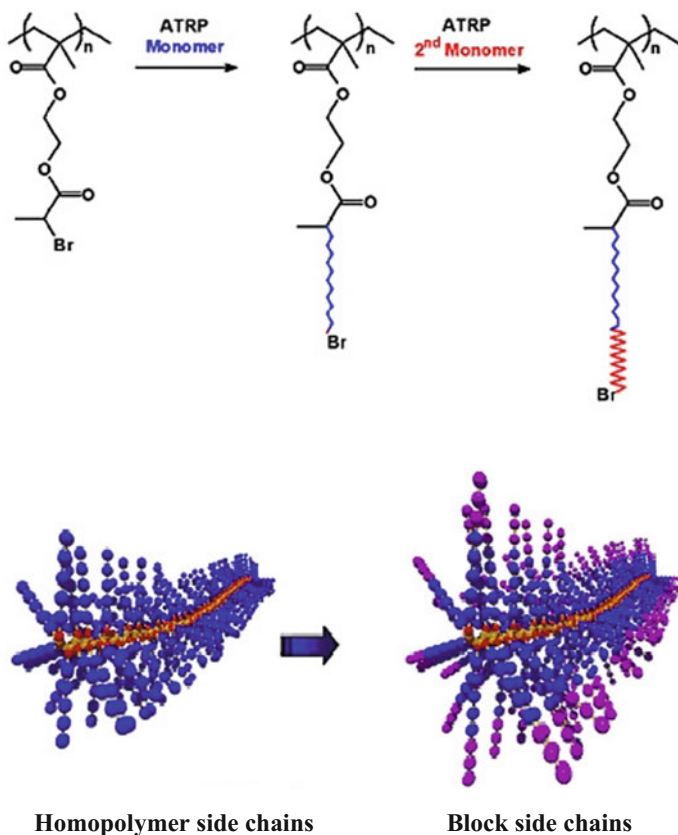

Fig. 2.18 Scheme of synthesis of bifunctional polymer brushes

Homopolymer side chains   **Block side chains**

The resulting nanostructured macromolecules can form soft/hard core/shell systems, macromolecular channels, stable worm-like micelles or inverse micelles, and other complicated architectures. It is important that these materials served as templates for production of gold nanowires [413].

Interesting approach to synthesis of a material, which can also be related to brush block copolymers, is formation of a precursor of macroinitiator with the following elongation of a chain by another monomer. This brings to «standard» for block-copolymers architecture along a brush matrix. Another block can be used for formation of a segment with separated phases for physical linking of brush-copolymer macromolecules, for example, shown in the following schematic drawing (Fig. 2.19).

To study self-assembly in large domain ordered nanostructures [414], PS-*b*-polylactide brush copolymers are synthesized by combination of three controlled methods of polymerization. A block-copolymer matrix for double grafted polymerization was prepared for RAFT polymerization of solketal MMA followed by polymerization of 2-(bromoisobutyryl) ethyl methacrylate. Branches of polylactide
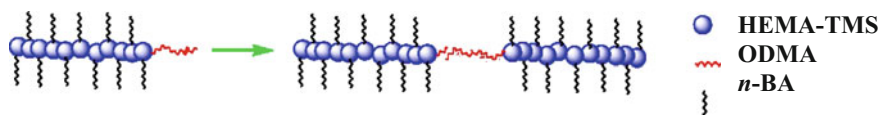
Fig. 2.19 Schematic image of brush copolymer with linear architecture of block-copolymer along matrix, where *n*-BA is *n*-butyl acrylate, ODMA is octadecyl methacrylate, HEMA-TMS is 2-(trimethylsilyloxy) ethyl methacrylate

were «grafted-from» from the first block after removal of a ketal groups, and PS branches were grafted by ATRP from the second block. A similar structure was obtained by consequent copolymerization of matrix precursor of a monomer-initiator and a macromonomer [415]. This results in formation of a block-copolymer brush synthesized by the «grafting-from» and «grafting-through» combination.

One more interesting topology of brush, which is important for PMC problems, is shown by synthesis of materials called hetero-grafted copolymer brushes. For example, brush copolymer with grafted PEO and poly(butyl acrylate) is obtained by the following scheme. First, precursor is prepared for CRP initiator by preliminary «grafting-through» polymerization of a macromonomer with low molecular weight co-monomer [416, 417]. Then, protecting groups on the precursor monomer units are transformed with formation of fragments capable of initiation of ATRP, and the final product is synthesized using «grafting-from» polymerization of a second monomer with initiated groups distributed along a brush copolymer chain.

Combination of copolymerization gradient and synthesis of macroinitiator provides access to brushes with controlled gradient of grafting density along the initial matrix [418, 419]. Gradient macroinitiators are prepared by spontaneous copolymerization of monomers with different reactivity or by controlled addition of one monomer to copolymerization of monomers with relatively similar copolymerization constants [420]. If macroinitiator with gradient of initiating centers along a matrix is used in grafting from copolymerization, the resulting molecule has higher density of side chains on one end of the matrix than on the other. Upon compression the rod-globule transition goes on the end where a brush is densely grafted, leaving a molecule with ball-like «head» and broadened «tail», so called «tadpole conformation» (Fig. 2.20) [419].

First, tadpole shape is formed of the block-grafted copolymers of bromide PS and methacryloyl-end poly(*tert*-butyl acrylates) and then hydrolysis of poly(*tert*-butyl acrylate) side chains to PAA side chains, which form pH-sensitive micelles in water [421].

Another combination of «grafting-from» and «grafting-through» methods can result in formation of such type of polymers, which are called «double grafted» brush copolymers. This topology appears when macromonomers are polymerized by «grafting-from» method of linear macroinitiator.
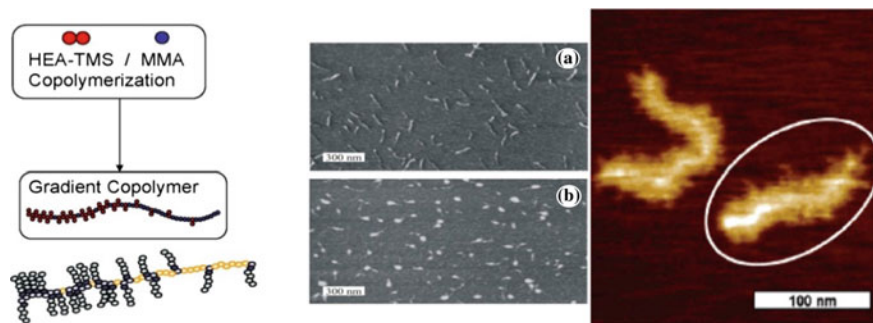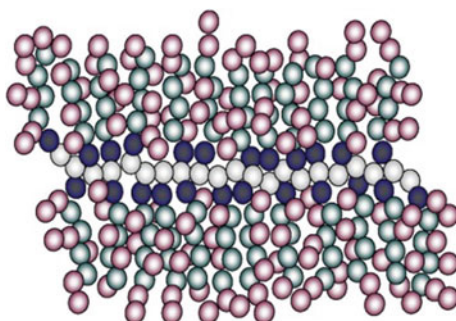
Fig. 2.20 Formation of a «tadpole» from block-grafted amphiphilic copolymers

In many cases, this can be considered as a brush copolymer in which each grafting is a brush copolymer [380].

Binary polymer brushes containing homopolymer and di-block copolymer brushes, which is the attractive class of ecologically sensitive nanostructured materials, should also be noted [422].

It is important that grafted polymerization is a convenient method for production of «tailored» polymers playing important role in PMC chemistry. For these purposes, for example, PEI was grafted to «tailored» polyurethane using the second 4,4′-diphenylmethane diisocyanate linked to carbamate half of polyurethane [423].

As is seen from this brief review, grafting polymerization methods are continuously improved, which advances fine control not over a polymer structure, but also over its chelating junction. At the same time, in many cases in these processes no proper attention is paid to the problems of formation of homopolymers and methods of their removal from products.
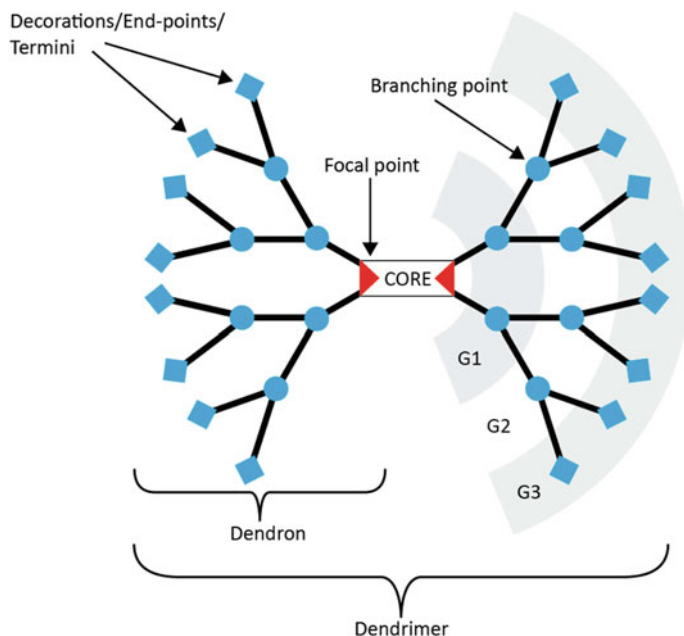
Fig. 2.21 Anatomy of a dendrimer. This example is the AB_2 type, where each branch is made from a monomer A which is divided into two monomers B

2.3   Dendrimers as Polymer Chelating Ligands

Dendrimers (originated from Greek «dendron», tree) relate to the class of polymer compounds, which have numerous branches [424–444]. Other proposed synonyms to these compounds were arbolors and cascade molecules; however, they occurred less commonly used. Dendrimers are multiply branched approximately spherical big molecules and have distinct chemical structures (Fig. 2.21) [445].

2.3.1   General Characteristics of Dendrimers

Considering chemistry of polymers, dendrimers are almost ideal monodisperse macromolecules with regular, highly branched 3D structure; they are even called polymers of the 21st century [446]. They consist of three architectural components, such as core, branches and end groups, and they are built from an initial atom, nitrogen, to which carbon and other elements are linked via repeated series of chemical reactions, forming spherical branched structure. A number of branches increase during their formation at each elementary act of monomer addition. As a result, while molecular weight of the dendrimers increases, shape and hardness of

molecules change, which is, as a rule, accompanied by change in physico-chemical properties of the dendrimers, such as intrinsic viscosity, solubility, density, etc. Reactions used till now in synthesis of polymers and dendrimer-like polymers are not, as a rule, chain reactions. Usually, these are well known reactions of condensation, substitution, and linking by multiple bonds.

As a result of the first stage of polymerization in the ends of branches free groups are formed, each of which can react with two additional monomers, thus forming first generation (G1) dendrimer. There can be a finite number of these consequent stages, since at some moment a close-packed structure of monomers is formed, which prevents further polymerization. For example, a layer of G9 dendrimer already contains 3069 monomers, and diameter of this molecule is ~ 10 nm. In other words, dendrimers are highly branched nanostructures with controlled composition and architecture, having functional groups incorporated in a regular «branched upon branched» structure. Such high density of functional groups confined in the limits of nanometer containers makes dendrimers especially attractive as chelating agents of high capacity for metal ions [447, 448].

The existing synthetic approaches provide production of regular dendrimers, whose macromolecules have strictly definite molecular weight. Besides, it should be noted that many properties of dendrimers, such as glass-transition temperature (T_g), depend strongly on chemical origin of terminal groups placed on the surface of the spherical molecules. All aforementioned facts attract interest of researchers-chemists to synthesis of dendritic macromolecules. Thus, by now dendrimers have been synthesized basing on polyethers and polyesters, polyamides, polyphenylenes, polysiloxanes, polycarbosilanes, etc.

Utmost sizes, configuration and molecular-weight characteristics of regular dendrimers can be predicted theoretically. Since growth of macromolecule branches in all directions is equally probable, they become almost spherical already after 3–4 generations. Then, hence molecular weight of all macromolecules at each stage of controlled synthesis increases by the same value, the formed polymers are almost monodispersing, i.e. they contain macromolecules of equal molecular weight and size. Thus, for PAMAM dendrimer the ratio of average-weight and average-number molecular weights is very close to unit (PDI = 1.001–1.005), which is a sign of monodisperse polymer.

The key parameters, which determine structure and size of dendrimer macro-molecules, are: N_c, functionality of a core (index of core branching), i.e. a number of dendrons grown from the core of a macromolecule: N_b, index of unit branching, a number of branches formed by each repeated unit; G, generation number. Ideal dendritic structures can be described by exact mathematic expressions using terminology of polymer chemistry. Thus, the number of terminal groups z is increased in accordance with the

$$z = N_c N_b{}^G,$$

which means that in the simplest case of trifunctional core and difunctional branching center ($N_c = 3$, $N_b = 2$) number of terminal groups increases from 2 to 48 in the core in the fourth generation.

The number of repeating units N_r greatly increases with the generation number even for the simplest case:

$$N_r = N_c \frac{N_b^{G+1} - 1}{N_b - 1} \tag{2.4}$$

and the molecular weight of M, respectively, increases exponentially with each generation:

$$M = M_c + N_c \left(N_r \frac{N_b^{G+1} - 1}{N_b - 1} + M_t N_b^{G+1} \right) \tag{2.5}$$

where M_c is weight of the core and M_t is weight of terminal units.

Using the aforementioned parameters, the following can be calculated theoretically: DP or a number of repeated units, a number of terminal groups, molecular weights of the core, repeated units, and end groups. In Table 2.4 calculated and experimentally found characteristics of macromolecules of a PAMAM dendrimer are compared. It is seen that the calculated and experimentally measured values of molecular weight for the samples with predetermined number of generations almost coincide.

Experimental data on sizes of macromolecules are in the range of the calculated data determined by two extreme conformations respecting to extended and corrugated dendrons.

The best results were obtained by now for PAMAM dendrimer, whose efficiency of branching reaches 95%. The cascade polymers produced by one-stage method display efficiency of branching of terminal groups no better than 70%. Probably, their most noticeable difference from polymers produced by controlled synthesis is higher polydispersity.

Table 2.4 Calculated and experimentally found values of molecular weight and diameter of macromolecules of PAMAM dendrimer

G	DP	$M_{theor.}$	M_{ex}	$d_{theor.}$	$d_{ex.}$
0	3	360		9.6–19.2	11
1	9	1044		12.8–28.8	16
2	21	2411		17.6–41.6	24
3	45	5154	5200	24.1–51.2	32
4	93	10,633	10,700	30.6–65.6	40
5	189	21,563	21,600	38.5–81.6	56
6	381	43,451	44,000	47.5–91.2	66
7	765	87,341	88,000	61.8–104.0	75
8	1533	174,779	174,000	78.0–117	90
9	3069	349,883		98.0–130.0	105
10	6141	700,091		123.0–143.0	124

2.3.2   The Main Types of Chelating Dendrimers

Among most widespread types of dendrimers with the highest value for CPL synthesis, we should mention the following.

1. PAMAM dendrimers are synthesized by divergent method taking ammonia or en as basic reagents. They are built using repeated consequent reactions consisting of (a) double Michael addition of methacrylate to primary amino group with the following (b) amidation of the forming carbomethoxy intermediate with great excess of en (Fig. 2.22).
2. Polypropylene imine (PPI) dendrimers are synthesized by the divergent method beginning from 1,4-diaminobutane (DAB). As an alternative name of PPI dendrimer the name POPAM dendrimers is sometimes used to describe of this class of dendrimers. POPAM denotes Poly(Propylene AMine), much like the acronym PPI. They grow by multiple repeated consequent reactions consisting (a) double Michael addition of AN to the primary amino group with the following (b) hydrogenation under pressure in presence of Raney-cobalt (Scheme 2.21).
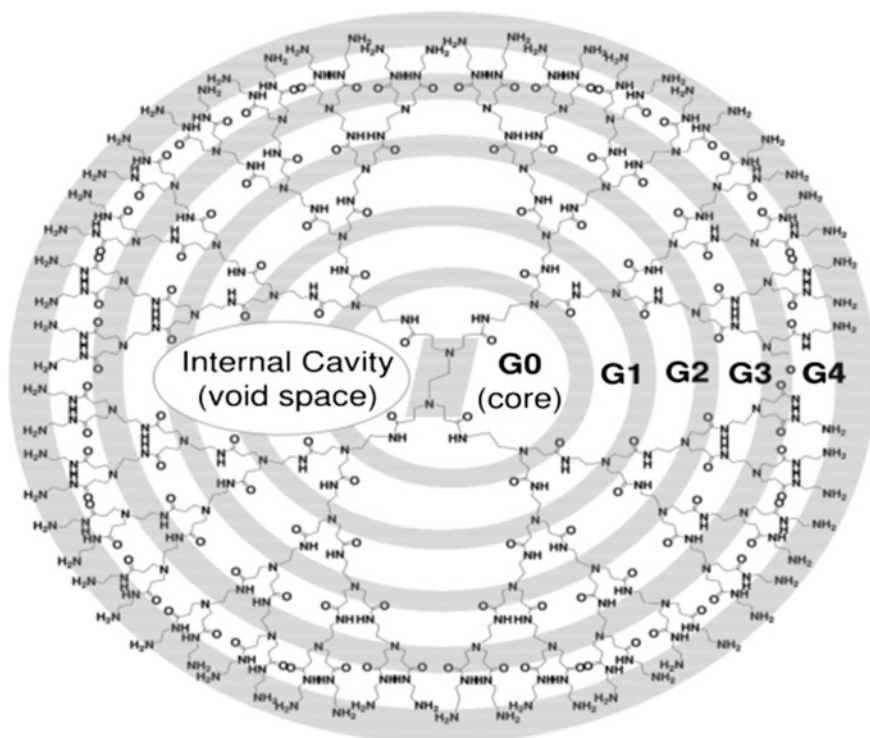
Fig. 2.22 Schematic representation of the G4 dendrimer with 64 amino groups at the periphery. This dendrimer begins from the en core; branches or arms have been attached by Michael addition to methacrylate followed by complete aminolysis of the methyl ester obtained using en [449]
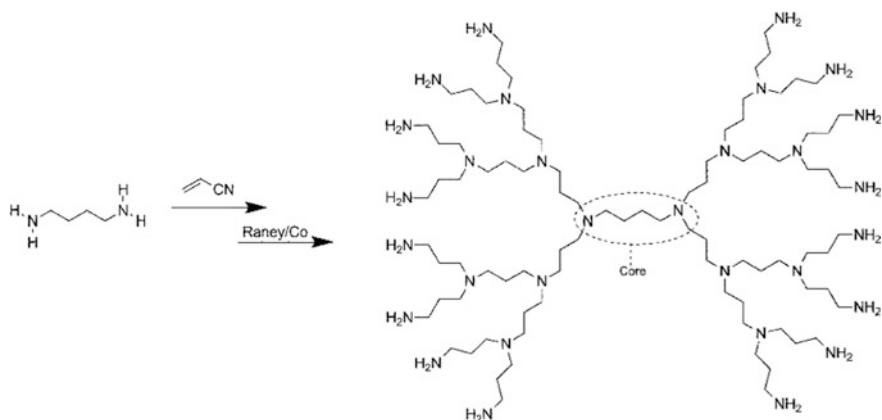
Scheme 2.21   PPI dendrimer synthesis scheme
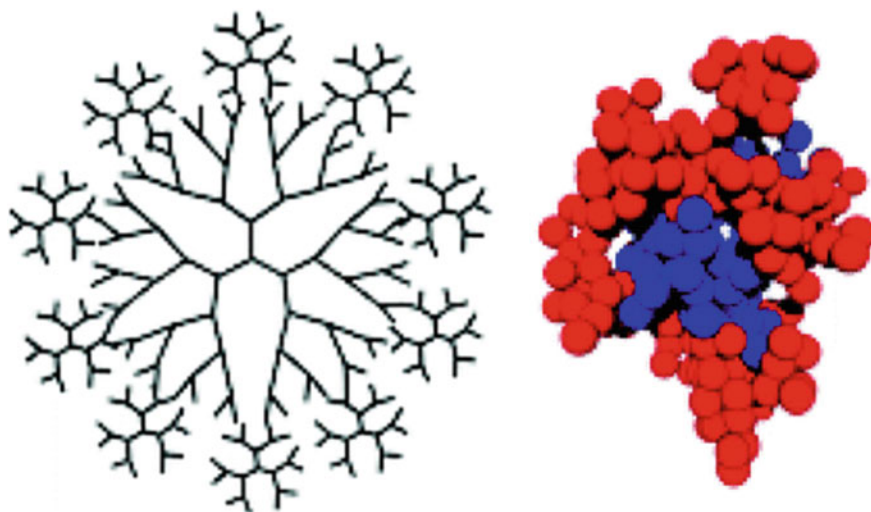
Fig. 2.23   Structure of tecto-dendrimers

3. Tecto-dendrimers. They consist of a dendrimer core surrounded by dendrimers
   of several generations (for each type of construction) designed for performing
   functions required for smart-therapeutic nanodevices [450–452]. Different com-
   pounds perform different functions, beginning from recognition of the diseased
   cells, diagnostics of illness, delivery of drugs, and ending by therapy results. It is
   important that dendrimer core of tecto-dendrimers may or may not contain a
   therapeutic agent surrounded by dendrimers (Fig. 2.23).

4. In multilingual dendrimers the surface contains several copies of certain functional groups [453].
5. Chiral dendrimers, in which chirality is based on design of constitutionally different but chemically similar branches of chiral cores (Fig. 2.24) [454–456]. As a practical matter, chiral dendrimers are especially interesting, because a combination of well-defined structure with chiral groups brings to a possibility of control over sizes and shapes of interior caverns in dendrimers. They provide development of different application fields, related to chirality, for example, molecular recognition, sensors, catalysts, enantioselective separation, etc. It is important that controlled 3D structure in these polymers resembles natural polymer systems and, consequently, offers new directions for biological and medical applications. Chiral dendritic molecules can be classified by four categories [457]: (a) dendrimer with chiral core; (b) dendrimer with chiral end units; (c) dendrimer with chiral building blocks, and (d) dendrimer with different branches linked to a nonplanar core.
6. Hybrid dendrimers include block or grafted polymers of dendritic and linear polymers (Fig. 2.25) [458]. Hybrid linear-dendritic (a copolymer formed with one or more dendritic fragments associated with one or more linear analogues) and dendronized polymer (a special type of a linear-dendritic hybrid, wherein the linear polymer contains dendrons attached to each repeating unit) are distinguished. To obtain this class of compounds two main approaches are used:
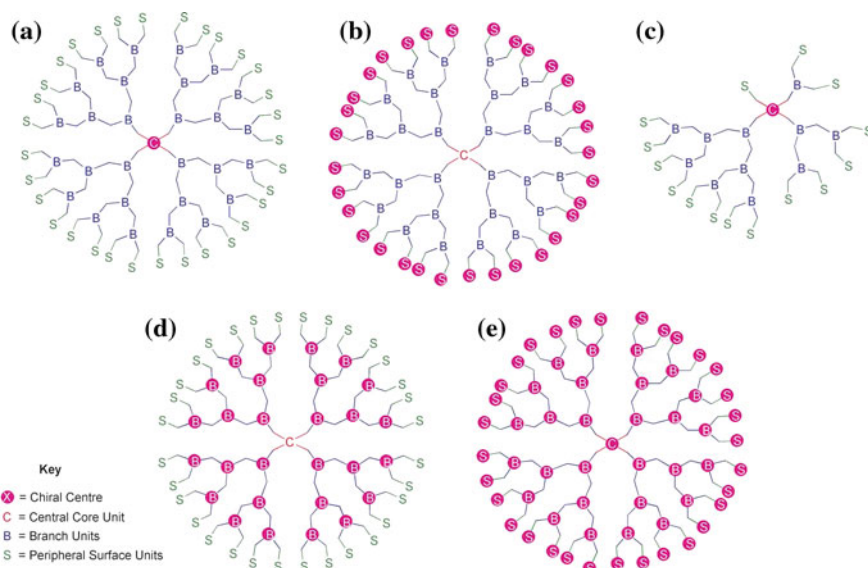

Fig. 2.24 A cartoon representation of the variety of possible formats for chiral dendrimers that feature: **a** a chiral central core, **b** chiral units at the peripheral surface, **c** achiral core coupled to constitutionally different branches, **d** chiral branching units and **e** chiral units at the core, branches and peripheral surface
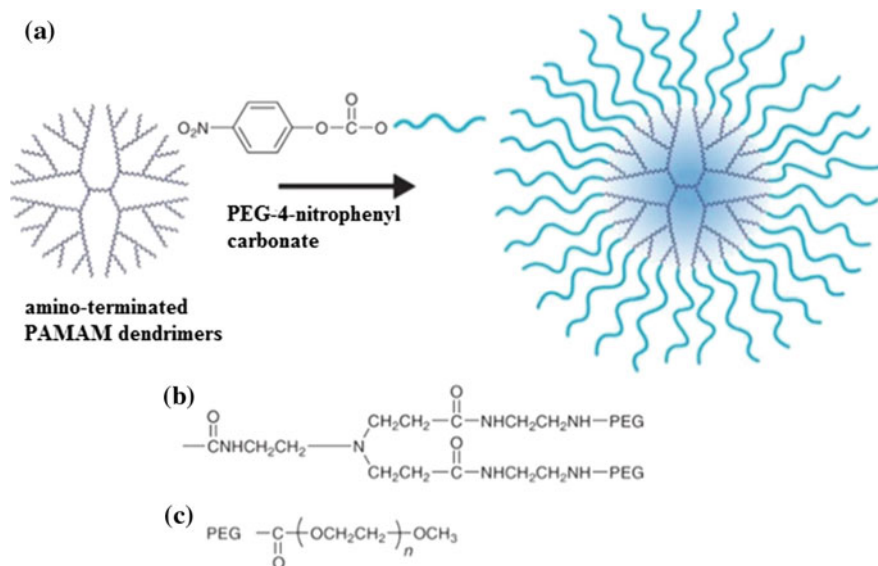
Fig. 2.25 Synthesis of PEG-modified PAMAM dendrimers (**a**). The chemical structures of the terminal units (**b**) and the PEG chain (**c**)
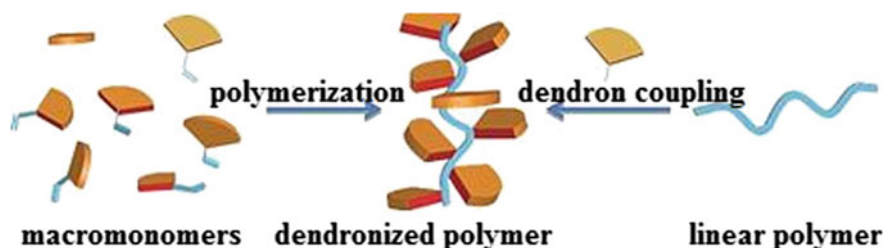

Fig. 2.26 Hybrids of dendritic and linear polymers

macromonomer and attach-to routes (Fig. 2.26). In the first case, a monomer is polymerized, which already carriers a dendrimer of a certain size, in the second case module synthesis is used according to traditional chemistry of dendrimers based on divergent or convergent methods, with linear polymers or macro-monomers used as building blocks [459].

For example, a series of photosensitive hybrid dendrimers G1–G3 is synthesized by the addition of amidoamines dendrons with end groups of *o*-nitrobenzyl alcohol to an alternating copolymer of St and maleic anhydride. It is found that the degrees of attachment of dendrons comprise 74, 42 and 26%, respectively, indicating that the number of attached dendrons decreases from G1 to G3 because of steric hindrance at the higher generation dendrons with large branches [460]. Hybrid

dendrimers with PAMAM units and surface groups of *N*-hexylamide type or poly (*N*-methylglycine) blocks are obtained by the ring-opening copolymerization of sarcosine-*N*-carboxyanhydride with the dendrimer. Aqueous solutions of copolymers with poly(2-methyl-2-oxazoline) and PAMAM blocks are synthesized by reaction of polyoxazoline with ω-terminal functional groups [461]. Such dendrimers have 3D hybrid architecture of nano-organized systems containing cavities inside and outside of the dendrimer, and interconnected, which gives them a controlled permeability. Self-assembled block copolymers such as «head to tail» are produced from PAMAM as head and blocks of poly(L-lysine) (PLL) as tail. At that, PL tail blocks undergo «helix-coil» transition as a result of changing the solvent from water to methanol, resulting in a 3D structure similar to the protein molecules [462]. Dendronized alternating copolymers containing crown ether units are synthesized by copolymerization of St having side chains of the polyether dendron (two generations) and maleimide having side units of dibenzo-24-crown-8 [463]. Hybrid dendrimers from PPI (core) and PAMAM (shell) are also described [464].

Design of biocompatible environment-sensitive dendrimers is carried out based on PEG and PAMAM G4 dendrimers with *N-tert*-butoxycarbonyl-*S*-acetamido-methylcysteine moiety [465]. PAMAM G4 dendrimers, whose end groups modified by L-phenylalanine or γ-benzyl-L-glutamate and PEO chains are attached to the amino acids units, are obtained for use as nanocapsules [466].

A synthetic route to thermosensitive molecules using alkylamide side groups is proposed. It was shown that the thus obtained PAMAM dendrimers have a lower critical solution temperature (LCST), and the accumulation of *N*-alkylamide groups on dendrimers periphery provides thermosensitivity initially thermo-insensitive dendrimers. It is noted the attempt to extend the application of the technique to lipids based on PAMAM dendrimers with two octadecyl chains as a head group and a hydrophobic tail [467].

An interesting class of hybrid dendritic molecules is dendrigraft polymers [468]. Size of dendrigraft polymers is usually by 1–2 orders of magnitude more than of their dendritic analogues and is from about 10 nm to several hundred nanometers. Another distinctive feature of these polymers is synthesis based on the reaction with grafting polymer side chains serving as building blocks. To obtain these compounds three different synthetic methodologies were used: (1) divergent «grafting-to» methods based on consequent reactions of coupling polymer chains with functionalized polymer-substrate; (2) divergent «grafting-from» methods using cyclopolymerization initiated from functional centers placed on a polymer-substrate; and (3) convergent «grafting-through» methods including coupling preliminary formed polymer chains in one-pot synthesis.

It should be also noted different structural classes of dendritic copolymers such as hyperbranched copolymers, linear-dendritic block copolymers, dendrimer-like star-branched block copolymer, multiarm dendritic initiators, dendritic focal point chain transfer agents etc. [469].

7. Amphiphilic (Janus) dendrimers consist of two insulated parts of a chain end, half of which are donors, and another half acceptors (Fig. 2.27). PAMAM dendrimers also

Fig. 2.27 Diagram of the structure of amphiphilic dendrimers
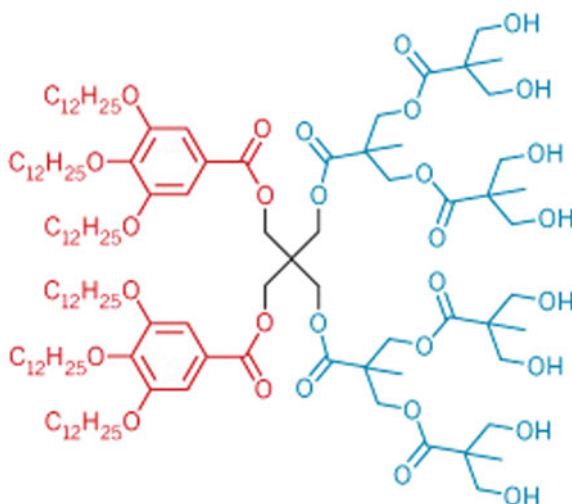
relate to amphiphilic dendrimers consisting of a hydrophilic core of a dendrimer and hydrophobic shells of stearyl acrylate type [470] or aromatic dansyl (1-dimethyl amino-1-naphthalene-5-sulfonyl) and 1-(naphthalenyl)-2-phenyldiazene [471]. Or, on the contrary, amphiphilic dendrimers consist of hydrophobic PEO core and hydrophilic carboxyl groups [472], and the latter can be used as polymer reagents in green technology of chemoremediation in liquid homogeneous phases [473].

8. Micellar dendrimer consists of unimolecular micells of water-soluble hyper-branched polyphenylenes [474].

9. Highly branched oligomers or polymers consisting of dendritic structures containing mesogen group, which can display meso-phase behavior, relate to liquid crystal dendrimers. They consist of mesogen monomers forming liquid crystal dendrimers in lamellar, columnar, and nematic phases (Fig. 2.28) [475].

It is noted co-dendrimers of Janus type G1 or G2, which combine the promesogenic bent-core and a rod-shaped molecular segments synthesized by universal CuAAC click reaction (Fig. 2.29) [476]. Depending on the ratio between the amount of rod-shaped and bent-core blocks these compounds form meso-phases in the range from nematic to complex polar smectic meso-phase, wherein the two kinds of mesogenic fragments are separated on a nanometer scale. If the ratio bent/rod 1:1, the materials form ferroelectric meso-phases and macroscopic polarization is stable in the absence of an applied electric field.

10. Frechet-type dendrimers designed Frechet based on poly(benzyl ether) hyper-branched skeleton (Scheme 2.22) [477–480]. Such dendrimers typically have surface carboxyl groups acting as a convenient anchor point for further surface functionalization or surface polar groups increasing the solubility of the hydrophobic type dendrimer in polar solvents or aqueous media.
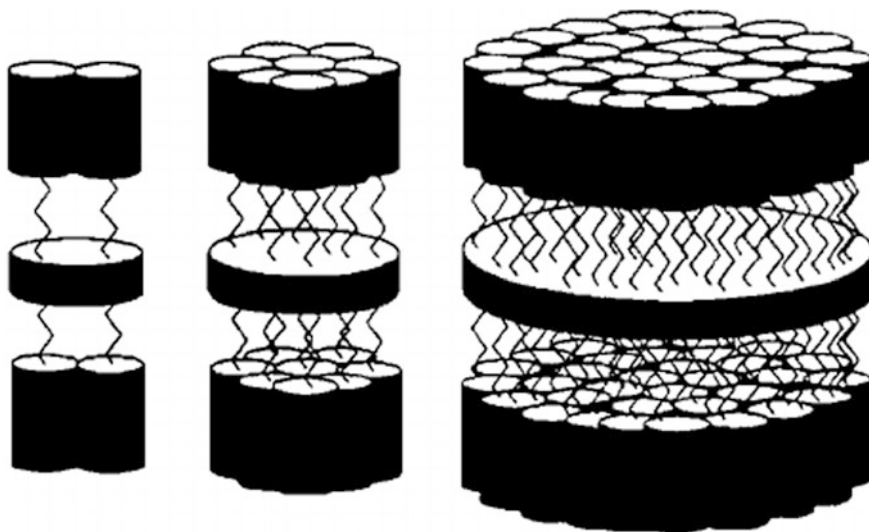
Fig. 2.28 Liquid crystal dendrimers

Fig. 2.29 Preparation of liquid crystal dendrimers via click-synthesis

11. Radially layered poly(amidoamine-organosilicon) (PAMAMOS) dendrimers are inverted unimolecular micelles, which consist of hydrophilic nucleophilic PAMAM interiors and hydrophobic organosilicon (OS) surface groups [481, 482]. Generalized 2D projection of the structure of these nano-sized globular macromolecules is shown in Fig. 2.30. This unique dendrimer family was discovered in 1990, and contains many compositional and functional variants, including dendrimers with terminal alkoxysilyl groups (X = Si–OR).

12. In the polysiloxane dendrimers, the key point in the synthesis of each generation is the alternation of two reactions: the formation of peripheral groups – SiOEt (actually chain growth) followed by substitution at –SiCl (Scheme 2.23) [483–485].
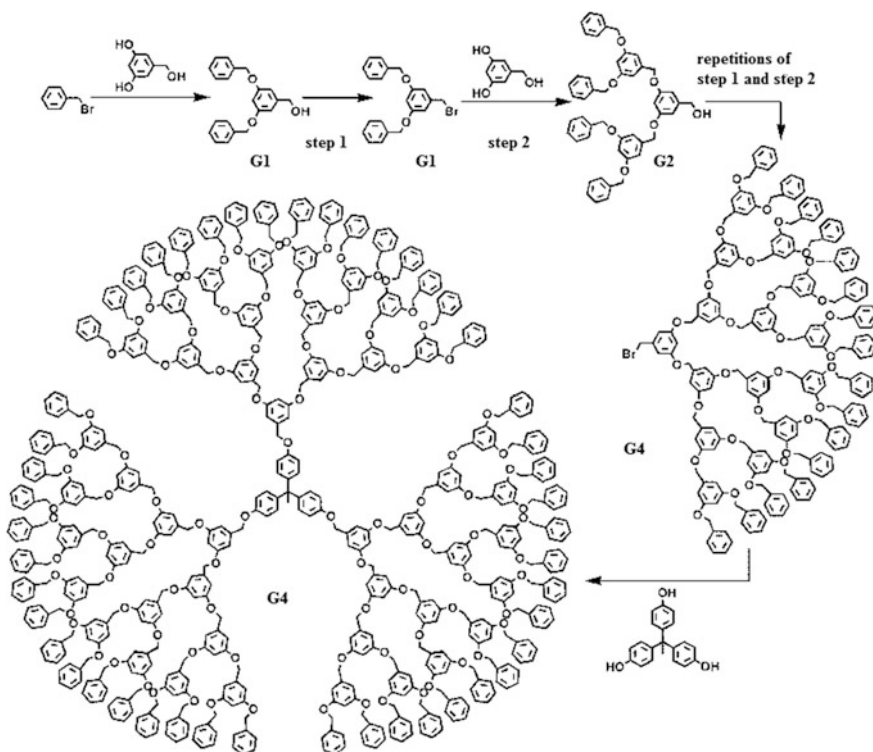
Scheme 2.22 Scheme of synthesis of Frechet-type dendrimers

13. Phosphorus-containing dendrimers represent a broad class of dendrimers containing phosphorus donor atoms in different parts of the dendritic architecture [486–488]. An interesting example is hexachlorocyclotriphosphazene that can be used as branch points for the rapid synthesis of dendrimers with high density of functionality as well as for the synthesis of dendrimers having exactly one function different from all others. These dendrimers are used as the materials providing reusable catalysts, chemical sensors or substrates for cell cultures (Fig. 2.31) [489]. Furthermore, these dendrimers were used for in vivo imaging and in order to clarify the biological mechanisms, particularly for anti-inflammatory dendrimers.

The binding of carbosilane dendrons with phosphine in the focal point with phosphorus-hydrazone dendrons having thiophosphoryl azide in the focal point was successfully carried using the click reactions (Scheme 2.24) [490]. Appropriate
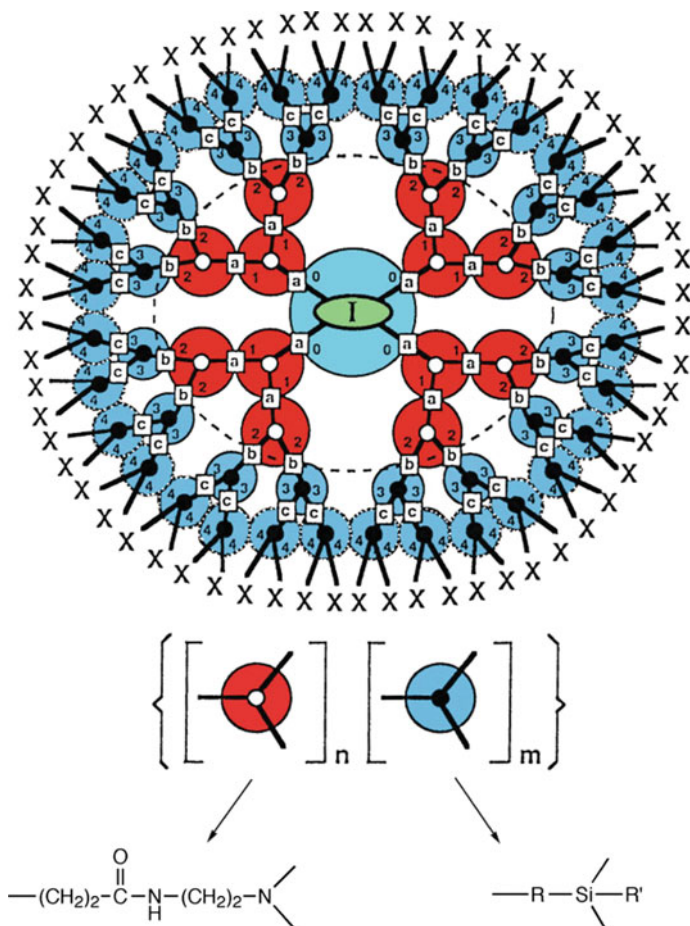
Fig. 2.30 A generalized representation of the structure of PAMAMOS dendrimer. Red: interiors cell s of PAMAM branches; blue: external cells of OS branches. I: Core atom or group of atoms; X: inert or reactive end groups; numbers 1, 2, 3, 4, … denote generation; letters: a, b and c represent PAMAM-PAMAM, PAMAM-OS and OS-OS chemical bonds, respectively

Janus dendrimers have characteristics of both components, thus they are fatty as a carbosilane dendrons and can be easily functionalized with a phosphorus-hydrazone dendrons.

It is noted chiral diphosphine-functionalized Janus dendrimers containing up to sixteen 2,2′-bis(diarylphosphino)-1,1′-binaphthyl (BINAP) units, readily synthesized via the liquid phase organic synthesis with G3 Frechet-type poly(aryl ether) dendron as the soluble substrate [491].
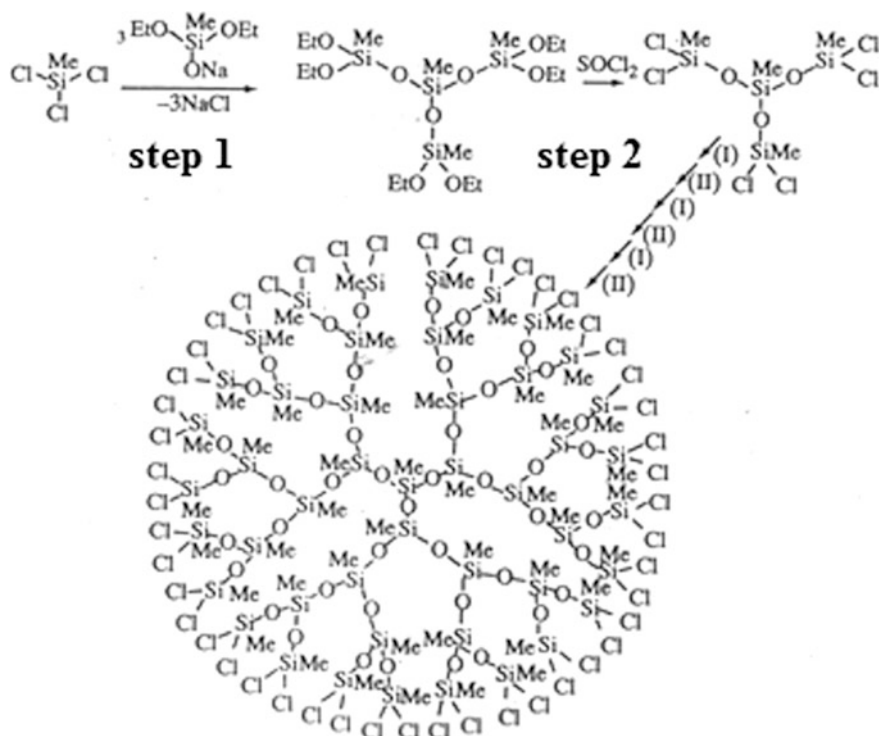
Scheme 2.23 Synthesis scheme of dendrimer based on polymethylsilsesquioxane
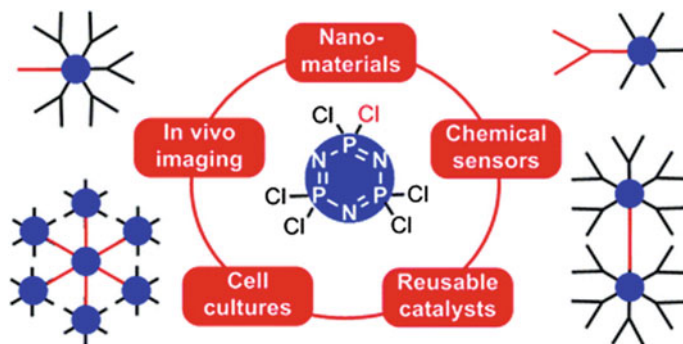
Fig. 2.31 The main directions of use of phosphorus-containing dendrimers based on hexachloro-cyclotriphosphazene
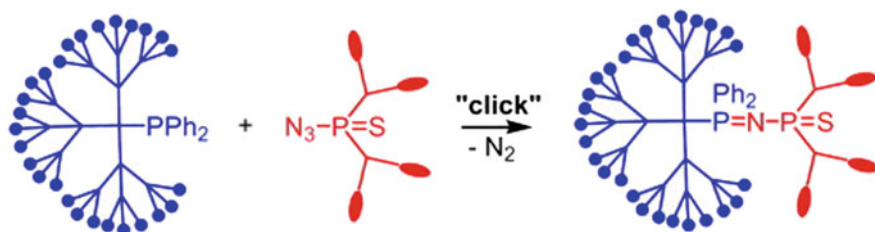
Scheme 2.24 The scheme of synthesis of phosphorus-containing Janus dendrimers via click-synthesis

2.3.3 Divergent and Convergent Synthesis

Dendrimers are obtained by controlled multi-staged synthesis, in which the main are two strategies of synthesis according to divergent and convergent schemes. The already becoming classical scheme of dendrimer synthesis (Fig. 2.32) beginning from an initial branching center following by repeated reactions of a layer growth and removal of protection is called divergent [492]. A distinctive feature of this scheme is fast increase in a number of reaction centers on the surface of a dendritic molecule associated with increase in a generation number. This, in turn, brings to difficulties of purification of the final compounds from the products of incomplete substitution of surface functional groups, if such are present in the system. The purification problem is caused by very little difference between molecular weights of dendrimers with completely reacted surface groups and products of incomplete substitution.

This difference does not exceed several percent. To overcome this drawback, another approach was proposed called convergent method [477]. If in the case of
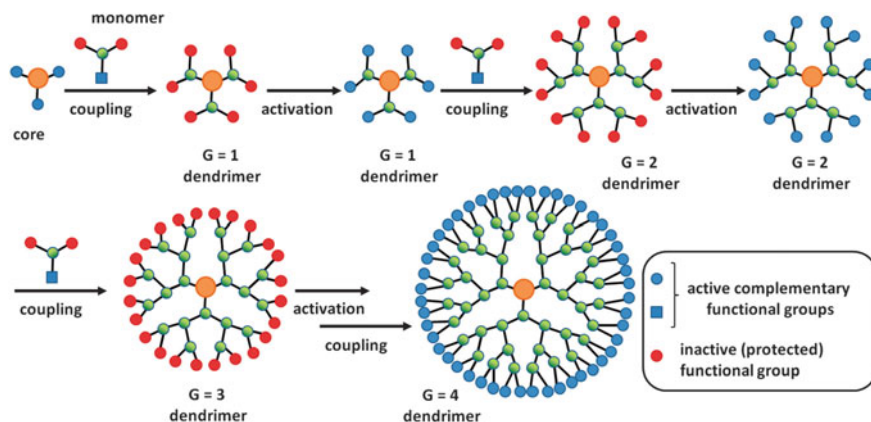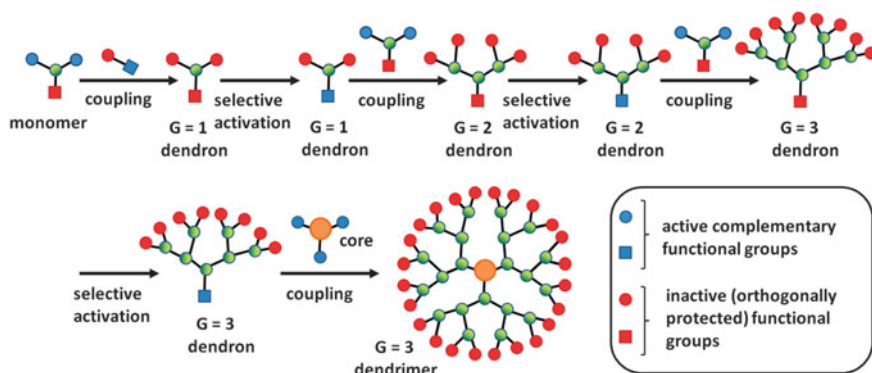

Fig. 2.32 Divergent growth method [492]

Fig. 2.33 Convergent growth method [492]

divergent synthesis, a dendritic molecule is growing from the center to periphery, in this case, on the contrary, a dendrimer is «collected» beginning from the surface groups. Taking to the notation system introduced before, the convergent growth of a monodendron can be represented by a scheme shown in Fig. 2.33.

An advantage of the convergent approach is a small number of reacting groups at each stage, which, in turn, brings to minimal number of intermediate compounds (products of incomplete substitution). Besides, a difference in molecular weight of initial, intermediate, and final products is so big (1.5–2 times) that it allows easily isolate a target compound in pure form. However, a significant drawback of this method is appearance of steric hindrances emerging at the stage of linking a monodendron to a branching center. There are such a small number of reactive groups (actually one for monodendron—a focal point), which plays a negative role. In the reaction system there is quite low concentration of reacting groups, whose activity is lowered even more due to a great number of «inert» (surface and other) groups, and reaction is impeded.

Most currently known chelating dendrimers are obtained by the two traditional methods and the number of these CPLs sufficiently large. Among the most interesting examples are variety dendrimers with tpy chelating moieties [10, 14]. A series of dendrimer polyallyl- and polyferrocenyl-containing chelating bpy ligands was obtained by the coupling reaction of 4,4′-bis(bromomethyl)-bpy with AB_3 and AB_9-dendrons [493]. Synthesis of G1 and G2 dendrimers with dibenzo-24-crown-8 groups serving as branching blocks is described [494]. A dendrimer with pseudocrown ether, which can chelate Ag(I) and Hg(II) ions, was obtained in the similar way [495].

It is doubtless that the dendrimers themselves are chelating ligands, since for them a considerable probability is typical of multiple-point metal ion coupling by monofunctional ligands due to their high density on the surface [496]. Metal chelates with dendrimers based on PEO and polypropylene oxide can be an example [472]. A consequence from this, in particular, is ability of crown ether groups to migrate over surface (Fig. 2.34), which was called «spacewalk» [497, 498].
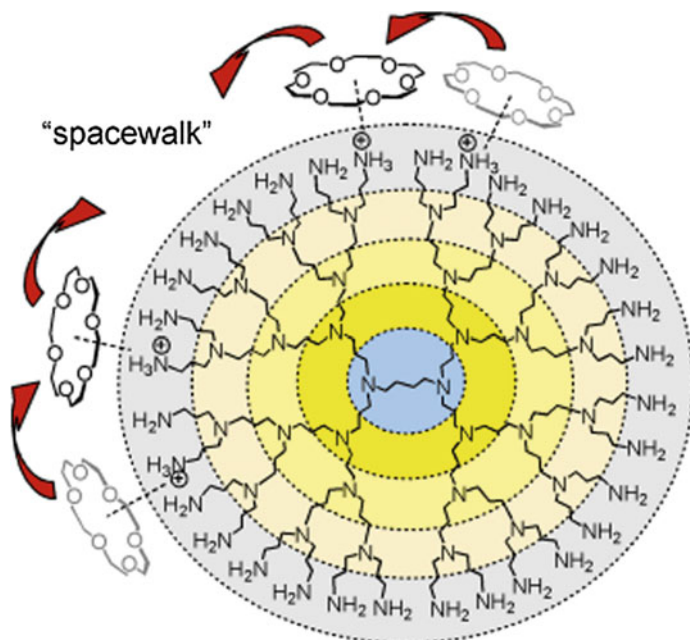
Fig. 2.34 Complex of crown ethers with G4 PAMAM dendrimer

It should be noted numerous examples of dendrimers with porphyrin and phthalocyanine fragments [499]. So, different Pp [500] including 5,10,15,20-tetrakis(4-hydroxyphenyl)-Pp and 5,10,15,20-tetrakis(3,5-dihydroxyphenyl)-Pp can be used as a core of dendrimer [501]. Pp-containing dendritic polymers up to G4 are obtained by Suzuki polycondensation of dendritic dibromide macromonomers and pinacolyl ethers of Pp-diboron acids [502]. Synthesis of the G2 poly(benzyl ether) dendrimers having N_3O Pp in a core (21-oxo-Pp core) is described [503]. Then phenyl-containing compounds (dendrons), from which branching of generations has already begun, can be linked to the Pp cores. At that superstable structure is obtained, which makes it possible to remove a Pp core from a micelle, as a result a cavity is formed, which is appropriate for catalytic and other reactions. Removal of Pp is executed by splitting of ether bonds, and the formed cavity is surrounded from inside by eight carboxyl groups. Something similar happens in depth of protein enzyme globules.

Possibilities of synthesis regarding architecture and chemical composition of produced polymers are broadened considerably at combination of the divergent and convergent schemes used. Taking into account the aforementioned advantages and disadvantages of both approaches, it should be noted that recently a tendency is observed of using a combined approach, which includes linking of monodendrons produced by the convergent method not to a pointed branching center, but to a dendrimer of G2–G3 synthesized beforehand by the divergent scheme.

2.3.4   Alternative Methods of Synthesis

For rapid studies of dendrimers, it is highly desirable to develop more efficient synthetic processes to avoid more elaborative and time-consuming stages of activation or protection of monomers in the reaction of condensation and purification using chromatographic separation. To these methods, which make it possible to reduce a number of synthetic stages and obtain a desired dendrimer with high yield, belong: a double-stage convergent growth approach, a hypermonomer approach, and double-exponential dendrimer growth, and orthogonal coupling strategies (Fig. 2.35) [504].

For example, in the double-exponential growth approach [505] first two functional groups of AB_2 monomer are disguised so that it would be possible to selectively take off protection. Then two growing monomers, one of which with protected functional group B, are obtained by removal of protection from the functional group A (divergent type of a monomer), and another one with protected functional group A is obtained by removal of protection from the functional group B (convergent type of a monomer) in individual reactions. The monomer of divergent type is condensed with the monomer of convergent type to produce protected dendritic molecules. Dendrimers of higher generations are synthesized by repetition of selective processes of de-protection and coupling. Therefore, DP depends on a number of generations increasing according to double exponential function from the initial generation (n), as $DP = 2^{2n} - 1$. Double exponential growth was used, in particular, to produce dendritic aliphatic G4 polyethers, beginning from 2,2-bis(hydroxymethyl)propionic acid in six stages with two purifications [506]. If macromolecules having the same generations were prepared by the ordinary divergent scheme, a number of purifications, corresponding to a
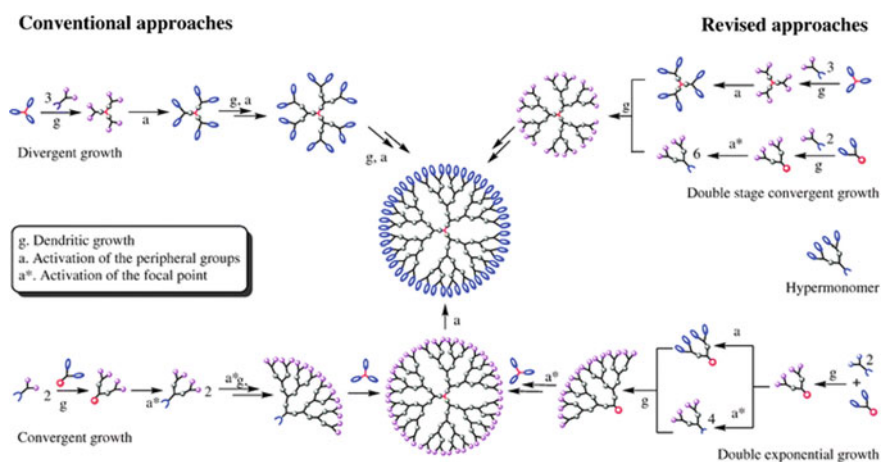

Fig. 2.35 Comparison of conventional and revised approaches

number of generations would be needed. Therefore, this method allows reducing a number of growth stages and simplification of purification of a final dendrimer.

The G6 dendrimer consisting of poly(phenylacetylene) linked with polyether was synthesized in three stages and two chromatographic separations based on orthogonal coupling strategy using Mitsunobu etherification or Sonogashira reaction [507]. Thus also coupling of efficient orthogonal ABC Passerini multicomponent reaction and ABB thiol-yne multicomponent reaction two kinds of dendrimers were synthesized efficiently: dendrimers with two generations in three steps and dendrimers with two generations containing one kind of internal functional group and two kinds of surface functional groups in five steps [508].

The hypercore or the branched monomer approach [509] specifies preliminary assembly of oligomer precursors, which can be linked with organic fragment. Linking of oligomer precursors goes in radial, branch-to-branch direction. A core interacts with two or more moles of a reagent containing, at least, two protected branching centers with the following removal of protective groups. The following release of reactive centers brings to the G1 dendrimers.

Contrary to these methods, the following two methods can exclude time-consuming processes of protection removal or activation. In the two monomer approach two different monomers are used, at that, one of the different functional groups of AB_2 monomer is prescribed for selective interaction with one of two different functional groups of CD_2 monomer, i.e. functional groups A and C react with reactive D and B centers, respectively. A typical example is synthesis of poly(ether-urethane) dendrimer from 3,5-diisocyanatobenzyl chloride and 3,5-dihydroxybenzyl alcohol [510]. Generations can grow in one reactor without intermediate purification stages.

One more approach, which helps to avoid the time-consuming purification process is using PS-PEG resin for synthesis of PAMAM dendrimers. It is a simple and efficient method for preparation of dendrimers up to the G3 [511].

One-pot synthesis of poly(amino carbonate) dendrimer from 2,6-dimethyl-4-heptanol and tert-butyl alcohol is performed using high-selective carbonyldiimidazole (CDI) reaction [512].

Introduction of energy using the microwave radiation is a widely used method in synthetic chemistry and is mainly in the organic chemistry [513–515]. Microwave synthesis is a highly effective technique for performing high-speed synthesis and is based on the interaction of electromagnetic waves with the mobile electrical charges, which may be polar solvent molecules or ions in solution. In a solution polar molecules try to align themselves in an electromagnetic and alternating field and so that the molecules are constantly changing their orientations. Thus, by applying the appropriate frequency, the collision between the molecules is achieved, which leads to an increase in the kinetic energy, i.e. system temperature. Therefore, high speeds of heating and uniform heating over the entire sample are possible. Synthesis of dendrimers using microwave radiation at low temperature reduces the reaction time, significantly reducing the occurrence of defects in the dendrimer backbone. For example, using microwave radiation PAMAM G1 dendrimers are

synthesized by divergent method in high yields, high purity and in nearly perfect regioselectivity [516].

It is noted the use of microwave amidation method for the synthesis of PAMAM dendrimers with Jeffamine polymer core up to G4 [517]. This method reduces the aminolysis time and minimizes excessive use of reagents and solvents. Quick, easy and one-step microwave synthesis of water-soluble PAMAM dendrimers with the same polymer Jeffamine® T-403 core and the two monomeric, en and dien, cores were achieved with high (90–96%) yields in a short time (110–140 min, from 3.5 to 4 times faster than normal reactions) and under mild conditions using methanol as the solvent [518].

Microwave synthesis allows quick access to the lower generations (one to three) triazine dendrimers with high yields [519]. Using microwave convergent synthetic approach, two reactions of nucleophilic aromatic substitution are performed on cyanuric chloride within 10 min at 60 °C using primary amines (Fig. 2.36). It is important that the substitution with the diamine obtained monochlorotriazine requires 95 °C for 30 min and the purification are performed by an automated chromatography system so G3 dendrimer can be prepared from starting materials in less than one day.

Similarly, starting from commercially available and inexpensive materials, accelerated synthesis of triazine dendrimers of odd generations up to G9 with high yields was performed using microwave radiation (Fig. 2.37) [520].

Unique SAMs, consisting of dendritic viologen-shaped molecules with ω-mercaptodecyl groups (G = 0–3) at the top of the dendritic structure, which can encapsulate a certain amount of metal anionic complexes, determined by dendritic structure, are noteworthy [521]. Such lower generation dendritic molecule is successfully synthesized by microwave heating, thereby providing easy access to the G3 dendrimers without requiring processes of protection/deprotection during generations growth. SAM of dendritic molecules themselves is made by soaking of gold substrates in solutions of molecules in a mixture of ethanol/acetonitrile at room temperature (Fig. 2.38).

A «dumb-bell» shaped molecule can be produced using a reaction of two dendrimers with a cross-linking agent, for example, hexanediol chloride [522]. The
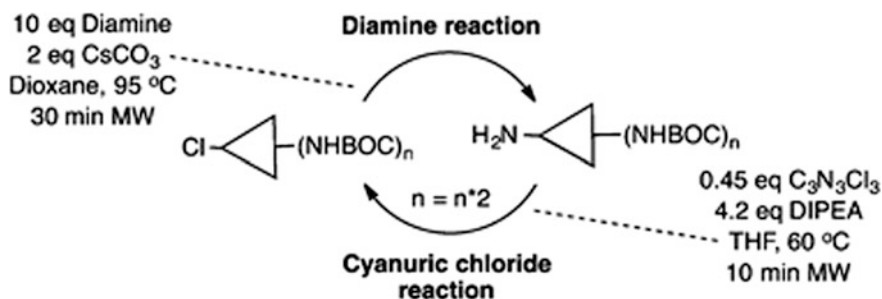

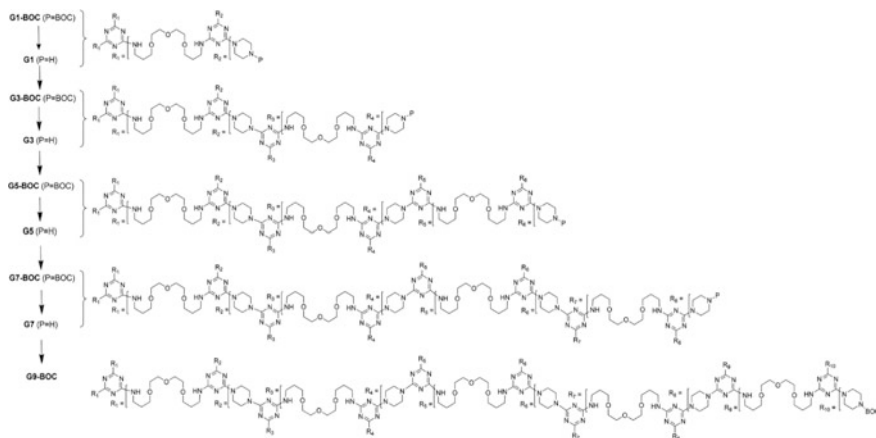**Fig. 2.36** Scheme of microwave synthesis of triazine dendrimers
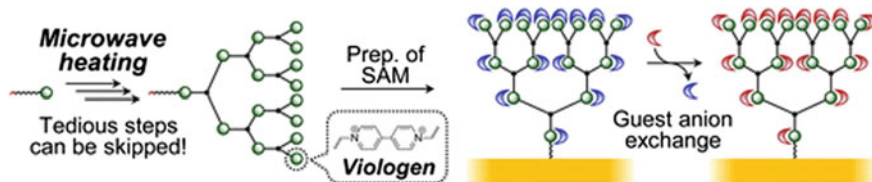
Fig. 2.37 Dendrimers with triazine core

Fig. 2.38 Preparation of dendrimers SAMs using a microwave synthesis

promising way is using 3D polycondensation method for dendrimer synthesis [63, 64, 523]. A solid phase synthesis of inverse PAMAM was developed, and when AB$_2$ type monomers were used, only one reaction was required for synthesis of each PAMAM generation [524].

2.3.5   Using the Click Chemistry in the Synthesis of Dendrimers

Recently design of dendritic macromolecules has reached a noticeable success, mainly due to extremely advantageous and elegant developed synthetic routes based on click chemistry [445, 525–527]. In particular, very efficient are click chemistry methods used in synthesis of dendrimers via Diels-Alder [528], thiol-yne [529], and azide-alkyne reactions [530–532]. Synthesis of some dendrimer that employs CuAAC and furan-maleimide Diels-Alder click chemistry in layer-by-layer (LbL) fashion can serve as an example shown in Fig. 2.39 [533]. Apparent
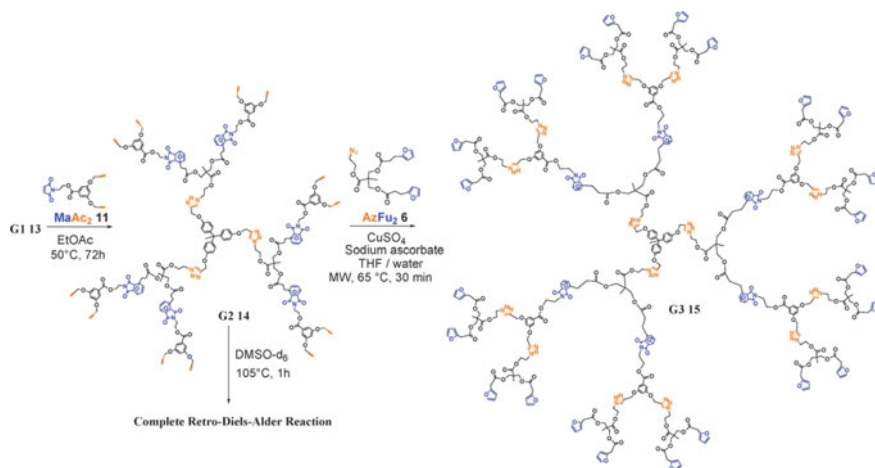
Fig. 2.39 Synthesis of G2 and G3 dendrimers and retro-Diels-Alder reaction
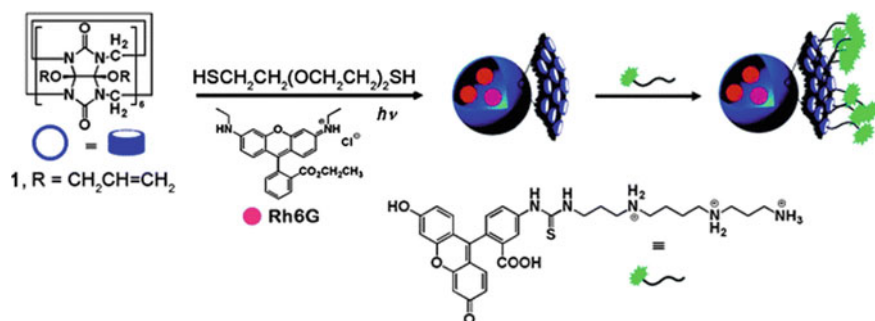
Fig. 2.40 Click-synthesis of *N,S*-chelating dendrimers

advantage is potentially «green» character of this methodology of design of macromolecular assembles.

The combination of controlled polymerization methods and click reactions creates an effective platform for the production of polymers with different architectures (Fig. 2.40) [534].

Usually performed CuAAC reaction in the synthesis of dendrimers requires stoichiometric use of the most common click-catalyst $CuSO_4 \cdot 5H_2O$ with sodium ascorbate. An effective, practical and easily accessible catalytic Cu(I) complex with hexabenzyl-tris(2-aminoethyl) amine was proposed to carry out this reaction under milder conditions for the synthesis of relatively large dendrimers. This catalyst can be used to form intradendritic [1,2,3]-triazole heterocycles coordinated with the transition metal ions through their nitrogen atoms (Fig. 2.41) [535].
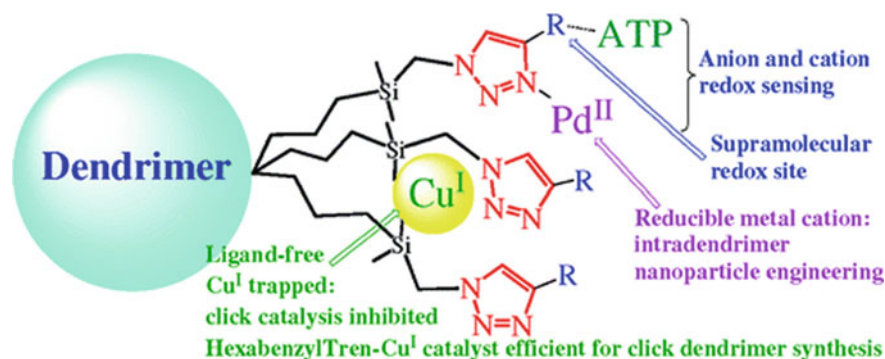
Fig. 2.41 Click-synthesis of dendrimer with [1,2,3]-triazole heterocycles
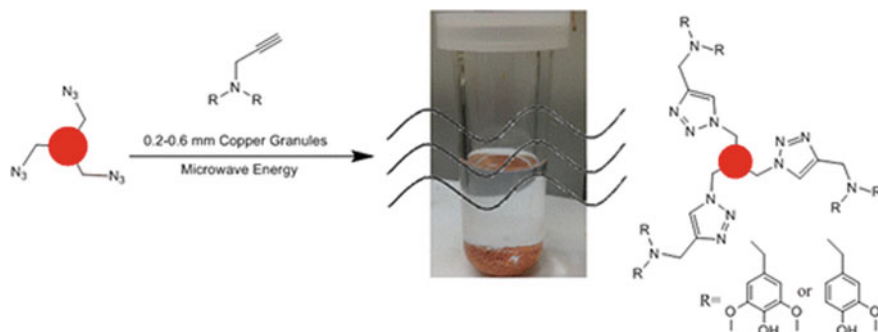

Fig. 2.42 Microwave click-synthesis of polyphenol dendrimers

It is noted the use of copper granules in held by microwave alkyne-azide 1,3-dipolar cycloaddition click-synthesis of antioxidant dendrimers based on lilac aldehyde and vanillin (Fig. 2.42) [536]. Importantly that the copper granules ineffective at both room temperature and at reflux (<5% yield). However, they have shown to be highly effective when synthesis of chelating dendrimer is performed under microwave radiation, giving yields up to 94% for 8 h. Equally important is the fact that the dendrimers obtained by using this method, practically showed no contamination by copper (9 ppm), which was the same as the background level.

2.3.6 The Post-synthetic Modification of Dendrimers

Numerous studies were performed for purposeful synthesis of chelating fragments in a core, inside, and on surface of dendrimers using post-synthetic modification (PSM) (Fig. 2.43) [537].
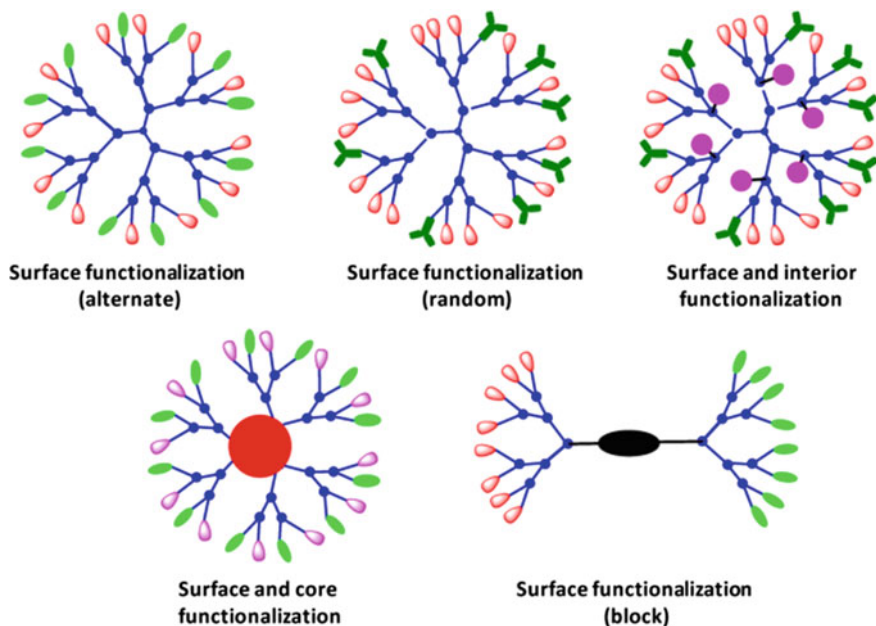
Fig. 2.43 Surface-, interior- and core-functionalized heterofunctional/multifunctional dendrimers

Selective modification of the dendrimer surface by different functional groups is very difficult [538]. However, derivatives of PAMAM dendrimers with acetamide, hydroxyl, and carboxyl terminal groups were successfully synthesized from the G4 PAMAM dendrimers with en core and five primary terminal amino groups [539]. The reaction of acetylation of G5 PAMAM dendrimers, containing reactive amino groups was carried out [540]. Terminal amino groups of G1 PAMAM dendrimer were used as initial material for synthesis of glycidol and acetamide-end-capped dendrimers [541]. Carboxylate-functionalized G5 PPI dendrimers were obtained by double Michael coupling of amine-functionalized PPI dendrimer to methacrylate with the following basic hydrolysis [542]. Modification of PAMAM dendrimers surface by benzoyl thiocarbamide was used to obtain ion-exchanged material having high selectivity to heavy metal ions [543]. Peripheral functionalization of G2 PAMAM dendrimers containing terminal amino groups was performed using 9-anthracenecarboxaldehyde [544]. G1 PPI dendrimer was modified by reaction of terminal amino groups with 2-pyridinecarboxaldehyde [545]. Dendritic chelating oxybatho-phen ligands (up to G3) were obtained by treatment of the respective Fréchet-type dendrons carrying benzyl-bromide groups in the focal point by 4,7-bis(4′-hydroxyphenyl)-phen, where phen is 1,10-phenanthroline [546].

Chemoselective substitution of surface groups in the range of phosphorus-containing dendrimers occurs successful [547, 548]. Reaction of dendrimers carrying $P(X)Cl_2$ (X=O, S) groups on periphery with allylamine and then with a sodium salt of *p*-hydroxybenzaldehyde brings to the aldehyde terminal groups,

which can be subjected to further modification, for example by Schiff and Wittig reaction. Thus, terminal functional groups $P(X)Cl_2$ are monosubstituted and then disubstituted not only by amines and aldehydes, but by phosphorus ylids, hydrazine, and chiral compounds. Inner layer of a dendrimer containing eighteen P-N(S) blocks can also be post-modified by allyl and propargyl triates, giving chemoselectively allylated and propargylated dendrimers pointing that accumulation of a certain number of functional groups is possible in well-defined globular macromolecule. These dendrimers with rich surface and internal functionalities can have applicability potential in different fields, especially, in catalysis.

Interaction between phenol, formaldehyde, and G0 and G1 PAMAM dendrimers brings to fabrication of two dendrimers containing benzoxazine side groups [549]. Interesting ion-chelating dendrimers are obtained on the basis of a benzene tricarbonyl core linked to three tripodal branching units, each of which contains a carboxyl, catechol, and 3-hydroxy-6-methyl-pyran-4-one fragments [550]. Surface groups of PAMAM and PPI dendrimers were modified by salicylate-, catecholate-, and hydroxypyridinonate-fragments [551]. A chelating ligand based on xanthate-functionalized PAMAM dendrimer was obtained from polyamidoamine dendrimer with terminal hydroxyl groups [552]. It is also noted surface modification of phosphorus-containing dendrimers for the preparation of (+)-cinchonine fragments [553].

A new family of poly(propylenamine) ferrocenyl dendrimers with azacrown ethers based on DAB was produced by the reaction of functionalized ferrocenyl derivative $\{[\eta^5\text{-}C_5H_4COCl]Fe[\eta^5\text{-}C_5H_4CONCH_2CH_2(OCH_2CH_2)_5]\}$ through amidoferrocenyl blocks [554].
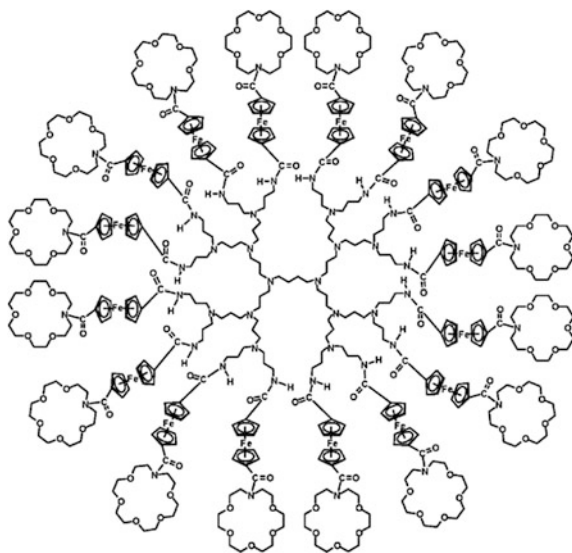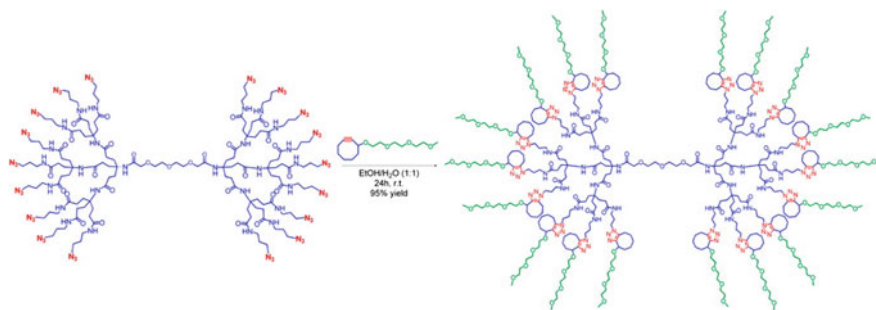
Fig. 2.44 Scheme of functionalization of PAMAM dendron by PEG chains

A copper-free strategy of strain-promoted azide-alkyne cycloaddition, which provides a quantitative functionalization under mild reaction conditions without any metal impurities, is developed for functionalization of poly(amido)-based dendron with PEG chains (Fig. 2.44) [555].

Effective precursors for PSM towards creating chelating fragments were mono-functionalized dendrimers based on polyamide with terminal azide or alkyne moieties derived using microwave 1,3-dipolar cycloaddition [556]. Microwave Huisgen 1,3-dipolar cycloaddition between azide-peptides and dendritic alkynes was used to produce multivalent dendrimeric peptides with yields ranging from 46 to 96% [557].

Strategy of in situ PSM was successfully applied for synthesis of AB_2C bifunctional dendrimers with inner acetylene/azide and outer hydroxyl groups [558]. These dendrimers can be easily transformed into dendritic nanoparticles or used as cross-linking agents for preparation of hydrogels.

Highly active surface of dendrimers serves as a basis for their self-assembly to supramolecular structures [559].

An example of modification of dendrimers in a core can be incorporation of resorcinarene [560], anthracene [561], and fluorene [562] cores in PAMAM dendrimer. We shall consider synthesis of two types of dendritic β-diketonate ligands, which contain dbm core and poly(aryl ether) dendron, and range of dendritic 2-(2-pyridyl) benzimidazole ligands [563]. Asymmetrically placed dendrimers with Cz and phenyl azomethine cores were obtained through Ullmann and dehydration reactions in presence of titanium tetrachloride [444]. Derivatives of tetrapyrazino-porphyrazine-containing flexible linear and rigid dendritic groups were synthesized [564].

Crown ethers and tpy ligands were successfully linked to the focal point of light-harvesting phenyl-acetylene monodendrons through Pd-catalyzed coupling reaction [565]. It is also noted dendritic chiral phosphorus ligands, including diphosphines monodentate phosphoramidites and N,P-ligands synthesized by fixing the respective chiral phosphorous units in the core or the focal point of Frechet-type dendrons [566].

It is important to emphasize that the purposeful creation of multi-functional dendrimers, with well-defined structures is necessary not only from the point of view of further chelation of metals, but also for the application of dendrimers in nanomedicine, light-harvesting systems, sensing and catalysis [567]. Furthermore, because of their unique steric structures and rich peripheral functional groups dendrimers are promising for various bioinspiring functions, including artificial proteins, viruses, enzymes, cell structure and light-harvesting antennas [568].

2.3.7   Fixing Dendrimers on Solid Surfaces

Dendrimers occurred to be convenient objects for fixation on different surfaces [569]. The special names dendritic-surface hybrid or dendronized surface were even introduced for such systems. Thus, PAMAM dendrimers with terminal amine groups are fixed on surfaces of carbon nanotubes [570], and PAMAM dendrimers modified by 1,8-naphtalamides are fixed on polyamide-6 used as a matrix for producing fluorescent materials [571, 572]. A detailed study of nanostructured G1–G3 dendrimer, supported on Merrifield resin with hydroxyl-, mesylate- and bromine-end groups showed [573] that particle diameter growth is associated with the end groups of samples and increases nonlinear with the dendrimer, wherein the dendrimer particles after G2 became denser.

Microwave technology is used for grafting PAMAM dendrimers on silica surface [574]. It was found that the amount of amino groups and nitrogen content increase with increasing generation PAMAM. Such dendronized surface links bovine serum albumin through glutaraldehyde, at that the immobilization efficiency increased with the increase in the generation of PAMAM.

Similarly, PAMAM G1–G7 dendrimers are constructed on the surface of ethylenediaminepropyl-functionalized magnesium phyllosilicate lamellas using a modified microwave synthesis [575]. The resulting solid materials showed an increase in their interlamellar space and disorganization of their lamellae packing with dendron growth.

In recent years, numerous studies are conducted with such interesting carrier as graphene oxide. Fixation of PAMAM dendrimers on graphene oxide surface using «grafting to» method can be cited as an example [576]. Obtained dendronized materials proved effective in the adsorption of a number of heavy metals.

2.3.8   Properties of Chelating Dendrimers

The study of the physico-chemical properties and architecture of dendrimers is one of the most promising approaches to solving the problem of designing and directed synthesis of MCD with predetermined properties. However, the dendrimer ligand, unlike low molecular weight analogues is characterized by a number of features that

make it difficult study of its physico-chemical characteristics. Oppositely to almost all other macromolecules, including even hyperbranched and star-like polymers, dendrimers do not obey the Mark-Coon-Houwink equation after reaching a certain molecular weight [577–580]. For example, in the case of polyether dendrimers after reaching of molecular weight about 5000, its further increase brings to a decrease in intrinsic viscosity. This phenomenon can be understood taking into account that as a generation number increases, volume of a dendritic macromolecule increases in cubic proportion of a linear size, while its weight increases as an exponent, which does not work for any other polymer. Unusual relations between intrinsic viscosity and molecular weight for the dendrimers correlate with a change in their shape from loose to globular structure with increase in molecular weight.

Dendrimers, like most linear polymers, are (depending on composition and molecular weight) viscous liquids, amorphous powders, or glassy resins, well soluble in most known organic solvents. Viscosity of their solutions is by several orders of magnitude lower than that of linear polymers with similar molecular weight. Unlikely to chain polymers, these ones do not have a crystal state; however, liquid crystal ordering is possible in polymer solutions and melts, containing mesogen groups.

Dendrimers of low generations (0, 1, and 2) have more asymmetric shape and have more open structure as compared with dendrimers of higher generations. As long as chains growing from a core become longer and more branched (in the G4 and higher dendrimer generations), a dendrimer molecule gains a globular shape. When critical branched state is reached, dendrimers cannot grow due to lack of space. This is called «star burst» effect [581]. For PAMAM dendrimer it is observed after G10, which contains 6141 monomer units and has diameter about 124 Å, at that the reaction rate decreases dramatically and no further reactions of terminal groups take place.

Numerous studies of the spectroscopic properties, melt rheology, solution properties of bio- or synthetic dendritic polymers have shown a special behavior of dendritic structures in bulk and in solution [582–586].

Presently there are more than fifty families of dendrimers, each of which have unique properties, surface, branching groups and cores, which can be adapted for different applications. Thus, dendrimers containing photoactive units can be used for probing of metal ions. For example, for these purposes G5 PPI dendrimers are applied, which are functionalized at periphery with strongly luminescent dansyl (1-dimethyl amino-1-naphthalene-5-sulfonyl) units [587].

High local orientation mobility of a dendrimer segments is typical of dendrimers [588]. Therefore, various reactions on a dendrimer surface or «guest-host» assemblies give a way to stoichiometric nanocompounds, such as dendrimer-dendrimer, dendrimer-protein, dendrimer-fullerene, metallodendrimer, etc. These examples convincingly confirm appearance of active dendritic modules based on the platform of synthetic nanochemistry [589].

One of the interesting features of dendrimers is formation of fractal structures, existence of a solid state with extremely low density [590]. Interest shown to chemical compounds with fractal structure is stipulated by, at least, two reasons.
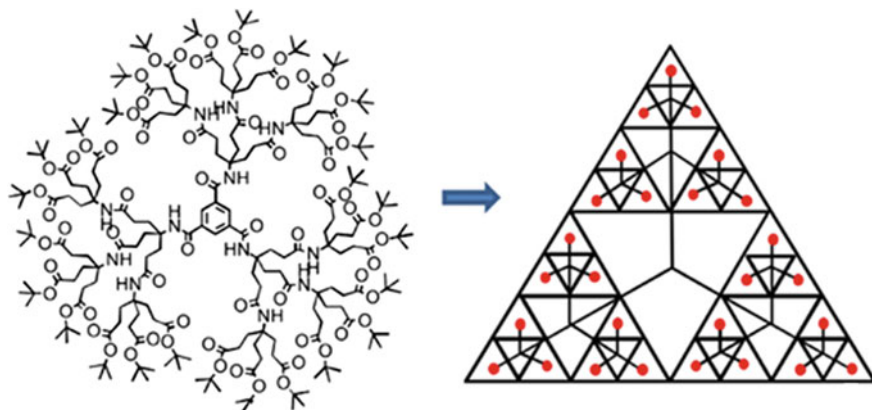
Fig. 2.45 Conceptual progression from branched dendrimer architecture to interrelated, non-tree-like fractal motifs

Firstly, these systems are rather wide spread in nature. Secondly, they are basic structural forming element for a range of macroscopic systems appeared as a result of physico-chemical processes and phenomena similar to fractal structures development. A fractal polymer with all features of Sierpinski triangle can be presented geometrically considering transformation proceeding from a 3-oriented 2D dendrimer to the triangular ($1 \rightarrow 3$) branched motif, which can be superimposed on the pattern of Sierpinski triangle predicted as early as in 1916. Dendritic branches divide in two the triangle sides, and these intersection points make a basis for development of Sierpinski triangle (Fig. 2.45) [591].

Dendrimers have specific properties, such as low density, highly developed structure of inner caverns, high specific surface, high sedimentation stability of disperse particles, etc., which characterize them as promising carriers of different substances, including drugs [592–596], and nanoreactors for production of nanometer metal particles [597]. Our interest to these structures is sustained by their high chelating capacity to a wide range of metals.

2.4   Chelating Hyperbranched Polymers

During two last decades a special attention has being attracted to such interesting CPLs as hyperbranched polymers, nanostructured polymers with complicated architecture of macromolecules [20, 53, 63, 64, 598–611]. Nano-dimensionality and polyfunctionality of hyperbranched polymers stipulates apparent attractiveness of these reagents as regards oriented synthesis of polymers with predetermined chelating properties. Possibilities of functioning coordinationally active structured ligands as nanocontainers encapsulating target compounds, or nanoplatforms retaining «host» molecules or functional groups on the surface, will make it possible to obtain and

characterize new hetero- and polynuclear metal chelates. The attention to hyper-branched polymers is attracted due to their unique chemical and physical properties, and a possibility of their application in coatings, additions, drug delivery, macro-molecular building blocks, nanotechnologies, and supramolecular systems.

Presence of technologically significant methods of hyperbranched polymer synthesis of several types (in particular, aliphatic polyether Boltorn® [52], poly (amidoester) Hybrane® [612] and PEI Lupasol® [613, 614], as well as a number of hyperbranched polyesters [615] and polyurethanes [616–618]) gives a possibility of implementation of their industrial production within the limits sufficient for further application in very different areas.

As well as dendrimers, hyperbranched polymers relate to group of polymers with densely branched structure and a great number of reactive groups (Fig. 2.46). They are alike also because they are obtained by polymerization of monomers with mixed functionalities, usually designated as A_2B or A_3B monomers, thus providing exponential growth of branched structures in two directions and with the same molecular weights. However, there are principal differences between them. Dendrimers are hyperbranched monodisperse polymers, while ordinary hyper-branched polymers are polydisperse. Moreover, absolutely different fundamental synthetic approaches are typical of them: whereas absolute control over all stages of chemical synthesis of dendrimers is required, a simplified approach is needed for production of hyperbranched polymers, similarly to ordinary synthetic polymers technology. Hyperbranched polymers obtained by controlled method in two or three stages, can work as well as dendrimers synthesized in 10 or 12 stages. Dendrimers are polymers with orderly branched structure, while hyperbranched polymers have randomly branched structure.
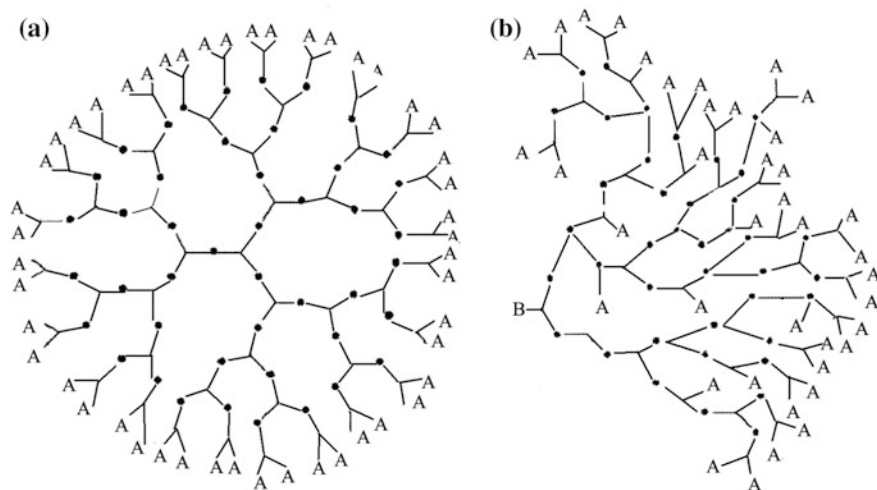

Fig. 2.46 a Dendrimer, **b** hyperbranched polymer with B core (functional groups A are on periphery)
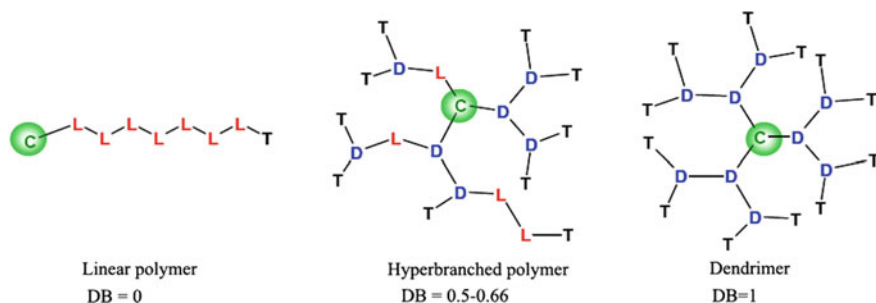
Fig. 2.47 Comparison of polymer architectures as a function of degree of branching

There are three main parameters for description of hyperbranched polymers: molecular weight, PDI and a degree of branching (DB). The later can be calculated using the following equation [619]: $DB = 2D \div (2D + L)$, where D is a number of dendritic units, L is a number of linear units. This parameter is used for topologic characteristic of hyperbranched polymers and can serve to determine a difference between linear polymers, dendrimers, and hyperbranched polymers (Fig. 2.47).

Dendrimers have no linear units, and in this case a degree of branching is 1. On the other hand, linear polymers have no dendritic units; therefore, DB has zero value. Respectively, hyperbranched polymers should have intermediate value of DB between 0 and 1. Control over branching degree is very complicated and usually non-regular, polydisperse macromolecules with DB = 0.4–0.7 are obtained. This brings to formation of a great number of geometrical isomers, whose number increases with increase in molecular weight and a number of reaction centers of monomers. DB has an extreme value 0.66 at slow addition of monomers and high degree of conversion.

2.4.1 Star Polymers

The simplest branched macromolecules are called star polymers, in which several linear polymer chains are fixed only on one fixation point (core) [620]. Based on chemical composition of the arms, star polymers can be divided into two categories: homoarm (or ordinary) star polymers and miktoarm (or heteroarm) star copolymers

Fig. 2.48 Star and miktoarm polymers

(Fig. 2.48). Homoarm star polymers consist of symmetric structure containing divergent stars with the same chemical composition and similar molecular weight. In contrast, miktoarm star molecule comprises two or more arms with different chemical compositions and/or molecular weight and/or different periphery functionality [621, 622].

To obtain star polymers, methods of controlled polymerization are actively used, which can be separated into three common synthetic approaches: (a) «core-first» approach («from-approach»), in which a polyfunctional initiator is simultaneously used for initiating polymerization of vinyl monomers, thus forming polymer stars (Fig. 2.49a); (b) «arm-first» approach includes reaction of a living macroinitiator (or) macromonomer, an arm, with bifunctional vinyl cross-linker, with formation of
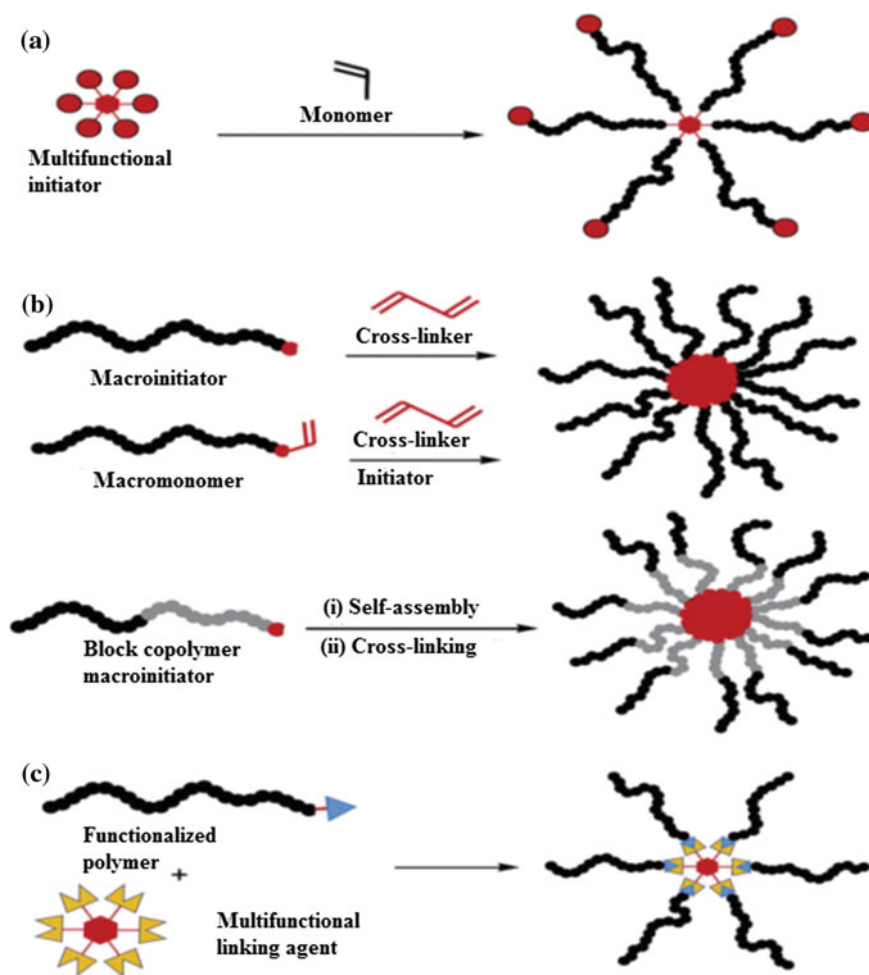
Fig. 2.49 Synthetic approaches to preparation of star polymers via controlled polymerization: **a** the core-first approach, **b** the arm-first approach, **c** grafting to approach
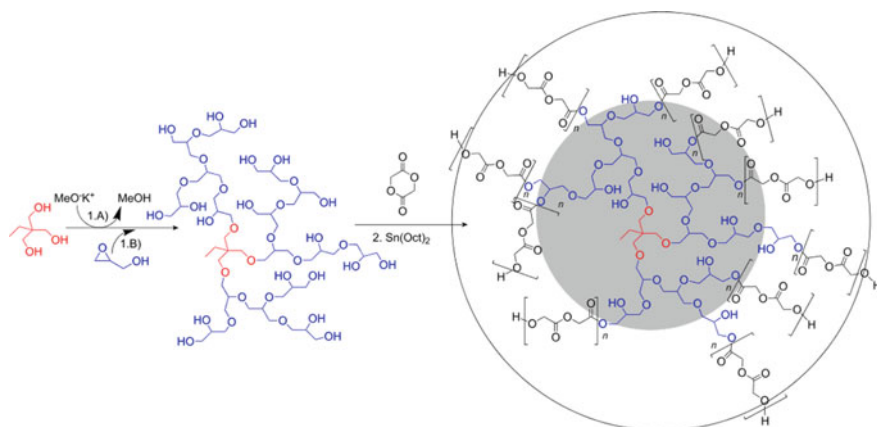
Scheme 2.25 Synthetic route to hyperbranched multi-arm star copolymers by two-stage method

a densely cross-linked core, from which arms are spread (Fig. 2.49b); (c) «grafting-to» approach can be considered as a combination of controlled polymerization and addition reactions, in which a preliminary formed polymer, arm, is prepared through controlled polymerization and introduced into the coupling reaction with polyfunctional cross-linking agent, which works as a core (Fig. 2.49c) [623].

We shall consider as an example a simple two-stage synthesis of multi-arm star poly(glycerols) with several poly(glycolide) arms (Scheme 2.25). At the first stage glycidol is polymerized in anion-type using trimethylolpropane as a tri-functioning initiator, and at the second stage polyethers-polyols are used as macroinitiators for the open-chain polymerization of a glycolide using $Sn(Oct)_2$ as a catalyst [624].

The combination of star-shaped dendrimers and linear chains reveals much more variation of polymer architectures and new molecular properties. Examples are hyperstar that can be obtained by different approaches, but usually «core-first», «grafting-from» or «grafting-onto» approaches used linear polymers for grafting to the dendrimer core [625–627]. For example, the synthesis of a number of dendrimer-like star-branched poly(methyl methacrylate) (PMMA) from G1 to G7 by stepwise iterative methodology based on the «arm-first» divergent approach (Scheme 2.26) [628].

Besides being able to use as chelating ligands, hyperstars actively studied in anion-cured epoxy thermosets [629], and in biomedical areas as the core-multishell nanocarriers [630, 631].

2.4.2 Methods of Synthesis of Hyperbranched Polymers

The developed by now methods of synthesis of hyperbranched polymers are divided into three categories [63, 64, 459, 632–635]:
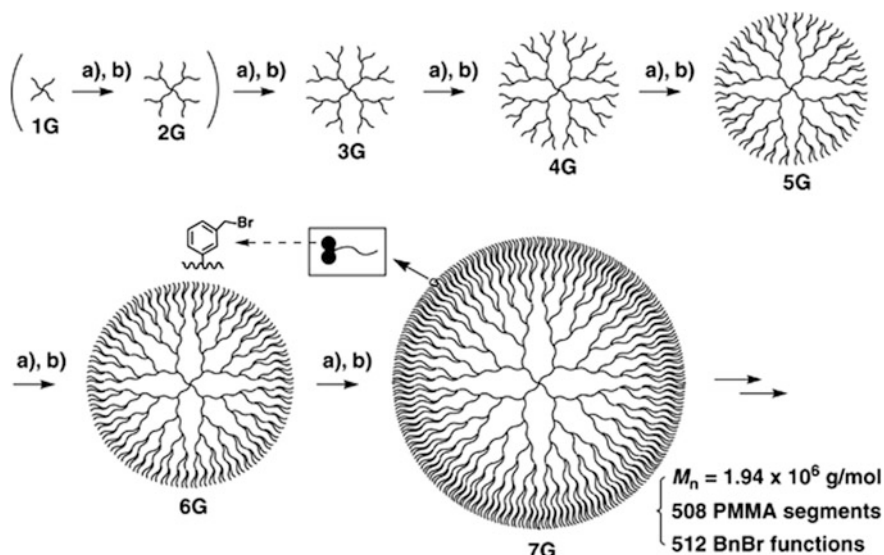
Scheme 2.26 Synthesis of dendrimer-like star-branched polymer by stepwise iterative methodology based on the «arm-first» divergent approach (BnBr—benzyl bromide)

– polymerization by the mechanism of stepwise poly-addition of polycondensation type;
– radical polymerization by the chain poly-addition mechanism;
– other methods (for example, radical polymerization under conditions of living chains, which is a special case of poly-addition, etc.).

The first method is a classical approach to synthesis of hyperbranched polymers, in which AB_x and $AB_x + B_y$ monomers with equal reactivity of B functional groups are used (Fig. 2.50). The reaction includes typical characteristics of a staged reaction of polyfunctional monomers and oligomers formed without linking. In this case growth of a polymer begins from the already existing A and B reaction centers, in other words, new centers do not form during polymerization. As a result of reaction, strongly branched macromolecules are formed, which contain dendritic units (completely reacted B groups), terminal units (non-reacted B groups), linear units (one reacted B group), and one focal point (A group).

Among synthetic approaches bringing to very wide structural variety of hyperbranched products, use of AB_2 monomers is the predominant. This method is used, in particular, for production of Boltorn® industrial polyethers based on commercially available AB_2 monomer 2,2-dimethylol-propionic acid (A = COOH; B = OH) by etherification reaction. In this case terminal hydroxyl groups form a shell of a hyperbranched polymer.

Hyperbranched polymers are synthesized from AB_2 monomer containing bis(*m*-phenylene)-32-crown-10 and two groups set on its opposite ends, linked with a benzene ring. The monomer is easily self-assembled and polymerized in solution,
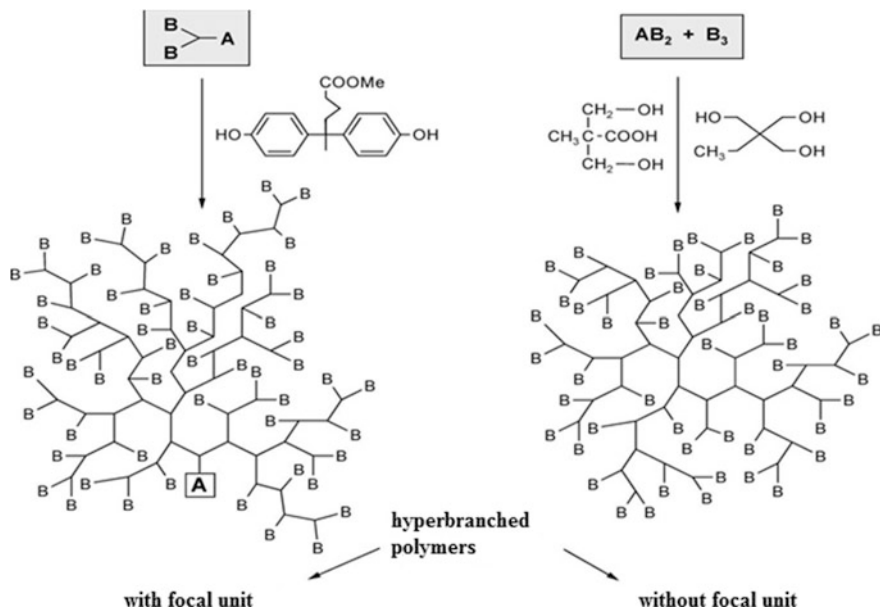
Fig. 2.50 General strategy of synthesis of hyperbranched polymers through AB_x and $AB_x + B_y$ approach ($x \geq 2$; here is 2; $y \geq 3$; here is 3)

at that, to obtain a polymer with high DP, high concentration of a monomer (150 g L^{-1}) is required [636].

Aromatic AB_2 bis-amino acid monomer **1** was used for production of hyperbranched PAMAM polymers as «dendrimer equivalents» [637]. The analysis showed that purified hyperbranched polymers have $M_n = 2000$ and PDI = 3.2 (Scheme 2.27).

The fraction deposition method with use of another AB_2 monomer, 3,5-bis-(4-aminophenoxy) benzoic acid, permits to prepare hyperbranched polymers with the end NH_2-groups [638]. For them, DB value increased as molecular weight of the formed polymers decreased.

It is noted hyperbranched polymer containing chelating β-ketoester fragments which is synthesized from 2-acetoacetoxyethyl acrylate by the Michael coupling reaction in presence of 1,8-diazabicyclo-[5.4.0]undec-7-ene (DBU) as a catalyst. DB in poly(β-ketoesters) was very high, about 82.9%, and M_n was between 2100 and 12,000 and it increased as temperature of the reaction and a degree of conversion increased [639].

Hyperbranched N,N′-substituted polycarbamides are obtained using 3,5-diamino benzoic acids containing methyl, benzene, and allyl substituents for AB_2 monomer [640]. This method of synthesis of hyperbranched polycarbamides can be used for creation of libraries of polymers with interior functional groups.

Condensation polymerization of 5-amino-isophthalic acid methyl ether containing chains of N-(triethylene glycol) methyl ether is performed [641]. The
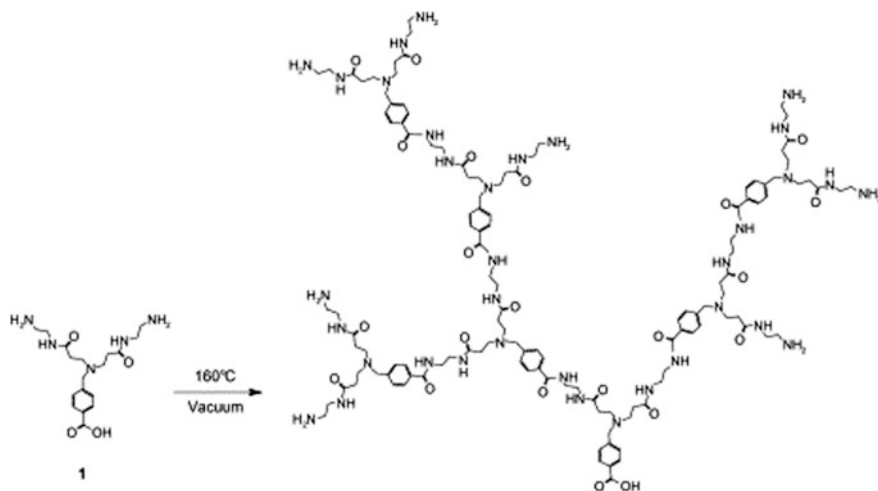
Scheme 2.27 Synthesis of PAMAM hyperbranched polymer

formed hyperbranched polymers have M_n = 3810–18,600, PDI = 1.11–1.19, are water-solved and are characterized by LCST.
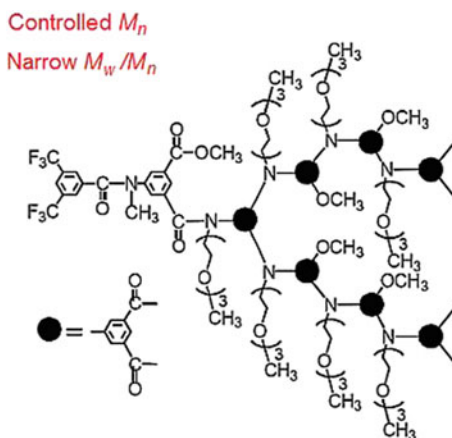
There is an interesting approach in which AB_x type monomer is formed in situ via interaction between primary amino groups of 2-amino-2-ethyl-1,3-propanediol *or* tris(hydroxymethyl)aminomethane with aliphatic carboxylic acid anhydride [642]. It is important to emphasize that the initial substances are commercially available, and the following thermal self-condensation is carried out without catalysts or solvents. DB of the formed polymers is in the range from 0.36 to 0.55. Among the obtained hyperbranched poly (ether-amides) polymer structures with

cyclohexyl molecular skeleton have the lowest DB, the highest T_g, and the best thermal stability.

Self-polycondensation of AB_2 monomers using different strategies was successfully applied to achieve DB = 100%, which is a typical property of dendrimers. Besides, due to a change in the reaction rate constants of the first reaction of the group B and the second reaction to the functional group A, hyperbranched polymers with controlled DB from 0 to 100% can be produced [643]. Moreover, molecular weight and molecular-weight distribution of the formed polymers can be controlled.

Also binuclear platinum complexes having one acetylene terminal group and two platinum-chloride groups can be used as AB_2 monomer [644]. Self-polycondensation of such monomer in presence of copper catalyst brings to hyperbranched platinum-polyyne polymers containing platinum-acetylide units and having high solubility in basic organic solvents. It is important to notice that such metal-containing hyperbranched polymers can then serve as precursors for PCMs.

For successful synthesis of classical hyperbranched polymers from AB_x and $AB_x + B_y$ monomers it is necessary to meet the following demands: first, A and B groups should react selectively with each other without side reactions, secondly, intermolecular cyclization should not take place, and thirdly, B groups should have equal reactivity.

This type of polymerization can be performed by slow addition of a monomer in presence of B_f molecule ($f \geq 3$) as a core, which provides structural control over a growing polymer. Thus, hyperbranched polyethers were synthesized from 2,2-bis (hydroxymethyl)propionic acid taken as AB_x monomer and triethanol amine used as a core molecule [645].

Another approach is copolymerization of A_2 monomer with B_n co-monomers ($n \geq 3$). Thus, hyperbranched polyethers with controlled molecular weight are obtained using $A_2 + B_3$ approach by interaction between glycerol and adipic acid without a solvent in presence of a tin catalyst (Fig. 2.51) [616].

The same $A_2 + B_3$ approach was successfully applied for production of hyperbranched polymers containing fragments of ferrocene (Fc) [646]. In this case diols, dithiols, or dichloroarenecomplexes were used as A_2 compounds, and B_3 compounds were preliminary prepared star-like molecules, as well as commercially available triols.

Slow addition of monomer, 2,2-bis(hydroxymethyl)propionic acid, to a trifunctional core gives a product with DB 47% [647].

$A_2 + B_4$ approach was used for production of hyperbranched conjugated poly (azomethines) via interaction between tetramines and dialdehydes [648]. Variation of the ratios between reagents and introduction of dopants, for example, $SnCl_2$ or β-cyclodextrin (CD), makes it possible to change content of terminal amino groups, which brings changes to interaction between the terminal amino groups and imine bonds of the main chain, and provides control over chelating properties of produced hyperbranched polymers.

Fluorescent hyperbranched polymer containing triphenylamine and divinyl-bpy units is obtained by Heck coupling reaction of 5,5′-divinyl-bpy with tris(4-bromophenyl)
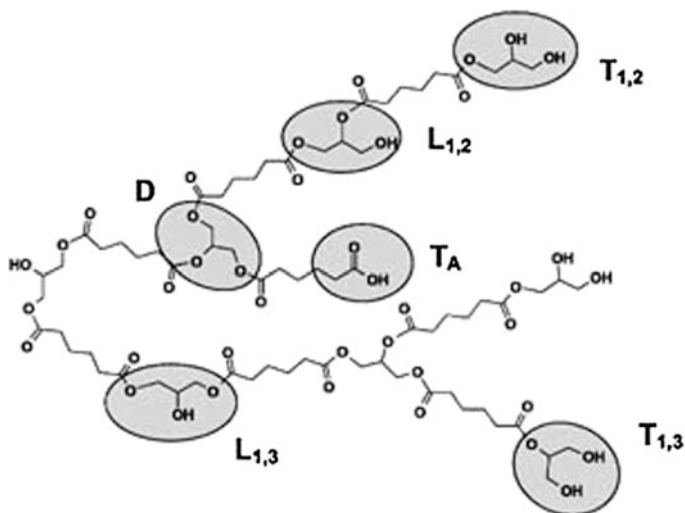
Fig. 2.51 Idealized structure of hyperbranched polyethers synthesized from adipic acid and glycerol in presence of tin catalyst

amine. It has $M_n = 1895$ and $M_w = 2315$, high thermal stability and is well solved in tetrahydrofuran (THF), chloroform, and dimethylsulfoxide (DMSO) [649, 650].

Hyperbranched polyyne with $M_w = 6.55 \times 10^4$ containing triphenylamine as the core, and diketone and pyrrol units is obtained by Glaser-Hay oxidative coupling reaction [651].

A series of water-soluble aliphatic hyperbranched PAMAM with the same or similar chemical structure of a PAMAM dendrimer is successfully synthesized from commercially available AB and C_n types of monomers using one-pot polymerization [652]. Methacrylate was used as AB monomer, and polyamino-compounds, such as en, dien, trien, tetraethylenepentamine and pentaethylenehexamine were used as C_n monomers. Hyperbranched polymers with different end groups and properties can be obtained via regulation of the initial ratio between AB and C_n. However, stoichiometric regulations between pairs of functional comonomers and potential risk of gelation assume serious drawbacks.

The chain growth mechanism for production of hyperbranched polymers has been widely developed after discovery of self-condensing vinyl polymerization (SCVP). Presently used monomer is designated as AB* and it contains an initiating radical in addition to a double bond. The initiating fragment is activated and reacts with the double bond forming a covalent bond and a new active center on the second carbon atom of the double bond (Scheme 2.28). A number of active centers increase in linear proportion to the growth reaction in SCVP, while two functional groups are always used during self-polycondensation of AB_x monomers. If new active centers formed during polymerization have different reactivity as compared
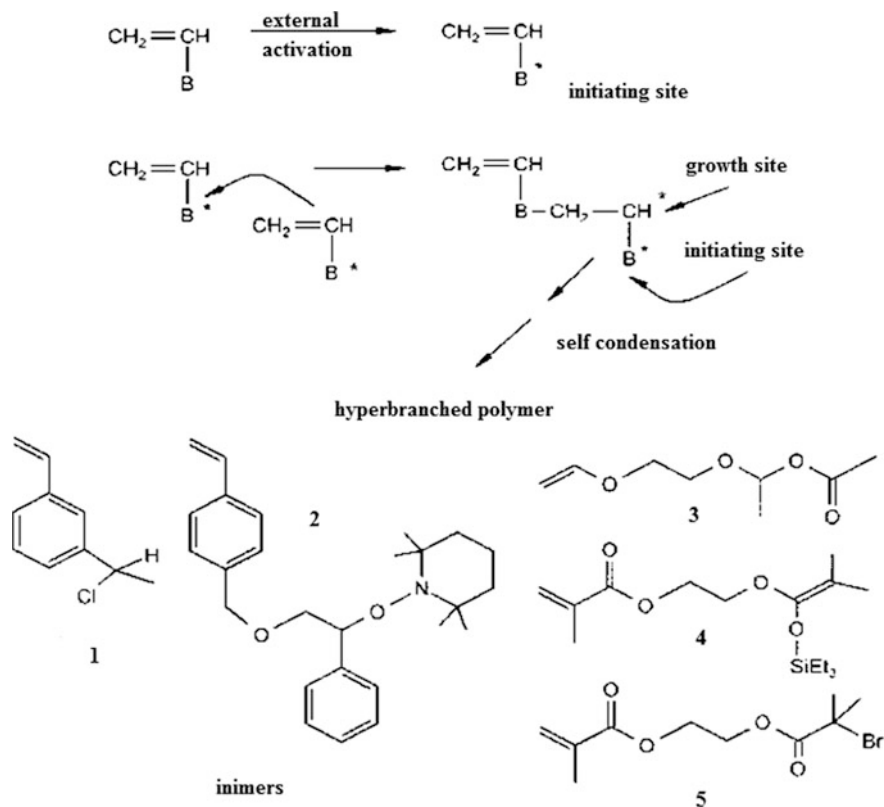
Scheme 2.28 Self-condensing vinyl polymerization (* is a reaction center, which can initiate polymerization) and some examples of AB* inimers ("inimer" = initiator + monomer)

with active centers in the initial monomer, this difference has a considerable effect on structure of obtained polymer. Living free radicals, electrophilic cation fragments and carbanion can serve as active centers.

A Pd-diimine catalytic inimer containing catalytic, initiating and monomer functionalities was used for synthesis of PE of hyperbranched-on-hyperbranched and star architectures by SCVP of ethylene (Fig. 2.52) [653]. It is important that it facilitates synthesis of star-shaped PE using tandem UV-coordination polymerization.

Aromatic polyamides with terminal NH_2-groups containing diphenylquinoxaline units are obtained by free radical polymerization of the 2,3-bis(4-aminophenyl)-quinoxaline-6-carboxylic acid and 2,3-bis[4-(4-aminophenoxy) phenyl] quinoxaline-6-carboxylic acid monomers at room temperature [654].

A variation of SCVP method is reversible addition-fragmentation chain transfer self-condensing vinyl polymerization (RAFT-SCVP), which is used for synthesis of segmented hyperbranched poly(GMA) (Scheme 2.29) [655].
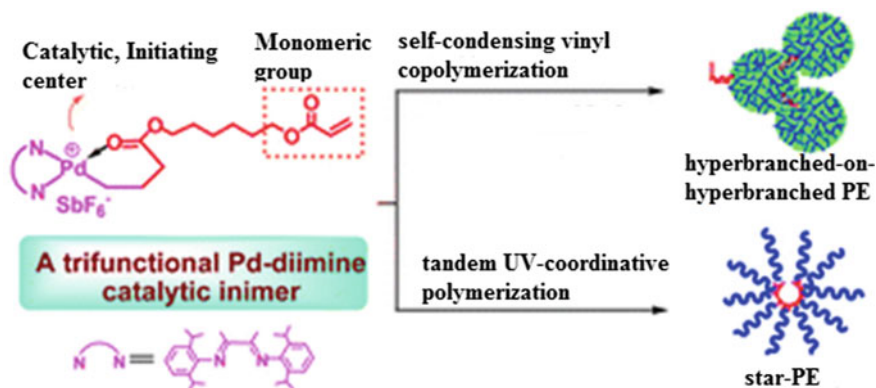
Fig. 2.52 Use of Pd-diimine catalytic inimer for synthesis of PE of hyperbranched-on-hyperbranched and star architectures
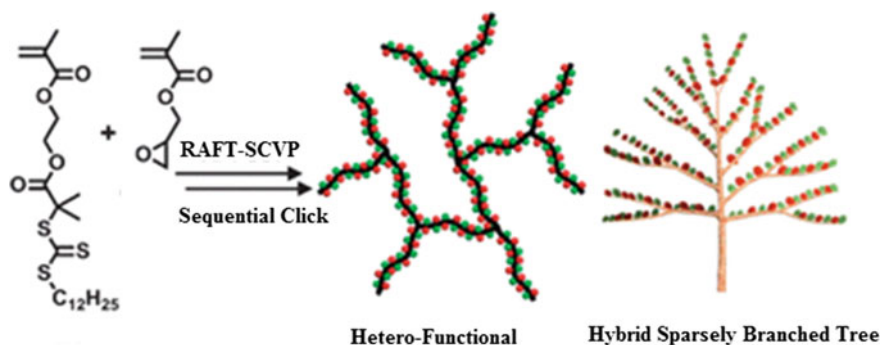
Scheme 2.29 RAFT-SCVP in synthesis of hyperbranched polymers

Apart from SCVP in the chain growth method other approaches are used, such as self-condensing ring-opening polymerization (SCROP), also known as ring-opening multibranching polymerization (ROMBP), proton-transfer polymerization (PTP), etc. For example, in ROMBP method branching units of blocks are generated during the ring-opening reaction, while initial AB monomers do not contain branching points. Polymerization is initiated by addition of respective initiators for generation of active centers, which can provide control over molecular weight and molecular-weight distribution of formed polymers (Scheme 2.30) [656].

PTP of thiol and epoxy groups was, in particular, applied to synthesis of hyperbranched water-soluble cation materials (Scheme 2.31) [657]. For this AB_2 monomer was synthesized, which contains two epoxy and thiol groups. PTP of this monomer catalyzed by bases brings to formation of polythioethers based on hyperbranched polymer with DB = 65–69% containing about 2% structural defects based on disulfide. This polymer contains two reactive centers, hydroxyl group, and
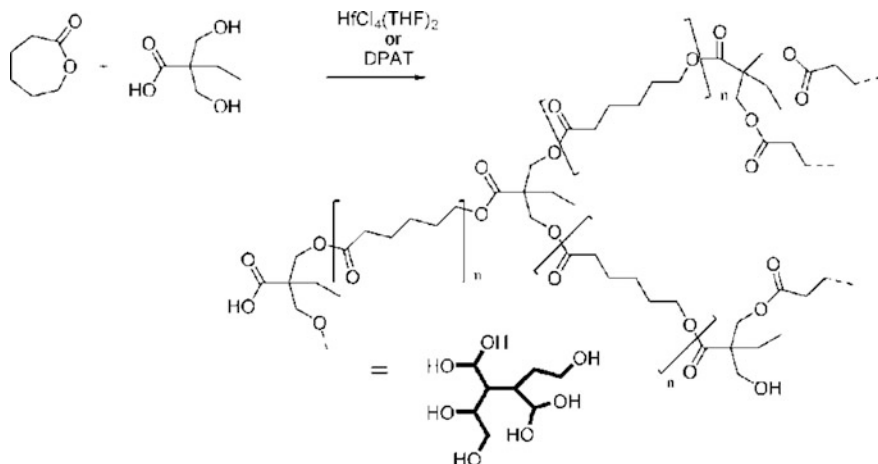
Scheme 2.30 Copolymerization of 2,2-bis(methylol)butyric acid with ε-caprolactone by ROMBP
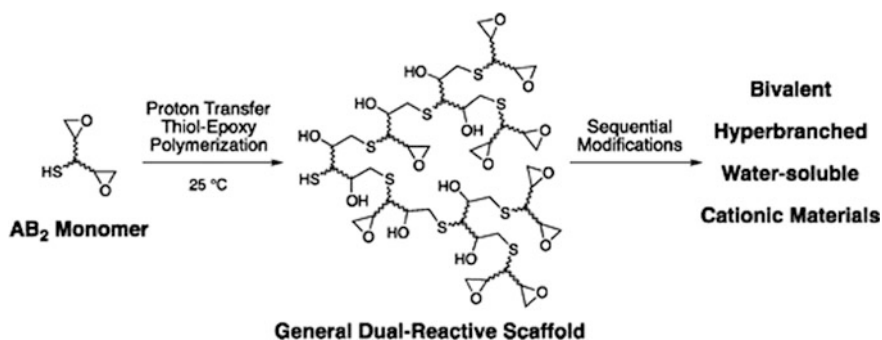
Scheme 2.31 Scheme of synthesis of hyperbranched polymer using PTP method

epoxy block distributed over all branched polymer carrier. Epoxy groups can be used in fixation of alkyl, aryl, and oxyethylene chains via thiol-epoxy reactions, while hydroxyl groups formed during polymerization or following functionalization can be involved in the coupling reactions of positively charged primary ammonium groups to branched polymer carrier.

The abovementioned synthetic approaches cover majority of general methods of preparation of hyperbranched structures. At the same time, in order to broaden structural variety and complexity of designed macromolecular structures, different building blocks are obtained by combination of strongly branched structures, which brings to linear-dendritic block-copolymers, hyperbranched core-star structures, dendrigrafts, and more complicated architectures [658].

Recently new efficient methods of synthesis of hyperbranched polymers have being used for different practical applications. For example, to obtain selective analytic reagents such methods as enzyme-catalyzed polymerization, click chemistry, or slow monomer addition are used [659].

An example of green synthesis of hyperbranched polymers is lipase-catalyzed production of polyfunctional poly(amine-ester)-type of hyperbranched polymers by polycondensation of triethanolamine with polyethers [660]. Another example of green synthesis is synthesis of hyperbranched polymer through thiol-yne photopolymerization of macromolecules carrying thiol group at one end of the chain and alkyne fragment at the other one (Scheme 2.32). These thiol-yne macromonomers were obtained by RAFT polymerization of St initiated by alkyne-containing agent of a chain transfer followed by aminolysis trithiocarbonate groups in thiol fragments. It has been shown that among different parameters of the process (size of used thiol-yne macromonomer, amount of added photoinitiator, or initial concentration of a used macromonomer), the latter is leading, having the effect on final size of hyperbranched structures [661]. However, structure of hyperbranched polymers can be controlled as in the case of dendrimers, and functional groups are not localized in a definite position. This is stipulated by statistic character of coupling stages, steric difficulties of growing chains, and reactivity of functional groups, i.e. growth takes place only from two centers among all branching units, which gives irregular and linear segments. At the same time, low cost of synthesis of hyperbranched polymers makes it possible to produce them in large quantities, giving them advantage against dendrimers in applications. Hyperbranched polymers are thus considered as alternative to dendrimers for different applications in researches and for practical using.
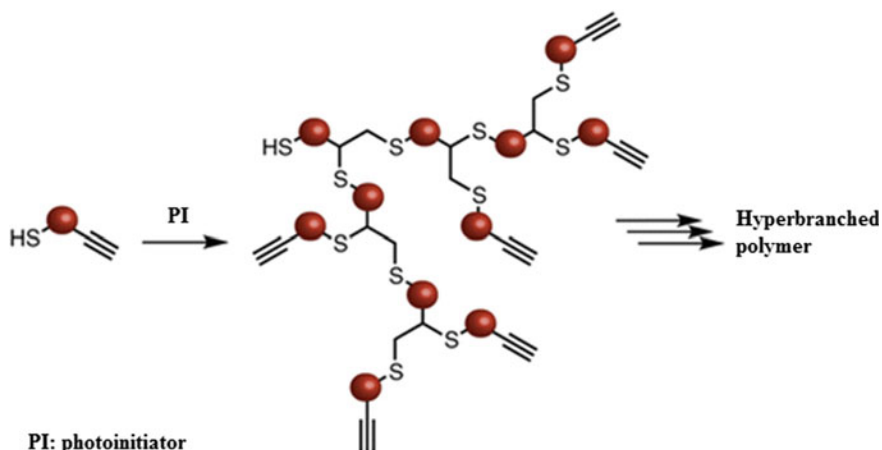
Scheme 2.32 Scheme of synthesis of hyperbranched polymer by thiol-yne photopolymerization method

It should be noted hyperbranched polymers with high DB and low dispersity values produced of slow monomer addition of a thiol/yne monomer to multifunctional core molecules in the presence of photoinitiator and under UV irradiation [662].

New strategy is developed [663], in frameworks of which small monomers can directly grow into big hyperbranched macromolecules under action of sunlight without any catalyst (Scheme 2.33).
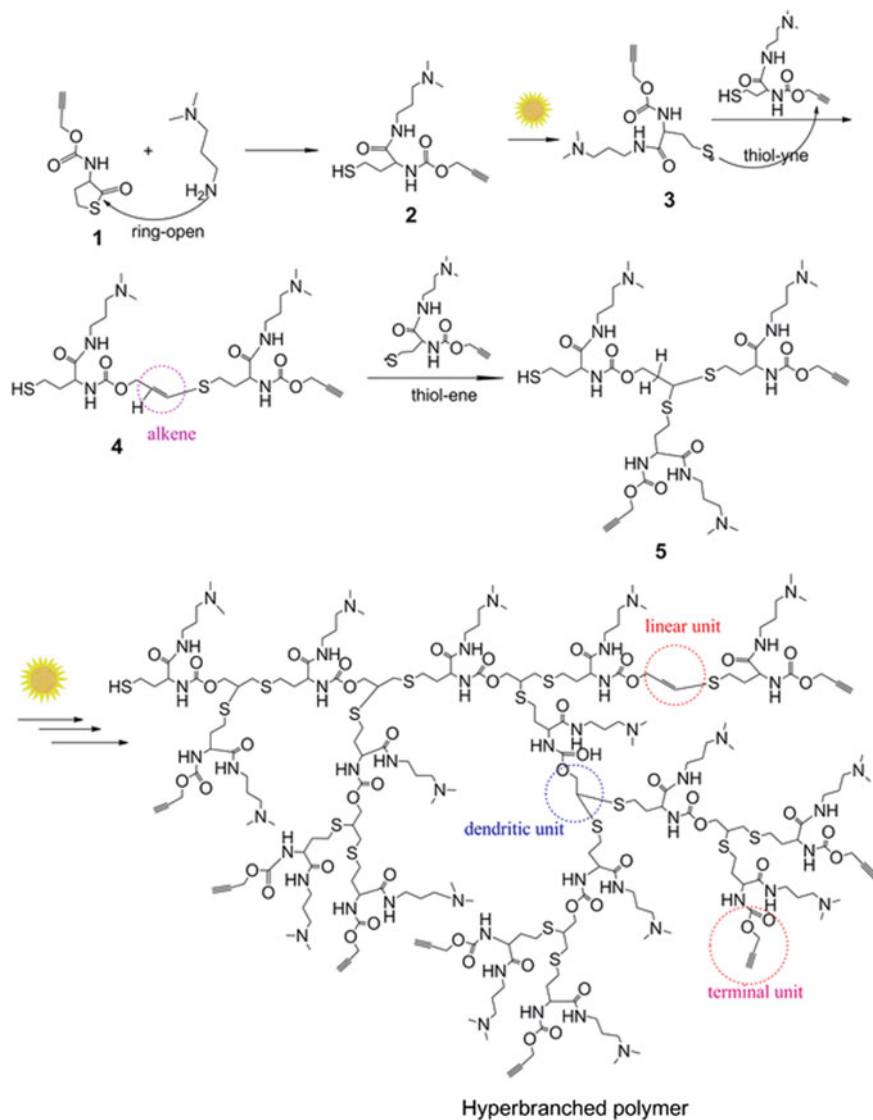

Scheme 2.33 Schematic image of growth of hyperbranched polymer under sunlight irradiation of the mixture of alkyne-containing thiolactone and primary amine

2.4.3   Post-synthetic Modification of Hyperbranched Polymers

Directed chemical modification of hyperbranched polymers makes it possible to perform architectural design of these compounds, determining size, shape, a ratio between length and density, and functionality of their surface. Besides, PSM is also an efficient method, which provides control of amphiphilic balance of polyfunctional macromolecules. High local specific weight of active groups bringing to existence of a number of identical ligands in a molecule is provided increased binding of a specific substrate. All this determines exactly hyperbranched polymers as a unique reagent for development of new composite materials of structural functions and a system for molecules transporting (chromophores, phototropes, catalysts, drugs) with a possibility of choice of delivery of specific compounds.

Four ways of PSM of hyperbranched polymers are based on highly branched architecture and a great number of terminal functional groups of these macromolecules: (1) end capping by short chains or organic molecules, (2) end grafting through living polymerization, (3) growth of hyperbranched polymers on a surface or grafting from/on a surface, and (4) hypergrafting for production of hyperbranched polymers with linear macromolecular core. End capping with small organic molecules can be used to obtain a great number of end chelating groups linked to linear and end units of hyperbranched polymers. Thus, hyperbranched polyamino-end glycidols were synthesized [664] using end modification of terminal hydroxyl groups with toluenesulfonyl chloride with the following nucleophilic substitution of the toluenesulfonyl groups with secondary aliphatic amines (Scheme 2.34).

The greatest number of studies considering the end modification is carried out using a hyperbranched commercial polymer Boltorn 2, 3, and 4 generations, H20, H30, and H40, respectively. Thus, Boltorn polymers are modified by incorporation of tertiary amino groups via interaction with diethylaminopropylamine using CDI
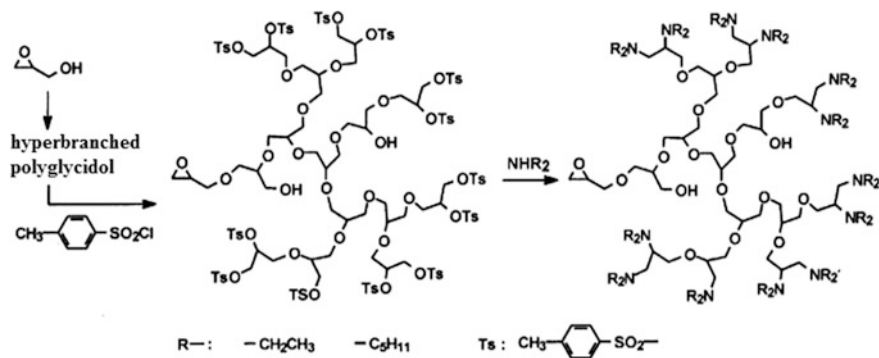
Scheme 2.34 Scheme of the end capping process

chemistry for development of non-toxic and biodegrading gene carriers [665]. Toxicity of modified hyperbranched polymers is lower than that of PEI. Boltorn H40 was subjected to interaction with hexamethylene or isophorone diisocyanates to obtain polyurethane containing soft hyperbranched polyether segments [666].

Interesting end capping modified amphiphilic hyperbranched polymers are synthesized on the basis of aliphatic polymer Boltorn H40, interior part and exterior shell of which contain hydrophobic PCL and hydrophilic PEG segments, respectively [667]. End capping of the surface of amphiphilic polymers using coupling reactions between hydroxyl group of the PEG segment and carboxylic group of folic acid provides carriers for cancer cells transport (Fig. 2.53).

Reaction of hyperbranched aliphatic polyester polyols of three generations with toluylene diisocyanate was used to synthesize respective hyperbranched poly(ester-urethanes) with end isocyanate groups [668].

Aliphatic hyperbranched polyethers synthesized from 2,2-bis(methylol)propi-onic acid and tris(methylol)propane are modified by end capping method using phthalic anhydride and trimellitic anhydride [587]. Oppositely to the initial, mod-ified polymers can form globular aggregates in the N,N-dimethylformamide (DMF)/ H_2O mixture due to their amphiphilic structure [669].

The end capping method was used for integration of reactive methacryloyl radicals to periphery of hyperbranched polymers produced from pentaerythritol as a «central core» and 1,2,4-benzenetricarboxylic anhydride and epichlorohydrin. The obtained hyperbranched polyethers have good solubility in alkalis and ability to photocuring.
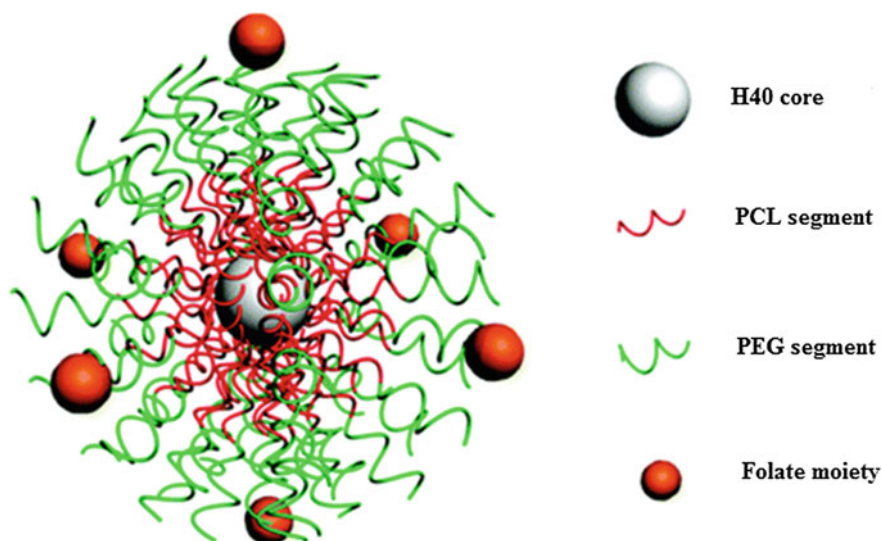
Fig. 2.53 End capping modified hyperbranched polymers

Hyperbranched poly(GMA) was efficiently functionalized along all polymer carrier by click chemistry methods such as azidation of oxiranes, thiol-epoxy, thiol-en, CuAAC and Menschutkin reaction (Fig. 2.54) [670]. This reactions bring to hyperbranched polymers containing chelating heterofunctional groups, including hydroxyl + azid, bi-hydroxyl, tri-hydroxyl, hydroxyl + tertiary amine, hydroxyl + alkene, hydroxyl + carboxyl, alkene + azid, alkyne + azid, hydroxyl + alkyne, bi-hydroxyl + alken, hydroxyl + carboxyl, alkene + azid, alkyne + azid, hydroxyl + alkyne, bi-hydroxyl + alkene, etc., and all of them with ∼100% conversion. Also double «thiol-epoxy + thiol-en» and triple «thiol-epoxy + Menschutkin reaction + CuAAC» click-sequences are possible, which makes modification of functional groups even more easily available.

The end capping method is also used for integration of chelating groups in arms of star polymers. Thus, DOTA (1,4,7,10-tetraazacyclododecane-1,4,7,10-tetraacetic acid) fragments were fixed on a polymer arms with a poly(dimethyl acrylamide-*co*-DVB) core with the following introduction of radioactive labels for biomedical purposes (Fig. 2.55) [671].

Terminal grafting relates to the «grafting-from» type of reactions. Grafted polymers from macromolecular initiators obtained by modifying functional groups of hyperbranched polymers give a core-shell poly-armed star polymers or hyperstars.
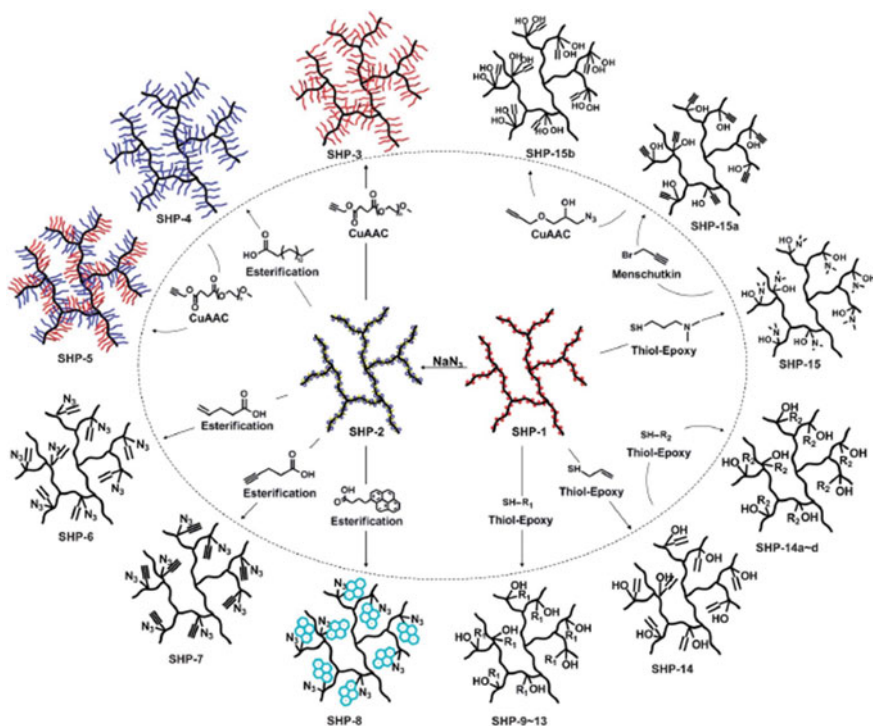
**Fig. 2.54** Click-sequences of functional groups of hyperbranched polymers
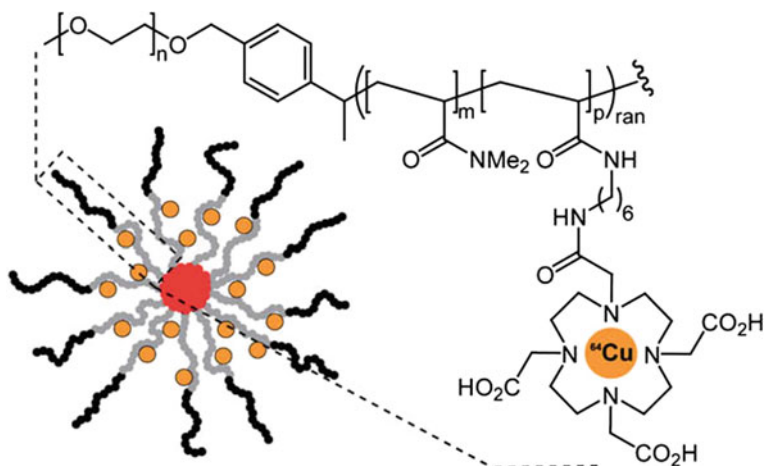
Fig. 2.55 Structure of DOTA-containing star polymers labeled with radioactive medium lived positron emitter ^{64}Cu

Some properties, such as polarity, solubility, and flexibility of the hyperbranched matrices can be controlled by modification using terminal grafting [672]. Three methods of polymerization (for example, anion, cation, and living/CRP) are applied to obtain hyperstars through reaction processes including macromolecular initiator and in situ grafting.

For example, series of liquid crystal copolymers with multi-armed star azobenzene side chains and hyperbranched core is synthesized by ATRP method via multifunctional hyperbranched polyether as initiator and chlorobenzene as a solvent [673]. Multifunctional hyperbranched polyether initiator is prepared based on poly(3-ethyl-3-(hydroxymethyl) oxetane) and 2-bromo-2-methylpropionyl bromide. Azobenzene side arms had liquid crystal conformation of poly [6-(4-methoxy-4′-oxy-azobenzene) hexyl methacrylate] with different molecular weights.

Method of modifying specific or interface surfaces with hyperbranched macromolecules or grafting hyperbranched polymers is called «surface growing» (Scheme 2.35). Hyperbranched grafted polymers can be considered as polymer brushes, which are usually linked to the surface with one end of a polymer chain, so that the polymer can spread from the surface. Surface grafting is efficient strategy for preparation of inorganic/organic hyperbranched polymer hybrid materials and functional devices for improvement of properties of surface objects.

Hypergrafting is a grafting of hyperbranched macromolecules to a multifunctional polymer core, and the obtained hybrid material is called hypergrafted polymer. If a linear polymer is used as a core, a new type of a comb-like polymer cylinder is formed. Hypergrafting method is used, for example, to obtain linear polyglycerol-*gr*-hyperbranched polyglycerol ($M_n = 1000$–4000) using AB_m monomers, from multifunctional, polydisperse macroinitiator cores by slow monomer addition [674].
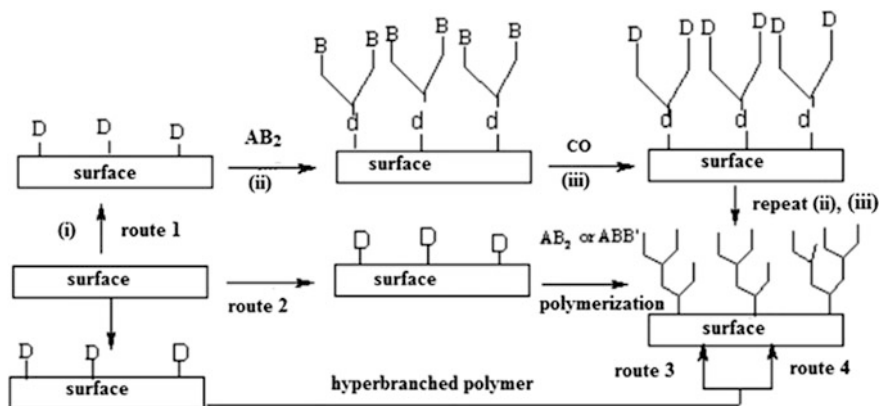
Scheme 2.35 Schematic representation of surface grafting

Hyperbranched polymers can be grafted also on other very different substrates. Thus, hyperbranched PAMAM is grafted on particles of resin powder from tire disposal, and the obtained product is well dispersed in water and can be used for curing and increase in impact resistance of epoxy resins [675]. It is noted grafting hyperbranched PEI of different molecular weight on the graphene oxide, which leads to promising adsorbents for potential use in the removal of Pb(II) ions from wastewater [676].

Design of biodegradable hyperbranched polymers are promising area of research, especially for biomedical applications. As an example, hyperbranched CPL synthesized using hybrid copolymerization of ε-caprolactone with GMA as the branching agent and (1-*tert*-butyl-4,4,4-tris(dimethylamino)-2,2-bis[tris(dimethylamino)phosphoranilideneamino]-2Λ^5,Λ^5-catenadi(phosphazene) as a catalyst in one step can be a typical example [677].

It can be concluded that though there is not yet complete clearness in many aspects of hyperbranched polymers formation, intensity of studies in this field guarantees that successful development of this task is beyond the question.

2.5   Polymeric Films as Chelating Macroligands

Recently a great attention has been given to such an interesting class of CPLs as polymer films [21, 678–685]. Apart from profoundly studied areas of practical applications of polymer films (semi-transparent membranes, electrode materials in chemical current sources, preserving and packing materials, including anticorrosive ones, etc.) incorporation of a rigidly bound metal in their structure opens more possibilities for practical usage. No less important is the fact that some conjugated

polymer films, polyaniline in particular, are commercially produced in large quantities, because, as compared with inorganic materials, they are less expensive to be applied in many electronic and optoelectronic devices such as semiconductor, transport, electroluminescent and photocell elements. It should be noted that many polymer films are related to nanometer materials; therefore, different nanometer effects can be used to produce films with considerably optimized or improved properties [686].

A wide range of practical tasks solved using polymer films or polymer coatings deposited on different substrates requires different fabrication methods, which can be divided into three groups. The first one supposes using of preliminary formed polymer having chelating functionalities for production of films. The second group includes different methods of assembling of polymer films from low molecular weight substances with chelating fragments. And, the last, third group includes different methods of PSM of preliminary produced inert or monofunctional films for development of chelating units.

2.5.1 Polymeric Films Based on Pre-formed Chelating Macroligands

The first group of these methods relates to multistage processes, because it includes stages of production of a CPL, its purification, and processing into a film or deposition on a substrate [21, 582, 684, 685, 687]. The main used approaches are: submerging method, «drop evaporation» method, oxidation or reduction deposition, spin-coating, etc.

The submerging method is based on holding of a substrate in a polymer solution for some time, during which molecules are adsorbed and a film is formed on a surface. Thus obtained films are stuck to the surface due to chemisorption and low solubility of the formed coatings in a solution applied. This method was used, for example, to obtain thin highly transparent homogeneous films based on copolymers containing alternating ion-conducting segments of 24-crown-8 conjugated with light-emitting fragments of 1,5-distyryl naphthalene [688]. Flexible transparent films are also prepared on the basis of polymers containing dibenzocrown ethers in the main chain, having aliphatic (C_{10-16}), aliphatic-aromatic, or oxyindole spacers. It should be noted that in these polymers supramolecular structures are formed [689].
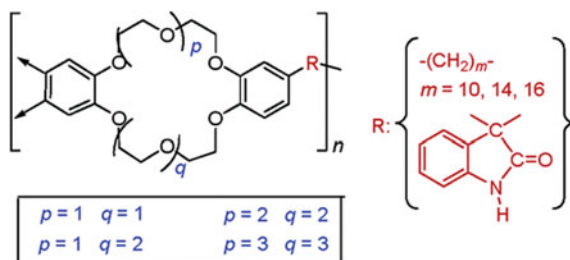
When forming polymer chelating films from solutions using the submerging method, one starts from very simple approaches for thick film fabrication to more sophisticated methods of thin film production, even to multilayered, and then to monolayers. However, when using this method, often films with non-uniform thickness are formed depending on viscosity of liquid, evaporation rate of a solvent, etc. Films with good processability caused by high solubility of polymers in polar aprotic solvents can be obtained by evaporation of a solvent from CPL solutions. Thus, for example, polyamide films were obtained from monomers based on isophthalic diacids, containing a benzo-12-crown-4 unit as a side group or benzo-dipodand subunit in the side structure, which represented an opposite part of alicyclic crown ether with an open chain [690]. To form films, solutions with 10% concentration of a polymer are needed, and a solvent is removed by heating at 100 °C for 4 h in air-circulating oven and then at 120 °C for 4 h in vacuum.

The drop evaporation method is used for modification of electrodes with small surface areas. Drop deposition of several micro-liters of a polymer solution of a certain concentration with the following evaporation of a solvent makes it possible to obtain a film, which is well reproducible by amount of the polymer and its composition. Structural homogeneity of a film depends to a great extent on the evaporation procedure: the latter should be rather slow. Composition of an initial film (including chelating groups) can be changed during its treatment by a respective reagent by the same «drop evaporation» method. Thus, to increase stability of PEI film in acid solutions, it is treated by dibromobutane solution in isopropyl alcohol, which brings to cross-linking of the polymer and decrease in its solubility with low pH [691].

The essence of the spin coating method is that a CPL is solved in appropriate solvent, and the solution is spun. A spin coating is the preferable way for deposition of thin, homogeneous films on plane substrates. It has been applied, in particular, for coating of a quartz glass by polymers containing chelating spun bpy and planar phen fragments. M_n of these polymers are 11,000 and 13,000 (PDI $\approx$ 1.5), respectively [692]. The chelating bpy fragment was incorporated into spin-coated films made of regioregular conjugated polymers including alternating 3-alkylated oligothiophene and bpy [693].
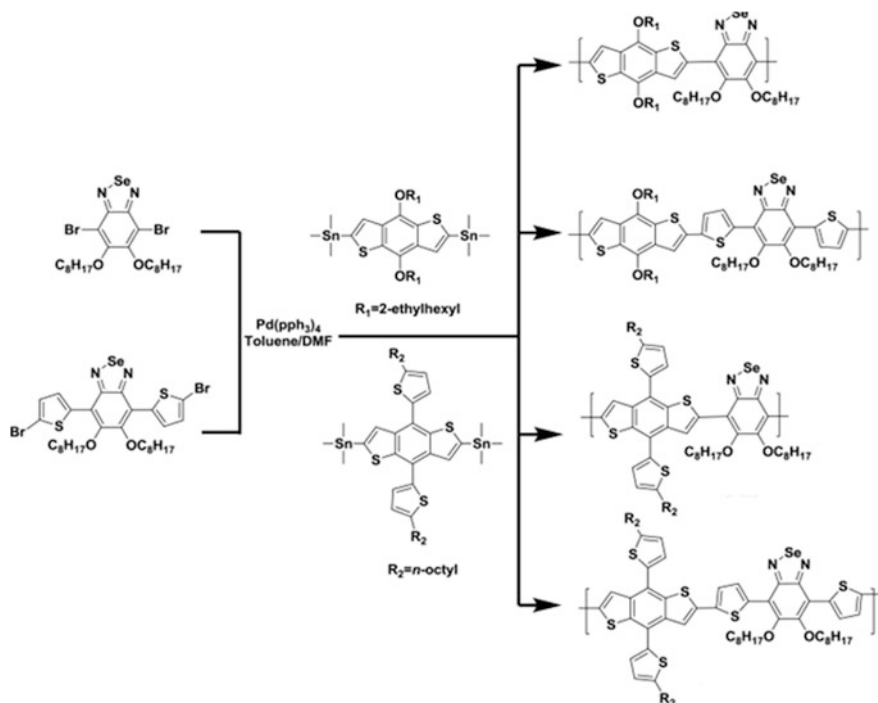
Scheme 2.36 Synthesis of 2,1,3-benzoselenadiazole-based conjugated polymers

Spin-coated thin films **I** and **II** are also obtained on the basis of 4-ethynyl-2,6-bis (pyrazolyl)pyridine (BPP) copolymers with fluorene in the main chain and M_n about 10,000 [694].

2,1,3-Benzoselenadiazole-based conjugated polymers are soluble in ordinary organic solvents and can be spin-cast for formation of smooth homogeneous thin films (Scheme 2.36) [695].
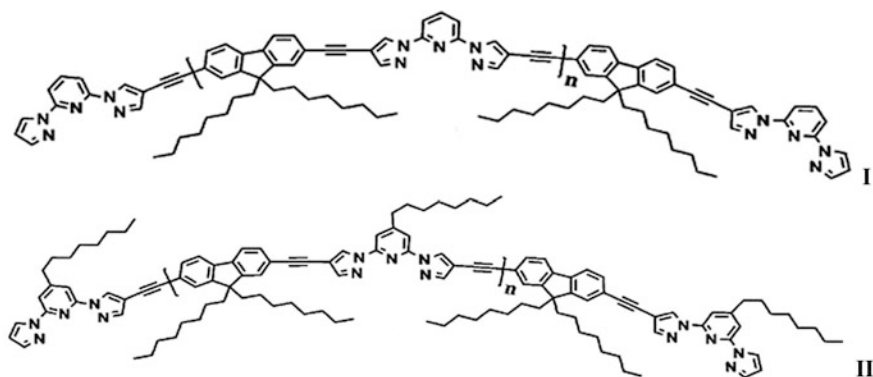
Thin films (9–70 nm) of a range of polymers, which contain in the main chain a dibenzo-18-crown-6 block linked with aliphatic spacer of different lengths (C_{10} or C_{14}) and origins, are prepared from chloroform solutions by spin coating on a silicon substrate. Geometry pattern of the grazing incidence small angle X-ray scattering (Fig. 2.56) correlates with a size of out-of-plane structure and with the length of repeated unit of the polymer. Heat treatment of the samples improves nanostructures due to increase in number of lamellate consistencies and vertical orientation of molecular columns [696].

Simultaneous copolymerization and film formation are performed in aqueous solution with addition of an oxidant (ammonium persulfate) for obtaining ultra-thin self-doped polyaniline films based on substrate of indium-tin oxide (ITO). The used monomers were aniline and its derivative o-aminobenzenesulfonic acid. Rate of the film formation depends on the monomers ratio: the rate is higher at higher concentration of aniline, and the film thickness is determined by duration of assembling and temperature [697].

In order to deposit monomolecular layers, Langmuir-Blodgett (LB) method is used, which gives name to thus obtained films. Phthalocyanines with substituents containing hydrophobic and hydrophilic groups are used for creation of monomolecular layers [698]. Soluble fluorine-containing polyamidoimides are obtained from 2,2-bis [N-(4-carboxyphenyl)-phthalimide-1,4-il] hexafluoropropane and different diamines as LB multilayers [699].

One of the methods of synthesis of multilayered films is based on gradual LbL deposition of molecular layers. For example, when designing solid solar cells of the sandwich type from polythiophene-Pp composite films, at the first stage a spin-coated film of poly(3-dodecylthiophene) on a gold electrode is obtained [700]. Then a layer of electrochemically produced bithiophene film is deposited on it, and at last, a tetrathienyl-Pp film is obtained on the top using the same electrochemical polymerization (1 or 10 cycles) in order to fabricate gold electrodes modified by polythiophene-Pp film. An aluminum electrode was deposited on the obtained polythiophene-Pp film by vacuum sputtering forming sandwich-like solid solar cells.
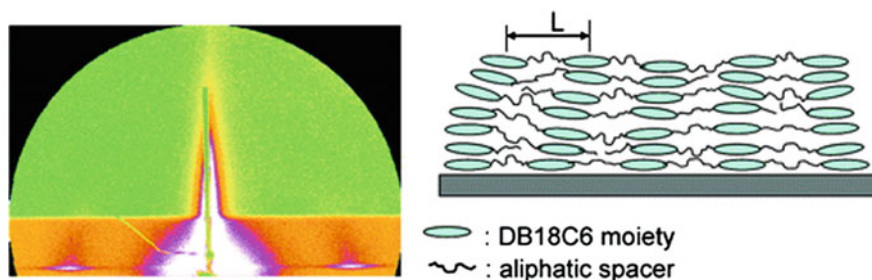

Fig. 2.56 The grazing incidence small-angle X-ray scattering patterns and out-of-plane structure (interference maximum near the horizon) of the polymer repeating unit in the main chain dibenzo-18-crown-6 linked to an aliphatic spacer of different length

2.5.2 Assembly of Polymeric Films from Chelating Monomers

The most widely spread methods of assembling polymeric films from low molecular weight compounds with chelating functionalities are chemical, electrochemical, plasma-chemical, and photopolymerization methods.

Thus, chemical polymerization was used to obtain films of poly(1,8-diaminonaphthalene) on a porous polycarbonate membrane, which can serve as a template for synthesis of nanometer structures [701]. At that, poly(1,8-diaminonaphthalene) obtained using the method of chemical polymerization is closer by its properties to electrically synthesized polymer. Moreover, in aqueous solutions nanowires were formed, as well as two types of structures, nanowires and round shaped structures not fitting to pore size, can be obtained by chemical polymerization in acetonitrile solution.

Resulting in optimal conditions of chemical polymerization (oxidizer—ammonium peroxydisulfate) film of aniline and o-aminophenol have good conductivity and high electrochemical activity to pH 11.0 with a wide potential region (from −0.20 to 0.80 V). Among all the factors that affect the properties of the copolymers, the ratio of o-aminophenol/aniline concentrations is a major [702].

Chemical co-polymerization of aniline with o-anthranilic acid in aqueous solution of hydrochloric acid can be applied for production of copolymer films in situ by submerging an object glass into polymerized medium [703, 704]. It is established that presence of o-anthranilic acid has an effect on the yield, the induction period, the time of transformation of monomers and the growth rate of film formation.
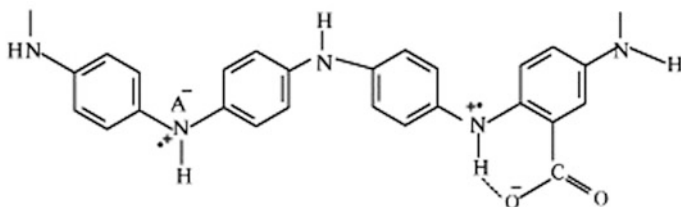
Electrochromic copolymers based on o-phenylenediamine and aniline are easily formed by chemical oxidized polymerization [705]. Coefficients of reactivity of o-phenylenediamine and aniline are 9.70 and 2.74, respectively, showing stronger tendency to homopolymerization than to copolymerization between them. The copolymers have a much greater plasticity and uniformity of the film, as well as higher electroactive and electrochromic best tricolor than homopolymers. Thus, the film of the copolymer containing 50 mol% of o-phenylenediamine is red at −0.5 to 0 V, then becomes green in the range of 0 to +0.6 V, and then blue from +0.6 to +1.35 V (Fig. 2.57).

Fig. 2.57 Current versus potential relationship and electrochromism of *o*-phenylenediamine/aniline copolymers
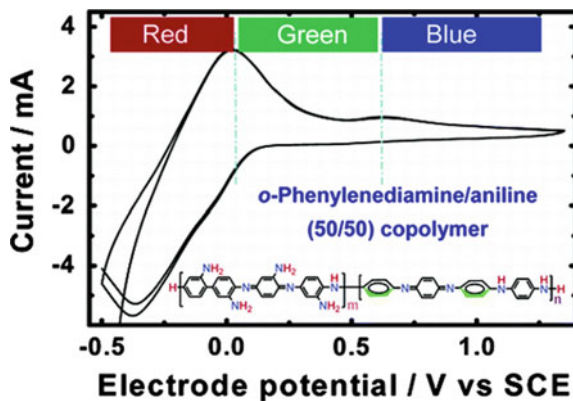
The method of electrochemical polymerization is most widely used for production of CPL films. First, films are formed directly on an electrode surface, and the product of reaction, electroactive film, has high electric conductivity. Secondly, electrosynthesis provides high current yield and strict stoichiometry of the process, therefore a film of a required weight and thickness is obtained. Thirdly, properties of a polymer film can be controlled during its synthesis [691].

Electrochemical polymerization is an elegant, attractive, and easy strategy for immobilizing chelating fragments on electrode surfaces [706]. This principle is based on electrochemical oxidation (or reduction) of preliminary obtained monomers for formation of polymer films containing chelating units. The obtained polymer films should be electron conductors to provide electron transport in matrix (and then following polymer growth). The most often used chelating monomers are derivatives of *o*-aminophenol [680] and *o*-phenylenediamine [184].

Mechanism of electrochemical polymerization of these substituted monomers is not completely explained, despite of a great number of data in this field. However, presently it is generally recognized that the first stage in the electropolymerization process is electro-oxidized formation of a cation-radical from a chosen monomer. The oxidation reaction is continued by dimerization process, and the following reactions of oxidation and coupling. This brings to formation of oligomers and polymers on the electrode surface. It is also clear that morphology and physical properties of CPL films depend, first of all, on conditions of electrochemical polymerization.

Using three methods (cyclic voltammetry, potentiostatic and potentiodynamic methods), electrocatalytic oxidative polymerization of *o*-phenylenediamine at the electrode reduced graphene oxide/glassy carbon, in which reduced graphene oxide acts as a catalyst, was carried [707].

5-Amino-phen can be polymerized electrochemically forming electro-conducting polymer using potentiodynamic or potentiostatic method on different electrode substrates: composite, formed by carbon paste in epoxy matrix, carbon glass, or an electrode made of polycrystalline gold [708]. Poly(aminoanthraquinone) films

which were successfully applied as analytical sensors for Ce(III) ions were obtained using the same methods [709].

Electropolymerization of 3-amino-5-mercapto-1,2,4-triazole on a carbon glass electrode in 0.1 M H_2SO_4 solution [710] is used to form nanostructured films, while uniformly conducting polymer films from poly(N-(1-naphthyl) ethylenediamine dihydrochloride) are easily and reproducibly prepared by anode oxidation of a monomer in the acid aqueous solution [711], and head-to-tail polymerization of the monomer was observed. One-stage method of potentiodynamic deposition is a convenient way for production of poly(1,5-diaminoanthraquinone)/reduced graphene oxide nanohybrides, in which 1,5-diaminoanthraquinone and graphene oxide are initial materials [712]. Poly(1,5-diaminoanthraquinone) displays a barleycorn-like structure and is covalent grafted to the surface of the reduced graphene oxide (Fig. 2.58).

Poly(o-aminophenol) films were potentiostatically produced at different potentials of electrodes in acid aqueous solution [713].

Numerous studies were performed on electrochemical polymerization of monomers containing chelating o-phenylenediamine fragment. Thus, electropolymerization of o-phenylenediamine on Pt electrode was carried out from deoxygenized water-acid medium by cyclic voltammetry method [714]. The kinetic equation $V = k$ [monomer]$^{1.19}$[acid]$^{1.23}$[electrolyte]$^{0.87}$ is obtained from the value of anode current density using cyclic voltammetry measurements. Apparent activation energy is 28.34 kJ mol^{-1}. Electrochemical polymerization of two derivatives of 2,5-di (2-thienyl)-1H-pyrrole, in pyrrol cycle of which of 3-pyridine or phen units are contained [715], was used for preparation of conducting polymer films on a carbon glass electrode, their maximum electric conductivity is $(6.5–9.2) \times 10^{-2}$ C cm^{-1} (1.4 V). Color of the pyridyl films changes from brown-yellow to deep blue at transition from the neutral state to the oxidized. Similarly, phen films were green-yellow ($\lambda_{max} = 451$ nm) in neutral state and light blue (1.4 V) in entirely oxidized
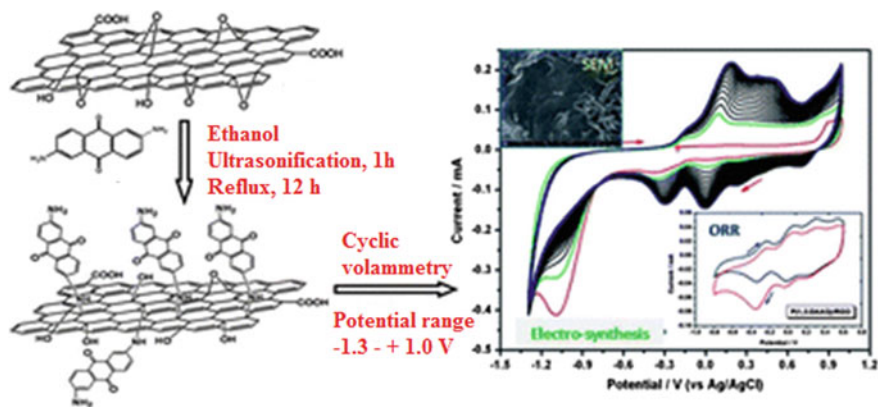
Fig. 2.58 Covalent grafting 1,5-diaminoanthraquinone to the surface of the reduced graphene oxide and current versus potential relationship of grafted polymers
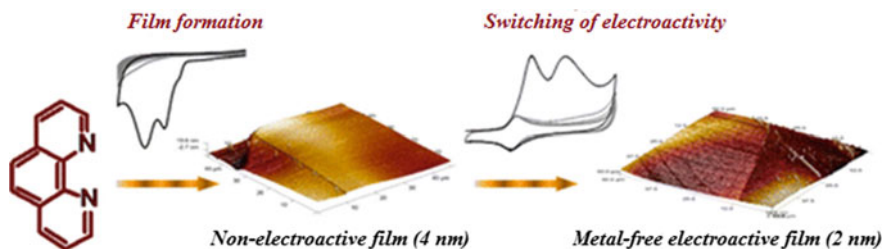
Fig. 2.59 Scheme of electrochemical reduction of phen

state. Electrochemical reduction of phen in water-acid electrolyte on a carbon glass electrode brings to covalent modification of the electrode (Fig. 2.59) [716]. After that, the deposited film can be switched to electroactive form using electrochemical oxidation. Electroactive film can also be generated by alternative reduction and oxidation voltammetry cycles of phen solution in aqueous sulfuric acid.

Electropolymerization of *o*-phenylenediamine in Ils, 1-ethyl-3-methylimidazolium bromide and *N*-methylimidazolium tetrafluoroborate, on a carbon glass electrode performed using cyclic voltammetry is interesting regarding green chemistry principles [717]. An example of biocatalytic electropolymerization can be polymerization of *o*-phenylenediamine on a carbon glass electrode, whose surface has been modified by grafting of L-tyrosine [40]. The obtained modified electrode has high electrocatalytic response to presence of ascorbic acid and is used to find concentration of ascorbic acid in vitamin C pills. It should be noted that a great number of CPL films, in particular, based on derivatives of *o*-phenylenediamine and 3,4-ethylenedioxythiophene are applied as biosensors [718].

Platinum disc microelectrode (50 μm in diameter) [719] and glassy carbon electrode [720], modified by PPD, were used for H_2O_2 sensors, and electrically synthesized PPD was used for support of Prussian blue high-disperse layer [721]. The observed high stability of Prussian blue as a catalyst of H_2O_2 decomposition is due to presence of organic polymer in the microstructured composite film. The results give an idea on design of high sensitive, stable, and free of noise biosensors.

Another interesting chelating monomer is 2,6-diaminopyridine, its electrochemical polymerization was performed using cyclic voltammetry in sodium hydroxide aqueous solution [722]. In the produced films interpenetrating network structure is formed, which is possible on doping of the polymer anions during oxidation, or, on the contrary, during reduction.
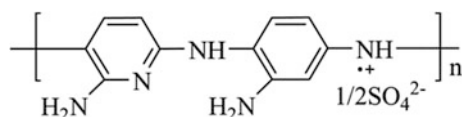
Based on this polymer, electrochemical sensor for detection of ascorbic acid is designed. First, a layer of poly(2,6-diaminopyridine) is deposited on the surface of a carbon glass electrode by electropolymerization technique, then negatively charged nano-gold and positively charged 2,6-diaminopyridine were alternately adsorbed on the modified electrode using LbL method. The sensor is characterized by high electrocatalytic activity of ascorbic acid oxidation by bi-layered 2,6-diaminopyridine film, thus providing abundant amino groups and positive charge, which advance electron transfer between the electrode and ascorbic acid, and increase sensitivity of the electrode [723]. Mediator-less ammeter biosensor of H_2O_2 is also prepared by immobilizing horseradish peroxidase enzyme on platinum wire electrodes coated by colloid gold and modified by 2,6-diaminopyridine. The studied biosensors show high selectivity, good stability, and reproducibility in design [724].

An example of electrochemically produced CPL with bpy fragment are stable polypyrrol films containing fragments of 4,4′-dimethoxy-bpy and are obtained using electropolymerization at the anode potential from −0.51 to −0.35 V and cathode wave value −0.77 V [725].

Numerous works are concerned with modification of surface of the electrodes with phen fragments. Thus, carbon glass surfaces are modified by phen derivatives, such as 5-amino-phen and 5,6-diamino-phen, using cyclic voltammetry scanning from +1.2 to +2.7 V [726]. Surfaces having phen chelating ligands with different functional groups are promising for detection of transition metal ions. Carbon glass electrodes are modified electrochemically by poly(5-nitro-phen) and poly(5-amino-6-nitro-phen) layers (Fig. 2.60) for designing sensors for heavy metal ions (new sensor platform) [727]. In particular, this was demonstrated by formation of
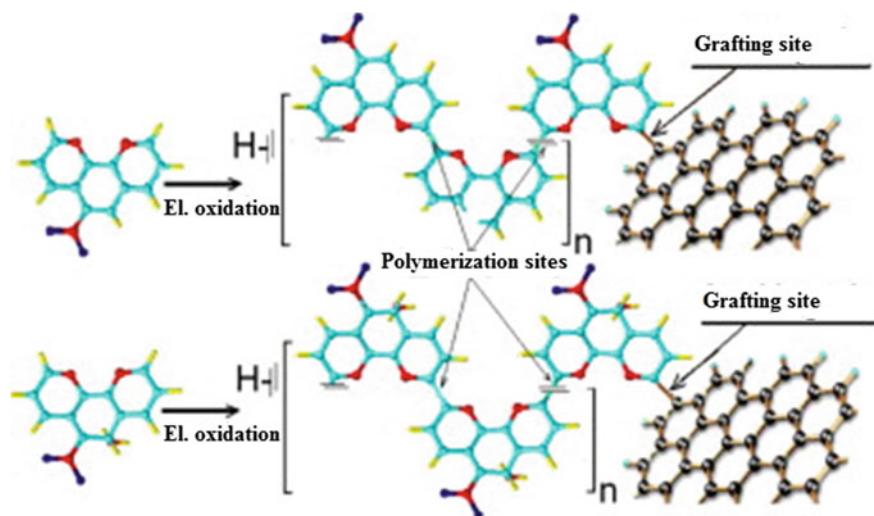
Fig. 2.60 Scheme of electrochemical polymerization of phen on carbon glass

chelates between carbon glassy-grafted poly(5-nitro-phen) and poly(5-amino-6-nitro-phen) layers and Cu(II) ions.

Electrochemical modification of a carbon glass electrode by phen groups is performed in two ways: reduction of respective diazonium ions and reduction of phen (Fig. 2.61) [728]. Initially grafted electrochemically inactive organic film becomes electrically active after it is subjected to electrochemical reduction and oxidation. At that thin homogenous phen films (<2 nm) are deposited on the surface of pyrolysis photoresist film electrode.

Electrochemical synthesis is used for production of a chelating ligand of *N,N*-type, poly(3-amino-1,2,4-triazole) on Pt electrode [729] in ammonium oxalate solution.

Poly(1-amino-9,10-anthraquinone) chelating films were prepared by electrochemical oxidation of a monomer in sulfuric acid solution [730] or in acetonitrile using $LiClO_4$ as a background electrolyte [731]. The same ligand also was electrically polymerized on platinum substrates from aqueous solution of hydrochloric acid or nonaqueous electrolytes [732, 733]. Both in water and in nonaqueous solutions the electropolymerization process obeys to the first order kinetics with respect to concentration of a monomer (Fig. 2.62).

Nanowires based on poly(1-amino-9,10-anthraquinone) were directly synthesized on a steel electrode preliminary modified by a thin film from poly(1-amino-9,10-anthraquinone-*co-o*-phenylenediamine) through SiO_2 mesoporous template (Fig. 2.63) [734]. It is shown that after removal of the template, nanowires of about 30 nm in diameter and 200 nm in length were fixed to the surface of poly(1-amino-9,10-anthraquinone) with high adhesive strength of polymer nanostructures.

A series of cross-linked poly(2-hydroxyethyl methacrylate) films containing 1,2-diaminoanthraquinone is synthesized for optical biomedical analysis of nitrites (nitrite-monitoring of biological liquids) and ecology (control over nitrite level in drinking water) [735].
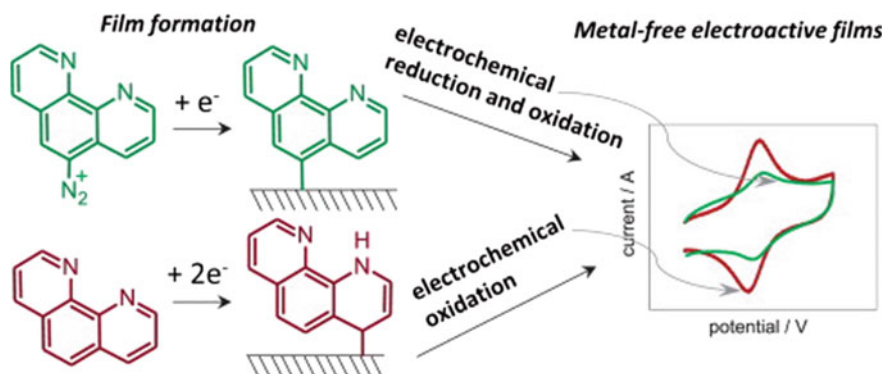
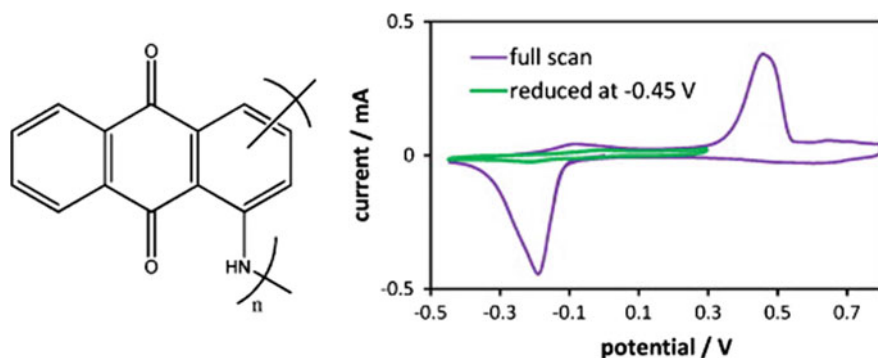

Fig. 2.61 Modification of carbon glass electrode

Fig. 2.62 Poly(1-amino-9,10-anthraquinone) synthesized using electropolymerization
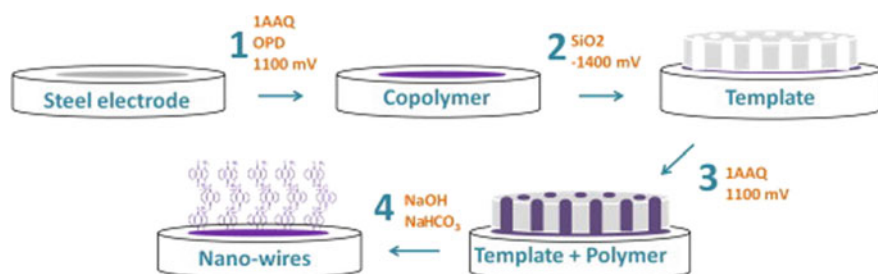

Fig. 2.63 Production of nanowires based on poly(1-amino-9,10-anthraquinone) through SiO₂ mesoporous template

Electrochemical method was used to obtain donor-acceptor π-conjugated polymers with 2,3-di(2-furyl) quinoxaline chelating fragment: poly [2,3-di(2-furyl)-5,8-bis(2-(3,4-ethylenedioxythiophene)) quinoxaline], poly [2,3-di(2-furyl)-5,8-bis(2-thienyl) quinoxaline] and poly[2,3-di(2-furyl)-5,8-bis(2-(3-methoxythiophene)) quinoxaline] [736]. All synthesized polymers contain 2,3-di(2-furyl) quinoxaline unit in the main chain as acceptor block and different derivatives of thiophene as donor aggregates. Colorimetric analysis showed that the first and third polymers were green in the neutral state unlike the second polymer, which has a light blue color.
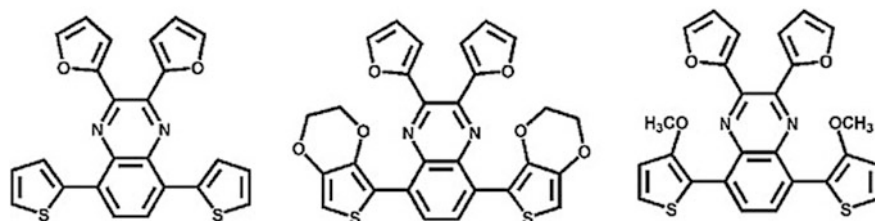
Poly(*o*-aminophenol) is produced electrochemically in previously deoxygenated acid medium. Initial rate of the reaction of electropolymerization on a platinum electrode is low and obeys to the equation $V = k_2[D]^{0.50}[HCl]^{1.125}[M]^{1.29}$. Apparent activation energy is 68.63 kJ mol^{-1} [737].

Electrochemical oxidation of *N,N′*-bis(3-methoxy-salicylidene)-1,3-propylendiamine brings to formation of a conducting CPL on the electrode surface [738, 739]. Similarly, 2,5-di-thienylpyrrole monomers containing salicylidenaniline fragments are electrically polymerized with formation of electrochromic conjugated films [740].
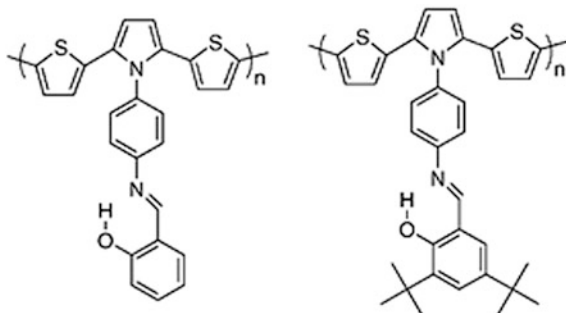
CPL films of N,S-type are deposited in situ on the surface of a carbon glass electrode using electrochemical oxidation of 2-mercapto-4-amino-5-cyano-6-phenylpyrimidine [741]; the polymer film consists of homogenous nanoparticles. Another chelating monomer of N,S-type, 2-aminothiazole is polymerized on Pt electrode using cyclic voltammetry from 0.01 M monomer solution containing 0.3 M ammonium oxalate solution with formation of homogenous and compacted film [742]. Poly(2-aminobenzothiazoles) are obtained by electropolymerization with 2-aminobenzothiazole and 6-ethoxy-2-aminobenzothiazole used as monomers [743].

Chelating 2,3-di(2-thienyl) quinoxaline fragment was included in an electrochemically synthesized conjugated polymer [744]. The similar chelating 2,3-di (2-thienyl) quinoxaline fragment is contained in some other monomers: 10,12-bis (4-hexylthiophen-2-yl)dibenzo[f,h]thieno[3,4-b] quinoxaline and 10,13-bis(4-hexyl thiophen-2-yl)dipyrido[3,2-a:2′,3′-c] phenazine [745]. We shall focus on electrochemical polymerization of sulfur monomers of 8,11-bis(4-octyl-2-thienyl)-acenaphthyl-[1,2-b] quinoxaline and 8,12-bis(4-octyl-2-thienyl)-acenaphthyl- [1,2,5] thiadiazolo[3,4,i]quinoxaline [746], as well as 6-(4-octyloxyphenyl)-4,8-bis(thiophene-2-yl)-3H-[d]imidazole [1,2,5] benzothiadiazole, and 4-(4-octyloxyphenyl)-2,6-bis (thiophene-2-yl)-3H-[d]imidazole-acenaphtho[1,2-b] quinoxaline [747]. The fluorescent polymer having reversible redox behavior, based on terthienyl with quinoxaline group directly linked to the third position of the central thiophene ring, is synthesized by electrochemical polymerization of 4-(2,5-bis(2,3-dihydrothieno[3,4-b] [1,4] dioxin-5-yl)thiophen-3-yl)pyrrolo[1,2-a] quinoxaline [748]. This polymer studied by fluorescence technique is selective with respect to Fe(III) ions (Fig. 2.64).
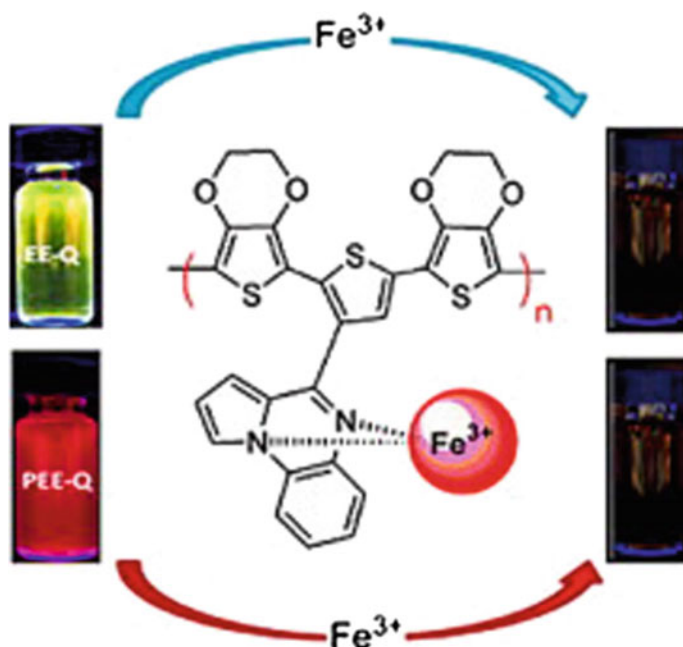
Fig. 2.64 The fluorescent polymer having reversible redox behavior, based on terthienyl with quinoxaline group, as a selective sensor with respect to Fe(III) ions

Electrochemical polymerization of 4-[(2,5-dithiophen-2-yl)thiophen-3-yl] pyrrol chelating monomer leads also to a fluorescent polymer [749].

Study of electropolymerization of protoporphyrin IX on highly oriented pyrolytic graphite (HOPG) showed [750] that Pp are adsorbed on electrode and are spontaneously self-assembled in ordered monolayers. Depending on origin of the substituents on periphery of the Pp ring, reduction of substituted tetraphenyl-Pp takes place in the range of negative potentials as a result of formation of π-anion radical and di-anion, and oxidation of Pp with formation of π-cation-radical and di-cation proceeds in the range of positive potentials [751]. In the case of tetrakis (*p*-aminophenyl)-Pp poly-Pp film is formed on electrode during electrooxidation. Electrochemical polymerization of the asymmetric 5,15-bis[4(-*N,N*-diphenylamino) phenyl]-10,20-bis[3-(*N*-ethylcarbazoyl)]-Pp with electrically active functionalities brings to formation of conjugate conductive and stable polymer films on the surface of semi-transparent ITO electrode [752], which makes them promising candidates for application in optoelectronic devices.

Electropolymerization of another Pp monomer, 5-(4′-aminophenylamino)-10,20-diphenyl-Pp, with amino group linking the Pp core and the aniline block makes it possible to obtain a polymer film forming a smooth layer on ITO and growing in

normal direction to the electrode surface [753]. ITO electrode coated by electrochemically prepared film of poly(tetrathienyl)-Pp is photoactive electrode in photoelectrochemical cell of Z-scheme type [754].

Electrochemical polymerization of tetra-(4-hydroxyphenyl)-Pp on ITO brings to formation of films with nanostructured morphology [755], the same is attributed to electropolymerization of poly-1,3-bisdithienyl benzene, having a Pp group as a side chain [756] and to electropolymerization of Pp-fullerene monomer [757]. In this polymer the Pp blocks are linked via amino-phenyl group with formation of a linear chain, in which Pp is integral part of the main chain of the polymer. Chelating monomers obtained by interaction between Pp in 5,15-positions with tetra- and bithiophene are electrochemically polymerized on gilt electrodes [168].

A crown ether ring is contained in tetra-methyl-substituted 14-crown-4-3,4-pyrrol chelating monomer, which has been electrochemically polymerized for studying a possibility of its using as a sensor for lithium ion [758].

Highly efficient CPL are formed during electrochemical co-polymerization of chelating monomers with traditional monomers. Thus, copolymers of *o*-phenylenediamine and other aniline derivatives (for example, *o*- and *m*-toluidines [759–764]) were widely studied for improvement of chelating properties of homopolymers. In particular, in the case of *o*-phenylenediamine and *o*-toluidine copolymer obtained in aqueous solution of acid on ITO-coated glass electrode, a band at $\lambda = 497$ nm was assigned to head-to-tail mixed copolymer formed as a result of a cross-reaction between *o*-phenylenediamine and *o*-toluidine cation-radicals.

Poly(1-amino-9,10-anthraquinone-*co-o*-phenylenediamine) is synthesized using electrochemical method on stainless steel electrodes [765]. Topographic and morphologic characteristics have shown that incorporation of *o*-phenylenediamine increases homogeneity of a copolymer. Electrochemical copolymerization of aniline with 1-amino-9,10-anthraquinone showed formation of a clear picture of nanometer polymer particles up to 100 nm formed in conducting copolymers [766].

Electroactive copolymers of aniline and *o*-aminophenol were obtained on ITO-coated glass and gold electrodes [767] as well as carbon glass electrode modified by multi-walled carbon nanotubes (MWCNT) [768]. Copolymerization rate and properties of a copolymer depend strongly on the ratio between aniline and *o*-aminophenol [769], as in the case of copolymerization of aniline with anthranilic acid [770, 771] or 2-aminodiphenylamine [772].

There is interesting electrochemical copolymerization proceeding through formation of a cation-radical of diphenylamine with chelating monomers 2,5-diaminobenzene-sulfonic acid [773], anthranilic acid [774, 775], and *o*-phenylenediamine [776].

Pyrrol and anthranilic acid copolymers with block structure have been produced by electrochemical method: order of the reaction by electric current density, HCl concentration, and monomer concentration is 1.02, 1.44, and 2.0, respectively. Pyrrol has the coefficient of relative reactivity to copolymerization 1.58, while anthranilic acid has 0.14 [777].

Photoluminescent and electroluminescent spectra of poly(N-vinyl-Cz) and 2,9-dimethyl-4,7-diphenyl-phen (1:1) films are studied [778].

Electrochemical copolymerization of Cz and dibenzo-18-crown-6 into pure boron trifluoride diethyl etherate was carried out using direct anode oxidation of monomer mixtures on electrodes made of platinum or stainless steel [779]. The copolymer films showed better electrochemical behavior as compared with homopolymers, they displayed excellent fluorescent properties, and good mechanical properties, and had higher thermal stability and higher electric conductivity.

Tuning of chelating groups of thin films of SP-containing copolymers for color-specific linking of a metal ion is performed using two monomers: SP-methacrylate and SP-methacrylate with methoxy-substitutent in 8′-position of benzopyran ring [780]. MMA and 2,2,2-trifluoroethyl methacrylate were chosen as comonomers. It has been shown that each metal ion generates unique calorimetric reaction for SP-containing copolymers.

A conducting polymer containing MC in the polymer backbone was prepared by electropolymerization of a SP fragment covalently linked between two alkoxythiophene units. Utilizing the known metal coordination capabilities of MCs, introduction of cobalt ions into the electropolymerization led to an enhancement of the morphology, conductivity and optical properties of the PMC films (Fig. 2.65) [781].

The main advantage of electrochemical methods is their one-stage approach, in particular, a possibility of exclusion from the technological scheme stages of preliminary synthesis of polymer material, it's following dissolution or dispersion and fixing on a substrate, uniting all these stages in one process. Another important property is that electropolymerization makes it possible to deposit at high rate uniform polymer coatings on substrates with complicated configuration. The third positive factor is a possibility of automation of these processes.

At the beginning of 1990s, when polymer films produced using chemical and electrochemical methods from aniline, pyrrol, Py, thiophene and their derivatives were already widely studied and produced on the industrial scale, a range of works appeared concerned with their plasma-chemical synthesis [21, 782]. Increased attention in this method is explained by the fact that is provides production of thin uniform in thickness structures with a small number of macroscopic defects on substrates of any form and origin. At that, because solvents, surfactants and oxidants are not used, the problem of polymer purification does not arise. Deposition of CPL using polymerization in low-temperature plasma provides fabrication of thin functional layers of thickness from 0.001 to 10 μm using a relatively simple technique of vacuum deposition. Thus, plasma polymerization of en is studied for modifying surface of quartz particles for optimization of concentration of nitrogen-containing coatings produced through rotating barrel of a plasma reactor [783]. Uniform distribution of chelating groups over all surface of a particle is shown. Plasma polymerization of 1-amino-9,10-anthraquinone in electric discharge to a conducting polymer (1×10^4–$1 \times 10^5\ \Omega\,\mathrm{cm}^{-1}$) of highly conjugated structure has been carried out [784].
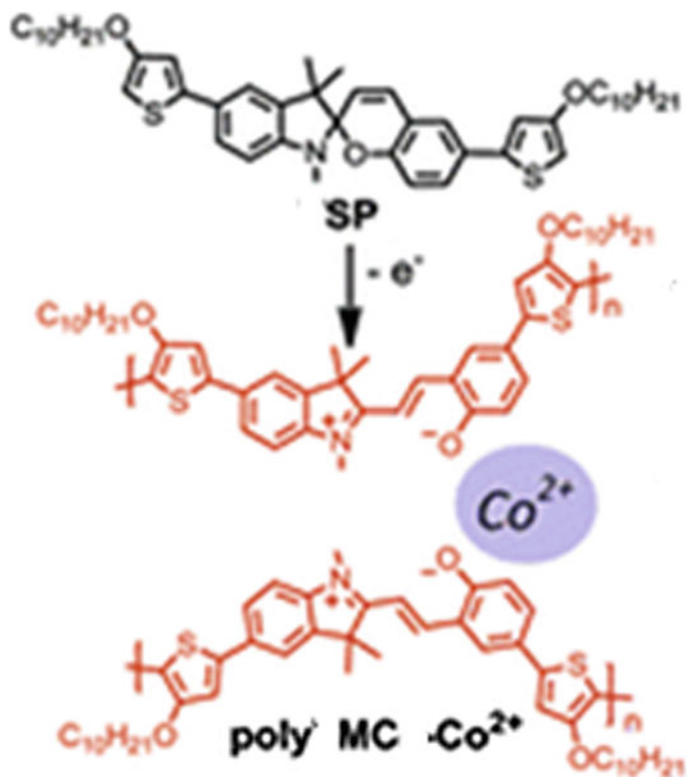
Fig. 2.65 A MC-based conductive polymer prepared by electropolymerization of a SP moiety covalently linked between two alkoxythiophene units and forming chelates with Co(II) ions

To produce CPL based on polymer films, cationic photopolymerization occurs to be a successful method. Thus, it has been shown that photopolymerization of tetra-alkylepoxy-Pp takes at least 10 min of illumination at 90 °C, while thermal polymerization of the same sample takes 10 min of heating in dark at the temperature 150 °C. Tetra-alkylepoxy-Pp acts as a self-sensitizer for cationic photopolymerization [785]. Cationic photopolymerization of liquid monomers based fullerene and Pc was used to obtain polymer films suitable for using in complex solar cell constructions (Fig. 2.66) [786].

2.5.3   Chemical Modification of Polymeric Films

A special place among methods of design of CPL films on solid surfaces has chemical modification (functionalization). Thus, modification method for surfaces of PE films by integration of chelating carboxylic acids, in particular, PAA (using
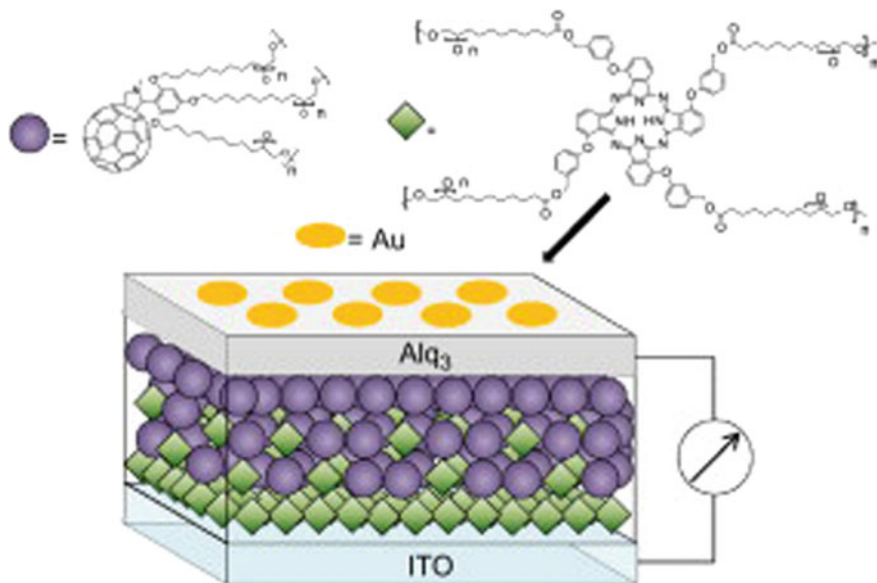
Fig. 2.66 Complex solar cell constructions using polymer films based on fullerene and Pc

PEI or en cross-linking agents) is proposed [787]. The modifying PAA content is
9.12 ± 0.71 mmol of carboxyl groups per 1 cm^2. Modified surface of a PE film has
higher affinity to Fe(III) ions than to Fe(II) ions at optimal binding pH 5. These
CPLs can be applied in chelatotherapy using heavy metals. Modification of PP films
can be performed in a similar way. Chelating ability of films is adapted by changing
conditions, for example, grafting density [788]. Even higher chelating activity
can be reached by transformation of carboxyl groups grafted to a PP film into
polyhydroxamic acids [1]. The obtained modified films show increased chelating
capacity with respect to iron ions (~ 80 nmol cm^{-2}). This is one of the ways of the
biomimetic design of chelating interface surface, which can broaden the application
field of PMC in restoring of environment, water purification and active packaging
cleaning.

A chelating ligand, IDA was covalently immobilized on poly(MMA-GMA)
films prepared using UV-initiated photopolymerization of epoxy groups [789].
Cu(II) ion was chelated by immobilized ligand.

Electrochemical sensor of lead ions was developed by modification of an elec-
trode based on carbon paste using polypyrrol, functionalized by IDA (Fig. 2.67)
[790].

The 5-nitroquinoxalines, substituted in 2 and 3 positions by 2-pyrrolyl, 2-furyl,
and 2-thienyl groups are used as active components in PVC membranes and
electrically polymerized electrodes, which were then tested as possible sensors for
different cations [791].
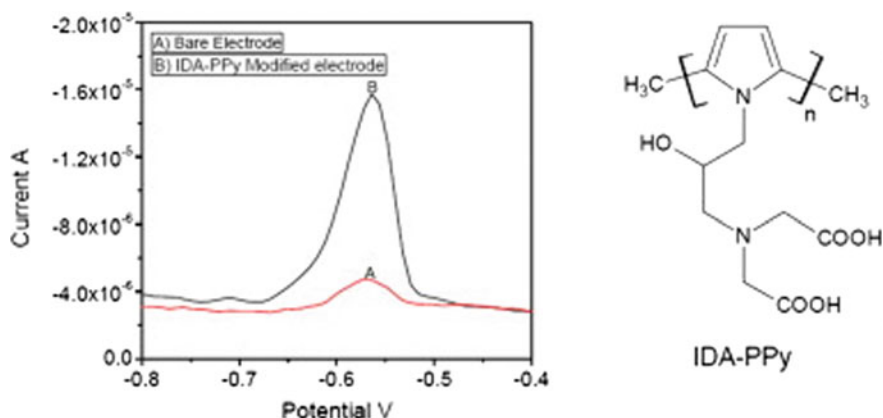
Fig. 2.67 Electrochemical sensing Pb(II) ions using carbon paste electrode modified with polypyrrol modified by IDA

An example of modification of the polymer films using macrocyclic unit can be (2,3,9,10,16,17,23,24-octa-[(4-carboxylate)-phenoxy]-Pc)-St-alkyl(meth)acrylate polymer films [792].

2.6 Liquid Crystal Chelating Polymers

Recently new area of CPLs, liquid crystal polymers (LCP), has being intensely developed. Macromolecular compounds capable of transforming into liquid crystal state under certain conditions (temperature, pressure, concentration in solution) belong to these polymers [793–798]. Since it takes an intermediate place between amorphous and crystal states, it is also often called mesomorphic or meso-phase (from Greek mesos, which means intermediate). Typical features of a meso-phase are presence of orientation ordering in macromolecular arrangement (or their fragments) and anisotropy of physical properties in absence of external actions. The main advantages of the LCP are stipulated by their dual nature, which provides in one material properties of macromolecular substances (with their ability to form films, glasses, fibers, and coatings), and mesomorphic properties of liquid crystals (which, in turn, display dualism of properties).

Similarly, to low molecular weight liquid crystals [799–802], LCP form the same structural types of meso-phases: nematics (N), smectics (S), and cholesterics (Ch) with typical for them arrangement of mesogenic fragments, presence of orientation order in nematics and layer order in smectics. In the cholesteric phase formed by optically active polymers, helical structure is formed, which determines special optical properties of cholesterics (Fig. 2.68).
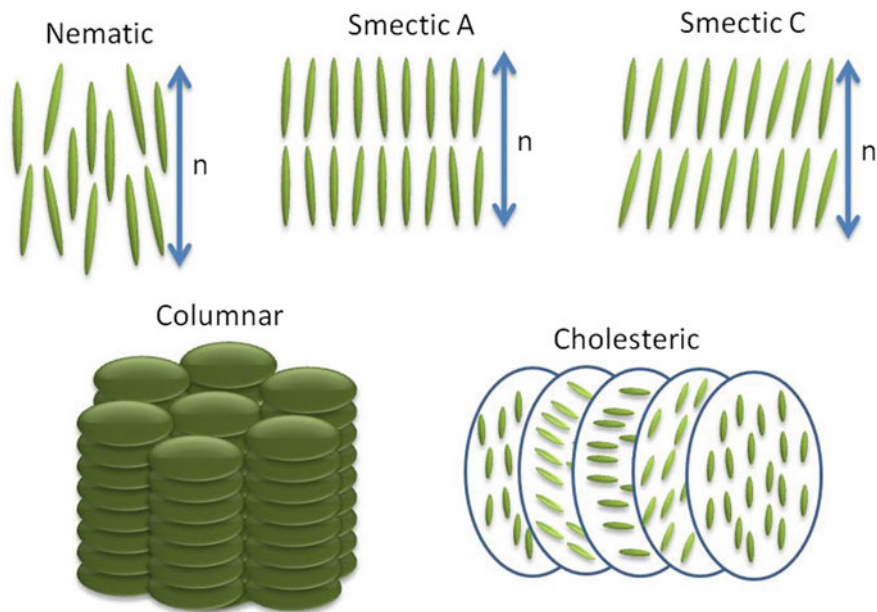
Fig. 2.68 Different phases of liquid crystals

Rod-like structure in a molecule consisting of several aromatic or heterocyclic rings linked directly or through different spacers predetermines behavior of a liquid crystal during heating or in a concentrated solution. If a meso-phase is formed during dissolution of polymers in certain solvents, they are called lyotropic LCP, and if polymers transform in the liquid crystal state or in meso-phase as a result of thermal treatment (heating or cooling), they are called thermotropic LCP. In the case of lyotropic LCP formed in solutions, a certain structural type of meso-phase is realized at exactly determined temperatures and concentrations of a polymer in solution and is displayed on their phase diagrams. Thermotropic LCP transit into the liquid crystal state above the melting point (T_m) or at higher than T_g or at the softening temperature if an initial polymer does not crystallize. These temperatures correspond with the lower boundary of a liquid crystal phase formation, while the upper boundary is so called isotropization temperature (T_i) above which a polymer transit into isotropic melt. Particularly in the temperature range T_g (or T_m)—T_i mesogenic fragments of a LCP organize spontaneously, forming a certain structural type of a meso-phase (N, S or Ch) with respect to molecular structure and molecular weight of a polymer.

Lyotropic liquid crystal state is most typical for rigid-chain polymers capable of very specific phase separation. The liquid crystals of this type are binary or ternary systems, which differ by a structural type as layered, rod-like, and cubic. Lyotropic LCP is characterized by high rigidity of macromolecules, high melting points being near temperatures of chemical decomposition, which excludes a possibility of appearance of a thermotropic meso-phase. However, despite this,
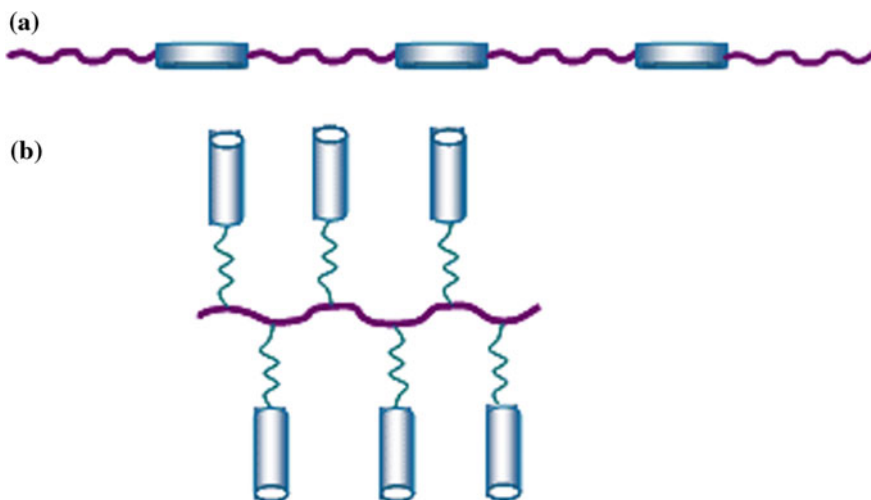
Fig. 2.69 Basic types of LCP: **a** polymers with mesogenic groups in main chain, **b** side-chain or comb liquid crystal polymers

rigid-chain polymers form lyotropic liquid crystal systems in such highly polar solvents, as sulfuric and chlorosulfonic acids, dimethylacetamide with lithium chloride, etc.

Thermotropic LCP is formed by chemical bonding of rigid and flexible fragments into one macromolecule, which can have linear or branched (comb-like) structure (Fig. 2.69). At that, molecules of low molecular weight liquid crystals or their mesogenic groups responsible for formation of a liquid crystal phase are usually used as rigid fragments. In turn, flexible fragments, usually called spacers, lowering rigidity of macromolecules due to their special dilution, decrease T_m of polymers, giving rather high autonomy to rigid mesogenic groups, which is necessary for their cooperative interaction with a meso-phase formation.

Instead of flexible fragments, other chemical groups can be used, which break linear structure of the rigid-chain macromolecules. In particular, a decrease in rigidity can be reached by integration of bulky substituents or chemical groups, which advance appearance of bends in a chain and break in their symmetrical linear structure (for example, due to presence of phenylene or naphthalene cores included in a chain not in *para*- but in *meta*- or *ortho*-positions).

2.6.1 Polycondensation in the Synthesis of Liquid Crystal Polymers

The main structural units of the rigid-chain polymers of linear structure are aromatic or heterocyclic fragments bound collinearly with each other via different spacers. Most

often such polymers are produced by polycondensation or co-polycondensation of similar or different bifunctional derivatives [803–814]. Thus, a wide range of poly-imines is synthesized by polycondensation of diamines or hydrazines with dialdehy-des, diketones or quinones [815–827]. Other known classes of LCP, such as polyimides and polyquinoxalines are produced on the basis of cyclic aliphatic, fluorinated, heterocyclic, Cz, perylene monomers of non-coplanar structure (loop, spiro, and cardo), chiral compounds and compounds with non-linear optical properties and non-symmetric structure [828, 829].

A series of semi-flexible homo- and co-polyazomethines containing imine bond in polymer backbone is synthesized based on hydroxyl-functionalized mesogenic cores with aliphatic spacers (Scheme 2.37) [805].

For polyazomethines containing p-substituted diamine, for example, 2-methyl-1,4-phenylenediamine and aliphatic chain with two CH_2-groups (polymer P2), the $T_m = 333$ °C was measured closely to decomposition, and no meso-phase was detected. However, with an increasing spacer length, the transition temperature decreases, and formation of a meso-phase is more probable. Thus, for P6 polymer two endothermic points are established, at 229 and 259 °C, and the polymer with ten methylene groups (P10) has shown only one T_m, 175 °C, at that, both homopolyazomethines (P6 and P10) have typical nematic textures.

Poly(azomethine ethers), which display thermotropic liquid crystal properties, are formed [807] at polycondensation of different diamines and 4,4′-diformyl-α,ω-(diphe-noxy) decane or 4,4′-diformyl-3,3-methoxy-α,ω-(diphenoxy)decane. The mesogenic transition temperatures decrease as a number of methylene groups increases from tetramethylene to hexamethylene; the similar tendency is observed for polymers con-taining aromatic segments. Nematic meso-phase formed only for the polymer syn-thesized from 1,4-phenylenediamine and benzidine, and for polymers based on tetramethylenediamine, there was absolutely no meso-phase observed. On the other hand, the polymer with six methylene spacers had a grainy texture.
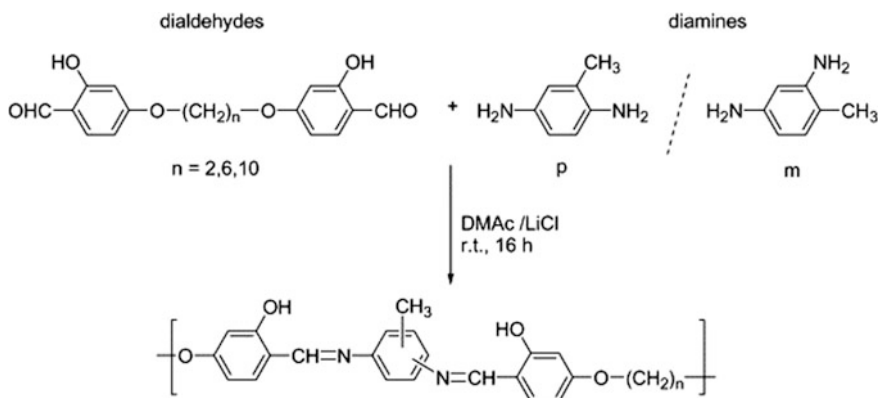
Scheme 2.37 Synthesis of co-polyazomethines based on hydroxyl-functionalized mesogenic cores and aliphatic spacers

Copolymers of polyazomethine ether obtained by polycondensation in solution with different diamines (for example, 1,4-phenylendiamine, 4,4′-diaminodiphenylmethane, etc.) show nematic liquid crystal thermotropic properties [830].

A study of the effect of length of methylene interchange on molecular mobility and dipole moment of polyazomethine ethers with azomethine-aromatic groups in *o*-position has shown that for them existence of four relaxation processes in solution is typical [831]. Parameters of molecular mobility (relaxation time and activation energy of three local processes) depend nonmonotonically on the methylene interchange length, showing the even-odd effect. In the case of the fourth large-scale process these parameters have high values and increase monotonically as the interchange length increases. This can be due to special features of conformation of the ester part of a macromolecule, which is also confirmed by theoretical analysis of geometric and electronic structure of coplanar conjugated polyazomethines [832].

Another group of polyazomethine ethers has been obtained using polycondensation of diformyl-*o*-diphenoxyalkanes and 2,7-bis-(*m*-aminobenzylidene) cycloheptanone or bis-(*m*-aminobenzylidene) acetone [808].

Mesomorphic properties of these polymers are determined by nature of diphenoxyalkane spacers (length of a spacer is 2, 4, 6, and 8 methylene units in the dialdehyde structure) independently of a diamine structure. At that, polymers synthesized from diamine with a cycloaliphatic core showed high T_m and T_i points as compared with polymers obtained from acetone-derivative diamine and the same dialdehydes [808].

Study of thermal behavior of a LCP including alternating polyazomethine and random poly-ester showed that it has the $T_g = 43$ °C, which is far lower than the crystallization temperature 97 °C, and two endotherms at 141 and 163 °C. This indicates the transition from half-crystalline nematics to nematic liquid.

Synthesis of twelve different azomethine polymers with the main chain containing banana-shaped mesogens is described (Scheme 2.38) [809].

Formation of a meso-phase also depends on length of aliphatic spacer and substituents in a mesogen ring. Thus, for polyazomethines with short (m = 6) spacer and carrying two or four halogen atoms, a nematic phase formation was observed, and longer aliphatic spacers (m = 12) governed formation of smectic meso-phase.

Also chiral salicylaldimine compounds including a fluorocarbon chain, with calamic molecular shapes are produced (Fig. 2.70) [833].

Liquid crystal polyazomethine ether with side dimethoxybenzylidene groups has been obtained by polycondensation of a diacid monomer benzalaniline-3′,4′-dimethoxy-terephthalic acid with two diol monomers [834].

Cross-linked LCP are obtained based on the liquid crystal twin epoxy monomers, containing azomethine groups, cured by aromatic diamines [810].
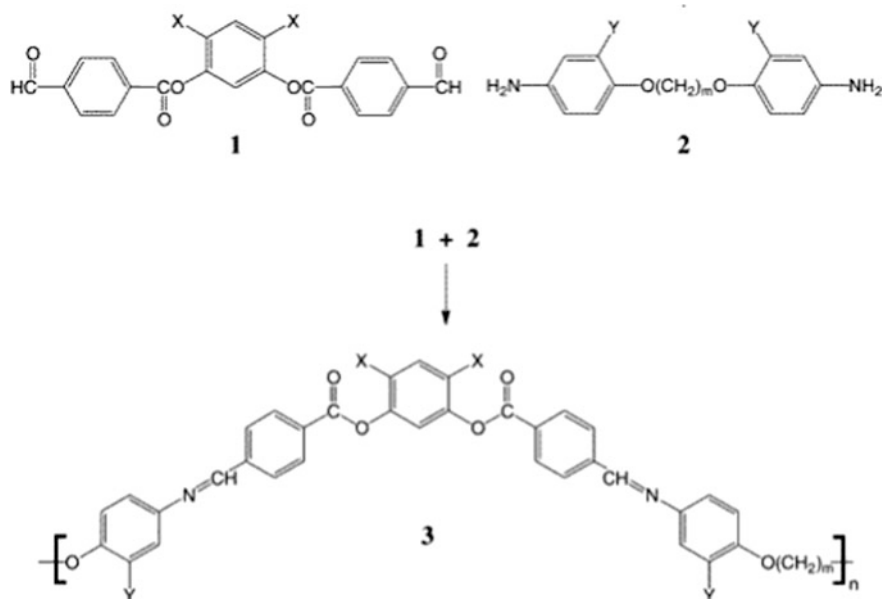
Scheme 2.38 Synthesis of azomethine polymers with the main chain containing banana-shaped mesogens
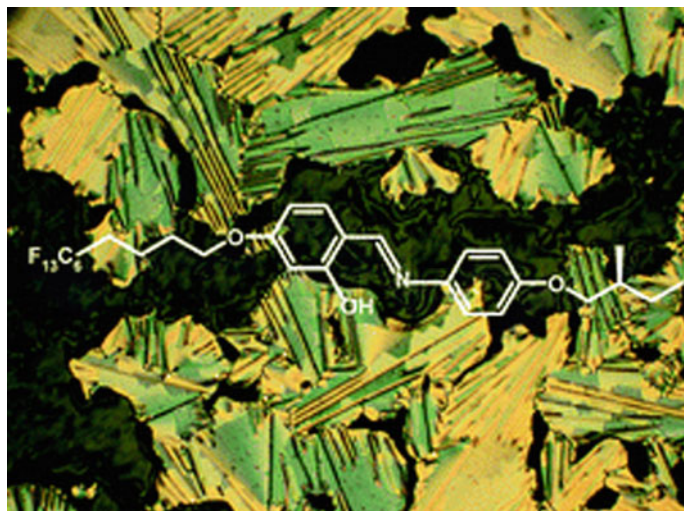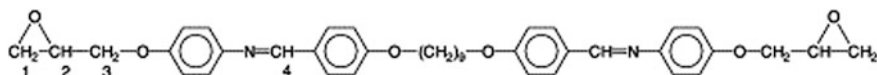

Fig. 2.70 Calamic molecular shapes of chiral salicylaldimine compounds including a fluorocarbon chain
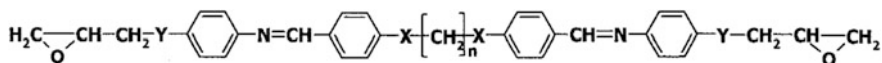
Nematic meso-phase showing schlieren textures was observed for all epoxy monomers after melting with the temperature of the meso-phase formation between 10 and 17 °C.

Another series of twin monomers with the end glycidyl group linked to the group of ester or ether and having aliphatic spacers of different lengths was used for producing rod-like aromatic imine structures with ester or ether bonds [811].

IAn

IBn

IIAn

IIBn
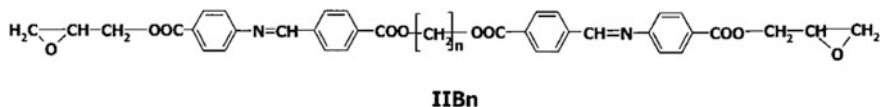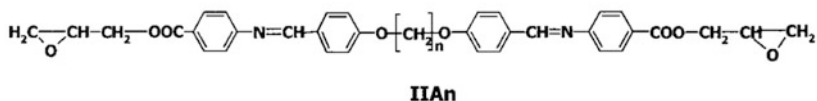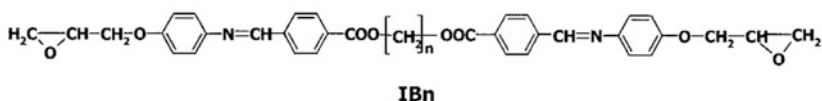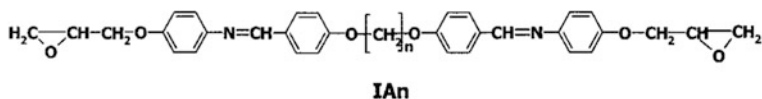
These monomers show mesogenic behavior, and their architecture influences a type of meso-phase. Thus, monomers of IA, IIA, and IIB series formed nematic meso-phases, and IB monomers formed smectic meso-phases depending on a length of aliphatic spacer. In particular, monomers with odd number of methylene groups formed smectic C meso-phases, while monomers with even number of methylenes formed smectic A meso-phases. After curing of homopolymer epoxy resin by 2,4-diaminotoluene and p-amino-acetophenone azine, a cross-linked epoxy resin is formed, which shows nematic meso-phase, excluding monomers of IB series with spacers of 8 and 10 methylene groups, for which smectic C meso-phase is formed. When the tertiary amine, 4-(N,N-dimethylamino) pyridine was used as a catalytic cross-linking agent, all monomers of IB range formed smectic C phases, whereas monomers of IIA series gave nematic phases [811].

Liquid crystal meso-phases [812] are formed in polyurethanes synthesized from diols containing four phenyl rings linked in p-position by azomethine and ether bonds and end spacers from 2 to 10 methylene groups and two isocyanates, hex-amethylene diisocyanate and methylene-bis(cyclohexyl isocyanate).

$$H_2C\!\!-\!\!CH\!\!-\!\!CH_2\!-\!Y\!-\!\!\bigcirc\!\!-\!N\!=\!CH\!-\!\!\bigcirc\!\!-\!X\!-\![CH_2]_{3n}\!-\!X\!-\!\!\bigcirc\!\!-\!CH\!=\!N\!-\!\!\bigcirc\!\!-\!Y\!-\!CH_2\!-\!CH\!-\!CH_2$$

Diols and polyurethanes produced from them showed formation of nematic meso-phase during heating. In both series of polyazomethines the transition temperature decreased as length of a flexible spacer increased, and it was somewhat higher for the polymers synthesized from hexamethylene diisocyanate than in the case of polymers produced from diisocyanates with cyclohexyl fragments [812].

A great number of liquid crystal polymeric crown ethers, as well as azacrown ethers, thiacrown ethers, and crown ethers with different heteroatoms is known [835]. Microcrystallinity in them is conditioned by substituents bound to crown ethers, depending of nature of which, rods, discs or tapers can form bringing to different types of meso-phases.

Thus, LCP of poly-esters containing dibenzo-18-crown-6 units are obtained by polycondensation in solution of 4,4′-(α,ω-alkandiol) dibiphenylyloyldichloride, *cis*-4,4′-bis-(4-hydroxyphenylazo) dibenzo-18-crown-6, *trans*-4,4′-bis(4-hydroxyphenylazo) dibenzo-18-crown-6, and 1,10-decandiol. Copolymers formed nematic meso-phase in melt, which has a texture of twisted fiber, grainy or schlieren-texture, and the T_m and T_i of the copolymer decreased as length of a flexible spacer increased [836].

Polycondensation of 4,4′-(alkylenedioloxy) dibenzaldehyde, *cis*-diaminodibenzo-14-crown-4, and *trans-cis*-diaminodibenzo-14-crown-4 in solution was used to produce LCP of Schiff base type and containing cyclic units of crown ether. These polymers have $M_n = 13{,}000\text{–}24{,}000$ and transform into liquid crystal state at the temperature above the T_m. Most synthesized polymers had wide meso-phase range, though some of them are liquid crystalline in nematic phase [837]. In the similar way polycondensation of 4,4′-(alkylenedioloxy) dibenzaldehyde and diamine-dibenzo-15-crown ether in solution were used to synthesize Schiff bases of liquid crystal polymeric crown ether. Their $M_n = 10{,}100\text{–}13{,}000$ and they transform into liquid crystal state at melting with formation of two types of textures, their T_m, T_g, and T_i depend on a type of flexible spacer [838].

Photochromic LCP, which contains azobenzene and crown ether groups, is synthesized [803]. Positions of the crown ether groups with respect to photochromic fragment have an effect on phase and spectral properties, and on kinetics of photo-orientation of the polymer thin films. These photo-oriented polymer films can be used as sensors of metal ions.

Polymeric liquid crystal crown ethers are formed using polycondensation in the solution consisting of 4,4′-(alkylenedioloxy) dibenzaldehyde, *cis*- and *trans*-4,4′-diaminodibenzo-18-crown-6. All obtained polymers transform in the liquid crystal state upon heating up to the T_m, at that nematic phase has typical schlieren texture, while the smectic phase is focal-conic, and the T_m and T_i depend on a type of flexible spacer [839].

2.6.2   Liquid Crystal Polymers Obtained by (Co) polymerization

Liquid crystal meso-phases can also be formed using polymers with mesogenic fragments linked to the main chain as side groups [809, 814–824, 840]. The principle of production of comb-like LCP with side mesogenic groups is in synthesis of monomers with mesogenic groups and their further homopolymerization or copolymerization with mesogenic or non-mesogenic compounds. Thus, LCP are obtained by free radical polymerization of salicylaldimine monomer 6-[3-hydroxy-4-(4-octadecyloxyphenyliminomethyl) phenoxy] hexyl methacrylate in presence of AIBN [841].

Different meso-phases have been found in methacrylate polymers with liquid crystal fragments in the side chain based on ω-hexyl-, ω-butyl-, and ω-undecyloxy-salicylaldimine with n-alkyl or n-alkyloxy end substituents [842, 843]. In particular, for decyloxy-, dodecyloxy-, and octyl-derivatives formation of smectic C_2 phase was observed in wide temperature range, while tetradecyl-derivative shows a complicated behavior: first smectic A_d phase appears, which transforms into smectic C_2 phase, and then into smectic C_d phase [842].

Liquid crystal oligomers with side salicylaldimine groups were obtained using free radical polymerization of respective monomers 5-(10-undecenyloxy)-2-[[(4-(hexyloxy) phenyl) imino] methyl] phenol and 5-(10-undecenyloxy)-2-[[(4-(hexyl) phenyl) imino] methyl] phenol [844, 845]. These oligomers form smectic meso-phases similar to those of the initial monomers, and displacement of hexyloxy-chain by hexyl-chain brings to the smectic C meso-phase.

Another way of production of comb-like LCP is linking low molecular weight liquid crystal molecules to a polymer chain. In this case, it is necessary that the polymer and mesogenic molecules involved in the reaction would have functional groups capable of interaction. Thus conducting copolymers of poly [1-(thiophene-3-methoxy)-6-(4-n-hexyloxy-2-oxybenzoic acid) hexane] and 3-n-hexylthiophene containing side mesogenic groups attached parallel to the backbone are synthesized. In this case transformation of non-mesogenic intermediate polymers to LCP with high temperature-dependent conductivity was observed, which pointed to a decrease in activation energy of the liquid crystal phase [846].

Liquid crystal thermosets epoxy resins with *bis*-azomethine biphenyl mesogenic groups are formed during co-polymerization with non-mesomorphic epoxy compounds. Under action of primary aromatic diamines, *tert*-amines, and during co-polymerization with non-mesomorphic epoxy monomers, a cross-linked network structures are formed [847].

Thermal and photopolymerization of mesogenic azomethine monomers with methacrylic and vinyl ether end groups have been carried out [814].

These monomers showed mesogenic behavior and, in most cases, a variety of smectic meso-phases. Photopolymerization was carried out in presence of a photoinitiator at the temperature, at which monomers formed smectic or nematic meso-phase. It has been established that mono- and di-acrylates have similar textures [814].

Formation of liquid crystal phases is significantly affected by structure of main chain of polymers having mesogenic side groups [815]. Thus, polymer **1** with MMA main chain formed nematic phase upon heating above T_g, and polymer **2** did not form a meso-phase, even if it had the same mesogenic side groups. However, copolymerization of MMA mesogenic monomer with MMA or methacrylic acid brought to polymers **3** and **4** with liquid crystal properties, whereas content of non-mesogenic monomer in copolymer did not exceed 20%.

Formation of symmetric azomethines of smectic A and B meso-phases is shown for the case of thermotropic symmetric azomethines based on poly-1,4-butanediol-bis(4-aminobenzoate) and 1,4-biphenyl carboxaldehyde [848].

A range of modified polyguanidines was synthesized, which were characterized by their liquid crystal properties (chirality, homogeneity of side chains length, linking mesogens to side chains) [849].

Studies of luminescent thermotropic liquid crystal polyazomethines containing a chromophore mesogen based on fluorene and/or oxadiazole, showed formation of nematic meso-phase containing alternating or statistical oxadiazole units. Mesomorphic state keeps ordering degree of semi-crystalline compounds, which confirms the liquid viscosity. Based on the obtained polymers, it is possible to produce monodomain or multidomain ordered thin films with good mechanical and luminescent properties [850].

The polymer with liquid crystal side chain has been obtained from tolane based on hemi-phasmid benzoic acid and poly-4-vinylpyridine (P4VP) [851]. It forms smectic and hexagonal columnar meso-phases with different compositions, which determine luminescent properties of the polymers.

Liquid crystal co-polyesters containing X-shaped 2D mesogenic units and crown ether cycles of *cis*-4,4′-bis(4-hydroxyphenylazo)-dibenzo-14-crown-4 in a side chain were obtained [852].

It should be noted that many studies have been performed with liquid crystal azomethine oligomers in order to incorporate them into a polymer chain [820–826]. For example, a series of semi-flexible liquid crystal tetramers was obtained [820], in which length of the central spacer was six methylene units, and lengths of exterior spacers varied from 3 to 12 methylene units.

All tetramers showed enantiotropic nematic phase, and the transition temperatures depend on length and ratios of external flexible spacers. Properties of this series of polymers were comparable with the respective series containing central pentamethylene spacer, and the transition temperatures showed pronounced odd-even effect with increase in lengths of the external spacers (even spacers gave higher values) [820].

For LCP based on fluorinated carbon chains with end SF_5 groups a transition from nematic to smectic A phase is detected [821].
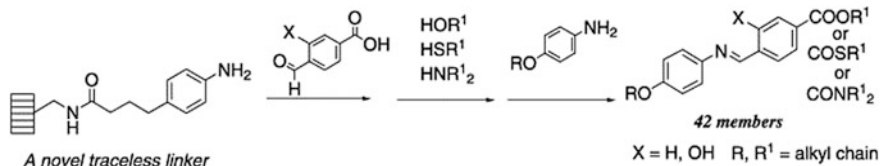
Recently LCP with very different topology, for example, block-copolymers, graft-copolymers, graft-block-copolymers, etc. (Fig. 2.71) were synthesized [794]. Thus, liquid crystal rod-coil di-block-copolymers (coil-conformation of St segments and rigid-rod conformation of mesogen-jacketed 2,5-bis[(4-methoxyphenyl)-oxy-carbonyl]-St segments) with different molecular weight and low PDI are obtained using ATRP method [853]. Liquid crystal behavior of polymers depends on molecular weight of a rigid segment. Thus, only copolymers with M_n of a rigid block above 9300 can form liquid crystal phases above T_g of the rigid block.

A range of liquid crystal block-copolymers of ABC_2 type with azobenzene fragments in the side chain has been obtained by combination of ATRP and chemical modification reaction (Scheme 2.39) [854].

Photopolymerization of polyfunctional liquid crystal monomers with ester spacers was applied to obtain monolithic ordered LCP nets [855]. Using different strategies of synthesis, it is possible to control molecular orientation of polymers in all three dimensions (Fig. 2.72). A film based on LCP has alternating plane chiral nematic areas near perpendicularly oriented (so called homeotropic) areas, and the
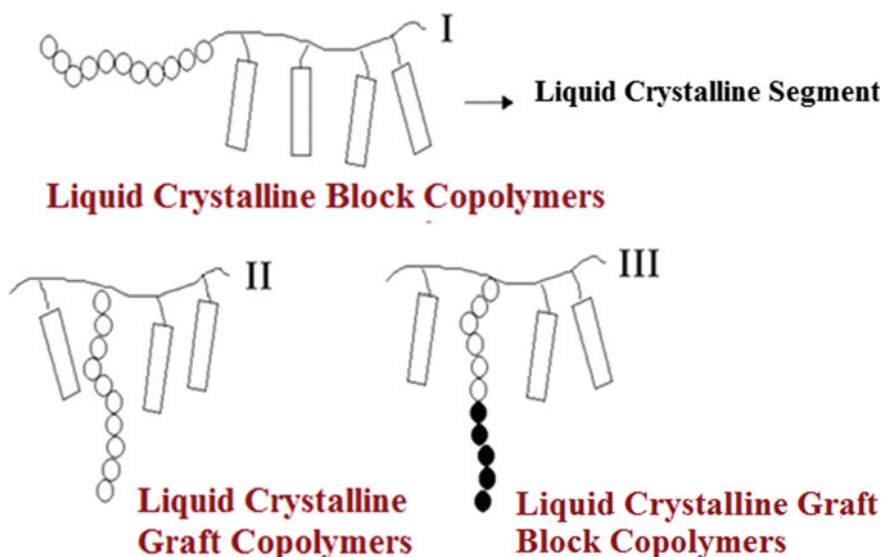
Fig. 2.71 Structures of liquid crystalline block copolymers, liquid crystalline graft copolymers, and liquid crystalline graft-block copolymers
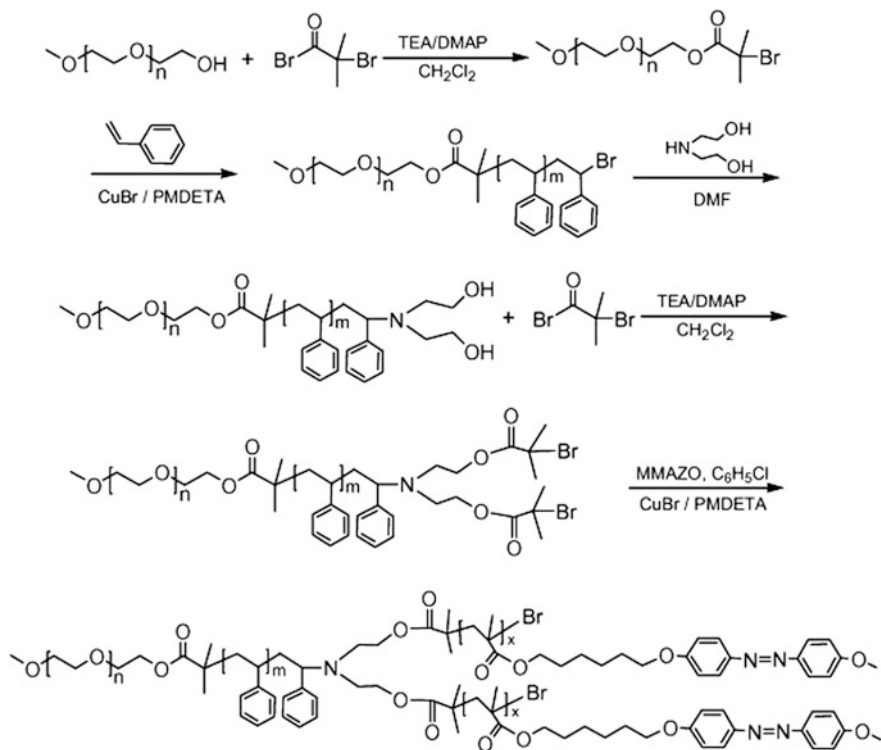
Scheme 2.39 Scheme of production of liquid crystal block-copolymers of ABC$_2$ type with azobenzene fragments in the side chain by combination of ATRP and chemical modification reaction

film changes its surface texture upon deposition as a coating. It is important to notice that during action of UV light it switches from plane to corrugated state.

Based on interpenetrated liquid crystal-hydrogel polymer nets, stimuli-responsive materials have been obtained [856]. These materials consist of cholesteric liquid crystal nets, which reflect light, and entangled polyacrylate nets, which provide humidity reaction, pH humidity, and pH response.

Numerous studies have been carried out on production of LCP nets of other types [857]. In particular, a cross-linked film based on polyarylamide with fiber morphology occurs photomechanically sensitive [858]. 3D shape of LCP nets prepared with different cross-linking density is determined by the cross-linking density and conditions of preparation, in particular, polymerization temperature [859].

LCP can also be obtained by the photoinduced surface relief grafting, which provides orientation control over meso-phases on surface [860]. In particular, plane, perpendicular and patterned orientation of meso-phases can be easily obtained, using photo-control, with a monomer, 4-propyldiphenylacetylenecarboxylic acid
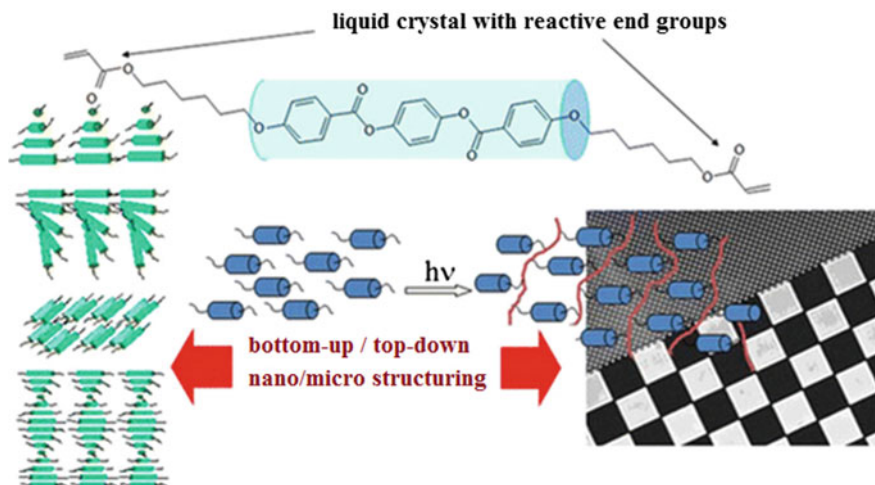
Fig. 2.72 Scheme of photopolymerization of polyfunctional liquid crystal monomers with ester spacers for the production of monolithic ordered LCP nets

cinnamon ester. 3D ordering in LCP is achieved during photopolymerization of the mixture of mesogens sandwiched between two patterned substrates [861].

2.6.3 Liquid Crystal Dendrimers and Hyperbranched Polymers

Recently much attention is focused on liquid crystal dendrimers and hyperbranched polymers [862–868]. Tuning of meso-phase structure of these polymers can be reached using respective molecular design depending on chemical nature of end mesogenic groups, dendritic core, and a number of generations of a dendrimer. Liquid crystal dendrimers can also contain mesogenic groups as a side or main chain, and in the latter case two types of dendrimers are formed: willow-like and octopus dendrimers. A range of other dendritic matrices is obtained: shape-persistent dendrimers, fullerodendrimers, polypedes and rod-coil block *co*-dendrimers [862, 867].

Thus, block *co*-dendrimers consisting of multifunctional mesogenic and Cz-containing 2,2-bis(hydroxymethyl)propionic acid of dendrons are synthesized [868]. Depending on chemical structure of composite dendrons, *co*-dendrimers formed lamellar or columnar meso-phases. Electrodeposition of Cz-containing dendrons afforded globular conformation, in which mesogenic molecular groups play the key role.

Many studies were concerned with dendrimers containing thermotropic liquid crystal fragments, because they can self-assemble in large organized assemblies

[817–819]. For this purpose, PAMAM and PPI dendrimers were functionalized by mesogenic fragments with azomethine groups [816]. Depending on generation of dendrimers, a number of mesogenic blocks varied from 4 to 64. Since mesogenic blocks contain one, two, or three end chains, a vast library of compounds displaying formation of a meso-phase is collected. General mesomorphism observed for all obtained dendrimers is based on chemical incompatibility between their constitutive parts (rigid aromatic parts, dendritic structure and aliphatic chains), and two possible conformations of molecules (parallel or radial) (Fig. 2.73). Presence of one aliphatic chain per mesogenic unit favors parallel arrangement of functionalized dendrimers and formation of smectic A or C meso-phases. Increase in a number of aliphatic chains (two or three) affords radial disposition bringing to formation of columnar structures. At that, temperatures of meso-phase transition depend on a dendritic core origin, a number of generations, and a number of terminal aliphatic chains [816].

Based on dendritic LCP, stimuli-responsive luminescent materials are obtained, which in future can be used as sensors of metal ions (Fig. 2.74) [869].
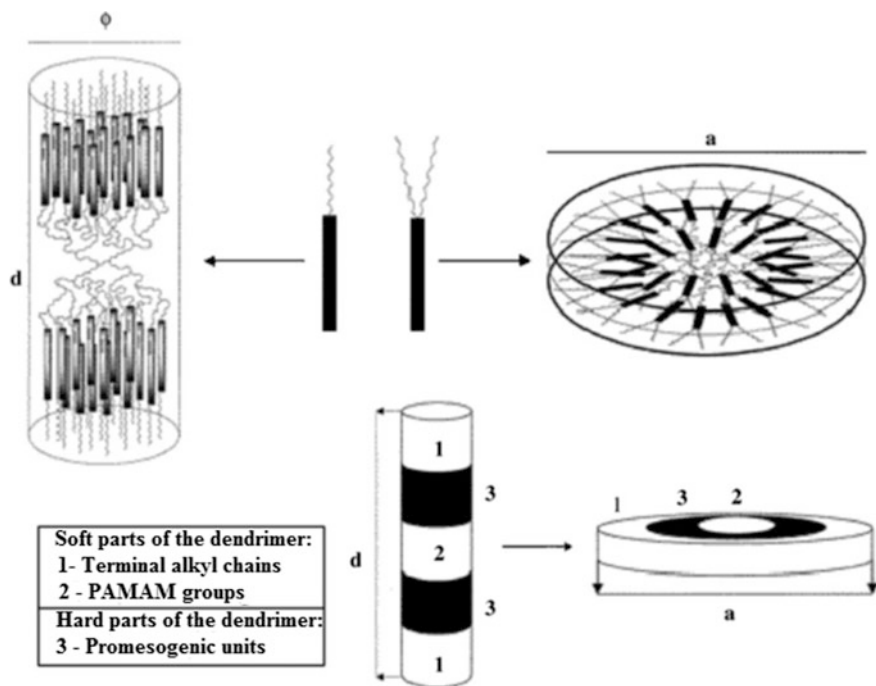
Fig. 2.73 Schematic presentation of two main molecular conformations (parallel and radial) by functioned at the end of liquid crystalline dendrimers and their correlation with a number of grafted terminal alkoxy-chains. Gigantic rods and discs are formed by microsegregation of incompatible segments by analogy with block-copolymers
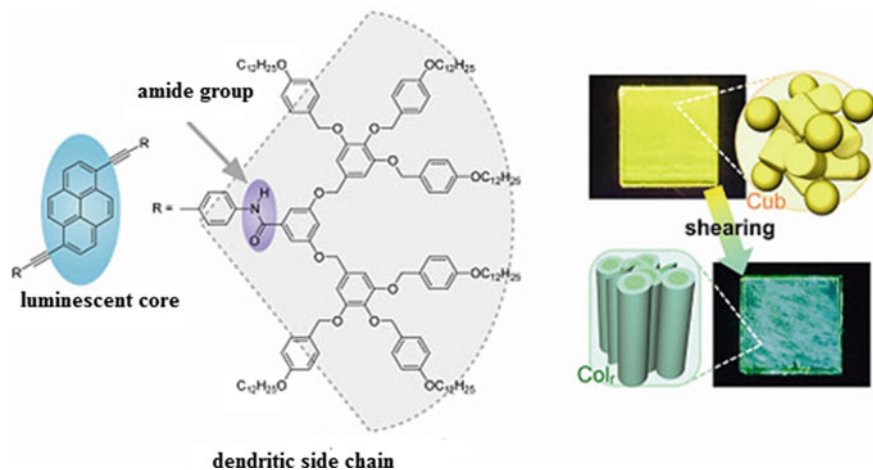
Fig. 2.74 Stimuli-responsible liquid crystals: change of photoluminescent colors triggered by a shear-induced phase transition

Order and frustration in the LCP are studied using the example of the G2 liquid crystal block- and statistic dendrimers with mixed aliphatic and mesogenic terminal groups, as well as homo-dendrimers from several generations containing only mesogenic end groups [870]. It has been established that homo-dendrimers from G1 to G4 show monolayer smectic phase, in G5 they show more ordered columnar phase, G2 block-dendrimer has bilayer smectic phase, while statistic G2 dendrimer does not show any mesogenic phase. The observed phase behavior is most convenient to be considered in terms of frustration due to competition between rigid geometry of the dendritic matrix and close-packing conditions of terminal chains.

Interesting chiral LCP were obtained by coupling methyl-α-d-glucoside (G) and methyl-α-d-mannoside (M) as different chiral structural fragments in a core and in branching centers within dendritic scaffolds surrounded by 12 cyanobiphenyl mesogenes (CB) (Fig. 2.75) [871]. Positional permutation approach of pyranose unit's G and M in the core and branching points was used for studies of mesomorphic properties of chiral homogenous dendrimers GG/MM and respective chiral heterogeneous dendritic homologues GM/MG. It occurs that the temperature profile and structure of the meso-phase of four dendrimers do not depend substantially on the origin of the central chiral core, and the external chirality on periphery predominates considerably over liquid crystal properties.

Liquid crystal co-polymers with multi-arm star azobenzene side chains and hyperbranched core are obtained by ATRP method through multifunctional hyperbranched polyether as initiator and benzene chloride as a solvent [812]. Multifunctional hyperbranched polyether initiator is produced from poly(3-ethyl-3-(hydroxymethyl)
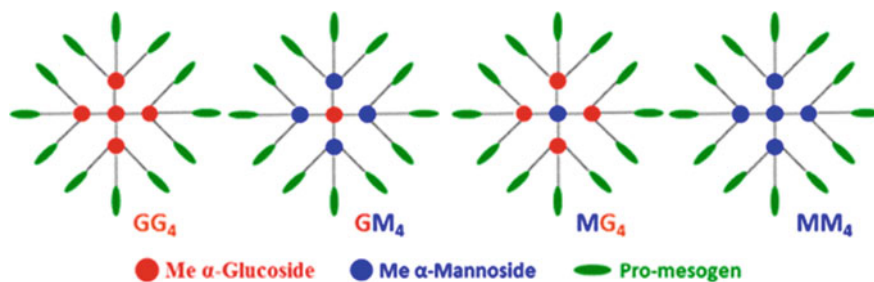
Fig. 2.75 Structures of chiral liquid crystal obtained by coupling methyl-α-d-glucoside (G) and methyl-α-d-mannoside (M) as different chiral structural fragments in a core and in branching centers within dendritic scaffolds surrounded by 12 cyanobiphenyl mesogens (CB)

oxetane) and 2-bromo-2-methylpropionyl bromide. Azobenzene side arms have liquid crystal conformation of poly [6-(4-methoxy-4′-oxy-azobenzene) hexyl methacrylate] with different molecular weights and they form smectic and nematic phases, and the phase transition temperatures from smectic to nematic phase and from the nematic to isotropic phase increase as molecular weight of the copolymers increases from 1.78×10^4 to 9.07×10^4.

Using very different methods of synthesis has brought to building of many thousands of different in structure LCP. Apart from classic linear and comb-like polymers, there is a great number of LCP containing paired mesogens, macromolecules with laterally bound mesogenic groups, disc-shaped and cross-shaped fragments, also alternation of different mesogenic groups is possible in the limits of one and the same polymer chain [872, 873]. The principal possibility of synthesis of LCP consisting of macromolecules of any combination between mesogenic and non-mesogenic fragments opens wide horizons for oriented design of PMC.

Analysis of the considered data points to the fact that by now a considerable experimental material on synthesis of CPL has been collected, which shows intensity of their chemistry development. Currently, the basic principles of design of the chelating polymers are formulated, their structural organization is understood, and development trends in the area are relatively well represented. It should be emphasized that design of CPL is important, and in some cases, a critical task in terms of both subsequent chelation reactions with a metal compound, and for subsequent PMC use.

However, until now a convenient classification of chelating polymers is not developed. For subsequent transformations the prehistory of formation of chelating fragments is important, since even the strict observance of all the intricacies of parallel experiments is not always possible to obtain reproducible results. Because very notion of "polymer structure" is a highly-valued and, as a first approximation, is determined by the conditions of its synthesis, CPL are to be classified according to the type of preparation thereof (polymerization, copolymerization of the corresponding monomers, polycondensation or PPM). Moreover, the chelating fragments are crucial in chelation of metal compound, so that the second parameter, reflected in the classification should be the nature, size and spatial arrangement of the chelating fragment, which may consist of both symmetrical and asymmetrical groups. Therefore, CPL classification adopted in this book includes, primarily, the method of preparation and structure of the base polymer and then its functionality. Although this classification is to some extent arbitrary, but two parameters, put in its foundation, more clearly characterize the CPL.

Table 2.5 shows the most typical derivatives of CPLs based on synthetic polymers, and methods of their production. They are classified by type of produced PMC as following the groups: ligands for molecular metal chelate, intracomplex compounds, and macrocyclic complexes. Apparently, this division is very conditional, since in many cases the same chelating fragments can participate in formation of metal chelates of different types, metal chelates with mixed ligands, a variety of bridge structures, and polynuclear metal chelates.

Obviously, presently there are no difficulties in synthesis of polymers with any chelating functionalities. Thus, a technique for producing polymers of chelating type is well developed and continues to improve. At the present stage of experimental studies design of CPL, which are analogues of low molecular weight ligands, for example, acetylacetonates (acac), Schiff bases, etc., does not constitute special synthetic difficulties.
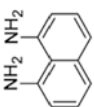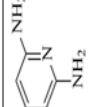
Polymer chelating ligands are often low-tonnage polymers for special purposes; therefore, PPM of industrial polymers such as PE, PP, PTFE, etc. is very perspective. Besides, in the last decade in spite of the well-known, cheap and widely used thermoplastics and elastomers the focus has shifted to more expensive materials.

Table 2.5 Main types of CPL based on synthetic polymers and methods of their preparation

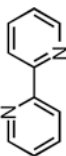| Chelating fragment	Polymer-support	Preparation method	Initial reagents	PCL characteristics	References
Ligands of molecular metal chelates					
$H_2NCH_2CH_2NH_2$	Homopolymer	EP	N-(1-naphthyl)ethylenediamine dihydrochloride	Film	[711]
	Homopolymer	Plasma polymerization	en	Film	[783]
	Copolymer	CoP	en + dimethyl amine + epichlorohydrin		[874]
	Polycondensate	PC	en + p-dichloromethylbenzene	Insoluble, 6.51 mmol $NH_2\ g^{-1}$	[875]
	Polycondensate	PC	en + 2-amino-6-nitrobenzothiazole		[876]
	PAAm	PPM	Support + en	[CF] = 0.87–2.78	[877]
	PCD-GMA	PPM	Support + en	2.68 mmol N g^{-1}	[878]
	PCD	PPM	Support + en	[CF] = 3.16, S_{BET} = 36.24, V_{pore} = 0.35, D_{pore} = 43.90	[879]
	Poly[4-vinyl benzyl (2-benzenesulfonate ethyl) sulfide]	PPM	Support + en	[CF] = 3.53	[880]
	2,4-dihydroxyacetophenone formaldehyde resin	PPM	Support + en	Yield = 75%	[881]
$(H_2NCH_2CH_2)_2NH$	PMA	ARGET ATRP	Methyl acrylate (MA) + dien	M_n > 1.5 million, PDI ~ 1.25	[882]
	Polycondensate	PC	Dien + urushiol + formaldehyde		[883]
	PMMA	PPM	Support + dien		[884]
	PAN	PPM	Support + dien		[885]
$(CH_2NHCH_2CH_2NH_2)_2$	Maleic anhydride-*co*-dicyclopentadiene	PPM	Support + trien	Yield = 63–65%, S_{BET} = 3.151	[886]
$NH_2(CH_2CH_2NH)_3CH_2CH_2NH_2$	Polycondensate	PC	Tetraethylenepentamine + 2,2'-biphenol + formaldehyde	Yield = 79%	[887]
$NH_2(CH_2)_6NH_2$	PAN	PPM	Support + hexamethylenediamine	Yield = 30–34%	[888]
benzene-1,2-diamine (NH_2, NH_2)	Homopolymer	Oxidative polymerization	*o*-phenylenediamine	Yield = 34–55%	[173]
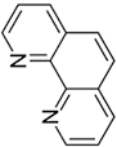
(continued)

Table 2.5 (continued)

Chelating fragment	Polymer-support	Preparation method	Initial reagents	PCL characteristics	References
	Homopolymer	Oxidative polymerization	Poly(1,8-diaminonapthalene)	Spherical grains with diameter about 300–500 nm, S_{BET} = 6.73	[178]
	Homopolymer	EP	2,6-pyridinediamine	Film	[722–724, 889]
	Homopolymer	Interface polymerization	2,6-pyridinediamine	Spherical microparticles with an average diameter of 1 μm	[179]
	GL	PPM	Support + N,N-di(2-pyridylmethyl)amine	[CF] = 1.15	[890]
	Homopolymer	ATRP	tpy monomers		[891]
	Poly(triphenylamine-alt-fluorene) or poly(triphenylamine-alt-N-ethylcarbazole)	Suzuki coupling polymerization	Triphenylamine-based conjugated monomer containing tpy ligands + corresponding diboronate	M_n = 20,950, PDI = 1.25 (M_n = 18,700, PDI = 1.06)	[892]
	Copolymer	CoP	Methacrylic acid 3-(tpy-4'-yloxy)-propyl ester + MMA + hydroxyethyl methacrylate (methacryloyl methacrylate or acryloyl methacrylate)	M_n = 3800, PDI = 3.98 (M_n = 8200, PDI = 1.58 or M_n =10,500, PDI = 1.70)	[132]
	Copolymer	CoP	4- or 4'-vinyl-tpy + tpy-functionalized MMA		[893]
	Copolymer	ROMP	ε-caprolactone + 4'-hydroxypropyloxy-tpy	M_n = 2500, M_w = 3100, PDI = 1.2	[156]
	PVC	PPM	Support + (2-mercaptophenyl)methanol + tpy bearing an isocyanate group		[894]
	PCD	PPM	Support + 4'-(4-hydroxyphenyl)-tpy		[895]
	PEO	PPM	Support + 6-(tpy-4'-yloxy)-hexylamine	M_n = 3400, M_w = 3700, PDI = 1.08, T_m = 57 °C	[896]
	PCS	PPM	Support + 4'-hydroxy-tpy	Yield = 100%, 6.83 mmol N g^{-1}	[229]

(continued)

Table 2.5 (continued)

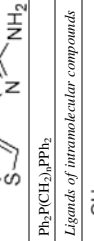| Chelating fragment	Polymer-support	Preparation method	Initial reagents	PCL characteristics	References
	Homopolymer	Biocatalytic polymerization	4-(phen-5-yl-iminomethyl)-phenol		[263]
	Homopolymer	EP	2,5-di(2-thienyl)-1H-pyrrol, containing phen in pyrrol cycle	Film	[715]
	Copolymer	CoP	5-acrylamido-phen + MMA	$M_n = 4.1 \times 10^4$, PDI = 1.33, T_g = 102.5 °C, [CF] = 2.35 wt%	[897]
	Polycondensate	PC	Poly(phen-3,8-diyl) and their 5,6-dialkoxyderivatives	M_n = 4300–6800	[898]
	Polyarylene ethers	PC	4,7-dichloro-3,8-diphenyl-phen or 4,7-dichloro-2,9-dimethyl-phen + bisphenol A	Soluble, [CF] <=70 mol.%, T_g = 278 °C	[899]
	Polycondensate	PC	5,6-diamino-phen + terephthaldehyde	Yield = 87.2%, [η] = 0.23 dl g^{-1}	[900]
	Polycondensate	PC	4,7-dihydroxy-phen + formaldehyde	Yield = 70%, T_m >300 °C	[901]
	Polycondensate	PC	3,8-dibromo-phen + 2,7-bis-(4,4,5,5-tetramethyl-1,3,2-dioxaborolan-2-yl)-9,9-dihexylfluorene (+ 1,4-dibromobenzene)	Yield = 42%, M_n = 6580, M_w = 21,700, PDI = 3.3, DP = 12.9 (yield = 74%, M_n = 4750, M_w = 26,500, PDI = 5.6, DP = 10.3)	[902]
	PCS	PPM	Support + 5-amino-phen		[903]
	PEG (PIB)	PPM	Support + 5-hydroxy-phen	Yield = 20–40%, M_n = 1550 and 1870 (yield = 20–40%, M_n = 1260 and 2460)	[904]

(continued)

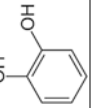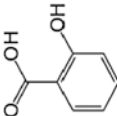**Table 2.5** (continued)

Chelating fragment	Polymer-support	Preparation method	Initial reagents	PCL characteristics	References
	Polyfluorene and poly(p-phenylene ethynylene)	CoP	p-arylene ethynylene or 7,7-dihexylfluorene + sterically enshrouded bpy monomer	PDI = M_w/M_n = 14,519/8026 = 1.8 and 24,714/7536 = 3.28 (38,716/9369 = 4.1 and 9757/3471 = 2.81)	[905]
	Polycondensate	PC	5,5'-dibromo-bpy + 9,9-dioctylfluorene-2,7-bis(trimethylene boronate); 5,5'-bis-(diethylphosphinatylmethyl)-bpy + 2,7-diformyl-9,9'-dioctylfluorene; 5,5'-dibromo-bpy + 2,7-diethynyl-9,9'-dioctylfluorene	Yield = 86, 29, 72%; M_n = 35,200 to 59,200; M_w = 55,300–113,500; PDI = 1.57–1.92	[906]
	Polycondensate	PC	5,5'-divinyl-bpy + (R)-5,5'-dibromo-6,6'-di(4-trifluoromethylphenyl)-2,2'-bisoctoxy-1,1'-binaphthyl	Yield = 72.4%; M_n = 3060; M_w = 6170; PDI = 2.02	[907]
	Polycondensate	PC	5,5'-bis(triphenylphosphoniomethyl)-bpy dibromide + 2,5-diformyl-1,4-didecyloxybenzene, 5,5'-bis(diethoxyphosphorylmethyl)-bpy + 2,5-diformyl-1,4-didecyloxybenzene, 5,5'-dibromo-bpy + 2,5-didecyloxy-1,4-phenylene diboronic acid	Yield = 36%; M_n = 1610; PDI = 1.63; yield = 63%; M_n = 6790; yield = 71%; M_n = 1950; PDI = 1.92	[908]
	Wang benzaldehyde resin	PPM	Support + calix[4]arene derivative incorporating two bpy groups	A grafting yield = 3.1%	[909]
	Phenol-formaldehyde and resorcinol-formaldehyde resins	PPM	Support + 3-(pyridin-2'-yl)-1,2,4-triazine-5(2H)-one	Yield = 75%	[910]
	Polycondensate	PC	2,7-bispinacolatoboron ester of 9,9-dihexylfluorene and a 1,4-dibromobenzene derivative carrying two o-BIP-substituted alkoxy groups in the 2- and 5-position (BIP is 2,6-bis(1'-methyl-benzimidazolyl)-4-hydroxypyridine)	Yield = 88%	[250]

(continued)
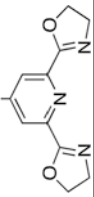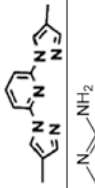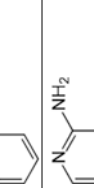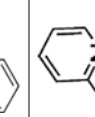
Table 2.5 (continued)

Chelating fragment	Polymer-support	Preparation method	Initial reagents	PCL characteristics	References
	Copolymer	CoP	Pyridine-bis(oxazoline) (pybox) + norbornene (dicyclopentadiene)		[911]
	Homopolymer (copolymer)	HP (CoP)	4-ethynyl-2,6-bis(pyrazolyl)pyridine (BPP) + (fluorine)	$M_n = 10,000$	[694]
	PCD	PPM	Support + 3-aminopyridine	[CF] = 0.96–1.04	[912]
	PCD	PPM	Support + 2-aminopyridine, 2-amino-5-methylthio-1,3,4-thiadiazole, 2-amino-5-ethyl-1,3,4-thiadiazole, and 2-mercaptobenzothiazole		[913, 914]
	Polycondensate	PC	4-(pyridinylimine)phenol + formaldehyde	Yield = 75%	[915]
	Polycondensate	PC	2,2′-diamino-4,4′-bithiazole + salicylic acid + paraformaldehyde	Yield = 90%, [η] = 0.231 dL g^{-1}	[916]
Ph$_2$P(CH$_2$)$_n$PPh$_2$	Copolymer	CoP	CH$_2$=CH$_2$(C$_2$H$_4$)CH$_2$OCH$_2$C(CH$_3$)(CH$_2$PPh$_2$)$_2$ + DVB + St	Yield = 96%	[917]
Ligands of intramolecular compounds					
	Polycondensate	Enzymatic PC	Catechol + pyrogallol	$M_n = 2000$, [CF] = 0.0082	[265]
	PAA	PPM	Support + pyrocatechin		[918, 919]

(continued)

Table 2.5 (continued)

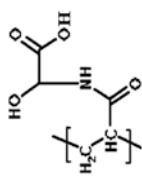| Chelating fragment	Polymer-support	Preparation method	Initial reagents	PCL characteristics	References
	Homopolymer	HP	o-benzoquinonemethacrylate	DP = 22–30 or 110–190	[76]
	Homopolymer	Photopolymerization	β-methacryloylacetone	$[\eta] = 25.0–37.5$ mL g^{-1}	[65]
	Homopolymer	HP	4-acetylacryloylethylacetate	$T_g = 48.2–61.8$ °C	[95]
	Homopolymer	HP	p-vinylbenzoylacetone	$[\eta] = 0.157$ и 1.26 L g^{-1}, yield = 80–98%	[100]
	Polycondensate	Sonogashira coupling reaction	3,7-dibromo-2,8-dimethoxy-5,5-dioctyl-5H-dibenzo[b,d]silole + (Z)-1,3-bis(4-ethynylphenyl)- hydroxyprop-en-1-one	Yield = 51%, M_w = 13 710, M_n = 11,050, PDI = 1.24	[920]
	Polycondensate	PC	acacH + terephthalaldehyde	$[\eta] = 0.92$ dL g^{-1}	[921]
	Polybenzimidazole	PPM	Support + 3-Br-acacH	Yield = 72%, $T_m > 30$ °C, $M_n = 6.1 \times 10^4$, $M_w = 1.6 \times 10^5$, PDI = 2.62	[922]
	Homopolymer	HP	Monomers based on (meth)acryloyl chloride and 2,4-dihydroxybenzophenone, 2,4-dihydroxybenzaldehyde, or 2,4-dihydroxyacetophenone	$[\eta]$ = 0.26–0.41, M_w = 20,300–31,000, M_n = 11,500–19,500, PDI = 1.41–1.76	[66]
	Homopolymer (copolymer)	CoP	2-hydroxy-4-acryloyloxybenzophenone (+ DVB)		[93, 96]
	Polycondensate	PC	2-hydroxy-4-methoxybenzophenone + ethanediol	T_m >270 °C, yield = 60.7%, M_n = 1156	[923]
	Polycondensate	PC	2-hydroxy-4-ethoxybenzophenone + 1,2-propylene glycol	$T_m > 270$ °C, yield = 57.85%	[924]
	Polycondensate	PC	2,4-dihydroxyacetophenone + formaldehyde + oxamide (biuret)	M_n = 10,500–14,400, $[\eta]$ = 1.14–1.22, yield = 84–88%, DP = 13–19 (soluble, yield = 84%, DP = 3.71, M_n = 1 035)	[241, 925]
	Poly(acryloyl chloride)	PPM	Support + salicylaldehyde		[926]

(continued)

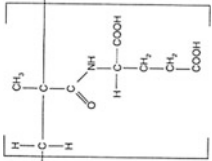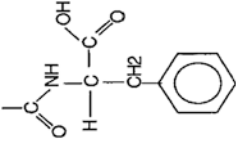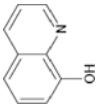**Table 2.5** (continued)

Chelating fragment	Polymer-support	Preparation method	Initial reagents	PCL characteristics	References
	Copolymer	ATRP	St + 5-chlorosulfonylsalicylic acid	M_n = 3590–11,240, PDI = 1.23–1.5	[927]
	Cyclic poly(salicylic acid)	ROP	Salicylic acid O-carboxyanhydride		[102]
	Copolymer	CoP	5,5'-azodisalicylic acid + PEO		[928]
	Polycondensate	Mechanochemical synthesis	Salicylic acid + formaldehyde		[245]
	Polycondensate	PC	Salicylic acid + formaldehyde + melamine (semicarbazide)	Yield = 72%	[929, 930]
	Polycondensate	PC	4-aminosalicylic acid + formaldehyde + urea	Yield = 85%	[931]
	Biodegradable poly (anhydride-ester)	Melt PC	Acetylated disalicylic acid	M_w = 6000, PDI = 1.2, T_g = 23.53 °C	[291]
	PCS	PPM	Support + 5-aminosalicylic acid	[CF] =1.88	[932]
	Chlorosulfonated PS	PPM	Support + 4-aminosalicylic acid	Yield = 98%, [CF] = 2.48, S_{BET} = 99.593, V_{pore} = 0.172, D_{pore} = 6.207 nm	[933]
	Amberlite XAD-4	PPM	Support + 2,3-dihydroxy benzoic acid (salicylic acid)	[CF] = 8.40	[934, 935]
	Polycondensate	Oxidative polycondensation	2-hydroxy-1-naphthaldehyde	M_n = 500, M_w = 1880, PDI = 3.75	[936]
	PCD	PPM	Support + morin	Yield > 95%	[937]
	Homopolymer	HP	GMA-IDA	$[\eta]$ = 0.688 dL g^{-1}	[938]
	Copolymer	CoP	GMA-IDA + MMA (St or St + DVB)	(water-soluble, D_{pore} = 118 or [CF] = 27.6%)	[104, 939, 940]
	Copolymer	CoP	Vinyl-IDA + NIPAM		[941, 942]
	PCS	PPM	Support + amine + acid	S_{BET} = 34.4–45.4	[943, 944]

(continued)
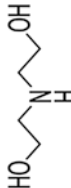
Table 2.5 (continued)

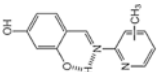| Chelating fragment	Polymer-support	Preparation method	Initial reagents	PCL characteristics	References
EDTA	Polycondensate	PC	Ethylenediaminetetraacetic acid (EDTA) dianhydrides + lactose	M = 132,000	[287]
	Poly(AAmr-AA)	γ-induced template polymerization	Support + EDTA disodium salt		[108]
DTPA	Polymer based on the diallyl ester of 1,1-cyclopropane Dicarboxylic acid and of 2-furanmethanethiol	PPM	Support + diethylenetriamine pentacetic acid (DTPA)	Yield = 75–90%, [CF] = 23–53%, PDI = 1.10–1.13	[945]
	Amino polymer–disulfide	PPM	Support + DTPA dianhydride	DP = 67 and 79, PDI = 1.17	[946]
	Poly(2-hydroxyethylmer-captomethyl-St)	PPM	Support + diethanolamine	[CF] = 4.95, yield = 92.8%	[947]
	Homopolymer (copolymer)	HP (CoP)	2-acrylamido glycolic acid (+ 2-acrylamido-2-methyl propane sulfonic acid)	Water-soluble, yield = 96%	[281, 948]
	Copolymer	Suspension CoP	2-methacryloylamidoglutamic acid + 2-hydroxyethyl methacrylate	S_{BET} = 56.7, a swelling ratio of 63%, [CF] = 3.5	[949]

(continued)

Table 2.5 (continued)

Chelating fragment	Polymer-support	Preparation method	Initial reagents	PCL characteristics	References
	Copolymer	CoP	Methacryloylamidophenylalanine + 2-hydroxyethyl methacrylate	S_{BET} = 19.1, [CF] = 3.2	[105]
	Homopolymer	HP	8-hydroxy-5-azoquinoline phenyl methacrylate-formaldehyde macromonomer	Yield = 77%, [η] = 0.64 dL g^{-1}, M_n = 1.85 × 10^4, M_w = 3.96 × 10^4, PDI = 2.1	[950]
	Copolymer	CoP	5-(2-methacryloylethyloxymethyl)-8-quinolinol + N-vinylcarbazole	M_n = 15,700, PDI = 2.09, T_g = 181, T_d = 383 °C	[951, 952]
	Polycondensate	PC	HQ + formaldehyde + catechol (dithiooxamide, pyrogallol or piperazine)	Yield = 50%, DP = 13.37–18.75, M_n = 4104–14,587, [η] = 0.144–0.158 dL g^{-1}	[953–956]
	Polycondensate	PC	HQ + formaldehyde + salicylic acid	T_m = 379.6 °C, 3850, 1.005	[957]
	Polycondensate	PC	HQ-5-sulphonic acid + formaldehyde + catechol (thiourea)	Yield = 84%, T_m = 391–394 K, DP = 16–23, M_n = 7475–17,188	[958, 959]
	PS	PPM	Support + 5-chloromethyl-HQ	[CF] = 5.88	[960]
	PVC	PPM	Support + HQ-5-sulphonic acid		[961]
	PCD (TosoHaas TSK vinyl polymer resin or GL)	PPM	Support + HQ	[CF] = 2.28, S_{BET} = 2.91 ([CF] = 1.43)	[962–964]
	Poly(p-nitro-St) and poly (p-amino-St)	PPM	Support + bis- HQ-terminated open-chain crown ether		[965]

(continued)

Table 2.5 (continued)
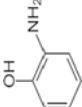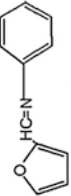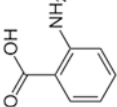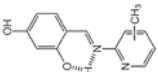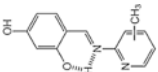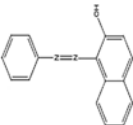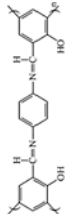
Chelating fragment	Polymer-support	Preparation method	Initial reagents	PCL characteristics	References
	Homopolymer (copolymer)	EP	o-aminophenol (+ aniline)	M_n = 5804–13,992, [η] = 0.89–1.27	[680, 737, 769]
	Polycondensate	PC	o-aminophenol + formaldehyde + urea		[966]
	Aminated PS or cross-linked poly(St-alt-maleic anhydride)	PPM	Support + o-aminophenol		[967, 968]
	4-benzyloxybenzaldehyde, polymer-bound	PPM	Support + o-aminophenol (2-amino-4-chlorophenol or 2-amino-4-methylphenol)	791/731, 1.1 (787/870, 0.9 or 664/641, 1.0)	[969, 970]
	Aminated PS	PPM	Support + furfural		[971]
	Copolymer	EP	Anthranilic acid + aniline		[972]
	Block-copolymers	EP	Anthranilic acid + pyrrol		[777]
	Homopolymer (copolymer)	Chemical polymerization	Anthranilic acid (or + aniline)	Yield = 49% (15.0% in acidic medium)	[703, 704]
	Polycondensate	PC	Anthranilic acid + formaldehyde + o-toluidine	M_n = 3600, [CF] = 6.18, yield = 80%	[973, 974]
	Poly(THF)	GP	Support + poly(caprolactone)-poly(anthranilic acid)-poly(caprolactone)		[333]
	Homopolymer	HP	Monomer based on 2,4-dihydroxy benzaldehyde, aniline and acryloyl chloride	[η] = 0.417 dL. g^{-1}, M_n = 1.89 × 10^4, M_w = 3.26 × 10^4, PDI = 1.72	[68]
	Copolymer	Oxidative PC	2-p-tolylazomethinephenol (o-phenylazomethinephenol) with air oxygen and sodium hypochloride	M_n = 6780, M_w = 7660, PDI = 1.13, [CF] = 0.5–20% (M_n = 1180, M_w = 1930, PDI = 1.64)	[950, 975]
	Polycondensate	PC	Salicylidene-3-amino-1,2,4-triazole (oligo-2-hydroxy naphthalidene-3-amino-1,2,4-triazole)	M_n = 1980, M_w = 5115, PDI = 2.58, (M_n = 1752, M_w = 4300, PDI = 2.45)	[976]
	Polycondensate	PC	5,5'-((2,5-dioctyloxy-1,4-phenylene)bis-(ethyne-2,1-diyl)bis(2-hydroxy-3-(piperidin-1-ylmethyl)-benzaldehyde + (S)-2,2'-binaphthyldiamine	M_w = 32,590, M_n = 18,180, PDI = 1.79	[977]

(continued)

Table 2.5 (continued)

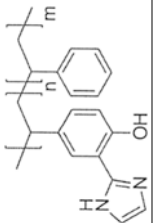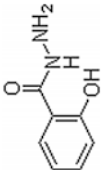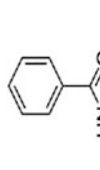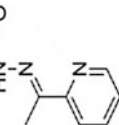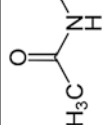| Chelating fragment	Polymer-support	Preparation method	Initial reagents	PCL characteristics	References
	Polycondensate	PC	Diethyleneglycol bis(2-aminophenyl ether) or triethyleneglycol bis(4-aminophenyl ether) with oligosalicylaldehyde	M_n = 1100, M_w = 5400, PDI = 4.90 (M_n = 1100, M_w = 5600, PDI = 5.01)	[978]
	PCS	PPM	Support + 3-formylsalicylic acid and ethanolamine		[979]
	Aminomethylated PS	PPM	Support + 3-ethoxysalicylaldehyde (salicylaldehyde)	[CF] = 0.28–0.75	[980, 981]
	Aminomethylated PS	PPM	Support + 2-hydroxyacetanilide		[982]
	Oligo-2-hydroxy-1-naphthaldehyde	PPM	Support + p-aminophenol (triethyleneglycol bis (4-aminophenyl ether) or aniline)	M_n = 670, M_w = 2490, PDI = 3.71 (M_n = 390, M_w = 1080, PDI = 2.77 or M_n = 320, M_w = 670, PDI = 1.85)	[936]
	Polycondensate	Oxidative PC	Schiff bases in an aqueous alkaline medium using NaOCl	M_n = 40,800–60,680, M_w = 43,840–63,500, PDI = 1.039–1.112	[983]
	Homopolymer	PC + oxidative polymerization	2-[[(6-aminopyridin-2-yl)imino]methyl]-phenol	M_n = 33,500, M_w = 78,900, PDI = 2.352	[984]
	Homopolymer	EP	N,N'-bis(3-methoxysalicylidene)-1,3-propylenediamine	Film	[738, 739]
	Polycondensate	PC	H=…=Ar-=…=H (Ar = fluorene or 2,5-dialkoxy-p-phenylene) + dibromo compounds of salphen (N,N'-phenylenebis (salicylideneimine))	Soluble, M_n = 9200–14,000, M_w = 27,000–49,700	[985]
	Polycondensate	PC	Salen + hydroquinone, 1,3,5-trihydroxybenzene or 1,1,1-tris (4-hydroxy phenyl)ethane dimeric dialdehyde derivatives with (1S, 2S)-(+)-1,2-diaminocyclohexane (or (1R, 2R)-(−)-1,2-diaminocyclohexane)	M_n = 6000	[986]
	Polycondensate	PC	Disalicylaldehyde + (R,R)-1,2-diaminocyclohexane or (R,R)-1,2-diphenylethylenediamine	DP = 27, M_w = 16,771, M_n = 12,261, PDI = 1.37 (DP = 23, M_w = 19,274, M_n = 12,449, PDI = 1.55)	[221]

(continued)

Table 2.5 (continued)

Chelating fragment	Polymer-support	Preparation method	Initial reagents	PCL characteristics	References
	Polycondensate	PC	A phenolic Schiff base derived from 4,4'-diaminodiphenylmethane and o-hydroxyacetophenone + formaldehyde or furfuraldehyde	Yield exceeded 70%	[987]
	Polycondensate	Oxidative PC	1,4-bis[(2-hydroxyphenyl)methylene] pyridinediamine	$M_n = 61,000$, $M_w = 94,200$, PDI = 1.54	[988]
	PCS	PPM	Support + 3-formylsalicylic acid, en and acacH		[885]
	PAAm	PPM	Support + 5-chloro-2-hydroxybenzaldehyde, 5-bromo-2-hydroxybenzaldehyde or 5-methyl-2-hydroxybenzaldehyde	Yield = 48–67%. M_n = 4480, 4630 or 4680	[989]
	Polycondensate	PC	1-(4-hydroxyphenylazo)-2-naphthol + formaldehyde	Yield = 70%, $[\eta]$ = 0.275 dL. g^{-1}. M_n = 1.32 × 10^4, M_w = 2.95 × 10^4, PDI = 2.23	[990]
	Oligo-1,4-bis [(2-hydroxyphenyl) methylene]phenylenediamine	Oxidative polycondensation	1,4-bis[(2-hydroxyphenyl)methylene]phenylenediamine by air, H_2O_2 and NaOCl oxidants	Yield = 99, 79 or 87%, M_n = 2430, M_w = 2550, PDI = 1.049 (M_n = 1 475, M_w = 1 640, PDI = 1.112 or M_n = 900, M_w = 975, PDI = 1.083)	[991]
	Amberlite IR P69	PPM	Support + Schiff base derived from 2-picolyl amine and 2-mercapto-4-methyl-benzaldehyde	Mesh size 16–45 mm	[992]

(continued)

Table 2.5 (continued)

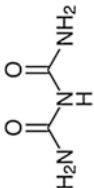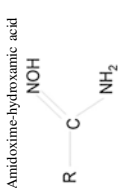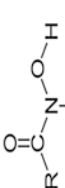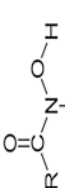| Chelating fragment	Polymer-support	Preparation method	Initial reagents	PCL characteristics	References
	Copolymer	CoP	St + 2-(2'-hydroxy-4'-ethenylphenyl)imidazole		[993]
	4-acryloxybenzaldehyde-co-DVB	PPM	Support + salicyloyl hydrazine	Yield = 51%	[994]
	Poly(methyl vinyl ether-alt-maleic anhydride)	PPM	Support + a Schiff base obtained in condensation of 2-acetylpyridine and 4-aminobenzoic hydrazide	M_w = 216,000, S_{BET} = 2,051, V_{pore} = 0.008, D_{pore} = 4.45 nm	[995]
	4-acryloxyacetophenone-co-DVB	PPM	Support + benzoyl hydrazone	Yield = 52%, the average particle size is 86.12 μm	[996]
	4-methacryloxy-acetophenone-co-MMA	PPM	Support + isonicotinoyl hydrazine	Yield = 41%	[997]
	PCS	PPM	Support + N,N'-bis(4-amino-o-hydroxy acetophenone) hydrazine	[CF] = 3.436	[998]
	Polycondensate	PC	Benzofuro[2,3-b]benzofuran-2,9-dicarboxylic acid + dihydrazides in ionic liquids	[η] = 0.21–0.47 dL g⁻¹, soluble	[44]
	Homopolymer	HP	Acryloyl benzoic hydrazide	Insoluble, yield = 55%	[999]

(continued)

Table 2.5 (continued)
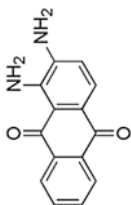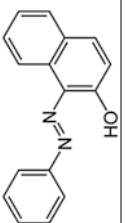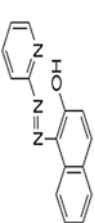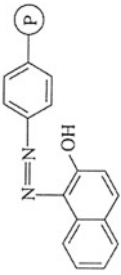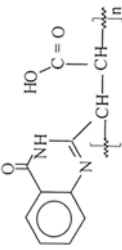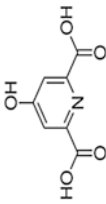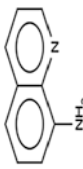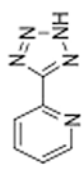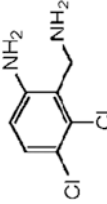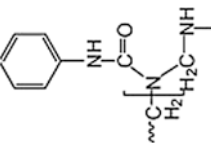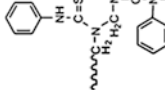
Chelating fragment	Polymer-support	Preparation method	Initial reagents	PCL characteristics	References
	Polycondensate	PC	Biuret + formaldehyde + 4-hydroxyacetophenone	Yield = 60–76%, M_n = 5230–12,019, [η] = 0.074–0.091 dL g^{-1}	[1000]
Amidoxime-hydroxamic acid	PAN	PPM	Support + amidoxime (or hydroxylamine)		[1001]
	Poly(AN-co-ethylacrylate)	PPM	Support + hydroxylamine (N-methylhydroxylamine)	T_m = 240 °C (260 °C)	[1002]
	PEI	PPM	Support + N-methylacrylamide	Soluble in water, yield = 64.0%	[274]
	Poly(GMA)	PPM	Support + iminodiacetonitrile + hydroxylamine		[236]
	PAN-co-DVB	PPM	Support + hydroxylamine	[CF] = 3.0	[1003]
	Homopolymer	EP	1-amino-9,10-anthraquinone	Film	[730, 731]
	Poly-2-hydroxyethyl-methacrylate	PPM	Support + 1,2-diaminoantraquinone		[1004]
	Polycondensate	PC	o-phenylazonaphthol linked with a phenylene or fluorine unit		[1005]
	PCD (Amberlite XAD-16)	PPM	Support + α-pyridylazo-β-naphthol	S_{BET} = 66	[235, 1006]

Table 2.5 (continued)

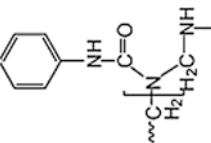| Chelating fragment	Polymer-support	Preparation method	Initial reagents	PCL characteristics	References
	Aminated PS	PPM	Support + 1-nitroso-2-naphthol		[1007]
	Homopolymer	HP	2-acroyl-4-quinazoline		[81]
	Polycondensate	PC	Chelidamic acid + Jeffamin ED® (polyester with end isopropylamino-groups)		[1008]
$RSO_2NHCONH_2$	PCD	PPM	Chlorosulphonated support + urea	3.5 mmol N g^{-1}	[1009]
	Copolymer	Oxidative polymerization	Aminoquinoline + ethylaniline (phenetidine)		[182, 183]
	PCS	PPM	Support + 5-aminopyridine-2-tetrazole	$S_{BET} = 23.72$, $D_{pore} = 18.74$, $V_{pore} = 0.11$	[1010]
	Homopolymer (copolymer)	Oxidative polymerization	o-amino benzyl amine (+ aniline)		[181]
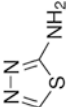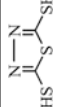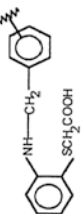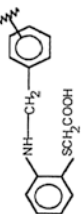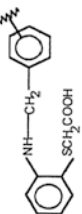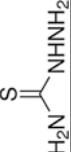
(continued)

Table 2.5 (continued)

Chelating fragment	Polymer-support	Preparation method	Initial reagents	PCL characteristics	References
	PCS	PPM	Support + 2-aminothiazole	[CF] = 2.52	[1011]
	Homopolymer	HP	4-acrylamido benzene sulphonyl guanidine		[1012]
	Polycondensate	PC	Guanidine hydrochloride + hexamethylene diamine + epichlorohydrin	$M_w = 5.8 \times 10^3$ – 1.66×10^6	[1013]
	St-co-DVB-co-N,N,N'-trimethyl-N'-(4-vinylbenzyl) cyanoguanidine	PPM	Support hydration		[1014]
	Polycondensate	PC	Phenylurea + formaldehyde	Yield = 75%, T_m >300 °C	[1015]
	Polycondensate	PC	Phenylthiourea + formaldehyde	Yield = 75%, M_w = 16,800	[1016]
	Polyallylamine with thiourea groups	PPM	Support + methyl isothiocyanate	Water-soluble	[280]
	Homopolymer	EP	3-amino-1,2,4-triazole	Film	[710]
	Polycondensate	PC	3-amino-1,2,4-triazole-5-thiol + glutaraldehyde (thiourea)	T_m > 300 °C, S_{BET} = 560 (687)	[1017]
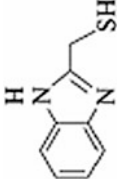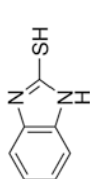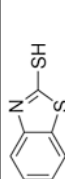
(continued)

Table 2.5 (continued)

Chelating fragment	Polymer-support	Preparation method	Initial reagents	PCL characteristics	References
	PAN (PCS)	PPM	Support + 2-amino-1,3,4-thiadiazole	[CF] = 3.55, yield = 34.92%, S_{BET} = 27.83, D_{pore} = 25.4 ([CF] = 3.65, yield = 88.6%)	[1018, 1019]
	PS-diethylene glycol or PS-triethylene glycol	PPM	Support + 2-amino-5-methylthio-1,3,4-thiadizole		[1020]
	PCS	PPM	Support + 2,5-dimercapto-1,3,4-thiadiazol	[CF] = 2.07	[1021]
	Copolymer	PC	2,5-bis(mercapto-acetichydrazide)-1,3,4-thiadiazole + 4,4'-biphenic, 3,3'-azodibenzoyl, 4,4'-azodibenzoyl dichlorides		[244]
	PCS	PPM	Support + 2-aminothiophenyl-S-acetic acid		[199]
	Copolymer	PC	Thiosemicarbazide + formaldehyde		[268]
	Amberlite IRC-50	PPM	Support + thiosemicarbazide		[1022]
	Polycondensate	PC	4-hydroxyacetophenone + oxamide + formaldehyde		[1023]
	PCD	PPM	Support + thiosemicarbazone		[1024]
	PCD	PPM	Support + dithiooxamide	[CF] = 0.97	[1025]

(continued)

Table 2.5 (continued)

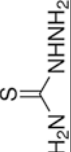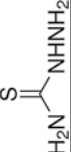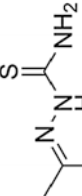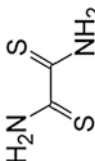| Chelating fragment	Polymer-support	Preparation method	Initial reagents	PCL characteristics	References
	PCD	PPM	Support + 2-thiomethylbenzimidazole		[1026]
	Copolymer	CoP	AA + 2-mercaptobenzimidazole		[107]
	PCD (PCS)	PPM	Support + 2-mercaptobenzothiazole	D_{pore} = 875–890, S_{BET} = 10.29–12.22 ([CF] = 3.67)	[232, 233, 1027]
	PAN	PPM	Support + 2-amino-2-thiazoline	S_{BET} = 27.80, D_{pore} = 25.1, [CF] = 2002	[1028]
	Homopolymer	EP	2-aminothiazole	Film	[1029]
	PCD	PPM	Support + 4-amino-5-methyl-3-thio-1,2,4-triazole	[CF] = 0.916	[1030]
	Poly(thiourea-amide)s	PC	Aromatic and aromatic-aliphatic diamines [isophthaloyl bis(3-(3-aminophenyl)thiourea), terephthaloyl bis(3-(3-aminophenyl)thiourea), adipoyl bis(3-(3-aminophenyl)thiourea), sebacoyl bis(3-(3-aminophenyl)thiourea)] + the diacid chlorides such as isophthaloyl, terephthaloyl and adipoyl chloride	0.92–1.56 dL g^{-1}, M_n = 607 × 10²-851 × 10², PDI = 1.62–1.88	[1031]

(continued)

Table 2.5 (continued)

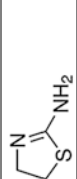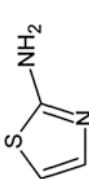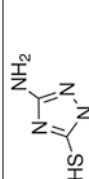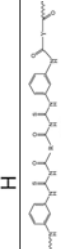| Chelating fragment	Polymer-support	Preparation method	Initial reagents	PCL characteristics	References
	Phenol-formaldehyde resin	PPM	Support + the disulfide carbon	Yield = 70%	[1032]
Ligands of macrocyclic complexes					
DOTA	GL	PPM	Support + DOTA	[CF] = 0.088	[1033]
	Homopolymer	HP	Monomer based on cyclam and acryloyl chloride	Swelling ratio 1400% at pH 12.0	[75]
	Vinylbenzyl chloride-co-DVB	PPM	Support + cyclam		[1034]
Tetraazacyclododecane (cyclen)	Poly(2-methyl-2-oxazoline) and poly(2-ethyl-2-oxazoline)	PPM	Support + N,N',N'',N'''-tetraazacyclododecane-1,4,7,10-tetraacetic acid	Water-soluble, 4500	[1035]
	Polycondensate	PC	Diester macrocycles + different aliphatic diamines		[1036]
Triazamacrocycle	Copolymer	CoP	(E,E,E)-1-[(4-methylphenyl)sulfonyl]-6-[(2-trimethylsilylethyl)sulfonyl]-11-[(4-vinylphenyl)sulfonyl]-1,6,11-triazacyclopentadeca-3,8,13-triene + St	[CF] = 1.15	[1037]
12-crown-4	Copolymer	CoP	NIPAM + benzo-12-crown-4-acrylamide		[86]
	Homopolymer	HP	1,4,7,10-tetraoxacyclododecan-2-ylmethyl methacrylate	Soluble, T_g = 35 °C	[1038]
	Polycondensate	PC	Isophthalic diacid-based monomers with 12-crown-4 ether group + aromatic diamines	T_m up to 349 °C, soluble	[1039]
15-crown-4	Copolymer	CoP	2,7-dibromo-9-(15-crown-4)-9H-fluoren + 2,4,7-trivinyl-9,9-dihexylfluoren		[1040]
15-crown-5	Copolymer	CoP	MMA + benzo-15-crown-5	M_n = 33,000–90,000, PDI = 2.1–2.5	[84]

(continued)

Table 2.5 (continued)

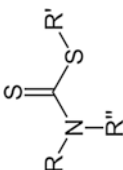| Chelating fragment	Polymer-support	Preparation method	Initial reagents	PCL characteristics	References
18-crown-6	Copolymer	CoP	AA + acrylamidomethyl-1-18-crown-6 (acrylamidomethyl 15-crown-5)	Yield = 70–72%, M_n = 37,500 (yield = 70%, M_n = 31,500)	[85]
	Copolymer	Oxidative coupling polymerization	Macromonomer containing dibenzo-18-crown-6 + p-phenylenediamine		[1041]
	Copolymer	CoP	NIPAM + benzo-18-crown-6-acrylamide		[1042]
	Copolymer	EP	Dibenzo-18-crown-6	Film	[1043]
	PP	PPM	Support + di-t-butylbenzo-18-crown-6		[1044]
32-crown-10	Homopolymer (copolymer)	HP (CoP)	5-vinyl-m-phenylene-m'-phenylene-32-crown-10 (+ AN or St)	M_n = 36,000 (M_n = 9900–14,300, T_g = 7–39 °C or M_n = 7300–11,800, T_g = 21–53 °C)	[83]
Azacrown ethers	Homopolymer	HP	16-membered α-methylenemacrolide monomers with monoazacrown ether	M_n > 5000	[1045]
	Copolymer	CoP	Crowned spirobenzopyran vinyl monomer + MMA	M_n = 5.7 × 10³, 8.1 × 10³, and 5.1 × 10⁴	[1046]
	Copolymer	CoP	N-2-ethyl-azacrown ether methacrylate (aza-12-crown-4, aza-15-crown-5 or aza-18-crown-6) + 9-anthryl methacrylate	[η] = 1.011, 0.599 or 0.573	[1047]
Monoaza dibenzo-18-crown-6	Amberlite XAD-4	PPM	Support + monoaza dibenzo-18-crown-6	[CF] = 1.34	[1048]
Diaza-18-crown-6	Polycondensate	PC	4,4′-(hexafluoroisopropylidene)diphthalic anhydride + macrocyclic diamine monomers		[1049]
Polymeric pseudo-crown ethers	Homopolymer	Cyclopoly-merization	PEG dimethacrylates		[1050]
Polyamine podand	Polycondensate	PC	1,3,5,7-tetrakis(2-glycidyloxypropyl)-1,3,5,7-tetramethylcyclotetrasiloxane + the corresponding amine	Yield = 79–87%, [CF] = 6.43–12.95	[1051]
Thiacrown ethers	Copolymer	ROP	3-thiopentyl glycidyl ether + diethylene glycol bisglycidyl ether	Yield = 74.6–95.1%	[159]
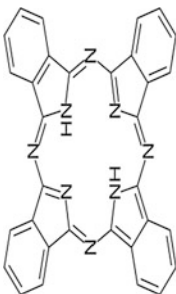
(continued)

Table 2.5 (continued)

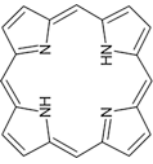| Chelating fragment	Polymer-support	Preparation method	Initial reagents	PCL characteristics	References
	Homopolymer	EP	Monomer containing fullerene and Pp units		[757]
	Copolymer	EP	Pp + tetra- or bithiophene		[754]
	Homopolymer	EP	5,10,15,20-tetrakis[3-(N-ethylcarbazoyl)]-Pp		[752]
	Homopolymer	EP	Tetra-(4-hydroxyphenyl)-Pp		[755]
	Homopolymer	EP	5-(4'-aminophenylamino)-10,20-diphenyl-Pp		[753]
	Homopolymer	HP	Ethynyl Pp monomers		[1052]
	Homopolymer	Polycycloaddition by click polymerization	Pp-containing dialkyne and 1,4-diazidobenzene		[667]
	Copolymer	ROMP	Pp + alkylnorbornene		[153]
	Block-copolymers	NMP	PSS + 5-(4-acryloyloxyphenyl)-10,15,20-tritolyl-Pp	Water-soluble	[145]
	Copolymer	CoP	Meso-tetrakis(pentafluorophenyl)-Pp + bis(catechol) monomer	S_{NET} = 900–1000	[1053]
	Copolymer	CoP	Pp + dithienothiophene	Soluble, T_m = 330–410 °C, T_g = 130–180 °C	[255]
	Copolymer	CoP	Pp, poly(p-phenylenevinylene) and/or a pendant fullerene	6.5×10^4 (2.3×10^5)	[1054]
	Copolymer	CoP	AAm (methacrylic acid) + disodium salt of protoporphyrin IX	M_n = 6000–23,000, PDI = 2.1–2.6	[1055]
	Polycondensate	PC	9,9'-dioctylfluorene + tetraphenyl-Pp by Pd-catalyzed Suzuki coupling reaction		[249]
	Poly(aryl isocyanide)	PPM	Support + tetraphenyl-Pp derivative	M_n = 10,300–19,000, PDI = 1.15–1.16	[217]

(continued)

Table 2.5 (continued)

Chelating fragment	Polymer-support	Preparation method	Initial reagents	PCL characteristics	References
	Homopolymer	Polymeric tetramerization	1,8-diazabicyclo[5.4.0]undec-7-ene + bisphthalonitrile monomer (N,N'-bis (2-oxyethyl-phthalonitrilo)-4,13-diaza-18-crown-6) (1,11-bis{3,4-dicyanophenylthio)-3,6,9-trithiaundecane or o-bis[3-(3,4-dicyanophenoxy) propyloxy]benzene)	$T_m > 300$ °C (yield = 70%, PDI = 2.76)	[205, 1056–1058]
	Poly[chlorotrifluoroethylene-alt-(2-iodoethyl vinyl ether)]	GP	Support + alkynyl CF_3-containing phthalocyanine		[1059]
	Polycondensate	PC	Tetranitrile monomer + 4,4'-[pyridine-2,6-diylbis (methyleneoxy)]diphthalonitrile	Yield = 51%, $T_m >$ 300 °C	[198]
	Cz-based polymer	PPM	Support + Pc	$M_n = 8729$, $M_w = 27$ 809, $T_g = 97$–110 °C, soluble	[1060]
	Allyloxy nonyl-phenoxy propanol polyoxyethylene ether ammonium sulfonate	PPM	Support + Pc		[1061]

Note *EP* Electropolymerization; *HP* Homopolymerization; *CoP* Copolymerization; *[CF]* Concentration of chelating fragments, mmol g^{-1}; S_{BET} Brunauer-Emmett-Teller (BET) surface area, m^2 g^{-1}; V_{pore} Volume of pores, cm^3 g^{-1}; D_{pore} Average pore diameter, nm

References

1. F. Tian, M.J. Roman, E.A. Decker, J.M. Goddard, J. Appl. Polym. Sci. **132**, 41232 (2015)
2. A.D. Pomogailo, I.E. Uflyand, *Makromolekulayrnye Metallokhelaty (Macromolecular Metal Chelates)* (Khimiya, Moscow, 1991)
3. D. Wohrle, A.D. Pomogailo, *Metal Complexes and Metals in Macromolecules* (Wiley-VCH, Weinheim, 2003)
4. I. Manners, *Synthetic Metal-Containing Polymers* (Wiley-VCH, Weinheim, 2004)
5. V. Chandrasekhar, *Inorganic and Organometallic Polymers* (Springer, Berlin, Heidelberg, 2005)
6. U.S. Schubert, G.R. Newkome, I. Manners (eds.), *Metal-Containing and Metallosupramolecular Polymers and Materials*, ACS Symposium Series, vol 928 (ACS, Washington, 2006)
7. Ch. Carraher Jr., C. Pittman Jr., A. Abd-El-Aziz, M. Zeldin, J. Sheats (eds.), *Metal and Metalloid Containing Macromolecules* (Wiley, NY, 2006)
8. A. Abd-El-Aziz, C.E. Carraher Jr., C.U. Pittman, M. Zeldin (eds.), *Macromolecules Containing Metal and Metal-Like Elements* (Wiley, New Jersey, 2006)
9. J.H. Zagal, F. Bedioui, J.P. Dodelet, *N₄-Macrocyclic Metal Complexes* (Springer, NY, 2006)
10. U.S. Schubert, H. Hofmeier, G.R. Newkome, *Modern Terpyridine Chemistry* (Wiley-VCH, Weinheim, 2006)
11. O.I. Koifman, T.A. Ageeva, *Porphyrinpolymers* (Fizmatlit, Moscow, 2006)
12. A.S. Abd-El-Aziz, I. Manners, *Frontiers in Transition Metal-Containing Polymers* (Wiley, Hoboken, New Jersey, 2007)
13. A.S. Abd-El-Aziz, C.E. Carraher, C.U. Pittman, *Inorganic and Organometallic Macromolecules: Design and Applications* (Springer, NY, 2008)
14. U.S. Schubert, A. Winter, G.R. Newkome, *Terpyridine-Based Materials. For Catalytic, Optoelectronic and Life Science Applications* (Wiley-VCH, Weinheim, 2011)
15. A.D. Pomogailo, Ros. Khim. Zh. (Mendeleev Chem. J.) **46**, 64 (2002)
16. P. Theato, H.-A. Klok (eds.), *Functional Polymers by Post-Polymerization Modification—Concepts, Guidelines, and Applications* (Wiley-VCH, Weinheim, 2012)
17. P. Zinck, F. Bonnet, A. Mortreux, M. Visseaux, Progr. Polym. Sci. **34**, 369 (2009)
18. M. Chanda, S.K. Roy, *Industrial Polymers, Specialty Polymers, and Their Applications* (CRC Press, Boca Raton, 2008)
19. E.A. Campo, *Industrial Polymers* (Hanser-Gardner, Cincinnati, 2008)
20. W. Wu, R. Tang, Q. Li, Z. Li, Chem. Soc. Rev. **44**, 3997 (2015)
21. W. Knoll, R.C. Advincula (eds.), *Functional Polymer Films* (Wiley-VCH, Weinheim, 2013)
22. M.I. Barroso (ed.), *Reactive and Functional Polymers Research Advances* (Nova Science Publishers, NY, 2008)
23. V. Jain, A. Kokil (eds.), *Optical Properties of Functional Polymers and Nano Engineering Applications* (CRC Press, Boca Raton, 2015)
24. J. Hu, *Adaptive and Functional Polymers, Textiles and Their Applications* (Imperial College Press, London, 2011)
25. W.-Y. Wong, A.S. Abd-El-Aziz (eds.), *Molecular Design and Applications of Photofunctional Polymers and Materials* (RSC Press, Cambridge, 2012)
26. H. Zhang, Eur. Polym. J. **49**, 579 (2013)
27. M.R. Aguilar, J.S. Román (eds.), *Smart Polymers and their Applications* (Woodhead Publishing, Cambridge, 2014)
28. E. Khosravi, Y. Yagci, Y. Savelyev (eds.), *New Smart Materials Via Metal Mediated Macromolecular Engineering* (Springer, Dordrecht, 2008)
29. H. Meng, G. Li, Polymer **54**, 2199 (2013)
30. T. Ueki, R. Yoshida, Phys. Chem. Chem. Phys. **16**, 10388 (2014)
31. A. Kumar, A. Srivastava, IYu. Galaev, B. Mattiasson, Prog. Polym. Sci. **32**, 1205 (2007)

32. P.T. Anastas, J.B. Zimmerman (eds.), *Innovations in Green Chemistry and Green Engineering* (Springer, NY, 2013)
33. R.A. Sheldon, I. Arends, U. Hanefeld, *Green Chemistry and Catalysis* (Wiley, Weinheim, 2007)
34. C. Jimenez-Gonzalez, D.J.C. Constable, *Green Chemistry and Engineering* (Wiley, Hoboken, New Jersey, 2011)
35. M. Lancaster, *Green Chemistry: An Introductory Text* (RSC, Cambridge, 2010)
36. S.C. Ameta, R. Ameta (eds.), *Green Chemistry: Fundamentals and Applications* (CRC Press, Boca Raton, 2013)
37. H. Pinkowska, Polimery **51**, 836 (2006)
38. T. Oshima, M. Sato, Y. Shikaze, K. Ohto, K. Inoue, Y. Baba, Biochem. Eng. J. **35**, 66 (2007)
39. Y. Yang, L. Mao, L. Li, X. Liu, J. Shi, S. Cao, Chem. Res. Chin. Univ. **20**, 240 (2004)
40. L. Zhang, J. Lian, J. Solid State Electrochem. **12**, 1 (2008)
41. B. Grignard, C. Jerome, C. Calberg, R. Jerome, C. Detrembleur, Eur. Polym. J. **44**, 861 (2008)
42. T. Ribaut, P. Lacroix-Desmazes, B. Fournel, S. Sarrade, J. Polym. Sci. A **47**, 5448 (2009)
43. J.M. DeSimone, W. Tumas (eds.), *Green Chemistry Using Liquid and Supercritical Carbon Dioxide* (Oxford University Press, Oxford, 2003)
44. A. Abdolmaleki, S.K. Varnamkhasti, J. Appl. Polym. Sci. **113**, 1935 (2009)
45. C.L. McCormick, A.B. Lowe, Acc. Chem. Res. **37**, 312 (2004)
46. D. Braun, H. Cherdron, M. Rehahn, H. Ritter, B. Voit, *Polymer Synthesis: Theory and Practice: Fundamentals, Methods, Experiments* (Springer, Berlin, 2012)
47. P.A. Williams (ed.), *Handbook of Industrial Water Soluble Polymers* (Wiley-Blackwell, Singapore, 2007)
48. B. Rieger, A. Künkel, G.W. Coates, R. Reichardt, E. Dinjus, T.A. Zevaco (eds.), *Synthetic Biodegradable Polymers* (Springer, Heidelberg, 2012)
49. T. Ma, Y. Liu, L. Sun, Gaofenzi Cailiao Kexue Yu Gongcheng **25**, 157 (2009)
50. K. Ishizu, K. Tsubaki, A. Mori, S. Uchida, Prog. Polym. Sci. **28**, 27 (2003)
51. S. Seiffert, Macromol. Chem. Phys. **216**, 9 (2015)
52. U.S. Schubert, A. Winter, *Supramolecular Assemblies: Polymers and Discrete Systems* (Wiley-VCH Verlag, Weinheim, 2015)
53. N. Hadjichristidis, A. Hirao, Y. Tezuka, F. Du Prez (eds.), *Complex Macromolecular Architectures: Synthesis, Characterization, and Self-Assembly* (John Wiley & Sons, Asia, Pte Ltd., 2011)
54. J.-M. Lehn, Chem. Soc. Rev. **36**, 151 (2007)
55. J.-M. Lehn, Aust. J. Chem. **63**, 611 (2010)
56. J.-M. Lehn, Constitutional dynamic chemistry: bridge from supramolecular chemistry to adaptive chemistry, in *Constitutional Dynamic Chemistry*, ed. by M. Barboiu (Springer, Berlin, Heidelberg, 2012)
57. J.-M. Lehn, Angew. Chem. Int. Ed. **127**, 4 (2015)
58. S.J. Rowan, S.J. Cantrill, G.R.L. Cousins, J.K.M. Sanders, J.F. Stoddart, Angew. Chem. Int. Ed. **41**, 898 (2002)
59. L. Hu, F. Schaufelberger, B.J.J. Timmer, M. Abellán Flos, O. Ramström, Constitutional dynamic chemistry, in *Kirk-Othmer Encyclopedia of Chemical Technology*, ed. by Kirk-Othmer (Wiley, NY, 2014)
60. J. Li, P. Nowak, S. Otto, J. Am. Chem. Soc. **135**, 9222 (2013)
61. J.C. Eslick, Q. Ye, J. Park, E.M. Topp, P. Spencer, K.V. Camarda, Comput. Chem. Eng. **33**, 954 (2009)
62. A.D. Pomogailo, I.E. Uflyand, E.F. Vainshtein, Russ. Chem. Rev. **64**, 857 (1995)
63. V.I. Irzhak, *Polymer Architecture* (Nauka, Moscow, 2012)
64. G.V. Korolyov, M.M. Mogilevich, *Three-Dimensional Free-Radical Polymerization* (Springer, Berlin, Heidelberg, 2009)
65. J. Zhao, T. Zhao, K. Qiu, Chin. J. Polym. Sci. **15**, 50 (1997)

66. T. Kaliyappan, S. Rajagopan, P. Kannan, J. Appl. Polym. Sci. **90**, 2083 (2003)
67. P. Kandasamy, M. Sasidaran, N. Janaki, T. Kaliyappan, J. Appl. Polym. Sci. **124**, 3600 (2012)
68. T. Kaliyappan, S. Rajagopan, P. Kannan, J. Appl. Polym. Sci. **91**, 494 (2004)
69. P.G. Ingole, H.C. Bajaj, K. Singh, J. Appl. Polym. Sci. **128**, 66 (2013)
70. R. Sankar, M. Sasidaran, T. Kaliyappan, High Perform. Polym. **23**, 32 (2011)
71. S. Vijayalakshmi, R. Sankar, S. Subramanian, S. Rajagopan, T. Kaliyappan, J. Appl. Polym. Sci. **104**, 797 (2007)
72. S. Vijayalakshmi, S. Subramanian, S. Rajagopan, T. Kaliyappan, J. Appl. Polym. Sci. **99**, 1516 (2006)
73. S. Vijayalakshmi, R. Sankar, S. Subramanian, S. Rajagopan, T. Kaliyappan, Des. Monomers Polym. **9**, 425 (2006)
74. R. Sankar, S. Vijayalakshmi, S. Subramanian, S. Rajagopan, T. Kaliyappan, Eur. Polym. J. **43**, 4639 (2007)
75. B. Salih, J. Appl. Polym. Sci. **83**, 1406 (2002)
76. M.V. Arsenyev, M.P. Shurygina, A.I. Poddel'sky, N.O. Druzhkov, S.A. Chesnokov, G.K. Fukin, V.K. Cherkasov, G.A. Abakumov, J. Polym. Res. **20**, 98 (2013)
77. A. Khazaei, D. Soudbar, M. Sadri, S.M.S. Mohaghegh, Iran. Polym. J. **16**, 309 (2007)
78. A.A. Khalil, J. Polym. Res. **20**, 28 (2013)
79. A.A. Khalil, J. Appl. Polym. Sci. **121**, 1160 (2011)
80. R.M. Issa, A.Z. El-Sonbati, A.A. El-Bindary, H.M. Kera, Eur. Polym. J. **38**, 561 (2002)
81. E.H. El-Mossalamy, Zaštita Materijala **49**, 23 (2008)
82. L.Y. Jin, T. Chien, M. Fang, S. Mah, B. Yin, Fibers Polym. **8**, 143 (2007)
83. L.Y. Jin, S. Mah, J. Appl. Polym. Sci. **84**, 2372 (2002)
84. A. Aydogan, D.J. Coady, K.S. Kuk, A. Akar, C.W. Bielawski, M. Marquez, J.L. Sessler, Angew. Chem. Int. Ed. **47**, 9648 (2008)
85. G.J. Price, P.L. Drake, React. Funct. Polym. **66**, 109 (2006)
86. Y.M. Wang, X.J. Ju, Z. Liu, R. Xie, W. Wang, J.F. Wu, Y.Q. Zhang, L.Y. Chu, Macromol. Rapid Commun. **35**, 1280 (2014)
87. P. Mi, L.Y. Chu, X.J. Ju, C.H. Niu, Macromol. Rapid Commun. **29**, 27 (2008)
88. H.R. Yu, X.J. Ju, R. Xie, W. Wang, B. Zhang, L.Y. Chu, Anal. Chem. **85**, 6477 (2013)
89. B. Zhang, X.J. Ju, R. Xie, Z. Liu, S.W. Pi, L.Y. Chu, J. Phys. Chem. B **116**, 5527 (2012)
90. R.M. Patel, M.B. Patel, P.M. Patel, K.J. Patel, Orient. J. Chem. **17**, 233 (2001)
91. S.A. Patel, B.S. Shah, R.M. Patel, P.M. Patel, Iran. Polym. J. **13**, 445 (2004)
92. P. Patel, B. Shah, A. Ray, R. Patel, J. Polym. Res. **11**, 65 (2004)
93. H.M. Zalloum, B. El-Eswed, R.M. Zalloum, M.S. Mubarak, J. Appl. Polym. Sci. **126**, 1008 (2012)
94. J. Bernard, C. Branger, I. Beurroies, R. Denoyel, S. Blanc, A. Margaillan, Polymer **51**, 2472 (2010)
95. C.-H. Yuan, S.-B. Lin, B. Liu, A.-R. Ke, Z.-L. Quan, Sens. Actuators B Chem. **140**, 155 (2009)
96. R.M. Zalloum, M.S. Mubarak, J. Appl. Polym. Sci. **109**, 3180 (2008)
97. L. Hauser, A.-C. Knall, M. Roth, G. Trimmel, M. Edler, T. Griesser, W. Kern, Monatsh. Chem. **143**, 1551 (2012)
98. T. Bilig, Y. Koyama, T. Takata, Chem. Lett. **37**, 468 (2008)
99. A.Z. Albayrak, D. Avci, J. Appl. Polym. Sci. **109**, 459 (2008)
100. S. Masuda, T. Tomida, M. Tanaka, Y. Asahi, Macromol. Chem. Phys. **196**, 621 (1995)
101. T. Tomida, M. Tomida, Y. Nishihara, I. Nakabayashi, T. Okazaki, S. Masuda, Polymer **31**, 102 (1990)
102. H.R. Kricheldorf, N. Lomadze, G. Schwarz, J. Macromol. Sci. Part A **46**, 346 (2009)
103. D.-F. Wei, R.-H. Zhou, Y.-W. Zhang, Y. Guan, A.-N. Zheng, J. Appl. Polym. Sci. **130**, 419 (2013)
104. C.-C. Wang, C.-Y. Chen, C.-Y. Chang, J. Appl. Polym. Sci. **84**, 1353 (2002)
105. R. Say, S. Emir, B. Garipcan, S. Patir, A. Denizli, Adv. Polym. Technol. **22**, 355 (2003)

106. A. Denizli, B. Garipean, A. Karabakan, R. Say, S. Emir, S. Patir, Sep. Purif. Technol. **30**, 3 (2003)
107. H.M.M.N. El-Din, J. Appl. Polym. Sci. **86**, 1607 (2002)
108. H.A. Hanafi, M. Abd Elsamad, Open J. Inorg. Chem. **5**, 19 (2015)
109. N. Şahiner, Ö. Çelikbıçak, S. Malc, Ö. Kantoğlu, B. Salih, J. Appl. Polym. Sci. **99**, 1657 (2006)
110. S. Döker, Ö. Çelikbıçak, M. Doğan, B. Salih, Microchem. J. **84**, 80 (2006)
111. N. Sandor, D. Gyorgy, K. Sandor, Z. Miklos, Magy. Kem. Lap. **57**, 410 (2002)
112. J. Jagur-Grodzinski (ed.), *Living and Controlled Polymerization, Synthesis, Characterization and Properties of the Respective Polymers and Copolymers* (Nova Science Publishers, NY, 2006)
113. N.V. Tsarevsky, B.S. Sumerlin (eds.), *Fundamentals of Controlled/Living Radical Polymerization* (RSC Publications, Cambridge, 2012)
114. K. Matyjaszewski, T.P. Davis, *Handbook of Radical Polymerization* (Wiley, Hoboken, 2002)
115. K.A. Aamer, G.N. Tew, Macromolecules **37**, 1990 (2004)
116. Y.-N. Zhou, Q. Zhang, Z.-H. Luo, Langmuir **30**, 1489 (2014)
117. K. Matyjaszewski, J. Xia, Chem. Rev. **101**, 2921 (2001)
118. M. Kamigaito, T. Ando, M. Sawamoto, Chem. Rev. **101**, 3689 (2001)
119. G. Moad, E. Rizzardo, S.H. Thang, Polymer **49**, 1079 (2008)
120. S. Perrier, P. Takolpuckdee, J. Polym. Sci. Part A Polym. Chem. **43**, 5347 (2005)
121. J.B. Mcleary, B. Klumperman, Soft Matter **2**, 45 (2006)
122. G. Moad, M. Chen, M. Häussler, A. Postma, E. Rizzardo, S.H. Thang, Polym. Chem. **2**, 492 (2011)
123. G. Moad, E. Rizzardo, S.H. Thang, Aust. J. Chem. **62**, 1402 (2009)
124. C.J. Hawker, A.W. Bosman, E. Harth, Chem. Rev. **101**, 3661 (2001)
125. Z. Yang, J. Lu, Gaofenzi Xuebao 838 (2008)
126. Z. Yang, J. Lu, L. Wang, Polym. Bull. **53**, 249 (2005)
127. C.-M. Liu, J.-J. Qiu, R. Bao, Y. Xu, X.-J. Cheng, F. Hu, Polymer **47**, 2962 (2006)
128. J. Zhou, L. Wang, X. Dong, T. Chen, Q. Yang, Q. Tan, J. Wang, Eur. Polym. J. **43**, 2088 (2007)
129. S. Li, H. Li, J. Guo, Huagong xuebao. SIESC J. **63**, 1967 (2012)
130. C. Wang, W. Zhang, N. Zhou, Y. Qiu, Z. Cheng, X. Zhu, Int. J. Polym. Sci. **2010**, article ID 340926 (2010)
131. J. Xu, X. Xiao, Y. Zhang, W. Zhang, J. Polym. Sci. Part A Polym. Chem. **51**, 1147 (2013)
132. H. Hofmeier, A. El-Ghayoury, U.S. Schubert, J. Polym. Sci. A **42**, 4028 (2004)
133. F.D. Jochum, J. Brassinne, C.-A. Fustin, J.-F. Gohy, Soft Matter **9**, 2314 (2013)
134. Q. He, J. Huang, H. Liang, J. Lu, Polym. Chem. **5**, 4348 (2014)
135. G. Zhou, I.I. Harruna, Macromolecules **37**, 7132 (2004)
136. G. Zhou, I.I. Harruna, Macromolecules **38**, 4114 (2005)
137. J. Zhang, L. Wang, C. Li, Y. Li, J. Liu, Y. Tu, W. Zhang, N. Zhou, X. Zhu, J. Polym. Sci. Part A Polym. Chem. **52**, 691 (2014)
138. S. Mukherjee, A.P. Bapat, M.R. Hill, B.S. Sumerlin, Polym. Chem. **5**, 6923 (2014)
139. S. Wang, B. Wu, F. Liu, Y. Gao, W. Zhang, Polym. Chem. **6**, 1127 (2015)
140. M. Demetriou, T. Krasia-Christoforou, J. Polym. Sci. Part A Polym. Chem. **50**, 52 (2012)
141. T. Krasia, R. Soula, H.G. Börner, H. Schlaad, Chem. Commun. **4**, 538 (2003)
142. T. Otsu, J. Polym. Sci. Part A Polym. Chem. **38**, 2121 (2000)
143. N. Metz, P. Theato, Eur. Polym. J. **43**, 1202 (2007)
144. U. Mansfeld, A. Winter, M.D. Hager, W. Günther, E. Altuntaş, U.S. Schubert, J. Polym. Sci. Part A Polym. Chem. **51**, 2006 (2013)
145. M. Nowakowska, A. Karewicz, M. Klos, Macromolecules **36**, 4134 (2003)
146. R. Shunmugam, K.A. Aamer, G.N. Tew, Polym. Prepr. **48**, 635 (2007)
147. B.G.G. Lohmeijer, U.S. Schubert, J. Polym. Sci. Part A Polym. Chem. **42**, 4016 (2004)

148. H.W. Gibson, Z. Ge, F. Huang, J.W. Jones, H. Lefebvre, M.J. Vergne, D.M. Hercules, Macromolecule **38**, 2626 (2005)
149. A. Farcas, M. Pinteala, V. Harabagiu, Rev. Roum. Chim. **52**, 143 (2007)
150. C.W. Bielawski, R.H. Grubbs, Prog. Polym. Sci. **32**, 1 (2007)
151. A.V. Rozhkov, L.N. Bochkarev, G.V. Basova, G.A. Abakumova, Zh. Prikl. Khim. **85**, 2046 (2012)
152. A.V. Rozhkov, L.N. Bochkarev, G.V. Basova, I.P. Malysheva, Y.E. Begantsova, E.O. Platonova, E.V. Baranov, Y.A. Kurskii, V.A. Il'ichev, M.A. Lopatin, G.A. Abakumov, M. N. Bochkarev, Zh. Obsch. Khim. **82**, 1937 (2012)
153. H. Li, K. Feng, L. Zhou, B. Chen, L. Zhang, Z. Tong (C. Tung), L. Wu, Yingxiang kexue yu guanghuaxue. Imaging Sci. Photochem. **30**, 429 (2012)
154. J.L. Bender, Q.-D. Shen, C.L. Fraser, Tetrahedron **60**, 7277 (2004)
155. A.A. Farah, W.J. Pietro, Can. J. Chem. **82**, 595 (2004)
156. H. Hofmeier, R. Hoogenboom, M.E.L. Wouters, U.S. Schubert, J. Am. Chem. Soc. **127**, 2913 (2005)
157. R.P. Sijbesma, F.H. Beier, L. Brunsveld, B.J.B. Folmer, J.H.K.K. Hirschberg, R.F.M. Lange, J.K.L. Lowe, E.W. Meijer, Science **278**, 1601 (1997)
158. R. Hoogenboom, D. Wouters, U.S. Schubert, Macromolecules **36**, 4743 (2003)
159. L.-Z. Meng, S.-L. Gong, Y.-H. Yin, Y.-Y. Chen, Y.-W. Wang, J. Appl. Polym. Sci. **87**, 1445 (2003)
160. J. Hu, J. He, M. Zhang, P. Ni, Gaofenzi Xuebao. Acta Polym. Sin. 300 (2013)
161. P. Espeel, F.E. Du Prez, Macromolecules **48**, 2 (2015)
162. H. Struthers, T.L. Mindt, R. Schibli, Dalton Trans. **39**, 675 (2010)
163. H. Chen, J. Zeng, F. Deng, X. Luo, Z. Lei, H. Li, J. Polym. Res. **19**, 9880 (2012)
164. W.H. Daly, S. Moulay, J. Polym. Sci. Polym. Symp. **74**, 227 (1986)
165. S.V. Amosova, L.P. Shaulina, G.V. Ratovskii, I.P. Golentovskaya, M.I. Smagunova, E.I. Birukova, S.A. Zhivetjeva, Khim. Inter. Ustoich. Razv. **11**, 831 (2003)
166. S. Habaue, M. Morita, Y. Okamoto, Kobunshi Ronbunshu **59**, 717 (2002)
167. H. Higashimura, S. Kobayashi, Oxidative polymerization, in *Encyclopedia of Polymer Science and Technology*, ed. by H.F. Mark, J.I. Kroschwitz (Wiley, Hoboken, 2002)
168. Z. Chen, C. Duanmu, L. Xiao, Wuhan Univ. J. Nat. Sci. **9**, 503 (2004)
169. T.C. Chang, C.C. Shih, C.P. Yin, H.B. Chen, T.R. Wu, Polym. Degrad. Stab. **87**, 87 (2005)
170. X.-G. Li, M.-R. Huang, Y.-M. Hua, M.-F. Zhu, Q. Chen, Polymer **45**, 4693 (2004)
171. X.-G. Li, M.-R. Huang, Y. Jin, Y.L. Yang, Polymer **42**, 3427 (2001)
172. X.-G. Li, M.-R. Huang, F. Li, W.J. Cai, Z. Jin, Y.L. Yang, J. Polym. Sci. Part A Polym. Chem. **38**, 4407 (2000)
173. C.O. Sánchez, B.L. Rivas, J. Appl. Polym. Sci. **85**, 2564 (2002)
174. H. Wang, A. Miyamoto, T. Hirano, M. Seno, T. Sato, Eur. Polym. J. **40**, 2287 (2004)
175. P. Savitha, P.S. Rao, D.N. Sathyanarayana, Polym. Int. **54**, 1243 (2005)
176. H.J. Salavagione, D.F. Acevedo, M.C. Miras, C. Barbero, Port. Electrochim. Acta **21**, 245 (2003)
177. B.L. Rivas, C.O. Sanchez, J. Appl. Polym. Sci. **89**, 2641 (2003)
178. J. Rutkowska, K. Kilian, K. Pyrzynska, Eur. Polym. J. **44**, 2108 (2008)
179. Z. Liu, Q. Liu, X. Dai, C. Shen-Tu, C. Yao, Y. Kong, ECS Electrochem. Lett. **2**, G1 (2013)
180. S. Huang, P. Du, C. Min, Y. Liao, H. Sun, Y. Jiang, J. Fluoresc. **23**, 621 (2013)
181. B.L. Rivas, C.O. Sanchez, J. Appl. Polym. Sci. **92**, 31 (2004)
182. X.-G. Li, Y.-M. Hua, M.-R. Huang, Chem. Eur. J. **11**, 4247 (2005)
183. X.-G. Li, M.-R. Huang, Y.-M. Hua, Macromolecules **38**, 4211 (2005)
184. X. Lu, H. Mao, D. Chao, X. Zhao, W. Zhang, Y. Wei, Mater. Lett. **61**, 1400 (2007)
185. X.-G. Li, M.-R. Huang, S.-X. Li, Acta Mater. **52**, 5363 (2004)
186. S. Huang, C. Min, Y. Liao, P. Du, H. Sun, Y. Zhu, A. Ren, RSC Adv. **4**, 47657 (2014)
187. J. Stejskal, Prog. Polym. Sci. **41**, 1 (2015)
188. S. Almeida, E. Rivera, J.M. Reyna-González, G. Huerta, F. Tapia, M. Aguilar-Martínez, Synth. Metals **159**, 1215 (2009)

189. A. Vázquez-Arce, G. Zaragoza-Galán, E. Aguilar-Ortíz, E.G. Morales-Espinoza, E. Rodríguez-Alba, E. Rivera, Des. Monom. Polym. **17**, 78 (2014)
190. E. Aguilar-Ortíz, G. Zaragoza-Galán, N. Solladié, R. Rein, M. Aguilar-Martínez, N. Macías-Ruvalcaba, E. Rivera, Synth. Metals **162**, 1000 (2012)
191. S.-M. Lee, S. Jung, C.-S. Ha, I. Chung, W.-K. Lee, Y.-H. Park, Macromol. Res. **16**, 510 (2008)
192. S.-M. Lee, N.-J. Lee, C.-S. Ha, W.-J. Cho, J. Appl. Polym. Sci. **94**, 57 (2004)
193. C. Ebner, T. Bodner, F. Stelzer, F. Wiesbrock, Macromol. Rapid Commun. **32**, 254 (2011)
194. S. Mallkpour, Z. Rafiee, Prog. Polym. Sci. **36**, 1754 (2011)
195. S. Mallkpour, M. Dinari, Polym. Adv. Technol. **19**, 1334 (2008)
196. S.D. Kukade, R.R. Naik, S.V. Bawankar, Orbital Electron. J. Chem. **6**, 240 (2014)
197. H. Kantekin, Z. Biyiklioğlu, Dyes Pigm. **77**, 432 (2008)
198. Y. Yang, D. Yu, Y. Liu, Y. Zhao, H. Fan, L. Jin, J. Zhou, Q. Jin, Liaoning Shiyou Huagong Daxue xuebao **26**, 56 (2006)
199. B.C. Mondal, A.K. Das, React. Funct. Polym. **53**, 45 (2002)
200. K. Faghihi, K. Zamani, A. Mirsamie, S.M. Reza, Eur. Polym. J. **39**, 247 (2003)
201. İ. Değirmencioğlu, R. Bayrak, M. Er, K. Serbest, Dyes Pigm. **83**, 51 (2009)
202. Q. Li, Q. Gao, H. Peng, Z. Xu, C. Yi, Gaofenzi Cailiao Kexue Yu Gongcheng **24**, 34 (2008)
203. A. Mahapatro, T.D.M. Negrón, Microwave-assisted biocatalytic polymerizations, in *Green Polymer Chemistry: Biocatalysis and Materials II*, ACS Symposium Series, vol. 1144, ed. by H.N. Cheng, R.A. Gross, P.B. Smith (ACS, Washington, 2013)
204. R. Kakuchi, R. Sakai, I. Otsuka, T. Satoh, H. Kaga, T. Kakuchi, Macromolecules **38**, 9441 (2005)
205. A. Bilgin, D. Yanmaz, C. Yagci, Turk. J. Chem. **38**, 1135 (2014)
206. K. Naka, T. Uemura, Y. Chujo, J. Polym. Sci. A **39**, 4083 (2001)
207. T. Narita, H. Hamana, M. Takeshita, H. Fujiwara, J. Fluorine Chem. **124**, 197 (2003)
208. M.H. Weston, O.K. Farha, B.G. Hauser, J.T. Hupp, S.T. Nguyen, Chem. Mater. **24**, 1292 (2012)
209. V. Borovkov, Symmetry **6**, 256 (2014)
210. M. Heller, U.S. Schubert, e-Polymers **2**, 375 (2002)
211. M. Azechi, K. Yamabuki, K. Onimura, T. Oishi, Polym. J. **42**, 632 (2010)
212. L. Feng, F.B. Zhao, Z.L. Liu, J.P. Sun, J.W. Hu, Chin. Chem. Lett. **18**, 875 (2007)
213. C. Zhang, Y. Zhang, H. Zhang, Y. Hu, X. Zhang, T. Masuda, React. Funct. Polym. **87**, 46 (2015)
214. Y. Zhang, K. Gao, Z. Zhao, D. Yue, Y. Hu, T. Masuda, J. Polym. Sci. Part A Polym. Chem. **51**, 5248 (2013)
215. R. Sakai, I. Otsuka, T. Satoh, R. Kakuchi, H. Kaga, T. Kakuchi, J. Polym. Sci. A **44**, 325 (2006)
216. R. Sakai, I. Otsuka, T. Satoh, R. Kakuchi, H. Kaga, T. Kakuchi, Macromolecules **39**, 4032 (2006)
217. F. Takei, H. Hayashi, K. Onitsuka, N. Kobayashi, S. Takahashi, Angew. Chem. Int. Ed. **40**, 4092 (2001)
218. P.A.J. De Witte, M. Castriciano, J.J.L.M. Cornelissen, L.M. Scolaro, R.J.M. Nolte, A.E. Rowan, Chem. Eur. J. **9**, 1775 (2003)
219. J. Tabei, M. Shiotsuki, F. Sanda, T. Masuda, Macromolecules **38**, 9448 (2005)
220. R. Sakai, T. Yonekawa, I. Otsuka, R. Kakuchi, T. Satoh, T. Kakuchi, J. Polym. Sci. A **48**, 1197 (2010)
221. S. Sakthivel, T. Punniyamurthy, Tetrahedron Asymmetry **23**, 570 (2012)
222. K. Günay, P. Theato, H.-A. Klok, J. Polym. Sci. A **51**, 1 (2013)
223. P.J. Roth, Macromol. Chem. Phys. **215**, 825 (2014)
224. M.D. Hossain, Z. Jia, M.J. Monteiro, Macromolecules **47**, 4955 (2014)
225. J. Romulus, J.T. Henssler, M. Weck, Macromolecules **47**, 5437 (2014)
226. N. Bensacia, S. Moulay, Int. J. Polym. Mater. **61**, 699 (2012)

227. I.M. Henderson, R.C. Hayward, Macromolecules **43**, 3249 (2010)
228. K. Uzun, E. Çevik, M. Şenel, Amer. J. Chem. **1**, 16 (2011)
229. H.A. Saadeh, E.A. Abu Shairah, N. Charef, M.S. Mubarak, J. Appl. Polym. Sci. **124**, 2717 (2012)
230. J.F. Lovell, A. Roxin, K.K. Ng, Q. Qi, J.D. McMullen, R.S. DaCosta, G. Zheng, Biomacromol **12**, 3115 (2011)
231. Y. de Gaetano, I. Clarota, J.-B. Regnouf-de-Vains, New J. Chem. **36**, 1339 (2012)
232. X. Wang, X. Zhang, H. Guo, L. Yuan, P. Liu, Polym. Eng. Sci. **52**, 972 (2012)
233. L.X. Yuan, X.M. Wang, X. Zhang, P.G. Liu, W.D. Yan, Chin. Chem. Lett. **21**, 1493 (2010)
234. R. Kumar, S.K. Jain, R.K. Misra, M. Kachchwaha, P.K. Khatri, Int. J. Environ. Sci. Technol. **9**, 79 (2012)
235. M.Y. Abdelaal, I.M.M. Kenawy, M.A.H. Hafez, J. Appl. Polym. Sci. **77**, 3044 (2000)
236. T. Çaykara, Ş.Ş. Alaslan, J. Appl. Polym. Sci. **106**, 2126 (2007)
237. K. Bester, A. Bukowska, W. Bukowski, J. Mol. Catal. A Chem. **378**, 124 (2013)
238. B. Gao, J. Zhang, J. Guo, J. Polym. Res. **17**, 301 (2010)
239. S.V. Vinogradova, V.A. Vasnev, Russ. Chem. Rev. **73**, 487 (2004)
240. S.V. Vinogradova, V.A. Vasnev, M.L. Keshtov, Vysokomol. Soedin. **49**, 2010 (2007)
241. S.S. Butoliya, A.B. Zade, W.B. Gurnule, J. Appl. Polym. Sci. **113**, 1 (2009)
242. A.S. Amarasekara, D. Green, L.D. Williams, Eur. Polym. J. **45**, 595 (2009)
243. H. Al-Adwani, A. Bishara, H. Shaban, J. Appl. Polym. Sci. **89**, 1 (2003)
244. N.S. Al-Muaikel, T.I. El-Emary, Eur. Polym. J. **39**, 211 (2003)
245. S. Lugovskoy, M. Nisnevitch, M. Zinigrad, D. Wolf, Clean Technol. Environ. Policy **10**, 279 (2008)
246. Y. Zhang, C.B. Murphy, W.E. Jones Jr., Macromolecules **35**, 630 (2002)
247. R.C. Smith, A.G. Tennyson, A.C. Won, S.J. Lippard, Inorg. Chem. **45**, 9367 (2006)
248. H. Huang, Q. Miao, Y. Kang, X. Huang, J. Xu, Y. Cheng, Bull. Chem. Soc. Jpn. **81**, 1116 (2008)
249. Q. Hou, Y. Zhang, R.Q. Yang, W. Yang, Y. Cao, Synth. Metals **153**, 193 (2005)
250. I. Welterlich, B. Tieke, Macromolecules **44**, 4194 (2011)
251. A.R. Rabindranath, A. Maier, M. Schafer, B. Tieke, Macromol. Chem. Phys. **210**, 659 (2009)
252. Q. Sun, H. Wang, C. Yang, Y. Li, J. Mater. Chem. **13**, 800 (2003)
253. M. Chiper, R. Hoogenboom, U.S. Schubert, Eur. Polym. J. **46**, 260 (2010)
254. H. Huang, Z. Cao, Z. Gu, X. Li, B. Zhao, P. Shen, S. Tan, Eur. Polym. J. **10**, 1805 (2012)
255. X. Huang, C. Zhu, S. Zhang, W. Li, Y. Guo, X. Zhan, Y. Liu, Macromolecules **41**, 6895 (2008)
256. Q.-H. Chu, Y. Pang, J. Polym. Sci. Part A Polym. Chem. **44**, 2338 (2006)
257. L. Florea, D. Diamond, F. Benito-Lopez, Macromol. Mater. Eng. **297**, 1148 (2012)
258. L. Bao, J. Sun, Q. Li, J. Polym. Res. **21**, 575 (2014)
259. H. Komber, S. Müllers, F. Lombeck, A. Held, M. Walter, M. Sommer, Polym. Chem. **5**, 443 (2014)
260. M. Sommer, H. Komber, Macromol. Rapid Commun. **34**, 57 (2013)
261. L. Metzler, T. Reichenbach, O. Brügner, H. Komber, F. Lombeck, S. Müllers, R. Hanselmann, H. Hillebrecht, M. Walter, M. Sommer, Polym. Chem. **6**, 3694 (2015)
262. S. Kobayashi, Adv. Polym. Sci. **262**, 141 (2013)
263. R. Mosurkal, S. Roy, J. Kumar, L.A. Samuelson, S.K. Tripathy, J. Macromol. Sci. A **39**, 1195 (2002)
264. L.N. Monsalve, F.M. Kaniz, H. Nonami, R. Erra-Balsells, A. Baldessari, Polymer **51**, 2998 (2010)
265. H. Kawakita, S. Nakano, K. Hamamoto, Y. Matsunaga, Y. Yoshimura, K. Ohto, K. Inoue, J. Appl. Polym. Sci. **118**, 247 (2010)
266. H. Duan, K. Zheng, Y. Cui, Y. Li, L. Zhang, Chin. J. Polym. Sci. **32**, 906 (2014)

267. D.-H. Yao, G.-J. Li, T. Kuila, P. Li, N.-H. Kim, S.-I. Kim, J.-H. Lee, J. Appl. Polym. Sci. **120**, 1114 (2011)
268. A. Mahapatro, B. Kalra, A. Kumar, R.A. Gross, Biomacromolecules **4**, 544 (2003)
269. A. Asati, D. Lehmkuhl, D. Diaz, J.M. Perez, Langmuir **36**, 13066 (2012)
270. T. Naolou, K. Busse, J. Kressler, Biomacromolecules **11**, 3660 (2010)
271. J. Zhang, H. Shi, D. Wu, Z. Xing, A. Zhang, Y. Yang, Q. Li, Process Biochem. **49**, 797 (2014)
272. E.A. Bekturov, *Polymeric Electrolytes, Hydrogels, Complexes and Catalysts* (Print-S, Almaty, Kazakhstan, 2007)
273. C.-Y. Chen, C.-Y. Chen, Eur. Polym. J. **39**, 991 (2003)
274. W. Bisset, H. Jacobs, N. Koshti, P. Stark, A. Gopalan, React. Funct. Polym. **55**, 109 (2003)
275. Y. Chen, Q.-L. Fan, P. Wang, B. Zhang, Y.-Q. Huang, G.-W. Zhang, X.-M. Lu, H.S.O. Chan, W. Huang, Polymer **47**, 5228 (2006)
276. Y. Chen, K.-Y. Pu, Q.-L. Fan, X.-Y. Qi, Y.-Q. Huang, X.-M. Lu, W. Huang, J. Polym. Sci. A **47**, 5057 (2009)
277. L. Zhang, C. Ni, C. Zhu, X. Jiang, Y. Liu, B. Huang, J. Appl. Polym. Sci. **112**, 2455 (2009)
278. H. Zhao, M. Deng, Synthesis. J. Mater. Civ. Eng. **25**, 112 (2013)
279. B. Zhou, J.Z. Li, C.H. He, S.Y. Qin, Chin. Chem. Lett. **16**, 27 (2005)
280. D. Nagai, M. Yoshida, T. Kishi, H. Morinaga, Y. Hara, M. Mori, S. Kawakami, K. Inoue, Chem. Commun. **49**, 6852 (2013)
281. B.L. Rivas, A. Maureira, Inorg. Chem. Commun. **10**, 151 (2007)
282. B.L. Rivas, C. Muñoz, Macromol. Symp. **304**, 40 (2011)
283. K. Ding, F. Wang, F. Wu, Chin. J. Polym. Sci. **30**, 63 (2012)
284. L. Do, R.C. Smith, A.G. Tennyson, S.J. Lippard, Inorg. Chem. **45**, 8998 (2006)
285. F. Gasc, S. Clerc, E. Gayon, J.-M. Campagne, P. Lacroix-Desmazes, J. Supercrit. Fluids **105**, 136 (2015)
286. L. Erdmann, K.E. Uhrich, Biomaterials **21**, 1941 (2000)
287. S.J. Choi, K.E. Geckeler, J. Appl. Polym. Sci. **90**, 650 (2003)
288. A. Okamura, T. Hirai, M. Tanihara, T. Yamaoka, Polymer **43**, 3549 (2002)
289. A.L. Carbone-Howell, N. Stebbins, K.E. Uhrich, Biomacromolecules **15**, 1889 (2014)
290. M.A. Rogers, Y.-F. Yan, K. Ben-Elazar, Y. Lan, J. Faig, K. Smith, K.E. Uhrich, Biomacromolecules **15**, 3406 (2014)
291. Y. Chandorkar, R.K. Bhagat, G. Madras, B. Basu, Biomacromolecules **15**, 863 (2014)
292. A. Zintchenko, L.J. van der Aa, J.F. Engbersen, Macromol. Rapid Commun. **32**, 321 (2011)
293. A.D. Pomogailo, *Catalysis by Polymer-Immobilized Metal Complexes* (Gordon & Breach Science Publishers, Amsterdam, 1998)
294. C. Feng, Y. Li, D. Yang, J. Hu, X. Zhang, X. Huang, Chem. Soc. Rev. **40**, 1282 (2011)
295. N. Hadjichristidis, S. Pispas, H. Iatrou, D.J. Lohse, Graft copolymers, in *Encyclopedia of Polymer Science and Technology*, ed. by K. Matyjaszewski (Wiley, Hoboken, 2007)
296. A. Bhattacharya, J.W. Rawlins, P. Ray (eds.), *Polymer Grafting and Crosslinking* (Wiley, Hoboken, New Jersey, 2009)
297. A. Bhattacharya, B.N. Misra, Prog. Polym. Sci. **29**, 767 (2004)
298. C.J. Galvin, J. Genzer, Prog. Polym. Sci. **37**, 871 (2012)
299. K. Kato, E. Uchida, E.-T. Kang, Y. Uyama, Y. Ikada, Prog. Polym. Sci. **28**, 209 (2003)
300. G. Gu, P. An, Gaofenzi Cailiao Kexue Yu Gongcheng **19**, 1 (2003)
301. H. Gao, K. Matyjaszewski, J. Am. Chem. Soc. **129**, 6633 (2007)
302. L. Wu, J. Baghdachi (eds.), *Functional Polymer Coatings: Principles, Methods, and Applications* (Wiley, Hoboken, NY, 2015)
303. F. Zhisheng, Z. Liang, Z. Jingxing, P. Huijie, S. Hongfu, W. Hua, J. Senyang, F. Zhiqiang, Suliao Keji. Plast. Sci. Technol. **38**, 89 (2010)
304. Y. Zeng, R. Jia, H. Yan, Suliao Keji. Plast. Sci. Technol. **40**, 123 (2012)
305. C. Pichot, Curr. Opin. Colloid Interface Sci. **9**, 213 (2004)
306. H. Wang, H. Zhang, Y. Lv, F. Svec, T. Tan, J. Chromatogr. A **1343**, 128 (2014)

307. L. Malovic, A. Nastasovic, Z. Sandic, J. Markovic, D. Dordevic, Z. Vukovic, J. Mater. Sci. **42**, 3326 (2007)
308. G. Bayramoğlu, M.Y. Arıca, Sep. Purif. Technol. **45**, 192 (2005)
309. J. Zu, S. He, Y.C. Nho, J.J. Pyo, F. Yan, J. Appl. Polym. Sci. **116**, 1414 (2010)
310. M. Barsbay, P.A. Kavakli, O. Güven, Radiat. Phys. Chem. **79**, 227 (2010)
311. K. Miyazaki, K. Hisada, T. Hori, Fiber **56**, 227 (2000)
312. M.J. Roman, E.A. Decker, J.M. Goddard, A.C.S. Appl, Mater. Interfaces **6**, 5383 (2014)
313. T. Shiraishi, M. Tamada, K. Saito, T. Sugo, Radiat. Phys. Chem. **66**, 43 (2003)
314. S. Das, A.K. Pandey, A. Athawale, V. Kumar, Y.K. Bhardwaj, S. Sabharwal, V.K. Manchanda, Desalination **232**, 243 (2008)
315. K. Saito, K. Saito, K. Sugita, M. Tamada, T. Sugo, Ind. Eng. Chem. Res. **41**, 5686 (2002)
316. I. Ozawa, K. Saito, K. Sugita, K. Sato, M. Akiba, T. Sugo, J. Chromatogr. A **888**, 43 (2000)
317. S.-Y. Nishiyama, K. Saito, K. Saito, K. Sugita, K. Sato, M. Akiba, T. Saito, S. Tsuneda, A. Hirata, M. Tamada, T. Sugo, J. Membr. Sci. **214**, 275 (2003)
318. A. Jyo, J. Kugara, H. Trobradovic, K. Yamabe, T. Sugo, M. Tamada, T. Kume, Ind. Eng. Chem. Res. **43**, 1599 (2004)
319. K. Saito, K. Saito, K. Sugita, M. Tamada, T. Sugo, J. Chromatogr. A **954**, 277 (2002)
320. P.A. Kavakli, C. Kavakli, O. Güven, Radiat. Phys. Chem. **94**, 105 (2014)
321. K. Ikeda, D. Umeno, K. Saito, F. Koide, E. Miyata, T. Sugo, Ind. Eng. Chem. Res. **50**, 5727 (2011)
322. G. Depecker, C. Branger, A. Margaillan, T. Pigot, S. Blanc, F. Robert-Peillard, B. Coulomb, J.-L. Boudenne, React. Funct. Polym. **69**, 877 (2009)
323. J. Bernard, C. Branger, I. Beurroies, R. Denoyel, A. Margaillan, React. Funct. Polym. **72**, 98 (2012)
324. X. Qiao, B. Yan, J. Phys. Chem. B **112**, 14742 (2008)
325. I.E. Uflyand, A.D. Pomogailo, J. Inorg. Organomet. Polym. **2**, 373 (1992)
326. S. Boussetta, C. Branger, A. Margaillan, J.-L. Boudenne, B. Coulomb, Eur. Polym. J. **43**, 416 (2007)
327. S. Boussetta, C. Branger, A. Margaillan, J.-L. Boudenne, B. Coulomb, React. Funct. Polym. **68**, 775 (2008)
328. N.M. Alotaibi, S. Lahsasni, T. Aouak, J. Appl. Polym. Sci. **127**, 1338 (2013)
329. I.E. Uflyand, A.S. Kuzharov, M.O. Gorbunova, V.N. Sheinker, A.D. Pomogailo, React. Polym. **13**, 145 (1990)
330. J. Feng, Q. Zhang, W. Li, Y. Li, M. Yang, Y. Cao, J. Appl. Polym. Sci. **109**, 2283 (2008)
331. S.D. Alexandratos, C.L. Stine, React. Funct. Polym. **60**, 3 (2004)
332. A. Khazaei, S. Saednia, M.K. Borazjani, J. Saien, M. Kiani, A. Afkhami, Supramol. Chem. **26** (2014)
333. A. Murugesan, B. Meenarathi, L. Kannammal, S. Palanikumar, R. Anbarasan, Synth. Metals **189**, 143 (2014)
334. L.-F. Wang, J.-C. Duan, W.-H. Miao, R.-J. Zhang, S.-Y. Pan, X.-Y. Xu, J. Hazard. Mater. **186**, 1681 (2011)
335. H.H. Abdel-Razik, M. Abbo, H.A. Almahy, J. Appl. Polym. Sci. **125**, 2102 (2012)
336. S. Liu, B. Gao, H. Fu, Gaofenzi Xuebao 727 (2010)
337. D. Madge, J. Ruhe, PMSE Prepr. 255 (2003)
338. P. Murugan, M. Krishnamurthy, S.N. Jaisankar, D. Samanta, A.B. Mandal, Chem. Soc. Rev. **44**, 3212 (2015)
339. S. Çetin, T. Tinçer, J. Appl. Polym. Sci. **108**, 414 (2008)
340. V.Y. Kabanov, V.N. Kudryavtsev, High Energy Chem. **37**, 1 (2003)
341. M.M. Nasef, O. Güven, Prog. Polym. Sci. **37**, 1597 (2012)
342. J.G. Drobny (ed.), *Radiation Technology for Polymers*, 2nd edn. (CRC Press, Boca Raton, London, NY, 2010)
343. B.I. Kharisov, O.V. Kharisova, U.O. Mendez (eds.), *Radiation Synthesis of Materials and Compounds* (CRC Press, Boca Raton, London, NY, 2013)

344. K. Yamashiro, K. Miyoshi, R. Ishihara, D. Umeno, K. Saito, T. Sugo, S. Yamada, H. Fukunaga, M. Nagai, J. Chromatogr. A **1176**, 37 (2007)
345. Y. Yang, N. Ma, Q. Zhang, S. Chen, J. Appl. Polym. Sci. **113**, 3638 (2009)
346. S. Francis, L. Varshney, Radiat. Phys. Chem. **74**, 310 (2005)
347. K. Yamada, R. Nagano, M. Hirata, J. Appl. Polym. Sci. **99**, 1895 (2006)
348. M. Taniguchi, G. Belfort, J. Membr. Sci. **231**, 147 (2004)
349. Z.P. Zhao, J.D. Li, D.X. Zhang, C.X. Chen, J. Membr. Sci. **232**, 1 (2004)
350. S. Ershov, F. Khelifa, M.-E. Druart, Y. Habibi, M.-G. Olivier, R. Snyders, P. Dubois, RSC Adv. **5**, 14256 (2015)
351. V.A. Titov, E.S. Krivykh, T.A. Ageeva, T.G. Shikova, A.B. Solov'eva, V.A. Timofeeva, I. A. Vershinina, V.V. Rybkin, H.-S. Choi, Polym. Sci. A **50**, 841 (2008)
352. Z.M. Liu, Z.K. Xu, J.Q. Wang, Q. Yang, J. Wu, P. Seta, Eur. Polym. J. **39**, 2291 (2003)
353. T. Ito, T. Hioki, T. Yamaguchi, T. Shinbo, S.-I. Nakao, S. Kimura, J. Am. Chem. Soc. **124**, 7840 (2002)
354. S. Edmondson, V.L. Osborne, W.T.S. Huck, Chem. Soc. Rev. **33**, 14 (2004)
355. R. Barbey, L. Lavanant, D. Paripovic, N. Schüwer, C. Sugnaux, S. Tugulu, H.-A. Klok, Chem. Rev. **109**, 5437 (2009)
356. H. Arslan, Block and graft copolymerization by controlled/living radical polymerization methods, in *Polymerization*, ed. by A. De Souza Gomes (InTech, Rijeka, Croatia, 2012)
357. R.R. Bhat, M.R. Tomlinson, J.J. Genzer, Polym. Sci. Part B Polym. Phys. **43**, 3384 (2005)
358. S. Banerjee, T.K. Paira, T.K. Mandal, Polym. Chem. **5**, 4153 (2014)
359. Q.-H. Wang, C.-Z. Wang, Y.-M. Wei, Gaodeng xuexiao huaxun xuebao. Chem. J. Chin. Univ. **33**, 2579 (2012)
360. F.J. Xu, J.P. Zhao, E.T. Kang, K.G. Neoh, J. Li, Langmuir **23**, 8585 (2007)
361. K. Matyjaszewski, D. Hongchen, W. Jakubowski, J. Pietrasik, A. Kusumo, Langmuir **23**, 4528 (2007)
362. M.P. Weir, A.J. Parnell, Polymers **3**, 2107 (2011)
363. G.-P. Jin, Y. Fu, X.-C. Bao, X.-S. Feng, Y. Wang, W.-H. Liu, J. Appl. Electrochem. **44**, 621 (2014)
364. Y. Inoue, T. Matsugi, N. Kashiwa, K. Matyjaszewski, Macromolecules **37**, 3651 (2004)
365. V. Percec, F. Asgarzadeh, J. Polym. Sci. Part A Polym. Chem. **39**, 1120 (2001)
366. S.C. Hong, T. Pakula, K. Matyjaszewski, Macromol. Chem. Phys. **202**, 3392 (2001)
367. S. Harrisson, X. Liu, J.-N. Ollagnier, O. Coutelier, J.-D. Marty, M. Destarac, Polymers **6**, 1437 (2014)
368. J. Bernard, A. Favier, T.P. Davis, C. Barner-Kowollik, M.H. Stenzel, Polymer **47**, 1073 (2006)
369. A. Nese, Y. Kwak, R. Nicolay, M. Barrett, S.S. Sheiko, K. Matyjaszewski, Macromolecules **43**, 4016 (2010)
370. A. Nese, Y. Li, S. Averick, Y. Kwak, D. Konkolewicz, S.S. Sheiko, K. Matyjaszewski, ACS Macro Lett. **1**, 227 (2011)
371. W. Zhang, M. Shiotsuki, T. Masuda, Macromol. Rapid Commun. **28**, 1115 (2007)
372. K. Maeda, N. Kamiya, E. Yashima, Chem. Eur. J. **10**, 4000 (2004)
373. V. Percec, E. Aqad, M. Peterca, J.G. Rudick, L. Lemon, J.C. Ronda, B.B. De, P.A. Heiney, E.W. Meijer, J. Am. Chem. Soc. **128**, 16365 (2006)
374. A. Bakandritsos, N. Bouropoulos, R. Zboril, K. Iliopoulos, N. Boukos, G. Chatzikyriakos, S. Couris, Adv. Funct. Mater. **18**, 1694 (2008)
375. L. Ding, Y.Y. Huang, Y.Y. Zhang, J.P. Deng, W.T. Yang, Macromolecules **44**, 736 (2011)
376. W. Sheng, B. Li, X. Wang, B. Dai, B. Yu, X. Jia, F. Zhou, Chem. Sci. **6**, 2068 (2015)
377. I. Gitsov, C. Zhu, J. Am. Chem. Soc. **125**, 11228 (2003)
378. Q. Li, X. Xiao, X. Zhang, W. Zhang, Polymer **54**, 3230 (2013)
379. N. Hadjichristidis, M. Pitsikalis, H. Iatrou, S. Pispas, Macromol. Rapid Commun. **24**, 979 (2003)
380. D. Neugebauer, Y. Zhang, T. Pakula, S.S. Sheiko, K. Matyjaszewski, Macromolecules **36**, 6746 (2003)

381. Z. Li, K. Zhang, J. Ma, C. Cheng, K.L. Wooley, J. Polym. Sci. Part A Polym. Chem. **47**, 5557 (2009)
382. J.-F. Lutz, N. Jahed, K. Matyjaszewski, J. Polym. Sci. Part A Polym. Chem. **42**, 1939 (2004)
383. R. Ranjan, W.J. Brittain, Macromolecules **40**, 6217 (2007)
384. R.M. Arnold, D.L. Patton, V.V. Popik, J. Locklin, Acc. Chem. Res. **47**, 2999 (2014)
385. Q. Fu, C. Liu, W. Lin, J. Huang, J. Polym. Sci. Part A Polym. Chem. **46**, 6770 (2008)
386. Y.-C. Li, A. Nese, N.V. Lebedeva, T. Davis, K. Matyjaszewski, S.S. Sheiko, J. Am. Chem. Soc. **133**, 17479 (2011)
387. J. Yin, Z.S. Ge, H. Liu, S.Y. Liu, J. Polym. Sci. Part A Polym. Chem. **47**, 2608 (2009)
388. D.H. Han, X. Tong, Y. Zhao, Macromolecules **44**, 5531 (2011)
389. N. Xu, R. Wang, F.S. Du, Z.C. Li, J. Polym. Sci. Part A Polym. Chem. **47**, 3583 (2009)
390. Y.Y. Yuan, Q. Du, Y.C. Wang, J. Wang, Macromolecules **43**, 1739 (2010)
391. A. Dag, H. Sahin, H. Durmaz, G. Hizal, U. Tunca, J. Polym. Sci. Part A Polym. Chem. **49**, 886 (2011)
392. Y. Li, M. Beija, S. Laurent, L. van der Elst, R.N. Muller, H.T.T. Duong, A.B. Lowe, T.P. Davis, C. Boyer, Macromolecules **45**, 4196 (2012)
393. X.S. Fan, G.W. Wang, J.L. Huang, J. Polym. Sci. Part A Polym. Chem. **49**, 1361 (2011)
394. M. Bertoldo, G. Zampano, F. Terra, V. Villari, V. Castelvetro, Biomacromolecules **12**, 388 (2011)
395. L. Ding, C. Chen, J. Deng, W. Yang, Polym. Bull. **69**, 1023 (2012)
396. H.Q. Huang, S.E. Rankin, L.S. Penn, R.P. Quirk, T.H. Cheong, Langmuir **20**, 5770 (2004)
397. V. Mittal (ed.), *Polymer Brushes: Substrates, Technologies, and Properties* (CRC Press, Boca Raton, 2013)
398. R.C. Advincula, W.J. Brittain, K.C. Caster, J. Rühe (eds.), *Polymer Brushes* (Wiley-VCH, Hoboken, New Jersey, 2004)
399. S.V. Orski, R.J. Sheridan, E.P. Chan, K.L. Beers, Polymer **72**, 471 (2015)
400. S.A. Egorov, H.-P. Hsu, A. Milchev, K. Binder, Soft Matter **11**, 2604 (2015)
401. J. Bünsow, T.S. Kelby, W.T.S. Huck, Acc. Chem. Res. **43**, 466 (2009)
402. O. Azzaroni, J. Polym. Sci. Part A Polym. Chem. **50**, 3225 (2012)
403. G. Liu, G. Zhang (eds.), *QCM-D Studies on Polymer Behavior at Interfaces* (Springer, Heidelberg, 2013)
404. S. Kawaguchi, K. Ito, Adv. Polym. Sci. **175**, 299 (2005)
405. R. Verduzco, X. Li, S.L. Pesek, G.E. Stein, Chem. Soc. Rev. **44**, 2405 (2015)
406. S.G. Boyes, A.M. Granville, M. Baum, B. Akgun, B.K. Mirous, W.J. Brittain, Surf. Sci. **570**, 1 (2004)
407. E. Mastan, L. Xu, S. Zhu, Macromol. Theor. Simul. **24**, 89 (2015)
408. J.R. Boyce, D. Shirvanyants, S.S. Sheiko, D.A. Ivanov, S. Qin, H. Boerner, K. Matyjaszewski, Langmuir **20**, 6005 (2004)
409. K. Fries, S. Samanta, S. Orski, J. Locklin, Chem. Commun. 6288 (2008)
410. R. Klajn, Chem. Soc. Rev. **43**, 148 (2014)
411. W.-H. Wang, J.-L. Dong, G.L. Baker, M.L. Bruening, Analyst **136**, 3595 (2011)
412. S. Rathgeber, T. Pakula, A. Wilk, K. Matyjaszewski, K.L. Beers, J. Chem. Phys. **122**, 124904/124901 (2005)
413. R. Djalali, S.-Y. Li, M. Schmidt, Macromolecules **35**, 4282 (2002)
414. J. Rzayev, Macromolecules **42**, 2135 (2009)
415. K. Ishizu, J. Satoh, A. Sogabe, J. Coll. Interface Sci. **274**, 472 (2004)
416. D. Neugebauer, Y. Zhang, T. Pakula, K. Matyjaszewski, Polymer **44**, 6863 (2003)
417. D. Neugebauer, M. Theis, T. Pakula, G. Wegner, K. Matyjaszewski, Macromolecules **39**, 584 (2006)
418. H.G. Boerner, K. Beers, K. Matyjaszewski, S.S. Sheiko, M. Moeller, Macromolecules **34**, 4375 (2001)
419. H.G. Boerner, D. Duran, K. Matyjaszewski, M. da Silva, S.S. Sheiko, Macromolecules **35**, 3387 (2002)

420. A. Kajiwara, K. Matyjaszewski, M. Kamachi, ACS Symp. Ser. **768**, 68 (2000)
421. S. Ohno, A. Nese, B. Cusick, T. Kowalski, K. Matyjaszewski, Vysokomol. Soedin. Ser. A Ser. B **51**, 1947 (2009)
422. C. Chen, P. Tang, F. Qiu, J. Polym. Sci. Part B Polym. Phys. **52**, 1583 (2014)
423. Y.-C. Chung, J.S. Park, C.H. Shin, J.W. Choi, B.C. Chun, Macromol. Res. **20**, 66 (2012)
424. D.A. Tomalia, J.B. Christensen, U. Boas, *Dendrimers, Dendrons, and Dendritic Polymers: Discovery, Applications, and the Future* (Cambridge University Press, Cambridge, 2012)
425. D.A. Tomalia, S.A. Henderson, M.S. Diallo, Ch. 24. Dendrimers—an enabling synthetic science to controlled organic nanostructures, in *Handbook of Nanoscience, Engineering, and Technology*, Second edn. ed. by W.A. Goddard III, D.W. Brenner, S.E. Lyshevski, G. J. Iafrate (CRC Press, Boca Raton, 2007)
426. V. Sujitha, B. Sayani, P. Kalyani, Int. Res. J. Pharm. **2**, 25 (2011)
427. Y. Cheng (ed.), *Dendrimer-based drug delivery systems: from theory to practice* (Wiley, Hoboken, New Jersey, 2012)
428. L.Y. Sklyarov, *Synthesis of Multifunctional Dendrimers and Their Precursors* (LAP LAMBERT Academic Publishing, Germany, 2014)
429. J.M.J. Frechet, D.A. Tomalia (eds.), *Dendrimers and Other Dendritic Polymers* (Wiley, NY, 2002)
430. G.R. Newkome, C.N. Moorefield, F. Vögtle, *Dendrimers and Dendrons: Concepts, Syntheses, Applications* (Wiley-VCH, Weinheim, 2001)
431. F. Vögtle, S. Gestermann, R. Hesse, H. Schwierz, B. Windisch, Prog. Polym. Sci. **25**, 987 (2000)
432. D.A. Tomalia, Progr. Polym. Sci. **30**, 294 (2005)
433. U. Gupta, H.B. Agashe, A. Asthana, N.K. Jain, Biomacromoles **7**, 649 (2006)
434. T. Furukawa, K. Ishizu, Multibranched polymers in solution: stars, dendrimers and hyperbranched polymers, in *Encyclopedia of Surface and Colloid Science*, vol. 1, ed. by P. Somasundara (CRC Press, Boca Raton, 2006)
435. M.V. Walter, M. Malkoch, Accelerated approaches to dendrimers, in *Synthesis of Polymers: New Structures and Methods*, ed. by D.A. Schlüter, C. Hawker, J. Sakamoto (Wiley-VCH, Hoboken, New Jersey, 2012)
436. K. Inoue, Progr. Polym. Sci. **25**, 453 (2000)
437. U. Singh, M. Maqbool Dar, A. Adil Hashmi, Orient. J. Chem. **30**, 911 (2014)
438. R.V. Tambe, S.S. Pakhare, M.G. Jadhav, S.S. Tiwari, C.R. Rai, IJRRPAS **2**, 513 (2010)
439. P.P. Takalkar, V.N. Deshmukh, D.M. Sakarkar, IJPRS **3**, 733 (2014)
440. F. Vögtle, G. Richardt, N. Werner, A.J. Rackstraw, *Dendrimer Chemistry* (Wiley-VCH, Hoboken, New Jersey, 2009)
441. D.A. Tomalia, I. Majoros, J. Macromol. Sci. C **43**, 411 (2003)
442. M. Seiler, Chem. Eng. Technol. **25**, 237 (2002)
443. R. Ceña-Diez, P. García-Broncano, F.J. de la Mata, R. Gómez, M.A. Muñoz-Fernández, Int. J. Nanomed. **11**, 2443 (2016)
444. A. Kimoto, J.-S. Cho, M. Higuchi, K. Yamamoto, Macromolecules **37**, 5531 (2004)
445. M. Arseneault, C. Wafer, J.-F. Morin, Molecules **20**, 9263 (2015)
446. L.P. Balogh, Dendrimer 101, in *Bio-Applications of Nanoparticles*, ed. by W.C.W. Chan, Adv. Exp. Med. Biol. **620**, 136 (2007)
447. R. Prajapat, B. Soni, S. Jain, A. Bhandari, WebmedCentral Pharm. Sci. **1**, WMC00745 (2010)
448. M. Galán, E. Fuentes-Paniagua, F. Javier de la Mata, R. Gómez, Organometallics **33**, 3977 (2014)
449. D.A. Tomalia, H. Baker, J. Dewald, M. Hall, G. Kallos, S. Martin, J. Roeck, J. Ryder, P. Smith, Macromolecules **19**, 2466 (1986)
450. F. Aulenta, W. Hayes, S. Rannard, Eur. Polym. J. **39**, 1741 (2003)
451. D.A. Tomalia, H.M. Brothers, L.T. Piehler, Y.D. Durst, D.R. Swanson, Proc. Nat. Acad. Sci. U S A **99**, 5081 (2002)
452. P.M. Welch, C.F. Welch, Macromolecules **42**, 7571 (2009)

453. A. Malik, S. Chaudhary, G. Garg, A. Tomar, Adv. Biol. Res. **6**, 165 (2012)
454. G.R. Newkome, C.N. Moorefield, F. Vögtle, Chiral dendritic macromolecules, in *Dendritic Molecules: Concepts, Syntheses, Perspectives*, ed. by G.R. Newkome, C.N. Moorefield, F. Vögtle (Wiley, NY, 2007)
455. B. Romagnoli, W. Hayes, J. Mater. Chem. **12**, 767 (2002)
456. A. Ritzén, T. Frejd, Chem. Commun. 207 (1999)
457. R. Stangenberg, D. Türp, K. Müllen, Tetrahedron **70**, 3178 (2014)
458. K. Kono, Polymer J. **44**, 531 (2012)
459. D. Konkolewicz, M.J. Monteiro, S. Perrier, Macromolecules **44**, 7067 (2011)
460. Z. Wang, M. Gao, J. Sun, D. Liang, X. Jia, Macromolecules **46**, 1723 (2013)
461. K. Aoi, A. Motoda, M. Ohno, K. Tsutsumiuchi, M. Okada, T. Imae, Polym. J. **11**, 1071 (1999)
462. A. Harada, K. Nakanishi, S. Ichimura, C. Kojima, K. Kono, J. Polym. Sci. A **47**, 1217 (2009)
463. X. Xiong, Y. Chen, S. Feng, W. Wang, J. Polym. Sci. A **48**, 3515 (2010)
464. I.J. Majoros, B. Keszler, S. Woehler, T. Bull, J.R. Baker, Macromolecules **36**, 5526 (2003)
465. K. Kono, T. Fukui, T. Takagishi, S. Sakurai, C. Kojima, Polymer **49**, 2832 (2008)
466. K. Kono, E. Murakami, Y. Hiranaka, E. Yuba, C. Kojima, A. Harada, K. Sakurai, Angew. Chem. Int. Ed. **50**, 6332 (2011)
467. E. Yuba, Y. Nakajima, K. Tsukamoto, S. Iwashita, C. Kojima, A. Harada, K. Kono, J. Control. Rel. **160**, 552 (2012)
468. S.J. Teertstra, M. Gauthier, Prog. Polym. Sci. **29**, 277 (2004)
469. S.R. Vinukonda, Dendritic copolymers, in *Synthesis and Applications of Copolymers*, ed. by A. Parthiban (Wiley, Hoboken, New Jersey, 2014)
470. S.K. Ghosh, S. Kawaguchi, Y. Jinbo, Y. Izumi, K. Yamaguchi, T. Taniguchi, K. Nagai, K. Koyama, Macromolecules **36**, 9162 (2003)
471. B.-B. Wang, X. Zhang, X.-R. Jia, Z.-C. Li, Y. Ji, Y. Wei, J. Polym. Sci. A **43**, 5512 (2005)
472. M. Tülü, M. Şenel, J. Appl. Polym. Sci. **109**, 2808 (2008)
473. V. Percec, D.A. Wilson, P. Leowanawat, C.J. Wilson, A.D. Hughes, M.S. Kaucher, D.A. Hammer, D.H. Levine, A.J. Kim, F.S. Bates, K.P. Davis, T.P. Lodge, M.L. Klein, R.H. DeVane, E. Aqad, B.M. Rosen, A.O. Argintaru, M.J. Sienkowska, K. Rissanen, S. Nummelin, J. Ropponen, Science **328**, 1009 (2010)
474. D. Guillon, R. Deschenaux, Curr. Opin. Solid State Mater. Sci. **6**, 515 (2002)
475. B. Donnio, S. Buathong, I. Bury, D. Guillon, Chem. Soc. Rev. **36**, 1495 (2007)
476. N. Gimeno, J. Vergara, M. Cano, J.L. Serrano, M.B. Ros, J. Ortega, C.L. Folcia, S. Rodríguez-Conde, G. Sanz-Enguita, J. Etxebarria, Chem. Mater. **25**, 286 (2013)
477. S.M. Grayson, J.M.J. Frechet, Chem. Rev. **101**, 3819 (2001)
478. S.J. Guillaudeu, M.E. Fox, Y.M. Haidar, E.E. Dy, F.C. Szoka, J.M. Fréchet, Bioconjug. Chem. **19**, 461 (2008)
479. A.-M. Stadler, Cryst. Growth Des. **10**, 5050 (2010)
480. J.W. Lee, J.H. Kim, B.-K. Kim, W.S. Shin, S.-H. Jin, Tetrahedron **62**, 894 (2006)
481. P.R. Dvornic, A.M. de Leuze-Jallouli, M.J. Owen, S.V. Perz, Macromolecules **33**, 5366 (2000)
482. P.R. Dvornic, M.J. Owen, in *Advances in Silicones and Silicone-Modified Materials*, ACS Symposium Series, vol. 1051 (ACS, Washington, 2010)
483. E.A. Rebrov, A.M. Muzafarov, A.A. Zhdanov, Dokl. Akad. Nauk **302**, 346 (1988)
484. A.M. Muzafarov, E.A. Rebrov, V.S. Pashkov, Uspehi Khim. **60**, 1596 (1991)
485. A.M. Muzafarov, E.A. Rebrov, J. Polym. Sci. Part A Polym. Chem. **46**, 4935 (2008)
486. A.-M. Caminade, A. Ouali, R. Laurent, C.-O. Turrin, J.-P. Majoral, Chem. Soc. Rev. **44**, 3890 (2015)
487. A.-M. Caminade, A. Ouali, R. Laurent, C.-O. Turrin, J.-P. Majoral, Coord. Chem. Rev. **308**, 478 (2016)
488. A.-M. Caminade, A. Ouali, R. Laurent, J.-P. Majoral, Inorg. Chim. Acta **431**, 3 (2015)
489. A.-M. Caminade, A. Hameau, J.-P. Majoral, Dalton Trans. **45**, 1810 (2016)

490. S. Gottis, L.-I. Rodriguez, R. Laurent, I. Angurell, M. Seco, O. Rossell, J.-P. Majoral, A.-M. Caminade, Tetrahedron Lett. **54**, 6864 (2013)
491. J. Liu, Y. Feng, B. Ma, Y.-M. He, Q.-H. Fan, Eur. J. Org. Chem. **2012**, 6737 (2012)
492. M. Sowinska, Z. Urbanczyk-Lipkowska, New J. Chem. **38**, 2168 (2014)
493. C. Jahier, S. Nlate, J. Organomet. Chem. **694**, 637 (2009)
494. A. Ossenbach, H. Rüegger, A. Zhang, K. Fischer, A.D. Schlüter, M. Schmidt, Macromolecules **42**, 8781 (2009)
495. J. Roeser, B. Heinrich, C. Bourgogne, M. Rawiso, S. Michel, V. Hubscher-Bruder, F. Arnaud-Neu, S. Méry, Macromolecules **46**, 7075 (2013)
496. M.S. Diallo, S. Christie, P. Swaminathan, L. Balogh, X. Shi, W. Um, C. Papelis, W.A. Goddard III, J.H. Johnson Jr., Langmuir **20**, 2640 (2004)
497. H.D.F. Winkler, D.P. Weimann, A. Springer, C.A. Schalley, Angew. Chem. Int. Ed. **48**, 7246 (2009)
498. W.P.L. Maurice, A. Baars, E.W. Meijer, Host-guest chemistry of dendritic molecules, in *Dendrimers II—Architecture, Nanostructure and Supramolecular Chemistry*, ed. by F. Vögtle (Springer, Berlin, Heidelberg, NY, 2000)
499. W.-S. Li, T. Aida, Chem. Rev. **109**, 6047 (2009)
500. D. Wang, M. Sun, H. Zhang, J. Wang, Jilin Daxue Xuebao. Lixue Ban **43**, 524 (2005)
501. S.C. Zimmerman, I. Zharov, M.S. Wendland, N.A. Rakow, K.S. Suslick, J. Am. Chem. Soc. **44**, 13504 (2003)
502. Z. Fei, Y. Han, Z. Bo, J. Polym. Sci. A **46**, 4030 (2008)
503. J.W. Lee, H.J. Kim, S.C. Han, J.H. Kim, S.-H. Jin, J. Nanosci. Nanotechnol. **8**, 4635 (2008)
504. M.V. Walter, M. Malkoch, Chem. Soc. Rev. **41**, 4593 (2012)
505. T. Kawaguchi, K.L. Walker, C.L. Wilkins, J.S. Moore, J. Am. Chem. Soc. **117**, 2159 (1995)
506. A.V. Hopper (ed.), *Recent Developments in Polymer Research* (Nova Science Publishers, NY, 2007)
507. F. Zeng, S.C. Zimmerman, J. Am. Chem. Soc. **118**, 5326 (1996)
508. X.-X. Deng, F.-S. Du, Z.-C. Li, ACS Macro Lett. **3**, 667 (2014)
509. K.L. Wooley, C.J. Hawker, J.M.J. Frechet, Angew. Chem. Int. Ed. **33**, 82 (1994)
510. R. Spindler, J.M.J. Fréchet, J. Chem. Soc. Perkin Trans. **1**, 913 (1993)
511. N.J. Wells, A. Basso, M. Bradlet, Biopolymers **47**, 381 (1998)
512. S.C. Stinson, Chem. Eng. News 28 (1997)
513. C.O. Kappe, D. Dallinger, S. Murphree, in *Practical Microwave Synthesis for Organic Chemists: Strategies, Instruments, and Protocols* (Wiley VCH: Weinheim, 2008)
514. C.O. Kappe, Chem. Soc. Rev. **37**, 1127 (2008)
515. S.C. Ameta, P.B. Punjabi, R. Ameta, C. Ameta (eds.), *Microwave-Assisted Organic Synthesis. A Green Chemical Approach* (Apple Academic Press, CRC Press, Toronto, New Jersey, 2014)
516. J. López-Andarias, J. Guerra, G. Castañeda, S. Merino, V. Ceña, P. Sánchez-Verdú, Eur. J. Org. Chem. **12**, 2331 (2012)
517. A.S. Ertürk, M. Tülü, A.E. Bozdoğan, T. Parali, Eur. Polym. J. **52**, 218 (2014)
518. A.S. Ertürk, M.U. Gürbüz, M. Tülü, A.E. Bozdoğan, RSC Adv. **5**, 60581 (2015)
519. A.E. Enciso, Z.M. Abid, E.E. Simanek, Polym. Chem. **5**, 4635 (2014)
520. A.E. Enciso, F. Ramirez-Crescencio, M. Zeiser, R. Redón, E.E. Simanek, Polym. Chem. **6**, 5219 (2015)
521. T. Kawauchi, Y. Oguchi, J. Sawayama, K. Nagai, T. Iyoda, Macromolecules **48**, 8090 (2015)
522. B. Wang, Y. Luo, X. Jia, Y. Gong, Y. Ji, L. Yang, W. Yen, Gaofenzi Xuebao 304 (2004)
523. G. Zhou, H. Tan, Y. Luo, Gaofenzi Cailiao Kexue Yu Gongcheng **21**, 85 (2005)
524. A.Y.-T. Huang, C.-H. Tsai, H.-Y. Chen, H.-T. Chen, C.-Y. Lu, Y.-T. Lin, C.-L. Kao, Chem. Commun. **49**, 5784 (2013)
525. D. Kushwaha, V.K. Tiwari, J. Org. Chem. **78**, 8184 (2013)

526. D.Q. McNerny, D.G. Mullen, I.J. Majoros, M.M. Banaszak Holl, J.R. Baker, Dendrimer synthesis and functionalization by click chemistry for biomedical applications. in *Click Chemistry for Biotechnology and Materials Science*, ed. by J. Lahann (Wiley, Singapore, 2009)
527. A. Carlmark, C. Hawker, A. Hult, M. Malkoch, Chem. Soc. Rev. **38**, 352 (2009)
528. G. Franc, A.K. Kakkar, Chem. Eur. J. **15**, 5630 (2009)
529. K.L. Killops, L.M. Campos, C.J. Hawker, J. Am. Chem. Soc. **130**, 5062 (2008)
530. S.P. Rannard, N.J. Davis, J. Am. Chem. Soc. **122**, 11729 (2000)
531. W.H. Binder, R. Sachsenhofer, Click chemistry on supramolecular materials, in *Click Chemistry for Biotechnology and Materials Science*, ed. by J. Lahann (Wiley, Singapore, 2009)
532. G. Franc, A. Kakkar, Chem. Commun. 5267 (2008)
533. A. Vieyres, T. Lam, R. Gillet, G. Franc, A. Castonguay, A. Kakkar, Chem. Commun. **46**, 1875 (2010)
534. K. Kempe, A. Krieg, C.R. Becer, U.S. Schubert, Chem. Soc. Rev. **41**, 176 (2012)
535. D. Astruc, L. Liang, A. Rapakousiou, J. Ruiz, Acc. Chem. Res. **45**, 630 (2012)
536. C.Y. Lee, R. Held, A. Sharma, R. Baral, C. Nanah, D. Dumas, S. Jenkins, S. Upadhaya, W. Du, J. Org. Chem. **78**, 11221 (2013)
537. A. Sharma, A. Kakkar, Molecules **20**, 16987 (2015)
538. A. Nazemi, E.R. Gillies, Braz. J. Pharm. Sci. **49**, 42 (2013)
539. X.Y. Shi, W. Lesniak, M.T. Islam, M.C. Muniz, L.P. Balogh, J.R. Baker, Colloids Surf. A Phys. Eng. Aspects **272**, 139 (2006)
540. C. Kojima, Y. Haba, T. Fukui, K. Kono, T. Takagishi, Macromolecules **36**, 2183 (2003)
541. X. Shi, I. Bányai, M.T. Islam, W. Lesniak, D.Z. Davis, J.R. Baker Jr., L.P. Balogh, Polymer **46**, 3022 (2005)
542. R.C. van Duijvenbode, A. Rajanayagam, G.J.M. Koper, M.W.P.L. Baars, B.F.M. de Waal, E.W. Meijer, M. Borkovec, Macromolecules **33**, 46 (2000)
543. A. Rether, M. Schuster, React. Funct. Polym. **57**, 13 (2003)
544. X.M. He, W. Zheng, P.X. Yang, H.P. Xia, Chin. Chem. Lett. **17**, 1251 (2006)
545. G. Smith, R. Chen, S. Mapolie, J. Organomet. Chem. **673**, 111 (2003)
546. H. Stephan, G. Geipel, G. Bernhard, P. Comba, G. Rajaraman, U. Hahn, F. Vogtle, Eur. J. Inorg. Chem. **22**, 4501 (2005)
547. M. Dasgupta, P.M. Brad, A.K. Kakkar, Coord. Chem. Rev. **233–234**, 223 (2002)
548. I.J. Majoros, C.R. Williams, D.A. Tomalia, J.R. Baker, Jr. Macromolecules **41**, 8372 (2008)
549. Y. Lu, J. Chen, Y. Lu, P. Gai, H. Zhong, J. Appl. Polym. Sci. **127**, 282 (2013)
550. U.E. Berndt, T. Zhou, R.C. Hider, Z.D. Liu, H. Neubert, J. Mass Spectrom. **40**, 1203 (2005)
551. S.M. Cohen, S. Petoud, K.N. Raymond, Chem. Eur. J. **7**, 272 (2001)
552. P. Ilaiyaraja, A.K.S. Deb, D. Ponraju, B. Venkatraman, J. Envir. Chem. Eng. **3**, 1047 (2015)
553. J. Rull, M. Casals, R.M. Sebastián, A. Vallribera, J.-P. Majoral, A.-M. Caminade, ChemCatChem **7**, 2698 (2015)
554. B. Gonzalez, B. Alonso, J. Losada, M.P. Garcia-Armada, C.M. Casado, Organometallics **25**, 3558 (2006)
555. C. Ornelas, J. Broichhagen, M. Weck, J. Am. Chem. Soc. **132**, 3923 (2010)
556. K. Yoon, P. Goyal, M. Weck, Org. Lett. **9**, 2051 (2007)
557. T.S. Dirk, G. Rijkers, W. van Esse, R. Merkx, A.J. Brouwer, H.J.F. Jacobs, R.J. Pieters, R.M.J. Liskamp, Chem. Commun. **36**, 4581 (2005)
558. P. Antoni, Y. Hed, A. Nordberg, D. Nyström, H. von Holst, A. Hult, M. Malkoch, Angew. Chem. Int. Ed. **48**, 2126 (2009)
559. F. Zeng, S.C. Zimmerman, S.V. Kolotuchin, D.E.C. Reichert, Y. Ma, Tetrahedron **58**, 825 (2002)

560. I.V. Lijanova, R.G. Monter, N.V. Likhanova, F.V. Garibay, X.O.C. Olivares, Supramol. Chem. **24**, 56 (2012)
561. Y. Takaguchi, Kagaku to Kogyo **78**, 25 (2004)
562. B.-L. Li, Z.-T. Liu, G.-J. Deng, Q.-H. Fan, Eur. J. Org. Chem. 508 (2007)
563. J. Li, J. Wang, T. Wang, L. Liu, Huaxue yanjiu **15**, 31 (2004)
564. C.K. Jang, J.Y. Jaung, J. Porphyrins Phthalocyanines **13**, 939 (2009)
565. Y. Pan, M. Lu, Z. Peng, J.S. Melinger, Org. Biomol. Chem. **1**, 4465 (2003)
566. Y.-M. He, Y. Feng, Q.-H. Fan, Acc. Chem. Res. **47**, 2894 (2014)
567. C. Ornelas, Macromol. Chem. Phys. **217**, 149 (2016)
568. X. Yang, H. Shang, C. Ding, J. Li, Polym. Chem. **6**, 668 (2015)
569. K. Goren, M. Portnoy, Dendritic molecules on solid support: solid-phase synthesis and applications, in *Solid-Phase Organic Synthesis: Concepts, Strategies, and Applications*, ed. by P.H. Toy, Y. Lam (Wiley, Hoboken, New Jersey, 2012)
570. B. Pan, D. Cui, F. Gao, R. He, Nanotechnology **17**, 2483 (2006)
571. I. Grabchev, J.-M. Chovelon, V. Bojinov, Polymer **44**, 4421 (2003)
572. I. Grabchev, J.-M. Chovelon, V. Bojinov, G. Ivanova, Tetrahedron **59**, 9591 (2003)
573. A. Olivas, T.A. Zepeda, D. Madrigal Peralta, Mater. Res. Innov. **12**, 12 (2008)
574. C. Zhang, P. Su, M.U. Farooq, Y. Yang, X. Gao, E. Hongjun, React. Funct. Polym. **70**, 129 (2010)
575. M.A. Andrade Jr., H.O. Pastore, A.C.S. Appl, Mater. Interfaces **27**, 1884 (2016)
576. F. Zhang, B. Wang, S. He, R. Man, J. Chem. Eng. Data **59**, 1719 (2014)
577. A.M. Caminade, R. Laurent, J.P. Majoral, Adv. Drug Deliv. Rev. **57**, 2130 (2005)
578. M. Ballauff, C.N. Likos, Angew. Chem. Int. Ed. **43**, 2998 (2004)
579. S. Uppuluri, F.A. Morrison, P.R. Dvornic, Macromolecules **33**, 2551 (2000)
580. P.K. Maiti, T. Cagin, S.T. Lin, W.A. Goddard III, Macromolecules **38**, 979 (2005)
581. D.A. Tomalia, H. Baker, J.R. Dewald, Polym. J. **17**, 117 (1985)
582. B.I. Voit, A. Lederer, Chem. Rev. **109**, 5924 (2009)
583. H. Mori, A.H.E. Müller, P.F.W. Simon, in *Macromolecular Engineering: Precise Synthesis, Materials, Properties, Applications*, vol. 2, ed. by K. Matyjaszewski, Y. Gnanou, L. Leibler (Wiley-VCH, Weinheim, 2007)
584. M.G. McKee, S. Unal, G.L. Wilkes, T.E. Long, Prog. Polym. Sci. **30**, 507 (2005)
585. M. Jikei, M.-A. Kakimoto, in *Progress in Polycondensation*, ed. by T. Matsumoto (Research Signpost, Trivandrum, India, 2002)
586. W. Burchard, Adv. Polym. Sci. **143**, 113 (1999)
587. V. Balzani, P. Ceroni, M. Maestri, C. Saudan, V. Vicinelli, Top. Curr. Chem. **228**, 159 (2003)
588. D.A. Tomalia, Soft Matter **6**, 456 (2010)
589. D.A. Tomalia, J. Nanopart. Res. **11**, 1251 (2009)
590. T. Zhong, P. Ai, J. Zhou, Fluid Phase Equilib. **302**, 43 (2011)
591. C.N. Moorefield, A. Schultz, G.R. Newkome, Braz. J. Pharm. Sci. **49**, 67 (2013)
592. M.S. Shinde, M.B. Bhalerao, S. Thakre, J. Franklin, A. Jain, Asian J. Pharm. Res. Dev. **2**, 24 (2014)
593. P. Bhattacharya, D. Du, Y. Lin, J.R. Soc, Interface **11**, 20131067 (2014)
594. C. Gao, D. Yan, Prog. Polym. Sci. **29**, 183 (2004)
595. D. Wang, T. Zhao, X. Zhu, D. Yan, W. Wang, Chem. Soc. Rev. **21**, 4023 (2015)
596. Q. Zhu, F. Qiu, B. Zhu, X. Zhu, RSC Adv. **3**, 2071 (2014)
597. I.N. Kurniasih, J. Keilitz, R. Haag, Chem. Soc. Rev. **44**, 4145 (2015)
598. D.A. Markelov, Yu.Ya. Gotlib, A.A. Darinskii, A.V. Lulin, S.V. Lulin, Vysokomol. Soedin. **51**, 469 (2009)
599. B.K. Nanjwade, H.M. Bechraa, G.K. Derkara, F.V. Manvia, V.K. Nanjwade, Eur. J. Pharm. Sci. **38**, 185 (2009)
600. P. Kesharwani, K. Jain, N.K. Jain, Prog. Polym. Sci. **39**, 268 (2014)
601. K. Madaan, S. Kumar, N. Poonia, V. Lather, D. Pandita, J. Pharm. Bioallied Sci. **6**, 139 (2014)

602. D. Yan, C. Gao, H. Frey (eds.), *Hyperbranched Polymers: Synthesis, Properties, and Applications* (Wiley, Hoboken, New Jersey, 2011)
603. X. Huang, S. Zheng, I. Kim, J. Nanosci. Nanotechnol. **14**, 1631 (2014)
604. M. Mishra, S. Kobayashi, *Star and Hyperbranched Polymers* (CRC Press, NY, Basel, 1999)
605. A. Lederer, W. Burchard, *Hyperbranched Polymers: Macromolecules in between Deterministic Linear Chains and Dendrimer Structures*, RSC Polymer Chemistry Series (RSC Publishing, Cambridge, 2015)
606. N. Karak, S. Maiti, *Dendrimers and Hyperbranched Polymers: Synthesis to Applications* (MD Publications Pvt Ltd, New Delhi, 2008)
607. J. Vukovic, *Hyperbranched Polymers Based on Aliphatic Polyesters, Synthesis and Characterization* (VDM Verlag Dr. Müller, Germany, 2008)
608. W.A. Braunecker, K. Matyjaszewski, Prog. Polym. Sci. **32**, 93 (2007)
609. S. Kuchanov, H. Slot, A. Stroeks, Prog. Polym. Sci. **29**, 563 (2004)
610. Y. Zheng, S. Li, Z. Weng, C. Gao, Chem. Soc. Rev. **44**, 4091 (2015)
611. J. Han, S. Li, A. Tang, C. Gao, Macromolecules **45**, 4966 (2012)
612. A. Hult, M. Johannson, E. Malmström, Adv. Polym. Sci. **143**, 1 (1999)
613. P. Froehling, J. Polym. Sci. Part A Polym. Chem. **42**, 3110 (2004)
614. B. Voit, J. Polym. Sci. Part A Polym. Chem. **38**, 2505 (2000)
615. M. Jikei, M. Kakimoto, J. Polym. Sci. Part A Polym. Chem. **42**, 1293 (2004)
616. J.-F. Stumbé, B. Bruchmann, Macromol. Rapid Commun. **25**, 921 (2004)
617. B. Bruchmann, Macromol. Mater. Eng. **292**, 981 (2007)
618. B. Bruchmann, R. Koeniger, H. Renz, Macromol. Symp. **187**, 271 (2002)
619. H. Holter, A. Burgath, H. Frey, Acta Polym. **48**, 30 (1997)
620. N. Hadjichristidis, M. Pitsikalis, S. Pispas, H. Iatrou, Chem. Rev. **101**, 3747 (2001)
621. C. Wei, H. Gao, Star polymers as unimolecular containers, in *Encyclopedia of Polymeric Nanomaterials*, ed. by S. Kobayashi, K. Müllen (Springer, Berlin, Heidelberg, 2013)
622. K. Khanna, S. Varshney, A. Kakkar, Polym. Chem. **1**, 1171 (2010)
623. A. Blencowe, J.F. Tan, T.K. Goh, G.G. Qiao, Polymer **50**, 5 (2009)
624. F.K. Wolf, A.M. Fischer, H. Frey, Beilstein J. Org. Chem. **6**, 67 (2010)
625. C. Gao, X. Zheng, Soft Matter **5**, 4788 (2009)
626. A. Kowalczuk, A. Vandendriessche, B. Trzebicka, B. Mendrek, U. Szeluga, G. Cholewiński, M. Smet, A. Dworak, W. Dehaen, J. Polym. Sci. Part A Polym. Chem. **47**, 1120 (2009)
627. H. Hong, Y. Mai, Y. Zhou, D. Yan, Y. Chen, J. Polym. Sci. Part A Polym. Chem. **46**, 668 (2008)
628. A. Hirao, H.-S. Yoo, Polymer J. **43**, 2 (2011)
629. M. Morell, A. Lederer, X. Ramis, B. Voit, A. Serra, J. Polym. Sci. Part A Polym. Chem. **49**, 2395 (2011)
630. M.A. Quadir, R. Haag, J. Control. Release **161**, 484 (2012)
631. M. Caldéron, M.A. Quadir, S.K. Sharma, R. Haag, Adv. Mater. **22**, 190 (2010)
632. C.R. Yates, W. Hayes, Eur. Polym. J. **40**, 1257 (2004)
633. A. Khan, M. Malkoch, M.F. Montague, C.J. Hawker, J. Polym. Sci. Polym. Chem. **46**, 6238 (2008)
634. B. Voit, H. Komber, A. Lederer, Hyperbranched polymers: synthesis and characterization aspects, in *Materials Science and Technology*, 701 (2013)
635. Y. Shi, R.W. Graff, X. Cao, X. Wang, H. Gao, Angew. Chem. Int. Ed. **54**, 7631 (2015)
636. F. Huang, H.W. Gibson, J. Am. Chem. Soc. **126**, 14738 (2004)
637. L.J. Twyman, A.S.H. King, J. Burnett, I.K. Martin, Tetrahedron Lett. **45**, 433 (2004)
638. A.S. Nasar, M. Jikei, M.A. Kakimoto, Eur. Polym. J. **39**, 1201 (2003)
639. Y.B. Kim, H.K. Kim, H. Nishida, T. Endo, Macromol. Mater. Eng. **289**, 923 (2004)
640. A.V. Ambade, A. Kumar, J. Polym. Sci. A **42**, 5134 (2004)
641. Y. Ohta, Y. Kamijyo, A. Yokoyama, T. Yokozawa, Polymer **4**, 1170 (2012)
642. X. Li, J. Zhan, Y. Li, Macromolecules **37**, 7584 (2004)
643. Y. Segawa, T. Higashihara, M. Ueda, Polym. Chem. **4**, 1746 (2013)

644. K. Onitsuka, N. Ohshiro, M. Fujimoto, F. Takei, S. Takahashi, Mol. Cryst. Liq. Cryst. **342**, 159 (2000)
645. T. Higashihara, Y. Segawa, W. Sinananwanich, M. Ueda, Polymer J. **44**, 14 (2012)
646. A.S. Abd-El-Aziz, S.A. Carruthers, P.M. Aguiar, S. Kroeker, J. Inorg. Organomet. Polym. **15**, 349 (2005)
647. H. Magnusson, E. Malmstrom, A. Hult, Macromolecules **33**, 3099 (2000)
648. L. Song, C. Tu, Y. Shi, F. Qiu, Y. Jiang, Q. Zhu, B. Zhu, D. Yan, X. Zhu, Macromol. Rapid Commun. **31**, 443 (2010)
649. J. Feng, Y. Li, M. Yang, Eur. Polym. J. **44**, 3314 (2008)
650. J. Feng, Y. Li, M. Yang, J. Polym. Sci. A **47**, 222 (2009)
651. Y. Jiang, Y. Wang, J. Hua, S. Qu, S. Qian, H. Tian, J. Polym. Sci. A **47**, 4400 (2009)
652. C. Liu, C. Gao, D. Yan, Chem. Res. Chin. Univ. **21**, 345 (2005)
653. L. Xu, Z. Ye, Chem. Commun. **49**, 8800 (2013)
654. J.-B. Baek, J.B. Ferguson, L.-S. Tan, Macromolecules **36**, 4385 (2003)
655. S. Li, J. Han, C. Gao, Polym. Chem. **4**, 1774 (2013)
656. M. Smet, C. Gottschalk, S. Skaria, H. Frey, Macromol. Chem. Phys. **206**, 2421 (2005)
657. I. Gadwal, S. Binder, M.C. Stuparu, A. Khan, Macromolecules **47**, 5070 (2014)
658. R.R. Barzegar, S. Akbari, M.H. Kish, Polym. Int. **62**, 1767 (2013)
659. F. Sun, X. Luo, L. Kang, X. Peng, C. Lu, Polym. Chem. **6**, 1214 (2015)
660. F. Xu, J. Zhong, X. Qian, Y. Li, X. Lin, Q. Wu, Polym. Chem. **4**, 3480 (2013)
661. R. Barbey, S. Perrier, Macromolecules **47**, 6697 (2014)
662. A.B. Cook, R. Barbey, J.A. Burns, S. Perrier, Macromolecules **49**, 1296 (2016)
663. J.-J. Yan, J.-T. Sun, Y.-Z. You, D.-C. Wu, C.-Y. Hong, Sci. Rep. **3**, Article number 2841 (2013)
664. R. Salazar, L. Fomina, S. Fomine, Polym. Bull. **47**, 151 (2001)
665. R. Reul, J. Nguyen, T. Kissel, J. Biomaterial. **30**, 5815 (2009)
666. G. Prevec, E. Zagar, M. Zigon, Chem. Ind. **55**, 365 (2006)
667. S. Chen, X.Z. Zhang, S.X. Cheng, R. Zhuo, Z.W. Gu, Biomacromolecules **9**, 2578 (2008)
668. N.S. Klimenko, A.V. Shevchuk, M.Ya. Vortman, E.G. Privalko, V.V. Shevchenko, Vysokomol. Soedin. Ser. A. **50**, 268 (2008)
669. Z. Feng, L. Lin, Sci. Photochem. **24**, 36 (2006)
670. T. Qiu, L. Tang, Z. Fu, X. Tuo, Y. Li, D. Liu, W. Yang, Polym. Adv. Technol. **15**, 65 (2004)
671. K. Fukukawa, R. Rossin, A. Hagooly, E.D. Pressly, J.N. Hunt, B.W. Messmore, K.L. Wooley, M.J. Welch, C.J. Hawker, Biomacromolecules **9**, 1329 (2008)
672. X. Wang, R.W. Graff, Y. Shi, H. Gao, Polym. Chem. **6**, 6739 (2015)
673. H. Xiaohua, Y. Deyue, M. Yiyong, Eur. Polym. J. **40**, 1759 (2004)
674. C. Schüll, H. Rabbel, F. Schmid, H. Frey, Macromolecules **46**, 5823 (2013)
675. P. Fan, C. Lu, Polym. Adv. Technol. **23**, 48 (2012)
676. Y. Liu, L. Xu, J. Liu, X. Liu, C. Chen, G. Li, Y. Meng, Chem. Eng. J. **285**, 698 (2016)
677. H. Yang, J. Xu, S. Pispas, G. Zhang, RSC Adv. **3**, 6853 (2013)
678. G.G. Wallace, P.R. Teasdale, G.M. Spinks, L.A.P. Kane-Maguire, *Conductive Electroactive Polymers: Intelligent Polymer Systems*, 3rd edn. (CRC Press, Boca Raton, 2008)
679. G. Inzelt, *Conducting Polymers: A New Era in Electrochemistry* (Springer, Heidenberg, 2012)
680. R. Tucceri, *Poly(o-aminophenol) Film Electrodes: Synthesis, Transport Properties and Practical Applications* (Springer, Cham, Heidelberg, NY, Dordrecht, London, 2013)
681. M.W. Urban (ed.), *Stimuli-Responsive Polymeric Films and Coatings*, ACS Symposium Series, vol. 912 (American Chemical Society, Washington, 2005)
682. A. Singh, *Structure and Dynamics of Ultrathin Polymeric Films* (Lap Lambert Academic Publishing, Germany, 2013)
683. H. Biederman (ed.), *Plasma Polymer Films* (Imperial College Press, London, 2004)
684. A. Heilmann, *Polymer Films with Embedded Metal Nanoparticles* (Springer, Berlin, 2003)

685. O.C. Tsui, T.P. Russell, *Polymer Thin Films* (World Scientific Publishing Co., Singapore, 2008)
686. D.R. Baer, P.E. Burrows, A.A. El-Azab, Prog. Org. Coat. **47**, 342 (2003)
687. L.A. Felton, Int. J. Pharm. **457**, 423 (2013)
688. J. Zhou, H. Wang, Zhongnan Minzu Daxue Xuebao. Ziran Kexue Ban **23**, 5 (2004)
689. M.G. Zolotukhin, M.C.G. Hernandez, A.M. Lopez, L. Fomina, G. Cedillo, A. Nogales, T. Ezquerra, D. Rueda, H.M. Colquhoun, K.M. Fromm, A. Ruiz-Trevino, M. Ree, Macromolecules **39**, 4696 (2006)
690. V. Calderon, F.C. Garcia, J.L. De la Pena, E.M. Maya, J.M. Garcia, J. Polym. Sci. A **44**, 2270 (2006)
691. B.I. Podlovchenko, V.N. Andreev, Uspekhi Khim. **71**, 950 (2002)
692. L. Tian, M. Zhang, P. Lu, W. Zhang, B. Yang, Y. Ma, Chin. Sci. Bull. **49**, 246 (2004)
693. S. Panozzo, F. Lafolet, L. Trouillet, J.-C. Vial, S. Guillerez, Synth. Metals **142**, 201 (2004)
694. S. Basak, Y.S.L.V. Narayana, M. Baumgarten, K. Müllen, R. Chandrasekar, Macromolecules **46**, 362 (2013)
695. S.A. Shin, J.B. Park, J.-H. Kim, D.-H. Hwang, Synth. Metals **172**, 54 (2013)
696. D.R. Rueda, A. Nogales, J.J. Hernández, M.-C. García-Gutiérrez, T.A. Ezquerra, S.V. Roth, M.G. Zolotukhin, R. Serna, Langmuir **23**, 12677 (2007)
697. C.-H. Yang, L.-R. Huang, Y.-K. Chih, S.-L. Chung, J. Phys. Chem. C **111**, 3786 (2007)
698. K. Fukuda, S. Lee, Polym. Prepr. (Japan) Engl. Ed. **45**, E 396 (1996)
699. E.J. Onah, U. Oertel, L. Hauszler, D. Voigt, C. Froeck, H. Komber, B.I. Voit, K. Lunkwitz, Eur. Polym. J. **39**, 127 (2003)
700. T. Akiyama, M. Matsushita, K. Kakutani, S. Yamada, K. Takechi, T. Shiga, T. Motohiro, H. Nakayama, K. Kohama, Jpn. J. Appl. Phys. Part 1 **44**, 2799 (2005)
701. M. Tagowska, B. PaLys, M. Mazur, M. Skompska, K. Jackowska, Electrochim. Acta **50**, 2363 (2005)
702. J. Zhang, D. Shan, S. Mu, J. Polym. Sci. A **45**, 5573 (2007)
703. M.M. Ayad, N.A. Salahuddin, A.K. Abou-Seif, M.O. Alghaysh, Eur. Polym. J. **44**, 426 (2008)
704. M.Y. Abed, A.M. Mazrouaa, Z. Abdeen, A. Ashery, Periodica Polytech. **58**, 35 (2014)
705. X.-G. Li, H.-Y. Wang, M.-R. Huang, Macromolecules **40**, 1489 (2007)
706. S. Cosnier, A. Karyakin (eds.), *Electropolymerization: Concepts, Materials and Applications* (Wiley, Weinheim, 2011)
707. S. Mu, Electrochim. Acta **56**, 3764 (2011)
708. J.A. Cobos-Murcia, L. Galicia, A. Rojas-Hernandez, M.T. Ramirez-Silva, R. Alvarez-Bustamante, M. Romero-Romo, G. Rosquete-Pina, M. Palomar-Pardave, Polymer **46**, 9053 (2005)
709. W. Badawy, K. Ismail, S. Medany, Z. Phys. Chem. **237**, 1741 (2013)
710. S.B. Revin, S.A. John, Electrochim. Acta **56**, 8934 (2011)
711. W.A. Badawy, K.M. Ismail, Z.M. Khalifa, J. Appl. Electrochem. **37**, 593 (2007)
712. H. Liu, G. Zhang, Y. Zhou, M. Gao, F. Yang, J. Mater. Chem. A **1**, 13902 (2013)
713. A.H.A. Shah, R. Holze, J. Electroanal. Chem. **597**, 95 (2006)
714. S.M. Sayyah, M.M. El-Deeb, S.M. Kamal, R.E. Azooz, J. Appl. Polym. Sci. **112**, 3695 (2009)
715. J. Hwang, J.I. Son, Y.-B. Shim, Sol. Energy Mater. Sol. Cells **94**, 1286 (2010)
716. G. Shul, M. Weissmann, D. Bélanger, Langmuir **30**, 6612 (2014)
717. Y.F. Du, X.M. Qi, P. Zhao, J.X. Lu, M.Y. He, Chin. Chem. Lett. **15**, 1098 (2004)
718. M. Ates, Mater. Sci. Eng. C **33**, 1853 (2013)
719. Z.M. Zain, N. Zakaria, Malays. J. Anal. Sci. **18**, 107 (2014)
720. W. Zhai, X. Tian, Y. Yan, Y. Zhao, Y. Liu, Canad. J. Chem. **91**, 1077 (2013)
721. A. Curulli, Sensor Lett. **6**, 682 (2008)
722. S.P. Luo, Q.X. Liu, Z. Liu, A.J. Xie, Y. Kong, X. Dai, Chin. Chem. Lett. **23**, 1311 (2012)
723. S.R. Cao, R. Yuan, Y.Q. Chai, L.Y. Zhang, X.L. Li, R. Chai, J. Electrochem. Soc. **153**, H223 (2006)

724. S.R. Cao, R. Yuan, Y.Q. Chai, L.Y. Zhang, X.L. Li, F.X. Gao, Bioproc. Biosyst. Eng. **30**, 71 (2007)
725. A. Merz, S. Anikin, B. Lieser, J. Heinze, H. John, Chem. Eur. J. **9**, 449 (2003)
726. Y. Oztekin, Z. Yazicigil, A.O. Solak, Z. Ustundag, Z. Kilic, S. Bilge, Surf. Interface Anal. **43**, 923 (2011)
727. Y. Oztekin, Z. Yazicigil, A.O. Solak, Z. Ustundag, A. Okumus, Z. Kilic, A. Ramanaviciene, A. Ramanavicius, Sens. Actuators B Chem. **166–167**, 117 (2012)
728. G. Shul, M. Weissmann, D. Bélanger, Electrochim. Acta **162**, 146 (2015)
729. B.D. Mert, M.E. Mert, G̣. Kardaṣ, B. Yazici, Appl. Surf. Sci. **258**, 9668 (2012)
730. W.A. Badawy, K.M. Ismail, S.S. Medany, Electrochim. Acta **51**, 6353 (2006)
731. K.M. Ismail, Z.M. Khalifa, M.A. Azzem, W.A. Badawy, Electrochim. Acta **47**, 1867 (2002)
732. W.A. Badawy, K.M. Ismail, S.S. Medany, Int. J. Chem. Kinet. **43**, 141 (2011)
733. Z. Algharaibeh, P.G. Pickup, Electrochim. Acta **93**, 87 (2013)
734. L.A. Hernández, M.A. del Valle, F.R. Díaz, D.J. Fermin, T.A.G. Risbridger, Electrochim. Acta **166**, 163 (2015)
735. I.M. Burguete, V. Fabregat, F. Galindo, A.M. Izquierdo, S.V. Luis, Eur. Polym. J. **45**, 1516 (2009)
736. Z. Xu, M. Wang, W. Fan, J. Zhao, H. Wang, Electrochim. Acta **160**, 271 (2015)
737. S.M. Sayyah, M.M. El-Rabiey, S.S. Abd El-Rehim, R.E. Azooz, J. Appl. Polym. Sci. **99**, 3093 (2006)
738. A.M. Golyakov, A.N. Borisov, G.A. Shagisultanova, F.L. Shpikev, Zh. Obsch. Khim. **81**, 1529 (2011)
739. A.M. Golyakov, A.V. Schukarev, V.N. Pak, G.A. Shagisultanova, A.N. Borisov, Zh. Prikl. Khim. **84**, 321 (2011)
740. B.C. Thompson, K.A. Abboud, J.R. Reynolds, K. Nakatani, P. Audebert, New J. Chem. **29**, 1128 (2005)
741. X. Tan, S. Zhang, X. Song, C. Li, Nanosci. Nanotechn. Lett. **6**, 333 (2014)
742. R. Solmaz, G. Kardas, Prog. Org. Coat. **64**, 81 (2009)
743. M. Yildirim, İ. Kaya, Synth. Metals **162**, 834 (2012)
744. F.R. Diaz, M.A. Del Valle, C. Nunez, A. Godoy, J.L. Mondaca, A. Toro-Labbe, J.C. Bernede, Polym. Bull. **56**, 155 (2006)
745. E.N. Esmer, S. Tarkuc, Y.A. Udum, L. Toppare, Mater. Chem. Phys. **131**, 519 (2011)
746. M. Mahmut, T. Awut, I. Nurulla, M. Mijit, J. Polym. Res. **21**, 403 (2014)
747. M. Mahmut, T. Awut, I. Nurulla, M. Mijit, J. Appl. Polym. Sci. **131**, 40861 (2014)
748. B.B. Carbas, A. Kivrak, M. Zora, A.M. Önal, J. Electroanal. Chem. **677–680**, 9 (2012)
749. K.A. Koparkar, B.B. ECarbaEs, A. Kivrak, M. Zora, A.M. Onal, React. Funct. Polym. **71**, 579 (2011)
750. B. Duong, R. Arechabaleta, N.J. Tao, J. Electroanal. Chem. **447**, 63 (1998)
751. M.V. Tesakova, I.A. Popov, V.I. Parfenyuk, Russ. J. Electrochem. **50**, 517 (2014)
752. J. Durantini, G.M. Morales, M. Santo, M. Funes, E.N. Durantini, F. Fungo, T. Dittrich, L. Otero, M. Gervaldo, Org. Electron. **13**, 604 (2012)
753. A. Uygun, R. Myjavcova, A.G. Yavuz, J.V. Ruppel, K.B. Fields, A. Frankhauser, X.P. Zhang, V.R. Bhethanbotla, P. Bednar, Electroanalysis **23**, 1158 (2011)
754. K. Takechi, T. Shiga, T. Akiyama, S. Yamada, Photochem. Photobiol. Sci. **9**, 1085 (2010)
755. P. Veerender, S.P. Koiry, V. Saxena, P. Jha, A.K. Chauhan, D.K. Aswal, S.K. Gupta, AIP Conf. Proc. **1447**, 727 (2012)
756. K. Iwasaki, A. Kimoto, S. Naya, F. Iwahori, J. Abe, Synth. Metals **159**, 880 (2009)
757. M. Gervaldo, P.A. Liddell, G. Kodis, B.J. Brennan, C.R. Johnson, J.W. Bridgewater, A.L. Moore, T.A. Moore, D. Gust, Photochem. Photobiol. Sci. **9**, 890 (2010)
758. J.-M. Pernaut, K. Zong, J.R. Reynolds, Synth. Metals **130**, 1 (2002)
759. S. Bilal, A.H.A. Shah, R. Holze, J. Electrochem. Soc. **155**, P89 (2008)
760. S. Bilal, R. Holze, J. Electroanal. Chem. **592**, 1 (2006)
761. S. Bilal, R. Holze, Electrochim. Acta **52**, 1247 (2006)

762. S. Bilal, R. Holze, Electrochim. Acta **52**, 5346 (2007)
763. S. Bilal, A. Ali Shah, R. Holze, Electrochim. Acta **97**, 364 (2013)
764. S. Bilal, A.H.A. Shah, R. Holze, Electrochim. Acta **85**, 358 (2012)
765. L.A. Hernandez, M.A. Del Valle, F.J. Armijo, F.R. Diaz, G. Louarn, Electrochemistry **81**, 954 (2013)
766. S. Palaniappan, P. Manisankar, J. Polym. Res. **18**, 311 (2011)
767. A.H.A. Shah, R. Holze, Electrochim. Acta **52**, 1374 (2006)
768. Y. Zhang, X. Liu, Q. Li, J. Appl. Polym. Sci. **128**, 1625 (2013)
769. S. Mu, Synth. Metals **143**, 259 (2004)
770. A. Benyoucef, S. Boussalem, M.I. Ferrahi, M. Belbachir, Synth. Metals **160**, 1591 (2010)
771. H.S.O. Chan, S.C. Ng, W.S. Sim, K.L. Tan, B.T.G. Tan, Macromolecules **25**, 6029 (1992)
772. W.C. Chen, T.C. Wen, A. Gopalan, J. Electrochem. Soc. **148**, E427 (2001)
773. C.-F. Chang, W.-C. Chen, T.-C. Wen, A. Gopalan, Acid J. Electrochem. Soc. **149**, E298 (2002)
774. M.S. Wu, T.C. Wen, A. Gopalan, Mat. Chem. Phys. **74**, 58 (2002)
775. M.S. Wu, T.C. Wen, A. Gopalan, J. Electrochem. Soc. **148**, D65 (2001)
776. L. Zhang, B. Hou, Q. Lang, Amer. J. Anal. Chem. **2**, 182 (2011)
777. S.M. Sayyah, M.M. El-Rabiey, S.S. Abd El-Rehim, R.E. Azooz, J. Appl. Polym. Sci. **109**, 1643 (2008)
778. Y. Wang, F. Teng, Z. Xu, Y. Hou, Y. Wang, X. Xu, Eur. Polym. J. **41**, 1020 (2005)
779. K. Wagner, M. Zanoni, A.B.S. Elliott, P. Wagner, R. Byrne, L.E. Florea, D. Diamond, K.C. Gordon, G.G. Wallace, D.L. Officer, J. Mater. Chem. C **1**, 3913 (2013)
780. J. Wang, B. Lu, C. Liu, J. Xu, M. Pei, J. Mater. Sci. **45**, 5769 (2010)
781. K.H. Fries, G.R. Sheppard, J.A. Bilbrey, J. Locklin, Polym. Chem. **5**, 2094 (2014)
782. K.A. Koparkar, Sens. Transducers J. **143**, 10 (2012)
783. K.L. Jarvis, P. Majewski, Plasma Proc. Polym. **10**, 619 (2013)
784. A.I. Drachev, A.B. Gil'man, E.S. Obolonkova, A.A. Kuznetsov, Synth. Metals **142**, 35 (2004)
785. K. Lintinen, L. Storbacka, A. Efimov, S. Hietala, R. Ahorinta, N. Tkachenko, H. Lemmetyinen, J. Polym. Sci. A **47**, 6095 (2009)
786. K. Lintinen, L. Storbacka, A. Efimov, A. Tolkki, N. Tkachenko, H. Lemmetyinen, Solar Energy Mater. Solar Cells **95**, 909 (2011)
787. F. Tian, E.A. Decker, J.M. Goddard, J. Agr. Food Chem. **60**, 2046 (2012)
788. M.J. Roman, F. Tian, E.A. Decker, J.M. Goddard, J. Appl. Polym. Sci. **131**, 39948 (2014)
789. G. Bayramoglu, M.Y. Arica, Fibers Polym. **13**, 1225 (2012)
790. A. Joseph, S. Subramanian, P.C. Ramamurthy, S. Sampath, R.V. Kumar, C. Schwandt, Electrochim. Acta **137**, 557 (2014)
791. H. Březnová, R. Volf, V. Král, J.L. Sessler, A.C. Try, T.V. Shishkanova, Anal. Bioanal. Chem. **375**, 1193 (2003)
792. T.R. Aslamazova, V.A. Kotenev, YuA Plachev, AYu. Tsivadze, Prot. Met. Phys. Chem. Surf. **48**, 627 (2012)
793. A.M. Donald, A.H. Windle, S. Hanna (eds.), *Liquid Crystalline Polymers*, 2nd edn. (Cambridge University Press, Cambridge, 2006)
794. D. Broer, G.P. Crawford, S. Zumer (eds.), *Cross-Linked Liquid Crystalline Systems: From Rigid Polymer Networks to Elastomers* (CRC Press, Boca Raton, London, NY, 2011)
795. V.P. Shibaev, L. Lam (eds.), *Liquid Crystalline and Mesomorphic Polymers* (Springer, NY, 1994)
796. X. Wang, Q. Zhou, Liquid crystalline polymers, in *Thermoplastic Materials: Properties, Manufacturing Methods, and Applications*, ed. by C.C. Ibeh (CRC Press, Boca Raton, 2011)
797. W.H. de Jeu (ed.), *Liquid Crystal Elastomers: Materials and Applications* (Springer, Berlin, 2012)
798. S. Kumar, *Chemistry of Discotic Liquid Crystals: From Monomers to Polymers* (CRC Press, Boca Raton, 2010)

799. S.J. Woltman, G.D. Jay, G.P. Crawford (eds.), *Liquid Crystals: Frontiers in Biomedical Applications* (World Scientific Publishing Co., Singapore, 2007)

800. P. Oswald, P. Pieranski, *Nematic and Cholesteric Liquid Crystals* (CRC Press, Boca Raton, 2005)

801. T. Rasing, I. Musevic (eds.), *Surfaces and Interfaces of Liquid Crystals* (Springer, Berlin, Heidelberg, 2004)

802. S.V. Pasechnik, V.G. Chigrinov, D.V. Shmeliova, *Liquid Crystals: Viscous and Elastic Properties in Theory and Applications* (Wiley, Weinheim, 2009)

803. S. Sudhakar, T. Narasimhaswamy, K.S.V. Srinivasan, Liq. Cryst. **27**, 1525 (2000)

804. B.B. Sauer, W.G. Kampert, R.S. McLean, Polymer **44**, 2721 (2003)

805. J.M. Adell, M.P. Alonso, J. Barbera, L. Oriol, M. Pinol, J.L. Serrano, Polymer **44**, 7829 (2003)

806. D. Pucci, A. Bellusci, A. Crispini, M. Ghedini, M. La Deda, Inorg. Chim. Acta **357**, 495 (2004)

807. P. Kannan, S. Raja, P. Sakthivel, Polymer **45**, 7895 (2004)

808. K.I. Aly, A.A. Khalaf, I.A. Alkskas, J. Appl. Polym. Sci. **88**, 153 (2003)

809. E.-J. Choi, J.-C. Ahn, L.-C. Chien, C.-K. Lee, W.-C. Zin, D.-C. Kim, S.-T. Shin, Macromolecules **37**, 71 (2004)

810. E.J. Choi, J.C. Ahn, C.K. Lee, J.I. Jin, Polymer **41**, 7617 (2000)

811. D. Ribera, A. Mantecon, A. Serra, Macromol. Symp. **199**, 267 (2003)

812. K.S.V. Srinivasan, T. Padmavathy, Macromol. Symp. **199**, 277 (2003)

813. M. Cano, L. Oriol, M. Pinol, J.L. Serrano, Chem. Mater. **11**, 94 (1999)

814. T. Sasaki, G. Fukunaga, Chem. Mater. **17**, 3433 (2005)

815. B. Donnio, J. Barbera, R. Gimenez, D. Guillon, M. Marcos, J.L. Serrano, Macromolecules **35**, 370 (2002)

816. J. Barbera, M. Marcos, J.L. Serrano, Chem. Eur. J. **5**, 1834 (1999)

817. J. Barbera, M. Marcos, A. Omenat, J.L. Serrano, J.I. Martinez, P.J. Alonso, Liq. Cryst. **27**, 255 (2000)

818. M. Marcos, R. Gimenez, J.L. Serrano, B. Donnio, B. Heinrich, D. Guillon, Chem. Eur. J. **7**, 1006 (2001)

819. V. Cozan, M. Gaspar, E. Butuc, A. Stoleriu, Eur. Polym. J. **37**, 1 (2001)

820. P.A. Henderson, C.T. Imrie, Macromolecules **38**, 3307 (2005)

821. H. Hioki, M. Fukutaka, H. Takahashi, M. Kubo, K. Matsushita, M. Kodama, K. Kubo, K. Ideta, A. Mori, Tetrahedron **61**, 10643 (2005)

822. T. Narasimhaswamy, N. Somanathan, D.K. Lee, A. Ramamoorthy, Chem. Mater. **17**, 2013 (2005)

823. J.A. Smith, R.A. DiStasio, N.A. Hannah, R.W. Winter, T.J.R. Weakley, G.L. Gard, S.B. Rananavare, J. Phys. Chem. B **108**, 19940 (2004)

824. R. Paschke, S. Liebsch, C. Tschierske, M.A. Oakley, E. Sinn, Inorg. Chem. **42**, 8230 (2003)

825. M. Grigoras, C.O. Catanescu, J. Macromol. Sci. C **44**, 131 (2004)

826. I.O. Savchenko, V.G. Siromyatnikov, Ukr. Khim. Zh. **80**, 44 (2014)

827. J.J. Wie, S. Chatterjee, D.H. Wang, L.-S. Tan, M.R. Shankar, T.J. White, Polymer **55**, 5915 (2014)

828. G. Rabilloud, High-performance polymers. Chemistry and applications, in *Polyquinoxalines and Polyimides*, vol. 2. (Editions Technip, Paris, 1997–2000)

829. D.-J. Liaw, K.-L. Wang, Y.-C. Huang, K.-R. Lee, J.-Y. Lai, C.-S. Ha, Prog. Polym. Sci. **37**, 907 (2012)

830. U. Shukla, K.V. Rao, A.K. Rakshit, J. Appl. Polym. Sci. **88**, 153 (2003)

831. V.P. Malinovskaya, T.I. Borisova, N.M. Geller, S.V. Fedorova, S.S. Skorokhodov, Vysokomol. Soedin. **48**, 34 (2006)

832. C.-L. Liu, F.-C. Tsai, C.-C. Chang, K.-H. Hsieh, J.-L. Lin, W.-C. Chen, Polymer **46**, 4950 (2005)

833. H. Ocak, B. Bilgin-Eran, C. Tschierske, U. Baumeister, G. Pelzl, J. Mater. Chem. **19**, 6995 (2009)
834. B.J. Vasanthi, L. Ravikumar, Open J. Polym. Chem. **3**, 70 (2013)
835. M. Kaller, S. Laschat, Top. Curr. Chem. **318**, 109 (2012)
836. S. Zhang, X. Zhang, T. Jia, G. Hao, Z. Li, Gaofenzi Xuebao 403 (2009)
837. S. Zheng, K. Guo, M. Niu, S. Zhang, Z. Li, Q. Zhou, L. Li, Gaofenzi Xuebao 32 (2004)
838. Z. Li, W. Zhu, K. Guo, S. Zhang, S. Zheng, Gaofenzi Cailiao Kexue Yu Gongcheng **20**, 81 (2004)
839. L. Marin, E. Perju, M.D. Damaceanu, Eur. Polym. J. **47**, 1284 (2011)
840. A. Iwan, D. Sek, Progr. Polym. Sci. **33**, 289 (2008)
841. E.A. Soto-Bustamante, C.M. Gonzalez-Henriquez, G.A. Rodriguez-Lehyt, R.O. Vergara-Toloza, Liq. Cryst. **31**, 1115 (2004)
842. E.A. Soto-Bustamante, D. Saldaño-Hurtado, R.O. Vergara-Toloza, P.A. Navarrete-Encina, M.A. Athanassopoulou, Liq. Cryst. **30**, 17 (2003)
843. A. Iwan, M. Palewicz, A. Sikora, J. Chmielowiec, A. Hreniak, G. Pasciak, P. Bilski, Synth. Met. **160**, 1856 (2010)
844. H.E. Gulbas, H. Ocak, Y.H. Gursel, B. Bilgin-Eran, Mol. Cryst. Liq. Cryst. **574**, 40 (2013)
845. H.E. Gulbas, D.G. Coskun, Y.H. Gurse, B. Bilgin-Eran, Adv. Mat. Lett. **5**, 333 (2014)
846. J.W. Brown, G.J. Lambe, P.J.S. Foot, J.A. Clipson, Macromol. Rapid Commun. **25**, 1000 (2004)
847. P. Castell, A. Serra, M. Galia, J. Polym. Sci. A **42**, 3631 (2004)
848. J. Kim, B.M. Novak, A.J. Waddon, Macromolecules **37**, 8286 (2004)
849. Z. Li, K. Guo, X. Zhang, T. Zhang, S. Zheng, S. Zhang, Q. Zhou, L. Li, Gaofenzi Xuebao 175 (2003)
850. A. Ryabchun, A. Bobrovsky, A. Medvedev, V. Shibaev, J. Polym. Sci. A **49**, 625 (2011)
851. S.-J. Wang, R.-Y. Zhao, S. Yang, Z.-Q. Yu, E.-Q. Chen, Chem. Commun. **50**, 8378 (2014)
852. V. Shibaev, A. Medvedev, A. Bobrovsky, J. Polym. Sci. A **46**, 6532 (2008)
853. H. Zhang, Y. Tu, X. Wan, Q.-F. Zhou, E.M. Woo, J. Polym. Res. **9**, 11 (2002)
854. X. He, W. Sun, D. Yan, L. Liang, Eur. Polym. J. **44**, 42 (2008)
855. J.E. Stumpel, E.R. Gil, A.B. Spoelstra, C.W.M. Bastiaansen, D.J. Broer, A.P.H. J. Schenning, Adv. Funct. Mater. **25**, 3314 (2015)
856. D. Zhao, Q. Wang, L. Guo, H. Yang, Liq. Cryst. **41**, 1510 (2014)
857. J.J. Wie, K.M. Lee, T.H. Ware, T.J. White, Macromolecules **48**, 1087 (2015)
858. M.E. McConney, A. Martinez, V.P. Tondiglia, K.M. Lee, D. Langley, I.I. Smalyukh, T.J. White, Adv. Mater. **25**, 5880 (2013)
859. D. Iqbal, M.H. Samiullah, Materials **6**, 116 (2013)
860. T. Seki, Polym. J. **46**, 751 (2014)
861. G. Fernández, Nature Mater. **12**, 12 (2013)
862. B. Donnio, D. Guillon, Adv. Polym. Sci. **201**, 45 (2006)
863. M. Higuchi, M. Tsuruta, H. Chiba, S. Shiki, K. Yamamoto, J. Am. Chem. Soc. **125**, 9988 (2003)
864. J.S. Cho, K. Takanashi, M. Higuchi, K. Yamamoto, Synth. Met. **150**, 79 (2005)
865. A. Kimoto, K. Masachika, J.S. Cho, M. Higuchi, K. Yamamoto, Chem. Mater. **16**, 5706 (2004)
866. X. Yan, T. Goodson, T. Imaoka, K. Yamamoto, J. Phys. Chem. B **109**, 9321 (2005)
867. M. Marcos, R. Martín-Rapún, A. Omenat, J.L. Serrano, Chem. Soc. Rev. **36**, 1889 (2007)
868. I. Gracia, B. Feringán, J.L. Serrano, R. Termine, A. Golemme, A. Omenat, J. Barbera, Chemistry **21**, 1359 (2015)
869. Y. Sagara, T. Kato, Angew. Chem. Int. Ed. **47**, 5175 (2008)
870. B.I. Ostrovskii, S.N. Sulyanov, N.A. Boiko, V.P. Shibaev, S.B. Astaf'ev, L.G. Yanusova, W.H. de Jeu, Eur. Phys. J. E. **36**, 134 (2013)
871. A. Belaissaoui, I.M. Saez, S.J. Cowling, J.W. Goodby, Macromolecules **46**, 1268 (2013)
872. V.P. Shibaev, Polym. Sci. Ser. A **51**, 1131 (2009)
873. V.P. Shibaev, Polym. Sci. Ser. A **56**, 727 (2014)

874. P. Argurio, R. Molinari, T. Poerio, Desalination **162**, 217 (2004)
875. I. Kaya, M. Yildiz, S. Koyuncu, Synth. Met. **128**, 267 (2002)
876. M.A.R. Ahamed, R. Subha, D. Jeyakumar, A.R. Burkanudeend, Polym. Int. **64**, 126 (2015)
877. H. Kasgoz, S. Ozgumus, M. Orbay, Polymer **44**, 1785 (2003)
878. M.-A. Kwon, G.-J. Kim, Catal. Today **87**, 145 (2003)
879. X. Liu, Y. Hu, B. Wang, Z. Su, Synth. Met. **159**, 1557 (2009)
880. R. Qu, C. Sun, J. Chen, H. Chen, C. Wang, C. Ji, L. Xu, Polym. Eng. Sci. 721 (2007)
881. K.H. Reddy, A.R. Reddy, J. Appl. Polym. Sci. **88**, 414 (2003)
882. Y. Kwak, A.J.D. Magenau, K. Matyjaszewski, Macromolecules **44**, 811 (2011)
883. Y. Xu, W. Bai, Z. Luo, Y. Jin, B. Peng, L. Feng, B. Hu, J. Lin, Appl. Surf. Sci. **258**, 5141 (2012)
884. Y.Q. Wang, Y.X. Sun, X.L. Xong, X.Z. Zhang, G.Y. Zhang, Mol. BioSyst. **6**, 256 (2010)
885. D. Kumar, P.K. Gupta, A. Syamal, J. Chem. Sci. **117**, 247 (2005)
886. A.M. Albu, M. Mocioi, C.D. Mateescu, A. Iosif, J. Appl. Polym. Sci. **121**, 1867 (2011)
887. P.U. Belsare, A.B. Zade, Der Pharma Chem. **5**, 325 (2013)
888. M.K. Othman, F.A. Al-Qadri, F.A. Al-Yusufy, Spectrochim. Acta Part A **78**, 1342 (2011)
889. F. Bakhtiarzaden, S.A. Ghani, Electroanalysis **22**, 549 (2010)
890. C. Sun, G. Zhang, R. Qu, Y. Yu, Chem. Eng. J. **170**, 250 (2011)
891. N.P. Tzanetos, A.K. Andreopoulou, J.K. Kallitsis, J. Polym. Sci. Part A Polym. Chem. **43**, 4838 (2005)
892. Y. Cui, Q. Chen, D.-D. Zhang, J. Cao, B.-H. Han, J. Polym. Sci. Part A Polym. Chem. **48**, 1310 (2010)
893. K.J. Calzia, G.N. Tew, Macromolecules **35**, 6090 (2002)
894. M.A.R. Meier, U.S. Schubert, J. Polym. Sci. Part A Polym. Chem. **41**, 2964 (2003)
895. D.-W. Yoo, S.-K. Yoo, C. Kim, J.-K. Lee, J. Chem. Soc. Dalton Trans. 3931 (2002)
896. E. Holder, V. Marin, M.A.R. Meier, U.S. Schubert, Macromol. Rapid Commun. **25**, 1491 (2004)
897. Q. Luo, Y. Guan, Y. Zhang, M. Siddiq, J. Polym. Sci. Part A Polym. Chem. **48**, 4120 (2010)
898. T. Yamamoto, Y. Saitoh, K. Anzai, H. Fukumoto, T. Yasuda, Y. Fujiwara, B.-K. Choi, K. Kubota, T. Miyamae, Macromolecules **36**, 6722 (2003)
899. N. Kang, A.S. Hay, J. Macromol. Sci. Part A Pure Appl. Chem. **40**, 881 (2003)
900. P. Yan, H. Jing, Adv. Synth. Catal. **351**, 1325 (2009)
901. T. Ahamad, S.M. Alshehri, Adv. Polym. Technol. **32**, 21350 (2013)
902. J. Ritchie, A. Ruseckas, P. Andre, C. Munther, M. Van Ryssen, D.E. Vize, J.A. Crayston, I.D.W. Samuel, Synth. Met. **159**, 583 (2009)
903. S.M. Islam, M. Mobarok, P. Mondal, A.S. Roy, S. Mondal, D. Hossain, J. Appl. Polym. Sci. **123**, 3789 (2012)
904. M. Nagy, M. Zsuga, D. Racz, S. Keki, J. Polym. Sci. Part A Polym. Chem. **48**, 2709 (2010)
905. S. He, A.A. Buelt, J.M. Hanley, B.P. Morgan, A.G. Tennyson, R.C. Smith, Macromolecules **45**, 6344 (2012)
906. B. Liu, W.-L. Yu, J. Pei, S.-Y. Liu, Y.-H. Lai, W. Huang, Macromolecules **34**, 7932 (2001)
907. L. Zong, Q. Miao, Y. Liu, J. Xu, X. Huang, Y. Cheng, Chin. J. Chem. **27**, 1179 (2009)
908. S.-I. Kato, K. Takagi, K. Suzuki, T. Kinoshita, Y. Yuki, J. Polym. Sci. Part A Polym. Chem. **42**, 2631 (2004)
909. Y. de Gaetano, I. Clarot, J.-B. Regnouf-de-Vains, Tetrahedron Lett. **50**, 5793 (2009)
910. A.V. Pestov, P.A. Slepukhin, Y.G. Yatluk, V.N. Charushin, O.N. Chupakhin, J. Appl. Polym. Sci. **125**, 1970 (2012)
911. A. de Bettencourt-Dias, J.S.K. Rossini, Inorg. Chem. **55**, 9954 (2016)
912. C. Ji, S. Song, C. Wang, C. Sun, R. Qu, C. Wang, H. Chen, Chem. Eng. J. **165**, 573 (2010)
913. C. Ji, R. Qu, C. Sun, C. Wang, Q. Xu, Y. Sun, C. Li, S. Guo, J. Appl. Polym. Sci. **103**, 3220 (2007)
914. C. Ji, R. Qu, Q. Xu, C. Sun, C. Wang, Y. Cheng, Y. Song, J. Appl. Polym. Sci. **111**, 2148 (2009)

915. T. Ahamad, S.M. Alshehri, Polym. Int. **61**, 1640 (2012)
916. J. Weng, L.M. Jiang, W.L. Sun, Z.Q. Shen, S.Q. Liang, Polymer **42**, 5491 (2001)
917. C. Bianchini, M. Frediani, G. Mantovani, F. Vizza, Organometallics **20**, 2660 (2001)
918. S. Moulay, R. Mehdaoui, React. Funct. Polym. **61**, 265 (2004)
919. A. Stepuk, J.G. Halter, A. Schaetz, R.N. Grass, W.J. Stark, Chem. Commun. **48**, 6238 (2012)
920. C. Dai, Y. Wang, Y. Quan, Q. Chen, Y. Cheng, C. Zhu, J. Polym. Sci. Part A Polym. Chem. **52**, 3080 (2014)
921. I.A. Alkskas, I.S. Moosa, Int. J. Polym. Mat. **61**, 1142 (2012)
922. R. Qu, C. Wang, C. Ji, C. Sun, X. Sun, G. Cheng, J. Appl. Polym. Sci. **95**, 1558 (2005)
923. M.M. Patel, M.A. Kapadia, G.P. Patel, J.D. Joshi, React. Funct. Polym. **67**, 746 (2007)
924. M.M. Patel, M.A. Kapadia, J.D. Joshi, Eur. Polym. J. **45**, 426 (2009)
925. S.S. Rahangdale, World Appl. Sci. J. **1**, 237 (2013)
926. G. Alagumuthu, P. Mariselvi, Int. J. Chem. Stud. **1**, 157 (2013)
927. Z. Yang, J. Lu, Acta Polym. Sinica **1**, 838 (2008)
928. J. Lai, L.-Q. Wang, K. Tu, C. Zhao, W. Sun, J. Appl. Polym. Sci. **26**, 1572 (2005)
929. W.B. Gurnule, H.D. Juneja, L.J. Paliwal, React. Funct. Polym. **50**, 95 (2002)
930. J. Dontulwar, K. Nandekara, W. Gurnule, Der Pharma Chem. **5**, 160 (2013)
931. M.S. Dhore, S.S. Butoliya, A.B. Zade1, ISRN Polym. Sci. **2014**, Article ID 873520 (2014)
932. B. Gao, W. Zhang, Z. Zhang, Q. Lei, J. Lumin. **132**, 2005 (2012)
933. A. El-Dissouky, A.-Z. Elassar, A.-H. Bu-Olian, J. Chem. Eng. Data **56**, 1827 (2011)
934. M.S. Hosseini, H. Raissi, S. Madarshahian, React. Funct. Polym. **66**, 1539 (2006)
935. A. Islam, A. Ahmad, M.A. Laskar, J. Appl. Polym. Sci. **123**, 3448 (2012)
936. I. Kaya, D. Senol, J. Appl. Polym. Sci. **90**, 442 (2003)
937. G. Pina-Luis, G.A. Rosquete Pina, A.C.V. Gonzalez, A.O. Teran, I.R. Espejel, M.E. Diaz-Garcia, React. Funct. Polym. **72**, 61 (2012)
938. C.-Y. Chen, C.-Y. Chen, J. Appl. Polym. Sci. **86**, 1986 (2002)
939. B. Gao, X. Wei, Y. Zhang, Opt. Mater. **35**, 536 (2013)
940. C.-Y. Chen, S.-Y. Chen, J. Appl. Polym. Sci. **94**, 2123 (2004)
941. G. Iyer, L.M.V. Tillekeratne, M.R. Coleman, A. Nadarajah, Polymer **49**, 3744 (2008)
942. G. Iyer, L.M.V. Tillekeratne, M.R. Coleman, A. Nadarajah, Polymer **49**, 3737 (2008)
943. L. Yang, Y. Li, X. Jin, Z. Yeb, X. Ma, L. Wang, Y. Liu, Chem. Eng. J. **168**, 115 (2011)
944. L.Q. Yang, Y.F. Li, L.Y. Wang, Y. Zhang, X.J. Ma, Z.F. Ye, J. Hazard. Mater. **180**, 98 (2010)
945. N. Illy, D. Majonis, I. Herrera, O. Ornatsky, M.A. Winnik, Biomacromolecules **13**, 2359 (2012)
946. D. Majonis, I. Herrera, O. Ornatsky, M. Schulze, X. Lou, M. Soleimani, M. Nitz, M.A. Winnik, Anal. Chem. **82**, 8961 (2010)
947. C. Sun, R. Qu, C. Ji, Q. Wang, C. Wang, Y. Sun, G. Cheng, Eur. Polym. J. **42**, 188 (2006)
948. B.L. Rivas, A. Maureira, C. Guzman, M.A. Mondaca, J. Appl. Polym. Sci. **111**, 78 (2009)
949. A. Denizli, R. Say, B. Garipcan, S. Patir, React. Funct. Polym. **58**, 123 (2004)
950. I. Kaya, A.R. Vilayetoglu, H. Topak, J. Appl. Polym. Sci. **85**, 2004 (2002)
951. X. Ma, Y. Li, Z. Ye, L. Yang, L. Zhou, L. Wang, J. Hazard. Mater. **185**, 1348 (2011)
952. J.X. Luo, C.L. Yang, J. Zheng, J.Y. Ma, L.Y. Liang, M.G. Lu, Eur. Polym. J. **47**, 385 (2011)
953. N.M. Salem, K.A.K. Ebraheem, M.S. Mubarak, React. Funct. Polym. **59**, 63 (2004)
954. S.S. Katkamwar, A.B. Zade, S.S. Rahangdale, W.B. Gurnule, J. Appl. Polym. Sci. **113**, 3330 (2009)
955. S. Gharbi, J. Khiari, B. Jamoussi, J. Chem. Eng. Process Technol. **5**, 198 (2014)
956. W.B. Gurnule, S.S. Katkamwar, Der Pharm. Lett. **4**, 1360 (2012)
957. R.S. Azarudeen, M.A.R. Ahamed, A.R. Burkanudeen, Desalination **268**, 90 (2011)
958. V.D. Mane, N.J. Wahane, W.B. Gurnule, J. Appl. Polym. Sci. **111**, 3039 (2009)
959. S.K. Mandavgade, J.R. Dontulwar, W.B. Gurnule, Der Pharma Chem. **4**, 1695 (2012)
960. W. Zhang, B. Gao, Y. Chen, Acta Polym. Sinica 1382 (2011)

961. M.N.A. Al-Jibouri, T.M. Musa, M. Mubarak, W.M. Al-Jibouri, Sci. J. Chem. **1**, 38 (2013)
962. H. Askun, B. Gülbakan, O. Celikbicak, C. Uzun, O. Güven, B. Salih, J. Appl. Polym. Sci. **107**, 2714 (2008)
963. H. Dierssen, W. Balzer, W.M. Landing, Mar. Chem. **73**, 173 (2001)
964. M. Hruby, J. Hradil, M.J. Bene, React. Funct. Polym. **59**, 105 (2004)
965. C. Sun, C. Li, C. Wang, R. Qu, Y. Niu, H. Geng, Chem. Eng. J. **200–202**, 291 (2012)
966. W.B. Gurnule, D.B. Patle, Elixir Appl. Chem. **50**, 10338 (2012)
967. S.M. Islam, A.S. Roy, P. Mondal, S. Paul, N. Salam, Inorg. Chem. Commun. **24**, 170 (2012)
968. S. Samal, S. Acharya, R.K. Dey, A.R. Ray, J. Appl. Polym. Sci. **88**, 570 (2003)
969. N. Samadi, R. Hasanzadeh, M. Rasad, J. Appl. Polym. Sci. **132**, 41642 (2015)
970. S.M. Islam, N. Salam, P. Mondal, A.S. Roy, J. Mol. Catal. A Chem. **366**, 321 (2013)
971. O. Melad, M. Esleem, Open J. Org. Polym. Mater. **5**, Article ID: 54864 (2015)
972. M.R. Nateghi, M. Borhani, React. Funct. Polym. **68**, 153 (2008)
973. R.S. Azarudeen, M.A.R. Ahamed, D. Jeyakumar, A.R. Burkanudeen, Iran. Polym. J. **18**, 821 (2009)
974. R.S. Azarudeen, M.A.R. Ahamed, N. Prabu, N.M. Kani, Appl. Organomet. Chem. **28**, 773 (2014)
975. I. Kaya, H.O. Demir, A.R. Vilayetoglu, Synth. Met. **126**, 183 (2002)
976. A. Ercag, I. Kaya, D. Senol, S. Koyunci, Polym. Plast. Technol. Eng. **44**, 265 (2005)
977. J. Hou, F. Song, L. Wang, G. Wei, Y. Cheng, C. Zhu, Macromolecules **45**, 7835 (2012)
978. S. Keesara, M.R. Mandapati, S. Parvathaneni, Appl. Catal. A Gen. **496**, 58 (2015)
979. J.P. Gangwar, P.N. Saxena, Orient. J. Chem. **27**, 119 (2011)
980. D. Kumar, P.K. Gupta, A. Syamal, J. Chil. Chem. Soc. **59**, 2260 (2014)
981. Y. Feng, M.E. Lydon, C.W. Jones, ChemCatChem **5**, 3636 (2013)
982. G.S.V. Kumar, B. Mathew, J. Appl. Polym. Sci. **92**, 1271 (2004)
983. I. Kaya, M. Yildirim, A. Avci, Synth. Met. **160**, 911 (2010)
984. F. Dogan, I. Kaya, A. Bilici, Synth. Met. **161**, 79 (2011)
985. H. Fukumoto, K. Yamane, Y. Kase, T. Yamamoto, Macromolecules **43**, 10366 (2010)
986. B. Liu, Y. Bao, F. Du, H. Wang, J. Tian, R. Bai, Chem. Commun. **47**, 1731 (2011)
987. R. Sankar, S. Vijayalakshmi, S. Rajagopan, T. Kaliyappan, J. Appl. Polym. Sci. **117**, 2146 (2010)
988. I. Kaya, F. Dogana, A. Bilici, Polym. Int. **58**, 570 (2009)
989. N. Sarı, S. Özcan, Chin. J. Polym. Sci. **27**, 675 (2009)
990. M. Sasidaran, R. Sankar, P. Kandasamy, S. Vijayalakshmi, T. Kaliyappan, High Perform. Polym. **23**, 602 (2011)
991. I. Kaya, A. Bilici, M. Sacak, Synth. Met. **159**, 1414 (2009)
992. M.N. Al-jibouri, T.M. Musa, IOSR J. Appl. Chem. (IOSR-JAC) **7**, 46 (2014)
993. R.S. Walmsley, C. Litwinski, E. Antunes, P. Hlangothi, E. Hosten, C. McCleland, T. Nyokong, N. Torto, Z.R. Tshentu, J. Mol. Catal. A Chem. **379**, 94 (2013)
994. T.R. Sankar, P.V. Ramana, J. Appl. Chem. **2**, 1459 (2013)
995. M. Cegłowski, G. Schroeder, Chem. Eng. J. **263**, 402 (2015)
996. T.R. Sankar, K. Kesavulu, P.V. Ramana, J. Chem. Sci. **126**, 597 (2014)
997. K. Kesavulu, T.R. Sankar, P.V. Ramana, Chem. Sci. Trans. **2**, 1318 (2013)
998. K.C. Gupta, A.K. Sutar, J. Mol. Catal. A Chem. **280**, 173 (2008)
999. A.M. Gad, A. El-Dissouky, E.M. Mansour, A. El-Maghraby, Polym. Degrad. Stab. **68**, 153 (2000)
1000. W.B. Gurnule, P.K. Rahangdale, L.J. Paliwal, R.B. Kharat, React. Funct. Polym. **55**, 255 (2003)
1001. S.M. Badawy, H.H. Sokker, A.M. Dessouki, J. Appl. Polym. Sci. **99**, 1180 (2006)
1002. F.A. Alakhras, K.A. Dari, M.S. Mubarak, J. Appl. Polym. Sci. **97**, 691 (2005)
1003. G. Zong, J. Ma, H. Chen, C. Wang, N. Ji, D. Liu, J. Appl. Polym. Sci. **124**, 2179 (2012)
1004. M. Bru, M.I. Burguete, F. Galindo, S.V. Luis, M.J, Marin, L. Vigara, Tetrahedron Lett. **47**, 1787 (2006)

1005. M.S. Choi, J.H. Lee, D.W. Kim, T.S. Lee, J. Polym. Sci. Part A Polym. Chem. **45**, 4430 (2007)
1006. M.B. Amran, A.S. Panggabean, A. Sulaeman, M. Rusnadi, Int. J. Environ. Res. **5**, 531 (2011)
1007. S.M. Islam, P. Mondal, A.S. Roy, S. Mondal, D. Hossain, Tetrahedron Lett. **51**, 2067 (2010)
1008. M. Ignatova, M. Sepulchre, N. Manolova, Eur. Polym. J. **38**, 33 (2002)
1009. B.F. Senkal, E. Yavuz, Monatsh. Chem. **137**, 929 (2006)
1010. Y. Zhang, Y. Chen, C. Wang, Y. Wei, J. Hazard. Mater. **276**, 129 (2014)
1011. C. Xiong, S. Zhou, X. Liu, Q. Jia, C. Ma, X. Zheng, Ind. Eng. Chem. Res. **53**, 2441 (2014)
1012. M.A. Diab, A.Z. El-Sonbati, R.H. Mohamed, Spectrochim. Acta. Part A Mol. Biomol. Spectrosc. **77**, 795 (2010)
1013. L. Qian, Y. Guan, B. He, H. Xiao, Polymer **49**, 2471 (2008)
1014. M. Hatanaka, M. Hoshi, R. Shiba, Kobunshi Ronbunshu **63**, 745 (2006)
1015. T. Ahamad, S.M. Alshehri, Spectrochim. Acta. Part A Mol. Biomol. Spectr. **96**, 179 (2012)
1016. T. Ahamad, S.M. Alshehri, Spectrochim. Acta. Part A Mol. Biomol. Spectr. **108**, 26 (2012)
1017. M.A.A. El-Ghaffar, M.H. Mohamed, K.Z. Elwakeel, Chem. Eng. J. **151**, 30 (2009)
1018. C. Xiong, Y. Zheng, Y. Feng, C. Yao, C. Ma, X. Zheng, J. Mater. Chem. A **2**, 5379 (2014)
1019. C. Xiong, Y. Li, G. Wang, L. Fang, S. Zhou, C. Yao, Q. Chen, X. Zheng, D. Qi, Y. Fu, Y. Zhu, Chem. Eng. J. **259**, 257 (2015)
1020. C. Wang, C. Ji, Y. Meng, L. Liu, R. Qu, C. Wang, J. Appl. Polym. Sci. **116**, 636 (2010)
1021. R. Qu, C. Sun, C. Ji, C. Wang, Q. Xu, S. Lu, C. Li, G. Xu, G. Cheng, J. Appl. Polym. Sci. **101**, 631 (2006)
1022. K. Roy, S. Basu, Ind. J. Chem. **44A**, 531 (2005)
1023. W.B. Gurnule, P.K. Rahangdale, L.J. Paliwal, R.B. Kharat, J. Appl. Polym. Sci. **89**, 787 (2003)
1024. K.S. Chettiyar, K. Sreekumar, Ind. J. Chem. **42A**, 499 (2003)
1025. S. Dutta, A.K. Das, J. Appl. Polym. Sci. **103**, 2281 (2007)
1026. M.R. Maurya, A. Arya, P. Adao, J.C. Pessoa, Appl. Catal. A Gen. **351**, 239 (2008)
1027. C. Ji, R. Qu, C. Sun, C. Wang, Y. Sun, N. Zhao, H. Xie, J. Appl. Polym. Sci. **100**, 5034 (2006)
1028. Y. Chen, Y. Zhao, React. Funct. Polym. **55**, 89 (2003)
1029. H. Ciftci, H.N. Testereci, Z. Oktem, Polym. Bull. **66**, 747 (2011)
1030. M. Bakherad, A. Keivanloo, B. Bahramian, S. Jajarmi, J. Organomet. Chem. **724**, 206 (2013)
1031. A. Kausar, S. Zulfiqar, Z. Ahmad, M. Ishaq, M.I. Sarwar, J. Appl. Polym. Sci. **124**, 373 (2012)
1032. A.R. Reddy, K.H. Reddy, J. Appl. Polym. Sci. **91**, 1932 (2004)
1033. M. Hruby, M. Skodova, H. Mackova, J. Skopal, M. Tomes, M. Kropacek, J. Zimova, J. Kucka, React. Funct. Polym. **71**, 1155 (2011)
1034. D. Jermakowicz-Bartkowiak, React. Funct. Polym. **67**, 1505 (2007)
1035. F.C. Gaertner, R. Luxenhofer, B. Blechert, R. Jordan, M. Essler, J. Control. Rel. **119**, 291 (2007)
1036. H. Mouaziz, J.-C. Soutif, V. Montembault, Eur. Polym. J. **39**, 1773 (2003)
1037. L. Garcia, A. Torrent, E. Anticó, C. Fontas, A. Roglans, React. Funct. Polym. **68**, 1088 (2008)
1038. M.J. Tapia, H.D. Burrows, J.M. Garcia, F. Garcia, A.A.C.C. Pais, Macromolecules **37**, 856 (2004)
1039. V. Calderon, F. Serna, F. García, J.L. de la Pena, J.M. Garcia, J. Appl. Polym. Sci. **106**, 2875 (2007)
1040. J.-M. Yu, Y. Chen, Macromolecules **42**, 8052 (2009)
1041. L. Cui, D. Chao, J. Zhang, H. Mao, Y. Li, C. Wang, Synth. Metals **160**, 400 (2010)
1042. X. Han, P. Xiao, H. Zhao, C. Zeng, J. Zhou, Appl. Spectrosc. **68**, 879 (2014)

1043. W. Zhou, M. Guo, J. Xu, X. Yuan, Eur. Polym. J. **44**, 656 (2008)
1044. P.K. Mohapatra, S. Lakshmi, D.M. Raju, V.K. Manchanda, J. Membr. Sci. **232**, 133 (2004)
1045. S. Habaue, Y. Akagi, M. Sato, A. Niimi, Polym. Bull. **54**, 237 (2005)
1046. K. Kimura, H. Sakamoto, R.M. Uda, Macromolecules **37**, 1871 (2004)
1047. H. Sakamoto, T. Anase, H. Osuga, K. Kimura, React. Funct. Polym. **71**, 569 (2011)
1048. S.R. Dave, H. Kaur, S.K. Menon, React. Funct. Polym. **70**, 692 (2010)
1049. S.H. Chan, W.T. Wong, W.K. Chan, Chem. Mater. **13**, 4635 (2001)
1050. T. Terashima, M. Kawabe, Y. Miyabara, H. Yoda, M. Sawamoto, Nat. Commun. **4**, 2321 (2013)
1051. B. Gierczyk, G. Schroeder, M. Cegłowski, React. Funct. Polym. **71**, 463 (2011)
1052. Z. Liu, I. Schmidt, P. Thamyongkit, R.S. Loewe, D. Syomin, J.R. Diers, A. Zhao, V. Misra, J.S. Lindsey, D.F. Bocian, Chem. Mater. **17**, 3728 (2005)
1053. N.B. McKeown, S. Hanif, K. Msayib, C.E. Tattershall, P.M. Budd, Chem. Commun. 2782 (2002)
1054. C. Huang, N. Wang, Y. Li, C. Li, J. Li, H. Liu, D. Zhu, Macromolecules **39**, 5319 (2006)
1055. T. Asano, P.-C. Wang, A. Iwasaki, Spectrochim. Acta. Part A **75**, 305 (2010)
1056. A. Bilgin, C. Yagci, A. Mendi, U. Yildiz, Polyhedron **26**, 617 (2007)
1057. A. Bilgin, C. Yagci, U. Yildiz, Macromol. Chem. Phys. **206**, 2257 (2005)
1058. A. Bilgin, A. Mendi, U. Yildiz, Polymer **47**, 8462 (2006)
1059. G. Tillet, P. De Leonardis, A. Alaaeddine, M. Umeda, S. Mori, N. Shibata, S.M. Ali, D. Fortin, P.D. Harvey, B. Ameduri, Macromol. Chem. Phys. **213**, 1559 (2012)
1060. H. Duan, L. Liu, X. Meng, D. Qin, X. Wang, X. Du, C. Wang, J. Tian, Synth. Met. **159**, 1512 (2009)
1061. S. Fu, K. Zhang, M. Zhang, L. Tian, Pigm. Resin Technol. **41**, 3 (2012)

Chapter 3
Metal Complexes with Polymer Chelating Ligands

Abstract Major advances and problems in the field of synthesis, properties, and structure of polymeric metal chelates prepared by the direct interaction of chelating polymer ligands with metal compounds are discussed. The polymeric metal chelates are subdivided into molecular, intracomplex, macrocyclic and polynuclear types which in turn are grouped depending on the nature of the donor atoms (N,N-, N,O-, N,S-, O,O-, O,S-, S,S-, P,P-chelates, etc.). The main attention is focused on similarities and differences between low and high molecular weight metal chelates. Special attention is paid to the spatial organization of polymeric metal chelates. The most important directions of the studies in the field of such compounds are highlighted.

The most PMCs were obtained by the direct interaction of metal ions with chelating polymers [1–35]. In most cases, this interaction takes place similar to the chelation process of metal compounds with low molecular weight chelating ligands. However, the chelation processes in polymeric systems are more complicated than monomer analogues and their description is associated with the need to consider a number of additional factors. Thus, during metal chelation with CPL, the complications associated with incomplete of the reactions; change the nature of the functional groups during the process, the heterogeneity of the system as well as the formation of the mixture of mixed-ligand products arise. In addition, originality of formed PMC consists in significant distortion of the chelate node, caused by specific steric strain due to the rigidity of the reaction centers. Effect of the polymer matrix on the central ion configuration in PMC is determined by the nature of the CPL, its crosslinking degree, reaction conditions, etc. The special role plays the spatial arrangement of chelating units on the polymer chain, which will provide the minimum geometric tension during the interaction of the CPL with MX_n and the maximum overlap of ligand orbitals with the bounded metal orbitals. As for low molecular weight analogues, the energy of the spatial organization of the chelate

nodes in PMC depends on a number of factors. These include the presence of steric stresses arising at the location of the functional groups at the tops of the polyhedron defined by the nature of the transition metal atom, the electrostatic interaction of the CPL and MX_n, as well as the orientation of the orbitals of reacting atoms, etc.

It should be noted that both reagents (CPL and MX_n) can undergo various transformations. For example, redox processes, decomposition of dimeric complexes, cluster formation, etc. often accompany MX_n chelation. At the same time, the conformation changes of polymeric chain, CPL destruction, adverse reactions of functional groups, displacement of tautomeric equilibrium, etc. are characteristic of the CPLs. In addition, PMC properties are largely determined by different character of chelate node distribution on a polymer ligand, difference in spatial geometries of metal ions, composition heterogeneity, etc. Well-directed attempts to synthesize PMCs are determined, on the one hand, the necessity to obtain PMC with homogeneous structures, and, on the other hand, their practical use as metal-containing materials. Moreover, the study of chelation reactions in systems containing a CPL is of further interest. First, for coordination chemistry, it is necessary to clarify the influence of the polymer chain on the character of the metal chelate units formed, their spatial organization and the nature of the bonds. From the polymer chemistry, it is interesting to study the peculiarities of the reactivity of macromolecules.

As well as the contributions from the entropy and enthalpy of chelation common to low and high molecular weight metal chelates, a series of specific contributions caused by the chain structure of CPL are characteristic of the PMC. The most essential ones are the following [36]:

- the "adjustment" of the local chelating fragment;
- the effect of "neighboring" groups;
- the effect of the "chain";
- the change in chain conformation in the course of the reaction;
- the cooperative effect.

Knowledge about effects of the chemical structure of CPL and the nature of ions on the efficiency of formation of PMC provides a means of targeted variation in the functional characteristics of PMC. Problem of the influence of the polymeric nature of ligand on the physico-chemical properties and the structure of metal chelate units connected to the polymer chain is currently under development. This problem, as well as many other problems of the PMC chemistry it is advisable to investigate from individual classes of PMCs. In this chapter, some representatives of the different types of PMCs will be reviewed in accordance with the classification proposed in Chap. 1. It does not attempt to provide an exhaustive analysis of all the available experimental data. The main attention will be focused on similarities and differences between low and high molecular weight metal chelates.

3.1 Molecular Metal Chelates

Nitrogen-containing polymeric chelating ligands are the most widely used class of compounds for the preparation of molecular metal chelates.

3.1.1 Chelation with Polyamine Ligands

The metal chelates with CPLs containing polyamine fragments are the typical representatives of PMCs with nitrogen-containing chelating ligands. Examples of such complex ligands mainly include en, dien, trien, etc. In most cases, they are characterized by the same spatial structure (especially in dilute solutions) as that for low molecular weight analogues. We note that a good model for such systems is PEI, which has good water solubility, suitable molecular weights, high content of chelating fragments as well as good physical and chemical stabilities [37–45]. PEI polymers are well known for their ability to bind metal ions, with commercially available branched PEI commonly having primary, secondary and tertiary amine groups in approximately 1:1:0.7 ratios. Both linear and branched PEIs show high chelating ability and the branched PEI is the most efficient in chelating copper and forms chelates with an N/Cu ratio of 4–5. Among commercial polymers such as PEI, poly (ethylene imine-epichlorohydrin), and poly (dimethyl amine-*co*-epichlorohydrin), PEI has the highest chelation abilities [46–48]. Theoretically the chelating ability of PEI is high (3.88 mmol g^{-1} is one assumes the transition metal ion coordinative number, CN, to be equal to 4). The reason lies in the fact that repeating –NH–CH$_2$–CH$_2$– group behavior is a first approximation similar to en (although trien is usually accepted as a monomer analogue). The study of Cu(II) chelation with PEI and poly (N-methyl ethylene imine) showed that up to 70% of the polymer units take part in chelation. The structure of chelates with the polymer and low molecular weight amines is identical. The difference in reactivity of low molecular weight ligands and CPLs is due to the different ability of functional groups to bind protons and the conformational changes of PEI. Stable PEI-Cu(II) chelates were reported where copper ions are hard to elute from the polymer domain to the bulk solution and binding constant values are 1–5 order magnitude greater in the PMC systems than in the monomeric Cu-chelate systems.

Four-coordinative chelates are formed in the Co(II)-PEI system. The high chelating ability of the units of the CPL is also confirmed by the fact that PEI units within all the examined reagents concentrations replace all ligand groups of LMC.
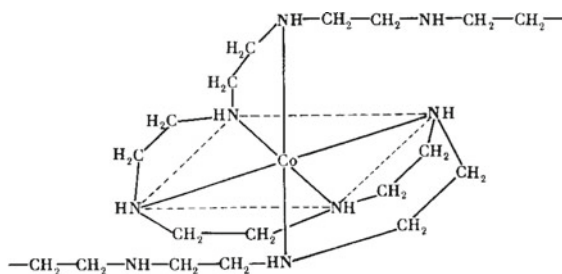
The process of Co(II) and Ni(II) chelation is assumed to be step-by-step and consists of progressive complexes (of the ratio L/M(II) = 2, 4, 5, and 6) formation. An analysis of the treatment of PEI with cobalt(II) and nickel(II) ions in concentrated solutions showed that the chelates with the CN = 2 and 4 are formed at low ratios of N/M(II) in solution. An increase of the ratio of N/M(II) in solution leads to formation of chelates with CN = 5 and 6. In this case, water is removed from the coordination sphere of metal ion. The absence of cooperative effect in those chelates is bound with the energetic expenses at the formation of inner-chain chelates with CN = 4 or 6 (apparently, due to the rigidity of the polymer chains and their weak amenability during metal chelation). The use of mono- and bidentate units of different polymer chains [49] realize the completion of these high-ligand chelates:
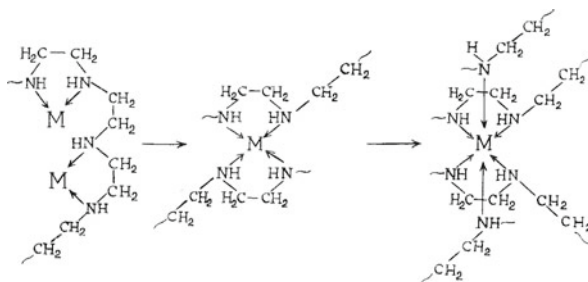
The adsorption capacity of such an interesting polymer ligand as poly (acrylamidino diethylenediamine) is equal to 11.4 mequiv g^{-1} [50]. It is important that the use of CPL with polyamine ligands in the binding of heavy metal ions is largely determined by the pH of the medium. In particular, at low pH values, adsorbed H^+ ions on the amino groups of the polymer ligand blocked the chelation of metal ions, and an increase in pH led to higher adsorption values (Scheme 3.1).

It should be noted a strategy to introduce acid-degradable linkages between the polymer backbone and the permanently bound en ligands of Pt(II)-based drugs (Fig. 3.1) [51]. The methodology exploited the high stability of the bonds between Pt and en ligands to enhance the pH responsiveness. It is important that the micelle
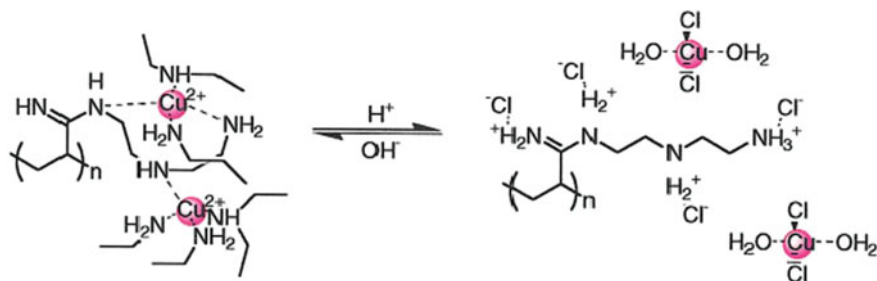
Scheme 3.1 Change of the structure of the poly (acryloamidino diethylenediamine)-Cu(II) chelate with increasing and decreasing pH
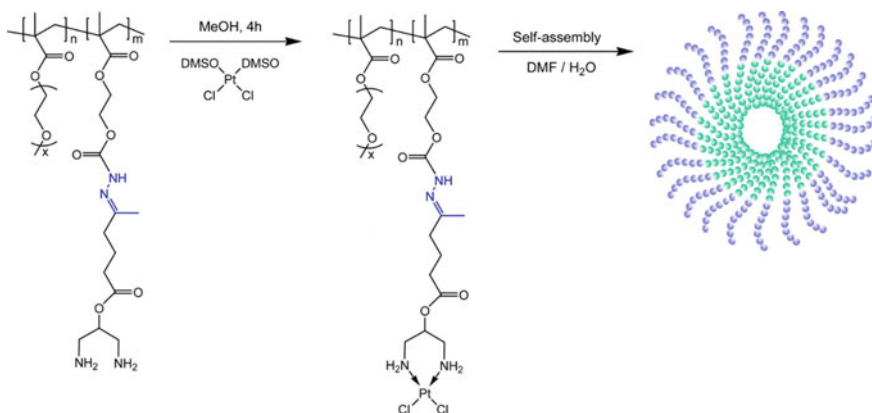
Fig. 3.1 Preparation of the hydrazone copolymer-Pt(II) en chelate and illustration of micelles through self-assembly of polymer-drug conjugates. The hydrazone bond was cleavable under acidic conditions, resulting in the release of Pt(II)

formed by self-assembly of pH-sensitive PMC-Pt(II) showed an acid-accelerated drug release behavior.

It should be emphasized that en-containing CPLs have excellent chelation properties against certain metal ions [52–54]. Thus, polymers synthesized by condensation of trien, *p*-nitrophenol, and formaldehyde were proved to be selective CPLs for Fe(III), Cu(II), Ni(II), Co(II), Zn(II), Cd(II), Hg(II), and Pb(II) ions [55]. In another interesting example, the aminated CPL prepared via surface-initiated ATRP of GMA to PCS and subsequent amination reaction (Scheme 3.2) was used for the chelation of copper(II) and lead(II) ions [56]. XPS spectra proved that chelation between the amine groups on the CPL and cationic heavy metals occurred.

Chelation experiments showed that polyamine-type CPLs containing sulfide (**I**) synthesized by the reaction of polyamines, such as en, dien, and trien, with poly
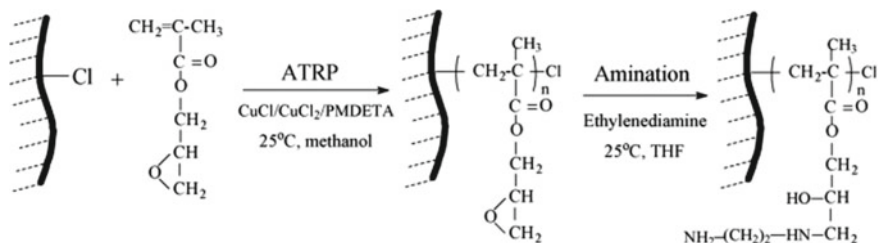
Scheme 3.2 Schematic diagram illustrating the preparation process of the aminated CPL by the combined surface-initiated ATRP and amination reactions

[4-vinylbenzyl (2-benzenesulfonate ethyl) sulfide] exhibit better chelation selectivity for noble metal ions and Hg(II) than other heavy ones [57]. It is important that the increase of length of polyamine chain was beneficial to the chelation of CPL with noble metal ions. The macroporous PSD beads (**II**) modified by en, dien, and trien (PS-en, PS-dien, and PS-trien) showed high chelation capacities to Hg(II) ions of 1.55, 1.73, and 1.84 mmol g^{-1} of polymer, respectively [58].

R = $C_2H_4NH_2$, $C_2H_4NHC_2H_4NH_2$, $C_2H_4NHC_2H_4NHC_2H_4NH_2$.
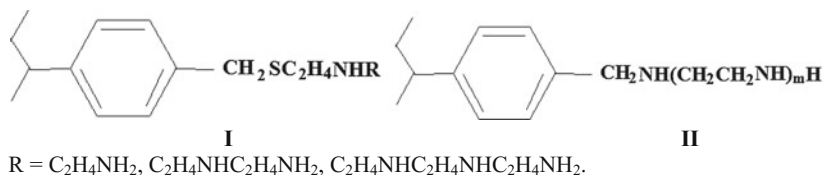
The initial high adsorption rate of PS-en, PS-dien, and PS-trien is explained by the abundance of chelating fragments, and their saturation over time leads to a decreasing adsorption rate. The PS-trien with to the longer polyamine chain has highest adsorption towards to Hg(II) ions. The thermodynamic parameters (Table 3.1) testify about the spontaneous and endothermic character of the metal chelation.

The amine functionalized CPLs (Scheme 3.3) based on low cross-linked terpolymers of GMA with St and DVB or diethylene glycol dimethacrylate chelate quickly Cu(II) ions from methanol solutions [59]. It is important that their chelation ability to Co(II), Fe(III), and Mn(II) ions depended on the mutual compatibility of solvents and CPL. In particular, it increases clearly, when the mixtures of methanol and methylene chloride are applied.

The formation of $[M(en)_2(H_2O)_2]$ chelates was shown in Cu(II)-, Ni(II)-, and Zn (II)-PMCs based on 2-amino-6-nitro-benzothiazole-en-formaldehyde polymer as CPL [60, 61].

Table 3.1 Thermodynamic data of Hg(II) adsorption by PS-en, PS-dien, and PS-trien

CPL	T (K)	ΔG^0 (kJ mol^{-1})	ΔH^0 (kJ mol^{-1})	ΔS^0 (J K^{-1} mol^{-1})	E_a (kJ mol^{-1})
PS-en	278	−1.25	4.13	9.81	6.24
	288	−1.38			
	298	−1.56			
	308	−1.62			
PS-dien	278	−1.36	2.19	3.49	6.08
	288	−1.46			
	298	−1.58			
	308	−1.65			
PS-trien	278	−1.38	2.15	3.49	4.86
	288	−1.48			
	298	−1.58			
	308	−1.68			
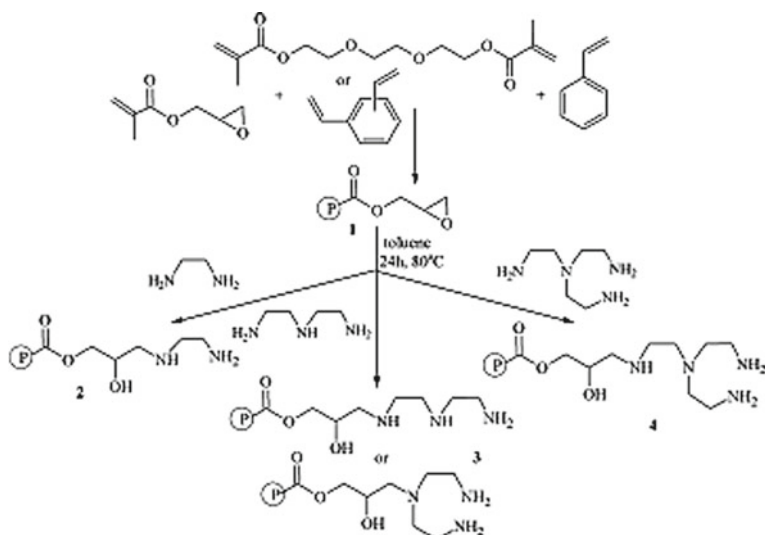
Scheme 3.3 Structures of the amine functionalized CPLs based on low cross-linked terpolymers of GMA with St and DVB or diethylene glycol dimethacrylate

M = Cu(II), Ni(II) and Zn(II).
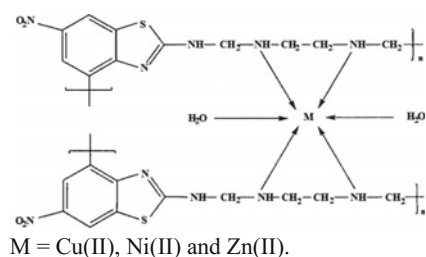
Another aminothiazole-functionalized CPL could exclusively chelate a copper [62]. In the predominant chelating mode simulated by density functional theory (DFT) calculation, a metal ion chelated with three nitrogen atoms and formed a PMC with two five-membered rings, and Cu(II) showed stronger chelation ability than Ni(II) did. Meanwhile, anions exerted significant beneficial effects by electrostatic screening, and thus strengthened the exclusive chelation of Cu(II).
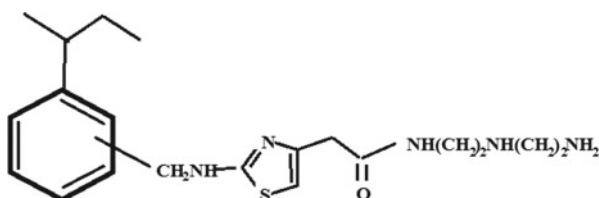
Other polycondensation CPLs such as hexamethylenediamine-salicylic acid-formaldehyde and phenylenediamine-p-hydroxybenzoic acid-formaldehyde polymers also have proven their chelation capacities [54, 63]. CPL synthesized by chemical modifications of maleic anhydride-dicyclopentadiene copolymer with trien was used in the chelation of Cr(III) ions [64]. In this case, the metal ions were linked with nitrogen atoms of trien fragment. Based on the experimental results, a possible chelating mechanism and the PMC structure was suggested (Scheme 3.4).
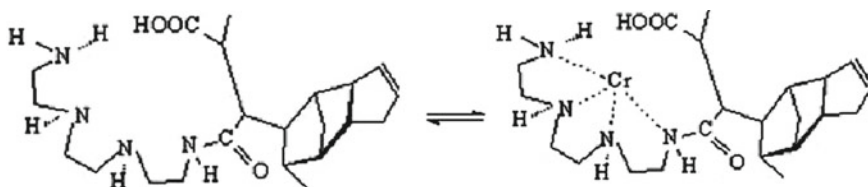
Scheme 3.4 Chelation process of chromium
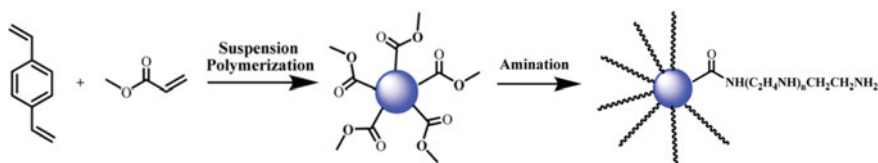
Scheme 3.5 Scheme of synthesis of polyamine CPL

PMC-Cr(III) was obtained by adding a suspension of CPL in DMF in drops under stirring to metal ion aqueous solution. The mechanism of chelation involves the chemical binding metal ions in fixed cages with the subsequent participation of chelating fragments from neighboring chains.

It should be noted CPL based on PMA-DVB with tetraethylenepentamine chelating fragments, which was purposefully obtained (Scheme 3.5) for enhanced binding copper(II) and nickel(II) ions [65]. It turned out that the maximum chelating capacity of CPL for copper(II) ions is equal to 1.21 mmol g^{-1}, which exceeds the commercial polyamine sorbent Purolite S984. Interestingly, the metal chelation leads to the formation of nitrogen-containing metal chelates without participation of oxygen atoms.

Studying the chelation behavior of PAN nanofiber modified by hexamethylenediamine showed that the maximum chelation capacities of the Pb(II), Cu(II) and Ni(II) ions were 175, 162.5, 48.5 mg g^{-1}, respectively [66]. At the lowest initial pH investigated, small amounts of metal ions could be chelated to the CPL, particularly due to the competitive adsorption between the prevalently available H^+ and the metal ions. Moreover, the positive charges as resulting from the protonation of the primary and the secondary amines of the 1,6-hexane diamine chelating ligands gave a strong electrostatic repulsive force to the positively charged metal ions.

In the case of poly (N-(5-methyl-4-imidazolyl) methylallylamine) (**I**) and poly (N-(5-methyl-4-imidazolyl) methylethylenimine) (**II**), the structure of polymer backbone plays a decisive role in metal chelation [67]. The coordination of Ag(I) ion proceeds through formation of two metal-nitrogen coordination bonds with participation of nitrogen atoms of imidazole fragment and amino group of the polymer chain. It is important that CPL **II** forms with Ni(II) four metal-nitrogen coordination bonds, while CPL **I** forms only three metal-nitrogen coordination bonds.
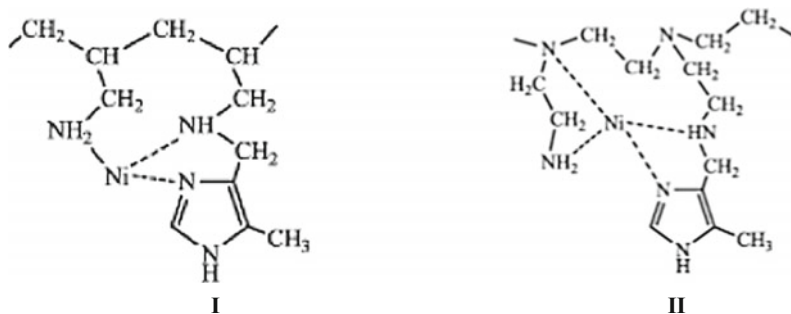
Of interest is the diaminesulfonamide CPL based on substituted alkenes, DVB and chiral 1,2-diamisulfonamide, which forms PMC when reacted with [RuCl$_2$(*p*-cymene)]$_2$ [68].
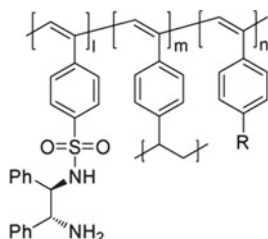
Microparticles of poly (1,8-diaminonapthalene) prepared by chemically oxidative polymerization showed good chelation capacity towards Cu(II) in comparison with the chelating sorbent Chelex 100 containing IDA functionalities [69]. It is well known that the rate-controlling mechanism may vary during the course of the adsorption process [70]. In this case, there is an external surface mass transfer or film diffusion that controls the early stages of the adsorption process, followed by a reaction between metal ions and chelating fragments of the CPL and finally by a diffusion stage where the adsorption process slows down considerably.

3.1.2   Metal Chelates Based on Schiff Bases

It should be noted the Fe(III) chelation by functionalized PS-Schiff base ligands with the maximum Fe loading in the freshly prepared PMC in the range of 5.3×10^{-5}–8.0×10^{-5} mmol g^{-1} polymer (Scheme 3.6) [71].

An easy chelation procedure for preparation of polymer-supported molybdenum carbonyl Schiff base (mixed carbonyl-imine-amine) chelate has been developed
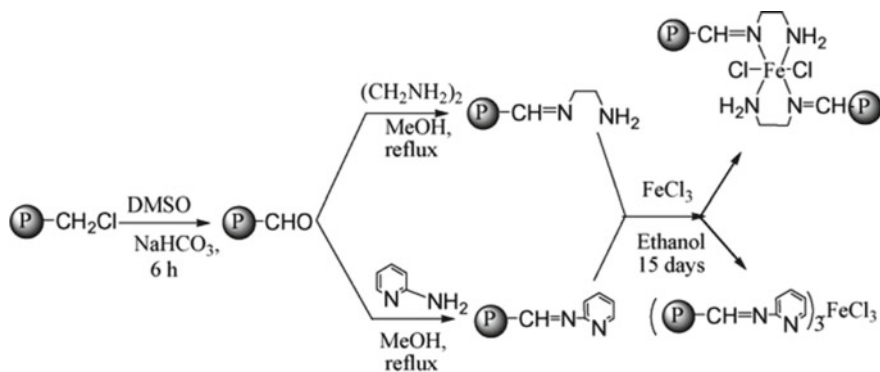
Scheme 3.6 Synthesis of PSD supported Fe(III) Schiff base chelates
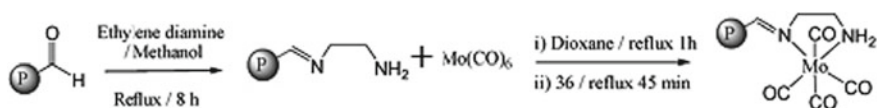
Scheme 3.7 Preparation procedures of Mo-PMC

(Scheme 3.7) [72]. The amount of molybdenum incorporated into the PMC showed value of about 3.64%.

Of interest is the synthesis of PS-supported Pd(II) 1-phenyl-1,2-propanedione-2-oxime thiosemicarbazone chelate (Scheme 3.8) [73, 74].
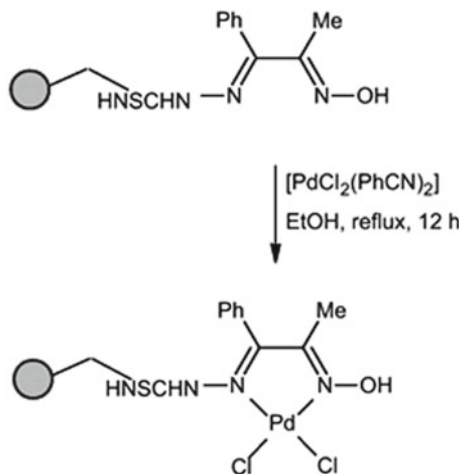
Scheme 3.8 Preparation of PMC-Pd(II) based on PS-supported 1-phenyl-1,2-propanedione-2-oxime thiosemicarbazone

The metal loading of the PMC-Pd(II) was obtained to be 4.38% (0.41 mmol g^{-1}).
Scanning electron microscopy (SEM) was recorded for a single bead of pure PCS and
PMC-Pd(II) to observe the morphological changes. As expected, the pure PS bead had
a smooth and flat surface, while the PMC-Pd(II) showed roughening of the top layer
(Fig. 3.2).

The Schiff base CPL prepared by reacting PCD with 5% crosslinking and
4-hydroxybenzaldehyde, followed by condensing with 2-aminopyridine, was loa-
ded with Ru(III) and Co(II) ions (Scheme 3.9) [75]. The loading of metal is
0.7–0.8%.

The similar Pd(II) chelate with iminopyridine ligand was anchored to PS via
nitration and then reduced to an amino functionality followed by Schiff base con-
densation (Scheme 3.10) [76]. The metal content of the PMC was equal to 5.3 wt%
Pd in the PMC-Pd(II).
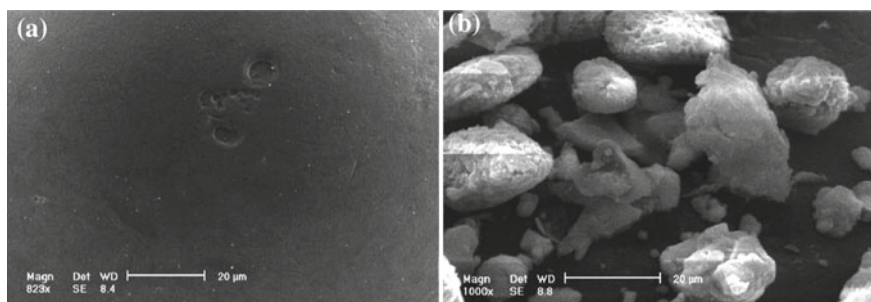
Fig. 3.2 SEM of **a** PCS and **b** PMC-Pd(II)

Scheme 3.9 Synthesis of
metal-supported PCD Schiff
base chelates
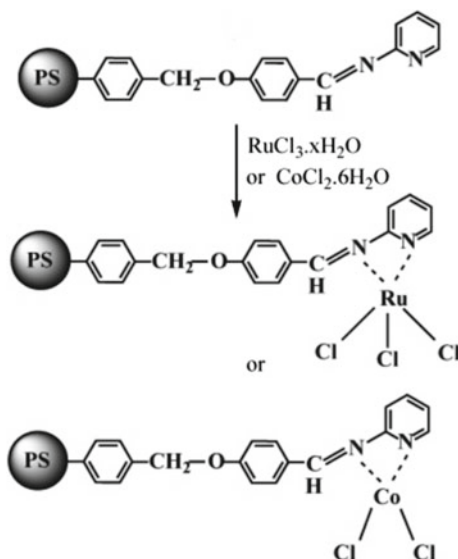
The SEM images of PS (Fig. 3.3a), amino-PS (Fig. 3.3b), azomethine CPL (Fig. 3.3c) and the PMC-Pd(II) (Fig. 3.3d) exhibited that the initial polymer beads have a smooth, flat surface. The fixing the chelating ligand onto the PS beads causes a roughening on the top layer of the beads. The metal chelation accommodates the fixed geometry of the chelate, whereupon image of the PMC-Pd(II) shows further roughening on the top layer.

CPL synthesized through the reaction of 4-(pyridinylimine) phenol and formaldehyde forms PMC-Ni in a 1:1 molar ratio [77].

3.1.3 Polymeric Five-Membered Nitrogenous Heterocycles in the Synthesis of Metal Chelates

Of interest is conjugated CPL obtained by the polymerization of 4,7-diethynylbenzo [1–3] thiadiazole with 1,4-diazidobenzene [78].

Scheme 3.10 Synthesis of the polymer-anchored Pd(II) chelate
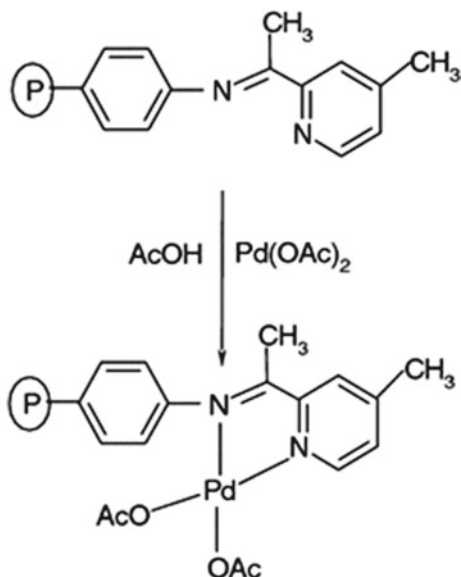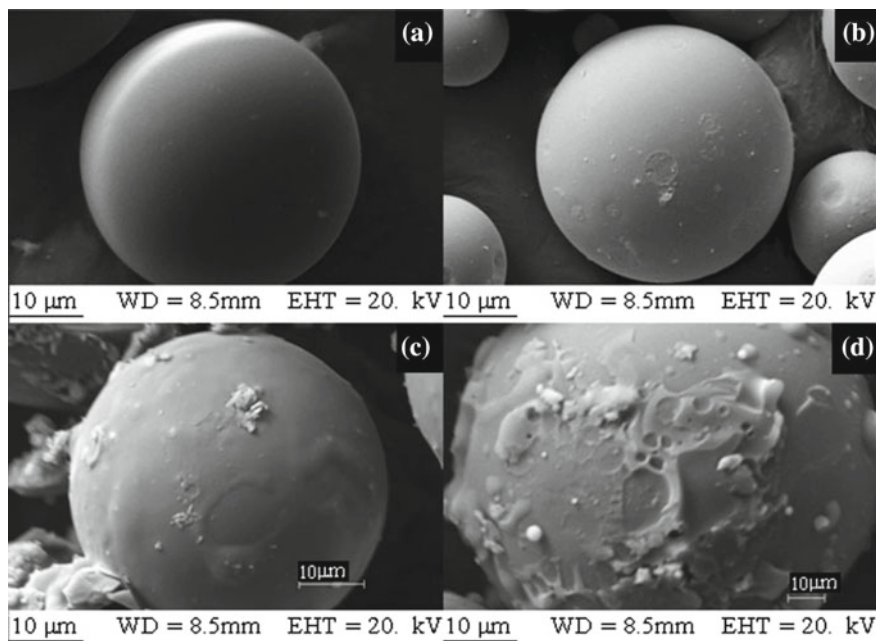
Fig. 3.3 FE SEM images of PS (**a**), amino-PS (**b**), azomethine CPL (**c**) and PMC-Pd(II) (**d**)
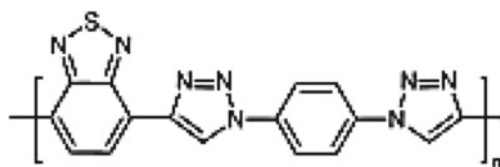
Compared with Co(II), Hg(II), Ag(I), Cd(II), Cu(II) and Zn(II) ions, Ni(II) ion showed the most pronounced fluorescence response in the presence of the conjugated CPL. The quenching could be ascribed to the intramolecular PET between the CPL backbone and the bonded metal chelate. The fluorescence intensity of the CPL possessed a linear correlation within the molar ratios from 0 to 0.6 (Ni(II)/the repeating unit) (Fig. 3.4). The fluorescence detection limit of the CPL solution for Ni(II) was determined to be as low as 1.1×10^{-7} mol L^{-1}.

It should be noted two conjugated CPLs based on benzohalcogendiazole and triazole chelating fragments, which are fluorescence sensors on Ni (II) ions [79]. Importantly, the first CPL exhibited higher sensitivity and selectivity than the second CPL, which is explained by the higher electronegativity of selenium (Fig. 3.5).
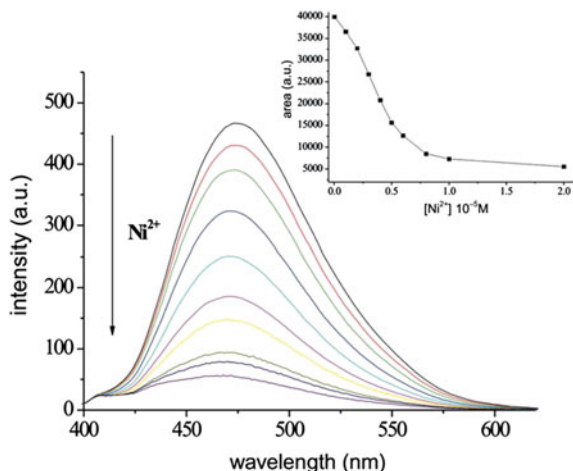
Fig. 3.4 Fluorescence spectra of the CPL (1.0×10^{-5} mol L^{-1}) in CHCl$_3$ with increasing amounts of Ni(II) in MeCN (0, 0.1×10^{-5}, 0.2×10^{-5}, 0.3×10^{-5}, 0.4×10^{-5}, 0.5×10^{-5}, 0.6×10^{-5}, 0.8×10^{-5}, 1.0×10^{-5}, 2.0×10^{-5} mol L^{-1}) ($\lambda_{ex} = 384$ nm). Inset: fluorimetric titration of the CPL with Ni(II)
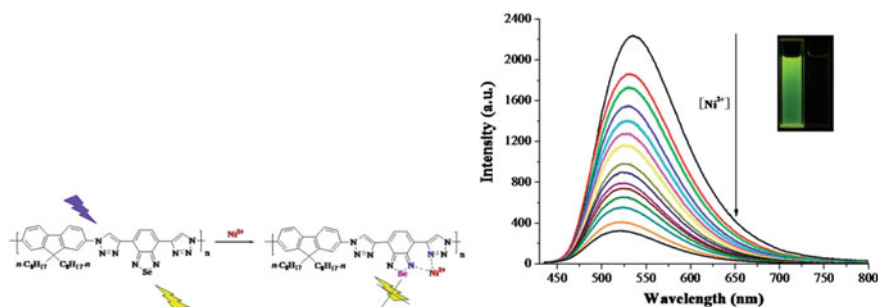
Fig. 3.5 (left) Possible binding mechanism of Ni(II) ion by the CPL based on benzohalcogendiazole chelating fragment. (right) Fluorescence spectra of the CPL with an increase of Ni(II) concentrations (0, 0.2, 0.4, 0.6, 0.8, 1, 1.2, 1.4, 1.6, 1.8, 2.0, 2.5, 3.0, 4.0, 5.0 mmol L^{-1} in CH$_3$CN) ($\lambda_{ex} = 425$ nm). Inset: visible fluorescence of the CPL before (left) and after (right) the addition of Ni(II) (5.0 mmol L^{-1}) under a 365 nm UV lamp

CPL containing cyanoguanidine fragment prepared by the functionalization of PCS with dicyandiamide displayed a marked advantage in Hg(II) chelation capacity, and the saturated chelation capacity estimated from the Langmuir model was dramatically up to 1077 mg g^{-1} at 45 °C (Fig. 3.6) [80].

The emission of linear and branched conjugated CPLs containing 2,2′-biimidazole chelating fragment (Fig. 3.7) can be efficiently quenched by Co(II) through a PET process with "turn off" character [81]. It was found that the fluorescence of the CPL solution had no change when the alkali as well as alkaline earth metal ions

(a)

(b)

CH$_2$ ——— NH ——— C ——— NH ——— CN
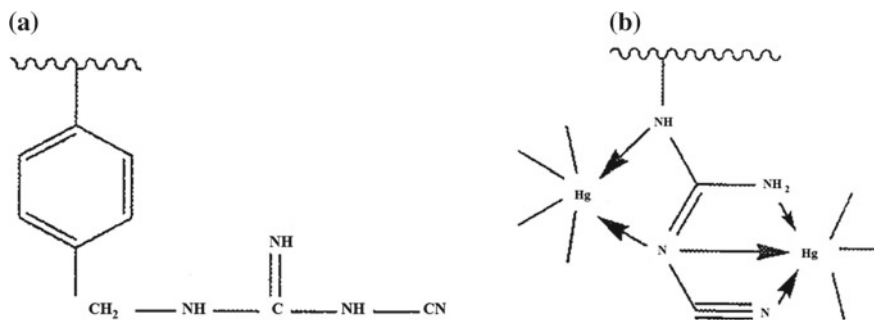
Fig. 3.6 Structure of the PS-cyanoguanidine polymer (**a**) and scheme of chelation of Hg(II) on CPL (**b**)

Linear polymer

R$_1$ = —B⟨O,O⟩   R$_2$ = ⟨O⟩

Branched polymer
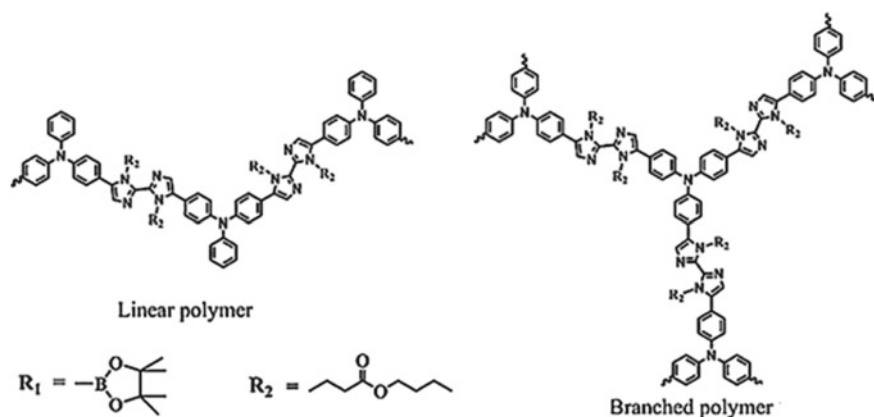
Fig. 3.7 Structures of the conjugated linear and branched CPLs

were added. However, upon the addition of Co(II), it showed remarkable quenching effect of fluorescence at 417 nm, and the quenching efficiency reached up to 95%.

It should be noted that the CPLs also show ratiometric fluorescence changes toward Ag(I). In particular, upon the addition of Ag(I), the emission peaks at 417 nm exhibited a red shift of 55 nm with a decreased intensity, which leads to an obvious change of the fluorescence color from bright blue to cyan. Such shift should be related to the change of the electron density in the CPL due to the chelation of Ag(I) to the biimidazole fragments. It is important that the sensitivity of the branched CPL to Ag(I) and Co(II) ions is much higher than that of the linear CPL. Since the conjugated polymer is considered as "molecular wire" [82], there are more exciton transport pathways in the branched CPL. Once a metal interacts with any of the chelating fragments on the CPL, the excitons in the branched CPL are easily affected, leading to a higher sensitivity. Thus, not only the chelating fragments, but also the architecture of the CPL is important in the preparation of
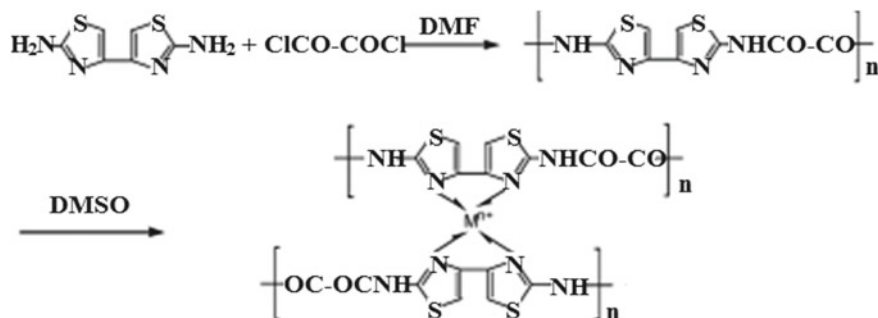
Scheme 3.11 Synthesis route of PMCs based on polyamide with bithiazole fragments, where M = Pr(III) and Sm(III)

chemical sensors. However, the chemical shift magnitude of the proton on the biimidazole fragment for the PMC-Co(II) was quite different from that for the PMC-Ag(I). These results suggest that Ag(I) and Co(II) have different impacts on the electronic structure of biimidazole fragment.

PMC containing bithiazole rings exhibited different types of magnetic behavior. It is well known that the magnetic property of PMC arises from the magnetic exchange interactions between metal ions in the PMC. Generally, this magnetic interaction is relatively strong through π-conjugated system compared with the space interaction. Thus, it turned out that the rare-earth PMCs based on the polyamide with bithiazole fragments synthesized by the polycondensation of 2,2′-diamino-4,4′-bithiazole and oxalyl chloride are ferromagnets at low temperature (Scheme 3.11) [83].

The physical properties of several n-type conjugated CPLs incorporating azadipyromethene (aza-DIPY) dyes in the main chain were tuned by chelation of the aza-DIPY fragment with Cu(I)PEt$_3$ or Ag(I)PEt$_3$ [84]. Chelation with the electron-rich Cu(I) and Ag(I) metals resulted in higher optical band gaps (1.5 eV) and higher HOMO (−5.3 eV) and LUMO (−4.0 eV) energy levels. X-ray diffraction of the PMC in the solid state showed a lamellar spacing that varied with the solubilizing groups.
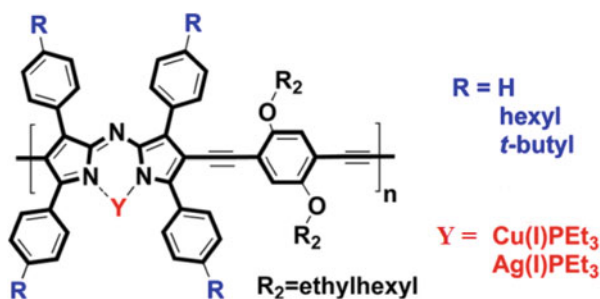
Of interest is the Ag(I), Cu(II), Zn(II), Cd(II), Hg(II) and Pb(II) chelation with the CPLs based on Merrifield resin containing the imidazolylazobenzene (**I**) and 1,4-bis(imidazolylazo)benzene (**II**) chelating fragments [85]. It is important that the azo-nitrogen along with pyridinic-nitrogen take part in the chelation with the formation of five-membered chelate nodes.
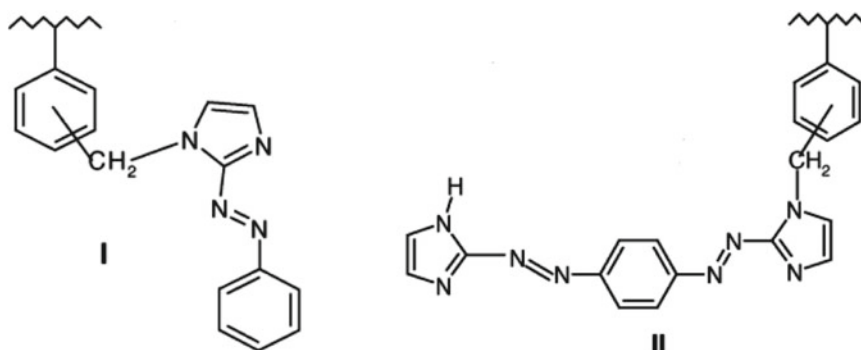
A multi-step PPM technique to attach Ru centers to CPL with the pendant pyrazole groups have been developed (Scheme 3.12) [86]. When metal content is less than 50%, the PMC is soluble in DMF, while the increasing Ru content up to 73% leads to insoluble PMC; and, finally, PMC with 97% Ru immediately precipitated from solution.

The interesting tris(imidazolyl)phosphine PMC-Cu(II) were prepared in three different ways: (a) homopolymerization of the N,N',N''-chelating ligand tris[2-(1-vinylimidazolyl)]phosphine (**1**) and subsequent chelation with CuCl$_2$ (**P1-Cu**); (b) copolymerization of **1** with ethylene glycol dimethacrylate and subsequent chelation with CuCl$_2$ (**P2-Cu**); or (c) molecular imprinting with the organometallic Mo-complex [Mo(μ_3-C$_4$H$_7$)(CO)$_2$(**1**)](TsO) and ethylene glycol dimethacrylate and subsequent replacement of Mo(II) by Cu(II) (**P3-Cu**) (Scheme 3.13) [87].
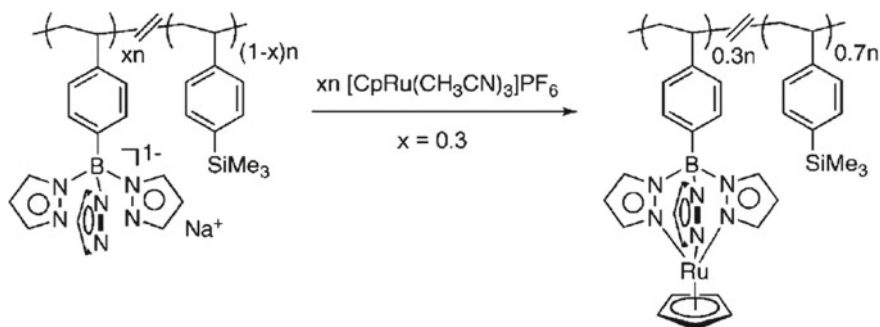
Scheme 3.12 Synthesis of tris (pyrazolyl)-functionalized PMC-Ru
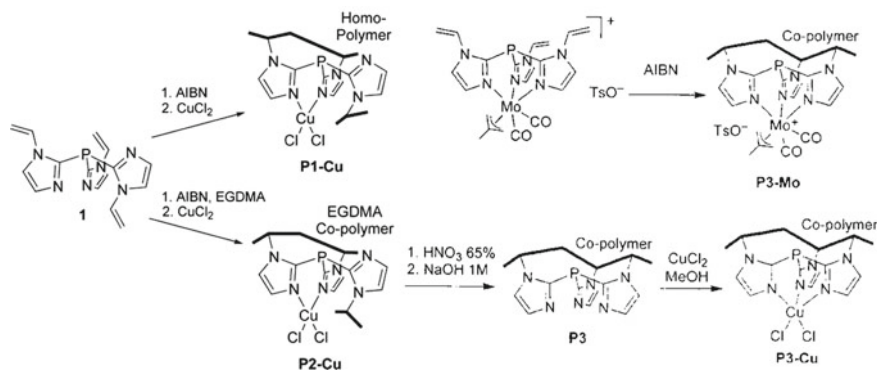
Scheme 3.13 Synthesis of copper-containing polymers **P1**-**Cu**, **P2**-**Cu** and **P3**-**Cu**

3.1.4 Specifics of Metal Chelation with Polypyridyl Ligands

CPL of polyaniline type, poly (dipyridylamine), with a chelation site and a chiral side chain formed PMC, and spatial structure of the PMC is controlled by the kind of the chelating metal species, as revealed by remarkable changes of the CD spectrum caused by chelation with the metal [88].

The chelating resin Dowex M-4195 containing dipyridylamine chelating fragments was applied to investigate the interaction nature toward Cu(II) ions [89]. In this case, the three nitrogen atoms of tridentate chelating fragment take part in the chelation with the formation of the two five-member metal chelate nodes (Scheme 3.14).

The reaction of CPL based on norborn-5-ene-(N,N-dipyrid-2-yl) carbamide and *exo*,*exo*-[2-(3-ethoxycarbonyl-7-oxabicyclo[2.2.1] hept-5-en-2-carbonyloxy) ethyl] trimethylammonium iodide with [Rh(COD)Cl]$_2$, where COD is 1,5-cyclooctadiene, gives PMC-Rh(I), with the critical concentration of micelle formation (CMC) $2,2 \times 10^{-6}$ mol L^{-1} (Scheme 3.15) [90].

Thermo-responsive CPLs carrying di(2-pyridyl) methyl chelating fragments showed to respond sensitively and selectively to the presence of heavy metal cations [91]. Polymer-metal chelation increases LCST transitions in water drastically (e.g. up to 22 °C) during addition of small amounts of Cu(II), Co(II), Fe(II) and Ag(I) salts (Fig. 3.8). Conversely, Mn(II) and Gd(III) salts did not affect CPL solubility.

Of interest is the study of the chelation properties of CPL carrying 2-amino-pyridine chelating fragment on macroporous cross-linked PS via a sulfur-containing spacer [92].

(I)

(II)
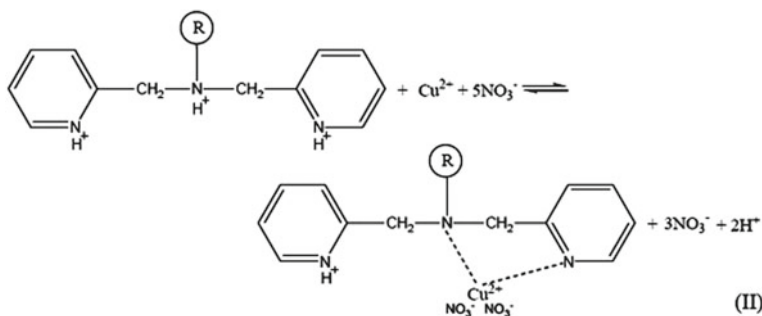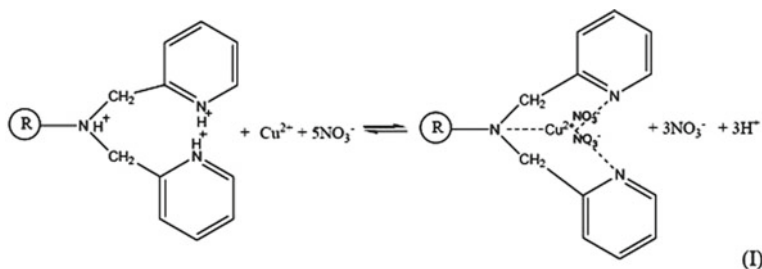
Scheme 3.14 The chelation modes of Dowex M-4195 containing dipyridylamine chelating fragments with Cu(II) ion (pH = 2)
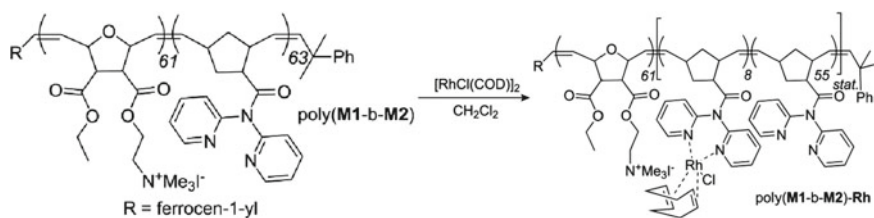
Scheme 3.15 Synthesis of PMC-Rh (R = ferrocen-1-yl)
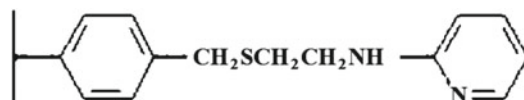
The study of the temperature dependence of the metal chelation (Fig. 3.9) indicates a rapid initial adsorption rate (for 0.5 h), especially at 350 °C, and after 2 h the adsorption process became very slow. In addition, an increase in temperature leads to an increase in adsorption capacity because CPL is strongly swollen in solution.
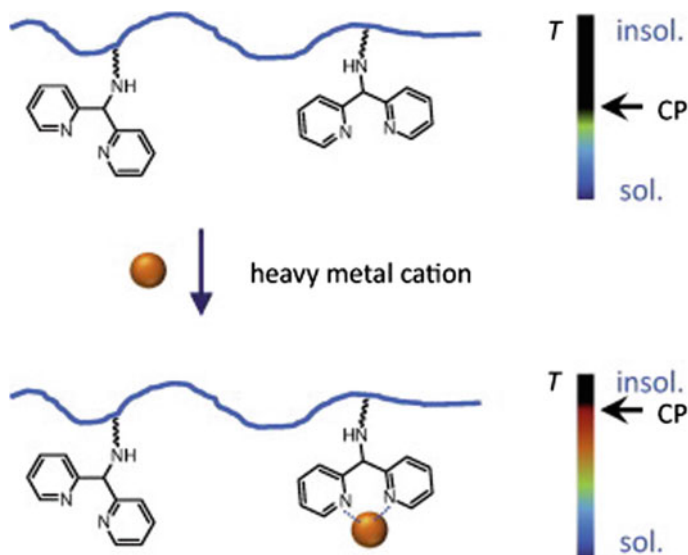
Fig. 3.8 Schematic of CPL, which cloud point increase with chelation of a metal cation

Fig. 3.9 Temperature dependence of Hg(II) ion adsorption by CPL
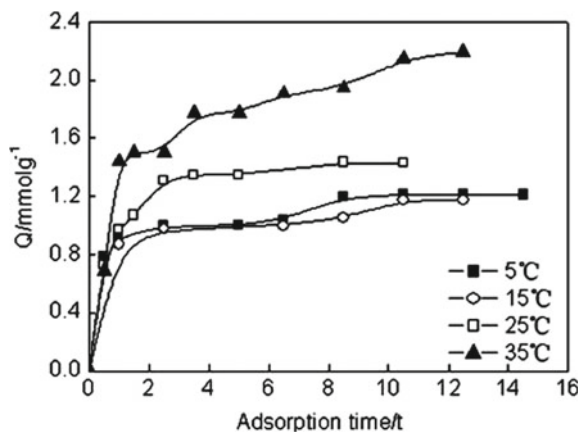
The best fit of chelation of Cd(II), Co(II), and Ni(II) ions on aminopyridine modified poly (St-*alt*-maleic anhydride) cross-linked by 1,2-diaminoethane (Fig. 3.10) was achieved with the Langmuir isotherm equation, yielding maximum chelation capacities of 81.30, 49.02, and 76.92 mg g^{-1} for Cd(II), Co(II), and Ni(II) ions, respectively [93]. The intra-particle diffusion study revealed that external diffusion might be involved in this case.

Polypyridyl ligands such as bpy, phen and tpy can be important building blocks for PMC because of their strong chelating affinity towards many metals. In particular,
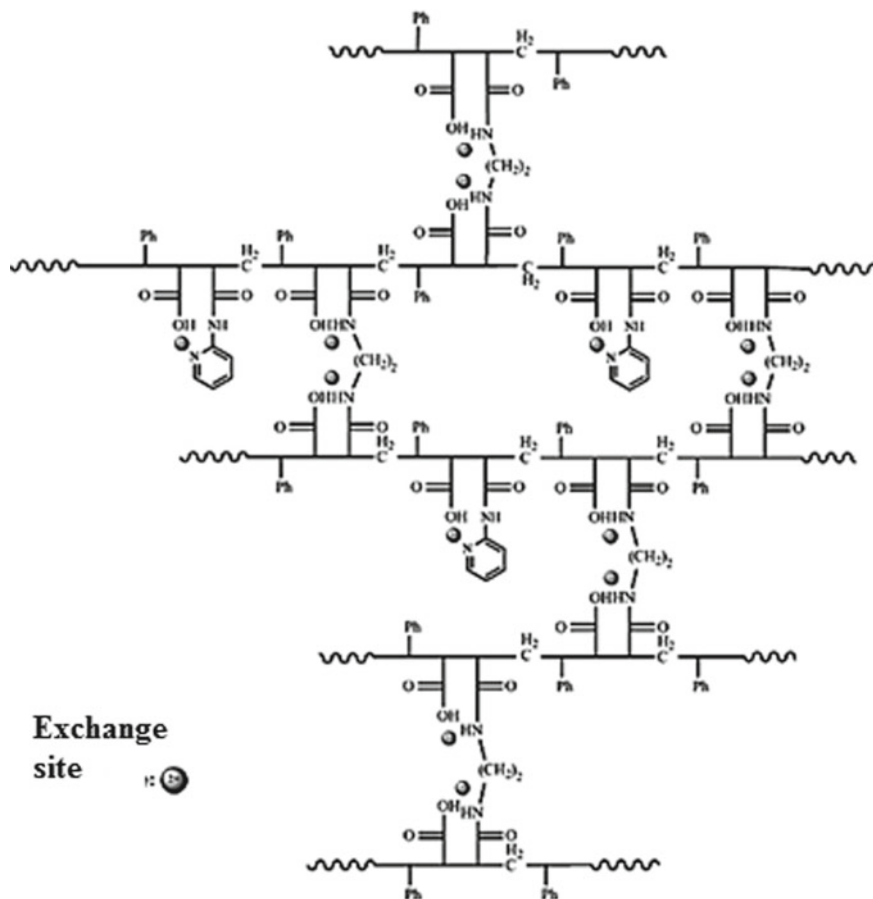
Fig. 3.10 The structure of cross-linked CPL

bpy is a highly versatile bidentate ligand for a variety of metal ions. Therefore, it was demonstrated the application of this chelating ligand in a variety of PMCs. For example, by introducing specific chelating ligands of bpy type [94–96] to the main backbones or side chains, conjugated CPLs have been widely employed for the metal ion detection owing to the characteristic metal-to-ligand charge transfer (MLCT). Thus, π-conjugated CPLs poly (bpy-5,5′-diyl) and poly (phen-3,8-diyl) prepared by organometallic polycondensations form PMCs with various metal compounds such as $[Ru(bpy)_2]^{2+}$ and $CuCl_2$ [97]. In another interesting example, Cu(II) and Ni(II) can form non-radiative MLCT chelates with the linear conjugated CPL based on 5,5′-divinyl-bpy and (R)-5,5′-dibromo-6,6′-di(4-methylphenyl)-2,2′-bisoctoxy-1,10-binaphthyl [94]. At the same time, Co(II), Mn(II), Cd(II), Zn(II), and Fe(II) effectively quench fluorescence due an energy transfer from the π-conjugated chiral CPL

to the metal chelate units. Thus, the substantial difference of the chelation processes of bpy-based CPLs with metal ions is observed.
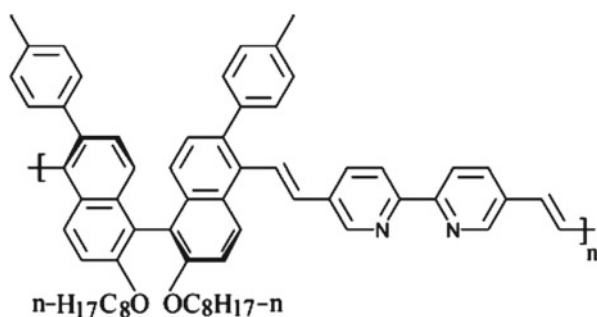
It should be noted a fluorescent conjugated CPL synthesized by the polymerization of 1,4-dibromo-2,3-bisbutoxynaphthalene with 5,5′-divinyl-bpy [95]. Cu(II) and Ni(II) ions can also form nonradiative MLCT chelates with the CPL, while Zn(II) and Cd(II) ions do not produce the pronounced differences from the CPL fluorescence and UV-vis spectra. The intramolecular PET or photoinduced charge transfer (PCT)) may probably be responsible for the fluorescent quenching. The results can also suggest that bpy fragment in the main chain backbone of the conjugated CPL can act as the recognition center of a special fluorescent chemosensor for sensitive detection of transition metal ions.

In contrast to LMCs, the advantage of using conjugated CPLs as fluorescent sensors is that they ensure collective interaction, which is very sensitive to minor changes in the electronic density in a macromolecule and makes it possible to determine minimum amounts of metal ions [98]. Bpy ligands form chelates with many metal ions; therefore, their introduction into conjugated CPL sensors is extremely promising because the chelation of metal ions causes electronic and conformational changes in starting CPL. As a result, the profiles of their adsorption and fluorescence spectra change significantly. If the interaction of metal ion with bpy leads to metal chelate, then chelation forces the noncoplanar (twisted) bpy to assume a fully planar conformation; as a result, the conjugation of polymer chains becomes more pronounced and facilitates a red shift in absorption and fluorescence spectra. As a typical example, we note the PMCs obtained by the bpy chelation of $Eu(TTA)_3.2H_2O$ and $Gd(TTA)_3.2H_2O$, where TTA^- is 1-(2-thenoyl)-3,3,3-trifluoroacetonate, with chiral CPL based on 5,5′-divinyl-bpy and (R)-5,5′-dibromo-6,6′-di(4-trifluoromethylphenyl)-2,2′-bisoctoxy-1,1′-binaphthyl (Fig. 3.11) [99].

Of considerable interest are conjugated CPLs in which the polymer chain contains 5,5′-divinyl-bpy chelating moiety with a well-defined spatial structure, which acts as a conjugated molecular spacer. In another interesting example, the vinylene bond between chelating bpy and naphthyl fragments allows to reducing the steric hindrance between the main chain rings and chelating fragments [100–102]. It is
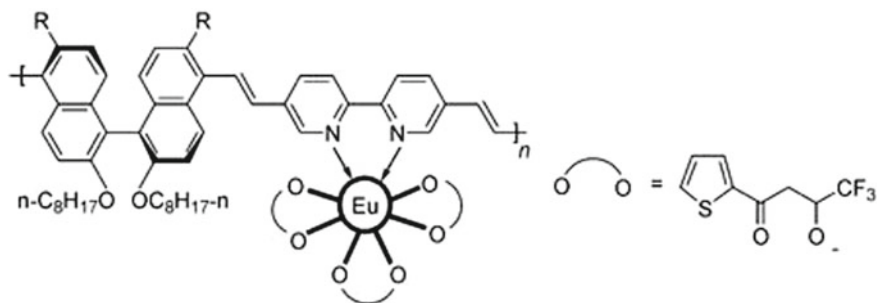
Fig. 3.11 Structure of PMC-Eu based of chiral CPL

important that the use of CPL with chelating bpy fragments in the main chain does not completely allow chelation of the metal compound, in particular, M(TTA)$_3$ [103].

Conjugated CPL bearing pendant bpy fragments, where the mole percentage of chelating fragments varied to levels of 25, 50, 75 and 100%, was reacted with a ruthenium complex to yield conjugated polymers bearing pendant bpy ruthenium chelates (Scheme 3.16) [104].

The order of reagent feed is very important to avoid the occurrence of interchain crosslinking through CPL chelation with metal ions. First, dichloro (*p*-cymene) Ru(II) dimer was reacted with low molecular weight bpy ligand in DMF, and then NH$_4$NCS was added. At this stage, four of the six coordination sites of the ruthenium ion are engaged in one bpy chelating ligand and two thiocyanate ligands, and only two coordination sites remain vacant for the chelation with the pendant bpy fragments in the CPL. Therefore, crosslinking through interchain chelation of CPL with ruthenium ion can be effectively prevented. The PMC-Ru show good solubility in some organic solvents indicating that interchain chelation does not occur. Thus, by modifying the synthetic procedure, PMC have been synthesized using a one-pot PPM, which is a simplified strategy to prepare this type of conjugated PMC with metal chelates linked to the pendant chelating fragment through a flexible chain.
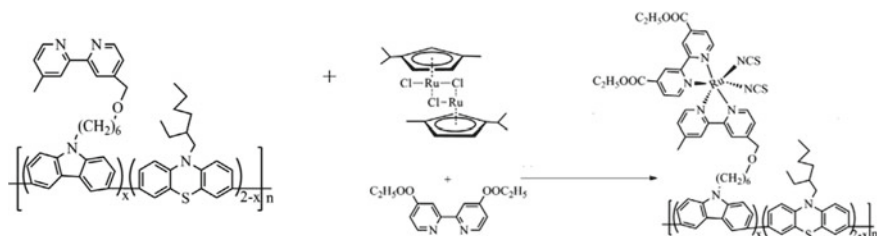
Scheme 3.16 Synthesis of PMC

It should be noted the preparation of bpy modified π-conjugated CPL having an average of one or three monomer units (*p*-arylene ethynylene or 7,7-dihexylfluorene) between metal-chelating fragments [105]. Strategic placement of sterically encumbered mesityl groups about the metal chelating fragments enforces a 1:1 metal to bpy chelating ratio.

Conjugated CPLs comprised of 9,9-dioctylfluorene and bpy fragments, which are alternatively linked by the C–C single bond (**P1**), vinylene bond (**P2**), or ethynylene bond (**P3**), are sensitive to transition metal ions [106].
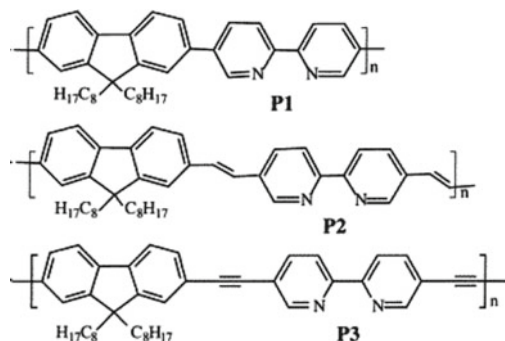
The different sensitivity is due to the various backbone rigidity of the three CPL, which is caused by the three different spacers. The chelation between the bpy fragments and the metal ions induces the conformation change (more conjugated) and the variation of electron density of CPL chains. Because the two pyridine rings in a bpy fragment are not coplanar, but with a 20° dihedral angle in its transoid-like conformation, effective chelation may force the two pyridine rings to be more coplanar. When the two pyridine rings become more coplanar by chelation, the coplanarity must determine the bonds, which link the fluorine and bpy fragments. A weak restriction allows the coplanarity of a bpy fragment to happen easier and thus to chelate metal ions more effectively, which corresponds to a stronger spectral response. Such a difference in chelation caused by the different linking bonds will be more pronounced in the chelation with the metal ions, which have weaker chelation ability with bpy fragments. The single C–C bond between the fluorene unit and the bpy chelating fragment (**P1**) provided the weakest forbiddance for the chelation of bpy fragment with metal ions, which was followed by the vinylene bond (**P2**), and the ethynylene spacer (**P3**) presented the highest resistance for the coplanarity of bpy fragment.

Of interest is chelation of Ni(II) and Cu(II) dithiolates by π-conjugated CPLs (**P1–P3**) with bpy-chelating fragments (Scheme 3.17) [107]. For example, during the formation of **P1**-NiCl$_2$, a red shift of the absorption band of **P1** (λ_{max} = 446 nm) at 36 nm is observed. At the same time, chelation of NiL1 with **P1** results in a greater bathochromic shift (λ_{max} = 499 nm) due to the expansion of the conjugate chain. A similar shift at 55 and 61 nm is also characteristic for the formation of
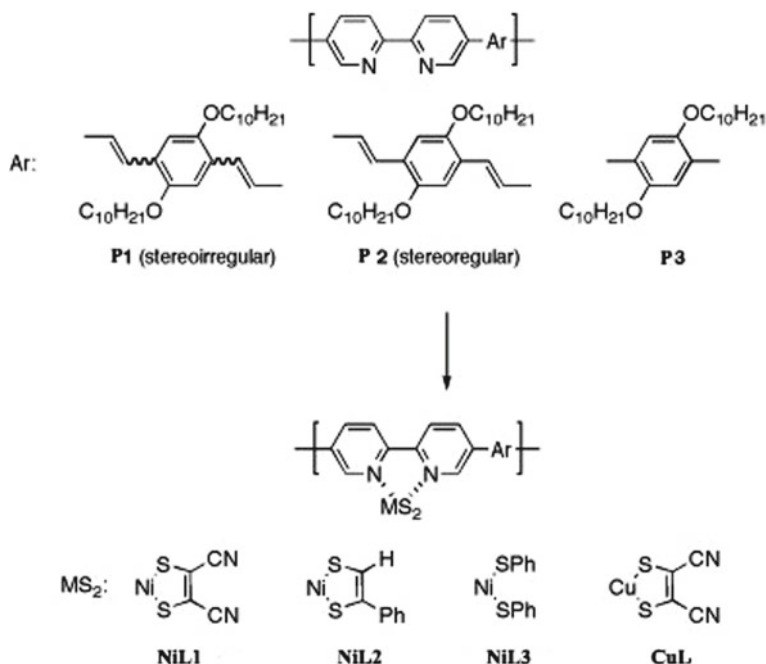
Scheme 3.17 Synthetic routes to PMCs

nickel dithiolate complexes with **P2** and **P3**, respectively. It is important that much smaller displacements at 28 and 20 nm are observed in the case of NiL2 and NiL3 complexes with **P1**, respectively. In the case of a similar complex **P1**-CuL1, the tetrahedral structure of the chelate node is established.

Water-soluble π-conjugated CPLs incorporating 5,5′-bpy (**P1**) or 6,6′-bpy (**P2**) fragments within the π-conjugated backbone were prepared as frameworks for polymer metal chelation (Fig. 3.12) [108]. The response of CPL emission to Cu(II) ions is the most efficient quenchers of CPL emission, with a Stern-Volmer constant $(K_{SV}) = 1.1 \times 10^5$ and 5.2×10^4 M^{-1} in water for **P1a** (40% bpy monomer fragments) and **P1b** (20% bpy monomer fragments), respectively. The quenching of **P1** with Cu(II) ion takes place by a static quenching mechanism. In contrast, **P2** emission is quenched by another mechanism, possibly because of aggregation in aqueous solution.

In Eu(III) chelated fluorine-bpy PMC, a level of ion content of 80% in molar basis was achieved, and according to the theoretical calculations it required a twist of 179° between the pyridine units to achieve the necessary planarity for the metal chelation [109]. The energy required for this transition is equal to 49 kJ mol^{-1}. Spectroscopy data showed that no electronic coupling between the main backbone and the chelation fragments has occurred, but these hindered the interchain aggregation are observed in the non-chelated CPL. The metal ion had a trapping effect in the charge transport.

R =

R' =

P1

P2
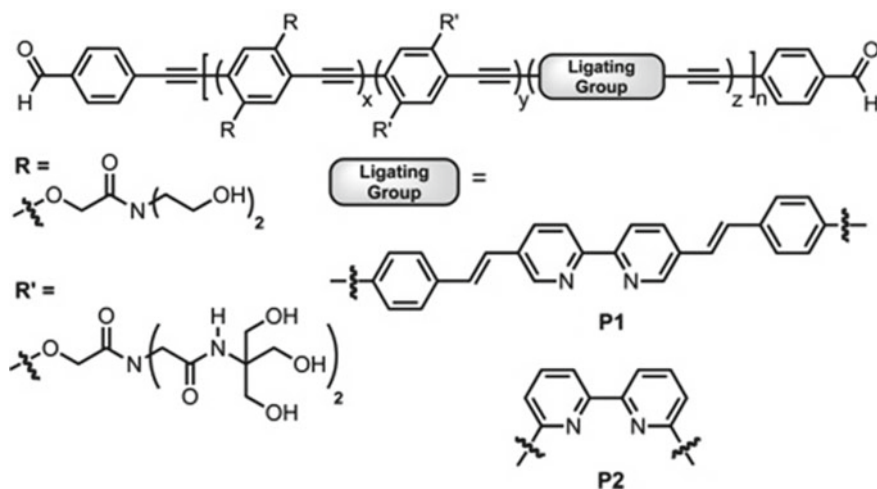
Fig. 3.12 Structures of π-conjugated chelating polymers **P1** and **P2**
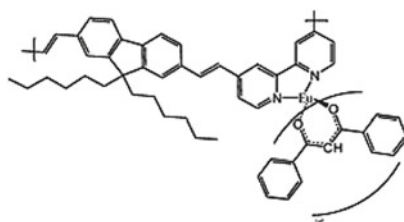
Two conjugated CPLs chelated with Co(II) ions were designed to combine functions of the conjugated backbone as a light-harvesting antenna and electron-transfer conduit with the in-chain bpy-chelated transition metal fragments as catalytic active centers to evolve hydrogen photocatalytically from water [110]. It is important that the PMCs are soluble in organic solvents, enabling detailed characterization.
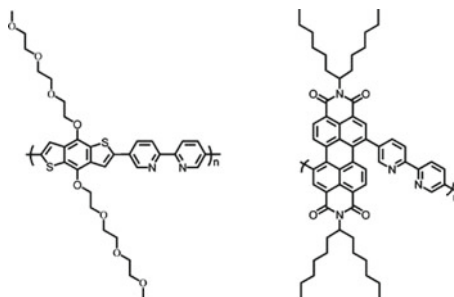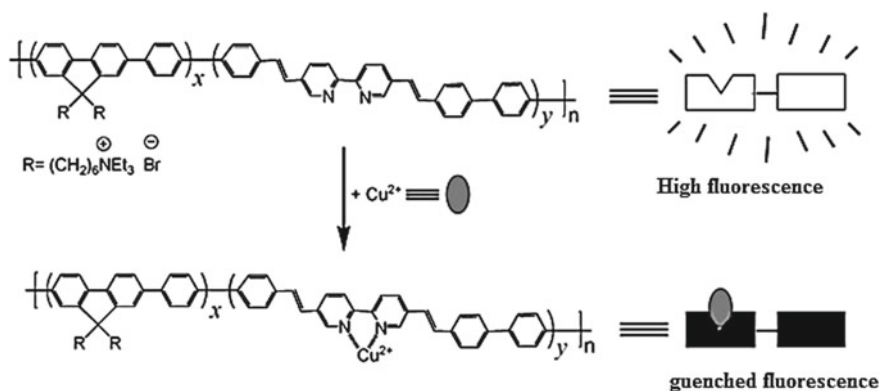
Fig. 3.13 Schematic representation of the Cu(II) ion assay based on the fluorescence quenching of the conjugated CPL

The water-soluble cationic polyfluorene CPLs containing bpy fragments in the backbone were used as the fluorescent probes for Cu(II) ions (Fig. 3.13) [111]. Upon adding the Cu(II) ion, the CPL chelates to Cu(II) ions through N–Cu interactions, and its fluorescence is efficiently quenched by the Cu(II) ion with K_{sv} of 1.44×10^7 M^{-1}. The fluorescence quenching of the conjugated CPL is mainly associated with the changes in the electron density along the CPL backbone.

Of interest is a copolymer of PMMA with bpy chelating fragments, whose side chains was reacted with ruthenium bpy and phen precursors [112]. It is important that the film-forming PMMA main chain increases the quantum efficiency in the range of 2–3%.

R = H, CH₃
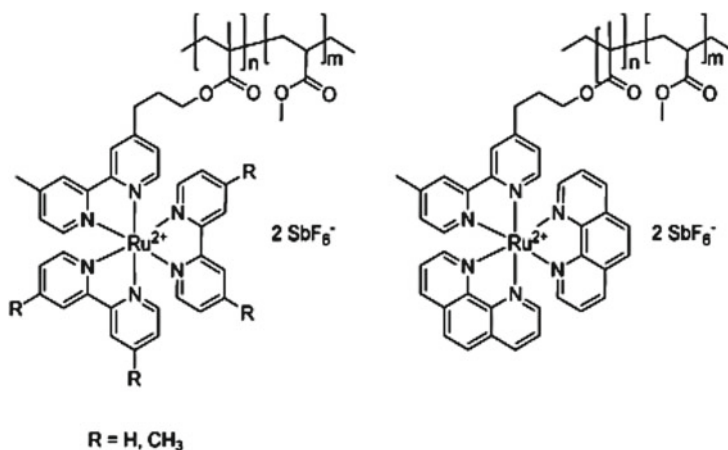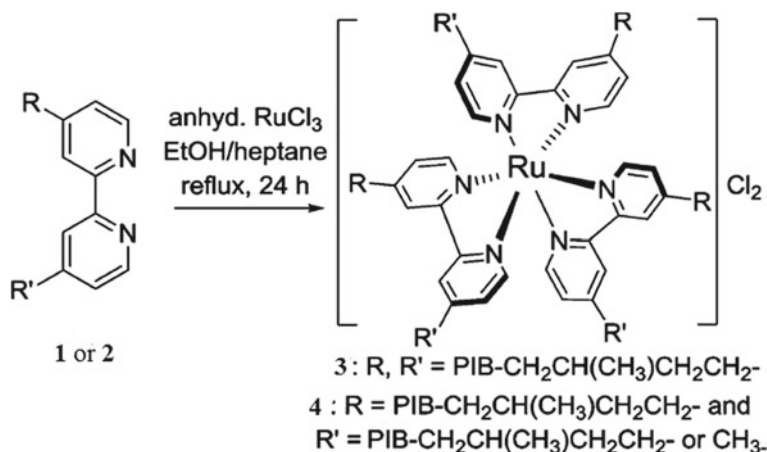
Scheme 3.18 Synthesis of Ru(PIB-bpy)$_3$Cl$_2$ chelates **3** and **4**

PIB-bound ruthenium bpy [Ru(PIB-bpy)$_3$]$^{2+}$ chelates were prepared from CPL formed by alkylation of 4,4′-dimethyl-bpy with PIB-bromide [113]. It is interesting that PMCs were synthesized from both **1** and the mixture of the PIB-containing bpy ligands **1** and **2** (Scheme 3.18). Pure **1** yielded the PMC **3**, and using the more readily obtainable mixture of **1:2** leads to PMC **4**. The PMC **3** and the mixture **4** had indistinguishable phase selective solubility and both PMCs were soluble in heptane and insoluble in polar solvents.

The study of the optical properties of a fluorene-bpy copolymers (P)(bpy)$_x$ in the presence of Zn(II) showed that by adjusting the bpy content in the CPL backbone, the emitting color of the CPL solution changed from initial blue to green to white and violet [114]. The counter-anions of Zn(II) ions also influence the optical properties of CPL greatly (Fig. 3.14).

It should be noted π-conjugated PMC-[Re]$_x$ (x = 0.1, 0.2, and 0.5) containing *fac*-(bpy)Re(I)(CO)$_3$Cl chromophores in the backbones [115]. It is interesting that neither the photoluminescence (PL) nor electroluminescence (EL) efficiency of PMC-[Re]$_x$ was satisfactory in comparison with the *fac*-(bpy)Re(I)(CO)$_3$Cl molecularly doped polymer.

During metal chelation by a bpy-functionalized CPL, multiple bpy fragments can chelate to some metal ions. The result is coordinative cross-link formation (Fig. 3.15, left) [116] and consequent preparation of the insoluble network. It is important that the coordination chemistry of bpy-containing CPL can be controlled by strategic distribution of sterically encumbering fragments. Positioning sterically encumbering fragments about a bpy chelating fragment can also provide steric compound [117] and in a bpy modified poly (phenylenevinylene) derivative [118]. The sterically enshrouded metal chelation fragments enforce a 1:1 M:L chelating ratio (Fig. 3.15, right), leading to impressive improvements in the solubility/processability of PMC
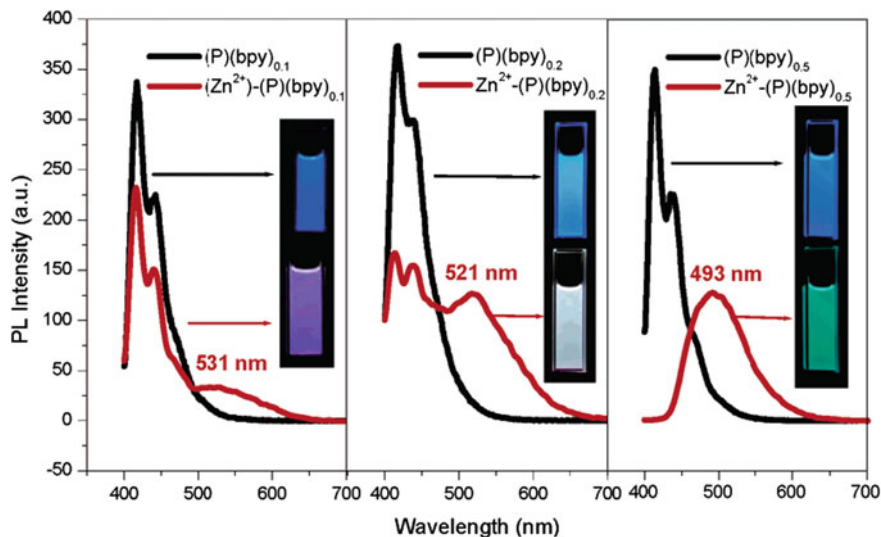
Fig. 3.14 Photoluminescence spectra of $(P)(bpy)_x$ and $Zn(II)-(P)(bpy)_x$ (excess $Zn(II)$) in THF solution were excited at 380 nm and the spectra were normalized. The colors of light emission from the CPL before and after $Zn(NO_3)_2$ chelation were recorded by photographs under UV light irradiation

versus coordinative cross-linked PMC which are formed upon chelation of non-sterically encumbered analogues. Furthermore, CPL bound a variety of transition metals with attendant changes in photophysical properties while remaining fully soluble and thus easier to characterize. Using this approach, bpy fragment was accessed that provides steric shielding from undesired cross-linking/network formation, while simultaneously leaving a cleft of free space about the bpy fragment to allow undistorted metal chelation environment. In addition, it allows the preparation of CPL with different ligand-to-ligand distances and selection of spacer identities from among commonly studies CPL backbones.

It should be noted a chelating calix[4]arene derivative incorporating two bpy fragments and one primary amino attachment function at the lower rim which was synthesized and coupled to Wang benzaldehyde resin (Fig. 3.16) [119]. The CPL effectively displayed chelation abilities towards Cu(I) and Zn(II) ions.

A partially soluble **PMC-1** was prepared by the interaction of poly(bpy) (**P1**) with $Ru(bpy)_2Cl_2$ (Scheme 3.19) [120]. It should be noted that emission from **PMC-1** occurred at 640 nm, red-shifted from $Ru(bpy)_3Cl_2$ by 30 nm. At the same time, poly (1,5-dinaphthyridine-2,6-diyl) (**P2**) shows a blue-shift of the absorption band during the formation of **PMC-2**, with a $\pi - \pi^*$ band at 300 nm and a broad MLCT band from 370 to 460 nm. It is important that the CPL exhibits an absorption band at 439 nm, because chelation induces twisting of the main chain.

It is important to emphasize that the suitable method for the formation of iridium PMC is the reaction of the binuclear bridge complex [121]. This method was applied
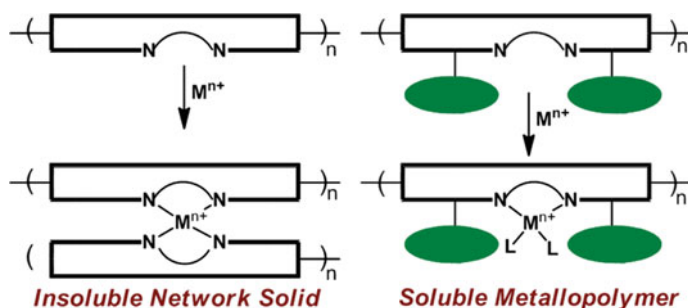
Fig. 3.15 Schematic illustrating how insoluble network formation (left) can be prevented by the steric coordination control strategy (right)

Fig. 3.16 Cu(II) chelate with calix[4]arene derivative incorporating two bpy fragments, which was obtained by grafting to Wang benzaldehyde resin (P = Wang benzaldehyde resin)
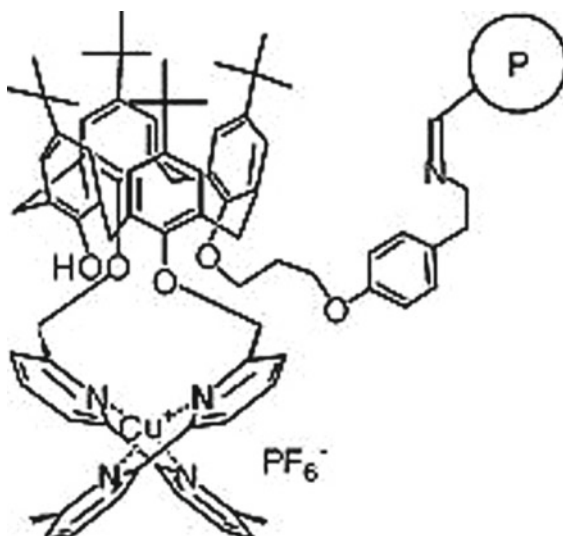
to the synthesis of the greenish-yellow-, yellow-, and orange-light-emitting Ir(III) bpy PMCs [122]. The respective dimeric precursor complexes, $[Ir(ppy)_2-\mu-Cl]_2$ and $[Ir(ppy-CHO)_2-\mu-Cl]_2$, where ppy is 2-phenylpyridine and ppy-CHO is 4-(2-pyridyl) benzaldehyde, were chelated to bpy carrying CPL tails with formation of PMCs, which were precipitated with a saturated methanol NH_4PF_6 solution (exchange of counter-ions).

The quantitative chelation was verified by both the photophysical and electrochemical properties of the mononuclear Ir(III) compounds. In particular, the PL spectra showed strong emissions at 535 and 570 nm. It is important that the color shifts depended on the substituents of the cyclometalating ligands. The molecular weight distributions were shifted toward higher molecular weights upon the chelation of CPL with the Ir(III) precursor complexes. For both PMCs, only one distribution was
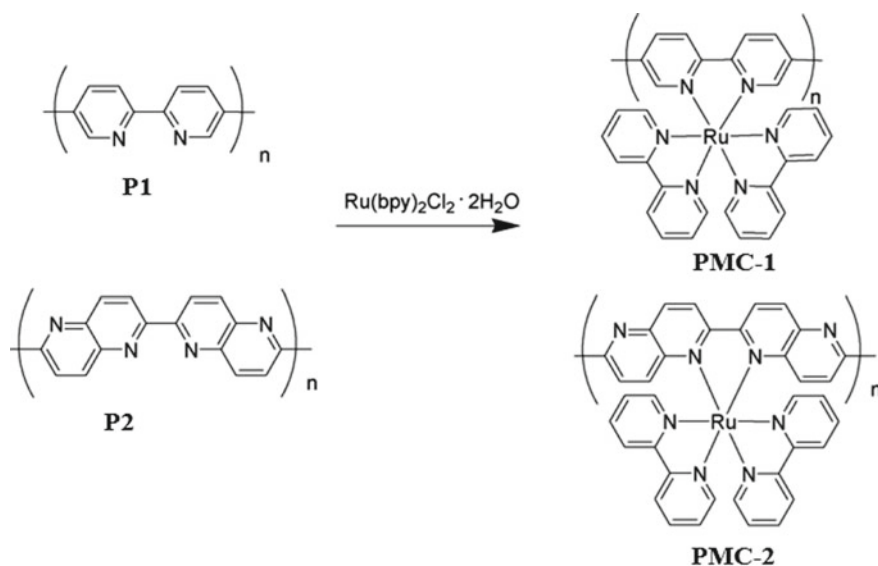
Scheme 3.19 Synthesis of **PMC-1** and **PMC-2**

Table 3.2 MALDI TOF-MS and GPC characterization data of CPL and PMC

Compound	MALDI TOF-MS			GPC			NMR
	M_n	M_w	PDI	M_n	M_w	PDI	M_n
CPL	3470	4340	1.25	4120	5800	1.40	5540
PMC-1	3950	4180	1.06	5300	6700	1.27	5806
PMC-2	3830	4050	1.06	7280	9400	1.29	5750

observed in the MALDI spectrum. Characterization by NMR, IR, gel-penetrating chromatography (GPC), and matrix-assisted laser desorption/ionization time-of-flight mass spectrometry (MALDI TOF-MS) proved the full chelation of the CPL with the respective metal precursors (Table 3.2).

Conjugated fluorescent bpy-containing polyfluorenes (**P-1**–**P-3**) feature fluorescence, can chelate with metal ions, combine solubility in organic solvents with high thermal characteristics, and exhibit high selectivity and sensitivity to terbium ions [123]. PMCs demonstrate a red shift in the spectra of absorption ($\Delta\lambda^{ab}$) and fluorescence ($\Delta\lambda^{fl}$), and the value of $\Delta\lambda^{ab}$ for the absorption of CPL varies in the range 3–30 nm, depending on the nature of metal ions. For example, for **P-3**, the value of $\Delta\lambda^{ab}$ varies from 12 for Ag(I) to 23 nm for Tb(III), whereas for polymer **P-1**, this parameter varies from 3 for Ag(I) to 19 nm for Tb(III). The difference in absorption maxima $\Delta\lambda$ results from the different chelation abilities of metal ions and bpy fragments. In particular, La(III) and Tb(III) noticeably quench fluorescence of the conjugated CPL. This effect is especially distinct when Tb(III) is added to polymer

P-2, whereas, in the case of Ag(I) or Mg(II), the fluorescence quenching is very slight.
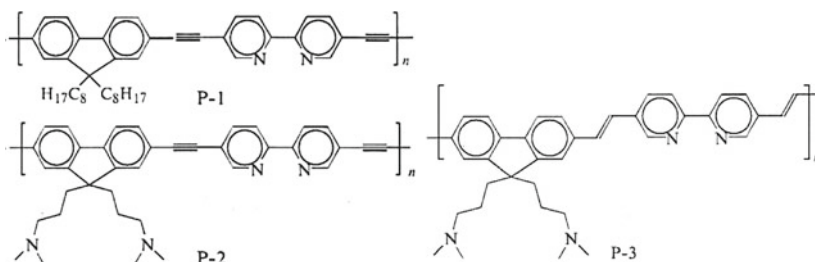
The interaction of copolyamides containing 5, 15, 30 and 45% of the side bpy fragments with the binuclear complex $[Ir(ppy)_2Cl]_2$ made it possible to obtain PMCs with different contents of $Ir(ppy)_2$ [124, 125]. It should be noted the significant influence of the flexibility of the polymer chain on the luminescence spectrum of PMC. In particular, increasing the flexibility of the chain leads to a decrease in the intensity of the luminescence band and its shift by approx. 30 nm to longer wavelengths, pointing to the excimer mechanism of energy transfer.
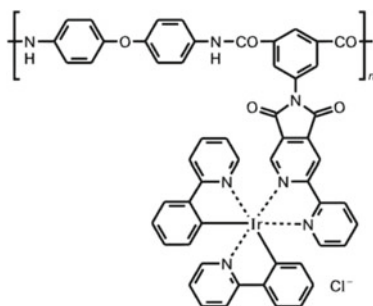
Of particular note is one of the few examples of using direct methods for PMC synthesis [126]. For example, PMC-Pd(II) based on polyamic acids containing the chelating biquinolyl fragments were prepared by electrosynthesis [127]. Compared with the conventional method of the PMC preparation, electrochemical synthesis is more preferred, because it allows to regulating chelation rate of Pd(II) ions and to preventing unwanted influence of counter-ions (Cl$^-$, OAc$^-$) in the solution. Usually, the formation of square planar metal chelates is characteristic for Pd(II) ion. However, in the case of biquinolyl LMC, the formation of a binuclear complex $(L)_2Pd_2X_2$ (X = Cl, OAc) with bridging anions (**I**) is characteristic due to the steric repulsion of two biquinolyl ligands. At the same time, the interaction of CPL with $PdCl_2$ or $Pd(OAc)_2$ salts leads to the mononuclear PMC $[LPdL'_n]^{2+}$ (**II**), where L' is the solvent molecule, N-methylpyrrolidone.
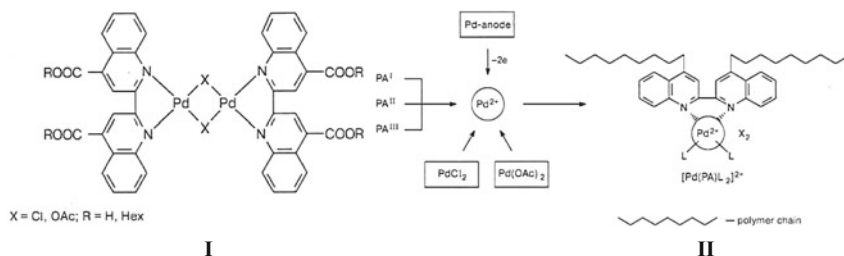
It should be noted that an electrosynthesis was also used to the preparation of Cu (I) chelates with CPL containing the same biquinolyl fragment [128].

The copolymers of N-vinylcarbazole and MMA carrying side pyridylquinoline fragments are shown to form stable PMC with Ir(ppy)$_2$Cl with interesting spectral and PL properties [129].
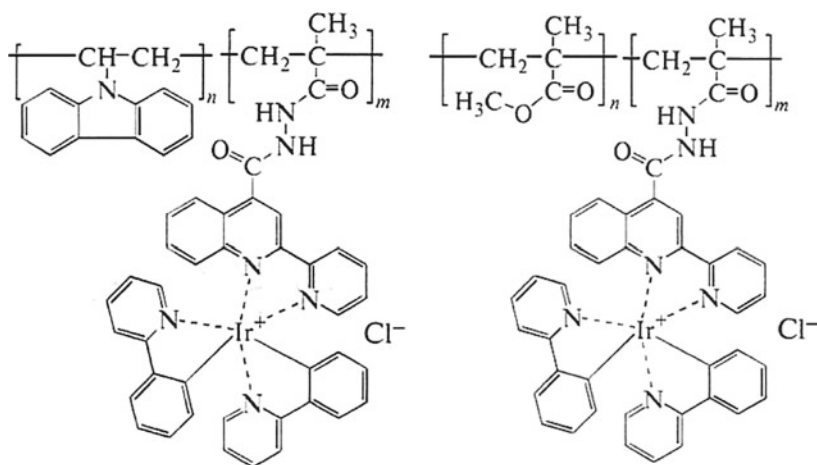
Of interest is a dipyrido-[3,2-*a*:2,3-*c*] phenazine-based metal ion-sensing conjugated CPL with unprecedented picomolar sensitivity and selectivity [96]. Such sensitivity was achieved due to a rigidly planar structure of the chelating fragments, which plays the essential role in the ion recognition process and rule out the chelation from the phenazine nitrogen atoms. The rigid planar structure of the chelating fragment prevents conformational change of the polymer backbone upon metal ion chelation, thus supporting the notion that conformational change is not required for achieving ionochromic response.
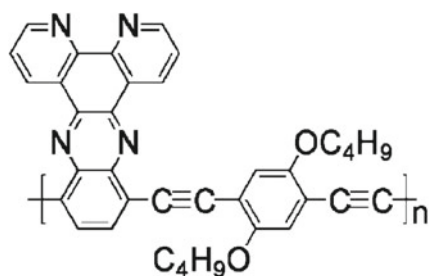
A synthetic approach to modify the structure of phenol-formaldehyde and resorcinol-formaldehyde polymers by the reaction with 3-(pyridin-2′-yl)-1,2,4-triazin-5(2H)-one was used to the preparation of CPL with a high selectivity [130]. Based on targeted synthesis of model compounds as structural fragments of the CPL and elucidation of the structure of their Cu(II) chelates, the most plausible type of metal chelation is formation of the bridge 1:1 chelates of the bpy type (Fig. 3.17).

Of interest are bidentate CPLs containing 2-phenyl-3-pyridin-2-yl-5,7-di-2-thienylthieno[3,4-b] pyrazine as intramolecular charge transfer dye, which form low band gap conjugated PMC-Re (Fig. 3.18) [131, 132]. It is important that the PMCs have good solubility due the solubilizing fragments even with high metal content.

The 5-aminopyridine-2-tetrazole-functionalized PS exhibited high chelation capacities for Cu(II), Pb(II) and Hg(II) ions, which increased sharply within 2 h and then
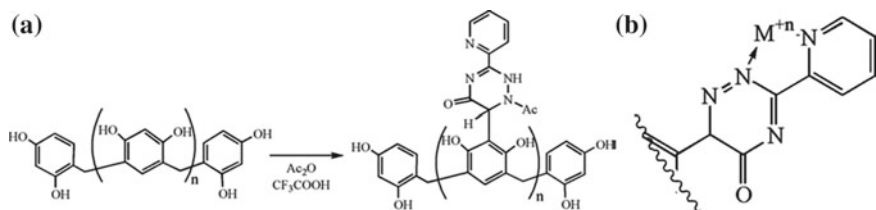
Fig. 3.17 a Modification of resorcinol-formaldehyde polymer with 3-(pyridin-2′-yl)-1,2,4-triazin-5(2H)-one and **b** formation of the chelate ring of the bpy type
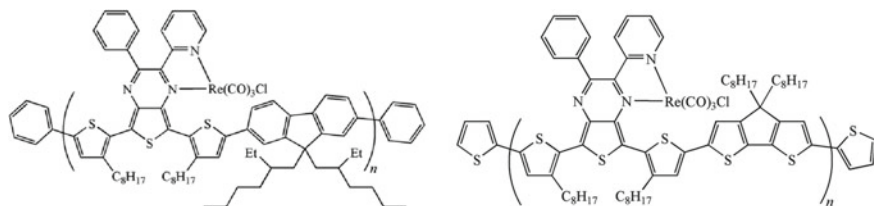
Fig. 3.18 Structures of light-harvesting rhenium PMC
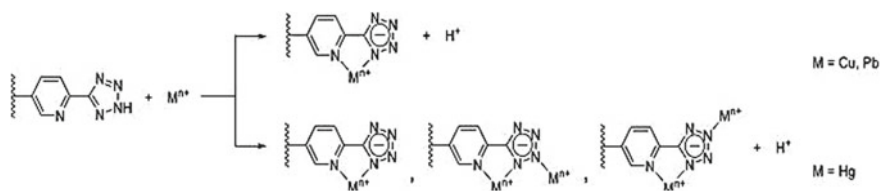
Fig. 3.19 The adsorption mechanism of metal ions on the 5-aminopyridine-2-tetrazole-functionalized PS

trended toward equilibrium until 12 h [133]. This phenomenon might be explained by the existence of plentiful centers at first, and as the chelation capacity increased, the available centers decreased, resulting in the rate reduction. The CPL would show a different chelation mode with Cu(II) and Pb(II) compared to Hg(II). In particular, there were three chelation modes for Hg(II), whereas for Cu(II) and Pb(II), only one chelation mode played an important role (Fig. 3.19). This speculated mechanism was supported by indirect evidence from the isotherm in which the adsorption of Cu(II) and Pb(II) belonged to mono-layer adsorption. In contrast, the adsorption of Hg(II) occurred on heterogeneous adsorption centers. After CPL was added into the solution containing Cu(II), Pb(II) or Hg(II), all pH values of the solution were found to decrease. This fact supported the participation of H^+ ions in the metal chelation, supporting the rationality of the speculated adsorption mechanism.

PS-based copolymers with Pd-chelating side fragments of 2-(1H-1,2,3-triazol-4-yl) pyridine were prepared ranging from 10 to 50% with respect to the fraction of the chelating comonomer [134]. The chelation of the CPL with $PdCl_2$ employing Pd (COD)Cl_2 as the metal source proceeds with very high conversions. Absolute molecular weights of the Pd-PMCs ranging from M_w = 16,000 to 20,000 and PDI = 1.3 were determined.

Of interest is using the hydrophobic luminescent PMC, poly (Ir-trifluoroethyl methacrylate), as an online dissolved-oxygen sensor [135]. The rational synthesis of the PMC through chelating CPL of phen-methacrylamide and trifluoroethyl methacrylate with iridium complex [(diphenylquinoline)$_2$IrCl]$_2$ rather than directly copolymerizing monomer [Ir(diphenylquinoline)$_2$phen]PF$_6$ with trifluoroethyl methacrylate can significantly reduce the cost. It is important that the fluorine-substituted trifluoroethyl methacrylate provide the polymeric hydrophobicity for preferable permeability to oxygen.
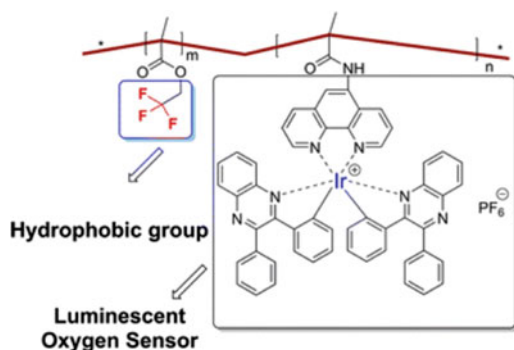
It should be noted PMC prepared by chelating bis(cyclometalated) Ir(ppy)$^{2+}$ to phen fragments of a PAMAM copolymer, in which the chelating fragments are $\sim 6\%$ of the repeating units [136]. It is important that the majority (88.3%) of the phen chelating ligands reacted with Ir(ppy)$_2$ fragments. In water, the PMC, in which the metal is surrounded by a lipophilic cage formed by the three large aromatic ligands, tend to segregate within the polymer to avoid contact with the water. Thus, the pendant Ir chelates are segregated into polymer pockets in which they experience less polar surroundings (thus giving a blue-shifted emission) and a more rigid environment than in solution. Besides, the emitting Ir chelates are very diluted along the polymer chains of PMC because the phen fragments are a minor component of the CPL. The best emitting features are often observed in systems where a rigid environment (rigidochromic effect) is joined to a low chelating fragment concentration.

The three kinds of luminescent polymers, Re-PMC, Re-Py-PMC, and Ru-PMC, were synthesized by the interaction of amphoteric CPL based on 4-(4′-aminobutyl)-phen, 2-methylpiperazine and bis(acrylamido)acetic acid (6% of phen-containing repeating fragments) with Re(CO)$_3^+$ or Ru(phen)$_2^{2+}$. They emit from ^{3}MLCT excited states with photoluminescence quantum yields (PLQY) = 0.7, 4.8, and 4.1%, in aerated aqueous solution, respectively [137]. It is important that the PMC maintained the nanometric size, water solubility, and biocompatibility of parent CPL. In fact, the properties of the PMC appear widely tunable, and it would be possible to modulate the wavelength, lifetime, and intensity of the emission by changing the substituents on the phen fragment or the metal itself.
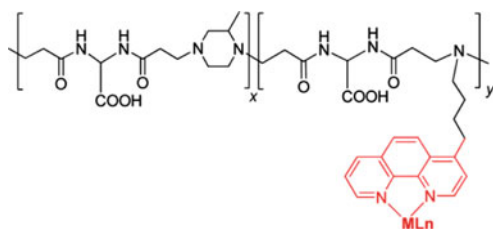
Well-defined mono- and bi-phen-terminated PIB and PEG underwent quantita-
tive chelation with Fe(II) ions in solution [138]. Since Fe(II) ions are hardly soluble
in nonpolar organic solvents preferred for PIB, the reaction was carried out in a
heterogeneous phase (CPL in CH_2Cl_2 and Mohr's salt in water). The color of the
mixture turned to red instantaneously, indicating a metal chelation and the pre-
cipitation of a large amount of red-colored gel occurred. After washing several
times with water, "strawberry jam"-like gel was obtained.
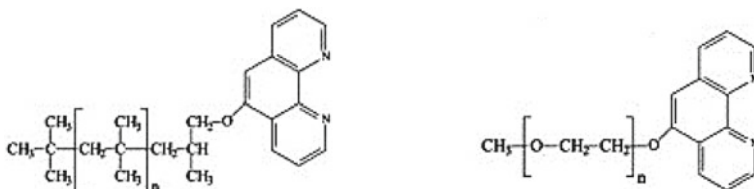
CPL containing alternating fluorene and phen fragments is capable of chelating
Eu(III) and Tb(III) ions in the presence of dbm or acac ligands to give PMC in
which all of the phen fragments are chelated [139]. For both PMC in dilute solution
there was no evidence for energy transfer along the CPL chain to the metal f-orbital
centered emission. However, sensitization of the Eu metal emission was observed
in thin films and at higher concentrations. At the same time, the Tb-containing PMC
shows only CPL-based emission, but there is a strongly red-shifted component
compared to the CPL. This red-shifted emission evolves rapidly from a new singlet
state of the phen fragment, which appears on metal chelation, and is more promi-
nent at higher metal content levels.
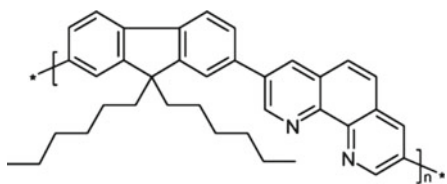
It is important that as in the case of protonation, the effect of a metal on the
absorption spectra of CPL is to cause a bathochromic shift in the absorption spectrum
[140, 141]. For example, when a metal such as Zn(II) is chelated a longer wavelength
emission appears. Although in polybipyridines such shifts were attributed to metal-
induced planarization of the CPL [142], this cannot operate on the already-planar
phen-containing CPL.

Of interest is the synthesis of a polymer-anchored Ni(II)-phen chelate with
content 1.1% of Ni ion [143].
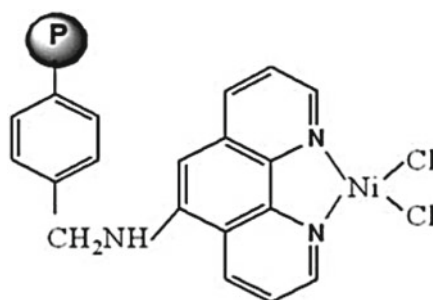
It should be noted the similar PMC that exhibit superior physical and biological activities to their LMC [144].

M = Co(II) and Ni(II).
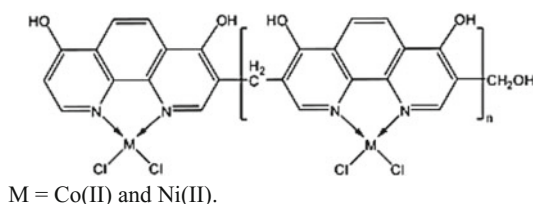
The interesting PMCs, in which about three or four repeating units incorporate one metal ion averagely in the PMC, were prepared by the reaction of $NiSO_4$, $CoCl_2$ or $FeSO_4$ with CPL synthesized by polycondensation of 5,6-diamine-phen with terephthalaldehyde [145]. The coordination structure of the PMC is composed of one metal ion and two phen units from adjacent polymer chains, in which nitrogen atoms act as coordinating centers (Scheme 3.20). It seems to be reasonable in view of the stiffness of polymer chain and the strong chelating tendency of bidentate N,N-donor ligands to metal ions.
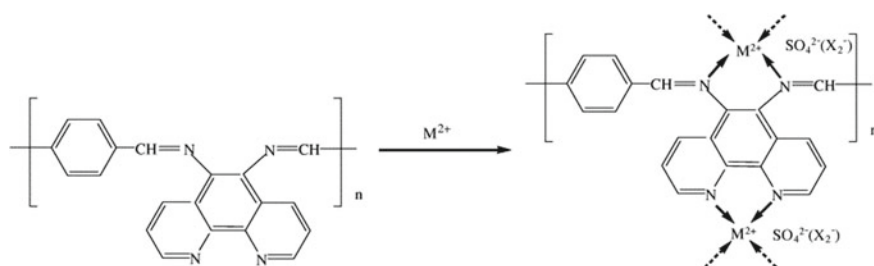
Scheme 3.20 Synthetic route of poly (Schiff base) metal chelates (M=Co, Ni, Fe)

Table 3.3 Magnetic data of PMC-Ni(II), PMC-Co(II) and PMC-Fe(II)

Chelate	Relative saturation magnetization (5 K) (emu/g)	Remanence magnetization (5 K) (emu/g)	Coercive field (5 K) (Oe)	Curie-Weiss temperature (30 kOe) (K)
PMC-Ni(II)	9.1	0.01	30	49
PMC-Co(II)	10.6	0.02	25	11
PMC-Fe(II)	5.9	0.05	200	−98

Based on the field and temperature dependence of magnetization and hysteresis loop (Table 3.3), it can be concluded that PMC-Ni(II) and PMC-Co(II) are soft ferromagnets, while PMC-Fe(II) exhibits features of an antiferromagnet.

A phen-based fluorescent sensor was introduced into poly (NIPAM-co-N-hydroxymethyl-AAm) nanofiber films via simple electrospinning technique [146]. The fragments of NIPAM and N-hydroxymethyl-AAm were designed to exhibit thermo-responsive and chemical crosslinking functions, respectively. It is important that CPL with 3 wt% of phen fragments showed significant quenching of fluorescence as chelating with Cu(II) ion with K_{sv} of 5.5×10^4 M^{-1}. As compared to dip-coating films, the downward deviation to linear Stern-Volmer plots of thin films was observed, indicating a fraction of phen fragments was inaccessible to the quencher Cu(II). The enhanced sensitivity of phen-containing electrospun nanofibers is attributed to their higher surface area compared to dip-coating films. Besides, the phen-containing nanofibers also exhibited an "ON-OFF" switchable sensing behavior due to the hydrophilic-hydrophobic change of PNIPAM as varying temperature that controlled the metal ions to be accessible to the sensors.

It should be noted that such N-donor ligand as tpy possesses a superb ability to chelate a large number of metal ions and forms stable tpy-metal chelates, so it is an important building block for the preparation of PMC [147]. As compared with the bpy-containing CPLs having a coiled conformation, structure of tpy-containing CPLs is determined by the nature of spacer between the two chelating fragments. As a typical example, we note CPL with tpy side fragment prepared by the interaction of 4′-hydroxy-tpy and the commercially available PCS [148]. It is important that the CPL has higher chelation ability toward Pb(II) and that the metal chelation follows the order: Pb(II) > Cu(II) > Zn(II) > Ni(II). This difference in metal chelation capacities observed among the metals by the CPL can be attributed to a combination of factors including M–L stability constants, metal ionic radii, and stereochemical configuration of active chelating fragments. At higher pH values, hydrolysis of the metal ions becomes significant and may compete with chelation reaction. The metal chelation increased with pH of the medium and approached a steady state at about pH 6.0. This behavior could be explained by the nature of the chelating fragments because at low pH values the nitrogens of the tpy group can be

protonated, which leads to less metal chelation. Therefore, at higher pH values, the amine group lone pairs will be more available for metal chelation and the metal ions compete favorably toward donor centers compared with hydrogen ions. It is important that the chelation abilities of these CPLs are largely dependent on the type of intervening spacer groups connecting the active chelating fragments.

Of interest is low molecular weight CPL (M_n < 3000) with low PDIs (<1.4) obtained by polymerization of a tpy-containing styrenic monomer by ATRP [149]. This CPL forms PMC with Ru ion and is well soluble in organic solvents. Proof for the complete attachment of Ru onto every side-chain tpy repeating unit can be found in the ^{1}H NMR spectra of the PMC. In particular, the characteristic downfield shift of the 3 and 3′ protons of the tpy moieties after chelation from 8.7 to 9 and 9.35 ppm, respectively, and the up field shift of the 6 tpy protons from 8.7 to 7.5 ppm can be noticed. Additionally, no peaks corresponding to the initial CPL were detected at 8.65–8.75 ppm attributable to the tpy fragments of the uncomplexed CPL. This work was extended by polymerization of the same tpy-carried monomer from both single- and MWCNT that allows to preparing the carbon nanotube-PMC composite material soluble in common organic solvents [150].

It should be noted the tpy-containing CPLs which were used to chelate Dy, Eu, Tb, and Sm [151]. Random PMC, which contains pendant Eu(III) chelates, showed two emission bands at 590 and 613 nm and had a pink color (Fig. 3.20a). At the same time, random PMC based on MMA and Tb(III) showed four emission bands, and their green color was attributed to the main transition band at 546 nm (Fig. 3.20b). Interestingly, the mixed-metal PMC emitted a yellow light (Fig. 3.20c).

Heating the mixed-metal PMC above 50 °C leads to the reversible thermochromism with a color change from yellow to orange/pink (Fig. 3.21). It is explained by the dissociation of the mixed-metal PMC to individual metal chelates. It is important that blends of PMC-Eu and PMC-Tb do not show reversible thermochromism, which indicates the determining role of the spatial organization of the PMCs for their fully reversible dissociation/association.

PMCs containing coordination-bonded ions of terbium in side chains were prepared via the synthesis using tpy anchor groups and the lanthanide pyrazolonate complex [152]. It is important that for the synthesis of the CPL, the monomer carrying Cz groups was used in the form of both individual *endo-* and *exo-*isomers and their mixture. In the PL spectra of the PMC in solutions and in thin films, intense bands at 492, 550, 586, and 624 nm, attributed to the $^5D_4 \rightarrow {}^7F_6$, $^5D_4 \rightarrow {}^7F_5$, $^5D_4 \rightarrow {}^7F_4$, and $^5D_4 \rightarrow {}^7F_3$ transitions in the Tb(III) ion, and low-intensity broad bands of the CPL were observed. The best EL properties were featured by the CPL prepared from a mixture of *endo-* and *exo-*isomers of the Ca-containing monomer. The EL spectrum of PMC showed only the metal-centered emission.

Of interest is the functionalization of nanophase-separated amphiphilic polymer co-networks with redox-responsive tpy-metal chelates and light-responsive SP derivatives, which leads to a novel material with tunable optical, redox and permeability properties [153]. The versatility of the CPL in chelation of various metal
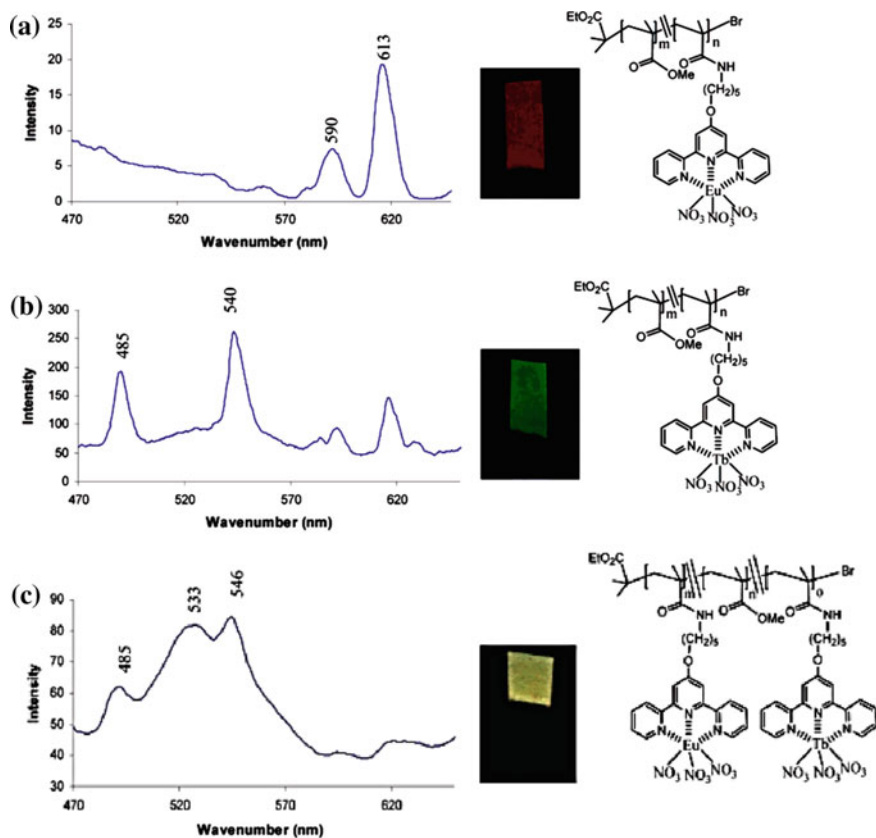
Fig. 3.20 Solid-state fluorescence spectrum of **a** PMC-Eu(III), **b** PMC-Tb(III), **c** PMC-Eu(III)/Tb (III) alloy. Only the alloy shown in spectrum c has the new emission band at 533 nm. Excitation wavelength is 350 nm

ions, in particular, cobalt or iron, results in a perfect monitoring over the degree of crosslinking of the hydrophilic poly (2-hydroxyethyl acrylate) channels. It is important that the reversibility of the chelation, the metal redox state and the isomerization to the MC form upon UV illumination was evidenced.

The interesting type of tpy chelation was observed in a mono-tpy-PEG-functionalized Ir(III) chelate successfully prepared by monomerization of a dimeric [Ir(ppy-CHO)$_2$-μ-Cl]$_2$ precursor complex (Scheme 3.21) [154]. It is important that the PDIs are shifted towards higher values after chelation of CPL with the phenyl-pyridine precursor complex.

Well-defined tpy-bearing poly (triphenylamine-*alt*-fluorene) fluorescent conjugated CPL shows much higher sensitivities toward Fe(III), Ni(II), and Cu(II) as compared with the other metal ions [155]. Especially, Fe(III) ion addition leads to fluorescence quenching of CPL. Whereas, the analogous CPL, in which N-ethylcarbazole repeat
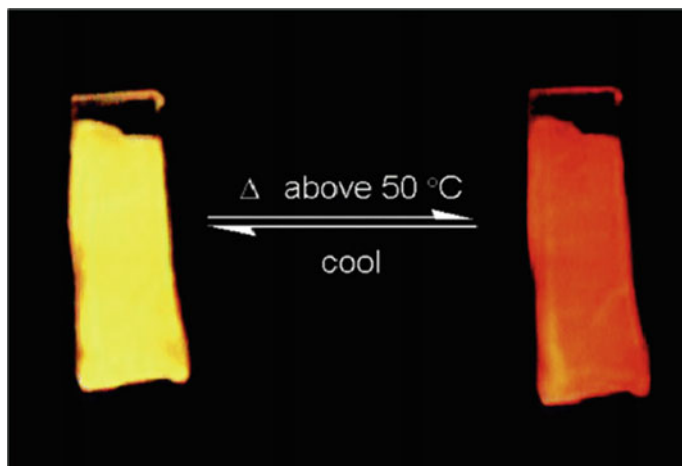
Fig. 3.21 Reversible thermochromism of mixed-metal PMC. Polymer was heated above 50 °C and thin films were excited with a UV lamp
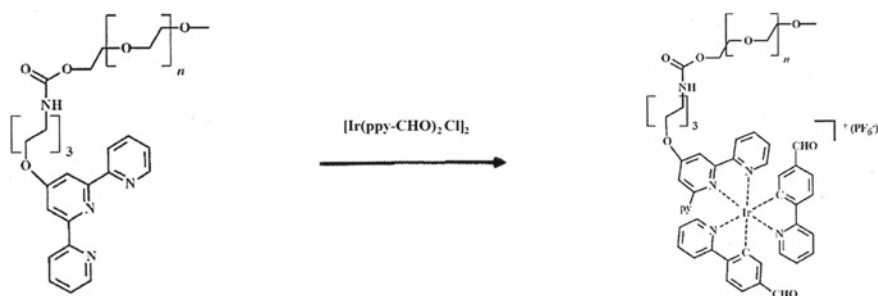
Scheme 3.21   Synthesis of the PEG-based mono-tpy Ir(III) chelate

units replace the fluorene fragments in CPL, shows a very poor selectivity. It demonstrates that CPL with same chelating fragments may show different sensitivity to metal ions owing to their different type of backbones.

CPL based on poly (phenylenevinylene) with tpy ligand shows the potential for some metal ion detection (Fig. 3.22) [156].

Resonance interaction extends to entire
conjugated polymer backbone

Resonance interaction is limited to *meta*-phenylene
bridge
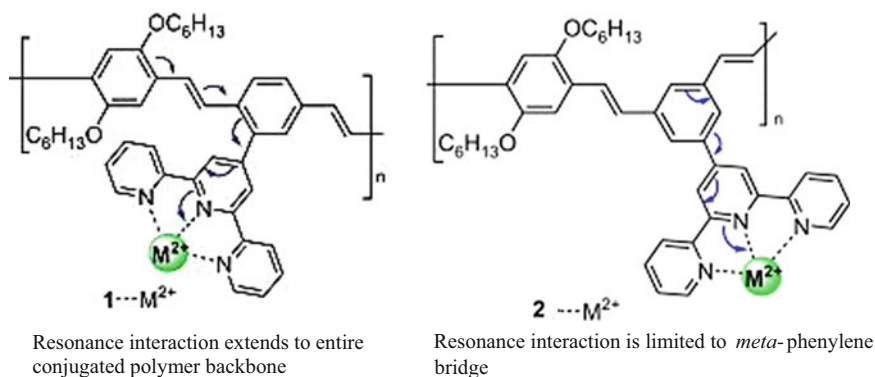
Fig. 3.22 Structures of PMC based on CPL **1** and **2**

It is interesting that the fluorescence of the CPL **1** was quenched completely by Fe (II), Fe(III), Ni(II), Cu(II), Cr(II), Mn(II), and Co(II). The indiscriminate fluorescence quenching, observed from the tpy-functionalized poly (phenylenevinylene), indicates strong coupling between the metal-chelating tpy and phenylenevinylene polymer backbone. It should be noted that the tpy in **1** is placed at *o*-position relative to one of the two vinylene bonds that allows the electronic resonance interaction between the tpy and conjugated main chain, which is easily extended to the entire conjugated backbone. At the same time, alternate occurrence of *m*-phenylene units along the poly [(*m*-phenylenevinylene)-*alt*-(*p*-phenylenevinylene)] chain effectively breaks the conjugated backbone into a sequence of well-defined chromophores (or isoenergetic molecular fragments). The tpy in CPL **2** is placed at the *m*-position relative to both vinylene bonds along the polymer chain; therefore, the resonance interaction from the tpy center is only transmitted up to the *m*-phenylene bridge. The fluorescence of the CPL with emission $\lambda_{em} = 460$ nm is selectively quenched by Cu(II) ion. The nature of the quenching process in **2** is probed by using Stern-Volmer analysis, revealing that the quenching results from both dynamic collision and metal chelation.

A level of Eu(II) chelation of 37% (molar basis) in the alternating CPL containing fluorine and tpy was achieved (Fig. 3.23) [157]. The PL studies showing the occurrence of polymer-to-Eu(III) energy transfer brought about by the spectral overlap between the absorption spectra of the Eu(III) chelate and the emission of the CPL. PMC showed a dominant pathway involving the energy transfer between the triplet of the dbm ligand and the $^5D_1$ and $^5D_0$ Eu(III) levels. The similar gadolinium chelate (PMC-Gd) was also synthesized to determine the triplet state of the chelate.

A tpy-carrying CPL, poly (N-vinylcarbazole)-*b*-poly [4′-((4-vinylphenyl) phenyl)-tpy], consisting of emission Cz and chelating tpy blocks exhibited higher sensitivities to Ni(II) and Mn(II) ions [158]. In this case, the Zn(II)-tpy chelate reduced the twist and vibration of the C–C main chain and increased the charge transfer from donors to acceptors due to the more rigid and planar architecture.
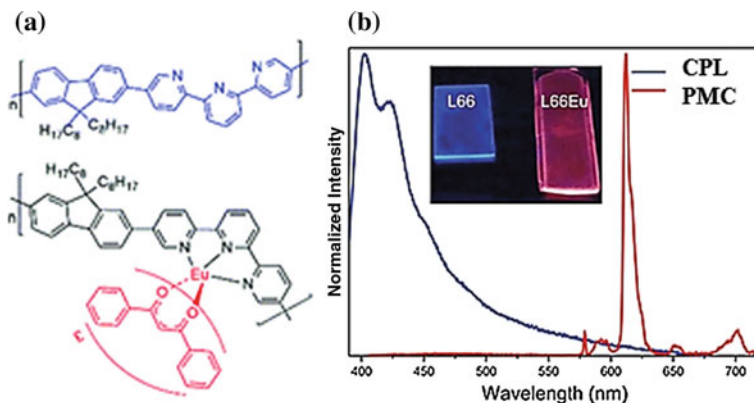
Fig. 3.23 **a** Structures of CPL and its PMC-Eu and **b** normalized emission spectra in the solid state. Blue line: PCL (λ_{exc} = 380 nm). Red line: PMC-Eu (λ_{exc} = 390 nm). The inset shows photographs of the films irradiated at 360 nm from an UV lamp

CPL with Pd-chelating fragments 2,6-bis(1H-1,2,3-triazol-4-yl) pyridine in the lateral chain were quantitatively loaded with Pd(II) ions, feature high molar weights of up to M_n = 30,000 [159]. The quantitative loading of the CPL with [Pd(COD)Cl$_2$] as a precursor was evidenced by ^{1}H NMR spectroscopy and elemental analysis.

Of interest is BPP-*co*-octylated phenylethynyl conjugated CPL with two cyan color (blue and green emission) [160]. The chelation of the BPP fixed on the surface of the CPL films and spheres was used to obtain red emitting PMC-Eu(III) layer (Fig. 3.24).

A scanning confocal fluorescence microscopy allows to confirming the appearance of cyan and white colors from initial CPL and CPL coated with PMC-Eu(III) (CPL/PMC spheres), respectively (Fig. 3.25a–f). In particular, CPL spheres showed a cyan color due to the mixing of blue and green emissions. At the same time, CPL/PMC spheres exhibited emission spectrum covering the entire visible region. The measured CIE (International Commission on Illumination) (*x*, *y*) purity of the emitted white-light spheres is nearly close to the designated coordinates for ideal white light (x = 0.33, y = 0.33) (Fig. 3.25f).

Of interest are alternating copolymers (**P1–P7** and **P9**) with the M_n in the range of 5300–11,000 prepared by copolymerization of the dialkynyl-functionalized olio (3-octylthiophene)$_m$ (m = 1–7 and 9, where m is the number of thiophene units) with BPP. The optical emission ranges of these PMCs were fine-tuned from blue to red and white by changing the chelation of red-emitting Eu(TTA)$_3$ and green-emitting Tb(acac)$_3$ complexes in both the solution and solid states [161].

MULTI−COLOR POLYMER MICRO−SPHERES
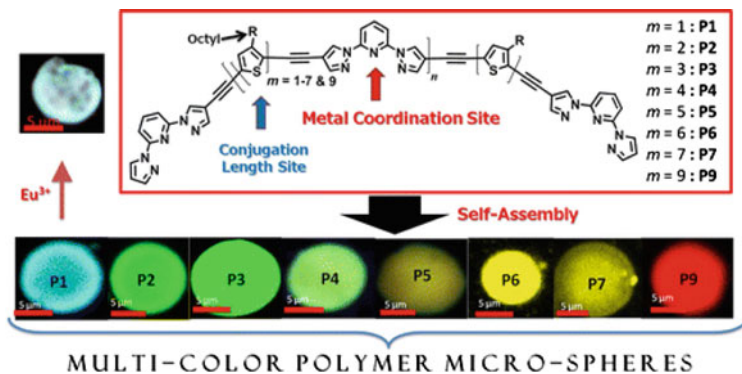
For example, a very dilute solution of **P1** showed blue color emission (Fig. 3.26a) and to this solution addition a 1:1 mixture of THF solution of Tb(acac)$_3$ and Eu (TTA)$_3$ displayed a white color light (Fig. 3.26a) with CIE (x, y) coordinates 0.29,
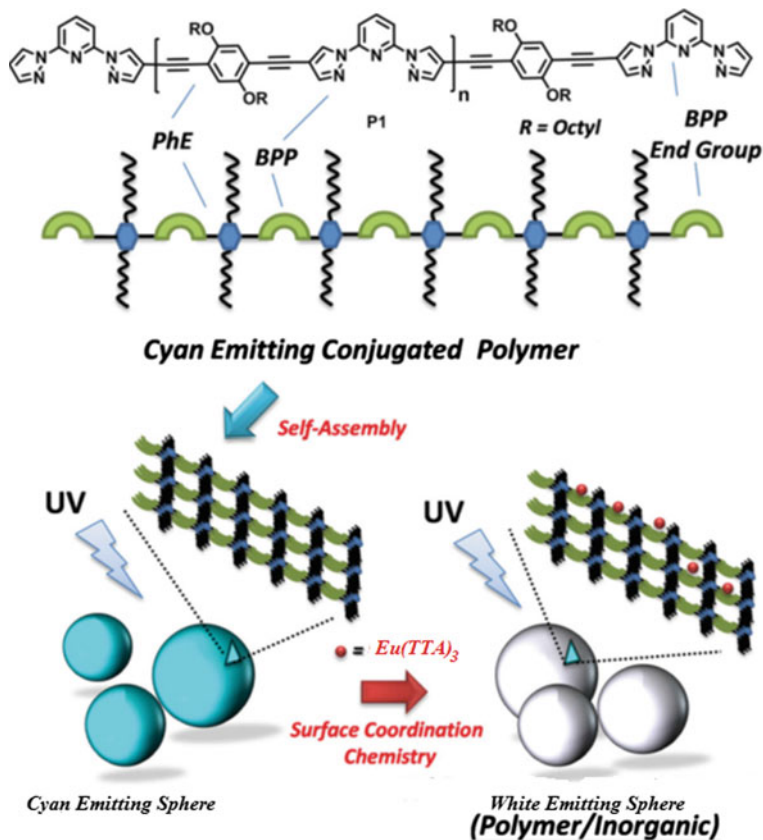

Fig. 3.24 Illustration of white emitting nano/microspheres prepared from PMC-Eu(III) via self-assembly, where PhE is octylated phenylethynyl
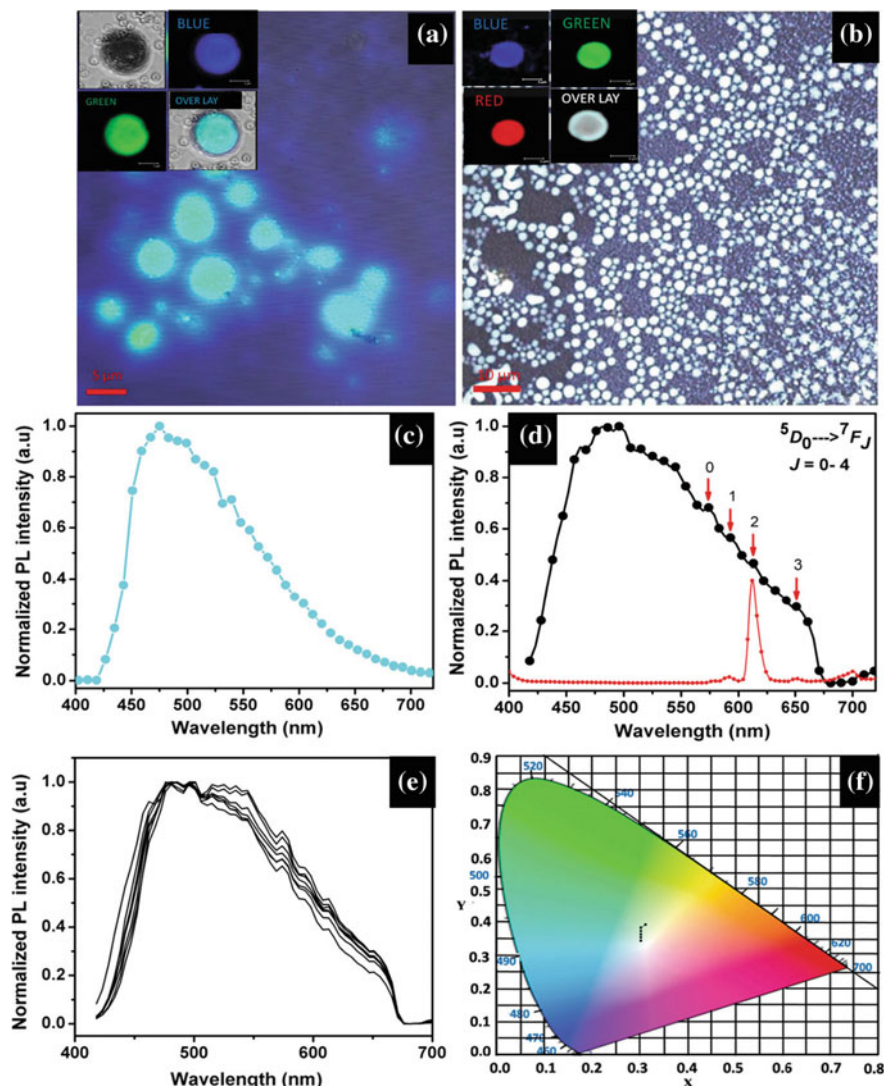
Fig. 3.25 Confocal fluorescence images of CPL and CPL/PMC spheres. **a** Cyan emitting CPL spheres (insets exhibit the bright field image of a single sphere, displaying mixed cyan emission due to blue and green dual emissions (scale bar is 5 μm). **b** White emission of CPL/PMC spheres (insets exhibit blue, green and red emissions from CPL/PMC spheres, and the final white color) (scale bar is 10 μm). **c–e** Confocal microscopy fluorescence spectra of cyan emitting CPL sphere, white emitting CPL/PMC sphere, and six various sized CPL/PMC spheres. **f** CIE chromaticity diagram of white emission color displayed by six PMC spheres ($x = 0.30$ and $y = 0.35, 0.36, 0.37, 0.38, 0.39, 0.40$), corresponding to their spectra shown in **e** ($\lambda_{ex} = 365$ nm)

0.35 (Fig. 3.26d). The emission spectra of Tb(III) ion exhibited sharp emissions at 490, 547, 585, and 620 nm due to $^5D_4 \rightarrow {}^7F_J$ (J = 3–6) f–f transitions and Eu(III) ion displayed peaks at 581, 594, 612, 653, 705 nm due to $^5D_0 \rightarrow {}^7F_J$ (J = 0–4) f–f transitions. The most intense emission was observed for Tb(III) ion at 547 nm, which corresponds to the $^5D_4 \rightarrow {}^7F_J$ transition. Among the peaks corresponding to that of Eu(III) ion, the strongest emission was observed at 612 nm ($^5D_0 \rightarrow {}^7F_2$) due to induced electronic dipole transition, which clearly indicates that the chemical environment around Eu(III) ions does not have an inversion center. White emission was also achieved by mixing highly concentrated solution of cyan emitting **P1** (Fig. 3.26b) with THF solution of Eu(TTA)$_3$. Similarly, white radiation was also obtained by simple mixing THF solutions of blue-emitting copolymer **P1** and
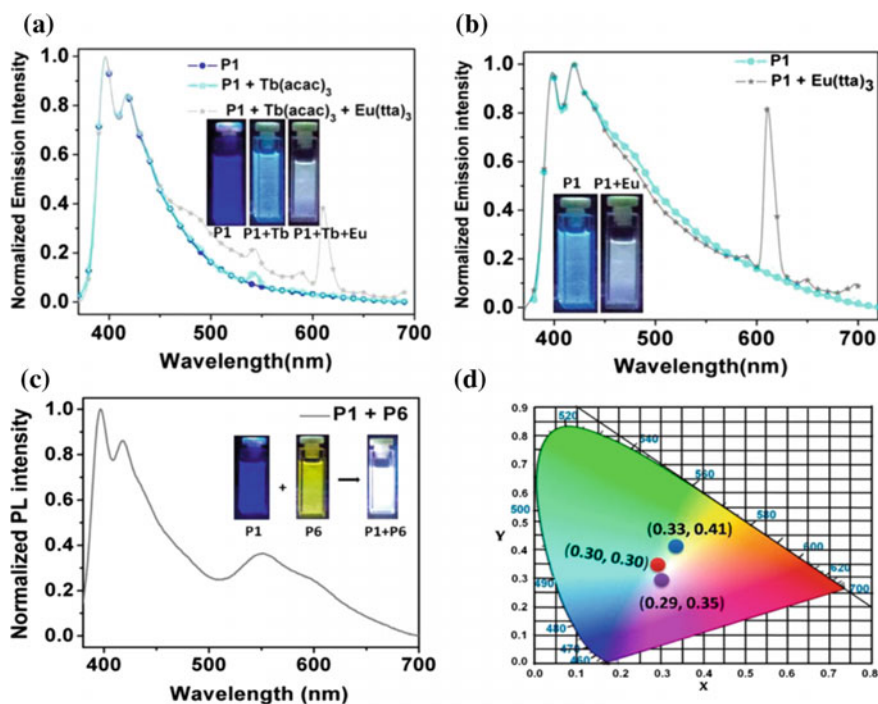
Fig. 3.26 **a** Emission spectra of **P1** without and with metals Tb(III), Eu(III) in CHCl$_3$. Insets show the photographs of emission colors from **P1**, **P1** + Tb(III), **P1** + Tb(III) + Eu(III) upon UV light irradiation. **b** Emission spectra of copolymer **P1** with and without Eu(III) in CHCl$_3$, and the insets show the emission colors of **P1** and **P1** + Eu(III) upon UV light irradiation. **c** Emission spectra of mixture of **P2** and **P6** in CHCl$_3$; the insets show the emission colors of **P1**, **P6**, **P1** + **P6** upon UV light irradiation. **d** Emission color of copolymers **P1** + Tb(III) + Eu(III) (0.29, 0.35), **P1** + Eu(III) (0.33, 0.41), and (**P1** + **P6**) (0.30, 0.30) in solution state CIE chromaticity diagram

yellow emitting copolymer **P6** in 1:1 ratio (Fig. 3.26c, d) corresponds to CIE (x, y) coordinates of 0.30, 0.30.

Of interest is other BPP end-capped fluorene main chain copolymers (**P1** and **P2**) with M_n around 10,000 [162]. By exploiting the metal chelation ability of tridentate BPP fragments in the main chain, a red emitting PMC-Eu(III) layer was formed on top of the **P1** and **P2** thin films via the dip-coating technique. This allows to achieve white color radiant films displaying triple emission with maxima at 425, 543, 614 nm and 428, 543, 611 nm for **P1** and **P2**, respectively (Fig. 3.27). The CIE coordinates were equal to (0.31, 0.35) and (0.31, 0.32) for white emitting films based on **P2** and **P3**, respectively.

To study the metal chelation properties of the tris(2-pyridyl)-borate-functionalized homo and block copolymers, prepared via ROMP of (bicyclo[2.2.1]hept-5-en-2-yl)-4-phenyl) (pyridin-1-ium-2-yl)di(pyridin-2-yl) borate and dimethyl-7-oxabicyclo[2.2.1]hept-5-ene-*exo,exo*-2,3-dicarboxylate, aggregate solutions of CPL in methanol were treated with a solution of $FeCl_2$ in methanol [163]. A red solid formed indicating successful chelation with Fe(II) and crosslinking of the CPL aggregates. SEM analysis of the PMC provided evidence for formation of an extended nanoparticle network as a result of Fe(II) cross-linking. The ligands in the Jahn-Teller d^9 complex Cu-PMC are much more weakly bound than in the low-spin d^6 complex Fe-PMC; therefore, Cu(II) should be readily replaced by addition of Fe (II). Indeed, treatment of a suspension of the cross-linked Cu-PMC in a solvent mixture of THF/MeOH with a solution of $FeCl_2$ in methanol led to a color change from green to light beige, indicating the successful transfer of the chelating ligands from Cu(II) to Fe(II) (Fig. 3.28).

Targeted functionalization of the initial polymers led to CPL with norbornene (**P1**) or dicyclopentadiene-based (**P2**) backbones and pyridine-bis(oxazoline) (pybox) pendants, which display red Eu(III)-based, green Tb(III)-based and blue Tm(III)-based emission [164].
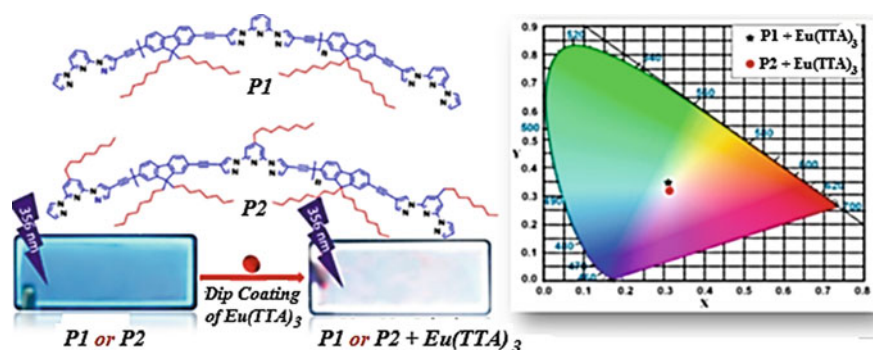

Fig. 3.27 Chemical structures of CPL **P1**–**P2** and emission color of $Eu(TTA)_3$-coated **P1** and **P2** film in a CIE 1931 2° standard observer chromaticity diagram
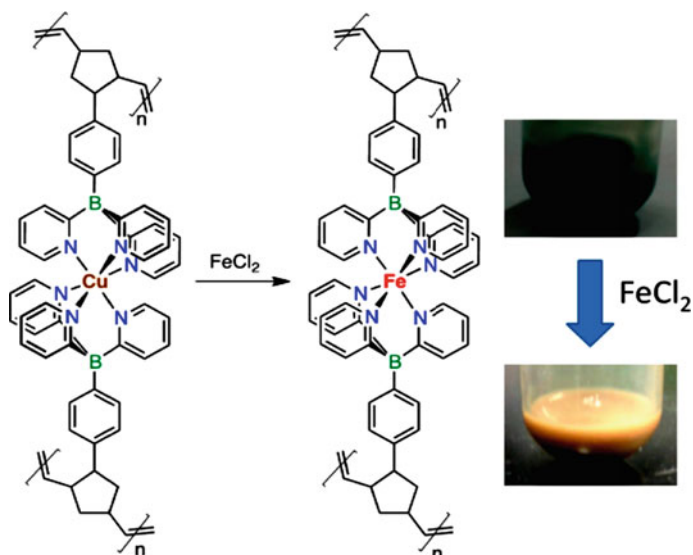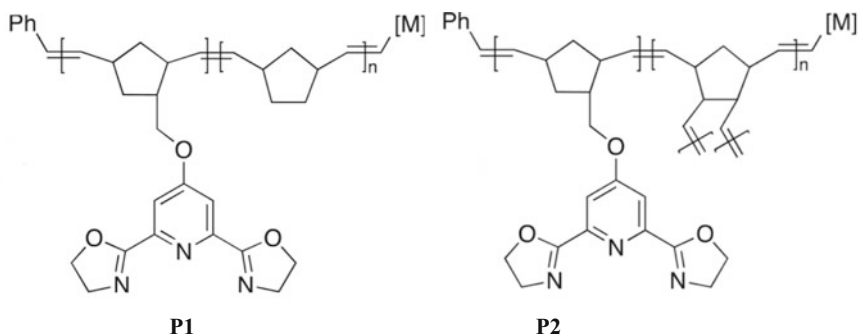
Fig. 3.28 Exchange of Cu(II) for Fe(II) in PMC network. Photographs of Cu(II)-PMC before and after treatment with $FeCl_2$

Red Eu(III) and green Tb(III) emission could be achieved in moderate-to-good quantum yields by mixing the two ions when the pendants are spaced enough apart does not lead to energy transfer between the two ions. Finally, these systems are the interesting examples of blue Tm(III)-centered emission in PMC (Fig. 3.29).
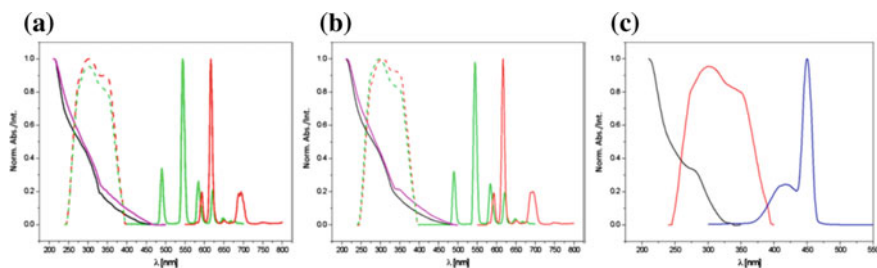
Fig. 3.29 **a** Absorption (solid magenta line), excitation (dashed red line), and emission (solid red line) spectra of Eu-**P1** and absorption (solid black line), excitation (dashed green line), and emission (solid green line) spectra of Tb-**P1**. **b** Absorbance (solid magenta line), excitation (dashed red line), and emission (solid red line) spectra of Eu-**P2** and reflectance (solid black line), excitation (dashed green line), and emission (solid green line) spectra of Tb-**P2**. **c** Absorbance (solid black line), excitation (solid red line), and emission (solid blue line) spectra of a Tm-**P1** film, measured at room temperature

3.1.5 Metal Chelates Formed by N,O-Containing Ligands

As an example of N,O-containing PMCs, we note Cu(II) chelates with poly [N-(thiazol-2-yl) methacrylamide] [165]. It is found that the Cu(II) chelated to CPL through the nitrogen of the thiazole ring and carbonyl oxygen to form stable six-membered ring in PMC-Cu (Fig. 3.30).

Of interest is a functionalized mesoporous CPL synthesized via organic-organic radical polymerization of 2,4,6-triallyloxy-1,3,5-triazine (Scheme 3.22) [166]. The CPL acts as an excellent support for chelation of Pd(II) at its surface. The metal content of Pd(II)-PMC suggested 5.16 wt%.
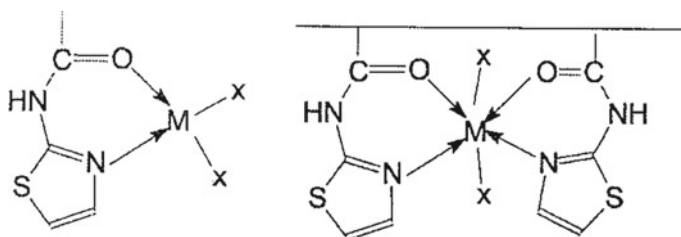
Fig. 3.30 Suggested structures of the metal chelates with poly [N-(thiazol-2-yl) methacrylamide] (X = Cl or Ac)
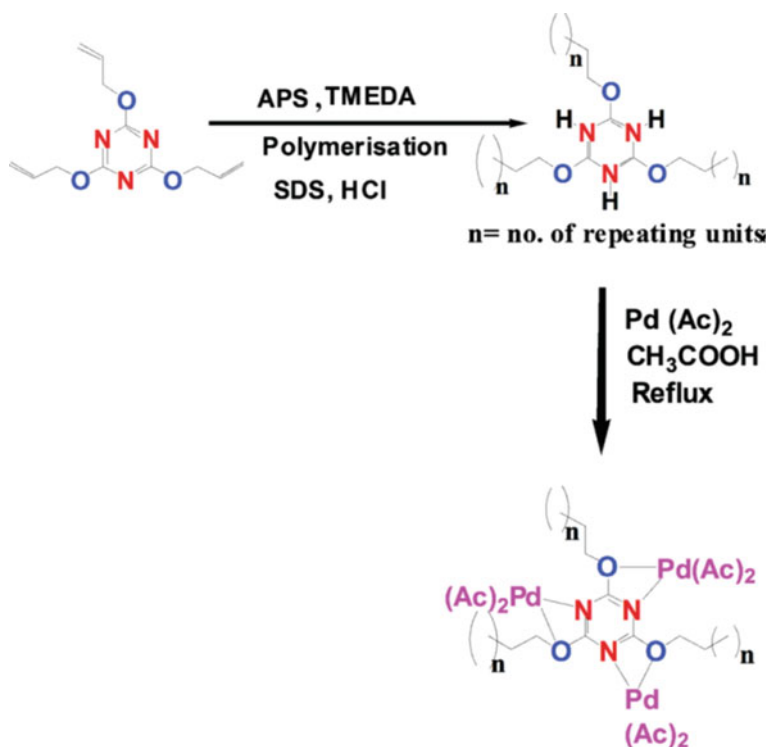
Scheme 3.22 Organic-organic in situ radical polymerization of 2,4,6-triallyloxy-1,3,5-triazine and grafting on Pd(II) in acetic acid medium

3.1.6 *Binding of Metal Compounds with O,O-Containing Ligands*

It should be noted PS-bearing di-bis(2-ethylhexyl) malonamide used for selective adsorption of U(VI) in the presence of Th(IV) due to sterical hindrance from the bulky alkyl chain for the chelation of Th(NO$_3$)$_4$ [167]. It is important that increasing acidity leads to increasing distribution ratios (D) values for both metal ions, and that trend was more characteristic for Th(IV).

CPLs synthesized by the condensation of biuret, formaldehyde and 4-hydroxy acetophenone [168], 4-hydroxybenzaldehyde [169] or 4-hydroxybenzophenone [170] were used for the preparation of PMC with O,O-chelating fragments.
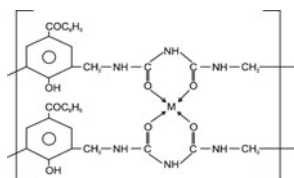
3.1.7 Metal Chelates with N,S-Containing Ligands

The PVC functionalized by phenyldithiocarbazate chelating fragments was reacted with PdCl$_2$(PhCN)$_2$ in DMF at 80 °C to yield the PVC anchored Pd(II) phenyldithiocarbazate chelate (Scheme 3.23) [171].

CPL obtained by inserting spacer ethylene oxide and ethylene sulfide, respectively, with 3-aminopyridine into PCD had higher chelation capacities and selectivity for Hg(II) [172]. The existence of the hydrophilic spacer was beneficial to enhance the hydrophilicity of the CPL and then increase the adsorption rate. The XPS results showed that not only 3-aminopyridine but also S atoms existed in the spacer arm could take part in the chelation with Hg(II).
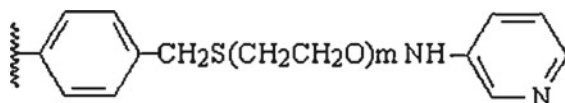
**Scheme 3.23** Preparation of the supported Pd-phenyldithiocarbazate chelate
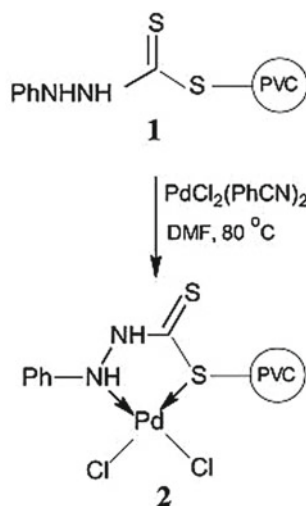
It should be noted the theoretical study of Hg(II)- and Pb(II)-PMC based on sulfur- and aminopyridine-bearing CPLs including sulfur- (**P1**), sulfoxide- (**P2**), and sulfone-containing (**P3**) spacers [173]. It is important that CPLs are tridentate ligands to chelate the metal ions by S and two N atoms (**P1**) or O and two N atoms (**P2** and **P3**).

The chelation capacity of CPL with amine-mercaptan groups reached 3.10 mmol g^{-1}, i.e. 621.8 mg g^{-1} [174]. The main factors determined the interaction of the metal ion and the CPL are the acidity of the medium and nature of the conjugate anion. It is important that such CPLs allow to selective separating of Hg(II) from Ca(II), Mg(II), Pb(II), Cd(II), Cu(II) and Zn(II) ions.
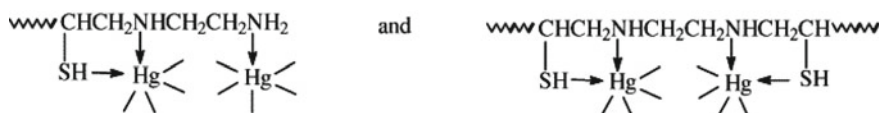
A conjugated CPL containing 2,6-bis(2-thienyl) pyridine exhibits a high sensitivity and selectivity for Pd(II) ion detection based on the fluorescent quenching effect [175].
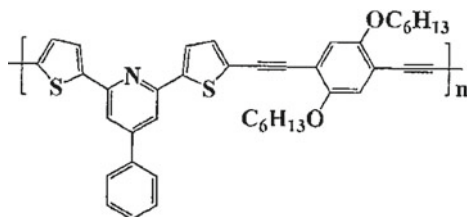

The CPL comprises two functional parts, one for the specific chelation of Pd(II) ions and another for signaling the response. Since a sulfur atom is considered as a "soft" donor atom in a chelating fragment, it generally increases the sensor's affinity and selectivity for "soft" metals such as Pd(II). A chelating block, 2,6-dithienyl-4-phenylpyridine, was introduced by combination of a pyridine group and a thiophene group, into the conjugated polymer, expecting to improve sensitivity and selectivity for Pd(II). After adding Pd(II) ions, the absorption spectra of CPL show no obvious red-shift, which might prove that the mode of linkage between the metal and the ligand is mostly intrachain linking instead of interchain linking. It is interesting that the CPL displays a selective chromogenic behavior towards the Pd(II) ion with a color change from yellow green to brown.

Of interest is the study of chelation capacity of CPL prepared from macroporous PCD by either direct attachment of the heterocyclic chelating fragments, such as 2-amino-5-methylthio-1,3,4-thiadizole, 2-amino-5-ethyl-1,3,4-thiadizole, and 2-mercaptobenzothiazole, to the polymeric matrix or through different hydrophilic spacer arms

[176–179]. As expected, these CPLs exhibited a high affinity for Hg(II) and Ag(I). It is important that the introduction of hydrophilic spacers between the polymeric matrix and heterocyclic chelating fragments resulted in an increase in the hydrophilicity, which allowed for better contact between the metal ion in solution and the chelating fragments and increased the chelation capacity. Besides, the introduction of spacer arms might the flexibility of the chelating fragments, which should help the functional group chelate the metal ions.

CPL synthesized simply by the reaction of PCS or PAN with 2-amino-1,3,4-thiadiazole was used for Pt(IV) [180] or Hg(II) adsorption [181]. In the case of Pt (IV) adsorption, the negative value of ΔG (-41.9 to -45.6 kJ mol^{-1}) confirms the spontaneity of the adsorption process with increasing temperature [182]. At the same time, PAN-2-amino-1,3,4-thiadiazole had the maximum adsorption capacity to Hg(II) ion of 526.9 mg g^{-1} at 308 K [181]. FT-IR analysis revealed that the nitrogen in –N–H, C–N, C=N and –C=NH contributed to the adsorption of Hg(II).
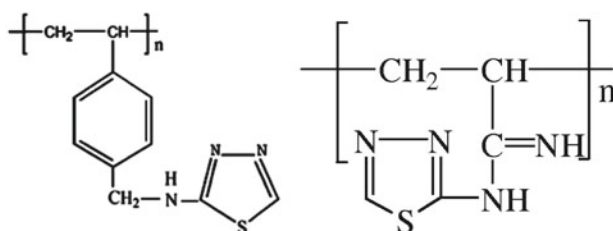
3D-ordered macroporous cross-linked PSs with 2-mercaptobenzothiazole chelating fragment attached directly or via hydrophilic spacer arms (PEG chains with three different lengths) to backbone were prepared for use as heavy metal ion CPLs [182]. CPLs are effective sorbents of heavy metals with chelation capacities ranging from 0.25 to 1.14 mmol g^{-1} for Ag(I) ion and 0.28 to 0.51 mmol g^{-1} for Hg(II) ion, respectively. The chelation capacities and adsorption kinetics improve by the introduction of hydrophilic spacers between the polymeric matrix and the heterocyclic chelating fragments. Moreover, the chelation capacities increase with the length of spacer arm.
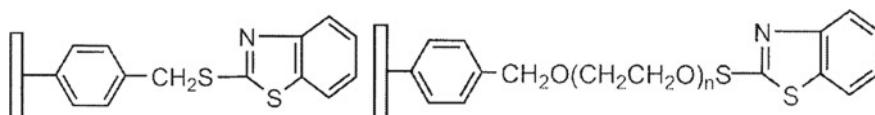
Of interest is such CPL as PS-2-aminothiazole with a high selectivity for Au(III) ions in comparison with Ni(II), Cu(II), Cd(II), and Co(II) ions [183]. It is important that chelation of gold chloride by PS-2-aminothiazole proceeds with participation of nitrogen and sulfur [184, 185].
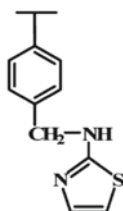
A *p*-bromophenyl substituted benzodithieno-imidazole based on soluble and rigid π-conjugated CPL with N and S donors exhibited outstanding sensitivity towards Cu(II) by emission quenching through PET [186]. The visually noticeable fluorescence quenching with the naked eye (under UV illumination at 365 nm) makes CPL an efficient sensor for Cu(II) (Fig. 3.31). However, the complete quenching of fluorescence of the CPL was not observed by the ligand-metal ion interaction in contrast to the monomer analogue, presumably due to the unavailability of all the chelation fragments to metal ions in the CPL.

It should be noted Pd(II)-PMC (0.28 mmol g^{-1} Pd in the polymer) prepared by stirring a suspension of CPL (4-amino-5-methyl-3-thio-1,2,4-triazole-functionalized PS) in a solution of $PdCl_2(PhCN)_2$ (Scheme 3.24) [187].

The study of the chelation behavior of the CPL synthesized through the reaction of 3-amino-1,2,4-triazole-5-thiol with glutaraldehyde in the absence and in the presence of thiourea (Fig. 3.32) towards Ag(I) from aqueous solutions showed that better chelation behavior was achieved for Ag(I) by thiourea-containing CPL [188]. The CPL obtained from a molar ratio of 2:1:3 of 3-amino-1,2,4-triazole-5-thiol, thiourea and glutaraldehyde, respectively, showed chelation capacity of 3.6 mmol g^{-1}. The data indicated that the adsorption process is an endothermic reaction and kinetically proceeds according to pseudo-first-order model.
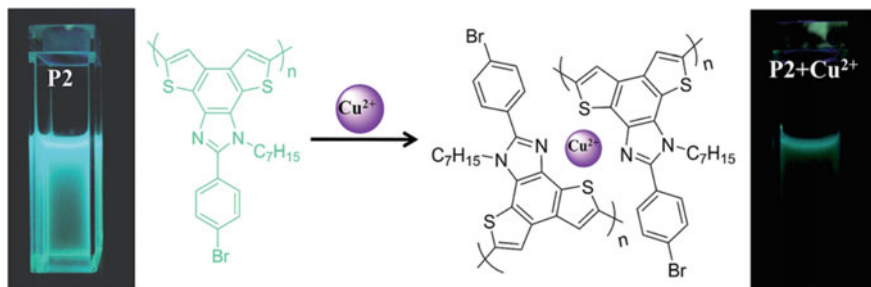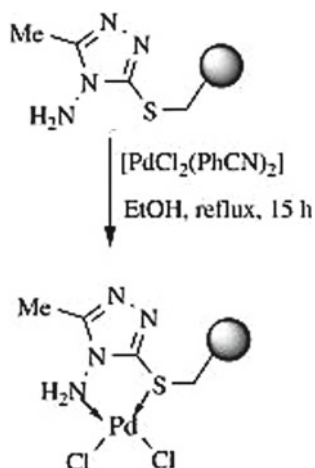

Fig. 3.31 Visual changes observed in emission of free **P2** (left) and Cu(II)-chelated **P2**. Cu(II) (right) under UV illumination at 365 nm
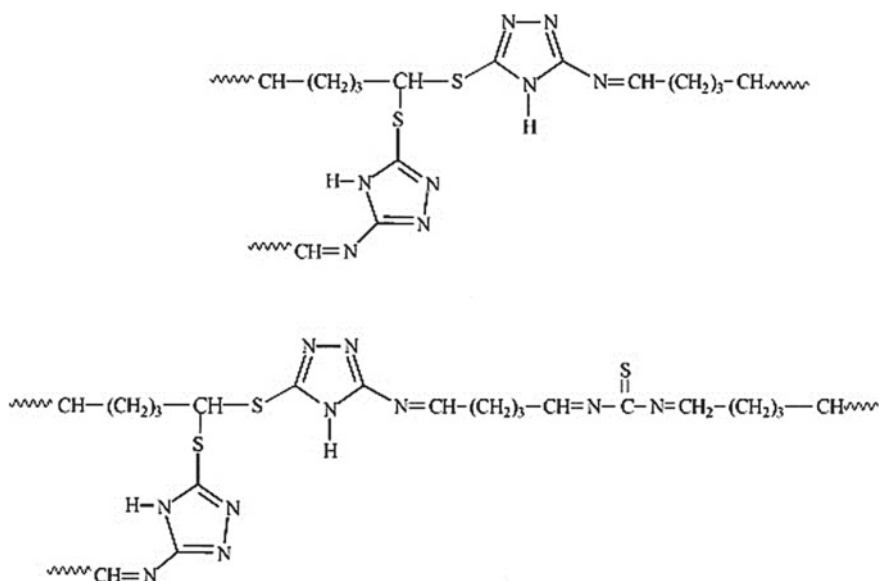
Scheme 3.24 Preparation of the PMC-Pd(II)

**Fig. 3.32** Proposed structures of the CPLs

The CPL based on PCS and 2-thiomethylbenzimidazole was reacted with VO (acac)$_2$, MoO$_2$(acac)$_2$ and Cu(CH$_3$COO)$_2$ to give corresponding PMCs [189]. It should be noted good dispersion of the VO(II) and Cu(II) centers in the PMC framework. In addition, the metal chelation proceeds with participation of nitrogen and sulfur atoms.
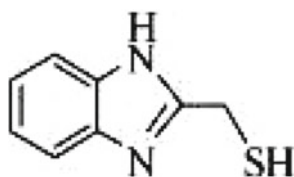
Of interest is the study of chelation capacity of CPL based on macroporous cross-linked PS with 2,5-dimercapto-1,3,4-thiodiazole chelating ligand linked via a hydrophilic tetraethylene glycol spacer [190]. It turned out that this CPL has higher chelation selectivity for Hg(II) and Ni(II) ions in comparison with other metal ions. It is important that the hydrophilic spacer allows to increasing chelation abilities of the CPL.

3.1.8 Some Examples of Metal Chelates with P-Containing Ligands

The supported complex [Rh(COD)(POLYDIPHOS)]PF$_6$ prepared by stirring a CH$_2$Cl$_2$ solution of [RhCl(COD)]$_2$ and Bu$_4$NPF$_6$ in the presence of POLYDIPHOS at room temperature for 24 h belongs to the metal chelates with polymeric P, P-ligand [191]. In this case, a p-styrenyl substituent attached to the ligand framework allows the diphosphine moiety –(C$_6$H$_4$)CH$_2$–OCH$_2$C(CH$_3$)(CH$_2$PPh$_2$)$_2$ to be introduced as a pendant group in PCD matrixes via free-radical copolymerization. The Rh loading in PMC was determined as 0.74 wt%.
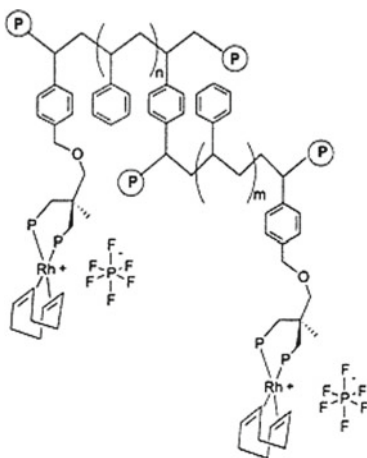
In another interesting example, the successive reaction of the optically active polyarylynes containing P-stereogenic bisphosphine as a chelating fragment in the main chain with Pd afforded the corresponding PMC [192]. The conformation of the CPL was controlled by the trigger of the metal chelation, and a new chirality was created by the metal-bisphosphine unit, which was locally transferred to the *m*-phenylene-ethynylene spacers.
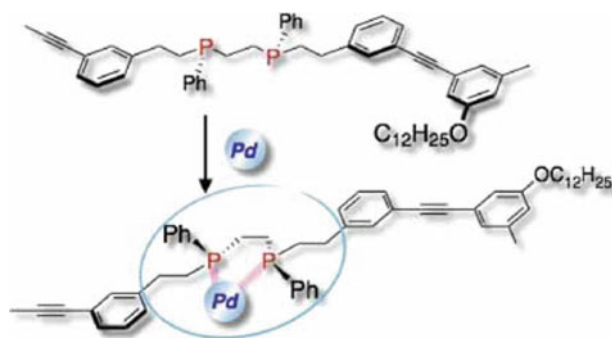
3.2 Intracomplex Compounds

This is the largest group of PMCs in which the metal ion associated with chelating fragment by both a covalent or coordination bonds. Not being able to describe in detail this class of PMCs, we list only the most important types of chelating nodes, as well as consider the peculiarities of their formation and structure of the resulting PMCs. Typically, these PMCs have relatively high thermal and chemical stability. Another feature is a complete saturation of the coordination sphere of the metal ion, except in certain cases, which will be given below.

3.2.1 Chelation with Polyphenol Ligands

Catechol (1,2-benzenediol) is important ligand in modern coordination chemistry because their two hydroxyl functions enable chelation of metals [193]. In particular, catechol can chelate Cd(II) and Cu(II) with relatively high stability constants (log K = 10.8 and 14.1 respectively). PMCs containing catechol-metal chelate fragments include mono-, bis- and tris-catechol-Fe(III) chelates [194–196]. It is important that the stoichiometry of the catechol-Fe(III) chelates is determined by pH (Fig. 3.33) [197] and the iron concentration [198].

It should be noted that the substituents on the catechol aromatic ring has the substantial effect on the chelation process due changing the pK_a values of the catechol fragments [199].
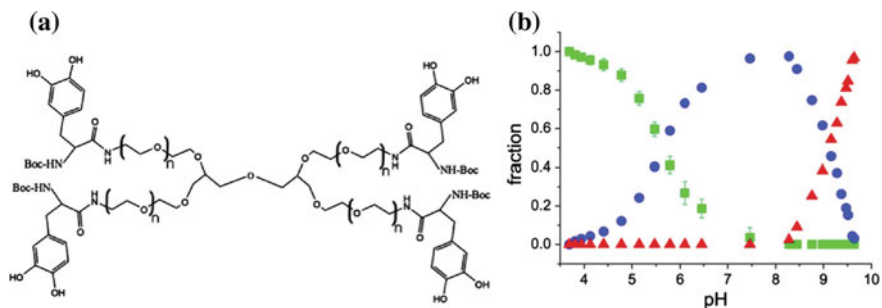
Fig. 3.33 a Catechol-functionalized PEG polymer. **b** Relative fractions of mono-, bis- and tris-chelates as a function of pH

The introduction of chelating catechol fragments onto the polymer backbone leads to a highly specific, isothermal solubility switch for poly (NIPAM) [200]. Due the possibility to tune the hydrophilicity of responsive polymers without the need for a temperature gradient, it is possible to obtaining increasingly selective, desired CPLs (Fig. 3.34).

It should be also noted the study of the Fe(III) and V(III) chelation by 4-arm PEG with terminal catechol fragments. It turned out that Fe(III) ion forms bis-chelates, while for V(III) the formation of tris-chelates is observed [201].

Of interest is the helical N-propargylamide CPL based on monomer **M1** with chelating catechol fragments and monomer **M2**, which provided the helical units (Scheme 3.25) [202].
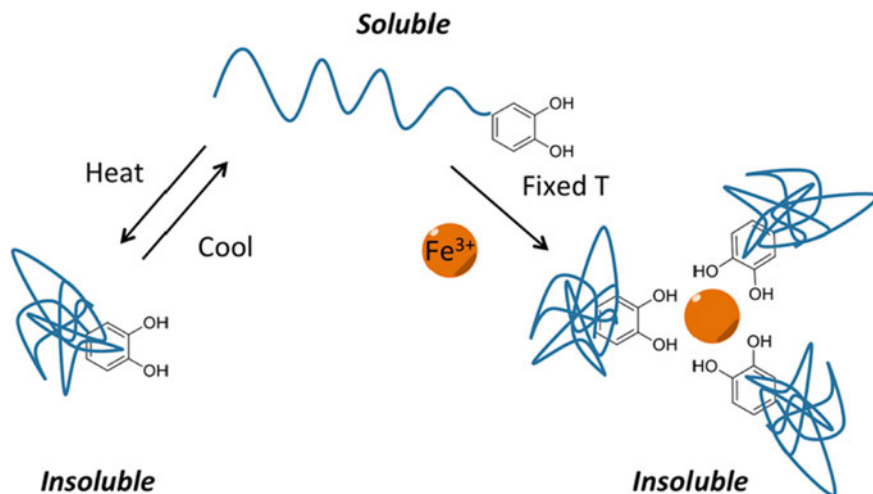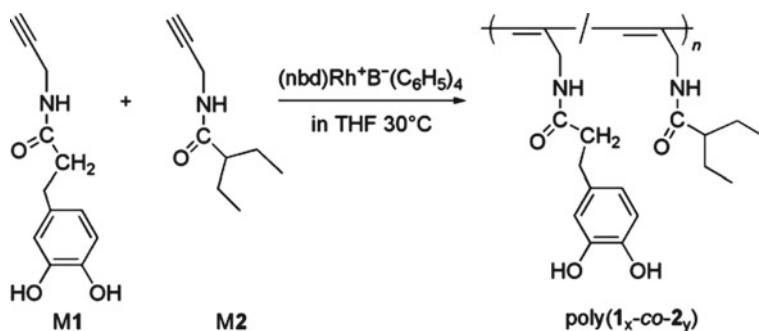

Fig. 3.34 Isothermal concept: an LCST and polymer conformational change can be induced through catechol-Fe(III) chelation, rather than by a temperature change

Scheme 3.25 Synthetic route to helical N-propargylamide CPL

Table 3.4 Chelation capacity (mg g^{-1}) of Fe(III) by poly($\mathbf{1}_x$-co-$\mathbf{2}_y$)s

x/y in poly($\mathbf{1}_x$-co-$\mathbf{2}_y$)s (mol mol^{-1})	100/0	40/60	30/70	20/80	10/90	0/100
Chelation capacity (mg g^{-1})	8	90	158	163	186	6

The chelating catechol fragments increased the hydrophilicity of the hydrophobic mono-substituted polyacetylenes and aided the helical N-propargylamide CPL to chelate the metal ions. For example, the maximum chelation ability of Fe(III) ion was equal to 186 mg g^{-1}, while the homopolymers of **M1** and **M2** weakly chelated Fe (III) (Table 3.4).

In the case of porous polymers, the formation of mono-catecholated PMCs is observed [203–206]. It is interesting that the charges of divalent metal will be compensated by the dinegative catecholate, resulting in the metal center and the polymer pores without charge-compensating anions.

The study of metal retention properties of porous PCD functionalized with catechol fragments towards Pb(II), Cu(II), Ni(II) and Cd(II) ions exhibited that at low metal concentration, interaction with the CPL is non-specific whereas at higher concentration catechol is responsible the retention properties [207, 208].

Poly(vinylcatechol-co-DVB)s prepared by suspension copolymerization of 3,4-dimethoxy-St with DVB and followed by deprotection of the catechol fragments show the chelation capacities 101.5 and 81.0 mmol g^{-1} for copper and cadmium, respectively [209]. This low accessibility can be the result of the morphology of the CPL beads and of the bottle-shape form of the pores (restricted connectivity between the pores). Moreover, catechol fragments may inaccessible units of highly crosslinked CPL because of the copolymerization process or of the post-crosslinking during methoxy deprotection step. It should be noted a significant variation of coloration upon chelation of copper by the CPL. Thus, the presence of three bands at 400, 570 and 750 nm in the diffuse reflectance spectrum of PMC-Cu(II) suggests that both mono and bis copper-catecholate chelates are formed with CPL. This indicates that two grafted catechol fragments are sufficiently closed to enable such a chelation.

It is interesting that the chelation of the cadmium in solution does not induce significant variations in the absorption spectra.

It should be noted that the chelation efficiency of metal ion through the chemically modified PAA with dihydroxybenzenes into the polymeric matrix is equal to 75 and 99% for Cr(VI) and Pb(II), respectively [210].

The saturation chelating ability of the polyphenols based on catechol and pyrogallol for Cu(II) ions were equal to 0.88 and 0.22 mol kg^{-1}, respectively [211]. Increasing the hydroxyl group content in the phenolic monomer increased the rate of adsorption and the saturation chelating capacity for copper ions. Besides, not all of the hydroxyl groups functioned as chelating fragments for copper. It shown that copper ion adsorbed to the polypyrogallol to release the two protons and the adsorption mechanism can be described by the following equation:
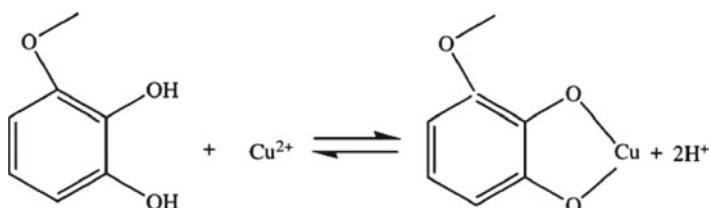

The polyelectrolyte chains in a PAA backbone functionalized with 30% catechol appendants can be reversibly cross-linked through metal chelation and irreversibly gelled by oxidative crosslinking [194]. Surprisingly, the reported "poor" metal chelator Zn(II) not only imparts this CPL compared to the one chelated by a stronger metal cross-linker, for example Fe(III), but also generates good mechanical performance of the self-healing hydrogel after the oxidation of catechol groups with a pH trigger.

It should be noted CPL based on Amberlite XAD-2 resin anchored with pyrocatechol through –N=C– group [212] and PAA chemically modified with 1,2,4,5-tetrahydroxybenzene or benzene-1,2,4,5-tetrol [213].

Metal chelation of catechol-carrying porous CPL proceeds readily with Cu(II), Mg(II), and Mn(II) ions, resulting in porous cavities including coordinative unsaturated, catechol mono-chelates (Scheme 3.26) [214]. In this case, hydroxy groups of the catechol fragments are available for metal chelation.

Treatment of CPL with excess of metal salts leads to the PMCs with high content of the catechol fragments, corresponding to a 1:1 M:L composition (Table 3.5).

It should be noted the chelation of Th(IV) and U(VI) ions by 9-phenyl-3-fluorone fixed on Duolite XAD-761 [215].
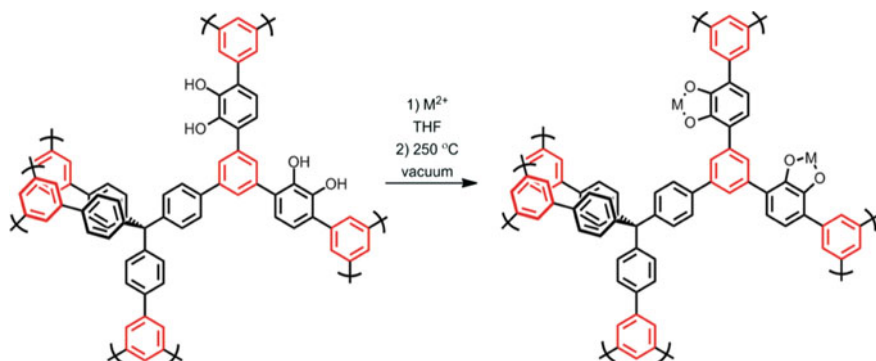
Scheme 3.26 Chelation of catechol-containing CPL

Table 3.5 Pore and surface characteristics of catechol-carrying CPLs and their PMCs

| Sample[a]	Theoretical metal content (wt%)	Actual metal content (wt%)	S_{BET} (m^2 g^{-1})	Total pore volume (cm^3 g^{-1})	Dominant DFT-calcd pore diameter (Å)
CPL-1			1050	0.41	12 ± 2
Mg-PMC-1	6.3	6.1	610	0.17	9 ± 2
Mn-PMC-1	12.8	10.9	600	0.16	9 ± 2
CPL-2			617	0.25	12 ± 2
Mg-PMC-2	10.9	10.6	205	0.08	11 ± 2
Mn-PMC-2	23.8	21.8	200	0.08	11 ± 2
Cu-PMC-2	24.3	21.3	195	0.08	12 ± 2

[a]The ratio of catechol-carrying monomer and comonomer is 2:1 for CPL-1 and 1:1 for CPL-2
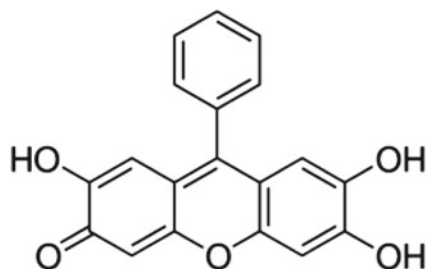
Chiral Ti-PMC was synthesized by the interaction of Ti(OiPr)$_4$ with a PEG bearing BINOL ligand, where BINOL is 1,1′-bi-2-naphtol [216].
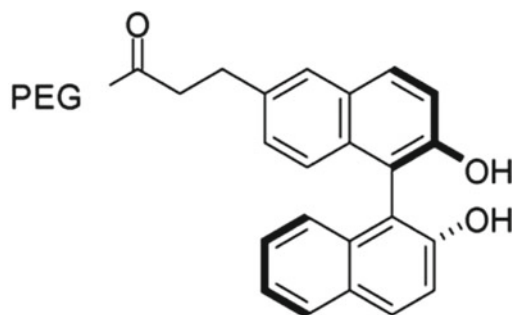
Of interest are highly porous chiral cross-linked CPLs based on the 1,10-binaphthyl building blocks with surface areas of 689 to 974 m^2 g^{-1} and pore volumes of 0.87 to 1.23 cm^3 g^{-1} [217]. The CPLs containing chiral dihydroxy functionalities were treated with $Ti(O^iPr)_4$ to generate chiral Lewis acid catalysts for the asymmetric diethyl zinc addition to aldehydes.
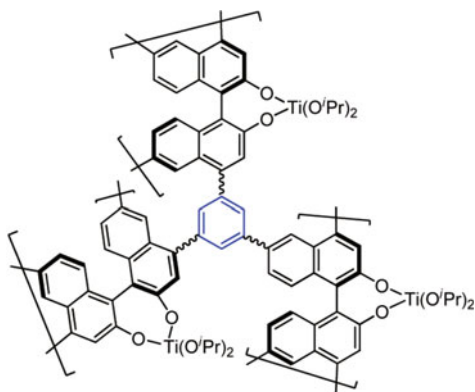
3.2.2   β-Diketonates

The β-diketone-based achiral CPL synthesized by the polymerization of 3,7-dibromo-2,8-dimethoxy-5,5-dioctyl-5H-dibenzo[b,d]silole with (Z)-1,3-bis(4-ethynylphenyl) 23-hydroxyprop-en-1-one can chelate with $Eu(L)_x$ [L^- = 4,4,4-trifluoro-1-(thiophen-2-yl)butane-1,3-dionate anion, x = 1, 2, 3] to afford corresponding Eu(III)-PMC as a yellow solid in 87% yield [218]. Moreover, the PMC with different L anion ligand content could be prepared by similar reaction procedures while the molar ratios of

[Eu]:[HL] were changed from 1:1 to 1:3 (x = 1, 2, 3). The content of Eu(L)$_x$ moiety is 87% for PMC (x = 2), indicating that the β-diketone fragment in the main chain of CPL does not undertake the complete chelation reaction with Eu(III) [219, 220]. The content of Eu(III) in PMC is 12.1%.
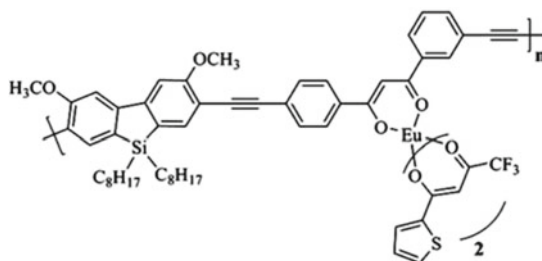

The pendant β-diketonate fragments of the CPL based on vinyltriphenylamine, vinyloxadiazole, and vinyl β-diketonate monomers allows to preparing Pt-PMCs [221]. Of interest is the study of the amino- and metal-ion sensing capability of CPLs based on 9-anthryl-MMA (hydrophobic, fluorescent) and 2-(acetoacetoxy) ethyl methacrylate (hydrophobic, metal chelating) [222]. For example, the Fe(III) cations have substantial effect on the fluorescence of the anthracene fragments due to chelation of the β-ketoester units of the 2-(acetoacetoxy)ethyl methacrylate fragment with the cations. On FeCl$_3$·6H$_2$O addition in the solution, a color change was observed within a few seconds from light yellow to deep wine red, attributed to the chelation between the Fe(III) ion and the β-ketoester groups. Presumably, the octahedral structure of the ferric salt preserved and only the four water molecules adjacent to the iron atoms are replaced by two chelating β-ketoester ligands.

It should be noted the CPL (polybenzimidazole containing β-diketone side fragment) and its corresponding PMCs of Dy(III) and Gd(III) [223]. The study of the influence of different second chelating ligands such as phen and bpy on the emission spectra of PMC-Dy and PMC-Gd showed that varying the second ligand does not substantially affect the characteristic emission of PMC.

3.2.3 Metal Chelates of Salicylaldehyde Type Ligands

Of interest is the preparation of PMC-Cu(II), PMC-Zn(II) and PMC-Co(II) based on oligosalicylaldehyde with the 1:2 M:L ratio, in which the formation of metal chelates proceeds through –OH and –CHO groups [224].
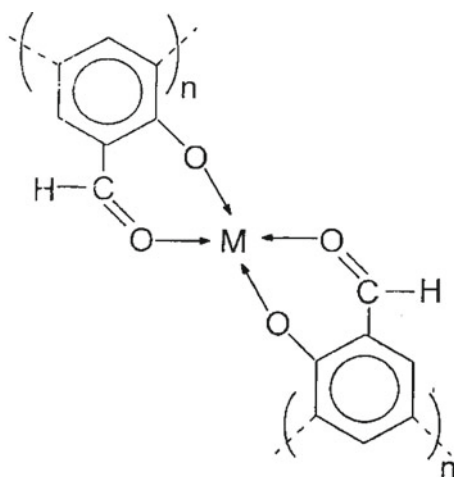
The similar PMCs were synthesized by the interaction of polyacryloyl salicy-laldehyde [140] and poly [5-(4-acryloyloxyphenylazo)-salicylaldehyde] with metal ions [225]. Elemental analysis of PMCs suggests that the M:L ratio is about 1:2. The chelation proceeded through oxygen of ligand and electronic and EPR spectra exhibited octahedral structure of the Ni(II), Cr(III), and Cr(VI) chelates, and square-planar structure of the Cu(II) chelate.
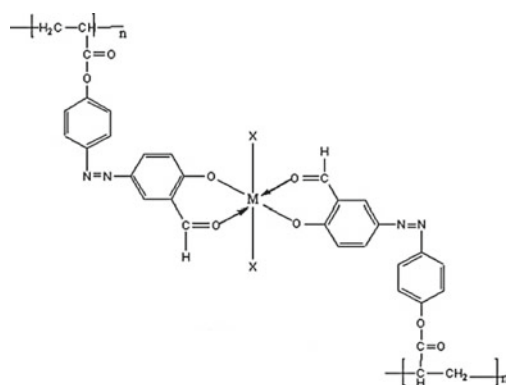
X = H$_2$O for Cr(III), Ni(II), Cr(VI)

Of interest are PMCs based on poly [(2-hydroxy-4-methoxybenzophenone)1,4-butylene] and lanthanide ions. Among these ions, La(III) ion has higher chelation by the CPL [226]. In the PMC, phenolic and carbonyl fragments are involved in metal chelation.
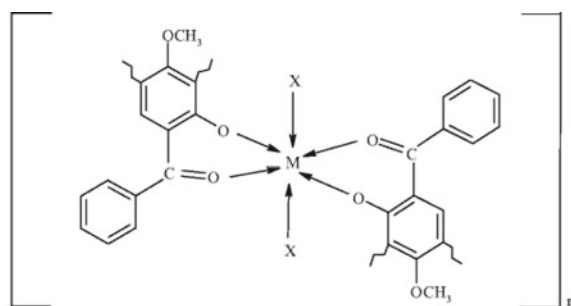
M = La(III), Pr(III), Sm(III), Gd(III), Tb(III) and Dy(III)
X = H_2O

3.2.4 Metal Chelates Based on Salicylic Acid Containing Polymers

There are numerous reports about the study of chelation capacity of various salicylic acid-containing CPLs, in particular, the phenolic-formaldehyde polymers, poly (2,4-dihydroxybenzoic acid-3,5-diylmethylene) and poly (2-hydroxybenzoic acid-3,5-diylmethylene), [227] as well as CPLs based on salicylic acid, formaldehyde and resorcinol [228, 229] and diaminonaphthalene [230], m-cresol [231] or en [232]. The maximum adsorption capacity of the CPL followed the order Pb(II) < Cd(II) < Cu (II) < Ni(II), which was related to the stability of chelation between carboxylic acid and phenolic active sites with metal ions.

The reaction between salicylic acid-formaldehyde polymer and diazonium salt of aniline [233], p-anisidine [234] or p-toluidine [235] yielded a CPLs, which after the treatment with metal ions form their PMCs.
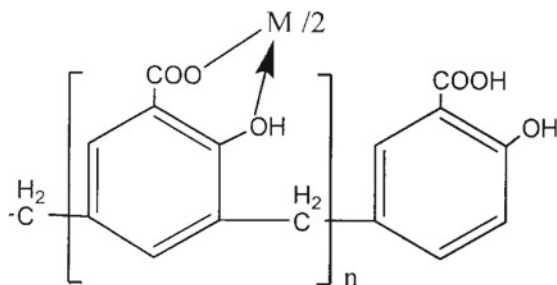
PMCs based on 3-carboxy-4-hydroxy acetophenone which was polycondensed with sodium hydrosulfide and formaldehyde with Cu(II), Fe(III), Co(II), Ni(II), UO_2(II) ions were synthesized [236]. In this case, the M:L ratio is also equal to 1:2 for the PMCs of all the divalent metals and is equal to 1:3 for the PMCs of Fe(III). It is important that the chelation capacity of all CPLs depends on the size of the CPL.

It should be noted the PMC based on salicylic acid loaded Amberlite XAD-4 [237–240].

PMC-Eu(III) based on CPL with salicylic acid chelating fragment (Scheme 3.27) [241] has substantial effect on the fluorescence emission of Eu(III) ion with the apparent "antenna effect". It is important that binary intrachain chelate PMC-Eu(III) is formed in the diluted solution of the CPL, and when a phen is added as an additional ligand, the ternary chelate PMC-Eu(III)-phen was formed.

Of interest are the rare earth PMCs of O,O-type prepared by the chelation of lanthanide ions by side chelating fragments of CPL [242–246]. The chlorosulfonated PS containing 4-aminosalicylic acid fragments forms octahedral complexes of Co(II), Ni(II), or Cu(II) ions through the carboxylato- and phenolato-O atoms [247, 248].
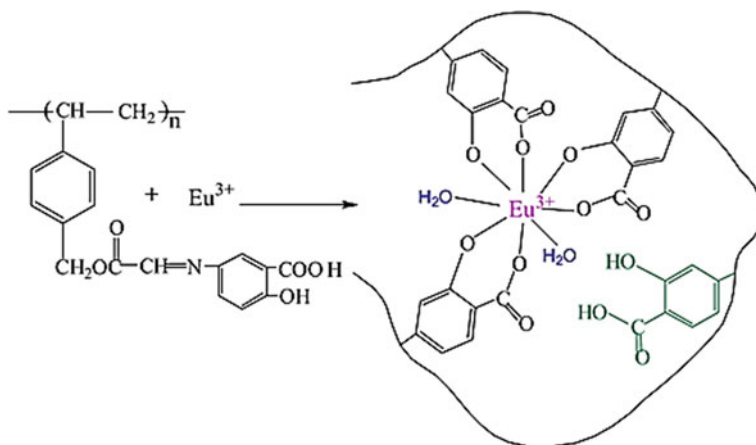
Scheme 3.27 The synthesis of PMC-Eu(III)

M = Cu(II), Ni(II) or Co(II)
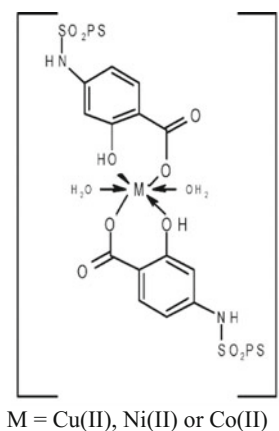
PS, modified salicylic acid adsorbs Pb(II) and Cu(II) ions quant. 0.13 mmol g^{-1} and 0.11 mmol g^{-1}, respectively. When the ion concentration <0.271 mmol L^{-1}, adsorption mechanism is ion exchange, and if it is >0.378 mmol L^{-1}, adsorption occurs through the formation of chelates [249].

The chelation behavior of poly(2-hydroxy-4-acryloyloxybenzophenone) (**I**) and its cross-linked CPLs with known amounts of the cross-linker DVB (4 mol% of DVB for **II**, 8 mol% of DVB for **III**, and 16 mol 16% of DVB for **IV**) toward the divalent metal ions was investigated [250]. The extent of metal-ion uptake by these CPLs toward the investigated divalent metal ions followed the order **I > II > III > IV**. The results reveal that the chelation process was highly affected by the relative amount of cross-linker; **I** (0% crosslinking) displayed the highest metal chelation capacity, whereas **IV** (16% crosslinking) showed the lowest metal chelation capacity. The decrease in the metal chelation capacity with crosslinking may be explained by the presence of steric hindrance of the DVB cross-linker, which hindered complete chelation with metal ions.

The PMCs were obtained by the reaction of chloroform solution of CPLs based on 3-acetyl-4-hydroxyphenyl acrylate with aqueous solution of Cu(II)/Ni(II) acetates [251]. The ratio of M:L was approximately 1:2, indicating metal chelation through two polymeric chains. The PMCs have a distorted octahedral and square planar structure for PMC-Ni(II) and PMC-Cu(II), respectively.
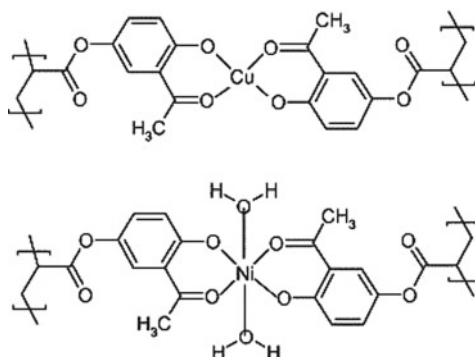
The similar PMCs were prepared by the metal chelation by CPL based on 2,4-dihydroxyacetophenone, biuret and formaldehyde [252]. The CPLs showed highest selectivity for Fe(III) and Cu(II) ions than for Ni(II), Co(II), Zn(II), Cd(II) and Pb(II) ions.

The CPLs synthesized by condensation of the derivatives of 2-hydroxybenzophenone with 1,2-propylene glycol [253], ethane diol [254] or oxamide with formaldehyde [255] form 1:2 M:L PMCs with some metal ions. In these PMCs, phenolic and carbonyl fragments take part in metal chelation.
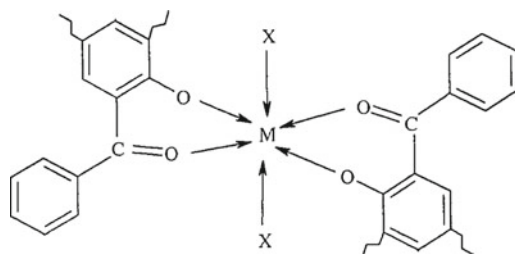
The potential in sensing and chelation properties of morin covalently attached to Merrifield's resin for Cu(II), Pb(II), Zn(II) and Cd(II) is outlined (Scheme 3.28) [256]. It was observed that CPL retained all the studied metals with high efficiency (90–95%). The fluorescence emission increased upon Zn(II) and Cd(II) interaction with a higher sensitivity for Zn(II). In contrast, fluorescence quenching was observed when Cu(II) and Pb(II) were injected and reacted with the CPL. These results confirm that the outermost electron layer structure of the metal cation was an important factor for quenching efficiency. In contrast to flavonoids, in morin the 3-hydroxy group (ring C) and the 2-hydroxy group in ring B have been proposed for metal chelation. Upon immobilization, these two hydroxy groups remained free for metal chelation without steric hindering.
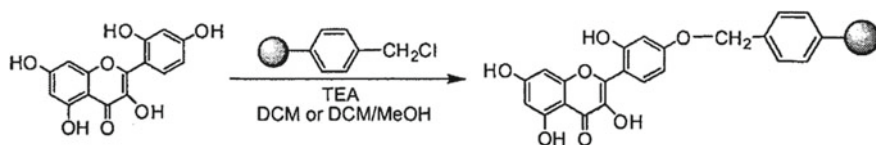
Scheme 3.28 Morin immobilization

3.2.5 Features of Metal Chelation with Spyropyran-Containing Ligands

SPs are one of the most popular classes of photochromic compounds that change their optical and structural properties in response to external inputs such as metal ions, making them ideal molecules for the fabrication of stimuli-responsive materials [257, 258]. In order to study the influence of increased chelation in SP-containing copolymers, two derivatives were used: SP methacrylate and SP methacrylate with a methoxy substituent in the 8′ position of the benzopyran ring. Additionally, the comonomer with which SP was polymerized is also varied between MMA and 2,2,2-trifluoroethyl methacrylate to tune the colorimetric response. In this system, the photoinduced conversion of SP to MC, as well as the MC–M(II) interaction occurs (Scheme 3.29). It is important that each metal ion gives rise to a unique colorimetric response for the various SP-containing CPL.

Upon chelation with each divalent metal ion, there is a decrease in the long wavelength absorbance band (λ_{max} at 600 nm), accompanied by a hypsochromic shift in absorbance maxima, that is dependent upon the metal ion nature. The MC–Fe(II), MC–Cu(II), and MC–Zn(II) complexes have very similar absorbance bands of $\lambda_{max} = 501$, 506 and 512 nm, respectively. The MC–Co(II) and MC–Ni(II) complexes have smaller hypsochromic shifts of 69 nm ($\lambda_{max} = 531$ nm) and 31 nm
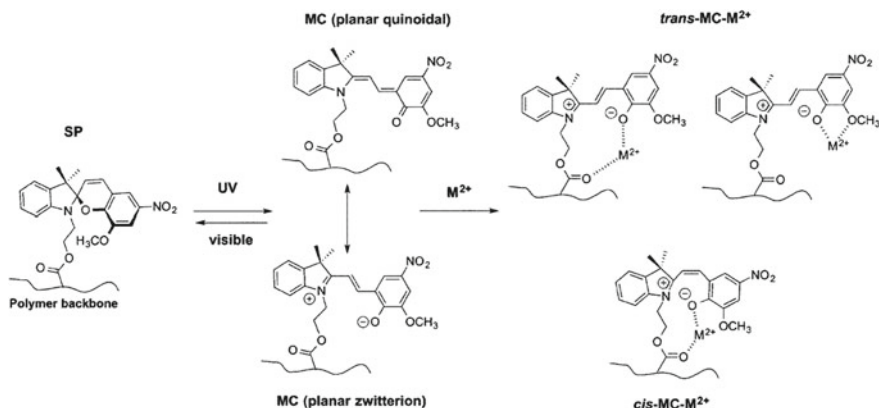
Scheme 3.29 Scheme of synthesis of the polymer-anchored MC-metal complexes

Fig. 3.35 SP monomer
electrochemical
polymerization and the
formation of MC–Co(II)
complex
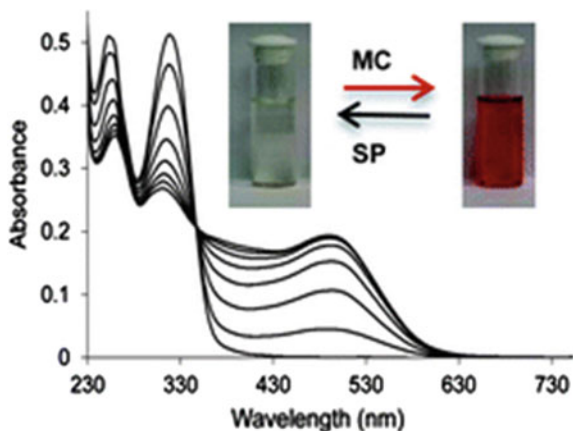
(λ_{max} = 569 nm), respectively. This shift to higher energy accompanying binding is
attributed to the disruption of planarity of the *trans*-MC^{2+} that occurs upon chelation.

Due the known metal coordination capabilities of MC, introduction of cobalt
ions into the electropolymerization of a SP fragment covalently linked between two
alkoxythiophene units led to an enhancement of the conductivity, morphology and
optical properties of the polymer films (Fig. 3.35) [259]. The presence of the conju-
gated MC in the polymer presented the opportunity to influence the polymer
properties by metal ion coordination. In particular, the addition of Co(II) to the MC
solution changes the spectrum with a decrease of the 490 nm peak and the appear-
ance of a low intensity peak at 415 nm. Apparently, the formation of a MC–Co(II)
complex is presumably a result of the interaction of two neighboring MC phenolate
groups with Co(II). However, the intensity of the 215 and 315 nm peaks, ascribed
to the SP, increased upon Co(II) addition, suggesting that Co(II) not only com-
plexed to MC but also augmented SP formation. Therefore, it is likely that the MC–
Co(II) complex is not particularly strong and the resulting solution is an equilibrium
mixture of SP/MC–Co(II).

It should be noted SP-containing microstructured optical fiber as the sensing
platform for the selective, dual sensor for Ca(II) and Cd(II) capable of detection at
100 pM concentrations [260] as well as SP-carrying polymer brushes as reversible,
photo switchable optical sensors that show selectivity for different metal ions [261].

## 3.2.6   Metal Chelates with Anthranilic Acid

Chelating ligands with oxygen and nitrogen as donor atoms are important class of
the CPLs. Thus, PMCs of few transition metals were prepared using the CPLs

formed from the polymerization of anthranilic acid and formaldehyde with thiosemi-carbazide [262], thiourea [263] or *o*-toluidine [264].
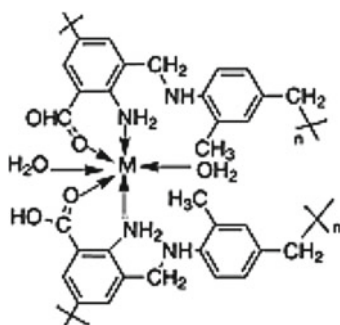
The M:L ratio in all the PMCs was found to be 1:2 and all the metal chelates have an octahedral geometry. The surface of the CPL is a woolen-like soft appearance with a dispersed nature. A close-packed arrangement is observed in the surface of the CPL. However, these arrangements are rigid with a lot of space in which the reactivity of chelating fragments is strongly obscured in the CPL. After the metal chelation takes place in the CPL, the surface of the PMCs is quite different from that of the CPL. The images of the PMCs show a rigid and more close-packed structure due to metal chelation. The image of the PMC-Zn clearly confirms the absence of any voids or holes. However, small holes presented in the PMC-Cu may be due to air voids, but it shows a stiff morphology (close-packed). The particle size of both CPL and PMCs is 1 μm at the surface.

Poly (anthranilic acid) and its copolymer with aniline were synthesized by chemical polymerization without or in the presence of different metal ions [265]. The amount of metal ions incorporated into the CPL during the polymerization varied between 0.01 and 0.4%. It is important that the percentage of metal ions in the CPL was higher in the copolymers than in the homopolymers. Moreover, when the acid/aniline ratio (f_1) increases, the percentage of Ni(II) and Co(II) increases. This could be attributed to a higher content of the 2-aminobenzoic acid fragments at the backbone as the f_1 rises. Besides, there is a relationship between the torsion angle of adjacent fragments ($\pi - \pi^*$ transition) and the amount of Cu(II) ions in the PMC. When the percentage of Cu(II) in the PMC increases the peak of λ_{max} of the benzenoid ring is shifted to a lower wavelength. Thus, it is possible to attribute the higher CPL metal ion interactions to the 2-aminobenzoic acid fragments. By increasing the presence of aniline, these interactions would be not favored.
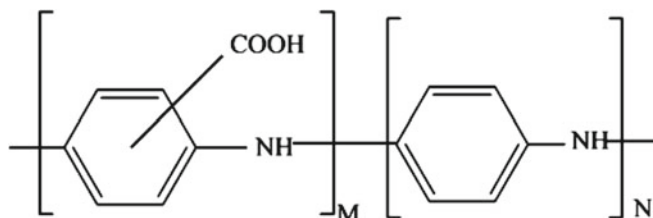
It should be noted the study of chelation ability of homo- and copolymers of
o-N-methacryloylaminobenzoic acid [266].

3.2.7 Polymeric o-Aminophenol and Its Derivatives in the Synthesis of Metal Chelates

Of interest is PMC-Cu prepared by the chelation of copper chloride with CPL
derived from *o*-aminophenol (Scheme 3.30) [267]. The square-planar spatial orga-
nization was established for PMC-Cu(II). The metal content in the PMC suggests
2.23 wt% Cu.

The comparison of SEM of CPL and PMC clearly indicates the morphological
change during metal chelation. Energy dispersive X-ray analysis (EDAX) data con-
firmed also the loading of Cu(II) ion on the CPL surface (Fig. 3.36a, b).
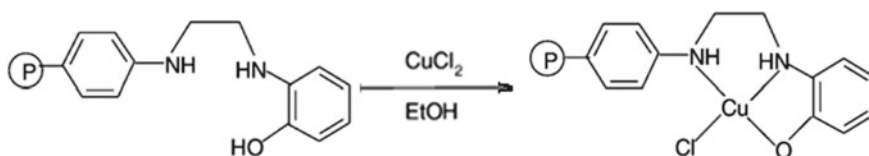
Scheme 3.30 Synthesis of polymer anchored Cu(II) chelate
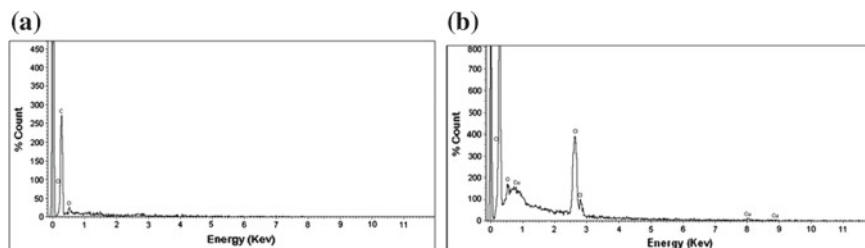
Fig. 3.36 EDAX data of CPL (**a**) and PMC-Cu(II) (**b**)

The similar PMCs were synthesized with CPLs based on *o*-aminophenol, formalde-hyde and urea [268] or melamine [269]. It is important that phenolic (–OH) and amino (–NH$_2$) fragments of CPL play a determining role in the chelation process.
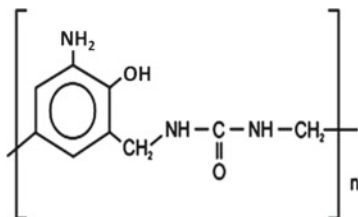
PMCs-Cr(III) were synthesized by the reaction of metal ion with azomethine CPLs based on polymer-supported 4-benzyloxybenzaldehyde, *o*-aminophenol, 2-amino-4-chlorophenol or 2-amino-4-methyl-phenol [270]. Octahedral geometry was proposed for azomethine PMC-Cr(III) according to magnetic susceptibility data. It is interesting that the PMCs had moderate or high antibacterial and antifungal activity.

X = -H, -Cl, -CH$_3$
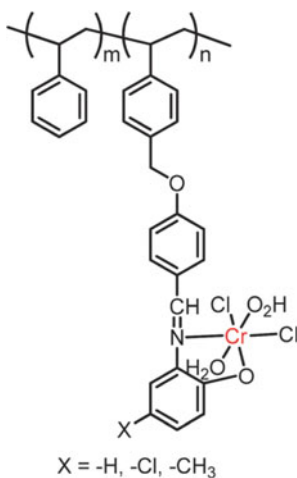
It should be noted PMC-Cu based on poly (2-hydroxyphenyliminomethyl-phenol) [271].
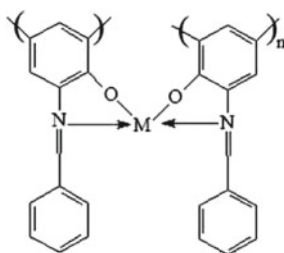
CPL based on PCD functionalized by pyridylazo-β-naphthol has been synthesized and its chelation properties toward some metal ions have been investigated [272, 273]. The chelation capacity of CPL is 7.5 mg g^{-1} at optimum pH and the CPL showed rapid kinetic adsorption. In particular, the adsorption equilibrium of Cd(II) on synthesized CPL was achieved just in 15 min.

PMCs were obtained when the DMF solution of the CPL based on 1-(4-hydroxyphenylazo)-2-naphthol and formaldehyde was reacted with Cu(II)/Ni(II) ions [274]. The metal chelation proceeds through the oxygen of the phenolic -OH group and nitrogen of the azo fragment.

M = Cu(II), Ni(II) (For Ni X = H$_2$O)
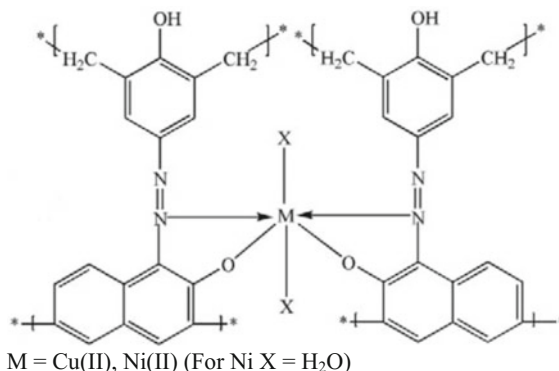
3.2.8 Specifics of Metal Chelation with Schiff Bases

Schiff bases are the most versatile and thoroughly studied ligands in coordination chemistry. Although metal chelates with poly (Schiff bases) known relatively long time, research in this direction is still relevant and the number of original works, especially with *o*-hydroxyazomethines, continuously growing. Poly (Schiff bases) metal chelates are studied extensively because of their attractive chemical and

physical properties, and their wide-ranging applications in numerous scientific areas. It should be noted that these PMCs have relatively high thermal and chemical stability. Their feature is connected with complete saturation of the coordination vacancies of the transition metal. Besides, polymer-supported Schiff base ligands are easily synthesized and loaded with different metal ions without any difficulty.

It is important that detection of isomeric forms of Schiff base metal chelates even for low molecular weight ligands presents known difficulties, and for Schiff base CPL this problem is almost insoluble. Therefore, usually, only the basic forms of the resulting PMC are analyzed.

Salicylidene Schiff bases have attracted considerable attention because of their facile preparation via salicylaldehyde-amine condensation, easy modification of their steric and electronic properties, and high binding affinity toward various metal ions. As an example, we note the reaction of aminomethylated PS and 2-hydroxyacetanilide in DMF resulting in the formation of PS-anchored monobasic bidentate Schiff base [275]. On the other hand, the reaction of PCS, 3-formylsalicylic acid, en and acacH in DMF produces another PS-anchored dibasic tetradentate Schiff base. Both CPLs react with a number of di-, tri- and hexavalent metal ions to form PS-anchored chelates.

Aminomethylated PS reacts with salicylaldehyde [276], 5-bromo-, 5-methyl-, 5-chloro- [277], and 3-ethoxysalicylaldehyde [278] to produce monobasic bidentate (N,O-donor) PS-anchored Schiff bases. The CPLs upon refluxing with metal the ions in 1:2 molar ratios give PS-anchored chelates. Co(II) and Cu(II) chelates are square-planar; Zn(II) and Cd(II) chelates are tetrahedral; Ni(II), Fe(III), MoO_2(VI) and UO_2(VI) chelates are octahedral.

A polymeric Schiff base prepared by condensation of salicylaldimine, formaldehyde and piperazine form PMCs with transition metal ions [279]. It should be noted that Mn(II)-, Co(II)- and Ni(II)-PMCs have octahedral structure, while Cu(II)- and Zn (II)-PMCs have square planar and tetrahedral structures.

Of interest is a nano-sized Schiff base PMC-Co(II) on cross-linked PAAm (Scheme 3.31) [280].

SEM and transmission electron microscopy (TEM) of the prepared PMC indicate their nano-sized fiber-like structure (Fig. 3.37). It is interesting that the PMC fiber lengths are from 50 to 250 nm in size.
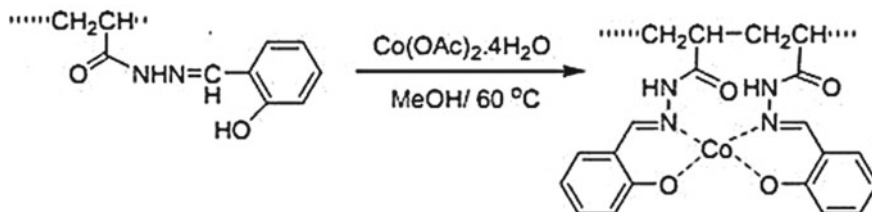
Scheme 3.31 Synthesis of modified PAAm loaded cobalt chelate
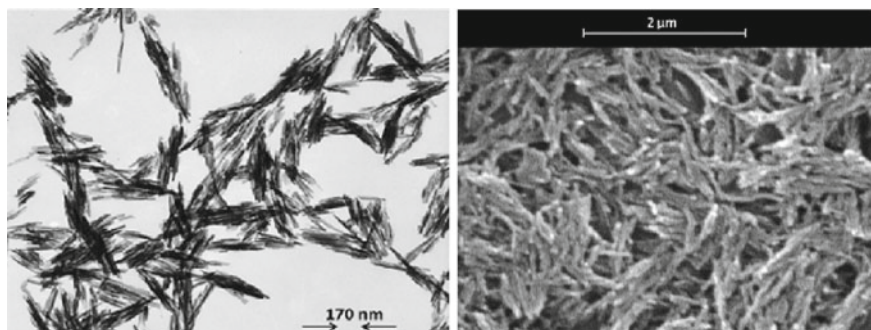
Fig. 3.37 TEM image (left) and SEM image (right) of cross-linked PAAm-anchored Schiff base-cobalt chelate

Acetylenic monomers containing salicylidene Schiff-base groups as well as Schiff-base and hydroxy groups were polymerized to afford the corresponding CPLs with high molecular weights (M_n = 2.6–7.2 × 10^5) in high yields (75–97%) [281]. Analyses indicated that the CPL formed helical structures with a predominantly one-handed screw sense. The addition of metal ions to salicylidene Schiff-base-containing CPLs produced insoluble PMCs through cross-linking as a result of salicylaldimine-metal ion chelation (Fig. 3.38).
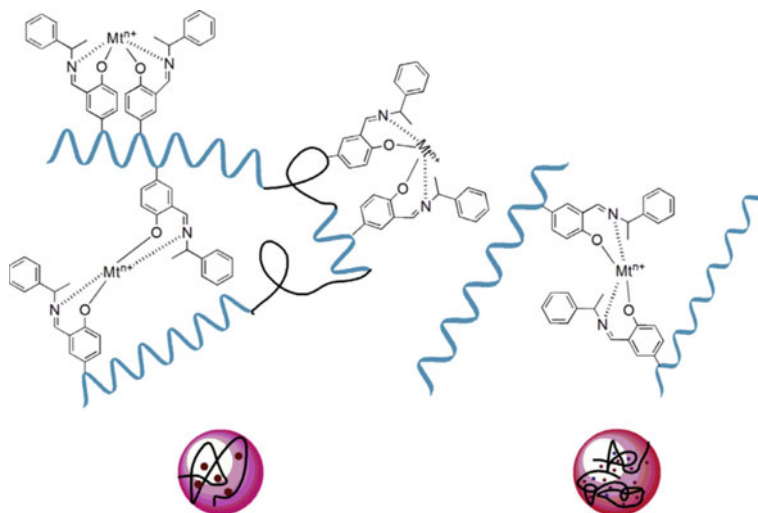
Fig. 3.38 Schematic drawing of PMC formed by the chelation of metal ion to salicylidene Schiff-base-containing CPL

It should be noted the Cu(II)-, Ni(II)-, Co(II)-, Cd(II)-, Mn(II)-, Ca(II)-, and Zn(II)-PMCs based on poly (3-hydroxy-4-((Z)-1-(phenylimino) ethyl) phenyl-3-methylbut-2-enoate) and poly (3-hydroxy-4-((Z)-phenyl(phenylimino)methyl) phenyl-3-methylbut-2-enoate [282]. Thorough investigations of PMCs indicated that functional groups of CPLs from different polymer chains involved in the chelation with the metal ions. However, metal ions do not occupy all the available centers in the CPLs due to steric restrictions. It is important that spectral data of the PMCs in association with magnetic moment suggest a distorted geometry for the metal chelates.

It is shown that the Fe(II), Fe(III), Co(II), Ni(II), and Cu(II) chelation of the azomethine supported on the cross-linked PS varied with the nature of the crosslinking in the PS backbone [283]. The metal chelation followed the order Cu(II) > Co(II) > Ni(II) > Fe(III) > Fe(II) and decreased with increasing hydrophilicity of the crosslinking agent in the polymer support.

Of interest is an immobilized bidentate Schiff base dioxomolybdenum(VI) chelate prepared with cross-linked PCS microspheres as starting carrier via two stepwise reactions with p-hydroxybenzaldehyde and glycine as reagents, respectively, as well as a chelation with $MoO_2(acac)_2$ [284].

Well-defined alternating CPLs with narrow PDI ($M_w/M_n < 1.35$) were synthesized via alternating RAFT copolymerization of p-methoxydiethylene glycol-substituted St and N-(2-salicylaldehyde-aminoethyl) maleimides [285]. It is interesting that alternating CPLs exhibit an excellent selective fluorescence "OFF-ON" response to Zn(II) by inhibiting the PET effect, while the monomer ligand almost has no fluorescence response to Zn(II) due to the PET process. Besides, the CPLs have very fast response (30 s) to Zn(II), 62-fold fluorescence enhancement in aqueous solution and a detection limit of about 0.25 μM.

PMCs with 1:2 M–L ratio were obtained in an alkaline solution of poly (2-hydroxy-4-acryloyloxy-N-phenylbenzylidine) with aqueous solutions of metal ions [286]. The IR spectral data of the PMCs indicated that the metals were chelated with the nitrogen of azomethine fragment and oxygen of the phenolic –OH fragment. The PMC-Cu(II) was square-planar, PMC-Ni(II), -Mn(II), and -Co(II) were octahedral, and PMC-Ca(II), -Cd(II), and -Zn(II) were tetrahedral.

The reaction of MX_n with the Schiff base CPL based on PCS, ethanolamine and 3-formylsalicylic acid leads to PS-supported chelates [287]. It is important that the Ti(III)-, V(III)-, Mn(III)-, Fe(III)-, Ru(II)- and Mo(V)-PMCs are paramagnetic while Mo(VI)- and U(VI)-PMCs are diamagnetic. In addition, all the PMC are octahedral and metal ions are coordinated through C=N of azomethine fragment, C–O of phenolic fragment and C–O of alcoholic fragment.

Reaction of the CPL based on monobasic bidentate ligand 2-(2′-hydroxyphenyl) benzimidazole and the PCS cross-linked with 5% DVB with $VO(acac)_2$, MoO_2 $(acac)_2$ and $Cu(CH_3COO)_2 \cdot H_2O$ gave the corresponding PMCs [288].
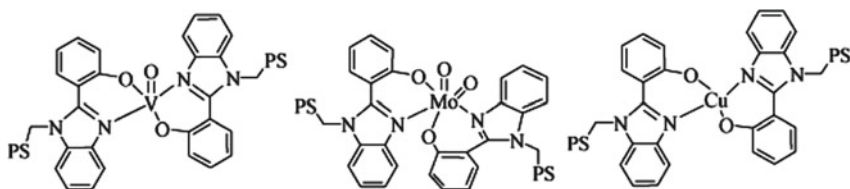
A chiral (S)-BINAM-based fluorescence CPL, where BINAM is 2,2′-binaphthyldiamine, based on (S)-2,2′-binaphthyldiamine and 5,5′-((2,5-dioctyloxy-1,4-phenylene)-bis-(ethyne-2,1-diyl)bis(2-hydroxy-3-(piperidin-1-ylmethyl)-benzaldehyde shows very weak fluorescence, while the chelation with Zn(II) leads to the obvious fluorescence enhancement response (Fig. 3.39) [289].

It should be noted that the BINAM-based chiral CPL can adopt a stable cisoids conformation due to the small groups of two imine substituents. The reversed Cotton effect can be attributed to the increase of the dihedral angle between two naphthalene rings of a binaphthyl molecule from cisoid to transoid conformation after the formation of the Zn(II)-PMC. It is important that the whole CPL backbone reverse need very high energy. However, the chelation between the CPL and Zn(II) is strong enough to cause the conformation reverse. Moreover, the dihedral angle gradually enlarges as the increase of Zn(II) molar ratios from 1:1 to 1:2 (Scheme 3.32), leading to greater Cotton effect change in the case of 1:2 Zn(II)-PMC than that of 1:1 Zn(II)-PMC.

Of interest are another chiral fluorescence CPLs incorporating (S)-2,2′-BINOL and (S)-2,2′-BINAM fragments in the main chain of the polymer backbone [290].

An AB type of clickable monomer, (S)-2-[2-azido-1-phenylethylimino) methyl]-5-propargyloxyphenol, was polymerized to yield a class of main-chain chiral poly (imine-triazole)s through the metal-free click reaction [291].

Fig. 3.39 Selectivity of the CPL (1.0×10^{-5} mol L^{-1} in THF, λ_{ex} = 362 nm, λ_{em} = 414 nm) toward Zn(II) and other metal ions (2.0×10^{-5} mol L^{-1}): relative fluorescence intensity of the chiral PMC
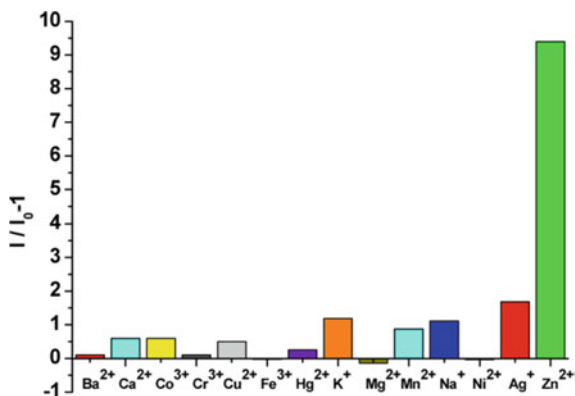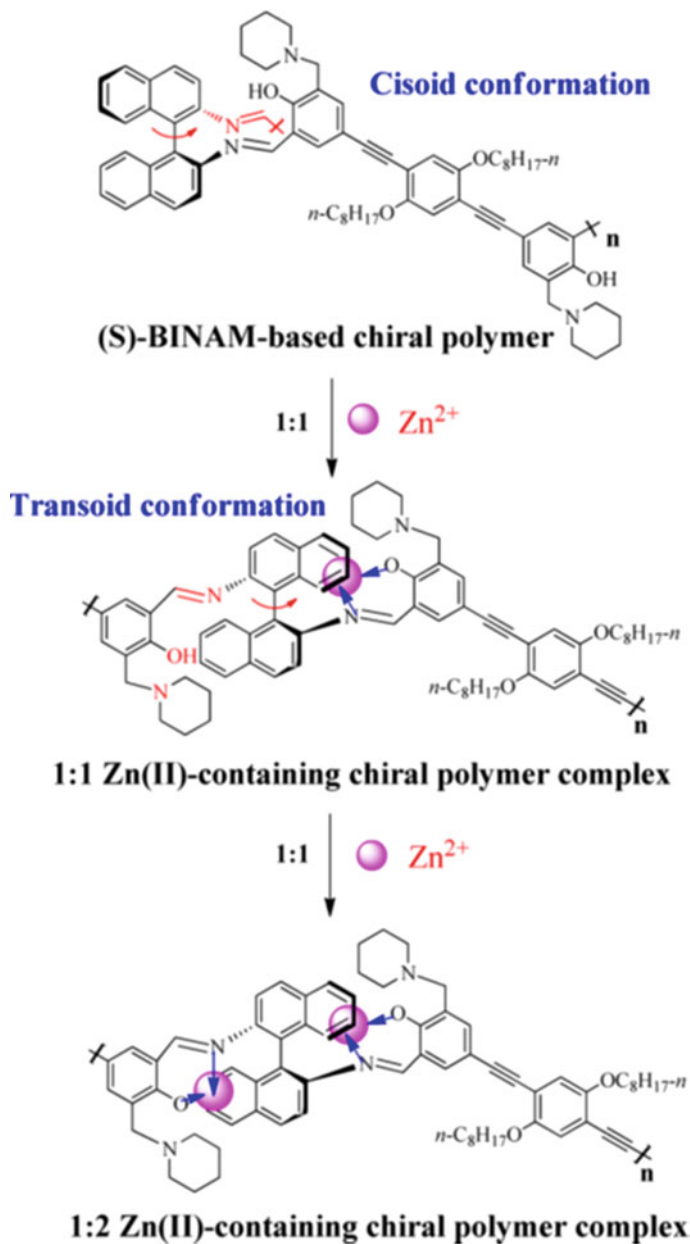
Scheme 3.32 Dihedral angle changes of chiral CPL with the increase of Zn(II) molar ratios
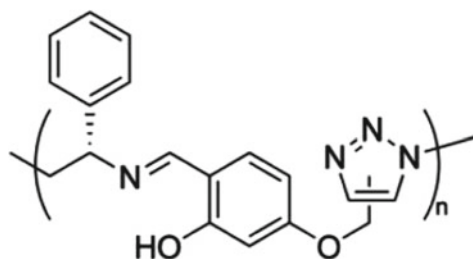
As the chemosensors, these CPLs exhibited a selective "turn-on" fluorescence enhancement response toward Zn(II) ion over other cations in DMSO (Fig. 3.40). Interestingly, the chiral CPLs showed distinctive changes in the CD spectra on chelation with Zn(II), which allowed for the discrimination of this ion in the presence of other species tested including those interfering ions observed in the fluorescent detection.

On account of their pronounced coordinating properties, a number of tridentate Schiff bases have been anchored to the PS matrix. For example, the cross-linked PCS reacts with 3-formylsalicylic acid and salicylhydrazide to form a PS-anchored Schiff base [292]. PMC is formed because of the interaction of the CPL with a number of metal ions. Shifts in band positions of the groups involved in chelation have been utilized to find tridentate ONO donor behavior of CPL. Of interest are also the polymer-supported vanadium chelates with tridentate Schiff bases [293, 294].
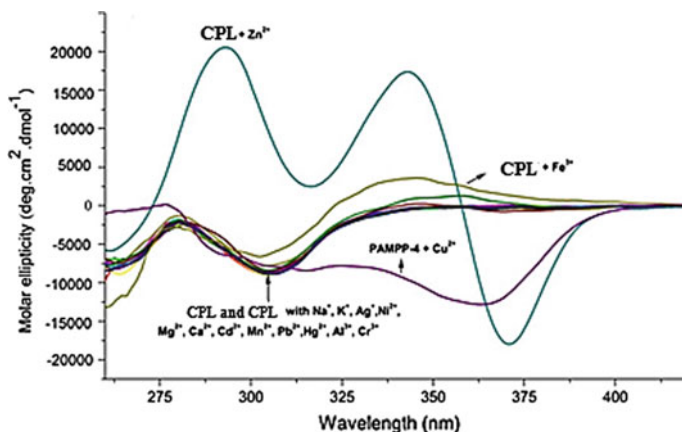
Fig. 3.40 CD responses of CPL to various metal ions in DMSO. Hg(II) as mercury perchlorate and other various metal ions as their nitrate salts were used in the detection
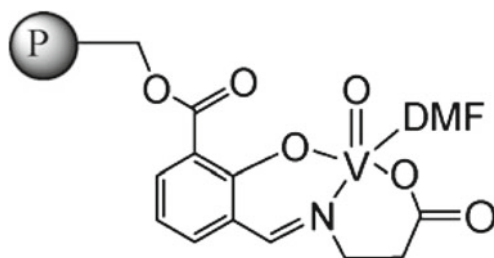
In another interesting example, the polymer-bound Schiff base manganese chelates have been prepared from the tridentate Schiff base CPL, a manganese salt and the second ligand, such as phen, bpy and HQ [295].

It should be noted CPL prepared by suspension copolymerization of 2-methacryloxy-5-methyl-benzophenone and DVB with consequent modification by isonicotinoyl hydrazine [296]. The network polymer based on 4-acryloxybenzaldehyde and DVB as a crosslinking agent was ligated with isonicotinoyl hydrazine [297] or salicyloyl hydrazine [298]. The prepared CPLs form PMC with Cu(II) and Ni(II) ions. It is important that the azomethine nitrogen, isonicotinoyl carbonyl group and chloride anions take part in metal chelation. The EPR spectra of the Cu(II) chelate showed that the M–L bond is covalent in nature. It should be noted the network polymer based on 4-acryloxy acetophenone and DVB which was ligated with benzoyl hydrazine [299]. The CPL was treated with Cu(II) and Fe(II) ions to form the corresponding PMCs. PMC-Cu(II) and PMC-Ni(II) based on copolymers of 4-methacryloxyacetophenone with MMA and following functionalization by incorporating an isonicotinoyl hydrazone fragment were also prepared [300].

The chelation capacity of the CPL based on poly (methyl vinyl ether-*alt*-maleic anhydride), 2-acetylpyridine and 4-aminobenzoic hydrazide for the Cu(II), Cd(II), Cr(III), Ni(II) and Co(II) ions was found in the range 29.95–157.25 mg g^{-1} [301]. It should be noted that the adsorption of metal ions onto CPL is driven by entropy [302].

M = Cu(II), Cd(II), Cr(III), Ni(II), Co(II).
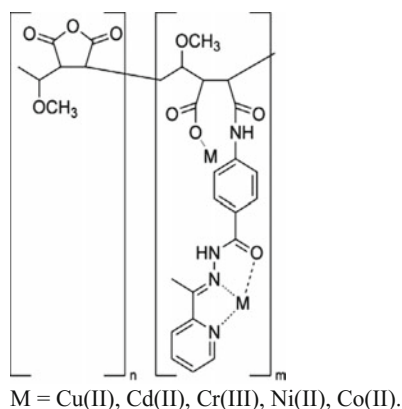
It should be noted PMC of 5-vinyl salicylidene anthranilic acid with europium, chromium and iron chlorides [303]. It is important that spectrophotometric studies proved the use of these CPLs for the microdetermination of Eu(III) ion in solutions. Besides, the spectral feature of PMC indicates the metal coordination with phenolic oxygen, carbonyl and azomethine groups.

M = Ni(II) and Cd(II)
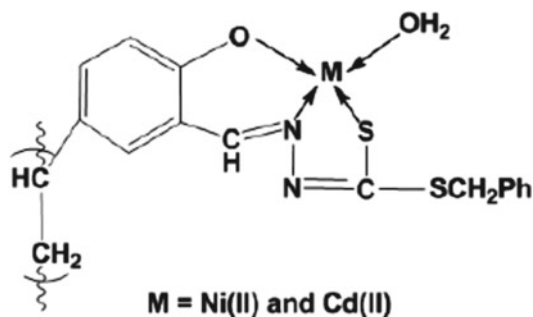
The determining factors of the metal chelation of the CPL prepared by the interaction of Schiff bases derived from 2-aminophenol, 2-hydroxy-5-chloroaniline and terephthalaldehyde with formaldehyde are the spatial organization of the CPL, the metal nature and the process conditions [304].
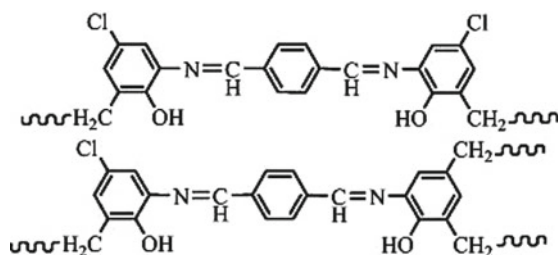
The PMCs were prepared by the reaction of the azomethine CPLs, poly (N,N′-bis(4-hydroxybenzylidene)-1,4-phenylenediamine) (**P1**) and poly(N,N′-bis(4-hydroxysalicylidene)-1,4-phenylenediamine) (**P2**), with Co(II), Mn(II) and Ru(III) salts (Fig. 3.41) [305].

It should be noted PMCs synthesized by the interaction of Cu(II) and Ni(II) ions with CPLs based on furfuraldehyde or formaldehyde and a phenolic Schiff base derived from 4,4′-diaminodiphenylmethane and *o*-hydroxyacetophenone [306]. It is important that the nature of the CPL has a significant impact on the metal chelation. In particular, the furfuraldehyde-based CPL was more effective in the metal chelation than the formaldehyde-based CPL.

Condensation of renewable resources-based monomer divanillin with alkyl diamines gives Schiff base CPL with DP ~ 25–32 in 88–95% yield [307]. CPL is shown to chelate with Cu(II), Fe(II), and Co(II) ions.
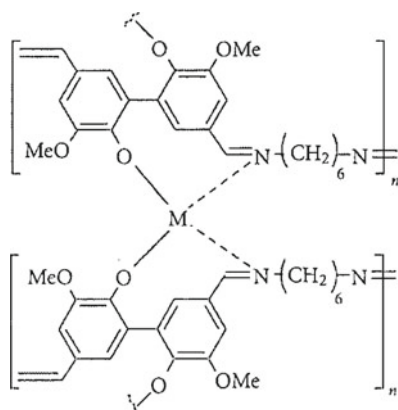
Metal chelates of a conjugated aromatic oligo(azomethine) derivative synthesized by oxidative polycondensation of 1,4-bis[(2-hydroxyphenyl) methylene] phenylenediamine were prepared with metal salts of Fe, Co, Ni, Cu, Zn, Cd, Mn, Cr, Pb and Hg (Scheme 3.33) [308]. Elemental analyses of PMCs suggested that the ratio of M:L is 1:1.

(a)   **(b)**

M= Co(II), Mn(II) and Ru(III); L = H$_2$O for Co(II) and Mn(II); L = Cl$^-$ for Ru(III)
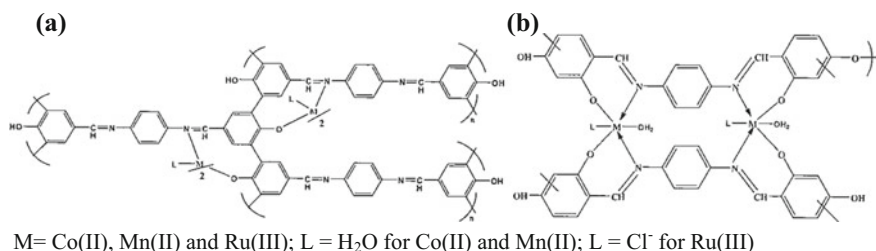
Fig. 3.41 The proposed structures of **P1**-metal chelate (**a**) and **P2**-metal chelates (**b**)
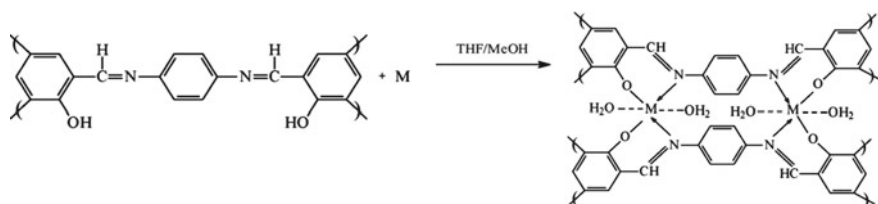
Scheme 3.33 The chelation mechanism of the oligomer with some metal ions

Another interesting CPL is N,O-containing chelating ligand poly(1-amino-5-chloroanthraquinone), which was developed as a fluorescent sensor for the determination of Fe(III) (Scheme 3.34) [309]. The CPL exhibited remarkably high sensitivity toward Fe(III) since the fluorescence of the CPL could be significantly quenched even though trace Fe(III) was added. It is interesting that the molar ratio of Fe(III) to CPL chelating fragments is approximately 1:5 at the complexing leap point. In other words, one ferric ion can cause remarkable fluorescence quenching of approximately five chelating fragments of CPL, probably due to the "molecular wire effect" for conjugated CPL [82].

Scheme 3.34 Synthesis of poly(1-amino-5-chloroanthraquinone)

3.2.9   Salen and Salphen Types of Metal Chelates

Numerous studies are devoted to salen and salphen types of PMCs. Thus, the flexible salen monomer **1**, with one ethylene glycol unit as the spacer, was copolymerized with DVB, yielding a highly rigid polymer-supported salen **2**, which, in turn, was reacted to Co(II) ions to form Co(II)-salen PMC **3** (Scheme 3.35) [310]. It is important that Co(II)-salen PMC can be oxidized to the Co(III)-salen PMC under the action lutidinium SbF_6.

In another interesting example, the (salen)Co chelate was prepared as a mixture of cyclic oligomers in a short, chromatography free synthesis from inexpensive, commercially available precursors [311].
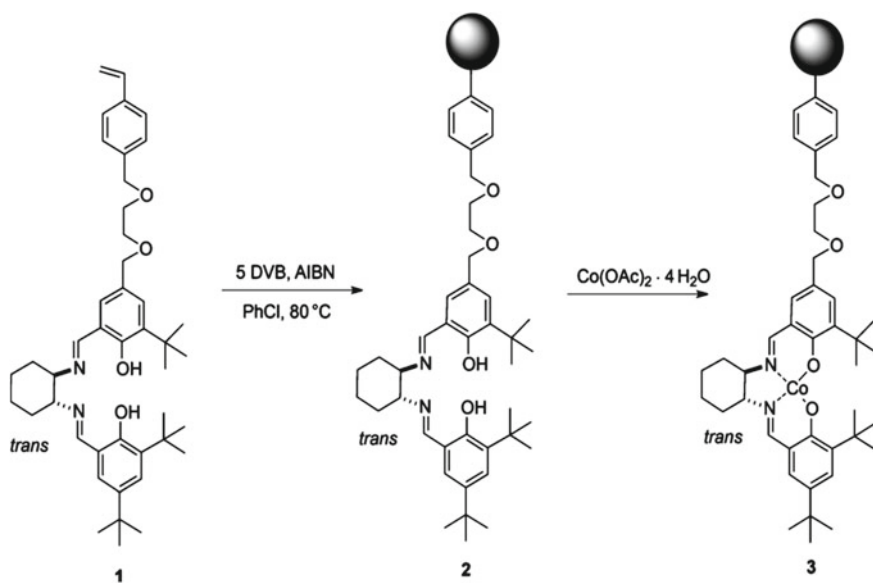
Scheme 3.35   Synthesis of Co(II)-salen PMC
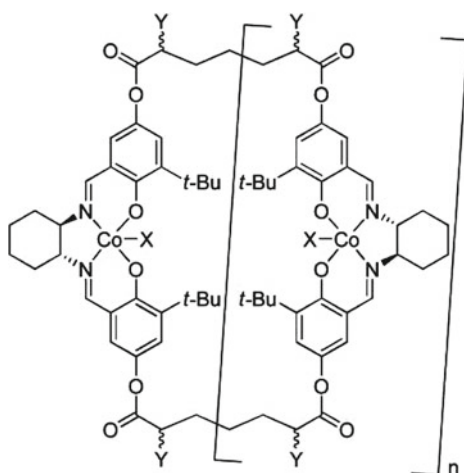
Of the interest is the methacrylate-based CPLs prepared by the interaction of 3-hydroxy-4-acetylphenyl methacrylate with amines (e.g., en, propylenediamine, and *o*-phenylenediamine), which possess appreciable selectivity for Pb(II) and Hg (II) compared with Cd(II) and Cr(VI) [312]. It is important that in this case the chelation ability of the CPLs towards the metal ions is a sensitive function of the substituent nature on the nitrogen atom.

Among the salen type polycondensation PMCs, we note the chelates prepared by incorporating the transition metal ions into polyazomethine-urethane-urea synthesized from 5,5′-methylene-bissalicylaldehyde by reaction with a urethane prepolymer based on PE adipate diol, hexamethylene diisocyanate and en [313]. It should be noted Cr(III)-, Mn(III)-, Fe(III)-, Ti(III)-, VO(IV)-, Zr(IV)-, MoO$_2$(VI)- and UO$_2$(VI)-PMCs with azomethine CPL prepared from 4,4′-bis-[(salycylaldehyde-5) azo] biphenyl and 1,3-diaminopropane [314]. Schiff base monomer, 2,3-bis[(2-hydroxy-naphtyl) methylene] diaminopyridine, was oxidized to give its corresponding oligomer which was converted into the PMCs of some divalent metals (Scheme 3.36) [315].

The CPL prepared by the polycondensation reaction of monomeric Schiff base derived from salicylaldehyde and 1,3-diaminopropane with formaldehyde and piperazine was found to form PMCs readily with Mn(II), Co(II), Ni(II), Cu(II), and Zn(II) ions (Scheme 3.37) [316].

The free and polymer-anchored metal chelates were synthesized by the reaction of Ni (II) with unsupported N,N′-bis(2-hydroxy-3-methoxybenzaldehyde) 4-methylbenzene-1,2-diamine or azomethine CPL [317]. The chelation of Ni(II) ion was higher on polymer-supported Schiff base (89.88 wt%) than free Schiff base (86.34 wt%). The structural study reveals that PMC-Ni(II) is square planar in geometry. The same -ONNO- tetradentate Schiff base ligand was used to chelate Zn(II) (Scheme 3.38) [318].
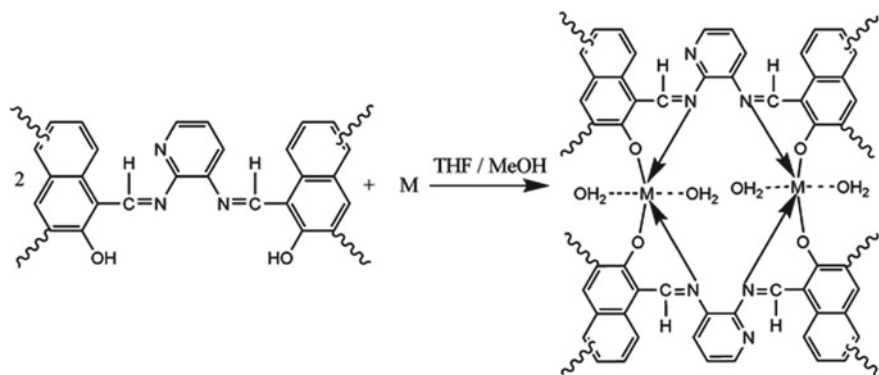
Scheme 3.36 Synthesis of PMCs based on polymeric 2,3-bis[(2-hydroxy-naphtyl) methylene] diaminopyridine
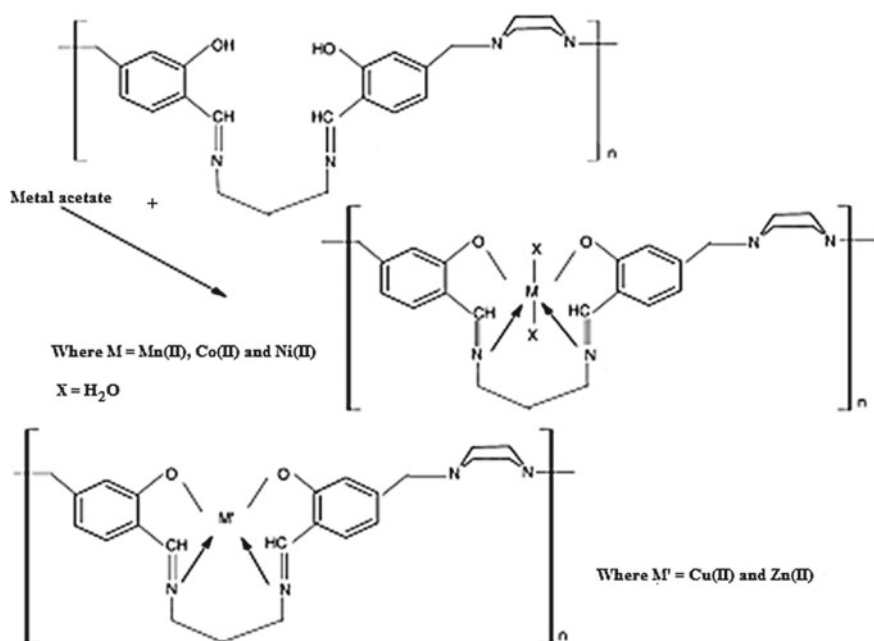
Scheme 3.37 Preparation of PMC using CPL based on Schiff base derived from salicylaldehyde and 1,3-diaminopropane with formaldehyde and piperazine

The structural study of the PMC based on similar poly [N,N′-bis (2-hydroxy-3-methylbenzaldehyde) 4-methylbenzene-1,2-diamine] ligand reveals that Fe(III) chelate has octahedral structure, whereas Co(II) chelate has square planar structure [319].
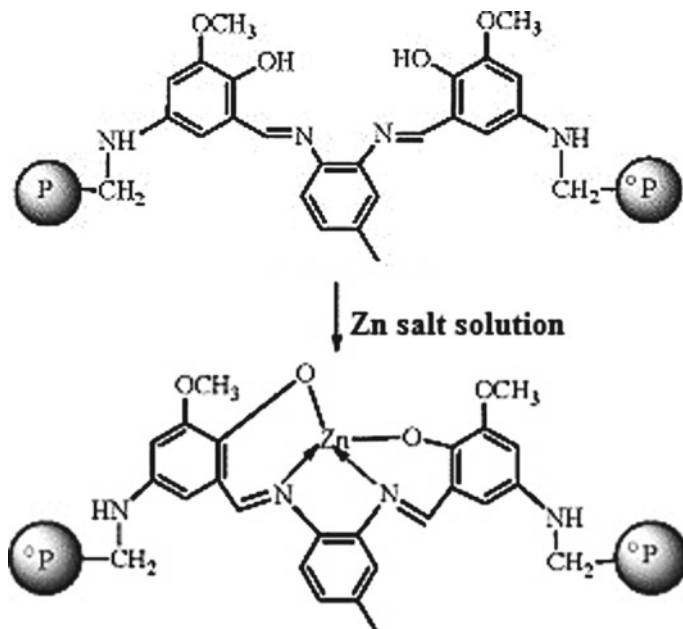
Scheme 3.38 Chelation of zinc ions with polymer-supported Schiff base

An interesting example of salen type PMC is N,N′-1,2-phenylenebis(3-(4-fluorobenzoyl)-2-benzyl-2-thiopseudourea) functionalized PS supported Pd(II) chelate (Fig. 3.42a) [320]. EDAX shows the presence of palladium metal in the PMC (Fig. 3.42b).

The CPL based on cross-linked PCS beads and N,N′-bis(4-amino-o-hydroxy acetophenone) ethylene diamine Schiff base was chelated with Fe(III), Co(II) and Ni(II) ions (Scheme 3.39) [321]. The Schiff base CPL beads showed 85, 86 and 89% chelation for Fe(III), Co(II) and Ni(II) ions, whereas monomer analogue exhibited 80, 88 and 77% chelation, respectively. Both the LMC and PMC have the octahedral structure for Fe(III) chelate and square planar structure for Co(II) and Ni(II) chelates.

Similar results were obtained for PMC-Fe(III), –Co(II), and –Ni(II) with a polymer-bound N,N′-bis(5-amino-o-hydroxy acetophenone) propylenediamine Schiff base [322]. In particular, the chelation of Fe(III), Co(II), and Ni(II) ions on the Schiff base CPL was 83.44, 82.92, and 89.58 wt%, respectively, whereas the unsupported Schiff base showed 82.29, 81.18, and 87.29 wt% chelation of these metal ions. The Fe(III) chelates of the Schiff base showed also octahedral geometry, whereas the Co(II) and Ni (II) chelates were square planar in shape.

PS with 2–20 mol% ethylene glycol dimethacrylate (**I**), 1,4-butanediol dimethacrylate (**II**) and 1,6-hexanediol diacrylate (**III**) were used as polymer supports enable incorporating dien and salicylaldehyde functions, which were then chelated with
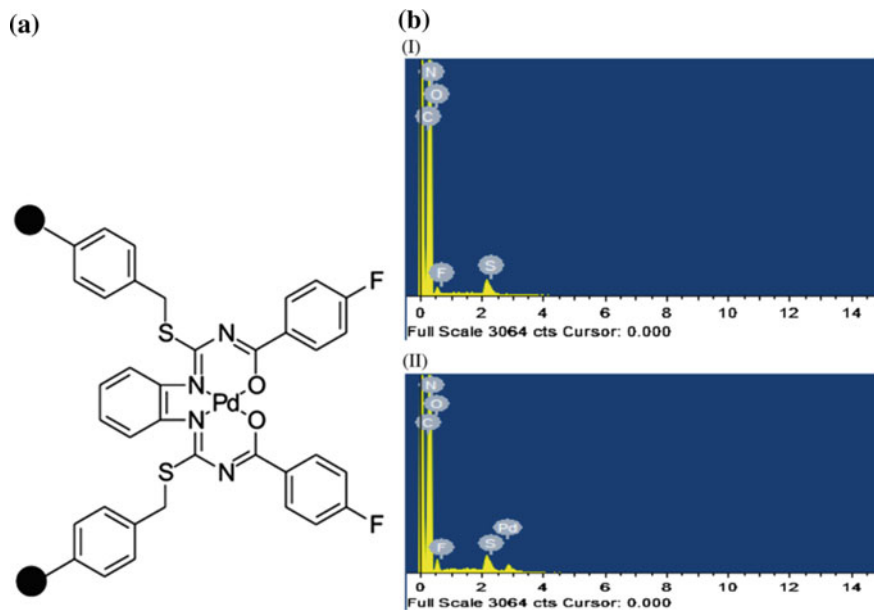
Fig. 3.42   a Structure of PS-supported Pd(II) chelate. **b** EDAX of PS-supported bis-thiopseudourea ligand (I) and PS-supported-Pd(II) chelate (**II**)
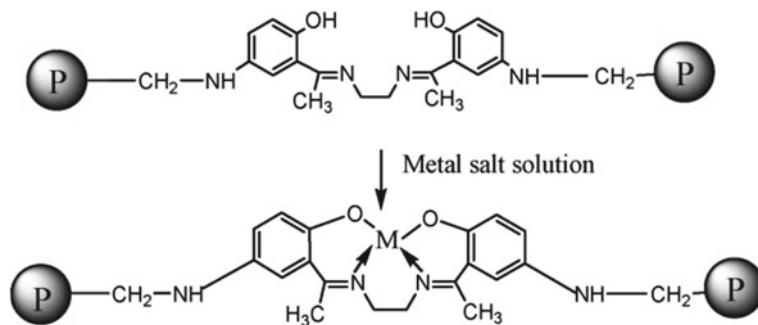
Scheme 3.39   Loading metal ions on Schiff base CPL

Fe(II), Fe(III), Co(II), Ni(II), and Cu(II) ions [323]. The metal chelation decreased in the order: Cu(II) > Co(II) > Ni(II) > Fe(III) > Fe(II), and extent of chelation by the various cross-linked CPL varied with the nature and degree of the crosslinking agent. The EPR data of Cu(II) chelates with differently cross-linked PS-supported Schiff bases are in agreement with the square planar geometry of Cu(II) chelate (Table 3.6). The $g_{\parallel}$ values almost coincide with the values of 2.3, indicating the covalent character of M–L bond. The values of α^2 Cu observed in the range of 0.47–0.56 support also the

Table 3.6 EPR parameters of various cross-linked PS-supported dien-salicylaldehyde Schiff base Cu(II) chelates

Crosslinking agent (mol%)	$g_\parallel$	$g_\perp$	$A_\parallel$	$A_\perp$	α^2	g_{av}
I						
2	2.2006	2.1044	190	126.7	0.5275	2.130
4	2.1890	2.1079	200	123.3	0.5556	2.140
8	2.1931	2.1044	195	128.3	0.5416	2.130
12	2.2080	2.1110	175	120.0	0.4861	2.140
20	2.2006	2.1010	190	130.0	0.5277	2.134
II						
2	2.1860	2.1110	200	126.7	0.5555	2.136
4	2.2010	2.1044	185	128.3	0.5319	2.137
8	2.2040	2.1010	180	130.0	0.4999	2.135
12	2.2156	2.1045	175	128.3	0.4861	2.141
20	2.2006	2.1044	190	126.7	0.5277	2.136
III						
2	2.1890	2.1110	200	121.7	0.5555	2.137
4	2.2120	2.1040	180	126.7	0.4999	2.140
8	2.2120	2.1010	175	123.3	0.4862	2.067
12	2.2160	2.1078	170	130.0	0.4722	2.108
20	2.2010	2.1010	190	123.3	0.5277	2.101

covalent character. Besides, the value of $g_\parallel > g_\perp$ shows the unpaired electron localized in the d_{x2-y2} orbital of Cu(II) ions and spectral characteristics of axial symmetry.

It should be noted Schiff bases 1,6-bis(2-carboxy aldehyde phenoxy) hexane and 1,5-bis(2-carboxy aldehyde phenoxy) pentane of amino methylated PS, which form Pd(II)-PMC [324].
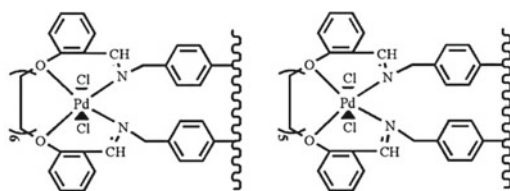
Significant place in the research of Schiff base PMCs takes chiral polymers. Thus, the chiral main chain polymers **1a–b** bonded alternatively with (R,R)-salen and 1,4-dioctyloxybenzene are a selective 'OFF-ON' fluorescent chemosensors toward Zn(II) (Fig. 3.43) [325].

As an example, Fig. 3.44 shows the graphical presentation of the selectivity of **1b** with different metal ions. It should be noted that CPL **1b** with Zn(II) emits a strong blue fluorescence, which could be attributed to the reduced non-radiative
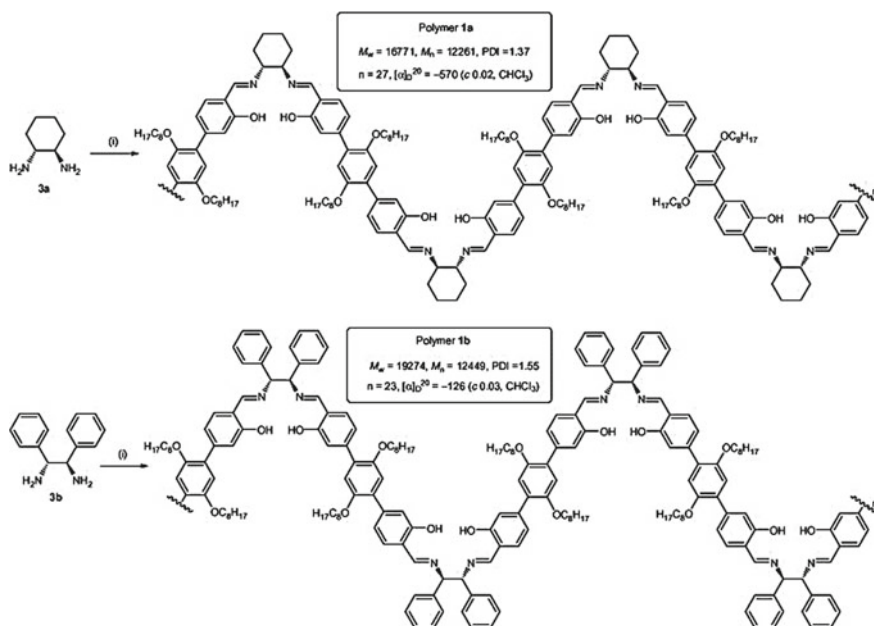
Fig. 3.43 Structures of CPLs **1a–b**

Fig. 3.44 The selectivity of **1b** (1×10^{-5} M in THF) with metal ions (3×10^{-4} M in water)
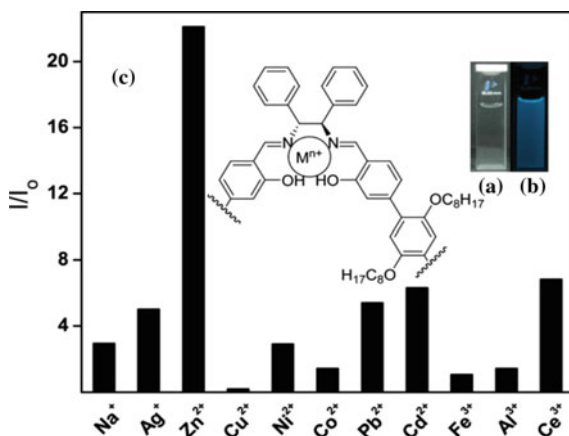
decay of the Zn(II)-PMC excited state and the quenching contributed from the lone pair of electrons of the nitrogen through internal charge transfer. In addition, a blue shift (~ 50 nm) in the emitted light was observed, which could be caused by a decrease in energy of the HOMO of the CPL upon the formation of the Zn(II)-PMC.
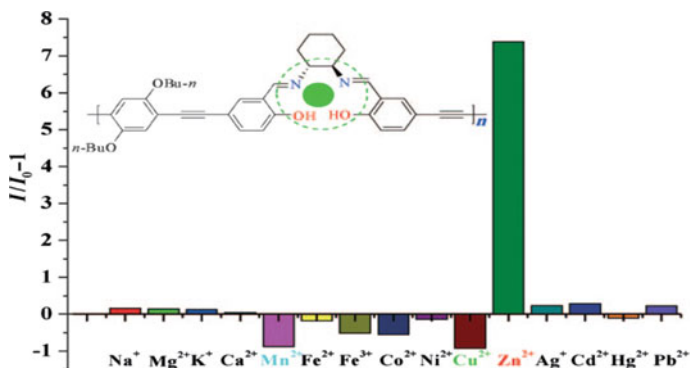
Fig. 3.45 The selectivity of the chiral CPL toward Zn(II) and other metal ions

Compared with other cations, Zn(II) can lead to a fluorescence enhancement as high as 7.8-fold together with a blue-shift change of the chiral CPL based on 2,5-dibutoxy-1,4-di (salicylaldehyde)-1,4-diethynyl-benzene and (R,R)-1,2-diaminocyclohexane (Fig. 3.45) [326].

Of interest is stereoregular non-linear chiral main chain CPLs **1a–b** bonded alternatively with (R,R)-salen and 1,4-diethynyl-2,5-dioctyloxybenzene fragments (Fig. 3.46) [327].

These CPLs are an effective chemosensors for the detection of Zn(II) with respect to other metal ions with enhanced fluorescence. The CD spectra observed for the CPLs **1a–b** could be attributed to the helical secondary structure with a low degree of inter-strand interactions. It is important that the CPL **1b** containing (R,R)-1,2-diphenylethylenediamine is superior to **1a** bearing (R,R)-1,2-diaminicyclohexane exhibiting the best result. In other words, the substituent on the salen fragment of the CPL has substantial effect on the sensitivity toward Zn(II). The Zn(II)-PMC based on CPL **1b** could exist in aggregated form through Zn–O interaction (Fig. 3.47).

It should be noted a chiral conjugated CPL with incorporated (R,R)-salen and perylenyl fragments in the main chain backbone which was obtained by the polymerization of 1,7-bis((3-formyl-4-hydroxyphenyl) ethynyl) perylene-3,4:9,10-tetracarboxylic tetrabutylate with (R,R)-1,2-diaminocyclohexane [328]. Compared with the other cations, only Hg(II) ion leads to the high response of the CPL and can be attributed to an ICT (intramolecular-charge-transfer). It is important that the fluorescent color of the CPL displays an obvious change from red to bright yellow upon addition of Hg(II) (Fig. 3.48).

Chiral poly (binaphthyl salen zinc chelates) were synthesized from an (R)-3,3′-diformylbinaphthol derivative, α,ω-diamines, and zinc acetate or diethyl zinc (Scheme 3.40) [329]. The underestimation of the molecular weights of PMC-Zn was attributable to the change in the molecular shape of the compact helices. The UV and CD spectra of PMC-Zn were quite different from those of the unit
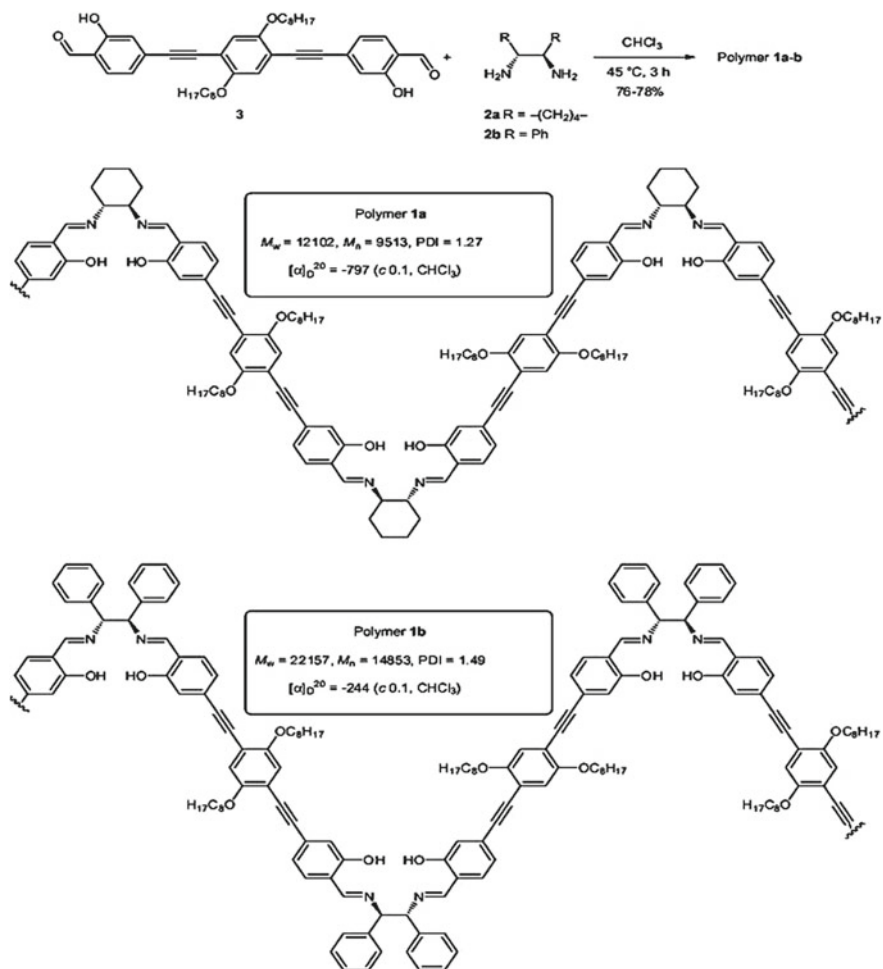
Fig. 3.46 Structures of CPLs **1a–b**

model, suggesting some regular polymer structure such as a helix, which is also suggested by the MD calculations.

Fig. 3.47 Illustration of inter-strand between the Zn (II)-polymer

Weak red color fluorescence   Bright orange color fluorescence
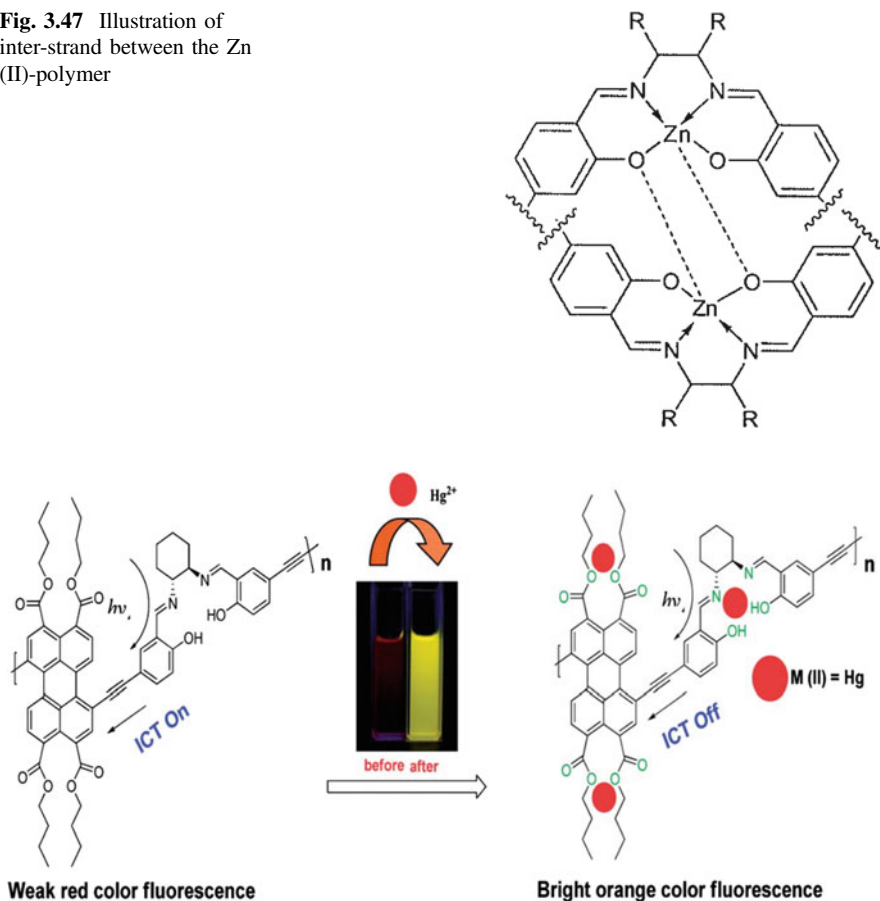
Fig. 3.48 Hg(II) induced ICT ON-OFF

It should be noted a poly(norbornene) tethered with chiral aluminum salen fragments [330].

a: R = (CH₂)₃

b: R = CH₂C(CH₃)₂CH₂

c: R = o-C₆H₄

d: R = (R,R)-

e: R = (S,S)-
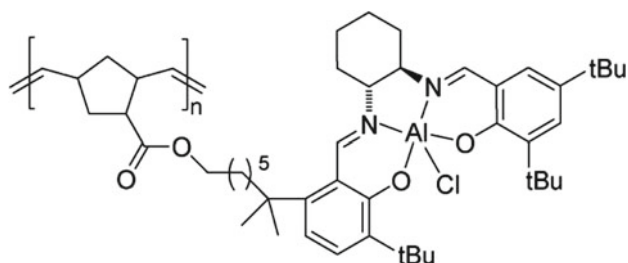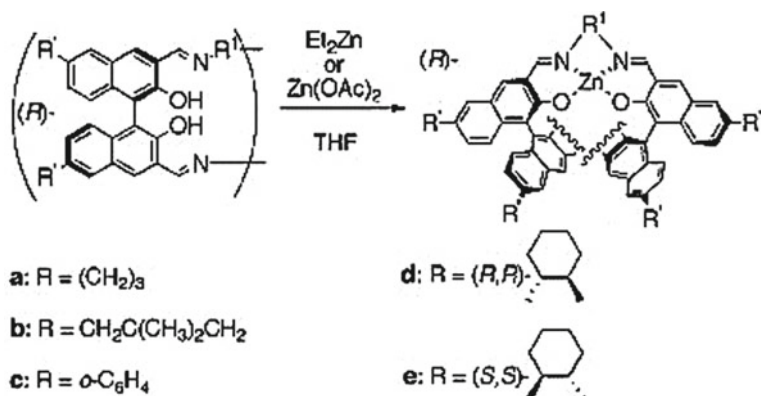
Scheme 3.40 Synthesis of PMC-Zn(II)

(R/R)-polymer **1**

(R/S)-polymer **2**

(S/S)-polymer **3**
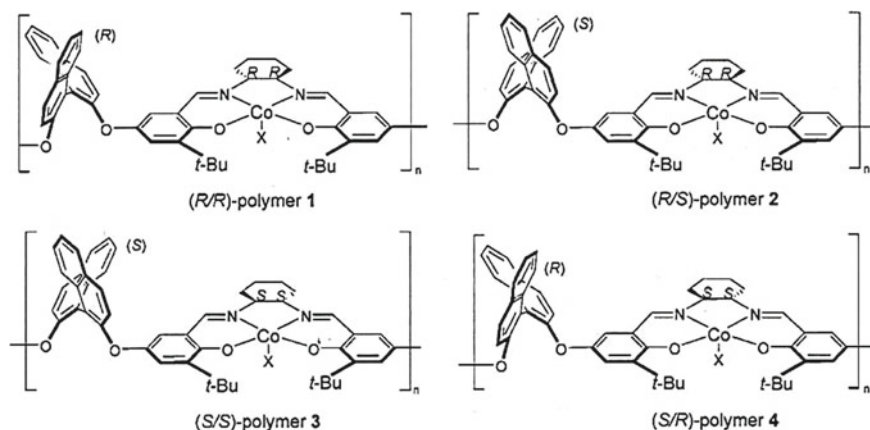
(S/R)-polymer **4**

Fig. 3.49 Configurations of polymer chelates BINOL-salen-Co(III)X

The synthesis of four polymer BINOL-salen-Co(III)X chelates: (R/R)-polymer **1**, (R/S)-polymer **2**, (S/S)-polymer **3** and (S/R)-polymer **4** (Fig. 3.49) with an auxiliary chiral site has been developed [331].

Initially of the polymeric salen ligand was chelated with Co(OAc)₂·4H₂O resulted in the corresponding diastereomeric isomer of the polymer BINOL-salen Co(II) chelate, which was subsequently oxidized with trichloroacetic acid and oxygen to obtain the corresponding BINOL-salen-Co(III)X PMC.

It should be noted the synthesis of Cu(II) and Ni(II) chelates of the CPL prepared by polycondensation of 5,5-methylene bis(2′-pyridinecarboxaldehyde) with 1,3-propylenediamine [332].
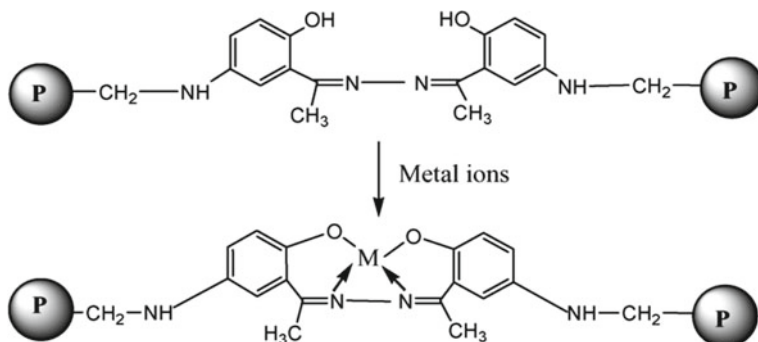
Scheme 3.41 Synthesis of PMCs based on polymer anchored Schiff base, where M = Fe(III), Cu(II), Zn(II)

CPL of N,N′-bis(*o*-hydroxy acetophenone) hydrazine Schiff base was loaded by Fe(III), Co(II) and Ni(II) ions in methanol (Scheme 3.41) [333, 334]. The chelation of the CPL was equal to 83.30, 84.20 and 87.80%, respectively, while the metal chelation with monomer analogue was equal to 80.3, 79.90 and 85.63%. The Fe(III) chelates of monomer Schiff base were octahedral in geometry, whereas Co(II) and Ni(II) chelates showed square planar structures.

PMCs were obtained by the interaction of the CPL, poly (2,4-dihydroxy benzophenone hydrazine-formaldehyde), with metal ions [335]. The X-ray diffraction pattern indicated that CPL was amorphous, whereas its PMC exhibited a number of reflection planes resulting in good crystallinity.
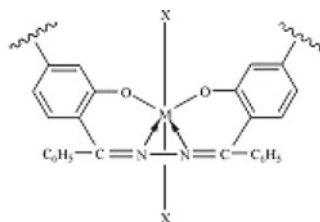
M = Cu(II), Ni(II) and for Ni(II) X = H₂O

3.2.10   8-Hydroxyquinoline Type of Metal Chelates

Polymers containing HQ fragments are one of the most common ligands for the preparation of PMCs [336–339]. Thus, the homopolymer and acrylic copolymer

based on 8-quinolinyl methacrylate are a good CPLs due to its pendant ester-bound quinolinyl fragment [340, 341]. It should be noted the targeted synthesis of metalloquinolate-functionalized polymers to improve the processability of AlQ$_3$ [342–344]. The interesting example is PMA having a pendent HQ fragment prepared using Kelex-100 (7-(4-ethyl-1-methyloctyl)-HQ) as a starting material [345]. A soluble PMC having AlQ$_3$-type side chains was obtained through the chelation of the CPL with Me$_3$Al in the presence of a monomeric Kelex-100. The fraction of AlQ$_3$ moieties in this PMC is calculated to be 42% by weight and GPC analysis indicated that PMC has M$_n$ = 1.35.10^4 and PDI = 1.65.
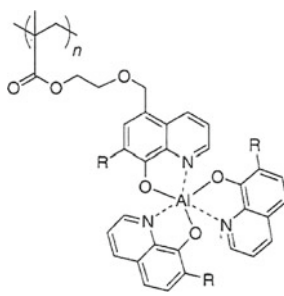
(R = 4-ethyl-1-methyloctyl)

Polycondensation type CPLs with HQ chelating fragments were synthesized from HQ and pyrogallol [346], catechol [347], dithiooxamide [348], salicylic acid [349] or anthranilic acid [350] using formaldehyde as a crosslinking agent. The PMCs of Cu(II), Zn(II), Mn(II), Ni(II) and Co(II) ions with the poly(ester-amide) obtained by polycondensation of 1,4-phenylenebisphthalamic acid and commercial epoxy resin (diglycidyl ether of bis phenol-A) with 5-chloromethyl-8-quinolinol hydrochloride were prepared [351].

Of interest is studying the chelates of the Mannich-type polymers, poly[HQ-5,7-(piperazine-N,N′-diyl-bismethylene)] (**I**) and poly[HQ-5,7-(N,N′-dimethylethylene-diamine-N,N′-diylbismethylene)] (**II**), with La(III), Nd(III), Sm(III), and Gd(III) ions [352] as well as Mg(II), Ca(II), Ni(II), Cu(II), Zn(II), and Cd(II) ions [353]. CPL **I** exhibited higher capacities and a more pronounced selectivity towards Cu(II) than CPL **II**. The faster equilibration rates observed for CPL **I** and **II** compared with that of their parent phenol-formaldehyde system, poly (HQ-5,7-diylmethylene), clearly reflect the effects of hydrophilic spacer groups (piperazine or N,N′-dime-thylethylenediamine), connecting HQ fragments, on the structural characteristic of these CPLs resulting in enhanced hydrophilic character. It is interesting that the replacement of a methylene (–CH$_2$–) by an ethylene (–CH$_2$CH$_2$–) spacer group in poly (HQ-5,7-diylethylene) also results in relatively faster rates of equilibration.

Thus, the nature and rigidity of the spacer group have determining effect on the chelation process; the use of piperazine as a spacer group considerably enhances the capacity and selectivity of this class of CPLs toward divalent metal ions.
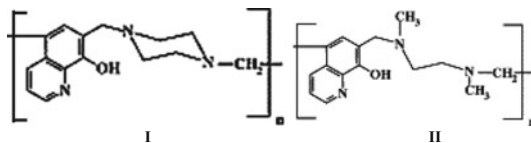
PMCs were obtained when the solutions of the poly (8-hydroxy-5-azoquinolinephenylmethacrylate-formaldehyde) [354], poly (8-hydroxy-5-azoquinolinephenylacrylate-formaldehyde) [355] or poly (8-hydroxy-4-azoquinolinephenol-formaldehyde) [356] were treated with the aqueous solution of Cu(II)/Ni(II) ions. The metals were chelated with the formation of a square planar structure for Cu(II)-PMC and octahedral structure for Ni(II)-PMC.
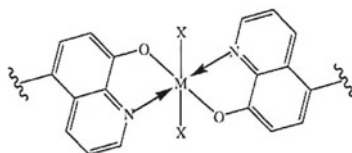
M = Cu(II), Ni(II) (X= H_2O)

CPL synthesized through copolymerization of HQ and dimethylolacetone monomers has been used to prepare PMCs of transition metal ions [357]. All PMCs with octahedral geometry are paramagnetic in nature except that of Zn(II) chelate, which is diamagnetic. PMCs were synthesized in alkaline solution of poly (8-hydroxy-4-azoquinolinephenylacrylate), prepared by the polymerization of the monomer based on acryloyl chloride, HQ and 4-aminophenol, with the aqueous solution of Cu(II) and Ni(II) [358]. Of interest are the oligomer Cu(II), Co(II), Ni(II), Mn(II) and Zn(II) chelates based on the ethanolyloxy *p*-cresol-formaldehyde polymer treated with 5-chloromethyl-HQ hydrochloride [359]. The value of the DP of all the PMC is in a range of 5–6.

M = Cu(II), Ni(II), Mn(II) and Zn(II)
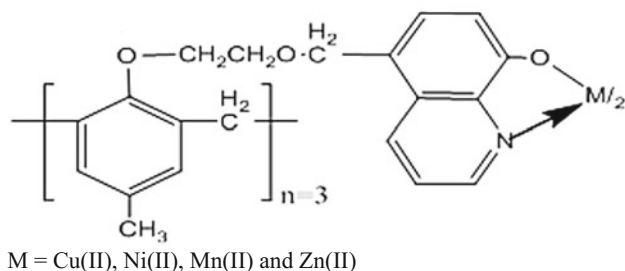
PMCs based on CPL having HQ as a pendent fragments prepared using phenylenebismaleimide-diamine polyimide and 5-chloromethyl-HQ hydrochloride were obtained using transition metal ions [360]. The CPL has good metal chelation capacity at varying pH range. Of interest are PMCs based on HQ containing polyester [361].

HQ-5-sulfonic acid-thiourea-formaldehyde copolymer is selective CPL for certain metals [362]. In particular, the CPL exhibited a higher selectivity for Fe(III) ions than for Cu(II), Ni(II), Co(II), and Pb(II) ions.
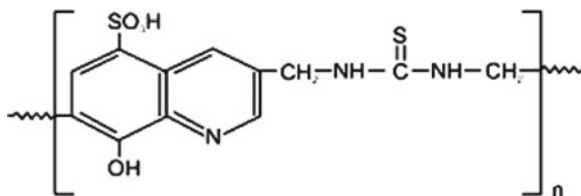
The polymer-supported HQ prepared by the reaction of PCS with 5-amino-HQ has a high chelation capacity for U(VI) over Th(IV) and La(III) [363]. It should be noted using the same chelating fragment for the solid-phase extraction of U(VI) by XAD-4 [364]. Nearly quantitative Cu(II) uptake within minutes was achieved with the chelating agent HQ or HQ-5-sulfonic acid (8HQ5S) bound to a methacrylate-based macroporous support (Scheme 3.42) [365, 366]. The macroporous nature of the microbeads assures full accessibility of the chelating fragments to the Cu(II) ions. It is important that the CPL demonstrated chelation selectivity for Cu(II) against Zn(II) with ratios of up to 1321 and sufficient stability of the copper chelates against rechelation using studies in the presence of chelating amino acids.

Of interest are three kinds of metalloquinolate-containing PS, AlQ$_3$-PS, ZnQ$_2$-PS and CuQ$_2$-PS, in which metal chelate units are linked with the side chains of PS [367]. It is important that these PMCs exhibit blue-green luminescence.

Heterocyclic compound and open-chain crown ether were combined together to form chelating fragments, open-chain crown ethers with "double" oxyquinoline end-groups, and they were loaded onto PS matrix to obtain CPL for the purpose
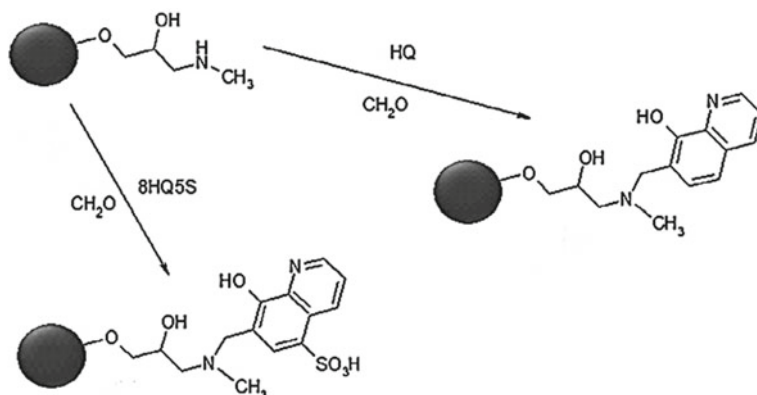
Scheme 3.42 Modification of a methacrylate-based macroporous support with the chelating agent HQ or 8HQ5S

of removing transition metal ions from aqueous solution [368]. The obtained PS-supported bis-HQ-terminated open-chain crown ether exhibited high chelation capabilities towards Hg(II) and Au(III), and the saturated chelation capacities could reach as high as 3.6 and 3.2 mmol g^{-1}, respectively. Both the adsorption rate and adsorption amount at equilibrium for Hg(II) were greater than those for Au(III) ions, which was probably caused by the differences in form and volume between the two kinds of absorbed ions. Besides, the adsorption for Hg(II) was physisorption while that for Au(III) was chemisorption.
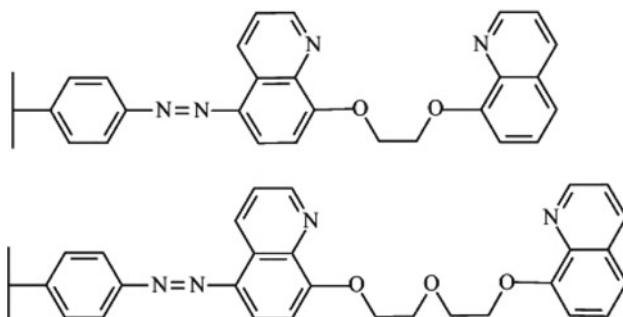
CPLs containing HQ fragments synthesized by the chemical transformation of macroporous GL were transformed into Ag(I)-, Cu(II)-, and Fe(III)-PMCs, respectively [369]. The metal contents found were 4.14% Ag (0.39 mmol g^{-1}), 3.42% Cu (0.54 mmol g^{-1}) and 1.66% Fe (0.29 mmol g^{-1}). It is important that only part of

the chelating fragments in CPL is utilized for metal chelation. As shown, immobilized HQ gives stable chelates with Ag(I), Cu(II) and Fe(III) ions in 1:1 and 1:2 ratios. Clearly, PMC with two ligands is almost certainly excluded due to steric hindrance on the highly cross-linked matrix.

CPL based on HQ-5-sulphonic acid and PVC has been used to prepare PMCs with transition metal ions [370]. It is important that oxygen atom of SO_3-H fragment and nitrogen of the quinolone ring take part in metal chelation. Of interest is using HQ-modified PCD microbeads to the chelation of Pb(II), Cd(II), Ni(II), and Co(II) ions [371]. It should be noted studying metal chelation with poly (aryleneethynylene)-type CPL containing 20% 8-quinolinol in the polymer chain (Scheme 3.43) [372]. It turned out that the addition of Zn(II) ions to the CPL **IIa** solution reduced the quantum yield of emission, but has not an effect on the emission maximum of the CPL. At the same time, Al(III) chelation by the same CPL leads to the emergence of a shoulder in the emission spectrum at 500 nm and an increase of quantum yield. It is interesting that Pd(II) chelation quenched all luminescence. Similar results were obtained with the CPLs **Ia** and **b** [373]. Reaction of both CPLs with complex **III** allows to preparing AlQ_3 chelates on the polymer chain, in which the energy is emitted from the aromatic groups before its transfer to the AlQ_3 chelate.

3.2.11 Metal Chelates with Amidoxime and Hydroxamic Acid

CPLs containing ligands of amidoxime groups have attracted much attention, for example, in the separation of uranium [374]. Amidoxime is supposed to be bidentate (Scheme 3.44); two amidoximes may be used for chelation with a metal ion, which makes a square planer chelate [375].

CPL, amidoximated poly (N,N′-dipropionitrile AAm), showed high adsorption properties for metal ions at very low concentration levels (ppb) in the following order: U(VI) > V(V) ≫ Co(II) = Cu(II) ≫ Ni(II) [376]. The chelation properties of the addition-type polymers poly (amidoxime-hydroxamic acid) and poly (N-methyl amidoxime-N-methyl hydroxamic acid) toward La(III), Nd(III), Sm(III), Gd(III), and Tb(III) ions depend largely on the cross-linker, DVB [377]. The
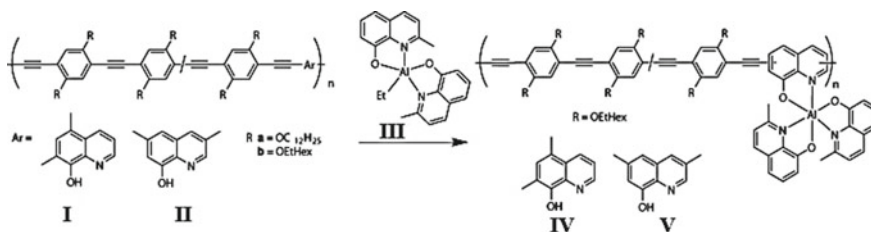
Scheme 3.43 Scheme of synthesis of PMCs IV and V
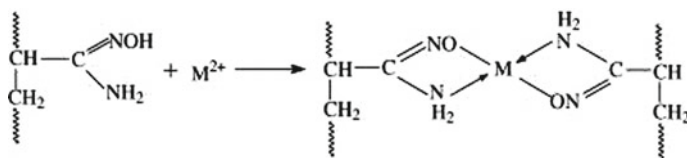
Scheme 3.44 Schematic diagram for chelation between M(II) and amidoxime-cross-linked PAN

chelated isothermal process and kinetics parameters of the amidoxime PAN nanofibers and PAN conventional fibers were compared [378]. It turned out that the saturated chelation capacity of amidoxime PAN nanofibers to Cu(II), Cd(II) was 3.4482 and 4.5408 mmol g^{-1} (dry fiber) respectively, nearly two times higher than that of amidoxime PAN conventional fibers. For poly (amidoxime) prepared by amidoximation reaction of PAN selective adsorption for uranium and low affinity for alkali and alkaline earth metals were observed [379]. The amidoxime-cross-linked PAN was used to chelation of Hg(II) [380] or Fe(III), Cu(II), Ni(II), Cd(II) ions [381] under different conditions.

Of interest is amidoximated nylon-66 fiber containing double amidoxime fragments per repeating unit for uranium removing of low concentrations (1–25 mg L^{-1}) [382]. In this case, the adsorption was spontaneous and endothermic.

It should be noted the ability of water-soluble PEI that incorporates N-methyl-hydroxamic acid chelating fragments (**I**) to achieve selective separation of target metal ions [383]. It is interesting that the CPL **I** selectively binds Fe(III) over Th(IV) at pH 1 in contrast to its primary hydroxamate analog **II**. A comparison of the chelation properties of **I** and **II** reveals the importance of the nature of the ligand in the chelation process.
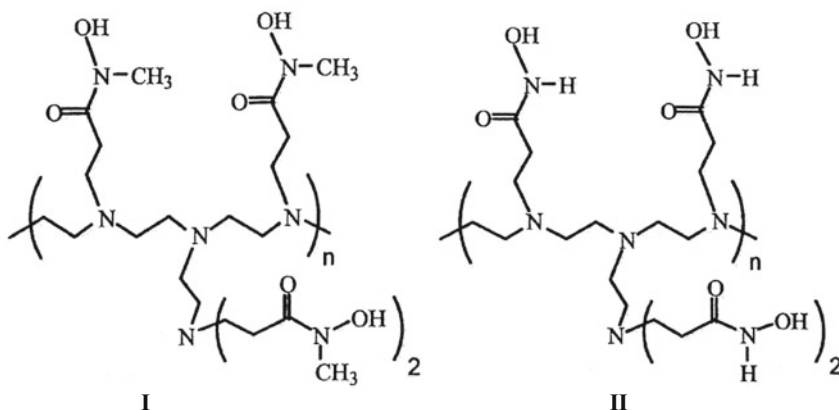
It is well known that the high stability constant (log K = 30.6) and specificity of deferoxamine to iron is a result of its unique chemical structure (Fig. 3.50).
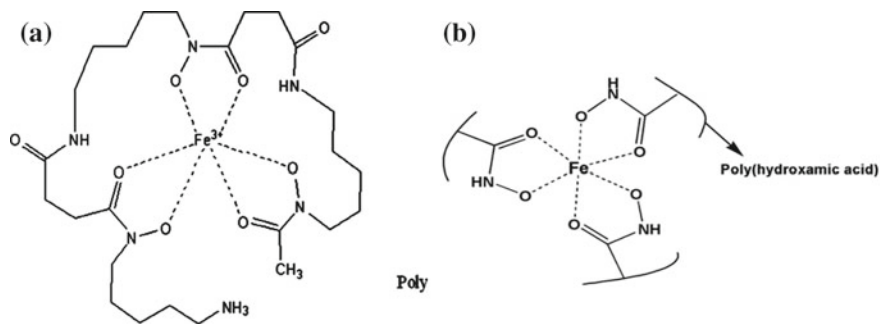
Fig. 3.50 Chemical structure of soluble deferoxamine/Fe(III) chelate (**a**) and poly (hydroxamic acid)/Fe(III) chelate (**b**)

Therefore, the numerous studies were devoted to the preparation of soluble [384] and grafted siderophore-mimetic CPLs [385]. It is hypothesized that the observed discrepancy between soluble and solid CPL bound hydroxamate fragments may be structure related. The grafted polyhydroxamate chelating fragments are expected to have similar chemistry to soluble hydroxamate chelators. However, difference in graft chain length, degree of cross-linking, and local chain mobility cause steric restrictions that may affect not only chelation kinetics and capacity, but also specificity.

In this regard, it should be noted PP-*gr*-poly (hydroxamic acid) films, obtained by grafting PMA followed by the conversion into poly (hydroxamic acid) [386]. CPL exhibited significant iron chelation activity (80 nmol cm^{-2}) with an equilibration time of 24 h. CPL based on fatty hydroxamic acid immobilized in PMMA is a sensor for V(V) [387].

3.2.12 Metal Ion Binding with Aminopolycarboxylic Acids

The aminopolycarboxylic acids bound to nitrogen atoms of the polymers are an important class of CPLs due to the high chelation capacity. Among them, the four aminopolycarboxylic acid, in particular, IDA, nitrilotriacetic acid (NTA), EDTA, and DTPA, are the most widely used in metal chelation.

3.2.12.1 Iminodiacetic Acid

Iminodiacetic acid is the simplest aminopolycarboxylic acid including two carboxyl groups and IDA-containing CPLs are widely studied during the last years. As a typical example, we note Cu(II)-PMC prepared by mixing CPL based on MMA and a chelating monomer GMA-IDA with copper sulfate solution [388].

Complex
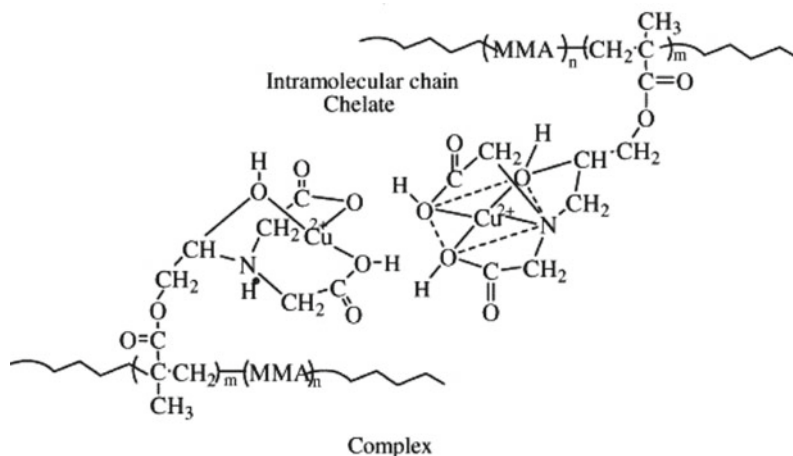
The comparison of proton spin-lattice relaxation time in the rotating frame ($T_{1\rho}^H$) of the IDA segments in PMC and CPL shows that metal chelation leads to a decrease of the mobility of the MMA segments with simultaneous increase of the mobility of the IDA segments. It is important that the effect of the Cu(II) ion on the mobility of the MMA and IDA segments can be evaluated from $T_{1\rho}^H$ value (Table 3.7). The domain size of the PMC is smaller than the spin-diffusion length (L) within $T_{1\rho}^H$ time. Furthermore, it suggests that the CPL and PMC are homogenous at a scale where the spin-diffusion occurs within the time $T_{1\rho}^H$.

Table 3.7 Spin-lattice relaxation times in the rotation frame $T_{1\rho}^H$ (ms) and the spin-diffusion path length L (nm) values of CPL and their PMC

PMC[a]	$T_{1\rho}^H$ (MMA unit)			L (MMA)	$T_{1\rho}^H$ (IDA unit)	L (IDA)
	45 ppm	52 ppm	178 ppm	178 ppm	178 ppm	178 ppm
Cu(II)-PMC$_{90}$	11.2 (10.9)[b]	11.1 (11.1)	21.8 (14.6)	3.6 (3.0)	6.4 (7.4)	2.0 (2.1)
Cu(II)-PMC$_{85}$	8.1 (8.1)	8.2 (7.1)	15.4 (12.7)	3.0 (2.8)	5.6 (7.3)	1.8 (2.1)
Cu(II)-PMC$_{80}$	10.5 (9.1)	10.8 (9.6)	17.5 (12.9)	3.2 (2.8)	7.7 (8.3)	2.1 (2.2)
Cu(II)-PMC$_{75}$	7.2 (7.0)	8.1 (7.2)	14.2 (12.3)	2.9 (2.7)	5.9 (6.9)	1.9 (2.0)
Cu(II)-PMC$_{70}$	10.0 (8.5)	10.6 (9.2)	15.4 (12.5)	3.0 (2.7)	6.7 (7.4)	2.0 (2.1)
Cu(II)-PMC$_{65}$	7.3 (6.3)	8.1 (6.2)	14.6 (12.5)	3.0 (2.7)	3.9 (7.6)	1.5 (2.1)

[a]The values at the bottom are the fraction of IDA units in CPL
[b]The values in parentheses are the $T_{1\rho}^H$ or L values of the GMA-IDA copolymers

Table 3.8 Stability constants of Ni(II), Zn(II), and Co(II) chelates with GMA-IDA or CPLs at I = 0.1 M and 25 °C

Chelating agent	Log K_s		
	Ni(II)	Zn(II)	Co(II)
IDA	8.13	7.24	6.94
GMA-IDA	8.29	7.83	7.63
PGMA-IDA	9.18	8.99	8.83
PGMA-IDA-co-MA$_{15}$	9.16	8.87	8.83
PGMA-IDA-co-MA$_{30}$	9.15	8.88	8.80
PGMA-IDA-co-MA$_{50}$	9.15	8.83	8.73
PGMA-IDA-co-MA$_{65}$	8.92	8.64	8.55
PGMA-IDA-co-AAm$_{15}$	9.83	9.57	9.39
PGMA-IDA-co-AAm$_{30}$	9.29	9.05	8.94
PGMA-IDA-co-AAm$_{65}$	8.83	8.52	8.24

The same chelating vinyl monomer GMA-IDA was used to the preparation three CPLs, PGMA-IDA, PGMA-IDA-co-MA, and PGMA-IDA-co-AAm [389]. The stability constants (K_S) of all the CPLs were larger than GMA-IDA (Table 3.8). Increasing the MA content within PGMA-IDA-co-MA affected the K_S only slightly. At a proper molar ratio of AAm in PGMA-IDA-co-AAm, K_S was 30–60 times greater than that of GMA-IDA. The CPL had a stereo and entanglement structure, which could, in turn, cage the metal ions and stabilize the intrachain and interchain chelation. For PGMA-IDA-co-MA, the incorporation of MA with GMA-IDA forced the GMA-IDA chelating fragments apart and decreased the K_S. The hydrophobic nature of PGMA-IDA-co-MA increased with increasing MA content. That is, the water-soluble CPL retained their stereo and entanglement structure with which to cage the metal ions. Hence, MA units did not cause remarkable changes in the K_S. As the AAm molar content within PGMA-IDA-co-AAm increased, the K_S decreased.

It should be noted two CPLs, water-soluble and latex types of poly (St-co-GMA-IDA), which are formed by reacting St with a chelating vinyl monomer GMA-IDA [390]. K_S are ordered, latex types > solution types > GMA-IDA. Latexes are surfactant-free, nearly nanoparticles and the mean size declines as the amount of metal ions increases, when the particles are chelated therewith. The K_S of the latex-PMC exceed those of the corresponding water-soluble PMC by a factor of 10^2–10^3, depending on the metal ions. Apparently, this is due the neighboring effect and high concentrations of GMA-IDA on latex's particulate surface (cooperative effect).

Of interest is CPL based on 2-(2-hydroxyethoxy) ethyl methacrylate and ethylene dimethacrylate modified by chelating groups of IDA in the form of homogeneous membrane sheets which showed high chelation capacity for Ni(II), Cu(II) and Fe(III) ions (up to 1.3 mmol g^{-1}) [391].

It should be noted that the amino-carboxyl fragment on an adsorbent is one of the most effective chelating groups for adsorption of heavy metal ions from an aqueous

solution [392–394]. In addition, it should be noted a wide variety of commercial IDA-containing CPLs including Purolite S390, Chelex 100, Amberlite IRC-748, and Lewatit TP 207 [395–400]. The chelation capacity of different IDA-containing CPLs depends on such parameters as the polymer substrate and metal nature as well as reaction conditions (Table 3.9).

Determined K_S values for IDA-PMC arrange in the following order of Cu > Ni > Zn > Co, as for IDA-LMC. The CPL with a long spacer arm has the selectivity towards to lanthanides close to that of the monomeric analogues. At the same time, the introduction of a short spacer arm leads to decreasing the PMC stabilities and, therefore, affects the adsorption selectivity. It should be noted that the adsorption process includes some steps: diffusion from the liquid phase to the polymer surface, film diffusion or boundary diffusion, diffusion in the pores of the polymer, and the surface reaction [394].

Table 3.9 Metal chelation properties of IDA-functionalized CPLs

Matrices modified with IDA	Surface coverage (mmol g^{-1})	Metal	Contact time (h)	pH	q_m (mmol g^{-1})	References
AN-DVB	–	Co(II)	8	5	2.51	[392]
		Ni(II)			2.81	
		Cu(II)			3.26	
	–	Cd(II)	24	5.5	0.99	[401]
		Pb(II)			0.69	
Polybenzylamine	–	Cu(II)	24	5	1.72	[402]
		Cd(II)			0.61	
		Pb(II)			1.12	
	–	Cu(II)	24	5	2.27	[403]
		Cd(II)			0.65	
		Pb(II)			1.27	
GMA	–	Cu(II)	48–72	–	0.43	[404]
		Cd(II)			0.40	
		Pb(II)			0.41	
		Cr(III)			0.45	
Amino methyl PS	–	Cu(II)	24	5	2.27	[405]
		Cd(II)			0.65	
		Pb(II)			1.30	

Of interest is the study of Cu(II) chelation by CPL containing IDA fragments [406]. The equilibrium isotherms showed that the CPL had a stronger affinity for Cu(II) ions. The CPL chelation capacity for Cu(II) increased relatively in the pH level range between 1.0 and 5.0, while for a higher initial concentration of Cu(II), the increase of the chelation capacity of the CPL reached a greater maximum equilibrium sorption of Cu(II) ions as 167 mg g^{-1}.

Porous CPL beads based on poly (AN-*co*-MBA) carrying IDA fragments were employed in chelation [407]. In particular, the CPL showed high adsorption capacity for Cu(II), Cd(II) and Pb(II) ions, and the its saturated value at 25 °C was equal to 2.43, 1.93 and 1.45 mmol g^{-1} CPL, respectively.
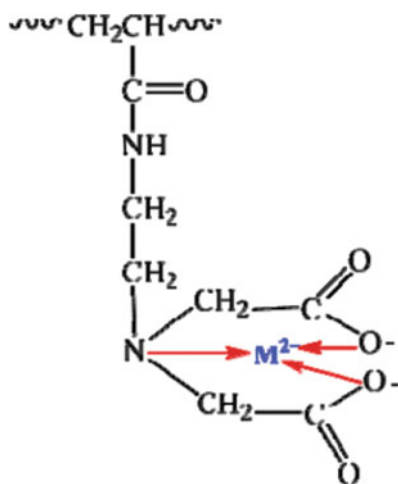
The comparative study of the chelation of Pb(II) on two CPLs containing different chelating fragments, the iminodiacetic Chelex 100 and the carboxylic Amberlite CG-50, showed that Pb(II) is strongly adsorbed on Chelex 100 through the formation of two complexes in the CPL phase: MHL with $\log_{10} \beta_{111i} = -0.3$ and ML with $\log_{10} \beta_{111i} = -3.7$ [408]. Furthermore, on Amberlite CG-50 the sorption is rather strong and involves the formation of the complex ML, in more acidic solution, with $\log_{10} \beta_{110i} = -2.0$.

A Fe(III)-loaded chelating fabric with IDA functional fragments was prepared by polymerization of GMA onto a nonwoven fabric made of PP coated by PE (PE/PP) and subsequent Fe(III) chelation [409]. Fe(III) chelation capacity of IDA fabric was determined to be 2.83 mmol Fe(III)/g of polymer.

$$L: H_2O \text{ or } Cl^-$$
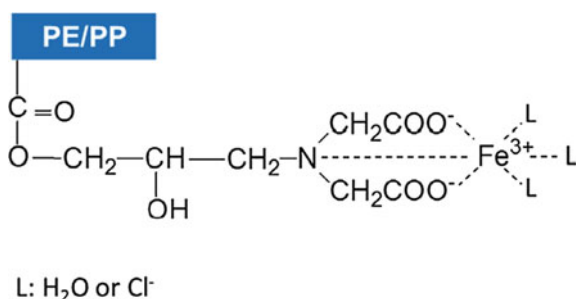
A thermoresponsive CPL with highly dense IDA fragments synthesized by condensation of poly (NIPAM-*co*-AA) with polyallylamine and the subsequent transformation of amino groups to IDA was used for the metal chelation (Fig. 3.51) [410]. Metal ions in water were collected by adding the thermoresponsive CPL and the nearly complete (99.8%) collection of seven metals (Ba, Co, Ni, Cu, Cd, In, and Pb) was reached.

Of interest is the hydrogel of poly (NIPAM-*co*-poly [2-methacrylic acid 3-(bis-carboxymethylamino)-2-hydroxypropyl ester] including a thermoresponsive fragment of poly (NIPAM) and a pH-responsive fragment of poly [2-methacrylic acid 3-(bis-carboxymethylamino)-2-hydroxypropyl ester], which contain a pendent ligand of IDA [411]. Because the IDA is strong chelating ligand [412], Pd(II) can be easily immobilized in the CPL hydrogel to form hydrogel/Pd(II) composite (Fig. 3.52). When a suitable amount of the CPL hydrogel is placed in PdCl$_2$ aqueous solution for about 5 min, the hydrogel becomes yellow, indicating immobilization of Pd(II) chelate in the hydrogel matrix.

Fig. 3.51 Conceptual illustration of designed thermoresponsive CPL
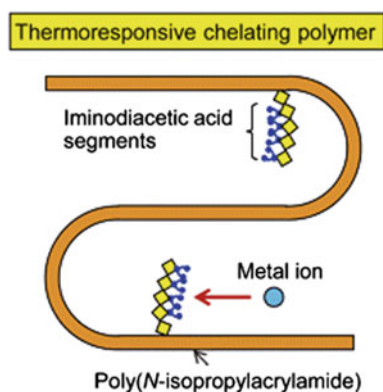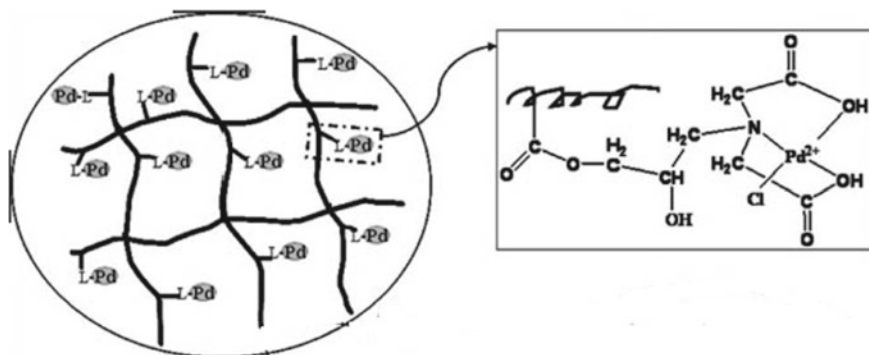
Fig. 3.52 Schematic structure of the CPL hydrogel/Pd(II) composite

It should be noted IDA ligand covalently immobilized to the poly (MMA-GMA) film which was chelated with Cu(II) ion [413].

3.2.12.2 Nitrilotriacetic Acid

It should be noted that some NTA-containing commercial CPLs are available [414]. However, NTA is not used as often in the metal chelation study as IDA. As a typical example, we note NTA-containing polycondensation CPL based on NTA, melamine, acetone, guaiacol, and formaldehyde which exhibited lower chelation capacity for Cu(II) in comparison with other similar CPLs [415].

3.2.12.3 Ethylenediaminetetraacetic Acid

It is well known that strong metal chelating ability, stability, local availability, and low price is characteristic for EDTA. Thus, CPL for transition metals were prepared by copolymerization of Allopurinol, a known drug for the treatment of gout and hyperuricaemia, with EDTA or cyclohexyldiaminetetraacetic acid [141].

Of interest is PS-based EDTA CPL which exhibits high chelation properties due a large number of chelating fragments and larger surface area [55, 162, 416]. The CPL shows as opaque, uniform and buff beads with the average diameter of approximately 900 μm (Fig. 3.53a) and exhibits a hyperbranched structure containing both carboxyl units and amino/imino units (Fig. 3.53d). The beads exhibit as a perfect ball, simultaneously, took a number of uniform apertures (Fig. 3.53b, c). These properties are favorable for producing good chelation properties.

The interesting approach was offered for improving the mechanical strength of the PS-EDTA CPL by wrapping it up in PVA beads [158]. It turned out that this CPL is an effective adsorbent for Zn(II) ions. It should be also noted using poly
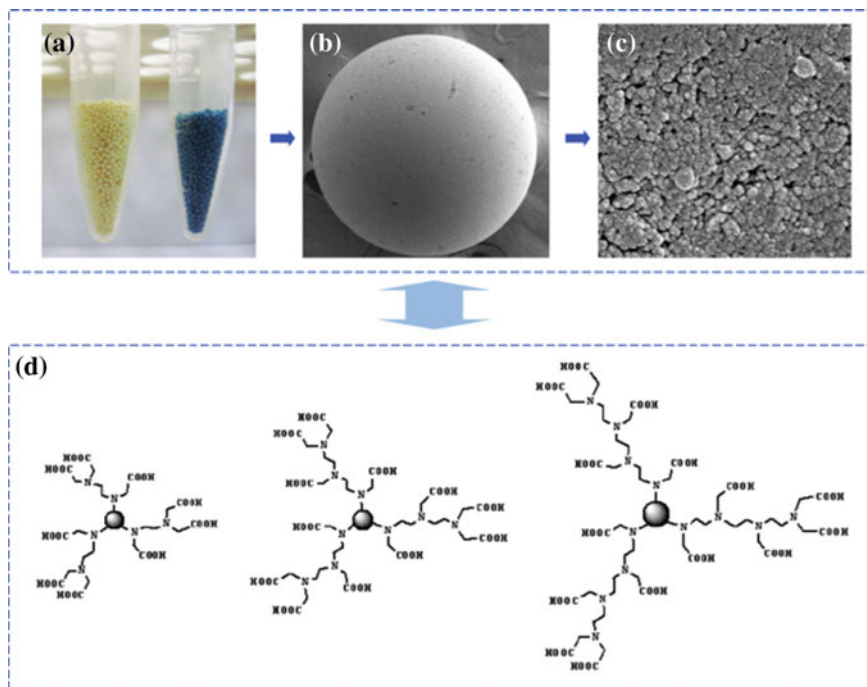
Fig. 3.53 The macro- and micro-structure of CPL: (**a**) color before and after chelating copper ions; (**b**) and (**c**) morphology of CPL; (**d**) the chelating fragments of the CPL

(AAm-AA)-EDTA disodium for the sorption of Ga(III), Cu(II), Ni(II) and Zn(II) ions [417].

3.2.12.4 Diethylenetriamine Pentacetic Acid

Among the DTPA-modified CPLs, it should be noted melamine-DTPA [418], melamine-formaldehyde-DTPA [419], and melamine-DTPA-polyvinylidene fluoride [420, 421]. It is important that the spatial organization of DTPA-PMCs is even more complex than EDTA-PMCs. Octahedral configuration of chelate node was suggested for Cu(II)- and Co(II)-PMCs based on DTPA-containing CPL [419]. DFT calculations confirmed the octahedral geometry of Ni(II)- and Cu(II)-PMCs based on DTPA-modified melamine with the participation of three carboxyl and three amine groups in the metal chelation [418].

During the last 25 years, the studies of metal chelation properties of DTPA-containing CPLs for biomedical applications, in particular, as contrast agents for magnetic resonance imaging (MRI), have received considerable attention [422–428]. In particular, polymeric DTPA-Gd(III) chelates have been developed to improve the pharmacokinetics and relaxivity of Gd(III)-based agents. Attaching the

Gd(III) chelates to CPL slows the rotational movement of the chelates, thereby increasing the relaxivities. Polymeric DTPA-Gd(III) chelates have relatively higher r_1 relaxivity on Gd(III) ion than Gd(III)-LMC. Besides, polymeric DTPA-Gd(III) chelates with higher relaxivity may generate more effective contrast enhancement and can be used at much reduced doses. Synthetic linear polymers have widely been studied for creating of polymeric DTPA-Gd(III) chelates as MR contrast media, citing characteristic advantages to exercise control over PDI and molecular weight. At present, commercially available PLL is widely used in MR imaging, in which conjugation with DTPA proceeds through the ε-amino group of lysine.
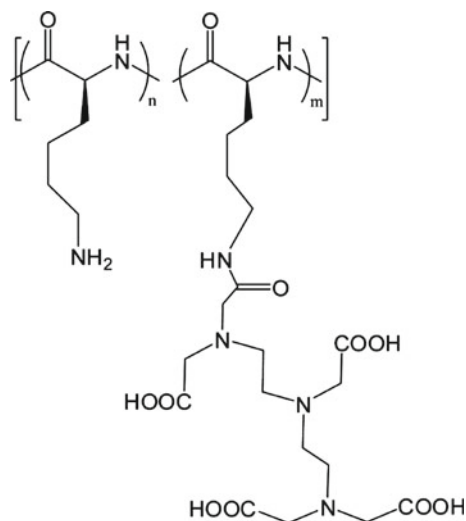
Another logical choice for DTPA-Gd(III)-chelate conjugation and building polymeric imaging agents is PEG due to its hydrophilicity, biocompatibility, and antiaggregation properties. It should be also noted Gd(III)-containing conjugates based on both PLL and PEG, which allow to improving solubility in blood and reducing the immunogenicity of PLL [429].

Of interest is the introduction of DTPA chelating fragments in the side chain or polymer chain, as in the case of CPL prepared by the condensation of DTPA and PEG-diamines or alkyldiamines [430]. A wide variety of polymer carriers were used, in particularly, PAMAM [431], polyglycerol [432], poly (AA-b-MA) [433], PVA [434], poly (p-phenylene ethylene) [435], and conjugated polymers [436]. It should be noted copolymers of DTPA-bisamide, in which increasing the rigidity in the hydrophobic comonomer by using more rigid linkages improved overall relaxivity likely due to the decrease in internal flexible bond movements in the polymer backbone [437]. Besides, as the length of the hydrophobic block increased, the relaxivity increased.

It should be noted a CPL with increased hydrophilicity and reduced toxicity prepared by copolymerization of DTPA with tartaric acid [438]. Of interest is also CPL prepared by copolymerization of DTPA with polysuccinimide derivatives including PEG, as a hydrophilic unit, and hexadecylamine, as a hydrophobic unit, which was used to obtain biocompatible micellar MR agents with improved in vivo stability [439].

Clinical application of polymeric DTPA-Gd(III)-based MRI agents is limited by their potential toxicity due to the slow body excretion. In order to minimize toxicity of polymeric DTPA-Gd(III) chelates, while maintaining their favorable properties such as high relaxivity and preferential accumulation in tumor, biodegradable macromolecular MRI agents have been developed [440, 441]. These polymeric DTPA-Gd(III)-based contrast agents contain disulfide bonds in polymer matrices [441]. In PMCs, these disulfide bonds can gradually recover by exogenous or endogenous thiols via thiol-disulfide exchange reactions. Consequently, polymeric DTPA-Gd(III) chelates have been restored in the LMC, to facilitate their removal from the body [442]. For example, polydisulfide Gd(III) chelates were synthesized by condensation polymerization of DTPA dianhydride and cystamine or other disulfide-containing monomers followed by Gd(III) chelation [441, 443]. The molecular weight of these PMCs varied in the range of 10,000–60,000 with relaxivity in the range from 4.4 to 12 mM^{-1} s^{-1} for Gd(III) at 3 T. The decomposition rate of polydisulfide Gd(III) chelates decreased with increasing steric hindrance around disulfide bonds.

R = H, COOH, COOET, CONH₂, CONHCH₂CH₂CH₃, CONHCH(CH₂)₃
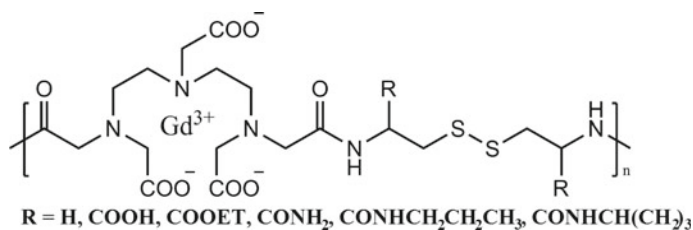
Of interest is the preparation of micelle based on a biodegradable poly (L-glutamic acid)-*b*-polylactide copolymer with shell-grafted DTPA-Gd(III) (Fig. 3.54) [444]. It is important that this DTPA-Gd(III) conjugate exhibited an r_1 of 7.90 mM^{-1} s^{-1} at 4.7 T, which is significantly higher than that of low molecular weight MRI contrast agent.

DTPA-containing CPLs are used for the preparation of multiplexed immunoassays based on mass cytometry [445]. In this case, CPL carries multiple copies of individual metal isotopes and provides functional groups for the conjugation with a monoclonal antibody (mAb)). As a typical example, we note the CPLs with a number average DP of 35 prepared by anionic ROP of an activated cyclopropane (the diallyl ester of 1,1-cyclopropane dicarboxylic acid). It is important that during
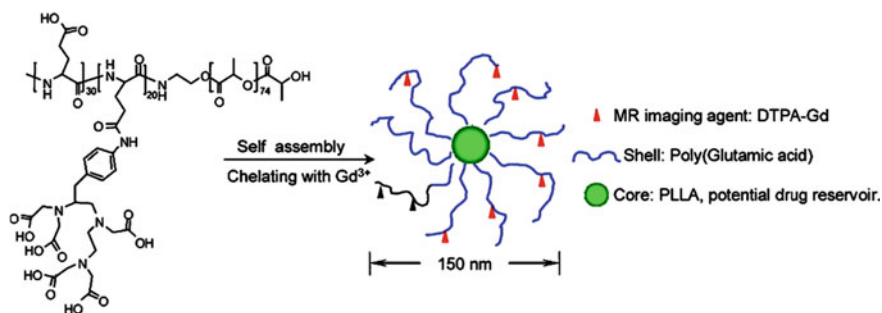
Fig. 3.54 Structure of poly (L-glutamic acid)(DTPA)-*b*-PLA and schematic model of the micellar structure with DTPA-Gd chelated to the shell layer

Gd(III) chelation the proximity of multiple DTPA fragments led to stronger chelation of metal ions at the beginning of the process and weaker chelation when the polymer approached saturation.

It should be noted the synthesis of CPL based on poly (2-aminoethylacrylamide) which has a DP of 67 and 79, high DTPA functionality, PDI $\leq$ 1.17, and a maleimide as an orthogonal functionality for conjugation to mAb [446]. It was shown that the CPL chelates an average of 50 Gd(III) ions per polymer that corresponds to the number of DTPA fragments per chain. Then, secondary goat antimouse IgG was covalently labeled with the maleimide fragment of the DTPA-containing CPL (DP_n = 79) bearing [159]Tb. It is important that each mAb carried an average of 161 $\pm$ 4 [159]Tb atoms, and there is an average of 2.4 $\pm$ 0.3 polymer chains linked to each mAb.
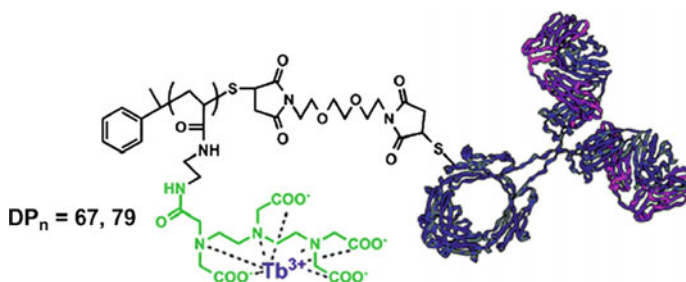
In another interesting example, CPL with hydrazide end groups was synthesized with a furan end group, and all pendant groups along the chain carried only DTPA fragments [447]. The immunoconjugates of these CPLs were radiolabeled with [111]In. It is well known that the preferred CN of In(III) is six, however, the DTPA-In(III) PMC has a CN of eight.
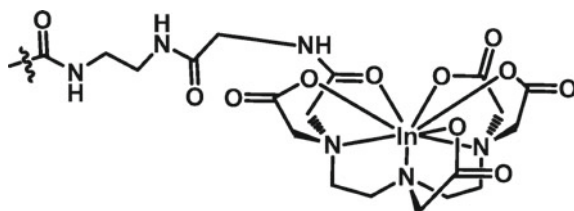
Of interest is biotin-functionalized CPL for ^{111}In chelation based on PAAm, polyaspartamide or polyglutamide backbone and harboured DTPA fragments [448]. It is important that PAAm-based CPL had a net negative charge; polyaspartamide- and polyglutamide-based CPLs were zwitter-ionic with a net neutral charge. The first CPL with a terminal biotin and a PAAm backbone harboring multiple DTPA chelating sites was conjugated to a streptavidin-modified Fab fragment of trastuzumab and subsequently complexed with ^{111}In through DTPA [449].

CPLs with pendant polyaminocarboxylate ligands and an orthogonal end-group, either a fluorescein molecule or a bismaleimide spacer for mAb attachment, were loaded with three different types of lanthanide ions as well as palladium and platinum ions [450]. It is important that at least one type of lanthanide ion, in particular, La(III) is capable of forming a bimetallic complex with pendant DTPA fragments. While the CPLs could be conjugated to mAb, the presence of Pd or Pt ions in the CPL interfered with the ability of the mAb to recognize its antigen.
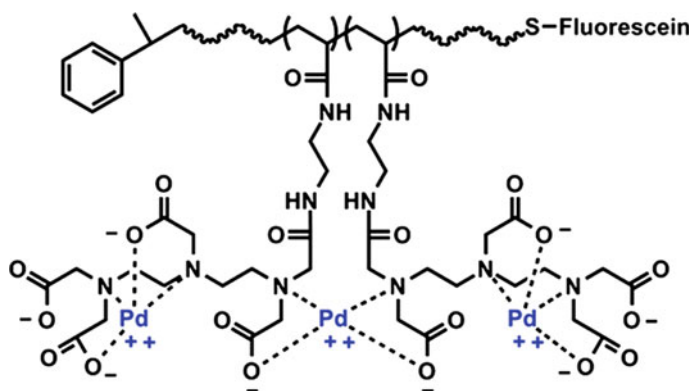
Pp-containing polyaspartamide CPL based on DTPA, 5-(4′-aminophenyl)-10,15, 20-tris(4′-sulfonatophenyl) Pp trisodium salt and poly-α,β-[N-(2-hydroxyethyl)-l-aspartamide] was used to prepare of PMC-Ga [451]. According to in vitro and in vivo tests, PMC-Gd has noticeably higher relaxation effectiveness than that of Gd-DTPA.
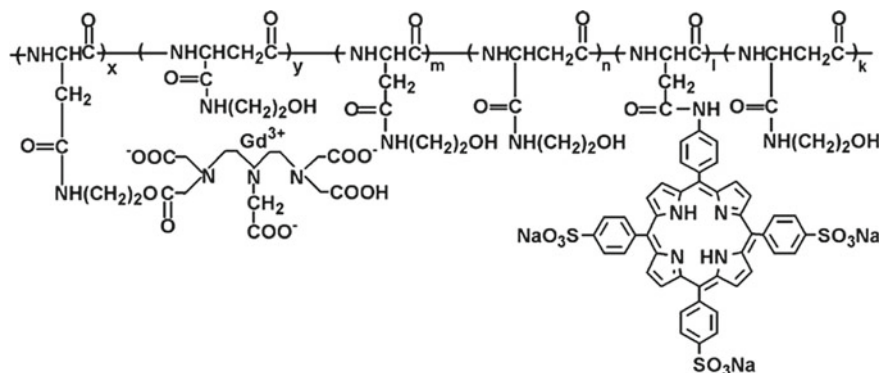
DTTA containing CPL obtained based on PEG-*gr*-α,β-poly (aspartic acid) derivatives, where DTTA is diethylenetriamine-tetra-*t*-butylacetate, formed PMC-Gd nanomicelles with gadolinium chloride (Scheme 3.45) [452].

The particle size of PMC-Gd (GD = 2%) nanomicelles was larger than that of PMC-Gd (GD = 7%), where GD is graft degree (Table 3.10). It is important that all the PMC-Gd nanomicelles have negative zeta-potentials. The mass percentage content of Gd in PMC-Gd (GD = 2%) was 16.1%, similar to its theoretic value of 16.8%.

3.2.13   Metal Chelates with Other N,O-Containing Ligands

Of interest the incorporation of the copper ions into the CPL prepared by functionalization of the polyaniline with imidazole (Scheme 3.46) [453].

The copper ion can chelate to the polyaniline CPL by either interchain copper chelation or intrachain copper chelation, which affects the effective molecular weight
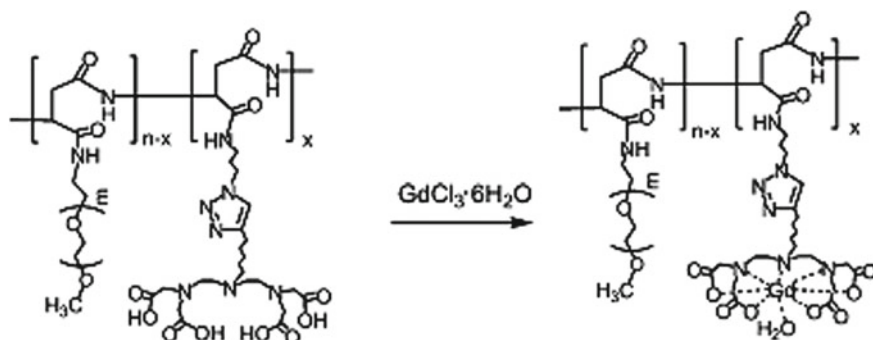
Scheme 3.45 Synthesis scheme of PEG-*gr*-α,β-poly (aspartic acid)-(DTTA-Gd)

Table 3.10 Characteristics of PMC-Gd nanomicelles

Nanomicelles	Gd (%)[a]	ξ potential (mV)[b]	Hydrodynamic diameter (nm)[b]	PDI[b]	CMC (mg mL^{-1})[c]
PMC-Gd (GD = 2%)	16.1	−3.4	82	0.10	1×10^{-6}
PMC-Gd (GD = 7%)	12.2	−3.0	63	0.10	1×10^{-7}

[a]Determined by inductively coupled plasma atomic emission spectroscopy
[b]PDI determined by dynamic light scattering
[c]Determined by fluorescence probe method using pyrene as fluorescent probe
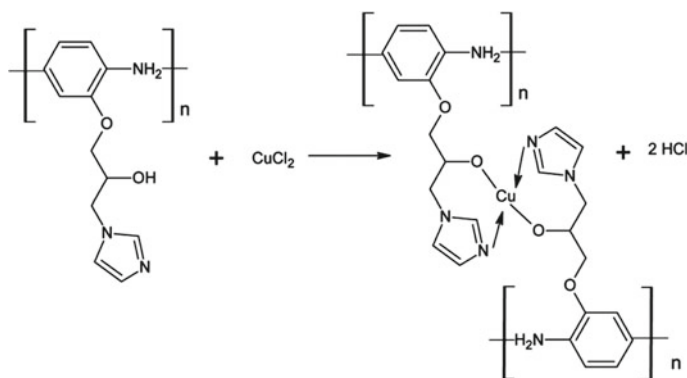
Scheme 3.46 Schematic of possible reaction pathway of chelation of Cu with polyaniline containing imidazole units and generation of secondary HCl

as well as the polymer aggregation. It is interesting that both CPL and PMC show characteristic unimodal distribution curves, with the values of the hydrodynamic radius centered at 108 and 121 nm, respectively (Table 3.11). This indicates the existence of globular submicrometer aggregates of CPL and PMC in the solution state. The observed molecular weight of PMC is higher than that of CPL due to the aggregation of the CPL chains because of the interchain copper chelation. It is important that the decrease in the percentage of PDI is associated with a tendency of the larger molecular weight polymer chains to aggregate preferentially with the low molecular weight polymer chains rather than the similar molecular weight chains. This is explained by the faster mobility of the low molecular weight fraction

Table 3.11 Dynamic light scattering (DLS) results of CPL and PMC

	Hydrodynamic radius (nm)	Molecular weight	PDI (%)
CPL	108.7	195,793	14
PMC	122.1	256,634	9.8

compared to that of the larger molecular weight, which kinetically favors chelation with copper.

Of interest are the fibers fabricated by the electrospinning of a St-*co*-2-(2′-hydroxy-4′-ethenylphenyl) imidazole which were reacted with a methanol vanadyl solution to afford the oxovanadium(IV)-PMC fibers [454]. Due to vanadyl chelation with the CPL, the BET surface area for initial fibers (0.6 μm diameter) is increased from 47.9 to 60.7 $m^2 g^{-1}$. The EPR analyses depicted complex speciation of vanadium ions within these PMCs.

Poly (N-2-aminoethylacrylamide)-*gr*-PS-Cu(II) chelate was synthesized (Scheme 3.47) [455]. The weight percentage of copper was found to be 6.62% (1.05 mmol g^{-1}).

It should be noted Mn(II)-, Co(II), Ni(II)-, Cu(II)-, and Zn(II)-PMCs based on CPL based on phenylurea and formaldehyde (Scheme 3.48) [456]. PMC-Mn(II), PMC-Co(II) and PMC-Ni(II) have octahedral structure, while PMC-Cu(II) and PMC-Zn(II) show square planar and tetrahedral structure, respectively.

CPL, the PS-supported N-(2-carbamoylfuranyl)-C-(3′-carboxy-2′-hydroxyphenyl) thiazolidin-4-one, reacts with Mn(II), Ni(II), Cd(II), Fe(III) and UO_2(VI) ions and forms the PS-anchored chelates [457]. CPL is a neutral tridentate ligand in PMC-Fe (II), a monobasic tridentate ligand in PMC-UO_2(II), a dibasic tridentate ligand in PMC-Mn(II), PMC-Ni(II) and PMC-Cd(II). A tetrahedral structure for Cd(II) and an octahedral structure for Mn(II), Ni(II), Fe(III), and a square-antiprism geometry for UO_2(VI) chelate are suggested (Fig. 3.55).

An approach using 2-methacryloylamidoglutamic acid as a chelating ligand was developed to obtaining high uranium chelation capacity [458]. CPL carrying these chelating fragments with a specific surface area of 56.7 $m^2 g^{-1}$, a swelling ratio of 63%, and containing 3.5 mmol chelating fragments/g were used in the chelation of UO_2(II). The chelating fragment incorporation significantly increased the uranium adsorption capacity (204.8 mg g^{-1}).

Scheme 3.47 Preparation of poly (N-2-amino ethylacrylamide)-*gr*-PS-Cu (II) chelate
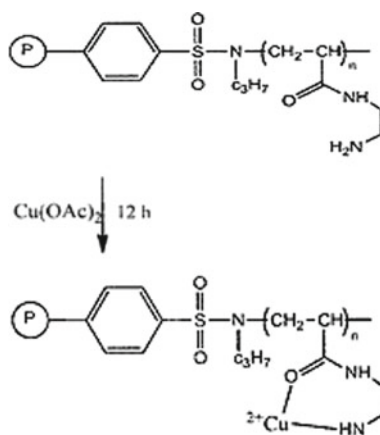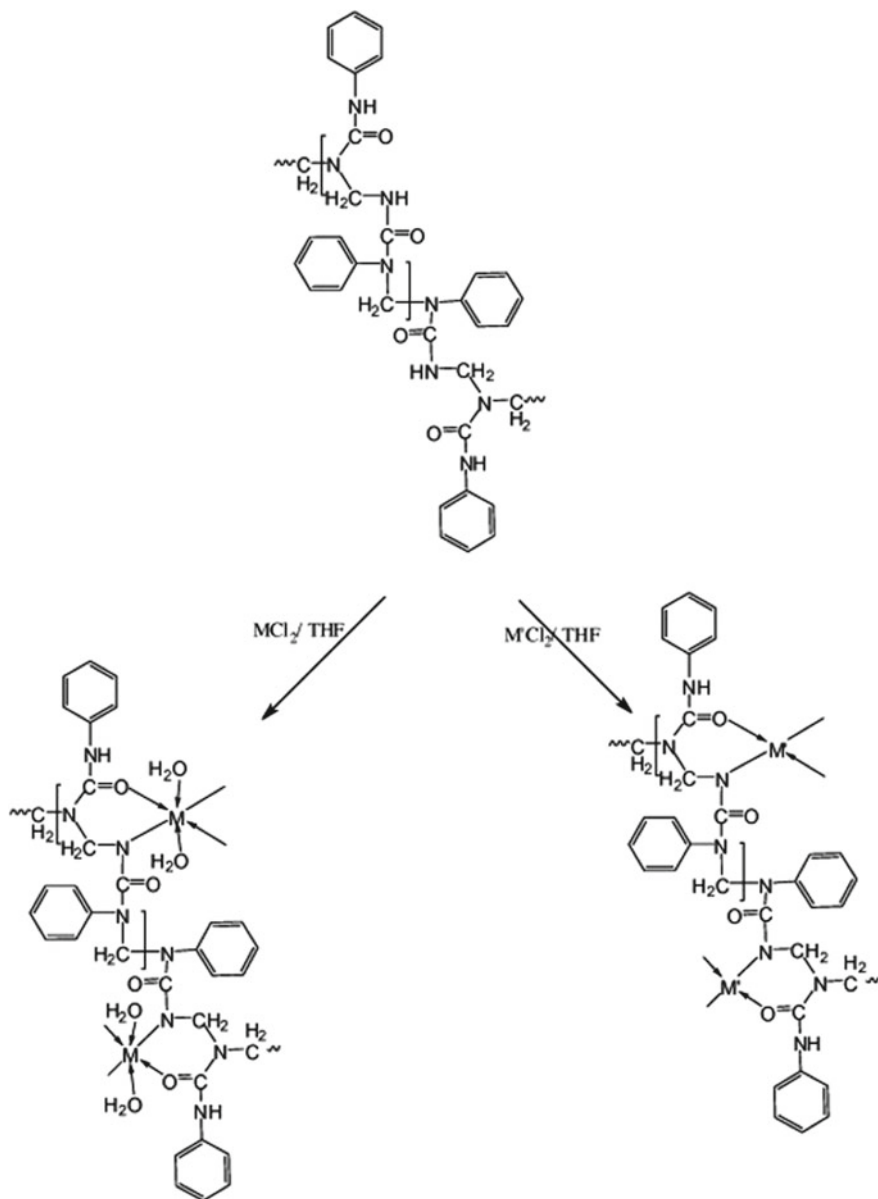
Scheme 3.48 Synthesis of metal chelates with CPL prepared by polycondensation of phenylurea and formaldehyde, where M = Mn(II), Co(II) and Ni(II); M′ = Cu(II) and Zn(II)
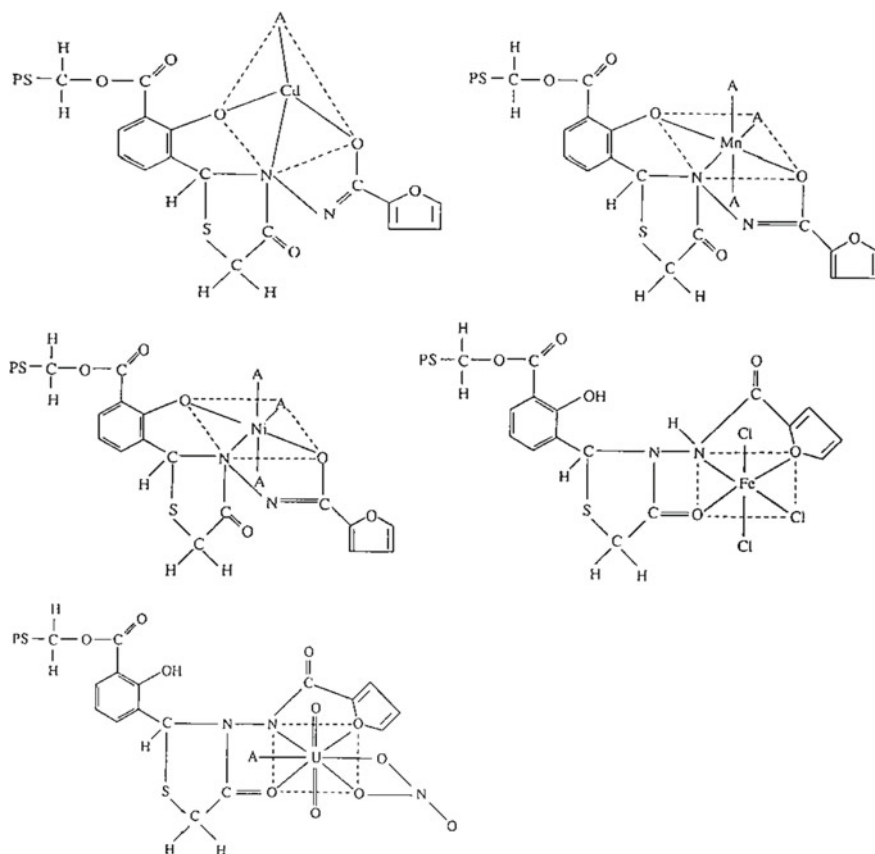
Fig. 3.55 Structure of PS-anchored chelates, where A is DMF
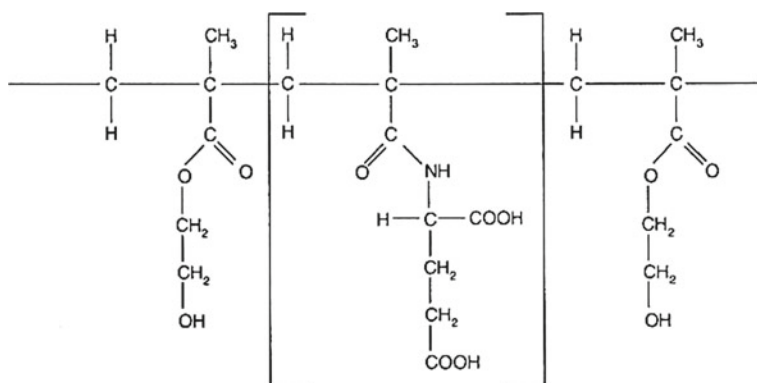
Of interest are PMC-Cu(II), -Pd(II), -Pt(II) and -Cd(II) based on homopolymer (4-acrylamido benzene sulphonyl guanidine) and different anions (SO_4^{2-}, CH_3COO^-, NO_3^-, Br^- or Cl^-) [459].
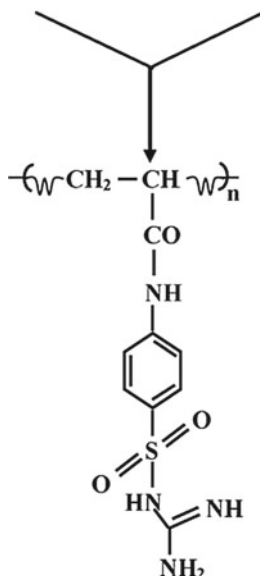
The metal chelation proceeds with the participation of oxygen (of O–S–O fragment) and nitrogen atom [of imino/nitrogen (NH/N) of the guanidine fragment]. It is interesting that the homopolymer acts as both neutral and monobasic bidentate ligand chelated through the –N and –O atoms. The PMCs have 1:1 or 1:2 (M–L) compositions and show four types of coordination (Fig. 3.56).

It should be noted Mn(II)-, UO_2(II)-, Zr(IV)- and Nb(V)-PMCs with CPL based on 2-acrolyl-quinazolin-carboxyl [460], in which the metal ions form octahedral complexes.
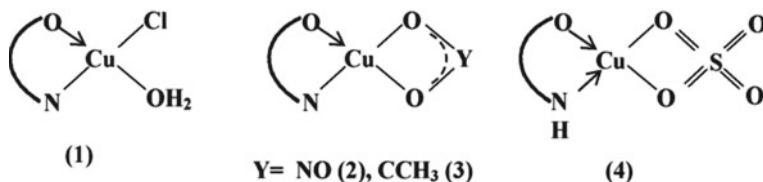
Fig. 3.56 Structures of PMCs: (**1**) $[Cu(L)Cl\cdot OH_2]$, (**2**) $[Cu(L)O_2NO]$, (**3**) $[Cu(L)OAc]$ and (**4**) $[Cu(HL)O_2SO_2]$
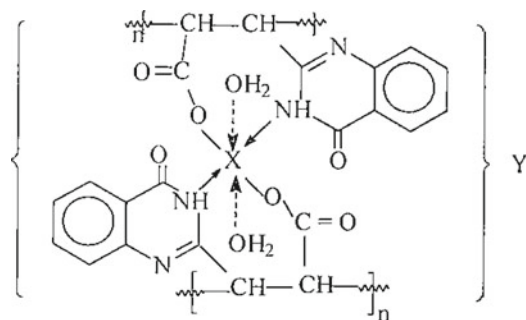
$X = UO_2$, $Y = -$; $X = Nb$, $Y = Cl_3$; $X = Zr$, $Y = Cl_3$.

Of interest are PMCs with the 2:1 (L:M) composition based on semicarbazide-formaldehyde resin [461].
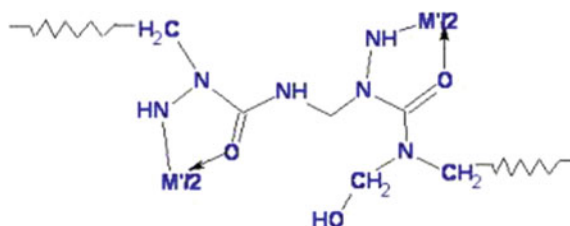
3.2.14 Chelation with N,S-Containing Ligands

CPLs bearing nitrogen and sulfur functionalities, especially polymers containing thiourea groups, have the ability of adsorbing precious ions (such as Au, Ag, Pt) and heavy metal ions (such as Cd, Pb, Cu) [462]. The interaction of thiourea with formaldehyde was used for the preparation of the CPL [463]. The experiment showed that the thiourea-formaldehyde CPL has better chelation ability to Pb, Au and Hg ions. On this basis, some CPL with thiourea as a main component also gets the corresponding development and application. Thus, a water-soluble thiourea-formaldehyde CPL chelated the heavy metal ions [464]. Formaldehyde, thiourea and melamine were used as raw materials to synthesize a CPL having chelation ability to Pd(II) [465]. It should be noted the CPL based on biphenol, thiourea and formalde-hyde [466] as well as CPLs such as thiourea-formaldehyde resin, semicarbazide-formaldehyde resin, and thiosemicarbazide-formaldehyde resin [467–470].
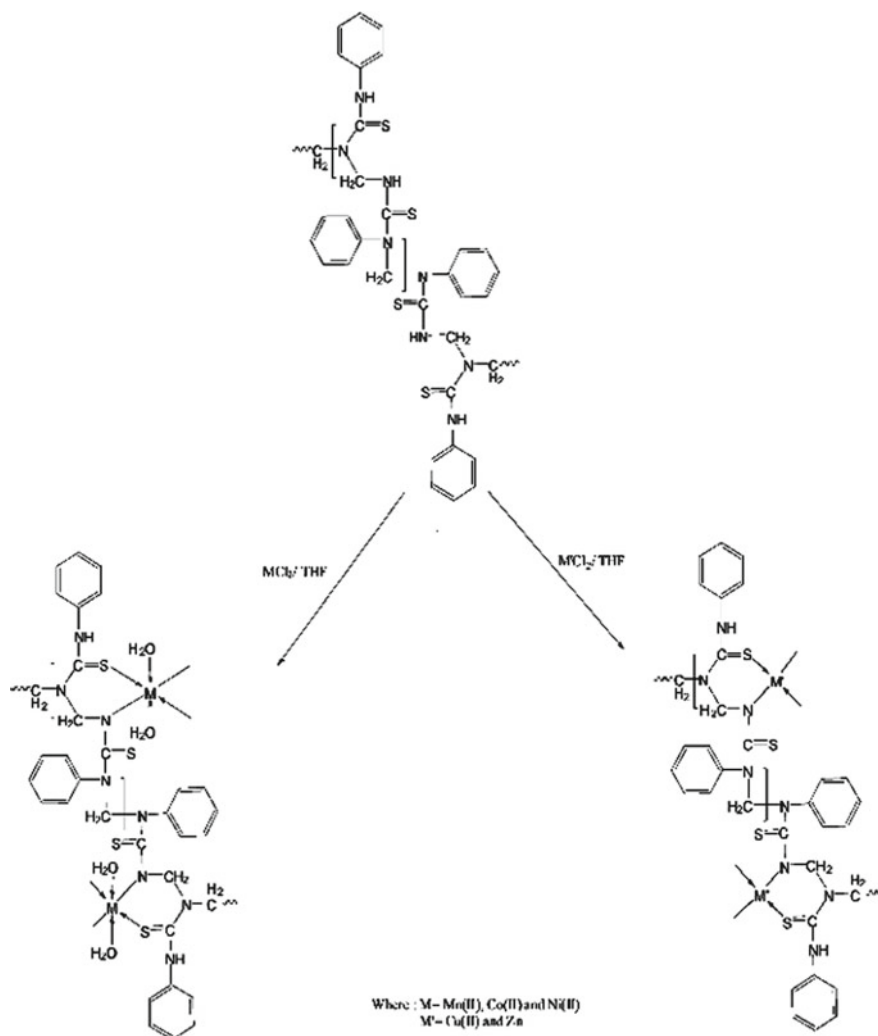
Scheme 3.49 Synthesis of PMCs with phenylthiourea-formaldehyde CPL

PMCs-M(II) were prepared by the interaction of Mn(II), Co(II), Ni(II), Cu(II), and Zn(II) ions with phenylthiourea-formaldehyde CPL (Scheme 3.49) [471]. It should be noted that Mn(II)-, Co(II)- and Ni(II)-PMCs have octahedral structure, while Cu(II)- and Zn(II)-PMCs exhibit square planar and tetrahedral structure, respectively.

Nearly 100% elimination of Pb(II) and Hg(II) ions was reached using poly (thiourea-amides) with C=S groups based on aromatic or aromatic-aliphatic diamines and the diacid chlorides [472].

It should be noted that the maximum chelation capacities of PCD functionalized with dithiooxamide found are 0.97, 0.12, 0.08, and 0.12 mmol g^{-1} for Cu(II), Zn (II), Cd(II), and Pb(II), respectively [473]. Assuming that all the nitrogen and sulfur are part of the chelating fragment, the capacity should be 1.0 mmol g^{-1}, but actually, it is 0.97 mmol g^{-1}. The lower value may be due to the rigidity of the polymeric matrix and inability of all the chelating fragments to participate in chelation for steric restriction.
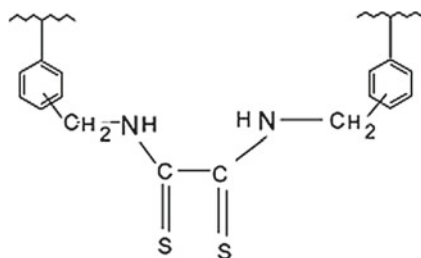
Dithiooxamide-formaldehyde CPL can be used in the separation of silver ions [474]. 2,4-Dihydroxyacetophenone-dithiooxamide-formaldehyde CPL is an example of CPL functionalized with dithiooxamide and was used for chelation of Fe(III), Cu(II), Ni(II), Co(II), and Zn(II) ions [475]. Sulphanilic acid-dithiooxamide-formaldehyde and dithiooxamide-formaldehyde CPL (Fig. 3.57) showed chelation capacity forward to Ni(II) ion of 188.3 and 99.8 mg g^{-1}, respectively [476].

CPL containing S, N and O atoms was synthesized by using poly (2-hydroxyethylmercaptomethyl-St) and diethanolamine [477]. The saturated chelation capacity of CPL for Hg(II) could reach to about 1.1 mmol g^{-1} at 25 °C. It is important that the adsorption was controlled by liquid film diffusion. In addition, both N and S atoms were electron donors, while O atom did not take part in the chelation with Hg(II) and the existence of it only increased the hydrophilicity of CPL.
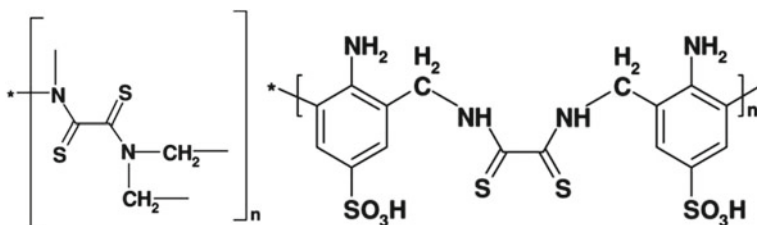
Fig. 3.57 The suggested chemical structures of dithiooxamide-formaldehyde CPL and sulphanilic acid-dithiooxamide-formaldehyde CPL
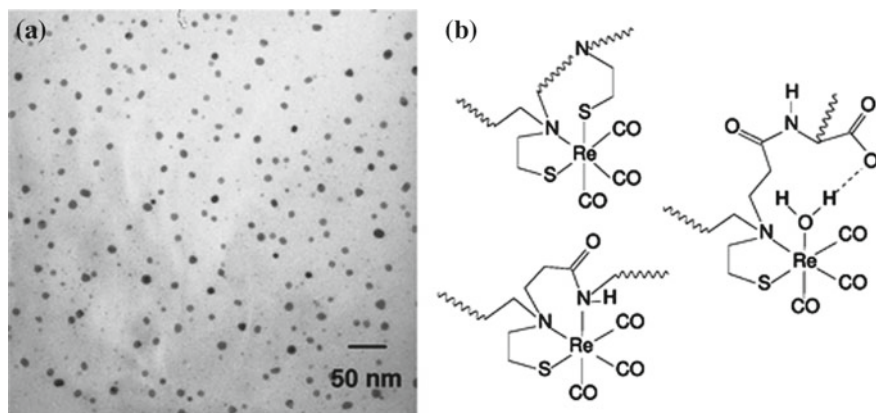
Fig. 3.58 a TEM photomicrograph of Re-PMC (magnification 105,000×) and **b** possible chelation environments of rhenium in PMC

Re-PMC was easily obtained by chelating an amphoteric thiol-functionalized PAMAM with $[Re(CO)_3(H_2O)_3](CF_3SO_3)$ [478]. It is important that both CPL and PMC-Re were soluble in water under physiological conditions. The radius of the Re-PMC was always slightly larger than that of the parent CPL and TEM analysis showed that PMC forms spherical nanoparticles with narrow size distributions (Fig. 3.58a). It should be noted that rhenium chelation proceeds with participation of the S and N atoms of the cysteamine fragment (Fig. 3.58b).

Upon treatment with $VO(acac)_2$ in DMF, the CPL based on salicylaldehyde and L-cysteine gave the oxidovanadium(IV) chelate (Scheme 3.50) [479]. According to the data of the EPR spectroscopy and magnetic susceptibility, there is antiferromagnetic exchange interaction between vanadium ions in the formed PMC.

Of interest is the Amberlite IR P69 modified with Schiff base derived from 2-picolyl amine and 2-mercapto-4-methyl-benzaldehyde and its PMC-Cr(III), -Co (II), -Ni(II) and -Cu(II) [480]. The results have deduced the coordination of nitrogen and sulphur atoms of Schiff base fragment of Amberlite IR P69 to the selected metal ions, as well as these data have confirmed the octahedral geometries for Cr (III)-PMC, tetrahedral symmetry for Co(II)- and square planner for Ni(II)- and Cu (II)-PMCs.
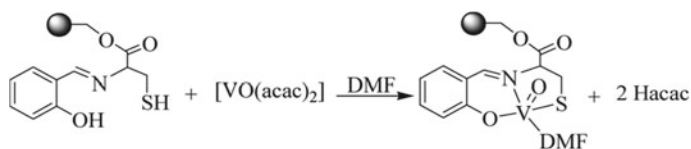
Scheme 3.50 Synthetic procedure for PMC
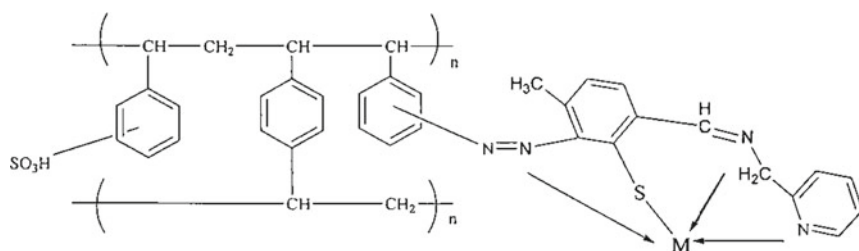
3.2.15 Metal Chelates Based on S,S-Containing Ligands

Among the S,S-containing CPLs, we note water-soluble CPLs including dithio-carbamate groups in PEI and in PAAm chains, which were used for chelation of heavy metal ions [481–483].

An interesting S,S-containing CPL is an amphoteric CPL flocculant [poly (dimethyl-diallylammonium chloride-*co*-AAm-*gr*-triethylenetetraminedithiocarbamate)], which the –CSS⁻ group reacted with Cu(II), Ni(II), Pb(II), and Cd(II) to form corresponding PMCs [484–488]. The K_S values of the PMC-Cu(II), PMC-Pb(II), PMC-Cd(II), and PMC-Ni(II) were $(1.37 \pm 0.35) \times 10^{12}, (3.26 \pm 0.39) \times 10^{11}, (2.05 \pm 0.27) \times 10^{11}$, and $(3.04 \pm 0.45) \times 10^{10}$, respectively. It is important that the –CSS⁻ fragments chelate with metal ions in several chelating modes (Fig. 3.59). Through the adjustment of spatial locations and conformation of the CPL chain, the –CSS⁻ fragments from the same or different CPL chains chelate with metal ions according to a molar ratio of 2:1, resulting in neutralization of the negative charges on CPL chains. The CPL chains twist to form microflocs, which further grow into larger ones through the adsorption of other flocs, bridging of CPL chains, or chelation of excess –CSS⁻ fragments from different flocs with the same metal ion. Excess negative floc charges caused by steric hindrance and spatial mismatch are effectively neutralized by the positive charges of the CPL chain. The positive charges of the CPL chains are conductive and bridge the flocs with negative charges, thus promoting the formation and growth of flocs and making them dense and thick.

The ability of the derivatives of PCD with N-ethylaminodithiocarbamate, N-ethanolaminodithiocarbamate, and N-*t*-butylaminodithiocarbamate fragments to form chelates with Hg(II), Pb(II), and Cd(II) ions is highest with Hg(II), followed by Pb(II), and then Cd(II) [489]. A general increase in the ability to chelate with metal ions was observed from the dithiocarbamate CPL derived from N-*t*-butylamino-PS to those derived from N-ethylamino-PS and N-ethanolamino-PS. In other words, the chelation level and preference among ions of these dithiocarbamate CPLs depends on the structures of their chelating fragments.
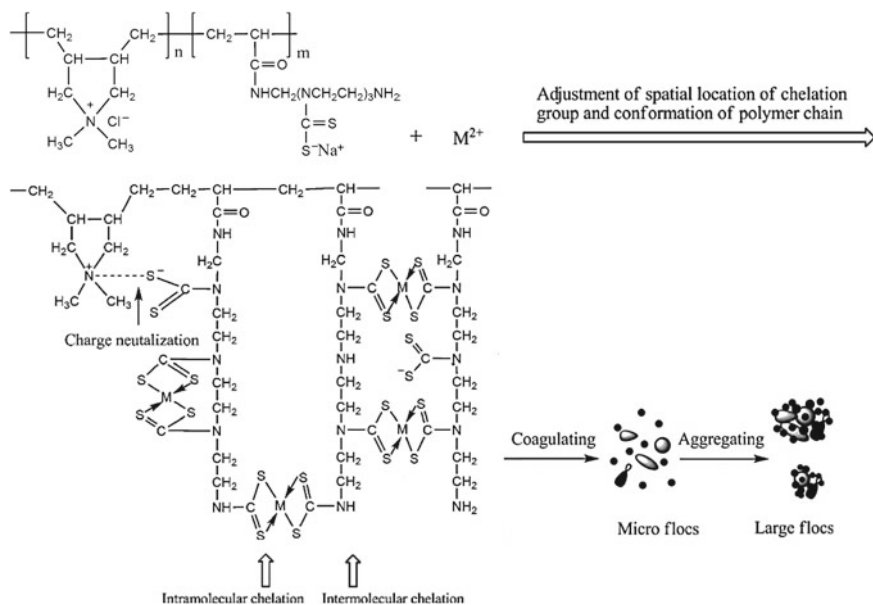
Fig. 3.59 Chelation mechanism of CPL with heavy metal ions, where M = Cu(II), Pb(II), Cd(II), Ni(II)

R = -CH₂CH₃, -CH₂CH₂OH, -C(CH₃)₃.
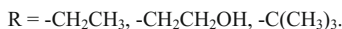
The interesting S,S-containing CPLs are polydithiocarbamates synthesized via Mannich-type polycondensation where aniline and a series of diaminoalkanes were linked together with paraformaldehyde and following treatment with carbon disulphide [490]. It is important that CPLs demonstrated high selectivity forward to Hg (II) ions. The CPL was dispersed into nanometer-size structures, which could explain the demonstrated improved affinity of the CPL towards Hg(II) ions and other toxic heavy metals.
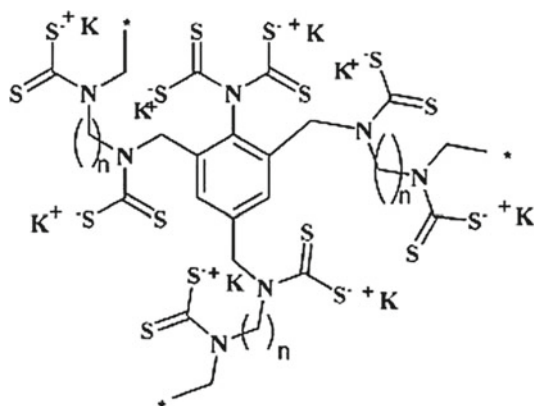
Of interest is a facile and high-recovery material for rare metals based on a CPL combining amino groups for water solubility and thiourea fragments for metal chelation (Fig. 3.60) [491]. The water-soluble CPL provides homogeneous chelation of metal ions in aqueous solution with high recovery efficiency at a high rate. It is important that as adsorption progresses, cross-linking between the thiocarbonyl sulfur atoms and the metal ions takes place, precipitating the PMC, which can be easily separated by filtration. For the recovery of Pd(II) by CPL, k was estimated to be 4.089 min^{-1}, which is 493 times greater than the equivalent value for CPL containing 99 mol% of thiourea fragments (0.0083 min^{-1}) due to its insolubility in the aqueous solution. Thus, improved CPL solubility significantly accelerated the recovery of Pd(II) from aqueous solution.
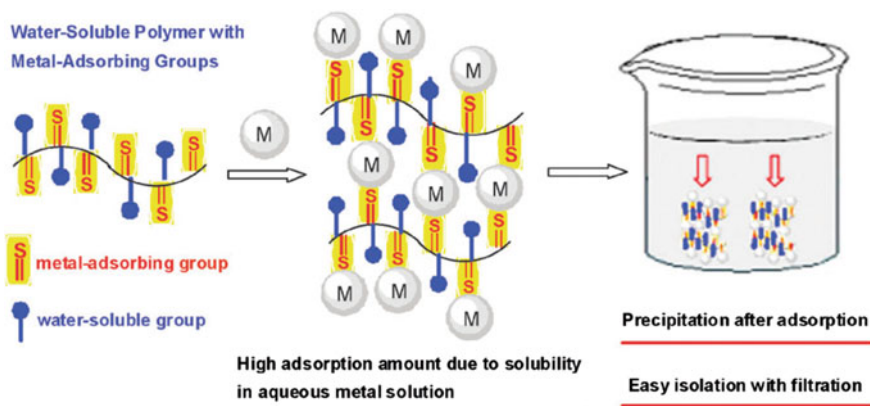
Fig. 3.60 Schematic representation of a facile and high-recovery system for rare metals using a water-soluble CPL

3.3   Macrocyclic Complexes

Here we will be examined the physicochemical properties and the structure of metal complexes with polymers containing macrocyclic fragments. PMCs of this type are of particular interest because, unlike other metal chelates, they are characterized by an increased stability due to the macrocyclic effect. The main attention will be paid to the macrocyclic complexes prepared by the direct interaction of CPL and MX_n.

3.3.1   Preparation of Metal Chelates with Participation of Cyclam-Containing Polymers

Among the macrocyclic complexes, the cyclam-containing PMCs occupy a significant place. Thus, the selective metal-chelating nanoparticles were prepared through the microemulsion copolymerization of a polymerizable tetraaza macrocycle, vinylbenzylcyclam, and the prepared CPLs showed a very high selectivity for Cu [492]. The cyclam modified with acryloyl chloride was polymerized to form the CPL, which was used for transition metal ion chelation studies [493]. This CPL showed high affinity for Cu(II) compared to the other metal ions.

Two macrocyclic ligands based on cyclam with *trans*-disposed N-methyl and N-(4-aminobenzyl) substituents as well as two methylphosphinic (H_2L1) or ethylphosphonic (H_4L2) acid pendant arms were employed in the modification of GL beads through a diazotization reaction (Fig. 3.61) [494]. The separation ability of the prepared CPL was tested with cold Cu(II) and non-carrier-added ^{64}Cu in the presence of a large excess of both Ni(II) and Zn(II). High overall separation efficiency was reached leading to 60–70% recovery of radiocopper with high selectivity over the other metal ions. It is important that the adsorption rate of metal ions on CPL beads generally depends on the chelation rate by CPL and on transport phenomena, especially on the diffusion rate and the accessibility of the chelating fragments.

It should be noted that the chelation of gold ions onto the cyclam-attached poly (*p*-chloromethylstyrene-ethylene glycol dimethacrylate) microbeads from solution was 6.18 mmol g^{-1} [495]. The selective adsorption of gold onto the CPL at pH 3.0 was very high compared to Cu(II), Ni(II), Co(II) and Zn(II). The similar results were obtained in studies of the adsorption of Au(III), Pt(IV) and Pd(II) ions on CPL prepared through a reaction between the vinylbenzyl chloride-DVB copolymer and the cyclam [496]. In this case, an outcome of up to 400 mg of noble metals per gram of dry CPL was reached.
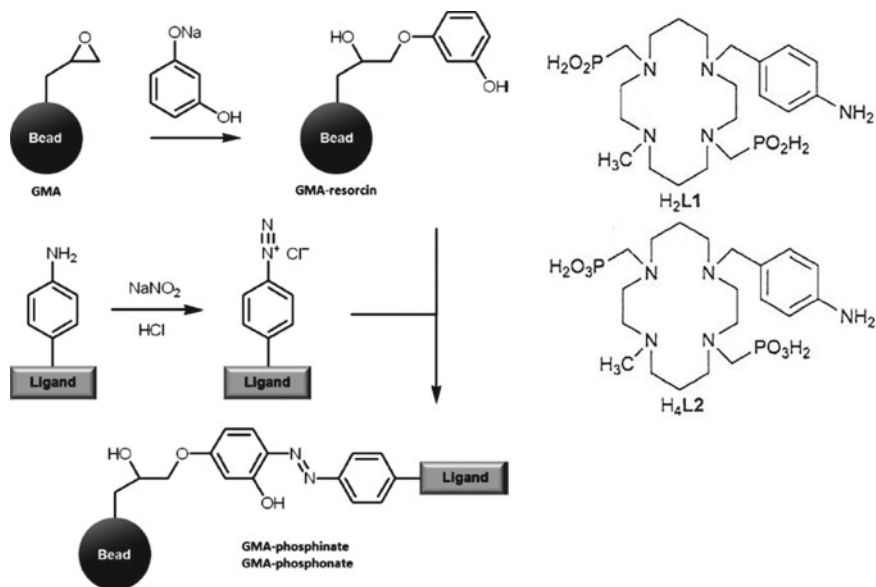
Fig. 3.61 Schematic representation of modification of macroporous polymer beads by ligands H_2L1 and H_4L2

3.3.2   Metal Chelates with Cyclen-Containing Polymers

The addition of metal salts to CPL containing cyclen, tri-*tert*-butyl-10-(2-(2-(2-(methacryloyloxy) ethoxy) ethoxy)-2-oxoethyl)-1,4,7,10-tetraazacyclododecane-1,4,7-tricarboxylate, leads to solid aggregates depending on metal salt nature (Scheme 3.51) [497]. In particular, $ZnCl_2$ formed a precipitate whereas NaCl and $Zn(OTf)_2$ did not.

The increasing metal salt-induced aggregation is easily monitored by DLS and turbidity data (Fig. 3.62). In particular, when mole ratios of metal salt to cyclen
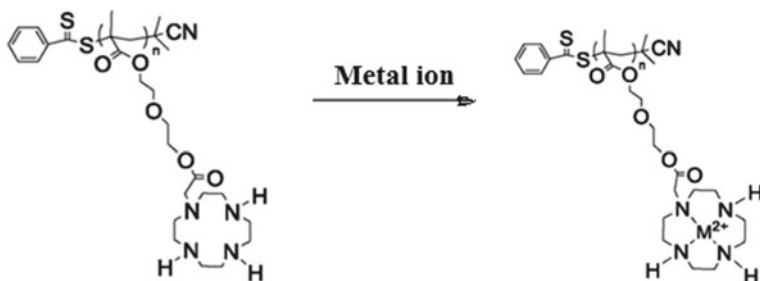
Scheme 3.51   The scheme of the synthesis of cyclen-based PMC
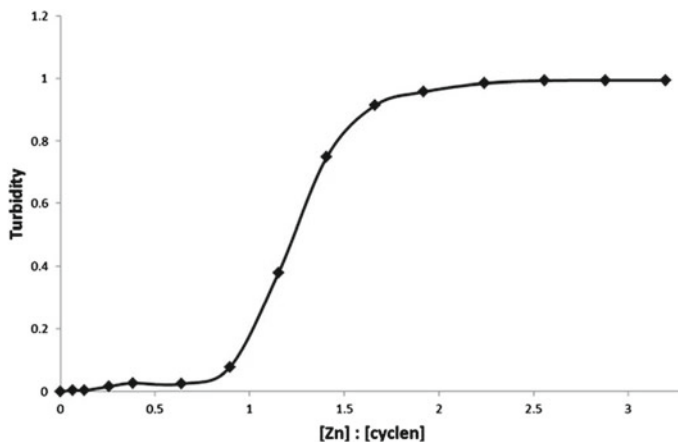
Fig. 3.62 DLS analysis of turbidity monitoring the self-assembly of the PMC-ZnCl$_2$ aggregates upon the addition of ZnCl$_2$ to CPL

fragments <0.8, the solution was transparent, and then turbidity rose rapidly with further addition of the salt.

It should be noted a Cu(II)-cyclen complex fixed on cross-linked poly (hydroxyethyl methacrylate) polymers [498] or derivatised polyurethane [499, 500]. Of interest is cyclen functionalization resulting in macromolecular (M$_w$ = 11,400) polycyclens [501].

3.3.3 Specifics of Chelation with DOTA and Related Ligands

Most studies of DOTA-containing polymers are devoted to the development of new polymeric contrast agents for MRT. Rational design of the chelating fragment, CPL or PMC allows to preparing polymeric contrast agents with desired biodistribution or to reflecting particular physiological phenomena. PLL is most widely used polymeric carrier for this purpose.
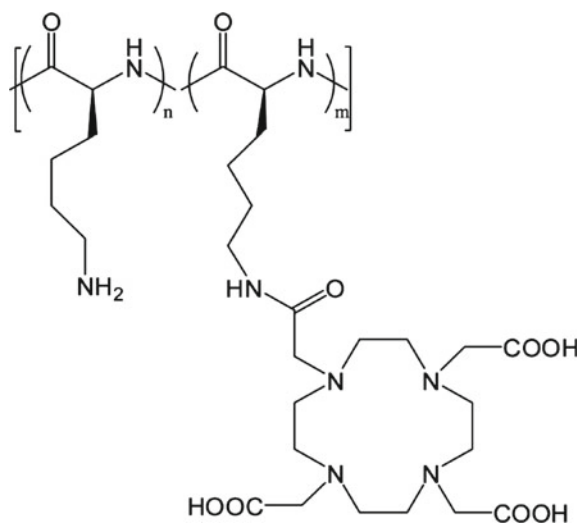
It should be noted the use of conjugated CPLs as contrast agent carriers [436]. Rigid architecture of the CPL leads to an increase in the τ_R and subsequently an increase in r_1. In particular, the r_1 of the CPL conjugated with DOTA-Gd(III) was 12.57 mM^{-1} s^{-1}, that higher than those of other polymers.
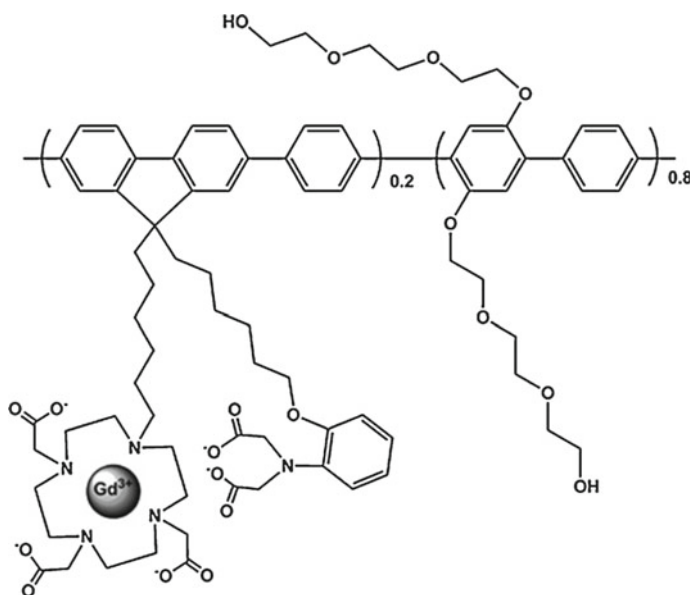
Copolymers of oligoethylene glycol methyl ether acrylate and an activated ester monomer, pentafluorophenyl acrylate, were modified with the DO3A-*t*-Bu-NH$_2$ chelate for the chelation of Gd(III), where DO3A is 1,4,7,10-tetraazacyclodocecane-1,4,7-triacetic acid [502]. It is important that the polymer architecture has a substantial effect on the relaxivity of the PMC-Gd(III) agents. In particular, CPL made from linear polymers showed a substantially increased relaxivity in comparison to existing commercial Gd(III) MRI contrast agents.

It should be noted poly [N-(3-aminopropyl) methacrylamide], which was coupled with DOTA, followed by conjugation with ^{64}Cu radionuclide (Scheme 3.52) [503]. It is interesting that prolonged retention of PMC-DOTA-^{64}Cu conjugates within the tumor tissues was demonstrated at 24 h, suggesting that the PMC-DOTA-^{64}Cu conjugates might be useful for interventional radionuclide therapy of locally recurrent prostate cancer in humans.

Of interest are safe and effective Gd-DOTA-based biodegradable polymeric MRI contrast agents for blood pool and cancer imaging [504]. The neutral biodegradable polymeric MRI contrast agent, N^1-lysylethylenediamine Gd-DOTA monoamide and dithiobispropionic acid copolymers, was synthesized through condensation polymerization of the DOTA monoamide and 3,3′-dithiobis[-sulfosuccinimidyl-propionate], followed by Gd(III) chelation (Scheme 3.53). The Gd(III) content in the agent was 16.1%, which corresponds to a chelation efficiency of 94.7% as compared with the calculated Gd content (17.0%). PMC-Ga has an apparent molecular weight of 23,000 a with T$_1$ relaxivities of 7.20 mM^{-1} s^{-1} per Gd at 1.5 T, and 6.62 mM^{-1} s^{-1} at 7.0 T. It should be emphasized that PMC-DOTA-Ga had high kinetic inertness against transmetallation with Zn(II) ions, and its polymer backbone was readily cleaved by L-cysteine.

Of interest is using copolymers of N,N-dimethyl-AAm with DOTA fragments for mass cytometry [505]. The CPLs had about 33 DOTA chelating fragments per chain.
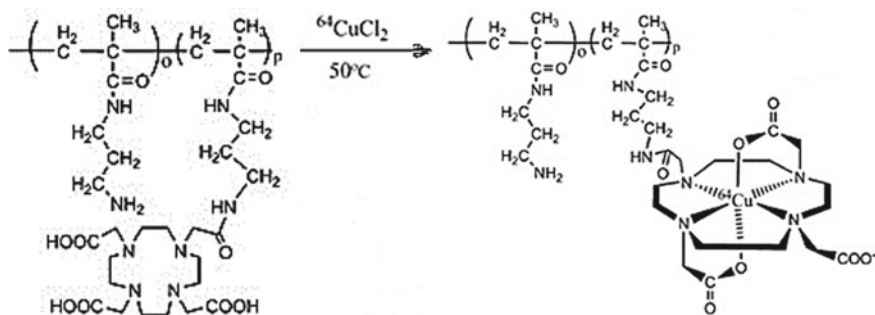
Scheme 3.52 The scheme of synthesis of PMC-DOTA-^{64}Cu conjugate
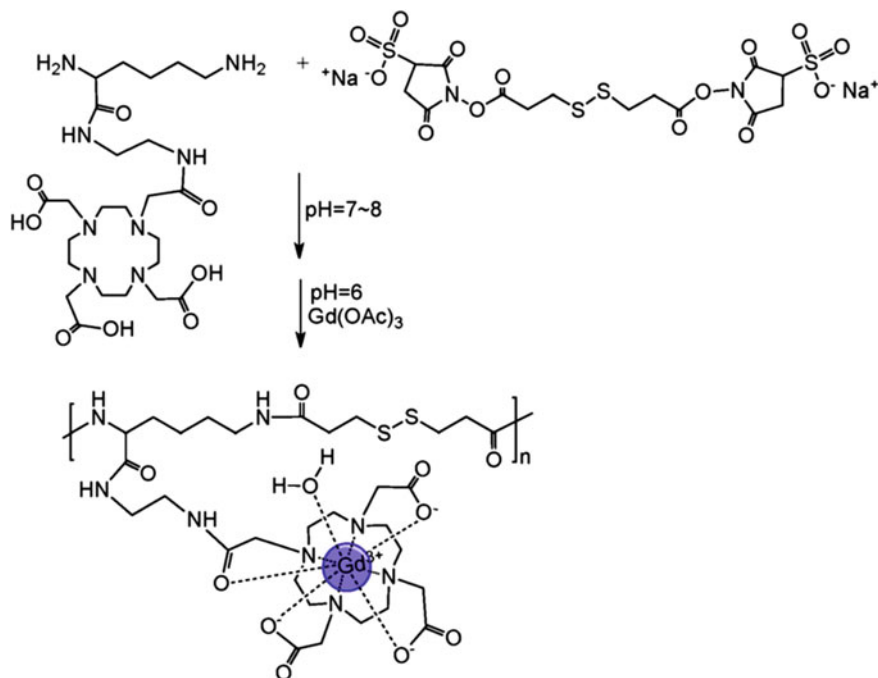
Scheme 3.53 Synthetic scheme of N^1-lysylethylenediamine Gd-DOTA monoamide and dithio-bispropionic acid copolymers

It should be noted Gd(III)-DOTA fixed on the copolymer of N-(2-hydroxypropyl) methacrylamide with mannosamine, which was used as a contrast agent specific for mannose receptors [506].

Special attention is paid to the macroporous CPLs as supports of β-emitters ^{177}Lu(III) and ^{131}I applied for radioembolization of liver tumors (Scheme 3.54) [507]. For example, GL carrying the primary amino groups was used for the fixing DOTA fragments, while HQ or HQ-5-sulfonic acid (8HQ5S) fragments, respectively, were linked with the polymer carrying secondary amino groups.

DOTA carrying CPL required heating to 80 °C while HQ or 8HQ5S fragments containing CPL were quantitatively radiolabeled within 1 h at room temperature (Table 3.12). It is important that HQ also allows to radiolabeling with ^{131}I. In addition, the ^{177}Lu(III) chelation rate for the DOTA carrying CPL is significantly slower than that for HQ or 8HQ5S carrying CPLs. Apparently, this is due by low conformational flexibility typical for chelation with participation of DOTA chelating ligands.
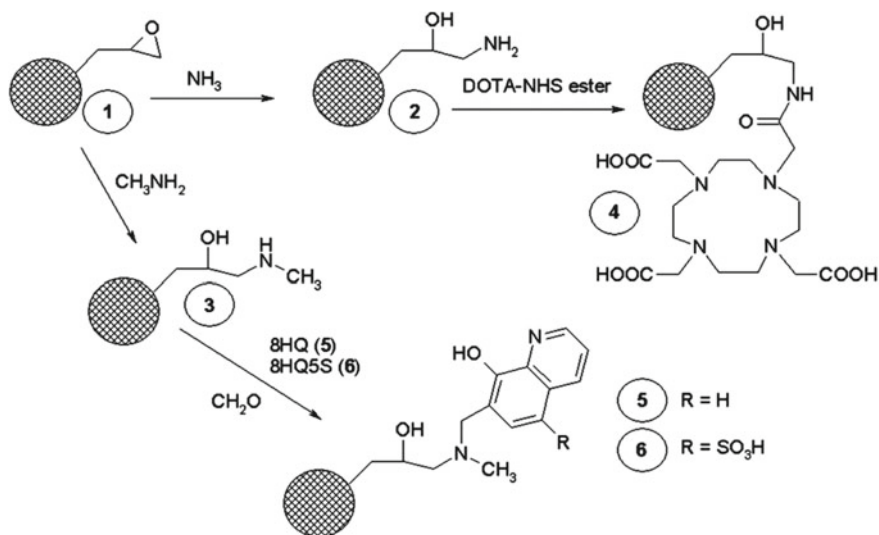
Scheme 3.54   Synthesis of CPLs

Table 3.12   Radiolabeling of the CPL beads with ^{177}Lu(III) as a function of pH at room temperature and at 80 °C; DOW is Dowex 50 W X8

Ligand	pH	Radiolabeling yield (%)				
		23 °C			80 °C	
		1 h	5 h	72 h	1 h	2 h
HQ	4.4	68	94	96	98	97
HQ	6.0	99	100	100	100	99
HQ	8.7	98	100	99	100	100
8HQ5S	4.4	100	100	100	100	100
8HQ5S	6.0	100	100	100	99	100
5HQ5S	8.7	99	100	100	100	100
DOW	4.4	44	64	64	77	86
DOW	6.0	16	47	46	52	48
DOW	8.7	75	83	80	51	50
DOTA	4.4	15	50	77	99	99
DOTA	6.0	29	72	99	99	99
DOTA	8.7	83	94	99	99	91

3.3.4   Metal Chelates Based on Polymeric Podands

CPLs containing podand polyamine arms bonded to gel polymeric matrix were effective CPLs of transition metal ions [508]. Their chelation capacities vary between 0.5 and 1.8 mmol g^{-1} depending on the CPL structure and metal nature. The complexes formed are analogous to those existing in the solutions containing

Table 3.13 ESR data for the CPL complexes with Cu (ClO$_4$)$_2$ at 77 K and metal ions concentration 0.5 mmol g^{-1}

Amine	g$_\parallel$	g$\perp$	A$_\parallel$ (mT)
H$_2$NCH$_2$CH$_2$NH$_2$	2.214	2.010	20.1
H$_2$N(CH$_2$CH$_2$NH)$_2$H	2.210	2.014	20.2
H$_2$N(CH$_2$CH$_2$NH)$_3$H	2.204	2.011	19.9
H$_2$N(CH$_2$CH$_2$NH)$_4$H	2.208	2.026	20.1
H$_2$N(CH$_2$CH$_2$NH)$_5$H	2.202	2.005	20.2

the appropriate metal and polyamine, but the rigidity of the CPL matrix causes a deformation of the coordination sphere and, in consequence, changes in some of spectral parameters. In particular, the anisotropic ESR spectra with two signals with g$_\parallel$ = 2.20–2.22 and g$\perp$ = 2.01–2.03 as well as a hyperfine coupling constant A$_\parallel$ = 19.9–20.2 mT were obtained (Table 3.13). The broadening of adsorption signals with increasing metal loading by the CPL indicates the dipolar interactions because of the small distances between the paramagnetic sites. The observed spectral parameters correspond to Cu(II) ion in slightly deformed square coordination (four nitrogen atoms in the equatorial plane), and the anion (ClO$_4$$^-$) or water molecules are weakly coordinated to Cu(II) ion in axial positions.

3.3.5   *Metal Chelates with Triolefinic Azamacrocycle*

It should be noted CPL prepared by the copolymerization of a 15-membered tri-olefinic azamacrocycle, named (E,E,E)-1-[(4-methylphenyl) sulfonyl]-6-[(2-trimethylsilylethyl) sulfonyl]-11-[(4-vinylphenyl) sulfonyl)]-1,6,11-triazacyclopentadeca-3,8,13-triene, with St, which was used for Pd and Pt adsorption [509]. The determined chelation capacity values are equal to 0.36 mmol g^{-1} of CPL for Pd(II) and 0.28 mmol g^{-1} of CPL for Pt(IV). Besides, the CPL presents a high selectivity towards precious metals over base metals such as Cu(II) and Ni(II).
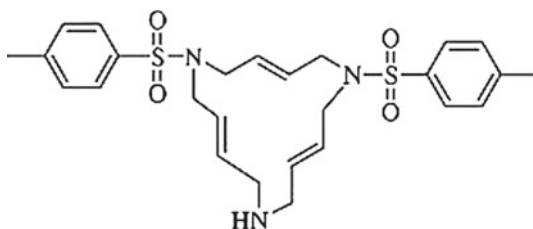
3.3.6 Porphyrin and Phthalocyanine Complexes

By now, a large number of Pp-based CPLs have been prepared, which are used in the synthesis of PMCs [510]. Metal incorporation into the "windows" of Pp-containing CPLs is often used to the preparation of the metalloporphyrin (M-Pp)) polymers. Thus, the Fe(III) chloride *meso*-tetraphenyl-Pp telechelic PS was obtained by metalation of CPL using FeCl$_2$ [511]. It should be noted an interesting route to macrocyclic PMC based on a unimolecular ring-closure process involving the direct end-to-end coupling of R,ω-bis[chloro-Fe(III) *meso*-tetraphenyl-Pp] telechelic linear PS with formation of a di-Fe(III)-μ-oxobis-(Pp) dimer as ring-closing fragment. It is important that addition of dilute HCl rapidly transforms the di-Fe(III)-μ-oxobis(Pp) fragment into the initial bis[chloro-Fe(III) Pp], indicating the selectivity and reversibility of this process.

The same processes proceed with participation of telechelic PEO bearing Fe(III) tetraphenyl-Pp chloride or Fe(II) tetraphenyl-Pp derivatives at their ends [512]. Such fully reversible chain end coupling processes take place under changes in acido-basic conditions, solvent nature, or the action of redox additives (Scheme 3.55). At low concentration, macrocyclic PEOs of same molar mass as the linear PEO precursors are almost exclusively formed via intramolecular coupling whereas increasing the PEO concentration yields both intra- and intermolecular chain coupling and formation of large macrocycles with [bis-Fe(III) μ-oxo-tetraphenyl-Pp PEO] repeating fragments.

Of interest are Pp-incorporated CPLs based on vinyl monomers and protoporphyrin IX disodium salt, which showed different metal chelation depending on pH (Scheme 3.56) [513].

Phthalocyanines, one of the best-known synthetic Pp analogues, are highly versatile and stable chelating fragments with unique physico-chemical properties that make them ideal building blocks for the construction of PMCs. Compared to low molecular weight Pc, relatively few reports describe the synthesis and properties of Pc-containing PMCs prepared by direct interaction of MX$_n$ and Pc-containing CPLs. As an example, we note *p*-xylylenebis-(oxa-thia-propan) bridged metal-free Pc polymer prepared by the reaction of a tetranitrile monomer with DBU in pentanol [514]. The metallophthalocyanine (M-Pc)) polymers were prepared by template method, including the reaction of the tetranitrile compound with the chlorides of Ni(II) and Co (II), acetates of Cu(II) and Zn(II), PbO and Fe(CO)$_5$, respectively. Besides, the extraction ability of CPL was also evaluated in THF using transition metal picrates, such as Ag(I), Hg(II), Pb(II), Cd(II), Cu(II) and Zn(II). It is important that the extraction affinity of CPL for Ag(I) is highest in the heterogeneous phase extraction experiments.

The similar results were obtained during the study of Pc-polymers based on *o*-bis [3-(3,4-dicyanophenoxy) propyloxy] benzene [515], bisphthalonitrile monomer [516] or tetranitrile monomer [517] and proper materials.

Of interest is the synthesis of an isoamethyrin derivative containing two CH$_2$CH$_2$CO$_2$CH$_3$ fragments in the β-pyrrolic positions and its use in the colorimetric
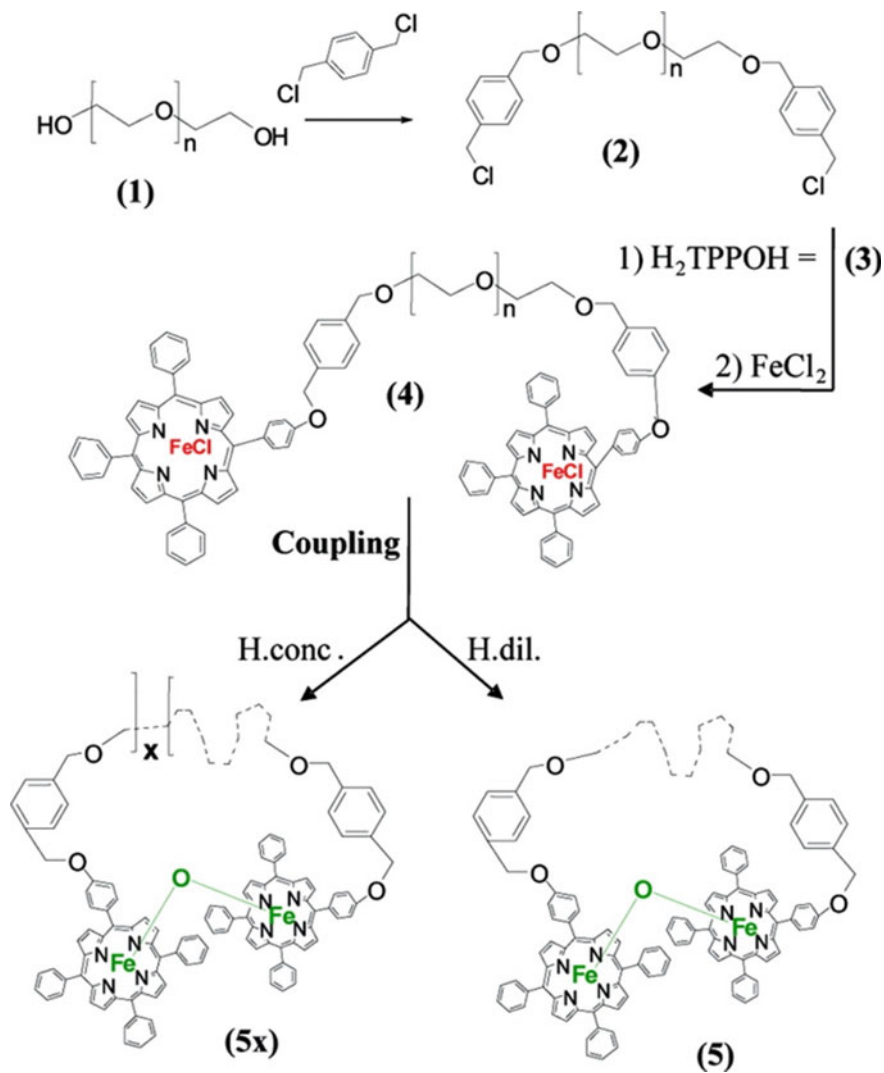
Scheme 3.55 Strategy of synthesis of telechelic PS with Fe(III) *meso*-tetraphenyl-Pp chloride ends and reversible switching between linear and macrocyclic PSs

detection of the uranyl cation after immobilization onto a solid support (a tentagel amino-terminated PS-PEG graft co-polymer resin) [518]. Isoamethyrin macrocycle has demonstrated greater specificity in terms of "sensing" the uranyl cation without interference from, e.g., lanthanide cations.

protoporphyrin IX disodium salt (PP)
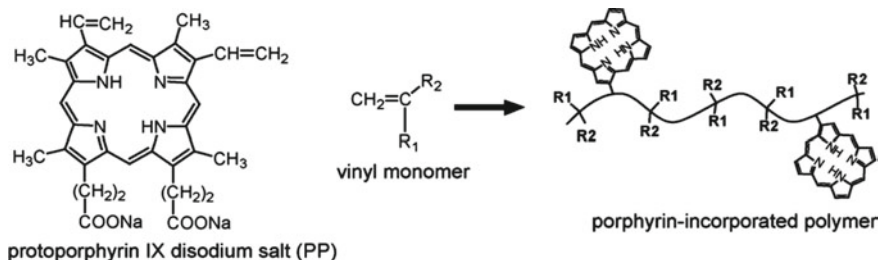
Scheme 3.56 Synthesis of Pp-incorporated PAAm (R_1: –$CONH_2$, R_2: –H) or PMMA (R_1: –COOH, R_2: –CH_3)
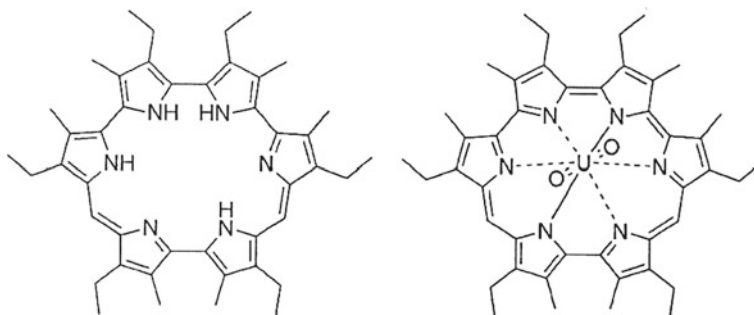
3.3.7 Metal Complexes Based on Crown Ethers

Crown ether polymers are among the thoroughly studied classes of CPLs, which can form stable complexes with many metal ions [519–521]. Thus, the covalent grafting of 4-amino benzo-9-crown-3 ether to poly (St-*alt*-maleic anhydride) allows to a considerable increasing the solubility of polymer in organic solvents, and the covalently linked 4-benzo-9-crown-3 ether allows the hosting of Li(I) ion [522]. Of interest is the study of the chelation of the lanthanides and poly(15-crown-5-2-yl-MMA) [523]. Addition of $KClO_4$ to the DMSO solutions of the CPL containing a benzo-15-crown-5-ether fragment caused the formation of the 2:1 inclusion between the 15-crown-5-ether ring and K(I) ion [524]. This inclusion led to a bathochromic shift in λ_{max} of the CPL. Besides, PL intensity of the CPL decreased after the addition of $KClO_4$ to solution.

$Ar = none,$ and   (structural fragments with C_8H_{17} substituents)
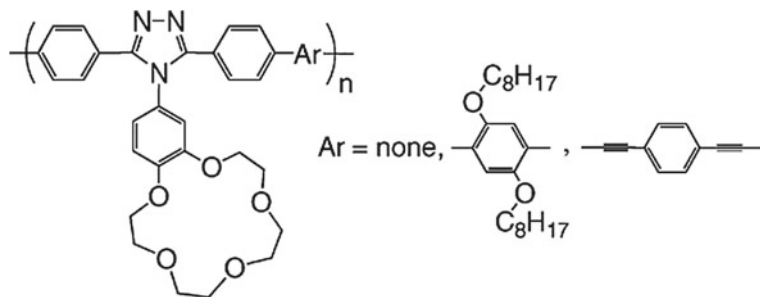
According to the theoretical study of interactions of Li(I), Na(I) and K(I) ions with poly(bithiophene) containing a 15-crown-5-ether bound to two adjacent thiophene rings, the substantial conformational flexibility of the CPL is reduced during the introduction of a metal ion in the cavity of the macrocycle [525]. It should be noted colorimetric self-assembled vesicular receptors with embedded receptor fragments for metal ions based on benzo-15-crown-5 functionalized polydiacetylene and 10,12-pentacosadiynoic acid [526]. Upon addition of alkali, alkaline earth and transition metal cations such as Na(I), K(I), Mg(II), Ca(II), Fe(II), Co(II), Cu(II), Mn(II), Ba(II), Cd(II), Ag(I), Pb(II) and Zn(II), only Pb(II) ion could induce a color change from blue to red observable by the naked eye. This change clearly showed that CPL vesicles could act as a highly selective and sensitive probe to detect Pb(II) ions in aqueous solution, which was mainly attributed to the stronger complexation interaction between the crown ether derivatives, Pb(II) ions and carboxylic acid functional groups with formation of sandwich complexes leading to the strong aggregation of the CPL vesicles. It is important that multivalent and strong coordination of benzo-15-crown-5 and carboxylate to Pb(II) ions could perturb the polydiacetylene backbone, which dominated the robust color and absorption spectral change of the CPL vesicles (Fig. 3.63).

A thermoresponsive hydrogel based on NIPAM and benzo-18-crown-6-acrylamide could respond to both temperature and ion stimuli (Scheme 3.57) [527]. When the crown ether fragments associated Ba(II) and formed stable complexes, the LCST of the hydrogel increased due to the repulsion among charged benzo-18-crown-6-acrylamide/ Ba(II) complex fragments and osmotic pressure within the hydrogel. Whereas crown ethers associated Cs(I) ion, the LCST shifted to a lower temperature because of the formation of 2:1 sandwich complexes.

The study of the Pb(II) responsibility to the same hydrogel in water has shown that the microgel size first decreases, followed by gradual increasing [528]. It should be noted that the addition of inorganic salt has two opposite effects on the swelling of microgel. On one hand, with increasing salt concentration and hence increasing ionic strength, water becomes gradually a relatively poor solution for CPL; therefore, the swelling degree of microgel may decrease with increasing salt concentration. On the other hand, the metal cations can bind with the crown ether fragments to form host-guest complex. As a result, the hydrophilicity of the

(a)

(b)
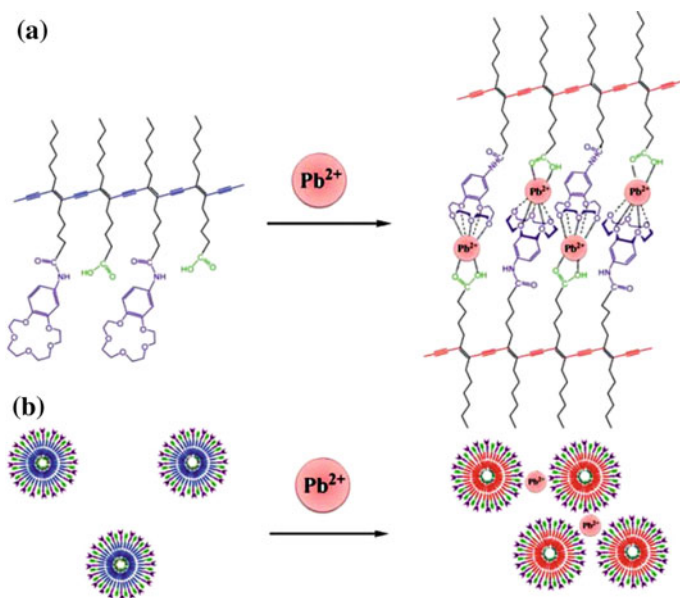
Fig. 3.63 Schematic representation of the Pb(II) ion response of self-assembled CPL vesicles
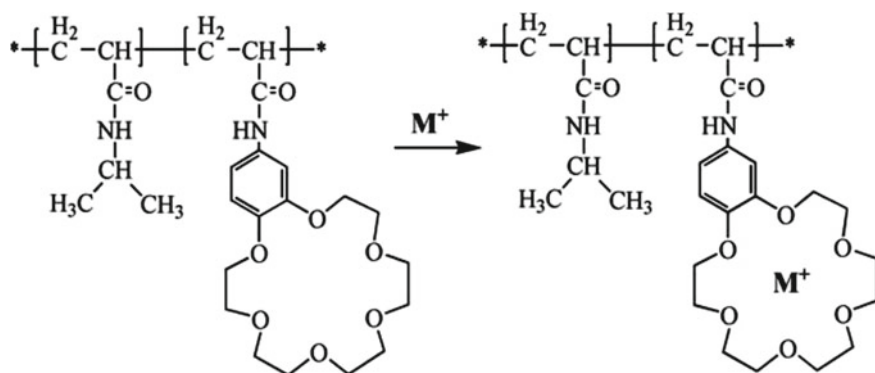
Scheme 3.57 Binding of metal cations with crown ether groups in hydrogel

polymer increases, so the swelling degree of microgel may increase with increasing salt concentration. As a combined result of the two opposite effects, the microgel size decreases with [Pb(II)] first but increases as [Pb(II)] continues to increase (Fig. 3.64).

When poly (NIPAM-*co*-benzo-18-crown-6-acrylamide) form stable host-guest complexes, the LCST of poly (NIPAM-*co*-benzo-18-crown-6-acrylamide) increases due to the repulsion among charged benzo-18-crown-6-acrylamide/M^{n+} complex
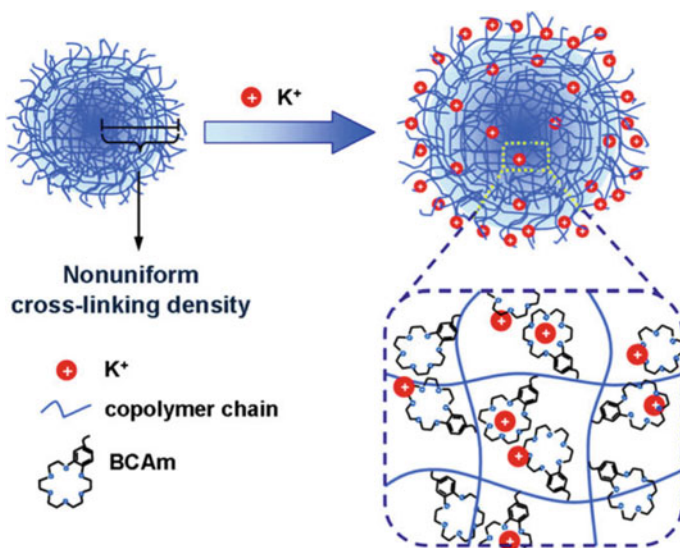
Fig. 3.64 The schematic illustration of ion-recognition behavior of poly (NIPAM-*co*-benzo-18-crown-6-acrylamide) microspheres

fragments and the enhancement of hydrophilicity, and the order of the shift degree of LCST of CPL is Pb(II) > Ba(II) > Sr(II) > Hg(II) > K(I) [529]. With increasing the content of pendent crown ether fragments, the LCST shift degree increases first and then stays unchanged when the benzo-18-crown-6-acrylamide content is higher than 20 mol%. It is interesting that there exists an optimal ion-responsive concentration for the CPL linear copolymer and cross-linked hydrogel in response to special metal ions, at which concentration the CPL exhibits the most significant ion-responsivity either in the form of linear copolymers or cross-linked hydrogels. With an increase of the content of crown ether fragments, the value of corresponding optimal ion-responsive concentration increases. It is important that an optimal molar ratio of metal ion to crown ether for the CPL in response to Pb(II) is around 4.5 (mol/mol). If the ion concentration is too high, the ion-responsive behaviors of CPL may even become surprisingly unobvious.

An electroactive polyamide with dibenzo-18-crown-6 and well-defined oligoaniline in the main chain showed the selectivity toward K(I) ions [530].
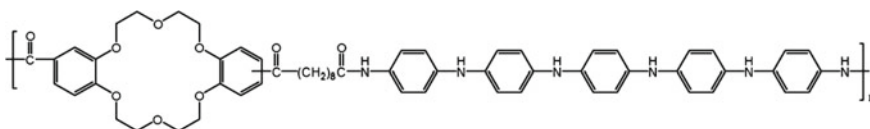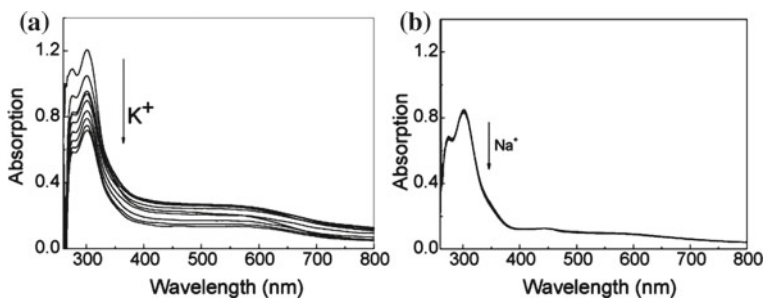
Fig. 3.65 UV-vis spectra of polyamide in solution in the absence (the uppermost curve) and presence of K(I) and Na(I) ions

In particular, the absorption attenuation of the polyamide solution is found upon K(I) binding (Fig. 3.65a). So it can conclude that with K(I) binding to the CPL can greatly impact electronic structure of the polymer. However, the absorption of the CPL solution to Na(I) ions (Fig. 3.65b) has almost no shift. Accordingly, the CPL shows a good selectivity toward K(I) ions compared to Na(I) ions.

Cross-linked copolymers based on PAA and functionalized with crown-ethers is selective sorbent for K(I) as compared on Li(I) and Na(I) [531] as well as on Cu(II) and for Ni(II) [532].

It should be noted that K(I), Pb(II), Cd(II) and Ba(II) ions enhance the fluorescence of the chiral conjugated CPL obtained by the polymerization of (S)-6,6′-dibromo-2,2′-binaphtho-20-crown-6 and 1,4-divinyl-2,5-dibutoxybenzene (Scheme 3.58) [533]. In contrast, Hg(II) causes effective quenching of the fluorescence of the CPL. The obvious influences on the fluorescence indicate that the 2,2′-binaphtho-20-crown-6 fragments plays an important role in fluorescence recognition for Hg(II).

The polyamides bearing benzo-12-crown-4, benzo-15-crown-5, benzo-18-crown-6 and oxyethylene dipodal arms as pendant structures acting as cation host fragments were used in competitive solid-phase extraction of nitrate cations [534]. The most

$M = Hg^{2+}, K^+, Pb^{2+}, Cd^{2+}, Ba^{2+}$
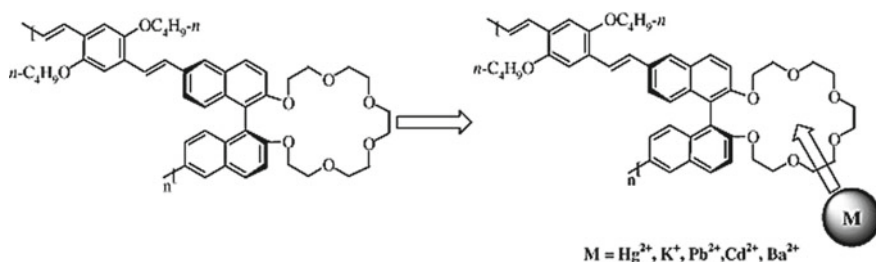
Scheme 3.58 Complexation of metal ion with chiral conjugated CPL containing 20-crown-6 fragments

striking result is the noteworthy extraction percentage, nigh on 100%, of Pb(II) by CPL bearing the benzo-18-crown-6 fragment with a remarkable selectivity. Besides, benzo-12-crown-4 CPL could be proposed for the extraction of Zn(II) in water solution.

Of interest are crown ether functionalized polythiophenes as chemical sensors [535, 536].
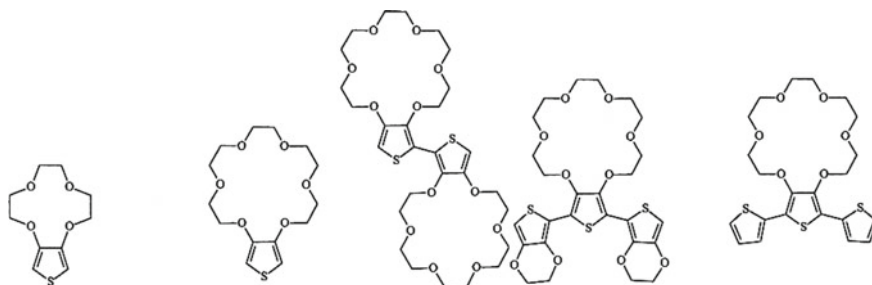
CPL prepared from MMA, calix[4]pyrrole, and the benzo-15-crown-5 derivative contains pendant benzo-15-crown-5 fragments capable of forming 2:1 sandwich complexes with potassium cations [537]. This, in turn, allows the CPL as a whole to overcome the relatively high hydration energies of KF and KCl and enables their extraction from aqueous media with efficiencies that exceed those expected on the basis of the effective concentration of the individual receptors (crown ether and calixpyrrole).
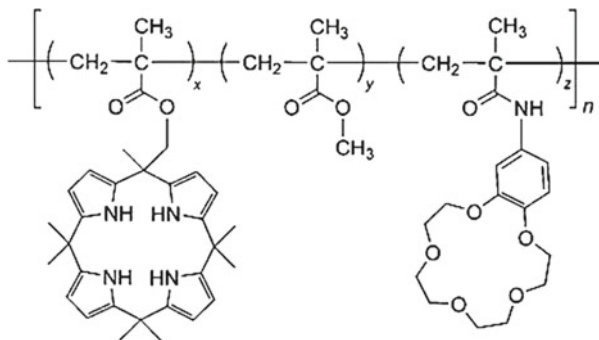
The calix[4]crown-4 oligomers, in particular, *p-tert*-butylcalix[4]crown-4 oligomer, *p-tert*-butylcalix[4]dioxacrown-4 oligomer, *p-tert*-butylcalix[4] diazacrown-4 oligomer, are good CPLs for metal ions as compared on with monomer analogues [538].

X

$CH_2OCH_2CH_2OCH_2$

$COCH_2CH_2OC$ (with O double bonds above both C)

$CONHCH_2CH_2NHCO$
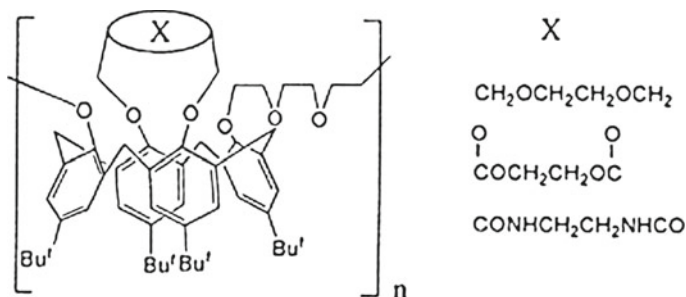
3.3.8   Polymeric Azacrown Ethers as Chelating Ligands

Copoly (*p*-phenylene) containing pendent azacrown ether and ethylene glycol ether was applied for chemical sensor [539]. The CPL exhibited specific selectivity and high sensitivity toward Zn(II), with the K_{sv} being 3.66×10^6 at low concentration. It is important that the CPL maintained high selectivity toward Zn(II) in the presence of fifteen interfering metal ions.
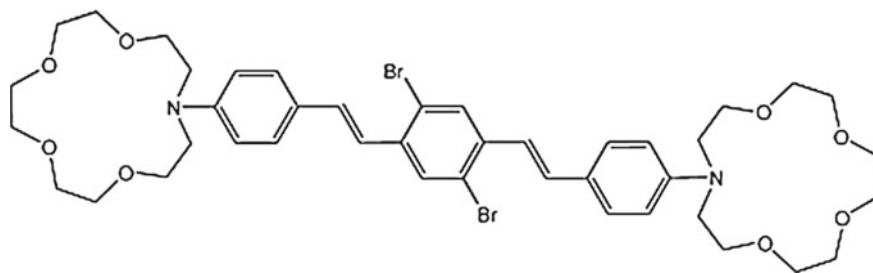
The fluorescence behaviors of the CPL bearing aza-12-crown-4, 15-crown-5 and 18-crown-6 ether and anthracene fragments were synthesized using methacrylates of N-2-ethyl-azacrown ether or 9-hydroxymethylanthracene (Fig. 3.66) [540]. The largest change in fluorescence behavior was observed for the CPL bearing aza-18-crown-6 in the presence of K(I). The magnitude of the increase in the fluorescence intensity was related to the content of the crown ether moiety. Thus, if the number of azacrown ether fragments in the CPL increases, PET from the nitrogen atom on the azacrown ether fragment to the anthracene fragment is more strongly interrupted when most of the azacrown ether fragments are chelated to metal ions.
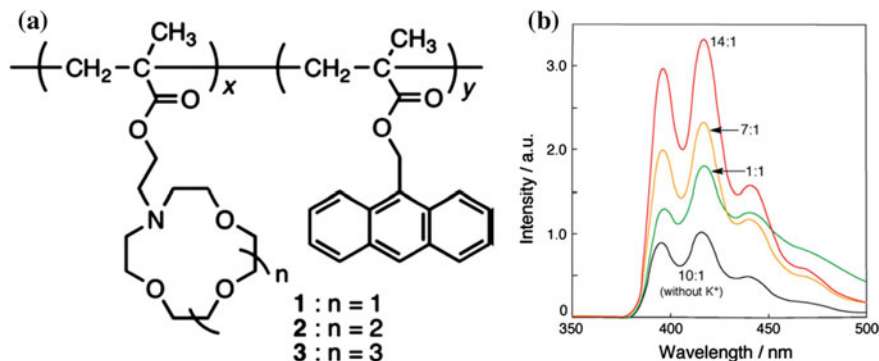
Fig. 3.66 **a** The structures of CPL. **b** Fluorescence spectral changes for aza-18-crown-6 CPL with different compositions of crown ether unit. The vertical axis units are normalized against the maximum fluorescence intensity of the copolymer in which the composition is crown ether: anthracene = 10:1 in the absence of K(I). $[KClO_4] = 1.0 \times 10^{-3}$ mol dm^{-3} and [anthracene unit] = 1.0×10^{-5} mol dm^{-3} in THF:H$_2$O = 10:1; λ_{ex} = 266 nm

It should be noted the segmented poly(ether-urethane-ureas) containing azacrown ether (cryptand) synthesized via the reaction of kryptofix 22 with 4,4′-methylene-bis-(4-phenylisocyanate), and different molecular weights of PEGs [541]. The obtained data confirmed chelation ability of these CPL for Li(I) ion and revealed the effect of Li(I) ion chelation on the morphology and thermal behavior of the CPL. In another example, a cross-linked poly (AA-co-cryptofix-22) superabsorbent copolymer was synthesized by the reaction of 4,13-dimethylacryloyl-1,7,10,16-tetraoxa-4,13-diazacyclooctadecane and AA [542]. It is important that the sorption rates decrease in the following row: Pb(II) > Cu(II) > Cr(III) = Cd(II) = Zn(II) > Ni(II) > Mn(II).
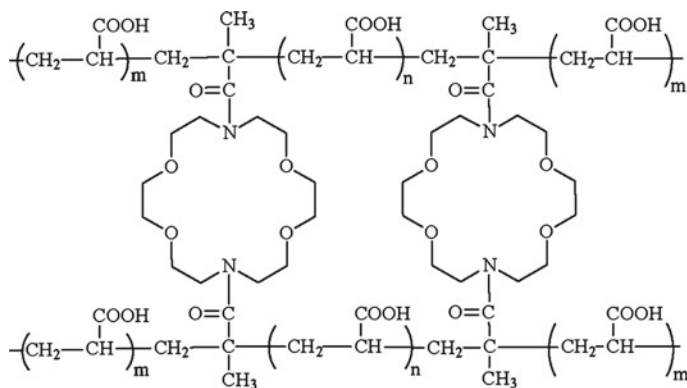
Of interest is CPL carrying monoaza-12-crown-4 and spirobenzopyran fragments at the side chains [543]. The CPL can bind alkali metal ions with their crown

ether fragment in the selectivity order of Na(I) > K(I) > Li(I). Besides, the spiroben-zopyran fragment undergoes UV-light-induced isomerization from its SP to the MC form, leading to MC aggregate formation. The metal-ion complexation of the crown ether fragment enhanced interchain MC aggregation by extending the polymer chain on the basis of the electrostatic repulsion between the associated metal ions.

Polyimides with diaza-18-crown-6 fragments on the main chain synthesized by the reaction between 4,4′-(hexafluoroisopropylidene) diphthalic anhydride and different macrocyclic diamine monomers formed the corresponding barium complexes [544]. The CPLs and their barium complexes exhibit different electronic absorption properties, which is attributed to the formation of charge-transfer excited states. The binding of barium ion to the polymer main chain may affect the energy level of the resulting charge transfer states. Besides, the emission properties of the CPL with and without barium ion are also different.

CPL prepared by fixing monoaza dibenzo18-crown-6 ether on modified Amberlite-XAD-4 is good adsorbent for rare earth metals [545].
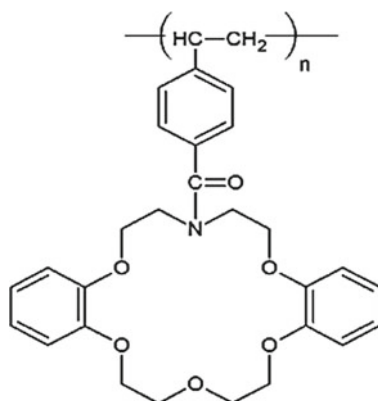
According to the obtained results (Table 3.14), the limits of detection (LOD at n = 5) and limits of quantification (LOQ at n = 5) for La(III), Nd(III) and Sm(III) were equal to 3.9, 4.2 and 7.4 µg L^{-1} and 13, 15 and 26 µg L^{-1}, respectively.

It should be noted CPL carrying monoazacrown side chain with a M_n of over 5000 which showed high chelation capacity for Na(I) and K(I), whereas K(I) was preferentially chelated by the monomers [546]. It should be noted that the CPL having the N-(2-naphthoyl) azacrown ether pendant fragments have a selective UV-responsive complexation with Li(I) in 1,2-dichloroethane-CH$_3$CN.

3.3.9   Metal Complexes with Thiacrown Ethers

Of interest are colorimetric and turn-on fluorescent dual-modal mercury sensors based on the styryl BODIPY scaffold attached to a hydrophilic PEG [547]. It is

Table 3.14 Parameters optimized for sorption and desorption of La(III), Nd(III) and Sm(III) on Amberlite XAD-4-monoaza dibenzo 18 crown-6

Parameters	Metal ions		
	La(III)	Nd(III)	Sm(III)
Sorption pH	4.5	4.5	4.5
Flow rate (mL min^{-1})	1.0	1.0	1.0
Eluting agent	2 M HCl	2 M HCl	2 M HCl
Sorption capacity (mmol g^{-1})	0.066	0.064	0.062
Distribution coefficient (K_d)	4272	4190	4076
Preconcentration factors (PF)	120	131	151
Breakthrough capacity (mg g^{-1})	2.1	2.2	2.3
R.S.D. (%)	1.3	1.5	2.6
LOD (µg L^{-1})	3.9	4.2	7.4
LOQ (µg L^{-1})	13	15	26

important that CPL exhibits an excellent spectral response to Hg(II) by inhibiting the intramolecular charge transfer effect from the Hg(II) specific ligand, dithia-dioxa-aza cyclopentadecane, to the BODIPY core. Upon addition of Hg(II), a significant fluorescence enhancing property in conjunction with a visible colorimetric change can be observed. These CPLs are highly selective for Hg(II) over other cations, whereas CPL with one Hg(II) binding fragment exhibits higher sensitivity than CPL with two Hg(II) binding fragment.
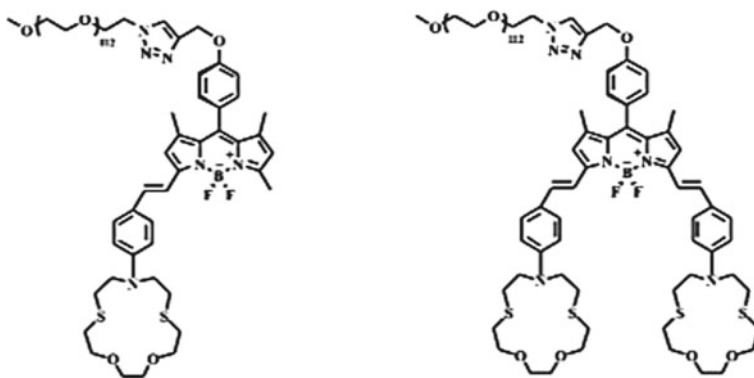
PCD microbeads modified by 1,5,9,13-tetrathiacyclohexadecane-3,11-diol (2.76 mmol g^{-1} polymer) were used for chelation of Au(III), Ag(I), Pt(II) and Pd (II) ions [548]. The crown ether CPLs with the pendent sulfur ether fragment prepared by ring-opening copolymerization of 3-thiopentyl glycidyl ether and diethylene glycol bisglycidyl ether show high adsorption capacity toward Cu(II), Pb (II), especially, Hg(II) ions, but poor adsorption capacity toward Mg(II) ions [549].

This is explained by the contribution of the sulfur atom in pendent sulfur ether fragment and the bigger cavity of CPL. The adsorption process is mainly coordination adsorption between sulfur ligand atom of pendent functional fragment and divalent mercury ion, and the coordination ratio is between 1 and 2.

Conformational transitions of macrocyclic oxyethylene-bridged oligo- and polythiophenes are observed in presence of Ba(II), Sr(II) and Pb(II) [550–552]. In particular, the electrochemical behavior of CPL in the presence of Li(I) can be interpreted as the result of two counteracting effects namely purely coulombic and inductive electronic effects which should increase a conformational effect in which cation complexation induces a planarization of the π-conjugated system and hence a decrease of the oxidation potential (Fig. 3.67) [551].

3.3.10   Calix[4]pyrrole[2]thiophene as Chelating Ligands

CPL based on macrocyclic ligand calix[4]pyrrole[2]thiophene attached to the polymeric backbone (a cross-linked vinylbenzyl chloride/DVB copolymer) exhibited strong affinity towards the noble metals over other transition metal ions [553]. This is due the presence of "soft" electron-donor sulfur atoms in the chelating fragment, which strongly interact with "soft" precious metals, and was caused by the fact that the size of the macrocyclic receptor and metal cations are comparable. It should be also noted that the uptake of gold, unlike other metals, is driven by the reduction of Au(III) to metallic gold on the surface of the CPL, resulting in considerably high values of uptake (up to 335 mg g^{-1} polymer).
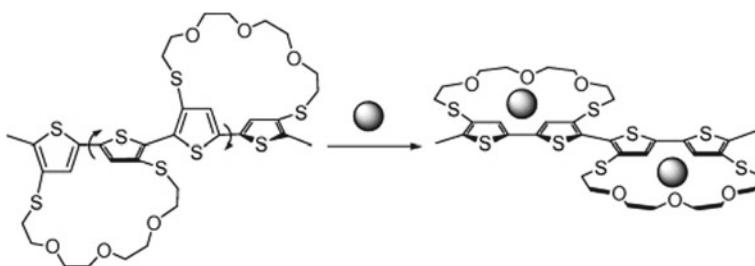
Fig. 3.67 Schematic representation of planarization of the π-conjugated system under the action of metal ion
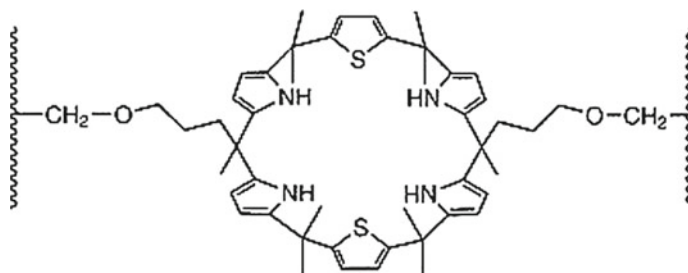
3.4 Polynuclear Polymeric Metal Chelates

The direct interaction of MX_n with polyfunctional CPLs is the one of the most popular methods for the preparation of polynuclear PMCs. The application of such techniques to high molecular weight compound chemistry is complicated by problems involved in the synthesis of the corresponding polyfunctional CPLs. Among the examples little in number is the preparation of binuclear Co(II) and Ni (II) chelates on PE-*gr*-poly(N-salicyloylacrylamide) [554, 555]. As in the case of LMC, such systems show the presence of exchange interaction of the antiferro-magnetic type between the paramagnetic sites. It should be noted that the existence of a PE-*gr*-poly (N-salicyloylacrylamide) as the *trans-trans*-form creates favorable conditions for the formation of binuclear bis-chelate structure.

Of interest is bithiazole-based PMC incorporating ferro ions and hexacyano-ferrate groups [556]. The CPL is a product of the polycondensation of salicylic acid with 2,2′-diamino-4,4′-bithiazole and paraformaldehyde. Its ferro-complex PMC-Fe (II) reacted with potassium ferricyanide ($K_3[Fe(CN)_6]$) in DMSO, producing the polymeric-inorganic complex PMC-Prussian blue (Scheme 3.59). PMC-Prussian blue exhibits a hysteresis cycle at 5 K, in which the observed coercive field is 40Oe and the remnant magnetization is 0.035 emu g^{-1}. It is important that PMC-Fe(II) is an antiferromagnet, while PMC-Prussian blue shows a soft-ferromagnetic behavior.

The polynuclear PMCs are formed during the interaction of metal ions with oligo-N,N′-bis[(2-hydroxy-1-naphthyl) methylene] urea (Scheme 3.60) [557].

An interesting route was offered for the preparation of polynuclear heterometallic PMCs (Scheme 3.61) [558]. Thus, a Zn-containing polymer **P-1** is synthesized by the interaction of the monomer 5,5′-divinyl-bpy (**M-1**) and salen-Zn(II) (**M-2**). Then, **P-1** was reacted with Eu(TTA)$_3$·2H$_2$O to form Eu(III)-Zn(II) copolymer **P-2**, including two different metal sites.

PS anchored binuclear Pd(II) azo complex was isolated [559]. The suspension of CPL with 1-nitroso-2-naphthol was reacted with Pd(II) acetate in glacial acetic acid to yield the PMC as light brown solid. A sharp peak at 1452 cm^{-1} due to the N=N
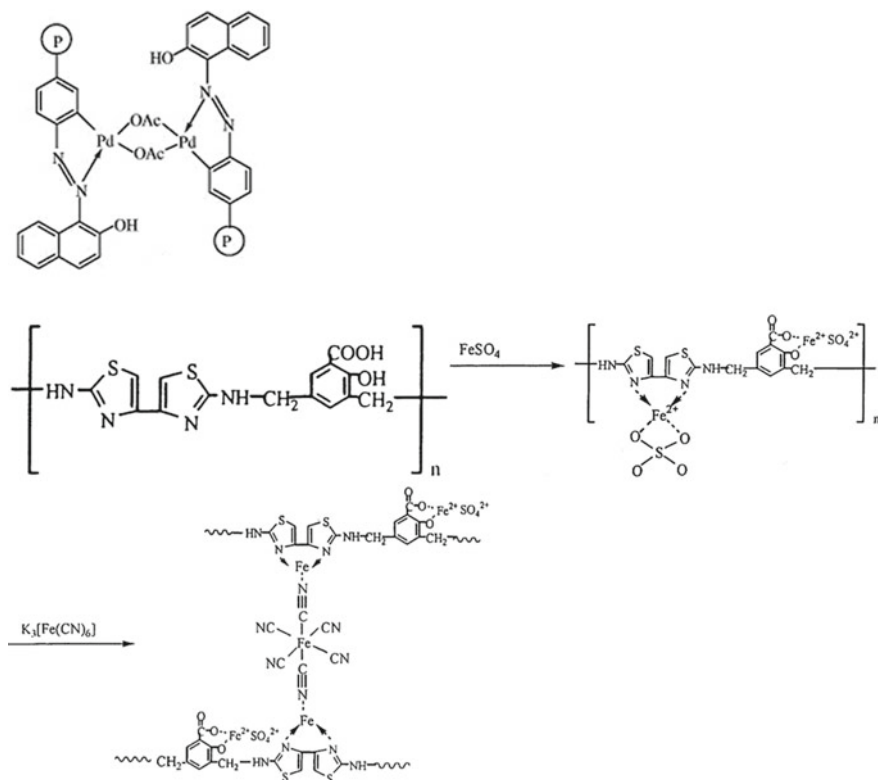
Scheme 3.59 Synthetic route of PMC-Fe(II) and PMC-Prussian blue and suggested structures
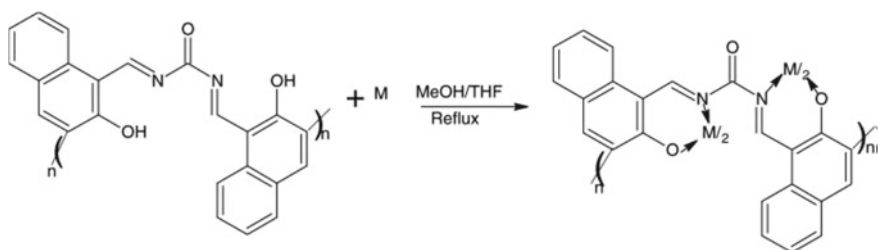
Scheme 3.60 Synthesis of oligo-N,N′-bis[(2-hydroxy-1-naphthyl) methylene] urea-metal chelates

bond in the CPL spectrum disappeared after the chelation with Pd and appeared as a band at 1440 cm^{-1}.

Of interest is PS-Pd(II)-furfural binuclear chelate prepared by the condensation of polymeric amine with furfural with subsequent interaction with Pd(OAc)$_2$ (Scheme 3.62) [560]. SEM images of the CPL and the Pd(II)-PMC exhibited a morphological difference between the azomethine CPL and the PMC.
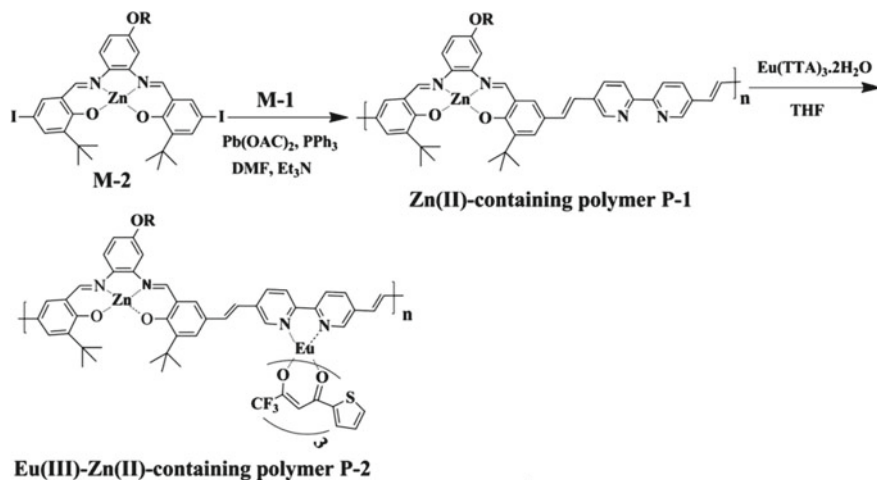
Scheme 3.61 A synthetic route to polynuclear heterometallic PMC

Scheme 3.62 Synthesis of binuclear polymer anchored Pd(II) chelate
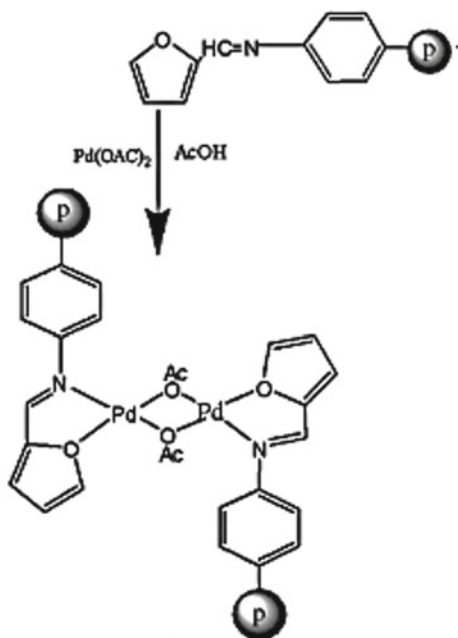
It should be noted Schiff bases 2-hydroxy-1-naphthaldehyde of amino methylated PS, which formed also binuclear PMC [324].
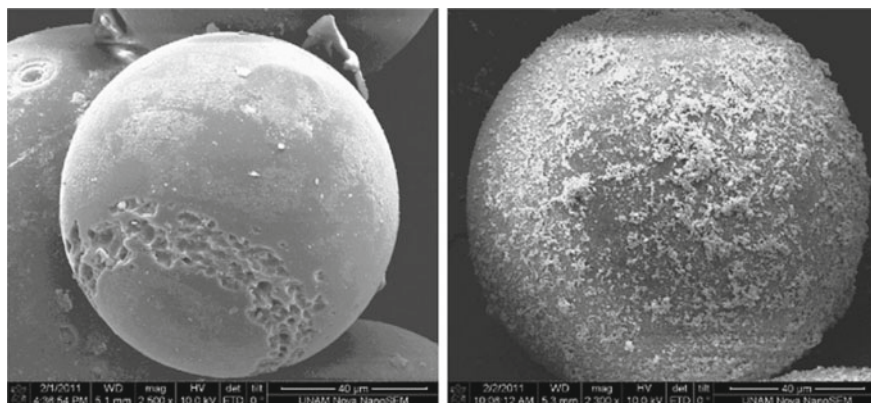
Fig. 3.68 SEM images of (left) CPL and (right) polymer anchored Pd(II) complex
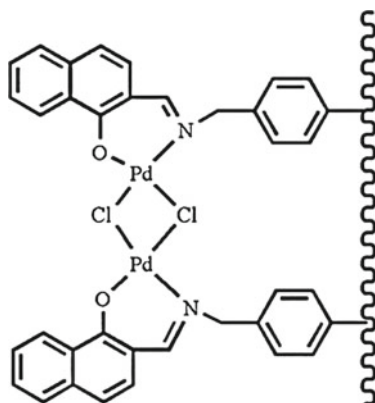
Analytical data of the PMC show 1:1 geometry. The comparison of SEM images of CPL and PMC showed the substantial morphological changes (Fig. 3.68). In particular, images of PMC beads exhibit roughening of the top layer due to the metal chelation to arrange in the fixed structure of the PMC.

References

1. A.D. Pomogailo, I.E. Uflyand, Adv. Polym. Sci. **97**, 61 (1990)
2. A.D. Pomogailo, I.E. Uflyand, *Makromolekulayrnye Metallokhelaty (Macromolecular Metal Chelates)* (Khimiya, Moscow, 1991)
3. D. Wohrle, A.D. Pomogailo, *Metal Complexes and Metals in Macromolecules* (Wiley-VCH, Weinheim, 2003)

4. I. Manners, *Synthetic Metal-Containing Polymers* (Wiley-VCH, Weinheim, 2004)
5. V. Chandrasekhar, *Inorganic and Organometallic Polymers* (Springer, Berlin, 2005)
6. M.A. Katkova, A.G. Vitukhnovskii, M.N. Bochkarev, Usp. Khim. **74**, 1193 (2005)
7. C. Carraher Jr., C. Pittman Jr., A. Abd-El-Aziz, M. Zeldin, J. Sheats (eds.), *Metal and Metalloid Containing Macromolecules* (Wiley, NY, 2006)
8. O.I. Koifman, T.A. Ageeva, *Porphyrinpolymers* (Fizmatlit, Moscow, 2006). (in Russian)
9. J.H. Zagal, F. Bedioui, J.P. Dodelet, N_4-*Macrocyclic Metal Complexes* (Springer, NY, 2006)
10. U.S. Schubert, H. Hofmeier, G.R. Newkome, *Modern Terpyridine Chemistry* (Wiley-VCH, Weinheim, 2006)
11. A.S. Abd-El-Aziz, I. Manners, *Frontiers in Transition Metal-Containing Polymers* (Wiley, Hoboken, New Jersey, 2007)
12. A.C.W. Leung, M.J. MacLachlan, J. Inorg. Organomet. Polym. **17**, 57 (2007)
13. W.K. Chan, Coord. Chem. Rev. **251**, 2104 (2007)
14. A.S. Abd-El-Aziz, C.E. Carraher Jr., C.U. Pittman Jr., M. Zeldin, *Macromolecules Containing Metal and Metal-Like Elements* (Wiley-Interscience, Wiley, NY, 2003–2007)
15. G.R. Whittell, I. Manners, Adv. Mater. **19**, 3439 (2007)
16. K.A. Williams, A.J. Boydston, C.W. Bielawski, Chem. Soc. Rev. **36**, 729 (2007)
17. A.S. Abd-El-Aziz, C.E. Carraher, C.U. Pittman, *Inorganic and Organometallic Macromolecules: Design and Applications* (Springer, NY, 2008)
18. J.-C. Eloi, L. Chabanne, G.R. Whittell, I. Manners, Mater. Today **11**, 28 (2008)
19. K.C. Gupta, A.K. Sutar, C.-C. Lin, Coord. Chem. Rev. **253**, 1926 (2009)
20. A.S. Abd-El-Aziz, P.O. Shipman, B.N. Boden, W.S. McNeil, Progr. Polym. Sci. **35**, 714 (2010)
21. B.M. Ibrahim, S.M. Magani, Afr. Sci. **11**, 217 (2010)
22. A.N. Pustam, S.D. Alexandratos, React. Funct. Polym. **70**, 545 (2010)
23. X. Wang, R. McHale, Macromol. Rapid Commun. **31**, 331 (2010)
24. U.S. Schubert, A. Winter, G.R. Newkome (eds.), *Terpyridine-Based Materials. For Catalytic, Optoelectronic and Life Science Applications* (Wiley-VCH, Weinheim, 2011)
25. A.Z. El-Sonbati, M.A. Diab, A.A. El-Bindary, Stoichiometry of polymer complexes, in *Stoichiometry and Research—The Importance of Quantity in Biomedicine*, ed. by A. Innocenti (InTech, Rijeka, Croatia, 2012)
26. A.S. Abd-El-Aziz, E.A. Strohm, Polymer **53**, 4879 (2012)
27. A.V. Yakimanskii, M.Y. Goikhman, I.V. Podeshvo, T.D. Anan'eva, T.N. Nekrasova, R.Y. Smyslov, Polym. Sci., Ser. A **54**, 921 (2012)
28. M. Ramanathan, Y.-C. Tseng, K. Ariga, S.B. Darling, J. Mater. Chem. C **1**, 2080 (2013)
29. M. Ramanathan, S.B. Darling, Polym. Int. **62**, 1123 (2013)
30. A.H. Ahmed, Int. J. Chem. Tech. Res. **6**, 36 (2014)
31. J. Zhou, G.R. Whittell, I. Manners, Macromolecules **47**, 3529 (2014)
32. C.G. Hardy, J. Zhang, Y. Yan, L. Ren, C. Tang, Progr. Polym. Sci. **39**, 1742 (2014)
33. L.N. Bochkarev, A.V. Rozhkov, M.N. Bochkarev, Polym. Sci. Ser. C **56**, 59 (2014)
34. J. Xiang, C.-L. Ho, W.-Y. Wong, Polym. Chem. **6**, 6905 (2015)
35. F. Xu, H.U. Kim, J.-H. Kim, B.J. Jung, A.C. Grimsdale, D.-H. Hwang, Progr. Polym. Sci. **47**, 92 (2015)
36. A.D. Pomogailo, E.F. Vainshtein, I.E. Uflyand, Russ. Chem. Rev. **64**, 913 (1995)
37. Z.P. Sandic, A.B. Nastasovic, Hem. Ind. **63**, 269 (2009)
38. S.I. Kadioglu, L. Yilmaz, N. Aydogan, O. Ozbelge, Separ. Sci. Technol. **45**, 1363 (2010)
39. B.L. Rivas, S. Hube, J. Sánchez, E. Pereira, Polym. Bull. **69**, 881 (2012)
40. Z. Yuan, N. Cai, Y. Du, Y. He, E.S. Yeung, Anal. Chem. **86**, 419 (2013)
41. J.B. Linden, M. Larsson, B.R. Coad, W.M. Skinner, M. Nyden, RSC Adv. **4**, 25063 (2014)
42. S. Nehru, S. Arunachalam, R. Arun, K. Premkumar, J. Biomol. Struct. Dynam. **32**, 1876 (2014)
43. J. Lakshmipraba, S. Arunachalam, A. Riyasdeen, R. Dhivya, M.A. Akbarsha, J. Photochem. Photobiol. B: Biol. **142**, 59 (2015)
44. C. Bertagnolli, A. Grishin, T. Vincent, E. Guibal, Ind. Eng. Chem. Res. **55**, 2461 (2016)

45. S. Kim, Y.-E. Choi, Y.-S. Yun, J. Hazard. Mater. **313**, 29 (2016)
46. C. McManamon, A.M. Burke, J.D. Holmes, M.A. Morris, J. Colloid Interface Sci. **369**, 330 (2012)
47. X. Guo, C.F. Wang, Y. Fang, L. Chen, S. Chen, J. Mater. Chem. **21**, 1124 (2011)
48. B.L. Rivas, S.A. Pooley, A.D. Pereira, R. Cid, M. Luna, M.A. Jara, K.E. Geckeler, J. Appl. Polym. Sci. **96**, 222 (2005)
49. A.D. Pomogailo, Type I: metal complexes bound to macromolecular carriers via ligands or metal ions, in *Macromolecule-Metal Complexes*, ed. by F. Ciardelli, E. Tsuchida, D. Wöhrle (Springer, Berlin, 1996)
50. Y.G. Ko, U.S. Choi, Y.S. Park, J.W. Woo, J. Polym. Sci., Part A: Polym. Chem. **42**, 2010 (2004)
51. S. Binauld, W. Scarano, M.H. Stenzel, Macromolecules **45**, 6989 (2012)
52. D.T. Masram, K.P. Kariya, N.S. Bhave, Der Pharm. Chem. **3**, 124 (2011)
53. D.T. Masram, K.P. Kariya, N.S. Bhave, Appl. Sci. Seg. **1**, APS/1513 (2010)
54. A. Burkanudeen, R. Azarudeen, M.R. Ahamed, P. Ramesh, N. Vijayan, Int. J. Chem. Environ. Eng. **1**, 29 (2010)
55. P.P. Kalbende, A.B. Zade, Sep. Sci. Techn. **50**, 965 (2015)
56. L. Niu, S. Deng, G. Yu, J. Huang, Chem. Eng. J. **165**, 751 (2010)
57. R. Qu, C. Wang, C. Ji, C. Sun, X. Sun, G. Cheng, J. Appl. Polym. Sci. **95**, 1558 (2005)
58. R. Qu, J. Liu, C. Sun, Y. Zhang, C. Ji, P. Yin, J. Chem. Eng. Data **55**, 4650 (2010)
59. A. Bukowska, W. Bukowski, J. Appl. Polym. Sci. **124**, 904 (2012)
60. M.A.R. Ahamed, R.S. Azarudeen, N.M. Kani, Bioinorg. Chem. Appl. **2014**, Article ID 764085 (2014)
61. M.A.R. Ahamed, R. Subha, D. Jeyakumar, A.R. Burkanudeen, Polym. Int. **64**, 126 (2015)
62. C. Xu, F. Liu, J. Gao, L. Li, Z. Bai, C. Ling, C. Zhu, D. Chen, A. Li, J. Hazard. Mater. **280**, 1 (2014)
63. D.T. Masram, K.P. Kariya, N.S. Bhave, Adv. Appl. Sci. Res. **2**, 156 (2011)
64. A.M. Albu, M. Mocioi, C.D. Mateescu, A. Iosif, J. Appl. Polym. Sci. **121**, 1867 (2011)
65. X.-P. Zhang, F.-Q. Liu, C.-Q. Zhu, C. Xu, D. Chen, M.-M. Wei, J. Liu, C.-H. Li, C. Ling, A.-M. Li, X.-Z. You, RSC Adv. **5**, 75985 (2015)
66. A.S. Mohamed, N.M. Fikry, T.I. Shalaby, A.I. Aloufy, M.M. Mohamed, Int. J. Chem. Appl. Biol. Sci. **1**, 52 (2014)
67. A.V. Pestov, Y.O. Privar, A.Y. Ustinov, A.V. Voit, Y.A. Azarova, A.V. Mekhaev, S.Y. Bratskaya, Chem. Eng. J. **283**, 323 (2016)
68. Y. Arakawa, A. Chiba, N. Haraguchi, S. Itsuno, Adv. Synth. Catal. **350**, 2295 (2008)
69. J. Rutkowska, K. Kilian, K. Pyrzynska, Eur. Polym. J. **44**, 2108 (2008)
70. K. Pyrzynska, K. Kilian, Microchim. Acta **142**, 67 (2002)
71. R. Antony, G.L. Tembe, M. Ravindranathan, R.N. Ram, J. Mol. Catal. A: Chem. **171**, 159 (2001)
72. G. Grivani, S. Tangestaninejad, A. Halili, Inorg. Chem. Commun. **10**, 914 (2007)
73. M. Bakherad, A. Keivanloo, B. Bahramian, S. Jajarmi, Synlett **3**, 311 (2011)
74. M. Bakherad, A. Keivanloo, B. Bahramian, S. Jajarmi, Appl. Catal. A **390**, 135 (2011)
75. W. Trakarnpruk, W. Kanjina, Ind. Eng. Chem. Res. **47**, 964 (2008)
76. S.M. Islam, P. Mondal, K. Tuhina, A.S. Roy, S. Mondal, D. Hossain, J. Inorg. Organometal. Polym. **20**, 264 (2010)
77. T. Ahamad, S.M. Alshehri, Polym. Int. **61**, 1640 (2012)
78. X. Huang, Y. Dong, J. Meng, Y. Cheng, C. Zhu, Synlett **12**, 1841 (2010)
79. Y.X. Lei, H. Li, W.X. Gao, M.C. Liu, J.X. Chen, J.C. Ding, X.B. Huang, H.Y. Wu, J. Mater. Chem. C **2**, 7402 (2014)
80. X. Ma, Y. Li, Z. Ye, L. Yang, L. Zhou, L. Wang, J. Hazard. Mater. **185**, 1348 (2011)
81. T. Wang, N. Zhang, Q. Li, Z. Li, Y. Bao, R. Bai, Sens. Actuators, B **225**, 81 (2016)
82. S.W. Thomas, G.D. Joly, T.M. Swager, Chem. Rev. **107**, 1339 (2007)
83. H. Gao, J. Yang, W. Sun, Z. Shen, J. Appl. Polym. Sci. **108**, 554 (2008)
84. L. Gao, S. Tang, L. Zhu, G. Sauvé, Macromolecules **45**, 7404 (2012)

85. S. Pramanik, S. Dhara, S.S. Bhattacharyya, P. Chattopadhyay, Anal. Chim. Acta **556**, 430 (2006)
86. Y. Qin, C. Cui, F. Jakle, Macromolecules **41**, 2972 (2008)
87. A. Schiller, R. Scopelliti, M. Benmelouka, K. Severin, Inorg. Chem. **44**, 6482 (2005)
88. M. Horie, I. Yamaguchi, A. Tanimoto, T. Yamamoto, Chem. Lett. **34**, 570 (2005)
89. J. Gao, F. Liu, P. Ling, J. Lei, L. Li, C. Li, A. Li, Chem. Eng. J. **222**, 240 (2013)
90. G.M. Pawar, J. Weckesser, S. Blechert, M.R. Buchmeiser, Beilstein J. Org. Chem. **6**, 28 (2010)
91. A. Kristanti, R. Batchelor, M. Albuszis, J. Yap, P.J. Roth, Eur. Polym. J. **69**, 499 (2015)
92. R. Qu, C. Sun, J. Chen, H. Chen, C. Wang, C. Ji, L. Xu, Polym. Eng. Sci. **47**, 721 (2007)
93. N. Samadi, R. Hasanzadeh, M. Rasad, J. Appl. Polym. Sci. **132**, 41642 (2015)
94. Y. Liu, Q. Miao, S.-W. Zhang, X.-B. Huang, L.-F. Zheng, Y.-X. Cheng, Macromol. Chem. Phys. **209**, 685 (2008)
95. Q. Miao, X.-B. Huang, Y.-Q. Cheng, Y. Liu, L.-L. Zeng, Y.-X. Cheng, J. Appl. Polym. Sci. **111**, 3137 (2009)
96. X. Liu, X. Zhou, X. Shu, J. Zhu, Macromolecules **42**, 7634 (2009)
97. T. Yamamoto, H. Fukumoto, T. Koizumi, J. Inorg. Organomet. Polym. **129**, 3 (2009)
98. M.O. Wolf, J. Inorg. Organomet. Polym. **16**, 189 (2006)
99. L. Zong, Q. Miao, Y. Liu, J. Xu, X. Huang, Y. Cheng, Chin. J. Chem. **27**, 1179 (2009)
100. Y. Liu, S.W. Zhang, Q. Miao, L.F. Zheng, L.L. Zong, Y.X. Cheng, Macromolecules **40**, 4839 (2007)
101. Y.X. Cheng, L.W. Chen, J.F. Song, X.W. Zou, T.D. Liu, Polym. J. **37**, 355 (2005)
102. J.F. Song, Y.X. Cheng, L.W. Chen, X.W. Zou, Z.L. Wang, Eur. Polym. J. **42**, 663 (2006)
103. Y.X. Cheng, X.W. Zou, D. Zhu, T.S. Zhu, Y. Liu, S.W. Zhang, H. Huang, J. Polym. Sci., Part A: Polym. Chem. **45**, 650 (2007)
104. Y. Jin, Y. Liu, W. Wu, Q. Wu, H. Gao, C. Wang, S. Xu, S. Cao, React. Funct. Polym. **90**, 7 (2015)
105. S. He, A.A. Buelt, J.M. Hanley, B.P. Morgan, A.G. Tennyson, R.C. Smith, Macromolecules **45**, 6344 (2012)
106. B. Liu, W.-L. Yu, J. Pei, S.-Y. Liu, Y.-H. Lai, W. Huang, Macromolecules **34**, 7932 (2001)
107. S.-I. Kato, K. Takagi, K. Suzuki, T. Kinoshita, Y. Yuki, J. Polym. Sci., Part A: Polym. Chem. **42**, 2631 (2004)
108. L. Do, R.C. Smith, A.G. Tennyson, S.J. Lippard, Inorg. Chem. **45**(8998), 2 (2006)
109. D.A. Turchetti, P.C. Rodrigues, L.S. Berlim, C. Zanlorenzi, G.C. Faria, T.D.Z. Atvars, W.H. Schreiner, L.C. Akcelrud, Synth. Met. **162**, 35 (2012)
110. L. Li, R.G. Hadt, S. Yao, W.-Y. Lo, Z. Cai, Q. Wu, B. Pandit, L.X. Chen, L. Yu, Chem. Mater. **28**, 5394 (2016)
111. C. Xing, Z. Shi, M. Yu, S. Wang, Polymer **49**, 2698 (2008)
112. V. Marin, E. Holder, U.S. Schubert, J. Polym. Sci., Part A: Polym. Chem. **42**, 374 (2004)
113. N. Priyadarshani, Y. Liang, J. Suriboot, H.S. Bazzi, D.E. Bergbreiter, ACS Macro Lett. **2**, 571 (2013)
114. L.L. Tian, W. Zhang, B. Yang, P. Lu, M. Zhang, D. Lu, Y.G. Ma, J.C. Shen, J. Phys. Chem. B **109**, 6944 (2005)
115. M. Zhang, P. Lu, X. Wang, L. He, H. Xia, W. Zhang, B. Yang, L. Liu, L. Yang, M. Yang, Y. Ma, J. Feng, D. Wang, N. Tamai, J. Phys. Chem. B **108**, 13185 (2004)
116. A. Kokil, P. Yao, C. Weder, Macromolecules **38**, 3800 (2005)
117. A.E. Dennis, R.C. Smith, Chem. Commun. **44**, 4641 (2007)
118. S. He, A.E. Dennis, R.C. Smith, Macromol. Rapid Commun. **30**, 2079 (2009)
119. Y. de Gaetano, I. Clarot, J.-B. Regnouf-de-Vains, Tetrahedron Lett. **50**, 5793 (2009)
120. T. Yamamoto, H. Nakajima, N. Hayashida, K. Shiraishii, H. Kokubo, Polym. Adv. Technol. **11**, 658 (2000)
121. M.C. De Rosa, D.J. Hodgson, G.D. Enright, B. Dawson, C.E.B. Evans, R.J. Crutchley, J. Am. Chem. Soc. **126**, 7619 (2004)

122. E. Holder, V. Marin, A. Alexeev, U.S. Schubert, J. Polym. Sci., Part A: Polym. Chem. **43**, 2765 (2005)
123. M.L. Keshtov, V.A. Vasnev, G.D. Markova, V.A. Barachevskii, A.R. Khokhlov, Polym. Sci. Ser. B **53**, 345 (2011)
124. M.Y. Goikhman, A.A. Polevoi, I.V. Podeshvo, N.L. Loretsyan, I.V. Gofman, R.Y. Smyslov, E.N. Popova, YuV Pokhvoshchev, V.D. Krasikov, Russ. J. Appl. Chem. **85**, 1703 (2012)
125. M.Y. Goikhman, I.V. Podeshvo, N.L. Loretsyan, I.V. Gofman, R.Y. Smyslov, T.N. Nekrasova, V.E. Smirnova, A.A. Polevoi, A.V. Yakimanskii, Izv. Akad. Nauk 961 (2012)
126. A.D. Garnovskii, B.I. Kharisov, *Direct Synthesis of Coordination and Organometallic Compounds* (Elsevier, Amsterdam, 1999)
127. T.V. Magdesieva, O.M. Nikitin, R.M. Abdullin, O.V. Polyakova, A.V. Yakimanskiy, M.Y. Goikhman, I.V. Podeshvo, Russ. Chem. Bull. **58**, 1423 (2009)
128. T.V. Magdesieva, A.V. Dolganov, A.V. Yakimansky, M.Y. Goikhman, I.V. Podeshvo, V.V. Kudryavtsev, Elektrokhimiya **43**, 1194 (2007)
129. M.Y. Goikhman, I.V. Podeshvo, N.L. Loretsyan, T.D. Anan'eva, R.Y. Smyslov, T.N. Nekrasova, M.A. Smirnov, E.N. Popova, A.V. Yakimanskii, Polym. Sci. Ser. B **53**, 89 (2011)
130. A.V. Pestov, P.A. Slepukhin, Y.G. Yatluk, V.N. Charushin, O.N. Chupakhin, J. Appl. Polym. Sci. **125**, 1970 (2012)
131. C.S.K. Mak, W.K. Cheung, Q.Y. Leung, W.K. Chan, Macromol. Rapid Commun. **31**, 875 (2010)
132. C.S.K. Mak, Q.Y. Leung, C.H. Li, W.K. Chan, J. Polym. Sci. A **48**, 2311 (2010)
133. Y. Zhang, Y. Chen, C. Wang, Y. Wei, J. Hazard. Mater. **276**, 129 (2014)
134. C. Lang, C. Kiefer, E. Lejeune, A.S. Goldmann, F. Breher, P.W. Roesky, C. Barner-Kowollik, Polym. Chem. **3**, 2413 (2012)
135. P. Jin, Z. Guo, J. Chu, J. Tan, S. Zhang, W. Zhu, Ind. Eng. Chem. Res. **52**, 3980 (2013)
136. D. Maggioni, M. Galli, L. D'Alfonso, D. Inverso, M.V. Dozzi, L. Sironi, M. Iannacone, M. Collini, P. Ferruti, E. Ranucci, G. D'Alfonso, Inorg. Chem. **54**, 544 (2015)
137. D. Maggioni, F. Fenili, L. D'Alfonso, D. Donghi, M. Panigati, I. Zanoni, R. Marzi, A. Manfredi, P. Ferruti, G. D'Alfonso, E. Ranucci, Inorg. Chem. **51**, 12776 (2012)
138. M. Nagy, M. Zsuga, D. Racz, S. Keki, J. Polym. Sci., Part A: Polym. Chem. **48**, 2709 (2010)
139. J. Ritchie, A. Ruseckas, P. André, C. Münther, M. Van Ryssen, D.E. Vize, J.A. Crayston, I. D.W. Samuel, Synth. Met. **159**, 583 (2009)
140. G. Alagumuthu, P. Mariselvi, Int. J. Chem. Stud. **1**, 157 (2013)
141. F.M. Al-Salami, H.H. Rashed, Iraq. Nat. J. Chem. **47**, 370 (2012)
142. C. Sun, C. Li, C. Wang, R. Qu, Y. Niu, H. Geng, Chem. Eng. J. **200–202**, 291 (2012)
143. S.M. Islam, M. Mobarok, P. Mondal, A.S. Roy, S. Mondal, D. Hossain, J. Appl. Polym. Sci. **123**, 3789 (2012)
144. T. Ahamad, S.M. Alshehri, Adv. Polym. Techn. **32**, 21350 (2013)
145. H. Jiang, W. Sun, R. Zheng, Eur. Polym. J. **42**, 425 (2006)
146. H.J. Lin, C.Y. Chen, J. Mater. Sci. **51**, 1620 (2016)
147. R. Shunmugam, K.A. Aamer, G.N. Tew, Polymer Preprints **48**, 635 (2007)
148. H.A. Saadeh, E.A.A. Shairah, N. Charef, M.S. Mubarak, J. Appl. Polym. Sci. **124**, 2717 (2012)
149. N.P. Tzanetos, A.K. Andreopoulou, J.K. Kallitsis, J. Polym. Sci. A: Polym. Chem. **43**, 4838 (2005)
150. A.A. Stefopoulos, E.K. Pefkianakis, K. Papagelis, A.K. Andreopoulou, J.K. Kallitsis, J. Polym. Sci. A: Polym. Chem. **47**, 2551 (2009)
151. R. Shunmugam, G.N. Tew, J. Am. Chem. Soc. **127**, 13567 (2005)
152. A.V. Rozhkov, L.N. Bochkarev, G.V. Basova, I.P. Malysheva, Y.I. Begantsova, E.O. Platonova, E.V. Baranov, Y.A. Kurskii, V.A. Il'ichev, M.A. Lopatin, G.A. Abakumov, M. N. Bochkarev, Russ. J. Gen. Chem. **82**, 1895 (2012)

153. K. Schoeller, C. Toncelli, J. Experton, S. Widmer, D. Rentsch, A. Vetushka, C.J. Martin, M. Heuberger, C.E. Housecroft, E.C. Constable, L.F. Boesel, L. Scherer, RSC Adv. **6**, 97921 (2016)
154. E. Holder, V. Marin, M.A.R. Meier, U.S. Schubert, Macromol. Rapid Commun. **25**, 1491 (2004)
155. Y. Cui, Q. Chen, D.-D. Zhang, J. Cao, B.-H. Han, J. Polym. Sci., Part A: Polym. Chem. **48**, 1310 (2010)
156. V. Banjoko, Y. Xu, E. Mintz, Y. Pang, Polymer **50**, 2001 (2009)
157. D.A. Turchetti, Phys. Chem. Chem. Phys. **17**, 26238 (2015)
158. R.-S. Juang, P.-C. Yang, H.-W. Wen, C.-Y. Lin, S.-C. Lee, T.-W. Chang, React. Funct. Polym. **93**, 130 (2015)
159. C. Lang, K. Pahnke, C. Kiefer, A.S. Goldmann, P.W. Roesky, C. Barner-Kowollik, Polym. Chem. **4**, 5456 (2013)
160. Y.S.L.V. Narayana, S. Basak, M. Baumgarten, K. Müllen, R. Chandrasekar, Adv. Funct. Mater. **23**, 5875 (2013)
161. Y.S.L.V. Narayana, M. Baumgarten, K. Müllen, R. Chandrasekar, Macromolecules **48**, 4801 (2015)
162. S. Basak, Y.S.L.V. Narayana, M. Baumgarten, K. Müllen, R. Chandrasekar, Macromolecules **46**, 362 (2013)
163. G.M. Pawar, R.A. Lalancette, E.M. Bonder, J.B. Sheridan, F. Jäkle, Macromolecules **48**, 6508 (2015)
164. A. de Bettencourt-Dias, J.S.K. Rossini, Inorg. Chem. **55**, 9954 (2016)
165. A.-Z.A. Elassar, A.H.A. Sughayer, F.A. Sagheer, J. Appl. Polym. Sci. **117**, 3679 (2010)
166. A. Modak, J. Mondal, M. Sasidharan, A. Bhaumik, Green Chem. **13**, 1317 (2011)
167. D. Prabhakaran, S.M. Subramanian, Talanta **65**, 179 (2005)
168. W.B. Gurnule, P.K. Rahangdale, L.J. Paliwal, R.B. Kharat, React. Funct. Polym. **55**, 255 (2003)
169. W.B. Gurnule, D.B. Patle, J. Chem. Pharm. Res. **4**, 2118 (2012)
170. W.B. Gurnule, Int. J. Envir. Res. **1**, 16 (2012)
171. M. Bakherad, A. Keivanloo, S. Samangooei, M. Omidian, J. Organomet. Chem. **740**, 78 (2013)
172. C. Ji, S. Song, C. Wang, C. Sun, R. Qu, C. Wang, H. Chen, Chem. Eng. J. **165**, 573 (2010)
173. Y. Niu, S. Feng, R. Qu, Y. Ding, D. Wang, Y. Wang, Int. J. Quantum Chem. **111**, 991 (2011)
174. A.A. Atia, A.M. Donia, K.Z. Elwakeel, React. Funct. Polym. **65**, 267 (2005)
175. B. Liu, Y. Bao, F. Du, H. Wang, J. Tian, R. Bai, Chem. Commun. **47**, 1731 (2011)
176. C. Wang, C. Ji, Y. Meng, L. Liu, R. Qu, C. Wang, J. Appl. Polym. Sci. **116**, 636 (2010)
177. C. Ji, R. Qu, C. Sun, C. Wang, Y. Sun, N. Zhao, H. Xie, J. Appl. Polym. Sci. **100**, 5034 (2006)
178. C. Ji, R. Qu, Q. Xu, C. Sun, C. Wang, Y. Cheng, Y. Song, J. Appl. Polym. Sci. **111**, 2148 (2009)
179. C.N. Ji, R.J. Qu, C.M. Sun, C.H. Wang, Q. Xu, Y.Z. Sun, C.X. Li, S.H. Guo, J. Appl. Polym. Sci. **103**, 3220 (2007)
180. C. Xiong, Y. Zheng, Y. Feng, C. Yao, C. Ma, X. Zheng, J. Jiang, J. Mater. Chem. A **2**, 5379 (2014)
181. C. Xiong, Y. Li, G. Wang, L. Fang, S. Zhou, C. Yao, Q. Chen, X. Zheng, D. Qi, Y. Fu, Y. Zhu, Chem. Eng. J. **259**, 257 (2015)
182. X. Wang, X. Zhang, H. Guo, L. Yuan, P. Liu, Polym. Eng. Sci. **52**, 972 (2012)
183. C. Xiong, S. Zhou, X. Liu, Q. Jia, C. Ma, X. Zheng, Ind. Eng. Chem. Res. **53**, 2441 (2014)
184. A. Sari, M. Tuzen, D. Citak, M. Soylak, J. Hazard. Mater. **149**, 283 (2007)
185. A.A. Shaikh, C.S. Othman, A. Hamouz, N.M. Hassan, J. Hazard. Mater. **248–249**, 47 (2013)
186. D. Giri, S.K. Patra, RSC Adv. **5**, 79011 (2015)
187. M. Bakherad, A. Keivanloo, B. Bahramian, S. Jajarmi, J. Organomet. Chem. **724**, 206 (2013)

188. M.A.A. El-Ghaffar, M.H. Mohamed, K.Z. Elwakeel, Chem. Eng. J. **151**, 30 (2009)
189. M.R. Maurya, A. Arya, P. Ada, J.C. Pessoa, Appl. Catal. A **351**, 239 (2008)
190. R.J. Qu, C.M. Sun, C.N. Ji, C.H. Wang, Z.G. Zhao, D.S. Yu, Polym. Eng. Sci. **45**, 1515 (2005)
191. C. Bianchini, M. Frediani, G. Mantovani, F. Vizza, Organometallics **20**, 2660 (2001)
192. Y. Morisaki, K. Suzuki, H. Imoto, Y. Chujo, Macromol. Rapid Commun. **31**, 1719 (2010)
193. C.G. Pierpont, C.W. Lange, Prog. Inorg. Chem. **41**, 331 (2007)
194. W. Wang, Y. Xu, A. Li, T. Li, M. Liu, R. von Klitzing, C.K. Ober, A.B. Kayitmazer, L. Li, X. Guo, RSC Adv. **5**, 66871 (2015)
195. D.E. Fullenkamp, D.G. Barrett, D.R. Miller, J.W. Kurutz, P.B. Messersmith, RSC Adv. **4**, 25127 (2014)
196. J. Yang, M.A.C. Stuart, M. Kamperman, Chem. Soc. Rev. **43**, 8271 (2014)
197. N. Holten-Andersen, M.J. Harrington, H. Birkedal, B.P. Lee, P.B. Messersmith, K.Y.C. Lee, J.H. Waite, Proc. Natl. Acad. Sci. U.S.A. **108**, 2651 (2011)
198. H.B. Zeng, D.S. Hwang, J.N. Israelachvili, J.H. Waite, Proc. Natl. Acad. Sci. U.S.A. **107**, 12850 (2010)
199. M.S. Menyo, C.J. Hawker, J.H. Waite, Soft Matter **9**, 10314 (2013)
200. D.J. Phillips, I. Prokes, G.-L. Davies, M.I. Gibson, ACS Macro Lett. **3**, 1225 (2014)
201. N. Holten-Andersen, A. Jaishankar, M.J. Harrington, D.E. Fullenkamp, G. DiMarco, L.H. He, G.H. McKinley, P.B. Messersmith, K.Y.C. Lee, J. Mater. Chem. B **2**, 2467 (2014)
202. L. Li, Y. Li, X. Luo, J. Deng, W. Yang, React. Funct. Polym. **70**, 938 (2010)
203. M.G. Schwab, B. Fassbender, H.W. Spiess, A. Thomas, X. Feng, K.J. Müllen, J. Am. Chem. Soc. **131**, 7216 (2009)
204. T. Tozawa, J.T.A. Jones, S.I. Swamy, S. Jiang, D.J. Adams, S. Shakespeare, R. Clowes, D. Bradshaw, T. Hasell, S.Y. Chong, C. Tang, S. Thompson, J. Parker, A. Trewin, J. Bacsa, A. M.Z. Slawin, A. Steiner, A.I. Cooper, Nat. Mater. **8**, 973 (2009)
205. N.B. McKeown, P.M. Budd, Macromolecules **43**, 5163 (2010)
206. J. Germain, F. Svec, J.M. Fréchet, J. Chem. Mater. **20**, 7069 (2008)
207. J. Bernard, C. Branger, T.L.A. Nguyen, R. Denoyel, A. Margaillan, React. Funct. Polym. **68**, 1362 (2008)
208. J. Bernard, C. Branger, I. Beurroies, R. Denoyel, A. Margaillan, React. Funct. Polym. **72**, 98 (2012)
209. J. Bernard, C. Branger, I. Beurroies, R. Denoyel, S. Blanc, A. Margaillan, Polymer **51**, 2472 (2010)
210. V. Vetriselvi, R.J. Santhi, Water Res. Ind. **10**, 39 (2015)
211. H. Kawakita, S. Nakano, K. Hamamoto, Y. Matsunaga, Y. Yoshimura, K. Ohto, K. Inoue, J. Appl. Polym. Sci. **118**, 247 (2010)
212. V.A. Lemos, D.G. da Silva, A.L. de Carvalho, D.D. Santana, G.D. Novaes, A.S. dos Passos, Microchem. J. **84**, 14 (2006)
213. N. Bensacia, S. Moulay, Int. J. Polym. Mater. **61**, 699 (2012)
214. M.H. Weston, O.K. Farha, B.G. Hauser, J.T. Hupp, S.T. Nguyen, Chem. Mater. **24**, 1292 (2012)
215. F.A. Aydin, M. Soylak, Talanta **72**, 187 (2007)
216. C. Larpent, S. Amigoni-Gerbier, A.P. De Sousa Delgado, C. R. Chim. **6** (2003)
217. L. Ma, M.M. Wanderley, W. Lin, ACS Catal. **1**, 691 (2011)
218. C. Dai, Y. Wang, Y. Quan, Q. Chen, Y. Cheng, C. Zhu, J. Polym. Sci., Part A: Polym. Chem. **52**, 3080 (2014)
219. F.Y. Song, G. Wei, X.X. Jiang, F. Li, C.J. Zhu, Y.X. Cheng, Chem. Commun. **49**, 5772 (2013)
220. J.F. Li, F. Li, X.X. Jiang, G. Wei, Y.X. Cheng, C.J. Zhu, Macromol. Rapid Commun. **34**, 1312 (2013)
221. P.T. Furuta, L. Deng, S. Garon, M.E. Thompson, J.M.J. Frechet, J. Am. Chem. Soc. **126**, 15388 (2004)
222. M. Demetriou, T. Krasia-Christoforou, J. Polym. Sci., Part A: Polym. Chem. **50**, 52 (2012)

223. W. Qian, Z. Chaofan, G. Rongfang, H. Aihong, H. Hualiang, J. Rare Earths **25**, 562 (2007)
224. H. Mart, A.R. Vilayetogu, Polym. Degrad. Stab. **83**, 255 (2004)
225. P. Kandasamy, M. Sasidaran, N. Janaki, T. Kaliyappan, J. Appl. Polym. Sci. **124**, 3600 (2012)
226. M. Kapadia, M. Patel, G. Patel, J. Joshi, J. Polym. Res. **15**, 285 (2008)
227. F. Al-Rimawi, A. Ahmad, F.I. Khalili, M.S. Mubarak, Solv. Extr. Ion Exch. **22**, 721 (2004)
228. B.A. Shah, A.V. Shah, R.R. Bhatt, Iran. Polym. J. **1**, 173 (2007)
229. A.B. Shah, A.A. Shah, B.N. Patel, Iran. Polym. J. **17**, 3 (2008)
230. D.T. Masram, N.S. Bhave, K.P. Kariya, J. Appl. Polym. Sci. **117**, 315 (2010)
231. P.M. Shah, B. Srinivasulu, S.C. Shit, Int. J. Res. Chem. Environ. **3**, 163 (2013)
232. W.B. Gurnule, S.S. Dhote, Der Pharma Chem. **4**, 791 (2012)
233. D.R. Gosai, K.S. Nimavat, K.B. Vyas, Int. J. Pharm. Res. Scholars (IJPRS) **1**, 86 (2012)
234. D.R. Gosai, K.S. Nimavat, K.B. Vyas, Arch. Appl. Sci. Res. **4**, 1395 (2012)
235. D.R. Gosai, K.S. Nimavat, K.B. Vyas, J. Chem. Pharm. Res. **3**, 490 (2011)
236. N.H. Parekh, R.T. Vashi, A.M. Patel, J. Environm. Res. Devel. **1**, 251 (2007)
237. M.S. Hosseini, H. Raissi, S. Madarshahian, React. Funct. Polym. **66**, 1539 (2006)
238. A. Islam, A. Ahmad, M.A. Laskar, J. Appl. Polym. Sci. **123**, 3448 (2012)
239. S. Boussetta, C. Branger, A. Margaillan, J.L. Boudenne, B. Coulomb, React. Funct. Polym. **68**, 775 (2008)
240. S. Khazaeli, N. Nezamabadi, M. Rabani, H.A. Panahi, Microchem. J. **106**, 147 (2013)
241. B. Gao, W. Zhang, Z. Zhang, Q. Lei, J. Lumin. **132**, 2005 (2012)
242. D. Liu, Z.-G. Wang, H. Yu, J. You, Eur. Polym. J. **45**, 2260 (2009)
243. C.-H. Yan, H.-H. Hu, C.-J. Xu, W. Zhu, M. Zhang, X.R. Bu, J. Photochem. Photobiol. A: Chem. **204**, 19 (2009)
244. D.-G. Li, J. Zhu, Z.-P. Cheng, W. Zhang, X.-L. Zhu, React. Funct. Polym. **69**, 240 (2009)
245. R. Shunmugam, G.N. Tew, Polym. Adv. Technol. **18**, 940 (2007)
246. L.-M. Zhao, B. Yan, J. Non-Cryst, Solids **353**, 4654 (2007)
247. A. El-Dissouky, A.-Z. Elassar, A.-H. Bu-Olian, J. Chem. Eng. Data **56**, 1827 (2011)
248. M.Q. Saima, M.S. Hasany, I.M. Bhanger, Y.M. Khuhawar, J. Colloid Interface Sci. **291**, 84 (2005)
249. G.-H. Meng, B.-H. Liu, J. Zhang, A.-M. Li, Yingyong Huaxue **26**, 219 (2009)
250. R.M. Zalloum, S.M. Mubarak, J. Appl. Polym. Sci. **109**, 3180 (2008)
251. S. Nanjundan, C.S.J. Selvamalar, R. Jayakumar, Eur. Polym. J. **40**, 2313 (2004)
252. S.S. Rahangdale, World Appl. Sci. J. **21**, 237 (2013)
253. M.M. Patel, M.A. Kapadia, J.D. Joshi, Eur. Polym. J. **45**, 426 (2009)
254. M.M. Patel, M.A. Kapadia, G.P. Patel, J.D. Joshi, React. Funct. Polym. **67**, 746 (2007)
255. S.S. Butoliya, A.B. Zade, W.B. Gurnule, J. Appl. Polym. Sci. **113**, 1 (2009)
256. G. Pina-Luis, G.A.R. Pina, A.C.V. Gonzalez, A.O. Teran, I.R. Espejel, M.E. Diaz-Garcia, React. Funct. Polym. **72**, 61 (2012)
257. L. Florea, D. Diamond, F. Benito-Lopez, Macromol. Mater. Eng. **297**, 1148 (2012)
258. K.H. Fries, G.R. Sheppard, J.A. Bilbrey, J. Locklin, Polym. Chem. **5**, 2094 (2014)
259. K.K. Wagner, M. Zanoni, A. Elliott, P.W. Wagner, R. Byrne, L. Florea, D. Diamond, K. Gordon, G.G. Wallace, D.L. Officer, J. Mater. Chem. C **1**, 3913 (2013)
260. S. Heng, A.M. Mak, D.B. Stubing, T.M. Monro, A.D. Abell, Anal. Chem. **86**, 3268 (2014)
261. K. Fries, S. Samanta, S. Orski, J. Locklin, Chem. Commun. **47**, 6288 (2008)
262. R.S. Azarudeen, M.A.R. Ahamed, A.R. Burkanudeen, J. Polym. Res. **18**, 1331 (2011)
263. R.S. Azarudeen, M.A.R. Ahamed, D. Jeyakumar, A.R. Burkanudeen, Iran. Polym. J. **18**, 821 (2009)
264. R.S. Azarudeen, M.A.R. Ahamed, N. Prabu, N.M. Kani, Appl. Organometal. Chem. **28**, 773 (2014)
265. B.L. Rivas, C.O. Sanchez, J. Appl. Polym. Sci. **89**, 2641 (2003)
266. V.D. Pautov, E.V. Anufrieva, T.D. Anan'eva, V.B. Lushchik, T.N. Nekrasova, R.Y. Smyslov, Polym. Sci. Ser. A **48**, 183 (2006)
267. S.M. Islam, A.S. Roy, P. Mondal, S. Paul, N. Salam, Inorg. Chem. Commun. **24**, 170 (2012)

268. W.B. Gurnule, D.B. Patle, Elixir Appl. Chem. **50**, 10338 (2012)
269. W.B. Gurnule, D.B. Patle, Polym. Bull. **66**, 803 (2011)
270. C. Selvi, D. Nartop, Spectrochim. Acta. Part A: Mol. Biomol. Spectr. **95**, 165 (2012)
271. A. Bilici, I. Kaya, F. Dogan, J. Polym. Sci., Part A: Polym. Chem. **47**, 2977 (2009)
272. A. Islam, M.A. Laskar, A. Ahmad, Environm. Monit. Assessm. **175**, 201 (2011)
273. M.B. Amran, A.S. Panggabean, A. Sulaeman, M. Rusnadi, Int. J. Environ. Res. **5**, 531 (2011)
274. M. Sasidaran, R. Sankar, P. Kandasamy, S. Vijayalakshmi, T. Kaliyappan, High Perform. Polym. **23**, 602 (2011)
275. D. Kumar, P.K. Gupta, A. Syamal, J. Chem. Sci. **117**, 247 (2005)
276. B. Gao, Y. Li, N. Shi, React. Funct. Polym. **73**, 1573 (2013)
277. D. Nartop, N. Sari, J. Inorg. Organomet. Polym. **22**, 772 (2012)
278. D. Kumar, P.K. Gupta, A. Syamal, J. Chil. Chem. Soc. **59**, 2260 (2014)
279. T. Ahamad, N. Nishat, S. Parveen, J. Coord. Chem. **61**, 1963 (2008)
280. B. Tamami, S. Ghasemi, Appl. Catal. A **393**, 242 (2011)
281. C. Zhang, Y. Zhang, H. Zhang, Y. Hu, X. Zhang, T. Masuda, React. Funct. Polym. **87**, 46 (2015)
282. P.G. Ingole, H.C. Bajaj, K. Singh, J. Appl. Polym. Sci. **128**, 66 (2013)
283. G.S.V. Kumar, B. Mathew, J. Macromol. Sci. Part A **41**, 1037 (2004)
284. B. Gao, J. Men, Y. Zhang, Synth. React. Inorg. Metal-Org. Nano-Metal Chem. **45**, 821 (2015)
285. S. Wang, B. Wu, F. Liu, Y. Gao, W. Zhang, Polym. Chem. **6**, 1127 (2015)
286. T. Kaliyappan, S. Rajagopan, P. Kannan, J. Appl. Polym. Sci. **91**, 494 (2004)
287. J.P. Gangwar, P.N. Saxena, Orient. J. Chem. **27**, 119 (2011)
288. D. Kalita, S. Sarmah, S.P. Das, D. Baishya, A. Patoway, N.S. Islam, React. Funct. Polym. **68**, 876 (2008)
289. J. Hou, F. Song, L. Wang, G. Wei, Y. Cheng, C. Zhu, Macromolecules **45**, 7835 (2012)
290. J. Meng, G. Wei, X.B. Huang, Y. Dong, Y.X. Cheng, C.J. Zhu, Polymer **52**, 363 (2011)
291. J. Zhou, W. Lu, F. Hu, M. Zhang, L. Jiang, Z. Shen, J. Polym. Sci., Part A: Polym. Chem. **52**, 2248 (2014)
292. D. Kumar, P.K. Gupta, A. Kumar, D. Dass, A. Syamal, J. Coord. Chem. **64**, 590 (2011)
293. R. Ando, T. Yagyu, M. Maeda, Inorg. Chim. Acta **357**, 2237 (2004)
294. A. Barbarini, R. Maggi, M. Muratori, G. Sartori, R. Sartorio, Tetrahedron: Asymm. **15**, 2467 (2004)
295. C. Hao, R. Wang, Y. He, Y. Wang, C. Xia, Chem. Res. Chin. Univ. **20**, 244 (2004)
296. T.R. Sankar, K. Kesavulu, P.V. Ramana, J. Mat. Sci. **42**, 8571 (2007)
297. T.R. Sankar, P.V. Ramana, Int. J. Pharm. Techn. **5**, 5713 (2013)
298. T.R. Sankar, P.V. Ramana, J. Appl. Chem. **2**, 1459 (2013)
299. T.R. Sankar, K. Kesavulu, P.V. Ramana, J. Chem. Sci. **126**, 597 (2014)
300. K. Kesavulu, T.R. Sankar, P.V. Ramana, Chem. Sci. Trans. **2**, 1318 (2013)
301. M. Cegłowski, G. Schroeder, Chem. Eng. J. **263**, 402 (2015)
302. S.A. Ali, O.C.S. Al Hamouz, N.M. Hassan, J. Hazard. Mater. **248–249**, 47 (2013)
303. E.H. El-Mossalamy, A.A. Khalil, Commun. Fac. Sci. Univ. Ank. B **53**, 1 (2004)
304. M.K. Othman, F.A. Al-Qadri, F.A. Al-Yusufy, Spectrochim. Acta, Part A **78**, 1342 (2011)
305. C. Demetgül, A. Delikanli, O.Y. Saribiyik, M. Karakaplan, S. Serin, Des. Monom. Polym. **15**, 75 (2012)
306. S. Samal, S. Acharya, R.K. Dey, A.R. Ray, J. Appl. Polym. Sci. **88**, 570 (2003)
307. A.S. Amarasekara, A. Razzaq, Int. Schol. Res. Network ISRN Polym. Sci. **2012**, Article ID 532171 (2012)
308. I. Kaya, A. Bilici, M. Sacak, Synth. Met. **159**, 1414 (2009)
309. S. Huang, P. Du, C. Min, Y. Liao, H. Sun, Y. Jiang, J. Fluoresc. **23**, 621 (2013)
310. Y. Feng, M.E. Lydon, C.W. Jones, ChemCatChem **5**, 3636 (2013)
311. D.E. White, P.M. Tadross, Z. Lu, E.N. Jacobsen, Tetrahedron **70**, 4165 (2014)
312. K.H. Reddy, A.R. Reddy, J. Appl. Polym. Sci. **88**, 414 (2003)

313. S. Vlad, A. Vlad, Mater. Plast. **45**, 172 (2008)
314. G.B. Pethe, A.R. Yaul, J.B. Devhade, A.S. Aswar, Der Pharma Chem. **2**, 301 (2010)
315. A. Bilici, İ. Kaya, M. Saçak, J. Inorg. Organomet. Polym. **20**, 124 (2010)
316. N. Nishat, S. Parveen, S. Dhyani, Asma, T. Ahamad, J. Appl. Polym. Sci. **113**, 1671 (2009)
317. A.K. Sutar, T. Maharana, Y. Das, P. Rath, J. Chem. Sci. **126**, 1695 (2014)
318. A.K. Sutar, Y. Das, S. Pattnaik, A. Routaray, N. Nath, P. Rath, T. Maharana, Chin. J. Catal. **35**, 1701 (2014)
319. A.K. Sutar, Y. Das, S. Pattanaik, A. Routaray, P. Rath, T. Maharana, Amer. J. Appl. Chem. **1**, 28 (2013)
320. S. Keesara, M.R. Mandapati, S. Parvathaneni, Appl. Catal. A: General **496**, 58 (2015)
321. K.C. Gupta, A.K. Sutar, J. Mol. Catal. A: Chem. **272**, 64 (2007)
322. K.C. Gupta, A.K. Sutar, J. Appl. Polym. Sci. **108**, 3927 (2008)
323. G.S.V. Kumar, B. Mathew, J. Appl. Polym. Sci. **92**, 1271 (2004)
324. F. Siga, H. Temel, M. Aydemir, Y.S. Ocak, S. Pasa, A. Baysal, Appl. Catal. A **449**, 172 (2012)
325. S. Sakthivel, T. Punniyamurthy, Tetrahedron Asymmetry **23**, 570 (2012)
326. Y. Xu, J. Meng, L. Meng, Y. Dong, Y. Cheng, C. Zhu, Chem. Eur. J. **16**, 12898 (2010)
327. S. Sakthivel, S. Jammi, T. Punniyamurthy, Tetrahedron Asymmetry **23**, 101 (2012)
328. J. Li, Y. Wu, F. Song, G. Wei, Y. Cheng, C. Zhu, J. Mater. Chem. **22**, 478 (2012)
329. T. Maeda, T. Takeuchi, Y. Furusho, T. Takata, J. Polym. Sci., Part A: Polym. Chem. **42**, 4693 (2004)
330. N. Madhavan, M. Weck, Adv. Synth. Catal. **350**, 419 (2008)
331. P. Yan, H. Jing, Adv. Synth. Catal. **351**, 1325 (2009)
332. M.A. Mughal, A. Mughal, G.Z. Memon, M.Y. Khuhawar, N.N. Memon, J. Chem. Soc. Pak. **35**, 1535 (2013)
333. K.C. Gupta, A.K. Sutar, J. Mol. Catal. A: Chem. **280**, 173 (2008)
334. K.C. Gupta, A.K. Sutar, J. Macromol. Sci. Part A Pure Appl. Chem. **44**, 1171 (2007)
335. R. Sankar, S. Vijayalakshmi, S. Rajagopan, T. Kaliyappan, J. Appl. Polym. Sci. **117**, 2146 (2010)
336. H.K. Sharma, N. Verma, J.K. Kapoor, Adv. Appl. Sci. Res. **2**, 522 (2011)
337. H.S. Patel, D.J. Pate, Int. J. Polym. Mater. **59**, 307 (2010)
338. D.K. Patel, A. Singh, E-J. Chem. **6**, 1017 (2009)
339. A.D. Patel, N.K. Prajapati, S.P. Patel, G.R. Patel, Der Chem. Sin. **2**, 130 (2011)
340. J.M. Patel, M.G. Patel, H.J. Patel, K.H. Patel, R.M. Patel, J. Macromol. Sci. **45**, 281 (2008)
341. P. Patel, B. Shah, A. Ray, R. Patel, J. Polym. Res. **11**, 65 (2004)
342. Q. Mei, N. Du, M. Lu, Eur. Polym. J. **43**, 2380 (2007)
343. C.-F. Zhong, Q. Wu, R.-F. Guo, H.-L. Zhang, Opt. Mater. **30**, 870 (2008)
344. C.-M. Liu, J.-J. Qiu, R. Bao, Y. Xu, X.-J. Cheng, F. Hu, Polymer **47**, 2962 (2006)
345. T. Takayama, M. Kitamura, Y. Kobayashi, Y. Arakawa, K. Kudo, Macromol. Rapid Commun. **25**, 1171 (2004)
346. S. Gharbi, J. Khiari, B. Jamoussi, J. Chem. Eng. Process. Technol. **5**, 198 (2014)
347. B.A. Shah, A.V. Shah, B.N. Bhandari, R.R. Bhatt, J. Iran. Chem. Soc. **5**, 252 (2008)
348. W.B. Gurnule, S.S. Katkamwar, Der Pharm. Lett. **4**, 1360 (2012)
349. R.S. Azarudeen, M.A.R. Ahamed, A.R. Burkanudeen, Desalination **268**, 90 (2011)
350. M.A.R. Ahamed, R.S. Azarudeen, D. Jeyakumar, A.R. Burkanudeen, Int. J. Polym. Mater. **60**, 124 (2010)
351. A. Singh, J. Bhanderi, Rasayan J. Chem. **2**, 846 (2009)
352. A.I. Ismail, K.A.K. Ebraheem, M.S. Mubarak, F.I. Khalili, Solv. Extr. Ion Exch. **21**, 125 (2003)
353. N.M. Salem, K.A.K. Ebraheem, M.S. Mubarak, React. Funct. Polym. **59**, 63 (2004)
354. R. Sankar, S. Vijayalakshmi, S. Subramanian, S. Rajagopan, T. Kaliyappan, Eur. Polym. J. **43**, 4639 (2007)
355. S. Vijayalakshmi, R. Sankar, S. Subramanian, S. Rajagopan, T. Kaliyappan, J. Appl. Polym. Sci. **104**, 797 (2007)

356. S. Vijayalakshmi, S. Subramanian, S. Rajagopan, T. Kaliyappan, J. Appl. Polym. Sci. **101**, 1506 (2006)
357. T.B. Shah, R.B. Dixit, B.C. Dixit, J. Therm. Anal. Calor. **92**, 505 (2008)
358. S. Vijayalakshmi, R. Sankar, S. Subramanian, S. Rajagopan, T. Kaliyappan, Des. Monom. Polym. **9**, 425 (2006)
359. S.M. Shah, F.B. Bux, V. Parmar, A. Singh, Der Chem. Sin. **2**, 304 (2011)
360. B.C. Dixit, R.B. Dixit, D.J. Desai, J. Polym. Res. **17**, 481 (2010)
361. W. Chouyyok, Y. Shin, J. Davidson, W.D. Samuels, N.H. LaFemina, R.D. Rutledge, G.E. Fryxell, Environ. Sci. Technol. **44**, 6390 (2010)
362. V.D. Mane, N.J. Wahane, W.B. Gurnule, J. Appl. Polym. Sci. **111**, 3039 (2009)
363. R.S. Praveen, P. Metilda, S. Daniel, T.P. Rao, Talanta **67**, 960 (2005)
364. B.N. Singh, B. Maiti, Talanta **69**, 393 (2006)
365. J. Mattova, P. Pouckova, J. Kucka, M. Škodova, M. Vetrik, P. Štepanek, P. Urbanek, M. Petrik, Z. Novy, M. Hruby, Eur. J. Pharm. Sci. **62**, 1 (2014)
366. M. Škodova, J. Kucka, M. Vetrik, J. Skopal, Z. Walterova, O. Sedlacek, P. Štepanek, J. Mattova, P. Pouckova, P. Urbanek, M. Hruby, React. Funct. Polym. **73**, 1426 (2013)
367. B. Gao, X. Wei, Y. Zhang, Opt. Mater. **35**, 536 (2013)
368. C. Sun, G. Zhang, R. Qu, Y. Yu, Chem. Eng. J. **170**, 250 (2011)
369. M. Hruby, J. Hradil, M.J. Benes, React. Funct. Polym. **59**, 105 (2004)
370. M.N.A. Al-Jibouri, T.M. Musa, M. Mubarak, W.M. Al-Jibouri, Sci. J. Chem. **1**, 38 (2013)
371. H. Askun, B. Gulbakan, O. Celikbıcak, C. Uzun, O. Guven, B. Salih, J. Appl. Polym. Sci. **107**, 2714 (2008)
372. T. Iijima, T. Yamamoto, Macromol. Rapid Commun. **25**, 669 (2004)
373. T. Iijima, S.-I. Kuroda, T. Yamamoto, Macromolecules **41**, 1654 (2008)
374. M.M. Nasef, O. Guven, Progr. Polym. Sci. **37**, 1597 (2012)
375. X. Liu, H. Chen, C.H. Wang, R.J. Qu, C.N. Ji, C.M. Sun, Y. Zhang, J. Hazard. Mater. **175**, 1014 (2009)
376. P.A. Kavakli, N. Seko, M. Tamada, O. Güven, Adsorption **10**, 309 (2005)
377. F.A. Alakhras, K.A. Dari, M.S. Mubarak, J. Appl. Polym. Sci. **97**, 691 (2005)
378. Q. Feng, X. Wang, A. Wei, Q. Wei, D. Hou, W. Luo, X. Liu, Z. Wang, Fibers Polym. **12**, 1025 (2011)
379. S.M. Badawy, H.H. Sokker, A.M. Dessouki, J. Appl. Polym. Sci. **99**, 1180 (2006)
380. G. Zong, J. Ma, H. Chen, C. Wang, N. Ji, D. Liu, J. Appl. Polym. Sci. **124**, 2179 (2012)
381. Q. Wang, J. Cui, G. Li, J. Zhang, F. Huang, Q. Wei, Polymers **6**, 2357 (2014)
382. M. Zhang, Q. Gao, C. Yang, L. Pang, H. Wang, H. Li, R. Li, L. Xu, Z. Xing, J. Hu, G. Wu, Ind. Eng. Chem. Res. **55**, 10523 (2016)
383. W. Bisset, H. Jacobs, N. Koshti, P. Stark, A. Gopalan, React. Funct. Polym. **55**, 109 (2003)
384. M.J. Roman, E.A. Decker, J.M. Goddard, A.C.S. Appl, Mater. Interfaces **6**, 5383 (2014)
385. Y. Ogiwara, M.J. Roman, E.A. Decker, J.M. Goddard, Food Chem. **196**, 842 (2016)
386. F. Tian, M.J. Roman, E.A. Decker, J.M. Goddard, J. Appl. Polym. Sci. **132**, 41231 (2015)
387. A. Isha, N.A. Yusof, M. Ahmad, D. Suhendra, Sensors Actuators, B **114**, 344 (2006)
388. T.C. Chang, C.C. Shih, C.P. Yin, H.B. Chen, T.R. Wu, Polym. Degrad. Stab. **87**, 87 (2005)
389. C.-Y. Chen, C.-Y. Chen, J. Appl. Polym. Sci. **86**, 1986 (2002)
390. C.-Y. Chen, C.-Y. Chen, Eur. Polym. J. **39**, 991 (2003)
391. K. Kráčalíková, M. Bleha, Polym. Bull. **61**, 147 (2008)
392. M.V. Dinu, E.S. Dragan, React. Funct. Polym. **68**, 1346 (2008)
393. D.H. Shin, Y.G. Ko, U.S. Choi, W.N. Kim, Ind. Eng. Chem. Res. **43**, 2060 (2004)
394. E. Repo, J.K. Warchoł, A. Bhatnagar, A. Mudhoo, M. Sillanpää, Water Res. **47**, 4812 (2013)
395. S. Hirata, T. Kajiya, M. Aihara, H. Honda, O. Shikino, Talanta **58**, 1185 (2002)
396. F. Gode, E. Pehlivan, J. Hazard. Mater. **100**, 231 (2003)
397. M. Seggiani, S. Vitolo, S. D'Antone, Hydrometallurgy **81**, 9 (2006)
398. L.C. Lin, R.S. Juang, Chem. Eng. J. **132**, 205 (2007)
399. D. Rahmi, Y. Zhu, E. Fujimori, T. Umemura, H. Haraguchi, Talanta **72**, 600 (2007)
400. E. Pehlivan, T. Altun, J. Hazard. Mater. **140**, 299 (2007)

401. M.V. Dinu, E.S. Dragan, A.W. Trochimczuk, Desalination **249**, 374 (2009)
402. P. Ling, F. Liu, L. Li, X. Jing, B. Yin, K. Chen, A. Li, Talanta **81**, 424 (2010)
403. L. Li, F. Liu, X. Jing, P. Ling, A. Li, Water Res. **45**, 1177 (2011)
404. C.C. Wang, C.Y. Chang, C.Y. Chen, Macromol. Chem. Phys. **202**, 882 (2001)
405. F. Liu, L. Li, P. Ling, X. Jing, C. Li, A. Li, X. You, Chem. Eng. J. **173**, 106 (2011)
406. S. Edebali, E. Pehlivan, Powder Technol. **301**, 520 (2016)
407. S.M. El-Bahy, Z.M. El-Bahy, Korean J. Chem. Eng. **33**, 2492 (2016)
408. R. Biesuz, G. Alberti, M. Pesavento, J. Solut. Chem. **37**, 527 (2008)
409. P.A. Kavakli, C. Kavakli, O. Güven, Radiat. Phys. Chem. **94**, 105 (2014)
410. T. Saitoh, A. Arakawa, M. Hiraide, Bull. Chem. Soc. Jpn **86**, 438 (2013)
411. Y. Wang, J. Zhang, W. Zhang, M. Zhang, J. Org. Chem. **74**, 1923 (2009)
412. C.-H. Tseng, C.-C. Wang, C.-Y. Chen, J. Phys. Chem. B **110**, 4020 (2006)
413. G. Bayramoglu, M.Y. Arica, Fibers Polym. **13**, 1225 (2012)
414. Q.Q. Liao, Y.J. Li, B. Xiang, L. Chen, W.N. He, Q.J. Zhang, Chin. J. Fine Chem. **25**, 281 (2008)
415. F.L. Fu, H.Y. Zeng, Q.H. Cai, R.L. Qiu, J. Yu, Y. Xiong, Chemosphere **69**, 1783 (2007)
416. L. Yang, Y. Li, X. Jin, Z. Ye, X. Ma, L. Wang, Y. Liu, Chem. Eng. J. **168**, 115 (2011)
417. H.A. Hanafi, M.A. Elsamad, Open J. Inorg. Chem. **5**, 19 (2015)
418. X. Zhao, L. Song, J. Fu, P. Tang, F. Liu, J. Hazard. Mater. **189**, 732 (2011)
419. A. Baraka, B.J. Hall, M.J. Heslop, React. Funct. Polym. **67**, 585 (2007)
420. X. Zhao, L. Song, Z. Zhang, R. Wang, J. Fu, J. Mol. Struct. **986**, 68 (2011)
421. L. Song, X. Zhao, J. Fu, X. Wang, Y. Sheng, X. Liu, J. Hazard. Mater. **199–200**, 433 (2012)
422. J.M. Bryson, J.W. Reineke, T.M. Reineke, Macromolecules **45**, 8939 (2012)
423. J. Tang, Y. Sheng, H. Hu, Y. Shen, Progr. Polym. Sci. **38**, 462 (2013)
424. C.F.G.C. Geraldes, S. Laurent, Contrast Media Mol. Imaging **4**, 1 (2009)
425. M.J. Moghaddam, L. de Campo, L.J. Waddington, C.J. Drummond, Soft Matter **6**, 5915 (2010)
426. A. Bumb, M.W. Brechbiel, P. Choyke, Acta Radiol. **51**, 751 (2010)
427. G. Anderegg, F. Arnaud-Neu, R. Delgado, J. Felcman, K. Popov, Pure Appl. Chem. **77**, 1445 (2005)
428. M. Botta, L. Tei, Eur. J. Inorg. Chem. 1945 (2012)
429. C.C. Cyran, Y. Fu, H.-J. Raatschen, V. Rogut, B. Chaopathomkul, D.M. Shames, M.F. Wendland, B.M. Yeh, R.C. Brasch, J. Magn. Reson. Imaging **27**, 581 (2008)
430. I. Pashkunova-Martic, C. Kremser, M. Galanski, P. Schluga, V. Arion, P. Debbage, W. Jaschke, B. Keppler, Mol. Imaging Biol. **13**, 432 (2011)
431. J. Rudovsky, P. Hermann, M. Botta, S. Aime, I. Lukes, Chem. Commun. **18**, 2390 (2005)
432. Z. Jaszberenyi, L. Moriggi, P. Schmidt, C. Weidensteiner, R. Kneuer, A.E. Merbach, L. Helm, E. Toth, J. Biol. Inorg. Chem. **12**, 406 (2007)
433. J.L. Turner, D.P.J. Pan, R. Plummer, Z.Y. Chen, A.K. Whittaker, K.L. Wooley, Adv. Funct. Mater. **15**, 1248 (2005)
434. Y. Tachibana, J. Enmi, A. Mahara, H. Iida, T. Yamaoka, Contrast Media Mol. Imaging **5**, 309 (2010)
435. K.M. Atkins, F.M. Martinez, A. Nazemi, T.J. Scholl, E.R. Gillies, Can. J. Chem. **89**, 47 (2011)
436. Q.L. Xu, L.T. Zhu, M.H. Yu, F.D. Feng, L.L. An, C.F. Xing, S. Wang, Polymer **51**, 1336 (2010)
437. Y. Zong, J. Guo, T. Ke, A.M. Mohs, D.L. Parker, Z.-R. Lu, J. Controlled Release **112**, 350 (2006)
438. R.L. Lucas, M. Benjamin, T.M. Reineke, Bioconjugate Chem. **19**, 24 (2008)
439. H.Y. Lee, H.W. Jee, S.M. Seo, B.K. Kwak, G. Khang, S.H. Cho, Bioconjugate Chem. **17**, 700 (2006)
440. Z.R. Lu, A.M. Mohs, Y. Zong, Y. Feng, Int. J. Nanomed. **1**, 31 (2006)
441. Z.R. Lu, X.M. Wu, Isr. J. Chem. **50**, 220 (2010)

442. Y.D. Zong, X.L. Wang, E.K. Jeong, D.L. Parker, Z.R. Lu, Magn. Reson. Imaging **27**, 503 (2009)
443. Y.D. Zong, X.H. Wang, K.C. Goodrich, A.M. Mohs, D.L. Parker, Z.R. Lu, Magn. Reson. Med. **53**, 835 (2005)
444. G. Zhang, R. Zhang, X. Wen, L. Li, C. Li, Biomacromol **9**, 36 (2007)
445. N. Illy, D. Majonis, I. Herrera, O. Ornatsky, M.A. Winnik, Biomacromol **13**, 2359 (2012)
446. D. Majonis, I. Herrera, O. Ornatsky, M. Schulze, X. Lou, M. Soleimani, M. Nitz, M.A. Winnik, Anal. Chem. **82**, 8961 (2010)
447. Y. Lu, G.N.N. Mbong, P. Liu, C. Chan, Z. Cai, D. Weinrich, A.J. Boyle, R.M. Reilly, M.A. Winnik, Biomacromol **15**, 2027 (2014)
448. A.J. Boyle, P. Liu, Y. Lu, D. Weinrich, D.A. Scollard, G.N.N. Mbong, M.A. Winnik, R.M. Reilly, Pharm. Res. **30**, 104 (2013)
449. P. Liu, A.J. Boyle, Y. Lu, R.M. Reilly, M.A. Winnik, Biomacromol **13**, 2831 (2012)
450. D. Majonis, O. Ornatsky, R. Kinach, M.A. Winnik, Biomacromol **12**, 3997 (2011)
451. G.-P. Yan, Z. Li, W. Xu, C.-K. Zhou, L. Yang, Q. Zhang, L. Li, F. Liu, L. Han, Y.-X. Ge, J.-F. Guo, Int. J. Pharm. **407**, 119 (2011)
452. W.-L. Zhang, D.-W. Yong, J. Huang, J.-H. Yu, S.-Y. Liu, M.-X. Fan, J. Appl. Polym. Sci. **120**, 2596 (2011)
453. A. Joseph, P.C. Ramamurthy, S. Subramanian, J. Appl. Polym. Sci. **123**, 526 (2012)
454. R.S. Walmsley, C. Litwinski, E. Antunes, P. Hlangothi, E. Hosten, C. McCleland, T. Nyokong, N. Torto, Z.R. Tshentu, J. Mol. Catal. A: Chem. **379**, 94 (2013)
455. D.K. Kurhe, R.V. Jayaram, Catal. Commun. **57**, 69 (2014)
456. T. Ahamad, S.M. Alshehri, Spectrochim. Acta. Part A: Mol. Biomol. Spectr. **96**, 179 (2012)
457. D. Kumar, A. Kumar, D. Dass, Bull. Chem. Soc. Ethiop. **28**, 29 (2014)
458. A. Denizli, R. Say, B. Garipcan, S. Patir, React. Funct. Polym. **58**, 123 (2004)
459. M.A. Diab, A.Z. El-Sonbati, R.H. Mohamed, Spectrochim. Acta, Part A **77**, 795 (2010)
460. E.H. El-Mossalamy, Zaštita Materijala **49**, 23 (2008)
461. N. Nahid, A. Tansir, M.A. Saad, P. Shadma, Eur. J. Med. Chem. **45**, 1287 (2010)
462. Z. Çelik, M. Gülfen, A.O. Aydin, J. Hazard. Mater. **174**, 556 (2010)
463. C. Ni, C. Yi, Z. Feng, J. Appl. Polym. Sci. **82**, 3127 (2001)
464. S.-J. Liu, Y.-P. Guo, H.-Y. Yang, S. Wang, H. Ding, Y. Qi, J. Environm. Manag. **182**, 328 (2016)
465. E. Birinci, M. Gulfen, A.O. Aydin, Hydrometallurgy **95**, 15 (2009)
466. M.M. Jadhao, L.J. Paliwal, N.S. Bhave, J. Appl. Polym. Sci. **118**, 1245 (2010)
467. N. Nishat, T. Ahamad, S.M. Alshehri, S. Parveen, Eur. J. Med. Chem. **45**, 1287 (2010)
468. N. Nishat, S. Ahmad, R. Ddin, T. Ahamad, J. Appl. Polym. Sci. **100**, 928 (2006)
469. T. Ahamad, V. Kumar, N. Nishat, Polym. Int. **55**, 1398 (2006)
470. L. Zhang, C. Zhu, X. Jiang, Y. Liu, B. Huang, Appl. Polym. Sci. **112**, 2455 (2009)
471. T. Ahamad, S.M. Alshehri, Spectrochim. Acta. Part A: Mol. Biomol. Spectr. **108**, 26 (2013)
472. A. Kausar, S. Zulfiqar, Z. Ahmad, M. Ishaq, M.I. Sarwar, J. Appl. Polym. Sci. **124**, 373 (2012)
473. S. Dutta, A.K. Das, J. Appl. Polym. Sci. **103**, 2281 (2007)
474. Z.C. Elik, M. Gulfen, A.O. Aydin, J. Hazard. Mater. **174**, 556 (2010)
475. S.S. Rahangdale, A.B. Zade, W.B. Gurnule, J. Appl. Polym. Sci. **108**, 747 (2008)
476. N.A. Abdelwahab, F.M. Helaly, Polym. Eng. Sci. **55**, 163 (2015)
477. C. Sun, R. Qu, C. Ji, Q. Wang, C. Wang, Y. Sun, G. Cheng, Eur. Polym. J. **42**, 188 (2006)
478. D. Donghi, D. Maggioni, G. D'Alfonso, F. Amigoni, E. Ranucci, P. Ferruti, A. Manfredi, F. Fenili, A. Bisazza, R. Cavalli, Biomacromol **10**, 3273 (2009)
479. M.R. Maurya, U. Kumar, I. Correia, P. Adão, J.C. Pessoa, Eur. J. Inorg. Chem. **4**, 577 (2008)
480. M.N. Al-jibouri, T.M. Musa, IOSR J. Appl. Chem. (IOSR-JAC) **7**, 46 (2014)
481. Q. Chang, G. Wang, Chem. Eng. Sci. **62**, 4636 (2007)
482. S. Tiwari, A. Bajpai, React. Funct. Polym. **64**, 47 (2005)
483. F.L. Fu, R.M. Chen, Y. Xiong, Sep. Purif. Technol. **52**, 388 (2006)

484. L. Liu, Y. Li, X. Liu, Z. Zhou, Y. Ling, Spectrochim. Acta. Part A: Mol. Biomol. Spectr. **118**, 765 (2014)
485. L. Liu, J. Wu, X. Li, Y. Ling, Sep. Purif. Technol. **103**, 92 (2013)
486. L. Liu, J. Wu, X. Li, Y. Ling, Chin. J. Environ. Chem. **30**, 843 (2011)
487. L. Liu, J. Wu, Y. Ling, X. Li, R. Zeng, J. Appl. Polym. Sci. **127**, 2082 (2013)
488. Q.Q. Liao, Z.Y. Wand, Y.J. Li, B. Xiang, R.M. Cheng, Q.J. Zhang, Spectrosc. Spect. Anal. **29**, 829 (2009)
489. A. McClain, Y.-L. Hsieh, J. Appl. Polym. Sci. **92**, 218 (2004)
490. O.S. Akintola, T.A. Saleh, M.M. Khaled, O.C.S. Al Hamouz, J. Taiwan Inst. Chem. Eng. **60**, 602 (2016)
491. D. Nagai, M. Yoshida, T. Kishi, H. Morinaga, Y. Hara, M. Mori, S. Kawakami, K. Inoue, Chem. Commun. **49**, 6852 (2013)
492. S. Amigoni-Gerbier, S. Desert, T. Gulik-Kryswicki, C. Larpent, Macromolecules **35**, 1644 (2002)
493. B. Salih, J. Appl. Polym. Sci. **83**, 1406 (2002)
494. M. Paurova, J. Havlickova, A. Pospisilova, M. Vetrik, I. Cisarova, H. Stephan, H.J. Pietzsch, M. Hruby, P. Hermann, J. Kotek, Chem. Eur. J. **21**, 4671 (2015)
495. C. Kavakli, N. Özvatan, S.A. Tuncel, B. Salih, Anal. Chim. Acta **464**, 313 (2002)
496. D. Jermakowicz-Bartkowiak, React. Funct. Polym. **67**, 1505 (2007)
497. C. Dolan, F. Drouet, D.C. Ware, P.J. Brothers, J. Jin, M.A. Brimble, D.E. Williams, RSC Adv. **6**, 23645 (2016)
498. S. Hwang, W. Cha, M.E. Meyerhoff, Angew. Chem. Int. Ed. **45**, 2745 (2006)
499. S.C. Puiu, Z. Zhou, C.C. White, L.J. Neubauer, Z. Zhang, L.E. Lange, J.A. Mansfeld, M.E. Meyerhoff, M.M. Reynolds, J. Biomed. Mater. Res., Part B **91**, 203 (2009)
500. K. Liu, M.E. Meyerhoff, J. Mater. Chem. **22**, 18784 (2012)
501. Y. Huang, D. Ou, C. Wang, C. Huang, Q. Li, Z. Li, Polym. Chem. **5**, 2041 (2014)
502. Y. Li, M. Bejia, S. Laurent, L.V. Elst, R.N. Muller, H.T.T. Duong, A.B. Low, T.P. Davis, C. Boyer, Macromolecules **45**, 4196 (2012)
503. J. Yuan, Y. You, X. Lu, O. Muzik, D. Oupicky, F. Peng, Mol. Imaging **6**, 1536 (2007)
504. Z. Ye, Z. Zhou, N. Ayat, X. Wu, E. Jin, X. Shi, Z.-R. Lu, Contrast Media Mol. Imaging **11**, 32 (2016)
505. X.D. Lou, G.H. Zhang, I. Herrera, R. Kinach, O. Ornatsky, V. Baranov, M. Nitz, M.A. Winnik, Angew. Chem. Int. Ed. **46**, 6111 (2007)
506. B. Zarabi, A. Nan, J. Zhuo, R. Gullapalli, H. Ghandehari, Mol. Pharm. **3**, 550 (2006)
507. M. Hruby, M. Skodova, H. Mackova, J. Skopal, M. Tomes, M. Kropacek, J. Zimova, J. Kucka, React. Funct. Polym. **71**, 1155 (2011)
508. B. Gierczyk, G. Schroeder, M. Cegłowski, React. Funct. Polym. **71**, 463 (2011)
509. L. Garcia, A. Torrent, E. Antico, C. Fontas, A. Roglans, React. Funct. Polym. **68**, 1088 (2008)
510. N.U. Day, C.C. Wamser, M.G. Walter, Polym. Int. **64**, 833 (2015)
511. M. Schappacher, A. Deffieux, J. Am. Chem. Soc. **133**, 1630 (2011)
512. M. Schappacher, A. Deffieux, Macromolecules **44**, 4503 (2011)
513. T. Asano, P.-C. Wang, A. Iwasakia, Spectrochim. Acta, Part A **75**, 305 (2010)
514. A. Bilgin, C. Yagcı, U. Yildiz, Macromol. Chem. Phys. **206**, 2257 (2005)
515. A. Bilgin, D. Yanmaz, C. Yagci, Turk. J. Chem. **38**, 1135 (2014)
516. A. Bilgin, A. Mendi, U. Yildiz, Polymer **47**, 8462 (2006)
517. A. Bilgin, C. Yagcı, A. Mendi, U. Yildiz, Polyhedron **26**, 617 (2007)
518. P.J. Melfi, S. Camiolo, J.T. Lee, M.F. Ali, J.T. McDevitt, V.M. Lynch, J.L. Sessler, Dalton Trans. **12**, 1538 (2008)
519. H. Huang, Q. Miao, Y. Kang, X. Huang, J. Xu, Y. Cheng, Bull. Chem. Soc. Jpn **81**, 1116 (2008)
520. M. Yu, F. He, Y. Tang, S. Wang, Y. Li, D. Zhu, Macromol. Rapid Commun. **28**, 133 (2007)
521. J. Yin, C.L. Wang, A. Liu, J. Phys. Chem. B **114**, 12213 (2010)

522. A. Khazaei, S. Saednia, M.K. Borazjani, J. Saien, M. Kiani, A. Afkhami, Supramol. Chem. **26**, 1 (2013)
523. F. Rubio, F. Garcia, H.D. Burrows, A.A.C.C. Pais, A.J.M. Valente, M.J. Tapia, J.M. Garcia, J. Polym. Sci., Part A: Polym. Chem. **45**, 1788 (2007)
524. I. Yamaguchi, H. Mitsuno, Macromolecules **43**, 9348 (2010)
525. J. Casanovas, F. Rodríguez-Ropero, D. Zanuy, C. Alemán, Polymer **51**, 4267 (2010)
526. X. Pan, Y. Wang, H. Jiang, G. Zou, Q. Zhang, J. Mater. Chem. **21**, 3604 (2011)
527. X.J. Ju, L.Y. Chu, L. Liu, P. Mi, Y.M. Lee, J. Phys. Chem. B **112**, 1112 (2008)
528. X.J. Ju, L. Liu, R. Xie, C.H. Niu, L.Y. Chu, Polymer **50**, 922 (2009)
529. B. Zhang, X.-J. Ju, R. Xie, Z. Liu, S.-W. Pi, L.-Y. Chu, J. Phys. Chem. B **116**, 5527 (2012)
530. L. Cui, D. Chao, J. Zhang, H. Mao, Y. Li, C. Wang, Synth. Met. **160**, 400 (2010)
531. G.J. Price, P.L. Drake, React. Funct. Polym. **66**, 109 (2006)
532. G.J. Price, A.A. Clifton, V.J. Burton, T.C. Hunter, Sensors Actuators, B **84**, 208 (2002)
533. Q. Miao, H. Huang, X. Huang, Y. Xu, L. Zong, Y. Cheng, Polym. Int. **59**, 712 (2010)
534. V. Calderon, F. Serna, F. Garcia, J.L. de la Pena, J.M. Garcia, J. Appl. Polym. Sci. **106**, 2875 (2007)
535. A. Mishra, C.-Q. Ma, P. Bäuerle, Chem. Rev. **109**, 1141 (2009)
536. A. Berlin, G. Zotti, S. Zecchin, G. Schiavon, Synth. Met. **131**, 149 (2002)
537. A. Aydogan, D.J. Coady, S.K. Kim, A. Akar, C.W. Bielawski, M. Marquez, J.L. Sessler, Angew. Chem. Int. Ed. **47**, 9648 (2008)
538. H. Li, D. Tian, D. Xiong, Z. Gao, J. Appl. Polym. Sci. **104**, 3201 (2007)
539. C.-S. Wu, C.-P. Chen, Y. Chen, J. Polym. Sci., Part A: Polym. Chem. **51**, 3975 (2013)
540. H. Sakamoto, T. Anase, H. Osuga, K. Kimura, React. Funct. Polym. **71**, 569 (2011)
541. S. Mallakpour, F. Rafiemanzelat, M.A. Zolfigol, P. Salehi, D.Y. Yang, Polym. Bull. **67**, 553 (2011)
542. S.S. Yilmaz, D. Kul, M. Erdol, M. Ozdemir, R. Abbasoglu, Eur. Polym. J. **43**, 1923 (2007)
543. K. Keiichi, M. Nakamura, H. Sakamoto, R.M. Uda, M. Sumida, M. Yokoyama, Bull. Chem. Soc. Jpn **76**, 209 (2003)
544. S.H. Chan, W.T. Wong, W.K. Chan, Chem. Mater. **13**, 4635 (2001)
545. S.R. Dave, H. Kaur, S.K. Menon, React. Funct. Polym. **70**, 692 (2010)
546. S. Habaue, Y. Akagi, M. Sato, A. Niimi, Polym. Bull. **54**, 237 (2005)
547. B. Wu, L. Xu, S. Wang, Y. Wang, W. Zhang, Polym. Chem. **6**, 4279 (2015)
548. C. Kavakli, S. Malci, S.A. Tuncel, B. Salih, React. Funct. Polym. **66**, 275 (2006)
549. L.-Z. Meng, S.-L. Gong, Y.-H. Yin, Y.-Y. Chen, Y.-W. Wang, J. Appl. Polym. Sci. **87**, 1445 (2003)
550. B. Jousselme, P. Blanchard, E. Levillain, J. Delaunay, M. Allain, P. Richomme, D. Rondeau, N. Gallego-Planas, J. Roncali, J. Am. Chem. Soc. **125**, 1364 (2003)
551. D. Demeter, P. Blanchard, I. Grosu, J. Roncali, Electrochem. Commun. **9**, 1587 (2007)
552. D. Demeter, P. Blanchard, M. Allain, I. Grosu, J. Roncali, J. Org. Chem. **72**, 5285 (2007)
553. A. Kałedkowski, A.W. Trochimczuk, React. Funct. Polym. **66**, 957 (2006)
554. A.D. Pomogailo, I.E. Uflyand, N.D. Golubeva, Kinet. Catal. **26**, 1404 (1985)
555. I.E. Uflyand, A.D. Pomogailo, M.O. Gorbunova, A.G. Starikov, V.N. Sheinker, Kinet. Catal. **28**, 613 (1987)
556. W. Sun, L. Jiang, J. Weng, B. He, Z. Shen, Mater. Chem. Phys. **78**, 676 (2003)
557. I. Kaya, A. Bilici, J. Appl. Polym. Sci. **105**, 1356 (2007)
558. J. Li, F. Song, L. Wang, J. Jiao, Y. Cheng, C. Zhu, Macromol. Rapid Commun. **33**, 1268 (2012)
559. S.M. Islam, P. Mondal, A.S. Roy, S. Mondal, D. Hossain, Tetrahedron Lett. **51**, 2067 (2010)
560. S.M. Islam, N. Salam, P. Mondal, A.S. Roy, J. Mol. Catal. A: Chem. **366**, 321 (2013)

Chapter 4
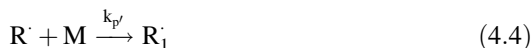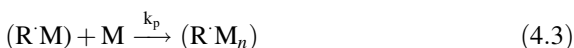# Polymer Complexes Based on Metal Chelate Monomers

Abstract The principal advances and problems of the preparation of polymeric metal complexes based on metal chelate monomers are analyzed. These monomers contain metal chelate cycle and multiple bonds for (co)polymerization or functionality, which can be involved in polycondensation. Use of metal chelate monomers allows to produce polymeric metal chelates in a single step, at that each chelating fragment contains a metal ion, and in most cases is characterized by a particular spatial configuration of the metal chelate cycle. The data are systematized according to methods for preparing polymeric metal chelates: homopolymerization, copolymerization, living and controlled polymerization, grafting polymerization, electropolymerization, polycondensation, as well as synthesis of dendrimers and hyperbranched polymers based on metal chelate monomers. Special attention is paid to the effect of a metal on reactivity of a multiple bond and functionalities containing in metal chelate monomers as well as the effect of double bond and functionalities on stereochemistry of a chelate node and electronic properties of a metal. The structural features of polymeric metal complexes based on metal chelate monomers are considered.

Polymerization transformations of metal chelate monomers (MCMs) are one of the most promising low-stage methods for the production of PMCs, in which each chelating fragment contains a metal ion in a predetermined spatial architecture [1–25]. Such monomers include a metal chelate unit and functional groups that allow MCMs to participate in homo- and copolymerization reactions as well as polycondensation. It is important that an undoubted advantage of MCMs is an increased stability in comparison with unchelated analogues due to a chelate or macrocyclic effect [4]. It should be noted that many theoretical problems of modern polymer (the reactivity of metallomonomers, the architecture of metal-containing polymers, etc.) and coordination chemistry (stereochemistry of metal chelates, electronic properties of metal complexes, etc.) are actively studied using MCMs as an example. MCMs proved to be convenient building blocks for the production of functional soft materials [26] or functional nanomaterials [27, 28], immobilized catalysts [29, 30], sensors, contrast agents, etc. [31].

4.1 Homopolymerization

Homopolymerization of MCMs is most widely studied with the example of metal complexes with vinyl derivatives of bpy, phen, and tpy, as well as metal chelates of molecular type with unsaturated monofunctional ligands, such as 4-vinylpyridine (4VP), bis-(4-pyridyl) ethylene, trans-4-stilbazole, N-(4-pyridyl) acrylamide, etc. [15, 23, 32]. It should be also noted numerous studies of the homopolymerization of MCM of an intracomplex type containing O,O– [33–36], N,O– [37–42], N,S– [43] and other chelating fragments.

The activity of MCM in free radical homopolymerization depends on such factors as a nature of a metal and a ligand, a distance of functionality from a metal, temperature, MCM and initiator concentrations, etc. Without going into details of profoundly studied polymerization kinetics of metal-containing monomers [20], it should be noted that the kinetic scheme of MCM radical polymerization can be described by the following equations:

$$I \xrightarrow{k_i} 2R_c^{\cdot} \tag{4.1}$$

$$R^{\cdot} + M \overset{K_{p_1}}{\leftrightarrow} (R^{\cdot}M) \tag{4.2}$$

$$(R^{\cdot}M) + M \xrightarrow{k_p} (R^{\cdot}M_n) \tag{4.3}$$

$$R^{\cdot} + M \xrightarrow{k_{p'}} R_1^{\cdot} \tag{4.4}$$

$$(R^{\cdot}M) + (R^{\cdot}M) \xrightarrow{k_t} P \tag{4.5}$$

$$(R^{\cdot}M) + R^{\cdot} \xrightarrow{k_{t'}} P \tag{4.6}$$

$$R^{\cdot} + R^{\cdot} \xrightarrow{k_{t''}} P \tag{4.7}$$

where

k_i	is the decomposition reaction rate constant of the initiator (I) into free radicals R_c;
k_{p1}	is equilibrium constant of the MCM (M) complexation reaction with a radical,
k_p and $k_{p'}$	are rate constants of the chain growth reaction with participation of M-coordinated and non-coordinated radicals,
k_t, $k_{t'}$, $k_{t''}$	are rate constants of the respective reactions of chain termination,
P	is products of the reaction.

This scheme takes into account interaction between a radical and MCM, and growth of the chain can be realized with participation of ordinary and MCM-

coordinated radicals. It should be noted that a chain termination occurs through a bimolecular mechanism, although along with recombination of ordinary radicals there plays an important role MCM-coordinated radicals formed by the reaction (4.2).

According to this scheme, the equation of the initial rate of polymerization (W_{n0}) looks as follows:

$$W_{n0} = (k_p K_{p_1}[M]_0 + k_{p'})\left(\frac{k_i[I]_0}{k_{t'}K_{p_1}[M]_0 + k_{t''}}\right)^{1/2}[M]_0 \qquad (4.8)$$

Upon fulfillment of the following conditions: $k_{p'} \gg k_p K_{p1}[M]_0$ and $k_t K_{p1}[M] \gg k_{t''}$, (4.8) is:

$$W_{n0} = k_{p'}\left(\frac{k_i[I]_0}{k_{t'}K_{p_1}}\right)^{1/2}[M]_0^{1/2} \qquad (4.9)$$

This scheme is confirmed also in dependence of conversion limit on initial concentration of initiator, and also by kinetics of a polymer accumulation according to (4.10):

$$\ln\left[[M]^{1/2} + k_{p'}\frac{[I]_0^{1/2}}{(k_{t'}K_{p_1}k_i)^{1/2}} - [M]_0^{1/2}\right] = \ln k_{p'}\left(\frac{[I]_0}{k_{t'}K_{p_1}k_i}\right)^{1/2} - k_i t/2 \qquad (4.10)$$

At the same time, presence of a metal ion in MCM can lead to different reactions of coordination and redistribution of electron density on a growing center, which can have an effect on elementary stages of a polymerization process. As a typical example, we note very slow homopolymerization of the MCM based on IDA due steric effect of a bulky IDA fragment close to double bond and participation of allylamino group of N,N-disubstituted methacrylamides in degradative chain transfer [42]. Low homopolymerization rate of some MCMs, in particular, Cu(II)-containing MCMs, is explained by intramolecular termination of a chain [4].
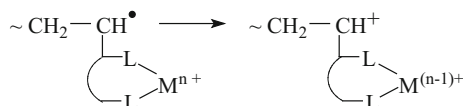
It should be noted that symmetry (C_{4v}) and configuration of a chelate node of Eu- and Nd-MCMs based on 2-methyl-5-phenylpentene-1-dione-3,5 do not change during polymerization [35, 44]. At the same time, weakening of metal-ligand bond during transition from a monomer to a polymer was shown.

Of interest is the comparison of two methods of PMC preparation based on direct reaction of MX_n with CPL and MCM homopolymerization. In particular,

complexation of bis-chlorine Ir dimer with a CPL based on 3-(4-vinyl benzyl)-pentane-2,4-dione lead to incomplete chelation of Ir(III) ions and preparation of insoluble product (A route). However, homopolymerization of a respective MCM allows to obtaining PMC in which each monomer unit contain bis(ppy)Ir(III)acac complex, where acac is acetylacetonate anion and ppy is 2-phenylpyridine (B route) [45].
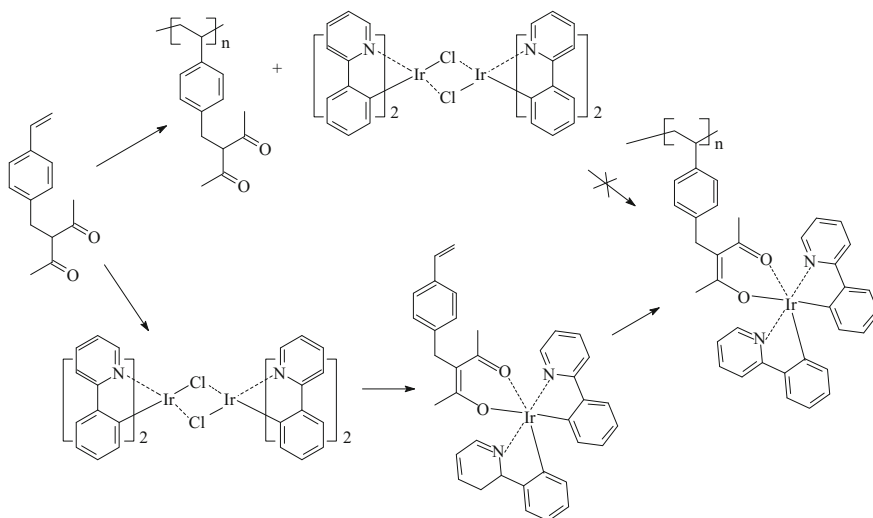

In this case, the formed PMC has $M_w = 5.0 \times 10^3$ and PDI = 1.4 in THF, and $M_w = 8.3 \times 10^3$ and PDI = 1.8 in N-methylpyrrolidone. It should be noted that monomerization of the dimeric complex takes place during MCM homopolymerization. However, monomerization of the Cu(I) dimeric complex with Cu_2I_2 block shaped as butterfly with bridged 2-(diphenylphosphino) pyridine N^P ligand was not observed (Scheme 4.1) [46]. It is important that pyridine in this N^P ligand can be functionalized or exchanged by quinoline or benzothiazole units, and various synthetic methodologies allows to preparing the polymers with different solution-processiable and photo-physical properties.

Of interest is PS with dendronized Ir(III) complexes in each monomer fragment prepared by homopolymerization of a «macromonomer» (Scheme 4.2) [47]. Such dendronized complex consists of phenyltriazolyl coligand and two ppy ligands bearing G1 bi-phenyl dendrons with terminal 2-ethylhexyloxy fragments.

It should be noted that 100% chelation is reached by homopolymerization of the respective metalloporphyrin (M-Pp), in particular, 5-(4-acryloyloxyphenyl)-10,15,20-trisphenyl-Pp Zn(II) [48]. It turned out that morphology and size of PMC microspheres are determined by the molar ratio of Zn-Pp and a solvent. In addition, PMCs exhibit new band of fluorescence emission and a new absorption band as
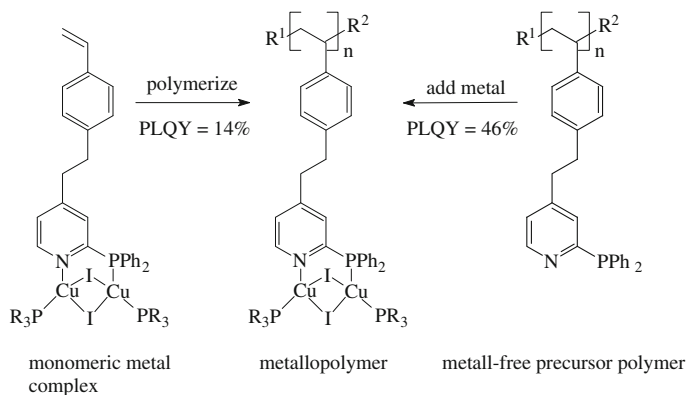
Scheme 4.1 Two main synthetic approaches to Cu(I)-containing polymers. Right: polymerization of metal-free monomer precursor and following loading of MX_n. Left: MCM polymerization
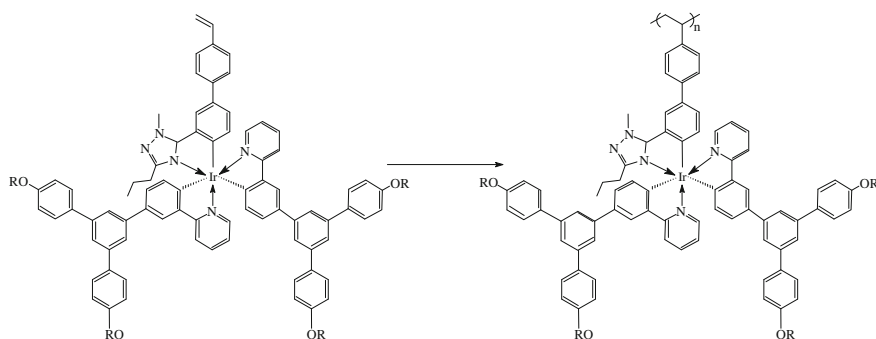
Scheme 4.2 Preparation of PS with pendant dendronized Ir(III) complexes (R = 2-ethylhexyl)

Fig. 4.1 Fluorescence emission spectra of Zn-Pp (1) and its polymer (2) (λ_{ex} = 423 nm, c_{Zn-Pp} = 1.02 × 10^{-6} mol L^{-1} and $c_{polymer}$ = 0.005 g mL^{-1})
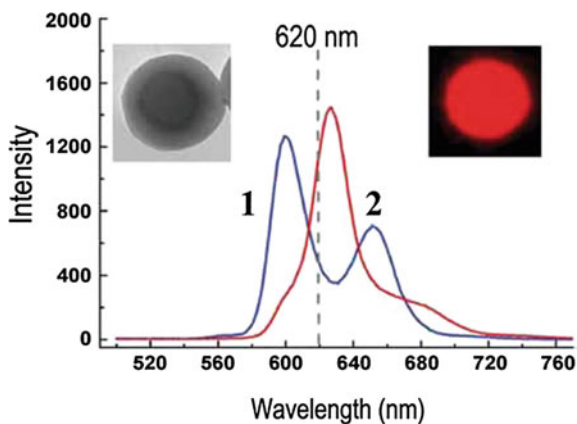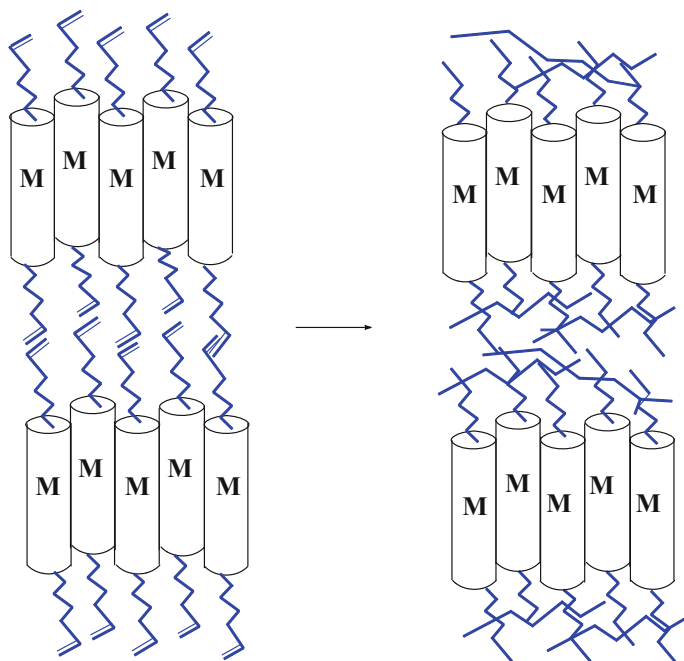
Scheme 4.3 Polymerization of 1,3-diene containing liquid crystalline MCM

compared with the initial MCM due to the formation of Pp assemblies, leading to improving color purity of their red fluorescence (Fig. 4.1).

Homopolymerization of liquid crystalline MCM containing 1,3-diene groups leads to the formation of liquid crystalline PMC (Scheme 4.3) [49].

The emulsion polymerization of Cr(VI)-MCM based on 2-methacryloyl histidine leads to Cr(VI)-imprinted nano-support used for adsorption of Cr(VI) from wastewater [50]. In particular, nano-support has shown higher chelation capacity to Cr (VI) ions than to Cr(III) ions.

It should be also noted chemically-initiated oxidized polymerization of thiophene- or pyrrol-containing chiral salen Co(III)-MCMs (Scheme 4.4) [51]. It is
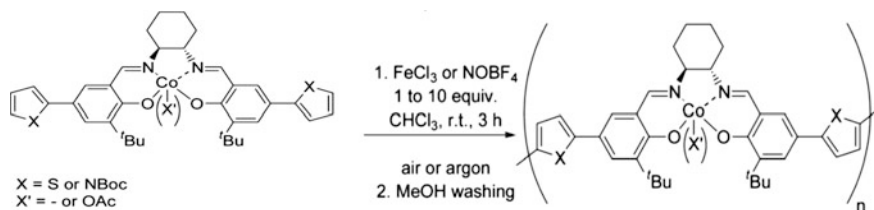
Scheme 4.4 Polymerization of thiophene- or pyrrol-modified chiral Co(III)-salen complexes

interesting that using of $FeCl_3$ as oxidant leads to the insoluble PMC with almost quantitative yield.

Using thermally-induced polymerization method, it is possible to obtain various metal-polymer coatings by deposition of MCM solution on electrode surface with their following thermal polymerization. Efficiency of this approach is shown on the example of polymerization of ethynyl Zn-Pp, which have different models of 1-4 ethyne or protected ethyne groups and different non-linking substituents. These MCM are subjected to thermal in situ polymerization on surface thus giving robust M-Pp films of controlled thickness, in particular, films prepared on different surfaces Si(100), SiO_2, Au(111) or glass, have thickness in the range from tens to hundreds nm [52].
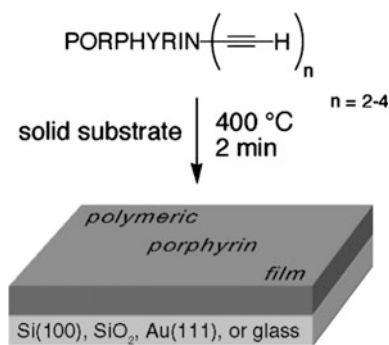
Physical vapor deposition polymerization is executed via evaporation of vinyl monomers with the following heat treatment [53]. This method is used to obtain hole-transport and emission layers of OLEDs (Fig. 4.2). In particular, emission layers were doped with red- or blue-emitting phosphorescent Ir complexes modified by styril fragments, and deposition polymerization was very promising for increase in efficiency of irradiation.

4.2 Copolymerization

The MCM copolymerization is a more popular process than their homopolymerization, because many MCMs easily copolymerize with traditional monomers. It is important that MCM copolymerization allows to preparing the new functional nanomaterials based on metalloblock copolymers [54].

For quantitative description of MCM copolymerization, the known Mayo-Lewis equation is used:
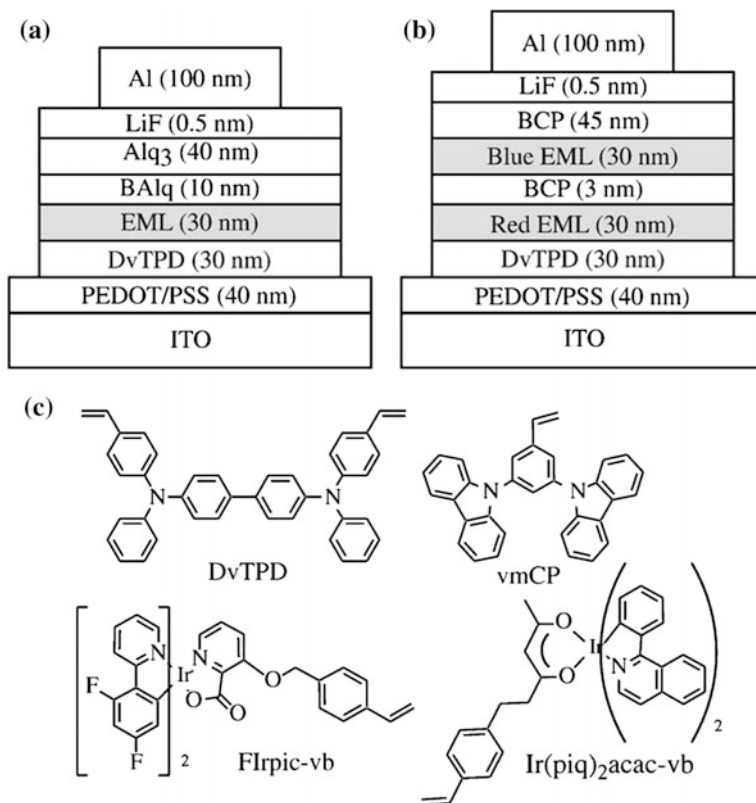
Fig. 4.2 OLED structures having **a** single emissive layers (EML) and **b** double EMLs, including hole-transport layer (HTL), tetraphenyldiaminobiphenyl (DvTPD), a vinyl derivative of bis(*N*-carbazolyl) benzene (vmCP), bis[(4,6-difluorophenyl) pyridinato-*N*,C2](picolinato) Ir(III) (FIrpic) or its styril derivative bis[(4,6-difluorophenyl)pyridinato-*N*,C2][3-(4-vinyl-benzyloxy)picolinato] Ir(III) (FIrpic-vb), bis(2-methyl-8-quinolinato)-4-phenylphenolate aluminum (BAlq), bathocuproine (BCP). Chemical structures of synthesized vinyl monomers are shown in (**c**)

$$\frac{[m_1]}{[m_2]} = \frac{[M_1]}{[M_2]} \frac{r_1[M_1] + [M_2]}{[M_1] + r_2[M_2]}, \tag{4.11}$$

where $r_2 = k_{22}/k_{21}$ is a copolymerization constant, characterizing relative activity of a monomer upon linking to «their» and «foreign» radicals, which relates to MCM, m_2 and M_2 is content of MCM in a copolymer and in a monomer mixture,

$$r_1 = k_{11} / k_{12},$$

m_1 and M_1 correspond to «metal-free» analogue.
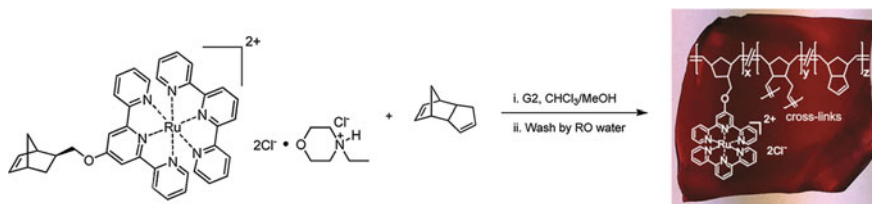
Fig. 4.3 Synthesis of the anion-exchanged membranes based on Ru-MCM. A photograph of a representative membrane is also shown

MCMs of molecular type are the most studied class of the monomers in copolymerization processes. As a typical example, we note copolymerization and cross-linking of dicyclopentadiene and norbornene monomer containing bis-tpy Ru(II) complex leading to anion-exchanged membranes based on metal cations [55]. It should be noted that each Ru(II) complex in this membrane has two linked with it counter-ions (Fig. 4.3).

Divergent approach is applied to copolymerization of St with hetero-[Ru(4′-vinyl-tpy)(4′-HOCH$_2$-tpy)]$^{2+}$ chelate functionalized on the one side with polymerized group using simple radical polymerization [56]. The product is deposited as a solid substance of orange color, which has M_n = 5170 with PDI = 1.62. There is no dissociation during passing PMC through a column of GPC, which shows stability of such polymeric hetero-Ru(II) chelates. It should be emphasized that using possible further functioning on hydroxymethyl-groups of ligands, diverse grafted or cross-linked systems can be obtained, and, furthermore, hetero-[Ru(4′-vinyl-tpy)(4′-HOCH$_2$-tpy)]$^{2+}$ chelates have interesting photophysical properties due to their high luminescence at room temperature as a result of conjugation in 4′-position of tpy.

Copolymerization of [Ru(4-vinyl-4′-methyl-bpy)bis(bpy)](PF$_6$)$_2$ with *N*-dodecyl acrylamide and NIPAM allows to preparing amphiphilic copolymers [57]. It is interesting that the films structured as honeycomb can be cast from PS solution of obtained PMCs.

Of interest is copolymerization of Ir- and Ru-MCMs with 5,5′-diethynyl-bpy ligand ([(ppy)$_2$Ir(5,5′-diethynyl-bpy)]Cl or [(ppy)$_2$Ru(5,5′-diethynyl-bpy)]Cl) and tetra(4-ethynylphenyl)methane through Co$_2$(CO)$_8$-indirect trimerization of terminal alkyne leading to the porous cross-linked PMCs (Scheme 4.5) [58]. The formed Ir- and Ru-PMCs with metal content of 4.5 and 2.2 wt%, respectively, are characterized by surface areas of 1547 and 1348 m^2 g^{-1}, as well as pore width in the range from 0.75 to 1.65 nm, respectively.

It should be noted the copolymerization of PEG-methyl ether methacrylate, NIPAM and Eu(AA)$_3$(phen) chelate leading to the copolymers, which form spherical micelles with more 100 nm size in aqueous solution and interact with DNA [59].
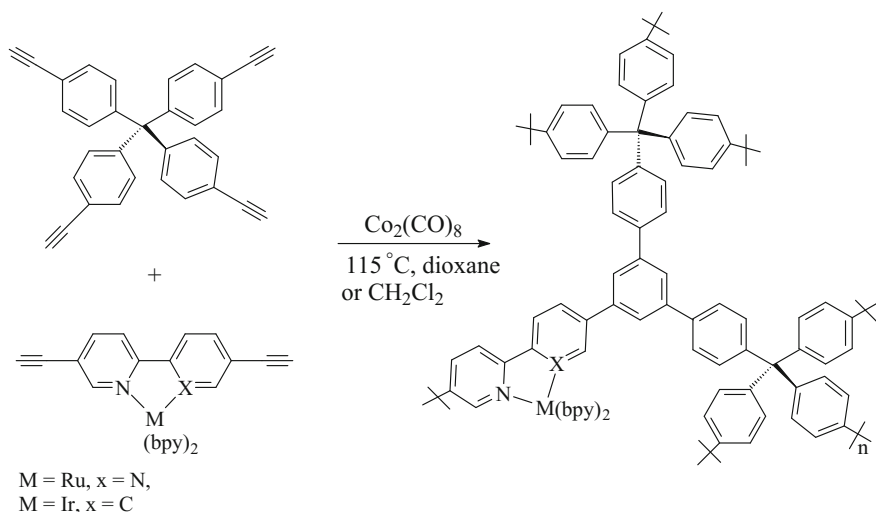
Scheme 4.5 Copolymerization of Ir and Ru chelates based on 5,5′-diethynyl-bpy ligand and tetra (4-ethynylphenyl)methane
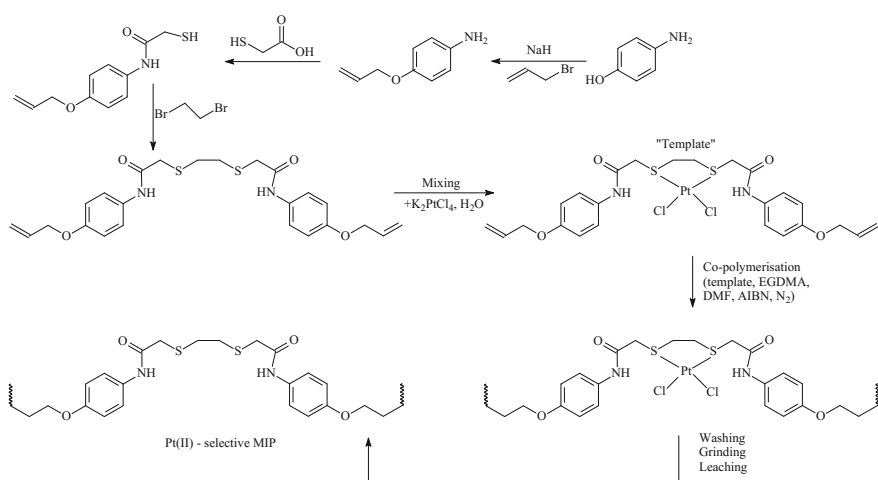
Scheme 4.6 Preparation of metal-selective molecular-imprinted polymer

Of interest is efficient metal-selective molecular-imprinted polymers prepared using Pt(II)-MCM of molecular type with S,S-chelating fragment (Scheme 4.6) [60].

Sequence-regulated polymerization with participation of a Pd-templated mono-mer leads to repeated ABA sequences in PMCs (Scheme 4.7) [61]. It is shown that π-π-stacking interaction between aromatic side fragments and the massif of three
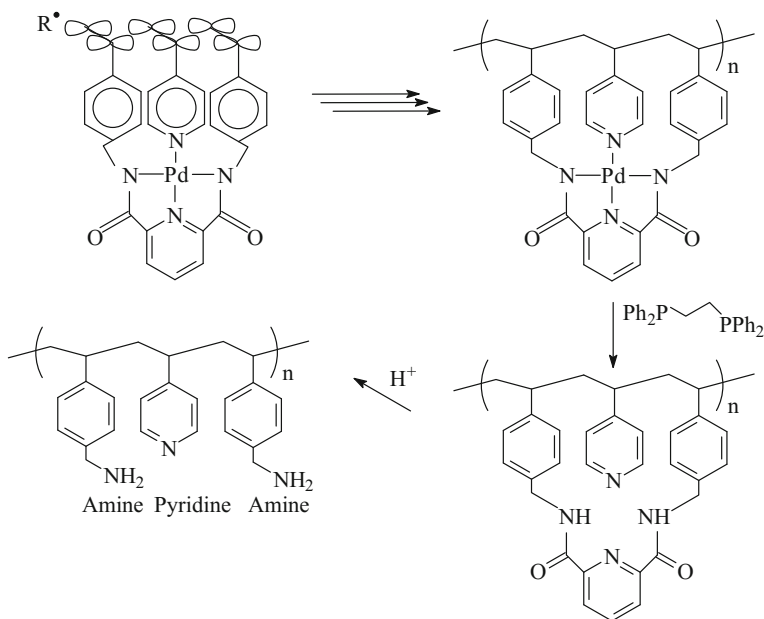
Scheme 4.7 Synthesis of repeated ABA sequences in metal-containing copolymers
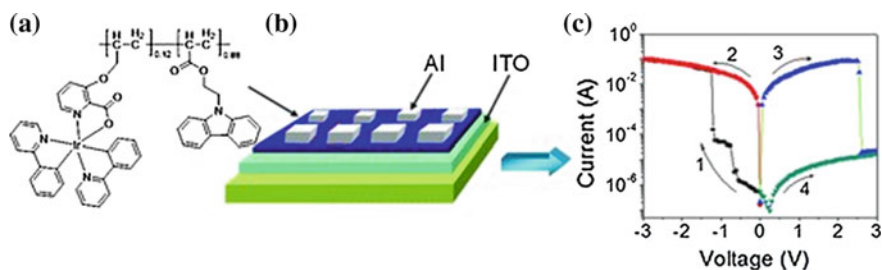
Fig. 4.4 **a** Structure of copolymers. **b** Memory device structure based on PMC (ITO/PMC/Al). **c** Typical *I–V* characteristics of an ITO/PMC/Al device

vinyl groups has the substantial effect on polymerization, and sequent removal of the metal-template allows to preparing sequence-regulated copolymers.

It should be also noted copolymers with stable di- and tertiary-memory containing of *N*-vinyl-Cz and mixed-ligand (phen and acac) fragments of Ir(III) chelates (Fig. 4.4) [62, 63]. Copolymers produced in the presence AIBN in THF at 70 °C show M_w of approximately 21,500 and PDI of approximately 1.33, as revealed by GPC measurement.

Recently significant advances have been made in the study of the copolymerization of MCM of intracomplex type. As a typical example, we note the copolymerization of Eu-MCMs based on β-diketones with MMA which leads to luminescent Eu-containing

PMC. It occurs that all Eu copolymers are completely soluble in ordinary organic solvents and can be re-processed into transparent thin films with good mechanical flexibility and thermal stability. Eu-copolymer luminophores display intense red color at 615 nm at UV excitation at room temperature corresponding to $5D^0 \rightarrow 7F^2$ transition of Eu(III) ions. Intensity of luminescence, lifetime and monochromaticities, $\eta(5D^0 \rightarrow 7F^2/5D^0 \rightarrow 7F^1)$ of Eu-copolymers are far higher than those of the respective Eu-MCMs and the PMMA/Eu-chelate mixture. It should be noted that intensity of luminescence increases almost linearly with increase in Eu content and the phenomenon of luminescence quenching is not observed at Eu content 0–6.38 mol%. This points to uniform distribution of metal chelate nodes in Eu-copolymers along a polymer chain, and is in good agreement with the result of analysis of the polymer structure [64].

Another example of β-diketonate MCM are chelates of rare earth metals (Sm, Eu, Tb, Dy) with 1-(2-furyl)-3-phenyl-1,3-propanedione and AA as a monofunctional ligand, which are copolymerized with MMA in presence of AIBN initiator [65]. It is interesting to note that this β-diketonate ligand can efficiently transfer energy in the obtained Sm(III) and Eu(III) copolymers, but it cannot sensitize Tb (III) and Dy(III) ions.

Copolymerization of luminescent Eu-MCM based on TTA and 5-acrylam ido-phen with MMA leads to the Eu-PMC emitting monochromatic light with increased lifetime and intensity (Scheme 4.8) [66].

Radical copolymerization was used to obtain non-conjugated copolymers containing N-vinyl-Cz units and other mixed-ligand MCM (phen)[Eu(β-diketonate)₃]. Multilayered PLED containing the obtained PMC emit monochrome red light (615 nm), whose spectral composition is independent on voltage [67].

Among MCM of intracomplex type we shall also note Eu(III) complex with acrylate-dbm, which was copolymerized with MMA to produce luminescent polymeric lanthanide chelates with chromophores [33]. Luminescence intensity of polymeric Eu(III) chelate containing dbm-ligands excess intensity of the monomeric complex by several times, which is explained by weakening of the quenching effect in low state of MLCT. In this case PMC differ considerably by properties from their low molecular weight analogues: during photolysis luminescence intensity of the studied Eu(III) chelates increases with the coefficient from 1.3 to 2.5 [68].

An interesting approach to the production of monochromatic PLED devices based on copolymerization of MCM of intracomplex type is developed (Scheme 4.9) [69]. First blue light-emitting fluorene monomer is copolymerized with a small amount of
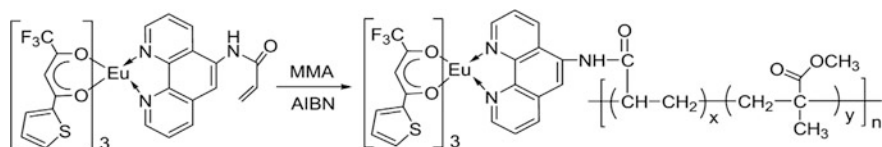
Scheme 4.8 Copolymerization of mixed-ligand Eu-chelate monomer with MMA
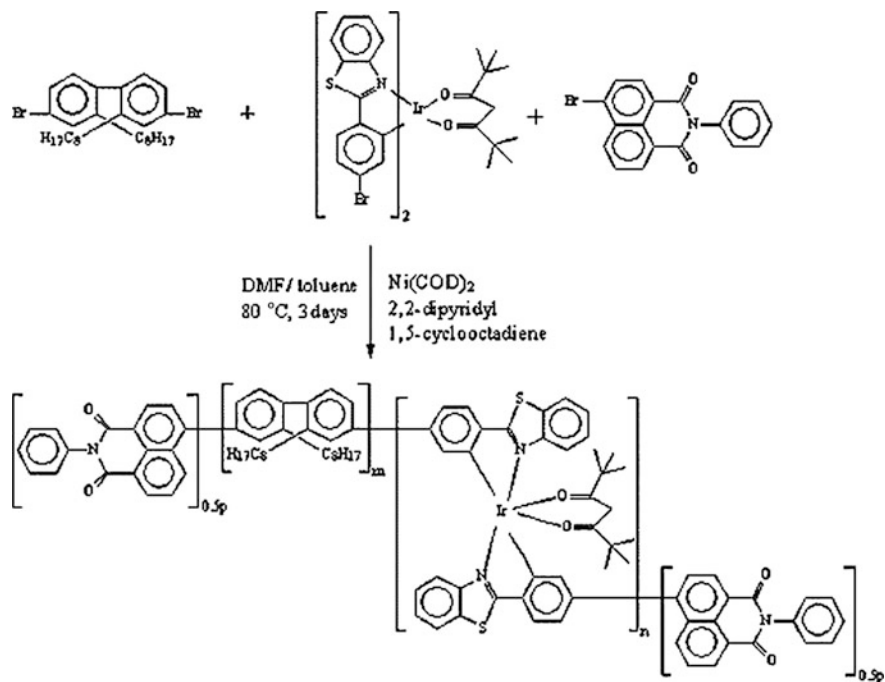
Scheme 4.9 Copolymerization of fluorene monomer, Ir-containing monomer and *N*-phenyl-1,8-naphthalimide

red light-emitting phosphorescent Ir-containing monomer, Ir-bis(4-bromophenyl ben-zothiazole)(acac), and then end-capped of the formed copolymer with green light-emitting *N*-phenyl-1,8-naphthalimide with PMC production is performed. By adjusting of molar ratio between three components, copolymers are obtained, which emit pure white light.

A series of copolymers containing metal-quinolates (AlQ$_3$, ZnQ$_2$ and LiQ) is obtained by radical copolymerization of MCM and MMA [70]. Free radical copolymerization of MCM containing AlQ$_3$ side fragments with acrylates [MMA, AN or 2-hydroxyethylmethacrylate] leads to acrylic copolymers containing AlQ$_3$ as a side group (25 wt%) [71].

The luminescent in the near-infrared (NIR) region PMCs containing of ErQ$_3$ chelate and Cz units were also prepared by the MCM copolymerization [72, 73]. In the obtained polymers, energy absorbed by light-harvesting Cz fragment is transferred to chelating Q fragment, and, at last, to photoluminescent Er(III) ion (Fig. 4.5).

It should be noted using MCM copolymerization for the preparation of PMC containing fragments of *N*-vinyl-Cz and Eu-chelate based on Q and dbm ligands [74]. It is interesting that the PMC solution emits Cz characteristic irradiation, while the solid PMC exhibits characteristic irradiation of Eu-quinolate (Fig. 4.6).
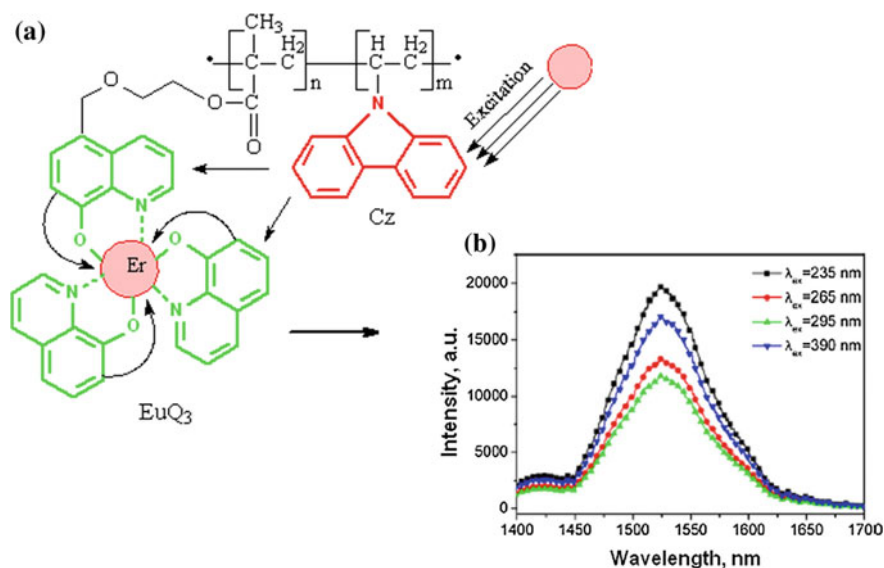
Fig. 4.5 **a** Structure of copolymers, containing of ErQ$_3$ and Cz fragments. **b** Photoluminescence emission spectra of the copolymer excited at different wavelength
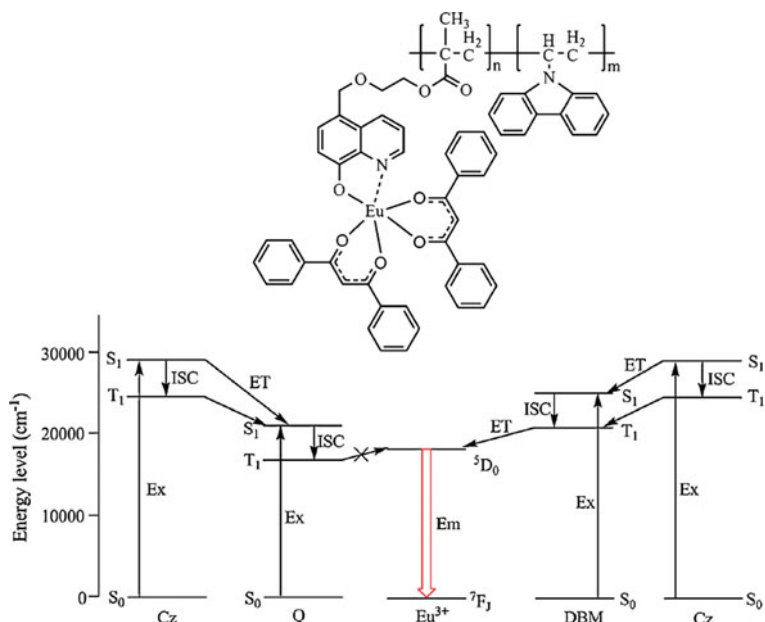
Fig. 4.6 Structure of Eu-chelate and *N*-vinyl-Cz copolymer and energy level diagram of Cz, Q, dbm and Eu(III) and energy transfer process in the photoluminescence of the copolymer

The copolymerization of Eu-MCM based on TTA and 5-acryloxyethoxy-methyl-Q with MMA leads to high-luminescent Eu-PMCs, which have good solubility, thermal stability, high T_g, and intense red emission at 612 nm [75].
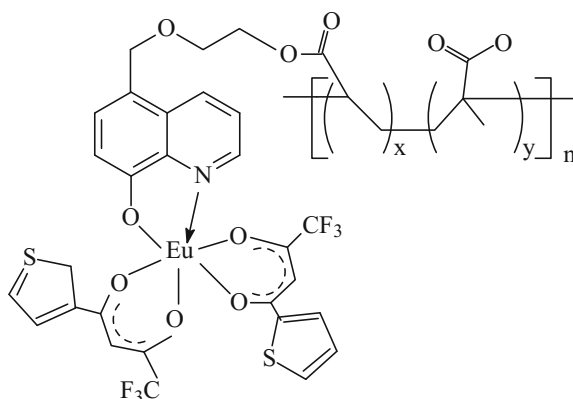
Of interest are PMCs containing AlQ_3 chelate and *N*-vinyl-Cz fragments with excellent PL performance and enhanced hole conductivity (Fig. 4.7) [76].

Of interest are NIR luminescent PMCs based on LnQ-MCMs (Ln = Er, Nd, and Yb), which exhibit appropriate molecular weight, good solubility-processability and thermal stability for PLEDs application [77]. It is important that *N*-vinyl-Cz fragments are not only used as light-harvesting groups, but also as a barrier to form a special microenvironment for the Ln-chelate moieties. In the PMC containing Cz fragments and Al chelate based on Q and salen ligands (Fig. 4.8) irradiation of the solution is generated from Q-site, and Cz segments are light-harvesting, hole transport, and luminescence preservation groups [78].
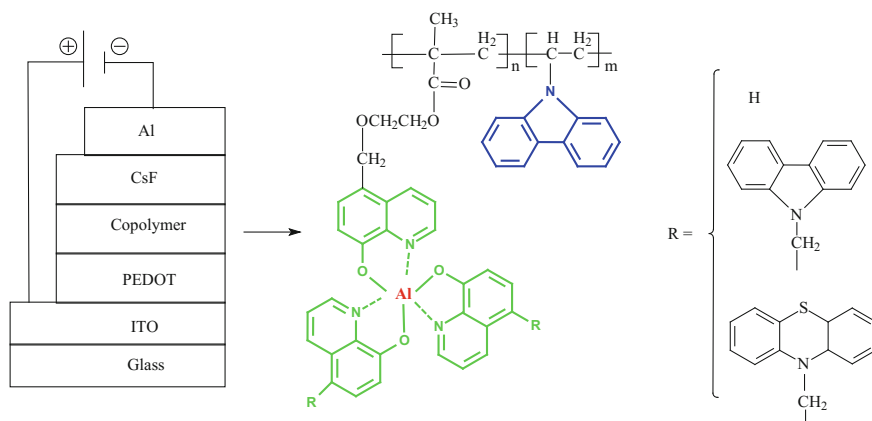
Device structure: Glass/ITO/PEDOT(40 nm)/Copolymer(80 nm)/CsF(1.5 nm)/Al(120 nm)

Fig. 4.7 The structures of the bipolar copolymers and the configuration of the devices, where PEDOT is poly (3,4-ethylenedioxy-thiophene)

Fig. 4.8 Structure of copolymer of mixed-ligand (Q and salen) Al chelate and *N*-vinyl-Cz
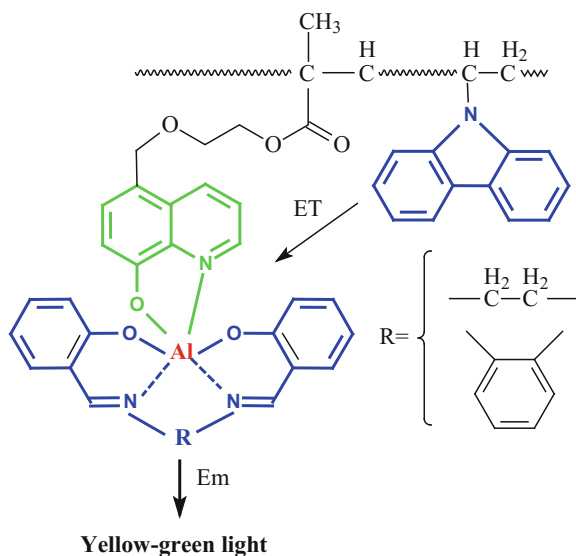
The heterometallic PMCs are produced by copolymerization of salen MCMs. For example, heterobinuclear Zn-Ln MCMs [Zn(L)(Py)Ln(NO$_3$)$_3$], where H$_2$L = *N,N'*-bis-(5-3′-vinylphenyl)-3-methoxy-salicylidene)cyclohexane-1,2-diamine, Ln = La, Nd, Yb, Er, Gd were copolymerized with MMA, St or *N*-vinyl-Cz to obtain Zn(II)-Ln (III) containing Wolf type II polymeric materials [79, 80].
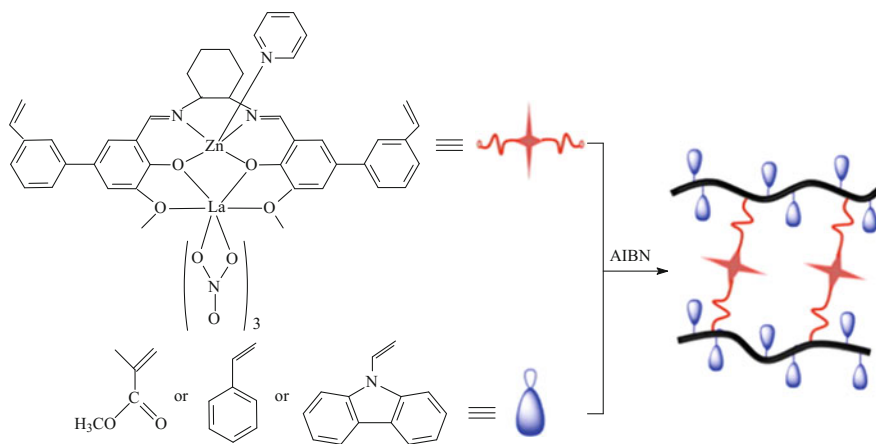
The copolymerization of MMA and MCM of Zn$_2$(salen)$_2$(4VP)$_2$Ln(NO$_3$)$_3$ type, where Ln = La, Nd, Yb, Er, Gd was used to the preparation of Wolf type II heterometallic trinuclear Zn$_2$Ln-containing polymers [81]. It should be also noted

that heterometallic quadronuclear $Zn_2(salen)_2Ln_2(4,4'-bpe)(NO_3)_6$ chelate, where Ln = La, Nd, Yb, Er, Gd, $4,4'$-bpe = $4,4'$-dipyridinethylene, is not copolymerized with MMA due to degradative chain transfer inside $4,4'$-bpe fragment, and allows to preparing PMMA-supported doped PMMA-$[Zn_2(salen)_2Ln_2(4,4'-bpe)(NO_3)_6]$ hybrid materials [82].

Ln = La, Nd, Yb, Er, Gd

PMMA-supported hybrid materials
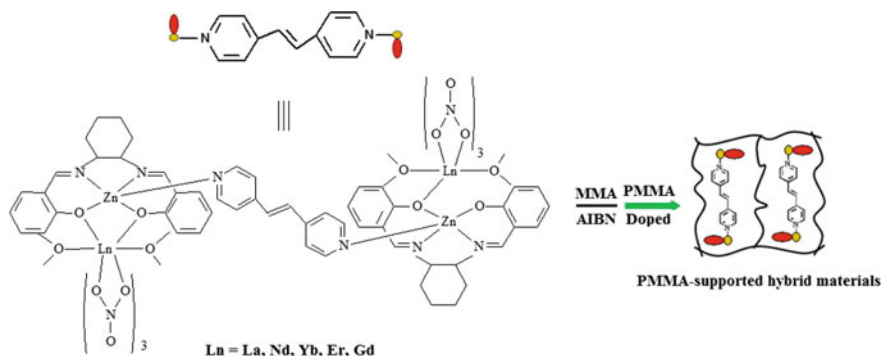
Of substantial interest is the copolymerization of M-Pp with traditional monomers for the preparation of PMCs of macrocyclic type [83–86]. In particular, it is shown that Cu(II)-Pp and Zn(II)-Pp comonomers containing one vinyl group at pyrrol or benzene ring decrease total rate of copolymerization with St and MMA and average molecular weight of the formed products, as compared to metal-free polymer analogues obtained under similar conditions. The main reason for this is attributed to termination of the M-Pp chain growth. In the obtained PMC Cu(II) centers are quite far from each other, in other words, metal-containing polymer systems are magnetically dissolved. Moreover, PLQY of Zn(II)-5-(4-vinyphenyl)-10,15,20-triphenyl-Pp copolymers is decreased as the mole fraction of Pp groups increases. Co- and Pd-2-vinyl-Pp were copolymerized with St [87].

It should be noted the copolymerization of methacryloyloxy-substituted M-Pc, for example, Cu(II)-2,9,16,23-tetra(methacryloxyethoxycarbonyl)-Pc and Cu(II)-2,9,16-tris(*tert*-butyl)-23-(methacryloxyethoxycarbonyl)-Pc [88].

4.3 Living and Controlled Polymerization

Like metal-free chelating monomers (Sect. 2.1.2), in the recent years, significant advances have been made in the study of the living and controlled polymerization of MCM, which include living anion polymerization, ROMP and controlled radical polymerization, such as ATRP, RAFT, and NMP [89].

For example, PMCs were prepared by RAFT polymerization of MCM with participation of functional RAFT agent or using metal chelate containing RAFT agent [90]. However, only few PMCs were synthesized directly from Z-C(=S)-SR RAFT

agents based on metal chelates for R-groups. In particular, we note St-coumarin homopolymer and block-copolymer of St-coumarin with NIPAM obtained using RAFT agents based on bpy Ru(II)-chelates [91–93].
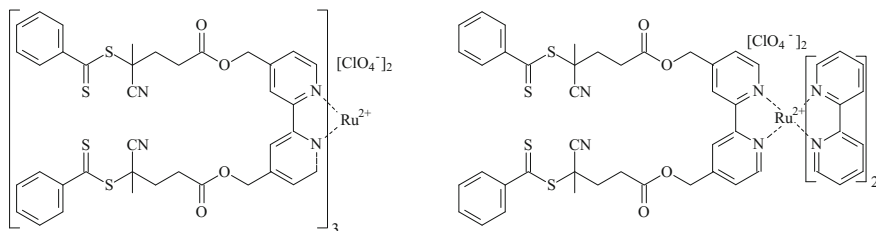
Of interest is the preparation of homo-, co-, and block-polymers based on MMA, GL, DVB, St, and (4-(3-butenyl)-St with participation RAFT agents containing Eu (III) β-diketonates [94, 95].
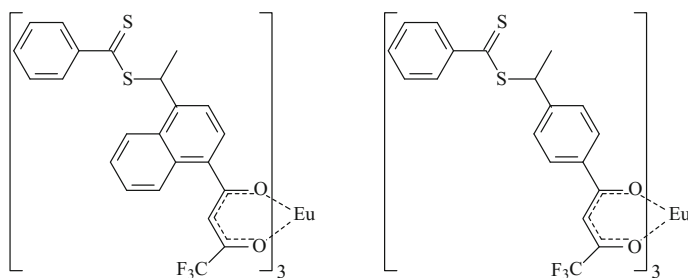
There are some examples of RAFT polymerization of the MCMs. As a typical example, we note using a RAFT agent during copolymerization of MMA and Ru (II)-MCM [96].
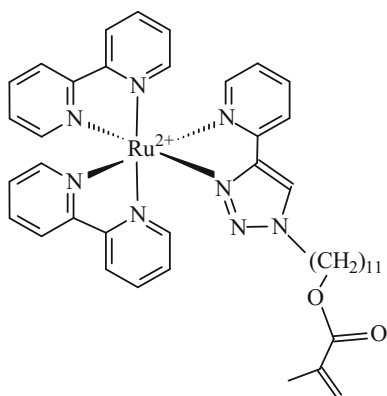
Of interest are PMCs prepared by RAFT polymerization of 4-hydroxy-1, 3-thiazole-based chromophore monomers and photoactive [Os(dimethyl-bpy)$_2$ (1,2,3-triazole-py)]$^{2+}$ MCM (Scheme 4.10) [97].

In the prepared PMCs, three metal-free dyer monomers (M_B, M_Y, and M_R) absorb and emit in different ranges of visible light: the blue-emitting first monomer emits in absorption maximum of the yellow-emitting second monomer, which emits in maximum of absorption of the red-emitting third monomer, which, in turn, emits in the absorption band of MLCT of photoactive M_{Os} MCM. 2D size-exclusion chromatography (SEC) segment of PMC (Fig. 4.9) confirms the introduction of all chromophore monomers into PMC.

It should be noted the preparation of block-copolymers of *N*-vinyl-Cz and Re-MCMs by the RAFT polymerization [98].
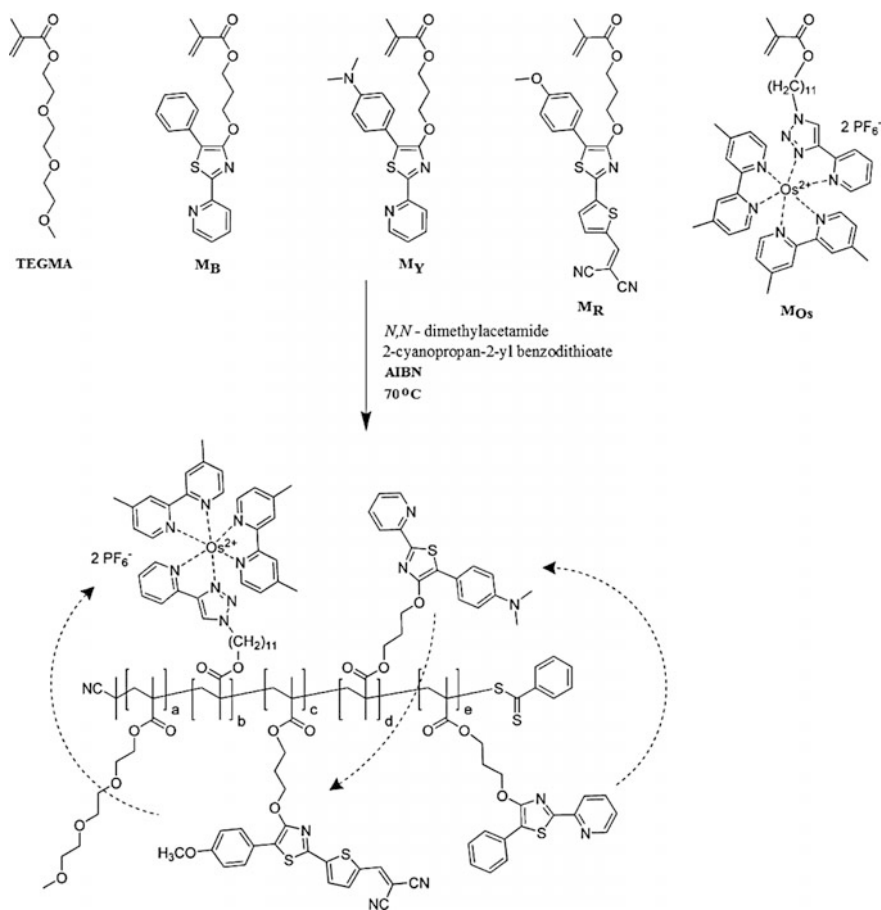
Scheme 4.10 RAFT polymerization of 4-hydroxy-1,3-thiazole-based chromophore monomers with [Os(dimethyl-bpy)$_2$(1,2,3-triazole-py)]$^{2+}$ metal complex
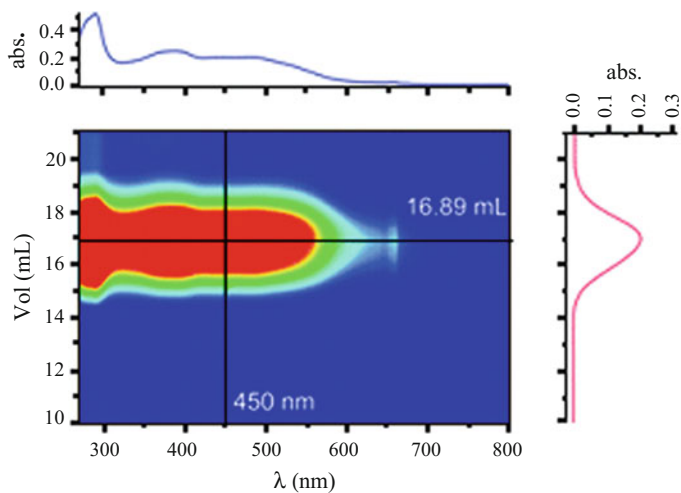
Fig. 4.9 2D SEC of PMC. The inserted lines display the corresponding profiles of the absorption spectrum (top) and the SEC trace (right)
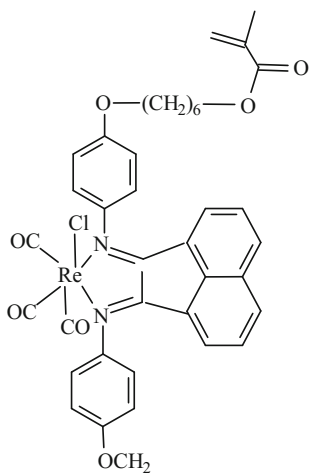
It should be noted the combination of RAFT polymerization and azide-alkyne click reaction. For example, such approach is applied to the preparation of PS-based polymers containing pendant Ru(II) polypyridine fragments [99].

Intrapolymer Excition Migration
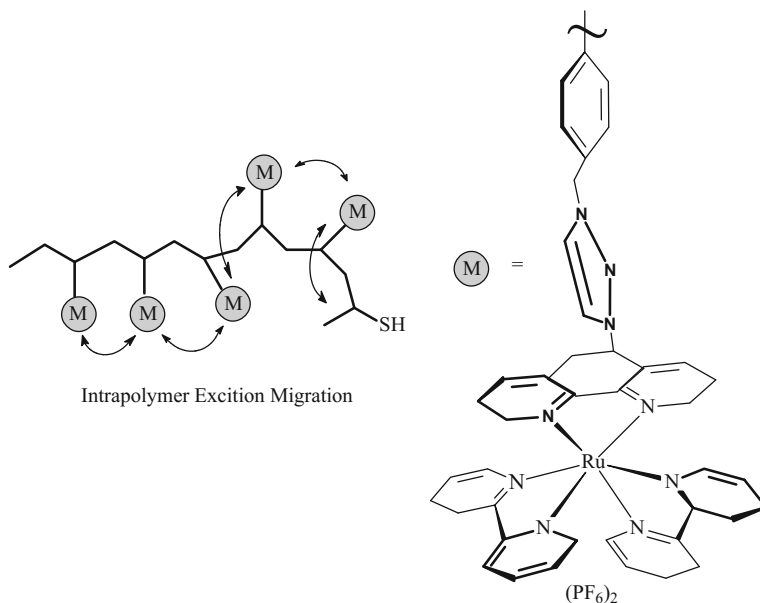
Of interest is the preparation of α-[Cu(II)-Pp]-PE with strongly-colored units using copper-catalyzed 1,3-dipolar azide-alkyne Huisgen cycloaddition (Fig. 4.10) [100].

An example of ATRP using is polymerization of 5-[(*p*-vinyl phenyl)-bpy]bis (bpy)Ru(II) with oxadiazole-type (2-{4-[(vinyl phenyl)methoxy]phenyl-5-phenyl-1,3,4-oxadiazole) or Cz-type (9-vinylcarbazole) monomers known for their electron or hole transporting properties with oxadiazole-type (2-{4-[(vinyl phenyl)methoxy] phenyl-5-phenyl-1,3,4-oxadiazole) or Cz-type (9-vinylcarbazole) monomers known
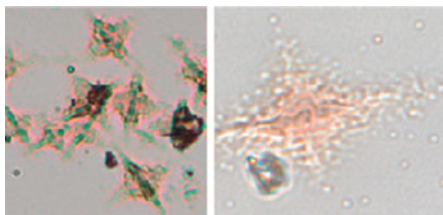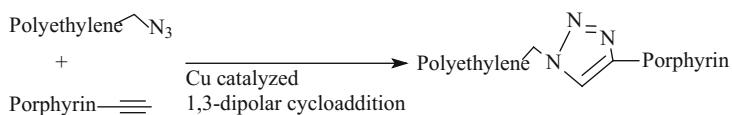
x50 and x100 magnifications

Fig. 4.10 Scheme of synthesis of α-[Cu(II)-Pp]-PE and its optical microscopy image

for their electron or hole transporting properties with formation of soluble PMC with high yields and high metal content with help of the initiator 5-[[4-(bromomethyl)benzene]oxy]benzene-1,3-dicarboxylic acid. Optical properties of metal-polymer materials are determined by intense optoelectronic characteristics of Ru(II) (bpy)$_3$ chelates in combination with optical properties of oxadiazole or Cz units [101].

Amphiphilic Zn-Pc-terminated PMCs with poly (triethylene glycol methyl ether methacrylate) main chain were obtained by ATRP of acrylates with Zn-Pc functionalized initiator. The PMCs aggregation in methanol leads to physical gel with dense fiber net-like structure, in which Zn-Pc fragments are stacked in 1D columnar aggregate via intermolecular π-π interactions (Fig. 4.11) [102].

Of interest is combination of ATRP with click chemistry, which allows to preparing a range of M-Pc-PMMA-*b*-PS with M$_n$ = 41,000, 66,000, or 86,000 (Fig. 4.12) [103]. The prepared PMCs are self-assembled in cylindrical morphology, in which M-Pc fragments exhibit π-π interactions in closed PMMA cylinders.

Click reaction of Zn-Pc and end functional polymers based on poly (*tert*-butyl acrylate) or PS produced by ATRP proceeds with efficiency 75 and 93%, respectively. It is important that in situ electrocolorimetric measurements allow to estimating color coordinates of each electrogenerated anion and cation redox type (Fig. 4.13) [104].
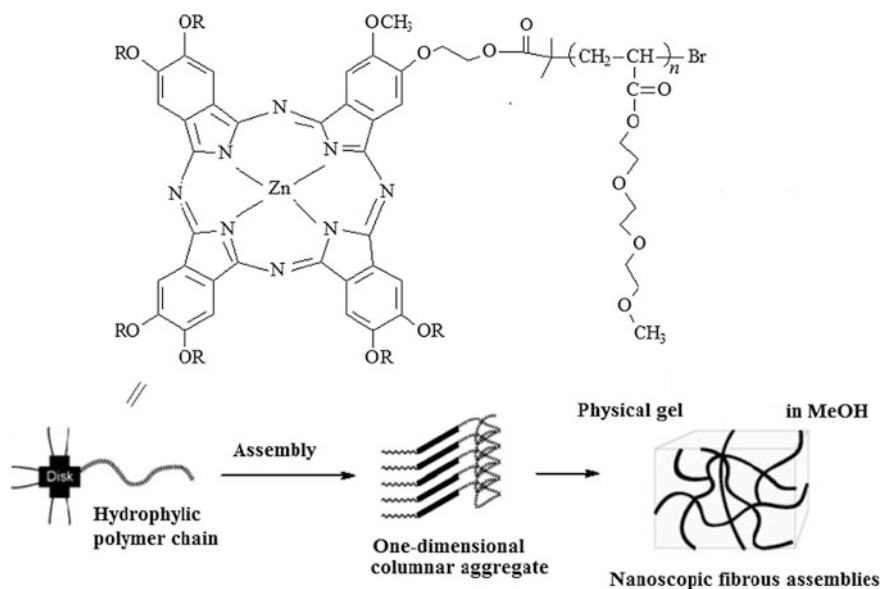
Fig. 4.11 Schematic illustration of the formation of nanoscopic fibrous assemblies of Zn-Pc-terminated polymer in methanol
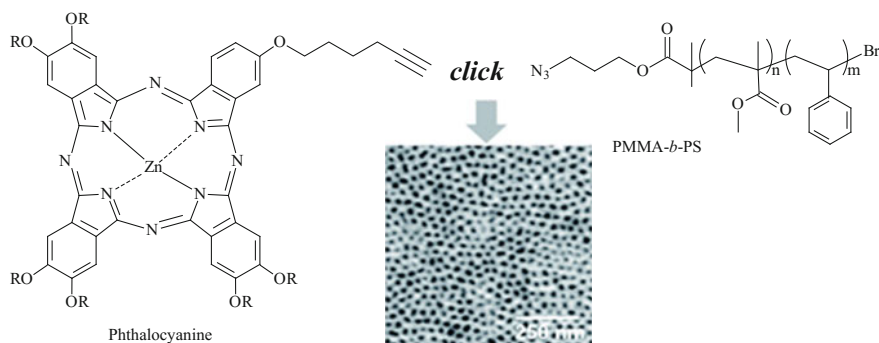
Fig. 4.12 Scheme of Zn-Pc copolymer synthesis and it atomic force microscopy phase images

Fig. 4.13 Chromaticity diagram (each symbol represents the color of electrogenerated species: Zn(II)-Pc^{-2}, square; Zn(II)-Pc^{-3}; circle; Zn(II)-Pc^{-4}; triangle; Zn(II)-Pc^{-1}, star)
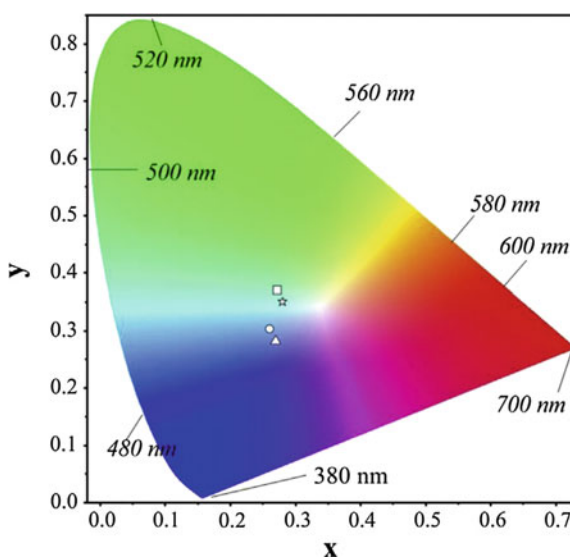
Double CuAAC click-reaction between end alkynyl-substituted Zn-Pc, azido-functional poly (MMA-*co*-2-(2-bromoisobutyryloxy) ethyl methacrylate), and 4-ethynyl-*N*,*N*-dimethylaniline was used for the preparation of photocured Zn-Pc PMC (Scheme 4.11) [105].

Cross-linking the prepared PMC in presence of a liquid crystalline mesogen 4′-(octyloxy)-4-biphenylcarbonitrile leads to the polymer disperse films with smectic A liquid crystal meso-phases. The textures of the meso-phase were identified during both heating and cooling cycles as being a smectic A meso-phase at 61.5 and 52.5 °C, respectively (Fig. 4.14).

EDMA = 4-ethynyl-*N*,*N*-dimethylaniline
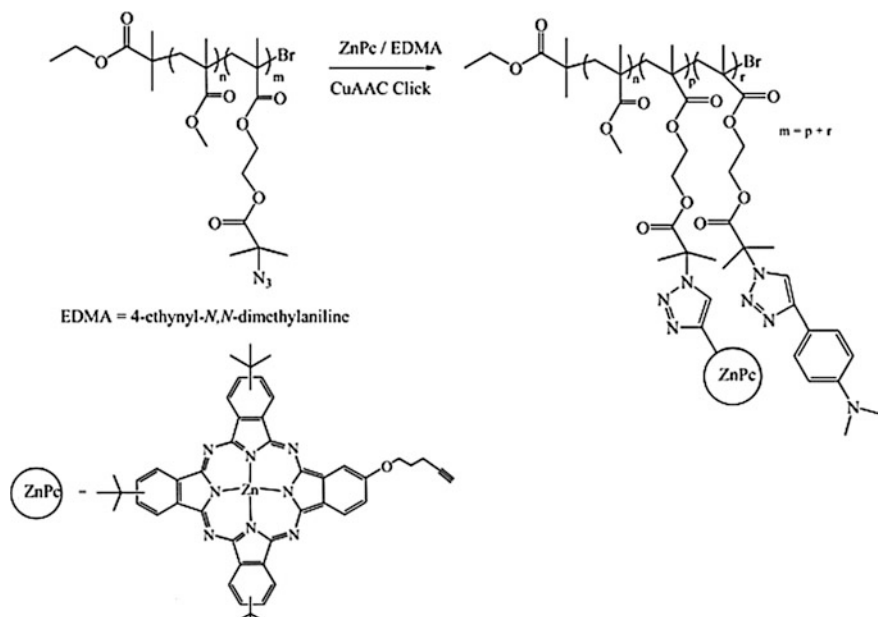
Scheme 4.11 CuAAC reaction between azido-functional poly (MMA-*co*-2-(2-bromoisobutyryl-oxy) ethyl methacrylate), alkynyl-substituted Zn-Pc and 4-ethynyl-*N*,*N*-dimethylaniline
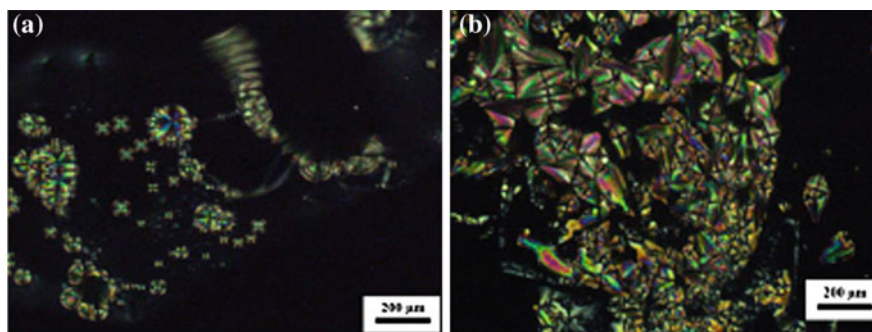
Fig. 4.14 Polarized optical micrographs of Zn-Pc-functional copolymer taken during heating at 61.5 °C (**a**) and cooling at 52.5 °C (**b**) at a rate 5 K min^{-1}. The scale bar in inset represents 200 mm
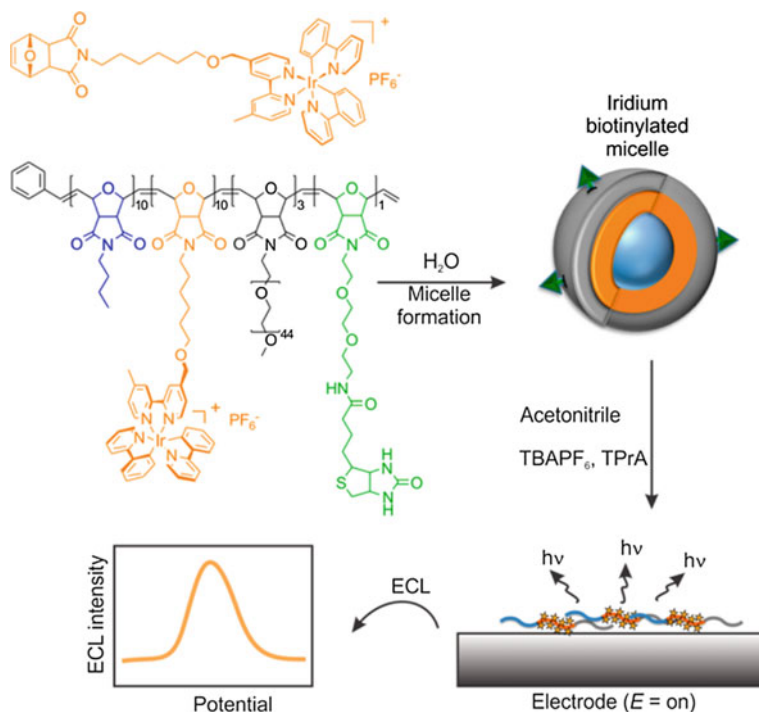
Fig. 4.15 The scheme of formation of Ir(ppy)$_2$(bpy) chelate block-copolymers' micelle. The polymer is composed of three main blocks and a biotin label. The blocks containing butyl chains and the Ir chelates are hydrophobic, while the PEG portion imparts water solubility

It should be noted using ROMP in PMC synthesis, in particular, norbornene-containing phosphorescent ppy-complexes of Ir type, Ir(ppy)$_3$ or Ir(ppy)$_2$(bpy) (PF$_6$), were copolymerized with alkyl norbornenes (Fig. 4.15) [106, 107]. Polymers preserve optical properties of phosphorescent chelates with maximum emission in yellow-green range and PLQY from 0.23 to 0.24 for polymers containing Ir (ppy)$_2$(bpy)(PF$_6$), and from 0.20 to 0.24 for polymers containing *fac*-Ir(ppy)$_3$.

Of interest are phosphorescent poly (dendrimers) with norbornene-based matrix prepared by ROMP with Grubbs III catalyst. They include heteroleptic Ir(III) complex based on two ppy ligands and phenyltriazolyl coligand as core, biphenyl-based dendrons, and 2-ethylhexyloxy terminal fragments. It is important that dendronized structure allows to control intra- and intermolecular interactions and inhibit triplet annihilation [108].

1 R = R' = H
2 R = D, R' = H
3 R = R' = D

D =
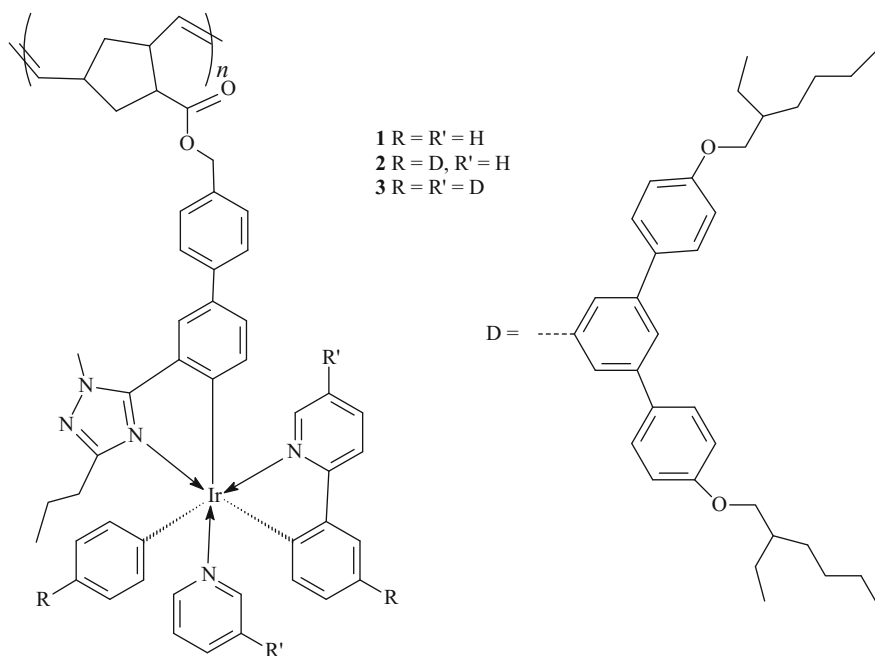
A cross-linked membrane was prepared by ROMP of water-soluble bis-tpy Ru(II) complex linked with norbornene monomer and dicyclopentadiene [109].

It should be noted polymeric Fe-tris(dbm-polylactide) complex prepared from D, L-lactide and Fe(dbmOH)$_3$ as metal-initiator (Scheme 4.12) [110]. It is important that high quality control of molecular weight (PDI < 1.1) at ∼60–70% conversion

Fe(dbmOH)$_3$ + $\xrightarrow{130^0C}$ Fe (dbmPLA)$_3$ $\xrightarrow[Fe]{aq\ HCl}$ 3 dbmPLA
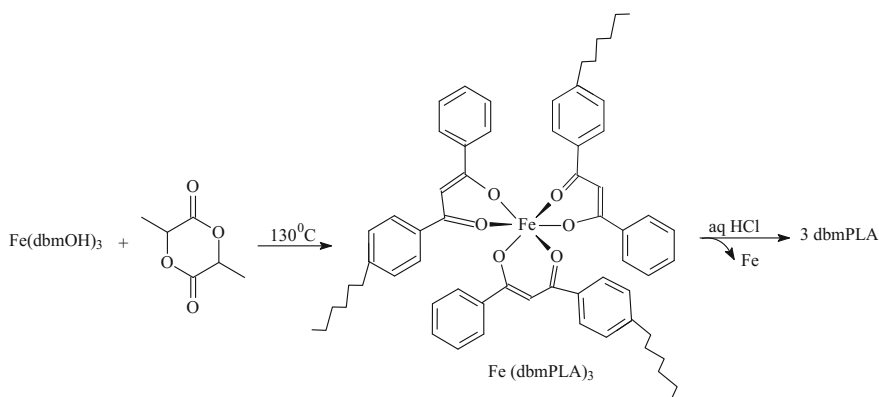
Scheme 4.12 Synthesis of polymeric Fe-tris(dbm-polylactide) complex

is guaranteed and de-metallization by diluted HCl leads to chelating polymers for consequent linking other metals.

ROMP of Eu-MCMs leads to statistical copolymers and amphiphilic block-copolymers with the characteristic bright-red long-lived Eu(III) luminescence [111]. Tb(III)- and Eu(III)-diketonates modified by primary alcohols are catalysts and ROMP initiators of lactide monomer under solvent-free conditions (Fig. 4.16) [112].

We shall also mention AlQ$_3$-functionalized polymer obtained by ROMP of norbornene-monomer containing AlQ$_3$ chelate fragment [113]. Al-salen complexes with asymmetric *O,N,O,N*-quadridentate hemi-salen ligands containing binaphthyl fragments were used in the stereoselective ROMP of *rac-* and L-lactides (Scheme 4.13) [114].

Dimeric Fe(III) chelates with acac-ligands and tridentate chiral azomethine ligand are efficient catalysts of lactides ROMP [115].

Zn(II)-2,3,9,10,16,17,23,24-octakis(3-hydroxypropylmercapto)-Pc was used as macrocyclic initiator in ROMP of ε-caprolactone leading to hydroxyl-containing octa-armed star PCLs [116].

We shall also consider ROMP of well-defined alkylidenes of VI and VII group transition metals [117], and also metal-functionalized cyclic monomers and catalytic systems based on W, Mo, and Ru for PMC production [118]. Moreover, PMC can also be obtained using ROMP reactions initiated by Schrock's Mo-carbene or Grubbs' Ru-carbene catalysts [119].

It should be noted ROMP of norbornene and homoleptic tetranuclear complexes based on diallyl-modified flexible hexadentate salen-type ligand, *N,N'*-bis(5-allyl-3-methoxysalicylidene)cyclohexane-1,2-diamine, leading to Wolf II type Ln(III)-containing polynuclear PMCs poly(norbornene)-*co*-poly[Ln$_4$(salen)$_4$], where Ln = La, Nd, Yb, Er or Gd (Scheme 4.14) [120].
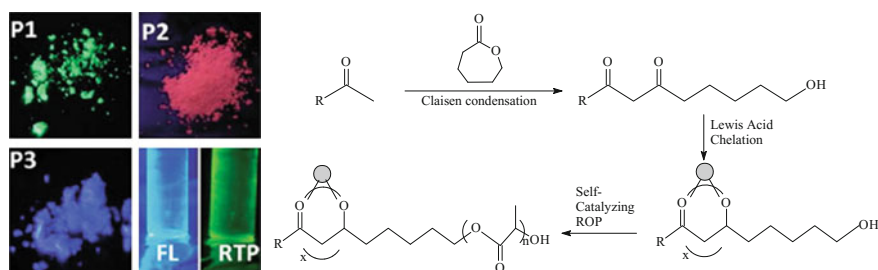
Fig. 4.16 Photos of **P1**–**P3** solids, where R = 4-methoxyphenyl (**P1**), naphthalen-2-yl (**P2**), thiophen-2-yl (**P3**), and fluorescence (FL)/room-temperature phosphorescence (RTP) of a thin film of **P3** in a glass vial filled with N$_2$ under 365 nm UV light (left) and scheme of synthesis of PMC (right)
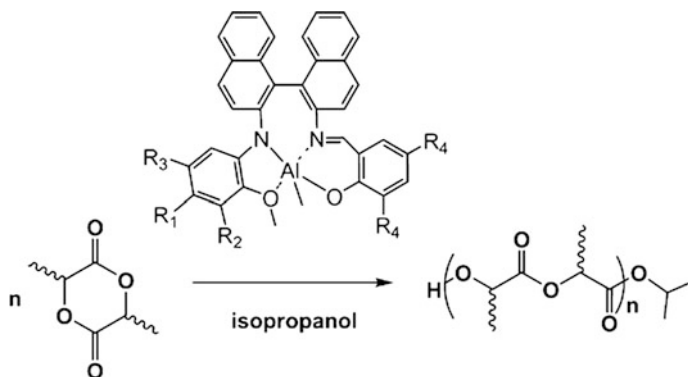
Scheme 4.13 ROMP of *rac*- and L-lactides under the action of Al-salen complexes
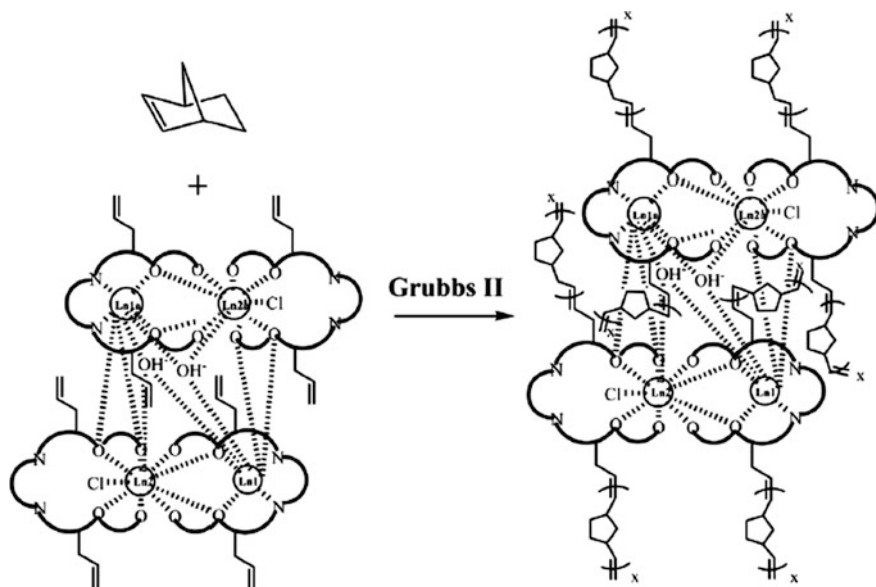
Scheme 4.14 Reaction scheme for the synthesis of poly [(norbornene)-*co*-Ln₄(salen)₄]

4.4 Electropolymerization

MCM electropolymerization is often used for synthesis of different PMCs, in particular, in the form of thin insoluble films with various areas of their further applications [121–123]. In particular, mechanism of reductive electropolymerization (Scheme 4.15) is studied in detail on the example of molecular type of MCM

containing a chelating bpy, phen, or tpy ligands and monofunctional monomer of 4VP, *trans*-4-stilbazole, etc. [121].

Reductive electropolymerization is carried out by repeated cyclic change in potential of an electrode (ITO, Pt, carbon glass, etc.) near a value corresponding to ligand reduction, that leads to coating an electrode surface by uniform polymer film. It was shown [123] that increase in a number of vinyl groups in MCM allows to increasing polymerization rate and introduction of a vinyl group in α-position of a pyridine ring with respect to coordinated nitrogen atom prevents MCM electropolymerization.

Of interest is electropolymerization of MCM based on 5,5′-divinyl-bpy and 4,4′-divinyl-bpy ligands [124]. It turned out that Ru-MCMs with one 5,5′-divinyl-bpy ligand are easily deposited on electrode surfaces by reductive electropolymerization (Fig. 4.17).

Ru-MCM based on one 4,4′-divinyl-bpy ligand does not polymerize under the same conditions, while Ru-MCMs with two or three 5,5′-divinyl-bpy ligands are also well polymerized. PMC films were obtained on the surface of Pt and ITO glass electrodes using reductive electropolymerization of tris-bidentate diruthenium MCM with 5-vinyl-bpy with phen-1,4-diyl-bridge [125]. It should be also noted reductive electropolymerization of bis-tridentate cyclometalated and non-cyclometalated Ru (II)-MCMs based on 5,5′-divinyl-4′-tolyl-tpy on carbon glass and on ITO glass electrodes [126]. PMC films were prepared by reductive electropolymerization of bis-cyclometalated Ru-MCM $[(4′-vinyl-tpy)Ru(L)Ru(4′-vinyl-tpy)]^{2+}$, where L = 1, 2,4,5-tetra(2-pyridyl)benzene (Fig. 4.18) [127]. Characteristic feature of these films is electrochromism, which is typical of many PMCs [128].
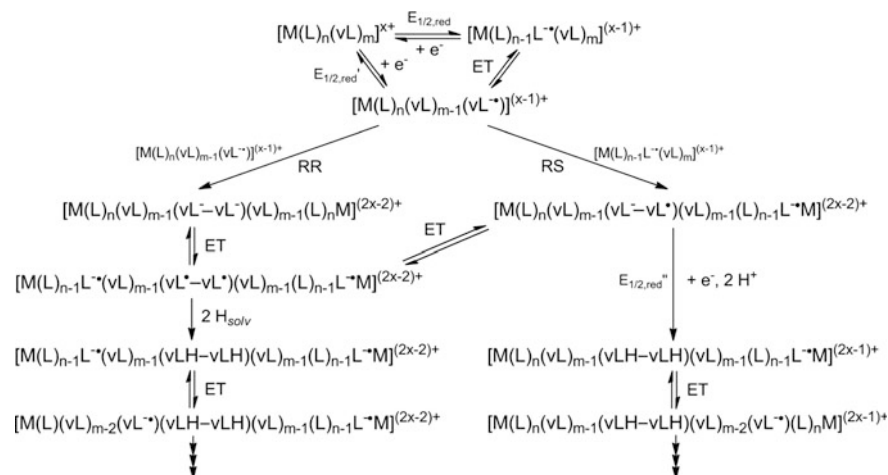
Scheme 4.15 Mechanism of reductive electropolymerization of vinyl-pyridyl transition metal chelates, where M: Fe, Ru, Os (x = 2) or Co, Cr (x = 3); L: Py, bpy, tpy; vL: vinyl-Py, vinyl-bpy; ET is electron transport: RR or RS are radical-radical or radical-substrate combination

However, in most cases oxidation methods are more widely used than reductive electropolymerization. They are performed using oxidation coupling of, mainly, 5-member heterocycles. The common mechanism of this process includes anode electropolymerization of MCM with the formation of cation-radicals through one-electron oxidation of aromatic ring followed by radical-radical route and de-protonation leading to dimeric species [121]. Oxidation and polymerization of organic fragment is greatly facilitated by the presence of a metal ion in the case of Ru-MCM [Ru(4′-[(2,2′:5′,2″-terthien-3′-yl)methoxy]-tpy)$_2$][PF$_6$]$_2$. Besides, presence of –O–CH$_2$-spacer between coordinating and polymerized blocks (tpy and terthiophene, respectively) decreases electron delocalization between these units. It is interesting that so called charge-trapping phenomenon is observed in the formed PMC that is also characteristic for a polymer ligand (Fig. 4.19) [129].

Electropolymerization of di-ruthenium MCM limited by two triphenylamine units leads to metal chelate polymer films with alternating di-ruthenium and tetraphenylbenzidine structures [122, 130]. The prepared PMCs consist of biphenyl-bridge *bis*-triarylamine segments and alternating structural units including 2,7-*bis*-deprotonated form of 1,3,6,8-tetra(pyrid-2-yl)pyrene or 3,6-*bis*-deprotonated form of 1,2,4,5-tetra(pyrid-2-yl)benzene cyclometalated *bis*-Ru units. Sandwich electric devices based on these PMC films exhibit excellent resistive memory switching with low operating voltage, high OFF/ON current coefficient, good stability and long confinement time (Fig. 4.20). It is interesting that devices with PMC films based on *mono*-Ru chelate show efficiency with far smaller memory. By controlling intervalence
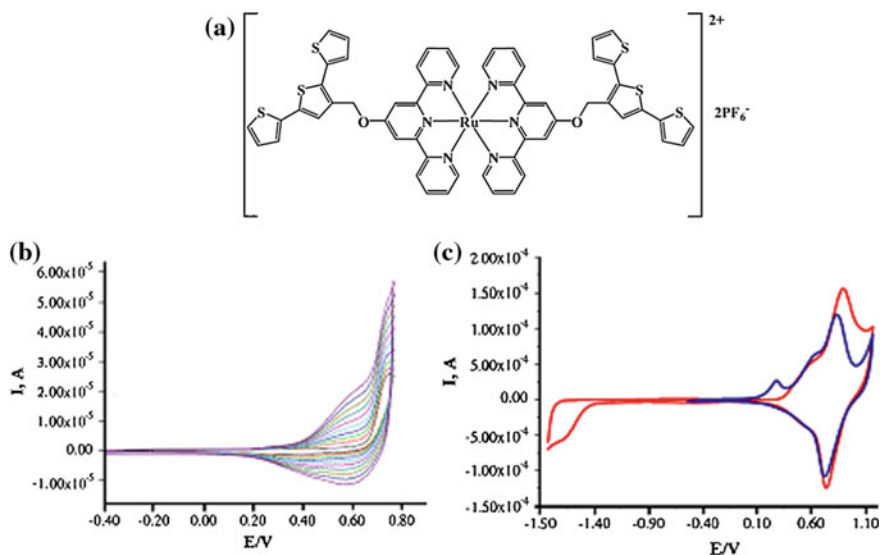
Fig. 4.19 **a** Structure of Ru(II) chelate. **b** Potentiodynamic growth of Ru chelate in 2×10^{-3} M solution of the monomer, CH$_3$CN/TEAPF$_6$ 0.1 M solvent system, scan rate = 50 mV s^{-1}. **c** Voltammetric response of Ru chelate in TEAPF$_6$/CH$_3$CN 0.1 M; potential scan rate 50 mV s^{-1}
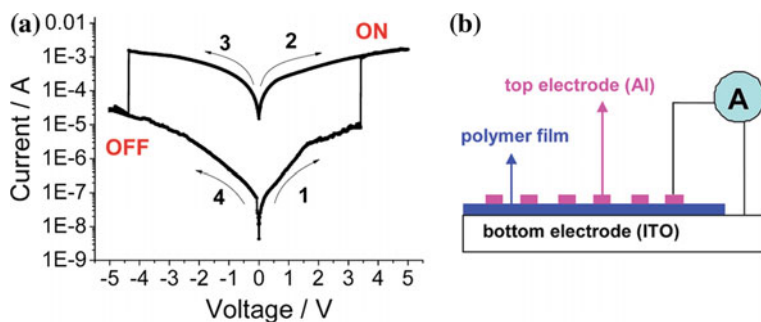
Fig. 4.20 a Typical I–V characteristics of the ITO/PMC/Al device with an active area of 6.0 mm^2. The arrows denote switching order and direction. The thicknesses of the polymer film and Al electrode are 100 and 80 nm, respectively. **b** Schematic representation of the memory device structure

transitions with charge transfer of mixed valence *bis*-Ru and *bis*-triarylamine blocks, the five-staged NIR electrochromism can be reached with stepwise color change, accompanied by good contrast and color efficiency (Fig. 4.21).

Electrochemical oxidation of thiols has become widespread as an easy method of the preparation of multilayered PMC films on Au surface [131]. Thus, MCMs [Ru (tpySH)$_2$]$^{2+}$ and [Fe(tpySH)$_2$]$^{2+}$ (tpySH = 4′-(2-(*p*-phenoxy) ethanethiol)-tpy) containing two anchor groups were used for surface fixing (Fig. 4.22). In the case of Ru-MCM two sequent oxidation processes are typical, first of which is associated with oxidation of thiol substituents and is irreversible, the second is reversible and respects to one-electron oxidation of a metal center. For Fe-MCM both processes are superimposed. The high degrees of a surface coating ($\Gamma = 6 \times 10^{-10}$ and 4×10^{-10} mol cm^{-2} for Ru- and Fe-MCMs, respectively) correspond to vertical
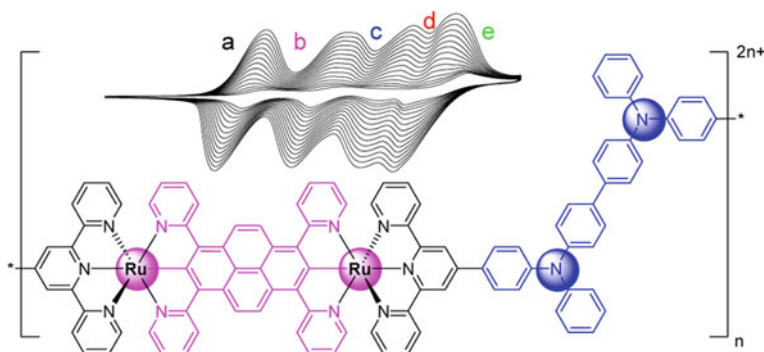
Fig. 4.21 Structure of PMC with alternating di-Ru and tetraphenylbenzidine fragments and oxidative electropolymerization of di-Ru chelate (0.5 mM in CH$_2$Cl$_2$) on a Pt disk electrode by 15 repeated potential scan cycles at 100 mV s^{-1}. The plots in red color are the steady state electrochemical response of di-Ru chelate in the potential window of 0.30–0.90 V

Fig. 4.22 Scheme of multilayer formation of PMC (bottom). Evolution of the signal during oxidative electropolymerization of $5 \times 10^{-4}\,M^{-1}$ in CH_3CN by repeated potential scans (1.06, −2.0 V) at a gold electrode (diameter = 2 mm), $v = 100\,mV\,s^{-1}$ (top)
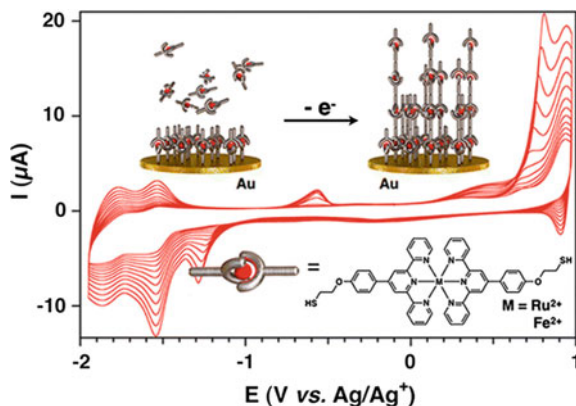
orientation of linked complexes. Thus, one thiol is bound to the gold electrode surface, with the second unreacted thiol moiety exposed to the outer surface. Successive cyclic voltammetry induced LbL nanostructured growth at the surface of the SAMs, and this is presumably due to the electrochemical formation of disulfide bonds, where the thiol moieties play a double role of both an anchoring group and an electroactive coupling agent.

It should be also noted anode electropolymerization of thiophene-functionalized cyclometalated Ru(II)-MCMs containing 1,2,3-triazole fragment [132] and cyclometalated Pt-MCM based on 4-[p-(diphenylamino) phenyl]-6-phenyl-bpy on working Pt and ITO electrodes [133]. Orange PMC film shows low-voltage controlled anode coloration of NIR electrochromism with a considerable coefficient of optical contrast, short response time, and high coloring efficiency (Fig. 4.23).
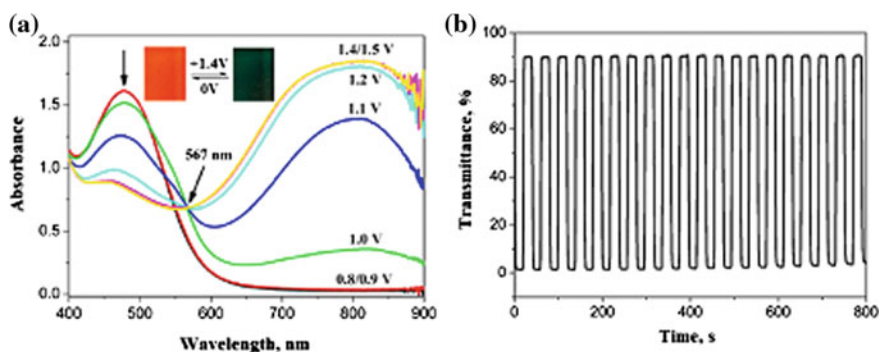
Fig. 4.23 a Spectroelectrochemical spectra of the PMC film/ITO electrode upon stepwise application of potential from 0 to +1.4 V versus Ag wire reference electrode. (Inset) Color changes at different potentials. b Transmittance changes monitored at $\lambda = 820$ nm as a function of time

Electropolymerization of Co(II)-MCM with *bis*-tpy ligand allows to prepare PMC films with even more interesting type of electrochromism called black-to-transmissive electrochromism [134]. During submersion in aqueous solution, the PMC films exhibit stable switching on the metal ion of the Co(II)/Co(I) redox reaction. It is important that almost black-to-transmissive electrochromic efficiency can be reached with the transmission difference 74.3% at 550 nm, and light absorption can be induced with lighter areas from visible to NIR with greater attenuation.

Of interest is the variant when the same MCMs, for example, homoleptic 2:1 Ru(II) chelate based on 4′-(2,2′:5′,2″-terthien-3′-ethynyl)-tpy is capable of anodic electropolymerization on the terthiophene moiety and cathodic polymerization on the tpy moiety [135].
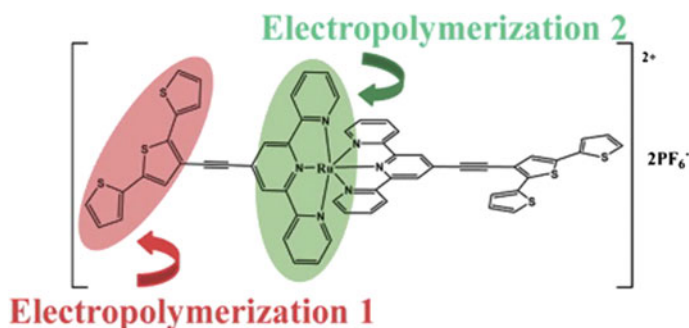
It should be noted electropolymerization of [Ir(ppy)₂L(PF₆)], [Ir(F-mppy)₂ L(PF₆)] and [Ir(Br-mppy)₂L(PF₆)] chelates, where L—ligand of 3,8-bis(2,2′-bithien-5-yl)-phen type, and F-mppy and Br-mppy are ancillary ligands based on phenylpyridine, which leads to electrically conducting PMCs with color control (from blue-green to red) of emitted light depending on a type of ancillary ligand [136].

The presence of donor-acceptor substituents, especially nitro group in the cyclometalated phenyl ring, has a special effect on the anode electropolymerization of thiophene-functionalized cyclometalated Ru(II)-MCMs [137]. We also note the electropolymerization of N-C-N-Pt-pincer complexes with electropolymerizable substituents (Scheme 4.16) [138]. It is important that LMCT degree can be controlled by changing oxidation state of metal-thiophene fragments to allow adjusting optical and conducting properties of polymer materials.

Electropolymerization of linear rod-like Ru(II)-MCMs with 2,6-di(quinoline-8-yl) pyridine containing two 2-thienyl groups bound in 4-position of quinoline fragment and 4-position of a pyridine ring leads to the formation of thin solid films on electrode surface [139]. The photoluminescence of the formed PMC is stipulated by a metal site, and electric conductivity by thiophene units [140].
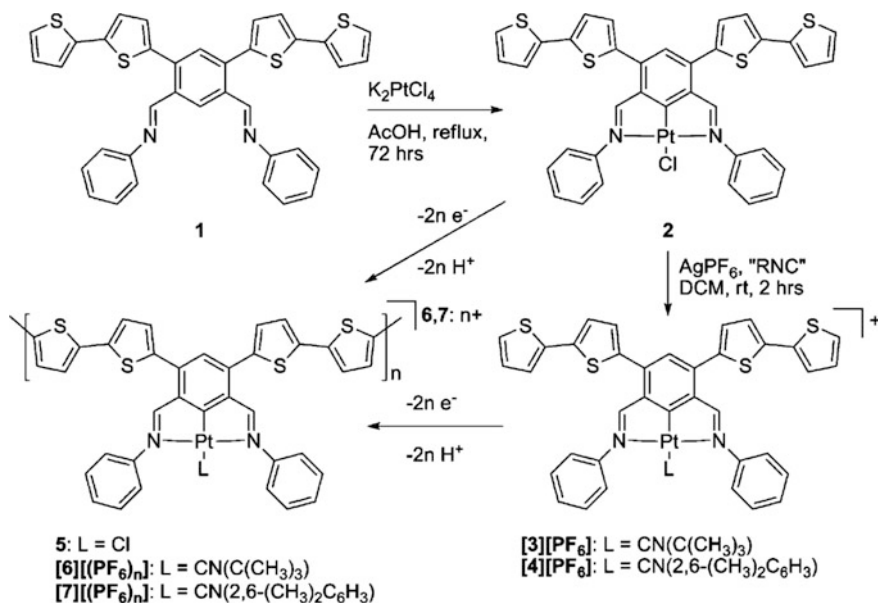
Scheme 4.16 Electropolymerization of N-C-N-Pt-pincer complexes with electropolymerizable substituents
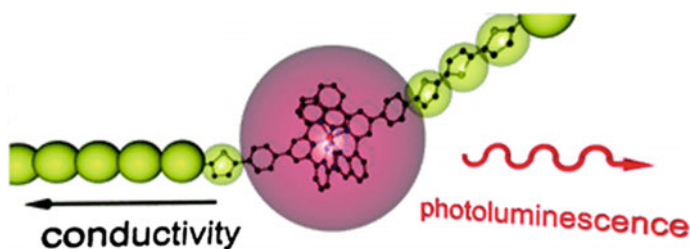
Electrochemical oxidation of $[RuL_3]^{2+}$ chelates (L is 8-aminoquinoline) proceeds by intermolecular coupling 8-aminoquinoline ligands with formation of electroactive polymers (Fig. 4.24) [141]. At the same time, $[Ru(bpy)_2L]^{2+}$ chelate containing only one 8-aminoquinoline ligand is absolutely not subjected to electrochemical polymerization.

In recent years, special attention has been paid to the electropolymerization of MCM salen-type [121, 142]. As a typical example, we note electropolymerization of Ni(salen)-MCM (Fig. 4.25) [143].

The Cu(salen) MCM was electropolymerized at Pt electrode in a 0.1 mol L^{-1} solution of tetrabutylammonium perchlorate in acetonitrile by cyclic voltammetry between 0 and 1.4 V versus SCE [144]. After cycling the modified electrode in a 0.50 mol L^{-1} KCl solutions the estimated surface concentration was found to be
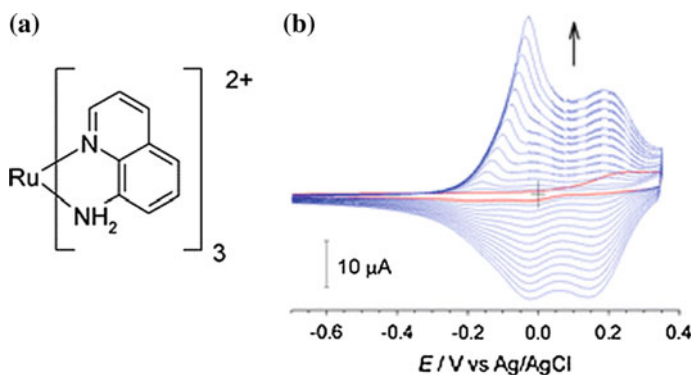
Fig. 4.24 Structure of $[RuL_3]^{2+}$ (**a**). Successive voltammetric scans for 1.0 mM $[RuL_3]^{2+}$ in pH 5.04 acetate buffer (**b**). Scans were recorded at 25 mV s^{-1} and each scan was paused at 0.350 V for 100 s
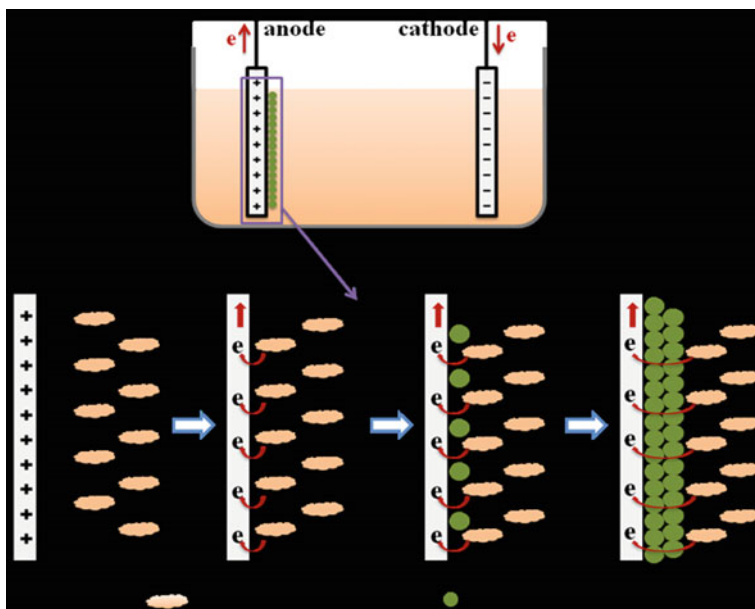
Fig. 4.25 Scheme of the electrochemical polymerization process of poly[Ni(salen)] films

equal to 2.2×10^{-9} mol cm^{-2}. The obtained results corroborate the hypothesis that the model for the structure of polymetal-salen on the electrode surface is the generation of stacked PMCs (charge transfer complexes) formed due to the donor-acceptor interaction between the ligand of one monomer fragment and the metal center of another (Fig. 4.26).
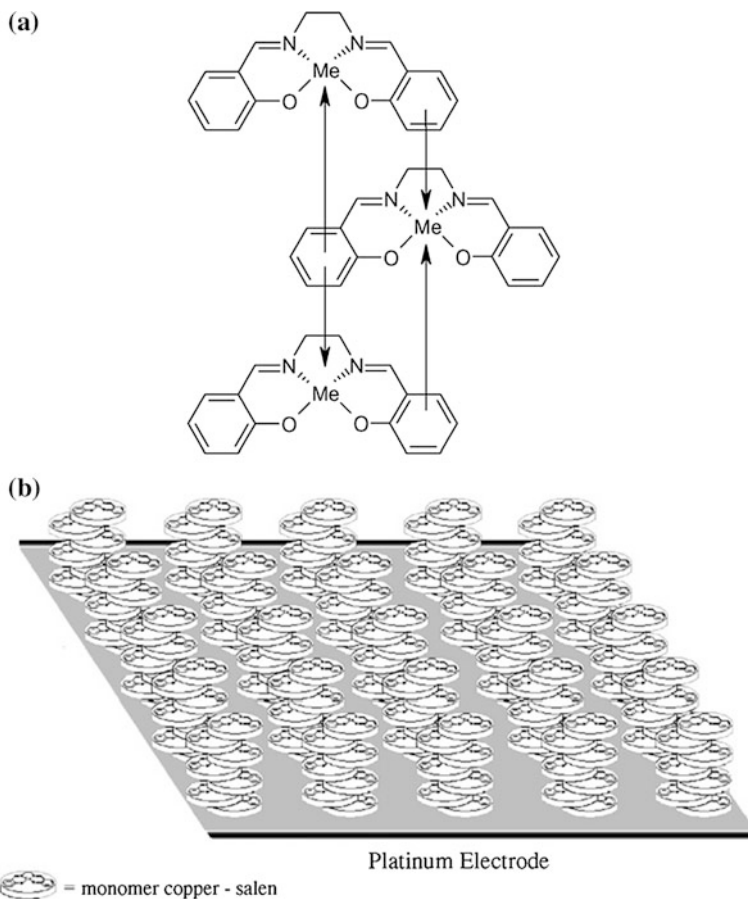
Fig. 4.26 Scheme of an electrode modified by nanostructured polymer: **a** stack polymer complexes; **b** polymer chain complexes

Thus, polymerization of Ni(II)-salen MCMs containing methoxy-substituents in phenyl rings and methyl substituents in bridge imino groups proceeds in two routes independently on ligand substituents. A positive charge in the first oxidized form is delocalized on phenyl fragments of the ligand. At the same time, the second oxidized form is stable only in coordinating solvents at high electrode polarizations, and, probably, has a charge localized on a metal atom stabilized by axial coordination of the solvent molecules. These data are corroborated by the results of calculations by the DFT for modeling chains consisting of one to four monomer units [145].

Nanobelt-like poly [Ni(salen)] electrodeposited by potentiometric method is proposed as a material for supercondensator electrodes for energy accumulation (Fig. 4.27) [146].
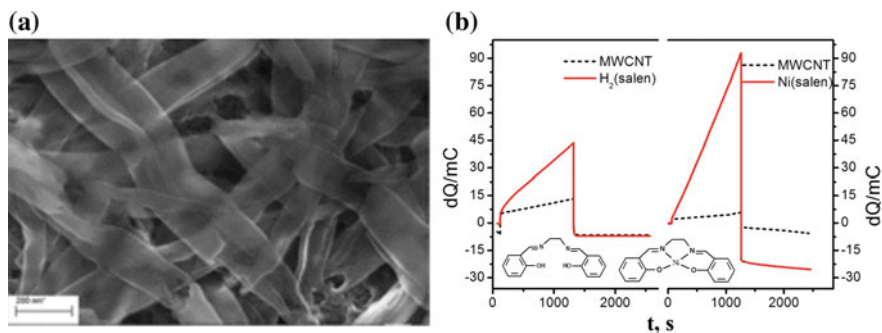
Fig. 4.27 a SEM image of poly [Ni(salen)] on MWCNTs electrode. **b** Charge variation during the constant-potential polymerization at 0.85 V for 20 min. (Left) H_2(salen); (right) Ni(salen)

It is interesting that anode electropolymerization of the same Ni(III)-MCM depends on the linear sweep rate of potentials. In particular, content of redox sites in poly [Ni(salen)] grown at the sweep rate 20 mV s^{-1} reaches maximum and then decreases with increasing the sweep rate, and the diffusion coefficient of charge at this sweep rate is the highest [147].

Conducting Cu(II)-PMCs with *o*-hydroxyaromatic azomethines based on salicylic and 3-methoxysalicylic aldehydes have photovoltaic activity depending on a layer thickness, redox-state of PMCs and incorporated in background solution electron-donor and electron-acceptor components [148, 149].

We also note electrochemically obtained a conducting PMC based on Cu(II)-MCM with *N,N'*-bis(salicylidene)-1,3-propylenediamine [150, 151].

Structuring of poly [M(salen)], where M = Ni or Pd, on molecular level, using purposeful selection of a composition of initial compounds and synthesis conditions (potential of film formation and origin of solvent and background electrolyte) allows, to great extent, accelerate the charge transfer process in PMC films and to improve stability of their electrochemical characteristics [152, 153].

A few works deal with electropolymerization of thiophene-containing MCM of the salen-type going through thiophene fragments [154].
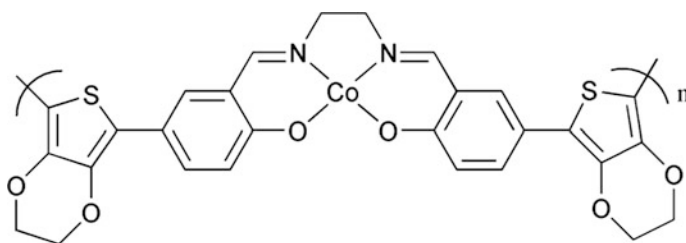
Thus, for example, in the case of salen-MCMs with thiophene substituents in diamine fragment electropolymerization goes through phenylene group or simultaneously, through phenylene and thiophene groups [155].
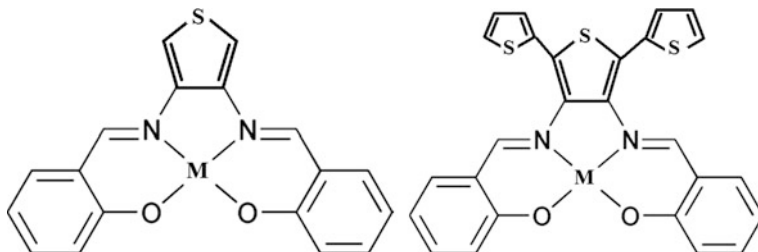
Of interest is using thieno[3,2-*b*]thiophene fragments in Ni(II)-salen MCMs, which makes it possible to obtain PMC films with high photostability (Fig. 4.28) [156], and also bithiophene fragments giving PMCs with uniform distribution of metal ions [157, 158].

Important observations are made during studying electropolymerization of Fe (III) MCM based on terthienyl-substituted Q-salen ligand [159]. Studies of temperature dependence of magnetic susceptibility showed that the polymer film is a spin-crossover, and resistivity measurements on ITO coated glass containing a polymer film shows intriguing profiles depending on temperature.

Special attention was given to studying electropolymerization of chiral salen-MCMs, in particular, for the production of polymer chiral catalysts [160–165]. For example, electropolymerization of thiophene-containing chiral Cr(III)-salen MCMs with the formation of respective salen-PMCs was carried out [160, 161]. The high
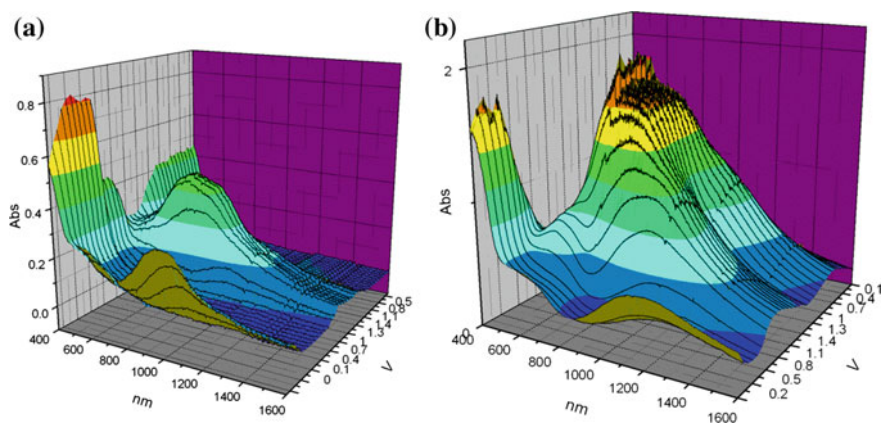
Fig. 4.28 Spectroelectrochemistry of polymer and PMC. The jaggedness at 800 nm on the PMC spectra is an artifact produced by the transition of the spectrometer lamps

stability of PMC films on the electrode surface and the effect of electropolymer-
ization conditions on their morphology are shown.

We shall also consider an example of electropolymerization of binuclear Ni(II)-
and Cu(II)-salen chelates with formation of rigid, conjugated shape-persistent PMC
[166].
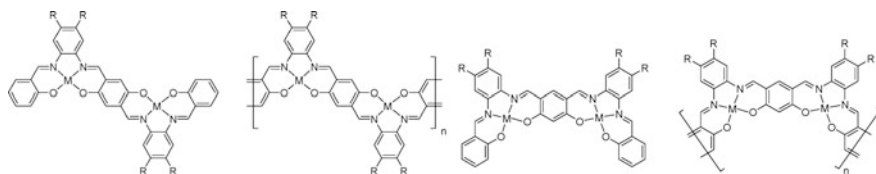
From the point of view of coordination chemistry, a considerable interest attracts
the possibility of chelation of several metal ions at once by salen-type polymers
containing apart from a salen-chelating center also other coordinating fragments. As
an example, we consider electroactive films obtained on Pt electrodes using poten-
tiodynamic polymerization of Cu-salen MCMs with the same 3-methoxy-
substituent in a salicylaldehyde fragment, but with different di-imine units [167].
The films had different i-E signatures during the polymerization process and the
following redox cycles (Fig. 4.29), although the imine bridge was theoretically
beyond the area of electroactivity (conjugated polymer spine). In this case a degree
of distortion of planarity of the salen fragment is the most considerable structural
effect from the character of participation of the imine bridge. The consequence is a
change in size of a pseudo-crown pocket formed by two O-donors separated by
Cu, two O-donors of methoxy groups, allowing thin films chelate Ba(II) ions. Thus,
the polymer containing pseudo-crown ether and Schiff base units is a redox sensor
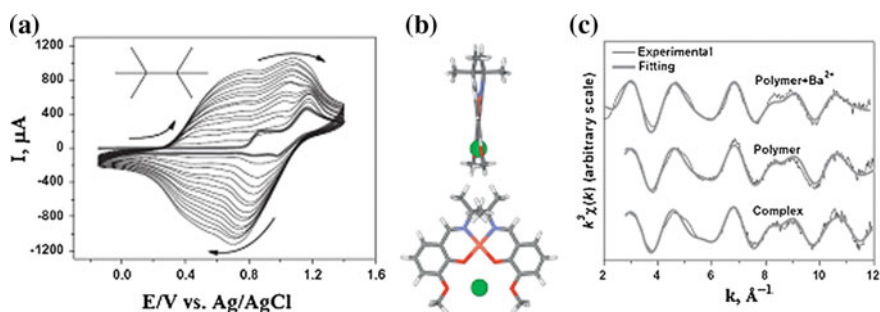
Fig. 4.29 a Voltammetry responses during potentiodynamic film deposition from 0.1 mol dm^{-3}
electrolyte solution containing MCM. Heavy line represents first cycle response; thereafter, for
presentational clarity, only responses for alternate cycles shown. Arrows indicate direction of
potential cycling. **b** Final optimized structures derived from DFT for Cu(salen):Ba(II) adducts.
c EXAFS functions (thin black trace: data; thick grey trace: fitting) for MCM (as powder), polymer
in air and polymer in air, after immersion in Ba(ClO$_4$)$_2$ solution

for Ba(II) ions (new polymeric metal-pseudomacrocyclic sensor for dual-ion cochelation).

Electropolymerization of MCMs allows to preparing different electrochromic materials of salen type, which are characterized by change in color under applied voltage [168]. For the electrogenerated polymers based on the salen type Cu(II)-, Ni (II)- and Pd(II)-MCMs, maximum efficiency of color for the coloration stage of 184 (Pd), 161 (Cu), 83 cm^2 C^{-1} (Ni) and the bleaching stage of 199 (Pd), 212 (Cu), 173 cm^2 C^{-1} (Ni) were determined, respectively. It is important that that reversibility and stability of polymer films based on salen-type MCMs depends on a metal character, and Pd is the most stable [168, 169].

It should be noted the preparation of conducting PMCs by electropolymerization of cell molecules synthesized by metal-template of [2 + 3] type cocondensation of π-extended boric acid and nioxime (1,2-cyclohexane-dione dioxime) [170]. The prepared polymeric materials exhibit metal-dependent electrochemical properties, as is seen from different redox windows observed for M = Co, Fe, Ru, although they have isostructural frameworks. Sequent electropolymerization using two different MCM allows to obtaining two-layered devices with different metals in each layer. It is interesting that the polymer can be used as heavy metal sensors, and redox-active metal sites participate in potential-dependent interlayer electron transfer, at that cyclic current-voltage characteristics differ distinctly for each layer or from statistic polymers. It is important that the proposed electrochemical method can be used as a simple diagnostic tool for the study of structural ordering of conducting layered polymeric materials (Fig. 4.30).

When studying mechanism of M-Pp electropolymerization, it is shown that π-cation-radical and π-dication-radical are formed at the initial stage of oxidizing of
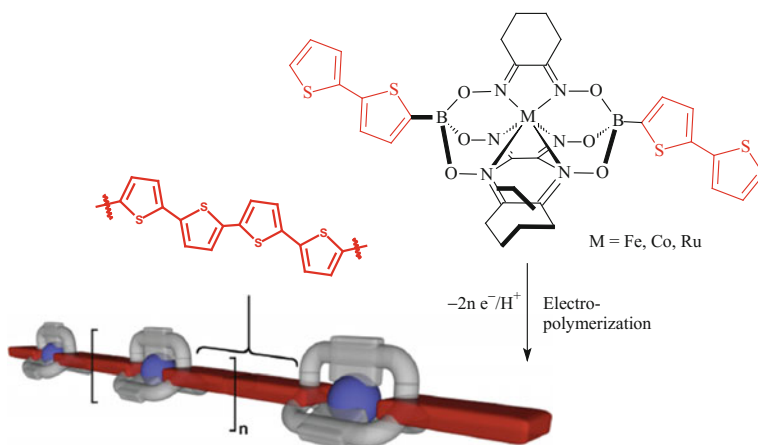
Fig. 4.30 Cage synthesis and electropolymerization

Mg-porphin synthesized by Lindsey method, and the main intermediate compound formed during electropolymerization is diprotonated di-isoporphin [171]. Poly (Zn-tetraphenyl-Pp), poly (Zn-tetradimethoxyphenyl-Pp), and poly (Pt-tetradim ethoxyphenyl-Pp) films are obtained using anode polymerization of appropriate MCMs on the surface of Pt electrodes [172]. The strongest effect on M-Pp electropolymerization have polymerization conditions and character of a metal, depending on which different models of film growth are possible, despite the fact that each of them has the same structure of Pp ring [173–176].

Electrically oxidative polymerization of a range of bi- and terthiophenes substituted by M-*meso*-tetraphenyl-Pp groups through individual oxaalkyl units brings to formation of M-Pp functionalized polythiophenes. Properties of the obtained polymer films point to imposing of electron properties of M-Pp and thiophene π-systems [177]. Electropolymerization of bromine-Fe(III)-*meso*-tetrakis(3-thienyl)-Pp brings to M-Pp PMC randomly linked at 2,5 positions of peripheral thienyl fragments [178]. The PMC has π-conjugated structure with moderate delocalization of π-electrons along thienyl-M-Pp units. M-Pp with 2-thienyl substituent was electrochemically copolymerized with 3-methylthiophene and 3-hexylthiophene [179].

M: Zn
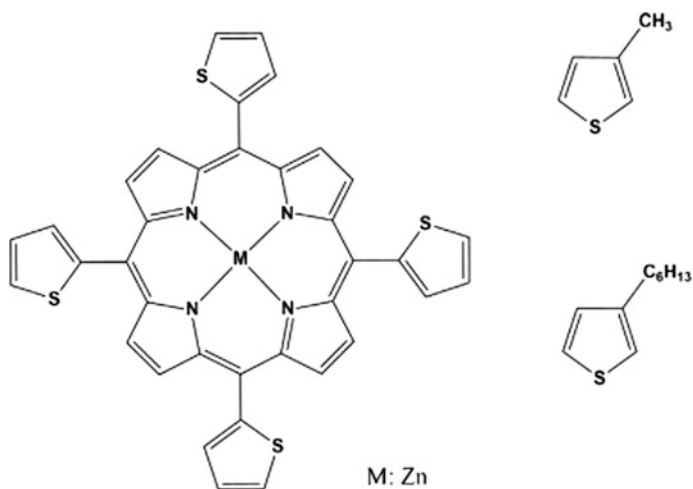
We should also notice *bis*-M-Pp copolymers synthesized using Zn-β-octaethyl-Pp and metal-free Pp functionalized by Py groups [180]. This process of electropolymerization is based on nucleophilic attack of Py-groups onto electrogenerated Zn-Pp dications and their *meso*-positions.
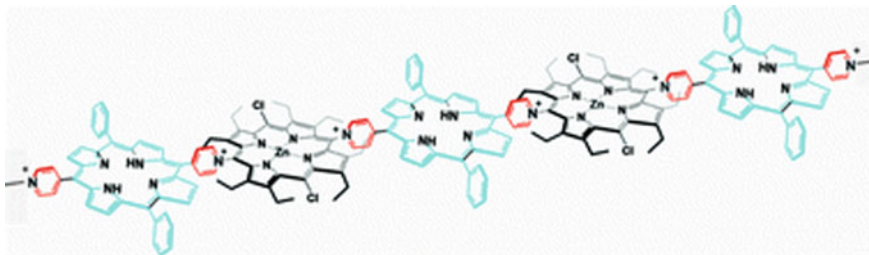
Polymers containing central metal-free Pp and peripheral Zn-Pp fragments were obtained in similar way, and electropolymerization allows to providing control over a number of macrocycles and architecture of polymers, whose properties are determined by Py spacers (Scheme 4.17) [181].

Electro-oxidation of Zn-octaethyl-Pp and Zn-5,15-dipyridinium-octaethyl-Pp in presence of polyoxometalate of Anderson-type $[MnMo_6O_{18}\{(OCH_2)_3CNHCO(4-C_5H_4N)\}_2]^{3-}$ allows to preparing such promising materials as hybrid polyoxometalate-M-Pp copolymers (Fig. 4.31) [182].

It should be noted the electropolymerization of M-Pc MCMs. For example, electropolymerization mechanism of peripherally-tetra-substituted Ni(II)-, Co(II)-, and Cu(II)-Pc with electropolymerized amino-, dimethylamino-, and diethylamino-groups is affected by applied potentials and a character of a metal site [183–186].
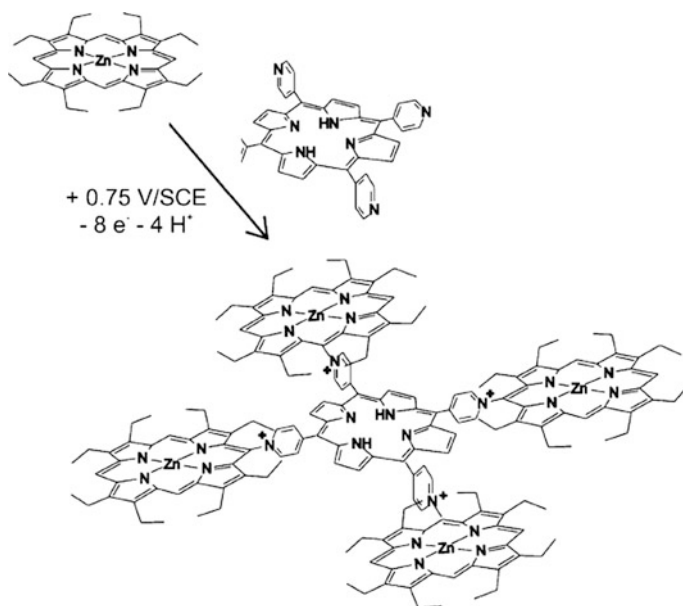
Scheme 4.17 Preparation of polymers with central metal-free Pp and peripheral Zn-Pp
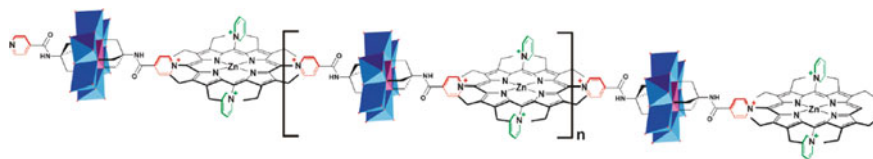
Fig. 4.31 Electropolymerization of the Zn-5,15-dipyridinium-octaethyl-Pp with the Anderson type polyoxometalate leading to the copolymer M-Pp-polyoxometalate

It is important that electrogenerated anion types of MCMs have considerable color differences, which are determinative factors for electrochromic application of polymeric materials (Fig. 4.32).

Polymer films obtained from M-Pc with (diphenylamino) phenyl substituents by deposition on ITO electrode also display reversible electrochromic switching between green, red-brown, and blue colors [187].

It is important that incorporation in the composition of M-Pc such redox-active and electropolymerized groups as tetrahydroquinoline [188], chromone, or coumarin [189] leads to significant increasing electropolymerization rate as compared with initial MCM.

Electrochemical polymerization of tetrakis-4-(2,5-di-2-thiophen-2-yl-pyrrol-1-yl) substituted Ni-Pc brings to a polymer film with electrochromic behavior: deep-olive green in neutral and dark-blue in oxidized states with the switching time 1.98 s. It should be noted that a gap band width of the prepared poly (Ni-Pc) was equal to 2.27 eV from the beginning of π-π^* transition of the conjugated polymer [190].

4.5 Grafted Polymerization

Among developed by now methods of grafted polymerization, considered in detail in Chap. 2, in chemistry of MCM radiation-stimulated «grafting from» method is the most often used. Technique of this polymerization includes preliminary growth of initiating particles on a polymer or another substrate, using for instance, γ-radiation of ^{60}Co source with the following polymerization of MCM. The main advantages of this method are almost entire absence of homopolymerization process, preservation of coordination and valence metal state, MCM fixation in thin surface layer, which is interesting for use of grafted metal chelate copolymers in catalytic reactions.

Among MCM of molecular type used for grafted polymerization, we note bpy- and phen-chelates of transition metals obtained by the reaction of chelating ligands with transition metal acrylates [191–193]:

$$M(CH_2 = CHCOO)_n \cdot mH_2O + L \rightarrow M(CH_2 = CHCOO)_n \cdot L \cdot pH_2O,$$
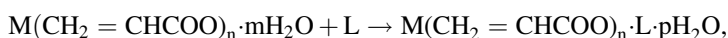
where M = Cu(II), Ni(II), Co(II), Cr(III); L is bpy or phen; n = 2, 3; m, p = 0–2.
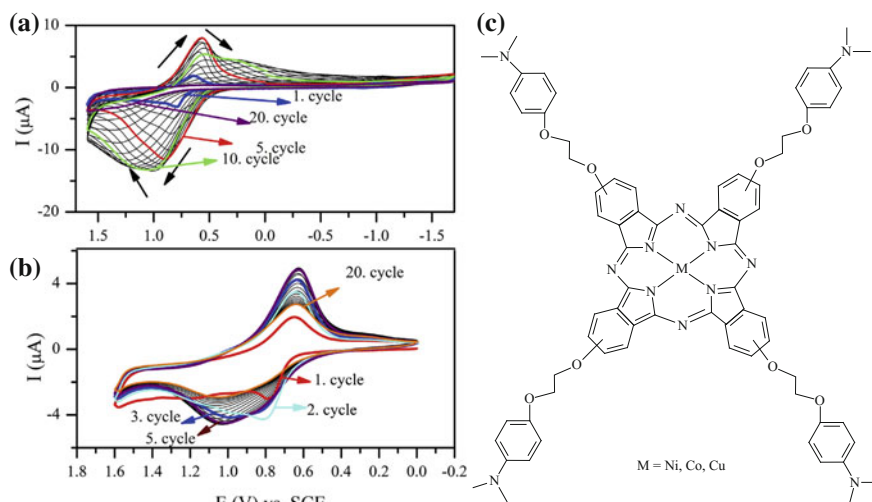
Fig. 4.32 **a** Repeated CVs of Cu-Pc recorded with in the whole potential windows of DCM/TBAP electrolyte system at 0.1 V s^{-1} scan rate on a Pt working electrode. **b** Repetitive CVs of CuPc recorded at anodic potential windows of DCM/TBAP electrolyte system at 0.1 V s^{-1} scan rate on a Pt working electrode. **c** Structure of peripherally-tetra-substituted Ni(II)-, Co(II)-, and Cu (II)-Pc with electropolymerized groups

Kinetic dependencies of grafting these MCM are similar to those, which are established for metal-containing monomers of other types [5, 194, 195], at that a special feature of grafting is almost entire absence of a homopolymer. Presence of C=C-bond absorption band at ∼1640 cm^{-1} in IR spectra of the grafted PMCs indicates some amount of non-polymerized vinyl groups. In other words, the grafted polymerization of MCM goes with participation of only part of vinyl groups present in initial MCM. Similarity of spectral and magnetic properties of MCMs and them based PMCs (Table 4.1) exhibits that in the grafting process geometric structure of a chelate node and valence state of a metal ion do not change. However, it should be noted a decrease in the value of the splitting parameter (Dq) and increase in Racah parameter of electron repulsion (B′) upon transition from MCM to PMCs. Taking into account that Dq ∼ l/d^6, one can assume that a decrease in the splitting parameter indicates an increase in the metal-ligand distance (d) in the abovementioned range. Besides, nephelauxetic β parameter increases in this range, which indicates a decrease in covalence degree of the metal-ligand bond.

Grafted polymerization of MCM of intracomplex type was studied for the example of MCMs based on methacryloyl acetophenone and N-(2-pyridyl) acry-lamide [196–202]. For all studied MCMs the same character of kinetic depen-dencies of the grafting is observed (Fig. 4.33): during first 0.5 h the rate is maximum about 1–15 × 10^{-5} mol MCM/g polymer h; then grafting rate decreases fast and, in most cases the process is completed in 2–3 h. This cannot be associated

with decomposition of initiating hydro-peroxide fragments, whose lifetime is 4.5 h, and can be explained by decrease in adsorption of MCM during transition from initial polymer-substrate to the same polymer covered with a layer of grafted metal chelate polymer. Besides, the grafting is considerably influenced by a nature of transition metals, and according to MCM activity, metals can be arranges as follows: Co(II) > Pd(II) > Mn(II) > Fe(III) $\sim$ Ni (II) > Cu(II) > Cr(III).

It is important that for Co(II)-, Ni(II)-, Mn(II)-, and Cr(III)-MCMs bimolecular character of termination of growing polymer chains is typical, and for Cu(II)- and Fe(III)-MCMs it is monomolecular, which is stipulated by strong oxidation ability of these ions and higher value of constant of intermolecular termination of the polymer chain of these MCM as compared with the constant of bimolecular termination.

It should be also noted amphiphilic copolymer prepared by grafted polymerization of macromonomer of PEG-methacrylate of methyl ether with 2,2,3,4,4, 4-hexafluorobutyl methacrylate and Eu(AA)(benzoic acid)$_2$phen MCM [203]. The obtained PMC can self-assemble in spherical micelles, and size and distribution of the micelles increase with increase in the PMC concentration.

4.6 Polycondensation

An efficient method of production of various polymeric metal chelate structures is polycondensation, for example, using different methods of metal-organic polycondensation [204]. This method, in particular, was applied to produce Ru and Cu chelates of molecular type with such π-conjugated chelating ligands as poly(bpy-5,5'-diyl) and poly(phen-3,8-diyl) [205]. Aromatic diimides react with dibromo-tpy Ru(II) chelates with formation of polymers with molecular weight up to 37,000. The obtained PMC are active in acetophenone hydrosilylation reaction and can be

Table 4.1 Data of IR-, electronic spectroscopy and magnetochemistry of MCM molecular type and their grafted polymers

Chelate	M	L	IR spectrum (basic frequencies), cm^{-1}			Dq, cm^{-1}	B', cm^{-1}	β	μ_{ef}, BM
			ν(C=C)	ν(heterocycle)	ν(COO$^-$)				
Monomer	Ni	bpy	1635	1605	1565	1134	773	0.743	3.16
Polymer	Ni	bpy	1639	1606	1560	1028	837	0.804	2.96
Monomer	Co	bpy	1637	1610	1560	1152	834	0.859	4.53
Polymer	Co	bpy	1638	1608	1560	1018	883	0.909	4.75
Monomer	Ni	phen	1637	1600	1565	1166	830	0.797	3.17
Polymer	Ni	phen	1640	1600	1560	990	857	0.823	2.95
Monomer	Co	phen	1635	1605	1565	1163	849	0.874	4.75
Polymer	Co	phen	1639	1608	1565	1016	884	0.911	4.87

Fig. 4.33 Kinetic dependencies of yield of grafted PMC based on MCM with methacryloyl acetophenone: Co(II) (1), Ni (II) (2), Pd(II) (3), Mn(II) (4), Cu(II) (5), Fe(III) (6) and Cr (III) (7) (ethyl acetate, $c_{MCM} = 0.04$ mol L^{-1}, 70 °C, D = 200 kJ kg^{-1})
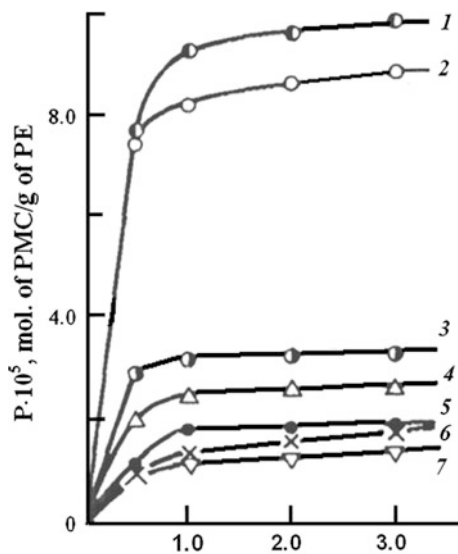
used several times repeatedly without substantial loss of activity (Scheme 4.18) [206].

Pd-catalyzed Stille cross-coupling reaction is used for synthesis of Ru(II) chelate π-conjugated polymers consisting of alternating units of regioregular quarter (3-octylthiophene) and bpy (Scheme 4.19) [207]. It should be noted that chelation of metal-free conjugated polymer by $Ru(bpy)_2Cl_2$ in boiling ethanol gives unsatisfactory results, while preliminary optimization of the cross-coupling reaction conditions between quarter(3-octylthiophene) and dibromo-substituted Ru(II) chelate makes it possible to synthesize macromolecular, structurally uniform and defect-free copolymers.

The Heck coupling reaction was used to obtain polyfunctional polymers containing Ru-bpy chelates and oxadiazole incorporated both in 5,5′-, and in 4,4′-positions of Ru-chelates (Scheme 4.20) [208]. Content of Ru chelates in a polymer
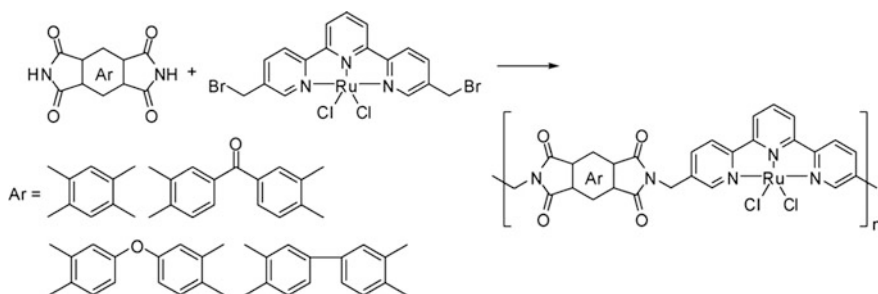
Scheme 4.18 Reaction of aromatic diimides with dibromo-tpy Ru(II) chelates
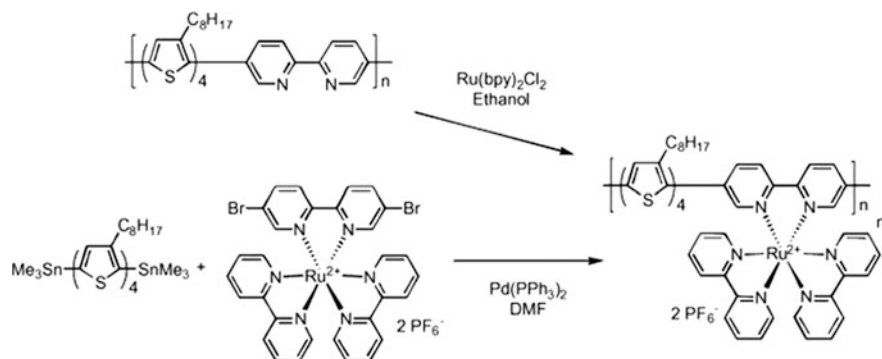
Scheme 4.19 Synthesis of π-conjugated Ru(II)-PMCs

can be easily controlled by initial ratio of monomers during the polycondensation reaction, and charge carrier mobility of polymers depends strongly on content of metal-chelate units.

High luminescent PMCs were obtained by the condensation of primary alkylamines contained in poly(St-*p*-aminomethyl-St) polymer chain and carboxyl groups of $[Ru(bpy)_2(L)](ClO_4)_2$, where L is 2-(4-carboxyphenyl)imidazo[4,5-e]-phen. Luminescent properties are very sensitive to occupation of metal sites on the polymer backbone, assuming weak electron interactions between neighboring centers and the polymer backbone. PMCs form continuous films at drop-cast on ITO electrode, and retain their strong luminescence. This effectiveness and intense luminescence make them potentially promising for applications in probing and imaging [209].

Of interest are heteroleptic $[Ru(L)(L')Cl_2]$ chelates (L and L′ = bidentate N^N ligands), which are polymerized by Stille cross-coupling with the following substitution of chloride ligands by thiocyanate [210]. Photosensitizing and tuning of the optical band gap properties of Ru(II)-PMCs showed their prospects for development of new class of optoelectronic materials.

Square-planar bis-(σ-acetylide) Pt(II)-PMCs with phen ligands of polycondensation type were used as colorimetric/luminescent sensors for detecting the vapor of benzene compounds (Fig. 4.34) [211].

A possibility of direct synthesis of microporous conjugated PMC is shown using Ir chelates. In particular, various metal chelate units were included in PMC frameworks with controlled content of metal, from 12.19 to 15.34 wt%, with the surface area from 652 to 859 $m^2\ g^{-1}$ and high porosity [212].
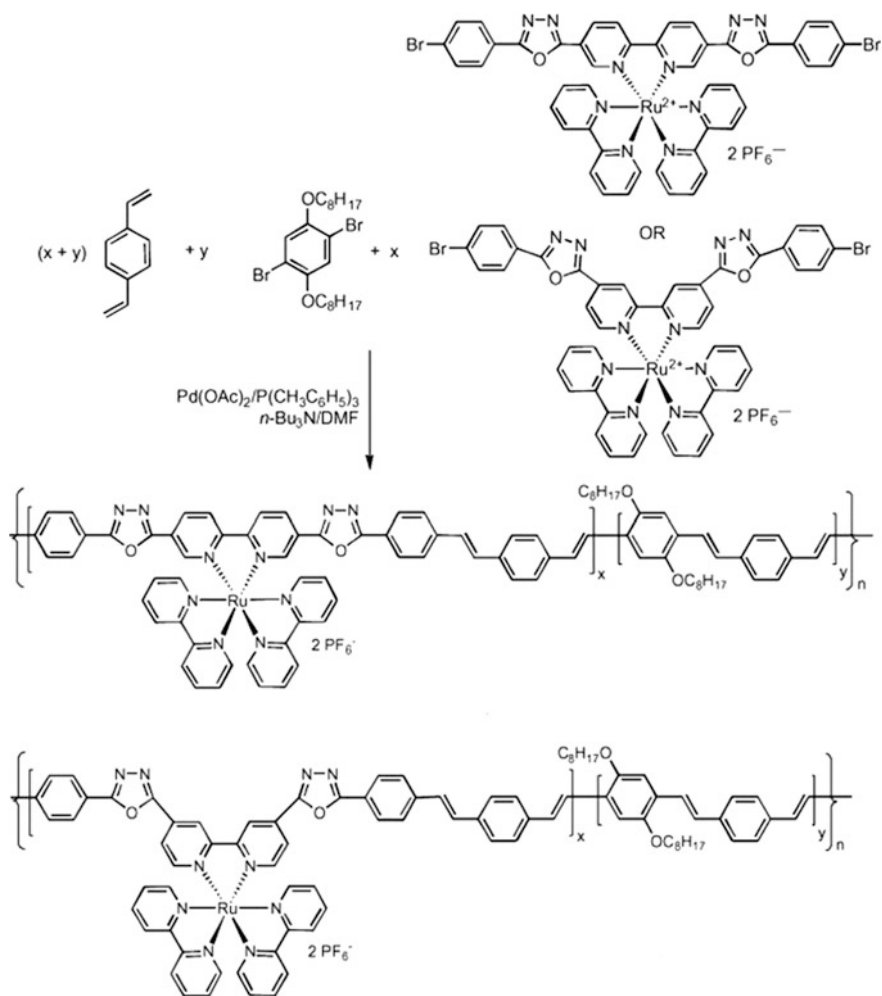
Scheme 4.20 Preparation of polyfunctional polymers containing Ru-bpy chelates and oxadiazole

Polycondensation is one of the most common methods of obtaining iridium-containing phosphorescent polymers for light-emitting diodes [213]. Thus, interesting copolymers functionalized by Ir-chelate in the side chain are obtained by Suzuki coupling [214, 215]. Color of these white-light emitting PMCs is regulated by concentrations of the emitting fragments.

Fig. 4.34 Polymeric square-planar bis-(σ-acetylide) Pt(II) chelates with phen ligands as colorimetric/luminescent sensors for detecting the vapor of benzene compounds
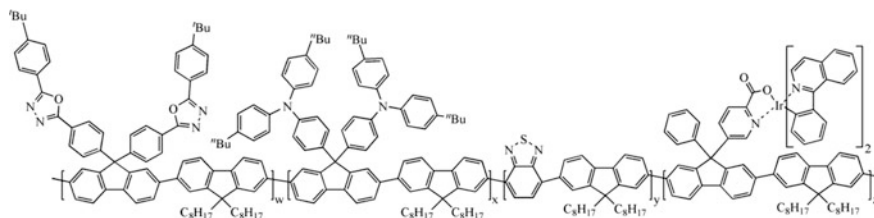
Of interest is using Pd-catalyzed Suzuki coupling in the synthesis of one-chained white light-emitting polyfluorene copolymers containing Ir complex with β-diketonate block, bis(2-benzothiazol-2-yl-N-ethyl-Cz)Ir-1,3-bis(p-bromophenyl)-1,3-propanedione as a fragment of red emission [216]. These PMCs are thermally stable, well soluble in ordinary organic solvents and exhibit two strong emission bands in both the blue and red spectral regions.
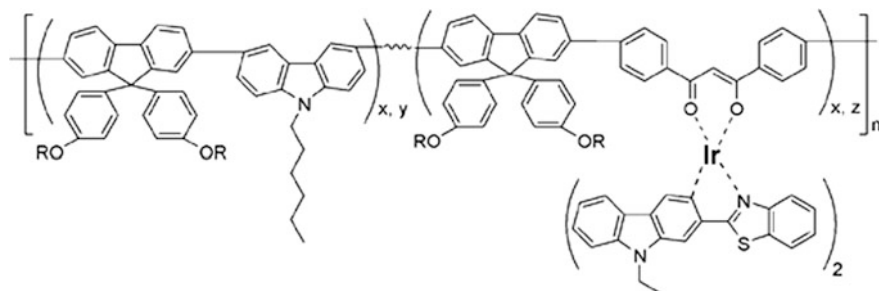
It should be noted that a range of polycondensated Pt-containing PMCs is applied in photovoltaic devices [217]. In particular, using Still and Suzuki reactions, cyclometalated Pt chelates are obtained, which show optical band gaps from 2.1 to

1.65 eV, depending on choice of a comonomer [218]. Ability of materials to sensitize singlet oxygen formation changes with excitation wavelength and during transition from solution to solid state.

Of interest are metal chelate alternating conjugated polymers consisting of indacenodithiophene and cyclometalated Pt(II) units [219]. One of devices including mixtures of these PMC and [6,6]-phenyl-C_{71}-oleic acid methyl ester in different mass ratios showed efficiency of energy transformation 2.9% with short circuit current 7.7 mA cm^{-2}, voltage of the open circuit 0.78 V.
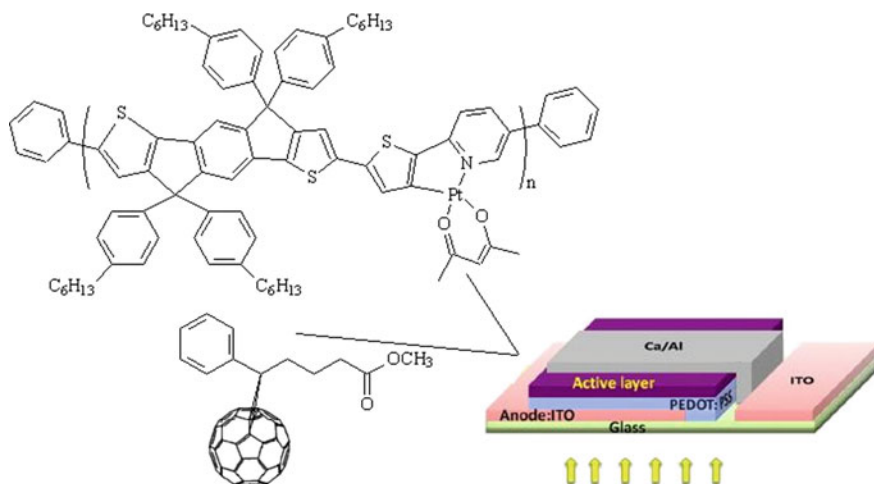
We shall notice Co(III)- and Fe(III)-PMCs with aromatic azoligands synthesized by polycondensation of diamino-substituted metal chelates with aromatic dialdehydes (Scheme 4.21). These PMCs are electrochemically active and exhibit reversible electrochromism [220].
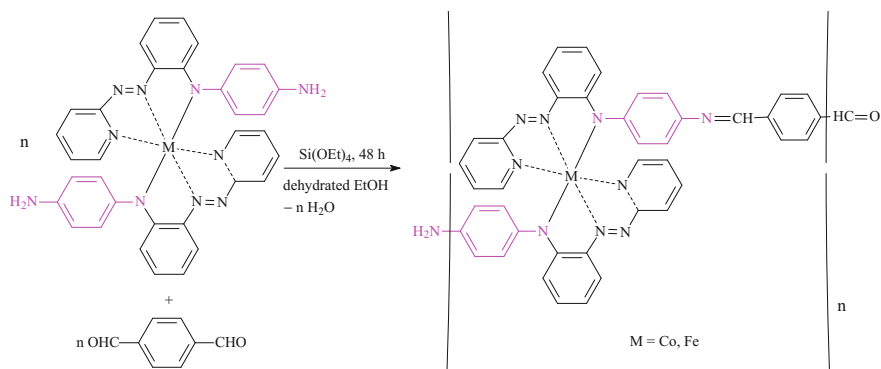
Scheme 4.21 Polycondensation of diamino-substituted metal chelates with aromatic dialdehydes
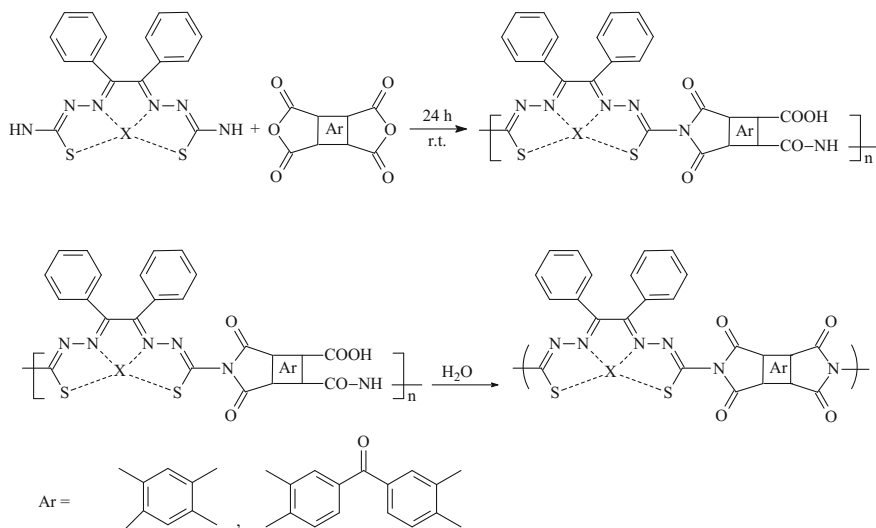
Scheme 4.22 Polycondensation of diamine MCM with aromatic dianhydrides

Polycondensation in solution of Ni and Cu chelates based on benzyl-bis-thio-semicarbazone with aromatic dianhydrides brings to soluble metal chelate azome-thine polyimide with inherent viscosity 0.98–1.33 dL g^{-1} (Scheme 4.22) [221].

Suzuki polycondensation was used for the preparation of red-light emitting polyfluorenes with bis(2,4-diphenylquinoline-N,C$^{2'}$)Ir(acac) grafted Ir-quinoline chelates in the side chain. Correlation between efficiency of luminescence and configuration of grafted polyfluorenes exhibits that polyfluorenes with covalently linked Ir-quinoline chelates are electroluminescent and emit red light effi-ciently: «simple polymeric chain, unexpected high efficiency» [222].

PMC containing HQ metal chelate conjugated with alkyl fluorene or alkoxy-benzene via C=N bond are obtained by Heck coupling reaction [223].

Of substantial interest is polycondensation of salen and salphen-type metal chelates. Thus, salen-containing polymers are synthesized from diglycidyl ether of bisphenol A and hydroxyl-functionalized azomethine chelates (Scheme 4.23) [224]. The following curing of polymers brings to linked epoxy resins.

Catalytic Pd polycondensation of H–≡–Ar–≡–H (Ar = fluorene or 2,5-dialko xy-p-phenylene) with dibromo-derivative Ni-salphen was used for the preparation of the π-conjugated poly (aryleneethynylene) including Ni-salphen chelate with high yield [225]. UV-visible spectra of the polymers are characterized by π-π* peaks of transition at about 420 nm, which correlates with poly (p-phenyle-neethynylene). The UV spectrum of Ni-PMC, apart from π-π* peak of a polymer ligand transition, also exhibits satellite intermediate and small peaks at about 480 and 600 nm, which are associated with MLCT and d-d transition, respectively.
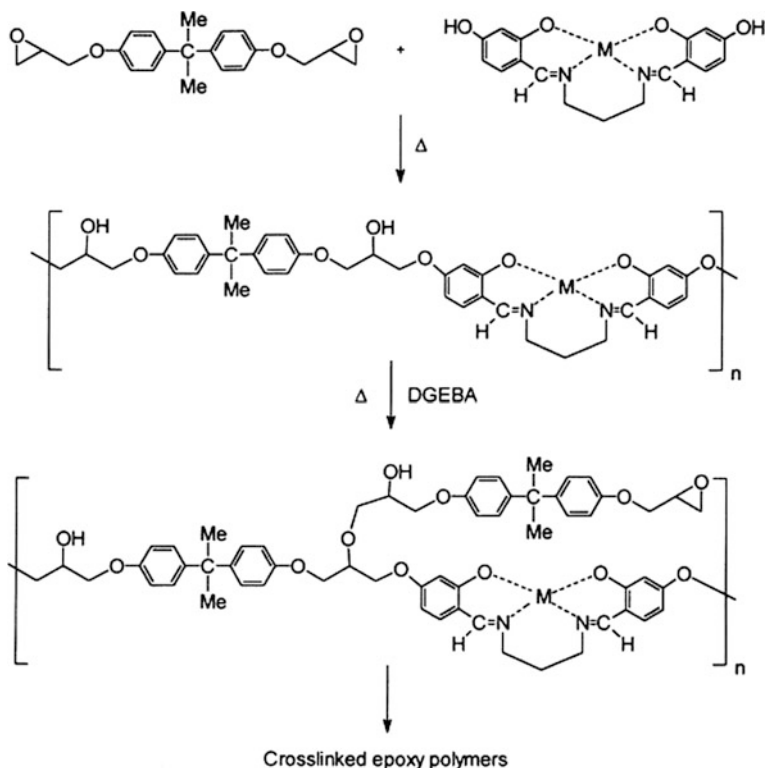
Scheme 4.23 Polycondensation of hydroxyl-functionalized azomethine chelates with diglycidyl ether of bisphenol A (DGEBA)

Polycondensation of Zn[bis(4-hydroxy)salicylidene-1,2-diaminoethane] and 4,4′-diphenylmethane diisocyanate was used to obtain PMC containing fragments of Zn-salen chelate and polyurethane [226]. In the similar reaction of salen-monomer, diisocyanate, poly(oxytetramethylene)glycol and 1,4-dihydroxybutane metal chelate polyurethanes form, which occur soluble and have molecular weights in the range from about 12,000 to 44,000 [227]. It is important that thermal and mechanical properties of polyurethanes improve markedly by the introduction of MCM based on tetradentate Schiff base into the polymer chain. Besides, the viscosity of the metal-containing polyurethane decreased abruptly upon increasing the metal content.

Complex [bis(pyridine)salen]Zn(II) interacts with biphenyl-4,4′-dicarboxylic acid in presence of $Zn(NO_3)_2.6H_2O$, leading to crystalline skeleton materials form, which are applied in enantioselective separations [228]. Statistic copolymers (M_n = 24,000–170,000) containing Pt-salen chelate are synthesized [229] by Yamamoto-type Ni(0)-mediated aryl-aryl-coupling using microwave irradiation (Table 4.2). Molar content of incorporated Pt-units is varied in the range 2.1–8%.
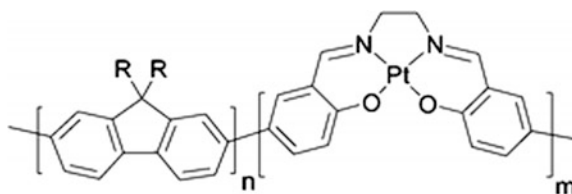
Condensation of epichlorohydrin with azomethine metal chelates in 2:1 and 1.25:1 molar ratios, respectively, in alkali medium was used for the preparation of epoxy resins containing azomethine metal chelates (Scheme 4.24) [230–232].

Metal chelate polyurea is obtained in a similar way by the polycondensation of diamine Schiff base chelates and toluene 2,4-diisocyanate (Scheme 4.25) [233].

Another type of metal chelates containing epoxypolymers is synthesized by condensation of epichlorohydrin with bis-phenol metal chelates based on 3-formyl-4,4′-dihydroxy-diphenylmethane and diamines (en or o-phenylenediamine) [231].

We shall notice polysiloxane-azomethine copolymers, which are formed during polycondensation of sodium salts of salen-diol Cu and Ni chelates with chloromethyl-substituted poly (dimethylsiloxane) [234].

Template method was used to obtain chiral conjugated hyperbranched azomethine polymer through one-pot condensation of aromatic trialdehyde and diamine in presence of Mn(OAc)$_2$ (Scheme 4.26) [235].

Another example of the template approach is design of crystalline Zn-salphen microporous frameworks with Urchin-like morphology (Fig. 4.35) [236].

It seems interesting to use interphase polycondensation to synthesize azomethine polymer including crown ether as well as Co-salphen complex (Scheme 4.27) [237].

This is an example of combination in one polymer both hard and soft acceptors of metal cations [238], which is very interesting as regards studying competitive coordination in polymer systems [239].

A range of soluble conjugative poly (salphenyleneethynylene) metal chelate polymers containing Zn-, Ni-, and Cu-salphen chelates is obtained [240]. It is established that Zn-chelate metal polymer displays strong aggregation behavior in solution and in solid state (unique supramolecular cross-linking), and dissociation

Table 4.2 Reaction conditions and polymer analysis for the copolymerization of 2,7-dibromo-9,9-dialkylfluorene and Pt-salen monomer

Sample	Solvent	Time (min)	M_w[a]	M_n[a]	PDI
R = ethylhexyl	THF	12	357,400	169,500	2.11
R = octyl	DMF-toluene	12	65,400	24,300	2.70

[a]After Soxhlet extraction with ethyl acetate
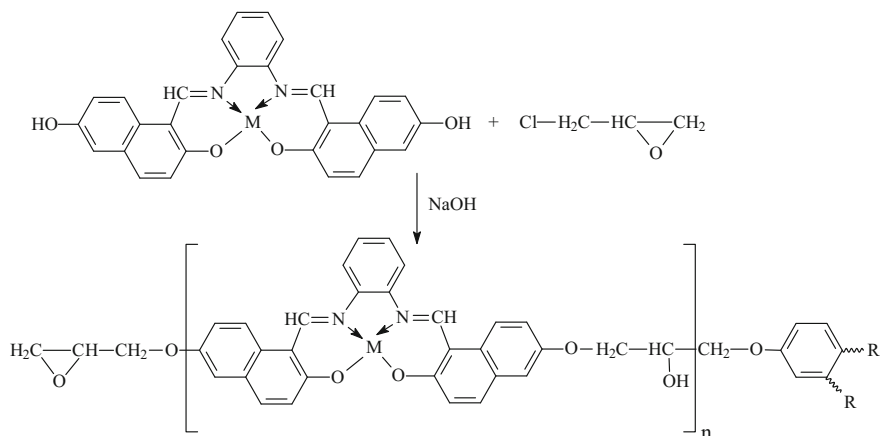
Scheme 4.24 Condensation of epichlorohydrin with azomethine metal chelates

M = Mn(II), Co(II), Ni(II), Cu(II), and Zn(II)
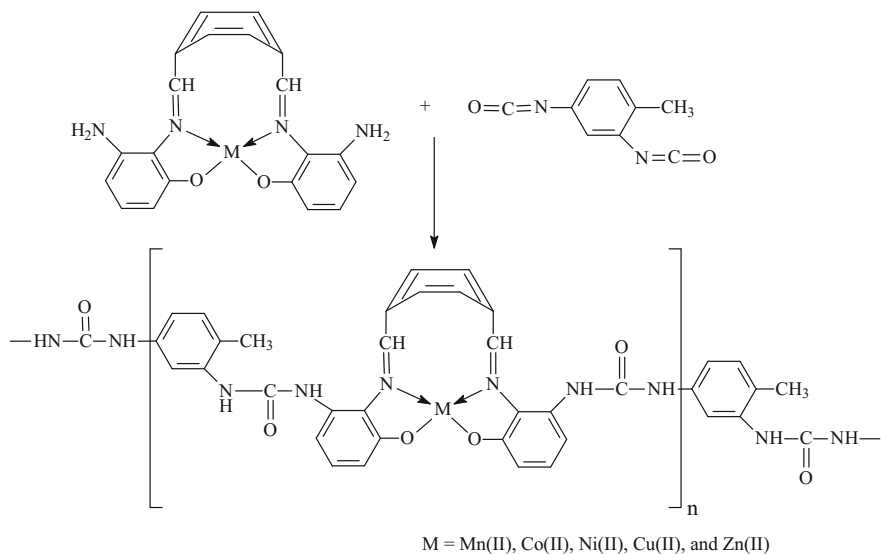
Scheme 4.25 Polycondensation of diamine Schiff base chelates and toluene 2,4-diisocyanate

of aggregates takes place only through ligation of such base as Py. It is important to notice that ligation is associated with considerable change in luminescence of PMC, which points to its potential application as a sensor for Lewis bases.
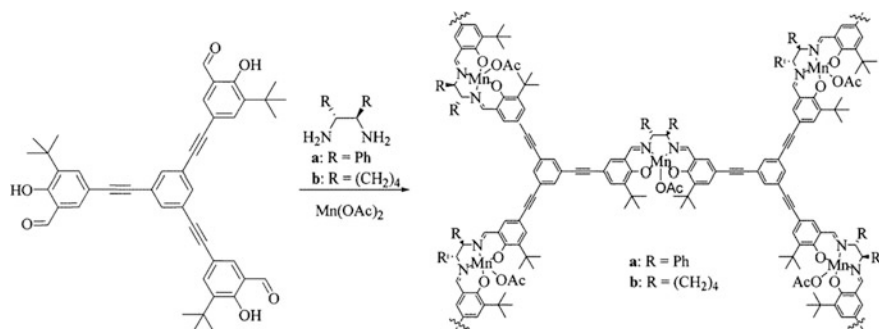
Scheme 4.26 Preparation of chiral conjugated hyperbranched azomethine polymer
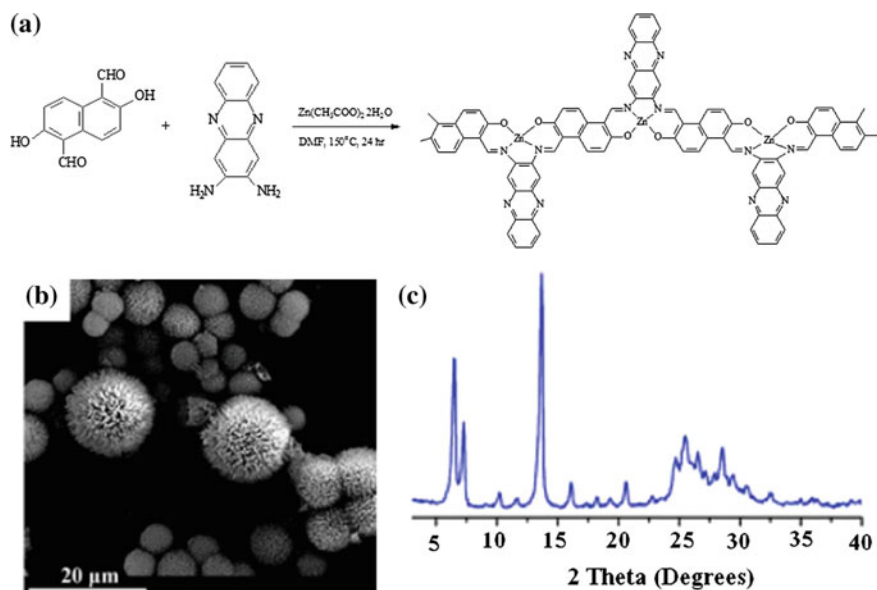
Fig. 4.35 a Synthesis of Zn-salphen microporous polymer frameworks. **b** SEM images of Zn-salphen microporous polymer frameworks Urchin-like microspheres. **c** XRD pattern of Zn-salphen microporous polymer frameworks
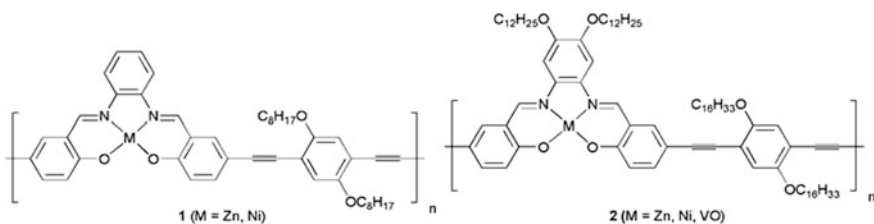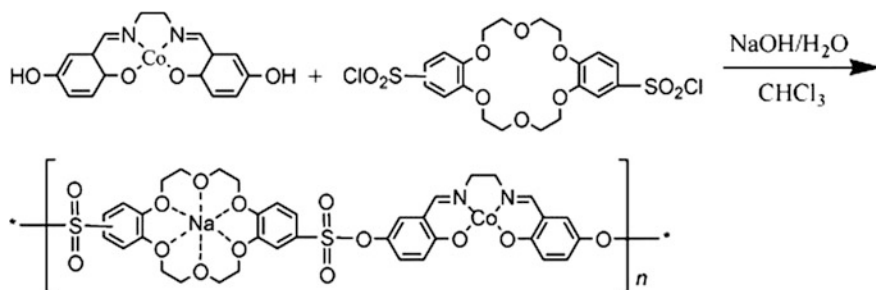
Scheme 4.27 Synthesis of azomethine polymer including crown ether as well as Co-salphen complex

Soluble macromolecular helical poly (phenyleneethynylenes) containing salphen-chelates, which can be used as chemical sensors, nano-lattices, and other supramolecular structures, were obtained by polycondensation of di-iodine substituted salphen-chelate monomers using Sonogashira coupling reaction (Scheme 4.28) [241].

It should be noted Ni-bis(bromobenzyl)salphen used in synthesis of metal chelate poly-*p*-phenylene-vinylene by Gilch polymerization (Scheme 4.29) [242]. Reaction with KO^tBu leads to gels and soluble conjugate oligomers, which are red-shifted in the absorption spectrum as compared to a monomer. This spectral change is closely connected to the extended conjugated length and exhibits that Gilch polymerization is a useful route for completely conjugate metal-containing polymers, if solubility of a product is achieved.

It was expected [243] that these PMC would be highly luminescent, however, it occurred that only in the case of Zn(II) with long solubilizing substituents, weakly luminescent polymers can be obtained [241]. Helical poly (phenyleneethynylenes) with *p*-ethynyl-groups have higher solubility and better conjugate capacity with respect to imine.
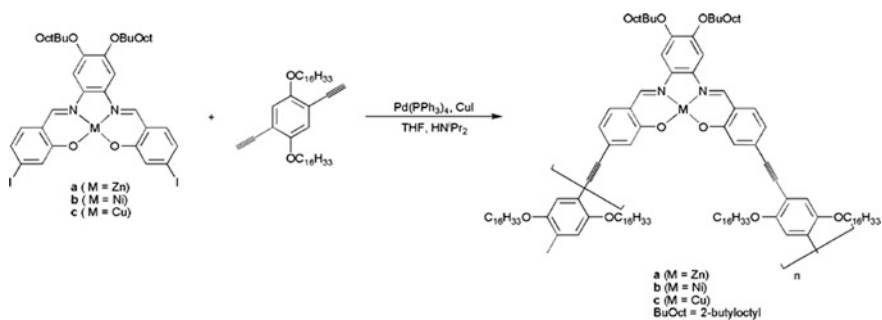
Scheme 4.28 Preparation of soluble polymeric helical poly (phenyleneethynylenes) containing salphen-chelates
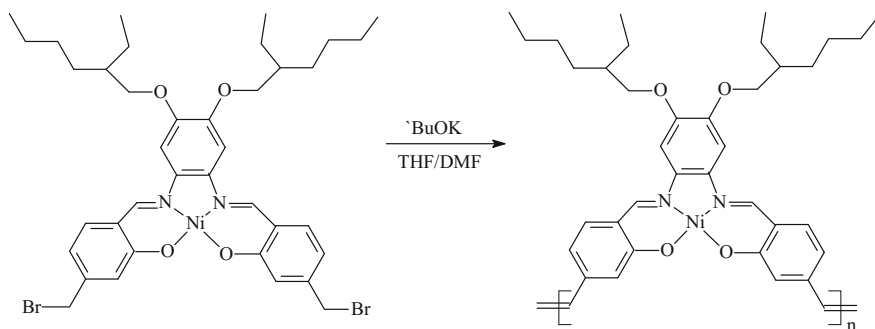
Scheme 4.29 Synthesis of metal chelate poly-*p*-phenylene-vinylene by Gilch polymerization

We note also phosphorescent conjugate PMCs (linear-rod and coilable sensor materials) consisting of alternating *p*-phenylethylene and *p*- or *m*-type Pt(II)-salphen phosphor units. In the prepared PMCS side arms carrying different *p*-alkoxy-substituents advance contrast emission properties stipulated by polymer conformation, a degree of π-stacking and differences in chemical structure [244].
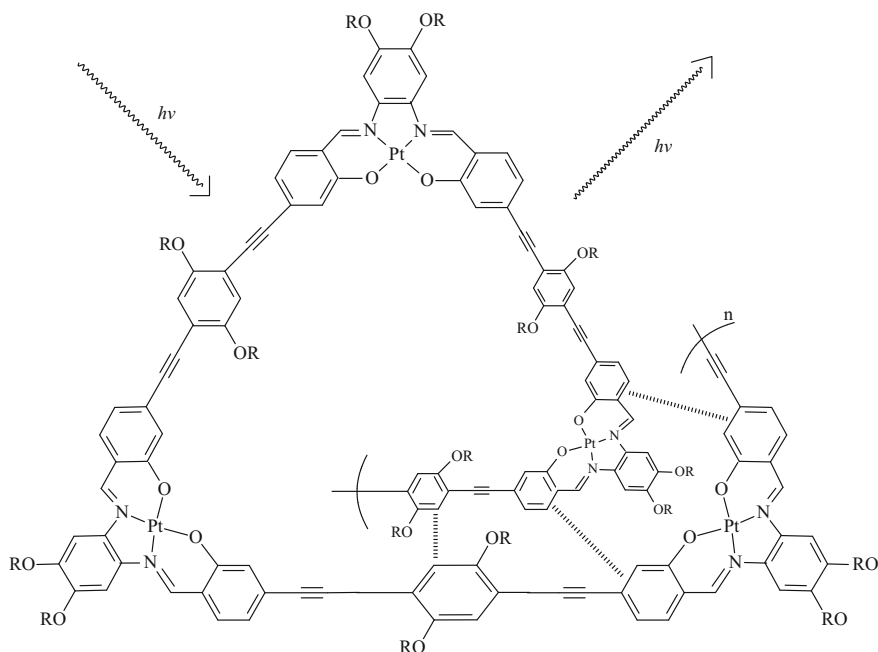
Pt(II)-salphen chelates are universal phosphorescent cores (signal component) in conjugate oligo(phenyleneethynylenes) [245], which can be used for sensor applications.
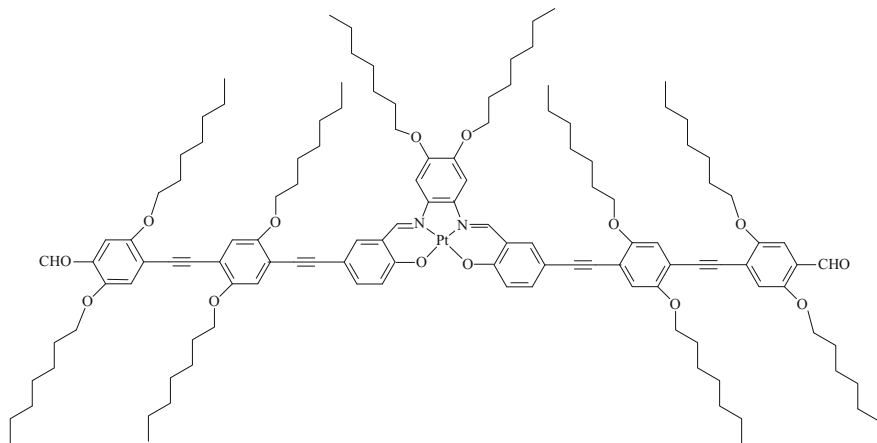
Based on azomethine metal chelates, completely conjugated ladder polymers are designed via condensation of derivatives from 1,4-dihydroxy-2,5-diformylbenzene and *o*-phenylenediamine [241].

Of interest is synthesis of organic microporous frameworks with incorporated metal sites in a skeleton by Sonogashira–Hagihara reaction with 1,3,5-triethynylb enzene and diverse metallosalen structural blocks [246]. These PMCs are insoluble in ordinary solvents and had high thermal and chemical stability. According to nitrogen physical absorption, the largest BET specific surface up to 1200 m^2 g^{-1} was obtained for three polymer frameworks with pores volume of 0.94 cm^3 g^{-1}. PMCs show high absorption potentials for carbon dioxide (up to 8.2 wt%) and good selectivity at 273 K and pressure 1 bar, which, to great extent, are determined by porosity of frameworks, nature of active heteroatoms, and coordination-unsaturated metal sites in the frameworks.

Chiral polymers based on BINOL Co(III)-salen salt complexes, which have been applied to direct synthesis of chiral propylene carbonate from racemic propylene oxide should also be noticed. Polymer (R/S)- and (S/R)-catalysts not only showed better enantioselectivity than (R/R)- and (S/S)-catalysts, but they were extracted and used repeatedly for more than ten times without loss of activity and enantioselectivity [247].
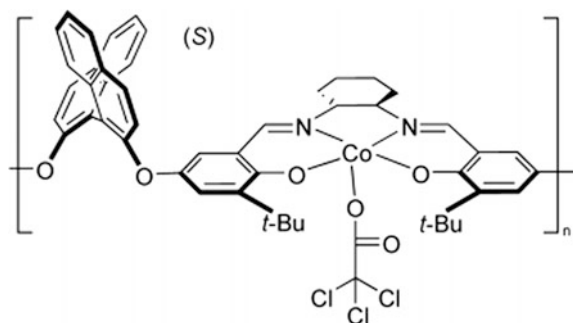
Copolymerization of alkyne-bearing Ni(II) complex based on Goedken macrocycle (4,11-dihydro-5,7,12,14-tetramethyldibenzo[b,i] [1, 4, 8, 11] tetraazacyclotetradecine) and brominated 9,9-dihexylfluorene gives polymers with potential application as functional redox-active materials. They exhibit exclusive thermal stability and interesting adsorption properties due to presence of Ni(II) macrocyclic complex and π-conjugated blocks incorporated in their polymer backbone (Fig. 4.36) [248].

Among PMC with M-Pp units, we shall mention π-conjugated Zn-Pp polymers with arylene and arylene-ethylene groups between Zn-Pp units obtained by metalorganic polycondensation [249]. Polymers with long alkyl substituents in arylene spacer fragments are soluble with the parameters η, M_n and M_w, which are 0.21–0.35 dL g^{-1}, 4.6–37.1 × 10^3 and 6.3–49.1 × 10^3, respectively.

It should be noted the preparation of molecular worms based on PMC: M-Pp polymers and oligomers are deposited on Au(111) surface using electrospray deposition, and accept such an arrangement, in which chains from neighboring molecules are interdigitated. Although flexible character of polymers brings to sharp kinks and the crossing of polymer strands (Fig. 4.37) a longer correlation length as compared to solvated oligomers was observed [250].
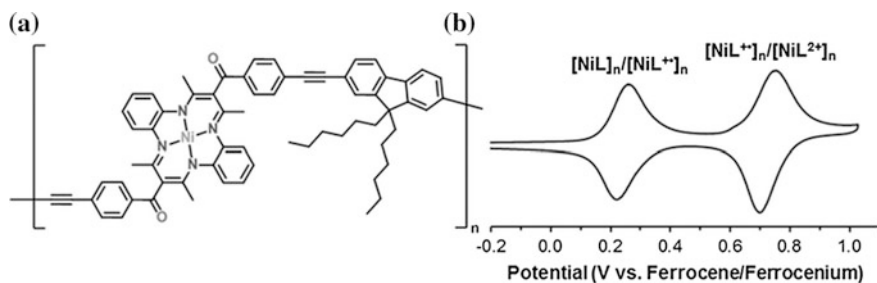
Fig. 4.36 **a** Structure of nickel-containing polymer. **b** Cyclic voltammograms acquired at a scan rate of 250 mV s^{-1} in a CH$_2$Cl$_2$ solution containing 1 × 10^{-3} M analyte and 0.1 M tetrabutylammonium hexafluorophosphate as supporting electrolyte
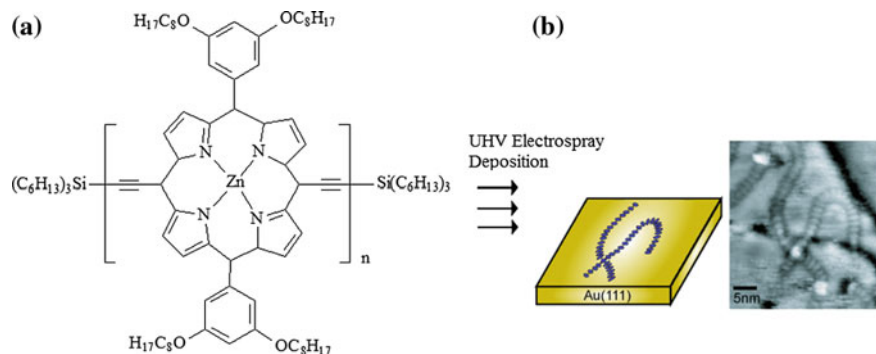
Fig. 4.37 a Electrospray deposition of M-Pp polymers on Au(111) surface. **b** Two polymer molecules P1 traverse a step edge, and cross at point P2 (twice the height of a single strand measured at P1)

Porous Fe-PMCs were synthesized by template method using easy one-pot bottom-top approach to M-Pp synthesis by reaction of expanded aromatic substitution between aromatic dialdehydes and pyrrol in presence of a small amount of Fe (III) ions. The obtained Fe-PMCs have very extensive area of BET surface, large micropores, and exhibit excellent CO_2 adsorption (19 wt%) at 273 K/l bar [251].

Pt(II) 5,15-bis(pentafluorophenyl)-10,20-bis(phenyl)-Pp-9,9-dioctylfluorene copolymers, in which relative intensities of blue and red phosphorescence are easily switched by a change in initial ratio of monomers or transfer energy between fluorescent and phosphorescent units, were synthesized by polycondensation reaction (Fig. 4.38) [252]. These PMCs can be used as radiometric dual emissive oxygen sensing.

There is an interesting synthesis using Pd(0)-catalyzed Stille coupling reaction of conjugated polymers with alternating Zn-Pp-furan or Zn-Pp-thiophene main chain [253].
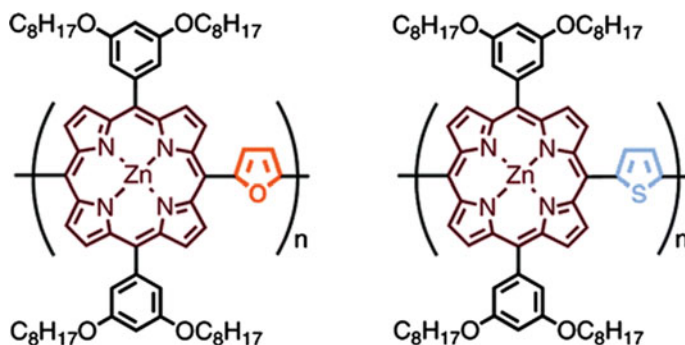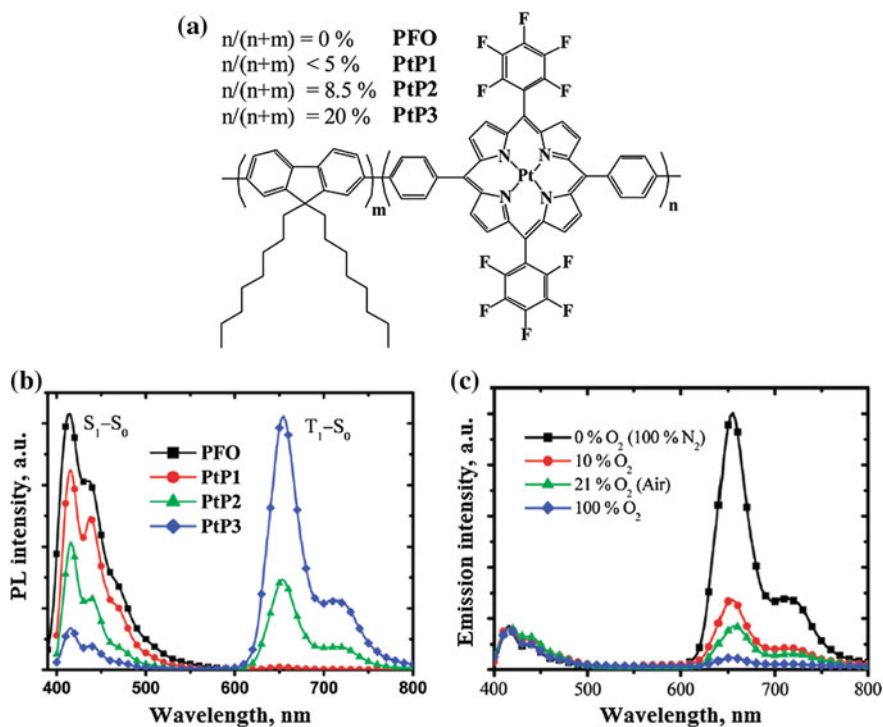
Fig. 4.38 a Structure of Pt-Pp copolymers. **b** PL spectra of polyfluorene (PFO) and Pt-Pp copolymers in CH_2Cl_2. **c** PL spectra of Pt-Pp copolymer in CH_2Cl_2 at room temperature at various oxygen concentrations

We shall notice soluble conjugated alternating M-Pp-dithienothiophene-copolymers, in which M-Pp and dithienothiophene fragments are bound by a single or triple bonds, synthesized by Pd(0)-catalyzed Stille and Sonogashira coupling reactions, respectively [254].
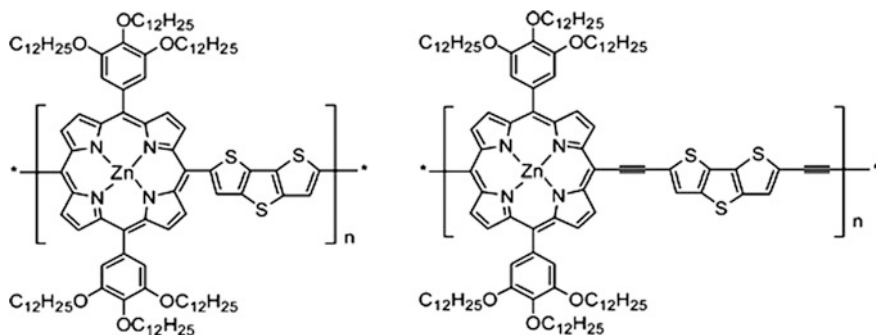
Polycondensation of Zn-Pp structures with conjugated fluorene segments by «$A_2 + A_2' + B_4$» approach based on an easy one-pot Suzuki polycondensation reaction, brings to branched polymer arrays (Fig. 4.39) with intense bright red luminescence (intensity = 740 cd m^{-2}) [255]. PMCs are easily soluble in ordinary organic solvents, thermally stable, and exhibit absorption and emitting properties depending on Zn-Pp content. The gap width of metal chelate polymers decreases as Zn-Pp increases, and emitted color changes from purple-pink to red.

Of interest is comparison of conjugated donor-acceptor (D-A) copolymers of Zn-Pp with 2,3-bis(4-trifluoromethyl phenyl)pyrido[3,4-b] pyrazine (**P1**) and perylene diimide (**P2**) prepared by Sonogashira polycondensation with Zn-Pp dithienothiophene D-D copolymer (**P3**) [256]. It is important that the PMCs **P1** and **P2** in films exhibit strong absorption in NIR region (820–950 nm) with optical gap lower than 1.15 eV. Besides, their Q-bands are shifted red by 60–190 nm as compared to PMC **P3**, while Cope bands are similar (Fig. 4.40).
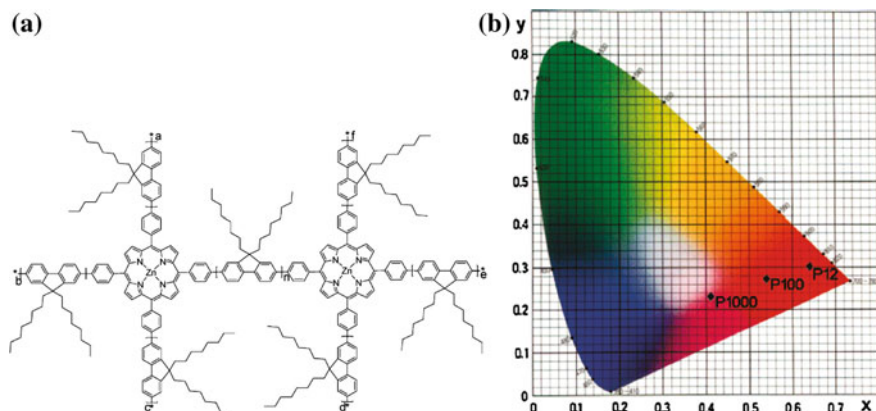
Fig. 4.39 a Molecular structures of the copolymers. **b** CIE chromaticity coordinates of the PLEDs based on copolymers with the molar ratio of Zn-Pp to fluorene units 5.50% for P12, 0.91% for P100, and 0.08% for P1000
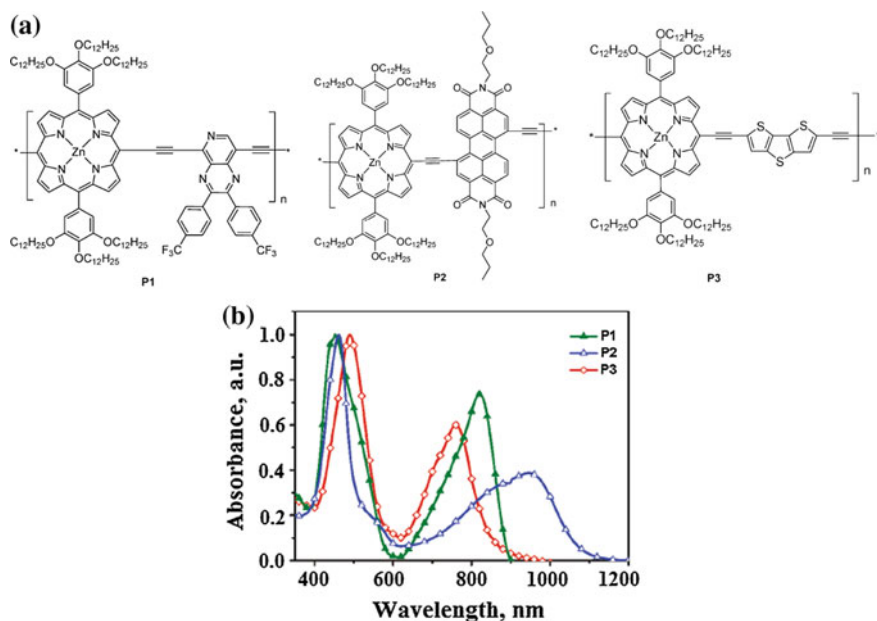
Fig. 4.40 a Chemical structures of Zn-Pp polymers. **b** UV-vis absorption spectra of the Zn-Pp polymers in thin film

Microporous M-Pp PMC with big pores and high surface area is obtained using Suzuki–Miyaura polycondensation by cross-coupling Fe(III)-tetrakis(4′-bromo-phenyl)-Pp and 1,4-phenyldiboronic acid in presence of Pd(0) catalyst (Scheme 4.30) [257]. Owing to such design, M-Pp PMC forms 2D frameworks, and packs in parallel with formation of polymer materials with 2.69 nm pore width and surface area 1270 m² g⁻¹. This well-developed porous organic polymer with M-Pp units in skeleton provides exclusive high loading of catalytic centers in different catalytic reactions.

In order to prevent aggregation of M-Pp polymers in solid state, a family of red-emitting dendronized M-Pp polymers is synthesized by Sonogashira coupling dendritic macromonomers and M-Pp monomers [258]. Dendritic edges of higher generations of Frechet dendrons (more than 2) can not only efficiently wrap polymer chains and reduce their aggregation, but also provide good solubility for conjugated M-Pp polymers working as red light-emitting materials.

PMCs, in which branched alkyl substituents (for example, 2-ethylhexyl) are incorporated in M-Pp fragments to improve their solubility, are synthesized by oxidative Glaser coupling [259, 260]. It is interesting that Zn-PMC aggregates in non-coordinating solvents due to coordination of the amide side-chains to the Zn centers (Scheme 4.31) [261].
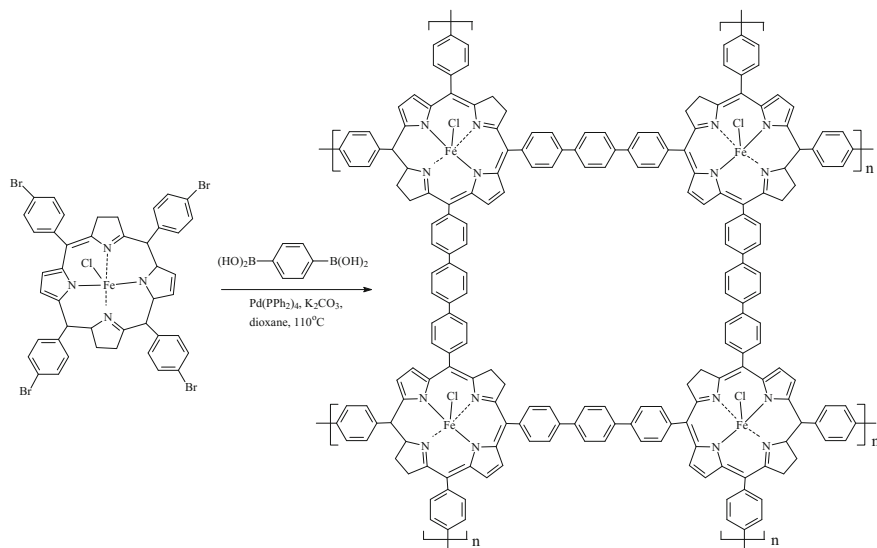
Scheme 4.30 Cross-coupling Fe(III)-tetrakis(4′-bromophenyl)-Pp and 1,4-phenyldiboronic acid using Suzuki–Miyaura polycondensation
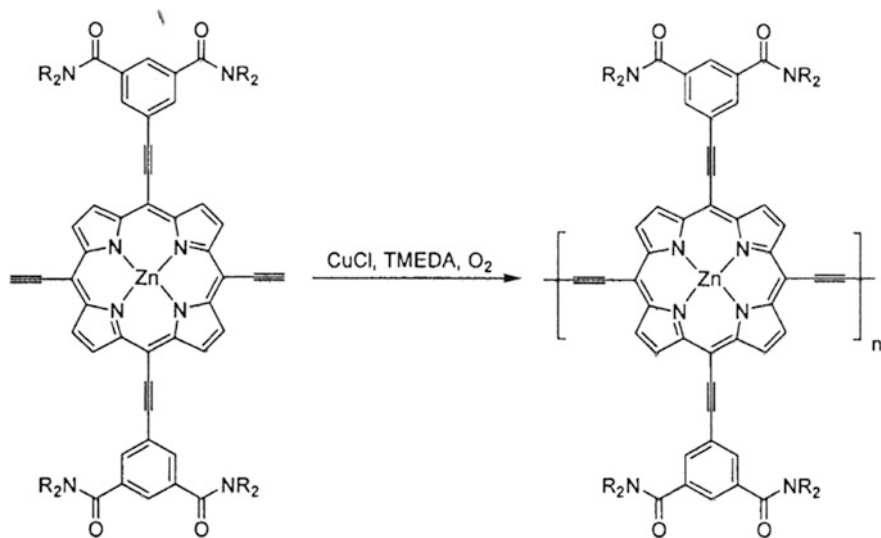
Scheme 4.31 Oxidative Glaser coupling of Zn-Pp

Fig. 4.41 Absorption (black) at 298 K and emission (various colors) spectra as a function of temperature of Zn-Pp polymers in the solid state
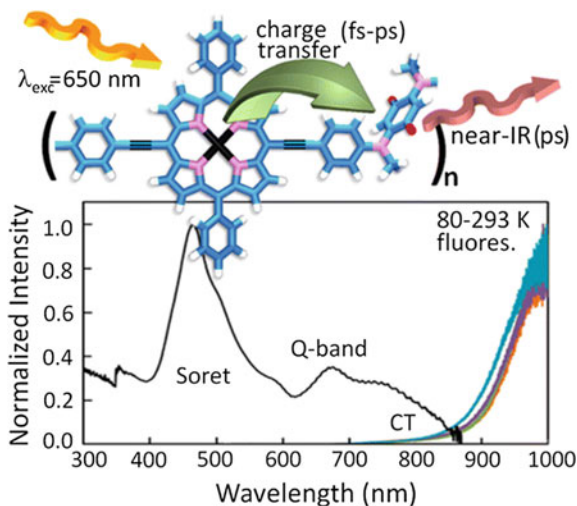
Of interest are four push-pull polymers (C≡C-[Zn-Pp]-C≡C-A)$_n$, where A = isoindigo (**P1**), bis(α-methylamino-1,4-benzene)quinone (**P2**), 2-(N-methylamino-1,4-benzene)-N-1,4-benzene-maleimide (**P3**), 2,2′-anthraquinone (**P4**), and [Zn-Pp] = bis(*meso*-aryl)-Pp-Zn(II) obtained in order to study a nature of low-lying singlet and triplet excited states (Fig. 4.41) [262]. It turned out that **P1** (completely conjugated polymer), **P2** (formally nonconjugated but exhibit strong electronic communication across the chain) and P4 (formally non-conjugated, but with local conjugation between donor and acceptor) are NIR emitters ($\lambda_{max} > 750$ nm). At the same time **P3** exhibits very modest charge transfer contribution (because maleamide is weak acceptor) and is not NIR emitter. High and low energy fluorescence are short- ($77 < \tau_F < 166$ ps) and long-living ($688 < \tau_F < 765$ ps), respectively, assuming that S1 energy transfers have rates (k_{ET}) 7.1 (**P1**), 12 (**P2**) and 4.5 ns^{-1} (**P4**). When cooling or increasing a solution concentration, new red-shifted fluorescence bands are appeared, which confirm an aggregate formation.

M-Pp have a great number of superior properties, which provide their successful incorporation in supramolecular systems and polymers, such as molecular wires and stacks [263, 264]. In particular, molecular wires are designed for different applications, such as organic conducting polymers and NLO materials [265]. For example, lead bis(ethynyl)-Pp polymer, consisting of ∼13 repeat units, possesses a strong and sharp absorption band (Q-band) that peaks at 858 nm (Fig. 4.42) [266].

For most molecular wires conjugation appears through linear π-π-superposition, and they become more and more attractive as long as drive of shorter chains is
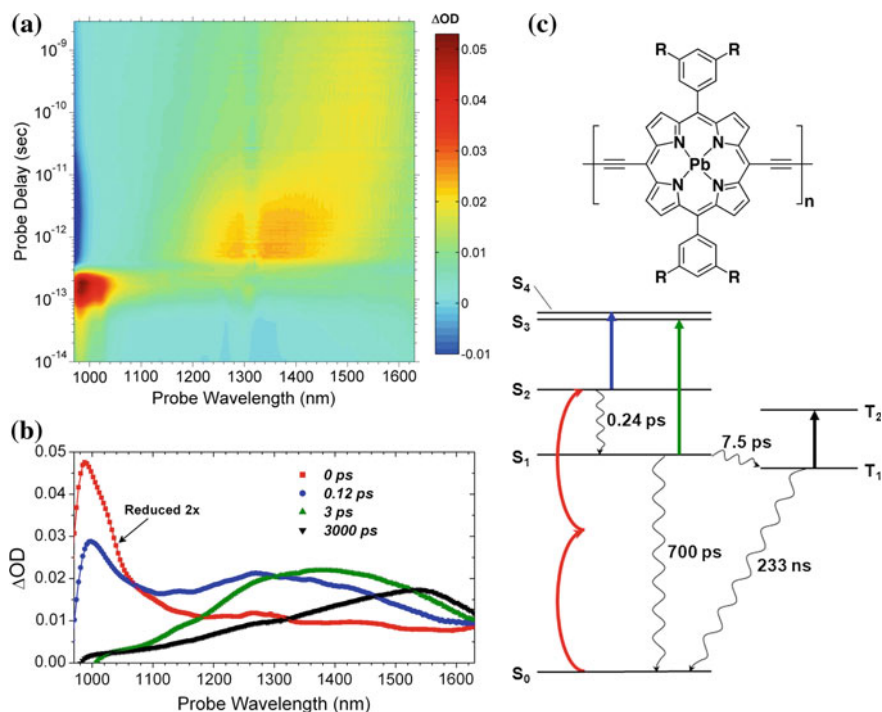
Fig. 4.42 Femtosecond transient absorption (TA) kinetics/spectra and state-level diagram for the M-Pp polymer. **a** Time-wavelength representation of fs-two-photon absorption following two-photon absorption (λ_{exc} = 1300 nm) into S2 and **b** representative transient spectra at various probe delays. Residual scattered light from the excitation beam is evident and early time spectra have been reduced in amplitude for ease of viewing. **c** Energetic level diagram and decay lifetimes determined from TA data. Upper-state lifetime decays were assumed to be fast ($\tau < 0.1$ ps). Inset (above) shows the chemical structure of the lead-based bis(ethynyl)-Pp polymer with R = CON (CH$_2$CHEtBu)$_2$

incremented [267]. π-Conjugated M-Pp are interesting, because they have small HOMO-LUMO gap, and therefore their properties can be purposefully changed for particular applications and non-covalently modified, causing self-assembled aggregates with a range of interesting properties [265]. Besides, they have high stability, which make them ideal for application in various devices at molecular level [266]. By changing character of M-Pp metal center, redox properties can be controlled [268], and modifying a ligand by Pp can be used to control stability, solubility, and self-organization properties of conjugated M-Pp [266].
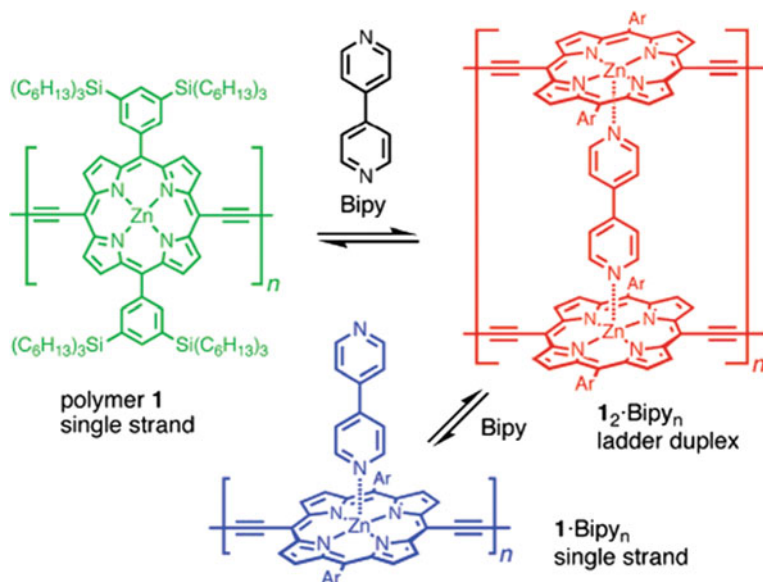
Acetylene, thiophene, phenylacetylene, and viologene were used as M-Pp spacers for production of uniform M-Pp wires of several micrometers in length and thickness no less than 4 nm (Scheme 4.32) [269].

One of examples of molecular wire can be PMC consisting of Zn-Pp units bound with butadiene fragments in 5,15-*meso*-positions.
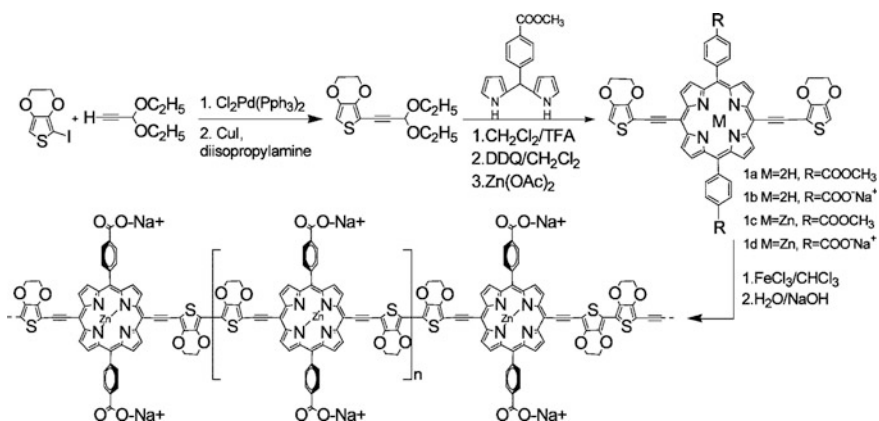
Scheme 4.32 Preparation of M-Pp molecular wires with acetylene, thiophene, phenylacetylene, and viologene spacers
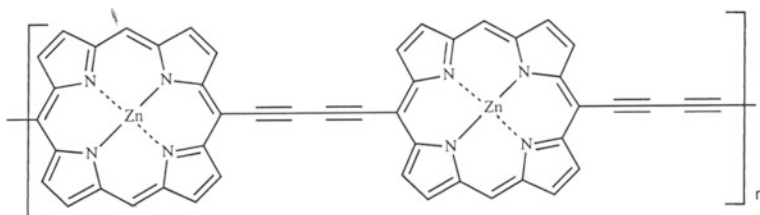
In particular, it is shown that this polymer can efficiently transfer a charge over long distances (mobility of positive charges along individual one-stranded M-Pp wires is 0.084 cm^2 V^{-1} s^{-1}), however, conjugation of these polymers is limited by rotation of one M-Pp block with respect to another. One of the possible methods of removal of this limitation can be, for example, linking of the wires using bidentate ligand, such as 4,4'-bipyridyl (4,4'-bipy), making a ladder-like conformation and enhancing conjugation, as a result charge carrier mobility increases by an order of magnitude up to 0.91 cm^2 V^{-1} s^{-1} [266].

single-strand
$n \approx 10$–15

double-strand: amplified $\chi^{(3)}$
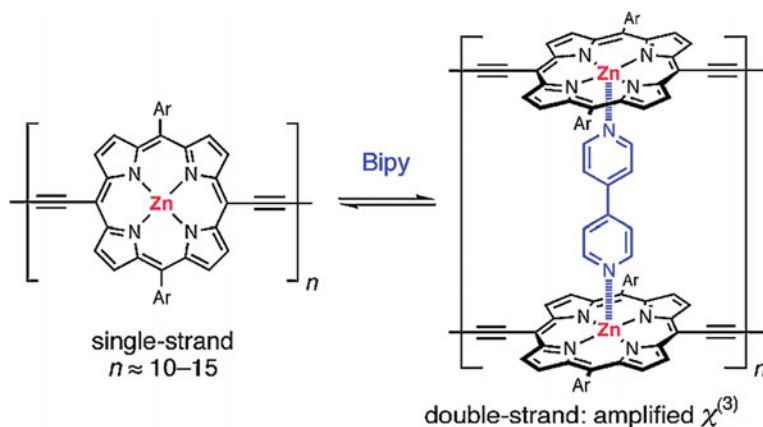
We shall note that for design of ladder M-Pp polymers different synthetic strategies are developed. Thus, completely conjugated rigid M-Pp-containing ladder polymer is obtained by Sc(III)-catalyzed oxidative coupling of *meso-meso*-Zn-Pp-linked polymer, which had adjacent M-Pp units normal to each other (Scheme 4.33) [270, 271].

Presence of multiple bonds throughout the polymer ladder provides planarity of conjugated metal chelate framework, which brings to considerable de-localization in the polymer matrix. These extremely extraordinary polymers should have important applications as molecular wires.

Diversified covalent-bound M-Pp aggregates have become more available after discovery of efficient technique of their preparation, for example, derived from dimeric structures [272].
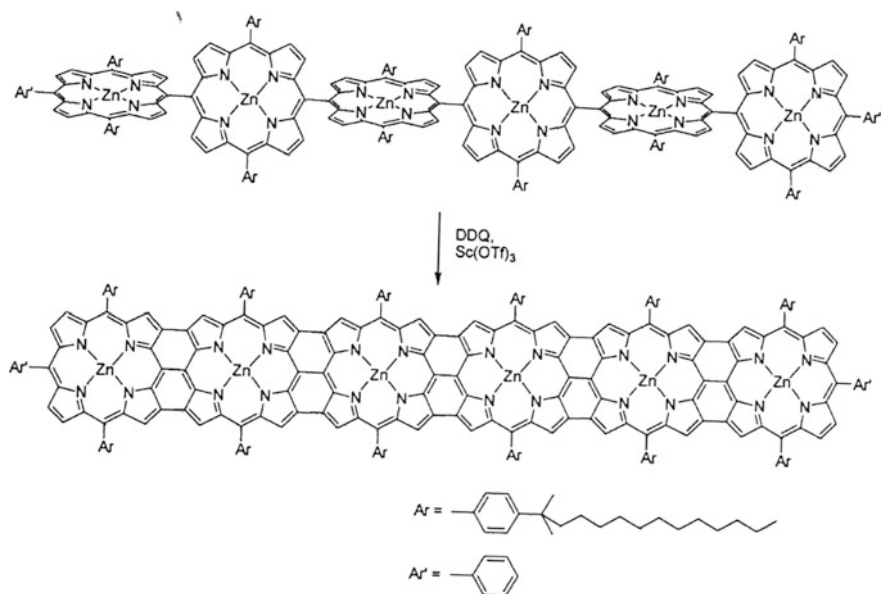
Scheme 4.33 Preparation of completely conjugated rigid M-Pp-containing ladder polymer
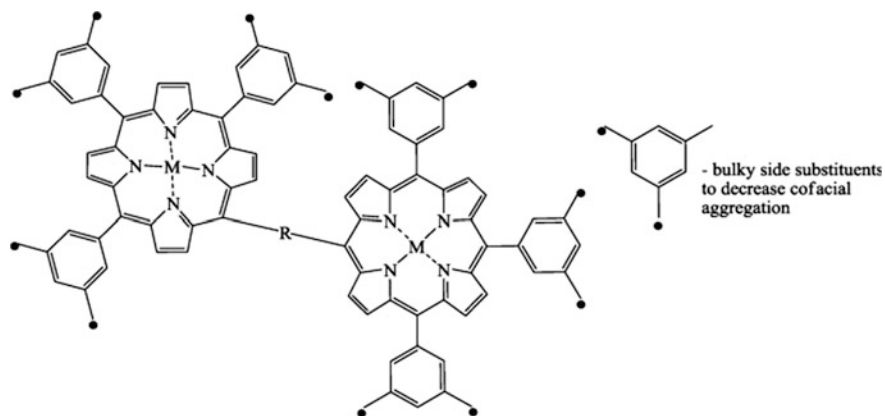
In particular, this route is used for producing windmills (A), lattices (B), rings (C), and boxes (D), which present models of light-harvesting antennas for photosynthesis.
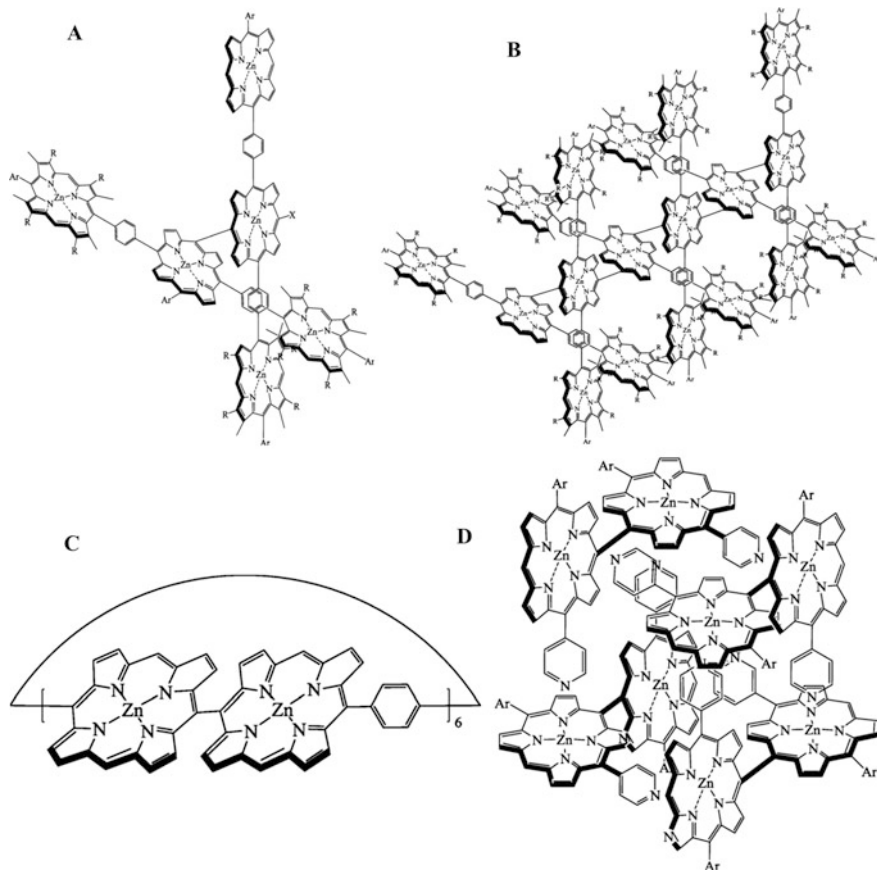
It should be noted that solution-processable Pt(II) polyyne polymers containing Zn (II)-Pp chromophores are synthesized using Cu(I)-catalyzed reaction of dehydrohalogenation of Pt(II) chloride precursor and respective bis(ethynyl)-Zn-Pp monomers [273]. This metal-polymer is an example of interesting class of polymetallayenes, which have metal-carbon σ-bonds in the main chain [3, 4, 274]. Due to rigid-rod geometry of the triple M≡C bond, these original metal-containing polymers can show NLO [275], luminescent, photovoltaic, and liquid crystalline properties [276].

Microporous polymeric net-like M-Pc structures with the surface area in the range 120–612 m^2 g^{-1} were obtained through condensation of Co-hexachloro-Pc with 5,5′,6,6′-tetrahydroxy-3,3,3′,3′-tetramethyl-1,1′-spirobisindane (Scheme 4.34) [277].
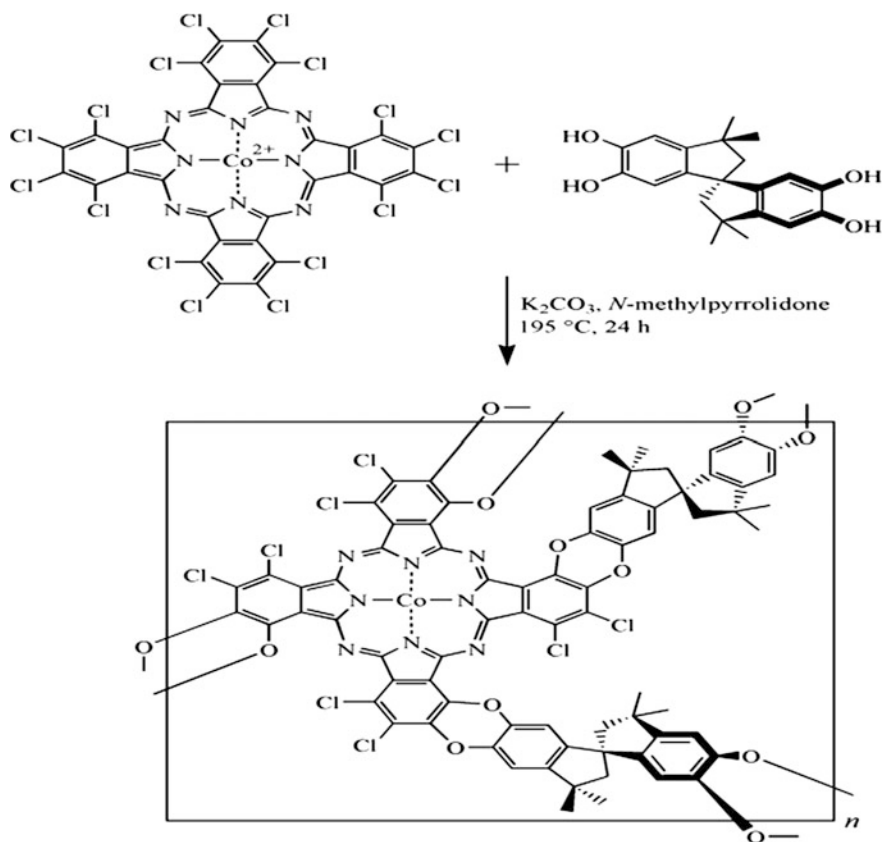
Scheme 4.34 Condensation of Co-hexachloro-Pc with 5,5′,6,6′-tetrahydroxy-3,3,3′,3′-tetramethyl-1,1′-spirobisindane

Of interest is the development of some synthetic approaches for production of mono-PEGylated Zn(II)-Pc, which are promising for PDT, which is minimally invasive procedure proved for treatment of some types of cancer with singlet oxygen [278]. It is well known that this procedure has advantages of cytotoxic activity of singlet oxygen ($^1O_2$) and other active forms of oxygen produced by visible and NIR radiation of light from sensitizers of a color after their accumulation in malignant cells. These PEGylated Zn(II)-Pc were prepared by substitution reactions of PEG monomethyl ether monotosylate with an average molecular weight of ca. 550, 2000, or 5000 with 2-hydroxyphthalocyaninatozinc(II) in the presence of K_2CO_3 in DMF.
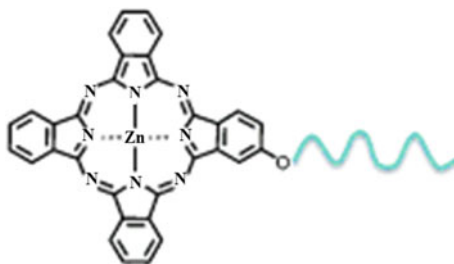
Homopolymer, block and random copolymers obtained based on methacrylate benzenedinitrile monomer using RAFT method, are used for synthesis of polymers with Zn-Pc containing side chains as a result of reaction with excess benzenedinitrile derivatives, 4-(octyloxy) phthalonitrile [279]. Zn-Pc-PMCs generate some species with high quantum yield of singlet oxygen, which are promising for PDT. Among them copolymers exhibit increased quantum yield of singlet oxygen ($\Phi_\Delta = 0.49$ and 0.40 in DMF, $\Phi_\Delta = 0.68$ and 0.73 in aqueous medium), as compared to a homopolymer ($\Phi_\Delta = 0.28$).

4.7   Synthesis of Dendrimers and Hyperbranched Polymers Based on Metal Chelate Monomers

It should be noted that LMC are convenient structural blocks for various MCD structures [16, 25, 280–293]. For these purposes two main methods of synthetic chemistry of dendrimer are applied: divergent and convergent approaches. As an example, Fig. 4.43 shows these two approaches for synthesis of dendrimers with M-Pp and M-Pc cores. Divergent synthesis based on an assembly from multi-functional metal chelate core, which spreads outwards through a series of reactions (Fig. 4.43a). Multistage character of this approach leads to accumulation of defects in chemical structure of MCD, and the more generations, the more accumulated defects.

This is explained by the fact that a number of functional groups, which should react to provide formation of next generation, increases exponentially with each following generation; therefore, a probability of side reactions increases. Besides, apart from statistic reasons, the effect of structural factor is increased, because a substantial fraction of peripheral units exists in folded state within a polymer volume. Usually a considerable molar excess of reagents is used in order to prevent formation of side products, and target polymers are carefully cleaned to avoid undesired directions of the reaction at the following stages. On the other hand, when using convergent approach MCD are built from small blocks connected with additional structural blocks to form a branched structure, therefore, the construction is prepared from peripheral dendrons to the central focal point. Then each dendron

(a) Divergent synthesis
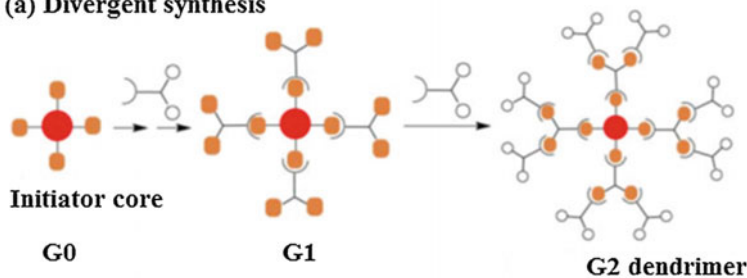
(b) Convergent synthesis
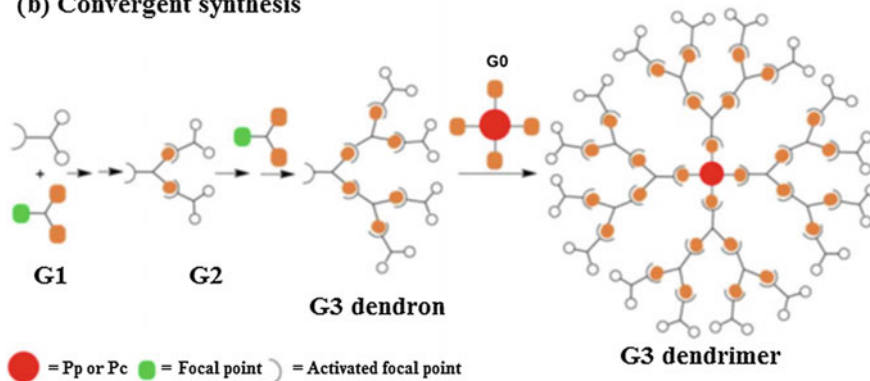
Fig. 4.43 Scheme of divergent and convergent methods, used for MCD synthesis

is linked to a metal chelate core through its focal point for the final MCD producing (Fig. 4.43b). This method makes allows to removing impurities and preventing MCD formation with shorter branches, so that a resulting polymer is more monodisperse.

Of substantial interest is synthesis of dendrimers containing metal chelates of molecular type based on polypyridyl Ru(II) complexes due to easy synthesis of functionalized pyridyl ligands, dendritic arms and Ru(II) sites. One of the first in this series MCDs with $[Ru(bpy)_3]^{2+}$ core were obtained, primarily for studying their photophysical and redox properties [294–305]. For example when $[Ru(bpy)_3]^{2+}$ is buried in a dendrimer core the quenching reaction rate by acceptor systems, such as molecular oxygen, tetrathiafulvalene, or methyl viologen was slower than in a free nondendritic complex. The Stern–Volmer equation gives a rate constant of quenching process (k_{SV}), which proceeds by diffusion mechanism, and luminescent studies have shown that the quenching process obeys to the equation:

$$\varphi_0/\varphi = 1 + k_{SV}\tau_0[Q],$$

where φ_0 and φ are fluorescence intensities in absence and in presence of quencher, respectively,

k_{SV} is bimolecular constant of the quenching reaction rate,

τ_0 is extinction time of fluorescence in absence of quencher,

[Q] is a concentration of the quencher.

In the $[Ru(bpy)_3]^{2+}$-core dendrimers containing units of dimethoxybenzene- and naphthyl types on branches the antenna effect is observed (Fig. 4.44), when absorbed energy hv (in red) migrates along a dendrimer skeleton until it reaches the core, from which emission goes [299]. MCD exhibit very efficient (90%) energy transfer from fluorescence of terminal units to the core, whose phosphorescence is sensitized (λ_{max} = 610 nm). As a result, strong emission in visible region at UV excitation of branch groups is observed [294, 297, 298, 300–303].

Fixation of carbohydrate groups at periphery of bpy-dendritic derivatives made it possible to integrate 6 or 18 units of mannose around Ru(II) centers for biomedical purposes [306]. Combination of high-sensitive luminescent Ru complex with peripheral centers generates MCD with excellent capacity of lectin-biosensors.
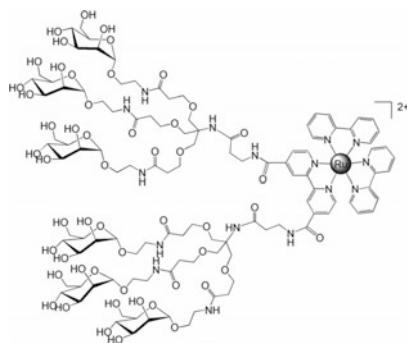
Similar $[Ru(bpy)_3]^{2+}$-core dendrimer (**I**) containing different carbohydrates are easily obtained using click chemistry by Huisgen [3 + 2] Cu(II)-catalyzed cycloaddition reaction [307].
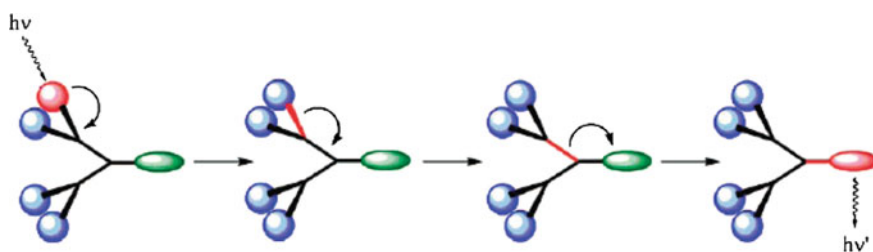
Fig. 4.44 Schematic illustration of a dendron as an antenna

In order to decrease total cytotoxicity of luminescent polypyridyl Ir complexes PEG branching arms were linked to Ir(III) sites (**II**) [308]. It turned out that incorporation of PEG branches not only decreases toxicity as compared to nonpegylated analogues, but also increases solubility in water and, consequently, cellular absorption of complexes.
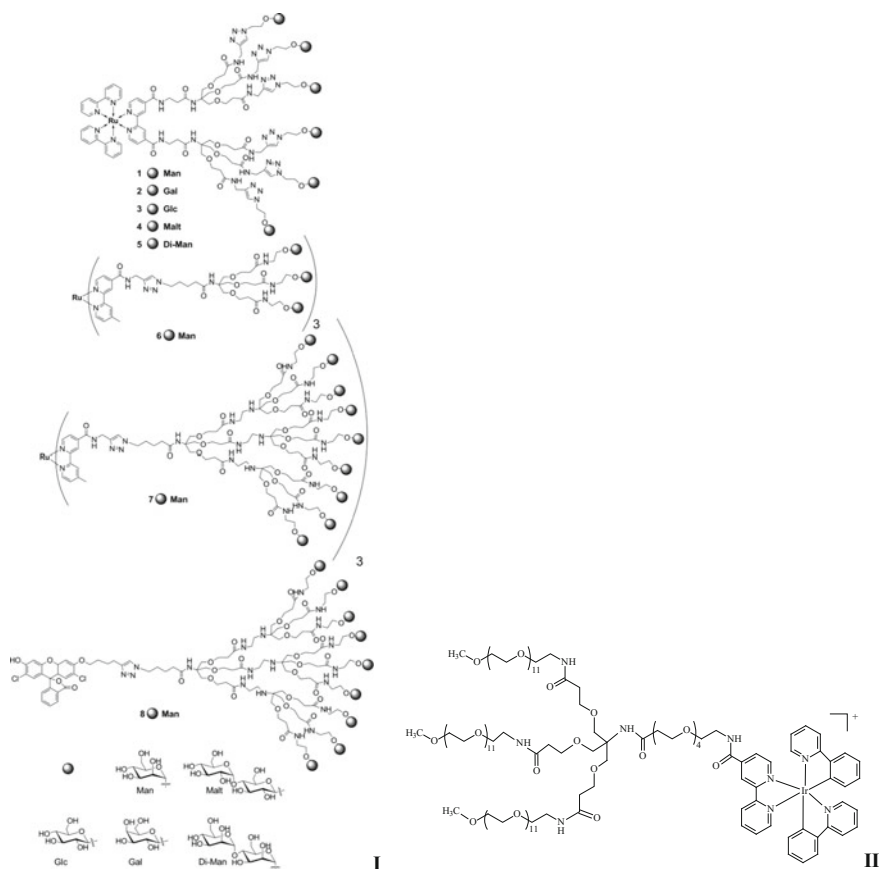
MCD of molecular type can also be obtained by end capped of monofunctional dendrimers with LMC. For example, luminescent PAMAM metal chelate dendrimers containing on periphery 32 polypyridyl Ru chelates with positive or negative charges are synthesized [309]. It is important that positively charged MCD are interesting for PDT, while negatively charged compounds are candidates for diagnostic analysis of fluorescence.
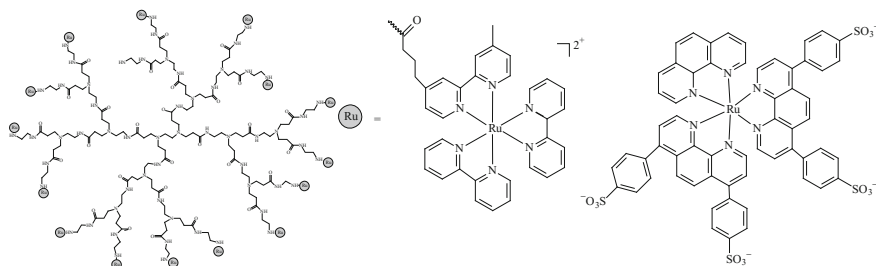
The same synthetic procedure is applied to production of tetranuclear MCD based on G1 PPI dendritic platform functionalized by [*meso*-1,2-bis(4-fluorophenyl)en]Pt (II) fragments on periphery, which is promising for biomedical applications [310].
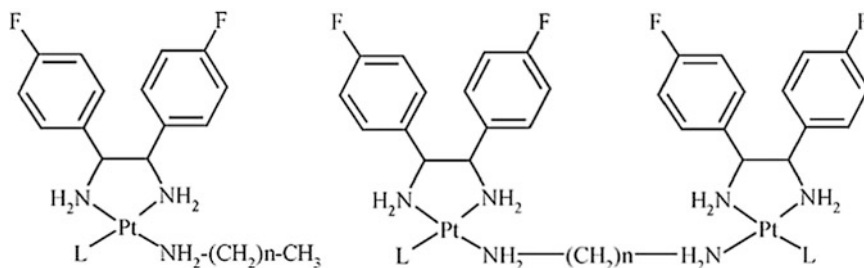
n = 2,3,5; L = DMSO or Cl   n = 6,9,12; L = DMSO or Cl

In particular, it occurs that conjugation affinity of dendrimer complexes with respect to DNA is by 700 times stronger than that of a *cis*-platinum. It is accepted that dendrimers are used as transport means, which transfer Pt complexes over barriers to reach a target center.

It should be also noted peripheral functionalization of PAMAM series of Pt(II) dendrimers by chelate fragments [311].

Of interesting are polythiophene dendrimers with $[Ru(bpy)_2(phen)]^{2+}$ and $[Ru(phen)_3]^{2+}$ cores, which are fluorescent in NIR region and exhibit extremely red shift ($\sim$165 nm) of MLCT emission [312].
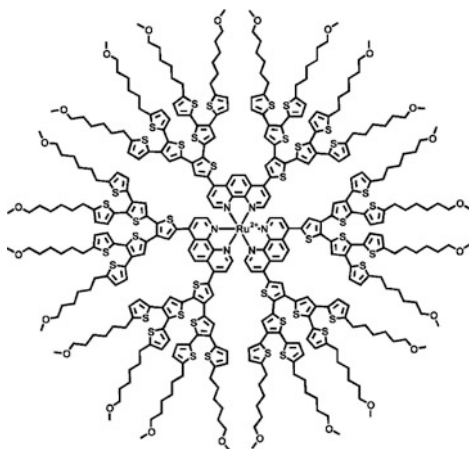
Studying kinetics of homogeneous electron transfer between oxidized and reduced tris(bpy)-metal-core dendrimers using NMR line-broadening showed that increase in a dendrimer generation is associated with decrease in self-exchange rate (Table 4.3) [313].
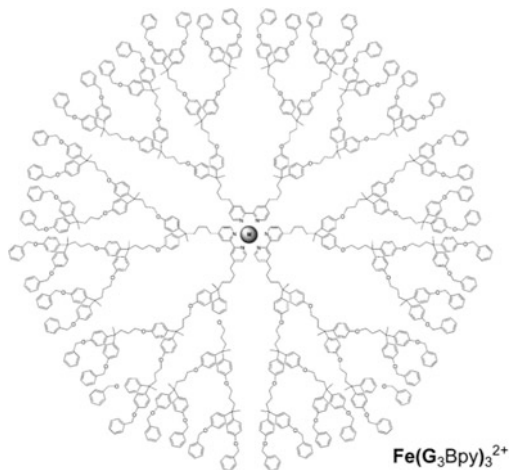
Fe(G$_3$Bpy)$_3$$^{2+}$

MCD with [Ru(bpy)$_3$]$^{2+}$-cores are convenient objects for the study of light-induced processes, which can be used for read and write of artificial molecular

Table 4.3 Electron self-exchange rate constants in CD_2Cl_2–CD_3CN (5:1) at 297 K

	Fe core, k_{ex} (M^{-1} s^{-1})	Ru core, k_{ex} (M^{-1} s^{-1})
G0	$2.59(0.19) \times 10^7$	$3.46(0.23) \times 10^7$
G1	$5.30(1.01) \times 10^4$	$7.26(0.89) \times 10^4$
G2	$2.72(1.03) \times 10^4$	$5.70(0.61) \times 10^4$
G3	$1.14(0.58) \times 10^4$	ND^a

Values in parentheses represent the magnitude of the 90% confidence interval
[a]Not determined

Fig. 4.45 a Structure of dendrimer with $[Ru(bpy)_3]^{2+}$-core. **b** Energy level diagram showing the excited states involved in the main photophysical processes (excitation: solid lines; radiative deactivation: dashed lines; non-radiative deactivation processes: wavy lines)

devices and machines. They present molecular and supramolecular systems, which work and/or fulfill useful functions using photoisomerization reaction, photoinduced processes of electron or energy transfer, or reaction of photoinduced proton transfer (Fig. 4.45) [314].

Presently, $[Ru(bpy)_3]^{2+}$-cores MCD containing different chromophoric groups can be designed and synthesized in order to obtain efficient light-harvesting devices potentially useful, in particular, for solar energy transformation [315].

Interesting dendrimers with a metal chelate core of molecular type are fluorescent Re dendrimers G1 obtained through interaction of (phen)Re(CO)₃Cl with dendrons containing biphenyl fragments and terminal 2-ethylhexyloxy-groups [316]. It should be emphasized that in this case properties of MCD are considerably dependent on a place of linking and a number of dendrons. For example, dendrons linked in 2- and 9-positions of metal chelate core showed high chemical stability as compared to other G1 dendrimers and provided control over electron interactions, which induce solvatochromism. Besides, they display lower solvatochromism as compared with other dendrimers due to ability of dendrons to protect a metal center. Also solution processability of materials appears, and PLQY of a solid substance is increased, as compared to solutions. As a result of electrochemical and photophysical properties, they can be potentially used for PLEDs production.

Another example is MCD with diimine carbonyl Re(I) complexes as a core and containing Cz fragments (Fig. 4.46) [317].

Fig. 4.46 Photoluminescence spectra of **P1**, **P2**, **D1**, and **D2** in CH_2Cl_2

It occurs that PLQY of **P1** and **P2** complexes containing mono-Cz fragments are 0.13 and 0.16, respectively, which is far higher than for Re(I) dendrimers with tri-Cz fragments **D1** (0.066) and **D2** (0.0048).

Of interest is synthesis with high yield (57–74%) of low generation of poly (alkylenediamine)-nitrile MCD peripherally functionalized with (diphenylphospino) ethylene (dppe) Ru chelates $[Ru(dppe)_2Cl]^+$ [318].

One of the important aspects of MCD that are to be considered for biological tests and clinical applications is the knowledge of their degradation/stability in solution along the time, as well as of the type of species resulting from the degradation process. ^{31}P NMR was performed to evaluate the degradation of the MCD/release of metallofragments (Fig. 4.47). MCD containing $[Ru(dppe)_2Cl]^+$ fragments are stable for 4 h, which provides potential of these compounds for biological applications.

It should be noted dendrimers with a [Fc(dppe)] fragment, which are used for target synthesis of MCD containing metal ions simultaneously in two degrees of oxidation: Fe(II) and Fe(III) (Scheme 4.35) [319].

There is an interesting approach to solid state synthesis of MCD fixed on polymer carriers of PS-type. Advantages of this approach are: easiness of the solid state synthesis with use of available structural blocks, a possibility to characterize the products fixed on carriers after detaching, better swelling properties in most solvents, and flexible polymer matrices. In accordance with this approach first structural blocks are obtained on the basis of pseudo-peptides with Fmoc-protected aminoacidic groups, and then synthesis of dendritic phosphines up to 8 units is performed using the divergent approach [320]. As occurred, these Rh complexes are excellent catalysts for hydroformylation of some olefins, in particular, G2 catalyst (4 units) is active for 5 cycles.

Fig. 4.47 ^{31}P NMR spectrum of MCD in [D6]DMSO at 37 °C at different time periods of incubation

Scheme 4.35 Oxidation of the MCD to the mixed-valence MCD(PF$_6$)$_3$ and fully oxidized MCD (PF$_6$)$_6$. The Fe(II) species are in red and the Fe(III) species are in blue

We shall notice shape-persistent N,C,N-pincer-Pd dendrimer complexes (Scheme 4.36) having one-, two-, and three-dimensional geometries obtained by interaction of pincer-complexes with poly-bromine-derivatives of dendrimers, which showed compatible activity with one-core catalyst in Michael reaction of ethyl cyanoacetate and methyl vinyl ketone [321].

Other SCS-pincer Pd-complexes were fixed on polar PAMAM dendrimers and showed more similar activity and higher selectivity as compared to a monomer

Scheme 4.36 Modular approach to the synthesis of multi(pincer-metal) complexes

analogue in the cross-coupling reaction of styryl boronic acid with epoxy vinyl [322]. This can be explained from the point of view of aggregation of a dendrimer and backfolding of peripheral groups.

The convergent «layer-block» synthesis of MCD containing hydrophobic shells of covalent dendritic wedges at periphery (Fig. 4.48) deserves consideration [323]. Using G1 and G2 Fréchet wedges having phosphines in the focal point, with using the convergent method, G3 and G4 MCD are obtained, in which nitriles, pyridines, and phosphines coordination to SCS-pincers-Pd(II) is used as assembly motif, and a number of terminal hydrophobic phosphine wedges increases with generation.

The two-staged so-called post-dendronization method was used in order to obtain processed in solution emitting green-blue light Ir-chelate dendrimers, containing ether dendrons based on *N*-phenyl-Cz (Scheme 4.37) [324].

At the first, reactive Ir core is obtained, for example, *m*-HO-difluorine-ppy-Ir complex with hydroxyl group in *meta*-position with respect to N atom in ppy ligand to exclude a possible resonance non-complex-forming keto-structure. Then, a synthesized ether core is functionalized by dendrons based on *N*-phenyl-Cz to obtain Ir dendrimers G1, G2, and G3 with high yield over 60% (Scheme 4.38). It is important that the obtained MCDs have high thermal stability with T_d above 380 °C and T_g above 200 °C. As the number of generation increases, intermolecular

Fig. 4.48 Schematic representation of the coupling dendrons to the core to produce the hybrid covalent-noncovalent MCD

Scheme 4.37 Two methods for the preparation of Ir-cored dendrimers

interactions between emissive Ir cores are efficiently suppressed, and do not bring to luminescence quenching, which is confirmed by blue shift of the emitting peak, and increase of lifetime in solid state.

The simple convergent synthetic approach is used to produce Ir(III)-core dendrimers with Cz dendrons, peripherally functionalized by β-diketone fragments [325]. Green-emitting MCD from G0 to G3 are synthesized by the reaction of respective β-diketonate dendrons with Ir(III) dimers under soft conditions with good yield, i.e. in

Scheme 4.38 Synthesis of greenish-blue-emitting Ir-cored dendrimers

this case, monomerization of the starting dimer complexes takes place during MCD formation. It is important to emphasize that this approach is modular and can be used for dendrimer formation either blue-green-emitting or red-emitting with the same β-diketonate dendrons, but different chelating ligands. The MCDs can be used as emitting layer in OLEDs with the increasing number of Cz dendrons, the efficiency improves from 6.7 cd A^{-1} for G1 to 23.4 cd A^{-1} for G1 [326].

For *fac*-Ir(ppy)$_3$-core dendrimers a positive dendritic effect is observed: PLQY increases during transition from non-dendritic film to G1 and further on to G2 MCD. Mono- and twice dendronized dendrimers have relatively narrow PDI about 1.4, and from them thin films can be obtained from solutions. Another important parameter for these highly efficient dendritic OLEDs is incorporation of biphenyl fragments and 2-ethylhexyloxy surface groups [327–330], which are used to control the intermolecular interactions.

Besides, *fac*-Ir(ppy)$_3$-core dendrimers are synthesized, which contain Müllen dendrons, however, due to their weak solubility, simple one-layer devices based on them showed low efficiency [331].

Presence of fluorene peripheral groups improves solubility and increases PLQY, especially in solid state. It should be noted that G1 and G2 MCD consisting of *fac*-Ir (ppy)$_3$ core and hole-transporting dendrons based on phenyl-Cz have provided very good devices [332–334].

From the point of view of a possible practical application, it is important that using MCD and OLED containing only the dendrimer/host mixture, light-emitting, and electron-transport layer brings to simplification of devices as compared to other OLEDs with five or six components in four or five layers. These simple devices based on MCD are highly efficient, since light-emitting processes from solution bring to a possible color variation, and exciton diffusion length in a dendrimer is far shorter than in a dendrimer film or in devices containing small molecules [335, 336]. Thus, highly efficient light-harvesting systems based on blue Ir(III)-core phosphorescent dendritic acceptor Ir(III)-bis-[(4,6-difluorophenyl) pyridinato-N,C$^{2'}$]-3-hydroxypicolinate in combination with dendron Cz-containing donors are developed through singlet-singlet and triplet-triplet energy transfer (efficiency more than 90%) [336].

It should be noted that in the phosphorescent MCD based on Ir complex core Cz dendrons, phosphorescence quenching can be prevented. In particular, the best phosphorescent light emission device had maximum luminance 13,060 cd m^{-2} at the driving voltage 11.5 V and peak current-efficiency of 4.3 cd A^{-1} at luminance 3400 cd m^{-2} [337].

Triplet-exciton jump is regulated by electron-exchange interaction and is 600 times faster than phosphorescence quenching in films of Ir(III) phosphorescent dendrimers [338].

Fixation of dendritic triphenylsilylphenyl groups on pyridine part of a ppy ligand causes stronger MLCT transition and lower energy gap than non-functionalized complex Ir(ppy)$_3$ (Fig. 4.49) [339]. In this case, as at increase in a number of substituents, excited state of intermolecular interactions, which bring to non-radiation decomposition, is suppressed more efficiently. These effects of center-isolation and improved solubility due to integration of triphenylsilylphenyl group make possible wet preparation of PLED based on these Ir(III) chelate dendrimers. Besides, it is interesting to emphasize that they considerably increase thermal stability of dendritic Ir(III) chelates.

It should be also noted PLED based on phosphorescent green solution-processing Ir(III) chelate, which exhibits external quantum efficiency (EQE) 5.1% and luminous efficiency 16.4 cd A^{-1} with brightness 100 cd m^{-2} at 15.8 V [340].

Fig. 4.49 Trend curves that show the T$_1$ energy level of Ir (III) chelates calculated by TD-DFT and optical band gap energy (E$_g$) obtained from absorption spectra of Ir(III) chelates

Of interest is synthesis of bipolar homoleptic Ir(III) dendrimer containing diphenylphosphoryl and diphenylamine dendrons (Fig. 4.50) [341]. It is important that devices based on it have maximum current efficiency 21.6 cd A^{-1}, which is the highest among single-layer self-host green PLED.

A series of dendron-jacket electrophosphorescent non-conjugated copolymers, in which Ir chelate and Cz [342] or oxadiazole [343] fragments is incorporated in a polymer, is prepared. In particular, St-based phosphorescent monomer with cyclometalated

$$k_{et-}/k_{et+} = 2.44 \qquad k_{et+}/k_{et-} = 2.37$$
$$\gamma = 0.55 \qquad\qquad \gamma = 0.61$$

Fig. 4.50   a Molecular structures of MCD (the parent Ir complex is shown in black color). **b** The predicted emission zones of single-layer devices based on MCD in which they possess similar degrees of charge balance

Ir complex was copolymerized with the G1 dendritic Cz monomer through the conventional free radical polymerization to obtain a series of electrophosphorescent random copolymers. With increasing iridium content, the EL of the copolymers shifted from blue to orange and passed through a near-white emission region (Fig. 4.51).

Fig. 4.51 Electroluminescence spectra (**a**) and CIE coordinate (**b**) of the MCD

It is important that large side groups can separate Ir chelates from each other and suppress quenching of triplet excitons at high Ir concentrations. Steric hindrances of large side groups in the dendron-jacket copolymers are far weaker than in the dendrimers.

A series of benzyl ether of branched dendritic fragments with terminal carbazolyl groups was integrated in heteroleptic Ir(III) chelates in order to increase PL (Scheme 4.39) [344]. In this case dendritic fragments play a double function as a donor of Förster resonance energy transfer (FRET) and shield of Ir(III) chelate core from oxygen. For example, peripheral carbazolyl groups absorb intensely UV light and efficiently transfer energy to Ir(III) chelate core through FRET effect. As a result, PL of Ir(III) chelate around 560 nm increases considerably. Besides, dendritic units shield Ir(III) chelate core to reduce the oxygen quenching effect, which brings to further increase in PL of Ir(III) chelate. It is interesting that the complexes contain chelating bpy ligand with a carboxyl group for further bioconjugation or functionalization and, therefore, they can be used for bioimaging and biolabeling.

Another route of producing light-emitting G3 phosphorescent Ir dendrimers containing Cz dendrons includes etherification of aryl Ir-chelate core of a dendrimer with 4-(dimethylamino)-pyridinium-4-toluenesulfonate in presence of DCC (Scheme 4.40) [345]. Thermal analysis showed good thermal stability reaching $T_d = 370$ °C and $T_g = 720$ °C.

Of interest is synthesis with good yield of red phosphorescent Ir dendrimers with two 2-(benzo[b]thiophen-2-yl) pyridine and 3-hydroxypicolinate as chelating and ancillary ligand [346]. Absorption of photons on picolinate dendrons was followed

Scheme 4.39 Preparation of heteroleptic Ir(III) chelates containing benzyl ether of branched dendritic fragments

by efficient energy transfer to Ir site, which resulted in high red emission at ~600 nm by MLCT. It is important that phosphorescence intensity increased substantially with the dendrimer generation. Based on phosphorescence quenching rates, efficiencies of energy transfer were calculated for G1, G2, and G3 dendrimers as 162, 223, and 334%, respectively.

Scheme 4.40 Preparation of light-emitting G3 phosphorescent Ir dendrimers

A special attention is given to divergent procedure of synthesis (yield > 80%) of polyphenyl dendrimers of high generations with Ir(III) core up to G4 with molecular diameter 8 nm (Fig. 4.52) [347]. It occurs that PLED based on G3 dendrimer has the highest efficiency as compared with other generations of dendrimers, since its size ($R_3 \approx 30$ Å) can not only prevent intermolecular triplet-triplet annihilation, thus increasing PLQY, but provide effective mobility of charge carriers from periphery to Ir(III) core.

We shall mention synthesis of green light emitting hyperbranched polymers with Ir chelate as a core and 3,6-Cz-*co*-2,6-pyridine as branches executed by Suzuki polycondensation (Scheme 4.41) [348].

The initial ratio of Ir complex and 2,6-pyridine fragment has a significant effect on molecular weight and PDI of the formed PMC (Table 4.4). The results indicated that the actual Ir contents in these copolymers are substantially lower than the feed ratios of the complex monomers, and the contents varied in a certain range even when the feed ratios of Ir complex monomers were the same.

It should be noted that hyperbranched structures can considerably suppress interchain interaction between facial Ir chelates and self-quenching of Ir complexes due to aggregation. Therefore, a hyperbranched framework balanced with 3,6-Cz-*co*-2,6-pyridine segment as a branch and Ir(ppy)$_3$ complex as a core, suggests a new molecular design for highly efficient phosphorescent green PLED.

Good prospects of using dendrimers with Ir(III) chelate core in PDT should be noted [349]. For example, using Ir(III) chelates allows increasing efficiency of $^1O_2$ production, and dendrimers serve for delivery of hydrophobic (lipophilic) and amphiphilic photosensitizers to target cells.

Eu-core dendritic OLED with Cz-containing groups on periphery shows white radiation (as a result of several emissions) [350]. In these chelates FRET from peripheral Cz units to β-diketonate fragments is established, as well as from ligands to central Eu(III) ions.

Commercial PAMAM dendrimers are functionalized with chiral Co-salen complexes and showed high activity with respect to monomer or dimer analogues in HKR of terminal epoxides. This was the first positive dendrimer effect in asymmetric catalysis with dendritic PAMAM-Co-salen chelates for HKR of terminal epoxide, which is due to cooperation in the key mechanical step: coordinated nucleophile attacks epoxide, in turn, with another Co atom. Therefore, proximity of two Co chelates advances the reaction, and this proximal state is best realized in dendrimers with four branches [351].

Fig. 4.52 MCD based on *fac*-tris[2-(3-ethynylphenyl) pyridyl]Ir(III) core

Scheme 4.41 Synthesis of hyperbranched polymers containing Ir chelate as a core by Suzuki polycondensation

Table 4.4 Molecular weight and composition of copolymers

2,6-pyridine moiety in polymer (mol%)	M_n ($\times$ 10^3)	PDI	Ir complex (mol%) in	
			Feed ratio	Polymer
0	7.66	1.4	1	0.55
0	11.84	1.3	3	1.24
10	4.99	1.6	3	1.79
20	7.02	1.6	3	2.02
30	6.66	1.7	3	2.17

Chiral MCD with rigid matrices containing three or six α-aminoalcohols on a branched chain ends can work as chiral catalysts for enantioselective linking of dialkyl-Zn to aldehydes, at that secondary alcohols were obtained with enantiomer excess to 86% [352].

Conjugation of arene Ru metallocycle containing 5,8-dioxydo-1,4-naphtho-quinonato-chelating fragment with pyrenil-functionalized poly (aryl ether) dendrimers carrying cyanobiphenyl terminal groups allows to prepare liquid crystalline MCD [353]. Multicomponent nature of dendrimers (terminal groups of mesogens, dendritic cores, pyrene blocks, aliphatic spacers and metallocycle) brings to the formation of highly segregated meso-phases with complex multilayered structure. Pyrenil dendrimers exhibited multilayered smectic A-like phase with unusual morphology. These systems showed also enhanced cytotoxicity compared to pyrenyl-containing polymers and the metallaprism itself, which might be attributed to the increased water solubility. It is important that the MCDs showed similar cytotoxicity for both the cisplatin-sensitive A2780 and cisplatin-resistant A2780cisR cancer cell lines, indicating that they behaved with a different mechanism from the reference drug, cisplatin.

We shall consider highly stable bis(P,O)-Ni-chelate incorporated in a core of carboxylate dendrimer [354], which showed increased activity in ethylene oligo-

merization as compared to the homogeneous analogue. This MCD proves that, though rarely, but core-functionalized dendritic catalysts can be far more efficient than LMC due to isolation of a catalytic center.

Of substantial interest is synthesis of MCD used as contrast agents in MRI, which is highly efficient non-invasive diagnostic technique for visualization of organs and blood vessels [355–371]. MRI has a number of significant advantages, since it does not use ionizing radiation and provides 3D imaging with high spatial resolution and high contrast. For this purpose, most clinically approved MRI contrast agents are LMC-Gd(III), which have effect on relaxivity of protons of bound water (Fig. 4.53) [372].

Penetrating different organs, contrast agents cause a change in the rate of water proton relaxation by coordination to paramagnetic contrast agent, i.e. to Gd(III) chelates, which then brings to increase in their imaging contrast with respect to neighboring tissues. Gd(III)-based contrast agents can increase longitudinal T_1 as well as transverse T_2 relaxation rates of water protons, which include contributions from relaxation rates $(1/T_{1,2})_d$ without a contrast agent and relaxation rates $(1/T_{1,2})_p$ from a contrast agent. Increase in relaxation rate of water protons is related linearly to concentration of a contrast agent in the range of clinically significant concentration. Relaxivity $(r_{1,2})$ is determined as concentration-dependent increase in relaxation rate of water protons under action of the contrast agent in $mM^{-1}\ s^{-1}$ units:

$$(1/T_{1,2})_{obs} = (1/T_{1,2})_d + r_{1,2}[Gd]$$

The main properties necessary for Gd(III) MRI contrast agents are good biocompatibility (low toxicity), using in low doze, good elimination from a system, and high thermodynamic and kinetic stability. This brings to the fact that Gd(III) chelates are by more than 10 million times more contrast than ordinary MRI scanning. Among Gd(III) MRI contrast agents most widely used are Gd(DTPA)

Macrocyclic Gd(III) chelates:

Gd-DOTA (DOTAREM®)   Gd(HP-DO3A) (Prohance®)   Gd(DO3A-butrol) (Gadovist®)

Linear Gd(III) chelates:

Gd-DTPA (MAGNEVIST®)   Gd(DTPA-BMA) (OMNISCAN®)   Gd(EOB-DTPA) (EOVIST®)

Gd-BOPTA (Multihance®)   MS-325 (Vasovist®)
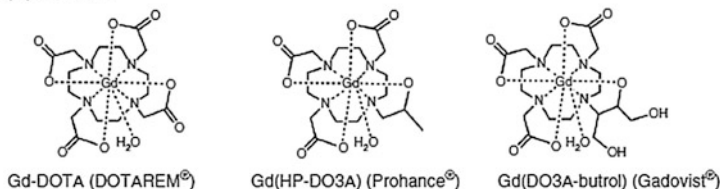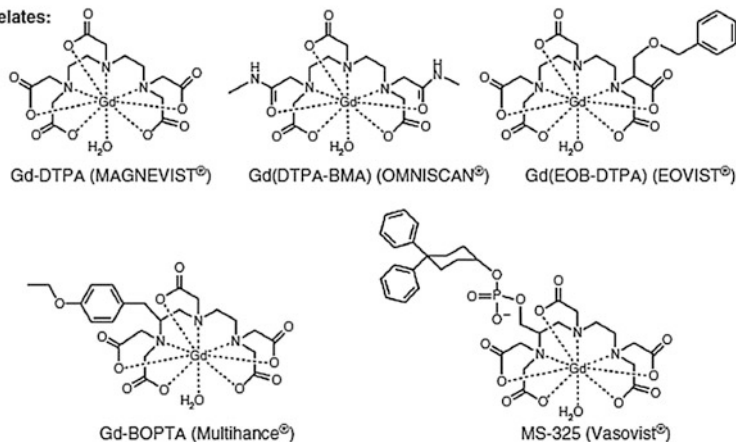
Fig. 4.53 Structures of the Gd(III)-based MRI contrast agents currently used in the clinical practice

and Gd(DOTA). Small size and monomer character of these agents, finally, impose limitation on resolution of images, which could be obtained both for enhancement of contrast and for pharmokinetics/biodispersion. Linking of LMC-Gd(III) to dendrimers increases considerably contrast and resolution of imaging due to their large sizes and ability to switch several Gd(III) chelate centers [373]. Moreover, dendrimer agents are profitable, because they are non-toxic, hydrophilic, are easily cleaned, are aggregation-stable, and have a controlled 3D polymer structure with several Gd(III) chelation centers. As compared to a small molecule of MRI agents, dendritic contrast agents provide high relaxivity and long retention in blood circulation. It should be also noted that dendrimers have many advantages as compared to linear polymers, including exact molecular structure and a great number of surface functionalities for linking of Gd(III) [374]. As a typical example, we consider one of numerous variants of linking of LMC-Gd(III) on PAMAM dendrimers [375].
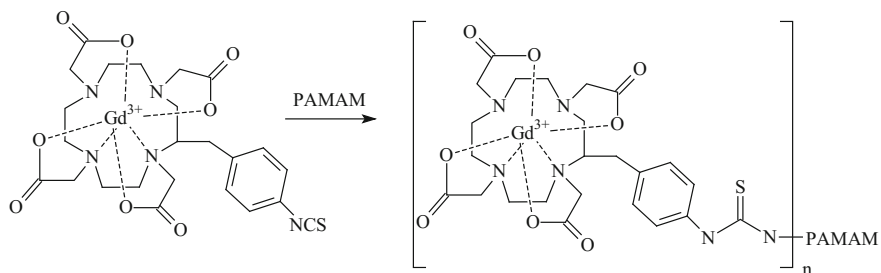
In particular, metal chelates were linked to G4, G5, and G6 PAMAM dendrimers with the ratios between chelates and dendrimers 28:1, 61:1, and 115:1, and molar relaxivity measured at pH 7.4, 22 °C and 3T were 29.6, 49.8 and 89.1 mM^{-1} s^{-1}, respectively.

It should be noted efficient methods of click chemistry for fixation of contrast agents on dendrimers (Fig. 4.54) [376, 377].

Dendrimer MRI contrast agents can be obtained using different dendrimers, for example, PAMAM [378], PPI [379, 380], PLL [381], etc. at that dendrimer Gd(III) chelates showed high relaxivity as compared with LMC. Thus, Gd-DTPA linked with G5 PPI dendrimers (M$_w$ = 51,000) had high r$_1$ relaxivity, 19.7 mM^{-1} s^{-1} per Gd(III)
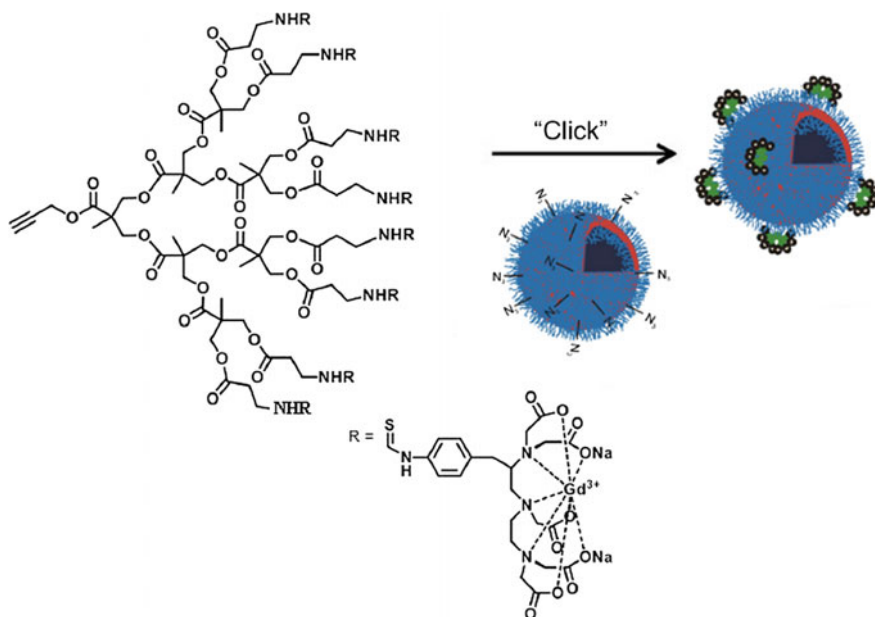
Fig. 4.54 Preparation of Gd(III) chelate functionalized dendrimers

ion (1.5 T, 20 °C), which was by 4.7 higher than Gd-DTPA [379]. Dendrimer based Gd(III) chelates are efficient for enhanced MRI contrast of kidneys, vessels, liver or a tumor [368, 382], and showed certain size-dependent pharmokinetic properties [383]. It is important that design of dendrimer-based contrast agents performed using respective generations and sizes are necessary for MRI.

We shall notice original MRI contrast agent called P792, which is Gd-DOTA compound substituted by hydrophilic arms [384].

Commercial applications of dendrimer contrast agents followed with Gadomer 17 dendrimer containing a core of trimesic acid linked with G2 PL dendron carrying 24 DTPA and 24 DOTA peripheral chelating Gd(III) groups, respectively [385–387]. The water-exchange rate was $1.0 \pm 0.1 \times 10^6$ s^{-1}, the value similar to measured value for other Gd-DOTA-monoamide complexes, and activation parameters were $\Delta H^{\neq} = 24.7 \pm 1.3$ kJ mol^{-1} and $\Delta S^{\neq} = -47.4 \pm 0.2$ J K^{-1} mol^{-1}. Interior flexibility of a macromolecule is characterized by Lipari-Szabo ordering parameter $s^2 = 0.5$ and time of rotational local correlation $\tau_1^{298} = 760$ ps, while time of global rotational correlation of the dendrimer is far longer $\tau_g^{298} = 3050$ ps. Analysis of proton relaxivities shows that interior flexibility is an important limitation factor for visualization of magnetic fields.

We should notice using convergent approach for production of Gd(III)-chelate-core dendrimers with branched-alcohol arms [388]. 1D amino-substituted dendrons of increased length and branching were linked to Gd(III)-DOTA-like chelate having a ligand with peripheral carboxylate groups. Disposition of Gd(III) ion in center of a dendrimer structure combines efficiently local motion of Gd(III)-OH$_2$ vector with rotation of a whole macromolecule, which results in increase in relaxivity [389].
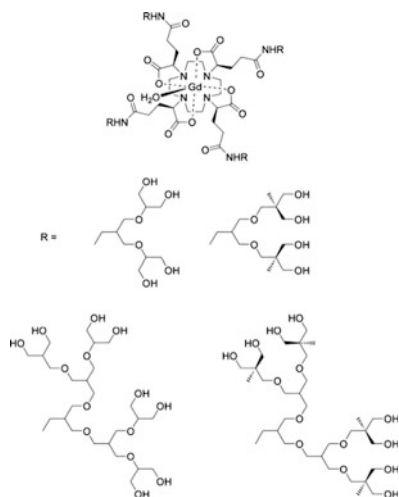
It is important to mention that behavior of dendritic Gd(III) contrast agents in vivo depends on modification of dendrimer properties, such as size [380, 390], chemistry of a core [391], and outer shell [392].

Among metal chelate dendrimers, MCD with M-Pp and M-Pc fragments are most extensive studied [393]. First messages about M-Pp and M-Pc dendrimers appeared in early days of dendrimer chemistry due to morphological similarity between these polymers and natural hemoproteins [378, 394].

Of interest are dendrimers containing Zn(II)-Pp and four *meso*-(tetra-*n*-hexyl-truxene) or -(tris-tetra-*n*-hexyltruxene) which showed increase in fluorescence and phosphorescence of the central M-Pp and abrupt quenching of emission of a dendron by S_1 and T_1 energy transition (Fig. 4.55) [395]. Transfer rates of singlet energy (k_{ET}) calculated by a change in lifetime of fluorescence of donors (mono- and tris-truxenes) in presence and in absence of acceptor (Zn(II)-Pp) are equal to 1.2 and 0.74 ns^{-1} at 298 K, and 2.6 and 1.2 ns^{-1} at 77 K, respectively. These slow rates are easily associated with weak orbital overlapping between truxene and the Zn(II)-Pp π-system.

Based on Zn-Pp as a core, a double layer-type MCD is obtained with Cz as outer layer and phenylazomethine as inner layer of dendrons using Ullmann dehydration reaction in presence of TiCl$_4$. Combination of both blocks provides thermally stable shell, for which temperature of 10% weight loss was more than 550 °C. This MCD is excellent hole-transporter in an OLED device with processability increasing with a generation increase (Fig. 4.56) [396].

It should be noted shape-stable carbosylane-functionalized M-Pp type Zn(II)-tetraphenyl-Pp(4-SiRR′Me)$_4$ (R and R′ = Me, CH$_2$CH=CH$_2$, CH$_2$CH$_2$CH$_2$OH) and Zn(II)-tetraphenyl-Pp(4-Si(C$_6$H$_4$-1,4-SiRR′Me)$_3$)$_4$ (R and R′ = Me, CH$_2$CH=CH$_2$), obtained by Lindsey condensation [397]. In this case, a number of M-Pp dendrimer structures were determined by X-ray diffraction analysis.

G1 and G2 Zn-Pp core dendrimers with triarylamine as a dendron were synthesized by Ullmann coupling reaction [398], for which differentiation of oxidation site of dendrimers is shown. For example, oxidation potential of Zn-Pp ring shifts

Fig. 4.55 Space filling model and scheme of light-harvesting, energy transfer and emission in truxene-Zn-Pp
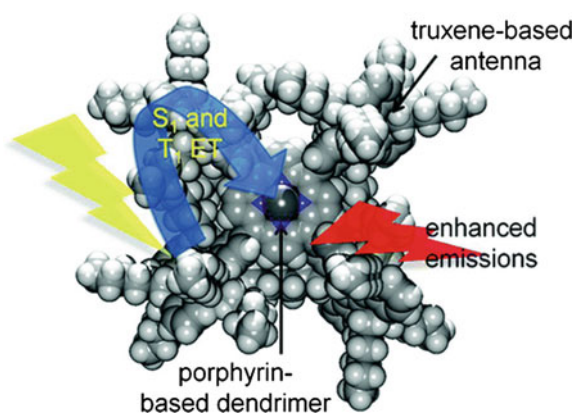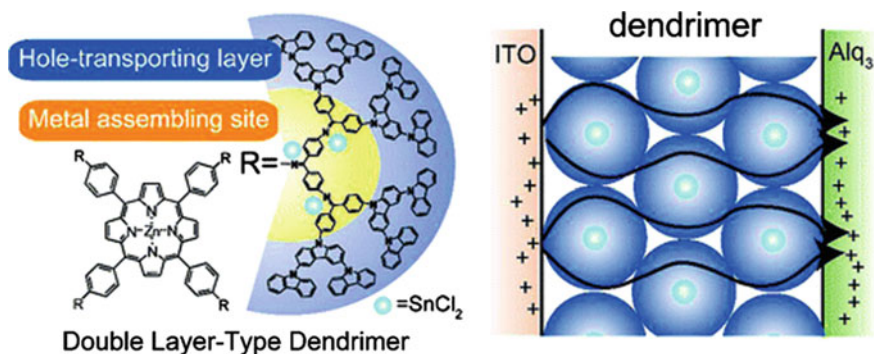
Fig. 4.56 Structure of double layer-type MCD

cathode-likely for G1 dendrimer, since periphery of dendrons has strong electron donor groups. At the same time, G2 dendrons are first oxidized and create an atmosphere of eight positive charges, and Zn-Pp core rings then oxidize with anode shift of potential in connection with electron acceptor effect of oxidized substituents.

Aryl ether dendrimers with M-Pp core are developed for using in PDT because of their potential for production of singlet oxygen under irradiation with light [399]. At that, aryl ether dendrimers with two types of peripheral groups are obtained: quaternary amines providing positive charge (+)Zn-Pp or carboxylate groups suggesting negative charge (−)Zn-Pp. Efficiency of $^1O_2$ generation of these Zn-Pp dendrimers was compatible with protoporphyrin IX, which is a low molecular photosensitizer used as a standard compound for comparison. At the same time toxicity of (+)Zn-Pp and (−)Zn-Pp in darkness was just 1% from toxicity of protoporphyrin IX.
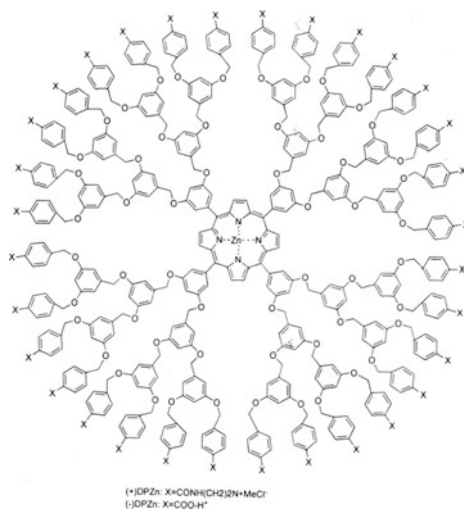
For similar medical purposes derivatives of M-Pp with 32 carboxyl terminal groups [400] or of primary amines [401] were obtained. These dendritic sensitizers show very low dark cytotoxicity and effective absorption by malignant cells, thus providing prominent therapeutic MCD.

Pd-Pp dendrimers based on Pd-*meso*-tetra-(4-carboxyphenyl)-Pp and on Pd-*meso*-tetra-(4-carboxyphenyl) tetrabenzo-Pp carrying sixteen carboxylate groups at periphery are soluble in physiological media, and in vivo studies showed oxygen distribution in a subcutaneous tumor growing in rats [402].

Using this synthetic strategy, functionalization is executed of phosphorescent Pt-Pp oxygen sensors by carboxylate terminal groups and fluorescent coumarin derivatives working as two-photon absorbing antenna [403]. It is assumed that dendritic arms play several roles, including shielding of Pp core, total solubility of the compound in water and structural support between a core and phosphorescent two-photon absorbing antenna.

PET is observed for snowflake-like MCD with Zn-Pp core and anthraquinonyl terminals, which have four rigid ethynyl-en-phenylene conjugated chains covered with soft branches of benzyl ether [404, 405].
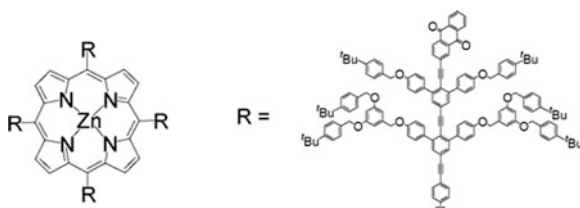
It is interesting that a considerable increase in rate constants of energy transfer under action of dendrimer architecture is observed («dendrimer effect»). This is explained by hydrophobic interactions between flexible benzyl ether chains in a dendrimer, which results in significant conformation changes in coplanar forms between the Zn-Pp plane and ethynyl-en-phenylene anthraquinone plane.
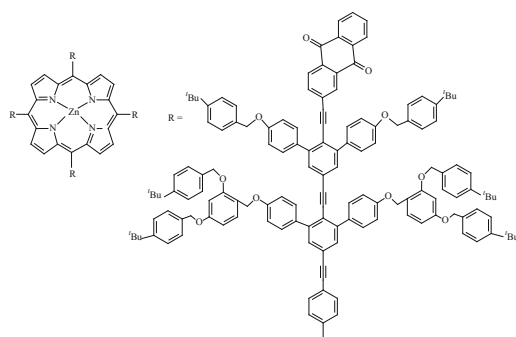
Dendritic Zn-Pc with ionic peripheral groups is obtained by template method from G2 dendritic phthalonitrile and Zn(OAc)$_2$ with addition of a few drops of

DBU [406, 407]. The following hydrolysis of fragments of external ethers brings to anionic Zn-Pc dendrimer.

Poly(ethylene glycol)-poly(L-lysine)
block copolymer (PEG-PLL)

anionic dendrimer phthalocyanine (DPc)
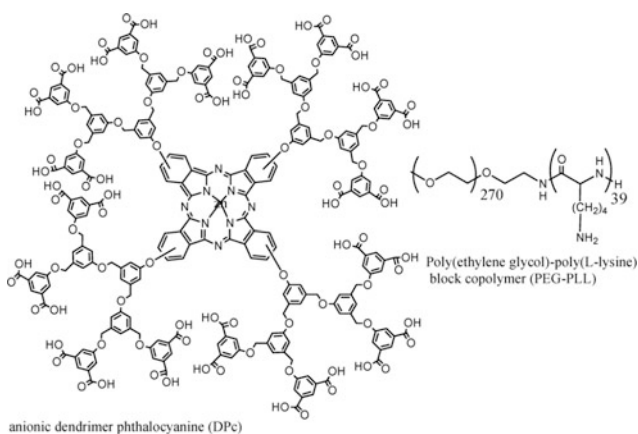
Of interest is Zn(II)-Pc containing four poly (aryl benzyl ether) dendritic substituent with terminal cyano groups does not aggregate completely in organic solvents, and with terminal carboxylic groups it decreases a tendency of aqua-aggregation with increase in dendron size [408].

In 1,4-dipegylated Zn(II)-Pc α-position of methyl ether of PEG chains is responsible for red shift of Q-band absorption and less aggregation in solution [409].

Similarly, MCD with ionic peripheral groups are obtained, in which M-Pp center is surrounded with poly (benzyl ether) G3 dendrons. In these dendrimers M-Pp core is spatially isolated aryl ether dendrimer framework, and they are interesting for their hydrophilic properties [410–412]. It is important that these M-Pp dendrimers provide high efficiency of production of singlet oxygen even at high concentration, because dendritic environment prevents aggregation of M-Pp center. Besides, peripheral character of ionic dendrimers can be modified with different functional groups providing solubility in water and practical functions, for example, as biomedical nano-devices.

A purposeful synthesis of MCD with Zn-Pp core linked to mono- and tetra-substituted benzyl aryl ether dendrons is performed in order to increase solubility [413].

Of practical interest are water-soluble MCD consisting of a central fragment Zn-Pc and dendritic wedges with terminal carboxylate groups [414]. The greatest polyelectrolyte includes 32 negative charges on the dendrimer surface. Strong correlation between a degree of dendritic environment, aggregation degree, and a capacity of singlet oxygen generation in aqueous media was observed. Functionalization over outer rim also considerably improves ability of Pc to photosensitize singlet oxygen as compared to dendrimers with axial ligation.
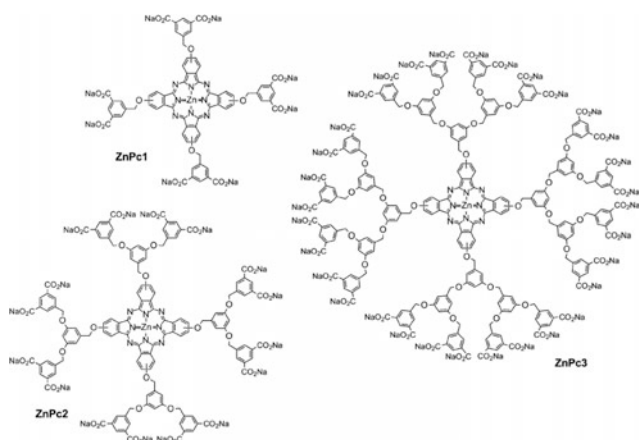
M-Pp are promising structural blocks for building of nano-sized architectures having excellent light-harvesting and photoinduced electron/energy transfer properties [415–419]. In the recent years, much attention is given to molecular assemblies with participation of M-Pp and macrocyclic receptors [279, 420]. For example, based on M-Pp, covalently bound M-Pp fullerene diads are obtained integrated into dendritic framework, which are units of PET including charge separation (Pp^+-C_{60}^- state) from M-Pp to C_{60}. Dendrons containing Zn-Pp units on branches and C_{60} in focal point shows Cope band, which becomes wider from 1 Zn-Pp-C_{60} to 3 Zn-Pp-C_{60}, and then to 7 Zn-Pp-C_{60} (a difference in FWHM is 54 cm^{-1}). Therefore, increase in generation points to electron interaction between Zn-Pp fragments in 7 Zn-Pp-C_{60}, and quenching fluorescence appears from Zn-Pp block to the focal point with formation of Zn-Pp^+-C_{60}^-. The process of reverse electron transfer, as has been shown, is retarded [421].

We shall also note a system, in which Zn-Pp fragment is bound with a fullerene via metal-free Pp [422].
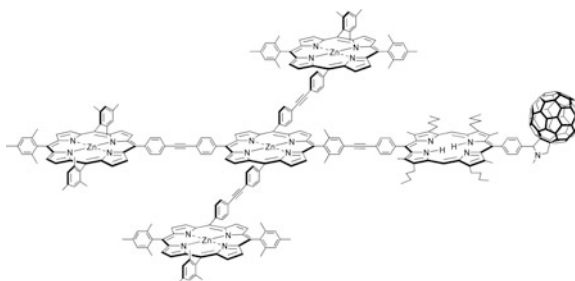
Several diads M-Pp-C_{60} are built successfully on a dendrimer surface [423, 424]. Thus, for example, on a dendrimer surface a light sensitive layer is collected with spatially separated sets, consisting of 6, 12, or 24 Zn-Pp units bound by bpy fragments carrying several (1–3) fullerene blocks (Fig. 4.57) [424]. The M-Pp-C_{60}
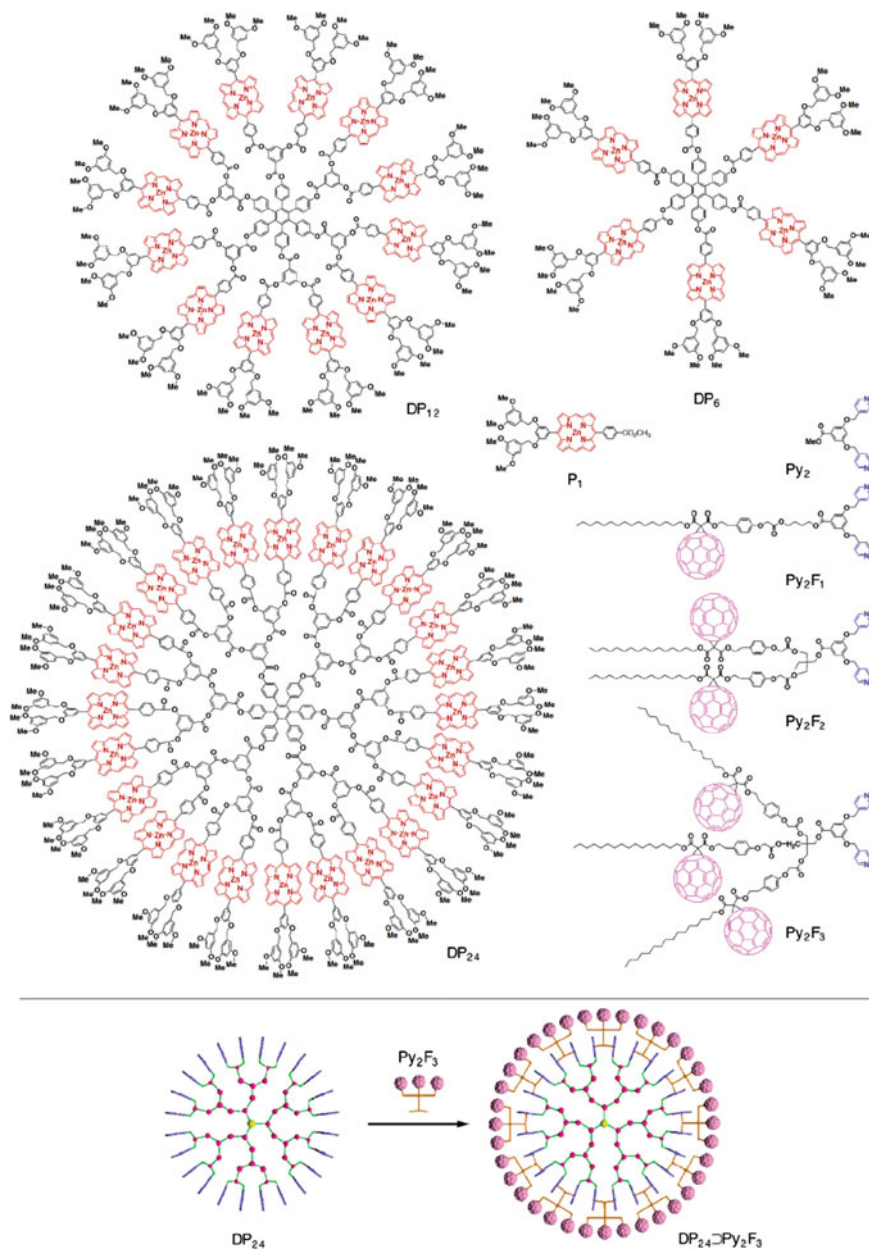
Fig. 4.57 Molecular structures of Zn complexes of multiporphyrin dendrimers DP_m (m = 6, 12, and 24), fullerene-appended bpy ligands Py_2F_n (n = 1 − 3), and reference compounds P1 and Py_2, and schematic representation of the complexation of DP_{24} with Py_2F_3

diads are quite stable: K (is average affinity of linking) = $1.1 \times 10^6 - 4.4 \times 10^6$ M^{-1}, and it occurs possible to visualize clearly structure of petals, as is shown in Fig. 4.63, for the diad consisting of 12 Zn-Pp blocks and 3 fullerene blocks. Photo-excitation of Zn-Pp fragments brings to transfer of electrons from Zn-Pp to C_{60} for generation of charge separation. The rate constant of charge separation increases from 0.26×10^{10} to 2.3×10^{10} s^{-1} as a number of Zn-Pp fragments to C_{60} blocks increases, while the rate constant of charge recombination remains almost unchanged in the range $4.5–6.7 \times 10^6$ s^{-1}.

The Zn-tetraphenyl-Pp dendrimer is obtained shaped as a snowflake containing peripheral C_{60} groups [425]. Rigid covalent bond of C_{60} linked through phenylethynyl fragments brings to considerable quenching of Zn-Pp fluorescence, mainly, because of energy transfer from Zn-Pp core to C_{60} terminal. Comparison of efficiencies of energy transfer with the similar dendrons exhibits that dendritic structures substantially retard the energy transfer rate.

X: R = C_{60}H   Y: R = Ph
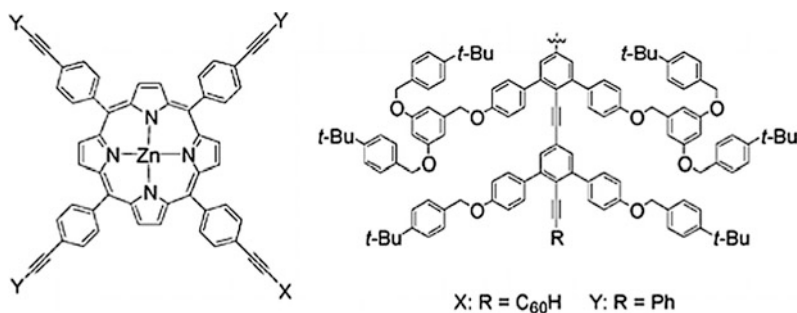
Of interest is water-soluble nanorod synthesized by self-assembly of C_{60} and two-sided Zn-Pp with four protruding β-CD on each side [426, 427], forming well-defined stable M-Pp nanowires, in which individual monomers do not aggregate through π-π-interactions [427].

Combination of MCD and carbon nanotubes in one object is very promising [289, 290, 428, 429]. It is interesting that these two nano-objects, independently from each other, are a popular subject for many studies, but their association is still not properly studied. For example, treatment of preliminary prepared Sn-Pp dendrimer with succinic acid and excess of Ag_2O leads to oligomerized dendrimer (tetramer and dodecamer with the respective molecular weights 23,000 and 72,600), whose amount to great extent depends on concentration of the reaction mixture, which is increased by the solvent evaporation (Fig. 4.58). It is important that the oligomer is immediately treated by Ru Grubbs catalyst for apparent increase in molecular weight with time. After the exchange reaction with the following metathesis reaction, the formed rod dendrimer is subjected to interaction with NaOMe for M-Pp core liberation and generation of real nanotubes (with «empty» interior) [430].

Fig. 4.58 Assembly of M-Pp dendrimers, then polymerization of the terminal alkene groups to rigidify the nanotube. The M-Pp can be removed by reaction with NaOMe to afford a real nanotube

As an example of covalent functionalization of MWCNTs with dendrimers, we shall consider click chemistry grafting Zn-Pp dendrons to triple bond of carbon nanotubes, preliminary functionalized by ethynyl aniline (Fig. 4.59). Appreciably strong electronic coupling between the photo- and electroactive constituents (i.e., MWCNT and Zn-Pp) led to rapid excited-state deactivation of Zn-Pp via charge transfer to the nanotubes. Upon selective photoexcitation of this nanostructure, formation of reduced carbon nanotubes and oxidized Zn-Pp is observed [431].

From the point of view of coordination chemistry, a considerable interest is given to M-Pp dendrimers with peripheral chelating fragments. As typical example, we note Zn-Pp dendrimer containing bpy units on peripheral ends of both conjugated and alkyl side chains [432]. Three terminal bpy fragments on both ends are linked with Fe(II) ions forming 1:2 complexes, which induces a great conformation change in alkyl side chains, and has a moderate effect on axial coordination of Zn-Pp core by imidazole ligand.

Fig. 4.59 Zn-Pp dendrons covalently linked to single-walled carbon nanotubes
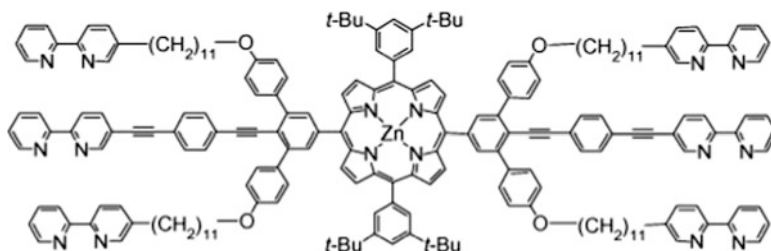
It should be noted a range of dendritic phenylazomethines based on Zn-tetraphenyl-Pp core, whose imine fragments can coordinate metal ions with formation of heteropolymetal structures (Fig. 4.60) [433, 434].

It is interesting that G4 dendrimer with Zn-Pp core has a sphere-like structure in the 1-nm scale ($R_h = 22$ Å) and works as a reservoir of metal ions for $SnCl_2$ and $FeCl_3$. Besides, LbL complexation on interior imines near the core towards the surface is
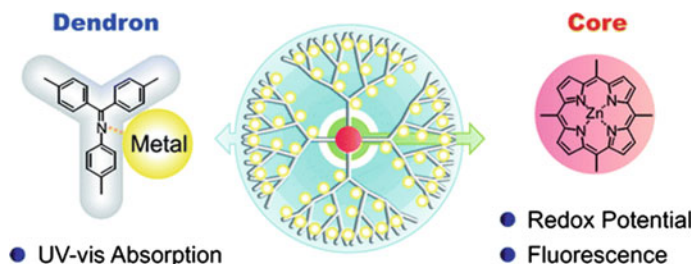
Fig. 4.60 Structure of G4 phenylazomethine dendrimers containing Zn-Pp core
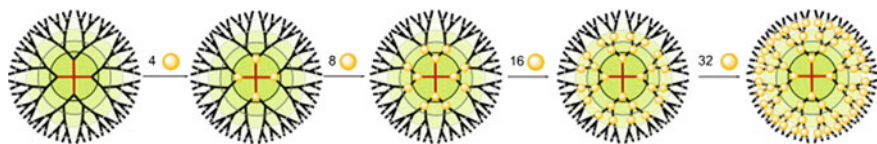
Fig. 4.61 Scheme of stepwise radial complexation of Zn-Pp-phenylazomethine G4 dendrimers with metal ions

observed and a dendrimer can link up to 60 molar amounts of metal compounds around the M-Pp core (Fig. 4.61). Fluorescence and redox behavior of the Zn-Pp core in the polymetallic dendrimers also confirm stepwise complexation with a metal ion. Thus, metal complexes in dendrimer architecture have a strong effect on electronic state of M-Pp core. The results indicate clearly very fast electron transfer between a core and incorporated metal complexes on sub picosecond time scale.

Similar inner-sphere coordination is found also in other phenylazomethine dendrimers, including those containing Co(II) and Co(III)-Pp cores [435]. At the same time, recently [436] inversion of the sequence caused by change a position of a substituent in phenylazomethine group from *para-* to *meta*-position was found (Fig. 4.62).

Due to using of semi-rigid dendritic phenylazomethine units, polymer nanocavities are designed for cooperative identification of a certain recognition of molecular aspect (size, contour shape, flexibility, and specific groups) of big guest molecules (as a rule, more than 1 nm) in wide 3D nanospace [437]. Conformationally fixed complex with the best position of a guest is described by 3D molecular-modeling based model. It is interesting that imitated structure of the cavity also predicts catalytic selectivity of Ru-Pp core, showing high shape-stability and wide applicability of the cavity.
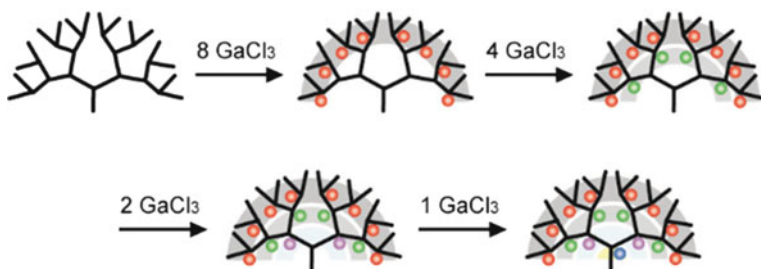
Fig. 4.62 Stepwise radial complexation from the outer layer to the inner layer
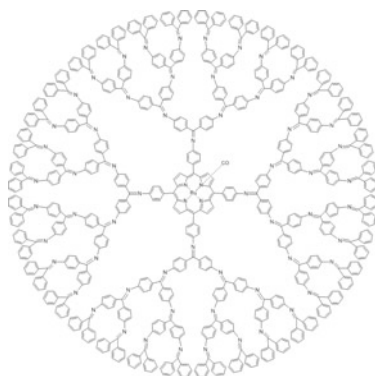
Apart from divergent and convergent synthesis for production of MCD, click chemistry methods are actively used [282, 306, 438–440]. In particular, CuAAC was applied to M-Pp synthesis to prepare sophisticated architectures and complex molecules with different applications. For example, water-soluble dendrimer like star-branched PEO G2 and G3 having Zn(II)-tetraphenyl-Pp units in the core and in each branching point were synthesized through the convergent approach using click chemistry [441]. At the first, four-arm star-like PEO is synthesized using CuAAC between Zn(II)-5,10,15,20-tetra(propargyl-oxyphenyl)-Pp core and α-azido PEO branches. Then, four-arm PEO star carrying Zn(II)-5-(4-phenoxy)-10,15,20-tris (propargyl-oxyphenyl)-Pp at each end of the branch is obtained using the divergent method through etherification reaction of Williamson type. By repeating of these two stages, high molecular weight G3 dendrimer-PEO carrying 36 ω-OH PEO terminal branches with uniform distribution of 17 Zn-Pp fragments as inner branching points was prepared. Obtained MCDs with poly (Zn-Pp) fragments showed their efficiency in singlet oxygen generation in organic or aqueous medium.

Of interest are dendritic Zn-Pp containing Cz units on terminals prepared via click-reaction of azide-substituted Zn-Pp precursors and Cz-based alkynes in presence of [Cu(NCCH$_3$)$_4$][PF$_6$] as a catalyst [442]. These M-Pp dendrimers exhibit double luminescence from the uppermost S$_2$ and the lowest S$_1$ singlet states. Spectral and photophysical properties of the MCDs can be regulated by a *meso*-spacer between a macrocyclic core and dendritic shell. The key feature of the *meso*-spacer is a degree of difficulties to rotation of aryl ring with respect to the midplane of M-Pp. In particular, dendrimer architectures with four steric hindered *meso*-aryl spacers are most appropriate for control over the processes related to axial coordination of a dendrimer core.

Using Cu-catalyzed cycloaddition of dendritic azides and end acetylene fragments linked to Zn-Pp core through 1,2,3-triazole units, a series of dendritic Zn-Pp with benzyl ether dendrons is synthesized functionalized (Fig. 4.63) [443]. Stable axial ligation with additional monofunctional ligands takes place on Zn-center, and
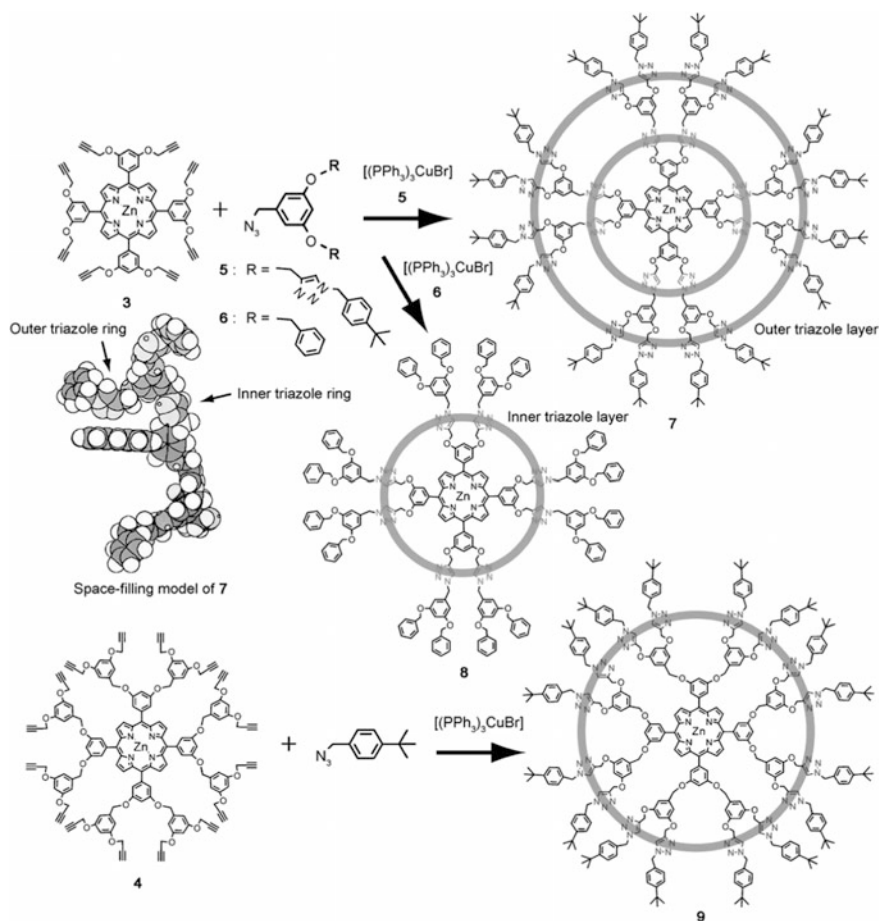
Fig. 4.63 Synthetic approach to a series of triazole-linked dendritic Zn-Pp

stability of the complex substantially depends on spatial position of 1,2,3-triazole units in dendritic Zn-Pp.

It should be noted that in the MCDs obtained using click-synthesis from AB$_2$- and AB$_4$-type multitopic Zn-Pp reversible self-assembly into short oligomers (2–6 units in length) through intermolecular Zn-Pp-triazole coordination is observed [444]. This is an example of successful combination of supramolecular and polymer chemistry for development of functional nanostructured materials. It is important that association constant of Zn-Pp triazole complexes can be increased by two orders of magnitude by varying length and density of grafting of polymer arms. Besides, self-assembly leads to an increase in T$_g$ by 6 K with respect to non-assembled dendrimers.

Series of special G1, G2, and G3 pair-dendron systems based on Zn(II)-tetra-*meso*-aryl-Pp polyimides designed on dimethylxanthenebis(Zn(II)- or Cu(II)-Pp)

central core were synthesized using click chemistry [445]. Dendrons work as acceptors or donors of singlet or triplet energy depending on nature of dendrimer systems. For example, presence of paramagnetic d^9 Cu(II) ion in dendrimers accelerates transfer of singlet-triplet energy from Zn(II)-tetra-*meso*-aryl-Pp to bis (Cu(II)-Pp) unit and slow transfer of triplet-triplet energy from the central bis(Cu (II)-Pp) unit to peripheral Zn(II)-tetra-*meso*-aryl-Pp. When bis(Zn(II)-Pp) is a central core, folding of the chain is observed, which unambiguously confirms transfer of triplet-triplet energy into heterobimetallic system, because such process can take place only at short distances.

Of interest is using click chemistry for the production of poly-Pp dendrimers including Pp core and different peripheral Pp, in which there is a logical gradient of transfer of energy or electrons between Pp units [446]. For example, excitation energy transfers to the core under visible light irradiation in the system consisting of central metal-free Pp and peripheral Zn-Pp acting as ancillary light absorbers. A series of similar dendrimers has been expanded by including Mg-Pp or Sn-Pp as chromophores. It should be noted that light-induced electron transfer becomes possible due to incorporation of Au(III)-Pp$^+$ into the massif, in particular, in three-level dendrimer containing Au-Pp$^+$ core, inner layer of four blocks of metal-free Pp and outer layer including 12 residuals of Zn-Pp. In such system irradiation in peripheral Zn-Pp brings to highly efficient electron energy transfer to the metal-free Pp with the following charge transfer to the central Au-Pp$^+$.

Water-soluble Zn-Pc dendrimers containing terminal triethylene glycol fragments as water solvating groups are obtained using CuAAC [447]. It is interesting that a non-peripherally substituted dendrimer is far less aggregated in water than its peripherally substituted isomer.

We note highly efficient oriented transfer of excitation energy reached using multipophyrin massifs [448], which are important for understanding energy migration in photosynthesizing organisms. At the same time, such massifs should have some important attributes, which imitate natural light-harvesting synthesis, i.e. organic solubility, architectural hardness, and a possibility of integration of various M-Pp and metal-free Pp into the system [449]. This massif is obtained, for example, with use of tetraaryl-Pp carrying peripheral iodine groups, which are then linked with Zn-Pp through homogeneous Pd-indirect coupling reaction [450]. Fluorescent spectrum of multi-Pp massif shows irradiation of a core of metal-free Pp, while emission yield of peripheral Zn-Pp decreases by 12 times as compared with respective monomer Zn-Pp. In this system energy transfer from peripheral Zn-Pp to the core of metal-free Pp proceeds with about 90% yield (Fig. 4.64).

A method is developed of stepwise building of shape-persistent assemblies using snowflake-shaped dendrimers as key modular blocks. The Sonogashira coupling reaction of A$_3$B type Zn-Pp with A$_4$-type metal-free Pp gives a cross-shaped covalent assembly **1** [451]. It is important that the distance between the terminal phenyl group and the diagonal phenyl group is approximately 12 nm and intramolecular singlet energy transfer from peripheral Zn-Pp core to a metal-free Pp core was observed.
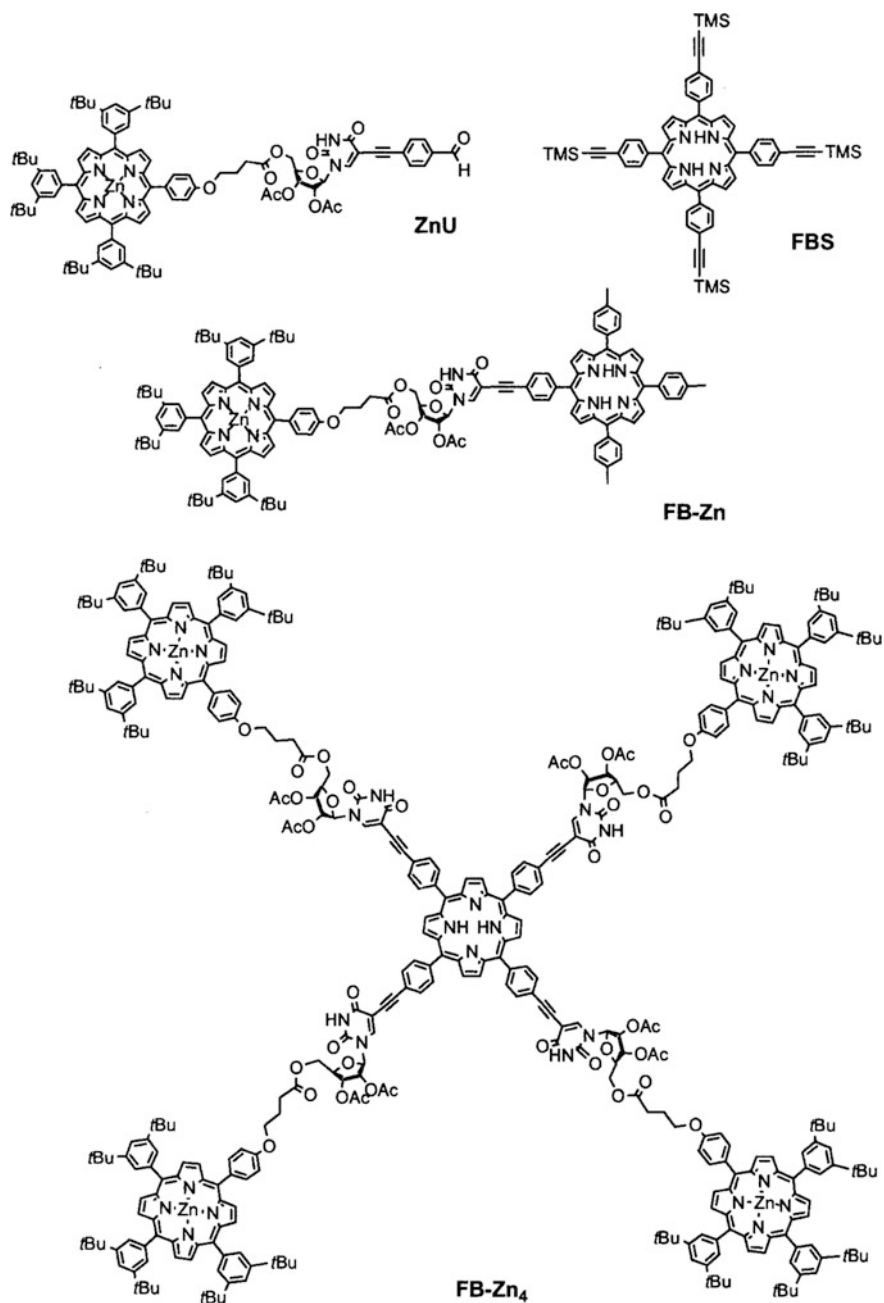
Fig. 4.64 The structures of the component models Zn-Pp and metal-free Pp, the dyad and the pentad
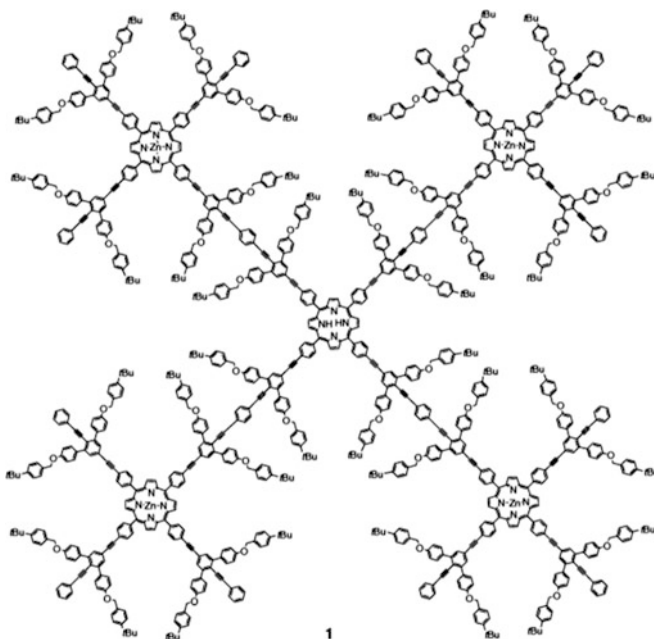
Studies these poly-Pp dendrimers showed their high efficiency in accumulation and transfer of light energy. In particular, there is almost 100% light energy transfer from four excited Zn-Pp fragments to a core of metal-free Pp. These properties determine good prospects of application of poly-Pp dendrimers in molecular electronics.

Such synthetic method is applied also for MCD production containing metal-free Pp core rigidly conjugated with phenylethynyle chains and terminal Zn-Pp blocks (Fig. 4.65) [452]. This dendritic M-Pp functions as light-harvesting antenna and has efficient singlet-energy transfer from end M-Pp fragments to metal-free Pp core.

Of interest is light-harvesting antenna consisting of three different Zn-Pp sets with a different number of ethynyle groups in their *meso*-positions [453]. Such antenna exhibits intense absorption in the visible spectrum up to 700 nm, energy transfer of the singlet-excited-state from peripheral M-Pp to central M-Pp with >90% efficiency and rate constants approximately 10^{10} s^{-1}.

We should notice that π-electron conjugation is not necessary for simplification of long-distance energy transfer: fast ($k_{ENT} = 1.04 \times 10^9$ s^{-1}) and efficient ($\Phi_{EXT} = 71\%$) energy transfer from 28 photoexcited Zn-Pp units to focal metal-free Pp block takes place in a big star-shaped dendritic multiporphyrin massif, in which chromophore units are bound through flexible ether groups [454].

It has been shown that four dendritic Zn-Pp wedges do not work individually, but cooperate completely in a large multi-Pp massif, thus making easier migration and energy transfer (Fig. 4.66) [261].

Ar = 3,5-di-*tert*-butylphenyl
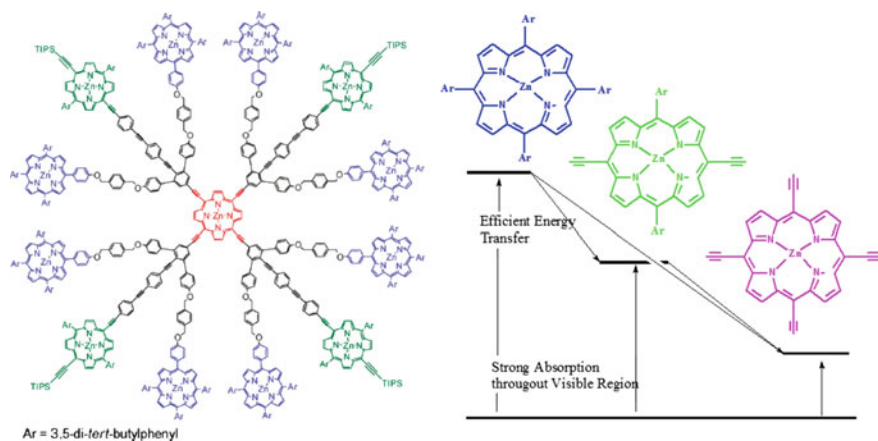
Fig. 4.65 Chemical structure of light-harvesting antenna

In other interesting example [455], dendron growth based on reactions of nucleophilic aromatic substitution of AB_2 monomers based on *meso*-dichloro pyrimidinyl substituted Pp, goes to G2 dendron. This convergent strategy of synthesis is applied to stepwise introduction of different metals into the following generations. In particular, three different metals (Pt, Zn, and Ni) can be integrated into hepta-Pp G2 dendron bringing to heterometallic Pp dendrimers.
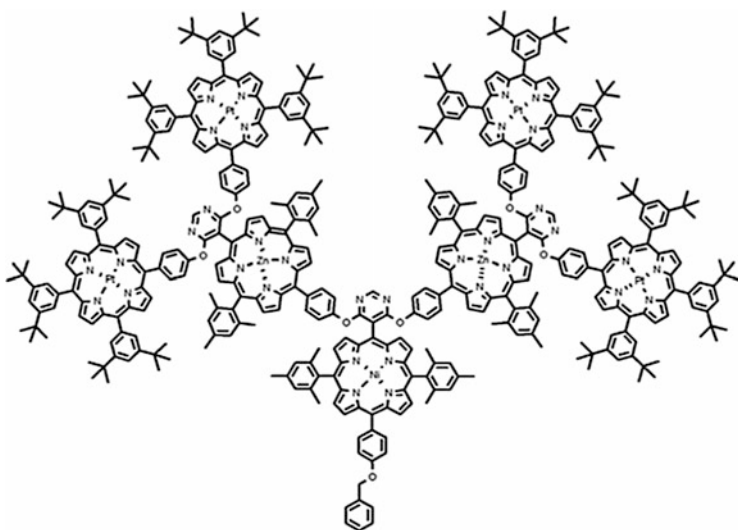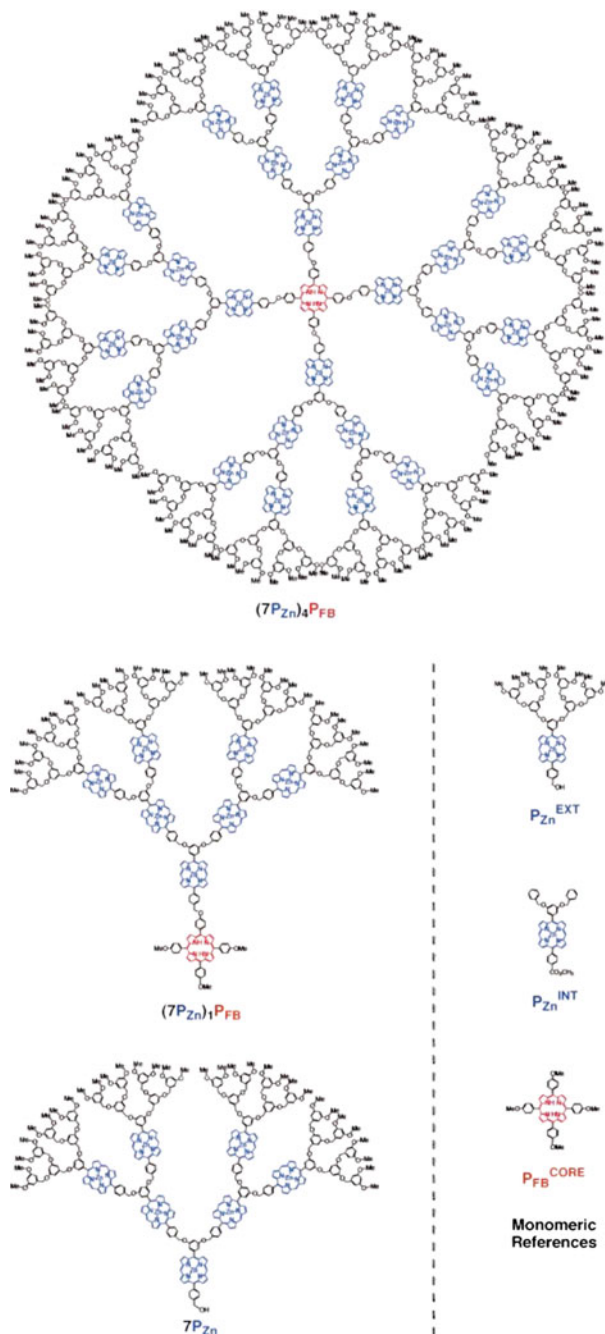
Fig. 4.66 Multiporphyrin array consisting of dendritic wedges of a Zn-Pp as the energy-donating units which are anchored by a focal free-base Pp unit which functions as the energy acceptor

We shall notice big hetero-massifs, such as hetero-dendrimers with terminal M-Pp and M-Pc core [456], which show interesting photophysical properties, i.e. wide absorption spectrum and energy transfer of excited singlet state from M-Pp to M-Pc core. Thus, synthesis of similar M-Pp-M-Pc dendrimers is fulfilled, in which four M-Pp fragments are covalently bound with M-Pc core through phenyl spacers. They show similar features with Pp-Pc diads in that they absorb in blue and red ranges and show fast, efficient energy transfer from M-Pp fragments to M-Pc core [457].

Poly (benzyl ether) dendrons were successfully linked to axial position, in order to obtain Rh(III)-Pp dendrimers G1, G3-G5 [458]. When excited by visible light, in CO atmosphere there is homolysis of alkyl-Rh bond with formation of respective acyl-Rh bonds, and rate of dendrimer consumption depends on a generation number of a dendron block. In particular, G5 dendrimer carrying the biggest dendron block is far less than others subjected to photochemical reactions, which is manifestation of the «dendrimer effect».
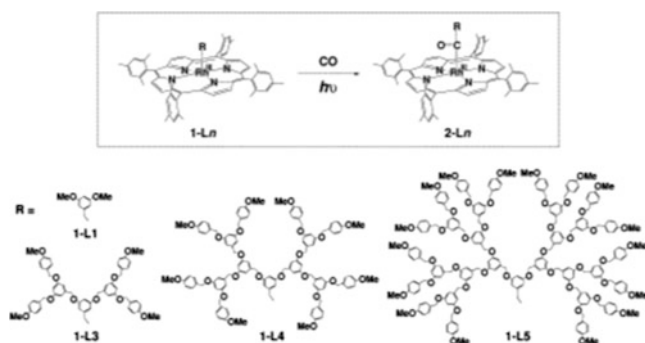
MCD can also be used in the interesting guest-host systems. For example, a range of non-symmetric Zn-Pp-containing dendrimers with benzyl ether type dendritic substituents are obtained, which are pocket MCD, because they contain dendritic wedges on three sides of M-Pp left a fourth side free of guest molecules for coordination with a metal center and formation of the guest-host system (Fig. 4.67) [459, 460]. When diamidopyridine moiety was introduced into the Zn-Pp dendrimer pocket, a thymine derivative was bound through complementary hydrogen bonding. Two different kinds of substrates, pyridine and thymine derivatives, were simultaneously accommodated in the nanoscale pocket and bimolecular guest accommodation was realized with the designed Zn-Pp dendrimer receptor.

Of interest is using M-Pp dendrimers as sensors of small heterocyclic substrates: 1,4-diazabicyclo[2.2.2]octane, Py, imidazole, N-methyl imidazole and 1,2,3-triazole [461]. Binding property of M-Pp receptors with respect to mono- and bidentate N-containing substrates depends on a nature, amount and generation of a dendrimer. In this case, axial ligation is accompanied by distinct and easily identified signal in spectra of reaction mixture.
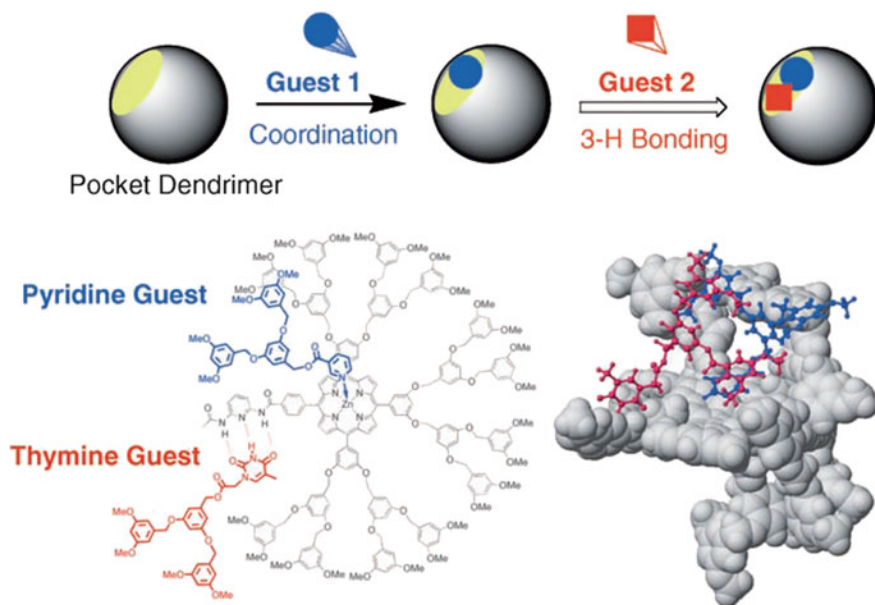
Fig. 4.67 Bimolecular guest accommodation with pocket dendrimer: zinc coordination plus complementary hydrogen bonding
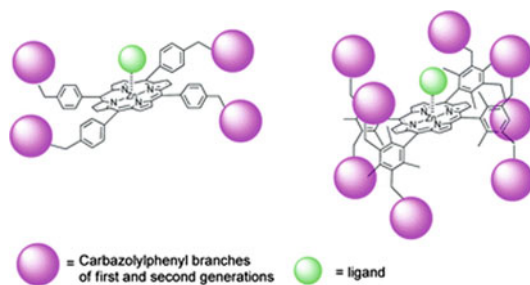
Using convergent synthetic strategy, pyridine-containing dendrons are obtained and then collected on a core through axial ligation of a metal center [462]. It is important that growing shell of oligo-ethylene glycol chains around the Ru-Pc lipophilic core provides MCD solubility in water. The obtained MCDs are strongly

phosphorescent and for them microenvironment-switchable singlet oxygen generation is typical. For example, M-Pc can generate singlet oxygen in such weakly polar media as $CHCl_3$ or THF, while generation of singlet oxygen in water is almost completely switched off.

It should be noted similar Ru-Pc and naphthalocyanines, axially ligated by dendronized pyridine ligands, which have high solubility in different solvents and exhibit spectra of solid state absorption comparable to the data obtained in diluted solution, that makes them interesting candidates for optical filtration in visible spectral range [463].
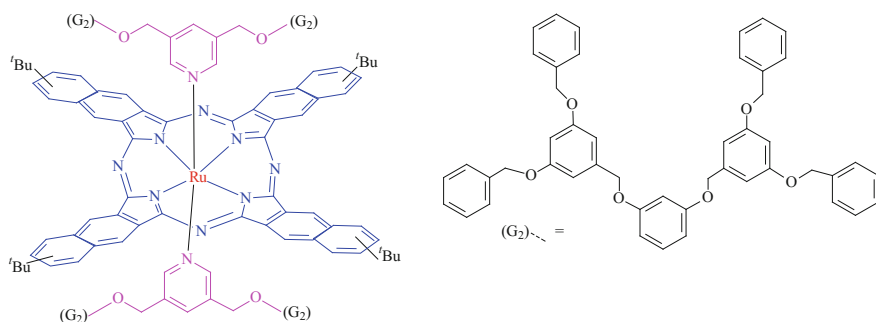
MCM are convenient initial structural blocks for synthesis of hyperbranched polymers [464]. For example, we note star-shaped polymers with linked Cz fragments and Zn-Pp core produced using ATRP method of St and methacrylate monomers (Scheme 4.42) [465]. It is interesting that two star-like homopolymers in solid state show red light emission, while the star-like copolymer exhibits blue light emission.

It should be noted production of hyperbranched π-conjugated light-emitting polymers containing Ir complex as a branching core and polyfluorene or poly (fluorene-*alt*-Cz) as branched fragments using Pd-catalyzed Suzuki polymerization [466]. In this case, FRET is observed in PL spectra of thin films, while no noticeable characteristic absorption and PL of Ir complex was detected in diluted solutions. EL spectra of the polymers showed typical emission of Ir complex with respective CIE coordinates (0.67 ± 0.01, 0.31). Thus, hyperbranched conjugated architectures can be promising strategy of molecular design of efficient electrophosphorescent light-emitting polymers.

Of interest is studying star-shaped polymers based triphenylamine-based Ir(III) dendritic complex with orange-emitting core and poly (9,9-dihexylfluorene) chains,
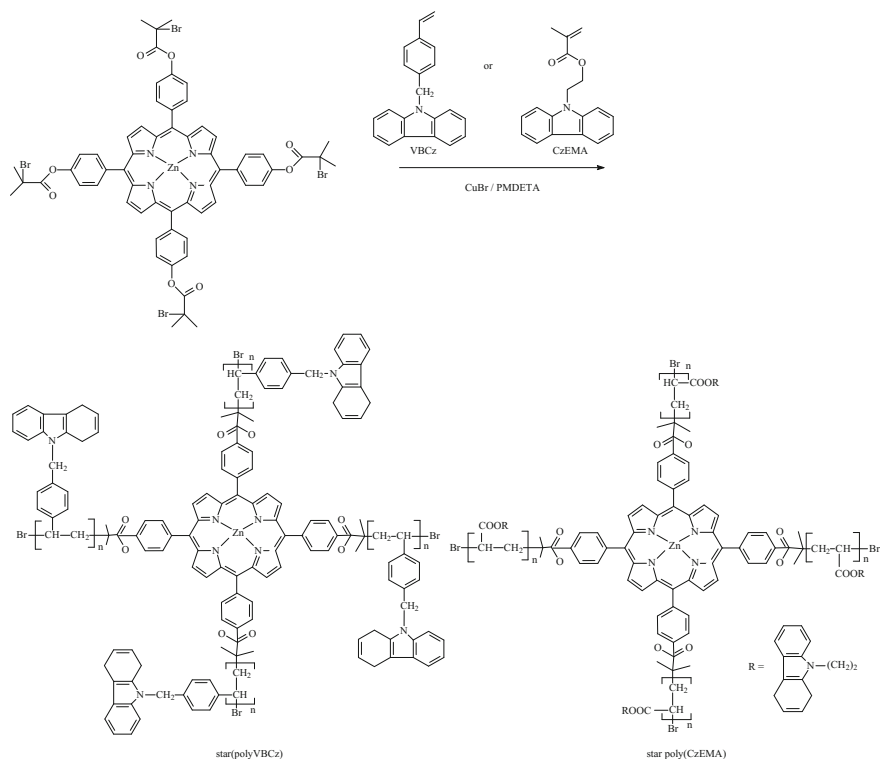
Scheme 4.42 Synthesis of star-shaped polymers with pendant Cz fragments and Zn-Pp core

as well as blue-emitting arms, which occur to be white-light PLED (Fig. 4.68) [467]. These PLED exhibited maximum current efficiency 1.69 cd A^{-1} and CIE coordinates (0.35, 0.33), which is very close to the clear white light point coordinates (0.33, 0.33).
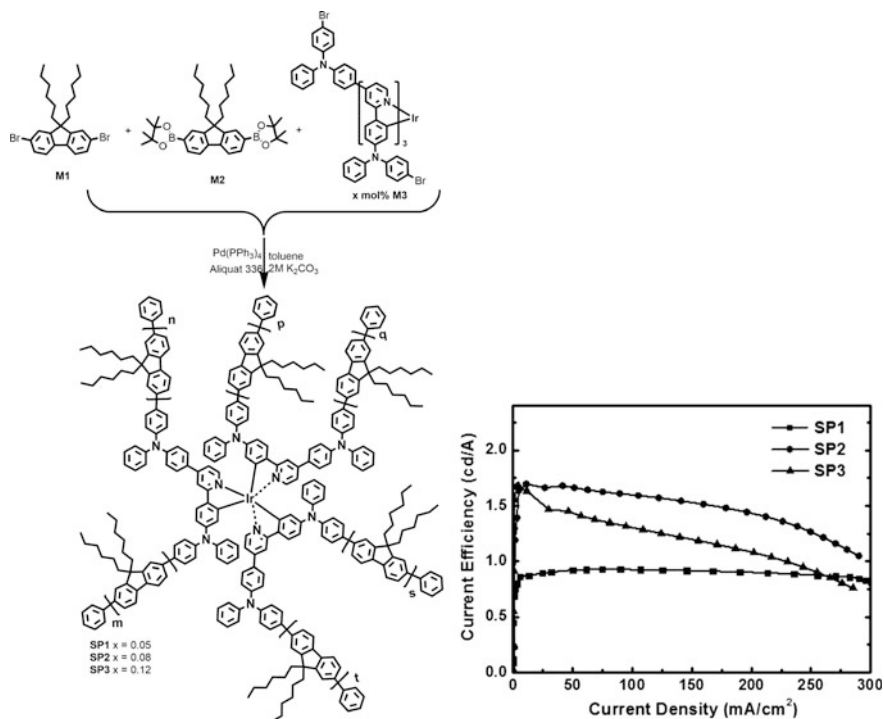
Fig. 4.68 Synthesis of star-shaped polymers with triphenyl amine-based Ir(III) dendritic complex and current efficiency versus current density curves of devices fabricated from Ir(III) polymer

References

1. A.D. Pomogailo, I.E. Uflyand, Adv. Polym. Sci. **97**, 61 (1990)
2. A.D. Pomogailo, I.E. Uflyand, J. Coord. Chem. **23**, 183 (1991)
3. I.E. Uflyand, A.D. Pomogailo, Russ. Chem. Rev. **60**, 773 (1991)
4. A.D. Pomogailo, I.E. Uflyand, *Makromolekulayrnye Metallokhelaty (Macromolecular Metal Chelates)* (Khimiya, Moscow, 1991)
5. A.D. Pomogailo, V.S. Savostyanov, *Synthesis and Polymerization of Metal-Containing Monomers* (CRC Press, Boca Raton, 1994)
6. D. Wohrle, A.D. Pomogailo, *Metal Complexes and Metals in Macromolecules* (Wiley-VCH, Weinheim, 2003)
7. I. Manners, *Synthetic Metal-containing Polymers* (Wiley-VCH, Weinheim, 2004)
8. V. Chandrasekhar, *Inorganic and Organometallic Polymers* (Springer, Berlin, 2005)
9. U.S. Schubert, G.R. Newkome, I. Manners (eds.), *Metal-Containing and Metallosupramolecular Polymers and Materials*. ACS Symposium Series, vol. 928 (American Chemical Society, Washington, DC, 2006)
10. Ch. Carraher Jr., C. Pittman Jr., A. Abd-El-Aziz, M. Zeldin, J. Sheats (eds.), *Metal and Metalloid Containing Macromolecules* (Wiley, New York, 2006)
11. O.I. Koifman, T.A. Ageeva, *Porphyrinpolymers* (Fizmatlit, Moscow, 2006)
12. A. Abd-El-Aziz, C.E. Carraher Jr., C.U. Pittman, M. Zeldin (eds.), *Macromolecules Containing Metal and Metal-like Elements* (Wiley, New Jersey, 2006)

13. J.H. Zagal, F. Bedioui, J.P. Dodelet, *N₄-Macrocyclic Metal Complexes* (Springer, NY, 2006)
14. I. Asselberghs, M.J. Therien, B.J. Coe, J.A. McCleverty, K. Clays, *Metal-Containing and Metallosupra-molecular Polymers and Materials*. ACS Symposium Series, vol. 928 (American Chemical Society, Washington, DC, 2006)
15. U.S. Schubert, H. Hofmeier, G.R. Newkome, *Modern Terpyridine Chemistry* (Wiley-VCH, Weinheim, 2006)
16. A.S. Abd-El-Aziz, I. Manners, *Frontiers in Transition Metal-Containing Polymers* (Wiley, Weinheim, 2007)
17. A.C.W. Leung, M.J. MacLachlan, J. Inorg. Organomet. Polym. **17**, 57 (2007)
18. W.K. Chan, Coord. Chem. Rev. **251**, 2104 (2007)
19. A.S. Abd-El-Aziz, C.E. Carraher, C.U. Pittman (eds.), *Inorganic and Organometallic Macromolecules: Design and Applications* (Springer, NY, 2008)
20. A.D. Pomogailo, G.I. Dzhardimalieva, *Monomer and Polymer Metal Carboxylates* (Fizmatlit, Moscow, 2009)
21. A.S. Abd-El-Aziz, P.O. Shipman, B.N. Boden, W.S. McNeil, Prog. Polym. Sci. **35**, 714 (2010)
22. A. Wild, A. Winter, F. Schlutter, U.S. Schubert, Chem. Soc. Rev. **40**, 1459 (2011)
23. U.S. Schubert, A. Winter, G.R. Newkome (eds.), *Terpyridine-based Materials. For Catalytic, Optoelectronic and Life Science Applications* (Wiley-VCH, Weinheim, 2011)
24. A.Z. El-Sonbati, M.A. Diab, A.A. El-Bindary, Stoichiometry of polymer complexes, in *Stoichiometry and Research—The Importance of Quantity in Biomedicine*, ed. by A. Innocenti (InTech, Rijeka, Croatia, 2012)
25. A.S. Abd-El-Aziz, E.A. Strohm, Polymer **53**, 4879 (2012)
26. G.R. Whittell, M.D. Hager, U.S. Schubert, I. Manners, Nat. Mat. **10**, 176 (2011)
27. X. Wang, R. McHale, Macromol. Rapid Commun. **31**, 331 (2010)
28. M. Ramanathan, S.B. Darling, Polym. Int. **62**, 1123 (2013)
29. A.D. Pomogailo, *Catalysis by Polymer-Immobilized Metal Complexes* (Gordon & Breach Science Publishers, Amsterdam, 1998)
30. M.M. Dell' Anna, G. Romanazzi, P. Mastrorilli, Curr. Org. Chem. **17**, 1236 (2013)
31. H. Xu, Q. Sun, Z. An, Y. Wei, X. Liu, Coord. Chem. Rev. **293–294**, 228 (2015)
32. X. Liu, Y. Hu, B. Wang, Z. Su, Synth. Met. **159**, 1557 (2009)
33. N.V. Petrochenkova, M.V. Petukhova, A.G. Mirochnik, V.E. Karasev, Russ. J. Coord. Chem. **27**, 676 (2001)
34. A.T. Mubarak, A.Z. El-Sonbati, A.A. El-Bindary, R.M. Issa, H.M. Kera, J. Appl. Organomet. Chem. **20**, 819 (2006)
35. I. Savchenko, A. Berezhnytska, Y. Fedorov, N. Rusakova, V. Syromyatnikov, S. Smola, Chem. Chem. Technol. **7**, 423 (2013)
36. T.I. Movchan, I.S. Voloshanovski, A.D. Pomogailo, Izv. Akad. Nauk, Ser. Khim. 2060 (1993)
37. A.Z. El-Sonbati, A.A. Al-Sarawy, A.M. Moqbal, Spectrochim. Acta Part A **74**, 463 (2009)
38. M.A. Diab, A.Z. El-Sonbati, M.E. Attallah, J. Coord. Chem. **65**, 539 (2012)
39. A.A. El-Bindary, A.Z. El-Sonbati, M.A. Diab, M.E. Attallah, Spectrochim. Acta Part A **79**, 1057 (2012)
40. A.Z. El-Sonbati, M.A. Diab, R.H. Mohamed, Polym. Int. **60**, 1467 (2011)
41. E.H. El-Mossalamy, A.A. Khalil, Commun. Fac. Sci. Univ. Ank. B **53**, 1 (2004)
42. A.Z. Albayrak, D. Avci, J. Appl. Polym. Sci. **109**, 459 (2008)
43. A.Z. El-Sonbati, A.S. Al-Shihri, A.A. El-Bindary, J. Inorg. Organomet. Polym. **13**, 99 (2003)
44. O.S. Berezhnytska, I.O. Savchenko, O.K. Trunova, O.O. Rogovtsov, N.B. Ivaha, Rep. Nat. Acad. Sci. Ukr. 132 (2012)
45. W.-Y. Lai, J.W. Levell, P.L. Burn, S.-C. Loa, I.D.W. Samuel, J. Mater. Chem. **19**, 4952 (2009)
46. D. Volz, A.F. Hirschbiel, D.M. Zink, J. Friedrichs, M. Nieger, T. Baumann, S. Bräse, C. Barner-Kowollik, J. Mater. Chem. C **2**, 1457 (2014)

47. W.Y. Lai, J.W. Levell, A.C. Jackson, S.C. Lo, P.V. Bernhardt, I.D.W. Samuel, P.L. Burn, Macromolecules **43**, 6986 (2010)
48. F. Wang, K. Ding, F. Wu, Macromol. Chem. Phys. **212**, 2087 (2011)
49. L. Oriol, J.L. Serano, Angew. Chem. Int. Ed. **44**, 6618 (2005)
50. M. Uygun, E. Feyzioğlu, E. Özçalişkan, M. Caka, A. Ergen, S. Akgöl, A. Denizli, J. Nanopart. Res. **15**, 1833 (2013)
51. X. Hong, L. Billon, M. Mellah, E. Schulz, Catal. Sci. Technol. **3**, 723 (2013)
52. Z. Liu, I. Schmidt, P. Thamyongkit, R.S. Loewe, D. Syomin, J.R. Diers, Q. Zhao, V. Misra, J.S. Lindsey, D.F. Bocian, Chem. Mater. **17**, 3728 (2005)
53. E. Otsuki, H. Sato, A. Kawakami, H. Taka, H. Kita, H. Usui, Thin Solid Films **518**, 703 (2009)
54. J. Zhou, G.R. Whittell, I. Manners, Macromolecules **47**, 3529 (2014)
55. Y. Zha, M.L. Disabb-Miller, Z.D. Johnson, M.A. Hickner, G.N. Tew, J. Am. Chem. Soc. **134**, 4493 (2012)
56. M. Heller, U.S. Schubert, Macromol. Rapid Commun. **23**, 411 (2002)
57. B.S. Kim, C. Basavaraja, E.A. Jo, D.G. Kim, D.S. Huh, Polymer **51**, 3365 (2010)
58. Z. Xie, C. Wang, K.E. de Krafft, W. Lin, J. Am. Chem. Soc. **133**, 2056 (2011)
59. X.-X. Hu, P.-H. Li, K.K. Yeung, P. Chu, S.-L. Wu, Z.-S. Xu, J. Polym. Sci. A **48**, 5961 (2010)
60. P.T. Kaye, S. Afr. J. Sci. **107**, Art. #439 (2011)
61. Y. Hibi, M. Ouchi, M. Sawamoto, Angew. Chem. Int. Ed. **50**, 7434 (2011)
62. Q. Ling, Y. Song, S.J. Ding, C. Zhu, D.S.H. Chan, D.-L. Kwong, E.-T. Kang, K.-G. Neoh, Adv. Mater. **17**, 455 (2005)
63. S.-J. Liu, P. Wang, Q. Zhao, H.-Y. Yang, J. Wong, H.-B. Sun, X.-C. Dong, W.-P. Lin, W. Huang, Adv. Mater. **24**, 2901 (2012)
64. L.-H. Wang, W. Wang, W.-G. Zhang, E.-T. Kang, W. Huang, Chem. Mater. **12**, 2212 (2000)
65. Q. Suo, F. Lu, J. Shi, H. Hong, J. Luo, J. Rare Earths **27**, 28 (2009)
66. C.-J. Xu, J.-T. Wan, B.-G. Li, Dyes Pigments **98**, 493 (2013)
67. Z.-G. Zhang, J.-B. Yuan, H.-J. Tang, H. Tang, L.-N. Wang, K.-L. J. Polym. Sci. A. **47**, 210 (2009)
68. N.V. Petrochenkova, A.G. Mirochnik, M.V. Petukhova, V.E. Karasev, Polym. Sci. Ser. B **48**, 194 (2006)
69. P.I. Lee, S.L.C. Hsu, J.F. Lee, J. Polym. Sci. A Polym. Chem. **46**, 464 (2008)
70. N. Du, R. Tian, J. Peng, M. Lu, J. Polym. Sci. A Polym. Chem. **43**, 397 (2005)
71. E.-Y. Kim, S.-H. Myung, Y.-H. Lee, H.-D. Kim, Clean Tech. **18**, 366 (2012)
72. J. Luo, C. Zhang, C. Yang, M. Lu, Synth. Met. **162**, 431 (2012)
73. C. Zhang, J. Luo, Acta Polym. Sinica **10**, 1289 (2012)
74. J. Luo, C. Zhang, W. Wang, X. Tang, L. Zhu, H. Hu, B. Hu, J. Photochem. Photobiol. A Chem. **252**, 93 (2013)
75. C.-J. Xu, B.-G. Li, Macromol. Chem. Phys. **211**, 1733 (2010)
76. J. Luo, C. Yang, D. Zhou, L. Liang, M. Lu, Synth. Met. **161**, 1771 (2011)
77. J. Luo, C. Zhang, C. Li, H. Hu, B. Hu, RSC Adv. **4**, 57393 (2014)
78. J. Luo, C. Zhang, X. Tang, W. Wang, H. Hu, B. Hu, Synth. Met. **185–186**, 137 (2013)
79. Z. Zhang, W. Feng, P. Su, L. Liu, X. Lü, J. Song, D. Fan, W.-K Wong, R.A. Jones, C. Su, Synth. Met. **199**, 128 (2015)
80. Z. Zhang, W. Feng, P. Su, X. Lu, J. Song, D. Fan, W.K. Wong, R.A. Jones, C. Su, Inorg. Chem. **53**, 5950 (2014)
81. T.-Z. Miao, W.-X. Feng, Z. Zhang, P.-Y. Su, X.-Q Lu, J.-R. Song, D.-D. Fan, W.-K. Wong, R.A. Jones, C.-Y. Su, Eur. J. Inorg. Chem. **2014**, 2839 (2014)
82. L. Liu, Z. Zhang, W. Feng, C. Yu, X. Lu, W.-K. Wong, R.A. Jones, Inorg. Chem. Commun. **49**, 124 (2014)
83. A.D. Pomogailo, N.M. Bravaya, V.F. Razumov, I.S. Voloshanovski, N.A. Kizhenko, V.V. Berezovskii, A.I. Kuzaev, A.G. Ivanchenko, Izv. Akad. Nauk. Ser. Khim. 2922 (1996)

84. V.F. Razumov, A.G. Ivanchenko, A.D. Pomogailo, I.S. Voloshanovski, A.I. Kuzaev, Vysokomol. Soed. Ser. B. **39**, 2046 (1997)

85. A.D. Pomogailo, V.F. Rasumov, I.S. Voloshanovsky, J. Porphyr. Phthalocyanines **4**, 45 (2000)

86. N.A. Kizhenko, Yu.V. Ishkov, I.S. Voloshanovski, Z.G. Aliev, A.D. Pomogailo, Izv. Akad. Nauk. Ser. Khim. 1827 (1995)

87. V.V. Berezovskii, D. Wöhrle, O. Tsaryova, S.G. Makarov, S.I. Pomogailo, N.N. Glagolev, Z.I. Zhilina, I.S. Voloshanovskii, V.P. Roshchupkin, A.D. Pomogailo, Russ. Chem. Bull. **56**, 160 (2007)

88. V. Kutureva, N. Baziakina, K. Maximova, V. Morozova, G. Schnurpfeil, D. Wöhrle, O. Suvorova, J. Porphyr. Phthalocyanines **12**, 832 (2008)

89. C.G. Hardy, J. Zhang, Y. Yan, L. Ren, C. Tang, Prog. Polym. Sci. **39**, 1742 (2014)

90. G. Moad, M. Chen, M. Haeussler, A. Postma, E. Rizzardo, S.H. Thang, Polym. Chem. **2**, 492 (2011)

91. M. Chen, K.P. Ghiggino, A. Launikonis, A.W.H. Mau, E. Rizzardo, W.H.F. Sasse, S.H. Thang, G.J. Wilson, J. Mater. Chem. **13**, 2696 (2003)

92. M. Chen, K.R. Ghiggino, S.H. Thang, G.J. Wilson, Angew. Chem. Int. Ed. **44**, 4368 (2005)

93. M. Chen, K.P. Ghiggino, S.H. Thang, G.J. Wilson, Polym. Int. **55**, 757 (2006)

94. G.E. Southard, K.A. Van Houten, G.M. Murray, Macromolecules **40**, 1395 (2007)

95. G.E. Southard, K.A. Van Houten, E.W. Ott Jr., G.M. Murray, Anal. Chim. Acta **581**, 202 (2007)

96. B. Happ, C. Friebe, A. Winter, M.D. Hager, U.S. Schubert, Eur. Polym. J. **45**, 3433 (2009)

97. A.M. Breul, I.R. de Moraes, R. Menzel, M. Pfeffer, A. Winter, M.D. Hager, S. Rau, B. Dietzek, R. Beckert, U.S. Schubert, Polym. Chem. **5**, 2715 (2014)

98. W.Y. Tam, C.S.K. Mak, A.M.C. Ng, A.B. Djurisic, W.K. Chan, Macromol. Rapid Commun. **30**, 622 (2009)

99. Y. Sun, Z. Chen, E. Puodziukynaite, D.M. Jenkins, J.R. Reynolds, K.S. Schanze, Macromolecules **45**, 2632 (2012)

100. M.M. Unterlass, E. Espinosa, F. Boisson, F. D'Agosto, C. Boisson, K. Ariga, I. Khalakhan, R. Charvet, J.P. Hill, Chem. Commun. **47**, 7057 (2011)

101. E.K. Pefkianakis, N.P. Tzanetos, J.K. Kallitsis, Chem. Mater. **20**, 6254 (2008)

102. M. Kimura, H. Ueki, K. Ohta, K. Hanabusa, H. Shirai, N. Kobayashi, Chem. Eur. J. **10**, 4954 (2004)

103. J. Aimi, M. Komura, T. Iyoda, A. Saeki, S. Seki, M. Takeuchi, T. Nakanishi, J. Mater. Chem. C **3**, 2484 (2015)

104. B.N. Şen, H. Mert, H. Dinçer, A. Koca, Dyes Pigments **100**, 1 (2014)

105. H. Mert, H. Dinçer, E. Çalişkan, B.N. Şen, Y.H. Gürsel, J. Appl. Polym. Sci. **132**, 41574 (2015)

106. J.R. Carlise, X.Y. Wang, M. Weck, Macromolecules **38**, 9000 (2005)

107. U.M. Tefashe, K. Metera, H. Sleiman, J. Mauzeroll, Langmuir **29**, 12866 (2013)

108. W.Y. Lai, M.N. Balfour, J.W. Levell, A.K. Bansal, P.L. Burn, S.C. Lo, I.D.W. Samuel, Macromolecules **45**, 2963 (2012)

109. M.S. Pawar, Y. Zha, M.L. Disabb-Miller, Z.D. Johnson, M.A. Hickner, G.N. Tew, Metal-ligand based anion exchange membranes, in *Polymer Composites for Energy Harvesting, Conversion, and Storage*. ACS Symposium Series, vol. 1161 (American Chemical Society, Washington, DC, 2014)

110. J. Chen, J.L. Gorczynski, G. Zhang, C.L. Fraser, Macromolecules **43**, 4909 (2010)

111. A.-C. Knal, C. Schinag, A. Pein, N. Noormofidi, R. Saf, C. Slugovc, Macromol. Chem. Phys. **213**, 2618 (2012)

112. X. Zhang, M. Cui, R. Zhou, C. Chen, G. Zhang, Macromol. Rapid Commun. **35**, 566 (2014)

113. A. Meyers, M. Weck, Macromolecules **36**, 1766 (2003)

114. B. Gao, R. Duan, X. Pang, X. Li, Z. Qu, Z. Tang, X. Zhuang, X. Chen, Organometallics **32**, 5435 (2013)

115. Y.Y. Kang, H.-R. Park, M.H. Lee, J. An, Y. Kim, J. Lee, Polyhedron **95**, 24 (2015)

116. A. Bilgin, Ç. Yağci, Eur. Polym. J. **61**, 240 (2014)
117. M.R. Buchmeiser, Chem. Rev. **100**, 1565 (2000)
118. V. Dragutan, I. Dragutan, H. Fischer, J. Inorg. Organomet. Polym. **18**, 18 (2008)
119. I. Dragutan, V. Dragutan, H. Fischer, J. Inorg. Organomet. Polym. **18**, 311 (2008)
120. W. Feng, Y. Zhang, Z. Zhang, P. Su, X. Lü, J. Song, D. Fan, W.-K. Wong, R.A. Jones, C. Su, J. Mater. Chem. C **2**, 1489 (2014)
121. C. Friebe, M.D. Hager, A. Winter, U.S. Schubert, Adv. Mater. **24**, 332 (2012)
122. C.-J. Yao, Y.-W. Zhong, J. Yao, Inorg. Chem. **52**, 10000 (2013)
123. Y.-W. Zhong, C.-J. Yao, H.-J. Nie, Coord. Chem. Rev. **257**, 1357 (2013)
124. H.-J. Nie, J.-Y. Shao, J. Wu, J. Yao, Y.-W. Zhong, Organometallics **31**, 6952 (2012)
125. H.J. Nie, Y.W. Zhong, Inorg. Chem. **53**, 11316 (2014)
126. B.-B. Cui, H.-J. Nie, C.-J. Yao, J.-Y. Shao, S.-H. Wu, Y.-W. Zhong, Dalton Trans. **42**, 14125 (2013)
127. C.-J. Yao, Y.-W. Zhong, H.-J. Nie, H.D. Abruña, J. Yao, J. Am. Chem. Soc. **133**, 20720 (2011)
128. Y.-W. Zhong, Electrochromism within transition-metal coordination complexes and polymers, in *Electrochromic Materials and Devices*, ed. by R.J. Mortimer, D.R. Rosseinsky, P.M.S. Monk (Wiley-VCH, Weinheim, 2015)
129. R. Scanu, P. Manca, A. Zucca, G. Sanna, N. Spano, R. Seeber, C. Zanardi, M.I. Pilo, Polyhedron **49**, 24 (2013)
130. B.-B. Cui, Z. Mao, Y. Chen, Y.-W. Zhong, G. Yu, C. Zhan, J. Yao, Chem. Sci. **6**, 1308 (2015)
131. S. Liatard, J. Chauvin, F. Balestro, D. Jouvenot, F. Loiseau, A. Deronzier, Langmuir **28**, 10916 (2012)
132. C. Friebe, B. Schulze, H. Görls, M. Jäger, U.S. Schubert, Chem. Eur. J. **20**, 8 (2014)
133. D. Qiu, X. Bao, Q. Zhao, Q. Yang, Y. Feng, H. Wang, C. Yang, K. Liu, Inorg. Chem. **54**, 8264 (2015)
134. C.-Y. Hsu, J. Zhang, T. Sato, S. Moriyama, M. Higuchi, A.C.S. Appl, Mater. Interfaces **7**, 18266 (2015)
135. P. Manca, R. Scanu, A. Zucca, G. Sanna, N. Spano, M.I. Pilo, Polymer **54**, 3504 (2013)
136. T.W. Hesterberg, X. Yang, B.J. Holliday, Polyhedron **29**, 110 (2010)
137. C. Friebe, B. Schulze, H. Görls, M. Jäger, U.S. Schubert, Chem. Eur. J. **20**, 2357 (2014)
138. K.M. Milum, Y.N. Kim, B.J. Holliday, Chem. Mater. **22**, 2414 (2010)
139. C. Friebe, H. Görls, M. Jäger, U.S. Schubert, Eur. J. Inorg. Chem. **2013**, 24 (2013)
140. C. Friebe, M. Jäger, U.S. Schubert, RSC Adv. **3**, 11686 (2013)
141. M.K. O'Neill, A.F. Trappey, P. Battle, C.L. Boswell, D.N. Blauch, Dalton Trans. 3391 (2009)
142. O. Fatibello-Filho, E.R. Dockal, L.H. Marcolino-Junior, M.F.S. Teixeira, Anal. Lett. **40**, 1825 (2007)
143. M. Li, H. Jiao, H. Zhang, S. Jiao, Int. J. Electrochem. Sci. **10**, 8797 (2015)
144. T.R.L. Dadamos, M.F.S. Teixeira, Electrochim. Acta **54**, 4552 (2009)
145. V.V. Sizov, M.V. Novozhilova, E.V. Alekseeva, M.P. Karushev, A.M. Timonov, S.N. Eliseeva, A.A. Vanin, V.V. Malev, O.V. Levin, J. Solid State Electrochem. **19**, 453 (2015)
146. G. Yan, J. Li, Y. Zhang, F. Gao, F. Kang, J. Phys. Chem. C **118**, 9911 (2014)
147. J.-L. Li, F. Gao, Y.-K. Zhang, L.-Z. He, G.-M. Han, X.-D. Wang, Acta Phys. Chim. Sin. **26**, 2647 (2010)
148. A.M. Golyakov, L.P. Ardasheva, A.N. Borisov, Zh. Prikl. Khim. **86**, 1162 (2013)
149. D. Deletioğlu, S. Yalçinkaya, C. Demetgül, M. Timur, S. Serin, Mater. Chem. Phys. **128**, 500 (2011)
150. A.M. Golyakov, A.V. Schukarev, L.P. Ardasheva, A.N. Borisov, Zh. Obsch. Khim. **83**, 368 (2013)
151. A.N. Borisov, A.V. Schukarev, Zh. Prikl. Khim. **82**, 1147 (2009)
152. S.V. Vasil'eva, I.A. Chepurnaya, S.A. Logvinov, P.V. Gaman'kov, A.M. Timonov, Russ. J. Electrochem. **39**, 310 (2003)

153. TYu. Rodyagina, P.V. Gaman'kov, E.A. Dmitrieva, I.A. Chepurnaya, S.V. Vasil'eva, A.M. Timonov, Russ. J. Electrochem. **41**, 1101 (2005)
154. T. Shioya, T.M. Swager, Chem. Commun. 1364 (2002)
155. J.L. Reddinger, J.R. Reynolds, Macromolecules **30**, 673 (1997)
156. J.D. Caraway, M.T. Nguyen, L.A. Mitchell, B.J. Holliday, Macromol. Rapid Commun. **36**, 665 (2015)
157. M.L. Mejía, J.H. Rivers, S.F. Swingle, Z. Lu, X. Yang, M. Findlater, G. Reeske, B. J. Holliday, Main Group Chem. **9**, 167 (2010)
158. K.R. Edelman, K.J. Stevenson, B.J. Holliday, Macromol. Rapid Commun. **33**, 610 (2012)
159. B. Djukic, M.T. Lemaire, Inorg. Chem. **48**, 10489 (2009)
160. A. Zulauf, M. Mellah, R. Guillot, E. Schulz, Eur. J. Org. Chem. **2008**, 2118 (2008)
161. A. Zulauf, X. Hong, F. Brisset, E. Schulz, M. Mellah, New J. Chem. **36**, 1399 (2012)
162. W. Rongmin, Z. Ming, H. Yufeng, H. Erxia, S. Guorui, Progr. Chem. **19**, 1783 (2007)
163. M. Mellah, B. Ansel, F. Patureau, A. Voituriez, E. Schulz, J. Mol. Catal. A Chem. **272**, 20 (2007)
164. A. Voituriez, M. Mellah, E. Schulz, Synth. Met. **156**, 166 (2006)
165. M.L. Mejía, K. Agapiou, X. Yang, B.J. Holliday, J. Am. Chem. Soc. **131**, 18196 (2009)
166. A.C.W. Leung, J.K.-H. Hui, J.H. Chong, M.J. MacLachlan, Dalton Trans. 5199 (2009)
167. J. Tedim, K. Biernacki, J. Fonseca, S. Patrício, A. Carneiro, A.L. Magalhães, S.J. Gurman, C. Freire, A.R. Hillman, J. Electroanal. Chem. **688**, 308 (2013)
168. C. Pinheiro, A.J. Parola, F. Pina, J. Fonseca, C. Freire, Sol. Energy Mater. Sol. Cells **92**, 980 (2008)
169. A. Branco, C. Pinheiro, J. Fonseca, J. Tedim, A. Carneiro, A.J. Parola, C. Freire, F. Pina, Electrochem. Solid-State Lett. **13**, J114 (2010)
170. W. Liu, W. Huang, M. Pink, D. Lee, J. Am. Chem. Soc. **132**, 11844 (2010)
171. S. Drouet, S. Ballut, J. Rault-Berthelot, P. Turban, C. Paul-Roth, Thin Solid Films **517**, 5474 (2009)
172. D. Quezada, J. Honores, M.J. Aguirre, M. Isaacs, J. Coord. Chem. **67**, 4090 (2014)
173. N. Phougat, P. Vasudevan, N. Jha, D. Bandhopadhyay, Transit. Met. Chem. **28**, 838 (2003)
174. G. Ramírez, M.C. Goya, L. Mendoza, B. Matsuhiro, M. Isaacs, Y.-Y. Chen, M.C. Arévalo, H. Cheuquepán, M.J. Aguirre, J. Coord. Chem. **62**, 2782 (2009)
175. M. Vago, V. Campodall'Orto, I. Rezzano, E.S. Forzani, E.J. Calvo, J. Electroanal. Chem. **566**, 177 (2004)
176. M. Schaferling, P. Bauerle, J. Mater. Chem. **14**, 1132 (2004)
177. M. Yuasa, K. Oyaizu, A. Yamaguchi, M. Ishikawa, K. Eguchi, T. Kobayashi, Y. Toyoda, S. Tsutsui, Polym. Adv. Technol. **16**, 616 (2005)
178. S. Cogal, M. Kiristi, K. Ocakoglu, L. Oksuz, A.U. Oksuz, Mater. Sci. Semicond. Process. **31**, 551 (2015)
179. Y. Xia, D. Schaming, R. Farha, M. Goldmann, L. Ruhlmann, New J. Chem. **36**, 588 (2012)
180. D. Schaming, Y. Xia, R. Thouvenot, L. Ruhlmann, Chem. Eur. J. **19**, 1712 (2013)
181. D. Schaming, C. Allain, R. Farha, M. Goldmann, S. Lobstein, A. Giraudeau, B. Hasenknopf, L. Ruhlmann, Langmuir **26**, 5101 (2010)
182. M. Aydemir, H.R.P. Karaoğlu, M.B. Koçak, A. Koca, J. Electrochem. Soc. **162**, H170 (2015)
183. V. Cakir, F. Demir, Z. Biyiklioğlu, A. Koca, H. Kantekin, Dyes Pigments **98**, 414 (2013)
184. F. Demir, Z. Biyiklioğlu, A. Koca, J. Electrochem. Soc. **161**, G1 (2014)
185. Z. Biyiklioğlu, V. Çakir, F. Demir, A. Koca, Synth. Met. **196**, 166 (2014)
186. V. Çakir, H. Kantekin, Z. Biyiklioğlu, A. Koca, Polyhedron **81**, 525 (2014)
187. M. Kimura, K. Yasuta, N. Adachi, Y. Tatewaki, T. Fukawa, H. Shirai, Chem. Lett. **38**, 82 (2009)
188. D. Arican, A. Aktaş, H. Kantekin, A. Koca, J. Electrochem. Soc. **161**, H670 (2014)
189. S. Chohan, I.N. Booysen, A. Mambanda, M.P. Akerman, J. Coord. Chem. **68**, 1829 (2015)
190. A. Yavuz, B.B. Çarbaş, L. Aras, A.M. Önal, J. Appl. Polym. Sci. **122**, 1293 (2011)

191. I.E. Uflyand, I.V. Kokoreva, A.S. Kuzharov, V.N. Sheinker, in *Advances in Surface Engineering—Processes, Fundamentals and Applications in Corrosion and Wear*, ed. by K. N. Strafford, P.K. Datta, J.S. Gray (Ellis Horwood Ltd., Sussex, Great Britain, 1990)
192. I.E. Uflyand, I.V. Kokoreva, A.G. Starikov, V.N. Sheinker, A.D. Pomogailo, React. Polym. **11**, 221 (1989)
193. I.E. Uflyand, I.V. Kokoreva, V.N. Sheinker, A.S. Kuzharov, Transit. Met. Chem. **17**, 360 (1992)
194. A.D. Pomogailo, React. Polym. **9**, 109 (1988)
195. V.S. Savostyanov, A.D. Pomogailo, D.A. Kritskaya, A.N. Ponomarev, J. Polym. Sci. Polym. Chem. A. **27**, 1935 (1989)
196. I.E. Uflyand, I.A. Ilchenko, V.N. Sheinker, A.V. Bulatov, React. Polym. **14**, 41 (1991)
197. I.E. Uflyand, I.A. Ilchenko, J. Inorg. Organomet. Polym. **3**, 89 (1993)
198. I.E. Uflyand, I.A. Ilchenko, V.N. Sheinker, V.S. Savostyanov, Transit. Met. Chem. **17**, 575 (1993)
199. I.E. Uflyand, I.A. Ilchenko, A.G. Starikov, V.N. Sheinker, V.S. Savostyanov, React. Polym. **17**, 458 (1993)
200. I.E. Uflyand, I.A. Ilchenko, V.N. Sheinker, V.S. Savostyanov, React. Polym. **17**, 289 (1992)
201. I.E. Uflyand, I.A. Ilchenko, A.G. Starikov, V.N. Sheinker, A.D. Pomogailo, Izv. Akad. Nauk, Ser. Khim. 451 (1990)
202. I.E. Uflyand, I.A. Ilchenko, A.G. Starikov, V.N. Sheinker, A.D. Pomogailo, Izv. Akad. Nauk. Ser. Khim. 2474 (1989)
203. Z. Ying-Jie, Z. Hai-E, Z. Jun, W. Shui-Lin, Y. Chang-Feng, X. Zu-Shun, Chem. J. Chin. Univ. **34**, 732 (2013)
204. T. Yamamoto, Bull. Chem. Soc. Jpn **83**, 431 (2010)
205. T. Yamamoto, H. Fukumoto, T. Koizumi, J. Inorg. Organomet. Polym. **19**, 3 (2009)
206. I. Uzdemir, S. Koytepe, N. Gurbuz, J. Inorg. Organomet. Polym. **19**, 143 (2009)
207. L. Trouillet, A. De Nicola, S. Guillerez, Chem. Mater. **12**, 1611 (2000)
208. P.K. Ng, X. Gong, S.H. Chan, L.S.M. Lam, W.K. Chan, Chem. Eur. J. **7**, 4358 (2001)
209. J.J. Walsh, Q. Zeng, R.J. Forster, T.E. Keyes, Photochem. Photobiol. Sci. **11**, 1547 (2012)
210. W.K. Cheung, C.S.K. Mak, W.K. Chan, Macromol. Rapid Commun. **33**, 585 (2012)
211. J. Ni, J.-J. Kang, H.-H. Wang, X.-Q. Gai, X.-X. Zhang, T. Jia, L. Xu, Y.-Z. Pan, J.-J. Zhang, RSC Adv. **5**, 65613 (2015)
212. J.-X. Jiang, C. Wang, A. Laybourn, T. Hasell, R. Clowes, Y.Z. Khimyak, J. Xiao, S. J. Higgins, D.J. Adams, A.I. Cooper, Angew. Chem. Int. Ed. **50**, 1072 (2011)
213. F. Xu, H.U. Kim, J.-H. Kim, B.J. Jung, A.C. Grimsdale, D.-H. Hwang, Prog. Polym. Sci. **47**, 92 (2015)
214. F.-I. Wu, X.-H. Yang, D. Neher, R. Dodda, Y.-H. Tseng, C.-F. Shu, Adv. Funct. Mater. **17**, 1085 (2007)
215. J. Jiang, Y. Xu, W. Yang, R. Guan, Z. Liu, H. Zhen, Y. Cao, Adv. Mater. **18**, 1769 (2006)
216. M.-J. Park, J. Kwak, J. Lee, I.H. Jung, H. Kong, C. Lee, D.-H. Hang, H.-K. Shim, Macromolecules **43**, 1379 (2010)
217. H. Xu, R. Chen, Q. Sun, W. Lai, Q. Su, W. Huang, X. Liu, Chem. Soc. Rev. **43**, 3259 (2014)
218. T.A. Clem, D.F.J. Kavulak, E.J. Westling, J.M.J. Frechet, Chem. Mater. **22**, 1977 (2009)
219. C.-Y. Liao, C.-P. Chen, C.-C. Chang, G.-W. Hwang, H.-H. Chou, C.-H. Cheng, Sol. Energy Mater. Sol. Cells **109**, 111 (2013)
220. A. Bandyopadhyay, M. Higuchi, Eur. Polym. J. **49**, 1688 (2013)
221. M. Ghaemy, H. Mighani, J. Appl. Polym. Sci. **118**, 2496 (2010)
222. Z. Ma, J. Ding, B. Zhang, C. Mei, Y. Cheng, Z. Xie, L. Wang, X. Jing, F. Wang, Adv. Funct. Mater. **20**, 138 (2010)
223. X. Jin, X. Yu, W. Zhang, J. Zhou, G. Tang, C. Zhong, Polym. Compos. **34**, 1629 (2013)
224. N. Chantarasiri, T. Tuntulani, P. Tongraung, R. Seangprasertkit-Magee, W. Wannarong, Eur. Polym. J. **36**, 695 (2000)
225. H. Fukumoto, K. Yamane, Y. Kase, T. Yamamoto, Macromolecules **43**, 10366 (2010)
226. H. Komatsu, B. Ochiai, T. Endo, J. Polym. Sci. A: Polym. Chem. **46**, 3673 (2008)

227. N. Senthilkumar, A. Raghavan, A.S. Nasar, Macromol. Chem. Phys. **206**, 2490 (2005)
228. S.H. Cho, T. Gadzikwa, G.A. Emberger, R.Q. Snurr, S.T. Nguyen, J.T. Hupp, PMSE Prepr. **97**, 95 (2007)
229. F. Galbrecht, X.H. Yang, B.S. Nehls, D. Neher, T. Farrell, U. Scherf, Chem. Commun. 2378 (2005)
230. T. Ahamad, N. Nishat, J. Appl. Polym. Sci. **107**, 2280 (2008)
231. N. Nishat, S. Ahmad, T. Ahamad, J. Appl. Polym. Sci. **101**, 1347 (2006)
232. T. Ahamad, V. Kumar, N. Nishat, J. Biomed. Mater. Res. **88A**, 288 (2009)
233. T. Ahamad, S.M. Alshehri, Bioinorg. Chem. Appl. **2010**, Article ID 976901 (2010)
234. M. Cazacu, M. Marcu, A. Viad, M. Vasiliu, J. Macromol. Sci.: Pure Appl. Chem. **A41**, 565 (2004)
235. M. Nielsen, A.H. Thomsen, T.R. Jensen, H.J. Jakobsen, J. Skibsted, K.V. Gothelf, Eur. J. Org. Chem. **2**, 342 (2005)
236. J. Wang, W. Huang, L. Pan, H. Wang, C. Zhang, X. Liu, Macromol. Res. **23**, 309 (2015)
237. R.-M. Wang, Z.-F. Duan, Y.-F. He, Z.-Q. Lei, J. Mol. Catal. A Chem. **260**, 280 (2006)
238. YuE Alexeev, B.I. Kharisov, T.C. Hernandez Garcia, A.D. Garnovskii, Coord. Chem. Rev. **254**, 794 (2010)
239. A.D. Garnovskii, B.I. Kharisov (eds.), *Synthetic Coordination and Organometallic Chemistry* (Marcel Dekker, NY/Basel, 2003)
240. A.C.W. Leung, M.J. MacLachlan, J. Mater. Chem. **17**, 1923 (2007)
241. A.C.W. Leung, J.H. Chong, B.O. Patrick, M.J. MacLachlan, Macromolecules **36**, 5051 (2003)
242. J. Jiang, A.C.W. Leung, M.J. MacLachlan, Dalton Trans. **39**, 6503 (2010)
243. O. Lavastre, I. Illitchev, G. Jegou, P. Dixneuf, J. Am. Chem. Soc. **124**, 5278 (2002)
244. S. Sun, W.-L. Tong, M.C.W. Chan, Macromol. Rapid Commun. **31**, 1965 (2010)
245. W.-L. Tong, L.-M. Lai, M.C.W. Chan, Dalton Trans. 1412 (2008)
246. H. Li, Z. Li, Y. Zhang, X. Luo, H. Xia, X. Liu, Y. Mu, RSC Adv. **4**, 37767 (2014)
247. P. Yan, H. Jing, Adv. Synth. Catal. **351**, 1325 (2009)
248. J.A. Paquette, E.R. Sauvé, J.B. Gilroy, Macromol. Rapid Commun. **36**, 621 (2015)
249. T. Yamamoto, N. Fukushima, H. Nakajima, T. Maruyama, I. Yamaguchi, Macromolecules **33**, 5988 (2000)
250. A. Saywell, J.K. Sprafke, L.J. Esdaile, A.J. Britton, A. Rienzo, H.L. Anderson, J.N.O' Shea, P.H. Beton, Angew. Chem. Int. Ed. **49**, 9136 (2010)
251. A. Modak, M. Nandi, J. Mondal, A. Bhaumik, Chem. Commun. **48**, 248 (2012)
252. H. Xiang, L. Zhou, Y. Feng, J. Cheng, D. Wu, X. Zhou, Inorg. Chem. **51**, 5208 (2012)
253. T. Umeyama, T. Takamatsu, N. Tezuka, Y. Matano, Y. Araki, T. Wada, O. Yoshikawa, T. Sagawa, S. Yoshikawa, H. Imahori, J. Phys. Chem. C **113**, 10798 (2009)
254. X. Huang, C. Zhu, S. Zhang, W. Li, Y. Guo, X. Zhan, Y. Liu, Z. Bo, Macromolecules **41**, 6895 (2008)
255. X. Wang, H. Wang, Y. Yang, Y. He, L. Zhang, Y. Li, X. Li, Macromolecules **43**, 709 (2010)
256. X. Huang, Q. Shi, W.-Q. Chen, C. Zhu, W. Zhou, Z. Zhao, X.-M. Duan, X. Zhan, Macromolecules **43**, 9620 (2010)
257. L. Chen, Y. Yang, D. Jiang, J. Am. Chem. Soc. **132**, 9138 (2010)
258. B.S. Li, Y.Q. Fu, Y. Han, Z.S. Bo, Macromol. Rapid Commun. **27**, 1355 (2006)
259. T.E.O. Screen, J.R.G. Thorne, R.G. Denning, D.G. Bucknall, H.L. Anderson, J. Am. Chem. Soc. **235**, 9712 (2002)
260. T.E.O. Screen, J.R.G. Thorne, R.G. Denning, D.G. Bucknall, H.L. Anderson, J. Mater. Chem. **13**, 2796 (2003)
261. H. Imahori, J. Phys. Chem. B **108**, 6130 (2004)
262. X. Wang, G. Brisard, D. Fortin, P.-L. Karsenti, P.D. Harvey, Macromolecules **48**, 7024 (2015)
263. J.M. Hales, M. Cozzuol, T.E.O. Screen, H.L. Anderson, J.W. Perry, Opt. Express **17**, 18478 (2009)
264. T. Tanaka, A. Osuka, Chem. Soc. Rev. **44**, 943 (2015)

265. M. Kawao, H. Ozawa, H. Tanaka, T. Ogawa, Thin Solid Films **499**, 23 (2006)
266. F.C. Grozema, C. Houarner-Rassin, P. Prins, L.D.A. Siebbeles, H.L. Anderson, J. Am. Chem. Soc. **129**, 13370 (2007)
267. A.N. Cammidge, P.J. Scaife, G. Berber, D.L. Hughes, Org. Lett. **7**, 3413 (2005)
268. K. Ogawa, T. Zhang, K. Yoshihara, Y. Kobuke, J. Am. Chem. Soc. **124**, 22 (2002)
269. G. Li, T. Wang, A. Schulz, S. Bhosale, M. Lauer, P. Espindola, J. Heinze, J. Fuhrhop, Chem. Commun. **5**, 552 (2004)
270. A. Tsuda, A. Osuka, Science **293**, 79 (2001)
271. N. Aratani, A. Osuka, Chem. Rec. **3**, 255 (2003)
272. D. Kim, A. Osaka, Acc. Chem. Res. **37**, 735 (2004)
273. H. Zhan, S. Lamare, A. Ng, T. Kenny, H. Guernon, W.-K. Chan, A.B. Djurišić, P.D. Harvey, W.-Y. Wong, Macromolecules **44**, 5155 (2011)
274. W.-Y. Wong, X.-Z. Wang, Z. He, A.B. Djurisic, C.-T. Yip, K.-Y. Cheung, H. Wang, C.S.K. Mak, W.-K. Chan, Nat. Mater. **6**, 521 (2007)
275. I.R. Whittall, A.M. McDonagh, M.G. Humphrey, M. Samoc, Adv. Organomet. Chem. **42**, 291 (1998)
276. W.-Y. Wong, J. Inorg. Organomet. Polym. **15**, 197 (2005)
277. H.J. Mackintosh, P.M. Budd, N.B. McKeown, J. Mater. Chem. **18**, 573 (2008)
278. B. Zhao, W. Duan, P.-C. Lo, L. Duan, C. Wu, D.K.P. Ng, Chem. Asian J. **8**, 55 (2013)
279. L. Wang, J. Li, W. Zhang, G. Chen, W. Zhang, X. Zhu, Polym. Chem. **5**, 2872 (2014)
280. W. Maes, W. Dehaen, Eur. J. Org. Chem. 4719 (2009)
281. D. Astruc, E. Boisselier, C. Ornelas, Chem. Rev. **110**, 1857 (2010)
282. D. Astruc, R. Ciganda, C. Deraedt, S. Gatard, L. Liang, N. Li, C. Ornelas, A. Rapakousiou, J. Ruiz, D. Wang, Y. Wang, P. Zhao, Synlett **26**, 1437 (2015)
283. S.-H. Hwang, C.D. Shreiner, C.N. Moorefield, G.R. Newkome, New J. Chem. **31**, 1192 (2007)
284. G.R. Newkome, C.N. Moorefield, F. Vögtle, *Dendrons and Dendrimers: Concepts, Synthesis and Applications* (Wiley-VCH, Weinheim, 2001)
285. D. Tomalia, J.M.J. Fréchet (eds.), *Dendrimers and other Dendritic Polymers* (Wiley-VCH, NY, 2002)
286. D. Astruc, J. Ruiz, J. Inorg. Organomet. Polym. **25**, 2 (2015)
287. A.S. Abd-El-Aziz, C. Agatemor, N. Etkin, Macromol. Rapid Commun. **35**, 513 (2014)
288. A.S. Abd-El-Aziz, S. Bernardin, Coord. Chem. Rev. **203**, 219 (2000)
289. S. Campagna, P. Ceroni, F. Puntoriero (eds.), *Designing Dendrimers* (Wiley, Hoboken, 2012)
290. L.H. Gade (ed.), *Dendrimer Catalysis* (Springer, Berlin, 2006)
291. A.-M. Caminade, R. Laurent, A. Ouali, J.-P. Majoral, Inorg. Chim. Acta **409**, 68 (2014)
292. A.-M. Caminade, A. Ouali, R. Laurent, C.-O. Turrin, J.-P. Majoral, Chem. Soc. Rev. **44**, 3890 (2015)
293. P. Govender, B. Therrien, G.S. Smith, Eur. J. Inorg. Chem. 2853 (2012)
294. V. Balzani, P. Ceroni, A. Juris, M. Venturi, S. Campagna, F. Puntoriero, S. Serroni, Coord. Chem. Rev. **219–221**, 545 (2001)
295. V. Balzani, A. Juris, Coord. Chem. Rev. **211**, 97 (2001)
296. S. Serroni, S. Campagna, F. Untorieri, F. Loiseau, V. Ricevuto, R. Passalacqua, M. Galletta, in *Dendrimers and Nanoscience*, ed. by D. Astruc (Elsevier/C. R. Chimie, Paris, 2003)
297. P. Ceroni, V. Vicinelli, M. Maestri, V. Balzani, S.-K. Lee, J. van Heyst, M. Gorka, F. Vögtle, J. Organomet. Chem. **689**, 4375 (2004)
298. P. Ceroni, G. Bergamini, F. Marchioni, V. Balzani, Prog. Polym. Sci. **30**, 453 (2005)
299. O. Flomenbom, R.J. Amir, D. Shabat, J. Klafter, J. Lumin. **111**, 315 (2005)
300. H. Tsukube, Y. Suzuki, D. Paul, Y. Kataoka, S. Shinoda, Chem. Commun. 2533 (2007)
301. S.-P. Yang, L. Lin, L.-Z. Yang, J.-M. Chen, Q.-Q. Chen, D. Cao, X.-B. Yu, J. Lumin. **126**, 515 (2007)
302. V. Balzani, G. Bergamini, P. Ceroni, F. Vögtle, Coord. Chem. Rev. **251**, 525 (2007)
303. C. Giansante, P. Ceroni, V. Balzani, F. Vögtle, Angew. Chem. Int. Ed. **47**, 5422 (2008)

304. D.N. Lee, B.K. Soh, S.H. Kim, Y.M. Jun, Y. Sook, W.Y. Lee, B.H. Kim, J. Organomet. Chem. **693**, 655 (2008)
305. G.D. D'Ambruoso, D.V. McGrath, Adv. Polym. Sci. **214**, 87 (2008)
306. R. Kikkeri, I. García-Rubio, P.H. Seeberger, Chem. Commun. 235 (2009)
307. R. Kikkeri, X. Liu, A. Adibekian, Y.-H. Tsai, P.H. Seeberger, Chem. Commun. **46**, 2197 (2010)
308. S.P.-Y. Li, H.-W. Liu, K.Y. Zhang, K.K.-W. Lo, Chem. Eur. J. **16**, 8329 (2010)
309. A. Ruggi, C. Beekman, D. Wasserberg, V. Subramaniam, D.N. Reinhoudt, F.W.B. van Leeuwen, A.H. Velders, Chem. Eur. J. **17**, 464 (2011)
310. T. Kapp, A. Dullin, R. Gust, J. Med. Chem. **49**, 1182 (2006)
311. T. Kapp, A. Dullin, R. Gust, Bioconjug. Chem. **21**, 328 (2010)
312. S. Deng, G. Krueger, P. Taranekar, S. Sriwichai, R. Zong, R.P. Thummel, R.C. Advincula, Chem. Mater. **23**, 3302 (2011)
313. Y.-R. Hong, C.B. Gorman, Chem. Commun. 3195 (2007)
314. P. Ceroni, A. Credi, M. Venturi, Chem. Soc. Rev. **43**, 4068 (2014)
315. V. Balzani, G. Bergamini, P. Ceroni, E. Marchi, New J. Chem. **35**, 1944 (2011)
316. Y.-J. Pu, R.E. Harding, S.G. Stevenson, E.B. Namdas, C. Tedeschi, J.P.J. Markham, P.L. Burn, I.D.W. Samuel, J. Mater. Chem. **17**, 4255 (2007)
317. Z. Si, X. Li, X. Li, G. Xu, C. Pan, Z. Guo, H. Zhang, L. Zhou, Dalton Trans. 10592 (2009)
318. J. Rodrigues, M.G. Jardim, J. Figueira, M. Gouveia, H. Tomás, K. Rissanen, New J. Chem. **35**, 1938 (2011)
319. Y. Wang, L. Salmon, J. Ruiz, D. Astruc, Nature Comm. **5**, Article number: 3489 (2014)
320. P. Arya, N.V. Rao, J. Singkhonrat, H. Alper, S.C. Bourque, L.E. Manzer, J. Org. Chem. **65**, 1881 (2000)
321. H.P. Dijkstra, C.A. Kruithof, N. Ronde, R. van de Coevering, D.J. Ramon, D. Vogt, G.P.M. van Klink, G. van Koten, J. Org. Chem. **68**, 675 (2003)
322. N.J.M. Pijnenburg, M. Lutz, M.A. Siegler, A. Spek, G. van Koten, R.J.M.K. Gebbink, New J. Chem. **35**, 2356 (2011)
323. H.-J. van Manen, R.H. Fokkens, N.M.M. Nibbering, F.C.J.M. van Veggel, D.N. Reinhoudt, J. Org. Chem. **66**, 4643 (2001)
324. Y. Wang, S. Wang, S. Shao, J. Ding, L. Wang, X. Jing, F. Wang, Dalton Trans. **44**, 1052 (2015)
325. B.-L. Li, L. Wu, Y.-M. He, Q.-H. Fan, Dalton Trans. 2048 (2007)
326. L. Chen, Z. Ma, J. Ding, L. Wang, X. Jing, F. Wang, Chem. Commun. **47**, 9519 (2011)
327. S.C. Lo, E.B. Nambdas, P.L. Burn, I.D.W. Samuel, Macromolecules **36**, 9721 (2003)
328. R.N. Bera, N. Cumpstey, P.L. Burn, I.D.W. Samuel, Adv. Funct. Mater. **17**, 1149 (2007)
329. E.B. Namdas, A. Ruseckas, I.D.W. Samuel, S.-C. Lo, P.L. Burn, Appl. Phys. Lett. **86**, 091104 (2005)
330. N. Cumpstey, R.N. Bera, P.L. Burn, I.D.W. Samuel, Macromolecules **38**, 9564 (2005)
331. S.-C. Lo, N.A.H. Male, J.P.J. Markam, S.W. Magennis, P.L. Burn, O.V. Salata, I.D.W. Samuel, Adv. Mater. **14**, 975 (2002)
332. T. Tsuzuki, N. Shirasawa, T. Suzuki, S. Tokito, Jpn. J. Appl. Phys. Part 1 **44**, 4151 (2005)
333. T.D. Anthopoulos, J.P.J. Markham, E.B. Namdas, I.D.W. Samuel, S.-C. Lo, P.L. Burn, Org. Electron. **7**, 85 (2006)
334. C.J. Yates, I.D.W. Samuel, P.L. Burn, S. Wedge, W.L. Barnes, Appl. Phys. Lett. **88**, 161105 (2006)
335. S.-C. Lo, R.N. Bera, R.E. Harding, P.L. Burn, I.D.W. Samuel, Adv. Funct. Mater. **18**, 3080 (2008)
336. T.-H. Kwon, M.K. Kim, M.K. Kim, J. Kwon, D.-Y. Shin, S.J. Park, C.-L. Lee, J.-J. Kim, J.-I. Hong, Chem. Mater. **19**, 3673 (2007)
337. Q.-D. Liu, J. Lu, J. Ding, Y. Tao, Macromol. Chem. Phys. **209**, 1931 (2008)
338. J.C. Ribiere, A. Ruseckas, K. Knights, S.V. Staton, N. Cumpstey, P.L. Burn, I.D.W. Samuel, Phys. Rev. Lett. **100**, 017402/1 (2008)
339. J.J. Kim, Y. You, Y.-S. Park, J.-J. Kim, S.Y. Park, J. Mater. Chem. **19**, 8347 (2009)

340. J.W. Levell, J.P. Gunning, P.L. Burn, J. Robertson, I.D.W. Samuel, Org. Electron. **11**, 1561 (2010)
341. W. Tian, Q. Qi, B. Song, C. Yi, W. Jiang, X. Cui, W. Shen, B. Huang, Y. Sun, J. Mater. Chem. C **3**, 981 (2015)
342. H. Jin, W. Zhang, D. Wang, Z. Chu, Z. Shen, D. Zou, X. Fan, Q. Zhou, Macromolecules **44**, 9556 (2011)
343. W. Zhang, H. Jin, F. Zhou, Z. Shen, D. Zou, X. Fan, J. Polym. Sci., Part A Polym. Chem. **50**, 3895 (2012)
344. Y. Li, Y. Liu, M. Zhou, Dalton Trans. **41**, 2582 (2012)
345. K.M. Jung, K.H. Kim, J.-I. Jin, M.J. Cho, D.H. Choi, J. Polym. Sci. Part A **46**, 7517 (2008)
346. Y.-J. Cho, S.A. Hong, H.-J. Son, W.-S. Han, D.W. Cho, S.O. Kang, Inorg. Chem. **53**, 13136 (2014)
347. T. Qin, J. Ding, L. Wang, M. Baumgarten, G. Zhou, K. Müllen, J. Am. Chem. Soc. **131**, 14329 (2009)
348. R. Guan, Y. Xu, L. Ying, W. Yang, H. Wu, Q. Chen, Y. Cao, J. Mater. Chem. **19**, 531 (2009)
349. N. Mehraban, H.S. Freeman, Materials **8**, 4421 (2015)
350. S. Li, G. Zhong, W. Zhu, F. Li, J. Pan, W. Huang, H. Tian, J. Mater. Chem. **15**, 3221 (2005)
351. R. Breinbauer, E.N. Jacobsen, Angew. Chem. Int. Ed. **39**, 3604 (2000)
352. I. Sato, T. Shibata, K. Ohtake, R. Kodaka, Y. Hirokawa, N. Shirai, K. Soai, Tetrahedron Lett. **41**, 3123 (2000)
353. A. Pitto-Barry, N.P.E. Barry, V. Russo, B. Heinrich, B. Donnio, B. Therrien, R. Deschenaux, J. Am. Chem. Soc. **136**, 17616 (2014)
354. C. Müller, L.J. Ackerman, J.N.H. Reek, P.C.J. Kamer, P.W.N.M. van Leeuwen, J. Am. Chem. Soc. **126**, 14960 (2004)
355. G.P. Yan, C.W. Ai, L. Li, R.F. Zong, F. Liu, Chin. Sci. Bull. **55**, 3085 (2010)
356. P. Verwilst, S. Park, B. Yoon, J.S. Kim, Chem. Soc. Rev. **44**, 1791 (2015)
357. A.J.L. Villaraza, A. Bumb, M.W. Brechbiel, Chem. Rev. **110**, 2921 (2010)
358. C.F.G.C. Geraldes, S. Laurent, Contrast Media Mol. Imaging **4**, 1 (2009)
359. Z. Qiao, X. Shi, Prog. Polym. Sci. **44**, 1 (2015)
360. E.J. Werner, A. Datta, C.J. Jocher, K.N. Raymond, Angew. Chem. Int. Ed. **47**, 8568 (2008)
361. S. Aime, S.G. Crich, E. Gianolio, G.B. Giovenzana, L. Tei, E. Terreno, Coord. Chem. Rev. **250**, 1562 (2006)
362. N. Kamaly, A.D. Miller, J.D. Bell, Curr. Top. Med. Chem. **10**, 1158 (2010)
363. J.C. Gore, H.C. Manning, C.C. Quarles, K.W. Waddell, T.E. Yankeelov, Magn. Reson. Imaging **29**, 587 (2011)
364. K. Glunde, D. Artemov, M.F. Penet, M.A. Jacobs, Z.M. Bhujwalla, Chem. Rev. **110**, 3043 (2010)
365. K. Gonsalves, C. Halberstadt, C.T. Laurencin, L. Nair (eds.), *Biomedical Nanostructures* (Wiley, Hoboken, 2007)
366. O. Rolland, C.-O. Turrin, A.-M. Caminade, J.-P. Majoral, New J. Chem. **33**, 1809 (2009)
367. B. Fadeel, A. Pietroiusti, A.A. Shvedova, *Adverse Effects of Engineered Nanomaterials: Exposure, Toxicology, and Impact on Human Health* (Elsevier, Amsterdam, 2012)
368. H. Kobayashi, M.W. Brechbiel, Mol. Imaging **2**, 1 (2003)
369. J.M. Bryson, J.W. Reineke, T.M. Reineke, Macromolecules **45**, 8939 (2012)
370. R.R. Amirov, *Metal Compounds as Magnetic Relaxation Probes for Highly Organized Media* (Novoe Znanie, Kazan, 2005)
371. U. Boas, J.B. Christensen, P.M.H. Heegaard, *Dendrimers in Medicine and Biotechnology: New Molecular Tools* (RSC, Cambridge, 2005)
372. Z. Zhou, Z.-R. Lu, Wiley Interdiscip. Rev. Nanomed. Nanobiotechnol. **5**, 1 (2013)
373. K. Nwe, M. Bernardo, C.A.S. Regino, M. Williams, M.W. Brechbiel, Bioorg. Med. Chem. **18**, 5925 (2010)
374. Y.-H. Tang, A.Y.-T. Huang, P.-Y. Chen, H.-T. Chen, C.-L. Kao, Curr. Pharm. Design **17**, 2308 (2011)

375. K. Nwe, H. Xu, C.A.S. Regino, M. Bernardo, L. Ileva, L. Riffle, K.J. Wong, M.W. Brechbiel, Bioconjug. Chem. **20**, 1412 (2009)
376. A. Nazemi, E.R. Gillies, Dendrimer bioconjugates: synthesis and application, in *Chemistry of Bioconjugates: Synthesis, Characterization, and Biomedical Applications*, ed. by R. Narain (Wiley, Hoboken, 2014)
377. A. Nazemi, E.R. Gillies, Braz. J. Pharm. Sci. **49**, 15 (2013)
378. V.J. Venditto, C.A.S. Regino, M.W. Brechbiel, Mol. Pharm. **2**, 302 (2005)
379. S. Langereis, Q.G. de Lussanet, M.H.P. van Genderen, W.H. Backes, E.W. Meijer, Macromolecules **37**, 3084 (2004)
380. S. Langereis, Q.G. de Lussanet, M.H.P. van Genderen, E.W. Meijer, R.G.H. Beets-Tan, A. W. Griffioen, J.M.A. van Engelshoven, W.H. Backes, NMR Biomed. **19**, 133 (2006)
381. K. Luo, G. Liu, W.C. She, Q.Y. Wang, G. Wang, B. He, H. Ai, Q.Y. Gong, B. Song, Z.W. Gu, Biomaterials **32**, 7951 (2011)
382. H. Kobayashi, M.W. Brechbiel, Adv. Drug Deliv. Rev. **57**, 2271 (2005)
383. N. Sato, H. Kobayashi, A. Hiraga, T. Saga, K. Togashi, J. Konishi, M.W. Brechbiel, Magn. Reson. Med. **46**, 1169 (2001)
384. M. Port, C. Corot, O. Rousseaux, I. Raynal, L. Devoldere, J.-M. Idée, A. Dencausse, S. Le Greneur, C. Simonot, D. Meyer, Magn. Res. Mater. Phys. Biol. Med. **12**, 121 (2001)
385. R. Kreiter, A.W. Kleij, R.J.M. Klein Gebbink, G. van Koten, Top. Curr. Chem. **217**, 163 (2001)
386. K. Vetterlein, U. Bergmann, K. Büche, M. Walker, J. Lehmann, M.W. Linsheid, G.K.E. Criba, M. Hildebrand, Electrophoresis **28**, 3088 (2007)
387. G.M. Nicolle, É. Tóth, H. Schmitt-Willich, B. Radüchel, A.E. Merbach, Chem. Eur. J. **8**, 1040 (2002)
388. D.A. Fulton, M. O'Halloran, D. Parker, K. Senanayake, M. Botta, S. Aime, Chem. Commun. **4**, 474 (2005)
389. A.E. Merbach, E. Toth (eds.), *The Chemistry of Contrast Agents in Medical Magnetic Resonance Imaging* (Wiley, Chichester, 2001)
390. A.T. Yordanov, H. Kobayashi, S.J. English, K. Reijnders, D. Milenic, M.C. Krishna, J.B. Mitchell, M.W. Brechbiel, J. Mat. Chem. **13**, 1523 (2003)
391. H. Kobayashi, N. Sato, S. Kawamoto, T. Saga, A. Hiraga, T.L. Haque, T. Ishimori, J. Konishi, K. Togashi, M.W. Brechbiel, Bioconjug. Chem. **12**, 100 (2001)
392. H. Kobayashi, S. Kawamoto, M. Bernardo, M.W. Brechbiel, M.V. Knopp, P.L. Choyke, J. Control. Release **111**, 343 (2006)
393. F. Figueira, P.M.R. Pereira, S. Silva, J.A.S. Cavaleiro, J.P.C. Tome, Curr. Org. Synth. **11**, 110 (2014)
394. W.S. Li, T. Aida, Chem. Rev. **109**, 6047 (2009)
395. D. Du, D. Fortin, P.D. Harvey, Inorg. Chem. **50**, 11493 (2011)
396. K. Albrecht, Y. Kasai, A. Kinoto, K. Yamamoto, Macromolecules **41**, 3793 (2008)
397. Z. Ishtaiwi, T. Rüffer, S. Klaib, R. Buschbeck, B. Walfort, H. Lang, Dalton Trans. **43**, 7868 (2014)
398. C.Y. Huang, Y.O. Su, Dalton Trans. **39**, 8306 (2010)
399. N. Nishiyama, H.R. Stapert, G.D. Zhang, D. Takasu, D.-L. Jiang, T. Nagano, T. Aida, K. Kataoka, Bioconjug. Chem. **14**, 58 (2003)
400. R. Ideta, F. Tasaka, W.-D. Jang, N. Nishiyama, G.-D. Zhang, A. Harada, Y. Yanagi, Y. Tamaki, T. Aida, K. Kataoka, Nano Lett. **5**, 2426 (2005)
401. G.-D. Zhang, A. Harada, N. Nishiyama, D.-L. Jiang, H. Koyama, T. Aida, K. Kataoka, J. Control. Release **93**, 141 (2003)
402. I. Dunphy, S.A. Vinogradov, D.F. Wilson, Anal. Biochem. **310**, 191 (2002)
403. R.P. Briñas, T. Troxler, R.M. Hochstrasser, S. Vinogradov, J. Am. Chem. Soc. **127**, 11851 (2005)
404. M. Kozaki, K. Akita, S. Suzuki, K. Okada, Org. Lett. **9**, 1509 (2007)
405. M. Kozaki, K. Akita, K. Okada, D.-M.S. Islam, O. Ito, Bull. Chem. Soc. Jpn **83**, 1223 (2010)

406. W.D. Jang, Y. Nakagishi, N. Nishiyama, S. Kawauchi, Y. Morimoto, M. Kikuchi, K. Kataoka, J. Control. Release **113**, 73 (2006)
407. S. Herlambang, M. Kumagai, T. Nomoto, S. Horie, S. Fukushima, M. Oba, K. Miyazaki, Y. Morimoto, N. Nishiyama, K. Kataoka, J. Control. Release **155**, 449 (2011)
408. Y. Peng, H. Zhang, H. Wu, B. Huang, L. Gan, Z. Chen, Dyes Pigments **87**, 10 (2010)
409. J.-Y. Liu, X.-J. Jiang, W.-P. Fong, D.K.P. Ng, Org. Biomol. Chem. **6**, 4560 (2008)
410. Y. Li, W.D. Jang, N. Nishiyama, A. Kishimura, S. Kawauchi, Y. Morimoto, S. Miake, T. Yamashita, M. Kikuchi, T. Aida, K. Kataoka, Chem. Mater. **19**, 5557 (2007)
411. W.D. Jang, N. Nishiyama, K. Kataoka, Supramol. Chem. **19**, 309 (2007)
412. K. Sugisaki, T. Usui, N. Nishiyama, W.D. Jang, Y. Yanagi, S. Yamagami, S. Amano, K. Kataoka, Invest. Ophthalmol. Vis. Sci. **49**, 894 (2008)
413. S. Lim, D. Choi, E.J. Shin, Bull. Korean Chem. Soc. **29**, 1353 (2008)
414. F. Setaro, R. Ruiz-González, S. Nonell, U. Hahn, T. Torres, J. Inorg. Biochem. **136**, 170 (2014)
415. C.J. Medforth, Z. Wang, K.E. Martin, Y. Song, J.L. Jacobsen, J. Allen Shelnutt, Chem. Commun. 7261 (2009)
416. T. Hasobe, J. Phys. Chem. Lett. **4**, 1771 (2013)
417. X. Zhang, Y. Zeng, T. Yu., J. Chen, G. Yang, Y. Li, J. Phys. Chem. Lett. **5**, 2340 (2014)
418. E. Antunes, C. Litwinski, T. Nyokong, Conjugates of nanomaterials with phthalocyanines, in *Intelligent Nanomaterials: Processes, Properties, and Applications*, eds. by A. Tiwari, A. K. Mishra, H. Kobayashi, A.P.F. Turner (Wiley-Scrivener Publishing LLC, Hoboken, 2012)
419. T. Hasobe, Y. Kashiwagi, M.A. Absalom, J. Sly, K. Hosomizu, M.J. Crossley, H. Imahori, P.V. Kamat. S. Fukuzumi, Adv. Mater. **16**, 975 (2004)
420. M. Vinodh, F.H. Alipour, A.A. Mohamod, T.F. Al-Azemi, Molecules **17**, 11763 (2012)
421. M.S. Choi, T. Aida, H. Luo, Y. Araki, O. Ito, Angew. Chem. Int. Ed. **42**, 4060 (2003)
422. D.M. Guldi, Chem. Soc. Rev. **31**, 22 (2002)
423. T. Hasobe, P.V. Kamat, M.A. Absolum, Y. Kashiwagi, J. Sly, M.J. Crossely, K. Hosomizu, H. Imahori, S. Fukuzumi, J. Phys. Chem. B **108**, 12865 (2004)
424. W.S. Li, K.S. Kim, D.L. Jiang, H. Tanaka, T. Kawai, J.H. Kwon, D. Kim, T. Aida, J. Am. Chem. Soc. **128**, 10527 (2006)
425. M. Kozaki, K. Akita, S. Suzuki, K. Okada, Org. Lett. **9**, 3315 (2007)
426. J. Zhao, H.-Y. Zhang, H.-L. Sun, Y. Liu, Chem. Eur. J. **21**, 4457 (2015)
427. M. Fathalla, A. Neuberger, S.-C. Li, R. Schmehl, U. Diebold, J. Jayawickramarajah, J. Am. Chem. Soc. **132**, 9966 (2010)
428. K. Ladomenou, V. Nikolaou, G. Charalambidis, A.G. Coutsolelos, Coord. Chem. Rev. **306**, 1 (2015)
429. A.-M. Caminade, J.-P. Majoral, Chem. Soc. Rev. **39**, 2034 (2010)
430. Y. Kim, M.F. Mayer, S.C. Zimmerman, Angew. Chem. Int. Ed. **42**, 1121 (2003)
431. T. Palacin, H. Le Khanh, B. Jousselme, P. Jegou, A. Filoramo, C. Ehli, D.M. Guldi, S. Campidelli, J. Am. Chem. Soc. **131**, 15394 (2009)
432. M. Kato, E. Hashimoto, M. Kozaki, S. Suzuki, K. Okada, Tetrahedron Lett. **53**, 309 (2012)
433. T. Imaoka, H. Horiguchi, K. Yamamoto, J. Am. Chem. Soc. **125**, 340 (2003)
434. T. Imaoka, R. Tanaka, S. Arimoto, M. Sakai, M. Fujii, K. Yamamoto, J. Am. Chem. Soc. **127**, 13896 (2005)
435. T. Imaoka, Y. Kawana, T. Kurokawa, K. Yamamoto, Nat. Commun. **4**, Article number: 2581 (2013)
436. K. Albrecht, N. Sakane, K. Yamamoto, Chem. Commun. **50**, 12177 (2014)
437. T. Imaoka, Y. Kawana, T. Kurokawa, K. Yamamoto, Nat. Commun. **4**, 2581 (2013)
438. D. Astruc, L. Liang, A. Rapakousiou, J. Ruiz, Acc. Chem. Res. **45**, 630 (2012)
439. U. Hahn, T. Torres, J. Porphyr. Phthalocyanines **15**, 364 (2011)
440. C.N. Moorefield, S. Perera, G.R. Newkome, Dendrimer chemistry: supramolecular perspectives and applications, in *Dendrimer-Based Drug Delivery Systems: From Theory to Practice*, ed. by Y. Cheng (Wiley, Hoboken, 2012)

441. A.-L. Wirotius, E. Ibarboure, L. Scarpantonio, M. Schappacher, N.D. McClenaghan, A. Deffieux, Polym. Chem. **4**, 1903 (2013)

442. N.T. Nguyen, J. Hofkens, I.G. Scheblykin, M. Kruk, W. Dehaen, Eur. J. Org. Chem. **2014**, 1766 (2014)

443. M. Kimura, Y. Nakano, N. Adachi, Y. Tatewaki, H. Shirai, N. Kobayashi, Chem. Eur. J. **15**, 2617 (2009)

444. D.A. Roberts, T.W. Schmidt, M.J. Crossley, S. Perrier, Chem. Eur. J. **19**, 12759 (2013)

445. F. Brégier, S.M. Aly, C.P. Gros, J.-M. Barbe, Y. Rousselin, P.D. Harvey, Chem. Eur. J. **17**, 14643 (2011)

446. L.L. Pleux, Y. Pellegrin, E. Blart, F. Odobel, A. Harriman, J. Phys. Chem. A **115**, 5069 (2011)

447. D.K. Muli, B.L. Carpenter, M. Mayukh, R.A. Ghiladi, D.V. McGrath, Tetrahedron Lett. **56**, 3541 (2015)

448. D. Kim (ed.), *Multiporphyrin Arrays: Fundamentals and Applications* (CRC, Singapore, 2012)

449. D.-L. Jiang, T. Aida, Prog. Polym. Chem. **30**, 403 (2005)

450. L. Flamigni, A.M. Talarico, B. Ventura, G. Marconi, C. Sooambar, N. Solladié, Eur. J. Inorg. Chem. **12**, 2557 (2004)

451. M. Kozaki, H. Tujimura, S. Suzuki, K. Okada, Tetrahedron Lett. **49**, 2931 (2008)

452. M. Kozaki, A. Uetomo, S. Suzuki, K. Okada, Org. Lett. **10**, 4477 (2008)

453. A. Uetomo, M. Kozaki, S. Suzuki, K. Yamanaka, O. Ito, K. Okada, J. Am. Chem. Soc. **133**, 13276 (2011)

454. M.S. Choi, T. Yamakaki, I. Yamazaki, T. Aida, Angew. Chem. Int. Ed. **40**, 3194 (2001)

455. W. Maes, J. Vanderhaeghen, S. Smeets, C.V. Asokan, L.M. Van Renterghem, F.E. Du Prez, M. Smet, W. Dehaen, J. Org. Chem. **71**, 2987 (2006)

456. P.C. Lo, X. Leng, D.K.P. Ng, Coord. Chem. Rev. **251**, 2334 (2007)

457. Z. Zhao, A.O. Ogunsipe, M.D. Maree, T. Nyokong, J. Porphyr Phthalocyanines **9**, 186 (2005)

458. S. Kimata, T. Aida, Tetrahedron Lett. **42**, 4187 (2001)

459. S. Shinoda, M. Ohashi, H. Tsukube, Chem. Eur. J. **13**, 81 (2007)

460. S. Shinoda, J. Incl. Phenom. Macrocyclic. Chem. **59**, 1 (2007)

461. N.T. Nguyen, G.M. Mamardashvili, O.M. Kulikova, I.G. Scheblykin, NZh Mamardashvili, W. Dehaen, RSC Adv. **4**, 19703 (2014)

462. U. Hahn, F. Setaro, X. Ragàs, A. Gray-Weale, S. Nonell, T. Torres, Phys. Chem. Chem. Phys. **13**, 3385 (2011)

463. R.R. Dasari, M.M. Sartin, M. Cozzuol, S. Barlow, J.W. Perry, S.R. Marder, Chem. Commun. **47**, 4547 (2011)

464. M. Häußler, H. Dong, B.Z. Tang, Hyperbranched polymers containing transition metals: synthetic pathways and potential applications, in: *Inorganic and Organometallic Macromolecules: Design and Applications*, ed. by A.S. Abd-El-Aziz, C.E. Carraher, C.U. Pittman (Springer, NY, 2008)

465. Y. Tao, Q. Xu, N. Li, J. Lu, L. Wang, X. Xia, Polymer **52**, 4261 (2011)

466. T. Guo, L. Yu, Y. Yang, Y. Li, Y. Tao, Q. Hou, L. Ying, W. Yang, H. Wu, Y. Cao, J. Lumin. **167**, 179 (2015)

467. M. Zhu, Y. Li, X. Cao, B. Jiang, H. Wu, J. Qin, Y. Cao, C. Yang, Macromol. Rapid Commun. **35**, 2071 (2014)

Chapter 5
Metal Chelate Dendrimers

Abstract In this chapter the synthetic methodologies, physico-chemical peculiarities, properties, and spatial organization of metal chelate dendrimers as a specific sub-class of polymeric metal chelates are considered. These compounds are subdivided into molecular, intracomplex, and macrocyclic types which in turn are grouped depending on the nature of the donor atoms (N,N-, N,O-, N,S-, O,O-, O,S-, S,S-, P,P-chelates, etc.). Special attention is paid to the features of the preparation of metal chelate star polymers by "arm-first", "core-first" and click-to-chelate approaches. The main data on the synthesis, spatial structure and properties of the metal chelates with hyperbranched dendrimers are summarized. The problems and future prospects of metal chelate dendrimers are outlined.

The creation of dendrimers becomes an important landmark in the development of contemporary coordination chemistry. Metallodendrimers are unique polymer compounds containing metals in different parts of dendritic architecture, which have been obtained in the first days of dendrimer chemistry and are objects of increasing interest of researchers [1–28]. Hierarchically dendrons and dendrimers are collections of 10^3–10^4 atoms with relative molar weights 10,000–100,000 and hydrodynamic sizes changing from 1 to 30 nm [29]. Due to presence of a great number of functional groups dendrimers form stoichiometric nanometer compounds of metallodendrimer type [30–33]. It is important to emphasize that following reduction of metals in these structures brings to production of nanocluster compounds covered by dendritic shell [14, 17–19, 29, 33–41]. Metallodendrimers are convenient precursors for light-harvesting molecular devices and machines: cables, switches, extenders, antennas, and nanomotors [42–44]. The use of controlled polymer architecture of dendrimers together with a suitable metal may lead to new functional materials based on well-designed redox-active sites [12], which can be used for development of molecular nanobatteries for redox probing, modified electrode surfaces, and redox catalysis [45].

In order to identify and predict the possible directions of practical use of metallodendrimers key is to incorporate the following effects: dendrimer (dendritic) effect, multivalency effect, and preorganization effect [46]. For all metallodendrimers more

or less typical is dendrimer (or dendritic) effect, when a functional group behaves differently depending on whether it is free or bound to a dendrimer [14]. At that, properties of metallodendrimers can even change depending on dendrimer generation. Usually all possible dendritic effects are interrelated and perhaps are determined by several parameters referred to as critical nanoscale design parameters [47–49]. Size, shape, flexibility/rigidity, architecture, surface chemistry, and elemental composition of the dendrimer are related to such parameters. Dendritic effect can be observed for all classes of metallodendrimers and for any type of properties, however, it is most commonly manifested in such areas as catalysis [8, 10, 12–14, 50–55], medicine [10, 14, 16, 56–65], and materials [10, 14, 66–70]. The multivalency (cooperative) effect is due to a decrease in entropy in successive chelation reactions of one metal by the polymer ligand [46, 71–73]. The preorganization effect is associated with a decrease in the degree of freedom in the transition from monomers to polymers [46].

Metallodendrimers are classified [17, 39] depending on a place of metal location in a dendrimer architecture (Fig. 5.1): (i) metal as a core, (ii) metal as branching centers, (iii) metal in multiple locations of a dendrimer, (iv) metal as a termini group, (v) metal as a connector, (vi) metal as a transformation auxiliaries or secondary element of a construction.
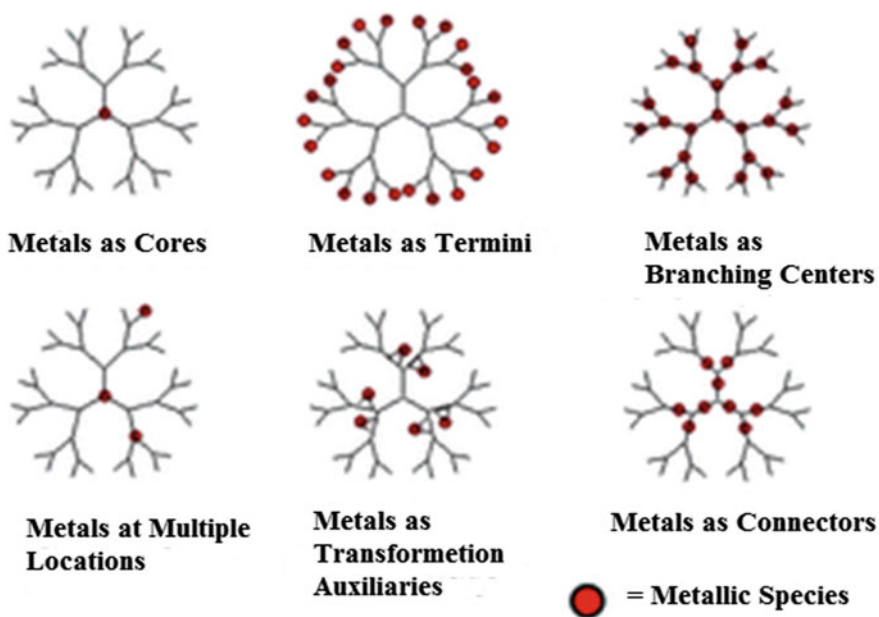
Fig. 5.1   The different roles metals can play in metallodendrimers

One of important subclasses of metallodendrimers is metal chelate dendrimers (MCDs), which contain metal chelate units in different parts of a dendritic structure. Metal chelate dendrimers are relatively young, but rapidly developed area of PMC chemistry.

Most widely used method of MCD production is direct interaction between MX_n and dendrimers containing chelating units [20]. This is substantially advanced by high solubility of dendrimers in different solvents, including water. One of efficient ways of enhancement of dendrimer solubility is fixing of different hydrophilic groups to their surface, for example, bulk oligo(oxyethylene) terminal group, which provides solubility in polar protonic solvents and prevents aggregation of dendrimers [74, 75]. Equally important is the fact the synthesis of MCD in most cases is carried out deliberately in view of their possible future applications. It should be noted that all chelating dendrimers in the synthesis process pass a number of successive chromatographic purifications, whereby the final product has a high purity. Therefore, it is possible to use the synthesis of MCD in situ without isolation of the metal chelates in a number of applications.

5.1   Molecular Metal Chelates

To date, it has accumulated considerable experimental material on the molecular MCD, and the range is wide enough chelating fragments.

5.1.1   Metal Chelates with N-Donor Ligands

The metal chelates with N-donor ligands occupy a significant place among MCD of molecular type. A typical example can be the family of pyridylimine chelates, which are located in various parts of the dendritic architecture. Thus, carbosilane dendritic mono-metallic Ni(II) chelates containing aryl-*N,N′*-iminopyridine ligand linked to Fréchet type dendrons are synthesized [76, 77]. It turned out that catalytic activity of these chelates with methylalumoxan (MAO) as co-catalyst is influenced more by metallic nuclearity than bulkiness of MCD. In addition, strong generation dependence concerning the topology and molecular weight of PE products is observed, at that, increasing generation leads to preferred oligomerization (chain transfer) over polymerization.
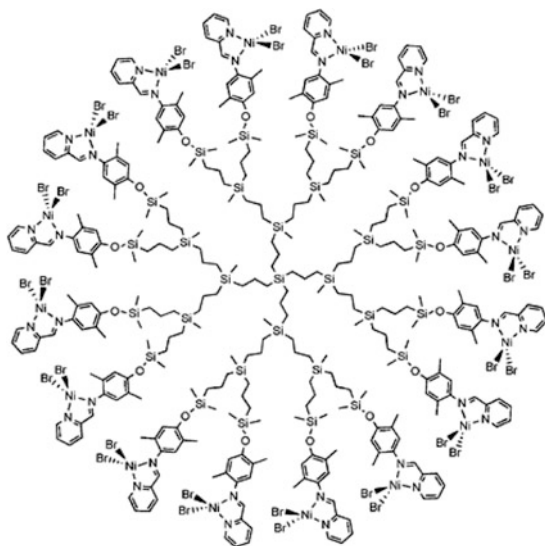
Of interest are Pd-MCDs, containing 4, 8 or 16 terminal pyridylimine chelates, which were used as catalysts for the alternating copolymerization of CO and 4-*tert*-butyl-St [78]. It should be noted that chloro methyl or cationic methyl Pd-MCDs are a *cis-trans* mixture of diastereoisomers. Besides, in this case the dendritic effect is observed: generation of the dendrimer affects the catalyst activity and the microstructure of the reaction products.
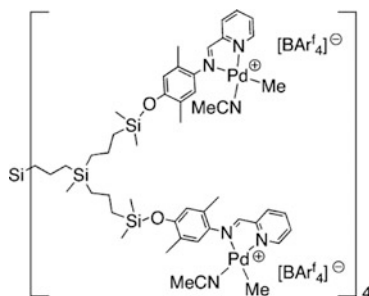
Chelation reaction of G1 PPI dendrimer modified through reaction of terminal amino groups and 2-pyridinecarboxaldehyde with PdCl$_2$(COD) in dry CH$_2$Cl$_2$ brings to production of MCD with pyridylimine Pd-containing chelates linked along perimeter [79]. The obtained MCD was isolated as a light orange, amorphous solid in 93% yield.
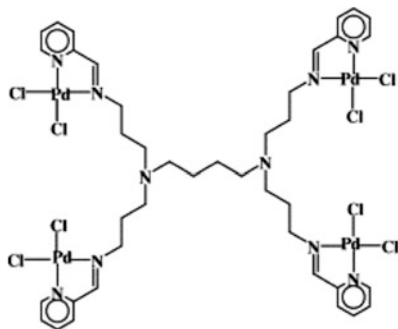
It should be noted that G1 and G2 Pd-containing pyridylimine MCD can be used as initial catalytic substance for ethylene polymerization resulted in high-molecular weight and high density PE production using MAO as co-catalyst [79] or for Heck coupling reaction [80].

Chelating dendrimer obtained by Schiff condensation reaction of tris-2-(ami-noethyl) amine with 2-pyridinecarboxaldehyde reacts reaction with [RhCl(CO)$_2$]$_2$ and [RhCl(COD)]$_2$ with formation of respective pyridylimine Rh MCD [81]. These Rh(I) chelate dendrimers are thermally stable, have high activity, and are chemo- and regioselective in hydroformylation of 1-octen.

G1 PAMAM dendrimers were modified by pyridylimine units to afford two MCD, a tetranuclear platinum chelate and a multinuclear copper chelate (Fig. 5.2) [82]. It is important that the cytotoxicity of these MCDs were evaluated in vitro against several cancer cell lines, namely MOLT-4 (cisplatin-sensitive cancer cell line), MCF-7 (cisplatin-resistant breast cancer cell line) and Chang Liver of benign origin.
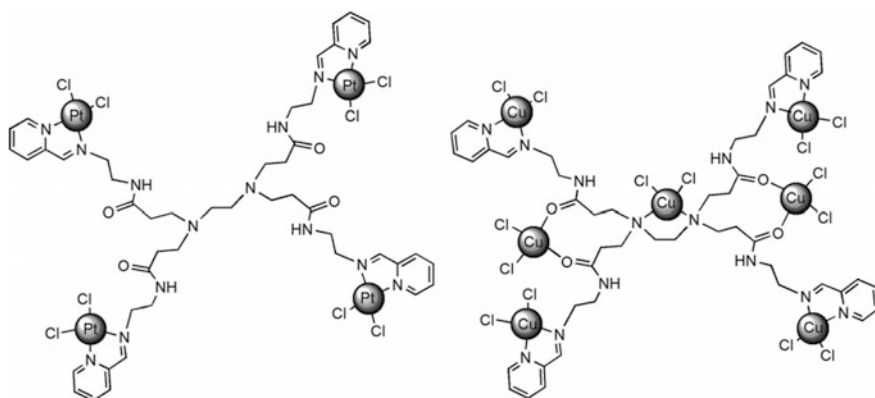
Fig. 5.2 Tetranuclear Pt-functionalized MCD (left) and a multinuclear Cu-functionalized MCD (right)
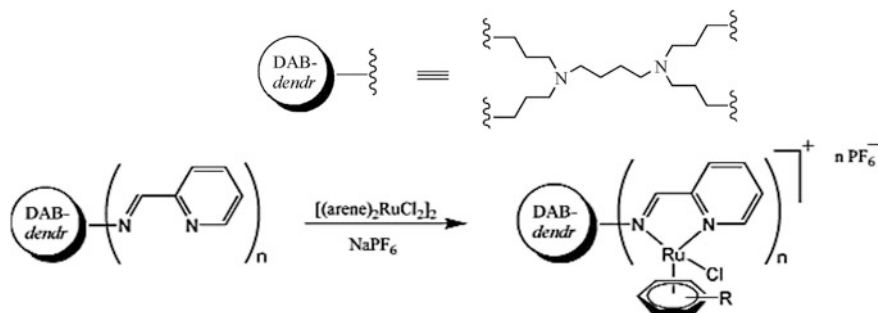
Scheme 5.1 Reaction of binuclear arene Ru precursors with pyridylimine dendritic ligands

G1–G2 Ru(II) arene MCDs based on PPI dendritic frameworks are obtained from binuclear arene Ru precursors (arene = *p*-cymene or hexamethylbenzene) as a result of reactions with pyridylimine dendritic ligands in form of hexafluorophosphate salts (Scheme 5.1) [56]. In this case structure of mononuclear Ru MCD was confirmed by X-ray diffraction analysis. These compounds are air-stable, soluble in DMSO, acetone and acetonitrile, and MALDI-TOF studies confirmed that all of the dendrimer end groups were functionalized with Ru(II) arene moieties.

Studies of cytotoxicity of MCD using A2780 and A2780cisR human ovarian carcinoma cancer cell lines in the range of concentrations 32–208 μM showed that distinct correlation is observed between MCD size and cytotoxicity, at that G2 MCD exhibited higher activity to both cell lines. The DNA binding studies confirmed high cytotoxicity observed for these chelates, because the MCD act, probably, via another mechanism than *cis*-platinum [56]. Therefore, definite positive dendritic effects are established for anti-proliferative activity and for DNA cleavage activity.

We note also the phosphorus chelating dendrimers bearing respectively 6, 12, or 24 pyridylimine end groups [83]. In situ chelation of CuI with these dendritic ligands gave catalysts, suitable for coupling of 3,5-dimethylphenol with PhI, as well as pyrazole with PhI and PhBr. In particular, the monomeric CuI complex was not efficient in the case of PhI, whereas all the MCDs were very efficient (95% yield). Besides, an increase of the efficiency was observed on going from the monomer (inefficient) to the G3 MCD (80% yield) in the case of PhBr, indicating a positive dendrimer effect.
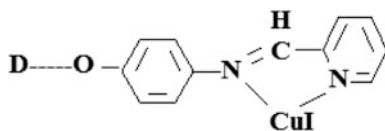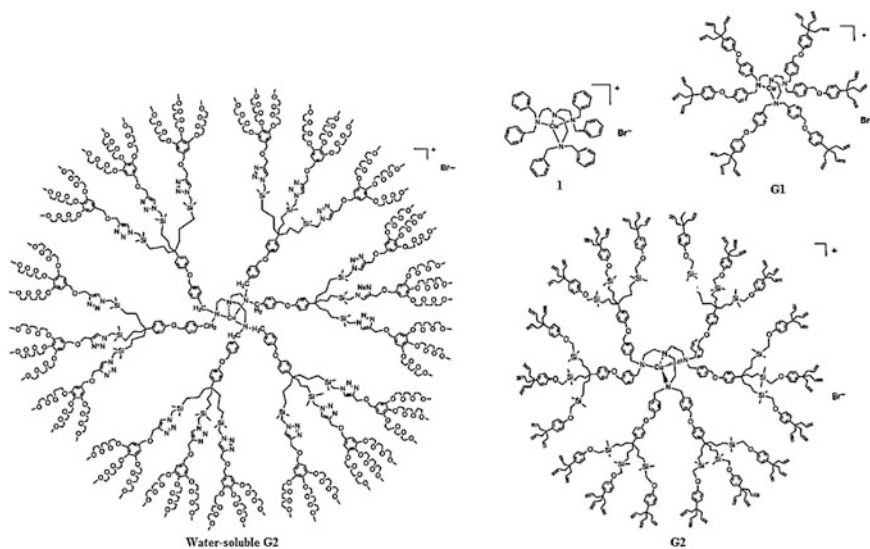
Fig. 5.3 Cu(I) (hexabenzyl)tris(en) chelate 1 and Cu(I) G1, G2, and water-soluble G2 MCD

Free pyridylimine G1–G3 dendrimer ligands and the copper MCDs have been used as anti-proliferative agents against different cancerous cells strains and it turned out that effectiveness depends on the type of end fragments. It is important that the free G1–G2 ligands and their copper chelates have nearly the same efficiency. At the same time, no cytotoxic effect was observed with metal-free G3 dendrimer, while the corresponding copper MCD has high activity [84].

It should be noted polyamine Ni MCDs active in ethylene oligomerization (with MAO as a co-catalyst) formed upon interaction of Ni salts with G1 and G2 polyamide dendrimers [85].

Of interest is a comparative study of Cu(I) (hexabenzyl)tris(en) complex and dendrimer analogues with 18 or 54 branch termini (Fig. 5.3) [86]. The Cu(I) MCDs were synthesized by heating CuBr with the chelating dendritic ligands G1, G2 and water-soluble G2 in freshly distilled dioxane at 60 °C overnight. Both parent and dendritic chelates exhibited high activities (yields and the turnover numbers) for click reactions with different substrates. MCDs also showed a positive dendrimer effect associated with steric protection against aerobic oxidation of Cu(I) to bis (μ-oxo)-bis-Cu(II) [86].

Chelation of MX_2 salts, where M = Co(II), Ni(II), Cu(II), Zn(II) and X = Cl, SCN, NO_3, to G0 and G1 multi-coordinating dendritic polyamine ligands (Fig. 5.4) derived from tris(2-aminoethyl) amine and modified on ends using di-3, 4-decyloxyphenyl groups, brings to MX_2L mononuclear MCDs [87]. All MCDs formed with mesogenic low generation ligand G0 are mesoformic apart from Ni(II) nitrate complex, and showed either smectic ambiguous or Col_h phase, depending on used salt. Temperature ranges of meso-phases also strongly depend on origin of a
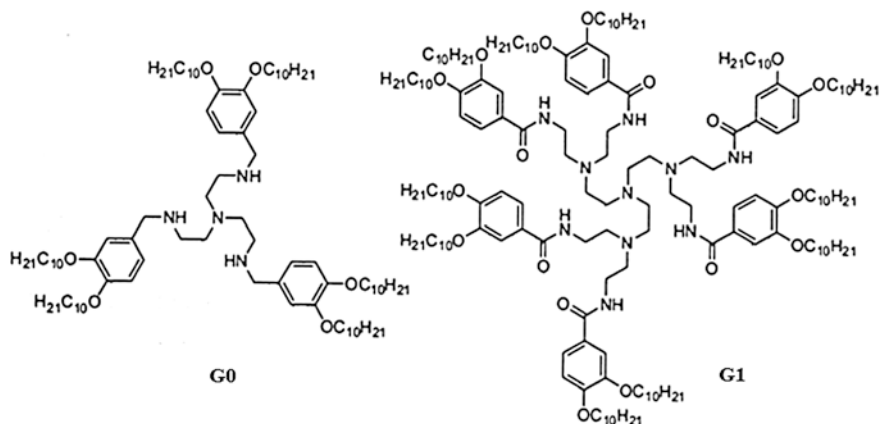
Fig. 5.4 Chemical structure of G0 and G1 dendritic ligands, forming liquid crystalline $MX_2 \cdot L$ MCDs by binding of metal salts

metal ion, and T_i decrease in sequence Zn(II) > Co(II) > Cu(II) > Ni(II). Chelation of $CuCl_2$ by a higher generation dendrimer G1, which itself shows monotropic Col$_h$ phase [88] and stabilizes a chelate by coordination with fourth central nitrogen atom in dendritic imino-junction, promotes increment of pure stability of Col$_h$ meso-phase from almost room temperature to 140 °C, at which the chelate clears into isotropic liquid. MCDs can have a trigonal bipyramidal coordination geometry, which brings to $[MX \cdot L]^+[X]^-$ penta-coordinated ionic chelates or exist as octahedral (and neutral) $MX_2 \cdot L$ chelates. The latter geometry was observed for Co(II) and Cu(II) chelates, Ni(II) chelates were octahedral; geometry of Zn(II) chelate was not identified. Here formation of columnar meso-phases (and smectic also) follows from nano-segregation between a strongly polar dendritic and metal fragments surrounded by aliphatic chains. With G2 dendrimer as a ligand or with Zn(II) as a central atom, columnar hexagonal phase is formed. In the opposite case lamellar meso-phases are formed.

It is important to notice that radionuclide MCDs are perfect nanoprobes for nuclear medical visualization, in particular, for Single Photon Emission Computed Tomography (SPECT) (^{99m}Tc, ^{111}In, ^{125}I), as well as for Positron Emission Tomography (^{68}Ga). Also a special attention is paid to radiolabeled (^{64}Cu, ^{18}F, [76]Br, ^{68}Ga, ^{111}In) MCDs targeting $\alpha_v\beta_3$ integrin, because this is a reliable strategy for estimation of angiogenesis presence, one of the best studied, and for targeted biological process.

In this view, very interesting precursors for development of chelating dendrimers are aliphatic G1–G8 polyether dendrons with a core of *p*-toluene sulfonyl ethyl ester as easily removed protective group, which can be efficiently replaced by different nucleophiles [89]. Thus, tridentate bis(pyridyl)amine chelating ligand, which forms stable complexes with Tc(I) and Re(I), was integrated into a dendrimer core using chemistry of amidation. Chelation of a ligand core with ^{99m}Tc radioactive element was achieved for G5–G7 within 10 min, and as a result, regioselective radiolabeling
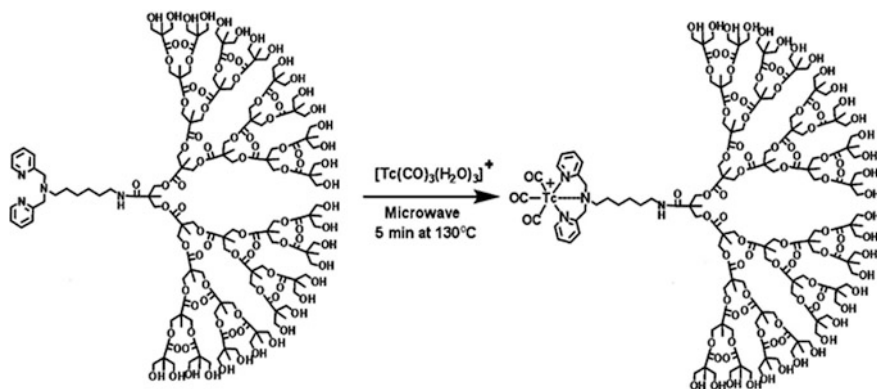
Scheme 5.2 Chelation of dendritic tridentate bis(pyridyl)amine ligand with [99mTc] radioactive element

of dendrimers was reached (Scheme 5.2). It is important that biodistribution of radiolabeled dendrimers can be easily estimated using SPECT.

It should be noted using CuAAC for the terminal functionalization of G1–G3 dendrons based on poly (2,2-bis(hydroxymethyl)propanoic acid) [59]. The subsequent modification of the prepared dendrons at the core by a dipicolylamine allows to radiolabeling with [99mTc] for biomedical applications.

Of interest are [111In]-radiolabeled dendritic nanoprobes, in vitro and in vivo tumor targeting efficiency of which was estimated in a mouse melanoma model [90]. It occurs that tumor uptake reaches such high values as $12.7 \pm 1.6\%$ ID g^{-1} at 4 h after intravenous injection in comparison with $1.5 \pm 0.5\%$ ID g^{-1} for non-functionalized nanoprobe, and correlates with a dendrimer multivalency.

The similar dendritic tridentate bis(pyridyl)amine ligands were reacted with a Cu (II) ion solution to form the targeted MCDs with 6, 12, 33, 104, and 232 Cu ions for G2–G6 dendrimers, respectively (Scheme 5.3) [91].

An important observation was made during studying chelation of Cu(I) salts with dendronized quinoline ligand containing terminal acid or ester groups [92]. It
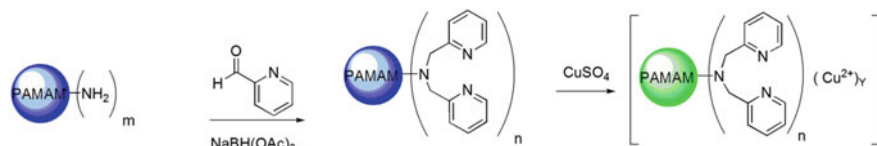
Scheme 5.3 Synthetic approach to prepare MCD based on tridentate bis(pyridyl)amine ligand
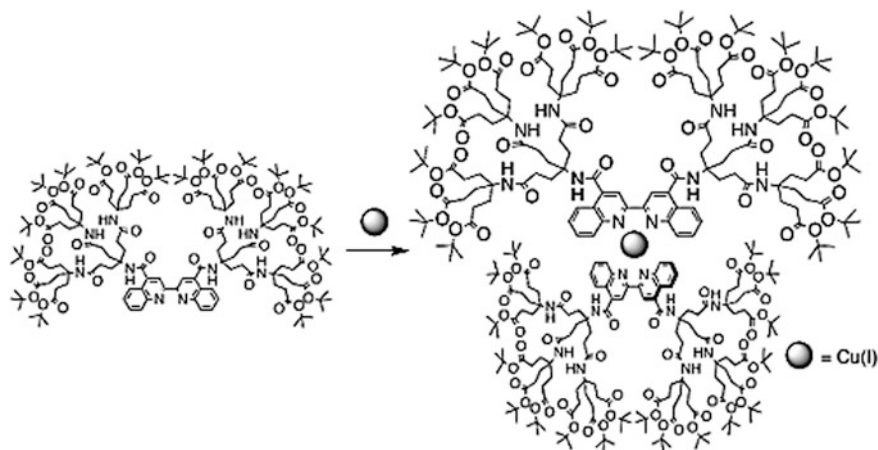
Scheme 5.4 Scheme of chelation of Cu(I) salts with dendronized quinoline ligand

is important that treatment of a ligand with Cu(I) salt brings to intermolecular cross-linking with quantitative formation of stable MCD with Cu(I) core (Scheme 5.4).

Among the numerous examples of MCD based on bpy chelating ligands, it should be noted a pH-switching metal coordination established during interaction between a chelating peptide dendrimer obtained via formation of double thioether bond between 5,5′-bis(bromomethyl)-bpy and two equivs of the peptide dendrimer (Ac-Glu-Ser)$_8$ (Dap-Glu-Ala)$_4$(Dap-Amb-Tyr)$_2$Dap-Cys-Asp-NH$_2$ (Dap = branching 2,3-diamino-propanoic acid, Amb = 4-aminomethylbenzoic acid) on the one hand, and Fe(II) salt on the other hand (Scheme 5.5) [93]. In particular, for pH 4.0, a dendrimer links Fe(II) with formation of expected tris-coordinated dendrimer complex FeL$_3$ (K$_f$ = 2.1 $\times$ 10^{15} M^{-3}), while for pH 6.5 mono-coordinated complex FeL (K$_f$ = 2.1 $\times$ 10^5 M^{-1}) is formed due to electrostatic repulsion between polyanionic dendrimer branches.

Of interest is the study a peptide dendrimer library with a 5,5′-disubstituted bpy core to determine the effect of the branched structure on the chelating ability of ligands at the core [94]. For this dendrimer, the main factor is the nature of amino acids placed at the dendrimer periphery, at that chelation is inhibited by cationic residues and promoted by anionic residues.

Studies of chelation of 6- and 18-armed dendritic polyallyl- and polyferrocenyl-containing bpy ligands produced by the coupling reaction of 4,4′-bis(bromo-methyl)-bpy with AB$_3$- and AB$_9$-dendrons and RuCl$_2$(bpy)$_2$ showed that, contrary to bulk 18-ferrocenyl-bpy ligand, 6-allyl and 18-allyl-bpy ligands take part in the chelation giving respective Ru(II) MCDs (Fig. 5.5) [95]. In the case of ferrocenyl-bpy ligand steric volume of two nonaferrocenyl wedges in 4,4′-position of a bpy fragment prevents transformation of a transoid structure of a ligand into a cissoid structure necessary for chelation with a metal. Therefore, 18-ferrocenyl Ru(II) dendrimer was not obtained.
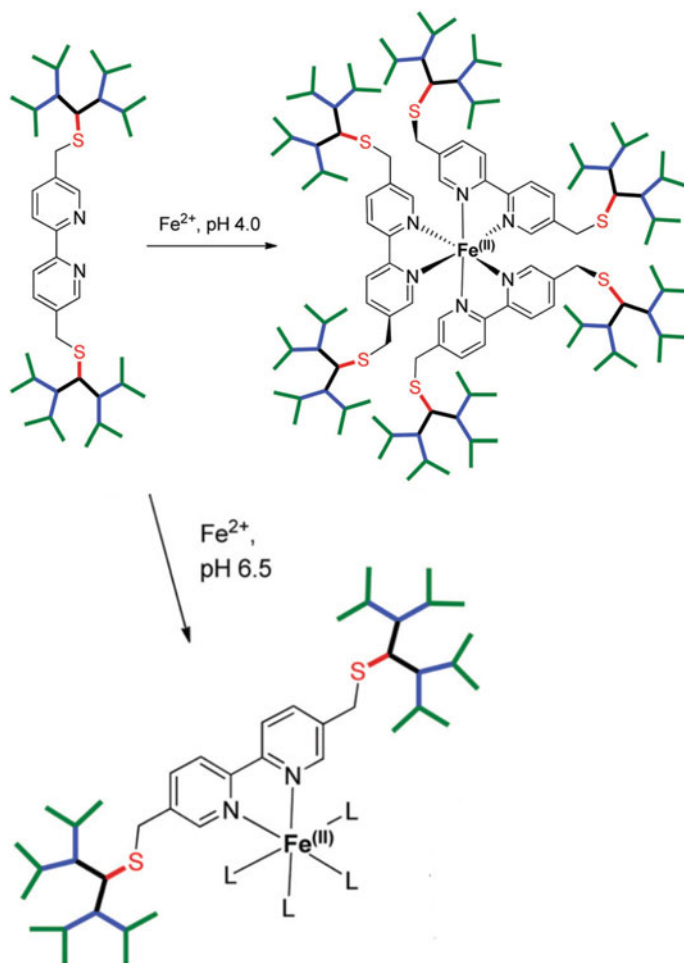
Scheme 5.5 A metallopeptide dendrimer peroxidase enzyme model. Monodentate ligand L = H_2O or amino acid side chains such as carboxylate from glutamate

MCD of molecular type with bpy ligands was obtained by reaction of MnBr $(CO)_3$ with chelating DAB-PPI dendrimers (Scheme 5.6) [96]. Dendrimers G1 contained 4 metal chelate units, and G2 contained 8 metal chelate fragments. It occurs that both dendrimer generations are stable in darkness in aqueous buffer solution during 16 h, but show photoactivated CO gas release upon excitation at 410 nm.

Luminescent Ir(III) MCDs with general formula $[\{Ir(ppy)_2\}_nL]^{n+}$, where n = 1, 3, 4, 8, L = poly(bpy)dendrimer, are obtained through placing the transition metal centers at the periphery of the dendritic core, thus increasing a fraction of metal complex per molecule and, probably, increasing photophysical response [97].
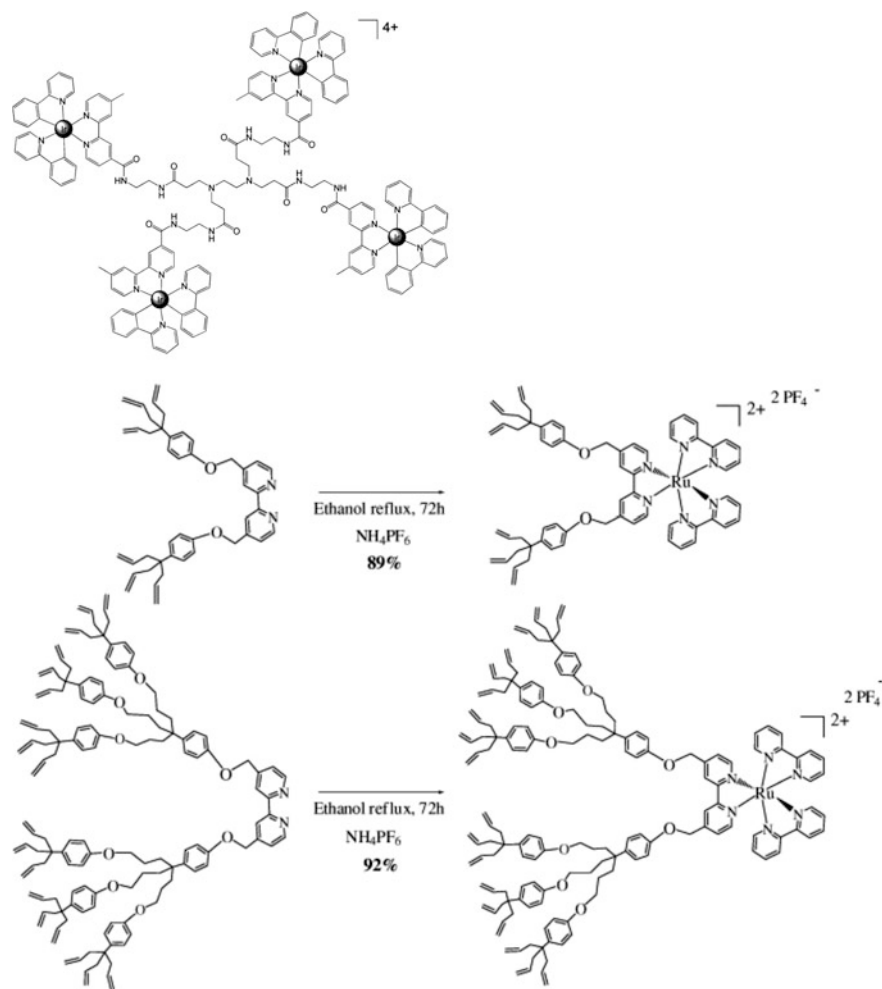
Fig. 5.5 Scheme of chelation of 6- and 18-armed dendritic polyallyl-containing bpy ligands with RuCl$_2$(bpy)$_2$

An assumption was pronounced that dendritic chelates are accumulated in the Golgi apparatus; therefore, they can be used as Golgi staining agents. These results confirm that integration of dendritic ligands can change biological properties of metal chelates.

Using the carbohydrate cancer marker linked to a bpy core, square planar chelates were obtained by simple addition of Cu(II) sulfate (Scheme 5.7) [98]. Cu(II)-chelated 2-acetamido-2-deoxy-D-galactopyranoside derivatives containing four and eight fragments were prepared from an aqueous solution in an efficient manner (H$_2$O, 48 h, 23 °C). After 48 h of stirring, the bluish solution was lyophilized to form light bluish-purple colored powder.
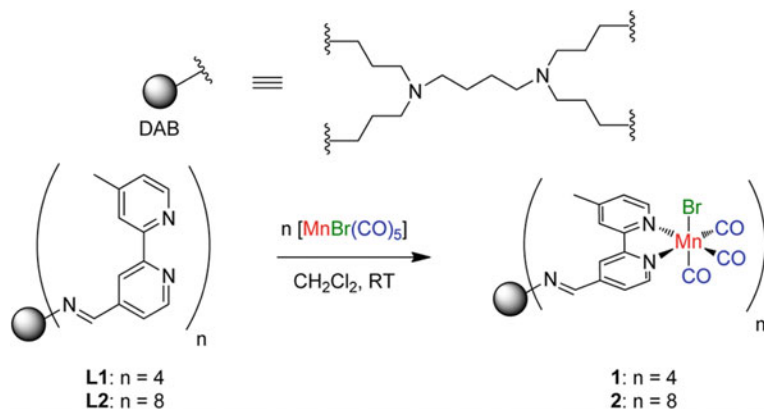
Scheme 5.6 Synthesis of tetra- and octanuclear Mn MCD **1** and **2**
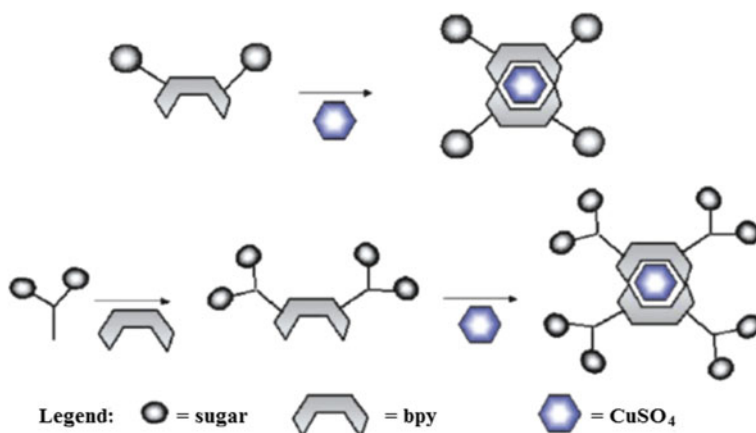
Scheme 5.7 Scheme of synthesis of Cu(II)-chelated 2-acetamido-2-deoxy-D-galactopyranoside derivatives

It should be noted using MCD based on poly (aryl ether) with a bpy core as catalysts for Diels-Alder and three-component condensation reactions [99]. The MCD was prepared in situ in dichloromethane by interaction of chelating dendrimer and Cu(OTf)$_2$.

Considerable interest is the study [100] of the coordination of Pt(II) ions by G4 PAMAM Ru-MCD containing 32 Ru bpy chelates at the periphery [101, 102]. Titration of Ru-MCD by K$_2$PtCl$_4$ solution leads to a decrease in the MLCT band and an increase in a tail below 500 nm (Fig. 5.6, left). Upon binding ~ 20 equivs of Pt(II) by Ru-MCD, a plateau at 620 nm is observed (Fig. 5.6, right, inset) that allows to calculating the stoichiometry of the heterometallic complex.
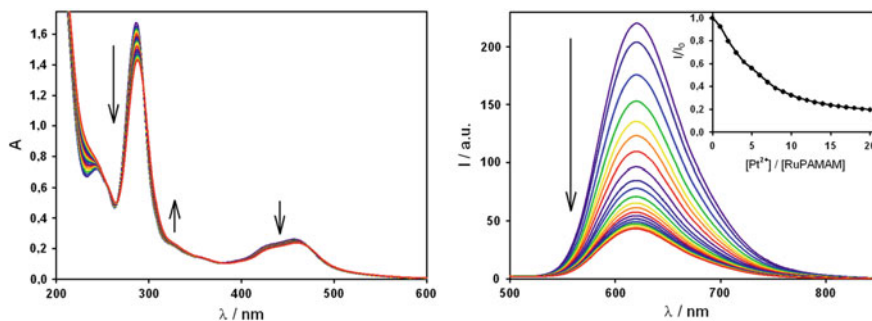
Fig. 5.6 Absorption spectra (left) and emission spectra (right) of a 1.47×10^{-6} M solution of MCD in H_2O upon titration with K_2PtCl_4. The inset shows the normalized emission intensity changes at 620 nm ($\lambda_{ex} = 375$ nm)

Table 5.1 Stability constants of the formed Cu(II) MCD

Generation	Metal	Stoichiometry	Log K	Solvent
G0	Cu(II)	3:1	16.4 ± 0.8	$CHCl_3$
G1	Cu(II)	3:1	17.5 ± 0.9	$CHCl_3$
G2	Cu(II)	3:1	15.6 ± 0.7	$CHCl_3$
G3	Cu(II)	3:1	16.6 ± 0.7	$CHCl_3$

Chelation of Cu(II) with dendritic oxybato-phen ligands (G0–G3) synthesized using 4,7-bis(4′-hydroxyphenyl)-phen treatment with respective Fréchet type dendrons carrying benzyl bromide function in a focal point was studied by liquid-liquid extraction using ^{64}Cu isotopes. Formation of 1:3 chelates (Cu:L) is shown, in which Cu(II) chromophor has an expected distorted square-planar geometry with two phen donor ligands coordinated with Cu(II) center. The third dendritic ligand, as is assumed, is bound by secondary interactions. Stability constants of 1:3 complexes are log K $\approx$ 16 in $CHCl_3$ (Table 5.1) [103].

The MCDs are obtained built around [Ru(4,7-diphenyl-phen)$_3$]$^{2+}$-type core containing peripheral phenyl residuals [104]. Convergent synthesis of ligands is reached by conjugation of dendritic branches containing focal amino group with chelating phen precursor bringing to formation of sulfonamide bonds. MCD G0 to G2 and monomer analogue (Fig. 5.7) were prepared by irradiation in a microwave oven. In particular, ethylene glycol solution of Ru(III) chloride and the corresponding ligands was heated for 2 min at 200 W in the presence of a few drops of water. The appearance of bright orange color indicates the formation of the [Ru(4,7-diphenyl-phen)$_3$]$^{2+}$-type complexes. Chelation of Ru ions gives respective MCDs containing up to 24 peripheral phenyl units in the case of the greatest dendritic structure. Dendritic effect is well seen during transition from G0 to G2, which is confirmed by increase in lifetime of excited state in aerated acetonitrile and increase in emission quantum yields as compared with low molecular weight analogues.
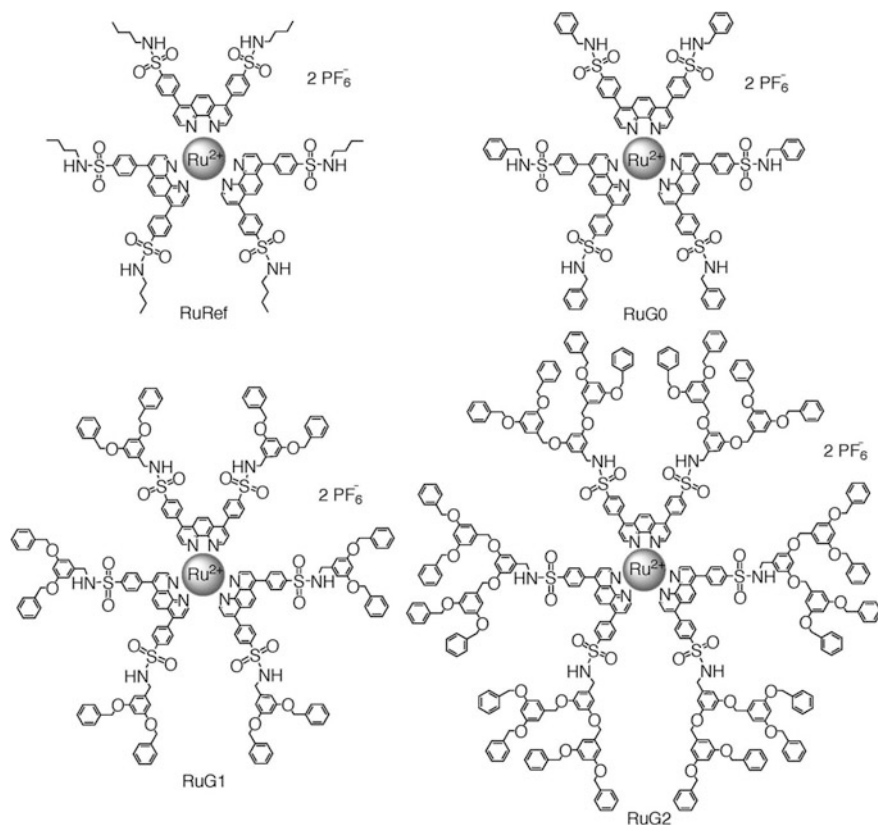
Fig. 5.7 G0–G2 MCD with phenyl end groups and reference chelate with butyl terminal groups

In contrast to chelating monomer, the Job plot for G2 of 2,9-dimethyl-phen grafted dendrimer shows two separated maxima which correspond to Cu(I) ions bound to one or two phen fragments (Fig. 5.8) [105]. This double maximum indicates that 2:1 or 1:1 chelates will predominantly exist for each Cu(I) ion depending on the molar ratio chosen.

Of substantial interest is study of tpy-containing MCD. At that, at present, it is possible to localize tpy chelating fragments in certain parts (core, cavities, focal or branching points, termini) of the dendritic architecture [5, 106].

As a typical example, we note the symmetric homoleptic and asymmetric heteroleptic benzyl ether dendrimers with $[Ru(tpy)_2]^{2+}$ core containing an electrochemically active fragment included in a polyether dendritic shell [107]. However, a purple colored side product of undefined structure was also formed together with the reddish brown bis(tpy)-Ru(II) MCD. It is important that main reaction product can be purified by column chromatography because the side product is much less polar.
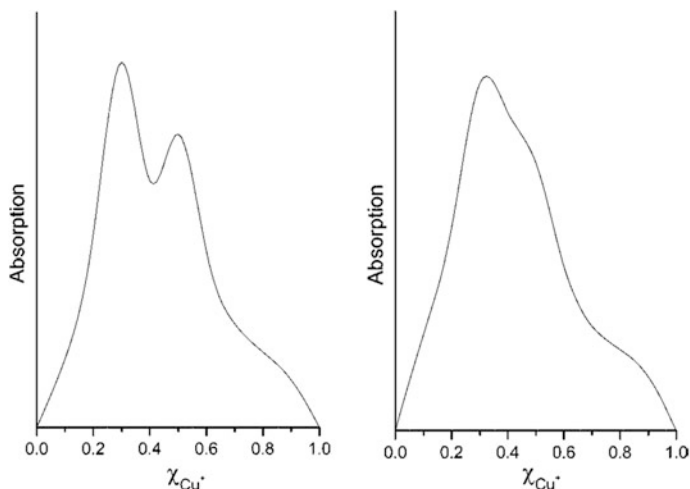
Fig. 5.8 Normalized Job plots for mixtures of the chelating phen dendrimer and $CuPF_6$ (left), and of the chelating phen monomer and $CuPF_6$ (right)
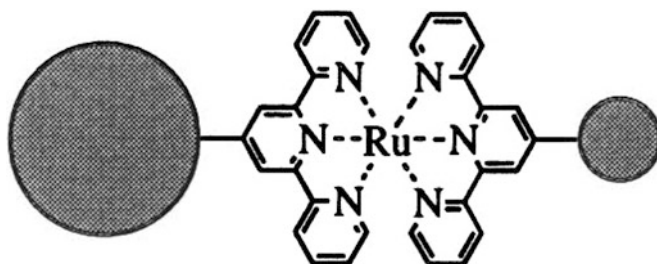
Treatment of G1–G3 dendrons with MX_n brings to formation of corresponding $[Co(tpy)_2]^{2+}$, $[Fe(tpy)_2]^{2+}$ and $[Ru(tpy)_2]^{2+}$ Fréchet type MCDs [108]. In this case the rotational freedom within the dendritic wedge leads to a rich diversity in conformational space. Studies of these structures containing a metal chelate core were carried out using X-ray diffraction analysis for G1 type.

It should be noted 1,3,5-phenylene-based MCD including a Ru-bis(tpy) complex, which was obtained by treatment of chelating dendrimer with $RuCl_3 \cdot 3H_2O$ with the following anion exchange with hexafluorophosphate ion [109]. The terminal *tert*-butyl groups allow to completely encapsulates the $Ru(tpy)_2$ cores and enhances the MCD hydrophobicity.

The homo- and heteroleptic $[Ru(tpy)_2]^{2+}$ chelates containing hydrophilic and hydrophobic dendrons were obtained [110] for development of amphiphilic vectors for potential gene delivery. Owing to staged assembly regime, dendrons can have the same or different degrees of lipophilic or hydrophilic character.
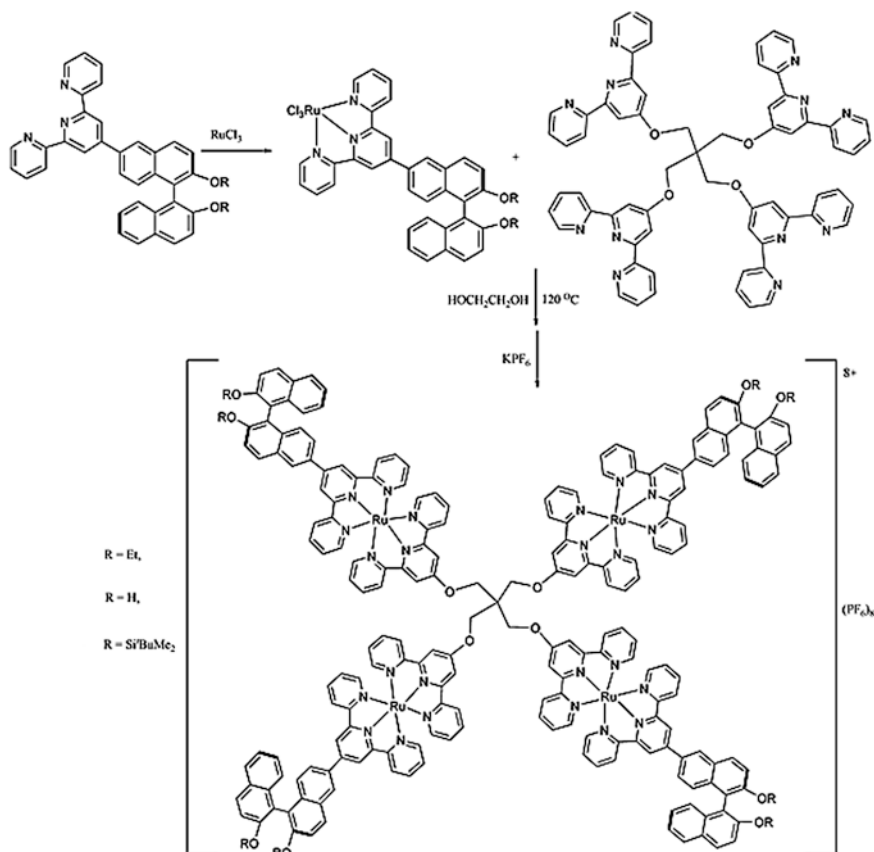
Scheme 5.8 Scheme of synthesis of Ru-tpy MCD with binaphthyl groups

Chelation of Ru(II) with π-conjugated oligothienylene-ethynylene dendrons containing tpy ligands has brought to MCDs with interesting spectroscopic properties [111]. In particular, broad absorption spectra covering from 250 to 600 nm and high molar extinction coefficients are characteristic for the prepared MCDs. The MLCT emission of the MCDs were significantly red-shifted (up to 115 nm) compared to the parent $[Ru(tpy)_2]^{2+}$ chelate.

Apart from abovementioned MCD with external counter-ions, generally neutral MCD was obtained [6, 112] containing four $[Ru(tpy)_2]^{2+}$-linked centers with internal carboxylate groups.

Undoubtedly introduction of chirality and also light-sensitive $[Ru(tpy)_2]^{2+}$ complexes into a dendritic sphere is interesting for production of new macromolecules with optical properties. For these purposes Fréchet type benzyl-bromide dendrons were functionalized with binaphthyl-tpy, which then formed a complex with tetrakis(tpy-4′-oxymethyl) methane through of Ru(III)/Ru(II) chemistry applied (Scheme 5.8) [113]. It is important that enantiopure compound is formed as a result of this reaction.
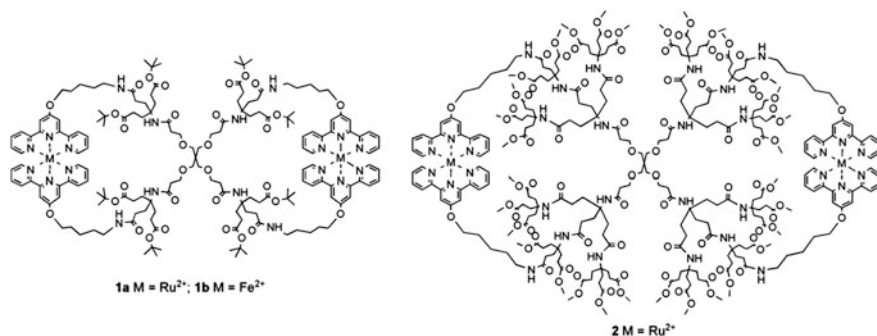
Fig. 5.9 Bis-Ru(II) spirometallodendrimers

Treatment of each generation of the chelating dendrimers with $RuCl_3 \cdot 3H_2O$ followed by addition of excess NH_4PF_6 gives after chromatography bis-Ru(II) spiro MCDs with 41 and 47% yields, respectively (Fig. 5.9) [114]. Additional evidence of easy intramolecular cyclization is obtained using the reaction of tetra-tpy dendrimer with two $FeCl_2 \cdot 4H_2O$ equivs giving (92%) respective pure Fe-spiro dendrimer. On the whole, these examples of macromolecular ring closures, are expected to provide entrance into dendrimer-based molecular devices using integration of different metals, ligands, and oxidized metal states.

PAMAM dendrimers containing en core with $[Ru(tpy)_2]^{2+}$ surface fragments are obtained by formation of peptide bond [115].

A method of production of series of MCDs based on mono-, bis-, and tris-Ru-tpy chelates with thiophene arms for photovoltaic applications is developed [116]. Energy levels of these MCD can be efficiently regulated not only by different generations of dendritic thiophene arms, but by their π-conjugated core ligands having different electron-donor (triphenylamine) and electron-acceptor (benzothiadiazole) fragments. Among different generations (G1–G3) of dendrimers, G3 has the highest efficiency of energy transformation in each series of dendrimers based on Ru chelates.

Most lanthanide ions in their stable trivalent state are luminescent and have high magnetic anisotropy [117] and are, therefore, promising basic components in projecting of multifunctional liquid crystals, for example, lanthanidomesogens [118, 119]. Therefore, using such a concept, G0 and G1 dendritic luminescent lanthanidomesogens are obtained by the reaction of $Ln(NO_3)_3$ with 2,6-bis-[(N-ethyl benzimidazol-2-yl)pyridine] fragments, specific central tridentate chelating ligand for Ln(III) ions [120], which has 5- and 5′-positions occupied by cyanobiphenyl-containing dendritic arms [121, 122].
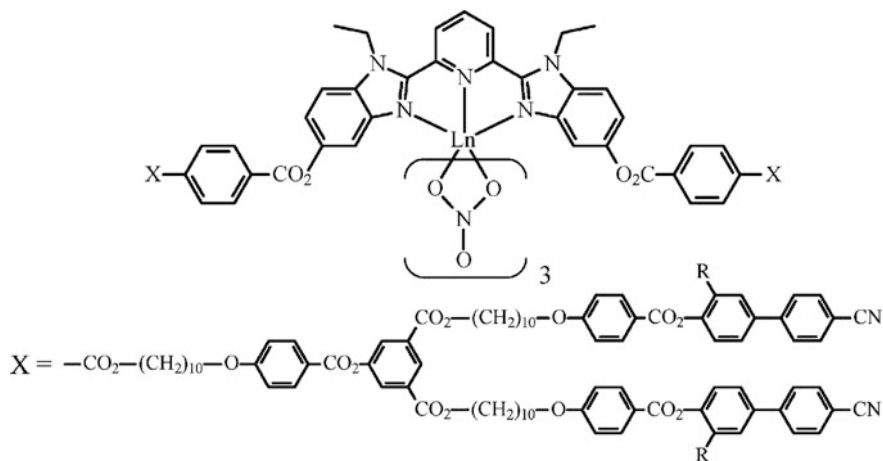
Ligands G1 show simple N single phase from 50–70 to 238 °C (R = H) and 197 °C (R = Me), and from 70–80 to 324 °C for non-methylated (R = H) and down to 205 °C for completely methylated (R = Me) G0 homologous chelates. This general thermal behavior implies some weakening of intermolecular cohesion in N phase as a result of limiting of lateral superposition between methyl-substituted cyanobiphenyl groups. In other words, peripheral cyanobiphenyl dendrimers impose microphase organization compatible with smectic mesomorphism, in which bulk nine coordinated lanthanide cores located between separated mesogenic sub-layers are composed of parallel cyanobiphenyl groups.

Independently on generation, $Ln(NO_3)_3$ coordination brings exclusively to formation of monomer chelates with the lowest lanthanide ions ($[Lu(NO_3)_3 \cdot L]$), while with intermediate (Ln = Eu–Tb) and big (Ln = Pr–La) lanthanide ions, monomer and dimer chelates exist in thermodynamic equilibrium ($2[Ln(NO_3)_3 \cdot L] \leftrightarrow [Ln(NO_3)_3 \cdot L]_2$). This equilibrium depends on formation of lanthanide-size-dependent construction of intermetallic nitrate-bridges and methyl substitution by dendritic ligand strands. Only G1 MCDs $[Ln(NO_3)_3 \cdot L]$ (R = H, Me) are meso-morphous. Bilayer SmA meso-phase is observed between 80–100 and 190–200 °C (R = H, Ln = Lu, Tb, Gd, Eu, Pr), whose structure consists of central cores located between decoupled mesogenic sublayers made by parallel alignment of cyanobi-phenyl groups. For methylated series (R = Me) polymorphism is observed between 80–100 and 145–160 °C: chelates with big lanthanide cations (Ln = La, Pr) give only bilayer SmA meso-phase (with periodicity d from 10 to 12 nm) over entire temperature range, while for the intermediate range and small lanthanide chelates, respectively, additional lamellar phase appears above SmA or SmA phase with comb-like interdigitated structure (Ln = Gd, Tb, d = 6 nm) was discovered, or N (Ln = Eu, Lu, Y) phase, though only in the range from 5 to 10 °C. The best segregation for different segments of molecules is reached in formation of nitrate bridges in $[Ln(NO_3)_3 \cdot L]_2$ dimer chelates, whereas intermolecular shift of strands is

responsible for decrease in interlayer separation in the lamellar phases and/or formation of N phase, probably correlates with a tendency of chelates to existence as monomer types, but not in a form of mixture of monomer and dimer types. Presence of N phase rarely observed in lanthanidomesogens [122] is also very interesting if it advances their solubilization with N hosts and their possible application in display devices.

It should be noted that tpy groups were grafted to phosphorus G1–G4 dendrimers, giving family of chelating dendrimers [123]. The catalytic system involving Sc (OTf)$_3$ and these dendritic tpy ligands promotes the Friedel-Crafts acylation of different aromatic compounds under microwave irradiation with high yields.
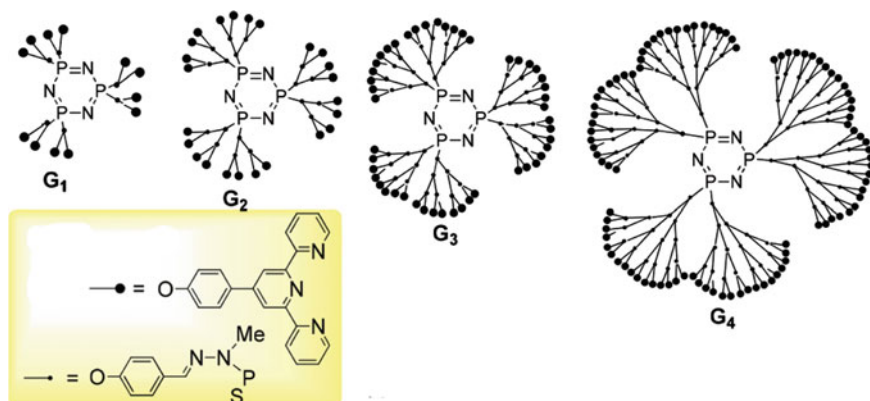
We note neutral and cationic bis(pyrazolyl)methane Pd(II) chelates with poly (aryl ether) of Fréchet type dendrons which were prepared by the interaction of [PdCl$_2$(COD)] with corresponding bis(pyrazolyl)methane, whereas the chlorido (methyl)Pd(II) chelates were synthesized using [PdClMe(COD)] (Scheme 5.9) [124].

Scheme 5.9 Palladium MCDs
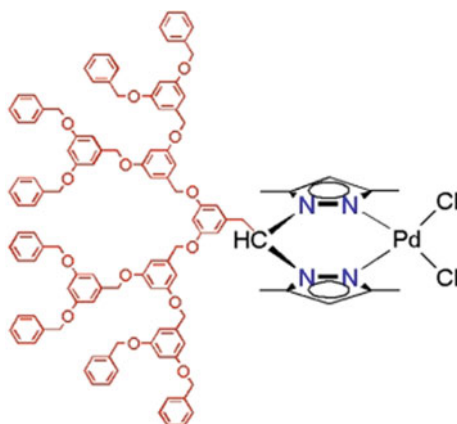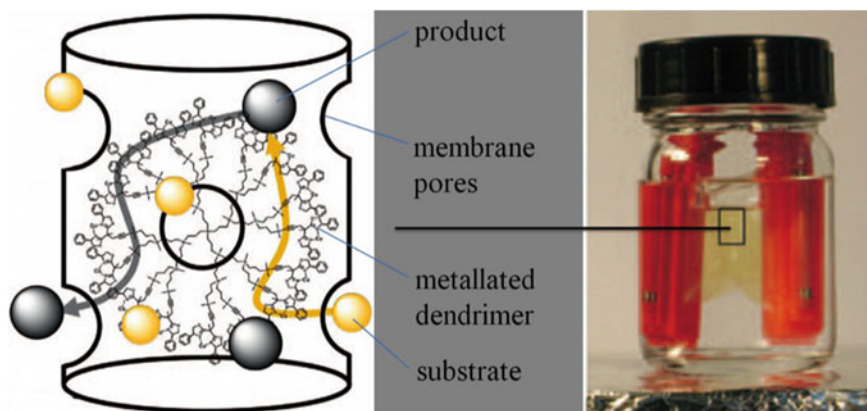
Fig. 5.10 General setup for the recycling using the «catalyst in a tea bag» principle

The Pd MCDs were used as precursors of a catalyst in Heck reaction between *p*-iodotoluene and MA.

An interesting example is the so-named «catalysis in a tea bag» (Fig. 5.10) [125]. At first, bis- and tris-oxazolines with a spacer in the ligand backbone are covalent fixed on carbosilane dendrimers, and then are used as chelating ligands for recyclable Cu(II) catalysts that were immobilized in a membrane bag.

It should be noted using dendritic azabis(oxazoline) ligands in Cu(II)-catalyzed asymmetric benzoylations [126].
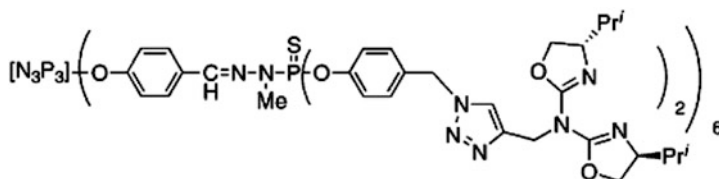
Of interest are mono- and polynuclear Pd-MCDs based on a 2-pyridyl-1,2,3-triazole chelating ligand in which solubility of the MCDs decreases with increasing metal number (Fig. 5.11) [127].

It should be noted water-soluble triazole dendrimers containing the two triazole rings at each bis-(methylol)propionic acid branching site, which are efficient chelating pockets for some transition metals. Thus, the [PdCl$_2$(PhCN)$_2$] chelation with these hydrophilic dendritic ligands is completed within 5 min according to ^{1}H NMR analysis in situ (Fig. 5.12) [128]. The signals of several protons are shifted downfield in comparison to the starting dendrimer, suggesting a deshielding process as a result of
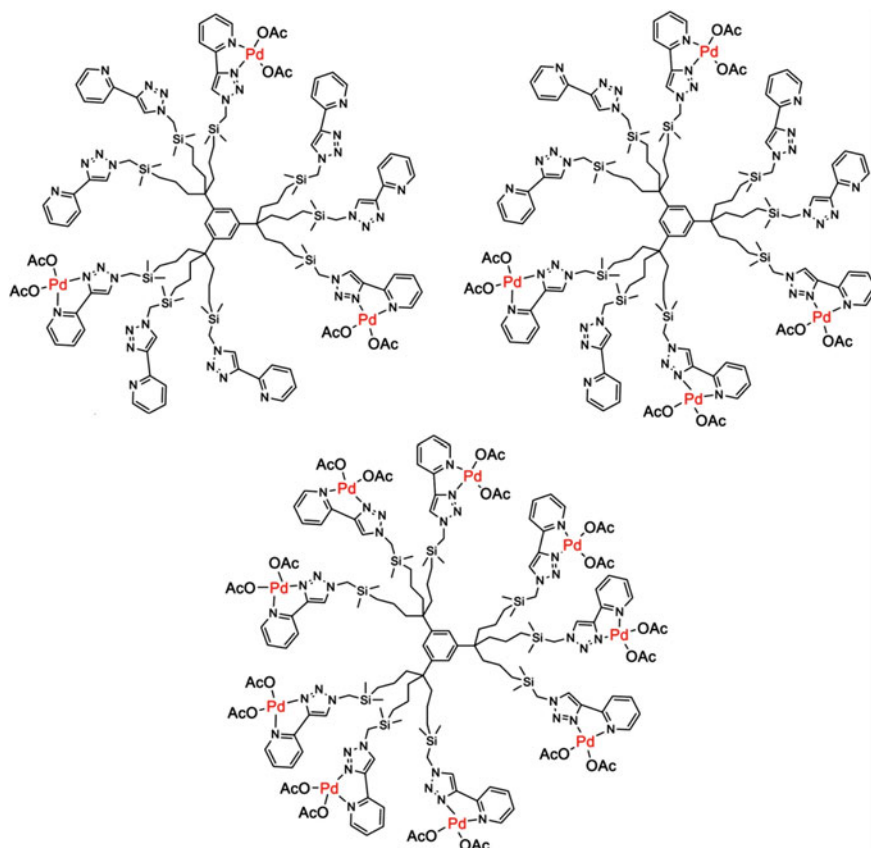
Fig. 5.11 Isolated MCD catalysts containing three, four, and nine metal centers with solubility decreasing with increasing their number

changes in dendrimer architecture and appearance of electron-withdrawing groups. Besides, the triazole protons (Fig. 5.12a, j) are facing inward in the chelating dendrimer but facing outward after the chelation with PdCl$_2$ (Fig. 5.12b). It is shown that the chelation efficiency (CE) is equal to 95 ± 5% for all dendrimers, suggesting the formation of MCDs with 3, 9, and 21 Pd-containing fragments for G1, G2, and G3, respectively.

Wide application in the synthesis of MCD has dendrimers containing chelating 2,6-bis(1,2,3-triazole-4-yl) pyridine (btp) fragment obtained through one-pot click-reaction [129].
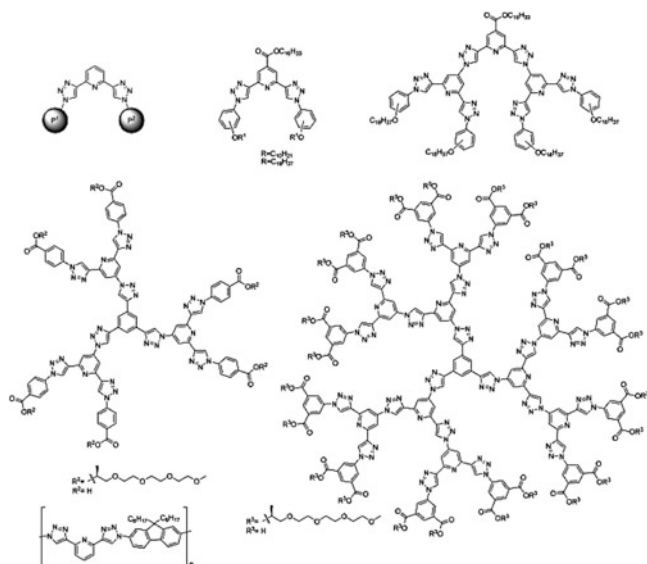
Also numerous examples of cyclometalated Ir(III) dendrimers should be noted, which are used as phosphorescent polymers for OLEDs [130]. These MCDs can be fixed on different substrates, for example, PS matrix, and additionally contain other
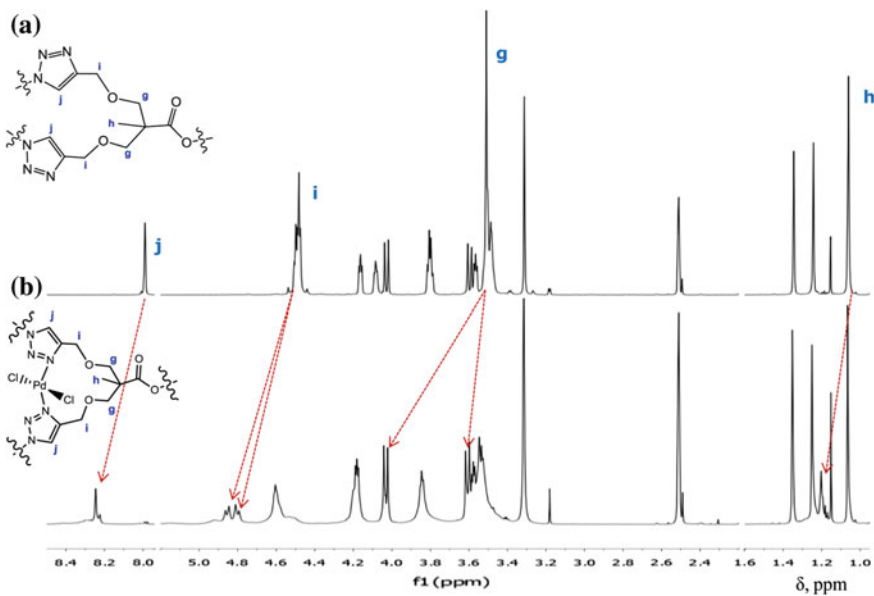
Fig. 5.12 ^{1}H NMR spectra of **a** chelating d-[G2] dendrimer and **b** Pd(II) MCD of d-[G2]. Analysis conditions: 600 MHz, DMSO-d$_6$, 298 K

interesting functional groups, such as, in particular, Cz charge-carrying fragments, which, besides, can prevent aggregation of chromophores [131].
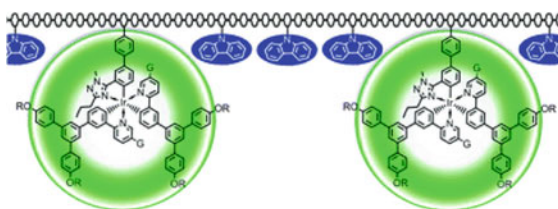
Devices produced using these MCDs, showed high EQE 11.0% (37.3 cd A^{-1}) at 100 cd m^{-2} and 8.3 V, at that, the best efficiency is achieved by mixing of twice dendronized copolymer with 50 wt% of 4,4′-bis(N-dicarbazolyl)biphenyl, which brings to 14,7% EQE (48.3 cd A^{-1}) at 100 cd m^{-2} and 9.3 V.

5.1.2   N,P-Ligands

Among MCD of molecular type, a substantial place has chelates with phosphorus-containing donor ligands [21, 22, 132–134]. One of the typical examples are the dendrimers incorporating γ-iminophosphine Pd chelates on the surface, which were obtained by the interaction of PdCl$_2$(COD) with N,P-donor chelating ligands (one Pd per N,P-ligand) [135]. An X-ray diffraction study corroborated the postulated structure in which the PdCl$_2$ unit is linked both to the imino nitrogen atom and to the phosphino group. The chelates were then used as catalysts for Stille couplings with various substrates.
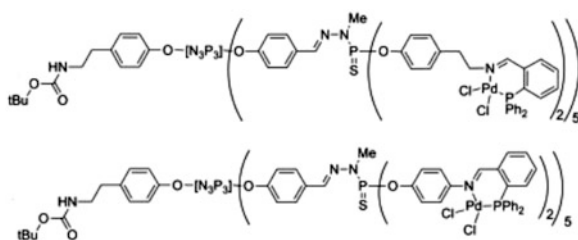
Of interest is using hexachlorocyclotriphosphazene for the preparation of bifunctional «off-center» dendrimers including one protected amine linked to the core and phosphine imines (N,P-ligands) as surface fragments [136]. The sequent interaction of the prepared dendrimers with PdCl$_2$(COD) leads to the MCD of the N,P-ligands.
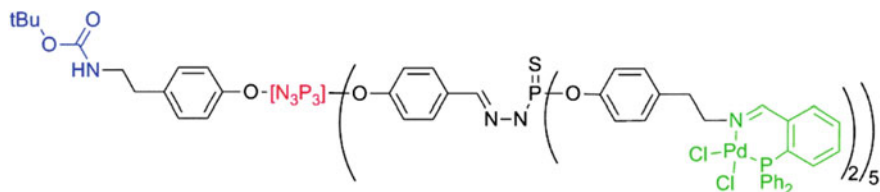
The condensation of the aldehyde terminal groups with (2S)-2-amino-1-(diphenylphosphinyl)-3-methylbutane gives the chiral G3 dendrimer, ended by 24 chelating N,P-ligands [137]. Dendrimer chelation of $[Pd(\eta^3-C_3H_5)Cl]_2$ in situ leads to a catalyst used in asymmetric allylic alkylations of *rac*-(E)-diphenyl-2-propenyl acetate and pivalate.
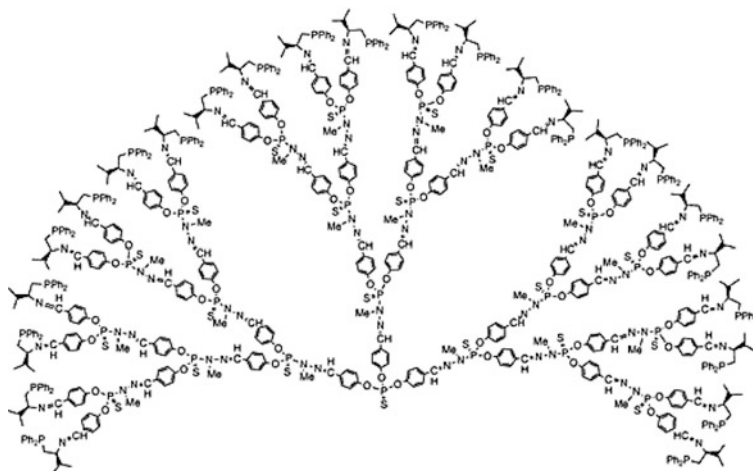
A family of N,P-chelating dendrimers up to G3 is obtained generated from a core based on 15-membered triolefinic azomacrocycle with the following fixing of γ-iminophosphane groups [138]. The dendrimers in dichloromethane solution were treated with stoichiometric amounts of PdCl$_2$(COD) for 3 h to form the targeted MCDs with good yields. It is interesting that the MCDs were synthesized in anhydrous THF; however, after precipitation and drying, their solubility changes and they are only soluble in DMF.
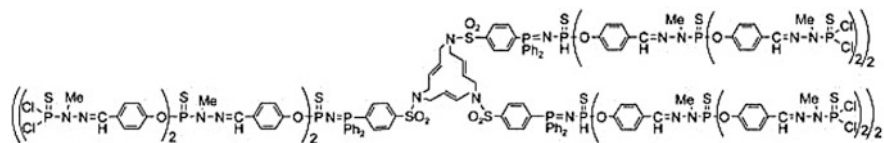
It should be noted the modular synthesis of dendritic phosphinooxazoline (PHOX) ligands and their iridium chelates with BArF$^-$ as the counter-anion [139]. The prepared MCDs were used in the Ir-catalyzed asymmetric hydrogenation of 2,4-diaryl-1,5-benzodiazepines, in which an obvious positive dendritic effect on catalytic activity was observed.

5.1.3   Metal Chelates with P,S-Ligands

A chiral ferrocenyl phosphine-thioether P,S-ligand, functionalized with a phenol group, was used for the substitution reaction on P(S)Cl$_2$ terminal groups, affording a series of chiral G1–G4 dendrimers [140]. The chelating dendrimers were used as ligands for the asymmetric allylic alkylation of *rac*-(E)-diphenyl-2-propenyl acetate. The chelation was carried out in situ by mixing the dendrimers ended by the ligands with [Pd(μ^3-C$_3$H$_5$)Cl]$_2$, using a stoichiometry of one Pd per P,S-ligand.
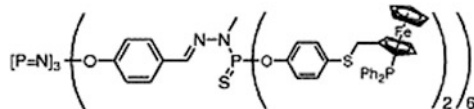
5.1.4   Metal Chelates with P,P-Ligands

The chiral diphosphine-functionalized dendrimers based on carboxyl-linked C2-chiral pyrphos ligand (pyrphos is 3,4-bis(diphenylphosphino)pyrrolidine) and G0–G4 PPI dendrimers form cationic rhododendrimers containing up to 32 metal centers (for the G4 species) [141]. The complete chelation was demonstrated by ^{31}P NMR spectroscopy and the observation of the coordination-shifted AB part of the ABX spin system (δ_A = 33.9, δ_B = 32.9; ^{1}J$_{Rh,P}$ = 150 Hz; ^{2}J$_{P,P}$ = 28 Hz). The similar Rh-MCDs were prepared with PPI and PAMAM dendrimers carrying from 4 to 64 chelating fragments at their periphery in dichloromethane (Scheme 5.10) [142]. It is interesting that the chelation was complete within seconds.

To explore the potential for a conformationally driven asymmetric induction of a catalytic dendrimer a pair of G1 dendrons at the 3 and 3′ positions of a 2,2′-bis
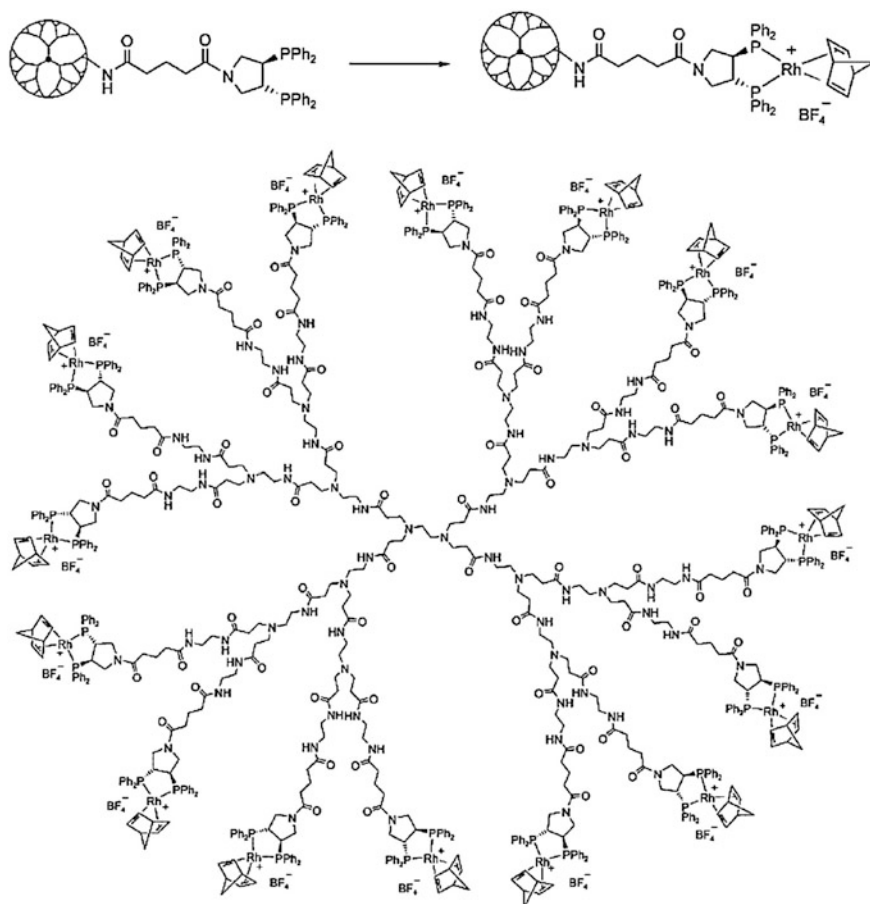
Scheme 5.10 General synthesis of the pyrphos-Rh(nbd) chelates, and {G2}-PAMAM-{glutaroyl-pyrphos-Rh(nbd)BF₄}₁₆

(diphenylphosphinoxy)biphenyl scaffold was prepared (Fig. 5.13) [143]. The rhodium MCDs based on these P,P-ligands interconvert among a minimum of six diastereomer conformations. Therefore, a dendritic catalyst directs the stereoselectivity of a catalytic process by dynamically transferring the conformational chirality of a dendritic architecture to the catalytic center.

PEI dendrimers up to the G3 modified by alkyldiphenyl phosphine ligand were chelated with Pd(COD)Cl₂ to give phosphine-Pd(II) MCDs (Fig. 5.14) [144]. The ^{31}P NMR spectra of Pd(II) chelates (4, 8, 12 and 16) indicated that all the phosphorus atoms were coordinated to the metal ion in an equivalent environment and MCDs have a similar bidentate mode of complexation, as in the monomer metal chelate.
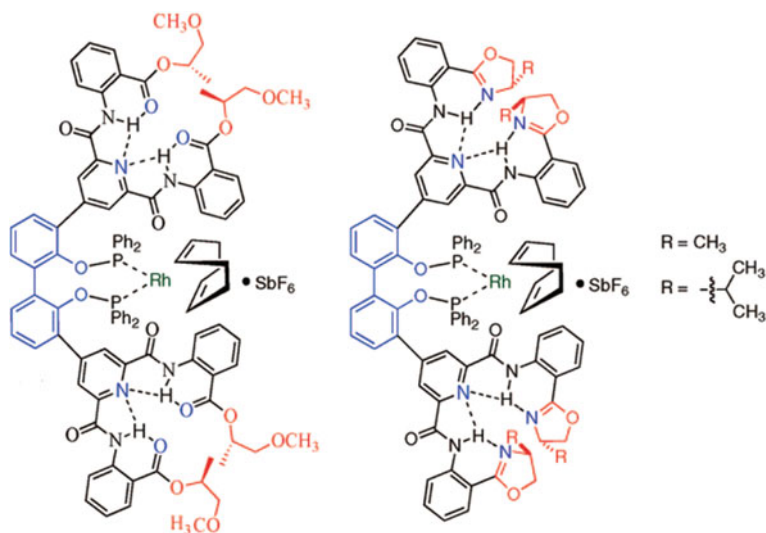
Fig. 5.13 Structure of LRh$^+$(COD)SbF$_6^-$ MCDs

It should be noted the chelating dendrimers with bis(diphenylphosphinomethyl) amino fragments linked to either L-tyrosine or tyramine methyl ester which form Pd-MCDs in situ [145].

Of interest is the chelation of RuCl$_2$(PPh$_3$)$_3$ by G1 dendron with diphosphine chelating fragments at the core [146]. It is important that in the MCD the metal has a square-based bi-pyramid configuration with the four phosphorus atoms of both diphosphines in a single plane and two chlorine atoms in axial positions.

Polyphosphines are used for integration of 32 or 64 [Ru$_3$(CO)$_{11}$] cluster units on the ends of phosphine branches. These reactions were carried out using electron-transfer-chain catalysis with 19-electron complex [FeCp(C$_6$Me$_6$)] as catalyst [147]. MCDs were obtained as a very air- and light-sensitive red powder in 50% yield after drying under vacuum for several days.

G3 MCDs with either 24 terminal palladium or ruthenium diphosphine chelates or one ruthenium diphosphine chelate located at the core were prepared by mixing the chelating dendrimers with PdCl$_2$ and RuH$_2$(PPh$_3$)$_4$, respectively [148]. The MCDs are efficient, recoverable catalysts in three general organic reactions: Stille couplings, Knoevenagel condensations, and Michael additions.
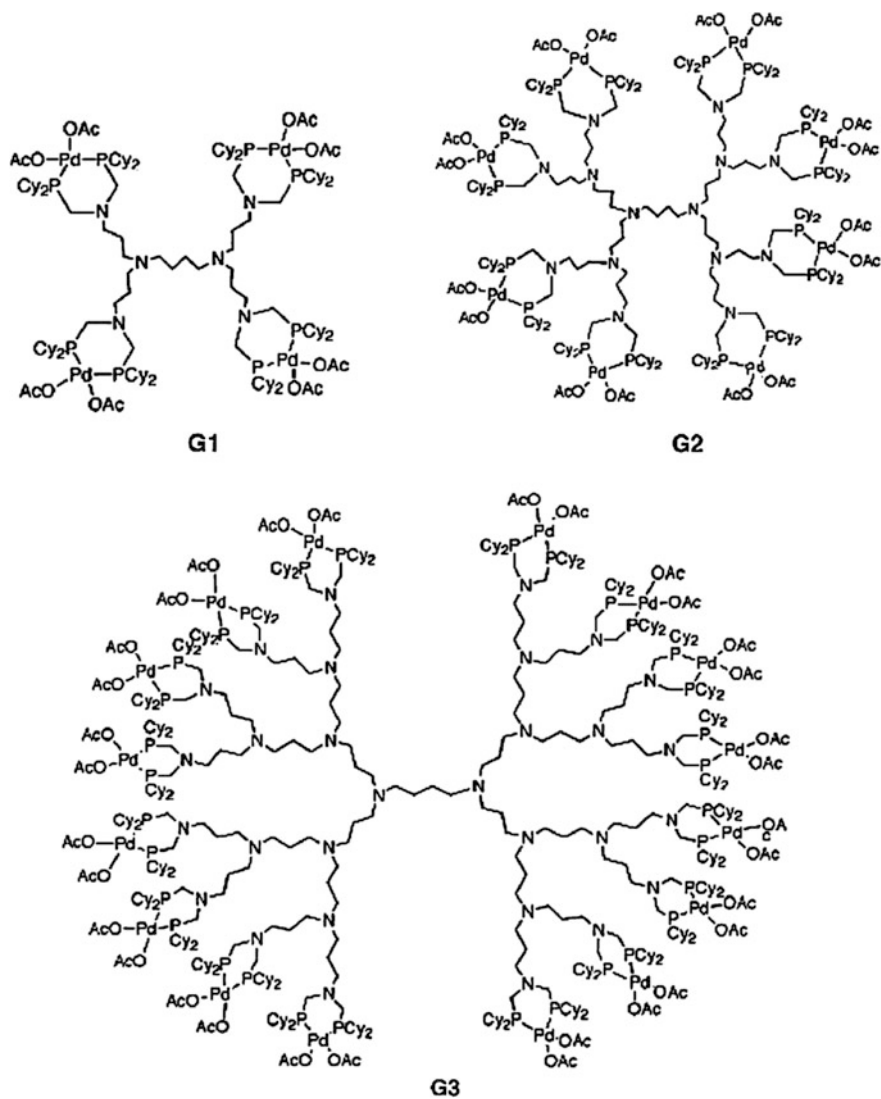
Fig. 5.14 Diphosphino Pd(II)-MCDs

[G₁]: [M] = PdCl₂
[G₁]: [M] = RuH₂(PPh₃)₂

[G₃]: [M] = PdCl₂
[G₃]: [M] = RuH₂(PPh₃)₂
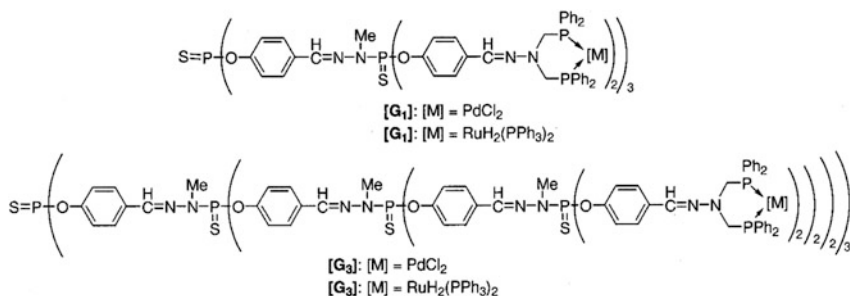
The fourteen multivalent MCDs containing diphosphine Pd(II) chelates both within and across the dendrimer generations were synthesized using G0–G3 poly (propyl ether imine) dendrimers (Fig. 5.15) [149]. The MCDs were obtained by the interaction of Pd(COD)₂Cl₂ with corresponding phosphines to form 6 Pd(II)-containing MCD **1**, 10 Pd(II)-containing MCD **2** and 16 Pd(II)-containing MCD **3**. The dendritic metal chelates **1–3** were amorphous solids, whereas initial chelating dendrimers were gums and foamy solids in general.

It should be noted Pd(II)-MCDs based on the commercial G1–G3 polyamino DAB-dendrimers with chelating bisphosphine ligands, in particular, bis(*tert*-butylphosphines) and bis(cyclohexylphosphines) [150]. It is important that complete conversion occurs within a few hours at most.

DAB G1–G3 dendrimers terminated by Ru benzylidene chelates were synthesized from the dendritic diphosphane and RuCl₂(=CH-*o*-Oi-PrC₆H₄)PPh₃ [151]. The MCDs undergo ROMP of norbornene to formation the metallodendrimer stars, in which each branch includes, for example, 100 norbornene units. Activity of MCD catalysts was higher than that of mono-Ru model catalyst and rate of metathesis polymerization decreases with increase in a dendrimer generation [151, 152].
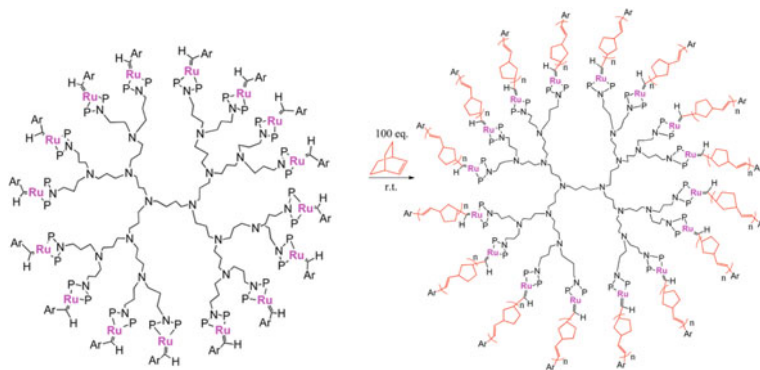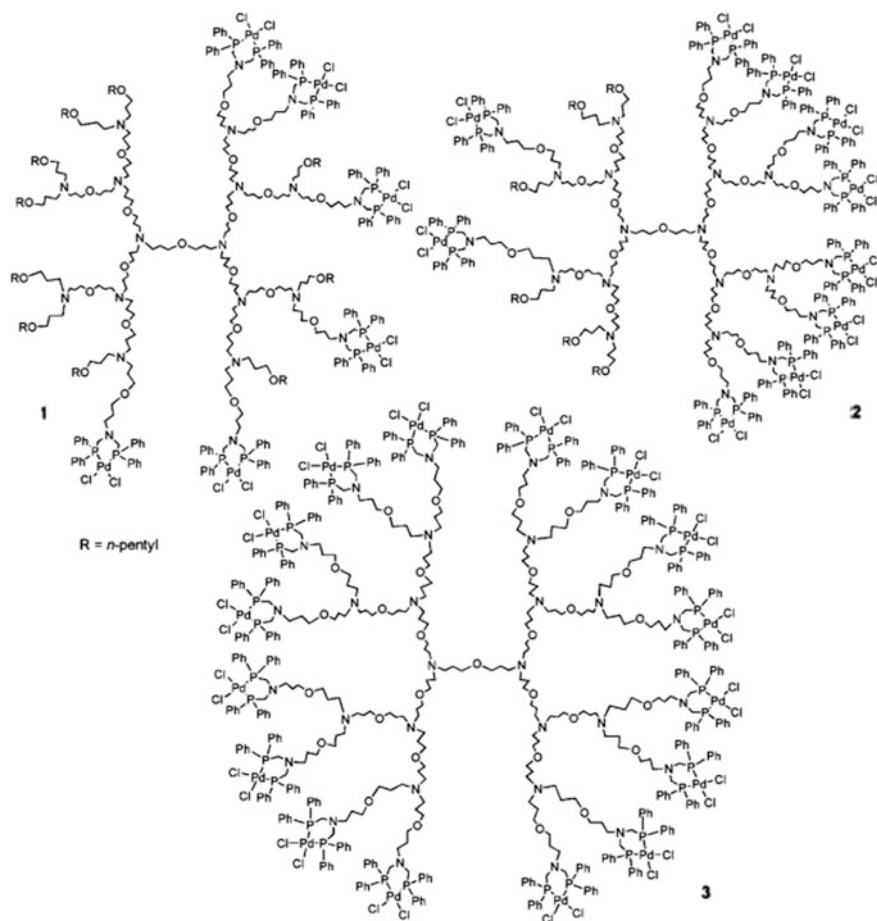
Fig. 5.15 Molecular structures of G3 partially and fully functionalized MCD

Dendrimers containing gem-bisphosphonate terminal fragments were used for the chelation of gadolinium salt Gd(triflate)$_3$ from monomer to G3 (Scheme 5.11). Magnetic susceptibility measurements indicate the presence of one gadolinium per the bisphosphonate group [153].

It should be noted Ir(BINAP)-cored dendrimers, which are used in enantiose-lective hydrogenation of quinolines [154]. The effects of the solvents, temperature, hydrogen pressure, and additive on the activity and enantioselectivity were inves-tigated by using the MCD catalyst, which was generated in situ from chelating BINAP dendrimer and [Ir(COD)Cl]$_2$.

Of interest are the chiral diphosphane-containing Janus dendrimers (up to 16 BINAP units) used for in situ catalyst preparation by mixing with [Ru(p-cymene)Cl$_2$]$_2$ [155]. The chemical shifts of Ru-MCDs in the ^{31}P NMR spectra were very similar, indicating that the introduction of sterically demanding dendritic wedges
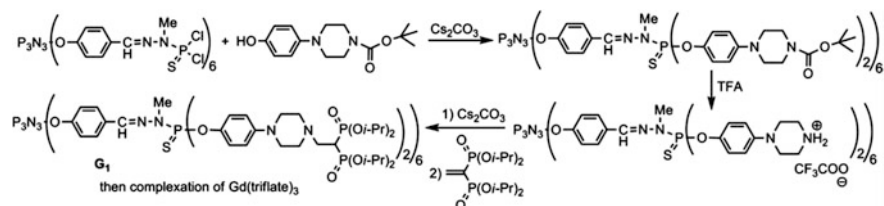
Scheme 5.11 Synthesis of dendrimers functionalized by gem-bisphosphonate end groups, used for the chelation of gadolinium salt
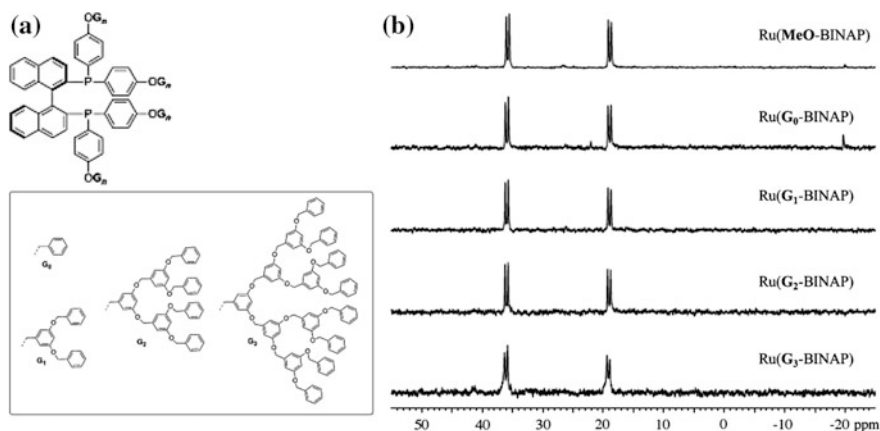
Fig. 5.16 a Structures of chiral Janus dendritic diphosphane ligands. **b** ^{31}P NMR spectra of dendritic [Ru(Gn-BINAP)] complexes and corresponding low molecular weight Ru complex

did not influence the chelation of ruthenium with the phosphorus atoms at the core of the dendrimer (Fig. 5.16).

Chiral copolymer with (S)-BINAP and fluorene as building blocks is used for design of chiral Ru/Ir bimetallic dendronized polymer catalysts based on Fréchet type dendritic DPEN (DPEN = 1,2-diphenylethylenediamine) ligands using M–L coordination strategy (Fig. 5.17) [156]. The prepared MCDs are applied to Ir-catalyzed asymmetric hydrogenation of quinaldine and showed perfect activity at moderate enantioselectivity. At that, the reaction rate is higher than that of a monomer catalyst and can be associated with efficient protection of catalytically active Ir center by bulk dendritic pendants, which decrease formation of inactive Ir dimer.

A kind of chiral dendritic [RuCl$_2$(BINAP)(DPEN)] catalysts with a «sandwich» multi-layer structure has been synthesized via metal chelation reactions of [RuCl$_2$
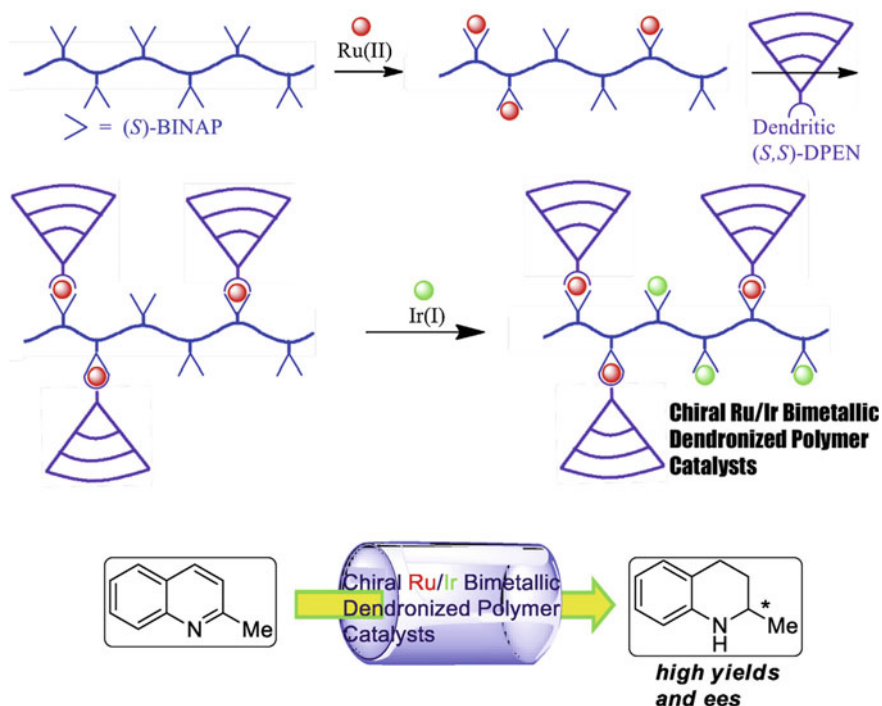
Fig. 5.17 Working hypothesis for catalyst design: synthesis of chiral Ru/Ir bimetallic dendronized polymer catalysts and their application in asymmetric hydrogenation of quinaldine

$(C_6H_6)]_2$ with dendritic chiral diamine and dendritic chiral diphosphine ligands [157]. In the MCDs the metal chelate layer is «cramped» between layers of poly (aryl ether) dendrons.

It should be noted some remarkable examples involving rhodium MCD with diphenylphosphino ligands on a solid support such as silica gel (Fig. 5.18) [158, 159]. The phosphonated dendrimers were chelated by simply stirring with chloro (dicarbonyl)rhodium(I) dimer in degassed dichloromethane at room temperature for 3 h under argon and the rhodium contents of G1 and G2 are 0.74 and 0.83 mmol g^{-1}, respectively.

Of interest are Pd-MCDs prepared by the interaction of the phosphonated G0–G3 dendrimers with dichlorobis(benzonitrile)palladium(II) [160, 161]. It is
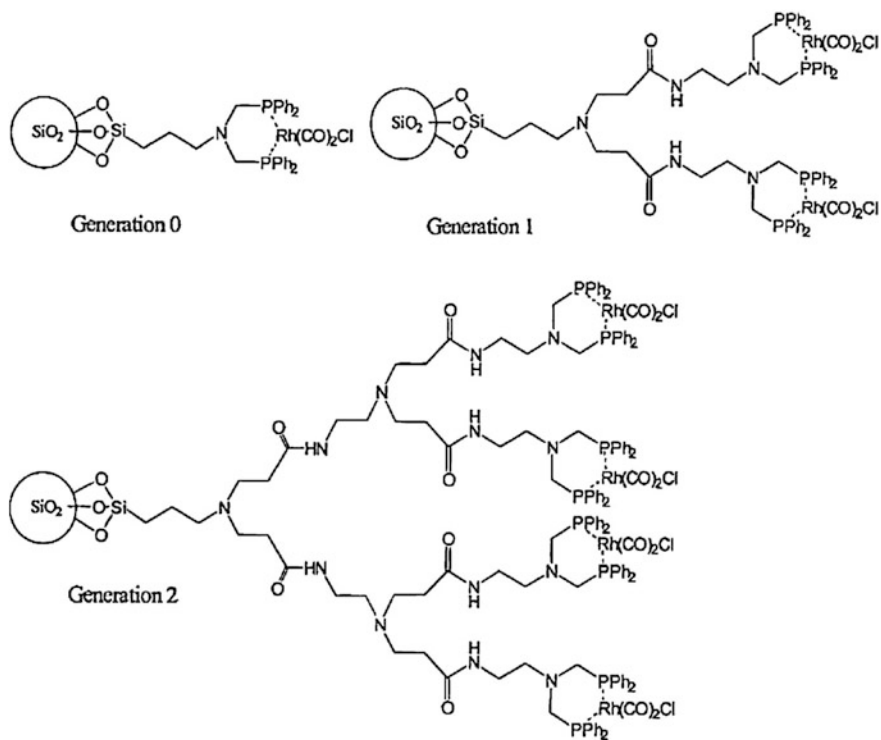
Fig. 5.18 Rhodium MCDs with diphenylphosphino ligands on a silica gel

important that extending the length of the PAMAM arms (Fig. 5.19) [160, 162] or using large pore PE-MCM-41 instead of amorphous silica [163] leads to an increasing metal content.

The Pd chelate based on 4-amino(N-methylendiphenylphosphino) pyridine has been reacted with the ruthenocarbosilane dendrimer to afford Ru–Pd concentric metal layered dendrimer [164].

5.1.5 Pincer Complexes

Dendritic SCS-pincer palladium chelates were prepared in good yields (60–89%) and high purity (palladium loading >97%) [165]. Palladation of dendrimer was achieved via direct C–H-activation with [Pd(MeCN)$_4$](BF$_4$)$_2$. The treatment of the formed cationic acetonitrile pincer complex by a saturated aqueous sodium chloride solution leads to replace the acetonitrile ligand by the stronger chloride ligand.
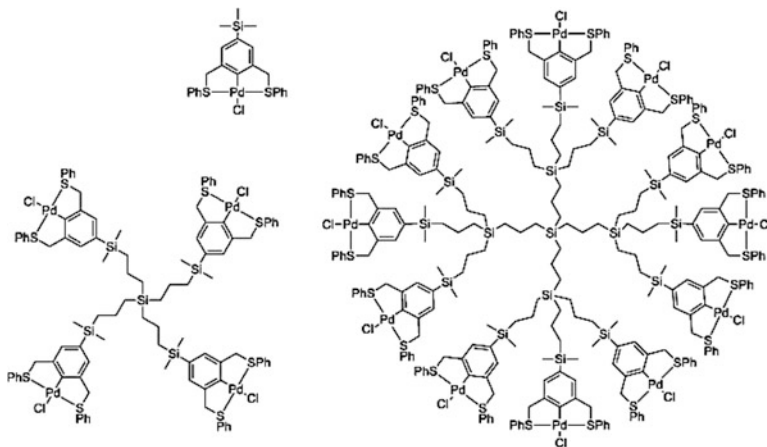
The dendritic SCS-pincer Pd-complexes were prepared by an amide coupling of an activated ester pincer derivative with a primary amine (commercially available amino-terminated PAMAM dendrimers) in order to investigate the effects of the dendrimer backbone on catalysis [166].

It should be noted the pincer-PCP Pd(II) complexes based on a tridentate diphosphinoaryl ligand immobilized on silica supported dendrimers [167].

A solid-phase synthetic approach to obtain dendritic PAMAM ligands anchored onto PS beads and their rhodium pincer complexes was developed [168]. The dendronized polymeric chelates were applied for the hydroformylation of several olefins. In another example the dendronized polymers up to the G3 containing NCN-pincer palladium complexes at the periphery were used as catalysts for the aldol condensation of benzaldehyde with methyl isocyanoacetate [169].

5.1.6 Chelating Dendrimers as Metal Sensors

Appropriately developed luminescent dendrimers can play a role of ligands and sensors for luminescent and non-luminescent metal ions [170]. Dendritic effects of dendrimers are useful for sensor development of specific metal ions using chelation with a selective ligand present on a dendrimer surface. Thus, PAMAM dendrimers functionalized by (4-dimethylaminoethyl) amine-1,8-naphtalimide on the surface were built for detection of divalent metal ions. Due to the fact that (4-dimethylamino-ethyl) amine groups quenched PET of 1,8-naphtalamide, a dendrimer does not provide fluorescence in the steady regime. After bonding with metal ions, (4-dimethyl-aminoethyl) amine does not function any more as quencher, and fluorescence can be observed generated by 1,8-naphtalimide. Increase in fluorescence depends on nature of coordinated metal ion because of difference in bonding force, at that, each size of PAMAM dendrimer provides selectivity of a certain type of a metal ion [171, 172].
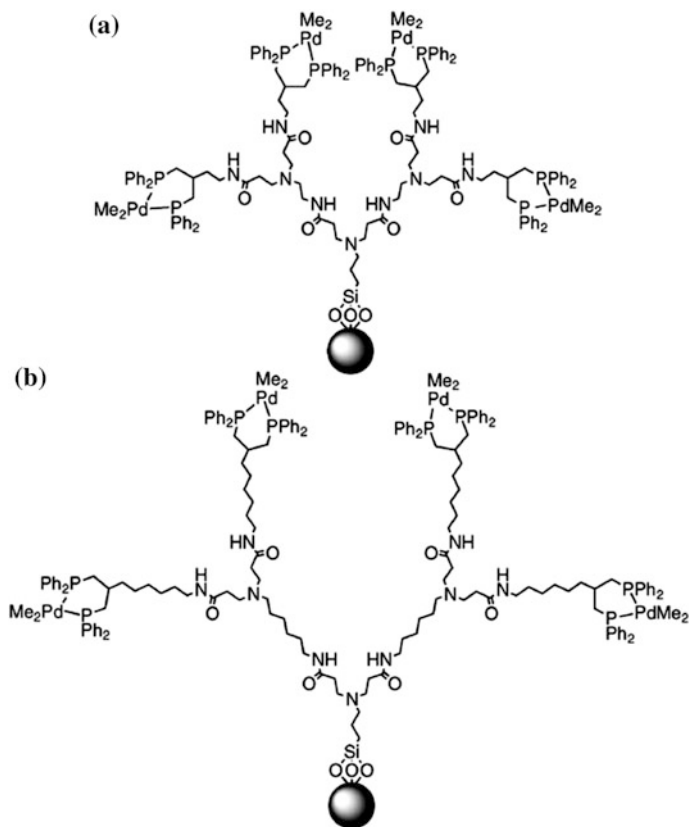
Fig. 5.19 **a** A G2 PAMAM Pd dendrimer supported on silica. **b** The PAMAM-C6 analogue, which differs in the number of carbon atoms separating the intermediate amido and the branching amine functionalities

Thus, G1 dendrimers with Fe(II) ions give the strongest increase in a signal, and G2 dendrimers are optimal as sensors of Cu(II) or Fe(II) [173, 174]. Other G0 and G2 PAMAM dendrimers with surface 4-allylamino-1,8-naphtalimide units showed the best results as sensors of Zn(II) ions [175].

High selectivity for detection of Cu cations found with green-yellow fluorescent PAMAM dendrimers peripherally modified by 1,8-naphtalimides (Fig. 5.20) [176].

The green fluorescence intensity of G1 PPI dendrimers with 1,8-naphthalimide fragments increases in the presence of different transition metal ions [177]. The quenching the fluorescence emission was observed during the interaction of the fluorophore (1,8-naphthalimide) and the receptor (*N,N*-dimethylamino group) initiating PET (Fig. 5.21a). The introduction of the metal ions in the dendrimer solution leads to a change of its properties (Fig. 5.21b). It is important that the *N,N*-dimethylaminoethylamine fragment at C-4 position of the 1,8-naphthalimide structure can coordinate with metal ions.
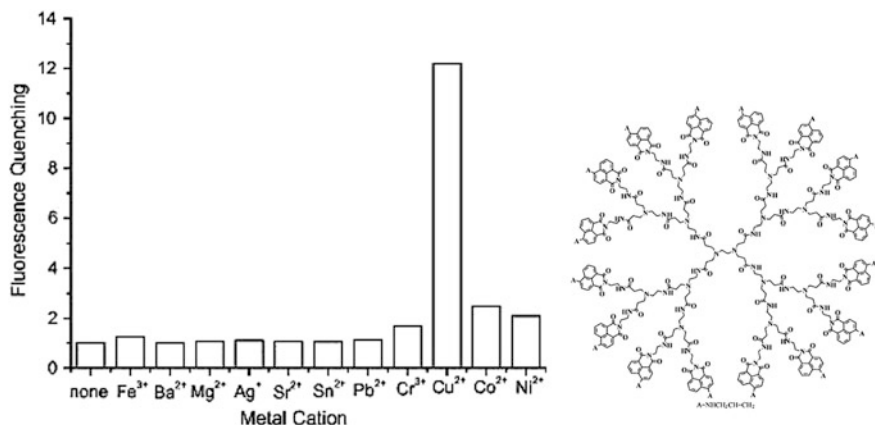
Fig. 5.20 Fluorescence quenching factor of PAMAM dendrimers with terminal 1,8-naphtalimides in presence of different metal cations (5×10^{-5} mol L^{-1}) in DMF solutions. The dendrimer concentration is c = 1×10^{-5} mol L^{-1}
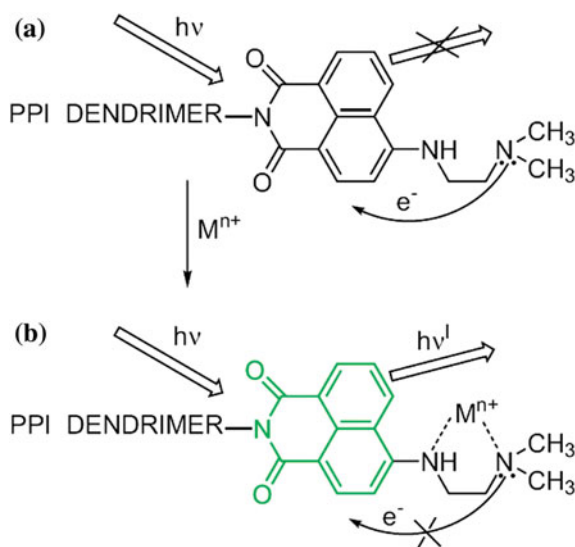
Fig. 5.21 Proposed mechanism of fluorescence enhancement of 4-*N,N*-dimethylaminoethylamino-1,8-naphthalimide-labeled PPI dendrimer

We shall also notice G3 PAMAM dendrimers functionalized with 2,3-naphthalimide chromophore groups on terminal branches, which with Eu(III) form luminescent complexes corresponding to the dendrimer:lanthanide ratio 1:8 [178]. For these MCDs an overall average CN of 7.5 was postulated. Luminescence lifetimes show that a metal cation is perfectly shielded from non-emitting deactivation by a dendritic structure.

Another often used label for studying chelation processes with participation of dendrimer ligands is a dansyl-group fixed on a dendrimer surface. It is important that the dansyl groups are independent from each other. If Co(II) salt is added, fluorescence quenching is due to Co(II) ion chelation in dendrimer interior, and this quenching is more distinguished with increase in a number of generations. Chelation showed that it is completely reversible. Fluorescence of all peripheral dansyl groups is quenched, when one Co(II) ion is incorporated in a dendrimer [179, 180], while in polyamide-core dendrimers a less number of dansyl units are quenched [181]. Lanthanide ions Nd(III), Eu(III), Gd(III), Tb(III), Er(III), and Yb(III) quenched dansyl fluorescence of dendrimers having PLL cores instead of PPI cores, and with Nd(III), Er(III), Yb(III) sensibilized NIR emission of a lanthanide ion was observed [182].
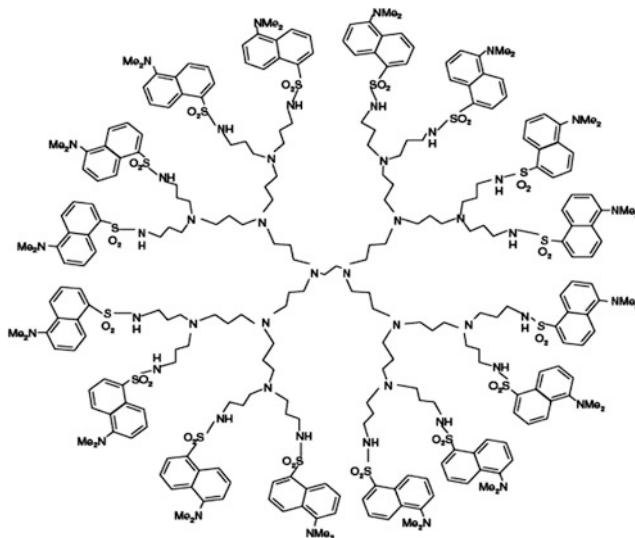
A family of POPAM dendrimers with terminal 4, 16, and 32 dansyl fragments and molecular clip consisting of two anthracene side walls and bridging block of benzene disulfate are good ligands for Zn(II) ions [183]. The interaction between dansyl dendrimer and anthracene-functionalized clips is mediated by Zn(II) ions and a number of metal ions and molecular clips linked to each dendrimer increases with a number of generations. It is important that energy transfer goes from anthracene, giving the fluorescent excited state with almost unitary efficiency.

5.2 Intracomplex Compounds

By now, a wide variety of MCD intracomplex type, including various metal chelate units, obtained.

5.2.1   Salen-Type Chelates

A large body of research concerning MCDs of intracomplex type with salicyl-laldimine ligands has been carried out. As a typical example, we note Ni dendrimer chelates obtained by chelation of a metal compound to periphery of salicylaldimine-containing G1–G3 DAB-PPI-dendrimers [184–186]. All three MCDs were isolated as green solids, with yields ranging from 75 to 85%. Using a catalytic system based on these MCDs with EtAlCl$_2$ co-catalyst, a tandem process has place, in which ethylene is oligomerized with following Friedel-Crafts alkylation of the reactive solvent, toluene, which brings to a range of alkylbenzenes.

G1–G2 salicylaldimine-containing PPI dendrimers was used to obtain some Cu and Co chelate dendrimers [187], which are efficient catalysts in aerobic hydroxylation of phenol using H$_2$O$_2$ and molecular oxygen as oxidants. It is important that the nature of the MCD as well as by the pH of the reaction medium have a substantial effect on the selectivity to the products.
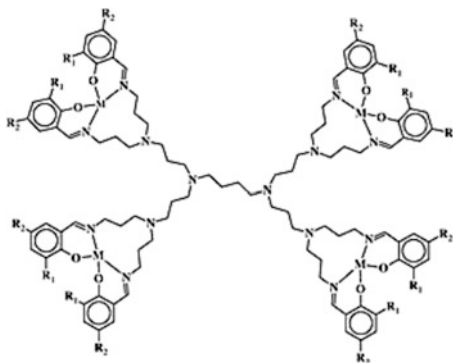
Ni-chelate dendrimer is synthesized with PAMAM, 3,5-di-*tert*-butyl-2-hydroxy-benzaldehyde and Ni chloride through Schiff base-forming reaction and chelation [188]. Studying catalytic activity of Ni MCD in ethylene oligomerization using MAO as a co-catalyst, showed that activity and selectivity is determined by dendritic structure, in particular, G2 metal chelates have higher activity. The dendritic salicylaldimine Cu and Zn chelates were similarly prepared by template method with 88.2 and 65.2% yield, respectively [189]. Studying salicylaldimine dendritic Cu complex as catalyst in oxidation reaction of ascorbic acid showed that this complex has good mimic enzyme catalytic kinetics. In particular, the catalytic reaction had the same features of the pseudo-first order reaction as the enzyme reaction, and the reaction rate increased under high concentration conditions of mimic enzyme complex and pH 7–7.5 [190].

Co(II)-salicylaldimine dendrimer and a 21-bases oligonucleotides (NH_2-5′-GAG GAGTTGGGGGGAGCACATT-3′ and 5′-AATGTGCTCCCCCAACTCC TC-3′) were assembled LbL on a gold electrode in order to generate electrochemical DNA-biosensor based on MCD [191]. In presence of complimentary oligonucleotide, formation of double-chained DNA increases impedimetric resistance of charge transfer from 6.52 to 12.85 kΩ. On the other hand, mismatched DNA fragments did not cause any changes in resistance, which resulted in stable and simple assembling of DNA biosensors.
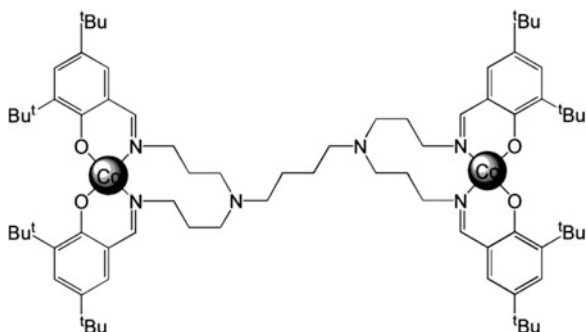
We shall notice dendritic salicylaldimine Ru chelates interesting for their biomedical applications [64]. Thus, MCD containing tetranuclear and octanuclear chelate G1–G2 Ru(II) arene dendrimers based on PPI frameworks is synthesized from binuclear arene precursors, $[Ru(arene)_2Cl_2]_2$ (arene = p-cumene, hexamethylbenzene) using the reaction with salicylaldimine dendritic ligands in ethanol at room temperature [48]. These compounds are stable in air, and MCDs are soluble in most polar organic solvents, and all terminal groups of a dendrimer are functionalized with Ru(II) arene fragments. In this case at chelation with participation of a polymer dendritic ligand dimeric Ru complexes are monomerized.

Cationic heterometallic ferrocenyl-derivatives MCDs of intracomplex N,O-type are obtained by the interaction of Ru(II)-arene-1,3,5-triaza-7-phosphatricyclo [3.3.1.1]decane with salicylaldimine ligand (Scheme 5.12) [192]. G1–G4 MCDs
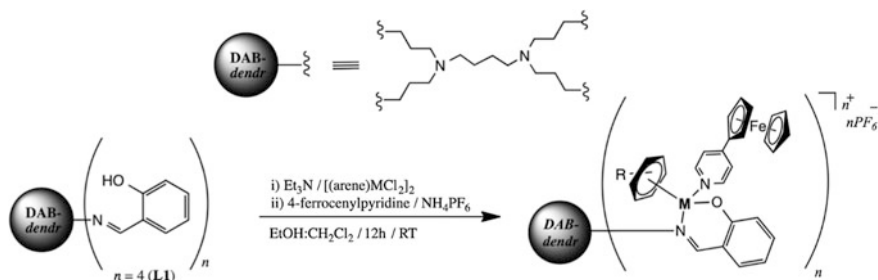
Scheme 5.12 Preparation of cationic heterometallic ferrocenyl-derivatives MCDs of intracomplex N,O-type
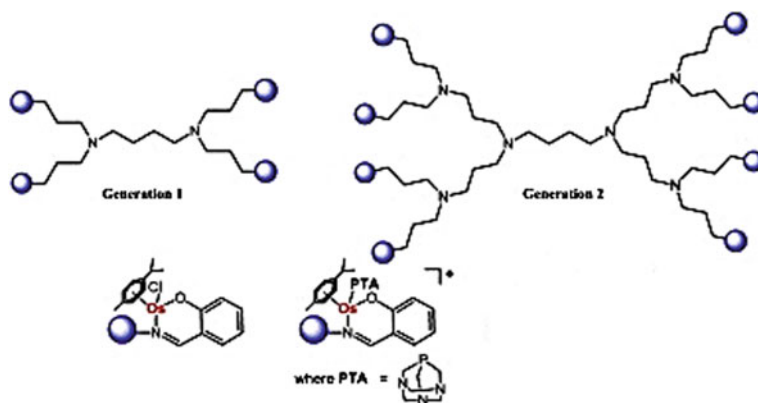
Fig. 5.22 Structure of Os(II) salicylaldimine dendritic chelates

contain up to 32 peripheral metal chelate units and show higher antiproliferative activity in vitro as compared to a monomer analogue.

Also similar salicylaldimine PPI dendrimers including Os-arene peripheral fragments have been synthesized, which showed high anticancer activity (Fig. 5.22) [193]. All MCDs were prepared as yellow solids, in moderate to high yields (48–88%). It is important that there is a loss of two-fold symmetry about the *p*-cymene fragment upon chelation of the bidentate *N,O*-salicylaldimine ligand.

Considerable attention is attracted to liquid crystalline salicylaldimine MCDs [194, 195]. Thus, VO(II) chelates formed with salen-ligands containing terminal G0–G1 lipophilic fragments show wide temperature ranges of hexagonal (Col$_h$) and rectangular (Col$_r$) columnar meso-phases [196]. As generation increases from G0 to G1, melting and clearing temperatures decrease more substantially for the latter, therefore, meso-phases exist in wider temperature ranges for G1. It also occurs that presence of two times more divergent aliphatic chains with increase in generation contributes to domination of rectangular symmetry over hexagonal. The main

structural parameter, which has an effect on thermal stability of meso-phases is, however, origin of a cross-linking spacer between two imine chelating fragments, because it has an effect on strength of molecular interactions through a dative bond between dipolar vanadyl groups, and therefore, determines reliability of the formed linear pseudo-polymer structure and helps to meso-phase stabilization. Optimum is reached when propylene spacer is considered, because chelates reflect stronger polymer linear chains with respect to higher clearing temperature and thermal stability of meso-phases (about 150–170 °C). In contrast to this, rigid ethylene spacer brings to monomer types, while a bulk spacer brings yet to polymer linear chains, but with weaker dipolar interactions, both show lower clearing temperatures (about 156 and 108–115 °C, respectively) than intermediate systems. It seems that additional steric factors related to protruding geminal methylene groups also contribute to considerable decrease in stability of a meso-phase, despite formation of a polymer chain, though less interconnected. Presence of this polymer chain in combination with a great number of divergent aliphatic chains also can be associated with unusual inversion of the meso-phase here observed, i.e. lower symmetry (rectangular against hexagonal) is discovered at higher temperatures. This, most probably, can be caused by limitation of core side diffusion, which impedes mesogens in tighter registry with limited conformation variants. As regards supramolecular organization in columnar meso-phases, G0 chelates should be coupled in correlated structures, which are then self-assembled into columns, while chelates with G1 dendritic ligands are packed directly in columns, as purely discotic compounds do. In both cases polar fragments are separated in the interior of columnar cores and surrounded with aliphatic medium.
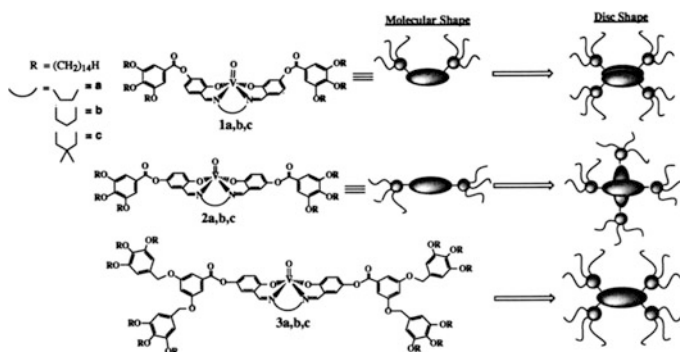
Similarly, binuclear Cu MCD are obtained through self-assembling two bidentate phenyl-iminopropyl ketone ligands containing divergent G1 dendron fragments in 3- and 5-positions of phenyl ring ($R_1 = R_2 = H/OC_nH_{2n+1}$, n = 5–8, 10, 12, 14, 16) [197].
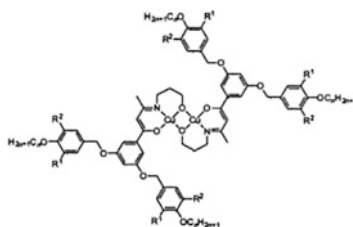
It is important that the ligands were not isomorphic themselves. Highly lipophilic bimetallic chelates ($R_1 = R_2 = OC_nH_{2n+1}$) with chain lengths between hexyl and dodecyl show Col_h phase between 83–99 and 97–117 °C. A decrease in a number of aliphatic chains ($R_1 = H$ and $R_2 = OC_nH_{2n+1}$ or $R_1 = R_2 = H$) or using other chain length has a negative effect on mesomorphism onset. Here also columnar formation follows from monomer chelate packaging.

PPI-based dendrimers functionalized at the end by four or eight coordinated 4-(alkoxybenzoyloxy)-salicylaldimines, respectively, were used as chelating ligands for the formation of bi- (G0) and tetranuclear (G1) Cu(II) MCDs, respectively [198]. Although all organic ligands show SmC and SmA phases [199], chelation of Cu(II) ions will stronger affect mesomorphic properties of respective multi-metallic MCDs. Suppression of mesomorphism (G0: n = 10, $T_m = 179$ °C; G1: n = 10, $T_m = 110$ °C; n = 14, $T_m = 80$ °C) or a decrease in temperature range of the meso-phase (G0: n = 14, Cr 163 SmC 197 I; n = 18, Cr 167 SmC 187 I; G1 n = 18, Cr 35 SmC 108 I) is observed more systematically for corresponding metal-free chelating dendrimers. Transition temperatures during chelation are slightly increased for dimetallic MCD, whereas for tetrametallic MCD temperature range is similar to that for ligands, at that only SmC phases are formed. Structure of smectic phases of dendritic chelating ligands is explained by parallel alignment of peripheral mesogenic blocks diverging up and down from a molecular center, while chelation brings to partial decomposition of this parallel disposition and opening of dendritic strands, thus decreasing micro-segregation with molecules located in neighboring layers. This model is confirmed by deterioration of periodicity of a layer, and widening of molecular range of chelates, as compared with ligands. Chelation of different amounts of Cu(II) ions with respective derivatives of liquid crystalline PPI G0–G1 dendrimers containing peripheral di-3,4-decyloxyphenyl amide groups, showed Col_h meso-phases (as well as metal-free chelating dendrimers [200]).
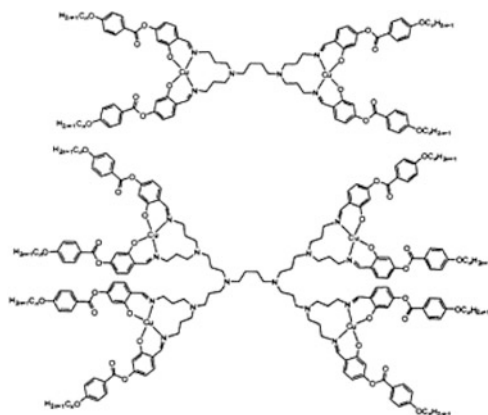
At low content of Cu(II) ions in dendritic ligand metal ions form monomer chelates having a columnar meso-phase with plane N_2O_2 coordination geometry with participation of carbonyl oxygen and amide nitrogen atom. At the same time at intermediate and high content of metal ions two metal chelate units were identified, in particular, pseudo-tetrahedral N_2O_2 mode with participation of the same donor atoms, and square-pyramidal N_2O_3 mode with additional bridge with tertiary amine nitrogen atom from internal core of a dendrimer with possible intermolecular interactions [201, 202].
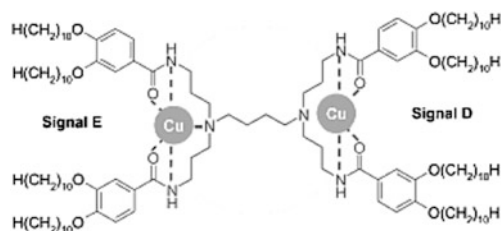
In blue salicylaldimine G1 Cu-MCD, having dimer structure, temperature activated effect of valence tautomerization accompanied by electron transport, with activation energy 0.35 meV is discovered [203].

In a spin-alternating Fe(III) chelate with G2 dendrimer branching of the salen-type a new phenomenon is found, «magneto-ferroelectric crossover», which is simultaneous synchronic change in spin state and electric polarization of Fe(III) centers during spin transition at $T_{1/2} = 312$ K. The chelate consists of three types of magnetic iron centers: one $S = \frac{1}{2}$ low-spin (LS) and two $S = 5/2$ high spin (HS) centers with strongly and weakly distorted octahedral crystal fields. Another prominent feature of this MCD is co-existence in one material of magnetic ordering

(4.2–50 K), magneto-electric effect (50–200 K), and spin-crossover of the transition (200–330 K) (Fig. 5.23) [204, 205].

It is interesting that Fe ions existing in HS state are chelated by decyloxybenzoate substituted G1–G5 PPI dendrimers in two types of iron-chelating centers with octahedral and tetrahedral symmetry (Fig. 5.24). Octahedral (high symmetry) centers are placed on a dendritic core boundary, while tetrahedral centers with strong rhomboid distortion of Fe environment are distributed over all branching of the dendritic core. It is found that all iron-containing dendromesogens display light-harvesting and fluorescent properties [206].

Co-existence of spin-crossover and magnetic ordering is found in dendritic Fe (III) chelate $[Fe(L)_2]^+PF_6^-$, where L = 3,5-di[3,4,5-tris(tetradecyloxy)benzoyloxy]
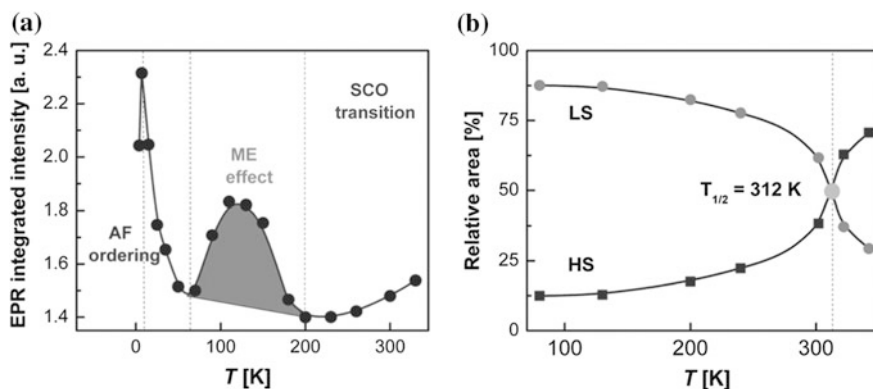
Fig. 5.23 **a** The temperature dependence of the EPR lines integrated intensity of the whole EPR spectrum. **b** The temperature dependence of the relative areas of HS and LS fractions
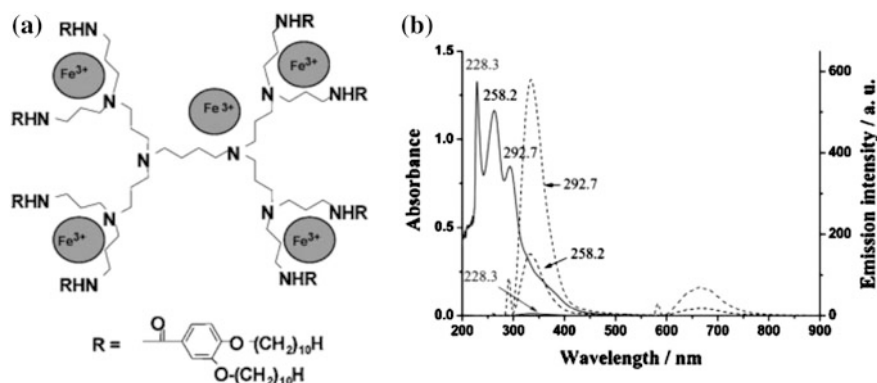
Fig. 5.24 **a** Structure of MCD with two types of iron-chelating centers. **b** Absorption (solid line) and fluorescence (dashed lines) spectra of MCD. The sample was excited at 292.7 (dashed line), 258.2 (dotted line) and 228.3 (short dotted line) nm

benzoyl-4-salicylidene-*N*-ethyl-*N*-ethylenediamine [207]. It should be noted that for this MCD antiferromagnetic exchange interactions predominate in the first temperature interval (4.2–70 K), while spin transitions between LS and HS centers predominate in the second temperature interval (70–300 K). Besides this MCD has antiferromagnetic ordering below 10 K.

5.2.2   8-Hydroxyquinoline Chelates

A dendritic HQ ligand, based on a PAMAM-type dendron, was chelated with Zn(II) by treating dendron by Zn(OAc)$_2$ [208]. The luminescence intensity of the G2 dendron was higher than that of G1, and upon chelation with Zn(II), a bathochromic shift was observed; the intensity of the Zn(II) MCD was higher than that of the analogous dendritic ligands. The emission spectra in visible region for monomeric chelate ZnQ$_2$, dendritic G1 and G2 chelates are quite similar, indicating that the shape and chemical properties of the dendrimer branches do not substantially affect the ZnQ$_2$-based chromophoric core.
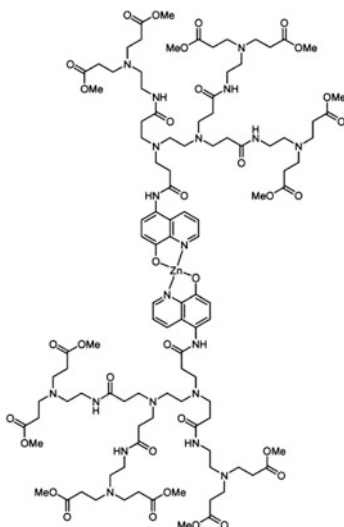
5.2.3   Pyrrolide-Imine Chelates

Bimetallic dendritic (pyrrolide-imine) Cu(II) and Ni(II) [DAB-{(N-CHC$_4$H$_3$N)$_4$} Cu$_2$], [DAB-{(N-CHC$_4$H$_3$N)$_4$}Ni$_2$] chelates have been obtained with good yield

[209]. Both the copper and nickel MCDs are fairly stable at room temperature in the solid state but show signs of decomposition in solution. The obtained MCDs are active catalysts of phenol hydroxylation using H_2O_2 and molecular oxygen as oxidants, at that Cu chelates showed generally higher activity as compared with their Ni analogues, however, Ni catalysts have far higher selectivity with respect to catechol than the Cu analogues.

M=Cu

M=Ni
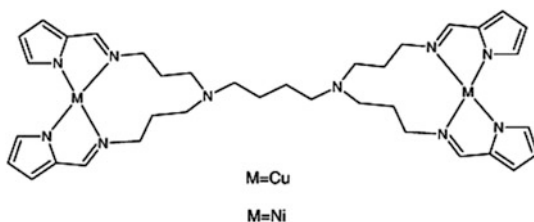
5.2.4 O,O-Chelates

Salicylate, catecholate, and hydroxypyridinonate bidentate chelators have been coupled to the surface of both PPI and PAMAM dendrimers up to the G4 (64 end groups) [210]. The metal-chelating properties of these dendrimers have been investigated by using batch spectrophotometric titrations. It is important that tris-bidentate and lower denticity modes of metal binding were identified. Metal chelation is specifically localized to the chelating end groups, with complexation halting at the formation of tris-bidentate complexes in the HOPO-based systems.

Studying chelation of Eu(III) with dendritic β-diketone ligands containing dbm core and poly (aryl ether) dendron obtained using the convergent method, showed that the linking point of a dendron to dbm plays important role in production of Eu MCD (Scheme 5.13) [211]. In particular, only dendritic β-diketonate ligands containing dendrons substituted in dbm phenyl group with $EuCl_3 \cdot 6H_2O$ form Eu (III) dendritic chelates from G1 to G3 with good yields. At the same time the β-diketonate ligands, which have dendrons linked to 2-position of dbm, can't form Eu(III) MCD, because the sterically demanding dendritic structure substituted in the 2-position might influence the formation of Eu(III) chelates. Integration of phen as a second ligand into these dendritic β-diketonate Eu(III) chelates gives mixed-ligand Eu(III) dendritic complexes with enhanced luminescence intensity.

The phonon-absorbing lanthanide chelates are synthesized by chelation of dendritic β-diketone ligands to Eu(III) [212]. Ligands are benzoyltrifluoroacetone units with poly (aryl ether) dendron branches. MCDs show Eu emission at the absence of residual emission with ligands with increase in generation from G0 to G3, which is associated with simultaneous manifestation of two effects: antenna and
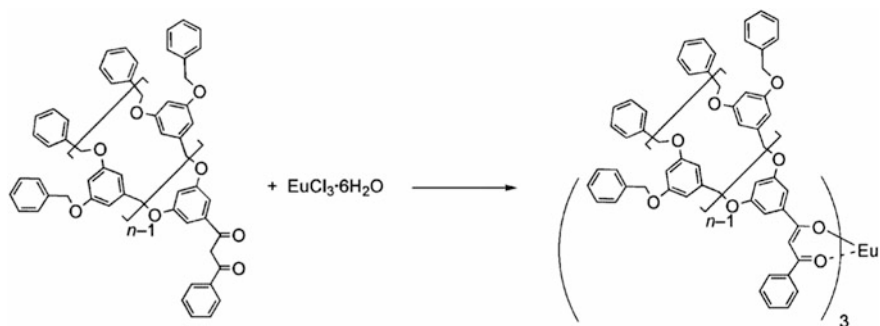
Scheme 5.13 Scheme of chelation of Eu(III) with dendritic β-diketone ligands

isolation of a metal center. The data on lifetimes show that G3 MCD is the longest lived type.

Phosphorus-based dendrimers with surface β-diketones is predominantly in the enol form obtained through intramolecular hydrogen transfer [213]. The chelating dendrimers were used for the in situ chelation of CuI, using either 2 or 4 diketone ligands per Cu. These MCDs catalyzed O-arylations of 3,5-dimethylphenol by aryl bromides. The absence of the dendrimer effect is explained by the decomposition of the dendrimer under the reaction conditions, which led to the release of the peripheral diketone moieties.
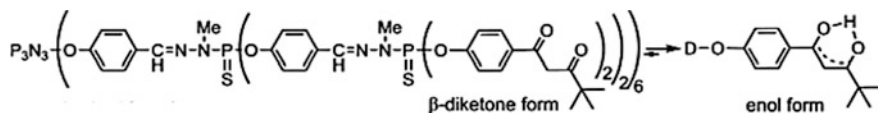
5.2.5 S,O-Chelates

Surface modifying PAMAM dendrimers with *N*-benzoylthiocarbamide brings to chelating ligands having high selectivity to ions of such metals as Co(II), Cu(II), Hg (II), Pb(II), and Zn(II) [214]. All metal ions can link quantitatively to chelating dendrimers at pH 9, however, most stable MCDs are formed with Cu and Hg ions, which can be selectively separated from other metal ions, and dendrimers can be regenerated and repeatedly used.

5.2.6 P,O-Chelates

Using dendritic or monomer P,O-ligand with an equimolar amount of Ni(COD)$_2$, mono-ligated chelates were formed [215]. When a second equivalent of monomer P,O-ligand was added to the solution of mono-ligated chelate an orange precipitate of bis (P,O)-nickel chelate immediately is formed. In contrast to the experiments with parent monomer ligand, addition of a second equivalent of dendritic P, O-ligand to the solution of mono-ligated chelates did not result in the formation of precipitate, and only a small amount (17%) of the bis(P,O)-nickel MCD is present in solution. These results demonstrate the ability of dendritic P,O-ligand to suppress the formation of inactive bis(P,O)-nickel MCD in toluene. Thus, dendritic P, O-ligand was anticipated to form a more productive catalyst than parent monomer ligand in the oligomerization of ethylene.
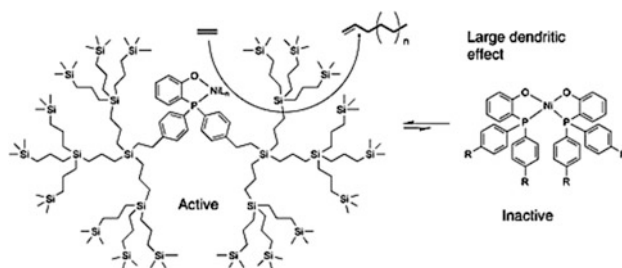
5.2.7 Metal Chelates with Polydentate Ligands

Recently much attention is given to chiral conformation order in dendritic structures [216]. In order to have a possibility to create and control chiral secondary structure in MCD, deep understanding the effect of chiral subunits on macroscopic structure is needed. Thus, chiral intramolecular H-bound dendrons, which are packed in dynamically biased helical conformation, can be «locked» in kinetically controlled conformation via chelation to Cu(II) ions [217]. Coordination of each chelating polydentate pyridine-2,6-dicarboxamide repeating dendron unit to Cu ion makes this subunit to exist only in syn-syn conformation and sharply rigidifies the dendron structure (Fig. 5.25).

The chelating polydentate dendritic structures was grafted to epoxy-activated mesoporous PMMA beads (Sepabeads EBEP-400) followed by metal coordination by terminal chelating groups for formation of MCD grafted catalysts (Fig. 5.26) [218]. The obtained catalyst was used for production of β-amino alcohols using regioselective method through nucleophilic opening of oxirane ring with different aromatic amines without solvents under soft conditions of reaction. It is found that
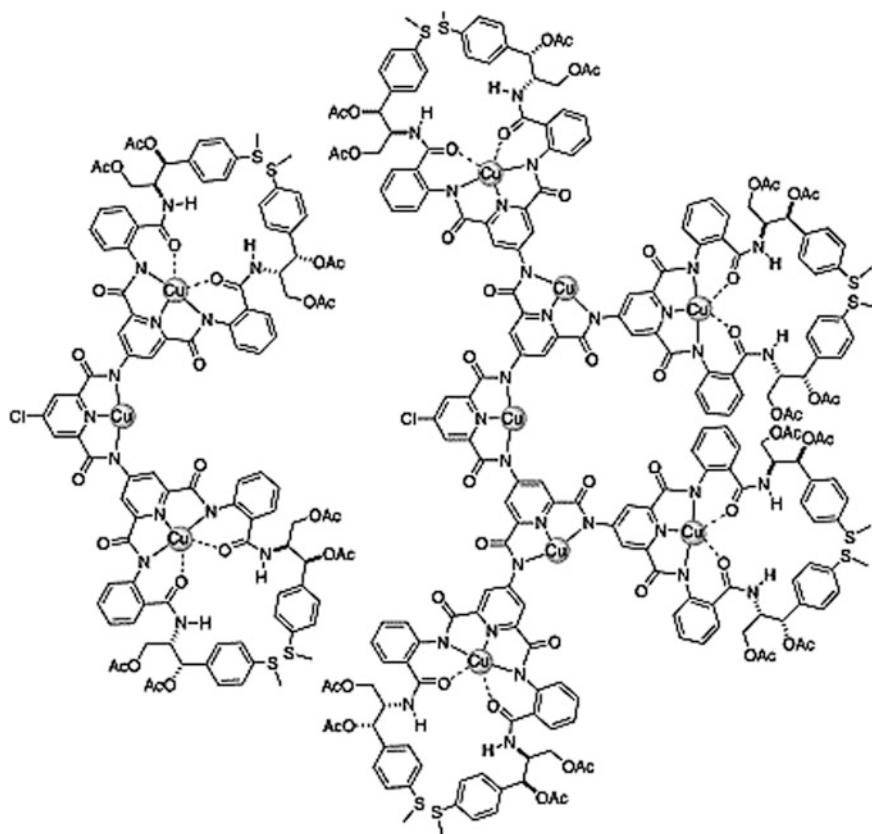
Fig. 5.25 G2 and G3 dendrons coordinated to three and seven copper(II) centers, respectively

MCD-based catalyst is efficient and is repeatedly used without loss of activity, selectivity, and efficiency.

It should be noted using of the dendrimers containing polydendate ligands for the preparation of contrast agents [219–223], in particular, through PSM (Scheme 5.14) [220, 221, 224, 225]. As a typical example, we note PSM of the commercially available PAMAM and PPI by DTPA with consequent chelation by GdCl$_3$ [226]. It is important that increasing generation of Gd-DTPA MCD leads to substantial increase of the r_1 and r_2 values.

The mixed gadolinium and yttrium chelates of the G5 DTPA-based dendrimer were obtained by changing the ratio between Gd-DTPA and Y-DTPA chelates along the periphery. It should be noted that yttrium was used as a diamagnetic probe
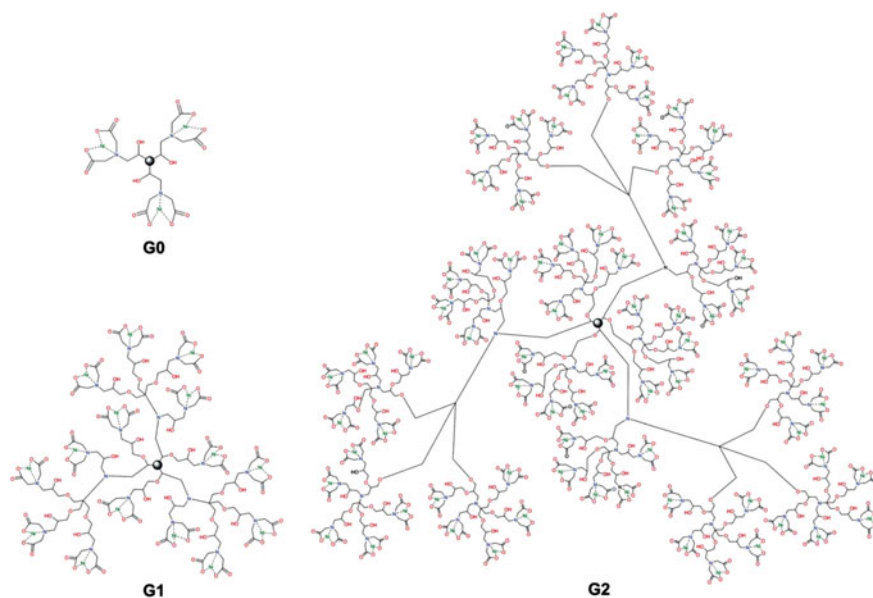
Fig. 5.26 Representation of Ni(II) loaded G0, G1, and G2 series of metallodendritic structures on surface of PMA-based Sepabeads EBEP-400
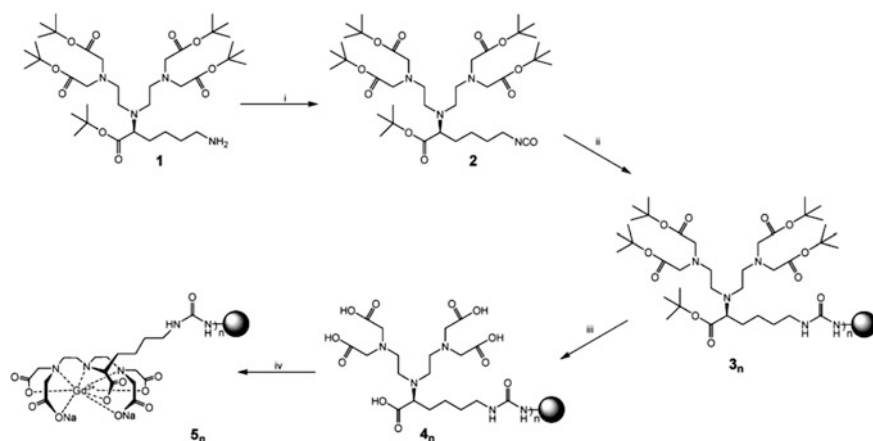
Scheme 5.14 Gd-DTPA-terminated PPI dendrimer

because it has a size similar to that of gadolinium, thus keeping the local mobility and molecular weight comparable. It is important that gadolinium was preferentially incorporated. Additionally, the heterometallic MCD exhibited a substantial increasing the ionic longitudinal relaxivity on going to higher fractions of gadolinium, indicating a real dendrimer effect.
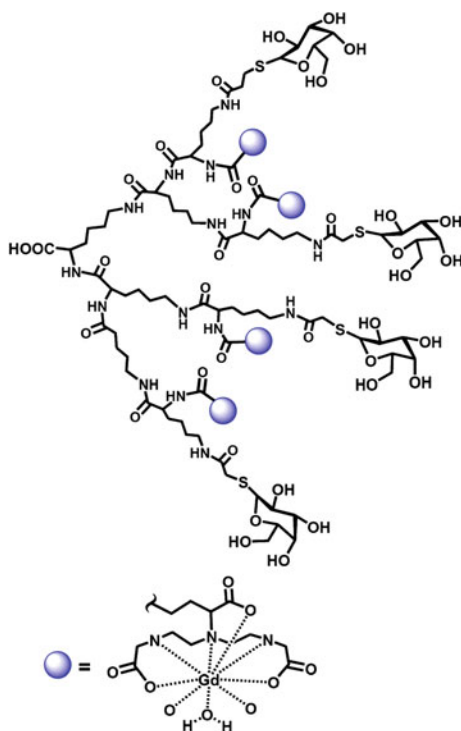
Fig. 5.27 PLL dendron bearing galactose and Gd chelates for cancer diagnosis

The *tert*-butyl ester-protected DTPA-terminated PPI dendrimers were chelated with $GdCl_3$, to create Gd-DTPA-terminated dendrimers [G1 (n = 4 Gd(III) ions per molecule), G3 (n = 16) and G5 (n = 64)] [227].

PLL dendron bearing galactosyl moieties and Gd-DTPA chelates was prepared by the mixing the chelating dendrimer with more than 1.5 equivs of $GdCl_3 \cdot 6H_2O$ at pH = 5.0–5.5 (Fig. 5.27) [228]. The MCDs having highly controlled structures and a single molecular weight show a two-fold increase in r_1 relaxivity to 9.1×10^3 $(Gd \ M)^{-1} s^{-1}$ compared to Gd-DTPA. It is important that no obvious cytotoxicity of this multifunctional dendritic agent is discovered in vitro.

The $EPTPA^{5-}$ chelate (H_5EPTPA is ethylenepropylenetriamine-*N,N,N′,N″,N″*-pentaacetic acid) was linked to PAMAM dendrimers of three different generations (5, 7, and 9) through benzylthiourea linkages [229]. The proton relaxivities measured at pH 7.4 for the MCDs G5-(Gd-EPTPA)$_{111}$, G7-(Gd-EPTPA)$_{253}$ and G9-(Gd-EPTPA)$_{1157}$ decrease with an increase of temperature, indicating that slow
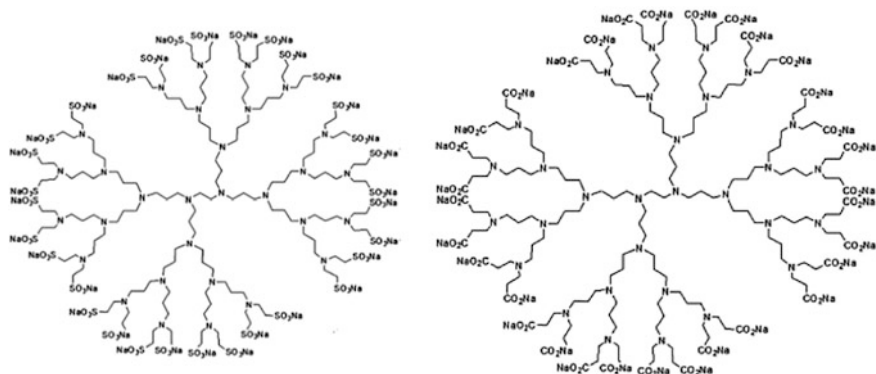
Fig. 5.28 Proposed structures for polysulfonate and polycarboxylate dendrimers

water exchange does not limit relaxivity. The Gd(III)-MCDs were prepared by mixing equimolar amounts of $Gd(ClO_4)_3$ and chelating dendritic ligand in water using a slight ligand excess (5%).
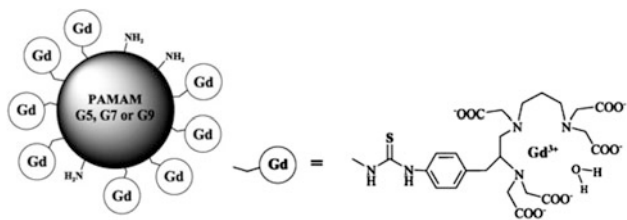
Among other polydentate dendritic ligands, we note G1–G3 sulfonated and carboxylated PPI-dendrimers with en core which showed specific picture in chelation of metal ions (Fig. 5.28) [230]. In particular, at low copper concentration up to 1:1 molar ratio between Cu(II) and dendrimer there is CuN_2O_2-mode on the dendrimer core. At higher concentrations of Cu(II) there is peripheral ion disposition coordinating one nitrogen atom and 3 oxygen atoms in square-planar geometry under limited mobility conditions. Finally, at high concentrations copper ions are timed to external dendrimer surface with CuO_4-mode. For sulfonate dendritic systems, weaker interaction of Cu(II) with nitrogen centers and stronger interaction with oxygen from SO_3^- groups is typical.

In another example, G3 triazine polydentate dendrimer (Fig. 5.29), containing multiple, iron-sequestering desferrioxamine B fragments is obtained in seven steps in 35% overall yield [231]. It is important that dendrimer chelates iron(III) ions with neither cooperativity nor significant interaction from the dendrimer backbone.
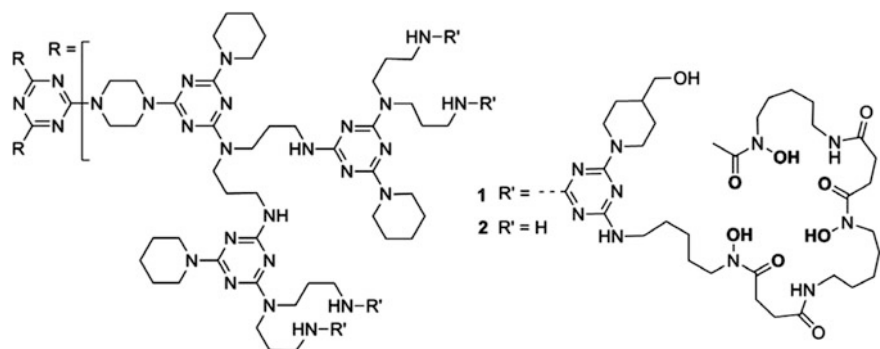
Fig. 5.29 Dendrimer displays 12 desferrioxamine B groups that form hexadentate chelates with Fe(III) using the groups shown in bold

The absorbance of Fe(III)-MCD is linear up to 11 mol equivs of Fe(III):L and this linear relationship suggests that iron chelation by this polydentate dendrimer is not cooperative.

5.3   Macrocyclic Complexes

The dendrimers and dendronized polymers containing macrocyclic complexes are the object of increased attention of researchers.

5.3.1   Metal Complexes with Pseudo-crown Ethers and Crown Ethers

The worm-like dendronized polymers having dendrons based on oxathiaethers showed high metal coordination properties [232]. Extensive characteristics of chelating properties with respect to a wide range of metal cations exhibited high and selective affinity of chelating dendrimers to Ag(I) and Hg(II) cations (Fig. 5.30). Its origin is explained by presence of specific M···S and M···O interactions (M = Ag or Hg) in a cage structure formed by dendritic fragments. Stoichiometry of complexation is determined by degree of steric hindrances in dendronized polymers. A result of complexation is Coulomb stabilization of charged dendronized polymers, which has a strong effect on their thermosensitive properties showing possible chemosensor applications.

Complexation of the dendronized PMAs with dibenzo-24-crown-8 branching blocks with K(I) ions brings to a significant expansion of a chain (Fig. 5.31) [233]. However, electrostatic repulsion does not contribute considerably into a chain expansion due to excessive bonding of counter-ions even far below Manning limit.
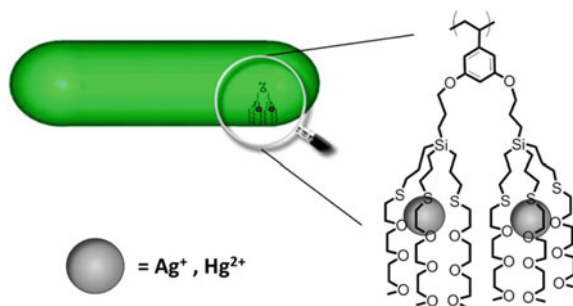
Fig. 5.30 Ag and Hg complexes with worm-like dendronized polymers bearing oxathiaether-based dendrons
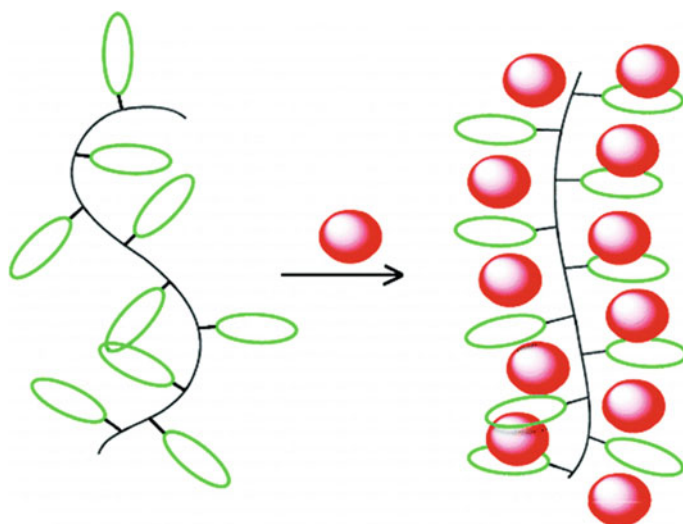
Fig. 5.31 Schematic representation of a potassium complexation with the dendronized PMAs with dibenzo-24-crown-8 branching blocks

Most probably, conformation change in fragments of the crown ether during coordination of K(I) ion in parallel to short-range interactions between ion pairs formed along a chain, causes the observed considerable increase in rigidity of the chain in terms of a Kuhn statistical segment length, l_k, with $l_k = 8$ to 19 nm and from $l_k = 19$ to 45 nm for G1 and G2 dendronized polymers, respectively. In other words, steric repulsion induced by guest-host interactions fits well for control over polymer conformation with densely grafted side chains.

We note also the dendrimer functionalized semi-crown ether incorporating up to 96 redox-active tetrathia-fulvalene moieties on the periphery, which was deposited onto a Pt electrode upon cycling. The macrocycle is suitable for the complexation of Ba(II) and the first dendrimer modified electrode able to reproduce the

electrochemical sensing of a metal cation thanks to the grafting crown ether/tetr athia-fulvalene units on the periphery of the dendrimer. It should be emphasized that this dendrimer constitutes one of the examples of sensing with organic redox active dendrimers [234].
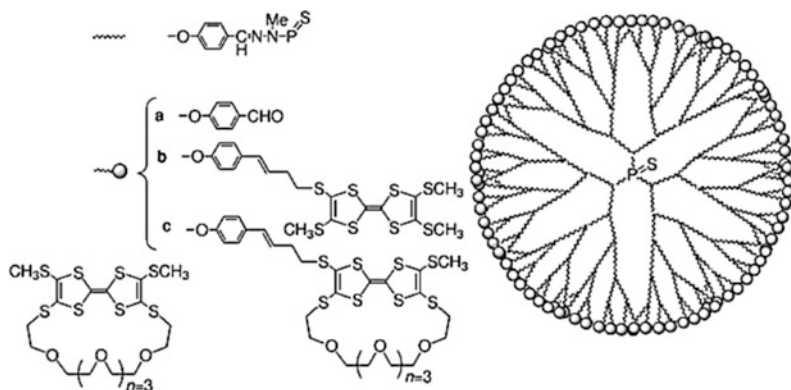
Of interest is using crown ether-functionalized dendrimers for extraction of alkali metal picrates [235]. It is important that depending on the generation of the dendrimer the positive and negative dendritic effects are observed.
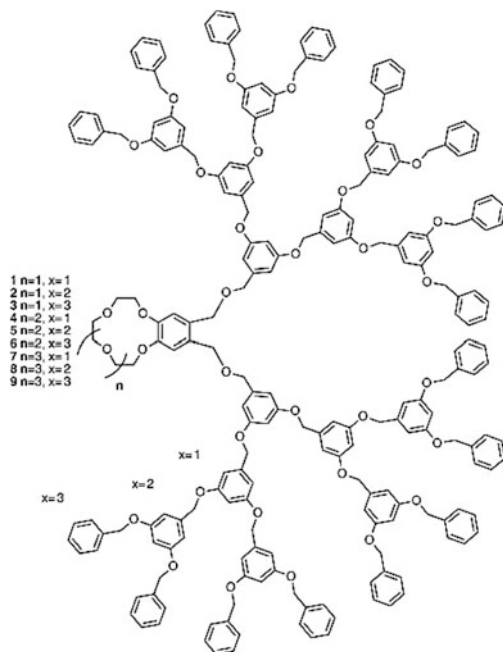
It should be noted the preparation of Na(I)-selective electrodes based on PVC membranes with silacrown modified carbosilane dendrimer, which works well over a wide concentration range with high selectivity [236].

Of interest is complexation of alkali ions with light-harvesting phenylacetylene monodendrons containing crown ether fragments [237].
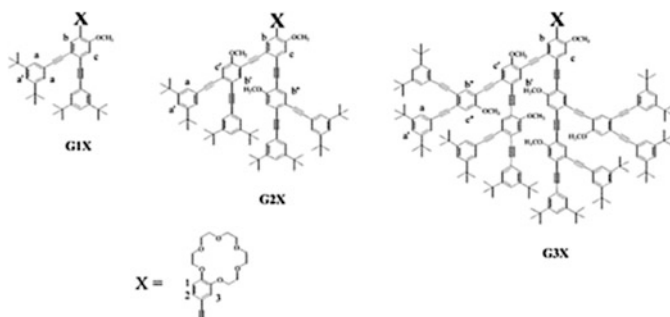
The crown ether-functionalized tetraphenylethene dendrimer was synthesized via the thiol-ene click reaction of thiol-derivatized tetraphenylethene with maleimide-functionalized benzo-15-crown-5 (Fig. 5.32) [238]. In the prepared com-pound the tetraphenylethene core and four outer benzo-15-crown-5 moieties serve as the AIE-active motif (AIE is aggregation-induced emission) and K(I)-binding function-alities, respectively. In particular, upon K(I) addition, dendrimer can be effectively induced to aggregate due to K(I)-mediated cross-linking via the formation of macro-cyclic complex in a sandwiched manner. This process is accompanied with the turn-on
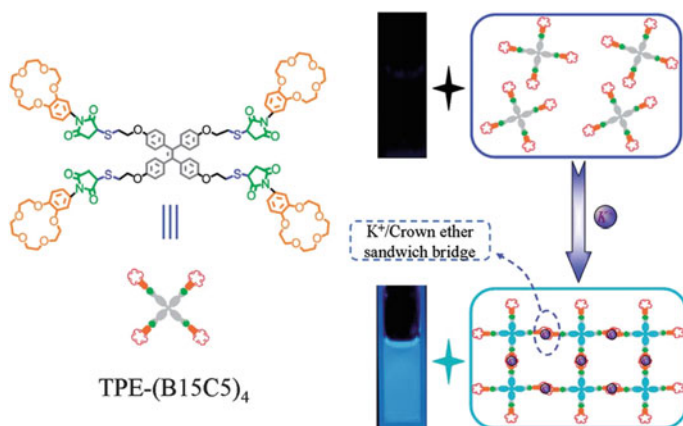
Fig. 5.32 Complexation of K(I) with crown ether-functionalized tetraphenylethene dendrimer

of fluorescence emission via the AIE mechanism. Thus, the prepared dendrimer can serve as highly sensitive and selective fluorometric off-on K(I) probes.

5.3.2   Metal Complexes with Cyclam-Containing Dendrimers

A large body of studies deals with MCD containing cyclam core [239–248]. Thus, a dendrimer with a cyclam core, dimethoxybenzene branches and naphthyl ends with Zn(II) gives bis-cyclam complexes [ZnL$_2$]$^{2+}$, which prevent formation of exiplexes as a result of naphthyl fluorescence [249, 250]. Similar photophysical results were obtained with lanthanide Nd(III), Eu(III), Gd(III), Tb(III), Dy(III) ion complexes, but data on emission correspond better with 1:3 and 1:2 dendritic complexes [251]. Upon titration of dendrimers containing two covalently bound cyclams as a core with [Zn(CF$_3$SO$_3$)$_2$] or [Cu(CF$_3$SO$_3$)$_2$], spectral emission changes, thus providing evidence of the 1:1 complexation, then substituted by 2:1 complex, though the results were different in absorption and emission spectra of these two metal ions [252]. Studying complexation between [Ru(bpy)(CN)$_6$]$^{2-}$ and dendrimer metal-cyclam core showed that the complex is formed with a dendrimer containing 12 dimethoxybenzene units and 16 naphthyl ends. In this complex a dendrimer plays a role of light-harvesting second coordination sphere and transfers collected energy to [Ru(bpy)(CN)$_6$]$^{2-}$. Moreover, the complex can be disrupted by addition of either acid or base exhibiting two distinct optical outputs according to an XOR and an XNOR logic, respectively [253, 254].

Cyclam-core G1 MCD with peripheral and in-core Ni centers is synthesized by interaction between tetrakis(salicylaldimine)cyclam ligand with Ni acetate [255]. MCD is cationic with two acetate groups as counter-ions and was isolated as a lime green solid in a yield of 63%. The trinuclear dendritic complex is used as a precursor of a catalyst in vinyl polymerization of norbornene using MAO as a co-catalyst with formation of macromolecular polynorbornene.
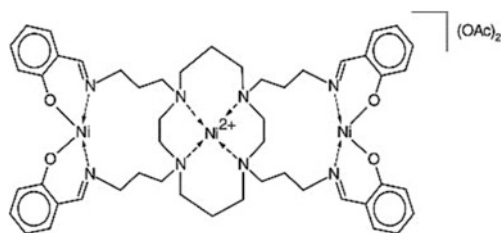
A dendrimer, which carries two cyclam units bound to azobenzene fragment and luminescent naphthalene peripheral blocks, was obtained (Fig. 5.33) [256]. It occurs that this dendrimer performs three different functions (light-harvesting,
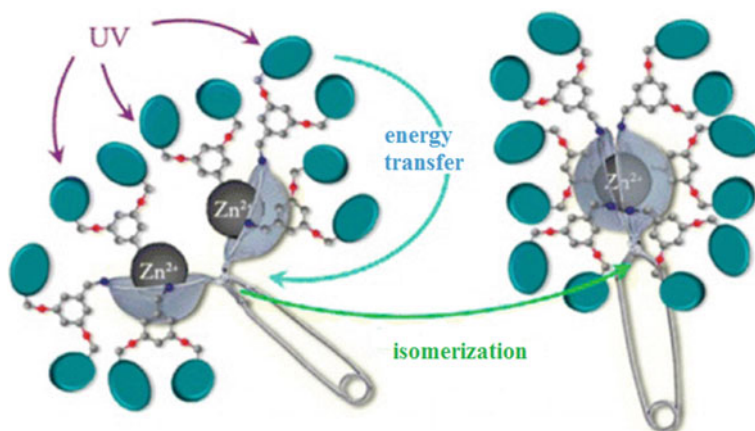
Fig. 5.33 Schematic representation of the functions performed by G1 dendrimer. Different coordination ability by the cyclam moieties (blue circles) of G1*(trans-azo)* (left) and G1*(cis-azo)* (right), light-harvesting by naphthalene units (grey ovals) and sensitized photoisomerization of the core azobenzene

photoisomerization, and metal ion coordination), which can interact or change depending on a metal ion nature. In other words, this is an example of easily controlled molecular tweezers, in which Zn(II) coordination provides 100% efficient photosensibilization of azobenzene switches, while Cu(II) switches off azobenzene isomerization.

Of substantial interest is the study of complexability of the dendrimers based on cyclam cores and linked PAMAM dendrons decorated along their perimeter with four or eight dansyl-chromophores [244]. It turned out that energy transfer to a central ion is a function of dendrimer generation. In addition, the energy transfer efficiency is determined by the geometry of the coordination node.
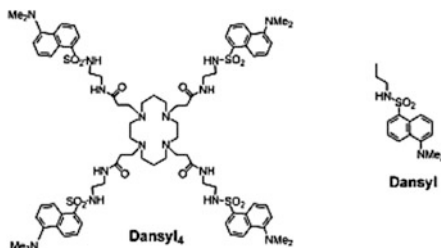
Nanolatexes of diameter 15 nm, having the cyclam fragment on the surface, were modified by a phosphorus dendritic compound containing an activated vinyl group at the core, and carrying Girard-T reagents as terminal fragments, for inducing
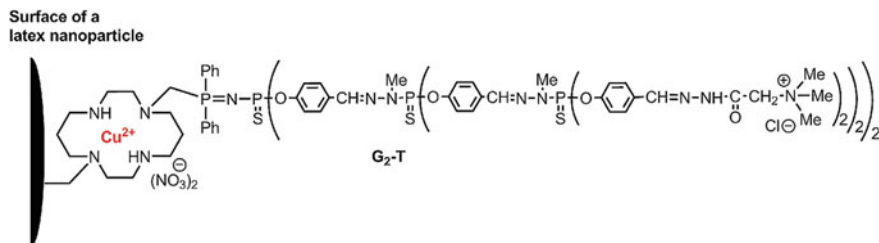
Fig. 5.34 A water-soluble dendritic structure linked to nanolatex through a tetraazamacrocycle suitable for the complexation of Cu(II)

solubility in water (Fig. 5.34) [257]. The dendronized nanoparticles retain the Cu(II) chelation ability, thus indicating the permeability of the dendritic shell.

5.3.3   Metal Complexes with Cyclen-Containing Dendrimers

In Eu-cyclen core dendrimers formed by click-reaction between dendrons carrying an azide group at the focal point and tetravalent cyclen core containing four alkyne groups, triazole not only acts as a stable spacer but also as a sensitizer, transferring their singlet-singlet excitation to UV range (270–290 nm) to partially occupied luminescent lanthanide 4f-shell (Fig. 5.35a) [240]. It should be noted that luminescence decay time from the lanthanide $^5D_0 \rightarrow {}^7F_2$ emission increases with increasing dendrimer generation, indicating that the shielding effect of the dendron wedges has a significant impact on the photo-excitation relaxation and energy transfer (Fig. 5.35b). Thus, the obtained triazoles intra-locked in close proximity to the macrocycle core promoted interesting photophysical properties.
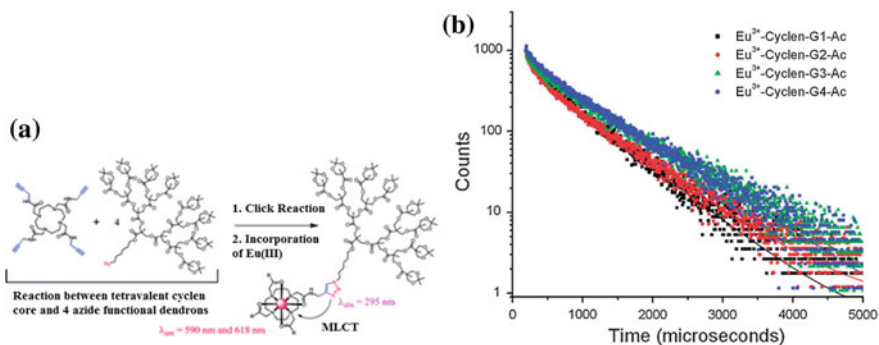
Fig. 5.35 a Scheme of synthesis of triazole sensitized Eu-dendrimer chelates. **b** Time-resolved luminescence recorded at 618 nm of various Eu(III)-cyclen dendrimers in THF solutions excited at 270 nm: G1 (black squares); G2 (red dots), G3 (green triangles), and G4 (blue diamonds)

5.3.4   Metal Chelates Based on Dendrimers with Triazacyclononane Fragments

Another example of macrocyclic MCD are PPI dendrimers with peripheral triaza-cyclononane fragments coordinated with Zn(II) ions [258]. Using control over molar ratio of triazacyclononane during production, 6 dendrimers were synthesized with 0, 20.5, 32.5, 53, 75, and 100% triazacyclononane groups on a surface. As occurs, a dendrimer with completely functionalized triazacyclononane groups is the most active catalyst of RNA model substrate cleavage, and its activity is by 270 times higher than that of the low molecular weight analogue and by five orders of magnitude more efficient than non-catalyzed reaction. Moreover, studies of coop-erative effects showed that each active center contains two Zn(II) chelates, pointing to the fact that two ions act cooperatively in the RNA cleavage reaction.
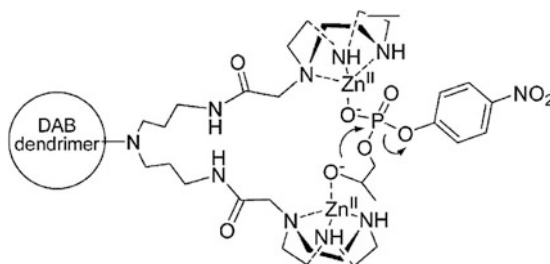
Lyzine-dendrons functionalized by triazacyclononane were fixed on Tentagel resin, and their Zn(II) MCDs were obtained (Fig. 5.36). It occurs that the cleavage reaction rate of RNA model substrate increases as a dendron size increases, at that increase in catalytic efficiency was determined by improved affinity of substrate conjugation. The obtained Michaelis-Menten parameters were in good agreement with the data obtained for homogeneous analogues, which points to the same type mechanism of catalytic reaction [259].

We should also notice peptide dendrons and dendrimers of increasing genera-tion, functionalized at periphery by triazacyclononane forming a strong complex with Zn(II) ions [260]. These MCD show higher increase in cleavage rate of RNA model displaying, for example, in the case of D_{32} dendrimer increase about 80,000 (k_{cat}/k_{uncat}) at the concentration 600 nM.

5.3.5   Tetrapyrazinoporphyrazine Complexes

Derivatives of tetrapyrazinoporphyrazine containing rigid dendritic fragments are used to produce macrocyclic MCDs [261]. Absorption spectra of Mg-porphyrazines
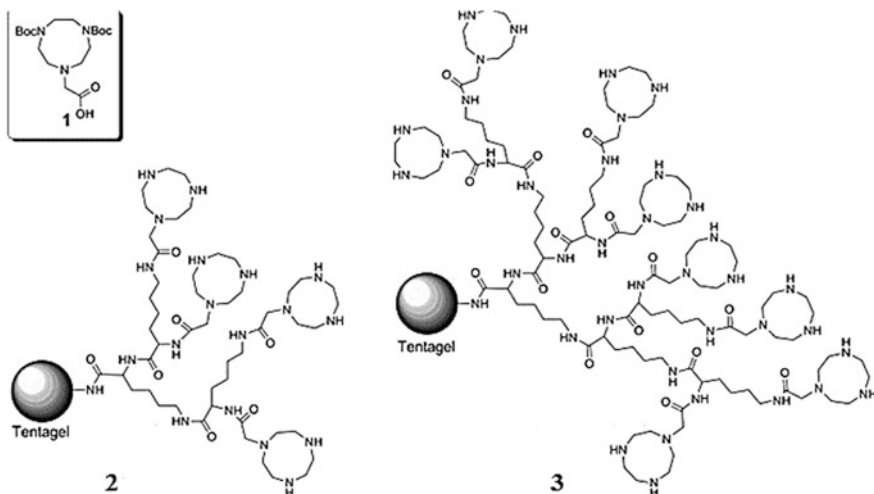
Fig. 5.36 Tentagel triazacyclononane resins **2** and **3** obtained in a single step by reacting Tentagel with triazacyclononane-derivative **1**

show that splitting of Q band for 653 and 737 nm is caused by a combination of a transition moment between a pair (or more) chromophores.
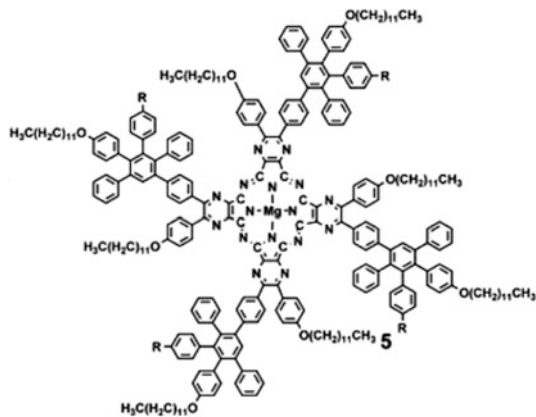
5.3.6   Porphyrin Complexes

Numerous studies are devoted to M-Pp dendrimers obtained by direct metallation of free-base Pp containing dendrimers [16, 21, 262]. The majority of M-Pp MCDs

possess a M-Pp unit as the interior core fragment only, although usually Pp units are mostly introduced at the surfaces of readily (commercially) available dendritic structures, such as PAMAM dendrimers.

As a typical example, we note the synthesis of photosensitizers by metallation of Pp core dendrimers with Al, Ag and Zn [263]. Experiments show effective two-photon excited FRET for Pp excited triplet state, which subsequently generates singlet oxygen by Al and Zn MCDs. In particular, efficiency of singlet oxygen photosensitization is most effective using Al, then using Zn, and the least effective then using Ag. In fact, Ag-metallated dendritic photosensitizers were non-fluorescing and unable to generate a measurable amount of singlet oxygen. With proper selection of the inserted metal, it was possible to tune efficiency two-photon induced singlet oxygen.
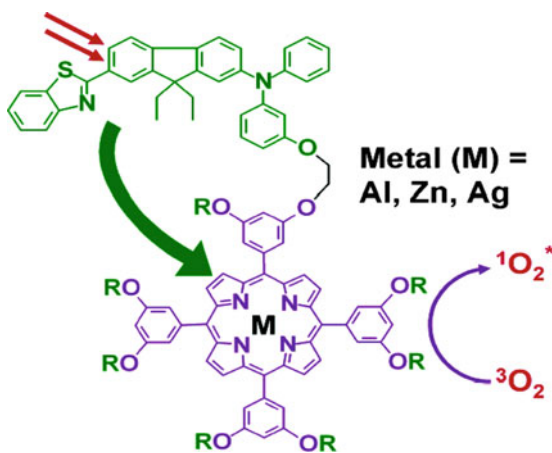
The corresponding free-base Pp dendrimer was metallated with $FeCl_2$ in dry THF to form the MCDs possessing a Fe-Pp catalytic core and polyether dendritic arms [264]. Lower generations of MCD show a normal hyperbolic kinetic behavior, whereas G3 and G4 MCDs exhibit a sigmoidal kinetic profile associated with cooperative effects due to aggregation phenomena. This behavior resembles that observed for Fe-Pp containing biomolecules such as cytochromes and hemoglobin.

It should be noted metal-chelating Pp-PAMAM dendrimers which were synthesized via the microwave method [265]. The metal-binding properties of the Pp-PAMAM dendrimers were studied by means of the polymer-supported nanofiltration technique. The nylon membranes modified with Pp-PAMAM dendrimers retained Pb(II), Cr(II) and Fe(II) with a retention rate of 99%, and Co(II) and Cd(II) with a retention rate above 50%.

Interesting examples are the complexes for optical amplification based on Er (III)-cored M-Pp dendrimers [70]. Initially, the 5,10,15-(G2)$_3$-20-(4-methoxy-carbonylphenyl)-Pp was metallated with $PtCl_2$ in anhydrous benzonitrile and then
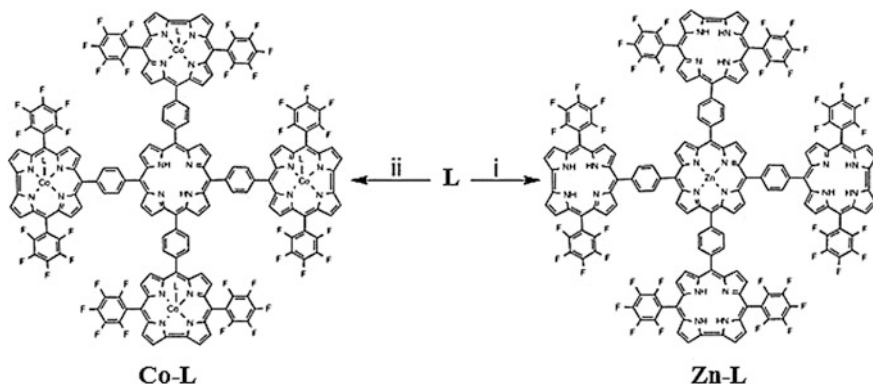
Fig. 5.37 The complexation of Co(II) or Zn(II) with dendritic Pp with four corroles

reacted with ErCl$_3$. The Er(III)-cored complex with Pt(II)-Pp bearing G2 Fréchet-type dendrons displayed intensity seven times greater than that of its parent Pt(II)-Pp. The emission lifetime of the Er(III)-cored dendritic complex was found to be 40 ms in deoxygenated THF solution. This result showed that energy transfer from the M-Pp to the Er(III) core proceeded through a triplet state.

It should be noted MCDs containing Fe-Pp core and boron ether end fragments [266]. It turned out that the end modification leads to changes in the conformation and catalytic behavior of the resulting MCDs, therefore these MCDs were called catalytic chameleon dendrimers.

An interesting observation was made in the study of complexation of dendritic Pp with four corroles [267]. It was found that different chelating properties of such macrocycles allow selective introduction of Zn(II) to the central Pp and Co(III) in the peripheral corroles (Fig. 5.37). The selective metallation is very important for the design of MCDs, in which one type of macrocycle is used as photosensitizer and the other for performing catalysis.

Selective metallation of the surrounding corroles under reaction conditions where the central Pp remained free indicates the known high affinity of corroles to cobalt(II). The ^{1}H NMR spectrum (Fig. 5.38) confirms the presence of four Co-PPh$_3$ moieties by the relative integrations of their *para*-H, *meta*-H, and *ortho*-H resonances (δ = 7.1, 6.7 and 4.7 ppm, respectively) with the Pp's β-pyrrole CH resonance (δ = 9.4 ppm). Finally, the two inner NH protons that appear at −2.3 ppm clearly testify that the central Pp was not metallated.

5.3.7 *Phthalocyanine Complexes*

The metal complexes with dendritic Pc obtained by direct metallation of free-base Pc have been little studied [16, 268]. For example, it should be noted the synthesis
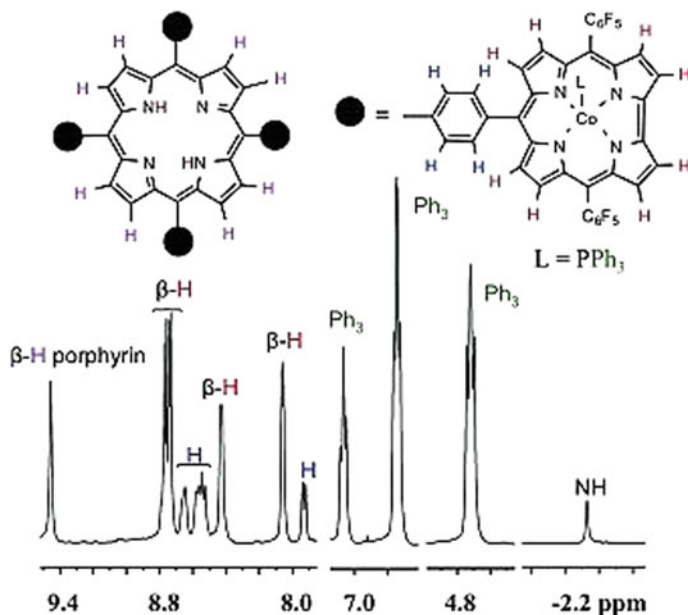
Fig. 5.38 ^{1}H NMR spectrum of Co-L in [D$_6$]benzene

of the G2 cobalt-metallated Pc dendrimer possessing Newkome-type dendrons (Fig. 5.39) to catalyze the oxidation of mercaptoethanol by dioxygen [269]. The dendritic structure around the Co-Pc prevented the molecular aggregation among Pc moieties in polar solvents and thin films. The electron-transfer process was hindered in the Co-Pc MCD that is the result of a shielding effect by the dendrimer branch on the Co-Pc core. The influence of Pc aggregation, resulting from strong inter-molecular stacking, led to increased catalytic activity, as well as enhanced catalytic stability.

Of interest is the study of the complexation of copper and cobalt chlorides with a G1 dendrimer containing an octa-substituted Pc core (Fig. 5.40a) [270]. The Pc core has D$_{2h}$ symmetry and corresponding Q-band splits into two main absorptions (ca. 670 and 700 nm). At the same time, Co-Pc dendrimer has D$_{4h}$ symmetry, for which a single Q-band at 674 nm and a vibrational band at 610 nm are characteristic (Fig. 5.40b). It should be noted that a broad band is observed between both bands due to a dendrimer aggregation. However, in the spectrum of G7 Co-Pc MCD (the insert in Fig. 5.40), the intermediate band has totally disappeared indicating an absence of any aggregation for a G7 dendrimer.

It should be noted that triplet quantum yields are substantially increased during transition from tetra-glycosylated Zn-Pc MCD to octa-galactosylated Zn-Pc MCD [271].
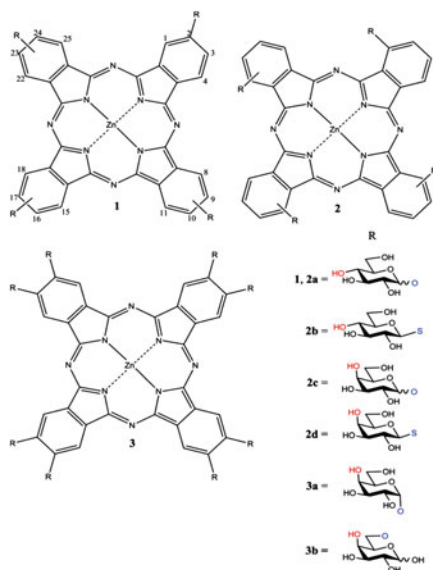
5.3.8   Metal Chelates with DOTA and Related Ligands

The DOTA ligand and its DO3A analogue are important chelators commonly used for biomedical applications as therapeutic radiopharmaceutical and/or MRI contrast agent [272]. MRI applications of dendrimers containing DOTA and DOTA-like ligands are particularly appealing, because the dendrimer can be labeled with multiple Gd chelates, creating a strongly paramagnetic macromolecule with higher relaxivities on a molar basis than conventional LMC, due to slower molecular tumbling rates of large macromolecules [10, 273]. The branched structure of the chelating dendrimers imparts rigidity and a high density of functional groups for the multivalent display of Gd for therapy and diagnosis [24, 219–225, 274, 275]. The dendrimers with DOTA or DO3A ligands have been mainly used as an alternative scaffold capable of carrying multiple chelating ligands (among them DOTA or DO3A) to incorporate radiopharmaceuticals at well-defined positions [219, 276]. It should be emphasized that the behavior of contrast agents based on Gd(III)-MCD in vivo depends on the modification of the properties of the dendrimer, such as the size of the core and the chemistry of the outer shell.

A more versatile topology within the dendritic structure is the dendrons, where the surface can be decorated with the same ionic groups as spherical dendrimers, but the focal point can be functionalized with different groups by orthogonal chemistry [6]. Very few examples have been reported conjugating a DOTA or
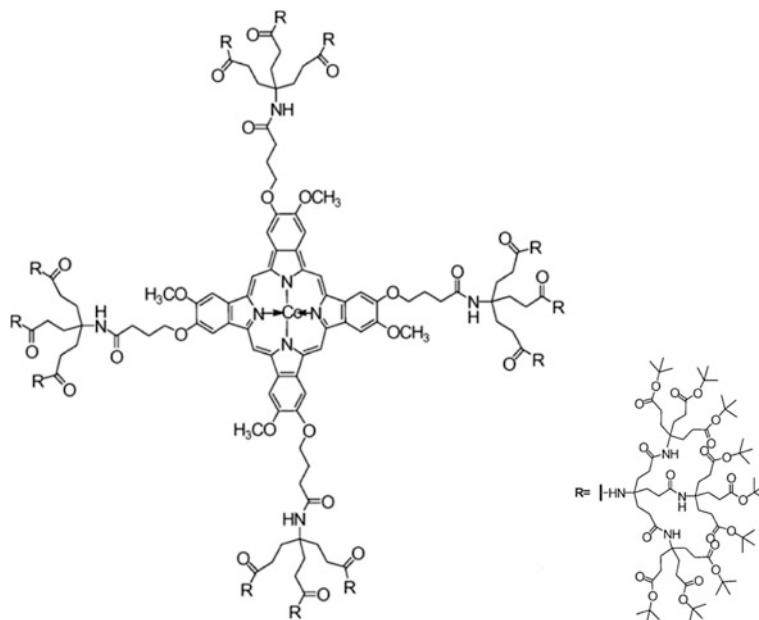
Fig. 5.39 M-Pc dendrimer possessing Newkome-type dendrons
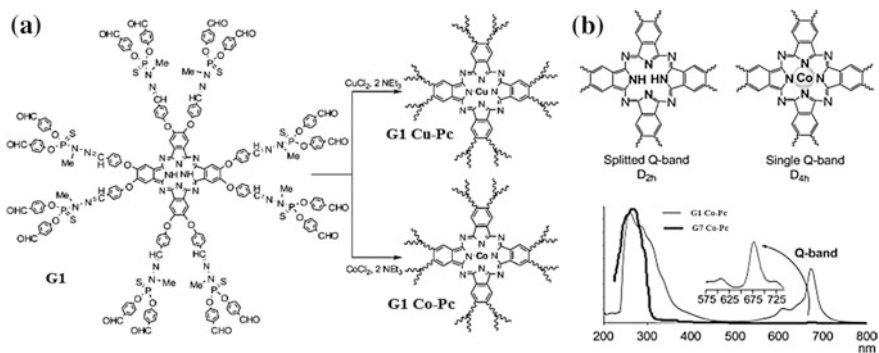
Fig. 5.40 a Synthesis of dendrimers having a Pc as core and the corresponding copper and cobalt complexes. **b** (top) Symmetry of free-base and complexed Pc cores, and spectroscopic consequences. (bottom) UV/Vis spectra of the G1 and G7 of the Co-Pc; both spectra are normalized to have the same intensity at 268 nm. The insert is an enlargement of the area of the Q-band of G7 Co-Pc in THF
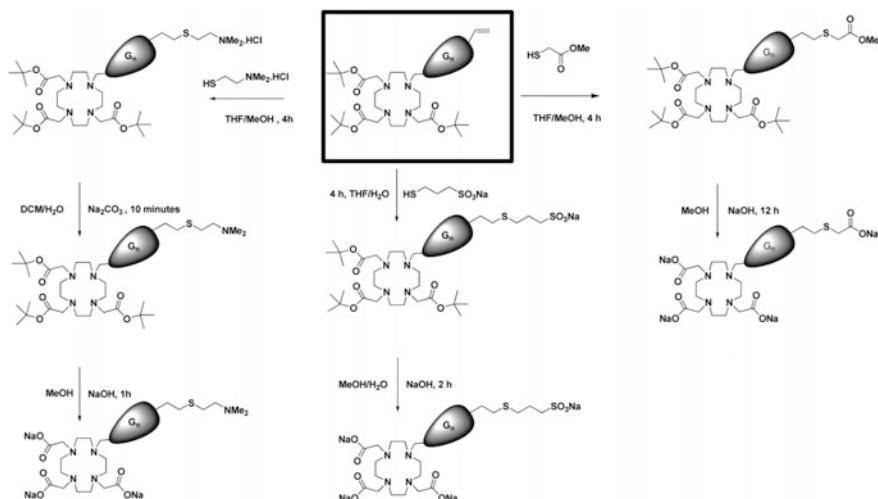
Scheme 5.15 Synthesis of neutral (amine or ester) and ionic (ammonium, carboxylate, or sulfonate)-terminated dendrons with protected and unprotected DO3A at the focal point

DO3A ligand at the focal point (Scheme 5.15) [277]. The presence of the dendron branches modifies the chelation capacity of the macrocyclic ring with respect to that of monomer DOTA ligand. In this situation, one can keep the periphery for the desired biomedical application while adding a new function at the focal point, normally as a radiolabeling moiety.

As a typical example, we note a readily and rapidly accessible triazine dendrimer prepared in four steps with 23% overall yield to give a structure showing four maleimide fragments and DOTA [278]. The functionalization of the chelating DOTA group with gadolinium was also accomplished easily.

In another interesting example, the Arg-Gly-Asp (RGD) peptide dendrimers were conjugated with a DOTA moiety and radiolabeled with ^{111}In to evaluate the in vitro receptor binding characteristics and in vivo tumor targeting properties [279]. The monovalent, divalent, and tetravalent dendrimers (Fig. 5.41) were radiolabeled by dissolving these compounds in an NH_4OAc buffer of pH 6.0 and 22.2–37 MBq [111]$InCl_3$ was added to each of the reaction mixtures. The radiochemical yield was more than 98% with a specific activity of 7.4 MBq μg^{-1} for monovalent (corresponding to 13.6 GBq μmol^{-1}) and divalent (22.7 GBq μmol^{-1}) ^{111}In-labeled dendrimers and was 80% for ^{111}In-labeled tetravalent dendrimer (43.3 GBq μmol^{-1}).

Of considerable interest is PAMAM G5-Gd-BnDOTA dendrimer synthesized in order to develop a clinically applicable analog [280]. Its main advantages are the greater inherent stability of the macrocyclic complex of Gd-BnDOTA under in vivo conditions, slightly smaller overall size, and ability to uniquely prepare a preformed Gd(III) chelate to attach to the dendrimer. Promising is the use of DAB core instead of en core because the slightly longer spacer will produce fewer cavities or defects
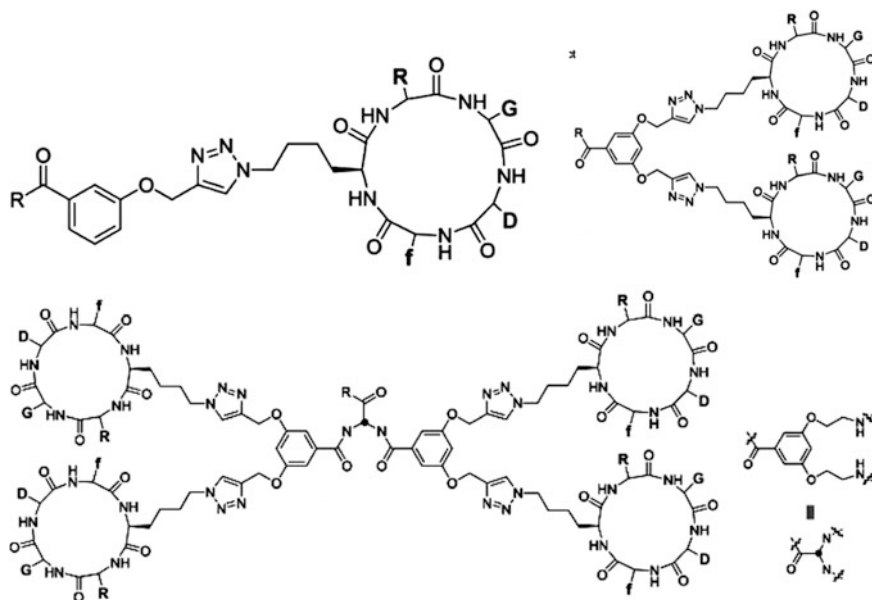
Fig. 5.41 Synthesis of the mono-, di- and tetravalent cyclo-peptide DOTA-conjugated dendrimers (R = DOTA-EtNH)

on the surface of the dendrimer into force less packed branches, and therefore more reproducible batch-to-batch production.

The conjugation of Gd-DOTA chelates to the PEG cored PLL dendrimer leads to a macromolecular MRI contrast agent for the differentiation of human breast cancer from benign soft tissue (Fig. 5.42a). No acute adverse effect was observed for this diagnostic agent in a long-term clinical trail [281]. It should be also noted the using the PAMAM framework to obtain a series of multivalent lanthanide(III)-glyco-conjugates, possessing DOTA monoamide functionalized chelators (Fig. 5.42b) [100]. The relaxivity of the Gd(III) chelates of the glycodendrimer in solution had a low value due to restrictions imposed by the flexibility and molecular weight of the dendrimer. At the same time, the lectin-glycoconjugated interaction was capable of retarding the tumbling rate considerably, therefore increasing the relaxivity of the Gd(III) chelates.

Of great interest is the relaxometric characterization of the fully loaded conjugate, containing 16 gadolinium chelates Gd-DO3AP^{ABn} based on monophosphinated DOTA-like ligand, where H$_4$DO3AP^{ABn} is 1,4,7,10-tetraazacyclododecane-4,7,10-triacetic-1-{methyl[(4-aminophenyl) methyl] phosphinic acid}, on the surface of a G2 PAMAM dendrimer (Scheme 5.16) [282]. The corresponding Gd(III) chelate was synthesized by mixing the conjugate with a twofold excess of GdCl$_3$ at pH 7.
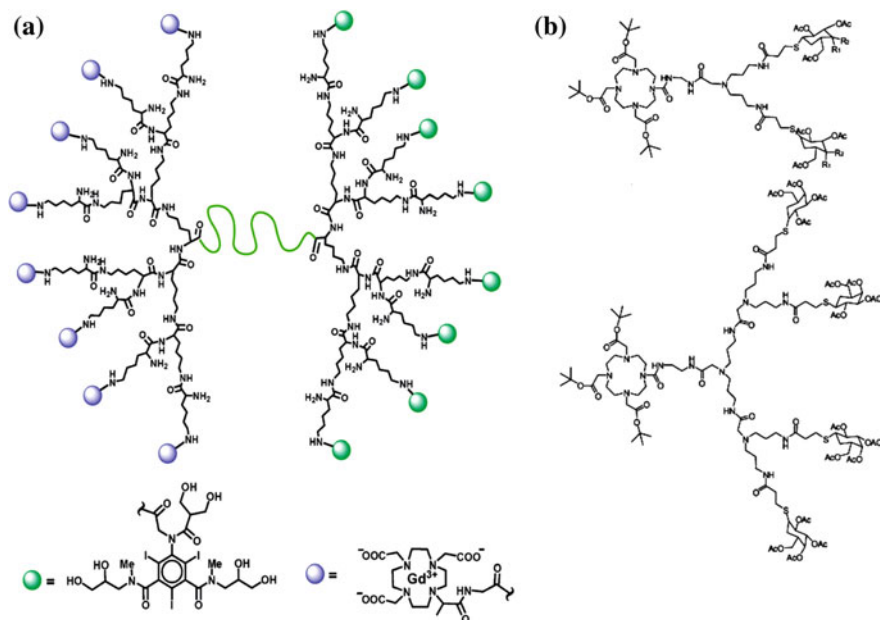
Fig. 5.42 a PEG-cored PLL dendrimers as MRI contrast agents. The green line represents PEG chain. **b** DOTA-Glycoconjugate ligands for lanthanide(III) chelation
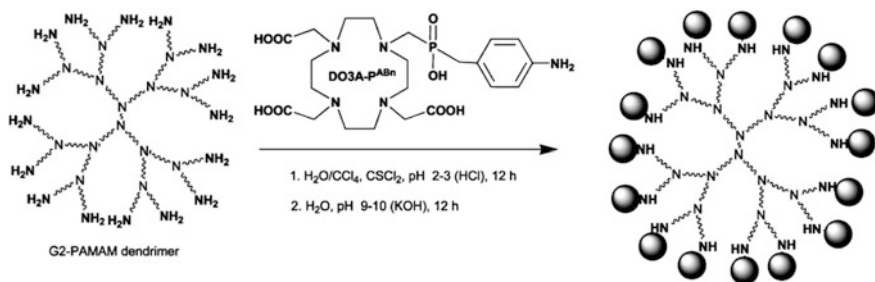
Scheme 5.16 Reaction sequence leading to the full-loaded G2-PAMAM dendritic conjugate

It is important that the proton relaxivity of this system was found to be pH dependent and, at pH = 6, it increased to ca. 24.8 mM^{-1} s^{-1}.

It should be noted G0 and G2 PPI dendrimers functionalized Yb(III)-DOTAM as pH-sensitive paramagnetic chemical exchange saturation transfer (CEST) agent [283].

5.4   Metal Chelate Star Polymers

One of the significant drawbacks of the MCDs is that their synthesis has usually required cumbersome multiple condensation reactions to increase the generation (molecular weight), which was even more complicated when a chelating functionality or metal chelate unit was introduced into the structure. As a similar 3D MCD, the metal chelates with hyperbranched polymers are the attracting alternative materials, because the synthesis is by simple addition polymerization, which is easy to prepare macromolecules with various chelating functionalities or metal chelate units through copolymerizations of functional monomers.

The simplest metal chelates with hyperbranched polymers are so-called star PMCs with more than three arms linked with the core. The undoubted advantages of star PMCs are simpler synthetic methodologies and a large number of terminal metal chelate units within a single polymer. As a typical example, we note star PMCs prepared by the modification of the different parts of star polymers using CRP method [284–292]. It is important that the size of star PMC can be tuned over a wide range by controlling the synthesis conditions.

The synthetic strategy of the star PMCs is based on the combination of star polymer synthesis and the coordination chemistry of metal chelates. There are two general methods for the synthesis of star PMCs: the «arm-first» and «core-first» methods (Scheme 5.17) [293]. Each of these has a select set of advantages and disadvantages inherently attached, and so care must be taken when planning the desired properties or targeted application for the star PMC prior to deciding which approach to employ. Advances in living/controlled polymerization methods have greatly improved the
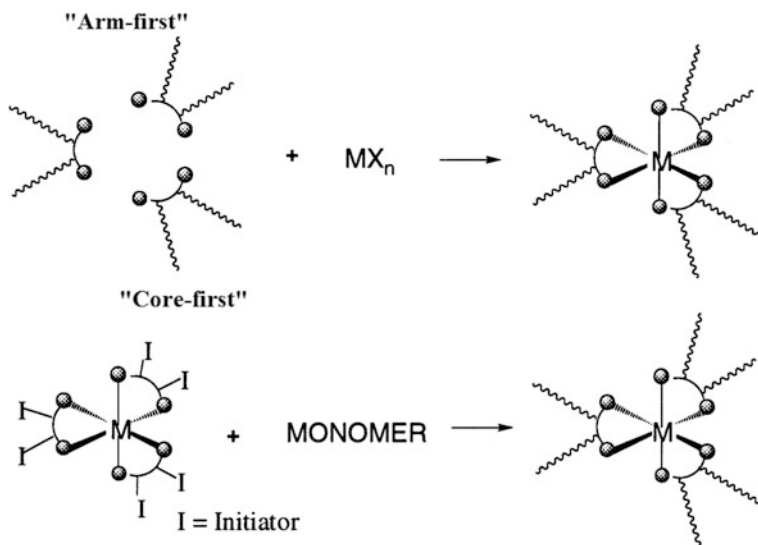
Scheme 5.17 Scheme presentation of «arm-first» and «core-first» methods

accessibility to star PMCs, with libraries of metal chelate stars of different size and/or functionality now able to be prepared for detailed assessment of structure-property relationships.

The «arm-first» method is based on MX_n chelation with the polymers containing terminal chelating fragments for preparing star PMCs. The different star PMCs including miktoarm star ones can be prepared by this method using various metal compounds and modifying polymer arms alone and their terminal fragments.

At the same time, «core-first» approach uses a metal chelate initiator for living polymerizations and, thus, becomes the core of the formed star PMC. This synthetic methodology allows to preparing star block PMCs and regulating number of arms.

5.4.1   «Arm-First» Method

The most frequently used ligand to prepare star PMCs is bpy. This ligand forms bis- or tris-chelates with a large variety of metal ions, and is an ideal candidate for the preparation of multiarm metal chelate stars because bpy functionalized at the 4- and/or 4′-position can be rather easily prepared. Thus, star iron(II) tris(bpy)-PMCs based on PS, PMMA, PCL, poly (DL-lactic acid) of different molecular weights with 3, 4, 5, or 6 arms can in principle be synthesized according to the functionality of the bpy used [294]. Iron tris(bpy)-chelate star formation is facile for macroligands <15,000; however, both the rate and extent of chelation are polymer dependent and decrease with increasing molecular weight.

The various star PMCs were prepared based on chelation of bpy-terminated PEO with Ru(II) [295] or Os(II) [296] ions. The star PMC obtained had a higher molecular weight than the pre-polymer and showed a narrow PDI. In the case of a Ni(II) or a Co(II) chelates, however, the star PMC is dissociated into three linear prepolymers under the conditions of GPC measurement.

Macromolecular PEG-containing iron tris(bpy)-chelates, presenting hydroxyl end groups for further modification as bioconjugates, copolymers, or cross-linking agents, were prepared via anionic ROP of ethylene oxide from hydroxyl-containing bpy initiators and subsequent chelation to iron(II) (Fig. 5.43a) [297]. Study of chelation of the bpy-centered PEGs with molecular weights from 4000 to 17,000 and low PDI (<1.1) to iron(II) sulfate revealed unexpected air sensitivity unlike iron tris(bpy)-LMC. In particular, red-violet aqueous solutions of $[Fe(bpyPEG_2)_3]^{2+}$ begin to bleach within hours when exposed to air and under argon, the chromophores are stable (Fig. 5.43b). Fe-PMCs are slower to form and faster to degrade in air with increasing molecular weight of $bpyPEG_2$.

$BpyPEG_2$ macroligands modified with methacrylate groups were also chelated with $FeSO_4$ to produce star PMCs [298]. In this case spontaneous gelation of iron (II) tris(bpy)-chelate PEG methacrylate was observed without the addition of a cross-linking agent. It is interesting that treatment of preformed hydrogels of chelating macroligands with aqueous solutions of $FeSO_4$, $CuBr_2$, and $CoCl_2$ also produced materials with color changes indicative of complexation.
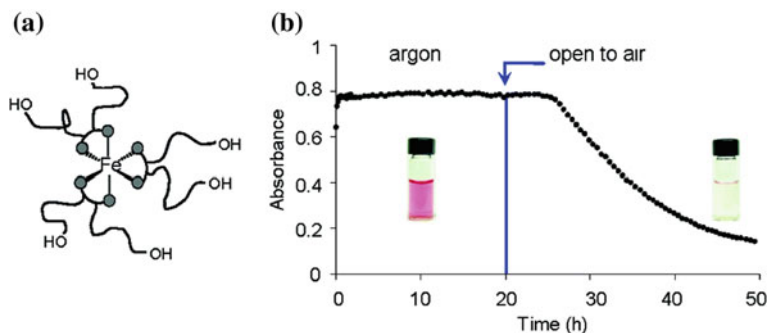
Fig. 5.43 Structure of $[Fe(bpyPEG_2)_3]^{2+}$ chelate with hydroxyl end groups (**a**). Rate comparison of $[Fe(bpyPEG_2)_3](SO_4)$ complexation in water under argon followed (after 20 h) by degradation under air for sample prepared from $bpyPEG_2$ macroligand of molecular weight $M_n = 6200$ (**b**)
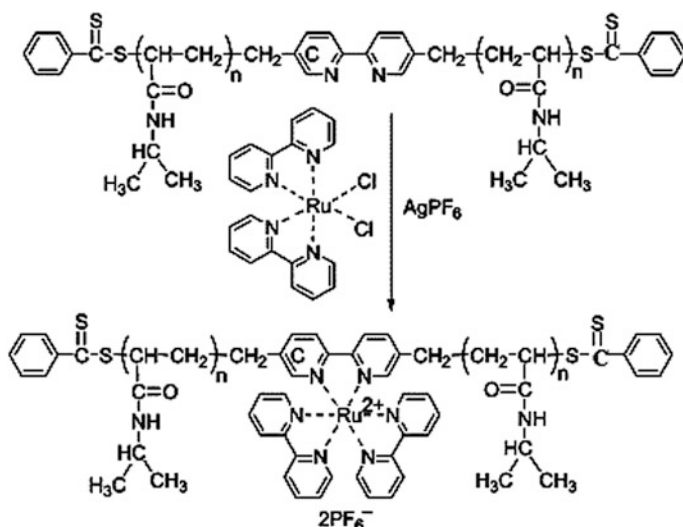
Scheme 5.18 Schematic representation for preparation of tris(bpy)Ru(II)-chelate poly(NIPAM) thermosensitive star polymers

«Arm-first» method was also employed for star PMCs with various arms including PS, PMMA, poly (propylene glycol), PCL, polylactides, and their block-copolymers [299–301]. Thus, macroligands $bpyPMMA_n$ (n = 1 or 2) were chelated to Fe(II) and Ru(II) with formation of star PMCs with one to six chains emanating from the central core, as well as different heteroarm star products [302]. Bpy-centered poly (NIPAM) polymers with controlled molecular weight and low PDI were chelated with ruthenium ion to produce thermosensitive star PMCs with well-defined structure (Scheme 5.18) [303].

Estimated CEs for formation of the Fe(II) and Ru(II) chelate stars, biocompatible polyesters, polylactides, PCL, and various copolymer analogues (M_n = 20,000–240,000 and 6000–30,000 for Fe and Ru chelates, accordingly) were high [300]. CE refers to the ratio of the extinction coefficient determined from λ_{max} for the PMC with that of Fe(II) and Ru(II) bpy-LMCs. Thin films of the red-violet colored iron-chelate stars exhibited reversible, thermochromic bleaching. Solutions and films of the polymers decolorize in response to some stimuli (heat, acid, bases, peroxides, ammonia), suggesting interesting possibilities for their use in qualitative and quantitative assays.

Narrow dispersity PS with bpy binding sites (bpyPS$_2$) were chelated to Ru precursor complexes, RuL$_2$Cl$_2$ (L = bpy, phen) or Ru(DMSO)$_4$Cl$_2$, to form star Ru-PMCs, [Ru (bpyPS$_n$)$_3$]$^{2+}$, with three and six arms, respectively [293]. More versatile were sequences involving chelation of 2 equiv of a bpyPS$_n$, followed by association of another ligand with the Ru(II) center (four-arm stars [Ru(bpyPS$_2$)$_2$(L)]$^{2+}$, where L = bpy, phen, 4,4′-bis(hydroxymethyl)-bpy, and 4,4′-bis(tricosanyl)-bpy) [304]. The determining factors of the reactivity at the Ru center are the CPL molecular weight, the position of the bpy donor in the PS chain, and solvent polarity. Homo-block star Ru-PMCs, [Ru(bpyPS)$_2$(bpyPS$_2$)]$^{2+}$ and [Ru(bpyPS$_2$)$_2$(bpyPS)]$^{2+}$, were synthesized by using two different kinds of bpyPS$_n$ macroligands.

The method has further permitted the synthesis of heteroarmed star PMCs [301]. Bis(bpy)Ru chelates were prepared with macroligands bearing one or two PS chains and then a second type of bpy-macroligand, bearing one or two PMMA chains, was attached to the bis-chelates, yielding hetero-arm star PMCs with 3 or 6 arms.

The bpy end-functionalized PS and poly (NIPAM)) polymers were used as macroligands for the preparation of star PMCs [305]. In this case, hydrophobic PS macroligand combined with hydrophiphilic poly (NIPAM) was chelated with Ru ions to produce amphiphilic star Ru-PMCs (Fig. 5.44).
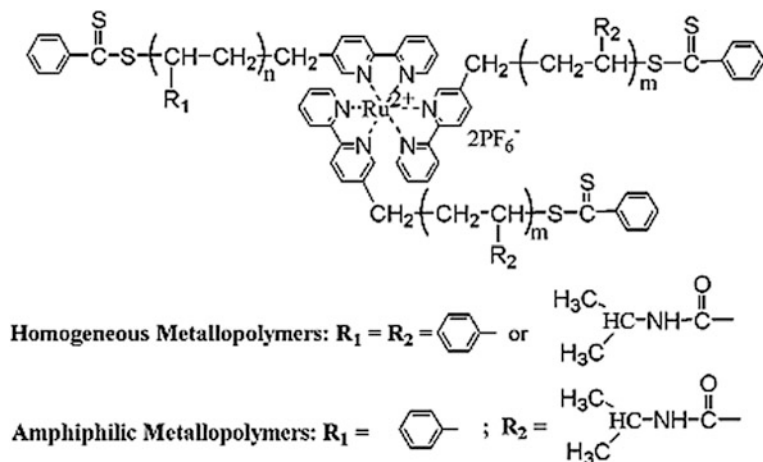
Fig. 5.44 Structure of star-shaped tris(bpy)-ruthenium-cored PMCs
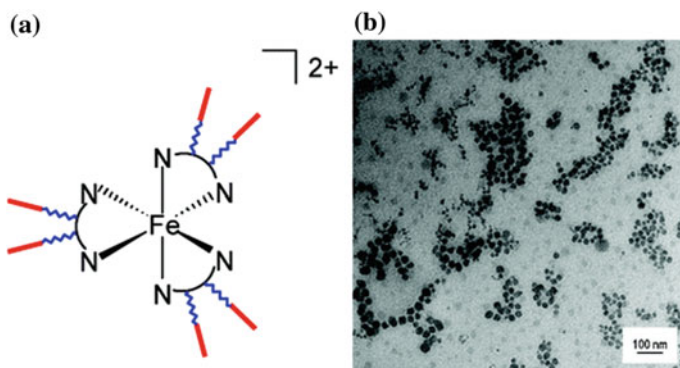
Fig. 5.45 a Schematic representation of star tris(bpy)-Fe(II) block-PMC: *N–N* bpy, zigzag PEG, straight poly(lactide). **b** TEM images of star Fe-PMC nanoparticles (M_n = 37,000)

It is important that the prepared amphiphilic star PMCs are able to form micelles in water, which morphology is determined by the polymer concentration and the hydrophilic poly (NIPAM) block length [306].

Bpy-centered block copolymers incorporating biocompatible PEG and poly (lactide) polymers with Fe(II) ions form star PMCs (Fig. 5.45a) [307]. Micelle-like nanoparticles of block copolymer macroligands and star Fe-PMCs were prepared via nanoprecipitation. The presence of spheroid particles (chelating macroligands, 111–253 nm in diameter; Fe-chelates, 37–75 nm in diameter) is shown (Fig. 5.45b). Halolike regions surrounding the nanoparticles and a distribution of lighter particles between the nanoparticles are observed, indicating that a fraction of the polymer is dissolved in the nanoparticle dispersion and aggregates during solvent evaporation.

The macroligands bpy(PMMA-PS)$_2$ and bpy(PS-PMMA)$_2$ were chelated with Fe(II) to yield six-arm star PMCs [308, 309]. However, for bpy[PCL-poly(*tert*-butyl acrylate)]2 and bpy[poly(lactic acid)-poly(*tert*-butyl acrylate)]2 macroligands, only bis(bpy)-chelates were formed. This is associated with variations in chain conformation in the solvent mixture used, inducing steric hindrance around the metal chelating site. CE is determined by polymer molecular weight and composition. It should be noted that most macroligands form tris-chelates efficiently (CE = 0.95–1.00) for lower molecular weights (20,000–25,000). At the same time, CEs decrease with increasing the molecular weights (e.g., for M_n = 115,000 only 62% tris-chelate formation is observed). Energetic preferences of polymer-polymer versus polymer-solvent interactions also play a role.

Hetero-arm star PMCs can also be produced by the chelation of the bpy (PS-PCL) macroligand with Fe(II) or Pt(II) [310]. In another example, a stepwise Ru chelation method was developed for synthesis of miktoarm star block-PMCs (Scheme 5.19) [311]. In this case six-arm metal chelate stars were obtained by first forming a Ru bis-chelate with bpy bearing two PCL chains as macroligands, followed by chelation with a bpy bearing either two PS chains or two PEG chains.
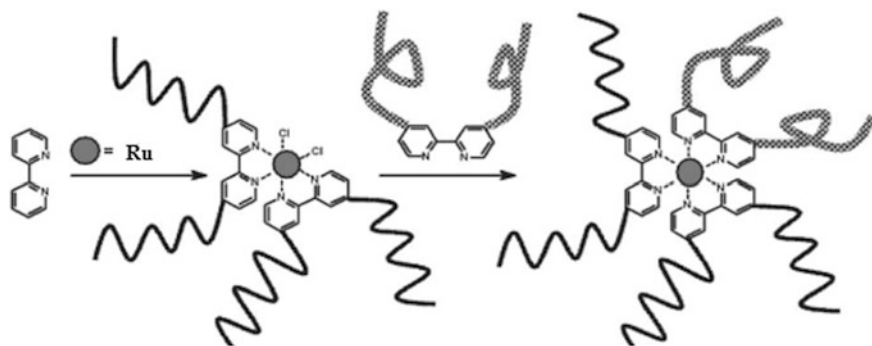
Scheme 5.19 Synthesis of hetero-arm metal chelate star polymers from bpy ligands
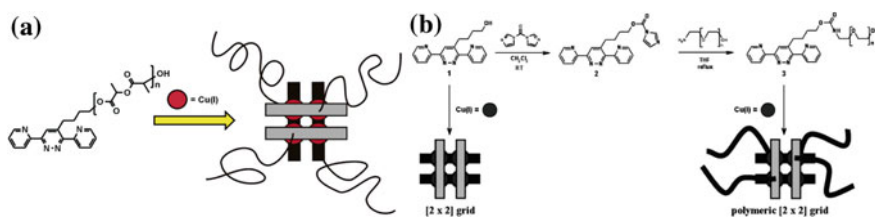
Fig. 5.46 a Schematic representation of the formation of polymeric grid-like complexes from the macroligands. **b** Schematic representation of the synthesis of PEG-DPP via activation of hydroxyl-DPP with CDI followed by coupling with α-hydroxy-ω-amino-PEG (top). The formation of grid-like [2 × 2] metal chelates upon addition of Cu(I) is also shown (bottom)

Four-arm stars were prepared by chelation to a Ru-bpy bis-chelate bearing one PS chain on each bpy, a bpy bearing either two poly (lactic acid) chains or two PEG chains.

Well-defined bpy-centered triblock and pentablock macroligands with low PDI were chelated with c FeCl$_2$ for preparation of star iron-PMCs [Fe{bpy (PEG-PCL)$_2$}$_3$]Cl$_2$, [Fe{bpy(PEG-PCL-L-poly(lactide))$_2$}$_3$]Cl$_2$, and [Fe{bpy(PEG-PCL-D,L-poly(lactide))$_2$}$_3$]Cl$_2$ with six diblock and three-block arms [312].

Among other chelating polymers, we note a poly (L-lactide) functionalized DPP which forms star polymeric [2 × 2] grids upon the addition of Cu(I) ions [313]. It is important that the chelation could be successfully performed in dichloromethane, thus, indicating that both the properties of the ligands (chelation) and the polymers (solubility) could be combined in one material since the Cu(I) grid of hydroxyl-DPP is insoluble in CH$_2$Cl$_2$. Besides, CPLs revealed strong cooperativity in the grid formation in the case of short polymer side-chains, the macroligands, whereas the larger CPLs formed polymeric [2 × 2] copper(I) grids without cooperativity [314].

This concept is expanded to metal chelate PCL-DPP (Fig. 5.46a) [315] and PEG-DPP star by end-functionalization of amine-containing PEG with DPP (Fig. 5.46b) [316].

Fig. 5.47 UV-vis spectra obtained during the titration of $Cu(CH_3CN)_4(PF_6)$ to solutions of PEG-DPP in dichloromethane. The insets show the increase of absorption with the addition of copper ions
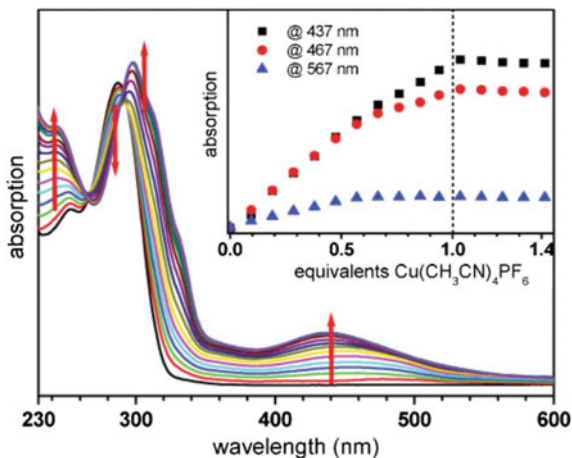
Addition of Cu(I) ions leads to the appearance of the characteristic MLCT band and the maximal absorption was reached at 1 equiv. of Cu(I) ions, which is associated with the formation of [2 × 2] Cu(I) grids (Fig. 5.47). Besides, the addition of 0.5 equiv. of Cu(I) ions resulted in a change in λ_{max} of the MLCT from 467 to 437 nm indicating that up to 0.5 equiv. of Cu(I), chelates containing two ligands and one Cu(I) ion are formed. Following addition of Cu(I) ions leads to the formation of the most stable structure, namely [2 × 2] grid-like chelates containing four ligands and four Cu(I) ions. Strong cooperativity is not observed in the grid formation due to sterical hindrance and/or entropic forces induced by the PEG-chains (Fig. 5.47, inset).

The self-diffusion dynamics of unentangled associating polymers based on four-arm PEG end-functionalized with tpy moieties chelated by Zn(II) in DMF (Fig. 5.48a) is measured by forced Rayleigh scattering at varying grating spacings ranging from 0.5 to 50 μm [317]. This model system is chosen for it's narrowly disperse molecular weight of the star polymer building blocks, its well-defined tpy-based sticker chemistry, and its robustly tunable strength of the metal-ligand bonds. Tracer diffusion of four-arm PEG polymers with just three associating arms is investigated through the same model transient network (Fig. 5.48b), providing insight into the diffusion mechanisms based on comparisons of self-diffusion and tracer diffusion.

Using 5-arm PEG polymer core with tpy end ligands on each arm (Fig. 5.49a), cross-linking network can be formed by introduction of different metal ions, including Mn(II), Fe(II), Co(II), Ni(II), Cu(II) and Zn(II) [318]. In particular, the increase of the π-π* band at 310 nm upon addition of Co(II) ions indicates the chelation (Fig. 5.49b). A similar behavior was found for the other investigated metal ions with π-π* bands in the region between 300 and 330 nm. However, no undesired effects such as precipitation were observed in the investigated concentration ranges.
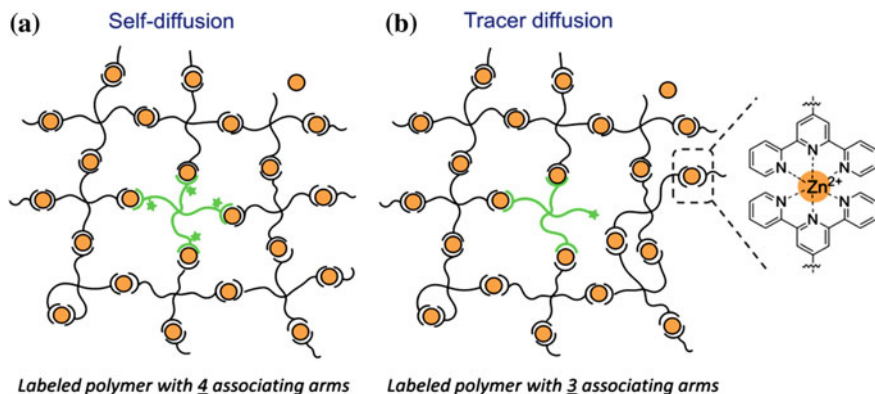
Fig. 5.48 Diffusion of fluorescently tagged four-arm PEG polymers with **a** four and **b** just three associating arms is probed in model transient networks formed by chelation between Zn(II) and tpy end-modified four-arm PEG polymers in (**a**) self-diffusion and (**b**) tracer diffusion configurations. Intramolecular primary loops and dangling chains are shown as two possible defects in the model transient networks. Green stars on the labeled polymers represent the locations of nitrobenzofurazan labels
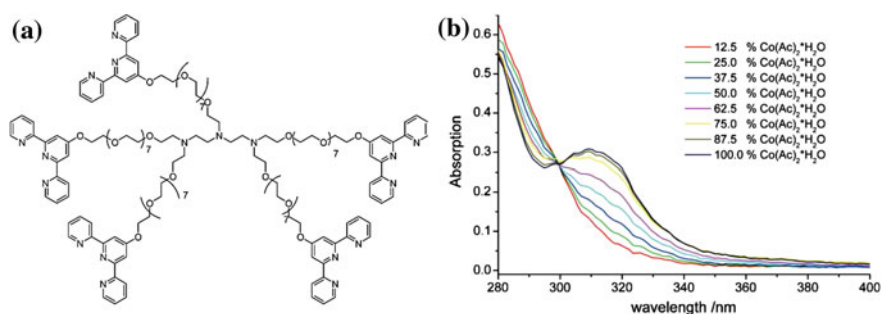
Fig. 5.49 **a** Structure of 5-arm PEG polymer core with tpy end ligands on each arm. **b** Chelation behavior of chelating macroligand with a variety of transition metal ions investigated in a parallel fashion in DMSO. The displayed spectra detail the case of Co(II) ions

The star PMC was obtained by coordination of *p*-(1,3-butanedionyl) phenyl-terminated PEO with Cr(III) ion [319]. It is important that the prepared star-shaped PMC exhibited film-forming properties, and the different star PMCs can be synthesized by coordination of this chelating macroligand with various transition metals.

Macroligands with β-diketone fragments were chelated to Eu, Fe, Cu and Ni metal ions to prepare star PMCs of various architectures (Fig. 5.50) [320]. «Arm-first» approach provides site-isolated PMCs with spectroscopic properties that correlate well with low molecular weight analogues. At the same time, the luminescence intensities of Eu-PMCs are substantially enhanced relative to Eu(dbm)₃
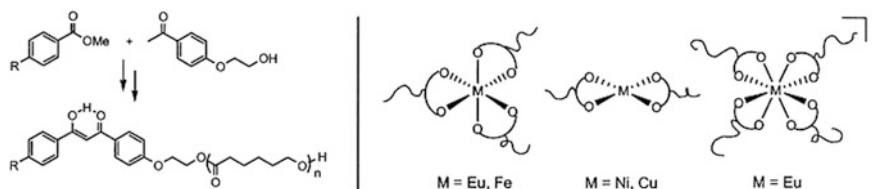
Fig. 5.50 Preparation of dbm initiators to generate dbm end-functionalized and dbm-centered PCL macroligands and structure of Eu, Fe, Cu and Ni metal chelate star polymers
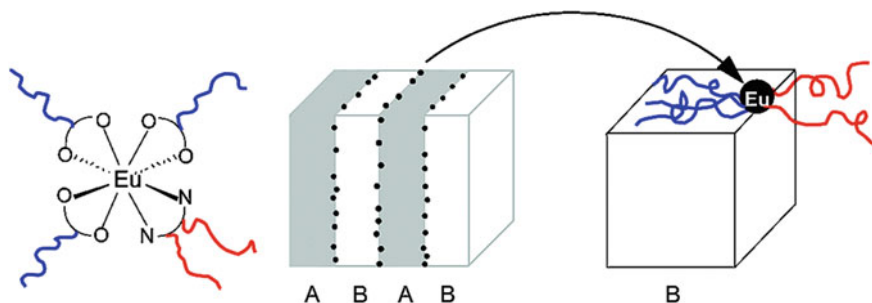
Fig. 5.51 A schematic representation of the lamellar morphology of a Eu[{dbm-poly(lactic acid)}3]{bpy-(PCL}2] block copolymer film (A = PCL, B = poly(lactic acid), filled circle = Eu center)

chelates. This is associated with the protective action of the polymer shell, determining luminescence quenching due to metal-metal interactions and access of water and other donor ligands to the metal site.

An Eu-chelate tri-armed star poly (lactic acid) was obtained by the «arm-first» approach using dbm-terminated poly (lactic acid) and EuCl$_3$ [321]. The three-armed star polymer was further turned into a five-armed one by addition of PCL containing the bpy fragment in the middle of the chain (Fig. 5.51). During transition from Eu (dbm)$_3$ solutions to Eu[dbm-poly(lactic acid)]$_3$ solutions to Eu[dbm-poly(lactic acid)]$_3$ films the increasing relative amounts of the longer lifetime component is observed due to the «polymer shell effect» and the decreasing aqua adducts known to shorten lifetimes. The sharpness of the feature at 579.7 nm, corresponding to the $^5D_0 \rightarrow {}^7F_0$ transition in the emission spectrum of PMC, lends further support for a homogeneous sample. This star PMC showed a lamellar morphology in thin films with the Eu(III) ions on the phase boundary. These microstructures containing Eu luminophores at the glassy poly (lactic acid)-crystalline PCL domain interfaces are modified by thermal treatment.

[Ln(dpa-PCL-PEG-OCH$_3$)$_3$](HNEt$_3$)$_3$, where Ln = Eu(III), Tb(III), were synthesized by the chelation of an amphiphilic block copolymer of PEG-*b*-PCL methyl ether functionalized with a dipicolinic acid (dpa) fragment with lanthanide ions (Scheme 5.20) [322]. Micelle-like nanoparticles of star PMCs were prepared by
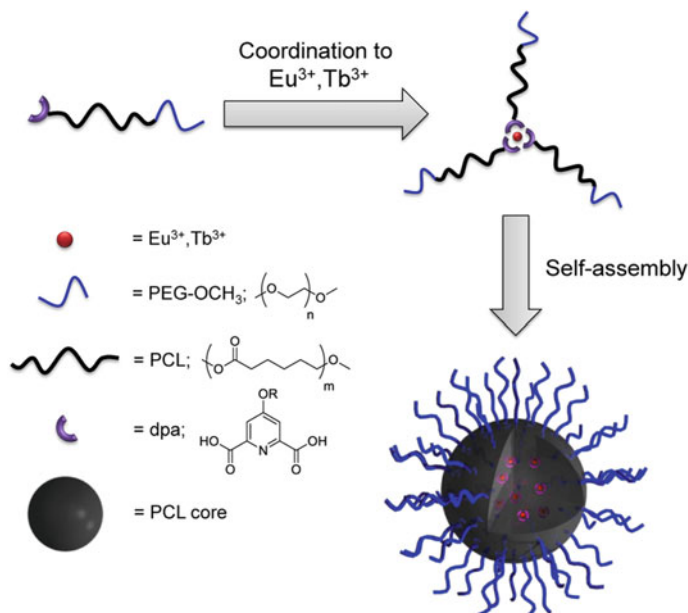
Scheme 5.20 Schematic representation for preparation of [Ln(dpa-PCL-PEG-OCH$_3$)$_3$](HNEt$_3$)$_3$ (Ln = Eu, Tb)

solvent displacement methods. The presence of solid sphere (<47 nm in diameter) and vesicle (>47 nm in diameter) morphologies was confirmed. The color of emission and morphology of the luminescent nanoparticles were tuned in a relatively straightforward approach by either changing the lanthanide ion or tuning the solution-assembly conditions, respectively.

The unique properties of star PMCs with a large number of functional arms make them suitable as fluorescent probes, contrast agents, and in vitro diagnostic systems [287, 323]. Star PMCs are highly desirable as MRI contrast agents owing to their well-defined architecture and potentially enhance MRI performance by reducing the rotational molecular tumbling rate (subsequently increasing the relaxivity). The results of the study of a series of MRI contrast agents based on star PMCs indicated the importance of the precise molecular location of Gd(III) in the optimization of MRI contrast at different magnetic field strengths [324, 325]. Thus, copolymers of oligoethylene glycol methyl ether acrylate and an activated ester monomer, pentafluorophenyl acrylate, were modified with the DO3A-tBu-NH$_2$ for the chelation of Gd(III) (Scheme 5.21) [324]. Star PMCs exhibited a substantially increased relaxivity in comparison to existing commercial Gd(III) MRI contrast agents.

Metal chelate based on DO3A-*t*Bu-NH$_2$ was also introduced into different parts (arms, cores, and end-groups) of the polymers using activated ester/amine nucleophilic substitutions, deprotected and chelated with Gd(III) [325]. In this case the precise placement of Gd(III) in the PMCs plays the determining role in optimizing
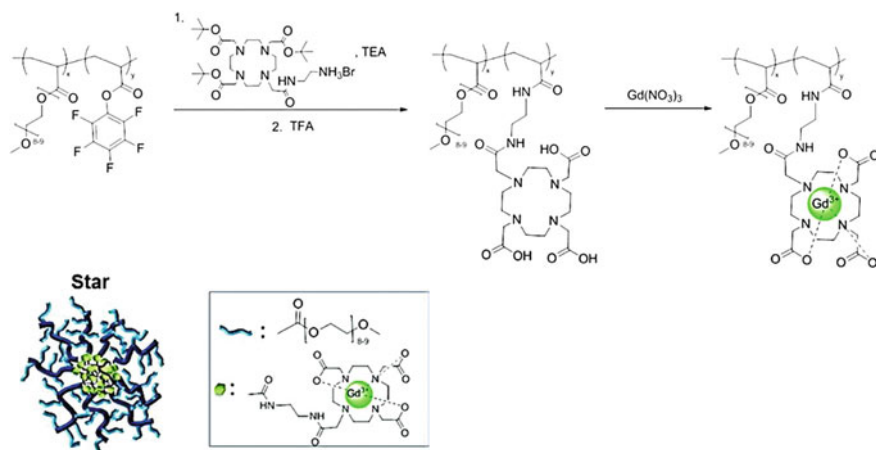
Scheme 5.21 General procedure for the preparation of metal chelate macromolecular star contrast agents

the performance of the PMCs as MRI contrast agents. The relaxivity varies from 11 to 22 $mM^{-1} s^{-1}$, 2–5 times higher than that of a commercial DOTA-Gd contrast agent when using a magnetic field strength of 0.47 T. Finally, the residence time of the coordinated water and the rotational correlation time of the final molecule were correlated with the polymeric structure.

Functionalization of 3D nanostructures having a PEG outer shell, a hydrophilic inner shell containing reactive functionalities, and a central hydrophobic core with a DOTA-ligand allows to chelating radioactive ^{64}Cu nuclei [323]. The biodistribution evaluation in normal rodents has shown a distinct correlation between the length of the PEG chains and the in vivo behavior of these nanostructures. Particularly, the cross-linked star PMCs with 2000 and 5000 PEG showed a much slower rate of blood clearance.

Of interest is the design of multifunctional drug delivery systems with bioimaging capabilities at the same time [326] as well as of multi-modality imaging [327] based on star polymers. Thus, acrylate star PMCs as fluorescence and MRI agents for multimodal imaging combining fluorescent and magnetic resonance features were developed (Fig. 5.52). Acrylate star polymers with hydrodynamic diameters of 10 ± 2 nm containing fluorene fragments as core units were functionalized with dopamine derivatives to chelate lanthanides such as Gd(III) and Eu (III) through the catechol moieties, which resulted in rapid water exchange of the highly hydrated star polymer. The in vitro and in vivo studies indicated that these multimodal imaging agents retained blue/red fluorescence and remarkable magnetic properties, with high relaxivity and high contrast features. The polymeric MRI agents based on a star architecture, where catechol chelates were fixed on the arms of stars, yielded contrast agents with a very high relaxivity (84 $mM^{-1} s^{-1}$) [328].
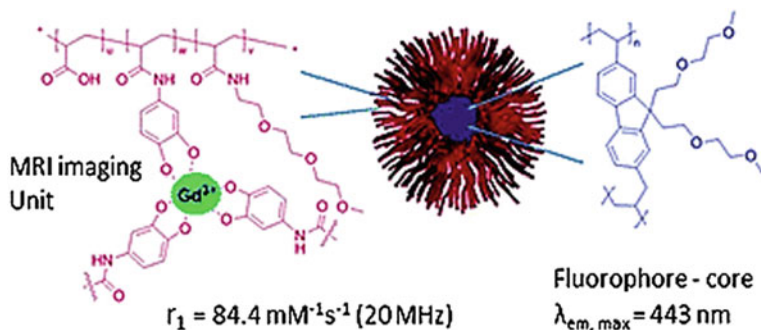
Fig. 5.52 Bimodal MRI star PMC imaging reagents
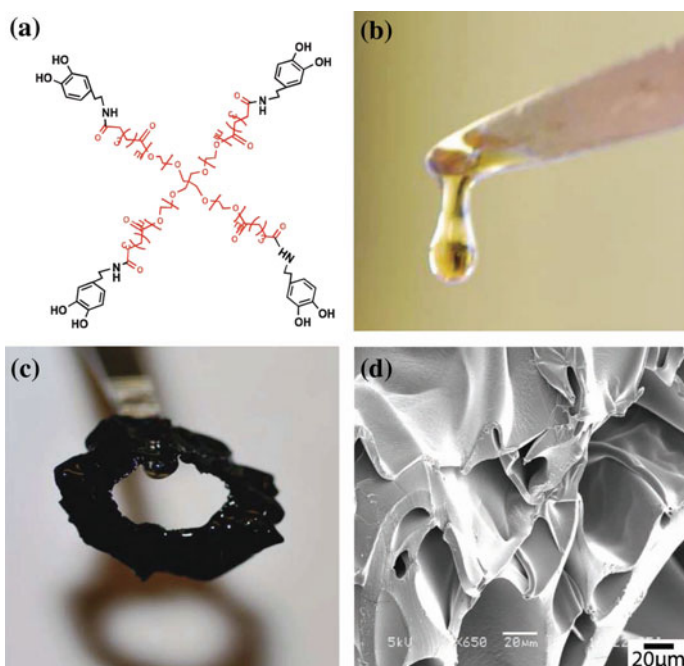
Fig. 5.53 a Chemical structure of PEG$_4$-dopamine (pentaerythritol-PEG$_4$ in red, dopamine in black). **b, c** Photograph of PEG$_4$-dopamine (20 mg) before (**b**) and after (**c**) the introduction of 2 M aqueous Fe(III) solution. **d** SEM image of the material in (**c**)

It should be noted a stiff injectable biodegradable elastomer based on a 4-arm PEG which was functionalized with dopamine terminal fragments (Fig. 5.53a). This chelating polymer was viscous and sticky (Fig. 5.53b). When PEG$_4$-dopamine was mixed with Fe(III) solution, a tough rubbery green-black polymer was formed within

a few seconds (Fig. 5.53c). The micrometer-scale morphology of this polymer (Fig. 5.53d) exhibited a rough surface with pores of different sizes and shapes [329].

5.4.2 «Core-First» Method

«Core-first» approach, which is faster, requires careful screening of initiator/ catalyst/solvent compositions to find reaction conditions, for which polymerization is controlled [330, 331]. For example, tris(dialkylaminostyryl-bpy) M(II) chelates (M = Fe, Ru, Zn) are used as multifunctional metalloinitiators for the ATRP of MMA with CuBr/*N*-propyl-2-pyridylmethanimine as a catalytic system (Scheme 5.22) [332]. The polymerization rate strongly depends on the nature of the metal-loinitiator : whereas a conversion of 94% was achieved after 4 h with Zn-initiator, only 50% conversion was reached when Ru-initiator was used. Kinetic curves of the polymerization exhibit a first-order behavior consistent with a living system. For the Fe and Ru chelates, an induction period of approximately 25 min is charac-teristic. The resulting star PMCs combine the optical properties of the monomers with good processability, which allow to preparing high optical quality thin films by the spin-coating method and thicknesses varying between 1 and 2 mm.

The bulk and solution (toluene) ATRP of MMA and methyl acrylate was per-formed using a Ru(II) tris(bpy) chelate bearing six α-bromoester initiating groups and $NiBr_2(PPh_3)_2$ and $NiBr_2(PBu_3)_2$ as catalysts resulting in well-defined polymers [333]. The molecular weight distributions of the PMMAs were narrow (toluene, PDI = 1.1–1.3; bulk, PDI < ~1.3 at <50% conversion). This method allows to preparing Ru chelate PMMA stars with molecular weights ranging from 2800 to ~350,000 (Table 5.2). It is interesting that the ε values were typically comparable to that of metalloinitiator (λ_{max} = 465 nm, ε = 16,607 M^{-1} cm^{-1}) and consistent with data for model structure containing a single Ru ion at the center.
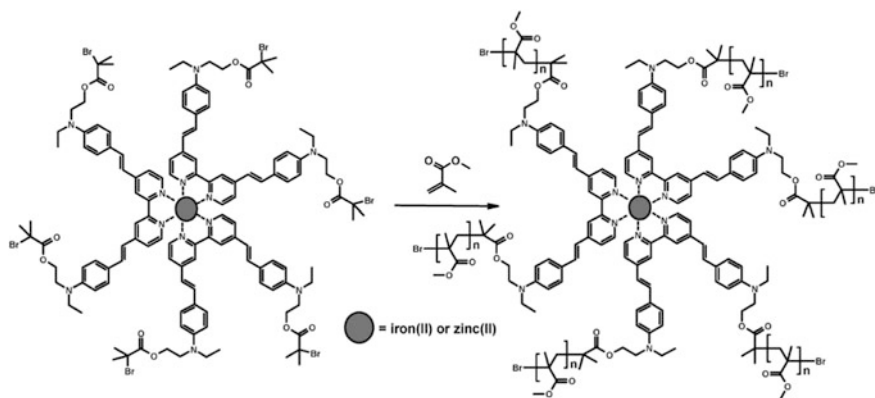
Scheme 5.22 Schematic representation of the synthesis of PMMA star PMCs

Table 5.2 Molecular weight and UV/vis data for a series of Ru chelate PMMA star polymers

$M_n^a \times 10^{-3}$	$M_w^a \times 10^{-3}$	PDI	$M_n(\text{lin})^b \times 10^{-3}$	$M_w(\text{lin})^b \times 10^{-3}$	PDI	$\varepsilon(465 \text{ nm})^c$ $(M^{-1} \text{ cm}^{-1})$
11.8	12.3	1.04	9.4	10.7	1.12	17,200
54.0	57.7	1.07	42.4	46.9	1.10	18,800
74.7	81.8	1.09	64.8	74.7	1.15	19,300
114.1	123.6	1.08	90.6	102.4	1.13	20,100
116.9	129.3	1.11	102.5	125.1	1.22	19,300

[a]Molecular weight determined by GPC in CHCl$_3$ at 25 °C using multi-angle laser light scattering/ refractive index detection
[b]Molecular weight determined by GPC in CHCl$_3$ at 25 °C using linear (lin) PMMA standards
[c]Molar extinction coefficient of the MLCT band determined using $M_n(\text{lin})$ to calculate sample concentration

The efficiency of initiation and controlled nature of these reactions are confirmed by low PDI of cleaved linear PMMA arms ($\sim$1.10–1.24) and $M_n^{\text{star}}/M_n^{\text{arm}} \approx 6$.

The poly(N-(ω'-alkylcarbazolyl) methacrylate) tris(bpy) bifunctional star Ru-PMCs were synthesized by ATRP of N-(ω'-alkylcarbazolyl) methacrylate in solution, where Ru chelates with one and three initiating sites acted as metal-loinitiators with NiBr$_2$(PPh$_3$)$_2$ as a catalyst [334]. Electronic absorption and emission spectra of the formed PMCs indicate the chromophore presence within a single polymeric chain.

A hexafunctional Ru complex initiator, [Ru{bpy(CH$_2$Cl)$_2$}$_3$](PF$_6$)$_2$ was employed as initiator in the ATRP of St to form star polymers containing chelating fragments and chromophores at discrete positions in the polymer structures [335, 336]. A polymer product with narrow molecular weight distribution ($M_n = 42,800$, PDI = 1.10) is obtained using DMF as a solvent, when the reaction is quenched at $\sim$20% monomer conversion. Di- and tetrafunctional metalloinitiators with alkyl chains, [Ru{bpy(C$_{13}$H$_{27}$)$_2$}$_n${bpy(CH$_2$Cl)$_2$}$_{3-n}$](PF$_6$)$_2$ (n = 1, 2), showed improved initiation and molecular weights closer to targeted values. The preparation of well-defined metal chelate PS star polymers demonstrates the compatibility of the ATRP process with the cationic ruthenium initiators.

A quenchometric oxygen sensor based on a low PDI star PMC [Ru(bpyPS$_2$)$_3$](PF$_6$)$_2$ is obtained [337]. The incorporation of the oxygen sensing Ru chelate in the PS support allows to reaching much higher doping levels without microcrystallization of the chelate than traditional two-component sensors. However, the luminescence decays were still multiexponentials, indicating that sensor heterogeneity was not completely eliminated despite the narrow PDI (1.10).

Three-arm star PMC was prepared by the «core-first» approach using ATRP method [338]. This PMC included charged Ir chelate as the luminescent core and 2-(carbazol-9-yl) ethylmethacrylate as the arm repeat fragment. The prepared PMC shows a relatively low PDI of 1.30 with high thermal stability. It demonstrated effective inter- and intra-molecular energy transfer from the arm Cz fragment to the
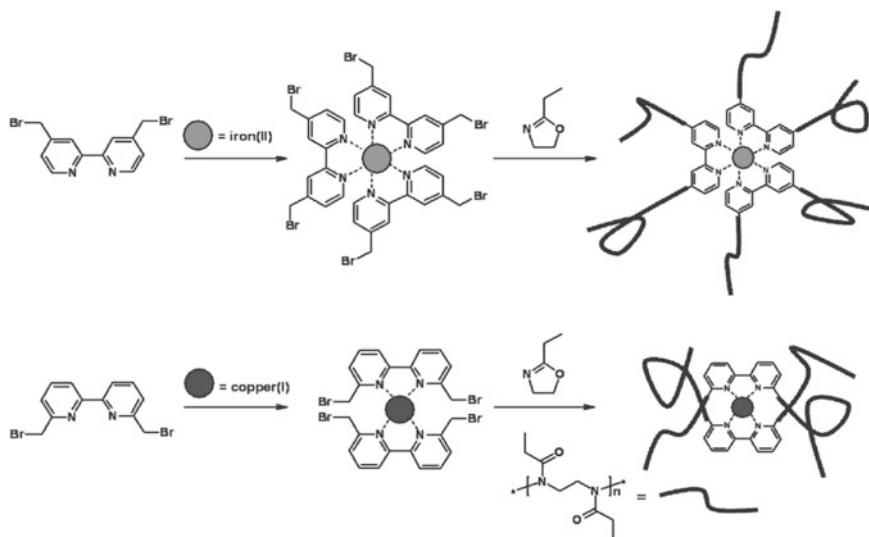
Scheme 5.23 Living ROP of 2-ethyl-2-oxazoline initiated with hexa-(halomethyl)tris(bpy) Fe(II) (top) and tetra-(halomethyl)bis(bpy) Cu(II) (bottom)

Ir chelate core in the host-guest system. It is important that good phosphorescent emission can be achieved at 565 nm by the design of the arm length.

A preformed Ru(II)bpy chelate was used as initiator for the direct polymerization of ε-caprolactone [339]. The resulting star PMCs showed both the electrochemical and optical properties of the Ru(II) chelate as well as the thermal properties of the polymers indicating the possibility of preparation of the materials with a novel combination of properties via the «core-first» method.

Metal chelate star polyoxazoline with six arms was prepared by living ROP of 2-ethyl-2-oxazoline initiated with di-, tetra- and hexa-(halomethyl)tris(bpy) Fe(II) and Ru(II) [340, 341] chelates as initiators resulting in well-defined star PMCs (Scheme 5.23, top). Dechelation of these star Fe(II)-PMCs was performed by reaction with potassium carbonate resulting in the free poly(2-ethyl-2-oxazoline) bpy macroligands. The decoloring of the polymer films was observed at 210 °C indicative of thermal dechelation, whereby the violet color of the Fe(II) chelate returned upon cooling. These metalloinitiators are also suitable for the polymerization of several other 2-oxazoline monomers including 2-methyl-, 2-phenyl- and 2-undecyl-2-oxazoline [342]. Samples were subjected to chemical cleavage in aqueous K_2CO_3 to generate metal-free bpy-centered polyoxazolines, which chelate to Fe(II), regenerating the $[Fe(bpy)_3]^{2+}$ chromophores. These experiments produce polymers with reasonably narrow molecular weight distributions (~ 1.1–1.5).

The cationic ROP of 2-ethyl-2-oxazoline with bis(bromomethyl)bpy Cu(I) initiators results in well-defined metal chelate four-arm star poly(2-ethyl-2-oxazoline) with central 6,6′-disubstituted bpy unit (Scheme 5.23, bottom) [343]. The living character of the polymerization was demonstrated with the linear relationship

between the M_w and the [monomer]/[initiator] ratio as well as in the synthesis of block copolymers. Thus, a metal chelate poly (2-ethyl-2-oxazoline-*b*-2-nonyl-2-oxazoline) star block copolymer was synthesized utilizing the same bis(bpy) Cu(I) initiator [344].

Amphiphilic six-arm star block-PMCs were prepared by the sequential addition of two different oxazoline monomers to the hexafunctional metalloinitiator, [Fe (4,4′-bis-(chloromethyl)-bpy)$_3$](PF$_6$)$_2$ [345]. The first block was made of the hydrophilic 2-ethyl-2-oxazoline, and the second, hydrophobic, block of either 2-phenyl-2-oxazoline or 2-undecyl-2-oxazoline. The star block-PMCs exhibit narrow molecular weight distributions (PDIs < 1.1) and molecular weights close to targeted values and T_g and T_m values that correlate well with those observed for the respective homopolymers. It was found that the hydrophilic poly (2-ethyl-2-oxazoline) block forms cylindrical microdomains in a matrix of hydrophobic block of poly (2-undecyl-2-oxazoline) [346].

A six-arm star PMC was prepared by a combination of ROP and ATRP [304]. At first, the polymerization of D,L-lactide by ROP using [Ru{bpy(CH$_2$OH)$_2$}$_3$] (PF$_6$)$_2$ as hexafunctional initiator was carried out. Then, the hydroxyl terminal groups were turned to bromoesters, and tert-butyl acrylate was polymerized by ATRP. Finally, conversion of poly(tert-butyl acrylate) to PAA via hydrolysis affords water-soluble polymers, [Ru(bpyPAA$_2$)$_3$]$^{2+}$ and [Ru{bpy(C$_{13}$H$_{27}$)$_2$}(bpy PAA$_2$)$_2$]$^{2+}$ and the amphiphilic star polymer [Ru{bpy(D,L-polylactide)-PAA)$_2$}$_3$)] (PF$_6$)$_2$.

Hexa(dithiobenzoate)-functionalized Ru(II) tris(bpy) chelate was used as chain transfer agents for the RAFT polymerization of St to obtain well-defined star light-harvesting block-PMCs containing an energy cascade of chromophores from the periphery to the core [347, 348]. RAFT polymerization of St functionalized coumarin monomers permits to introduce the first block with an average length of two St-coumarin units into each arm [348]. Then, the prepared polymer was used as a macro-RAFT agent for the polymerization of acenaphthylene to synthesizing the star diblock-PMC with a narrow PDI and an average length of 36 acenaphthenyl repeat fragments in each arm. A third block was introduced for synthesis a star triblock-PMC with an average length of 44 NIPAM repeat fragments in each arm (Fig. 5.54). It was demonstrated that the energy transfer proceeds mainly through a stepwise energy cascade from the initially excited acenaphthyl fragments to the coumarin chromophores and hence to the Ru(II) chelate core.

It should be noted numerous examples of the use of tpy metal chelates as metalloinitiators for star PMC preparation [349]. Thus, Fe(II) and Co(II) chelates of mono- and bis(bromomethyl)tpy were applied as initiators for the cationic ROP of 2-ethyl-2-oxazoline resulting in defined hydrophilic polymers with a central chelate unit and star-like architectures [350–352]. The living character of the polymerization allows an exact control of the molecular weight as well as the incorporation of additional (chelating) units at the polymer chain ends. Dechelation of both the Fe (II) and Co(II) star PMCs was carried out by refluxing the PMC with potassium carbonate in acetonitrile leading to the tpy-containing poly (2-ethyl-2-oxazoline). Rechelation of the CPLs with Fe(II) ions was effective up to 94%. Besides, an
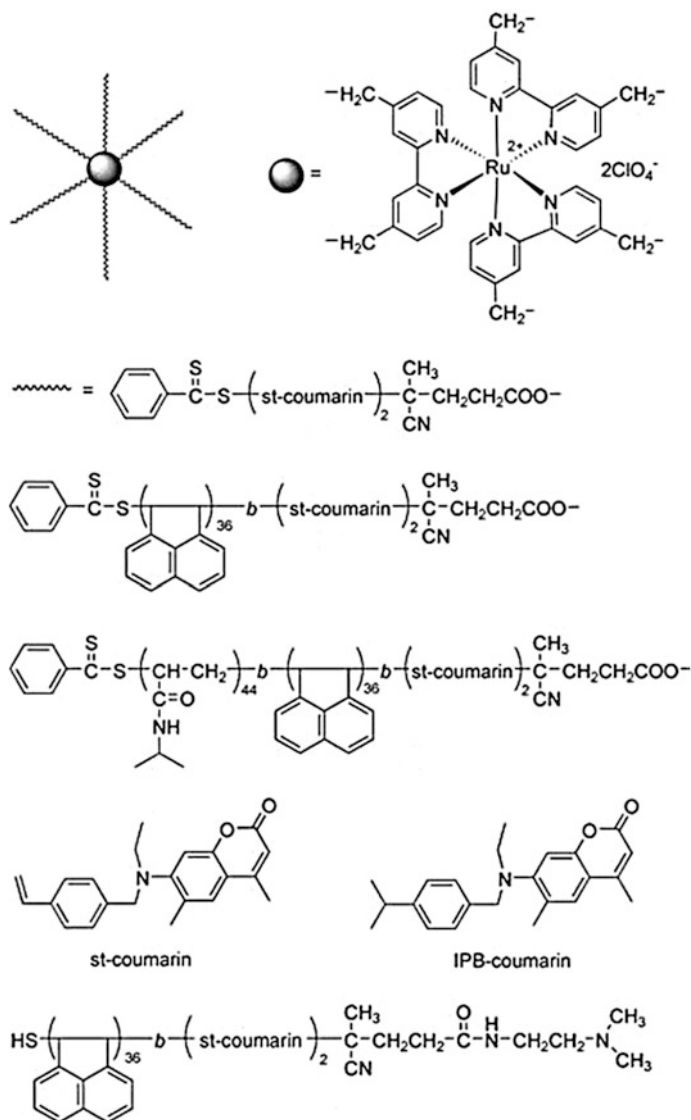
Fig. 5.54 Star light-harvesting PMCs

increase in viscosity was observed upon rechelation due to the coupling of the polymer chains by the metal chelation.

Of interest are amphiphilic PMCs containing a tri-arm or tetra-arm, conjugated, rigid core and flexible PEG coil blocks [353]. The synthesis of the PMCs includes the formation of heteroleptic bis-tpy Ru(II) chelates between the tpy-containing rigid cores and mono-tpy containing PEG chains. It should be noted the synthesis of
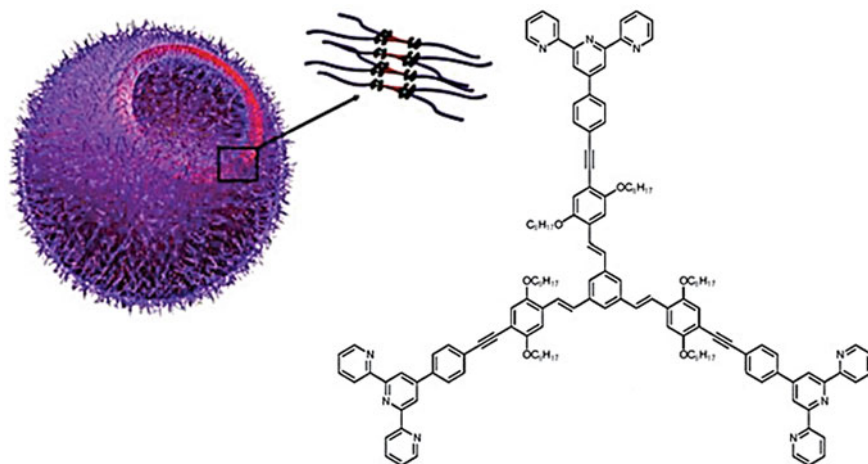
Fig. 5.55 Schematic representation of a vesicle formed from a tri-arm metal chelate star copolymer in acetone

the tri- and tetra-arm star block-PMCs by first preparing the PEG-Ru(II) mono-chelate with its following interaction with the tpy-containing rigid core. The self-organization in selective solvents leads to well-defined vesicles with thin walls for the tri-arm derivative in acetone and acetone/water mixtures in which the vesicular wall is formed by the rigid cores and both its inner and outer surfaces are decorated with the PEG blocks (Fig. 5.55).

The chelate $Fe(dbmOH)_3$ was used as an initiator in lactide polymerization [354]. Short reaction times (10 min) were noted with this trifunctional metalloinitiator and $Sn(Oct)_2$, and high molecular weights were achievable. Besides, reactions with $Sn(Oct)_2$ were controlled to high monomer conversion. Fe(III) tris(dbm) chelates play multiple roles in the synthesis and properties of poly (lactic acid) star PMCs. In particular, iron chelate acts as a dbm protecting group, a ROP initiator, catalyst and activating group, and as responsive fragments (i.e., chromophores, reactive centers) in the formed PMCs.

The same $Fe(dbmOH)_3$ chelate initiated ROP of D,L-lactide in the absence of additional catalysts (Fig. 5.56a) [355]. As a result, the $Fe(dbmOH)_3$-mediated ROP of D,L-lactide was fast and highly efficient, and it afforded well-defined tri-arm star PMCs in excellent purity and yield (Fig. 5.56b, c). It should be noted high quality control of molecular weight (PDI < 1.1) at ∼60–70% conversion. Besides, demetalation by diluted HCl leads to dbm-functionalized polylactide CPLs for other metals chelation.

Star oxime palladacycle complexes were prepared from star-shaped oxime-based ligands and lithium tetrachloropalladate in methanol (Fig. 5.57a) [356]. Indeed, a brown solid quickly precipitated due to the formation of cross-linkages among star-shaped fragments. SEM images exhibited that the solids include micrometer particles with the individual scales about 0.5–5 mm (Fig. 5.57b). It was calculated
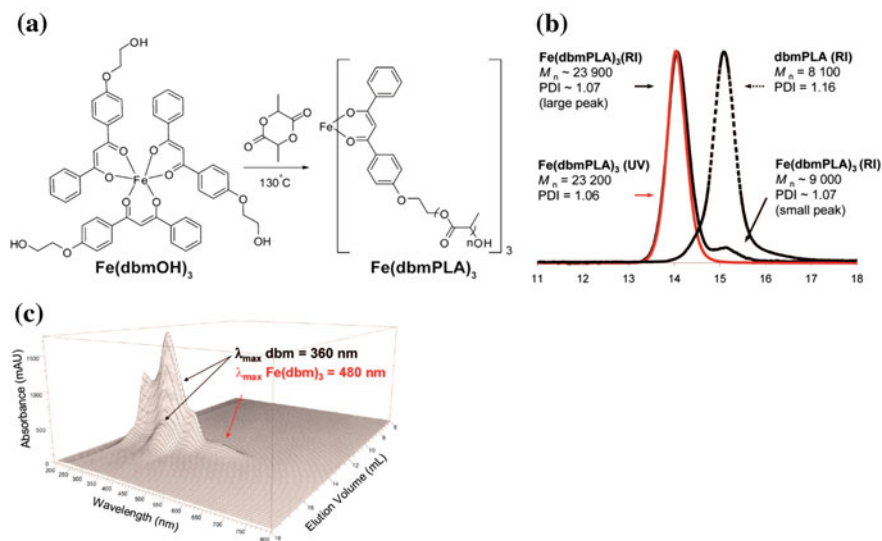
Fig. 5.56 a Schematic illustration for the synthesis of Fe(dbm-(poly (lactide acid)))₃ three-arm star polymer. **b** GPC overlay of star PMC and the corresponding dbm-(poly (lactide acid) macroligand obtained after demetalation by acid treatment. **c** 3D GPC plot of metal chelate star polymer from a UV-vis diode-array detector [PLA is poly (lactide acid)]
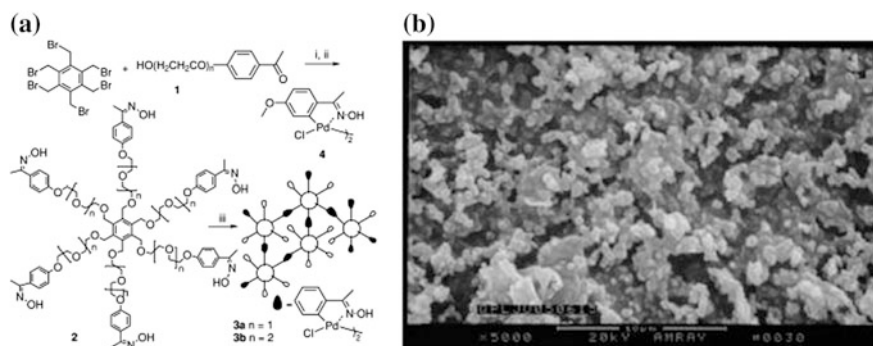
Fig. 5.57 Synthesis (**a**) and SEM image (**b**) of self-supported star-shaped oxime-palladacycles

that the Pd-loading was 1.98–2.03 mmol Pd $\times$ g^{-1} and about 48.2–55.2% oxime ligands were coordinated with Pd through chloro-bridges (molar ratio of Pd/N).

Various functional four-arm star PMCs were synthesized via ROPs of rac-β-butyrolactone, ε-caprolactone, rac-lactide acid, and allyl- or propargyl-functionalized trimethylene carbonates using tetrahydroxyl-functionalized tetraphenylethene/salan lutetium chelate as the initiator/catalyst (Fig. 5.58a) [357]. The prepared star AIE functional PMCs can be cast into thin solid films or devices by spin coating under
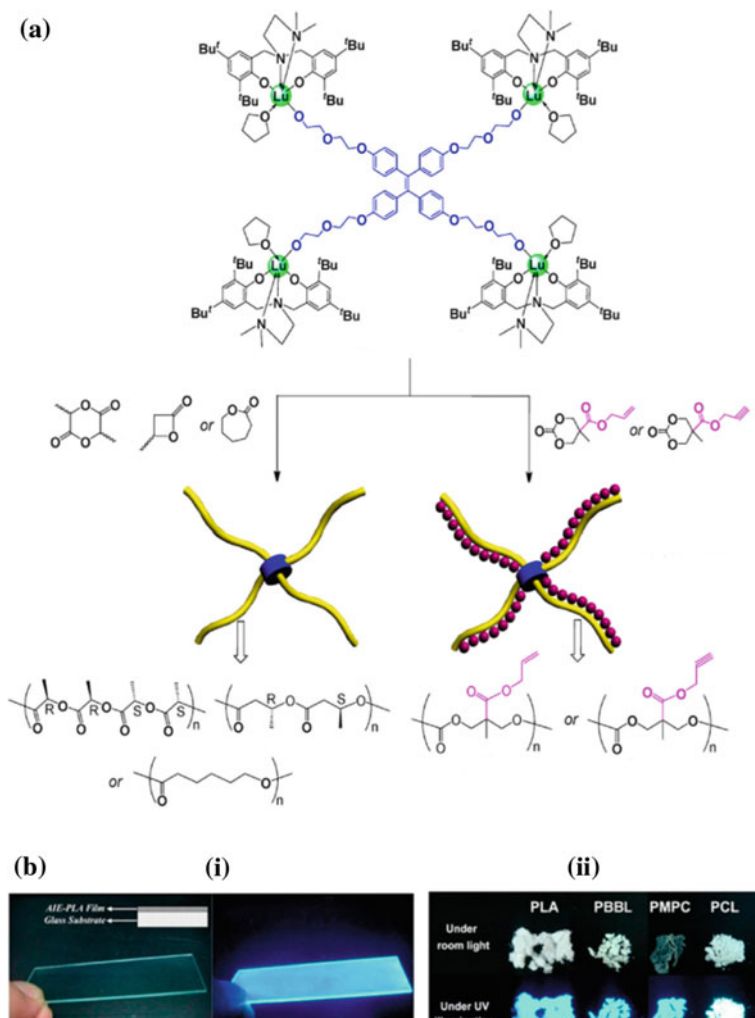
Fig. 5.58 **a** Schematic illustration for the synthesis of four-armed star AIE-active biocompatible polymers using salan lutetium alkoxide chelates. **b** Photographs of (i) AIE-active poly (lactide acid)-coated glass substrate taken under room light and UV illumination, and (ii) star luminogenic biocompatible polymers under room light and UV illumination

simple conditions (Fig. 5.58b). It is important that click functionalities (i.e., C=C and C≡C bonds) can be conveniently installed into the arm segments of the stars via (co) polymerization of functional monomers with pendent allyl or propargyl moieties.

It should be noted other cores used for «core-first» star PMC synthesis, for example different M-Pp (e.g., Zn [358, 359], Sn [360, 361], and Pd [362]). Many of these M-Pp star polymers are of interest because of the photocatalytic abilities of the core, with benefits derived from the polymeric arms including increased

solubility characteristics and improved recoverability, as well as potential modulation of the photoactivity or fluorescence intensity when the use of stimuli-responsive polymers is employed. The incorporation of copper during the polymerization of monomer hinders subsequent chelation of other metals. It is important that only a limited number of metals inside the Pp core can be used due to the interaction of these metals with the copper catalyst. In addition, removing the copper from the Pp core is difficult and often leads to the decomposition of the polymer.

Thus, the synthesis of star poly (2-ethyl-2-oxazoline) containing a Pp core starting from alkyne-functionalized Pp and azide-functionalized poly (2-ethyl-2-oxazoline) via CuAAC was developed [363]. The Pp core was further chelate Cu or Fe within the central cavity. For Cu chelate, the introduction of the metal ion proceeds through a one-pot reaction during the CuAAC reaction for fixing the azide-containing poly (2-ethyl-2-oxazoline) arms.

Of interest is using ATRP catalyzed by transition metals for the synthesis of well-defined Pp polymers. However, only some metal-containing (Zn(II) [364], Pd (II) [365]) Pp initiators were used for the preparation of star PMCs by ATRP. Unfortunately, attempts to synthesize polymers with free-base Pp using ATRP was unsuccessful due to a complexation of Cu(II) (formed by the Cu(I) catalyst) by the Pp core during the polymerization [364]. As a typical example, we note four-arm M-Pp star polymer of St and alkyl (meth)acrylates prepared from tetrabromo Pp-based initiators via ATRP because the coordination of zinc ion and Pp initiator allows avoiding copper ion as catalyst into Pp in star polymers [364]. Zn(II) 10,15,20-tetrakis(4-(2-methyl-2-bromopropoxy) phenyl)-21H,23H-porphine was used as an initiator in the ATRP of MMA, leading to the Zn-Pp-core star-PMMA. It should be noted using Pd(II) 10,15,20-tetrakis(4-(2-methyl-2-bromopropoxy) phenyl)-21H,23H-porphine as an initiator in the ATRP of MMA, however, the polymerization was completely inhibited. Star polymers containing M-Pp-core were prepared by *trans*-metalation of the Zn-Pp or by metal incorporation into the free-base Pp, for example, by heating the Pp-core star polymers in $PdCl_2$ or $PtCl_2$ solution.

The polymerization of St-type monomer 9-(4-vinylbenzyl)-9H-carbazole and methacrylate-type monomer 2-(9H-carbazole-9-yl)-ethyl methacrylate leads to M-Pp star polymers respectively via ATRP with participation of zinc 5,10,15,20-tetrakis(4-(2-methyl-2-bromopropoxy) phenyl)-Pp as an initiator [358]. PDI of M-Pp star polymers are relatively narrow (PDI = 1.09–1.32), that suggest a «living» polymerization process (Table 5.3). It is important that the content of Zn-Pp in the star PMCs depends on the arm length and the flexible arms effectively impede π-π stacking, thus preventing aggregation and fluorescent self-quenching in the solid state. In contrast to the initial monomers showing blue light emission, red light emission is observed in the emission spectra of M-Pp star polymers in the solid state, indicating the effective energy transfer from the Cz to the Zn-Pp core. At the same time, emission spectra of M-Pp star polymers in DMF solution exhibit weak red light emission and strong UV light emission at 350–400 nm that is associated with inefficient energy transfer from the Cz to the Zn-Pp core.

Table 5.3 Monomer, reaction time, molecular weight parameters and monomer conversion of the star PMCs made by ATRP

Monomer	Time (h)	Conversion (%)	M_n, GPC	M_w/M_n
St-type	1	3.4	7600	1.12
St-type	2	5.1	9200	1.09
St-type	3	7.3	15,800	1.18
St-type	4	8.7	17,900	1.23
St-type	5	11.7	24,700	1.25
St-type	6	14.1	30,100	1.20
St-type	7	15.3	32,900	1.24
Methacrylate-type	2	5.4	9300	1.32
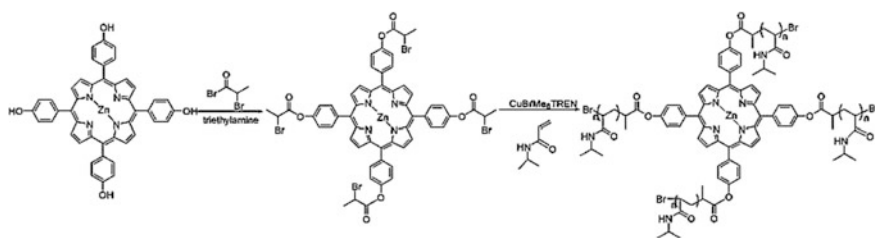
Scheme 5.24 Synthesis route of metal chelate star polymer with Zn-Pp core

A well-defined star poly (NIPAM) with Zn-Pp as the core was synthesized by ATRP with Zn(II)-*meso*-tetra(*p*-bromopropionylphenyl)-Pp as the initiator, and CuBr/tris(2-(dimethylamino) ethyl) amine as the catalytic system for 12 h at 60 °C (Scheme 5.24) [359]. The PDI was narrow and the polymerization was well controlled. The result exhibited lower value of lower critical solution temperatures for the aqueous solutions of M-Pp star polymers as compared to that of poly (NIPAM) homopolymer, which arose from the incorporation of the hydrophobic Pp core.

It should be noted free-base Pp cored star polymers and amphiphilic star block copolymers with controlled molecular weights and narrow PDI prepared by RAFT polymerization of the monomers containing *N,N*-dimethylacrylamide and St [366]. The formed polymers aggregated into star-like or flower-like micelles and their optical response to Zn(II) ions was a function of micellar structures. In particular, the formation of a Zn-Pp complex leads to the substantial UV-vis spectral changes within 17 h for Pp-[poly (*N,N*-dimethylacrylamide)$_{96}$-PS$_{33}$]$_4$ flower-like micelles (Fig. 5.59a). At the same time, for Pp-[PS$_{34}$-poly (*N,N*-dimethylacrylamide)$_{239}$]$_4$ star micelles the unchanged UV-vis absorption is characteristic after three days, which indicates an absence of Zn(II) coordination with Pp trapped in the micelle core (Fig. 5.59b).

Using of Sn(Oct)$_2$ as a catalyst in the synthesis of the free-base Pp star polymers leads to Sn incorporation into Pp core [360, 361]. Thus, Sn-containing star amphiphilic
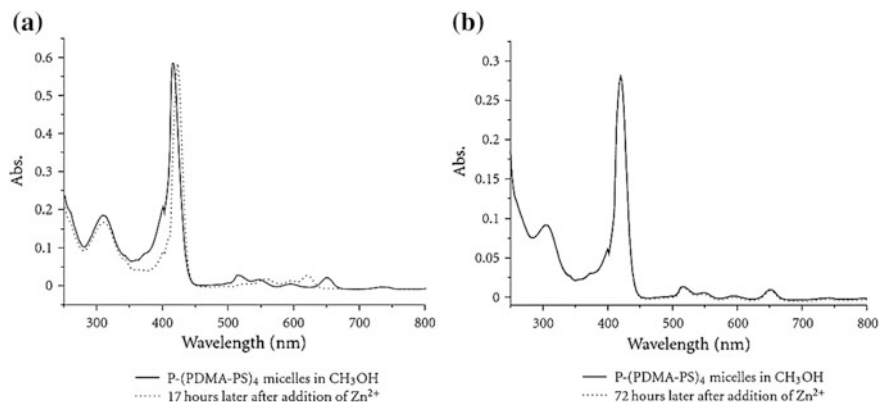
Fig. 5.59 UV-vis spectra of the micelles in methanol in the absence and in the presence of Zn (II) (5×10^{-4} M). **a** Pp-[poly (N,N-dimethylacrylamide)$_{96}$-PS$_{33}$]$_4$ micelles. **b** Pp-[PS$_{34}$-poly (N,N-dimethylacrylamide)$_{239}$]$_4$ micelles

PCL-*b*-poly [oligo (ethylene glycol) methyl ether methacrylate] with Pp core was synthesized by combination of ROP and ATRP (Scheme 5.25). The M-Pp star polymer can easily self-assemble into micelles in aqueous solution and the micelles can reversibly swell and shrink in response to external temperature. It should be noted that π-stacking and hydrophobic interactions in aqueous media leads to the aggregation of M-Pp and the resulting reduce in effectiveness of photodynamic effect.

The star CPL with Sn-Pp core was used for the preparation of the star CPL containing adamantyl terminal fragments with Sn-Pp core using DCC reaction with adamantaneacetic acid (Fig. 5.60a) [361]. The successful preparation of targeted star CPL confirms by disappearance of the signal at 3,65 ppm assigned to the methylene protons next to the terminal hydroxyl groups and appearance of the new peaks at 2.05 ppm (l), 1.96 ppm (j), and 1.65 ppm (peaks k, m were overlapped by peak g) assigned to adamantyl group in ^{1}H NMR spectrum (Fig. 5.60b).

Star diblock-PMCs were prepared via ATRP from a Pd-Pp macroinitiator (Scheme 5.26) [365]. It is interesting that the formed PMCs include the central Pd-Pp surrounded by a hydrophobic block of poly (butyl acrylate) and terminal hydrophilic block of poly (oligoethyleneglycol monomethylether monomethacrylate).

Of interest are star block copolymers with a hydrophilic pH sensitive shell and photosensitive hydrophobic core structure prepared by Cu-based ATRP [362]. At first, a multi-functionalized initiator containing Pd-Pp was used for the preparation of photosensitive *n*-butyl acrylate star PMC, which then was polymerized with N,N'-dimethylamino ethyl methacrylate or *tert*-butyl acrylate to synthesize the star block PMCs (Fig. 5.61). It is important that the prepared PMCs are characterized by well-defined molecular weights with narrow polydispersities (PDI < 1.23).
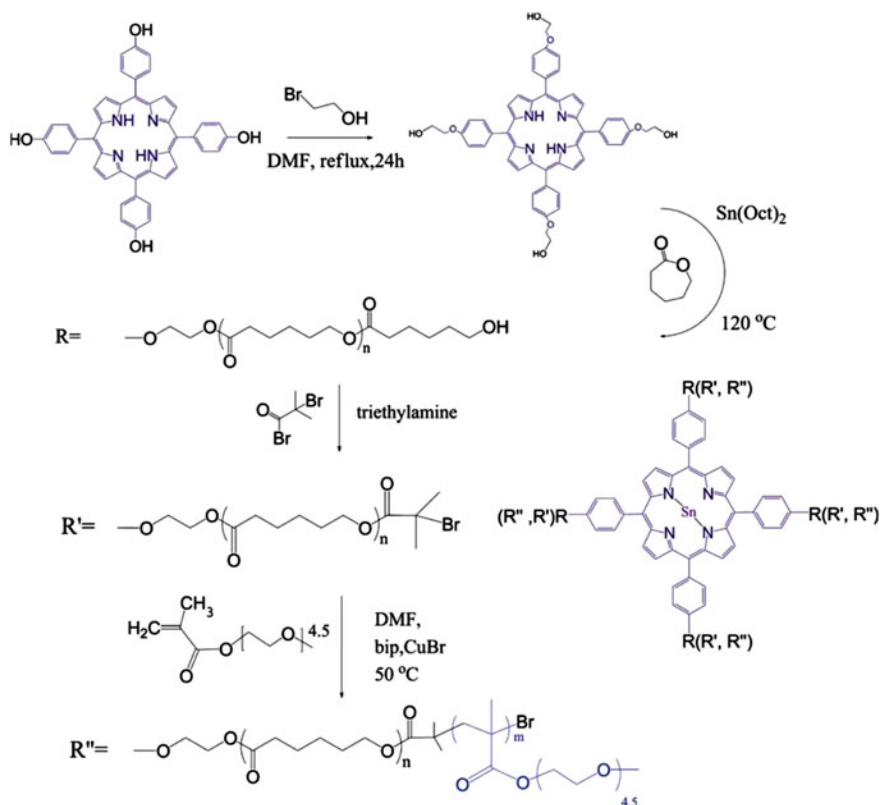
Scheme 5.25 Synthesis of Sn-containing star amphiphilic copolymers by the combination of ROP and ATRP

The hydroxyl-terminated star-shaped PCL with eight arms and different arm length ([M]/[I] = 30, 60, 90) with an initiator core of 2,3,9,10,16,17,23,24-octakis (3-hydroxypropylmercapto)-Pc-Zn(II) was prepared by the bulk ROP of ε-caprolactone (Fig. 5.62, top) [367]. The intrinsic viscosity and M_w of star PMCs (0.09–0.112 and 4542–6064, respectively) depend on concentration of polymer compounds and the [M]/[I] ratio. The addition of AgNO$_3$ causes the aggregation of the polymers and a slight shift in the electronic spectra is observed with the addition of Hg(NO$_3$)$_2$. At the same time, the addition of methanol and Pb(NO$_3$)$_2$ did not lead to any shift or optical change in the electronic spectra.

The «core-first» approach was used to the preparation of the M-Pc star polymer, with Zn-Pc as the core and poly (NIPAM) as the arms, via ATRP using Zn(II) tetra-(2-chloropropionylamido)-Pc as the initiator (Fig. 5.62, bottom) [368]. The thermo-responsive PMC has low PDI and photocatalytic activity. The introduction of the Pc core leads to increasing the lower critical solution temperatures for the M-Pc star polymer aqueous solutions.
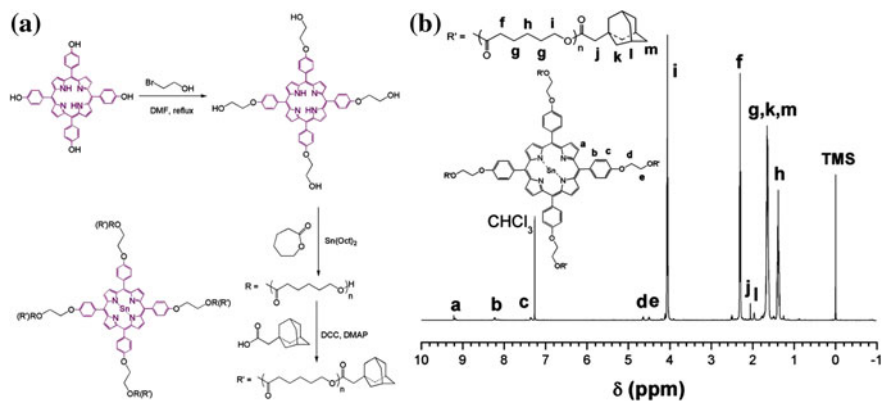
Fig. 5.60 a Synthesis and **b** ^{1}H NMR spectrum of adamantyl groups-terminated star PCL with Sn-Pp core
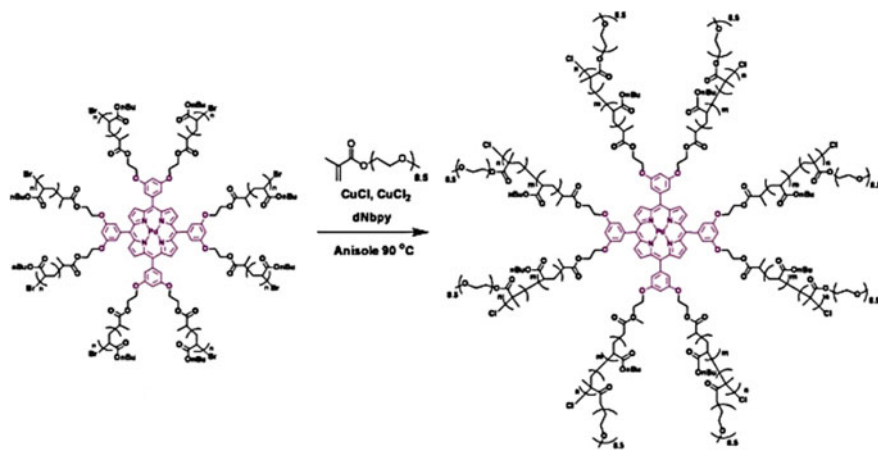
Scheme 5.26 Schematic representation of the synthesis of a diblock star polymer containing a Pd-Pp core, a hydrophobic interior block and a hydrophilic exterior block

5.4.3 Click-to-Chelate Approach

A new method called click-to-chelate approach to introduce chelating moieties on polymers using a 1,2,3-triazole ring as a coordinating functionality, which is easily prepared by CuAAC, was developed [369–371]. This method is a promising approach to incorporate bpy-like chelating fragment to macromolecules due to the excellent feasibility of azide substitution and click chemistry. Thus, a series of AB$_2$-, ABC-, (AB)$_2$-, A$_2$B$_2$- and ABCD-type miktoarm Ru(II)-PMCs was prepared by a click-to-chelate approach, which involved at first the chelation of Ru(II)(DMSO)$_4$Cl$_2$ by a
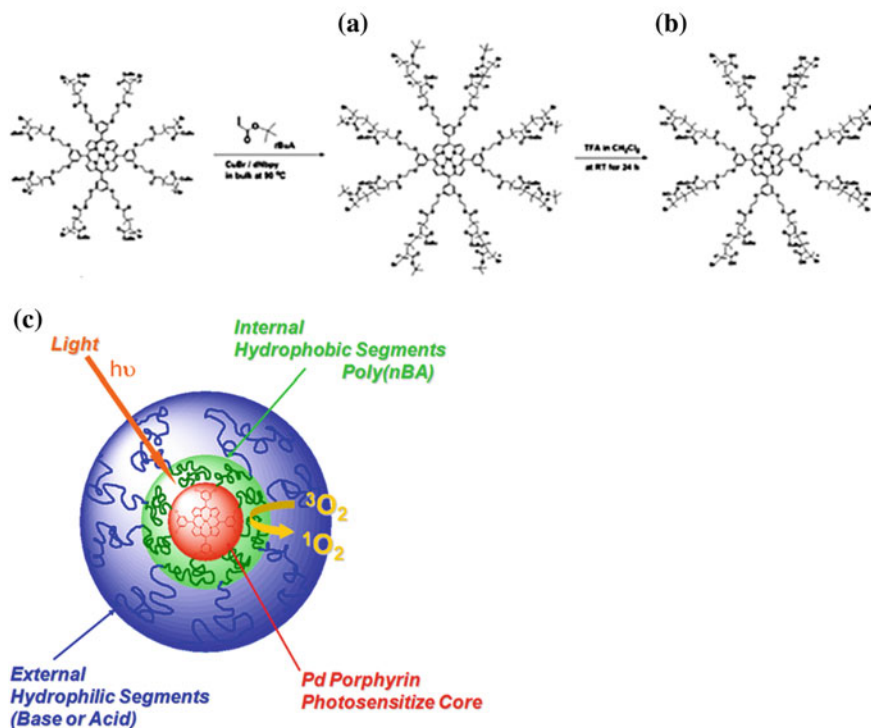
Fig. 5.61 Synthesis of poly (*n*-butyl acrylate)-*b*-poly (*N*,*N*′-dimethylamino ethyl methacrylate) (**a**) or of poly (*n*-butyl acrylate))-*b*-PAA (**b**) star PMCs from poly (*n*-butyl acrylate) star polymer macroinitiator by Cu-catalyzed living radical polymerization in bulk at 90 °C under argon. Structure of amphiphilic star block copolymer photosensitizers for photooxidation reactions (**c**)

polymer-substituted 2-(1H-1,2,3-triazol-4-yl)pyridine or 2,6-bis(1H-1,2,3-triazol-4-yl)pyridine to obtain a stable polymer Ru(II) *mono*-complex, and the chelation of the formed PMC with another polymer-substituted similar chelating ligands to afford the miktoarm Ru(II)-PMCs [372].

Of interest is using the click-to-chelate approach to incorporate chelating fragment in PS and chelation of Ru(II) ions to prepare 3-arm and 4-arm star-branched PS Ru(II) chelates [373]. The CuAAC of PS-N$_3$ with 2-ethynylpyridine or 2,6-diethynylpyridine leads to 2-(1H-1,2,3-triazol-4-yl) pyridine or 2,6-bis(1H-1,2,3-triazol-4-yl) pyridine ligands containing one or two PS chains at the first-position of the triazole rings. Star Ru(II)-PMCs as yellow solids were prepared by conventional procedure by heating of chelating macroligands with RuCl$_3$ with following addition of NaPF$_6$. The M$_n$ of these chelates were equal to 6740 and 10,400, respectively, which correspond to 3-arm and 4-arm star-branched PS Ru(II) chelates.

It should be noted the preparation of 3-, 4-, 5-, 6-, 7-, 8-, 9-, 10-, 11-, and 12-armed star poly (styrene oxide)) (PSO) Ru(II) chelates by a click-to-chelate method including the combination of the click reaction and stepwise chelation of
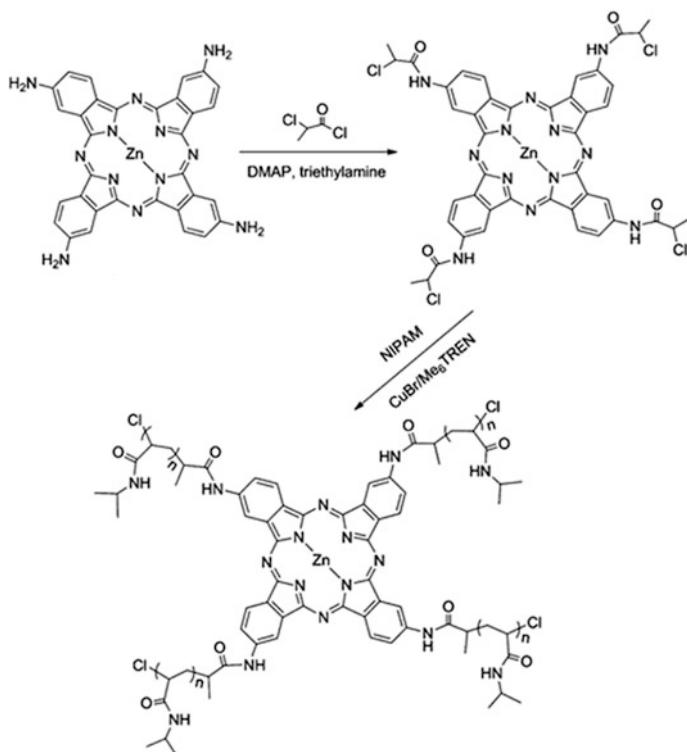
Fig. 5.62 Synthesis of star shaped PCL compounds with a Zn-Pc core (top) and synthetic route for the Zn-Pc star polymer (bottom)
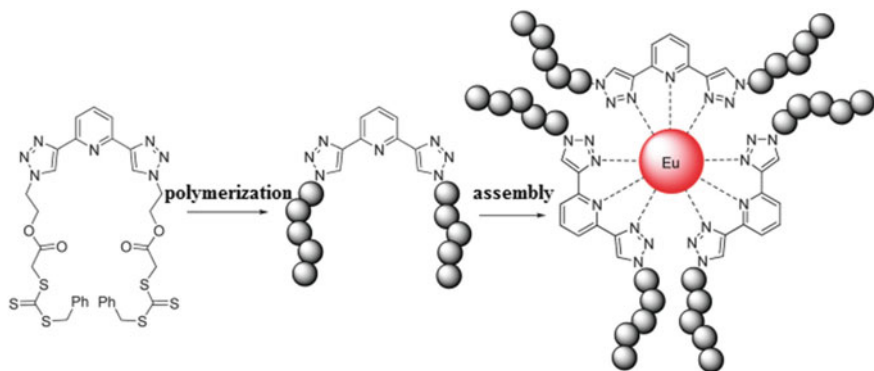
Fig. 5.63 Illustration of the polymerization-assembly strategy leading to formation of 6-arm star-branched PMC templated by Eu(III)

Ru(II)(DMSO)$_4$Cl$_2$ by 2-(1-PSO$_n$-1,2,3-triazol-4-yl) pyridine or 2-(1-PSO$_m$-1,2, 3-triazol-4-yl)-6-(1-PSO$_n$-1,2,3-triazol-4-yl) pyridine (m, n = 1, 2, or 3) [374].

A click-to-chelate approach, including the click reaction of poly (NIPAM) with 2,6-diethynylpyridine to prepare the btp CPL and the following chelation of RuCl$_3$, was used to the preparation of the four-arm star poly (NIPAM) Ru chelate [375]. The study of the thermoresponsive properties of the PMCs demonstrated the effects of the polymer terminal and core linkage and constituents of the four-arm star poly (NIPAM) Ru chelate on the T$_c$.

A combination of metal chelation, RAFT and click chemistry was used to obtain of star polymers with the terdentate btp core [376]. RAFT polymerization (e.g. with St or MMA) with following chelation of Ru(II) or Eu(III) ions led to 4- or 6-arm star PMCs (Fig. 5.63). Interestingly, metal chelation is accompanied by significant increasing a hydrodynamic diameter of ca. 2 nm of initial CPL (indicating single polymer chains) to 180 nm (for the Ru analogue) and 240 nm (for the Eu analogue).

5.5   Metal Chelates with Hyperbranched Polymers

At present, great attention is given to the PMCs based on hyperbranched polymers [39, 377–381]. Undoubted advantages of these CPLs as compared on the dendrimer ligands are low cost, better accessibility of chelating fragments, similar properties, and the possibility of large-scale synthesis [382]. Of no small importance is the fact that some hyperbranched CPLs are commercially available.

Widely ubiquitous platform for creating hyperbranched CPLs is soluble hyperbranched polyglycerol (PG), an aliphatic polyether polyol, which is prepared by anionic ROP of glycidol [383]. A distinctive feature of PG is a chemically stable polymer chain allowing easily to modifying terminal functional groups. As a typical example, we note the transformation of the end hydroxyl groups of PG to form diethylamine or di-*n*-pentylamine substituted hyperbranched CPLs [384].

It should be noted the using Cu(I) chelation in situ with hyperbranched CPLs PG-triamine and PG-tetramine for the preparation of the catalysts for ATRP of MMA or St [385].

Of interest is the method of the modification of PG derivatives with ethylethylene diamine [386, 387]. For example, the fixing hydrophilic PEG chains to amine-containing fragments leads to a core-multishell architecture (ligand II) or to the PG core for core-random shell structure (ligand III) (Fig. 5.64). Besides, PG fully modified by trimethylethylene diamine (ligand I) was used as a reference system. These efficient Cu-chelating hyperbranched polymers have a low toxicity and high water solubility as well as bind high amounts of Cu(II), which makes them good candidates for balancing Cu levels in neurodegenerative diseases. In this case, the determining factor to control the binding degree, the chelation strength, and the release profile of copper is the spatial organization of the core-shell structure. It should be noted that the hyperbranched CPL II is the most promising system for Cu chelation and release.
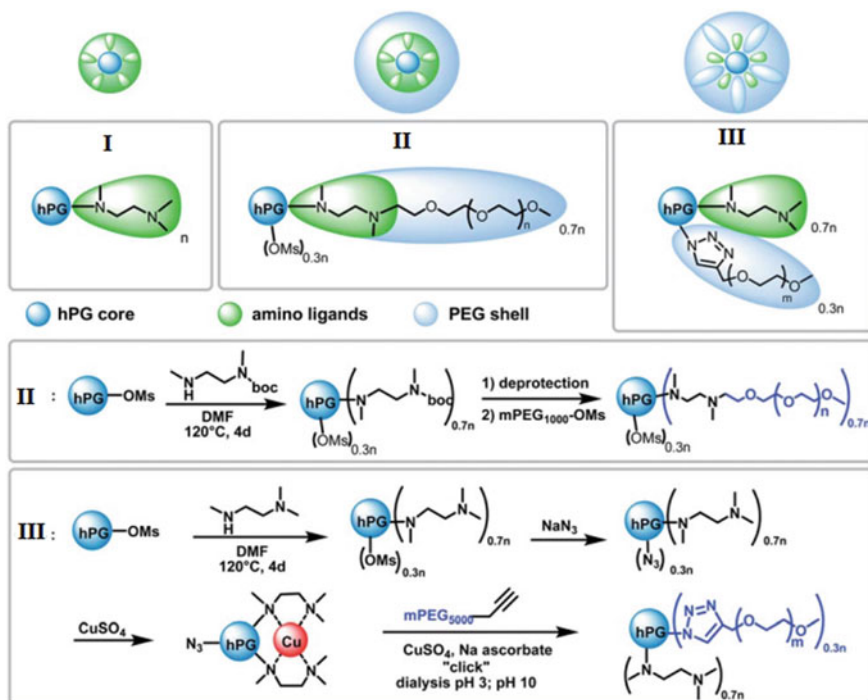
Fig. 5.64 Structure and synthesis scheme of ligands I, II and III (hPG is hyperbranched PG)

The hyperbranched CPL was synthesized by the interaction of trimethylethylene diamine possessing strong chelating ability to Cu(II) ions with hyperbranched PG [387]. The CPL links Cu(II) ions in the similar way as PEI (Fig. 5.65), however the formed Cu-PMC have a four times lower cytotoxicity. Besides, the chelation in the outer shell of the CPL based on PG core promotes the intracellular Cu release. At the same time, CPL based on PEI core links Cu(II) ions by amines in the core of the hyperbranched polymer, hindering the release of Cu.

The similar PG-based Cu-chelating ligands were prepared by covalent attachment of the N-methyl-N-picolylglycine amide, 2,6-Py-dicarboxylic acid mono-amide, and cyclam tetraacetic acid, to the hyperbranched PG (M_w = 16,800) with amide bonds [388]. Among these CPLs, the cyclam-containing CPL shows the highest chelation capacity (29 Cu ions/polymer), lowest cytotoxicity, and best stability with respect to pH and EDTA.

Of interest are hyperbranched polyamines with s-triazine fragments (Fig. 5.66a), which link metal ions and are metal ion sensors. In particular, a decrease in the intensity of fluorescence of the these CPLs with the increase of Cu(II) concentration is observed in contrast to other metal ions (Fig. 5.66b) [389, 390]. Such selectivity for Cu(II) can be explained by the square planar spatial organization of Cu(II) chelate, while other metal chelates have octahedral structures.
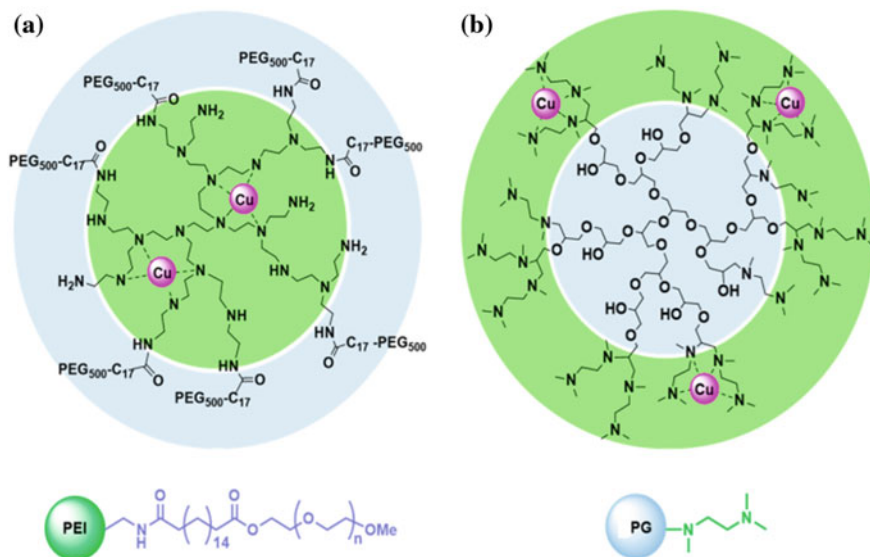
Fig. 5.65 Structures and Cu(II) chelation of the different hyperbranched architectures: **a** complexes Cu(II) inside the PEI core; **b** macroligand based on PEG core stabilizes Cu(II) ions in its amino ligand shell
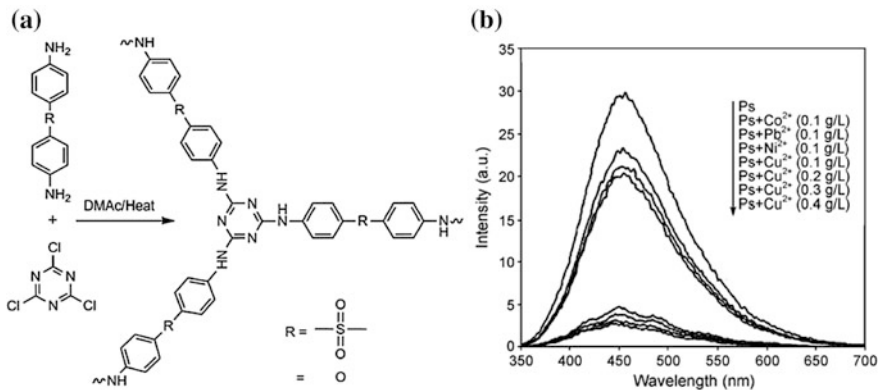
Fig. 5.66 Synthesis (**a**) and effect of metal ions on fluorescence (**b**) of hyperbranched polyamines

It should be noted the hyperbranched PEI with terminal amino or carbohydrate fragments (Scheme 5.27) which form the complexes with metal salts (CuSO$_4$, HAuCl$_4$, H$_2$PtCl$_6$, or AgNO$_3$) [391]. It turned out that the chelation capacity of the hyperbranched CPL is close to that of a G4 PAMAM dendrimer, although its molecular weight is only half of latter. Apparently, the hyperbranched CPL can link
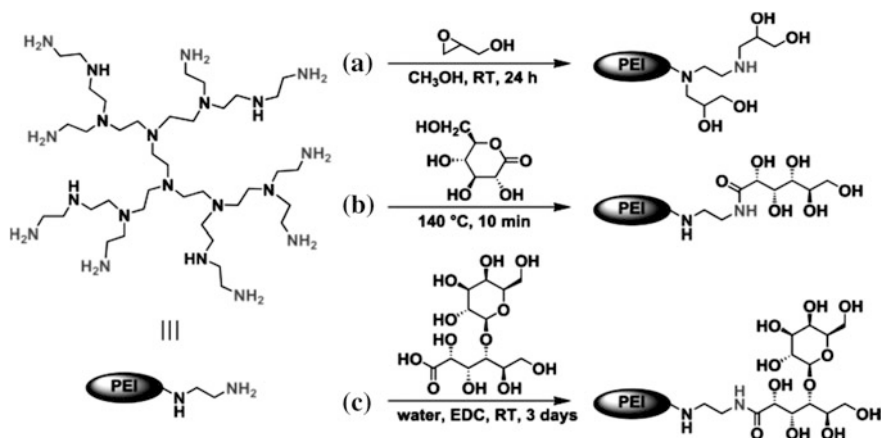
Scheme 5.27 Functionalization of hyperbranched PEI with **a** glycidol, **b** gluconic acid, and **c** lactobionic acid

metal ions by the internal chelating fragments. It is interesting that chelation capacity of the CPLs did not substantially change after the modification of the polymer ligand by gluconamide.

Hyperbranched PAMAM-*gr*-PTFE microfiltration membranes adsorbed 1.42 g m^{-2} Cu(II) ions from aqueous solution, with up to 90% desorption under acidic conditions and highly preserved adsorption capacity for Cu(II) ions with re-using cycles (Fig. 5.67) [392]. The results clearly indicate that hyperbranched PAMAM-*gr*-PTFE membrane is stable under the adsorption-desorption operating conditions and demonstrates its reusability in this environmental application.
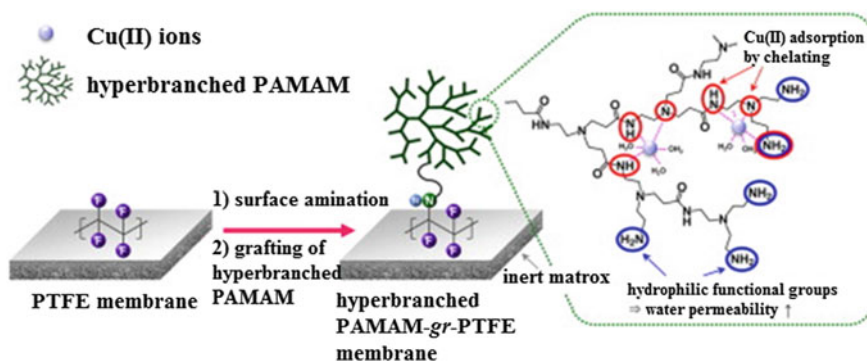
Fig. 5.67 Schematic illustration of the procedure used for the preparation of hyperbranched PAMAM-gr-PTFE microfiltration membranes for Cu(II) chelation
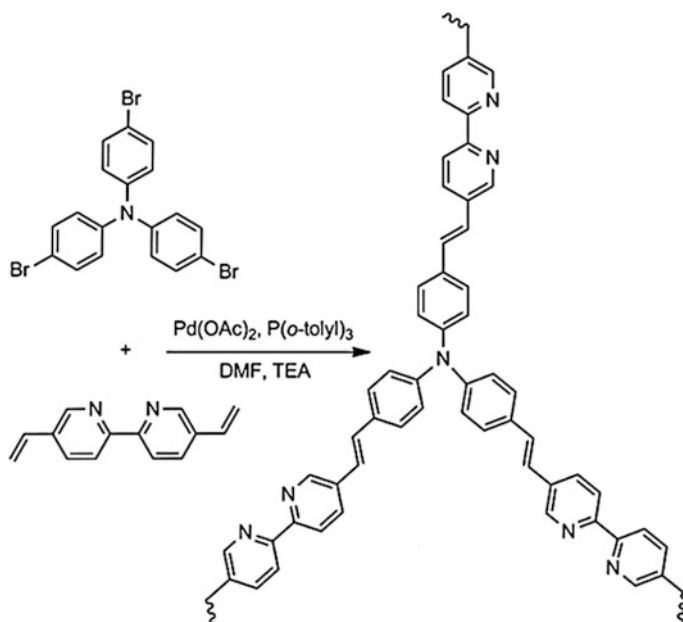
Scheme 5.28 The synthetic route of hyperbranched copolymer containing triphenylamine and divinyl-bpy units by Heck coupling reaction

Table 5.4 The K_{SV} of different metal ions

Ions	Co(II)	Ni(II)	Fe(II)	Mn(II)	Zn(II)
K_{SV} (M^{-1})	1.29×10^6	1.78×10^6	6.8×10^4	3.2×10^5	1.1×10^5

An amphiphilic derivative based on hyperbranched PAMAM was applied to the preparation of functional polysulfone membrane with heavy metal ion chelation [393]. It should be noted that the prepared membranes could provide high chelating capacity, effective regeneration of adsorption ability, and chemically inert matrices, which were the essential requirements in removing heavy metal ions from water.

A fluorescent hyperbranched copolymer with M_n of 1895 and M_w of 2315 containing triphenylamine and divinyl-bpy chelating fragments was prepared via the Heck cross-coupling reaction (Scheme 5.28) [394, 395].

Interestingly, hyperbranched copolymer has the higher K_{SV} for metal ions in comparison with similar linear polymer (Table 5.4). For example, for Mn(II), the K_{SV} of hyperbranched copolymer were equal to 3.2×10^5 M^{-1} that is 32 times high then that of linear analogue due to the «superamplified effect» of hyperbranched copolymer.

Of interest is a hyperbranched chelating aromatic polyamide with DB of 52% based on bifunctional 2,2′-diamino-4,4′-bithiazole and trifunctional 1,3,5-benzenetricarbonyl trichloride (Scheme 5.29) [396]. Two kinds of hyperbranched PMCs were synthesized
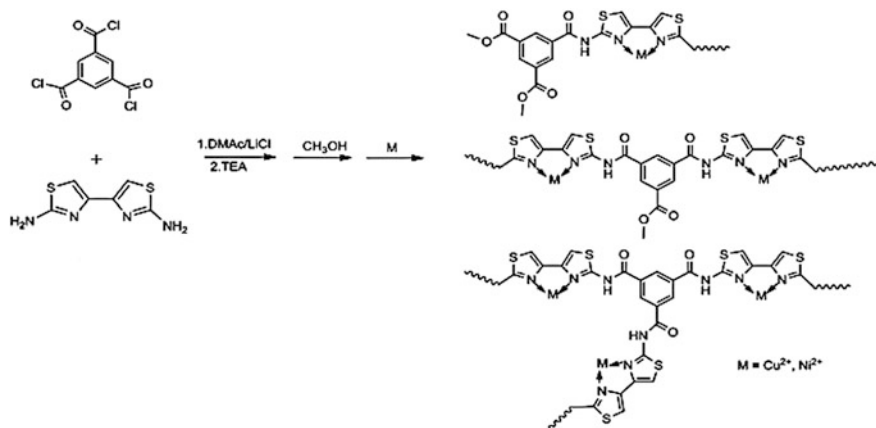
Scheme 5.29 The route of polymers' synthesis and preparation of metal chelate hyperbranched polymers

by the interaction of the hyperbranched CPL with Cu(II) and Ni(II) ions with the yields of 64.3 and 68.5%, respectively. It is important that PMCs were soft ferromagnets having Curie-Weiss temperature at 102 and 53 K, respectively.

The similar conjugated hyperbranched CPL based on 1,3,5-benzenetricarboxalde-hyde and 2,2′-diamino-4,4′-bithiazole forms PMCs with Co(II) and Sm(III) ions [397]. In this case, the magnetic hysteresis loops the Co- and Sm-PMCs have the typical «S» shape at 5 K with the Curie-Weiss temperature T_θ = 96 and 41 K, respectively. It is important that the prepared PMCs are also soft ferromagnets.

It should be noted two conjugated hyperbranched polymer fluorescent sensors with benzochalcogendiazole and triazole chelating fragments (Fig. 5.68) [398]. It is interesting that benzoselenadiazole-based CPL has higher sensitivity and selectivity with detection limit of 2.4 nM.

Of interest is fluorescence sensor based on a hyperbranched poly (phenylene sulfide) with M_w = 6 × 10^3 to 1 × 10^5 [399]. It is important that the K_{SV} is equal to 1.443 × 10^4 mL g^{-1} and the quenching efficiency is 20% at Cu(II) concentration of about 10 ppm.

It should be noted that Cu(II) and Fe(III) ions have substantial effect on fluorescence quenching of hyperbranched poly (hydroxyl ether) modified by *p-N, N*-dimethylaminobenzaldehyde [400]. For example, increasing the concentration of Fe(NO$_3$)$_3$ leads to a decrease of the intensity of the peak at 360 nm of the hyper-branched CPL with appearance of a new peak at 420 nm (Fig. 5.69a). This is explained by «complex quenching effect» . At the same time, the addition of Ni (NO$_3$)$_2$ and Co(NO$_3$)$_2$ does not lead to substantial change of the fluorescence intensity (Fig. 5.69b).
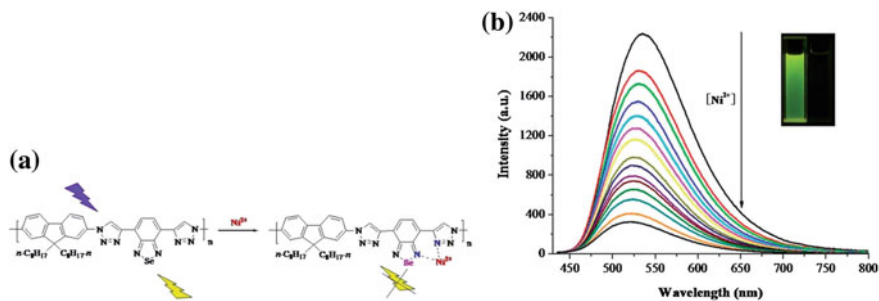
Fig. 5.68 Possible benzoselenadiazole-based polymer nickel ion detection mechanism (**a**). Fluorescence spectra of benzoselenadiazole-based polymer with increasing concentrations of Ni(II) (0, 0.2, 0.4, 0.6, 0.8, 1, 1.2, 1.4, 1.6, 1.8, 2.0, 2.5, 3.0, 4.0, 5.0 mmol L^{-1}) (λ_{ex} = 425 nm). Inset: visible fluorescence of benzoselenadiazole-based polymer before (left) and after (right) the addition of Ni(II) (5.0 mmol L^{-1}) under a 365 nm UV lamp (**b**)
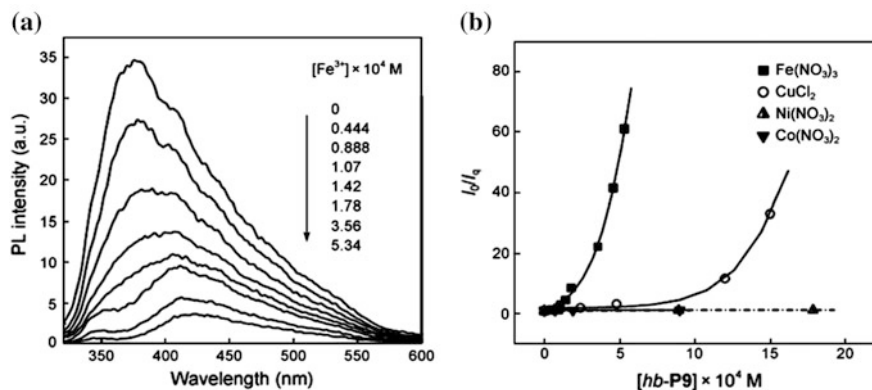
Fig. 5.69 **a** Quenching effect of $Fe(NO_3)_3$ on the fluorescence of hyperbranched polymer. **b** Stern-Volmer plots of hyperbranched polymer quenched by various quenchers in ethanol solution, c = 3.01 × 10^{-3} g mL^{-1}, λ_{ex} = 310 nm

A «complex quenching effect» was also shown in the case of fluorescent hyperbranched poly (sulfone-amine) modified by N,N'-dimethylaminoaniline [401]. It is important to emphasize that Ag(I), Cu(II) and Fe(III) ions quenched fluorescence in contrast to alkali and alkaline earth metal ions.

It should be noted the dual (thermal and metal ion) stimuli-responsiveness of oligo (ethylene glycol)-terminated hyperbranched poly (triazole) prepared by CuAAC [402]. It is important that the metal ion nature has substantial effect on the cloud point of hyperbranched polymer solution.

Of interest is the preparation of heterogeneous Pd catalysts using a hyperbranched poly (phenylacetylene) with side alkyne fragments (Fig. 5.70) [403].
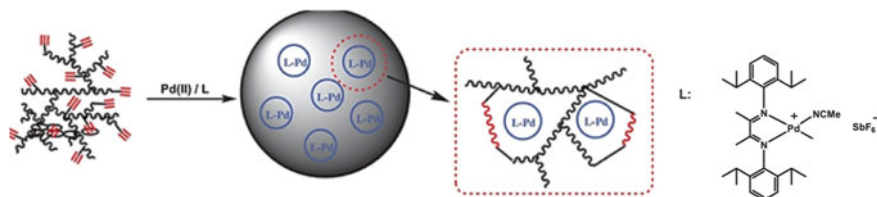
Fig. 5.70 Synthesis of heterogeneous Pd catalysts containing Pd chelate by Pd-catalyzed cross-linking of hyperbranched poly (phenylacetylene)

Under the action of Pd(II) diimine chelate, the cross-linking of the initial polymer and simultaneous linking metal compound into the cross-linked polymer matrix is carried out.

Three graphene oxide-hyperbranched PEI gels were used for Pb(II) adsorption which is determined by such parameters as Pb(II) concentration, pH value, contact time, the amino group concentration and the cross-link density [404]. The prepared CPL showed high adsorption capacity of 438.6 mg g^{-1} for Pb(II) ions.

Of interest is using carbo-BINAP and glutaroyl-AMINAP (methylene amino-substituted BINAP) functionalized hyperbranched PEI, as soluble carriers in the Cu-catalyzed hydrosilylation of acetophenone [405].
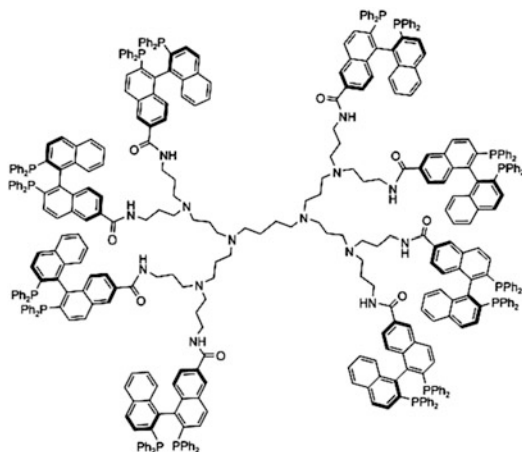
Cationic hyperbranched pyrphos-Rh(nbd) chelates have been synthesized using hyperbranched PEI containing on average 9–139 chelating fragments [142]. All hyperbranched metal chelates have been obtained in excellent yields of between 88 and 99%. It is important that the initial chelate nodes retain their spatial configuration, although the symmetry of the hyperbranched PMCs is much lower due to their PDI.

Of considerable interest is various pincer complexes attached to hyperbranched polymers [406, 407]. As a typical example, we note pincer-metal complexes fixed on a hyperbranched polyethers based on racemic hyperbranched PG (M_n = 2000) as well as chiral hyperbranched (−)-PG (M_n = 3000) and (+)-PG (M_n = 5500) [408, 409]. It should be noted that core-shell structures and a small size-distribution (15–20 nm) are characteristic for these PMCs, and thickness of the corona correlates with the content of pincer-Pt fragments.

In another interesting example, a hyperbranched carbosilane was functionalized with aryl diamine $[C_6H_3(CH_2NMe_2)_2$-2,6]-(NCN)-Pd(II) complex, using a lithiation-transmetalation method [410].

The hyperbranched conjugated polymers based on substituted *p*-phenylenes as the host fragments with *fac*-Ir(ppy)$_3$ or Ir(III) bi(2-tolyl-pyridine)acac as a light-emitting unit was synthesized by Yamamoto polycondensation [411]. For all the obtained hyperbranched PMCs, the efficient energy transfer from poly (*p*-phenylene) fragments to the Ir-complex was shown. It is interesting that Ir complex completely quenched EL emission from poly (*p*-phenylene) fragments.

It should be noted green-light-emitting hyperbranched PMC containing *fac*-Ir (ppy)$_3$ core and 3,6-Cz-*co*-2,6-Py branch [412] as well as PMCs with the 3,6-Cz-*co*-2,8-dioctyldibenzothiophene-S,S-dioxide-3,7-diyl as the main chain [413]. The emission color of the hyperbranched PMCs changes during the transition from *fac*-Ir (ppy)$_3$ fragments to other Ir chelates. In particular, hyperbranched PMCs containing an Ir chelate core and fluorene-*alt*-Cz branches are red light-emitted [414]. The other red-emitting hyperbranched PMCs contain polyfluorene and poly (fluorene-alt-Cz) branches and the Ir chelate $[(L')_2IrL]$ core (where L′ is 1-phenylisoquinoline and L is 3-(pyridin-2-yl)-1H-1,2,4-triazole) [415]. It is important that the same Ir complex was used to preparation of the hyperbranched π-conjugated light-emitting polymers [416–418].

Of interest are hyperbranched PMCs containing chlorotricarbonyl Rh(I) bis (stilbazoylimino)acenaphthene chelates [419]. It is important that the multilayer films for photovoltaic cells can be prepared from these PMCs.

PG-supported salen analogues were synthesized for the incorporation of Cr(II) ion in situ with subsequent air oxidation to the Cr(III) chelates (Scheme 5.30) [420]. The same route was used for the preparation of other hyperbranched Cr(III) salen chelates with subsequent substitution of the counter-anion Cl to SbF$_6$ using AgSbF$_6$.

It should be noted hyperbranched chromium chelate based on a PG-fixed unsymmetrical salen ligand used as catalyst for asymmetric Diels-Alder reactions [420].

Hyperbranched PG-fixed salen forms red PG-salen-Co(II) after the interaction with Co(OAc)$_2$ under inert atmosphere (Scheme 5.31) [421]. Then, the Co(II) chelate will oxidized into the Co(III) chelate, and a color changes from red to dark brown. The similar PG-fixed Mn-salen was synthesized by reacting hyperbranched ligand with Mn(II) ions. According to elemental analysis, 54 and 71% of salen sites are occupied by cobalt and manganese, respectively.
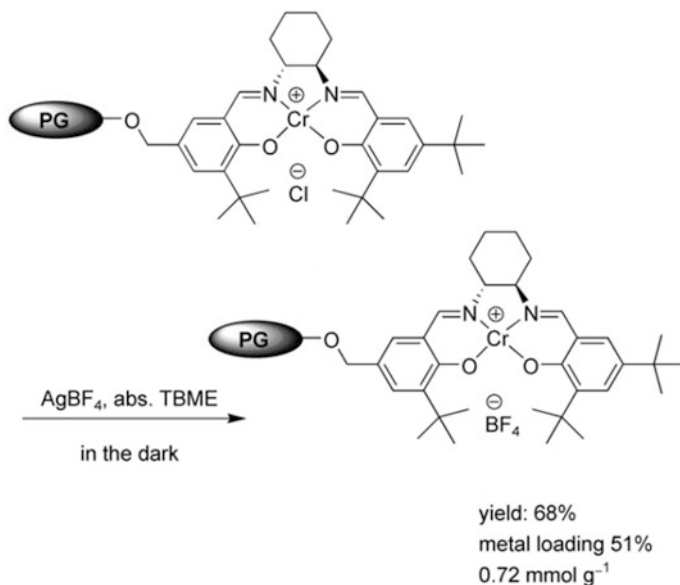
Scheme 5.30 Synthesis of a PG-supported chromium(III) salen complex with tetrafluoroborate counter-anions
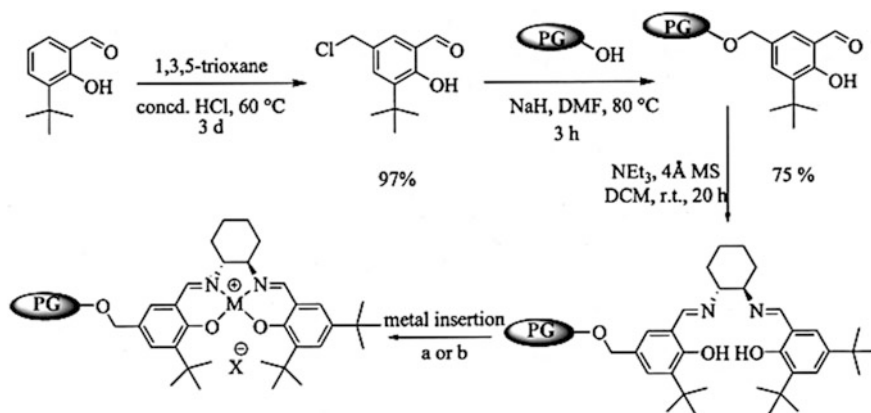
Scheme 5.31 Preparation of PG-supported Co- and Mn-salen chelates

The same PG-supported Mn-salen chelate is used as a catalyst in the epoxidation of 6-cyano-2,2-dimethylchromene [422].

Of considerable interest are the symmetrical hyperbranched (pyrrolidine-salen)-Cr(III) PMCs with spacers of different lengths (Fig. 5.71, top), which showed a positive dendritic effect in the asymmetric ring-opening of *meso*-epoxides [423].
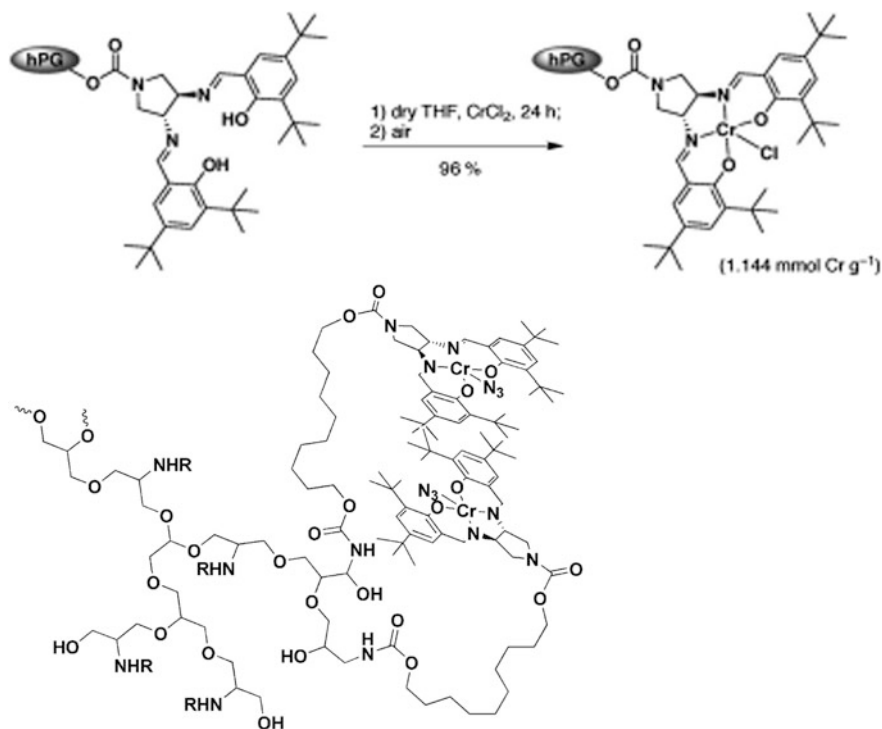
Fig. 5.71 Synthesis of PG-C1-CrCl (top). Possible back-folding mechanism for the favored head-to-tail orientation with a C10 spacer (bottom)
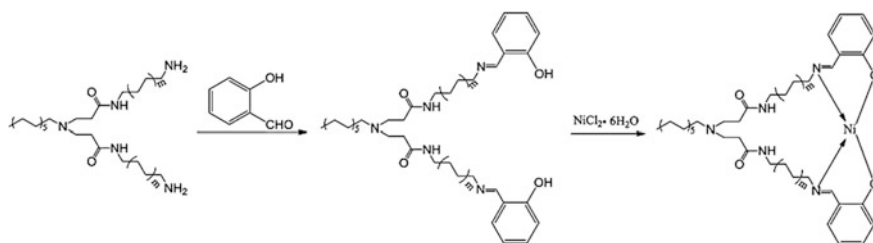
Scheme 5.32 Synthesis of hyperbranched ligand and nickel chelate

It is important that long spacers promote the favored head-to-tail orientation of two molecules (Fig. 5.71, bottom).

The hyperbranched salicylaldimine nickel chelates were synthesized by the Schiff's base and the chelation reactions with G1 hyperbranched macromolecules, salicyladehyde and nickel chloride hexahydrate as materials by employing two-step synthesis and one-pot synthesis, respectively (Scheme 5.32) [424, 425]. All nickel
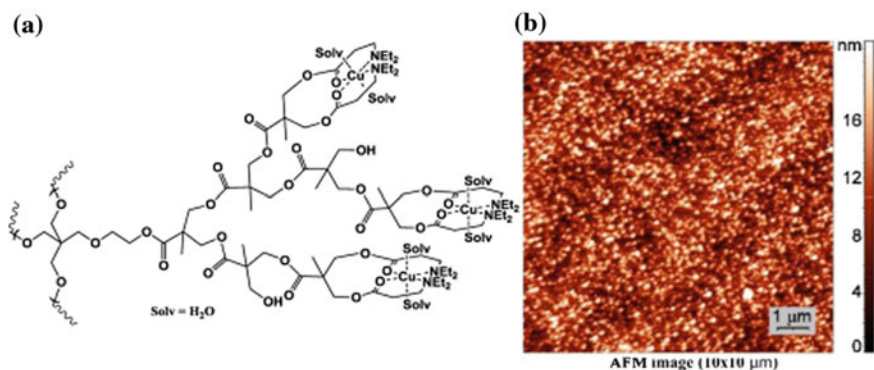
Fig. 5.72 a Scheme of synthesis of G2 and G3 copper(II) chelates of amine-modified hyperbranched polyesters ligands. **b** AFM image (10 × 10 μm) of the G3 Cu(II) chelate

chelates, activated with MAO, exhibited high activities for ethylene oligomerization and good selectivities for the longer chain oligomers produced.

It should be noted the fixing Hoveyda-Grubbs type I and II metathesis catalysts onto hyperbranched PG with a degree of functionalization of 3.85% [426].
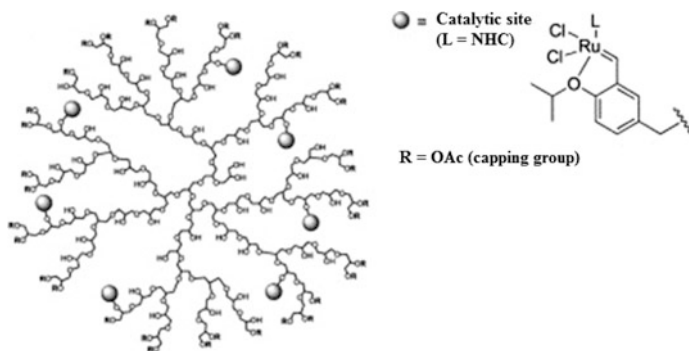
The polynuclear copper(II) chelates with hyperbranched G2 and G3 polyesters carrying end (3-diethylamino) propionate units were synthesized (Fig. 5.72a) [427]. A chelate node has composition $CuN_2O_2Solv_2$ where Solv is H_2O or DMSO. We note the preparation of a thin film composed of nanoparticles by dropping the solution of Cu(II)-PMC in methanol on the highly oriented pyrolytic graphite surface. The mean square roughness for 10 × 10 μm scan is 4 nm, variation in height is 20 nm (Fig. 5.72b).

Hyperbranched poly(ester-amide) Sm(III)-PMC was obtained by coordinating Sm(III) ions to hyperbranched CPL via a dissolution-distillation process [428]. The study of ^{13}C NMR spectra (Fig. 5.73a, b) shown disappearance of the peaks at 175.71 and 175.15 ppm assigned to the –CO–OH group and –CO–O– structure of
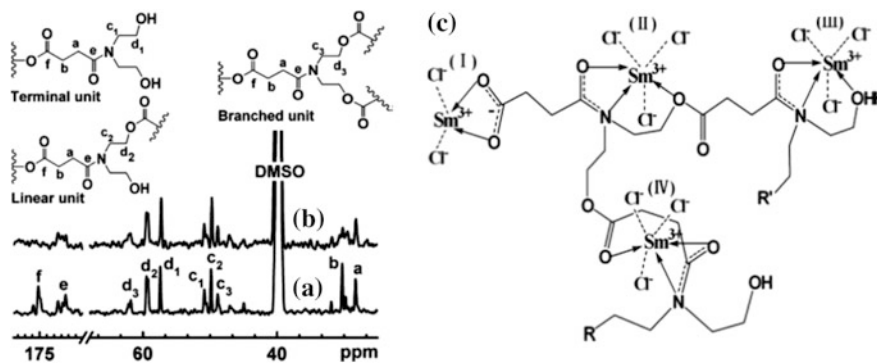
Fig. 5.73 ^{13}C NMR spectra of **a** hyperbranched poly (ester-amide) and **b** Sm(III)-hyperbranched poly(ester-amide) complex. Modes of chelation of hyperbranched poly (ester-amide) ligand with Sm(III) ions (**c**)

Fig. 5.74 The fluorescence response of hyperbranched polyfluorenes upon titration of various metal ions ([metal ion] = 50 × 10^{-6} M) at pH 7.0 in 10 mM NaH$_2$PO$_4$–Na$_2$HPO$_4$ buffer solution
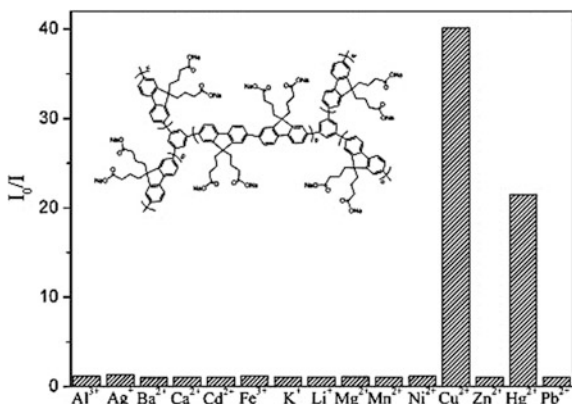
the CPL after chelation of Sm(III) ions. Other peaks, those of –COOH group, –CO–RN–CH$_2$– structure and –CH$_2$–OH group, are downfield shifted or upfield shifted due to the participation of the oxygen and nitrogen atoms in chelation (Fig. 5.73c).

Hyperbranched polyfluorenes containing carboxylate fragments showed high selectivity toward Hg(II) and Cu(II) ions in aqueous solution with the K$_{sv}$ of 0.8 × 10^6 M^{-1} and 3.11 × 10^6 M^{-1}, respectively (Fig. 5.74) [429].

Of interest is studying adsorption of metal ions by the hyperbranched polyesters based on 2,2-bis(hydroxymethyl)propionic acid and triethanol amine (Table 5.5), in which the ester groups and terminal hydroxyl groups take part in chelation [430]. The extent of binding (EOB)is determined by the number of moles of a metal ion linked per mole of CPL. It is important that the maximum EOB followed the order G2 < G3 < G4 < G5 for all metal ions. It should be noted that chelating ability of the prepared CPLs is better than that of Boltorn ones.

Table 5.5 The EOB of G2, G3, G4 and G5 for the metal ions

Metal ion	Efficiency of binding									
	G2	RSD (%)	G3	RSD (%)	G4	RSD (%)	G5	RSD (%)	Boltorn H30	RSD (%)
Cu(II)	4.5	2.8	10.1	1.2	18.0	1.2	26.1	1.0	10.8	2.5
Fe(III)	4.0	3.2	9.0	1.4	18.0	0.7	25.0	1.0	9.4	3.8
Pb(II)	3.5	4.5	8.0	3.2	16.0	1.5	20.0	1.1	9.1	2.9
Co(II)	2.4	4.6	7.0	1.0	15.6	1.7	22.4	1.0	7.8	3.1
Ni(II)	2.0	4.6	4.0	3.3	10.9	0.9	21.2	1.1	5.4	1.9
Cd(II)	2.0	4.7	7.0	1.6	14.0	2.5	22.5	0.9	8.3	2.7
Zn(II)	0.6	5.9	1.7	4.8	4.5	2.8	6.8	1.7	2.3	2.0

Table 5.6 Characterization and EOB values for Cd(II) ion of all prepared polymers

Sample	^{1}H NMR M_n g mol^{-1}	Number of (OH) mole/mole	Number of (COOH) mole/mole	EOB for Cd (II) ion
G1-OH	590	6	–	1
G2-OH	1170	11	–	2
G3-OH	1900	17	–	3
G4-OH	3200	28	–	5
G1-COOH	1457	–	10	4
G2-COOH	2760	–	18	8
G3-COOH	4653	–	32	14
G4-COOH	7100	–	44	20

The aliphatic hyperbranched polyesters based on 1,3,5-tris(2-hydroxyethyl) cyanuric acid with terminal hydroxyl and aromatic carboxylic groups were used for removal of heavy metal ions from waste water [431–433]. The increasing generation of the CPLs leads to an increase of their chelating ability, irrespective of the nature of end fragments (Table 5.6). It is interesting that two carboxyl fragments take part in chelation of one Cd(II) ion in the case of carboxyl containing polymers, whereas four OH groups coordinated with each Cd(II) ion for hydroxyl containing CPLs.

The carboxyl-terminated hyperbranched oligomer (M_w = 2125 and narrow PDI = 1.21) containing citric acid fragments was used to the absorption of chrome and reduce chromium emission [434]. It is interesting that prepared PMC retained chelation ability of citric acid that led to the formation of stable PMCs.

It should be noted biomedical applications of hyperbranched PMCs, for example, in bioimaging and contrast agents having reduced toxicity, prolonged plasma half-life, enhanced stability, and improved targeting specificity [435, 436]. In particular, hyperbranched conjugated polyelectrolyte was subsequently reacted with DTPA dianhydride in anhydrous DMSO at room temperature overnight to afford
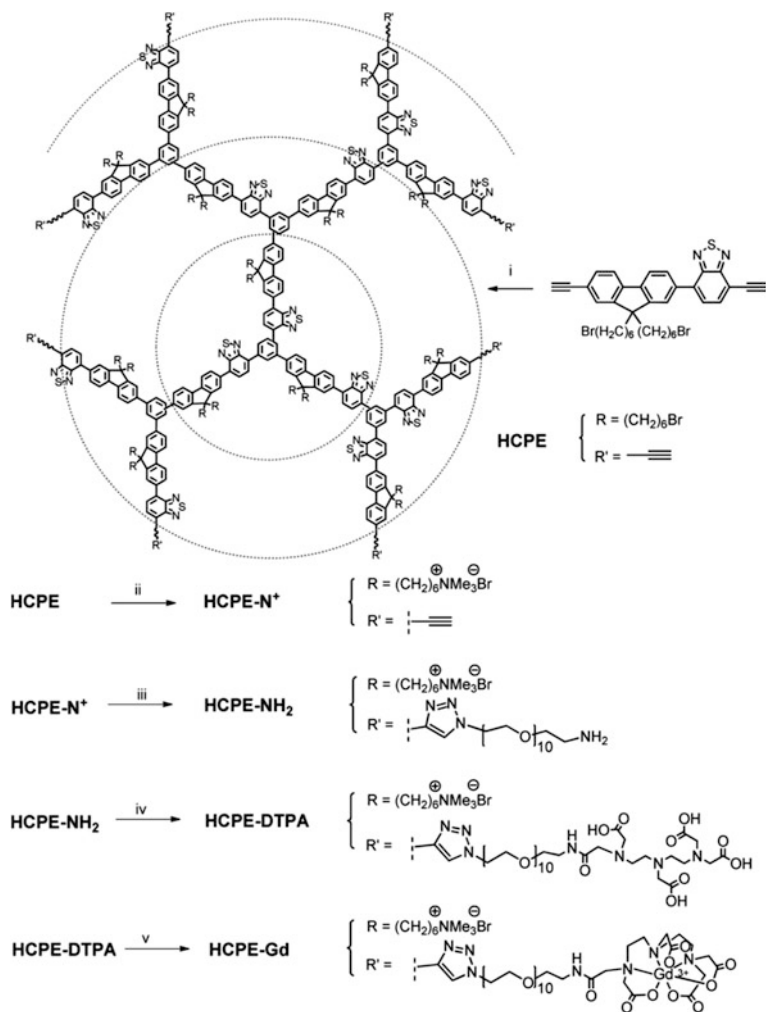
Scheme 5.33 Synthetic route to Gd-DTPA hyperbranched polymer

DTPA-containing hyperbranched polymer in 92% yield (Scheme 5.33) [437]. The final product Gd-DTPA hyperbranched polymer was obtained by chelation of Gd (III) to the DTPA moieties of the hyperbranched polymer. The prepared Gd-DTPA hyperbranched polymer is an efficient dual-modal (optical/MR) imaging agent for in vivo cancer diagnosis.

Numerous studies have been devoted to macrocyclic complexes with hyperbranched polymers, in particular, M-Pp [438]. In a typical example, iron was inserted within the Pp core by reacting hyperbranched polymer with FeCl$_2$. The solution was refluxed for 4 h and subsequently exposed to air to convert the Fe(II)-Pp to the Fe(III)-Pp hyperbranched polymer [439]. Fe-Pp hyperbranched polymer

was fractionated to prepare three different PMCs with M_n = 5400, 10,000 and 16,000, corresponding to the G2, G3 and G4 dendrimers.

1 X=H₂
2 X=Fe(III)Cl
a
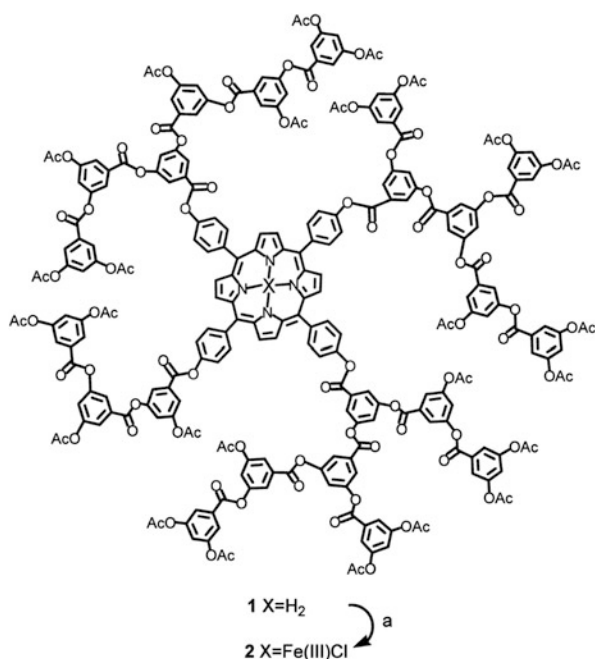
Hyperbranched poly (arylene ether ketones) containing M-Pp were synthesized by mixing of the ligand and excesses metal chlorides ($MgCl_2 \cdot 6H_2O$, $ZnCl_2$ or $MnCl_2 \cdot 4H_2O$) in the mixed solvent of $CHCl_3$ and DMF (yield 96%) [440]. It is important that dendritic architecture allowed for maximum dispersion of the chromophores, avoided aggregation, more optical limiting property was obtained. Besides, they retained the excellent properties of the materials, particularly in thermal stability.

It should be noted a narrowly dispersed tetra (acetoxyphenyl)-Pp cored hyperbranched polymer containing chelating and catalytic sites [441]. The interaction of the CPL and zinc acetate leads to the Zn-Pp hyperbranched polymer, which had a very similar molecular weight (11,710) to the initial Pp cored polymer (11,306).

A hyperbranched poly (aryl ester) with molecular weights between 4500 and 30 000 that possesses a number of free-base Pp units within its globular structure was synthesized [442]. The number of free-base Pp increased with molecular weight with the largest polymer containing ∼6 Pp. Metalation was carried out into the internal free-base Pp without harming or damaging the polymeric backbone. For example, Zn-Pp hyperbranched poly (aryl ester) was prepared by mixing of the Pp cored hyperbranched polymer with excess $Zn(OAc)_2 \cdot 3H_2O$ at room temperature for 30 min (yield 72%) (Scheme 5.34). As iron is slightly larger than zinc, a more
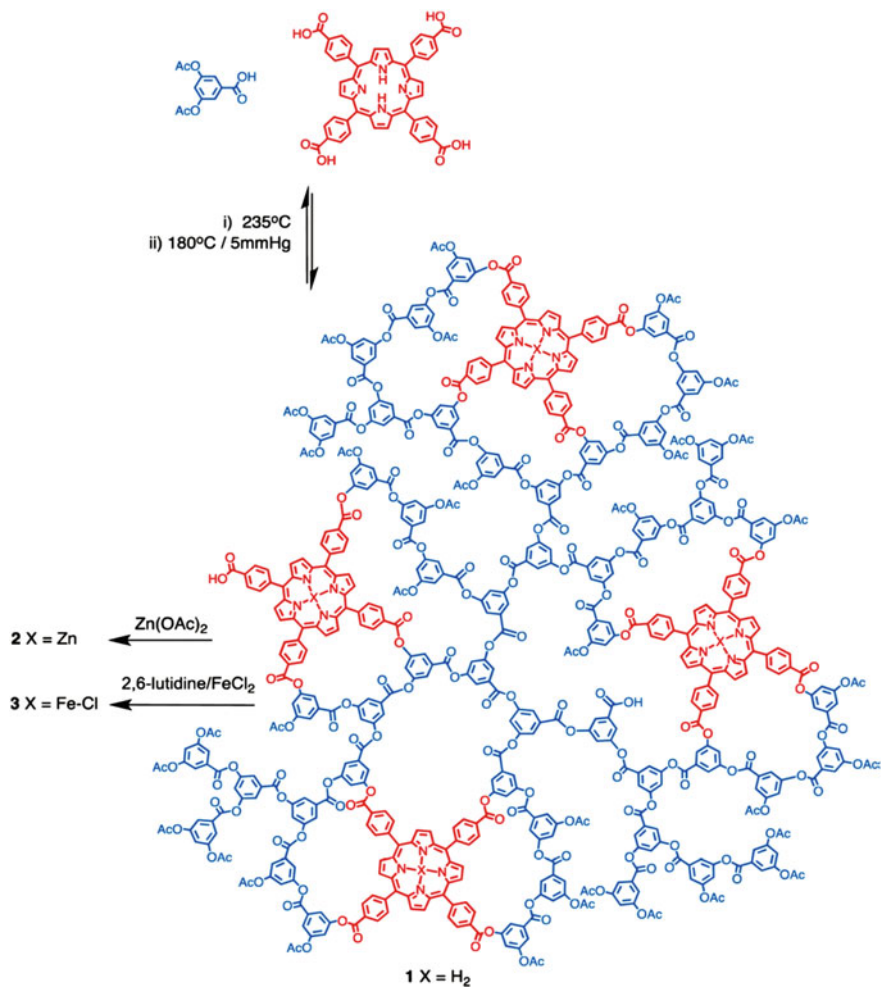
Scheme 5.34 Synthesis of multi-Pp hyperbranched poly (3,5-diacetoxybenzoic acid)

rigorous reaction procedure was required. In particular, the initial Pp cored polymer was dissolved in THF, and an excess of $FeCl_2$ was added together with 2,6-lutidine (yield 75%). It is important that the zinc- and iron-containing hyperbranched polymers confirmed that metalation had not destroyed or damaged the polymer: the M_n of both products remained unchanged, although the PDI was slightly reduced due to the additional purification step that also removed small oligomers.

It should be noted the one-stage preparation of a Fe(II)-Pp hyperbranched polymer similar the natural heme-based proteins [443]. Incorporation of iron was reached by the interaction of free-base Pp cored CPL and $FeBr_2$ with consequent oxidation to form Fe(III)-Pp cored PMC with values of 16,650 and 2.08 for M_n and PDI respectively.

Of interest is the preparation of pyridine-cored hyperbranched polymer by the polymerization of 3,5-diacetoxybenzoic acid followed by coordination of Zn-Pp (Scheme 5.35) [444].

Scheme 5.35 Synthesis of the Py-cored hyperbranched polymer and its Zn-Pp complex
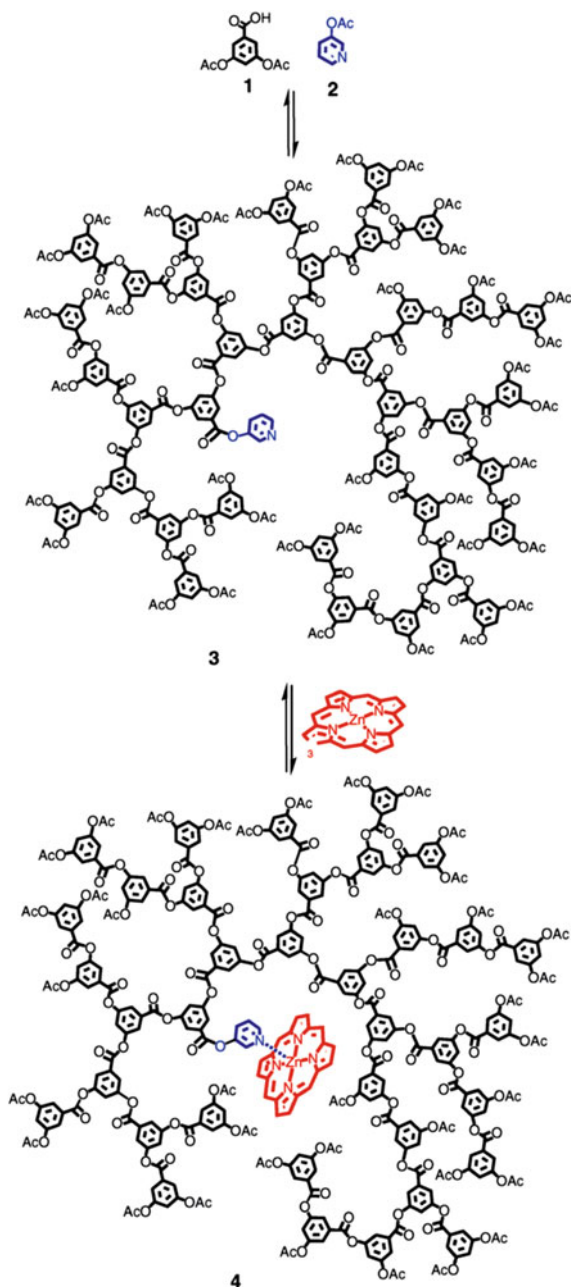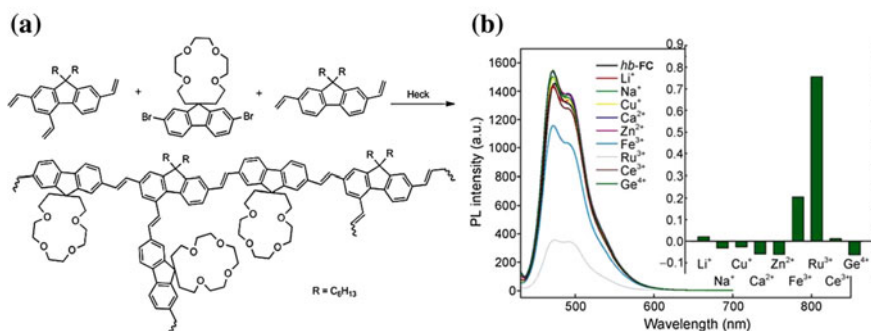
Fig. 5.75 a Synthesis of fluorescent hyperbranched polymers by Heck coupling copolymerization. **b** Photoluminescence spectra of fluorescent hyperbranched polymers in the presence of various metal cations. λ_{ex} = 423 nm, c = 10^{-6} M in DMF/H_2O = 9/1 (v/v), [ions] = 2.2 × 10^{-4} M. Inset figure is the photoluminescence spectra response profile by adding different metal cations

A range of M-Pc hyperbranched polymers was prepared using template method [445–448].
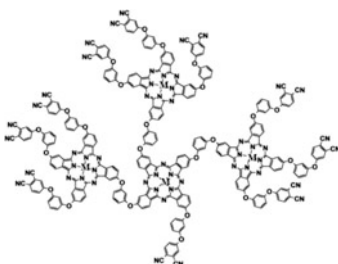
In a typical example, 1,3-bis(3,4-dicyanophenoxy) benzene or its mixture with $Ti(OC_4H_9)_4$ or $Cu(acac)_2$, in 1-pentanol in the presence of DBU, was heated at 90 to 110 °C for 2 to 4 h under a slow stream of nitrogen. The dark green powder was dried in the air for 6 h and then kept under vacuum for another 12 h [448]. A soluble Cu-Pc hyperbranched polymer was synthesized by Cu fusion technique from 1,2-bis(3,4-dicyanophenoxy) benzene and CuCl [446]. It should be noted the preparation of high-performance programmable memory devices [447] and organic-inorganic hybrid solar cells [448] based on M-Pc hyperbranched polymers.

Of considerable interest is using stimulus-responsive fluorescent hyperbranched CPLs as metal sensors [449]. As a typical example, we note metal ions responsive fluorescent hyperbranched polymers with 15-crown-4 fragments (Fig. 5.75a) [450]. Binding of crown ether receptor with conjugated polymer main chain leads to amplified fluorescence spectral change in the presence of different metal ions (Fig. 5.75b). In particular, the fluorescent hyperbranched polymers exhibit selective

fluorescence quenching toward Fe(III) and Ru(III), with the K_{sv} of 2×10^4 and 1.9×10^4 M^{-1}, respectively.

The PL intensity of another fluorescent hyperbranched polymer containing 18-crown-6 fragment was quenched by Cu(II), Ag(I), Ni(II) and Na(I) ions, whereas K(I) addition led to the emission enhancing without a noticeable absorption change [451]. Such behavior is explained by the strong coordination of K(I) with crown fragments due perfect size matching.

References

1. A.S. Abd-El-Aziz, I. Manners, *Frontiers in Transition-Metal Containing Polymers* (Wiley, NY, 2007)
2. S. Campagna, P. Ceroni, F. Puntoriero (eds.), *Designing Dendrimers* (Wiley, Hoboken, 2012)
3. L.H. Gade (ed.), *Dendrimer Catalysis* (Springer, Berlin, Heidelberg, NY, 2006)
4. Y. Cheng (ed.), *Dendrimer-based Drug Delivery Systems: From Theory to Practice* (Wiley, Hoboken, New Jersey, 2012)
5. U.S. Schubert, H. Hofmeier, G.R. Newkome, *Modern Terpyridine Chemistry* (Wiley-VCH Verlag GmbH & Co. KGaA, Weinheim, 2006)
6. D.A. Tomalia, J.B. Christensen, U. Boas, *Dendrimers, Dendrons, and Dendritic Polymers: Discovery, Applications, and the Future* (Cambridge University Press, Cambridge, 2012)
7. F. Vögtle, G. Richardt, N. Werner, *Dendrimer Chemistry: Concepts, Syntheses, Properties, Applications* (Wiley, Weinheim, 2009)
8. R. Andrés, E. de Jesus, J.C. Flores, New J. Chem. **31**, 1161 (2007)
9. I. Angurell, O. Rossell, M. Seco, Inorg. Chim. Acta, Part A **409**, 2 (2014)
10. D. Astruc, E. Boisselier, C. Ornelas, Chem. Rev. **110**, 1857 (2010)
11. D. Astruc, R. Ciganda, C. Deraedt, S. Gatard, L. Liang, N. Li, C. Ornelas, A. Rapakousiou, J. Ruiz, D. Wang, Y. Wang, P. Zhao, Synlett **26**, 1437 (2015)
12. D. Astruc, J. Ruiz, J. Inorg. Organomet. Polym. **25**, 2 (2015)
13. A.-M. Caminade, A. Ouali, R. Laurent, J.-P. Majoral, Inorg. Chim. Acta **431**, 3 (2015)
14. A.-M. Caminade, A. Ouali, R. Laurent, C.-O. Turrin, J.-P. Majoral, Chem. Soc. Rev. **44**, 3890 (2015)
15. E. de Jesus, J.C. Flores, Ind. Eng. Chem. Res. **47**, 7968 (2008)
16. F. Figueira, P.M.R. Pereira, S. Silva, J.A.S. Cavaleiro, J.P.C. Tome, Curr. Org. Synth. **11**, 110 (2014)
17. S.-H. Hwang, C.D. Shreiner, C.N. Moorefield, G.R. Newkome, New J. Chem. **31**, 1192 (2007)
18. W. Huang, Curr. Trends Surf. Sci. Catal. **1**, 65 (2014)
19. D.-L. Jiang, T. Aida, Prog. Polym. Sci. **39**, 403 (2005)
20. R.S. Kalhapure, M.K. Kathiravan, K.G. Akamanchi, T. Govender, Pharm. Dev. Technol. **20**, 22 (2015)
21. W.-S. Li, T. Aida, Chem. Rev. **109**, 6047 (2009)
22. F. Martinez-Olid, J.M. Benito, J.C. Flores, E. de Jesus, Isr. J. Chem. **49**, 99 (2009)
23. D. Méry, D. Astruc, Coord. Chem. Rev. **250**, 1965 (2006)
24. Z. Qiao, X. Shi, Prog. Polym. Sci. **44**, 1 (2015)
25. J.N.H. Reek, S. Arevalo, R. van Heerbeeck, P.C.J. Kamer, P.W.N.M. van Leeuwen, Adv. Catal. **49**, 71 (2006)
26. L. Xu, L.-J. Chen, H.-B. Yang, Chem. Commun. **50**, 5156 (2014)

27. X. Wang, G. Guérin, H. Wang, Y. Wang, I. Manners, M.A. Winnik, Science **317**, 644 (2007)
28. H. Frauenrath, Prog. Polym. Sci. **30**, 325 (2005)
29. D.A. Tomalia, Soft Matter **6**, 456 (2010)
30. N. Satoh, T. Nakashima, K. Kamikura, K. Yamamoto, Nat. Nanotechnol. **3**, 106 (2008)
31. K. Yamamoto, T. Imaoka, W.-J. Chun, O. Enoki, H. Katoh, M. Takenaga, A. Sonoi, Nat. Chem. **1**, 397 (2009)
32. M.S. Diallo, L. Balogh, S. Christie, P. Swaminathan, X. Shi, W.A. Goddard III, J.H. Johnson Jr., Dendritic nanoscale chelating agents: synthesis, characterization and environmental applications, in *Nanotechnology and the Environment*, vol. 890, Sect. VI, Ch. 7, ed. by B. Karn, T. Masciangioli, W.-X. Zhang, (Oxford University Press, NY, 2004), p. 238 (ACS Symp. Ser.)
33. C.N.R. Rao, A. Müller, A.K. Cheetham, dendrimers and their use as nanoscale sensors, in *Nanomaterials Chemistry: Recent Developments and New Directions*, ed. by N. Jayaraman (Wiley-VCH Verlag GmbH & Co. KGaA, Weinheim, 2007)
34. D. Astruc (ed.), *Dendrimers and Nanoscience* (Elsevier/C.R. Chimie, Paris, 2003)
35. A.-M. Caminade, R. Laurent, A. Ouali, J.-P. Majoral, Inorg. Chim. Acta **409**, 68 (2014)
36. F.G. Zhao, W.S. Li, Sci. Chin. Chem. **54**, 286 (2011)
37. R.W.J. Scott, O.M. Wilson, R.M. Crooks, J. Phys. Chem. B **109**, 692 (2005)
38. W. Lesniak, A.U. Bielinska, L.P. Balogh, Nano Lett. **5**, 2123 (2005)
39. X. Huang, S. Zheng, I. Kim, J. Nanosci. Nanotechnol. **14**, 1631 (2014)
40. Y. Shirota, H. Kageyama, Chem. Rev. **107**, 953 (2007)
41. R.W. Saalfrank, A. Scheurer (eds.), *Chemistry of Nanocontainers* (Springer, Berlin, Heidelberg, 2012)
42. V. Balzani, E. Marchi, M. Semeraro, Rendiconti Lincei **21**, 91 (2010)
43. V. Balzani, A. Credi, M. Venturi, *Molecular Devices and Machines—A Journey into the Nano World* (Wiley-VCH Verlag GmbH & Co, Weinheim, 2003)
44. B. Champin, P. Mobian, J.-P. Sauvage, Chem. Soc. Rev. **36**, 358 (2007)
45. D. Astruc, P. Zhao, L. Liang, A. Rapakousiou, R. Djeda, A. Diallo, T. Kusamoto, J. Ruiz, C. Ornelas, J. Inorg. Organomet. Polym. **23**, 41 (2013)
46. Y.-H. Tang, A.Y.-T. Huang, P.-Y. Chen, H.-T. Chen, C.-L. Kao, Curr. Pharm. Design **17**, 2308 (2011)
47. D.A. Tomalia, New J. Chem. **36**, 264 (2012)
48. B.M. Rosen, D.A. Wilson, C.J. Wilson, M. Peterca, B.C. Won, C. Huang, L.R. Lipski, X. Zeng, G. Ungar, P.A. Heiney, V. Percec, J. Am. Chem. Soc. **131**, 17500 (2009)
49. D.A. Tomalia, S.N. Khanna, Chem. Rev. **116**, 2705 (2016)
50. R.S. Bagul, N. Jayaraman, Inorg. Chim. Acta Part A **409**, 34 (2014)
51. A.M. Caminade, A. Hameau, J.P. Majoral, Chem. Eur. J. **15**, 9270 (2009)
52. A.W. Kleij, A. Ford, J.T.B.H. Jastrzebski, G. van Koten, Dendritic polymer applications: catalysts, in*: Dendrimers and Other Dendritic Polymers* (Wiley, West Sussex, UK, 2001)
53. J. Wang, H. Wang, C. Li, H. Li, Acta Petrolei Sinica (Petroleum Processing Section) **29**, 920 (2013)
54. S.A. Chavan, W. Maes, L.E.M. Gevers, J. Wahlen, I.F.J. Vankelecom, P.A. Jacobs, W. Dehaen, D.E. De Vos, Chem. Eur. J. **11**, 6754 (2005)
55. D. Wang, C. Deraedt, J. Ruiz, D. Astruc, Acc. Chem. Res. **48**, 1871 (2015)
56. P. Govender, A.K. Renfrew, C.M. Clavel, P.J. Dyson, B. Therrien, G.S. Smith, Dalton Trans. **40**, 1158 (2011)
57. P. Govender, B. Therrien, G.S. Smith, Eur. J. Inorg. Chem. **2012**, 2853 (2012)
58. N.C. Antonels, J.R. Moss, G.S. Smith, J. Organomet. Chem. **696**, 2003 (2011)
59. L.P. Sadowski, P.E. Edem, J.F. Valliant, A. Adronov, Macromol. Biosci. **14**, 1475 (2016)
60. C. Ghobril, G. Lamanna, M. Kueny-Stotz, A. Garofalo, C. Billotey, D. Felder-Flesch, New J. Chem. **36**, 310 (2012)
61. A. Parat, C. Bordeianu, H. Dib, A. Garofalo, A. Walter, S. Bégin-Colin, D. Felder-Flesch, Nanomedicine **10**, 977 (2015)

62. R.K. Tekade, P.V. Kumar, N.K. Jain, Chem. Rev. **109**, 49 (2009)
63. M.A. Oar, J.M. Serin, W.R. Dichtel, J.M.J. Fréchet, T.Y. Ohulchanskyy, P.N. Prasad, Chem. Mater. **17**, 2267 (2005)
64. A. Valente, M.H. Garcia, Inorganics **2**, 96 (2014)
65. V. Gajbhiye, V.K. Palanirajan, R.K. Tekade, N.K. Jain, J. Pharm. Pharmacol. **61**, 989 (2009)
66. A.B. Nepomnyashchii, M.A. Alpuche-Aviles, S. Pan, D. Zhan, F.-R.F. Fan, A.J. Bard, J. Electroanal. Chem. **621**, 286 (2008)
67. A. Tsuda, M.A. Alam, T. Harada, T. Yamaguchi, N. Ishii, Angew. Chem. Int. Ed. **46**, 8198 (2007)
68. D.-I. Lee, T. Goodson III, J. Phys. Chem. B **110**, 25582 (2006)
69. Y. Li, A. Rizzo, M. Salerno, M. Mazzeo, C. Huo, Y. Wang, K. Li, R. Cingolani, G. Gigli, Appl. Phys. Lett. **89**, 061125 (2006)
70. J.B. Oh, Y.H. Kim, M.K. Nah, H.K.J. Kim, J. Lumin. **111**, 255 (2005)
71. A.S. Mahadevi, G.N. Sastry, Chem. Rev. **116**, 2775 (2016)
72. L. Babel, T.N.Y. Hoang, L. Guénée, C. Besnard, T.A. Wesolowski, M. Humbert-Droz, C. Piguet, Chem. Eur. J. **22**, 8113 (2016)
73. W. Jiang, K. Nowosinski, N.L. Löw, E.V. Dzyuba, F. Klautzsch, A. Schäfer, J. Huuskonen, K. Rissanen, C.A. Schalley, J. Am. Chem. Soc. **134**, 1860 (2012)
74. M. Brewis, M. Helliwell, N.B. McKeown, Tetrahedron **59**, 3863 (2003)
75. M. Brewis, M. Helliwell, N.B. McKeown, S. Reynolds, A. Shawcross, Tetrahedron Lett. **42**, 813 (2001)
76. J.M. Benito, E. de Jesús, F.J. de La Mata, J.C. Flores, R. Gómez, Chem. Commun. 5217 (2005)
77. J.M. Benito, E. de Jesús, F.J. de la Mata, J.C. Flores, R. Gómez, P. Gómez-Sal, Organometallics **25**, 3876 (2006)
78. J.M. Benito, E. de Jesús, F.J. de la Mata, J.C. Flores, R. Gómez, Organometallics **25**, 3045 (2006)
79. G. Smith, R. Chen, S. Mapolie, J. Organomet. Chem. **673**, 111 (2003)
80. G.S. Smith, S.F. Mapolie, J. Mol. Catal. A Chem. **213**, 187 (2004)
81. B.C. Makhubela, A.M. Jardine, G. Westman, G.S. Smith, Dalton Trans. **41**, 10715 (2012)
82. X. Zhao, A.C.J. Loo, P.P.-F. Lee, T.T.Y. Tan, C.K. Chu, J. Inorg. Biochem. **104**, 105 (2010)
83. A. Ouali, R. Laurent, A.M. Caminade, J.P. Majoral, M. Taillefer, J. Am. Chem. Soc. **128**, 15990 (2006)
84. N. El Brahmi, S. El Kazzouli, S.M. Mignani, E.M. Essassi, G. Aubert, R. Laurent, A.M. Caminade, M.M. Bousmina, T. Cresteil, J.P. Majoral, Mol. Pharm. **10**, 1459 (2013)
85. T. Ahamad, S.M. Alshehri, S.F. Mapolie, Catal. Lett. **138**, 171 (2010)
86. L. Liang, J. Ruiz, D. Astruc, Adv. Synth. Catal. **353**, 3434 (2011)
87. U. Stebani, G. Lattermann, M. Wittenberg, J.H. Wendorff, Angew. Chem. Int. Ed. **35**, 1858 (1996)
88. U. Stebani, G. Lattermann, Adv. Mater. **7**, 578 (1995)
89. M.C. Parrot, S.R. Benhabbour, C. Saab, J.A. Lemon, S. Parker, J.F. Valliant, A. Andrianoov, J. Am. Chem. Soc. **131**, 2906 (2009)
90. A. Parat, D. Kryza, F. Degoul, J. Taleb, C. Viallard, M. Janier, A. Garofalo, P. Bonazza, L. Heinrich-Balard, R. Cohen, E. Miot-Noirault, J.-M. Chezal, C. Billotey, D. Felder-Flesch, J. Mater. Chem. B **3**, 2560 (2015)
91. C.-L. Kao, Y.-H. Tang, Y.C. Lina, L.-T. Chiu, H.-T. Chen, S.C.N. Hsu, K.-C. Hsieh, C.-Y. Lu, Y.-L. Chen, Nanomedicine. NBM **7**, 273 (2011)
92. A. Patri, C.N. Moorefield, G.R. Newkome, e-Journal **84**, 1023 (2012)
93. P. Geotti-Bianchini, T. Darbre, J.-L. Reymond, Org. Biomol. Chem. **11**, 344 (2013)
94. N.A. Uhlich, P. Sommer, C. Bühr, S. Schürch, J.-L. Reymond, T. Darbre, Chem. Commun. 6237 (2009)
95. A. Jahier, S. Nlate, J. Organomet. Chem. **694**, 637 (2009)
96. P. Govender, S. Pai, U. Schatzschneider, G.S. Smith, Inorg. Chem. **52**, 5470 (2013)

97. K.Y. Zhang, H.-W. Liu, T.T.-H. Fong, X.-G. Chen, K.K.-W. Lo, Inorg. Chem. **49**, 5432 (2010)

98. R. Roy, J.M. Kim, Tetrahedron **59**, 3881 (2003)

99. T. Muraki, K.-I. Fujita, M. Kujime, J. Org. Chem. **72**, 7863 (2007)

100. J.P. André, C.F.G.C. Geraldes, J.A. Martins, A.E. Merbach, M.I.M. Prata, A.C. Santos, J.J.P. de Lima, É. Tóth, Chem. Eur. J. **10**, 5804 (2004)

101. U.S. Schubert, A. Winter, G.R. Newkome (eds.), *Terpyridine-based Materials. For Catalytic, Optoelectronic and Life Science Applications* (Wiley-VCH, Weinheim, 2011)

102. S. Glazier, J.A. Barron, P.L. Houston, H.D. Abruña, J. Phys. Chem. B **106**, 9993 (2002)

103. H. Stephan, G. Geipel, G. Bernhard, P. Comba, G. Rajaraman, U. Hahn, F. Vogtle, Eur. J. Inorg. Chem. **2005**, 4501 (2005)

104. U. Hahn, F. Vögtle, G. De Paoli, M. Staffilani, L. De Cola, Eur. J. Inorg. Chem. **2009**, 2639 (2009)

105. U. Luning, J.P.W. Eggert, K. Hagemann, Eur. J. Org. Chem. **2006**, 2747 (2006)

106. A. Astruc, Nat. Chem. **4**, 255 (2012)

107. H.F. Chow, I.Y.K. Chan, P.S. Fung, T.K.K. Mong, M.F. Nongrum, Tetrahedron **57**, 1565 (2001)

108. E.C. Constable, C.E. Housecroft, M. Neuburger, S. Schaffner, L.J. Scherer, Dalton Trans. 2635 (2004)

109. M. Kimura, T. Shiba, T. Muto, K. Hanabusa, H. Shirai, Chem. Commun. 11 (2000)

110. A. Joester, V. Gramlich, F. Diederich, Helv. Chim. Acta **87**, 2896 (2004)

111. A. Mishra, E. Mena-Osteritz, P. Bäuerle, Beilstein J. Org. Chem. **9**, 866 (2013)

112. G.R. Newkome, E. He, L.A. Godinez, G.R. Baker, J. Am. Chem. Soc. **122**, 9993 (2000)

113. H. Jiang, S.J. Lee, W. Lin, J. Chem. Soc. Dalton Trans. 3429 (2002)

114. G.R. Newkome, K.S. Yoo, C.N. Moorefield, Chem. Commun. 2164 (2002)

115. G.D. Storrier, K. Takada, H.D. Abruna, Langmuir **15**, 872 (1999)

116. R. Satapathy, M. Ramesh, H. Padhy, I.-H. Chiang, C.-W. Chu, K.-H. Wei, H.-C. Lin, Polym. Chem. **5**, 5423 (2014)

117. J.-C.G. Bünzli, C. Piguet, Chem. Soc. Rev. **34**, 1048 (2005)

118. C. Piguet, J.-C.G. Bünzli, B. Donnio, D. Guillon, Chem. Commun. 3755 (2006)

119. A. Pucci, B. Donnio, in *Metal-Containing Liquid Crystals, in Handbook of Liquid Crystals*, ed. by J.W. Goodby, P.J. Collings, T. Kato, C. Tschierske, H. Gleeson, P. Raynes (Wiley-VCH Verlag GmbH & Co, Weinheim, 2014)

120. A. Terazzi, B. Bocquet, S. Campidelli, B. Donnio, D. Guillon, R. Deschenaux, C. Piguet, Chem. Commun. 2922 (2006)

121. T.B. Jensen, E. Terazzi, K.L. Buchwalder, L. Guénée, H. Nozary, K. Schenk, B. Heinrich, B. Donnio, D. Guillon, C. Piguet, Inorg. Chem. **49**, 8601 (2010)

122. K. Binnemans, in *Molecular Materials*, ed. by D.W. Bruce, D. O'Hare, R.J. Walton (Wiley, Weinheim, 2010)

123. A. Perrier, M. Keller, A.-M. Caminade, J.-P. Majoral, A. Oualli, Green Chem. **15**, 2075 (2013)

124. A. Sánchez-Méndez, E. de Jesús, J.C. Flores, P. Gómez-Sal, Eur. J. Inorg. Chem. **2010**, 141 (2010)

125. M. Gaab, S. Bellemin-Laponnaz, L.H. Gade, Chem. Eur. J. **15**, 5450 (2009)

126. A. Gissibl, C. Padie, M. Hager, F. Jaroschik, R. Rasappan, E. Cuevas-Yanez, C.O. Turrin, A.M. Caminade, J.P. Majoral, O. Reiser, Org. Lett. **9**, 2895 (2007)

127. D. Wang, D. Denux, J. Ruiz, D. Astruc, Adv. Synth. Catal. **355**, 129 (2013)

128. M. Koprowski, R.M. Sebastian, V. Maraval, M. Zablocka, V. Cadierno, B. Donnadieu, A. Igau, A.M. Caminade, J.P. Majoral, Organometallics **21**, 4680 (2002)

129. J.P. Byrne, J.A. Kitchen, T. Gunnlaugsson, Chem. Soc. Rev. **43**, 5302 (2014)

130. A. Xu, H.U. Kim, J.-H. Kim, B.J. Jung, A.C. Grimsdale, D.-H. Hwang, Progr. Polym. Sci. **47**, 92 (2015)

131. J.W. Levell, W.-Y. Lai, R.J. Borthwick, P.L. Burn, S.-C. Lo, I.D.W. Samuel, New J. Chem. **36**, 407 (2012)

132. M. Dasgupta, P.M. Brad, A.K. Kakkar, Coord. Chem. Rev. **233–234**, 223 (2002)
133. A.-M. Caminade, J.-P. Majoral, Molecules **21**, 538 (2016)
134. A.-M. Caminade, A. Ouali, R. Laurent, C.-O. Turrin, J.-P. Majoral, Coord. Chem. Rev. **308**, 478 (2016)
135. M. Tristany, R. Laurent, H. Dib, L. Gonsalvi, M. Peruzzini, J.P. Majoral, A.M. Caminade, Inorg. Chim. Acta **409**, 121 (2014)
136. A.-M. Caminade, A. Hameau, J.-P. Majoral, Dalton Trans. **45**, 1810 (2016)
137. R. Laurent, A.M. Caminade, J.P. Majoral, Tetrahedron Lett. **46**, 6503 (2005)
138. E. Badetti, G. Franc, J.-P. Majoral, A.-M. Caminade, R.M. Sebastián, M. Moreno-Mañas, Eur. J. Org. Chem. **2011**, 1256 (2011)
139. B. Ma, Z. Ding, J. Liu, Y. He, Q.-H. Fan, Chem. Asian J. **8**, 1101 (2013)
140. L. Routaboul, S. Vincendeau, C.O. Turrin, A.M. Caminade, J.P. Majoral, J.C. Daran, E. Manoury, J. Organomet. Chem. **692**, 1064 (2007)
141. P. Servin, R. Laurent, A. Romerosa, M. Peruzzini, J.P. Majoral, A.M. Caminade, Organometallics **27**, 2066 (2008)
142. J.K. Kassube, L.H. Gade, Adv. Synth. Catal. **351**, 739 (2009)
143. J. Yu, T.V. RajanBabu, J.R. Parquette, J. Am. Chem. Soc. **130**, 7845 (2008)
144. J. Lemo, K. Heuzé, D. Astruc, Org. Lett. **7**, 2253 (2005)
145. G. Engel, L.H. Gade, Chem. Eur. J. **8**, 4319 (2002)
146. V. Maraval, R. Laurent, B. Donnadieu, A.M. Caminade, J.P. Majoral, Phosphorus. Sulfur Silicon Relat. Elem. **184**, 1612 (2009)
147. E. Alonso, D. Astruc, J. Am. Chem. Soc. **122**, 3222 (2000)
148. V. Maraval, R. Laurent, A.-M. Caminade, J.-P. Majoral, Organometallics **19**, 4025 (2000)
149. K. Heuze, D. Mery, D. Gauss, J.-C. Blais, D. Astruc, Chem. Eur. J. **10**, 3936 (2004)
150. R.S. Bagul, N. Jayaraman, J. Organomet. Chem. **701**, 27 (2012)
151. S. Gatard, S. Nlate, E. Cloutet, G. Bravic, J.-C. Blais, D. Astruc, Angew. Chem. Int. Ed. **42**, 452 (2003)
152. G. Franc, C.O. Turrin, E. Cavero, J.P. Costes, C. Duhayon, A.M. Caminade, J.P. Majoral, Eur. J. Org. Chem. 4290 (2009)
153. Z.-J. Wang, G.-J. Deng, Y. Li, Y.-M. He, W.-J. Tang, Q.-H. Fan, Org. Lett. **9**, 1243 (2007)
154. J. Liu, Y. Feng, B. Ma, Y.-M. He, Q.-H. Fan, Eur. J. Org. Chem. **2012**, 6737 (2012)
155. B. Ma, T. Miao, Y. Sun, Y. He, J. Liu, Y. Feng, H. Chen, Q.-H. Fan, Chem. Eur. J. **20**, 9969 (2014)
156. Y.-Y. Huang, X. Yang, Y. Feng, F. Verpoort, Q.-H. Fan, J. Mol. Catal. A Chem. **393**, 150 (2014)
157. J. Liu, B. Ma, Y. Feng, Y. He, Q.-H. Fan, Inorg. Chim. Acta **409**, 106 (2014)
158. S.C. Bourque, H. Alper, L.E. Manzer, P. Arya, J. Am. Chem. Soc. **122**, 956 (2000)
159. S.-M. Lu, H. Alper, J. Am. Chem. Soc. **125**, 13126 (2003)
160. S.-M. Lu, H. Alper, J. Am. Chem. Soc. **127**, 14776 (2005)
161. S.-M. Lu, H. Alper, Chem. Eur. J. **13**, 5908 (2007)
162. P.P. Zweni, H. Alper, Adv. Synth. Catal. **346**, 849 (2004)
163. J.P.K. Reynhardt, Y. Yang, A. Sayari, H. Alper, Adv. Funct. Mater. **15**, 1641 (2005)
164. I. Angurell, E. Puig, O. Rossell, M. Seco, P. Ġomez-Sal, A. Martin. J. Organomet. Chem. **716**, 129 (2012)
165. R. Chanthateyanonth, H. Alper, Adv. Synth. Catal. **346**, 1375 (2004)
166. N.J.M. Pijnenburg, H.P. Dijkstra, G. van Koten, R.J.M.K. Gebbink, Dalton Trans. **40**, 8896 (2011)
167. N.J.M. Pijnenburg, M. Lutz, M.A. Siegler, A. Spek, G. van Koten, R.J.M.K. Gebbink, New J. Chem. **35**, 2356 (2011)
168. P. Arya, N.V. Rao, J. Singkhonrat, H. Alper, S.C. Bourque, L.E. Manzer, J. Org. Chem. **65**, 1881 (2000)
169. B.M.J.M. Suijkerbuijk, L.J. Shu, R.J.M. Klein Gebbink, A.D. Schlüter, G. van Koten, Organometallics **22**, 4175 (2003)

170. A. Bergamini, E. Marchi, P. Ceroni, in *Advanced Fluorescence Reporters in Chemistry and Biology II*, ed. by A.P. Demchenko (Springer, Berlin, Heidelberg, 2010)
171. I. Grabchev, J.-M. Chovelon, X. Qian, New J. Chem. **27**, 337 (2003)
172. I. Grabchev, J.-M. Chovelon, V. Bojinov, G. Ivanova, Tetrahedron **48**, 9591 (2003)
173. I. Grabchev, J.-P. Soumillion, B. Muls, G. Ivanova, Photochem. Photobiol. Sci. **3**, 1032 (2004)
174. I. Grabchev, D. Staneva, V. Bojinov, R. Betcheva, V. Gregoriou, Spectrochim. Acta. Part A Mol. Biomol. Spectr. **70**, 532 (2008)
175. S. Sali, I. Grabchev, J.-M. Chovelon, G. Ivanova, Spectrochim. Acta. Part A Mol. Biomol. Spectr. **65**, 591 (2006)
176. S. Yordanova, I. Grabchev, S. Stoyanov, V. Milusheva, I. Petkov, Inorg. Chim. Acta **409**, 89 (2014)
177. I. Grabchev, S. Dumas, J.-M. Chovelon, A. Nedelcheva, Tetrahedron **64**, 2113 (2008)
178. J.P. Cross, M. Lauz, P.D. Badger, S. Petoud, J. Am. Chem. Soc. **126**, 16278 (2004)
179. V. Balzani, P. Ceroni, S. Gestermann, C. Kauffmann, M. Gorka, F. Vögtle, Chem. Commun. 853 (2000)
180. F. Vögtle, S. Gestermann, C. Kauffmann, P. Ceroni, V. Vicinelli, V. Balzani, J. Am. Chem. Soc. **122**, 10398 (2000)
181. A. Prodi, F. Bolletta, M. Montalti, N. Zaccheroni, Eur. J. Chem. **3**, 455 (1999)
182. V. Vivinelli, P. Ceroni, M. Maestri, V. Balzani, M. Gorka, F. Vögtle, J. Am. Chem. Soc. **124**, 6461 (2002)
183. B. Branchi, P. Ceroni, V. Balzani, G. Bergamini, F.G. Klaerner, F. Vögtle, Chem. Eur. J. **15**, 7876 (2009)
184. R. Malgas-Enus, S.F. Mapolie, Inorg. Chim. Acta **409**, 96 (2014)
185. R. Malgas, S.F. Mapolie, S.O. Ojwach, G.S. Smith, J. Darkwa, Catal. Commun. **9**, 1612 (2008)
186. P. Govender, H. Lemmerhirt, A.T. Hutton, B. Therrien, P.J. Bednarski, G.S. Smith, Organometallics **33**, 5535 (2014)
187. S.F. Mapolie, J.L. van Wyk, Inorg. Chim. Acta **394**, 649 (2013)
188. J. Wang, G. Yang, C.-Q. Li, W.-G. Shi, S.-H. Wang, Chem. Pap. **11**, 1532 (2014)
189. J. Wang, P. Zhang, S. Chen, C.Q. Li, Adv. Mater. Res. **160–162**, 529 (2010)
190. J. Wang, G. Yang, C. Li, P. Zhangi, Asian J. Chem. **27**, 407 (2015)
191. J. Martinovic, J.v. Wyk, S. Mapolie, N. Jahed, P. Baker, E. Iwuhoa, Electrochim. Acta **55**, 4296 (2010)
192. P. Govender, L.C. Sudding, C.M. Clavel, P.J. Dyson, B. Therrien, G.S. Smith, Dalton Trans. **42**, 1267 (2013)
193. P. Govender, F. Edafe, B.C.E. Makhubela, P.J. Dyson, B. Therrien, G.S. Smith, Inorg. Chim. Acta **409**, 112 (2014)
194. B. Donnio, Inorg. Chim. Acta **409**, 53 (2014)
195. B. Donnio, D. Guillon, Adv. Polym. Sci. **201**, 45 (2006)
196. A.G. Serrette, T.M. Swager, J. Am. Chem. Soc. **115**, 8879 (1993)
197. C.K. Lai, M.Y. Lu, F.J. Lin, Liq. Cryst. **23**, 313 (1997)
198. J. Barberá, M. Marcos, A. Omenat, J.-L. Serrano, J.I. Martinez, P.J. Alonso, Liq. Cryst. **27**, 255 (2000)
199. B. Donnio, J. Barberá, R. Giménez, D. Guillon, M. Marcos, J.L. Serrano, Macromolecules **35**, 370 (2002)
200. J.H. Cameron, A. Facher, G. Lattermann, S. Diele, Mol. Cryst. Liq. Cryst. **409**, 29 (2004)
201. N. Domracheva, A. Mirea, M. Schwoerer, L. Torre-Lorente, ChemPhysChem **6**, 110 (2005)
202. N. Domracheva, A. Mirea, M. Schwoerer, L. Torre-Lorente, ChemPhysChem **7**, 2567 (2006)
203. N.E. Domracheva, A. Mirea, M. Schwoerer, L. Torre-Lorente, G. Lattermann, Phys. Solid States **49**, 110 (2007)
204. N.E. Domracheva, A.V. Pyataev, V.E. Vorobeva, E.M. Zueva, J. Phys. Chem. B **117**, 7833 (2013)

205. M.S. Gruzdev, N.E. Domracheva, U.V. Chervonova, A.M. Kolker, A.S. Golubeva, J. Coord. Chem. **65**, 1812 (2012)
206. N.E. Domracheva, V.I. Morozov, M.S. Gruzdev, R.A. Manapov, A.V. Pyataev, G. Lattermann, Macromol. Chem. Phys. **211**, 791 (2010)
207. V.E. Vorobeva, N.E. Domracheva, A.V. Pyataev, M.S. Gruzdev, U.V. Chervonova, Low Temp. Phys. **41**, 15 (2015)
208. L. Shen, F. Li, Y. Sha, X. Hong, C. Huang, Tetrahedron Lett. **45**, 3961 (2004)
209. J.N. Mugo, S.F. Mapolie, J.L. van Wyk, Inorg. Chim. Acta **363**, 2643 (2010)
210. S.M. Cohen, S. Petoud, K.N. Raymond, Chem. Eur. J. **7**, 272 (2001)
211. B.-L. Li, Z.-T. Liu, G.-J. Deng, Q.-H. Fan, Eur. J. Org. Chem. 508 (2007)
212. P.J. Case, A.W. Harper, MRS Proceedings **771**(L4), 10 (2003)
213. A. Keller, M. Ianchuk, S. Ladeira, M. Taillefer, A.-M. Caminade, J.-P. Majoral, A. Ouali, Eur. J. Org. Chem. **2012**, 1056 (2012)
214. C. Müller, L.J. Ackerman, J.N.H. Reek, P.C.J. Kamer, P.W.N.M. van Leeuwen, J. Am. Chem. Soc. **126**, 14960 (2004)
215. A. Rether, M. Schuster, React. Funct. Polym. **57**, 13 (2003)
216. S.E. Gibson, J.T. Rendell, Chem. Commun. 922 (2008)
217. M.R. Rauckhorst, P.J. Wilson, S.A. Hatcher, C.M. Hadad, J.R. Parquette, Tetrahedron **59**, 3917 (2003)
218. R. Tiwari, S.H. Daware, S.B. Kale, RSC Adv. **5**, 42526 (2015)
219. F. Fernández-Trillo, J. Pacheco-Torres, J. Correa, P. Ballesteros, P. Lopez-Larrubia, S. Cerdán, R. Riguera, E. Fernandez-Megia, Biomacromol **12**, 2902 (2011)
220. A.J.L. Villaraza, A. Bumb, M.W. Brechbiel, Chem. Rev. **110**, 2921 (2010)
221. A.R. Menjoge, R.M. Kannan, D.A. Tomalia, Drug Discov. Today **15**, 171 (2010)
222. A. Louie, Chem. Rev. **110**, 3146 (2010)
223. C. Khemtong, C.W. Kessinger, J. Gao, Chem. Commun. 3497 (2009)
224. A. Bumb, M.W. Brechbiel, P. Choyke, Acta Radiol. **51**, 751 (2010)
225. J.L. Major, T.J. Meade, Acc. Chem. Res. **42**, 893 (2009)
226. S. Langereis, Q.G. de Lussanet, M.H.P. van Genderen, W.H. Beckes, E.W. Meijer, Macromolecules **37**, 3084 (2004)
227. S. Langereis, Q.G. de Lussanet, M.H.P. van Genderen, E.W. Meijer, R.G. Beets-Tan, A.W. Griffioen, J.M. van Engelshoven, W.H. Backes, NMR Biomed. **19**, 133 (2006)
228. K. Luo, G. Liu, X. Zhang, W. She, B. He, Y. Nie, L. Li, Y. Wu, Z. Zhang, Q. Gong, F. Gao, B. Song, H. Ai, Z. Gu, Macromol. Biosci. **9**, 1227 (2009)
229. S. Laus, A. Sour, R. Ruloff, É. Tóth, A.E. Merbach, Chem. Eur. J. **11**, 3064 (2005)
230. S. Garcıa-Gallego, M. Cangiotti, L. Fiorani, A. Fattori, M.A. Mũnoz-Feŕnandez, R. Gomez, M.F. Ottaviani, F.J. De la Mata, Dalton Trans. **42**, 5874 (2013)
231. J. Lim, V.J. Venditto, E.E. Simanek, Bioorg. Med. Chem. **18**, 5749 (2010)
232. J. Roeser, B. Heinrich, C. Bourgogne, M. Rawiso, S. Michel, V. Hubscher-Bruder, F. Arnaud-Neu, S. Méry, Macromolecules **46**, 7075 (2013)
233. A. Ossenbach, H. Rüegger, A. Zhang, K. Fischer, A.D. Schlüter, M. Schmidt, Macromolecules **42**, 8781 (2009)
234. F. Le Derf, E. Levillain, G. Trippé, A. Gorgues, M. Sallé, R.-M. Sebastian, A.-M. Caminade, J.P. Majoral, Angew. Chem. Int. Ed. **40**, 224 (2001)
235. D. Alivertis, G. Paraskevopoulos, V. Theodorou, K. Skobridis, Tetrahedron Lett. **50**, 6019 (2009)
236. B. Sethi, S. Chandra, S. Kumar, R. Singh, L.P. Singh, J. Electroanal. Chem. **651**, 185 (2011)
237. Y. Pan, M. Lu, Z. Peng, J.S. Melinger, Org. Biomol. Chem. **1**, 4465 (2003)
238. X. Wang, J. Hu, T. Liu, G. Zhang, S. Liu, J. Mater. Chem. **22**, 8622 (2012)
239. V. Balzani, G. Bergamini, P. Ceroni, F. Vogtle, Coord. Chem. Rev. **251**, 525 (2007)
240. P. Antoni, M. Malkoch, G. Vamvounis, D. Nyström, A. Nyström, M. Lindgren, A. Hult, J. Mater. Chem. **18**, 2545 (2008)
241. B. Branchi, P. Ceroni, G. Bergamini, V. Balzani, M. Maestri, J. van Heyst, S.K. Lee, F. Luppertz, F. Vögtle, Chem. Eur. J. **12**, 8926 (2006)

242. G. Bergamini, A. Sottilotta, M. Maestri, P. Ceroni, F. Vögtle, Chem. Asian J. **5**, 1884 (2010)
243. L.M. Lima, R. Delgado, M.G. Drew, P. Brandão, V. Félix, Dalton Trans. 6593 (2008)
244. Z.S. Pillai, P. Ceroni, M. Kubeil, J.M. Heldt, H. Stephan, G. Bergamini, Chem. Asian J. **8**, 771 (2013)
245. J.V. Ros-Lis, R. Martínez-Máñez, F. Sancenón, J. Soto, M. Spieles, K. Rurack, Chem. Eur. J. **14**, 10101 (2008)
246. J. Havlíčková, H. Medová, T. Vitha, J. Kotek, I. Císařová, P. Hermann, Dalton Trans. 5378 (2008)
247. B. Branchi, G. Bergamini, L. Fiandro, P. Ceroni, A. Alvino, G. Doddi, F. Vögtle, F.G. Klärner, Dalton Trans. **40**, 1356 (2011)
248. B. Branchi, P. Ceroni, V. Balzani, F.G. Klärner, F. Vögtle, Chem. Eur. J. **16**, 6048 (2010)
249. C. Saudan, V. Balzani, M. Gorka, S.K. Lee, M. Maestri, V. Vicinelli, F. Vögtle, J. Am. Chem. Soc. **125**, 4424 (2003)
250. C. Saudan, V. Balzani, M. Gorka, S.K. Lee, J. van Heyst, M. Maestri, P. Ceroni, V. Vicinelli, F. Vögtle, Chem. Eur. J. **10**, 899 (2004)
251. C. Saudan, P. Ceroni, V. Vicinelli, M. Maestri, V. Balzani, M. Gorka, S.K. Lee, J. van Heyst, F. Vögtle, Dalton Trans. 1597 (2004)
252. G. Bergamini, P. Ceroni, V. Balzani, L. Cornelissen, J. van Heyst, S.-K. Lee, F. Vögtle, J. Mater. Chem. **15**, 2959 (2005)
253. G. Bergamini, C. Saudan, P. Ceroni, M. Maestri, V. Balzani, M. Gorka, S.K. Lee, J. van Heyst, F. Vögtle, J. Am. Chem. Soc. **126**, 16466 (2004)
254. C. Saudan, V. Balzani, P. Ceroni, M. Gorka, M. Maestri, V. Vicinelli, F. Vogtle, Tetrahedron **59**, 3845 (2003)
255. R. Malgas-Enus, S.F. Mapolie, Polyhedron **47**, 87 (2012)
256. E. Marchi, M. Baroncini, G. Bergamini, J. Van Heyst, F. Vögtle, P. Ceroni, J. Am. Chem. Soc. **134**, 15277 (2012)
257. C. Larpent, C. Genies, A.P.D. Delgado, A.M. Caminade, J.P. Majoral, J.F. Sassi, F. Leising, Chem. Commun. 1816 (2004)
258. A. Martin, F. Manea, R. Fiammengo, L.J. Prins, L. Pasquato, P. Scrimin, J. Am. Chem. Soc. **129**, 6982 (2007)
259. G. Zaupa, L.J. Prins, P. Scrimin, Bioorg. Med. Chem. Lett. **19**, 3816 (2009)
260. G. Zaupa, P. Scrimin, L.J. Prins, J. Am. Chem. Soc. **130**, 5699 (2008)
261. C.K. Jang, J.Y. Jaung, Mater. Lett. **62**, 3209 (2008)
262. W. Maes, W. Dehaen, Eur. J. Org. Chem. 4719 (2009)
263. M.A. Oar, W.R. Dichtel, J.M. Serin, J.M.J. Fréchet, Chem. Mater. **18**, 3682 (2006)
264. P. Vinš, A. de Cózar, I. Rivilla, K. Nováková, R. Zangi, J. Cvačka, I. Arrastia, A. Arrieta, P. Drašar, J.I. Miranda, F.P. Cossío, Tetrahedron **72**, 1120 (2016)
265. R.E.H. Ramirez, I.V. Lijanova, N.V. Likhanova, O.O. Xometl, J. Incl. Phenom. Macrocycl. Chem. **84**, 49 (2016)
266. M. Shema-Mizrachi, G.M. Pavan, E. Levin, A. Danani, N.G. Lemcoff, J. Am. Chem. Soc. **133**, 14359 (2011)
267. N. Semenishyn, A. Mahammed, Z. Gross, Eur. J. Org. Chem. **2015**, 5079 (2015)
268. D.K.P. Ng, C. R. Chimie **6**, 903 (2003)
269. M. Kimura, Y. Sugihara, T. Muto, K. Hanabusa, H. Shirai, N. Kobayashi, Chem. Eur. J. **5**, 3495 (1999)
270. J. Leclaire, R. Dagiral, A. Pla-Quintana, A.M. Caminade, J.P. Majoral, Eur. J. Inorg. Chem. 2890 (2007)
271. Z. Iqbal, N. Masilela, T. Nyokong, A. Lyubimtsev, M. Hanack, T. Ziegler, Photochem. Photobiol. Sci. **11**, 679 (2012)
272. T.J. Wadas, E.H. Wong, G.R. Weisman, C.J. Anderson, Chem. Rev. **110**, 2858 (2010)
273. O. Rolland, C.-O. Turrin, A.-M. Caminade, J.-P. Majoral, New J. Chem. **33**, 1809 (2009)
274. V.J. Venditto, C. Aida, S. Regino, M.W. Brechbiel, Mol. Pharm. **2**, 302 (2005)
275. G.P. Yan, C.W. Ai, L. Li, R.F. Zong, F. Liu, Chin. Sci. Bull. **55**, 3085 (2010)
276. M. Longmire, P.L. Choyke, H. Kobayashi, Curr. Top. Med. Chem. **8**, 1180 (2008)

277. S. Moreno, P. Ortega, F.J. de la Mata, M.F. Ottaviani, M. Cangiotti, A. Fattori, M.Á. Muñoz-Fernández, R. Gómez, Inorg. Chem. **54**, 8943 (2015)
278. C. Lee, K. Ji, E.E. Simanek, Molecules **21**, 335 (2016)
279. I. Dijkgraaf, A.Y. Rijnders, A. Soede, A.C. Dechesne, G.W. van Esse, A.J. Brouwer, F.H.M. Corstens, O.C. Boerman, D.T.S. Rijkers, R.M.J. Liskamp, Org. Biomol. Chem. **5**, 935 (2007)
280. L.M. Sena, S.J. Fishman, K.J. Jenkins, H. Xu, M.W. Brechbiel, C.A. Regino, N. Kosaka, M. Bernardo, P.L. Choyke, H. Kobayashi, Nanomedicine **5**, 1183 (2010)
281. C.C. Cyran, Y.J. Fu, H.J. Raatschen, V. Rogut, B. Chaopathomkul, D.M. Shames, J. Magn. Reson. Imaging **27**, 581 (2008)
282. J. Rudovský, P. Hermann, M. Botta, S. Aime, I. Lukeš, Chem. Commun. 2390 (2005)
283. J.A. Pikkemaat, R.T. Wegh, R. Lamerichs, R.A. van de Molengraaf, S. Langereis, D. Burdinski, A.Y.F. Raymond, H.M. Janssen, D.F.M. de Waal, N.P. Willard, E.W. Meijer, H. Grüll, Contrast Media Mol. Imaging **2**, 229 (2007)
284. J.M. Ren, T.G. McKenzie, Q. Fu, E.H.H. Wong, J. Xu, Z. An, S. Shanmugam, T.P. Davis, C. Boyer, G.G. Qiao, Chem. Rev. **116**, 6743 (2016)
285. C.L. Fraser, G.L. Fiore, Adapting polymeric metal complexes for biomedical applications, in *Polymers for Biomedical Applications*, vol. 977, Ch. 7 (2008), p. 95 (ACS Symp. Ser.)
286. B. Zhang, L.-H. Zhang, X. Huagong, Modern. Chem. Ind. **34**, 58 (2014)
287. W. Wu, W. Wang, J. Li, Prog. Polym. Sci. **46**, 55 (2015)
288. A. Winter, U.S. Schubert, Chem. Soc. Rev. **45**, 5311 (2016)
289. L. He, W. Bu, Synthesis, Design, Characterization, and application of metallo-supramolecular polymers, in *Non-covalent Interactions in the Synthesis and Design of New Compounds*, ed. by A.M. Maharramov, K.T. Mahmudov, M.N. Kopylovich, A.J.L. Pombeiro (Wiley, Weinheim, 2016)
290. V. Marin, E. Holder, R. Hoogenboom, U.S. Schubert, Chem. Soc. Rev. **36**, 618 (2007)
291. M. Kamigaito, Metal-containing star and hyperbranched polymers, in *Redox Systems Under Nano-Space Control*, ed. by T. Hirao (Springer, Berlin, Heidelberg, NY, 2006)
292. C.-A. Fustin, P. Guillet, U.S. Schubert, J.-F. Gohy, Adv. Mater. **19**, 1665 (2007)
293. X. Wu, C.L. Fraser, Macromolecules **33**, 4053 (2000)
294. R.M. Johnson, A. Pfister, C.L. Fraser, in *Metal-Containing and Metallosupramolecular Polymers and Materials*, vol. 928, Ch. 2 (2006), p. 17 (ACS Symp. Ser.)
295. Y. Chujo, A. Naka, M. Kramer, K. Sada, T. Saegusa, J. Macromol. Sci. Pure Appl. Chem. A **32**, 1213 (1995)
296. G.-I. Konishi, Y. Chujo, Macromol. Res. **16**, 70 (2008)
297. A. Pfister, C.L. Fraser, Biomacromol **7**, 459 (2006)
298. G.L. Fiore, J.L. Klinkenberg, A. Pfister, C.L. Fraser, Biomacromol **10**, 128 (2009)
299. G. Konishi, Y. Chujo, Polym. Bull. **9**, 43 (1999)
300. P.S. Corbin, M.P. Webb, J.E. McAlvin, C.L. Fraser, Biomacromol **2**, 223 (2001)
301. C.L. Fraser, A.P. Smith, X. Wu, J. Am. Chem. Soc. **122**, 9026 (2000)
302. C.L. Fraser, A.P. Smith, J. Polym. Sci. Part A Polym. Chem. **38**, 4704 (2000)
303. G. Zhou, I.I. Harruna, C.W. Ingram, Polymer **46**, 10672 (2005)
304. R.M. Johnson, C.L. Fraser, Biomacromol **5**, 580 (2004)
305. G. Zhou, J. He, I.I. Harruna, J. Polym. Sci. Part A Polym. Chem. **45**, 4225 (2007)
306. G. Zhou, J. He, I.I. Harruna, J. Polym. Sci. Part A Polym. Chem. **45**, 4204 (2007)
307. G.L. Fiore, J.L. Klinkenberg, C.L. Fraser, Macromolecules **41**, 9397 (2008)
308. R.M. Johnson, C.L. Fraser, Macromolecules **37**, 2718 (2004)
309. A.P. Smith, C.L. Fraser, J. Polym. Sci. Part A Polym. Chem. **40**, 4250 (2002)
310. A.P. Smith, C.L. Fraser, Macromolecules **35**, 594 (2002)
311. A.P. Smith, C.L. Fraser, Macromolecules **36**, 5520 (2003)
312. G.L. Fiore, C.L. Fraser, Macromolecules **41**, 7892 (2008)
313. R. Hoogenboom, D. Wouters, U.S. Schubert, Macromolecules **36**, 4743 (2003)
314. R. Hoogenboom, J. Huskens, U.S. Schubert, ACS Symp. Ser. **928**, 62 (2005)
315. R. Hoogenboom, B.C. Moore, U.S. Schubert, Chem. Commun. 4010 (2006)

316. R. Hoogenboom, B.C. Moore, U.S. Schubert, Macromol. Rapid Commun. **31**, 840 (2010)
317. S. Tang, A. Habicht, S. Li, S. Seiffert, B.D. Olsen, Macromolecules **49**, 5599 (2016)
318. M.A.R. Meier, U.S. Schubert, Chem. Commun. 4610 (2005)
319. K. Naka, G. Konishi, K. Kotera, Y. Chujo, Polym. Bull. **41**, 263 (1998)
320. J.L. Bender, Q.-D. Shen, C.L. Fraser, Tetrahedron **60**, 7277 (2004)
321. J.L. Bender, P.S. Corbin, C.L. Fraser, D.H. Metcalf, F.S. Richardson, E.L. Thomas, A.M. Urbas, J. Am. Chem. Soc. **124**, 8526 (2002)
322. D.C. Thévenaz, C.A. Monnier, S. Balog, G.L. Fiore, Biomacromol **15**, 3994 (2014)
323. K.-I. Fukukawa, R. Rossin, A. Hagooly, E.D. Pressly, J.N. Hunt, B.W. Messmore, K.L. Wooley, M.J. Welch, C.J. Hawker, Biomacromol **9**, 1329 (2008)
324. Y. Li, M. Beija, S. Laurent, L. vander Elst, R.N. Muller, H.T.T. Duong, A.B. Lowe, T.P. Davis, C. Boyer, Macromolecules **45**, 4196 (2012)
325. Y. Li, S. Laurent, L. Esser, L.V. Elst, R.N. Muller, A.B. Lowe, C. Boyer, T.P. Davis, Polym. Chem. **5**, 2592 (2014)
326. T. Zhang, C. Zhang, J. Xing, J. Xu, C. Li, P.C. Wang, X.-J. Liang, Multifunctional dendrimers for drug nanocarriers, in *Novel Approaches for Drug Delivery*, ed. by R.K. Keservani, A.K. Sharma, R.K. Kesharwani (IGI Global, Hershey, 2017)
327. L. Zhang, R. Liu, H. Peng, P. Li, Z. Xu, A.K. Whittaker, Nanoscale **8**, 10491 (2016)
328. C.T. Adkins, J.N. Dobish, C.S. Brown, B. Mayrsohn, S.K. Hamilton, F. Udoji, K. Radford, T.E. Yankeelov, J.C. Gore, E. Harth, Polym. Chem. **3**, 390 (2012)
329. B. Mizrahi, S.A. Shankarappa, J.M. Hickey, J.C. Dohlman, B.P. Timko, K.A. Whitehead, J.-J. Lee, R. Langer, D.G. Anderson, D.S. Kohane, Adv. Funct. Mater. **23**, 1527 (2013)
330. L. Viau, M. Even, O. Maury, D.M. Haddleton, H. Le Bozec, Macromol. Rapid Commun. **24**, 630 (2003)
331. R. Hoogenboom, U.S. Schubert, Chem. Soc. Rev. **35**, 622 (2006)
332. L. Viau, M. Even, O. Maury, D.M. Haddleton, H. Le Bozec, C. R. Chimie **8**, 1298 (2005)
333. R.M. Johnson, P.S. Corbin, C. Ng, C.L. Fraser, Macromolecules **33**, 7404 (2000)
334. A.A. Farah, W.J. Pietro, J. Polym. Sci. Part A Polym. Chem. **43**, 6057 (2005)
335. X. Wu, J.E. Collins, J.E. McAlvin, R.W. Cutts, C.L. Fraser, Macromolecules **34**, 2812 (2001)
336. J.E. Collins, C.L. Fraser, Macromolecules **31**, 6715 (1998)
337. S.J. Payne, G.L. Fiore, C.L. Fraser, J.N. Demas, Anal. Chem. **82**, 917 (2010)
338. Y. Deng, S.-J. Liu, B.-M. Zhao, P. Wang, Q.-L. Fan, W. Huang, L.-H. Wang, J. Lumin. **131**, 2166 (2011)
339. A.A. Farah, W.J. Pietro, Can. J. Chem. **82**, 595 (2004)
340. J.J.S. Lamba, C.L. Fraser, J. Am. Chem. Soc. **119**, 1801 (1997)
341. J.E. McAlvin, C.L. Fraser, Macromolecules **32**, 6925 (1999)
342. J.E. McAlvin, S.B. Scott, C.L. Fraser, Macromolecules **33**, 6953 (2000)
343. G. Hochwimmer, O. Nuyken, U.S. Schubert, Macromol. Rapid Commun. **19**, 309 (1998)
344. U.S. Schubert, O. Nuyken, G. Hochwimmer, Des. Monom. Polym. **3**, 245 (2000)
345. J.E. McAlvin, C.L. Fraser, Macromolecules **32**, 1341 (1999)
346. C. Park, J.E. McAlvin, C.L. Fraser, E.L. Thomas, Chem. Mater. **14**, 1225 (2002)
347. M. Chen, K.P. Ghiggino, S.H. Thang, G.J. Wilson, Angew. Chem. Int. Ed. **44**, 4368 (2005)
348. M. Chen, K.P. Ghiggino, A. Launikonis, A.W.H. Mau, E. Rizzardo, W.H.F. Sasse, S.H. Thang, G.J. Wilson, J. Mater. Chem. **13**, 2696 (2003)
349. A. Wild, A. Winter, F. Schlütter, U.S. Schubert, Chem. Soc. Rev. **40**, 1459 (2011)
350. U.S. Schubert, C. Eschbaumer, O. Nuyken, G. Hochwimmer, J. Incl. Phenom. **35**, 23 (1999)
351. U.S. Schubert, G. Hochwimmer, M. Heller, A.C.S. Symp. Ser. **812**, 163 (2002)
352. M. Heller, U.S. Schubert, Macromol. Symp. **177**, 87 (2002)
353. J.-F. Gohy, M. Chiper, P. Guillet, C.-A. Fustin, S. Hoeppener, A. Winter, R. Hoogenboom, U.S. Schubert, Soft Matter **5**, 2954 (2009)
354. J.L. Gorczynski, J. Chen, C.L. Fraser, J. Am. Chem. Soc. **127**, 14956 (2005)
355. J. Chen, J.L. Gorczynski, G. Zhang, C.L. Fraser, Macromolecules **43**, 4909 (2010)
356. Q.P. Liu, Y.C. Chen, Y. Wu, J. Zhu, J.G. Deng, Synlett 1503 (2006)

357. W. Zhao, C. Li, B. Liu, X. Wang, P. Li, Y. Wang, C. Wu, C. Yao, T. Tang, X. Liu, D. Cui, Macromolecules **47**, 5586 (2014)
358. Y. Tao, Q. Xu, N. Li, J. Lu, L. Wang, X. Xia, Polymer **52**, 4261 (2011)
359. N. Qiu, Y. Li, S. Han, G. Cui, T. Satoh, T. Kakuchi, Q. Duan, J. Photochem. Photobiol. A Chem. **283**, 38 (2014)
360. T. Ren, A. Wang, W. Yuan, L. Li, Y. Feng, J. Polym. Sci. Part A Polym. Chem. **49**, 2303 (2011)
361. W. Yuan, H. Zou, W. Guo, A. Wang, J. Ren, J. Mater. Chem. **22**, 24783 (2012)
362. K.-Y. Baek, S.-H. Lee, S.S. Hwang, Macromol. Res. **19**, 461 (2011)
363. T. Rudolph, S. Crotty, U.S. Schubert, F.H. Schacher, e-Polymers **15**, 227 (2015)
364. L.R.H. High, S.J. Holder, H.V. Penfold, Macromolecules **40**, 7157 (2007)
365. W.R. Dichtel, K.Y. Baek, J.M.J. Fréchet, I.B. Rietveld, S.A. Vinogradov, J. Polym. Sci. Part A Polym. Chem. **44**, 4939 (2006)
366. L. Wu, R. McHale, G. Feng, X. Wang, Int. J. Polym. Sci. **2011**, Article ID 109693, 11 pp. (2011)
367. A. Bilgin, C. Yagcı, Eur. Polym. J. **61**, 240 (2014)
368. Z. Gao, J. Liang, X. Tao, Y. Cui, T. Satoh, T. Kakuchi, Q. Duan, Macromol. Res. **20**, 508 (2012)
369. T.L. Mindt, H. Struthers, L. Brans, T. Anguelov, C. Schweinsberg, V. Maes, D. Tourwé, R. Schibli, J. Am. Chem. Soc. **128**, 15096 (2006)
370. T.L. Mindt, C. Müller, M. Melis, M. de Jong, R. Schibli, Bioconjugate Chem. **19**, 1689 (2008)
371. H. Struthers, B. Spingler, T.L. Mindt, R. Schibli, Chem. Eur. J. **14**, 6173 (2008)
372. N. Xiao, Y. Chen, X. Shen, C. Zhang, S. Yano, M. Gottschaldt, U.S. Schubert, T. Kakuchi, T, Satoh. Polym. J. **45**, 216 (2013)
373. C. Zhang, X. Shen, R. Sakai, M. Gottschald, U. Schubert, S. Hirohara, M. Tanihara, S. Yano, M. Obata, N. Xiao, T. Satoh, T. Kakuchi, J. Polym. Sci. A **49**, 746 (2011)
374. Y. Chen, N. Xiao, T. Satoh, T. Kakuchi, Polym. Chem. **5**, 4993 (2014)
375. Y. Chen, N. Xiao, M. Fukuoka, K. Yoshida, Q. Duan, T. Satoh, T. Kakuchi, Polym. Chem. **6**, 3608 (2015)
376. L. Munuera, R.K. O'Reilly, Dalton Trans. **39**, 388 (2010)
377. W. Wu, R. Tang, Q. Li, Z. Li, Chem. Soc. Rev. **44**, 3997 (2015)
378. F. Sun, X. Luo, L. Kang, X. Peng, C. Lu, Polym. Chem. **6**, 1214 (2015)
379. M. HaiiBler, H. Dong, B.Z. Tang, Hyperbranched polymer containing transition metals: synthetic pathways and potential applications, in *Inorganic and Organometallic Macromolecules*: *Design and Applications*, ed. by A.S. Abd-El-Aziz, C.E. Carraher, C.U. Pittman, M. Zeldin (Springer, NY, 2008)
380. C. Hajji, R. Haag, Top. Organomet. Chem. **20**, 149 (2006)
381. Y. Zheng, S. Li, Z. Weng, C. Gao, Chem. Soc. Rev. **44**, 4091 (2015)
382. A. Lederer, W. Burchard, *Hyperbranched Polymers: Macromolecules in between Deterministic Linear Chains and Dendrimer Structures* (RSC Polymer Chemistry Series, Cambridge, 2015)
383. I.N. Kurniasih, J. Keilitz, R. Haag, Chem. Soc. Rev. **44**, 4145 (2015)
384. R. Salazar, L. Fomina, S. Fomine, Polym. Bull. **47**, 151 (2001)
385. K.R. Kumar, J.N. Kizhakkedathu, D.E. Brooks, Macromol. Chem. Phys. **205**, 567 (2004)
386. S. Nowag, C. Frangville, G. Multhaup, J.D. Marty, C. Mingotaud, R. Haag, J. Mater. Chem. B **2**, 3915 (2014)
387. S. Fehse, S. Nowag, M. Quadir, K.S. Kim, R. Haag, G. Multhaup, Biomacromol **15**, 1910 (2014)
388. R. Albrecht, S. Fehse, K. Pant, S. Nowag, H. Stephan, R. Haag, C.C. Tzschucke, Macromol. Biosci. **16**, 412 (2016)
389. S.S. Mahapatra, U. Das, N. Karak, J. Lumin. **128**, 1917 (2008)
390. S.S. Mahapatra, N. Karak, Polym. J. **41**, 20 (2009)

391. M. Krämer, N. Pérignon, R. Haag, J.-D. Marty, R. Thomann, N. Lauth-de Viguerie, C. Mingotaud, Macromolecules **38**, 8308 (2005)
392. H. Yoo, S.-Y. Kwak, J. Membr. Sci. **448**, 125 (2013)
393. K.N. Han, B.Y. Yu, S.Y. Kwak, J. Membrane Sci. **396**, 83 (2012)
394. J. Feng, Y. Li, M. Yang, Eur. Polym. J. **44**, 3314 (2008)
395. J. Feng, Y. Li, M. Yang, J. Polym. Sci. A **47**, 222 (2009)
396. N.W. Ding, W.H. Lin, W.L. Sun, Z.Q. Shen, Sci. China Chem. **54**, 320 (2011)
397. N. Ding, W. Sun, Y. Lin, Z. Shen, Chin. J. Polym. Sci. **30**, 759 (2012)
398. Y. Lei, H. Li, W. Gao, M. Liu, J. Chen, J. Ding, X. Huang, H. Wu, J. Mater. Chem. C **2**, 7402 (2014)
399. R.L. Xu, H.W. Liu, W.F. Shi, J. Polym. Sci. Part B Polym. Phys. **44**, 826 (2006)
400. C. Gao, J. Hou, D.Y. Yan, Z.J. Wang, React. Funct. Polym. **58**, 65 (2004)
401. C. Gao, D.Y. Yan, Chin. Sci. Bull. **45**, 1760 (2000)
402. J. Wu, W. Liu, H. Han, R. Sun, M. Xie, X. Liao, Polym. Chem. **6**, 4801 (2015)
403. Z. Dong, Z. Ye, Appl. Catal. A General **489**, 61 (2015)
404. Y. Liu, L. Xu, J. Liu, X. Liu, C. Chen, G. Li, Y. Meng, Chem. Eng. J. **285**, 698 (2016)
405. J.K. Kassube, H. Wadepohl, L.H. Gade, Adv. Synth. Catal. **351**, 607 (2009)
406. G. van Koten, D. Milstein (eds.), *Organometallic Pincer Complexes* (Springer, Heidelberg, NY, Dordrecht, London, 2012)
407. G. van Koten, R.A. Gossage (eds.), *The Privileged Pincer-Metal Platform: Coordination Chemistry & Applications* (Springer, Heidelberg, NY, Dordrecht, London, 2016)
408. S.-E. Stiriba, M.Q. Slagt, H. Kautz, R.J.M.K. Gebbink, R. Thomann, H. Frey, G. van Koten, Chem. Eur. J. **10**, 1267 (2004)
409. M.Q. Slagt, S.-E. Stiriba, H. Kautz, R.J.M.K. Gebbink, H. Frey, G. Van Koten, Organometallics **23**, 1525 (2004)
410. C. Schlenk, A.W. Kleij, H. Frey, G. van Koten, Angew. Chem. Int. Ed. **39**, 3445 (2000)
411. W. Yang, H.Y. Zhen, C.Y. Jiang, L.J. Su, J.X. Jiang, H.H. Shi, Y. Cao, Synth. Met. **153**, 189 (2005)
412. R. Guan, Y. Xu, L. Ying, W. Yang, H. Wu, Q. Chen, Y. Cao, J. Mater. Chem. **19**, 531 (2009)
413. J. Liu, L. Yu, C. Zhong, R. He, W. Yang, H. Wu, Y. Cao, RSC Adv. **2**, 689 (2012)
414. T. Guo, R. Guan, J. Zou, J. Liu, L. Ying, W. Yang, H. Wu, Y. Cao, Polym. Chem. **2**, 2193 (2011)
415. T. Guo, L. Yu, B. Zhao, Y. Li, Y. Tao, W. Yang, Q. Hou, H. Wu, Y. Cao, Macromol. Chem. Phys. **213**, 820 (2012)
416. T. Guo, L. Yu, Y. Yang, Y. Li, Y. Tao, Q. Hou, L. Ying, W. Yang, H. Wu, Y. Cao, J. Lumin. **167**, 179 (2015)
417. J. Sun, J. Yang, C. Zhang, H. Wang, J. Li, S. Su, H. Xu, T. Zhang, Y. Wu, W.-Y. Wong, B. Xu, New J. Chem. **39**, 5180 (2015)
418. J. Sun, H. Wang, T. Yang, X. Zhang, J. Li, T. Zhang, Y. Wu, W. Chen, W.-Y. Wong, Dyes Pigm. **125**, 339 (2016)
419. C.W. Tse, K.W. Cheng, W.K. Chan, J. Inorg. Organomet. Polym. **18**, 59 (2008)
420. C. Hajji, S. Roller, M. Beigi, A. Liese, R. Haag, Adv. Synth. Catal. **348**, 1760 (2006)
421. M. Beigi, S. Roller, R. Haag, A. Liese, Eur. J. Org. Chem. 2135 (2008)
422. M. Beigi, R. Haag, A. Liese, Adv. Synth. Catal. **350**, 919 (2008)
423. J. Keilitz, R. Haag, Eur. J. Org. Chem. 3272 (2009)
424. J. Wang, G. Yang, C.Q. Li, W.G. Shi, Chem. J. Chin. Univ. **35**, 1536 (2014)
425. J. Wang, N. Zhang, C.Q. Li, W.G. Shi, Z.Y. Lin, J. Organomet. Chem. **822**, 104 (2016)
426. V.S. Thengarai, J. Keilitz, R. Haag, Inorg. Chim. Acta **409**, 179 (2014)
427. M.P. Kutyreva, A.R. Gataulina, G.A. Kutyrev, N.A. Ulakhovich, T. Newman, E.M. Khasanova, O.V. Bondar, S.V. Yurtaeva, S.A. Ziganshina, E.V. Khaldeeva, Inorg. Chim. Acta **450**, 101 (2016)
428. X. Fang, R. Chen, L. Xiao, Q. Chen, Polym. Int. **61**, 136 (2011)
429. B. Bao, L. Yuwen, X. Zhan, L. Wang, J. Polym. Sci. Part A Polym. Chem. **48**, 3431 (2010)

430. A. Goswami, A.K. Singh, React. Funct. Polym. **61**, 255 (2004)
431. J.N. Asaad, N.E. Ikladious, F. Awad, T. Müller, Canad. J. Chem. Eng. **91**, 257 (2013)
432. N.E. Ikladious, S.H. Mansour, N. Rozik, K. Dirnberger, C.D. Eisenbach, J. Polym. Sci. Part A Polym. Chem. **46**, 5568 (2008)
433. N.E. Ikladious, J.N. Asaad, N.N. Rozik, Des. Monom. Polym. **12**, 469 (2009)
434. C. Li, H. Chen, B. Liu, B. Wang, R. Luo, N. Shan, J. Appl. Polym. Sci. **131**, 40117 (2014)
435. Q. Zhu, F. Qiu, B. Zhu, X. Zhu, RSC Adv. **3**, 2071 (2013)
436. M. Elsabahy, G.S. Heo, S.-M. Lim, G. Sun, K.L. Wooley, Chem. Rev. **115**, 10967 (2015)
437. D. Ding, G. Wang, J. Liu, K. Li, K.Y. Pu, Y. Hu, J.C.Y. Ng, B.Z. Tang, B. Liu, Small **8**, 3523 (2012)
438. K. Kirkorian, A. Ellis, L.J. Twyman, Chem. Soc. Rev. **41**, 6138 (2012)
439. X. Zheng, I.R. Oviedo, L.J. Twyman, Macromolecules **41**, 7776 (2008)
440. X. Jiang, Y. Du, C. Liu, P. Huo, Z. Geng, S. Zhang, G. Wang, Chin. J. Polym. Sci. **32**, 73 (2014)
441. A. Ellis, L.J. Twyman, Macromolecules **46**, 7055 (2013)
442. L.J. Twyman, A. Ellis, P.J. Gittins, Macromolecules **44**, 6365 (2011)
443. L.J. Twyman, Y. Ge, Chem. Comm. **15**, 1658 (2006)
444. L.J. Twyman, A. Ellis, P.J. Gittins, Chem. Commun. **48**, 154 (2012)
445. M. Guo, X. Yan, T. Goodsoon III, Adv. Mater. **20**, 4167 (2008)
446. Y. Kwon, T. Hayakawa, M. Kakimoto, Chem. Lett. **35**, 1306 (2006)
447. S. Choi, S.-H. Hong, S.H. Cho, S.-D. Park, S.-M. Park, O. Kim, M. Ree, Adv. Mater. **20**, 1766 (2008)
448. Y. Li, M. Yan, M. Jiang, R. Dhakal, P.S. Thapaliya, X. Yan, J. Photon, Energy **1**, 011115 (2011)
449. J. Wang, J. Mei, A. Qin, J. Sun, B. Zhong, Sci. China Chem. **53**, 2409 (2010)
450. J.M. Yu, Y. Chen, Macromolecules **42**, 8052 (2009)
451. F.L. Bai, Q.G. He, H.M. Huang, H.Z. Lin, J.L. Yang, Synthetic Met. **137**, 971 (2003)

Chapter 6
Coordination Polymers Containing Metal Chelate Units

Abstract In this chapter the advances and problems associated with the preparation, properties and structure of coordination polymers containing metal chelate units are presented and assessed. The crystal engineering, reticular chemistry, metalloligand strategy, columnar-layered strategy, as well as approaches based on supramolecular building blocks and supramolecular building layers in the chemistry of coordination polymers containing metal chelate units are considered. The conventional (solvent evaporation, diffusion, hydro(solvo)thermal, urothermal, ionothermal, microfluidic, surfactant-thermal, in situ spacer methods as well as synthesis in supercritical CO_2) and alternative (microwave-assisted, electrochemical, mechanochemical, and sonochemical methods) synthesis routes are described. Special attention is paid to the post-synthetic approaches to the preparation of coordination polymers containing metal chelate units including post-synthetic modification, post-synthetic deprotection, and post-synthetic exchange.

Extended hybrid crystalline complex compounds formed by organic ligands (also called spacers) and metal ions expanding in one (1D), two (2D) or three (3D) dimensions due to formation of metal–ligand (M–L) coordination bond (Fig. 6.1) are called coordination polymers (CPs) [1–19]. CPs relate to a special class of polymeric metal complexes containing metal in the main chain, whose special feature is breaking of a polymer chain after a metal is removed. First time the term «coordination polymer» was used in 1964 [20]. At the first stage of the studies, CPs were obtained using a simple mixing of components or the template method, as a result, insoluble substances formed, whose exact structure was non-improvable. Therefore, they were regarded, by the figurative expression [2], as «vaguely defined «insoluble material» at the bottom of your vessel that spells death for your reaction». A great jump in directed design of CPs was done in 1990s by wide implementation of new techniques of synthesis of such materials, first of all, solvothermal method [21, 22], which made it possible to obtain pure substances, which can be studied by X-ray diffraction analysis.

Polymer coordination networks (PCNs) are metal complexes extended due to repeated coordination units within one chain, and at the same time with cross-links
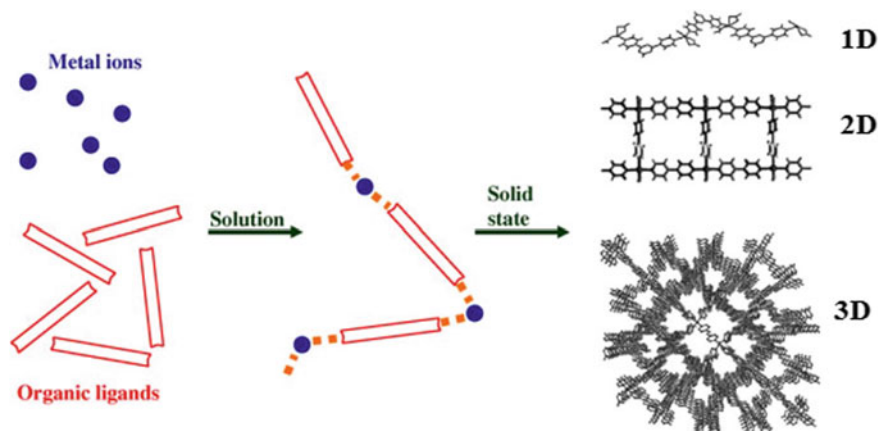
Fig. 6.1 Formation of coordination polymers

between two or more separate chains. CPs containing in their structure cavities and channels, whose sizes are enough for reversible incorporation of different guest molecules, are called porous CPs. Porous materials by IUPAC nomenclature are divided into three classes: microporous (linear sizes of cavities is up to 20 Å), mesoporous (cross section from 2 to 50 nm), and macroporous (cross section more than 50 nm). In the case of CPs most often microporous compounds [1–9] and far more rarely mesoporous compounds [23] form. Macroporous coordination compounds are not known. For the compounds with pore sizes greater than 1 nm a special term nanoporous CP is used. If a porous CP shows reversible gas adsorption and specific surface and porous volume based on sorption data coincide or are close to the calculated ones, it is called permanently porous.

Metal-organic frameworks (MOFs) are usually called CPs excluding guest molecules regardless of a possibility to eliminate these guest molecules without breaking the structure or not. This term MOF was popularized around 1995 [24, 25] and it highlights their similarity to traditional structure of solids, in particular, zeolite framework materials, and thus characterizes reliability and porosity. More formally, MOFs are polymer coordination networks consisting of metal ions or clusters linked by rigid organic ligands, so that 1D, 2D, and 3D structures containing potential voids—pores would form [26–40]. Integration of MOFs become a real outbreak in science and served a powerful catalyst of intense development of CP chemistry.

In order to avoid a confusion with names of these compounds, IUPAC has recommended [41] hierarchical terminology, where most common term is CP (Fig. 6.2). Then follows coordination networks as subsets of CPs, and MOFs, in turn, are a subset of coordination networks. It should be noted that MOF is often
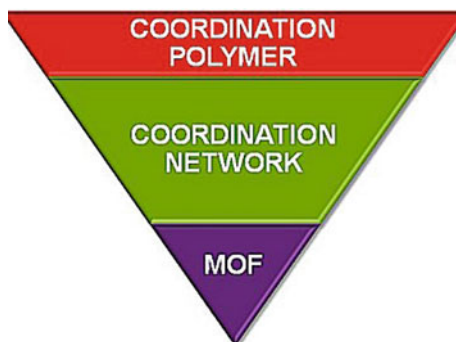
called either by order of their discovery (MOF-1, MOF-2, etc.) or using trivial
names, which relate to a place, where a material was first synthesized: Hong Kong
University of Science and Technology (HKUST), Matériaux de l'Institut Lavoisier
(MIL), Porphyrinic Illinois Zeolite Analogue (PIZA), University of Michigan
Crystalline Material (UMCM), Jilin University China (JUC), etc.

By controlling the process of CP molecular self-assembling, it is possible to obtain
new crystalline functional materials with given practical properties. Therefore, CPs
have progressed from «polymer disposal» to «materials of future» [42], which was
conditioned also by similar achievements in adjacent areas, such as crystal engi-
neering, supramolecular chemistry and X-ray diffraction. This is due to the fact that
CPs are porous materials with adjusted size of pores [43, 44], have vast surface areas
and intriguing structural topologies [45–55], which brings to universal architectures
[56]. Location of components in CP exists predominantly only in solid state [57, 58],
at that solid products are, as a rule, insoluble or decompose during solution. The CP
structures can be defined only by methods of X-ray crystallography, and their char-
acteristics in solution, as a rule, prove existence of oligomer fragments.

A great interest in development of new CPs rises from their promising appli-
cations [11, 30, 33, 42, 59–68], especially in such areas as ion exchange, adsorp-
tion, and separation processes [34, 35, 37, 38, 69–81], biomedical applications
[82–85], drug delivery [29, 86–88], sensor technologies [78, 87–90], heterogeneous
[77, 91–103] and biomimetic catalysis [104–106], luminescence [87, 89, 107–110],
proton conductivity [77, 104–106], light-harvesting [111], and in other areas [34,
75, 112–117].

Presently MOFs are industrially produced, for example, BASF (trade mark
BASOLITETM), and are commercially available through Aldrich (Fig. 6.3).

Taking into account the idea of this book, in the following paragraphs of this
chapter only those CPs will be considered, which contain metal chelate units.
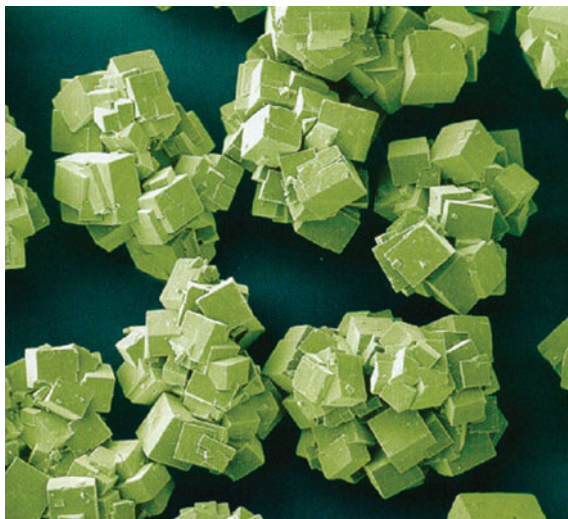
6.1 Crystal Engineering of Coordination Polymers

The essence of crystal engineering, design of molecular solids is in achievement of ordered materials with preliminary defined dimensionality and bonding through deliberate synthesis strategies. In its classic definition crystal engineering is the understanding of the intermolecular interactions in context of crystal stacking and using of such understanding in design of new solids with desired physical and chemical properties [118–120]. Though the term was initially conceived for purely supramolecular organic materials, it propagated very fast to inorganic and hybrid solids [121] and then has shown its efficiency in CP construction, and is now considered as a basis for modern strategies of CP design [43]. Crystal engineering provides efficient means for purposed development of a wide range of extended CP architectures with given structures and desired properties based on intermolecular interactions, especially M–L bonds. Modularity and amenability of MOFs stipulated by crystal engineering are the driving force of their fast progress.

A concrete application of crystal engineering to CP is implementation of efficient and widely used design strategy called node-and-spacer approach [122, 123]. It can be compared with supramolecular chemistry and self-assembling function, if crystals are considered as individual chemical objects [124]. In its simplest description it consists of metal ions or conglomerates (nodes) linked with bridging ligands (spacers) into 1D, 2D, and 3D massifs, some of which have no inorganic analogues. In other words, nodes and spacers are simplified as topological points and lines, and networks are presented in their respective combinations. Using metal ions with different coordination numbers as nodes, makes the structural topology controlled (Fig. 6.4) [43]. Variety of nodes and spacers provides infinite number of possibilities for design of new species with intriguing architectures, topologies, and properties,

Fig. 6.4 Schematic illustration of the node (red) and linear spacer (blue) approach for design of networks based upon tetrahedral (above left cubic diamondoid, above right hexagonal diamondoid) or octahedral metal nodes (below left square grid, below right octahedral network) [43]
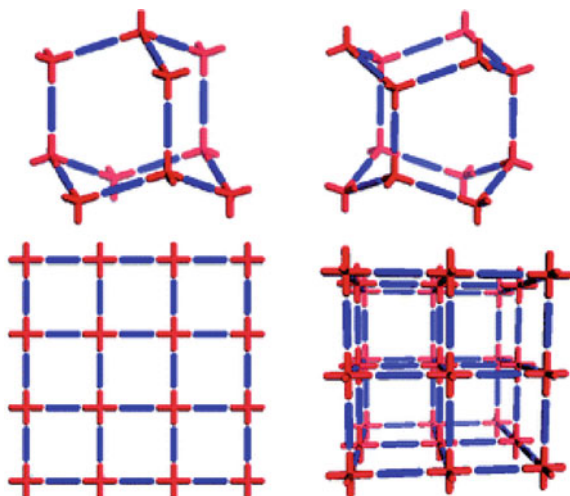
which provides wide possibilities for design of materials with high porosity as compared to traditional dense solid materials.

The CP design can be considered as «construction games»: the final architecture depends on building bricks (organic ligands, metal ions, counter-ions, solvent molecules) and their compatibilities [30]. Metal ions included in CP differ by size, ligand-field stabilization energy, hardness or softness, and coordination geometries (linear, tetrahedral, square-planar, octahedral, trigonal-planar, etc.). Dimensionality of CP is mostly determined by nodes (metal ions): in 1D motifs a metal ion is coordinated with two ligand molecules, at that metal ions and organic ligands are connected alternate; 2D compounds are obtained with three or four molecules of the ligand coordinated around a metal ion, and the monomer motif extends in two directions; 3D networks are built with metal ions of the highest coordination numbers (tetrahedral and octahedral nodes). These architectures can be schematized using nodes and links (Fig. 6.5).

Organic ligands act as bridging organic groups between metal ions, which should be polydentate with minimum two donor atoms, mainly N-, O-, or S-donors for CP production. They differ from each other by their charges, in particular, mostly used are neutral or anion ligands. One more structure-defining factor is a body of ligands: shape (rigid or flexible), length (space between chelating fragments), functionality (presence of heteroatoms, alkyl chains, aromatic rings, etc.). And, finally, ligand molecules can be symmetrical, chiral, etc., i.e. combining different functionalities in one molecule. It is suggested [14] that ligands should be classified as ditopic, tritopic, tetratopic, hexatopic, octatopic, mixed, desymmetrized, metallo- and N-heterocyclic spacers.

Apparently, elementary units are not always simple, and there are many 1D, 2D or 3D spatial types with various architectures and functions depending on building
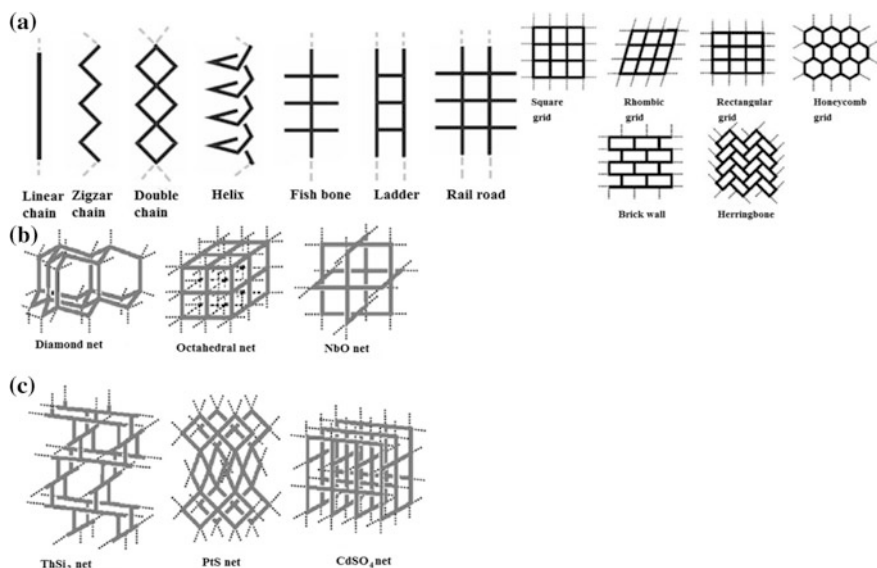
Fig. 6.5 1D (**a**), 2D (**b**), 3D (**c**) polymers motif

units and experimental conditions [95, 124], therefore, the task of prediction structures and properties of the purposed CPs is still important [64, 125–129].

Though the node-and-spacer approach can provide controlled MOF design and synthesis, at least, to a certain degree, under real conditions of synthesis control over different probable coordination geometries of metal ions and coordination bonds is not always possible.

6.2 Reticular Chemistry

A substantial progress is in using of the molecular building unit approach [130–135], which considers some discrete components with known characteristics as individual building units for design of the CP final structure. Actually, efficient coordination geometry of ions of one metal and/or inorganic cluster, as well as a shape of respective polydentate organic ligands, directs MOF formation, as a rule, on the basis of known targeted network topologies. This strategy proposes a promising way not only to design and building of desired CPs, but to purposed functional materials, since necessary functions or properties can be included at the stage of a molecular building unit design. For primary design of the targeted structures, it is necessary to use molecular building units, which have rigidity and desired orientation before the assembling process. Since inorganic molecular building units are, as a rule, formed in situ, it is principally important to define the

respective conditions of the reaction, under which they are consistently generated. After this aspect is realized, the targeted CPs can be created by combination of inorganic molecular building unit and reasonably chosen organic ligands (which can work as bridging spacers or additional rigid guide molecular building units depending on a targeted framework).

Building of MOFs from molecular building units advanced the designing process and has a set of necessary conditions for assembling of purposed networks [136]. In particular, substitution of metal ions by organic clusters known as secondary building units (SBUs), made it possible to substantially widen a range of rigid ligands, which can be used as spacers. If, for example, carboxylate building units are considered (which are most often realized in MOF structures), several basic and well known in classic coordination chemistry SBUs can be chosen: paddlewheel $M_2(OOCR)_4L_2$, $M_3O(OOCR)_6$, $M_4O(OOCR)_8$. Among them paddlewheel $[M_2(OOCR)_4]$ fragments are most widely used in CP design, since they are ubiquitous in coordination chemistry and their square geometry is versatile in this context. Metal clusters based on carboxylates have proven their efficiency in generation of targeted molecular building units in situ, which allows access to expected and new MOFs. This strategy is called reticular chemistry [132], which provides strong bonds between inorganic and organic fragments. In fact, reticular synthesis can be described as the self-assembling process assigned by reasonably rigid SBUs into beforehand determined ordered structures (networks), which are held together by strong bonds. Its main difference from retrosynthesis of organic compounds is in preserving of structural integrity and rigidity of building units remained unchanged during the entire building process, this is the important aspect that can help realize completely advantages of crystal engineering. Just in the same way reticular synthesis should be distinguished from supramolecular assembling, since in the first case building units are connected by strong bonds throughout a crystal. Therefore, design of MOFs requires not only respective choice of necessary building units, but predicting of formed structure. It is principally important that different spacers give the same framework topology, which makes it possible to use isoreticular principle for systematic generation of MOFs series with different pore size, and to adjust desired properties of a framework. Using bridging organic ligands of different length, but containing similar by nature, position and type functional group substituents, provides production of porous MOFs with the same method of metal centers linking, but different geometric characteristics of a structure (unit cell parameters, linear sizes, volume of voids, etc.), which are called isoreticular [137]. These isoreticular series are designed from similar general framework topologies, at that in these series the surface area can be proportional to a ligand size [138]. New directions of design can be reached using augmentation or decoration of MOFs ligands, which has also been shown for production of porous materials focused on open frameworks for maximally available surface area.

The main driving force of fast progress of MOFs is in their capacity for design: desired structure can be a target for reasonable choice of organic spacer and SBU [14, 44, 139–142]. SBUs have obvious advantages over simple metal ions as nodes; in particular, their larger sizes and higher rigidity make it possible to obtain greater

pores available for prevention of decomposition of highly porous structures and destabilization of interpenetrating frameworks. By now a great number of SBUs of different shapes is obtained [143]; however, search for new SBUs continues and, as is expected will advance designing of MOFs aimed at certain applications.

Reticular chemistry works best with rigid spacers, which give precise fixation of metal ions in a lattice sites or SBUs, which provide rigidity of MOF structure and determine a framework topology [144]. Despite of considerable progress achieved in rational design of porous MOFs, serious problems remain, especially as regards using of flexible spacer and projecting of highly thermally stable structures. By comparison CP structures with flexible and rigid spacers, isoreticular principle limit is defined [145]. Presently it is necessary to study more profoundly interaction between inorganic and organic building units in several length scales, in order to overcome these problems [29].

It is important to highlight that in accordance with the concept of reticular synthesis, properties of prototype MOF platforms can be directed through universal functioning or custom-design of organic spacers. As an example, we shall consider synthesis of some mesoporous M-Pp-based MOFs, in particular, polymer coordination networks PCN-600(M) (M = Mn, Fe, Co, Ni, Cu) using preliminary assembled $[Fe_3O(OOCCH_3)_6]$ building unit (Fig. 6.6) [146]. PCN-600 has shown 1D channel, as big as 3.1 nm, and experimental porous volume of 1.80 cm^3 g^{-1}, and also very high stability in water solutions at changing pH value from 2 to 11. Another example is 1D CP with $[Fe_4O_2(O_2CCMe_3)_8(L)]_4$ block (L = hexamethylenetetramine), which contains deliberately chosen central core $[Fe_4(\mu_3-O)_2]^{8+}$ and has zigzag shape [147].

Using preliminary choice of molecular building units containing given structural and geometric information, which is coded by the main network, MOFs with deliberate properties and functionalities are obtained [28, 148, 149]. The assembling process
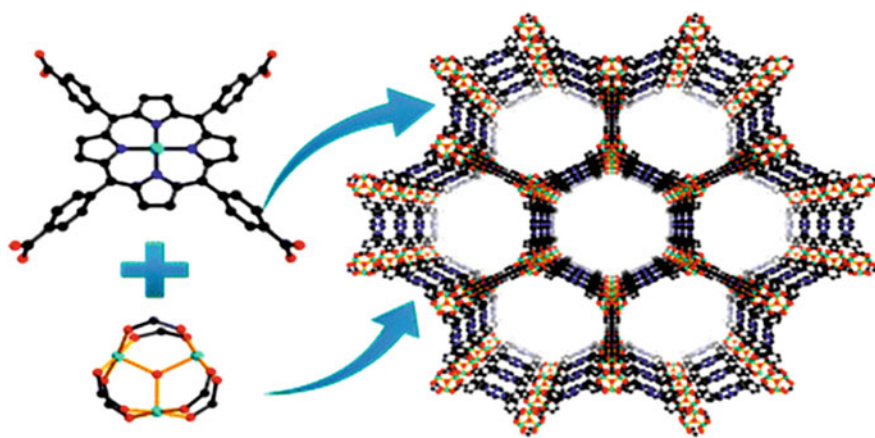
Fig. 6.6 The structure of PCN-600(M) synthesized from M-Pp (C: black, N: blue, O: red, metal: cyan) and preformed metal cluster (C: black, O: red, metal: cyan) [146]

based on the approach of molecular building unit, provides access to MOFs with simple topologies, such as edge-transitive networks (networks with one type of edge). Among MOFs primary emphasis was done on 3-periodical networks due to their potential for applications, at that most widespread types of 3-periodical MOFs are based on the simplest 4-connected nodes, such as **dia**, **nbo**, **cds**, and **1vt** [150]. Moreover, their modulus nature assumes that prototype MOFs can be blueprints or platforms for a great variety of derivatives offering controlled pore sizes and adjusted surfaces of pores. Successful incorporation of molecular building unit approach for rational MOF design requires meeting the following demands: choice of ideal blueprint of a network, which is exclusive for assembling of its respective basic building constructions, and finding of reaction conditions, which provide consistent in situ formation of targeted inorganic molecular building unit corresponding to extended basic building units (figure vertices) of the targeted network.

Ideal blueprint begins from a network, which is singular, exclusive for assembling of these building units, predominantly includes polyhedral cavities with 3D adjacent channels, and is insensitive to self-interpenetration after extending and/or decoration of a network. All necessary demands are met by **rht** network, which is a special singular network for assembling of 24-connected vertices (rhombobicuboctahedral (**rco**) figure vertices) and 3-connected vertices (triangular vertex of a figure) [151]. Exclusive character of **rht**-MOF provides extending without thinking of interpenetration, and substitution/decoration and functioning of a building unit.

It should be noted that uninodal and binodal networks with high connection, which have at least one node with $n \leq 8$ connectivity, are most appropriate for CP design, since they propose limited amount of possible networks for assembling of their nearby highly-connected molecular building units [152]. A difficulty in finding the reaction conditions, which provide formation of highly-connected molecular building units ($n \geq 12$) is directly characterized by relatively small amount of MOFs with high connectivity [77, 148, 153–159].

This strategy is expanded using preliminary formed homo- and heterometallic polynuclear complexes used as node [160]. Presence of two or more metal ions in a node brings to new network topologies and new properties following intra- and inter-node interactions. One of main tasks in this approach is prediction of topology of a polymer structure, since many factors take part in a framework formation (stoichiometric prevalence of metal ions, nature of ligands, M–L ratio, temperature of reaction, solvent and pH of solution) [161–172].

6.3   Metalloligand Strategy

Though a great amount of building units has brought to vast variety of target materials, using of well-defined metal complex as a building unit (i.e. metalloligand) is unique for building of projected architecture [173–179]. CP assembling based on

metalloligand approach goes mainly in two stages: (1) synthesis of a metalloligand by interaction between well-defined ligands and metal ions (mostly 3d metal ions), and (2) reaction of the metalloligand with a second type of a metal ion, which plays a role of nodal units in a framework. The metalloligand used as a building unit provides structural rigidity, which puts ancillary functional groups in predetermined conformation. These ancillary functionalities can then coordinate a secondary metal ion and take part in self-assembling through such weak intermolecular interactions as H-bonds. Two classes of metalloligands are respectively distinguished, which have competitive M–L-bond sensitive groups, and H-bond sensitive functional groups. This is how a metalloligand differs from a simple complex, in which a metal ion is coordinated with a certain number of «ordinary ligands», which do not contain appended functional group.

CP design based on the metalloligand approach has some advantages as compared with traditional mixing of a respective ligand and metal. One of the advantages is precise control over location of applied functional groups offered by a metalloligand; therefore a typical tendency for it is to generate highly ordered architectures. Moreover, metalloligand is, as a rule, rigid than traditional organic ligand, therefore it induces structural rigidity in a purposed CPs and gives durable and stable networks with permanent pores. It is also important that a metalloligand can rationally adjust pore sizes and their environment by interaction between ligands and spacers, therefore, topology and interior surface functionality of a network can be updated. Rather important is the fact that a metalloligand provides linking centers for coordination of a secondary metal ion, which facilitates positioning of two or more metals in immediate proximity to each other. This results in easy building of heterometallic CPs, whose synthesis is a complicated problem. And, finally, the metalloligand approach is very attractive for targeting of functional porous materials, since it allows double chemical functioning of obtained architecture by incorporation either of metal- or ligand-based functional groups into a network.

Among metalloligands the widest used as building units are M-Pp [180–217]. By integration of different functional peripheral substituents into β-pyrrol and/or *meso*-positions, M-Pp can have several multifunctional properties. With M-Pp used as building units for MOFs, easy molecular modification of Pp widens possibilities of structural design. Since most elements of periodic table can be included in Pp, different metal centers can be integrated into porous surface of MOFs without changing a framework topology. Moreover, using of M-Pp as building units for MOFs gives an opportunity to adapt photochemical, redox, catalytic, and other properties of frameworks.

Most widely used Pp-based ligands for CPs building are tetrakis(4-carboxyphenyl)-Pp (L^1) and tetrakis(4-pyridyl)-Pp (L^2). Using those various multiporphyrin frameworks with different topology and dimensionality are built on the basis of coordination of their peripheral carboxyphenyl or Py fragments. Therefore, L^1 и L^2 are almost inexhaustible sources for building of either H-bonding or M–L-driven CPs. It should be noted that for design of Pp-based MOFs, clusters formed with rigid Lewis acid metals, such as Zr_6, Hf_6, Zr_8, Hf_8 and Fe_3, are used as most stable SBU [146]. Thus,

systematic study of Zr and Hf-Pp MOFs has brought to discovery of isostructural PCN-221(M) based on metalloligands and Zr_8 или Hf_8 clusters [197]. In particular, cluster Zr_8O_6 is characterized by idealized Zr_8 cube, in which each Zr atom is in one vertex and each face of the cube is crowned with one μ_4-oxygen atom. On each face of the cube carboxylate from Pp ligands bridges two Zr atoms thus obtaining 3D MOF with very rare (4,12)-connected **ftw** topology, in which two types of polyhedral cages with diameters ~ 1.1 and ~ 2.0 nm and cage opening ~ 0.8 nm are found. As another example we shall notice a solvothermal reaction of Fe–L^1, $ZrCl_4$ and benzoic acid in DEF during 48 h at 120 °C, which brings to PCN-222(Fe) with a framework consisting of square-planar Pp ligands linked to Zr_6 clusters [180]. In this CP each Fe–L^1 block is coordinated with four 8-connected clusters Zr_6 with twisted angle forming 3D network with Kagome-like topology (Fig. 6.7). It is remarkable that the framework is mesoporous containing large 1D hexagonal open channels with a larger diameter 3.7 nm ranking among the largest for MOFs [218, 219]. Besides, this framework is preserved even after immersion in concentrated HCl, which is rarely seen in MOF materials. We shall also notice highly stable MOFs with 3D nanochannels PCN-224
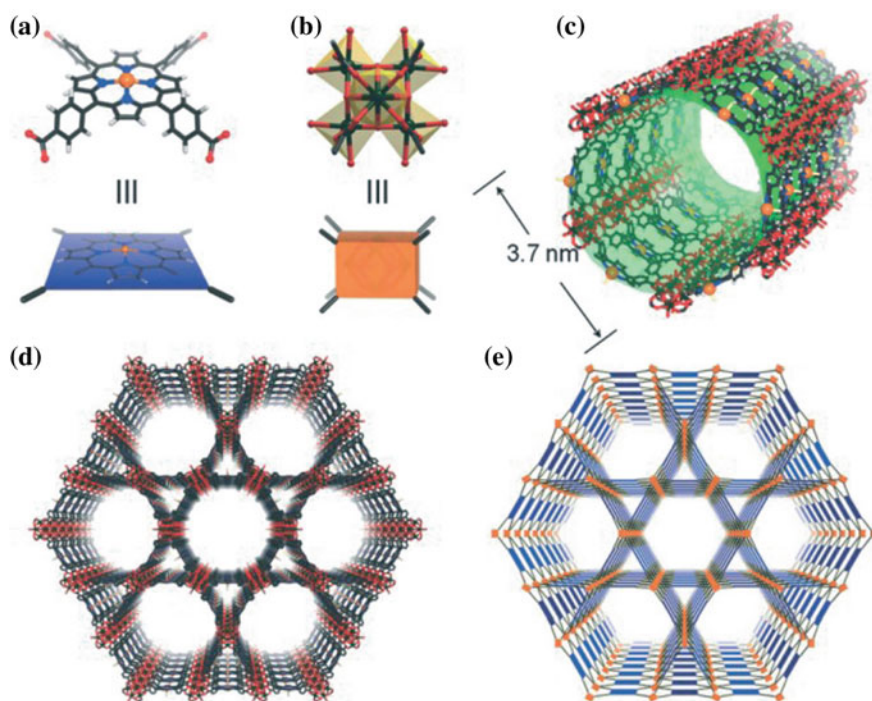
Fig. 6.7 The crystal structure and underlying network topology of PCN-222(Fe). The Fe-L^1 (**a** blue square) is connected to four 8-connected Zr_6 clusters (**b** light orange cuboid), generating a 3D network with Kagome-like topology (**d, e**) and large 1D channels (**c**; green pillar). Zr: black spheres, C: gray, O: red, N: blue, and Fe: orange [180]

(Ni, Co, Fe) assembled with six-connected Zr_6 cluster and M–L^1 metalloligands [220]. The PCN-224 series not only demonstrates high BET surface area (2600 m^2 g^{-1}), but also stays unchanged at pH of aqueous solution from 0 to 11.

Metal-metalloporphyrin frameworks (MMPFs) form a class of coordination networks self-assembled using reasonable choice of metal-containing SBUs and specially developed M-Pp metalloligands [31]. As an example among CP of MMPF series we shall consider MMPF-6 based on FeL^1–Cl metalloligand and SBU Zr oxide cluster, which is obtained under solvothermal conditions (Fig. 6.8) [181].

Porous MMPFs including $[Zn_2(HCOO)_2(MnL^1)]$, $[Cd_2(HCOO)_2(MnL^1)]$, $[Zn_2(HCOO)(FeL^1)]$ and $[Cd_3(H_2O)_6(\mu_2\text{-}O)(FeL^1)_2]$ blocks are synthesized by heating the mixture MCl–L^1 (M = Mn and Fe) and nitrates M′ (M′ = Zn or Cd) in DMF and acetic acid mixed solvent [221]. First three compounds are built from M′$_2$(COO)$_4$ paddlewheel subunits linked with ML^1 bridge and formate ligands for formation of their 3D connectivity. Formate column is heterogeneously connected with M and M′ cations in two first CPs and links homogeneously M′ cations in third CP. A μ_2-O bridging FeL^1 dimer plays a role of decadentate ligand for linking of 10 Cd cations with formation of interesting 3D coordination network of fourth CP (Fig. 6.9).

An example of PPF series is PPF-1 (PPF is porphyrin-paddlewheel framework) with $[Zn_2(Zn\text{-}L^1)]$ block which is assembled from Zn–L^1 metalloligand, linked by Zn paddlewheel clusters, $Zn_2(COO)_4$ as inorganic SBU with formation of 2D square network packed in AB packing pattern (Fig. 6.10) [193].

The reaction of M–L^1 (M = Co, Ni, Cu, VO) with lead nitrate gives MOFs with $[Pb_2(M\text{-}L^1)]$ blocks, which differ in framework topologies and Pp configurations changing from flat to wavy to bowl-shaped [222]. It is important that Pp cores play pivotal role in the formation of different coordination frameworks by controlling Pp stacking, L^1 coordination modes and the coordination spheres of the Pb(II) cations.

We should also notice CZJ-1 (CZJ = Chemistry Department of Zhejiang University) with $[Zn_2(MnOH\text{-}L^1)(L')]$ block, where L′ = N,N′-di(4-pyridyl)-1,4,5,
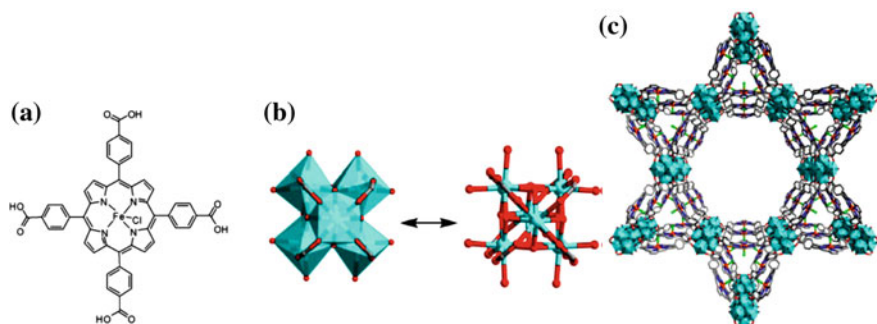
Fig. 6.8 **a** FeL^1-Cl metalloligand. **b** $Zr_6O_8(CO_2)_8(H_2O)_8$ SBU. **c** Hexagonal and triangular 1D channels of MMPF-6. Color scheme: C, gray; O, red; Cl, green; Zr, turquoise
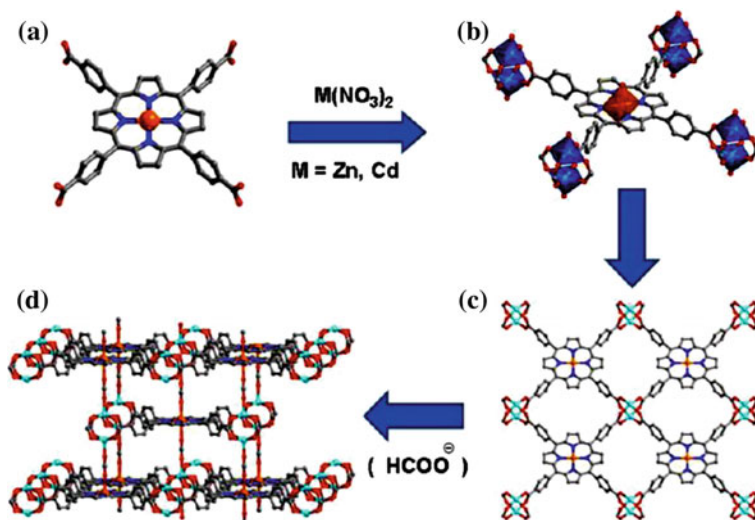
Fig. 6.9 **a** Deprotonated Mn-Pp ligand, **b** view of the coordination mode of Mn-Pp and the coordination environments of M′ and Mn atoms, **c** lamellar network of Mn-Pp linking up M′$_2$(COO)$_4$ paddlewheel SBUs, **d** perspective view of the 3D Pp framework. Color codes: M′, cyan or light-blue square pyramids; Mn, orange; O, red; N, blue; C, gray

8-naphthalenetetracarboxydiimide [223]. This porous MOF has a type of twice interpenetrated cubic α-Po topology, in which Zn$_2$(COO)$_4$ paddlewheel clusters are bridged by MnOH–L^1 in 2D sheets additionally linked by bridging organic pillared spacer L′ with formation of 3D porous structure.

Functional MOF assembled from Pd–L^1 metalloligand and Cd(II) connecting nodes is an interesting topologic network structure and has high framework stability [224]. In particular, in this CP each Pd–L^1 metalloligand plays a role of octadentate ligand coordinated by seven Cd atoms from four neighboring Cd chains, which brings to formation of 3D framework structure (Fig. 6.11) containing two types of channels with dimensions 4.61 × 12.55 Å^2 and 8.27 × 9.32 Å^2 along *a* axis. Besides, the framework remains undamaged after solvents are removed or exchanged with other guests showing its good framework stability.

An example of using Pp ligand L^2 is 3D porous MOF with [Zn$_2$Sn(IV)(L^2)] block synthesized by heating of mixture of Sn(IV)(OH)$_2$L^2 and Zn nitrate in DMF and CH$_2$Cl$_2$ at 50 °C during five days [225]. Each Sn(IV)–L^2 metalloligand is coordinated with four Zn atoms with formation of 2D framework structure, at those lamellae plates spread into a porous 3D network through links between formates and Sn atoms in Pp cores (Fig. 6.12).

Among other used Pp ligand, we shall notice 5,15-bis(dicarboxyphenyl)-Pp. Thus, for example, frameworks with [Cu$_2$(ML)]$_n$ block have been obtained from ML metalloligands, where M = Zn, Ni, Pd, MnCl, Ru(CO) [226] using two different methods: interaction between Cu nitrate and ML in DMF at 80 °C during 24 h or by

Fig. 6.10 a Building units of
PPF-1, Zn(COO)$_4$
paddlewheel (left) and Zn-L^1
(right) (C-gray, N-blue,
O-red, Zn-light gray). b 2D
Pp paddlewheel sheet. c View
along the [001] direction
showing two layers of PPF-1
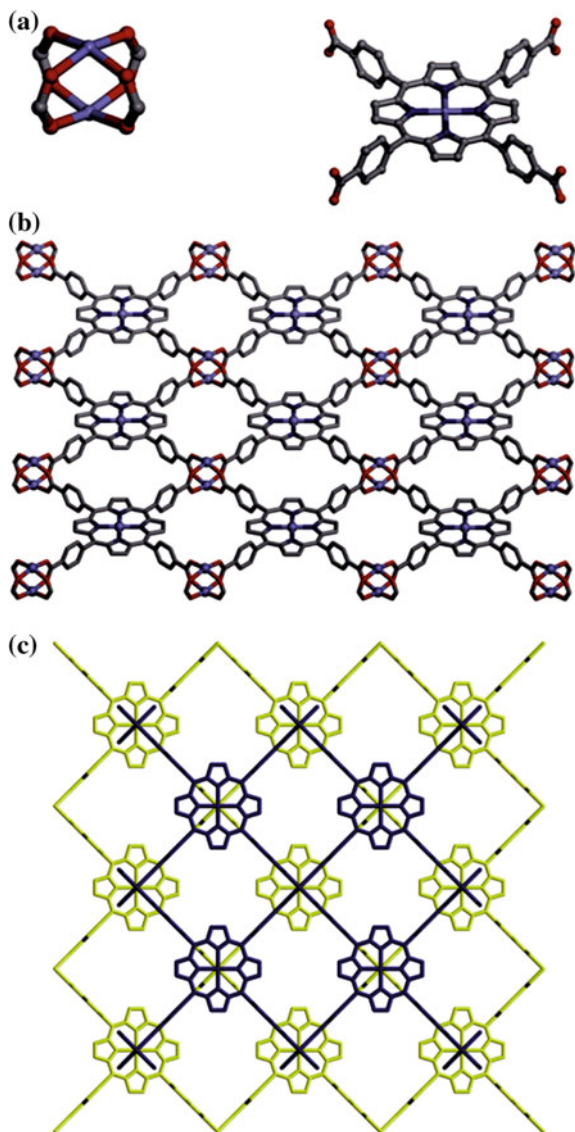
diffusion of triethylamine vapor into the abovementioned mixture. It is interesting
that this framework forms 3D network consisting of two-component combination
(Cu$_2$ paddlewheel nodes and ZnL building units) and having internal spherical cavity
of 20 Å in diameter. This interior cavity is surrounded totally by 16 available metal
centers of two different metals, i.e. with eight Zn atoms from ZnL blocks and eight
Cu atoms from paddlewheel units (Fig. 6.13). In another example, narrowly dis-
tributed nano- and micro-meter CPs are obtained from Mn(III)–L metalloligand and
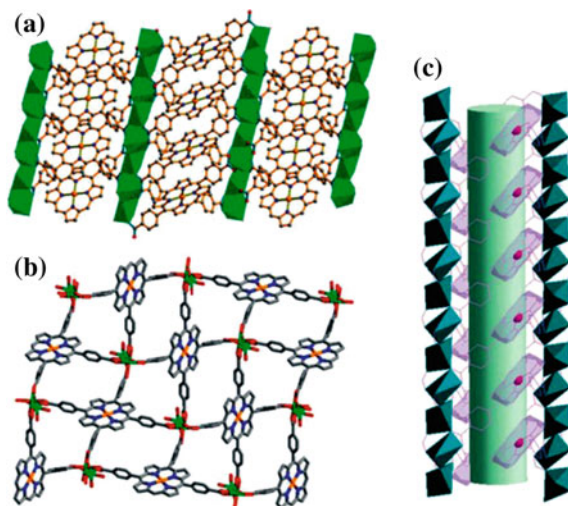
Co acetate, in which morphologies are diversified from amorphous spheres in crystalline cubes through different periods of reaction (Fig. 6.14) [227].

In order to develop CPs based on Pp ligands with a possibility to coordinate more metal centers, more than four carboxyl or Py groups were involved as, for example, in octatopic Pp-ligand 5,10,15,20-tetrakis(3,5-biscarboxyl-phenyl)-Pp [185, 189]. In particular, it is used for building of three porous M-Pp frameworks ZJU-18, ZJU-19 and ZJU-20 (ZJU = Zhejiang University) [189], whose structures are 3-periodical, binodal, edge-transitive **tbo** networks (Fig. 6.15) showing inter-crossed porous windows of about 11.5 Å and porous cavities of about 21.3 Å in diameter. These three isostructural MOFs were synthesized by heating of Mn(III) Cl–L and MnCl$_2$, NiCl$_2$ or CdCl$_2$ mixture, respectively, in mixed solvent DMF and acetic acid at 80 °C during a week.

We shall also notice MOF based on tetrazolyl-Pp with {[Mn(II)]$_4$Cl[Mn(III) Cl-L]$_2$} block, called UTSA-57 (UTSA = University of Texas at San Antonio), which is built from Mn$_4$Cl(L)$_8$(H$_2$O)$_4$ clusters, linked with metalloligand Mn(III) Cl–L (Scheme 6.1) [228]. UTSA-57 is a rare **scu** MOF topology and is built of 8-connected bridging SBUs with 1D square nanotube-like 20 Å channels along *c* axis. Besides, UTSA-57 presents 3D stable microporous structure.

An example of metalloligand for MOF formation through H-bonds can be Co(II)-5,10,15,20-tetra(4-(4-acetateethyl) phenoxy) phenyl-Pp [229]. In it M-Pp molecules are linked with each other by intermolecular H-bonds with formation of 2D layer, which is additionally linked by π···π interactions for formation of 3D supramolecular structure having one type of micropores with 3.98×6.47 Å^2. MOF has a permanent porosity with Langmuir surface area 158.79 m^2 g^{-1} and BET surface area 97.70 m^2 g^{-1}. In other example M-Pp coordination framework [Co(H$_3$L)]$_n$, where H$_6$L = *meso*-tetra(4-carboxyphenyl)-Pp having 2D layered coordination network structure, shows
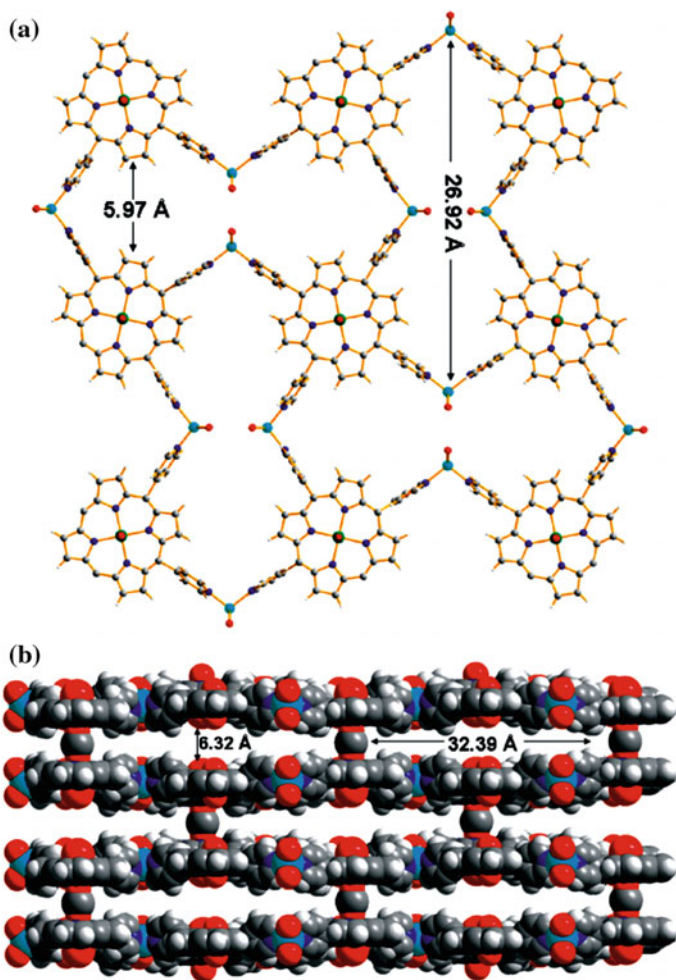
Fig. 6.12 a The lamellar network of Zn(II) atoms linking Sn(IV)-Pp as viewed along the *c* axis; and **b** a side view of the 3D network of the lamellae linked by the formate struts along the *b* axis [225]

H-bonds between carboxyl groups within 2D layer as well as between neighboring layers.

The popular metalloligands are metallosalens [138, 175, 230–238], in which additional functional groups, such as carboxylate [174, 175, 235, 239–242], Py [236, 237, 243] and benzoate-groups [138, 230] are in *para-* and *meta*-positions with respect to OH-groups on aromatic ring. As an example it can be noted using solvothermal synthetic strategy for CPs building based on metallosalens as spacers [78, 244, 245]. In this strategy a metalloligand based on carboxy-functionalized salen spacer 2,6-bis[(4-carboxy-anilino) carbonyl] pyridine and a metal salt are
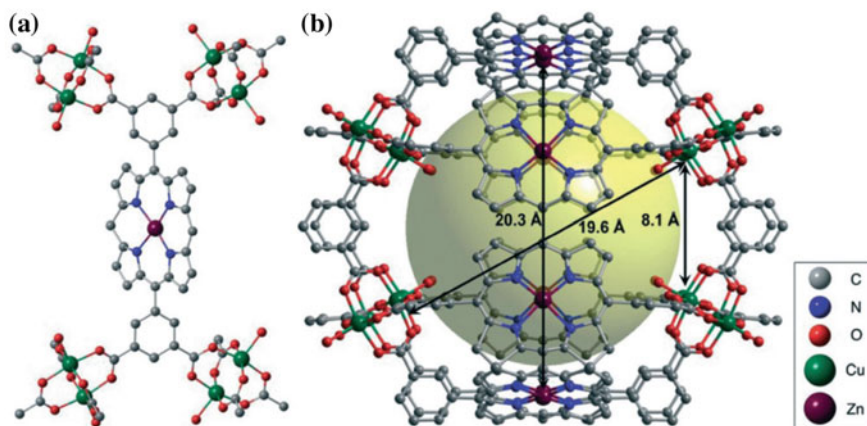
Fig. 6.13 **a** A ZnL moiety of [Cu$_2$(ZnL)]; and **b** a cage consisting of eight ZnL ligands and eight paddlewheel Cu$_2$ nodes [226]
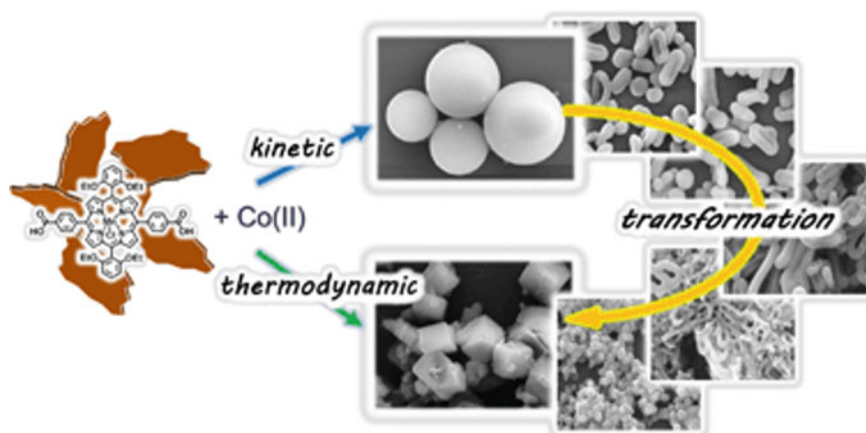
Fig. 6.14 A series of narrowly dispersed nano- and microsized CPs prepared from a Mn(III)-Pp metalloligand acid and Co(OAc)$_2$, which morphologies diversified from amorphous spheres to crystalline cubes by varying reaction periods [227]

solved in DMSO/DMF mixture, and then heated, which brings to CPs formation with governed size from nano- to micro-meter level [235]. The ligand chelates metal cations in the center of the structure and provides two terminal carboxylate groups for CP growth. The particle size is regulated by changing the reaction temperature, so that a temperature rise leads to bigger particles. First formed nanowires aggregate with formation of cub-like clusters, which undergo intrastructural fusion into uniform cubic-shaped particles (Fig. 6.16). Besides, the size of the formed structures is influenced by DMSO/DMF ratio, at that higher content of DSMO brings to bigger cubes.
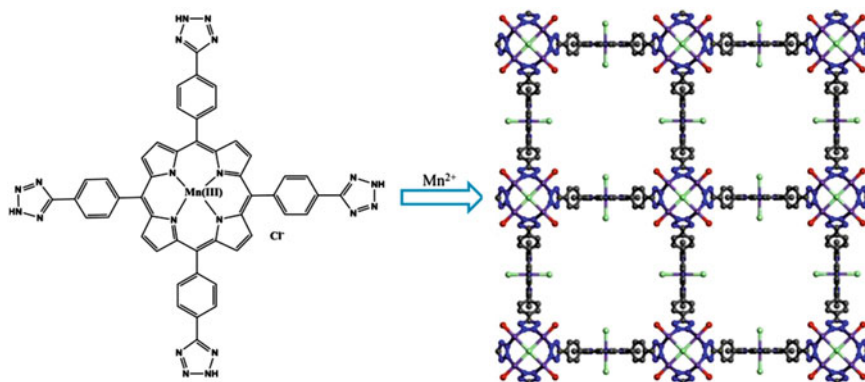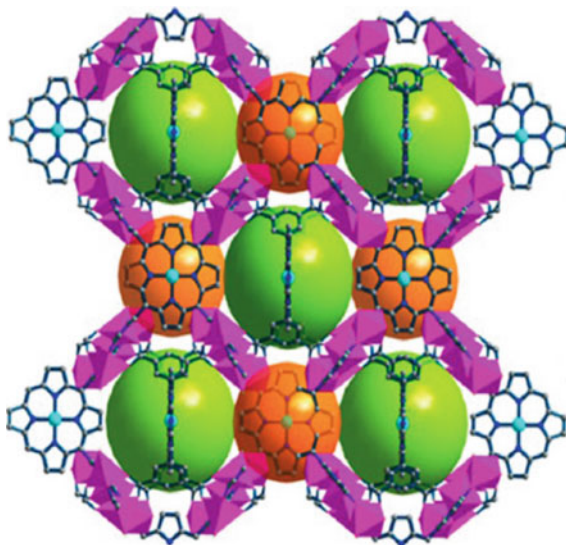
Scheme 6.1 A representation of processes from metalloligand Mn(III)Cl-L to a 3D crystal structure of UTSA-57 [228]

Substantial interest is in fabrication of chiral CPs based on salen-type metalloligands. Thus 1D homochiral CPs with $[Ni_3L(L')_2]_n$ block are based on enantiopure Py-functionalized NiL metalloligand with (R,R)–(−)–1,2-cyclohexanediamino-N,N′-bis(3-*tert*-butyl-5-(4-pyridyl)salicylidene) or (S,S)–(−)–1,2-cyclohexanediamino-N, N′-bis(3-*tert*-butyl-5-(4-pyridyl)salicylidene), where L′ = 4,4′-biphenyldicarboxylic acid [245]. Each NiL uses one terminal Py group as un-bridging pendant metalloligand for coordination of achiral NiL block and L′ with a helical chain formation, while another Py group remains non-coordinated. It is important that both L ligands should contain left- and right-hand helical chains formed from achiral building units, while
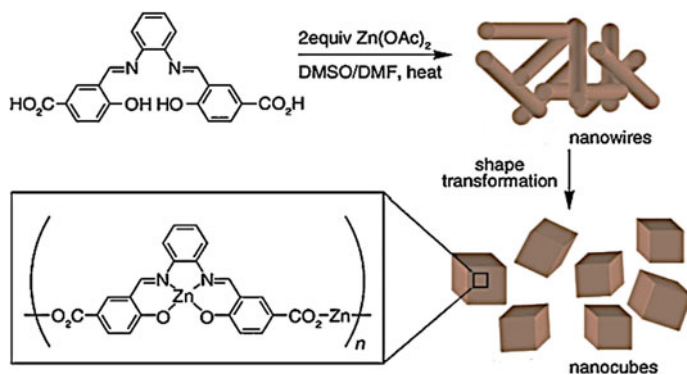
Fig. 6.16 Preparation of Zn-ML-Zn CP as nanowires and their subsequent transformation into nanocubes [235]

Fig. 6.17 View of left-handed (**a**) and right-handed (**b**) helix polymeric chains of [Ni₃L(L′)₂]ₙ
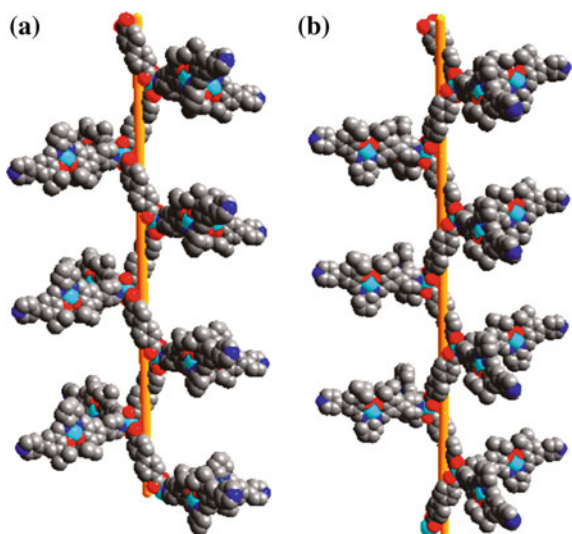
NiL as remote external chiral source is perpendicular to the main chain of helixes (Fig. 6.17).

Widely used in the metalloligand approach is pseudo-reversible solvent-induced process, in which metalloligand and a metal cation are solved in a solvent, in which they and the resulting CPs are well solved, and then another solvent (sometimes called «poor» or «weak» solvent) is integrated into a system for CPs deposition [177]. It highly important that this method provides control over particle size through fine changes under the reaction conditions. As an example, production of homochiral salen-based CPs particles and crystalline rods using acid-functionalized metallosalen ligands can be considered [138]. Spherical particles are obtained by

slow diffusion of diethyl ether in Py solution containing 1:1 mixture of Ni acetate and metallosalen (Fig. 6.18). The process is reversible at addition of excess of initial solvent, which is often coordinated with metal nodes and competes with ligands taking part in CP assembling. It is interesting that polarity of a depositing solvent also has effect on size of forming particles: using of diethyl ether as a depositing solvent brings to formation of coarse micrometer sized amorphous spherical particles, while using of methanol provides production of crystalline rod-like structures.

A special attention should be given to the metalloligand strategy in synthesis of heterometallic CPs, since used metalloligand already containing ion of an initial metal fits ideally for interaction between respective secondary metal ions [78, 244–248]. In conventional synthesis using the reaction between mixture of metal salts and organic ligands it is very difficult to control synthesis of heterometallic complexes, since there is always high probability of formation of homometallic polynuclear complexes. At the same time, when metalloligand strategy is used, side reaction is minimal, and exclusively heterometallic CP can be obtained. A great number of metalloligands is developed, which provide targeted production of ordered heterometallic architectures [249–261]. As an example of using metallosalens in synthesis of heterometallic CPs we shall consider dipyridyl [236] and dicarboxylate [230] functionalized (salen)MnCl metalloligands incorporated in the framework of Zn-MOFs structure, and also CPs formed via interaction between [bis(catechine)-salen]Mn(III) with several di- and trivalent metal ions [231]. The reaction of *mer*-[Ru(III)(CN-L)(CN)$_3$]$^{2-}$ tricyanoruthenium(III) salen complex with MnCl$_2$ or CoCl$_2$ brings to 1D double chain
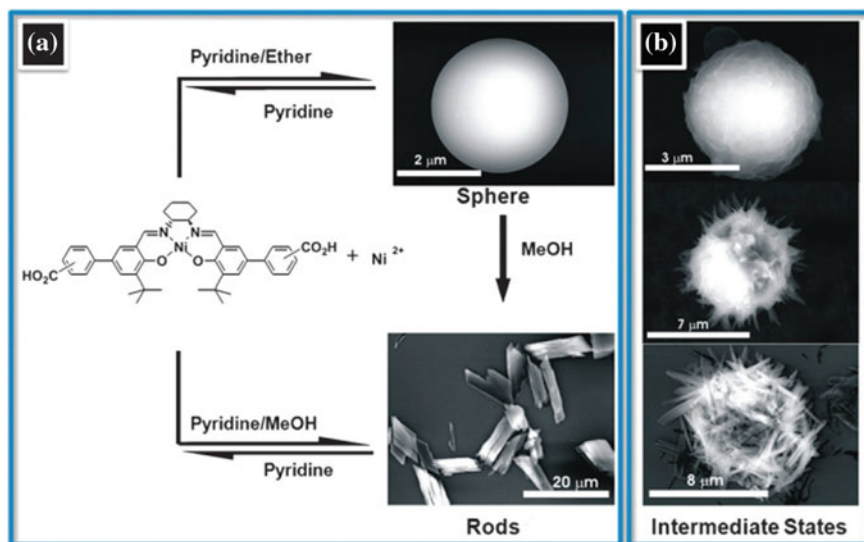
Fig. 6.18 Dynamic interconversion of salen-based CP spherical particles into rods (**a**) from precursors to spheres to rods and (**b**) intermediate states

of cyan-bridged heterometallic CP (Fig. 6.19) [262]. Interesting heterometallic Cu (II)–Zn(II) CPs **2A** and **2B** are synthesized by interaction between CuL metalloligand, where H_2L = N,N'-bis(salicylidene)-1,3-propanediamine with Zn perchlorate and sodium dicyanamide (dca) using different molar ratios of reagents (Scheme 6.2) [263]. The obtained compounds are 2D and 3D CPs, respectively, with a common $[(CuL)_2Zn(N(CN)_2)_2]$ trinuclear block, in which dca fragments get $\mu_{1,5}$-bridging coordination regime. It is interesting that the isomeric CPs is a rare example of «genuine supramolecular isomerism». It should be noted that the similar $[CuL^1]$ metalloligand (where H_2L^1 is *N,N'*-bis(α-methylsalicylidene)-1,3-propanediamine) on reaction with zinc perchlorate hexahydrate and sodium dicyanamide, in a 2:1:2 molar ratio at room temperature, resulted in a hetero-metallic discrete trinuclear complex, $[(CuL^1)_2Zn(N(CN)_2)_2]$ (**1**).

Cu(I)-salen CPs $\{[NiL]_2[Cu(I)CN]_9\}_n$, $\{[Cu(II)L]_2[Cu(I)CN]_9\}_n$ and $\{[NiL][Cu(I)I]_2\}_n$ are obtained by direct linking of metallosalen precursors with $[Cu(I)CN]_n$ chains and Cu_2I_2 clusters using the metalloligand strategy (Scheme 6.3) [264]. In these CPs efficient integration of catalytically active transition metals of Ni(II)/Cu (II)(salen) blocks and photoactive Cu(I) species in one solid polymer is achieved, which makes it possible to obtain materials with double catalytic properties.

We shall also notice using of the metalloligand strategy for combination of 3d- and 4f-metal ions, which differ by coordination chemistry and stereochemical geometry, which results in a vast variety of heterometallic complexes beginning from discrete
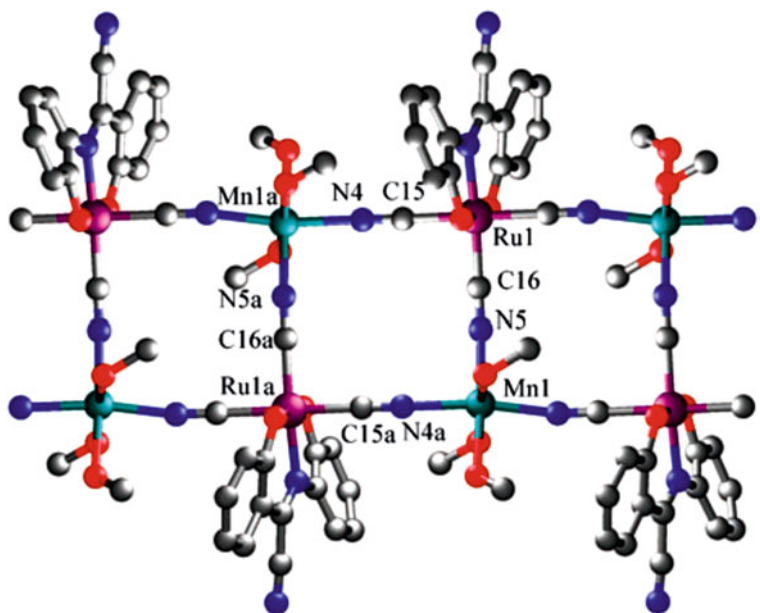
Fig. 6.19 The perspective view of CP based on salen chelate *mer*-[Ru(III)(CN-L)(CN)$_3$]$^{2-}$ c MnCl$_2$
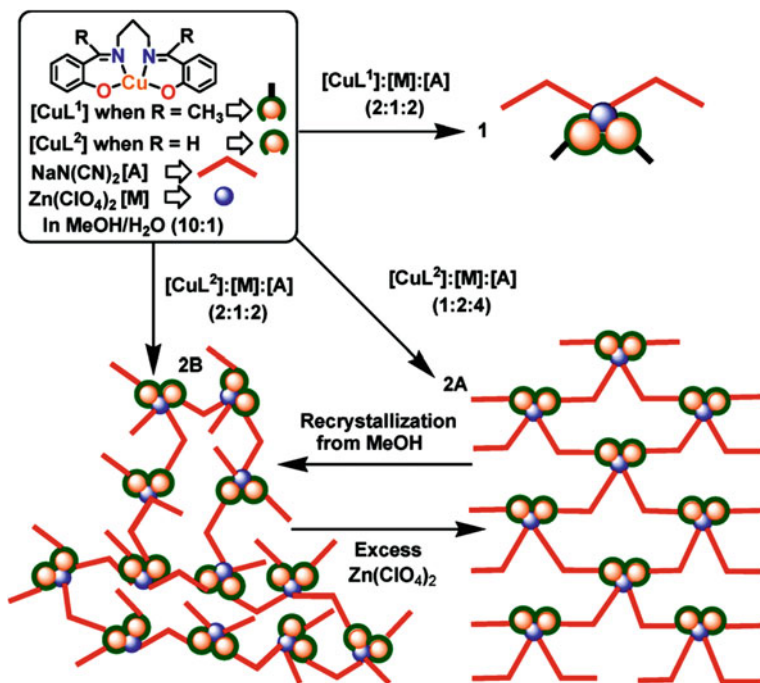
Scheme 6.2 Formation of the compounds **1**, **2A** and **2B**
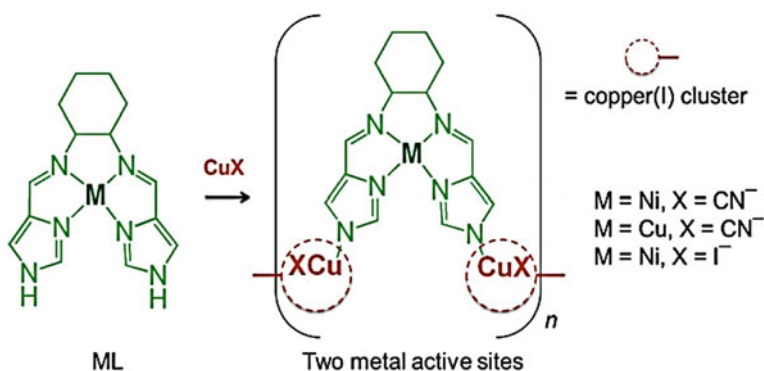
Scheme 6.3 Synthesis of $\{[NiL]_2[Cu(I)CN]_9\}_n$, $\{[Cu(II)L]_2[Cu(I)CN]_9\}_n$ and $\{[NiL][Cu(I)I]_2\}_n$

species to 3D CPs [265]. An example may be using of a Ni-salen complex as a metalloligand for formation of rare-earth element-based CPs with $[Ln_2(NiL)_3]_n$ (Ln = Er, Lu) and $[Dy(NiL)]_n$ [266], $[YbNiLCl]_n$ and $[YbNiLCl_3]_n$ blocks [267]. We shall also notice a Fe-rare-earth element CPs with $[Ln_2(FeLCl)_2]_n$ (Ln = Y, Eu, Gd, Tb, Dy) blocks [268].

Heterometallic CPs based on metallosalens have shown their efficiency in a range of catalytic processes: Mn(II)/Cu(II)-salen MOFs in asymmetric catalysis [178, 230, 236] and separation of chiral and achiral small molecules [248], Mn(II)/Ni(II)-salen 1D CPs in olefin epoxidation [245, 247], Cu(II)/Cu(II)-salen-based 1D CP in three-component Strecker reaction [269].

The interest is strategy of in situ immobilization of metalloligands used for targeted production of homometallic mixed valence Cu(I)/Cu(II) Schiff base CPs [270]. For this purpose, for example, two Cu(II) bulk metalloligands based on three structurally relative isomeric Schiff bases [HL(1-3) = o-, m-, p-pyridinecarbaldehyde isonicotinoyl hydrazone, respectively] are used, which contain chelating and bridging units. Using integration of dca-bridging spacers in one-pot solvothermal reactions, Cu(II) Schiff bases metalloligands are in situ immobilized in two different mixed valence Cu(I)/Cu(II) CPs with $[Cu_4(CN)_3(L1)_2]_n$ and $[Cu_4(CN)_3(L3)_2]_n$ blocks. Besides, formation of three unexpected CPs with $[Cu(L3)_2]_n$, $[Cu(L2)_2]_n$ and $[Cu_2(CN)_2(HL2)]_n$ blocks points to the fact that coordinating segments of ligands and symmetry of metalloligands play a substantial role in this synthetic algorithm.

Wide range of metalloligands is presented by acac-complexes, which are used, for example, in synthesis of heterometallic CPs with $[NiAg_3(acac)_3(NO_3)_2]_n$, $[NiAg_3(acac)_3 (ClO_4)_2]_n$ and $[NiAg_2(acac)_2(CF_3SO_3)_2]_n$ blocks through integration of respective Ag salts into the reaction with $Ni(acac)_2$ metalloligand (Scheme 6.4) [271]. It is important that anions in CPs are decisive factors for formation of different structures. In particular, first CP is outstanding 3D chiral framework, second CP has 2D inorganic layers, third CP shows 2D (4,5)-connected layered architecture.
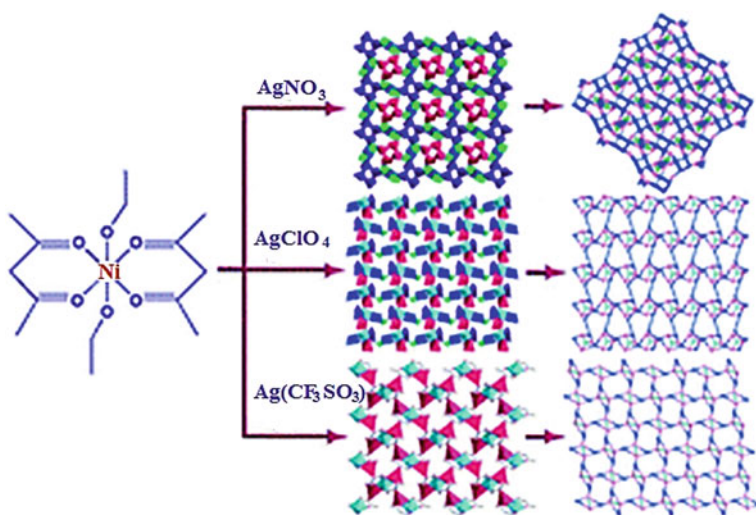
Scheme 6.4 The assembly of three Ag-Ni heterometallic CP

We shall notice crystal engineering of heterometallic CPs based on FeL$_3$ and Fe (L')$_3$ chelates, where L = 1,3-di(4-pyridyl)propane-1,3-dionato and L' = 1,3-di (3-pyridyl)propane-1,3-dionato, which act as metalloligands in reactions with Ag salts forming CPs with [AgFeL$_3$]$_n$ and [AgFe(L')$_3$]$_n$ blocks [272]. It is important that structure of obtained CPs depends on nature of used counter-ions. Thus, reaction between FeL$_3$ and AgBF$_4$ brings to CP, in which Ag centers link metalloligands in discrete nanotubes, while the reactions with AgPF$_6$ and AgSbF$_6$ have given CPs, in which metalloligands are bound in sheets. At the same time interaction between Fe(L')$_3$ and AgNO$_3$ gives layered CP with [Ag$_2$Fe(L')$_3$]$_n$ block. Similar dependence of CP structure on nature of counter-ions is found in reactions of FeL$_3$ with AgX (X = BF$_4^-$, ClO$_4^-$, PF$_6^-$, AsF$_6^-$, SbF$_6^-$, NO$_3^-$, CF$_3$SO$_3^-$, tosylate) (Scheme 6.5) [273]. In particular, 2D CPs [FeL$_3$Ag]X are obtained with pseudospherical anions (BF$_4^-$, ClO$_4^-$, PF$_6^-$, AsF$_6^-$ and SbF$_6^-$), while interaction with Ag(CF$_3$SO$_3$) gives absolutely different type of [FeL$_3$Ag]$^+$ 2D polymer framework, i.e. double layered types consisting of two imposed honeycomb sheets. Using AgNO$_3$, 3D framework [Fe$_2$L$_6$Ag$_3$](NO$_3$)$_3$ is obtained, which consists of double layers linked through Ag bridges from both sides with formation of binodal 5,4-connected 2-fold interpenetrating network. The reaction with Ag p-toluene sulfonate brings to a complicated 3D nanoporous network [Fe$_3$L$_9$Ag$_5$](tosylate)$_5$ with 6-connected metalloligands and 3- or 4-connected Ag ions. Similar ML$_3$, где M = Al or Ga are used for production of mixed MOFs containing interpenetrated primitive cubic networks [274].

An interesting example is self-assembling of 5,10,15,20-tetra(4-pyridyl)-Pp and *trans*-[CuL$_2$(H$_2$O)$_2$] (L = 1,1,1,5,5,5-hexafluoro-acac), including in situ Cu(II) metalation of Pp core, which gives rhomboidally distorted (4,4)-network-based polymer 2D layered structure (Scheme 6.6) [275].
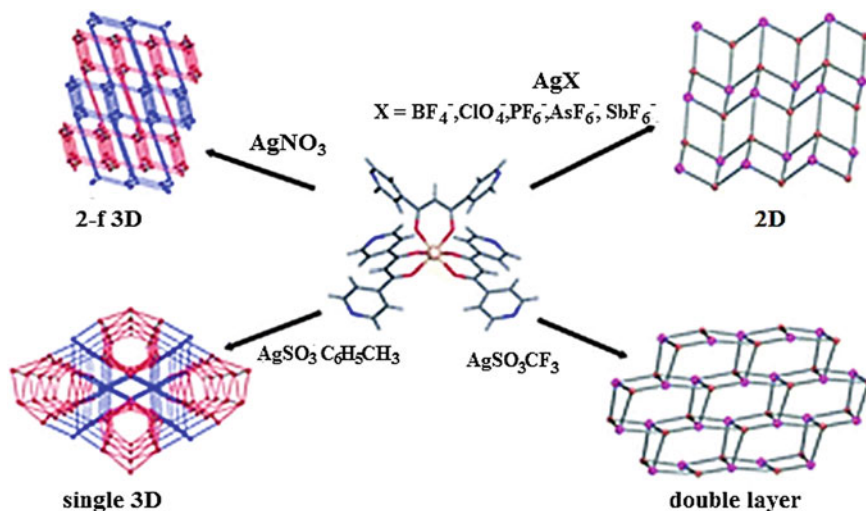
Scheme 6.5 *A* dependence of CP structure on nature of counter-ions during the reactions of FeL$_3$ with AgX (X = BF$_4^-$, ClO$_4^-$, PF$_6^-$, AsF$_6^-$, SbF$_6^-$, NO$_3^-$, CF$_3$SO$_3^-$, tosylate)

Heterobimetallic CPs with $[M(Mo_2O_5L_2)]_n$ (H_2L = 2-(3,5-di-*tert*-butyl-2-hydroxybenzylamino)acetic acid, M = Mn, Co, Zn, Cd и Ni) block are synthesized by simple mixing of Mo metalloligand with respective metal salts [276]. In other Co [277] and Ni [278] polymers based on Mo metalloligand $[MoO_2L]^-$ [L = carboxymethyl-(3,5-di-*tert*-butyl-2-hydroxybenzyl) aminoacetate] H-bonds form between helical chains in solid state. We shall also notice Na [279], K [280] and Li [281] complexes of another metalloligand $[MoO_3L]^{2-}$ (H_2L = iminodiacetic acid).

Metalloligand strategy is used for production of heterometallic 3D CPs containing Cu(II) and trimethyltin as nodes [282]. The first step of this synthetic way was in situ preparation of generated 2D CP with $[Cu(\mu\text{-}LH)_2]_n$ block (LH_2 = Py-2,5-dicarbonic acid), whose reaction with Me_3SnCl has given heterometallic 3D CP with $[Cu(Me_3Sn)_2(\mu\text{-}L)_2]_n$ block (Scheme 6.7). The obtained CP is 4,4-connected polymer with **sqc** topology, which contains the paddlewheel-shaped core consisting of two heterometallic Sn(IV)/Cu(II) macrocycles. In another example, 3d-4d heterometallic Co(III)–Zn(II) and Co(III)–Cd(II) CPs are obtained from two Co(III)-based metalloligands containing appended groups of arylcarboxylic acids 5-(picolinamido)-isophthalic acid and 4-[(pyridine-2-carbonyl)-amino]benzoic acid in different positions [283]. Arylcarboxylate groups coordinate secondary metal ions, Zn(II) and Cd(II) with production of different 3D networks (Fig. 6.20). It is important that all networks show ordered positions of secondary metal ions and unique, even unprecedented network topologies.
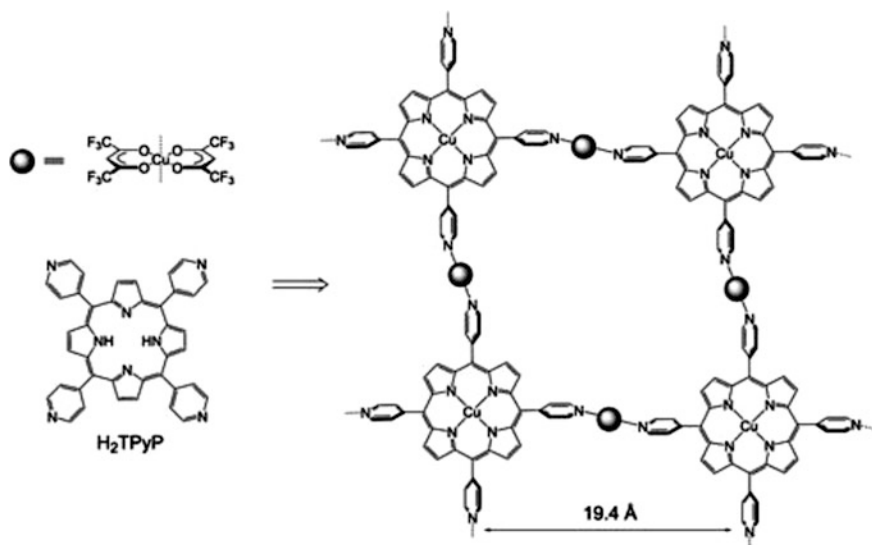
Scheme 6.6 A self-assembling of 5,10,15,20-tetra(4-pyridyl)-Pp (H_2TPyP) and trans-$[CuL_2(H_2O)_2]$ (L = 1,1,1,5,5,5-hexafluoro-acac)
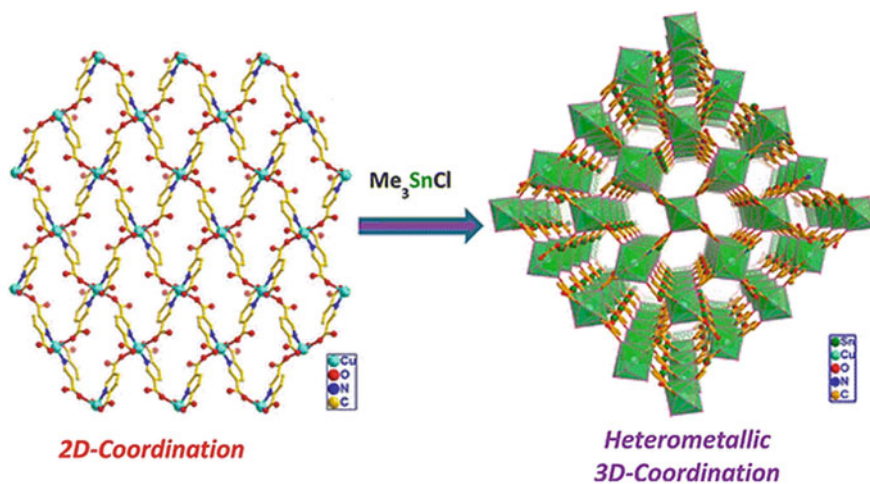
Scheme 6.7 A metalloligand type of synthetic route for production of heterometallic 3D CP containing Cu(II) and trimethyltin as nodes [283]
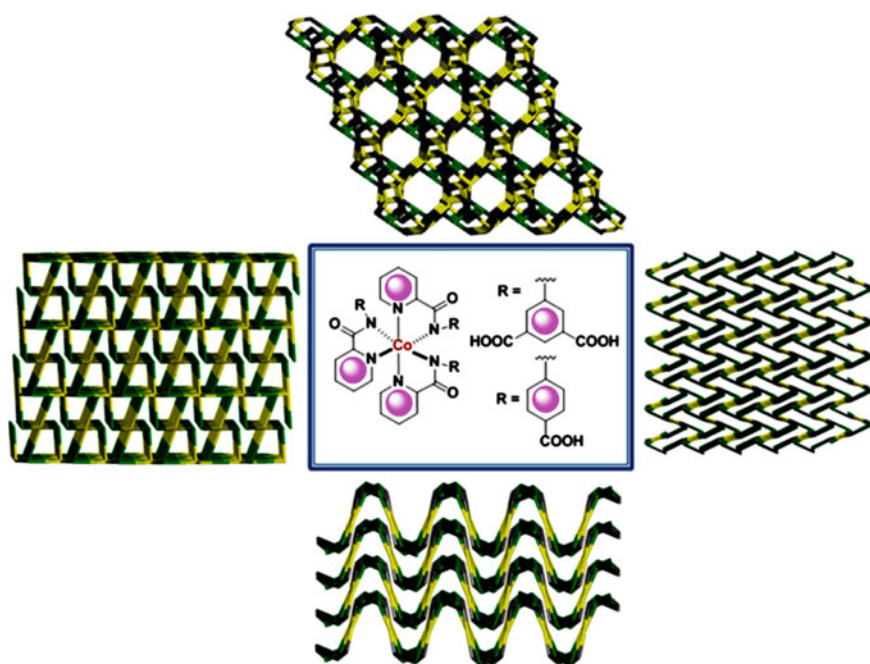
Fig. 6.20 The synthesis of Co(III)–Zn(II) and Co(III)–Cd(II) heterometallic coordination networks

An example of using chelating bpy ligands is porous 3D CP with $[La_2Cu]_n$ block based on tetranuclear La_4 cluster and Cu(I)-metalloligand, including 6,6′-dimethyl-5,5′-dicarboxy-bpy [284]. It is important that this CP shows reversible guest adsorption-desorption of different vapors with reversible structural transformations. In flexible porous heterometallic MOFs of rock-salt-type based on $[CoL_3]^{3-}$ metalloligand ($H_2L = 4,4′$-dicarboxy-bpy) and trivalent lanthanide cations La, Ce, Pr, Nd, Sm, Eu, Gd, Tb, Er, six carboxylates in the upper part of each coordination octahedron of Co(III)-metalloligand are bound with M cations [285]. If a MOF contains M cation smaller than Nd(III), the MOF is crystallized in cubic spatial group **Fm-3m**, while other MOFs with larger M are crystallized in low-symmetric rhombic spatial group **Fddd** due to asymmetric 10-coordinated bicapped structure of square antiprism of larger M cation.

There is an interesting using of macrocyclic metalloligand NiL (H_2L = 1,4-dihydro-2,3-dioxo-5,6:-9,10:13,14-tribenzo [1, 4, 8, 11] tetraazacyclotetradeca-7,11-diene-7,12-dicarboxylate) for production of CPs with $[Mg(NiL)]_n$, $[Zr_2(NiL)_2]_n$ and $[Pb(NiL)_2]_n$ blocks having infinite one-chained helical structures [286]. All NiL metalloligands in CPs are located in head-to-tail positions (Fig. 6.21, left column), in order to form very similar single-twisted helical CPs (Fig. 6.21, right column).

6.4 Pillar-Layered Strategy

Pillared MOFs are widely studied platforms with numerous applications, they consist of 2D layers, which have ligating sites for linking with ditopic columns, as a rule, derivatives of 4,4′-bipy bringing to 3D architectures. Functioning either with spacers within 2D layers or ditopic columnar ligands easily adjust structures and properties of pillared MOFs [200, 287].

Most widely used for building of pillared-layered CPs are M-Pp, since they form rigid 2D sheets, which are easily bound by pillared ligands. Thus, for example, Pp paddlewheel frameworks (PPF family) are obtained using M-Pp and columnar molecules for connection paddlewheel SBUs [199, 288]. The PPF assembling can be considered as two-staged process. At the first stage carboxyl groups M-Pp, where Pp = tetra-(4-carboxyphenyl)-Pp are linked to $M_2(COO)_4$ paddlewheel SBUs (M = Zn, Co), which are insensitive to Pp metals (Fig. 6.22) [194]. In the resulting 2D layer consisting of M-Pp and paddlewheel SBUs, axial paddlewheel directions are easily available for connection with ancillary ligands. Therefore, at the second stage the class of bipyridyl molecules is used as pillars for linking 2D layers occupying axial sites.

By choosing M-Pp spacers and bipyridyl pillars, three stacking patterns are found in these materials, including AA, AB, and ABBA types (Fig. 6.23) [192, 215]. In this case homogeneous or heterogeneous pillaring of 2D sheets is possible using 4,4′-bipy molecules. In the case of homogeneous pillaring two paddlewheel $M_2(COO)_4$ SBUs
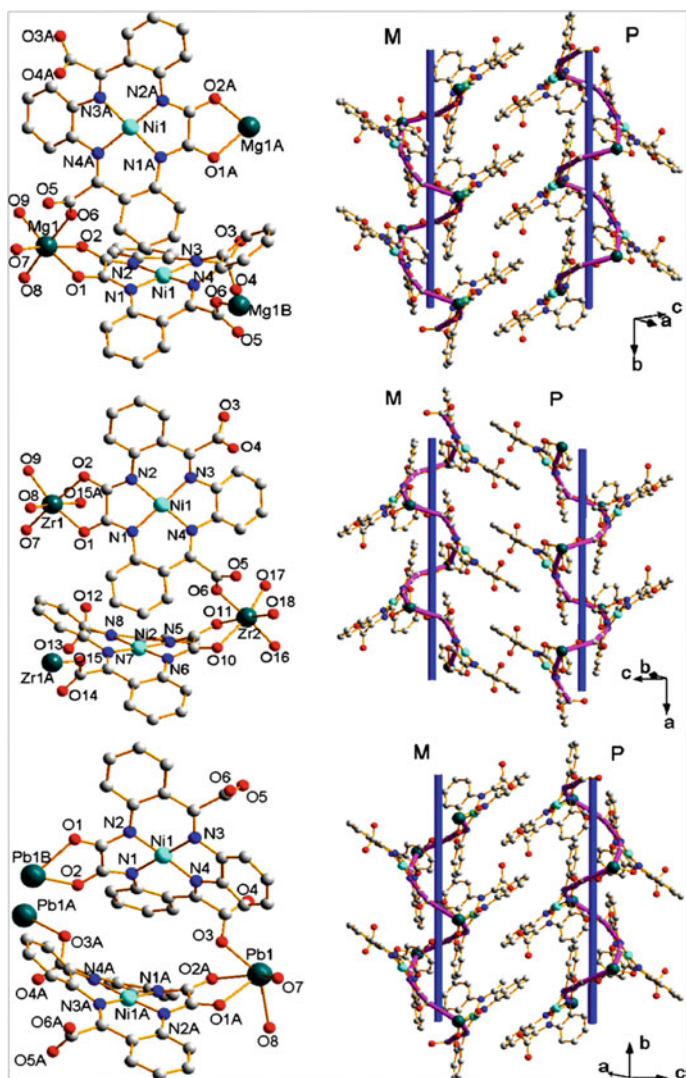
Fig. 6.21 Coordination environments of metal centers, and metal-binding mode, «head-to-tail» arrangement and saddle shape of NiL (left column) and left- (M) and right-handed (P) helical chains (right column) in [Mg(NiL)] (top), [Zr₂(NiL)₂] (middle) and [Pb(NiL)₂] (bottom). Mg, Zr, and Pb, pine green; Ni, cyan; N, blue; O, red; C, grey

are linked with 4,4′-bipy pillar, and in the case of heterogeneous pillaring 4,4′-bipy pillars are linked with $Co_2(COO)_4$ SBUs, as well as with Co-Pp in AB stacking pattern 3D networks [192]. A case is possible when 4,4′-bipy columns are linked with 2D Pp layers alternatively in homogeneous and heterogeneous models of
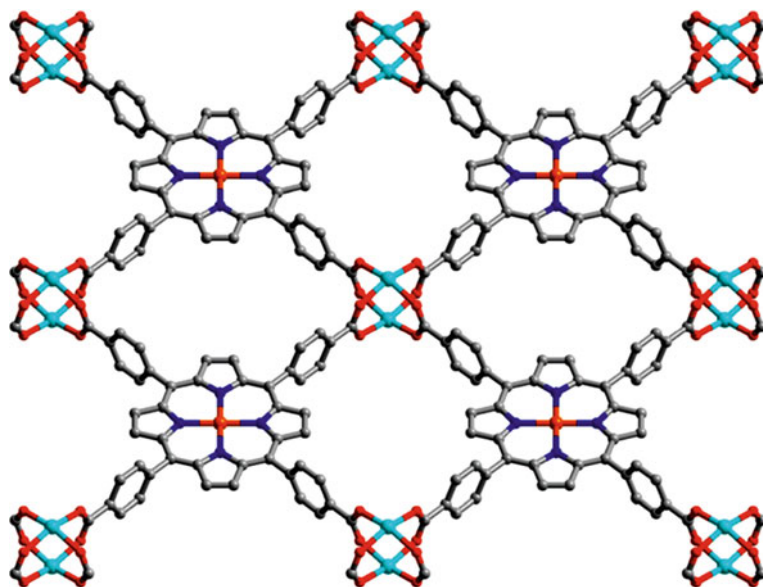
Fig. 6.22 The 2D Pp sheet and SBUs typically found in the PPF series
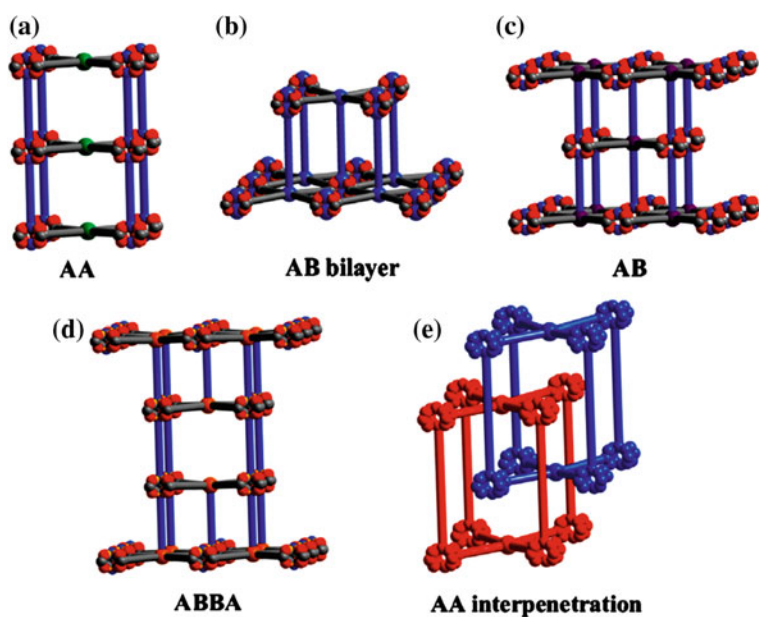
Fig. 6.23 Classification of the stacking patterns found in the PPFs series with different dipyridyl pillars

pillaring pattern forming ABBA stacking. Using Pd-Pp instead of Zn-Pp or Co-Pp only homogeneous pillaring is realized between two adjacent paddlewheels, because d^8 metal Pd(II) prefers square coordination geometry. In other words, stacking patterns of 3D pillared Pp frameworks are controlled by coordination geometry of Pp metals. As a rule, the pillars cannot distinct metal centers in paddlewheel SBUs or M-Pp if in both cases coordination sites are available. Therefore, for demonstration of targeted M-Pp pillaring the controlled strategy of production of Pp-based pillared-paddlewheel frameworks PPF-11, including metal pairs Zn/Zn, Co/Co, Mn/Zn and Fe/Zn is developed, where first and second metal are the metal center in a Pp core and in a paddlewheel cluster, respectively, by changing pillaring ligands from 4,4′-bipy to 2,2′-dimethyl-4,4′-bipy [194]. These compounds have 3D framework, in which 2D layers are pillared with a steric controlled 2,2′-dimethyl-4,4′-bipy remaining structurally unbound metal centers inside Pp. Therefore, using this approach, a desired control over pillar coordination is reached.

While small pillars like triethylene diamine and 4,4′-bipy rarely bring to interpenetrating frameworks, longer pillars N,N′-di-(4-pyridyl)-1,4,5,8-naphthalen etetracarboxydiimide and 3,6-di-4-pyridyl-1,2,4,5-tetrazine often bring to appearance of such structural topologies as bilayers and interpenetrating AA stacking patterns [201].

Noninterpenetrated, pillared-paddlewheel MOF are obtained through combination of 1,2,4,5-tetrakis(4-carboxyphenyl) benzene as the main building unit and 5,15-dipyridyl-10,20-bis(pentafluorophenyl)-Pp dipyridyl Pp struts with Zn salt (Scheme 6.8) [191]. The obtained crystalline compound is characterized by high porosity and contains entirely reagent-accessible M-Pp sites. It is worth noticing that this compound was the first M-Pp based MOF, which had shown catalytic activity in a material interior. However, when Mn-Pp is used instead free base of dipyridyl Pp, Mn ions act as structural nodes for production of 2D material without incorporation of tetratopic carboxylate.

The substantial interest is in light-harvesting pillared-paddlewheel MOFs using BODIPY- and Pp-based pillars where BODIPY spacers work as antenna chromophors for excitation of Pp pillars [188]. Efficient (practically quantitative) strut-to-strut energy transfer (antenna-like behavior) was observed in well-organized donor-acceptor assembling forming ordered MOF structure. Almost black MOF crystals can absorb most light from visible spectrum.

Another example is F-MOF and DA-MOF, which consist of two Zn(II)-Pp columns of [5,15-dipyridyl-10,20-bis(pentafluorophenyl)porphyrin]-Zn(II) and [5,15-bis [4-(pyridyl)ethynyl]-10,20-diphenylporphinato]-Zn(II), respectively (Scheme 6.9) [73]. Photogenerated exciton migrates at a pure distance up to ∼45 Pp pillars during its lifetime in DA-MOF, and only at ∼3 Pp pillars in F-MOF with high anisotropy along specific direction. This means that Pp molecular structures play important role in exciton jump. Great distance and directed energy transfer in DA-MOF suggest promising applications of this compound for development of efficient light-harvesting and energy-transporting materials.

1D helical CPs with $[M(HL)]_n$ (H_3L = 4,6-dihydroxy-1,3,5-triazine-2-carboxylic acid; M = Mn, Co, Zn, M = Ni) blocks were obtained by slow addition of a metal
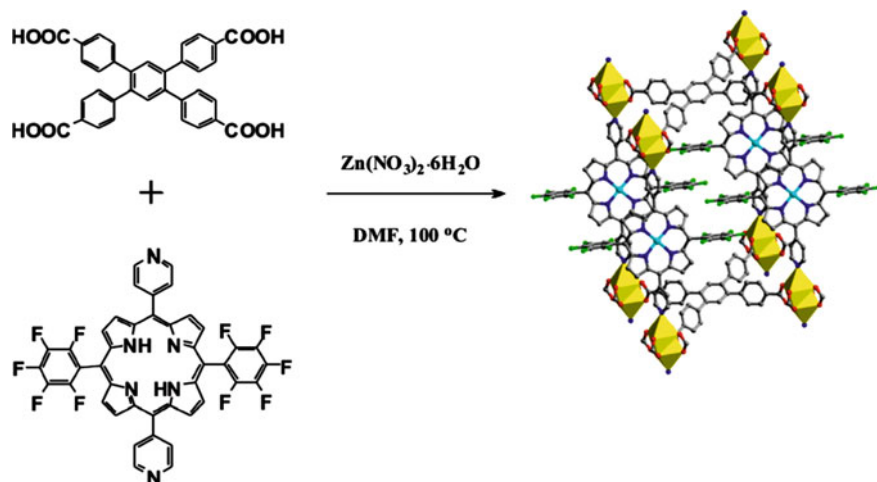
Scheme 6.8 Schematic representation of the synthesis of porous Zn-MOF
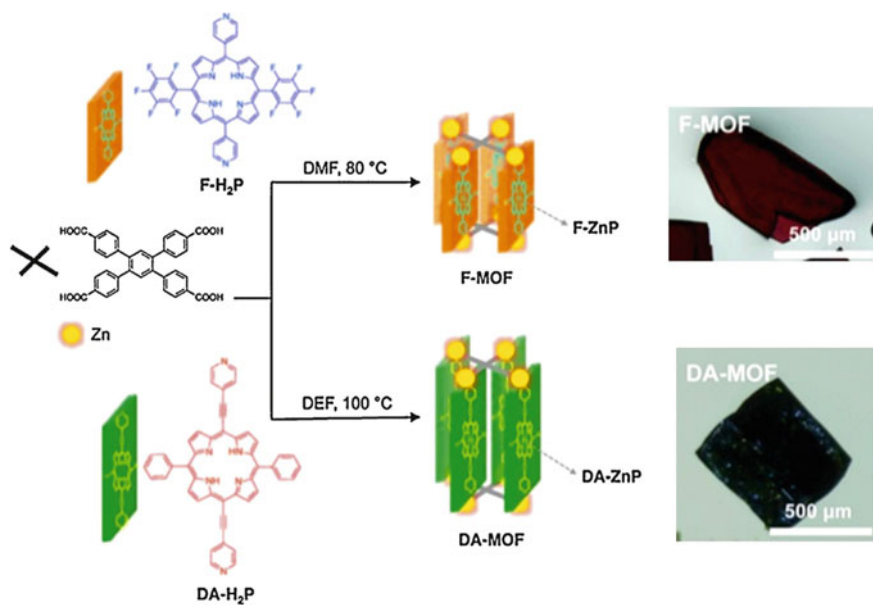
Scheme 6.9 Synthesis routes of the isostructural F-MOF and DA-MOF compounds and photographs of resulting crystals [73]
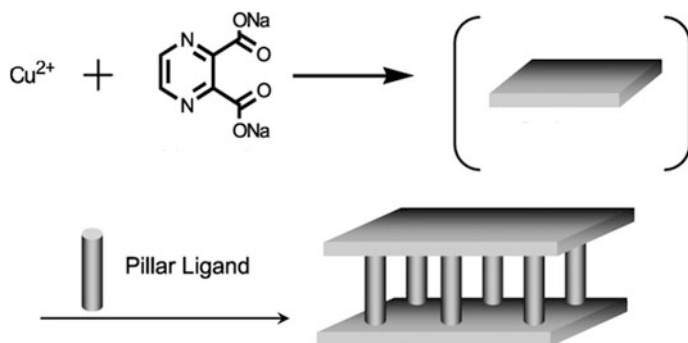
Scheme 6.10 Synthetic scheme of $[Cu_2L_2(P)]_n$

salt methanol solution to water solution of oxonic acid potassium salt with the following evaporation of the solution at room temperature. To increase dimensionality of these systems, $[M(HL)]_n$ SBU is linked to a rod-like N,N′-spacer, which makes it possible to isolate an CP with $[Zn(HL)(4,4'\text{-bipy})_{0.5}]_n$ and $[Ni(HL)(4,4'\text{-}$ bipy)$]_n$ blocks. $[M(HL)]_n$ chains pillared by 4,4′-bipy spacers within 2D corrugated layers in the first and 2D rectangular grid layers in the latter case [289]. In analogous flexible CP with $[Cu(HL)(4,4'\text{-bipy})_{0.5}]_n$ block, 2D corrugated $[Cu(HL)]_n$ layers are pillared by 4,4′-bipy spacers into 3D architectures [290].

We shall notice porous coordinated pillared layer structures with $[Cu_2L_2(P)]_n$ block, where L = pyrazine-2,3-dicarboxylate and P = pillar ligands in which channel dimensions (size and shape), and surface functionality can be controlled systematically by modifying columnar ligands [291–294]. They are synthesized using a simple procedure: mixtures of ethanol and aqueous Na_2L solutions and columnar P ligand are slowly added to aqueous solution containing Cu(II) ion at room temperature in air. Mixing provides making desired compounds for one day with high yield (Scheme 6.10).

6.5   Approach Based on Supramolecular Building Blocks

Other approaches to MOFs design were inspired by success in supramolecular chemistry. Thus, supramolecular building blocks (SBB) approach is a powerful method for achievement of hierarchical assembling, which provide qualitatively far higher level of control over structural properties and porous structures [43, 141, 295]. This concept is based on using of preliminary chosen 0-periodical metal-organic polyhedron (MOP) as a building unit, which allows self-assembling of MOFs at the supramolecular level of greater and more complicated ensembles of several metallic nodes and organic spacers

[296]. As compared with molecular building units, these supramolecular cages or clusters can sharply increment porous architecture, and very often they have well-defined coordination geometry, which results in considerable degree of predictability in synthetic design [297–302]. MOFs having high symmetry based on highly-connected polyhedral cage of molecular building units, which actually are SBBs, can provide elegant control over a structure due to their high connectivity, and also can design themselves features of limited nanospace [43, 303, 304] and very high surface area [305, 306]. In most detail this approach is studied for the example of M-Pp CP by MOP building using [M_2(carboxylate)$_4$] paddlewheel fragments [297, 298, 307, 308]. The examples are differently faceted MOPs obtained by vertex-linking of square SBUs with isophthalate ligands [43, 309, 310]. These faceted MOPs are used as SBBs for production of highly porous and symmetrical MOFs bridged with isophtalates with different organic fragments through their 5-positions, as in the example of the MOP based on isophtalate derivatives and square dicopper paddlewheel SBUs [43, 156, 300]. It is important that MOPs can be functionalized either on vertices, or on faces.

Using MOPs as building units promotes scale of MOFs to higher complexity level, and can give interesting MOF platforms. Thus, for example, were used 24-, 18-, or 12-connected MOPs as SBBs for formation of highly connected **rht**-MOFs [148, 151, 311, 312], **gea**-MOFs [155], and **fcu**-MOFs, respectively [300, 313]. Obviously, the more oriented and structured information can be included in SBB, the higher is degree of predictability and possibilities for design [302, 314]. As an example, we shall notice a MOP-based MMPF-1 built based on specially developed Pp ligand 5,15-bis(3,5-dicarboxyphenyl)-porphine, in which two isophthalates are incorporated for building of confined nanometer polyhedral cavity-containing metal-metalloporphyrin framework (Fig. 6.24) [183]. In this compound eight paddlewheel SBUs are linked with sixteen Pp ligands forming a nanometer cage. MOP works as SBB, which supports 3D porous M-Pp framework structure, which shows very high density of 16 open Cu sites in closed nanometer polyhedral cage. Four dicopper paddlewheel SBUs are linked with four isophthalate fragments of four different Pp ligands and give a cage vertex; they are pillared with four dicopper paddlewheel SBUs at the bottom of the cage through eight different Pp ligands. Pp cages are arranged as ABAB stacking pattern, thus narrowing its pore sizes.

Moreover, successfully strutted are several isophthalate derived Pp ligands during building of nanometer polyhedral cage-containing MMPFs [186]. Thus, MMPF-3 were obtained solvothermally from Pp ligand 5,15-bis(3,5-dicarboxyphenyl)-10,20-bis(2,6-dibromophenyl)-Pp and $Co_2(\mu_2\text{-}H_2O)(H_2O)_4(COO)_4$ molecular building units, which afford cubohemioctahedral SBBs serving as 12-connected nodes in the resulting network of **fcu** topology. It is worth noticing that MMPF-3 shows three types of polyhedral cage (Fig. 6.25): a cubohemioctahedron, truncated tetrahedron, and truncated octahedron, which are interlinked.

Based on custom-designed tetra-dicarboxy-Pp, self-assembled with M(II) (M = Zn and Cd) cations, SBBs are obtained, which are uniform polyhedrons based on Pp
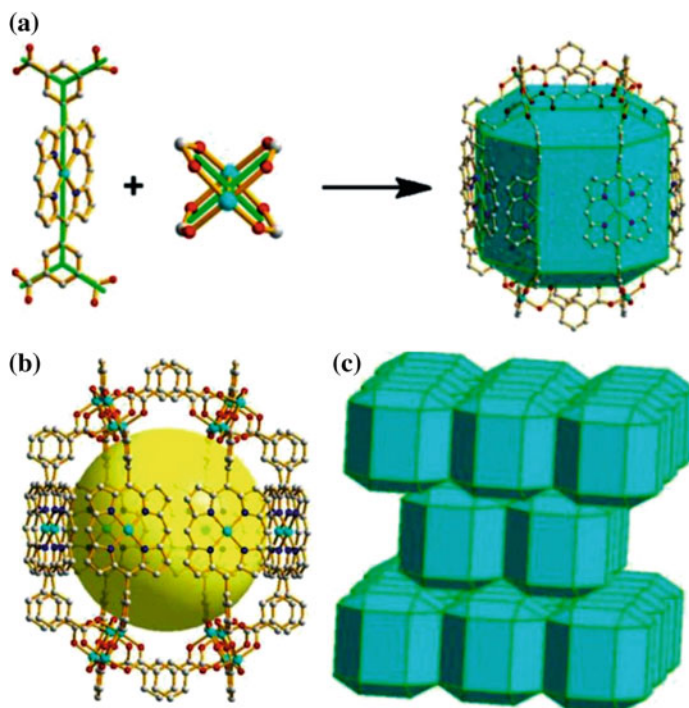
Fig. 6.24 **a** Illustration of the linking of a Pp ligand and a dicopper paddlewheel to form the irregular rhombicuboctahedral cage; **b** a nanoscopic cage enclosed by eight dicopper paddlewheel SBUs and 16 Pp ligands (eight are face-to-face Pp, and the other eight only provide isophthalate units); and **c** ABAB packing of rhombicuboctahedron layers in MMPF-1 [183]

molecular building units [184]. Faces of Pp fragments link triangular $M_2(CO_2)_3$ or $M(CO_2)_3$ fragments with formation of small cubicuboctahedral SBBs, which, in turn, are fused with adjacent SBBs on opposite faces of each Pp fragment. The resulting highly symmetric broadened topology **pcu** networks, MMPF-4 (M = Zn) and MMPF-5 (M = Cd) show two different polyhedral cages and are permanent microporous (Scheme 6.11).

6.6 Approach Based on Supramolecular Building Layers

We shall also notice another conceptual strategy, in particular, the approach based on supramolecular building layers (SBLs), which made it possible to design and produce pillared MOFs with far higher complexity (Fig. 6.26) [140, 315]. This unique and powerful assembling strategy is based on using of pre-targeted 2-periodical MOF layers as SBLs for deliberate building of 3-periodical functional MOFs. This is carried out by chemical cross-linking of layers through available bridging sites on
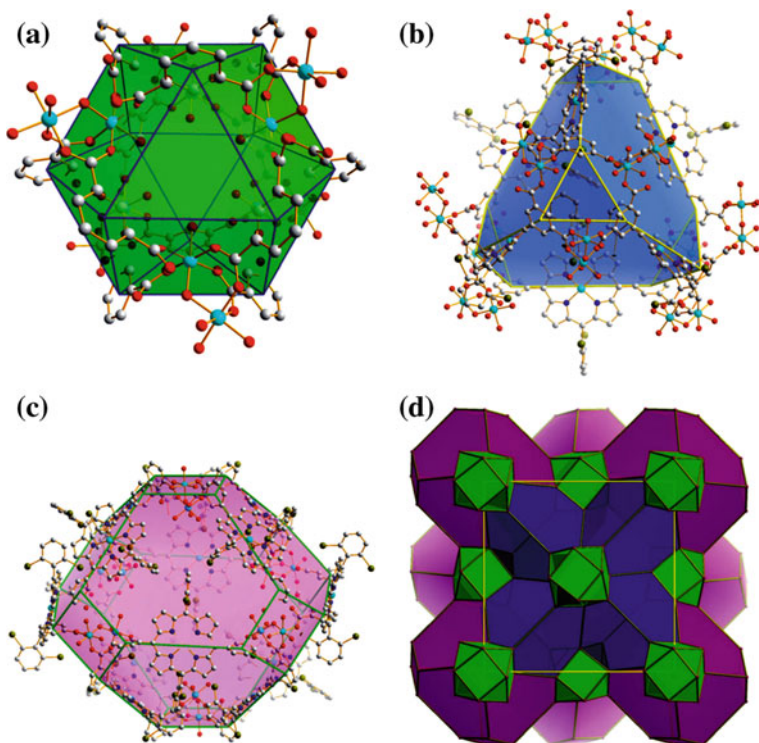
Fig. 6.25 The three types of polyhedral cages present in MMPF-3: **a** cubohemioctahedron, **b** truncated tetrahedron, and **c** truncated octahedron. **d** 3D structure of MMPF-3 illustrating how its polyhedral cages are connected
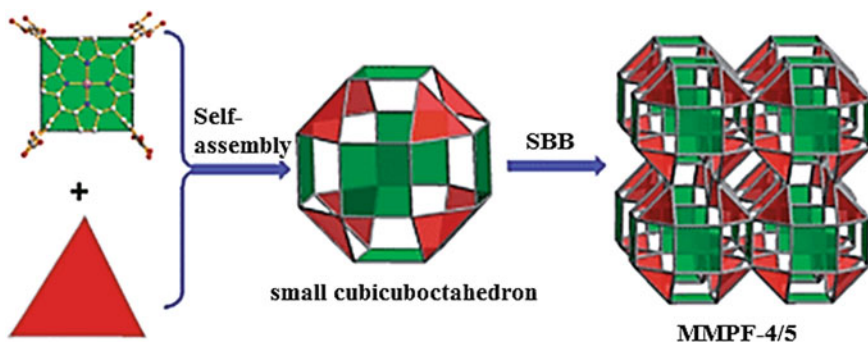
Scheme 6.11 The scheme of synthesis of MMPF-4 (M = Zn) and MMPF-5 (M = Cd) based on small cubicuboctahedral SBBs
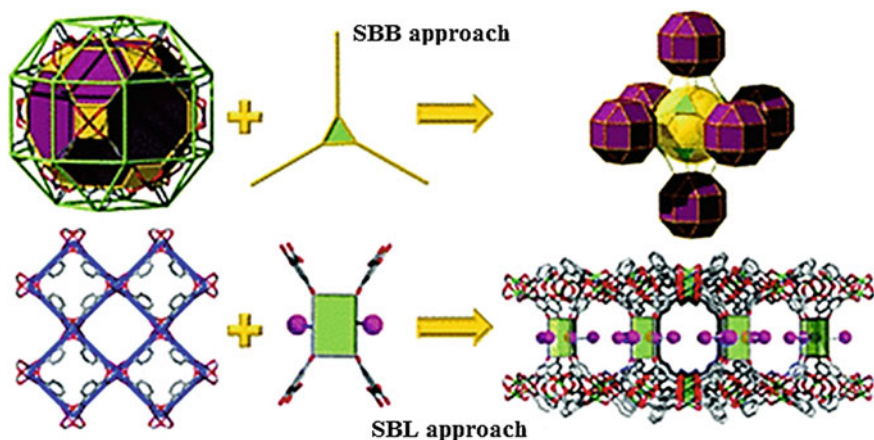
Fig. 6.26 Two implemented conceptual SBB and SBL approaches facilitating the design and deliberate construction of MOFs

layers (for example, open metal site or modified positions of organic spacer). SBL structural method requires reasonable choice of organic ligands, which will be pillars for layers. Definitely, this unique strategy is not confined to complicated pillaring; it is also applied to simple pillaring. As a result of countless combinations of cross-linkings, numerous MOFs with certain 3D network topologies can be pre-targeted developed and synthesized using preliminary obtained SBLs. Additional advantage of this approach is the fact that the common framework and topology of the network will remain unchanged basing on pillared layers, which provides almost unlimited expansion of the limited space (for example, cavities and porosity). Besides, it should be noted that if pores or windows of the layers remain unexpanded (i.e. expansion takes place only due to pillars), interpenetration of MOFs is excluded. No less important is the fact that modularity typical of this method provides easy functioning or introduction of additional functionalities for deliberate applications.

Axial-to-axial, ligand-to-ligand and ligand-to-axial pillaring strategies are developed for introduction of required functionalities in final MOFs through pillar fragments, which provide design, availability, and building of higher dimensionality MOFs [32–322]. Thus, trigonal heterofunctional ligands, for example, isophthalic acid cores functionalized in 5th position with N-donor (for example, pyridyl- or triazolyl-type) units are applied to pillar pre-targeted 2D layers (SBLs) [320]. SBLs based on edge-transitive Kagome and square networks are cross-linked into targeted 3D MOFs with restructured big cavities, which results in isoreticular platforms.

SBL approach is used for deliberate synthesis of MOF with open massif of amide or amine functionalities inside the porous system [323]. Two MOF platforms, eea-MOF and rtl-MOF based on pillaring kgm-a or sql-a layers with heterofunctional 3-connected organic building units are directed and built deliberately for desired incorporation and demonstration of amide or amine functionalities

(Figs. 6.27 and 6.28). Distinctive kgm-a and sql-a networks can be considered as ideal blueprints for targeted 2-periodical MOFs based on assembling of square building units produced from well-known metal paddlewheel clusters used as molecular building units.

SBL approach was successfully applied to target and building of isoreticular **tbo**-MOFs [315], functionalized and/or expanded, which contain very big nanocapsule-like cages have high porosity and potential for gas separation and storage. Similarly, another 3-periodical porous MOFs can be potentially targeted through pillaring SBLs based on one of five edge-transitive 2-periodical networks: **sql** (square lattice), **kgm** (Kagomé), **hcb** (honeycomb), **kgd** (Kagomé double), and **hex** (hexagonal lattice). Further on the obtained MOF layers can be perceived as SBLs, which are subjected to pillaring through 2-, 3-, 4-, or 6-connected organic building units for building of desired 3-periodical MOF platforms [140].

Initial studies in MOFs were focused on design of a wide range of the compounds with new topologies and architectures. Although the design of new structures is still very relevant, and a great number of works are still concerned with discovery of unique network topologies, the primary motivation in crystal engineering of MOFs has shifted to design of functional materials having specific physical properties and wide potential for applications.
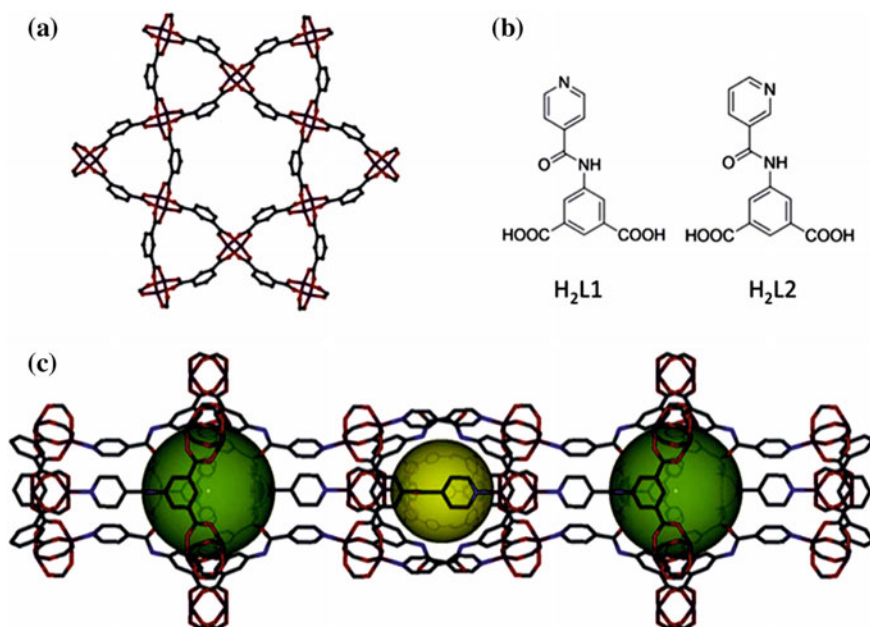
Fig. 6.27 **a** Layer segment of a kgm-MOF. **b** Left: 5-(isonicotinamido) isophthalic acid (H₂L1) and right: 5-(nicotinamido) isophthalic acid (H₂L2). **c** Hourglass-shaped channels with two primary types of cavities. C—gray, O—red, N—blue, Cu—plum
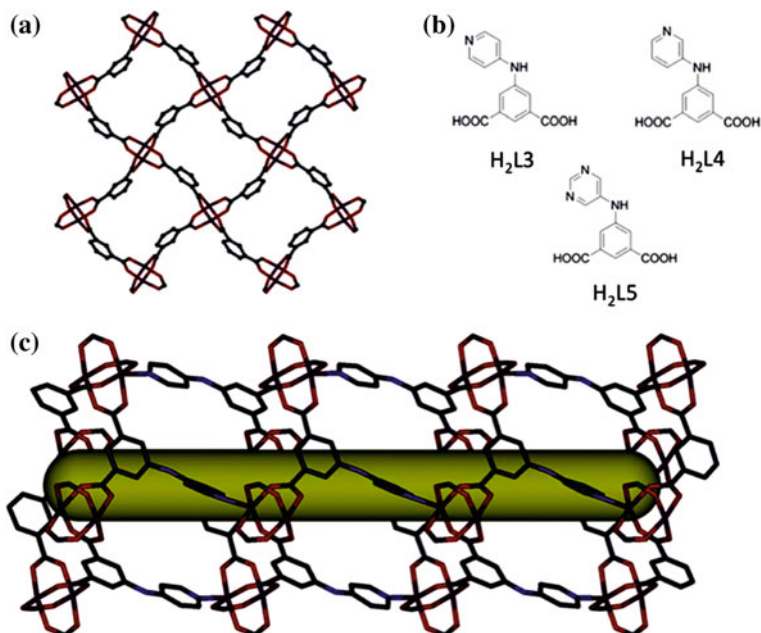
Fig. 6.28 a Layer segment of a sql-MOF. **b** Left, up: 5-(pyridin-4-ylamino) isophthalic acid (H$_2$L3). Right, up: 5-(pyridin-3-ylamino) isophthalic acid (H$_2$L4). Bottom: 5-(pyrimidin-5-ylamino) isophthalic acid (H$_2$L5). **c** Projection along the *a*-axis of the rtl-MOF-2 displaying channel. C—gray, O—red, N—blue, and Cu—plum

6.7   Conventional Synthesis

By now quite many approaches to MOF synthesis have been developed (Fig. 6.29), which are usually conventionally divided into two big groups: conventional synthesis and alternative methods of synthesis [16, 29, 33, 324–328]. The term conventional synthesis is applied to reactions performed without heating or using traditional electric heating without parallelization of reactions. Most MOF synthesis are liquid phase, in which separate solutions of metal salt and ligand are mixed together or a solvent is added to a solid salt and a ligand mixture in a reaction vessel [125, 329–337]. In order to obtain new MOFs, different factors should be taken into account during synthesis, such as nature of a metal ion [338, 339], structural features of organic ligand [340–342], counter-ion [343, 344], and some experimental variables including temperature of reaction, ratio of reacting agents and their concentrations, pH, system of solvents, crystallization methods, etc. [345–349]. It is important to notice that different processes with the same initial materials can bring to different products, for example, isomeric or polymorphous types [350–352]. Even small variations of only one from several factors having effect on the synthesis process, can change dramatically structure of the formed MOFs [353–363].
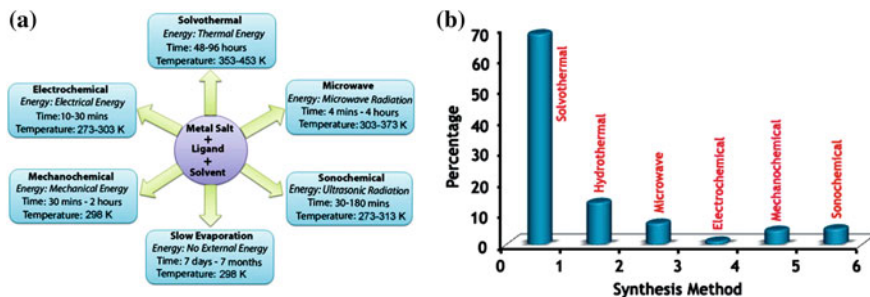
Fig. 6.29 a Synthesis conditions commonly used for MOF preparation; **b** indicative summary of the percentage of MOFs synthesized using the various preparation routes [328]

Thus, if reactions between metal(II) acetates and a [1-(2-hydroxyphenyl)propylidene]-hydrazide ligand is performed in 1:2 (M:L) molar ratio, only Mn(II) forms 1:2 complex in ethanol, while Cu(II) and Zn(II) form 1:1 1D CPs in methanol (Scheme 6.12) [364]. Interaction of ligand with Mn(II) acetate in methanol instead of formation of expected Mn(II) complex brings to heterocyclic derivative of quinazoline 2,2-dimethyl-3-[1-(2-hydroxy-phenyl)-propylideneamino]-2,2-dimethyl-2, 3-dihydro-1H-quinazolin-4-one.

Using interaction between 2-substituted 8-hydroxyquinolinate ligand (HL) including Py group, and Zn or Cd salts, CPs with $[ZnL_2]_n$ and $[CdL]_n$ blocks are produced (Scheme 6.13) [365]. The first CP has 2D square network containing *meso*-helical chains, while the second CP is a 2D network made of binuclear Zn_2 SBUs. By incorporation of two dicarboxylate anions into the reaction system, four CPs are
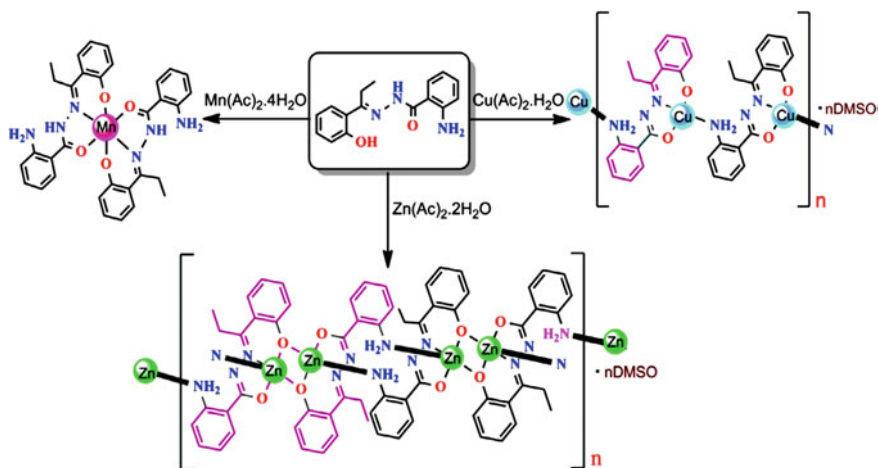
Scheme 6.12 Versatile coordination behavior of Schiff base ligand, 2-amino-benzoic acid [1-(2-hydroxy-phenyl)-propylidene]-hydrazide and results the formation of mono-/polynuclear complexes of Mn(II), Cu(II) and Zn(II)
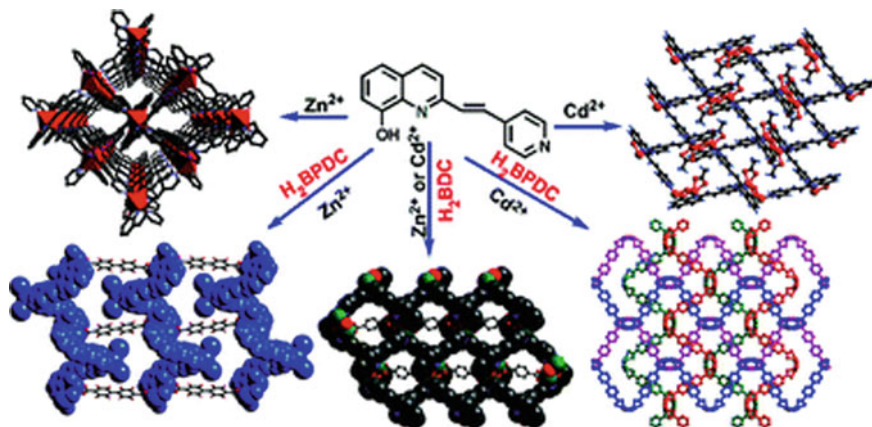
Scheme 6.13 Synthesis of CPs based on 2-substituted 8-hydroxyquinolinate ligand including Py group, where H_2BDC is 1,4-benzenedicarboxylic acid and H_2BPDC is 4,4'-biphenyldicarboxylic acid

obtained with $[Zn_2L_2(L')]_n$, $[Zn_3L_2I_2(L'')]_n$, $[Cd_2L_2(L')]_n$, and $[Cd_2L_2(L'')]_n$ blocks (H_2L' = 1,4-benzenedicarboxylic acid, H_2L'' = 4,4'-biphenyldicarboxylic acid). The L'-based CPs show 2D structures built by cyclic hexamers Zn_6L_4, which are divided in half by coordinated H_2L. In CPs based on L'' four ligands bridge 1D ML chains into 2D layered structure or present an interesting 3D structure in which L'' ligands link binuclear Cd units into multiple *meso*-helical chains along *a* and *b* axes, respectively. Therefore, skeletons of dicaboxylate anions play important role in assembling of different MOF structures.

In the case of using organic acid, a base is needed, usually, amine, which is necessary to deprotonate the acid (future bridging fragment) and initiate the reaction. At that it is important to exclude competitive coordination of the base and organic acid.

6.7.1   Solvent Evaporation Method

A solvent evaporation is most conventional and widely used method of crystal growth which carried out by evaporation or cooling of a saturated solution. For this method the following conditions are needed: crystals grow in saturated solutions, solubility increases as temperature rises, and crystals can appear during cooling, which should be well controlled, since the cooling rate and final temperature are concerned. The evaporation method is a regular process of crystallization, which is applied for preparation of MOF crystals. In this method a solution of initial reagents is concentrated by slow evaporation of a solvent at a fixed temperature, mainly, at room temperature. Sometimes a mixture of solvents is used in the process, which

can increase solubility of the reagents and make the process faster due to more rapid evaporation of low boiling solvents [366, 367]. Though this method is sometimes preferable, since it goes at room temperature, its main drawback is long duration of the process as compared to other known ordinary methods.

As an example of a simple water-based method of solution-slow evaporation we shall consider synthesis of Pb-based CP with $[Pb_2Cl_2(HL)_2]_n$ block, where $H_2L =$ pyrazine-2,3-dicarboxylic acid under optimized conditions [368]. It is 1D CP consisting of Pb_2Cl_2 dimers with monoprotonated dicarboxylic acids between chains. In the same way the CP with $[Pb_3L_3]_n$ block is obtained without any additives. Using the direct way of mixing, 1D linear Zn(II)-based CP with $[ZnL]_n$ block (L = pyrazine-2,5-dicarboxylate ligand) is obtained [369]. At room temperature CPs with $[Cd(L)_{1/2}]_n$ and $[SmCu_2K(L)_2]_n$ (H_4L = 1,2,3,4-butanetetracarboxylic acid) blocks are synthesized, which form 2D network and heterometallic 3D framework, respectively [370]. The CPs with $[MnL(phen)_2]_n$ block are obtained by mixing of aqueous solutions of Mn acetate, bpy-5,5′-dicarboxylic acid (HL) and phen [371]. In the CP Mn(II) atom is coordinated with four nitrogen atoms from two phen molecules and two oxygen atoms from two L molecules with distorted octahedral geometry. The complex was dibridged with L ligand forming 1D infinite chain, and 3D supramolecular framework is built by intermolecular weak interactions such as H-bonds and $\pi\cdots\pi$-stacking. Reactions between Zr(IV) salt and Pp-tetracarboxylic acid bring to MOF with two types of open channels presenting MOF distinguished by (4,8)-connected **sqc** network. It is interesting to notice that MOF remains unchanged in boiling water and in aqueous solutions with pH changing from 1 to 11, surprisingly wide range, which MOF can endure [372].

One of widespread methods of CP production with metal chelate units is incorporation of bridging anions (i.e. carboxylate, azide, and dca), which advances formation of CP with unusual network architectures and interesting properties through various linking regimes [373]. Thus, 3D heterobimetallic CP with $[MnL_2Hg(SCN)_4]_n$ asymmetric block (L = 2-benzoylpyridine) is synthesized by slow addition of NH_4SCN and $Hg(SCN)_2$ aqueous solution to methanol solution of Mn chloride and L followed by mixing at room temperature during 12 h [374]. The 2D hexaazamacrocyclic complex *trans*-$[NiL(N_3)_2]$ (L = 1,3,6,9,11,14-hexaazatricyclo [12.2.1.16,9]octadecane) is obtained from mononuclear complex $[NiL]Cl_2 \cdot 2H_2O$ and sodium azide in methanol [375]. The crystal structure of this CP is centrosymmetric and Ni(II) atom has axially elongated octahedral geometry with four nitrogen atoms from hexaazamacrocycle and two nitrogen atoms from azido ligands. Each *trans*-$[NiL(N_3)_2]$ block expands its structure to form 2D network of the «brick wall» type based on H-bonds interactions between nitrogen atoms of the azido ligand and secondary amine of macrocycle in four adjacent units (Fig. 6.30).

The final dimensionality of crystal structure depends on such important factor as M–L ratio. It is known that 1:1 ratio often brings to 1D structures, and high coefficients, as a rule, advance CP of higher dimensionality [376–379]. Not only covalence has relation to these structures: bridging action of non-covalent interactions
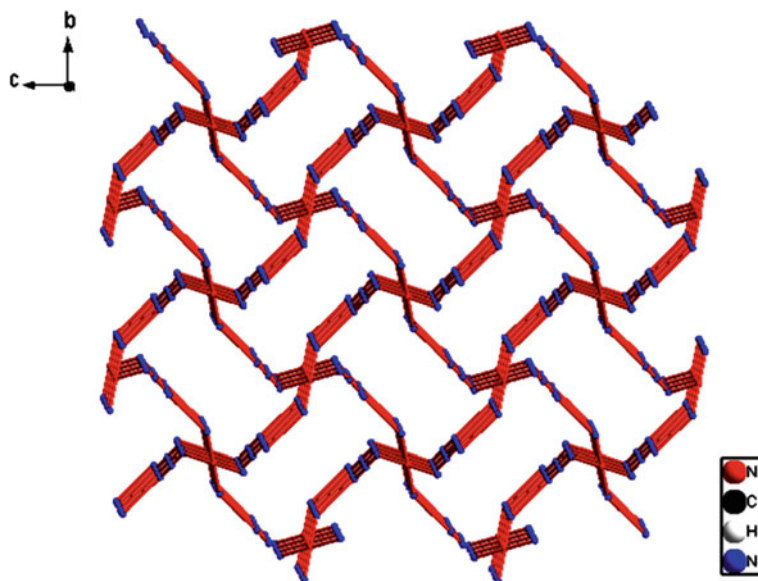
Fig. 6.30 «Brick wall» structure of the 2D CP (macrocyclic molecules are omitted for clarity)

such as H-bonds or π–π stacking can change final structures even with very similar components. This result depends strongly on eagerness of involved types and H-bonded donor/acceptor interactions.

Reactions of alkyl substituted aromatic monocarboxylic acids (HL) with transition metal ions in presence of chelating and bridging N,N-donor ligands (L') give either discrete or polymer complexes depending on position of a substituent on benzoic acid and ability of ancillary ligand to work as chelating or bridging ligand [380]. For example, when phen was used as an ancillary ligand, and for carboxylic acid was taken 4-*tert*-butylbenzoic acid, discrete complexes were deposited. However, for the same ancillary ligand with 2,4,6-trimethylbenzoic acid, 1D helical polymers with $[ML_2(L')]_n$ block (M = Mn, Co, Cu and Zn) were obtained. This clearly shows ability of *o,o*-disubstituted benzoic acids to form helical polymers, while *p*-substitution on aryl ring brings to discrete complexes.

The reaction temperature is very important parameter, which has effect on CP formation with variable topologies based on ligand conformations [381–383]. Especially this relates to flexible organic spacers, which take various conformations at different temperatures [384–388]. Thus, thermodynamically preferred conformer prevails at high temperature, while low temperatures advance kinetic conformer. In other words, by exhaustive control over the reaction temperature, thermodynamically or kinetically preferred conformers can be obtained [27, 389, 390]. From this point of view, the temperature of the reaction should be one of key factors in determining topology of CP and dimensionality of structures through control over conformation of a ligand. Rather important is the fact that higher temperatures can

enhance solubility of the reagents and, therefore, to slow down kinetics of crystal formation and bring to bigger and better detected particles [93, 114]. Moreover, choice of respective temperature of the reaction can have effect on morphology of the crystals [391] and evolution of colloid solutions [129], and long reaction time can bring to MOF degradation [392]. We shall also notice that a change in temperature of the reaction has a significant effect on formation of a product and often more condensed/dense structures are observed at higher temperatures [393, 394]. Depending on temperature of the reaction, two temperature ranges of MOF synthesis are distinguished, solvothermal and nonsolvothermal, that determines the type of reaction equipment, which should be used. Respectively, nonsolvothermal reactions take place below or at the boiling temperature of a solvent at atmospheric pressure, which simplifies the synthetic demands. Low temperature routes are widely used for growth of simple molecular or ionic crystals, since it is possible to adjust the reaction conditions, i.e. nucleation and growth rates of crystals. Therefore, using these methods, it is possible to obtain large crystals suitable for structural analysis.

Ancillary ligands, such as bpy and phen are often used with multicarboxylate ligands for building of new functional CP architectures containing metal chelate units [395]. Phen as an ancillary ligand is most preferable since it generates 3D supramolecular interactions, such as aromatic π–π stacking and –CH–π interaction stacking, which provides stability of supramolecular ensembles [396–398]. In this connection, reasonable combination of bridging carboxylates with phen-like chelating ligands and metal ions has generated many interesting coordinated architectures. As length of a linear spacer increases, a tendency to interpenetration of 3D CP also increases, and if a structure is already penetrated, a degree of interpenetration, as a rule, increases with length of a spacer ligand [29, 60, 399–402]. From the point of view of CP production with metal chelate units, a great attention was attracted by heterocyclic carboxylate ligands, such as pyridine-, pyrazole-, imidazole-, and benzimidazole-carboxylate ligands [403–407]. It should be noted that pyridylcarboxylic acid is the «ligand star» in coordination chemistry of MOFs containing metal chelate units at all times. In this view flexible heterocyclic carboxylate ligands receive far less attention [408–413].

Most studies of CPs are still concentrated on CPs of transition and lanthanide metals [1–9], and CPs of p-block metals is relatively studied less [414–422].

Counter-ions are present in CP structure, when neutral ligands are used. They can have effect on geometrical environment of a metal ion (more or less coordinating counter-ions), and can control generally CP structure by involving into weak interactions or acting as guest molecules in voids of a crystal architecture. As a typical example we shall consider assembling of tripyridyltriazole ligand 3,4-bis (2-pyridyl)-5-(3-pyridyl)1,2,4-triazole (L) with dca anion and different Cd(II) salts in CH_3OH–H_2O medium, which brings to CPs with $[Cd_2L_2(dca)_4(H_2O)]_n$, $[CdL(dca)(ClO_4)]_n$ and $[CdL(dca)X]_n$ ($X^- = Cl^-$ and Br^-) blocks [423]. In the first two CPs Cd(II) centers are linked by L spacers forming $[Cd_2L_2]$ bimetal units, which are bridged with dca anions, thus bringing to 1D motif and 2D layer, respectively. The latter two CPs reflect 3D isostructural homochiral coordination networks built by 1D $[CdL]_n$ helical units and dca bridges. Therefore, Cd(II) salt counter-ions are

responsible for different CP structures. We shall also notice that assemblies of the same ligand with Cu(II) chloride and dca anion at different M–L ratios give CPs with $[Cu_5L_4(dca)_{10}]_n$ and $[CuL(dca)Cl]_n$ blocks displaying 1D double-chained massif and 3D chiral, network, respectively (Scheme 6.14) [424].

Depending on nature of anion of the initial metal salt $Cu(NO_3)_2$ or $Cu(ClO_4)_2$, mixing of their aqueous solutions with methanol L solution [L = 3-(2-pyridyl)-4-(4-pyridyl)1,2,4-triazole] brings either to a mononuclear complex $[CuL_2(H_2O)_2]$ $(NO_3)_2$, or to 1D linear CP with $[CuL_2]_n$ block, respectively [425]. It is interesting that incorporation of NaN_3 in these assembled systems under similar conditions gives two different 2D layered networks with $[CuL(N_3)]_n$ blocks, both of which contain double inorganic anions as counter-ions (NO_3^-/N_3^- and ClO_4^-/N_3^-, respectively). Besides, with subtle change in reaction conditions, 1D linear massif $[CuL(N_3)_2]_n$ is obtained with N_3^-, compensating positive charges. It should be noted that stepwise structural transformations between these crystal phases can also be achieved by direction of azide anion (Scheme 6.15). In other example, Cd(II) CPs with $[CdLCl_2]_n$, $[CdLBr_2]_n$ and $[CdLI_2]_2$ blocks are assembled from CdX_2 (X = Cl, Br, I) and the same ligand [426]. The first two CPs are isostructural and show 1D loop-like chain, while the third complex has prominent dimeric macrocyclic motif. It is interesting that another 1D chain $[CdLI(SCN)]_n$ can be reached when NH_4SCN is incorporated in the assembled system of third complex. Thus, halogenide- and thiocyanate-anions in these coordination complexes act not only as counter-ions, but as structure-directing agents.

We shall also notice 3,3'-di(pyrazinamoyl)-bpy (H_2L) ligand consisting of different linking units, which can facilitate CP formation [427]. Reaction of the ligand with Cu acetate in presence of $Et_3N \cdot HCl$ gives CP with $[Cu_6L_2Cl_2(OAc)_6]_n$ block, at that *trans*-configuration of bpy-unit present in the ligand, remains in the resulting CP. In other words, a bpy fragment is not chelating, and L^{2-} anion coordinates two
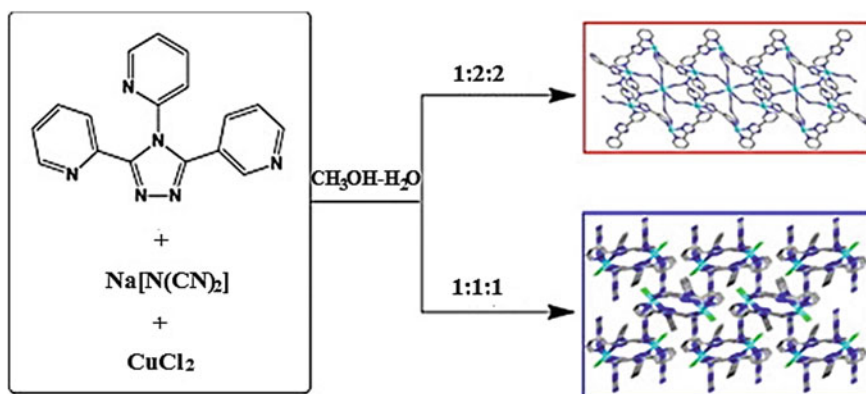
Scheme 6.14 The assemblies of the tripyridyltriazole ligand 3,4-bis(2-pyridyl)-5-(3-pyridyl) 1,2,4-triazole with Cu(II) chloride and dca anion at different M–L ratios into CPs, displaying 1D double-chained massif and 3D chiral **dia** network, respectively
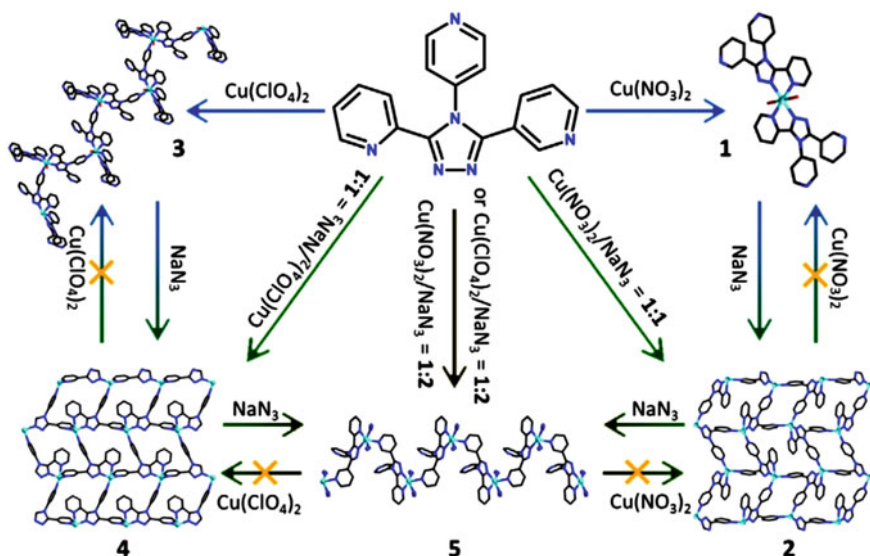
Scheme 6.15 A diagram illustrating self-assembled and structural transforming processes including 3-(2-pyridyl)-4-(4-pyridyl)1,2,4-triazole, metal salt $Cu(NO_3)_2$ or $Cu(ClO_4)_2$, and NaN_3

Cu ions by bis-tridentate mode through amide and pyridine nitrogen atoms (Fig. 6.31). Bimetallic unit is linked to equivalent unit through a pair of 1,3-acetate and μ-chlorine bridges with resulting tetrameric $[Cu_4L_2Cl_2(OAc)_2]$ core. Coordination of one of pyrazole substituents from each ligand to the third Cu center of rigid paddlewheel $[Cu_2(OAc)_4]$ unit brings to unique 1D polymer structure.

Choice of a solvent for the liquid phase CP synthesis is based on different aspects, such as reactivity, solubility, redox potential, stability constant, etc. A solvent also plays important role in determining thermodynamics and activation energy for a certain reaction, and also solvents can act as ligands during the synthesis. Molecules of a solvent can co-crystallize due to increase in a number of possible weak interactions, and also work as guest-molecules in vacant space of a porous structure. Therefore, character of a solvent may determine, ultimately, the final shape and size of the crystals. Thus, for example, correlation between crystal size and solubility of building units/reagents is established for the CPs based on In (III), 4,4′-bipy and 2,6-bis[(4-carboxyanilino) carbonyl] pyridine, which chelates other metal atom in center (Fig. 6.32) [428]. Increasing DMF content brings to increase in solubility in water and coarse octahedral particles, definitely shaped, while diluted systems provide nucleation on multiple sites and growth of rounded crystals appeared as a result of incomplete growth/stacking process.

As the chosen solvents change, the reactions between 2,5-thiophenedicarboxylic acid (H_2L) and Mg nitrate give four different CPs $Mg_2L_2(Sol)_{2.5} \cdot 0.5Sol$, MgL (DMSO), $[Mg_2L_2(Ac)]$ and $[Mg_2L_2(DMF)_2(EtOH)(H_2O)_2]$ (Sol = ethylene glycol) [429]. Coordinated molecules of solvents take different coordination regimes,
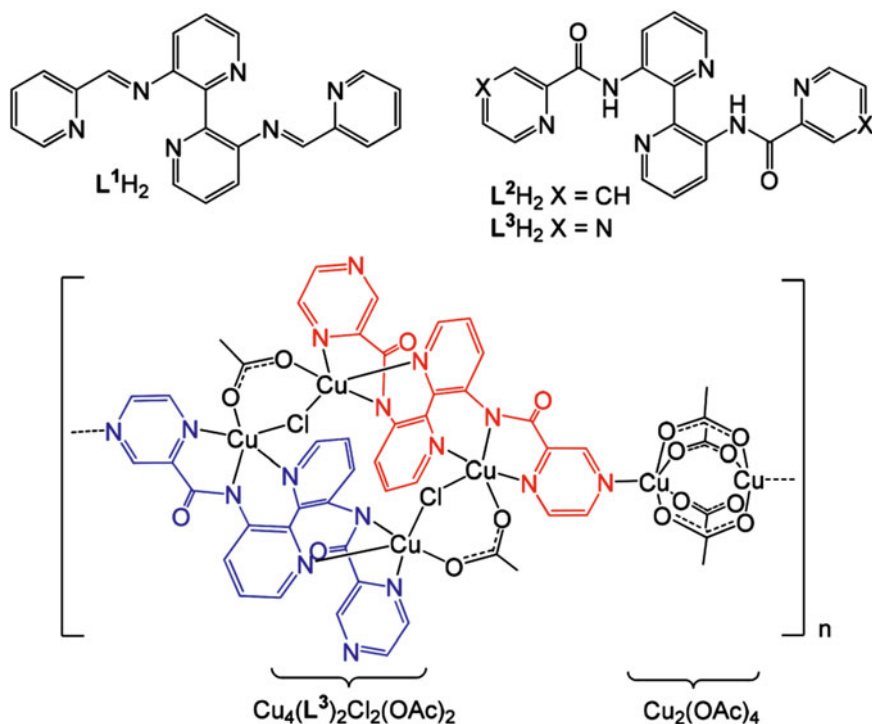
Fig. 6.31 (Top) Heterocyclic bis-imine and bis-amide ligands prepared from 3,3′-diamino-bpy. (Bottom) The molecular structure of CP comprised of a 1D arrangement of $[Cu_4L_2Cl_2(OAc)_2]$ and paddle wheel $[Cu_2(OAc)_4]$ units; for ease, the two ligands within the Cu_4 unit are shown in red and blue

which play important role in building of CP structure. Thus, in the first CP the Sol molecules as bidentate bridging ligands advance linking of MgL layers in 3D framework. DMSO molecules in the second CP and Ac^- anions in the third CP are coordinated in μ_2-way and $(k^2$–$k^2)$-μ_3 regime, respectively, bringing to infinite chains as SBU. And, finally, in layered 2D structure of the fourth CP coordination of DMF, EtOH and H_2O molecules provides induction of the non-centrosymmertical structure.

There is interest in fast, inexpensive, and ecological method of production of high quality MOFs with properties rarely obtained under normal conditions [430]. The method is based on using of organic salts (instead of their homological protonated organic ligands) as sources of anion spacers, so that their solubility and deprotonating stage, which present compulsory in MOF formation, are achieved substantially in aqueous solution. For example, high quality MOF-74 based on zinc acetate and 2,5-dihydroterephthalic acid usually obtained in organic solvents can also be synthesized in water and at room temperature.

Fig. 6.32 **a** Dark-field and **b** bright-field OM images. **c** Red region, **d** green region, and **e** blue region FM images of the micro-sized octahedron CP. **f** and **g** SEM images of the micro-sized octahedron CP and **h** and **i** of the nano-sized rounded-octahedron CPs [428]
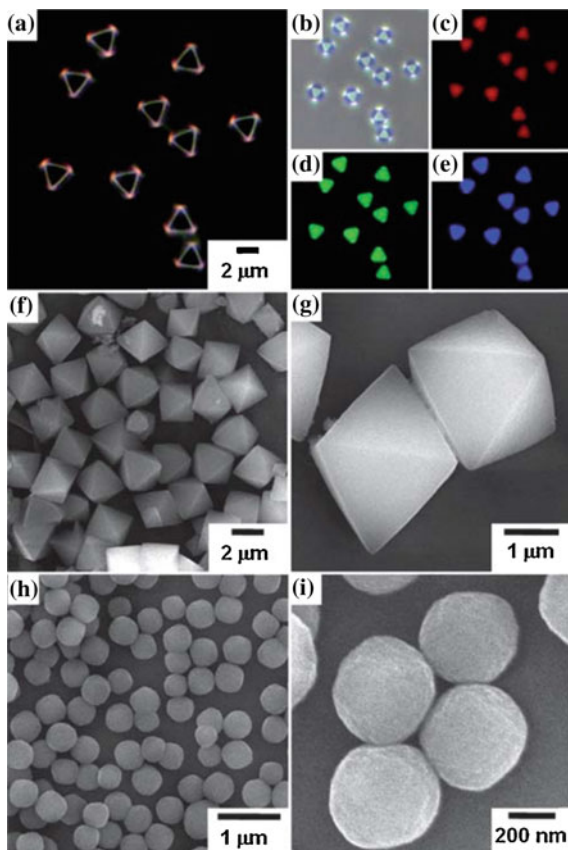
We shall also notice «green coordination modulation method» for CP synthesis using ecological ethanol and alkali additive [431]. In particular, most variable architectures, including rod crystals, dual-core shelled peanut-like crystals and double-head dandelion-like crystals are obtained through changes in parameters of the reaction.

For synthesis of phase-pure MOFs an easy seed-mediated approach is developed, which allows skipping the MOF nucleation stage, which generates mixed cores (Fig. 6.33) [432]. Besides, using this method, phase-pure MOF isomers with separate porous structures are obtained, thus showing universality of the method.

6.7.2 Diffusion Methods

Diffusion method is one of classic methods for synthesis of well-defined crystalline materials [433–435]. The most often used procedure is liquid-liquid diffusion, also
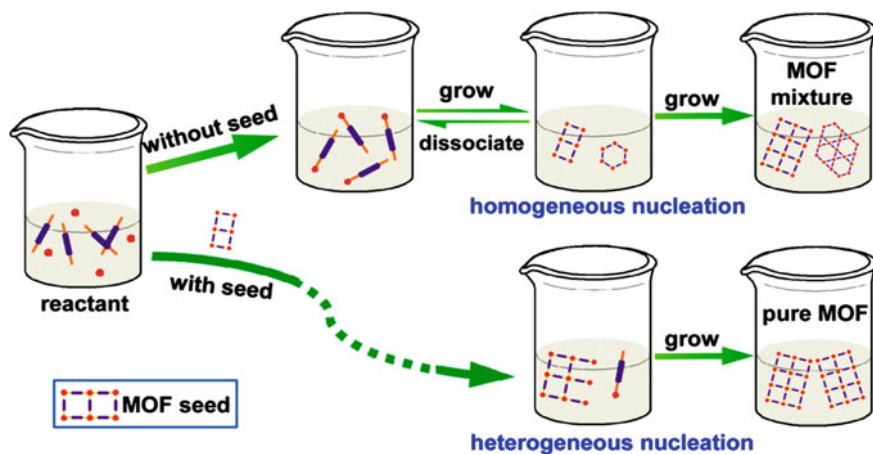
Fig. 6.33 Schematic illustration of the traditional process of MOF crystal growth (homogeneous nucleation) and the strategy for seed-mediated growth of phase-pure MOFs (heterogeneous nucleation)

known as free interface diffusion, in which two or more solutions containing solved reagents are used. Usually solutions of reagents are added in a vessel, so that different layers form in a certain consequence: denser solution in lower part, and a lighter one above it. Addition of a layer of inert solvent increases the diffusion area and prevents fast interaction between the reacting layers. The process begins by slow diffusion of one solution into another, generating crystal nuclei. As compared with fast mixing of solutions containing metal ions and bridging ligands, which makes it possible to obtain microcrystalline product, slow diffusion brings to formation of crystals with pronounced morphologies.

As an example, we shall notice 3d-4d heterometallic CPs with $\{[Cu_3(bpy)_3][Ag_6L_6]\}_n$ and $\{[Zn_3(en)_3][Ag_6L_6]\}_n$ blocks, where H_2L = 2-mercaptonicotinic acid produced based on hexanuclear Ag metalloligands by three-step synthetic method: synthesis of hexanuclear anionic Ag metalloligand, then cationic metalloligand containing centers of 3d-block transition metals, and finally, assembling of two preliminary synthesized components into expanded framework through liquid-liquid diffusion method [436].

It should be noted that growth on the liquid-liquid interface is time-dependent kinetic process, which depends on change in concentration as reactions goes on. Thus, evolution in time is shown from spherical particles to well-defined microribbons in the case of MOF with $[HgClL]_n$ block, where L = 2-[3-(pyridylamino)-phenylazo] pyridine, in methanol-aqua/methanol diffusion system [437]. Besides, fascinating monolithic CP nanofibers with $[CuL(H_2O)]_n$ block (L = aspartic acid) are synthesized [438] in double-layer ethanol-water system. The nanofibers up to one centimeter in length can be obtained by diffusion-controlled growth on the
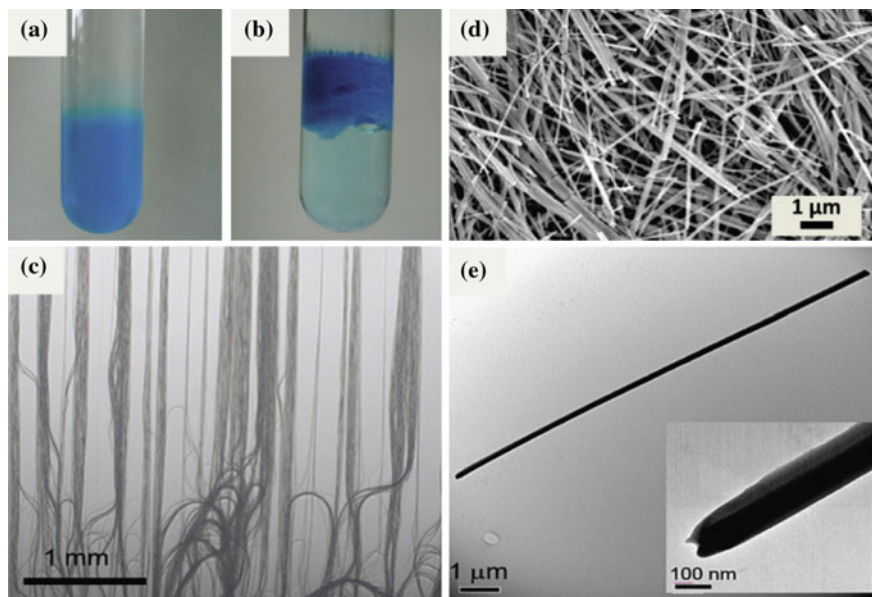
Fig. 6.34 (**a** and **b**) Illustration of the aqueous/organic interfacial growing used to fabricate [CuL (H$_2$O)]$_n$ nanofibers with lengths on the order of centimeters, and their corresponding **c** optical microscope, **d** FESEM, and **e** TEM images [438]

liquid-liquid interface during two weeks (Fig. 6.34). It should be noted that [CuL (H$_2$O)]$_n$ block shorter by tens microns are isolated by addition of the solutions of both reagents during mixing. Slow diffusion of reagents between two non-mixed phases brings to very efficient interphase reaction and provides defect-free junction. Thus, slow diffusion of chloroform solution of two ligands tetrapyridyl-Pp and tris (4-pyridyl)1,3,5-triazine into HgCl$_2$ aqueous solution at room temperature brings to well defined nanotube structures with diameter about 60–80 nm and wall thickness about 15–25 nm [439].

Of interest is a production of 3D plywood-like Ni(II) hexaazamacrocyclic CP with [NiL(H$_2$L′)]$_n$ block (L = 1,3,6,9,11,14-hexaazatricyclo[12.2.1.16,9]octade-cane, H$_4$L′ = 1,2,4,5-benzenetetracarboxylic acid) using slow diffusion [440]. The CP structure includes [NiL]$^{2+}$ cation and [H$_2$L′]$^{2-}$ anion in molar ratio 1:1, in which Ni(II) ions are connected through bridging ligand [H$_2$L′]$^{2-}$ based on weak Ni...O coordination interactions with 1D chain formation. Alternating cross-like 1D chains are stacked in the plywood structure and connected with each other through H-bonds, giving 3D network (Fig. 6.35).

There is such interesting synthetic method as vapor diffusion, which includes solution of a metal source and a ligand in a solvent, for example, DMF, and its positioning in an open container surrounded with a volatile base solution, such as
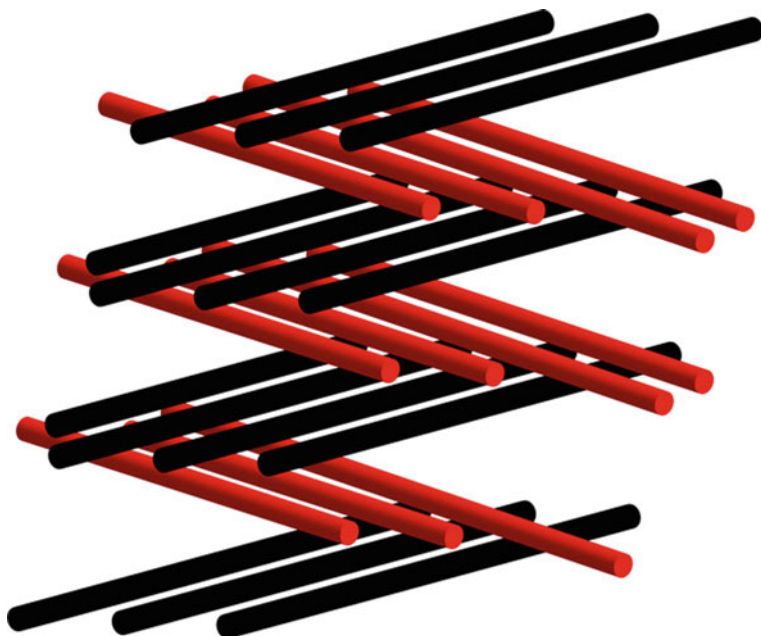
Fig. 6.35 Representation of cross-like arrangement of 1D chains in ABAB fashion to generate 3D plywood-like array in CP

triethylamine. During the synthesis slow diffusion of a volatile amine into diluted solution of the metal salt and ligand takes place at room temperature and atmospheric pressure, thus increasing the ratio acid ligand: conjugated base through deprotonating, and advancing MOF growth. This strategy makes it possible to form large crystals due to decrease in the reaction time [325].

In some cases, also gels are used as diffusion and crystallization media, especially to slow down diffusion and avoid bulk material deposition. Initially, a metal salt is solved in water in a test tube, than a gelating agent (for example, tetramethoxysilane) is added to this solution, and the mixture is shaken until it becomes homogeneous. Then the solution is kept to gel and aqueous solution of ligand layered above this gel and left for several weeks. This method is rather slow to obtain bulk crystals.

The diffusion method is preferred to grow single crystals suitable for X-ray diffraction analysis instead of non-crystalline or polycrystalline products, especially, if they are poorly solved. However, a drawback of diffusion methods is too long time of synthesis (1–2 weeks). Moreover, the diffusion method is to produce bulk crystals (several hundred microns), which are mainly used for structural studies, but are not good, as a rule, for practical applications because of impeded mass transport.

6.7.3   *Hydro(Solvo)Thermal Methods*

Hydro(solvo)thermal methods are the most efficient way for production of various CPs. Initially these methods were developed for synthesis of zeolites, but then they were adapted to synthesis of MOFs and occur so efficient that by now the majority of CPs is obtained particularly using these methods. Hydro(solvo)thermal methods are widely applied in synthesis of new CPs, since their products have high purity, good dispersion, are easily controlled, etc. (Fig. 6.36) [18, 21, 35–37, 84, 325, 441–451]. The hydro(solvo)thermal reactions are associated with using of organic or inorganic solvent at high temperature (usually 80–260 °C) and autogeneous pressure in a closed system (as a rule, Teflon-lined autoclaves or glass vessels) [38] and high throughput hydro(solvo)thermal syntheses are powerful tools for acceleration of discovery of new MOF structures and optimization of synthesis procedures [452, 453]. The apparent advantage of hydro(solvo)thermal methods is that they make it possible to facilitate problems of chelating ligands solubility and improve reactivity of reagents during crystallization process [454]. Undoubtedly, during the synthesis it is necessary to take into account some parameters of the reaction, including composition of reagents, temperature and pressure, concentration, time of reaction, pH, solubility, etc. [40]. Since crystallization under hydro(solvo)thermal conditions is often non-equilibrium process and can bring to metastable products, very important parameter is also the cooling rate at the end of reaction. It is important that many initial materials can be subjected to unexpected chemical changes under hydro(solvo)thermal conditions, which are often accompanied by formation of nanometer morphologies and are usually unachievable with traditional methods. Besides, as compared with traditional solution methods, such as evaporation, diffusion, and cooling, hydro(solvo)thermal reactions relate to relatively complicated processes, and final products in this set of conditions are often unpredictable. In most cases in hydro(solvo)thermal reactions highly boiling organic solvents are used, in particular, DMF, diethylformamide (DEF), acetonitrile, acetone, ethanol, methanol, etc. We shall notice also mixtures of solvents used in order to avoid problems of different solubility for various initial materials. This method allows
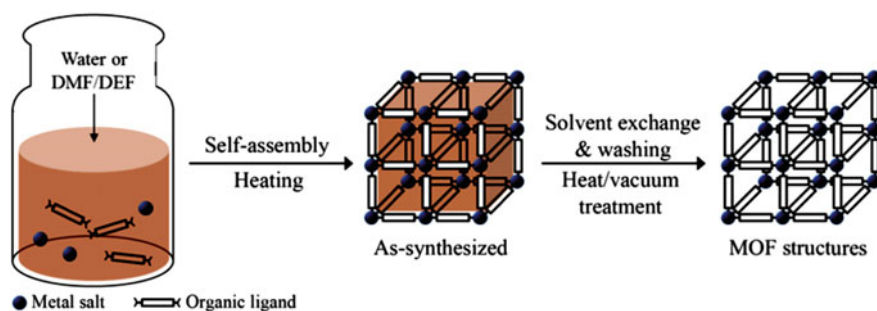
Fig. 6.36 Conventional hydro(solvo)thermal synthesis of MOF structures

reducing the synthesis time as compared with «diffusion» method to 24 h and in some cases to 4 h. As a rule, MOF crystals formed by hydro(solvo)thermal method are more suited to solving technological problems. Besides, clear advantages of hydro(solvo)thermal methods as compared to more complicated methods include larger crystal size, easy scaling and availability of the methods with high throughput. Drawbacks of this method are long time of reaction, low percentage yield, necessity in high temperatures and use of toxic solvents (for example, DMF) [325].

Among a vast variety of polytopic ligands used in hydro(solvo)thermal MOF synthesis, the leading role, undoubtedly belongs to carboxylate ligands [1–9], therefore they, first of all, were used in design of CPs containing metal chelate units. Thus, solvothermal reaction of Co(II) or Zn(II) salts with dianhydride of 1,2,4,5-benzenetetracarboxylic acid (H_4L) brings to formation of 3D CPs with $[Co_2L]_n$ and $[Zn_4L_2]_n$ blocks, at that in the first polymer 1D Co(II) carboxylate chains are interconnected by organic fragment of L^{4-} ligands. In the second polymer 1D ZnL^{4-} ribbons are interconnected by $[Zn_2(H_2O)_3]$ building units creating 3D porous framework with 1D rectangular channels [455]. With the same ligand CP with $[ZnL]_n$ block is obtained, which presents a 3D network containing 1D rhombic channels, window sizes about 8 Å in the widest and 4.5 Å in the narrowest spacing along c axis [379]. Often in similar synthesis, apart from the main also ancillary ligands are used, such as, for example, 1,2-di(4-pyridyl) ethylene (L′). Just with this ligand CP is obtained with $[ZnL_{0.5}(L')_{0.5}]_n$ block, which has a complicated 3D framework with (3,4)-connected **fsh** topology [456]. An interesting example is 3D CP with $[Cd_3(L')_2L_2]_n$ block synthesized based on a main ligand of 1,2,4-benzenetricarboxylic acid (H_3L) and ancillary ligand of 1,4-bis(imidazolyl) butane (L′) under hydrothermal conditions. The obtained CP relates to extraordinary examples of trinodal (4,6)-connected network with **fsc** topology [457]. We shall also notice 3D microporous MOF with $[ZnL(L')_{0.5}]_n$ block including 2-hydroxybenzenedicarboxylic acid (H_2L) and 1,4-diazabicyclo(2.2.2)octane (L′) with OH-functional groups on pore surfaces synthesized under solvothermal conditions [458]. It is worth paying attention to CP with $[MgL]_n$ block (L = perylene-3,4,9,10-tetracarboxylic acid dianhydride) with special hexagonal tube-like morphology, which is produced by self-assembling by hydrothermal method [459]. It is interesting that this morphology of $[MgL]_n$ is mostly controlled by Ostwald ripening and self-structuring mechanism, at that using organic solvents as additives, the preparation of CPs of different morphologies, for example, hexagonal rings and snowflakes, and also CP sizes from micro- to nanometers can be controlled.

Hydrothermal reaction of $La(NO_3)_3$ with 2-pyrimidinecarbonitrile in water gives 3D MOF with $[La_2L_3(H_2L)]_n$ block (L = oxalate), which has channels with accepted inside water molecules [460]. The crystal structure consists of 3D MOF with channels that propagate along a, b, and c crystallographic axes and locate water molecules inside the channels. It is important that CP is built from La atoms linking with bis-chelating oxalate ligands.

La-based CPs microplates are prepared using a simple «bottom-up» method by hydrothermal reaction of La(III) and «green ligand» EDTA [461]. Under similar conditions analogous Ce-EDTA CPs microplates are also prepared. It is important that the mechanism of La-EDTA CPs formation follows the Ostwald ripening mechanism, and its morphology can be easily adjusted by variation the amount of EDTA, and the total concentration of reagents. Besides, also several types of micro/ nanostructures have been obtained, such as nanocluster particles, nanofibers, big or uniform microplates.

In the design of the CPs containing metal chelate units a considerable attention was paid to combination of bridging mono- or polycarboxylates and ancillary chelating ligands with metal ions using hydro(solvo)thermal methods, which generated many interesting coordination architectures. This way was used, for example, to obtain of mixed-ligand Co(II) CPs with $[Co_2(\mu_2\text{-}L)(bpy)_2]$ and $[Co_2(\mu_2\text{-}L)(phen)_2]$ blocks based on 1,2,4,5-benzenetetracarboxylic acid (H_4L) [462]. It is worth noticing that both complexes are bridged using L^{4-} ligands with formation of binuclear structures, and H-bonds make it possible for them to join into 2D and 3D networks.

MOF with $[CdL(phen)]_n$ block is hydrothermally synthesized by heterocyclic 2,2′-biquinoline-4,4′-dicarboxylate ligand (L) and N-containing ancillary ligand [463]. The complex is infinite 2D framework networks containing aesthetic *meso*-helix, which are linked with formation of 6-connected 3D supramolecular architecture through aromatic π–π stacking and C–H···O–H-bonds interactions.

CPs with $[ZnL(L'')]_n$, $[ZnL(L'')]_n$, $[Cd_2(L')(L'')]_n$ and $[Cd(L')(L'')]_n$ blocks are obtained through interaction under solvothermal conditions between 1,2-phenylenedioxydiacetic acid (H_2L) and hydroquinone-O,O′-diacetic acid (H_2L') with Zn and Cd nitrates in presence of ancillary ligand 1,1′-(1,4-butanediyl)bis(imidazole) (L″) [464]. We shall also notice hydro(solvo)thermal synthesized CPs with $[Cd(HL)(phen)]_n$, $\{[Cd(HL)(bpy)]_2\}_n$ and $[Cd(HL')(bpy)]_n$ blocks based on 2-methyl (H_3L) and 2-ethyl-1H-imidazole-4,5-dicarboxylic acid (H_3L') [465]. The CPs are infinite chains, in which HL and HL′ in μ_2-regime are linked with Cd(II) atoms, while phen or bpy chelate central ions (Fig. 6.37).

An interesting example is hydro(solvo)thermally synthesized CPs with $[Mn_2L_2$ $(phen)_2]_n$, $[Mn_2L_2(phen)]_n$ and $[Mn_4L_4(phen)_4]_n$ blocks based on 1,4-naphthalene dicarboxylic acid (H_2L) [466]. L^{2-} ligands take various coordination regimes in different solvents and concentrations, which provides formation of various crystal structures. Thus, first CP has Mn_2 dimers linked with L^{2-} spacers, and stacked in 2D structures of grid pattern. The next CP has 3D framework, which is formed by Mn_2 dimers and L^{2-} spacers, and each MnO_4N_2 node of the third CP is linked with other node through L^{2-} ligands with formation of 2D structure (Scheme 6.16).

We shall also notice synthesized under hydrothermal conditions CPs with $[CdL$ $(L')_{0.5}]$ (**1**), $[NiL(L')]$ (**2**), $[Cd_2L_2(L')_2]$ (**3**), $[CdL(L')]$ (**4**), $[NiL(L')]$ (**5**), $[NiL(L')]$ (**6**), $[CdL(L')_{0.5}]$ (**7**), $[CdL(phen)]$ (**8**), $[Cd_3L_3(H_2O)]$ (**9**), and $[Cd_3L_3(L')_{0.5}]$ (**10**) blocks including the main ligand 3-carboxy-1-(4′-(2″-carboxy)biphenylmethyl)-2-oxidopyridinium (H_2L) and ancillary (L′) ligands 1,4-bis(imidazol-1-ylmethyl)
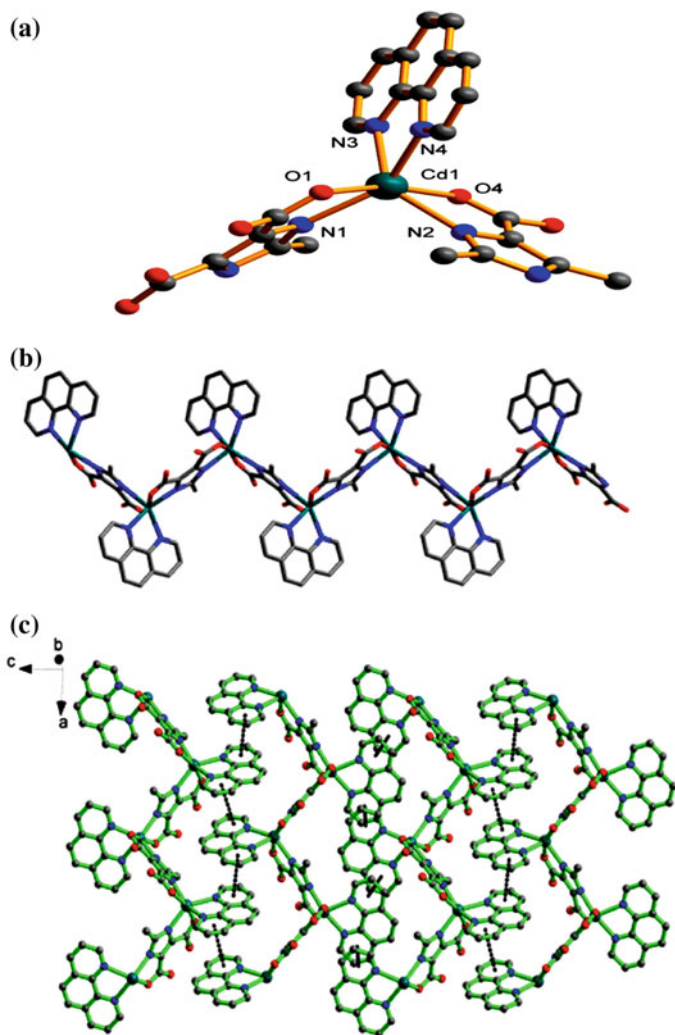
Fig. 6.37 a Molecular square structure of CP with $[Cd(HL)(phen)]_n$ block based on 2-ethyl-1H-imidazole-4,5-dicarboxylic acid. **b** 1D chain of CP. (c) 2D sheet of CP supported by π–π stacking interactions

benzene (compounds **1** and **2**), 2-(6′-(pyridin-2″-yl)-4′-p-tolylpyridin-20-yl)pyridine (compounds **3** and **5**), 2-(4′-(4″-*tert*-butylphenyl)-6′-(pyridin-2″-yl)pyridin-20-yl) pyridine (compounds **4** and **6**), 1,10-(1,6-hexanediyl)bis(imidazole) (compound **7**), 1,10-(1,4-butanediyl)bis(imidazole) (compound **10**) [467]. Compounds **1** and **2** have layered structures, in which adjacent layers are additionally linked through π–π stacking interactions with formation of supramolecular 3D architectures. The compound **3** consists of two crystallographically different dimers, which are later linked

$$H_2L + phen + MnCl_2 \cdot 4H_2O$$
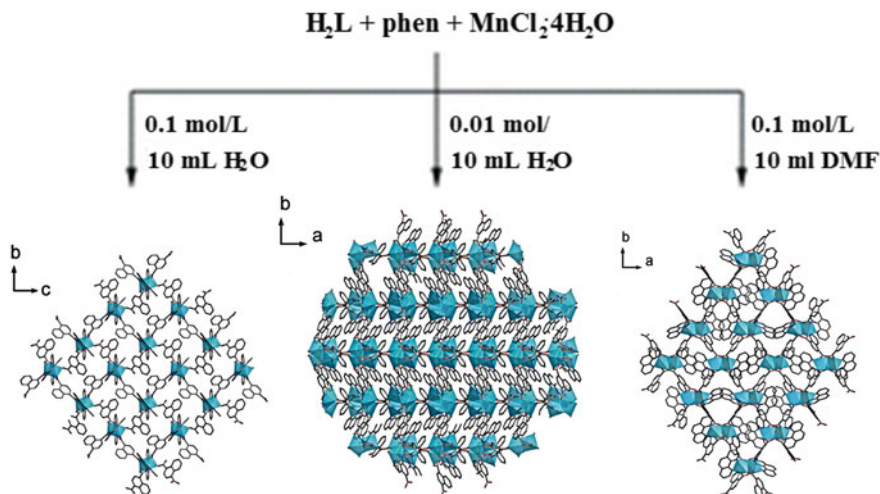
Scheme 6.16 The formation of various crystal structures in different solvents and concentrations during interaction of 1,4-naphthalene dicarboxylic acid, phen and MnCl$_2$

through π–π and H-bonding interactions into 2D supramolecular architecture. The compounds **4-6** are distinguished by chain structures and in the compound **4** adjacent chains are folded through π–π interactions, bringing to 2D supramolecular architecture. In the compound **5** adjacent chains are linked through π–π interactions bringing to 3D supramolecular architecture. In the compound **6** adjacent chains are further linked through H-bonds interactions into 3D supramolecular architecture. The compound **7** shows 2D 63-**hcb** network, in which the adjacent networks are prolonged by π–π stacking interactions into 3D molecular supramolecular architecture. The compound **8** reflects a (4,4) sheet. The compound **9** has 2D network (4,4). And, finally, the compound **10** shows 3D 5-connected framework with $(4^6 \cdot 6^4)$ topology. It is important that the crystal structures of the obtained CPs are to a great extent determined by the effect of L-anions and N-donor ligands.

Solvothermal reactions of terphenyl-2,5,2′,5′-tetracarboxylic acid (H$_4$L) and M (II) in presence of bpy give three CPs with [ML$_{0.5}$(bpy)]$_n$ (M = Co, Ni) and [Cu (H$_2$L)(bpy)]$_n$ blocks [468]. First two CPs are isostructural and represent 2D layer, in which L^{4-} is a twisted H-like ligand linking Co(II) centers. Moreover, 3D structures are formed using interchain π–π interactions between adjacent bpy ligands. In the third CP two deprotonated carboxyl groups of H$_2$L^{2-} represent Z-like ligand linking Cu(II) centers into 1D zigzag polymer chain. The 2D layered structure is built using interchain π–π interactions between bpy and H$_2$L^{2-}.

Of interest are systematic arrays of CPs including bpy chelating ligand and different derivatives of isophthalic acid, including, for example, C(CH$_3$)$_3$ group (tetranuclear clusters and linked by H-bonding to form a 3D supramolecular structure) [469], 5-(4′-methylphenyl) group (1D linear chain, linked with L bridge) [470], OH group (1D zigzag chains and linked by H-bonding and π–π stacking interactions to form a 3D
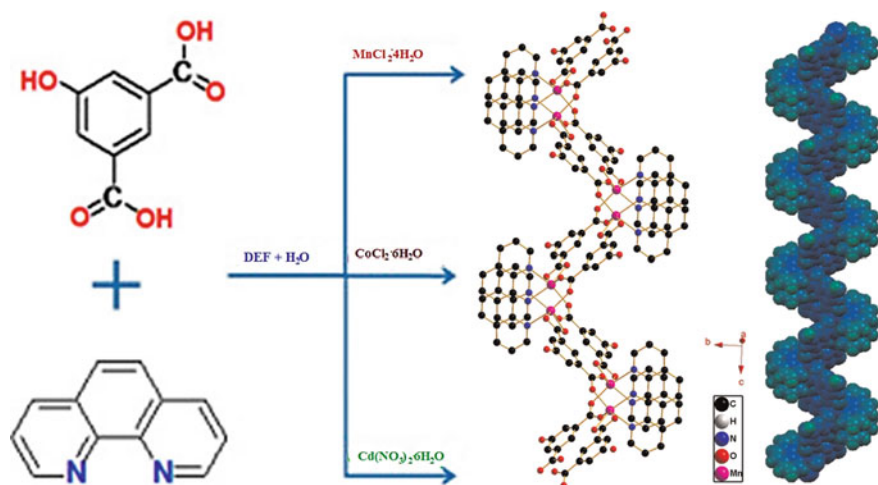
Scheme 6.17 1D helical chains of CPs synthesized by hydro(solvo)thermal reaction of 5-hydroxyisopthalic acid and phen with $MnCl_2 \cdot 4H_2O$, $CoCl_2 \cdot 6H_2O$ or $Cd(NO_3)_2 \cdot 6H_2O$

supramolecular structure, Scheme 6.17) [471], 5-(4-carboxybenzylamino) group (1D, 2D and 3D frameworks, Fig. 6.38) [472], 5-(imidazol-1-yl-methyl) group (double-chained and 3D supramolecular structures through H-bond/π–π interactions) [473], 4,5-di(3′-carboxylphenyl) group (0D, 1D, 2D and 3D structures, Fig. 6.39) [474] etc. Such arrays make it possible to reveal fundamental structure-properties relations to define possible directions of practical applications for CPs.

We shall also notice using of 3,5-disulfobenzoate (L) in hydrothermal synthesis of Ln-based 2D MOFs with $[LnL(phen)]_n$ block, where Ln = La, Pr, Nd [475]. They belong to two 2D structural types, and their networks have different topologies: the isostructural La and Pr compounds are uninodal 5-connected SP 2-periodical (6,3) networks and the Nd compound has a binodal 3- and 6-connected **kgd** network.

It is interesting to use flexible fatty carboxylic acids, for example heptane and hexane diacids, as bridging ligands, and phen derivatives, for example, 2-(3-pyridyl (imidazo[4,5-f]phen and 2-(4-pyridyl)imidazo[4,5-f]phen, as chelating ligands [476].

1D CP zigzag chain $[ZnL(L')]_n$ based on 5-amino-2,4,6-triiodoisophthalic acid (H_2L) and 2,2′-dipyridylamine (L′) is synthesized under solvothermal conditions [477].

Another direction of hydro(solvo)thermal synthesis of CPs containing metal chelate units is linking of low molecular weight metal chelates with various bridging ligands. Thus, CP with $[Co_2(\mu_{1,1}-N_3)_2(phen)_2(N_3)_2]_n$ block has been obtained by hydrothermal method using a phen as ancillary chelating ligand and
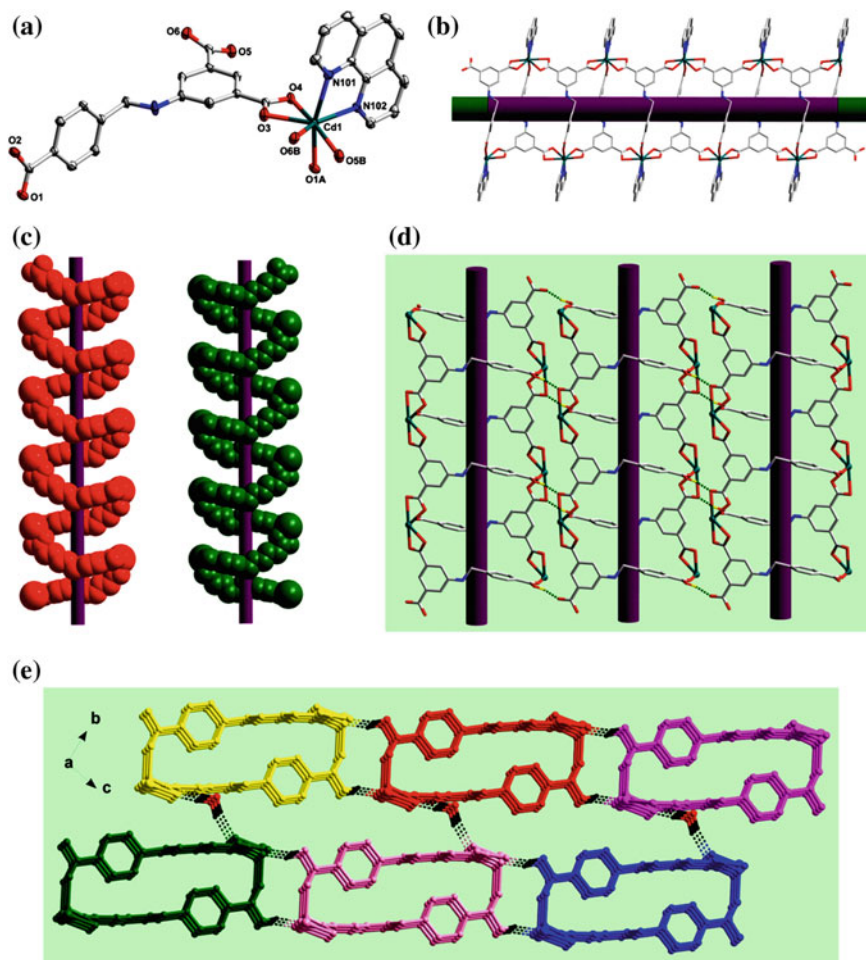
Fig. 6.38 a The coordination environment of the Cd(II) ions in CP. **b** The 1D neutral double-stranded chain of CP. **c** Schematic view of the right- and left-handed helical chains in CP. **d** The 2D network of CP extended by H-bonding interactions. **e** The 3D framework of CP constructed through H-bonding interactions

bridging azide-linking ligand [376]. Macrocyclic ML complexes based on 2,3-dioxo-5,6,15,15-dibenzo-1,4,8,12-tetraazacyclo-pentadeca-7,13-diene (H$_2$L) are applied as main building units for preparation of CPs with [Cd(L′)(NiL)]$_n$ and [Mn(L″)(NiL)$_2$]$_n$ blocks including bridging ligands 5-aminoisophthalic acid (H$_2$L′) or 5-aminoisophthalic acid (H$_2$L″). It is important that CPs consist of different 1D chains formed by L and L′ or L″ bridge, and they are bound through H-bonds into 2D architecture [478].

We shall also notice using of metal-organic coordination compound Cd(phen)$_2$(NO$_3$)$_2$ as a source of metal instead of inorganic metal salt for synthesis of CPs with
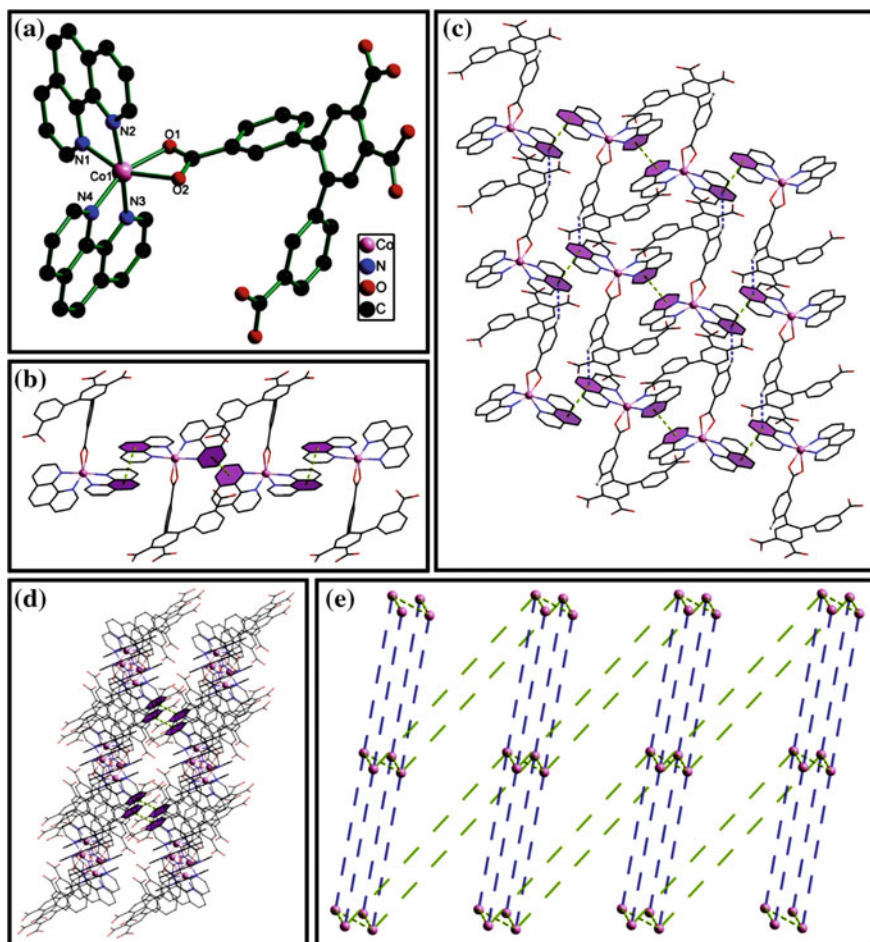
Fig. 6.39 a The coordination environment around Co(II) in CP. **b** The formation of 1D zigzag chain through π–π stacking of adjacent 0D units. **c** The construction of 1D to 2D layer through C–H⋯π interaction. **d** View of 2D to 3D through π–π stacking. **e** The 3D topological structure

[CdL(phen)$_2$]$_n$ blocks based on biphenyl-4,4′-dicarboxylic acid, benzene-1,4-dicarboxylic acid and 1,2,4,5-benzenetetracarboxylic acid (Scheme 6.18). The first CP is 1D zigzag chain, and the second CP is 2D layered network. The third CP is a supramolecular 3D framework, which is especially interesting for its two independent Cd atoms forming separately 1D polymer chains locating alternately with formation of 3D supramolecular framework through interchain H-bonds [479]. The 2D CPs with {[ZnL(phen)]$_2$}$_n$, {[CdL(phen)]$_2$}$_n$, {[Zn(L′)(phen)]$_2$}$_n$ and [Zn(L′)(phen)]$_n$ blocks are obtained as a result of reaction of Zn(II)- or Cd(II)-phen with biphenyl-4,4′-dicarbonic acid (H$_2$L) and 4,4′-azodibenzoic acid (H$_2$L′)] [480]. The coordination-induced effect of their morphology is shown, in particular, grain and
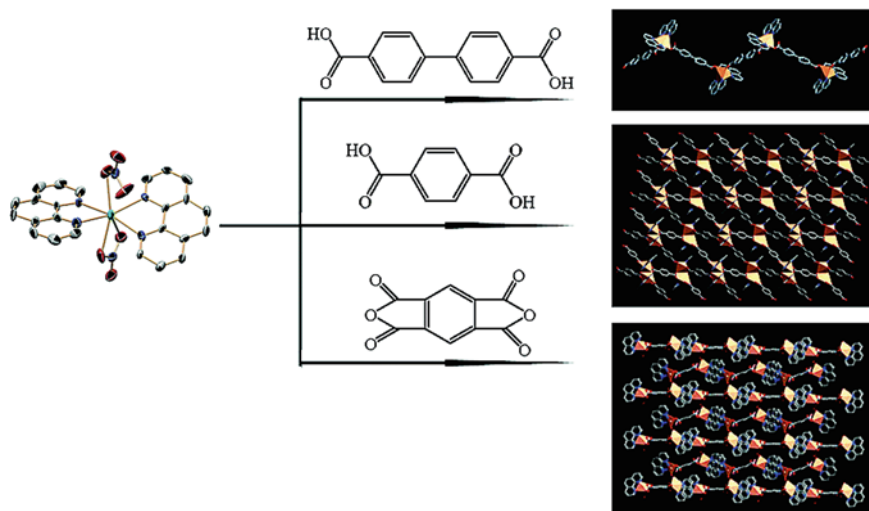
Scheme 6.18 The CPs based on biphenyl-4,4′-dicarboxylic acid, benzene-1,4-dicarboxylic acid and 1,2,4,5-benzenetetracarboxylic acid synthesized under different conditions by using the metal-organic coordination compound Cd(phen)$_2$(NO$_3$)$_2$ as the metal source instead of inorganic metal salt

flowery morphology of non-coordinated ligands H$_2$L and H$_2$L′, respectively, changes with coordination of metal salts. The ridged surface, cracks of 2 μm width, parallelepiped structure and feathery appearance are established for the CPs, respectively (Scheme 6.19).

Unexpected result is reached by studying of hydrothermal reaction of [Mn(III) (salen)(H$_2$O)$_2$](ClO$_4$) complex with phen and 4,4′-dicarboxy-bpy (H$_2$L) [481]. It occurs that during the reaction Mn is reduced to divalent state and 3D Mn(II) MOF with [MnL(phen)]$_n$ block forms. In these compounds neighboring Mn(II) ions are linked with carboxylate bridges in μ$_2$-coordinating regime for generation of 1D zigzag chains interlinked with dicarboxylate groups of long L ligands for production of 3D (4,4)-connected structure. Each Mn(II) ion is coordinated with four molecules of a ligand and one phen molecule and reflects distorted octahedral environment. It is important to emphasize that potentially chelating bpy fragment does not take part in chelation with Mn(II) ion. The similar absence of a bpy fragment chelation is also found in lanthanide CPs with [La$_2$L$_3$]$_n$ and [Sm$_2$L$_3$]$_n$ blocks based on bpy-3,3′-dicarboxylic acid (H$_2$L), in which only coordination of carboxylate fragments is realized [377]. The CPs are 2D network structures based on zigzag-like chains, which are linked by L ligands, and adjacent zigzag chains are symmetrical in mirror reflections forming ABAB stacking.

At the same time, when using bpy-4,4′-dicarboxylate (H$_2$L) and the respective transition metal(II) salt under hydrothermal conditions CPs with [MnL(H$_2$O)$_2$]$_n$, {[Ni(L(H$_2$O)$_2$]·2H$_2$O}$_n$, [NiL(H$_2$O)$_2$]$_n$, and [CuL(H$_2$O)]$_n$ blocks are obtained, in which each metal ion is coordinated with chelating bpy fragment, two carboxylate
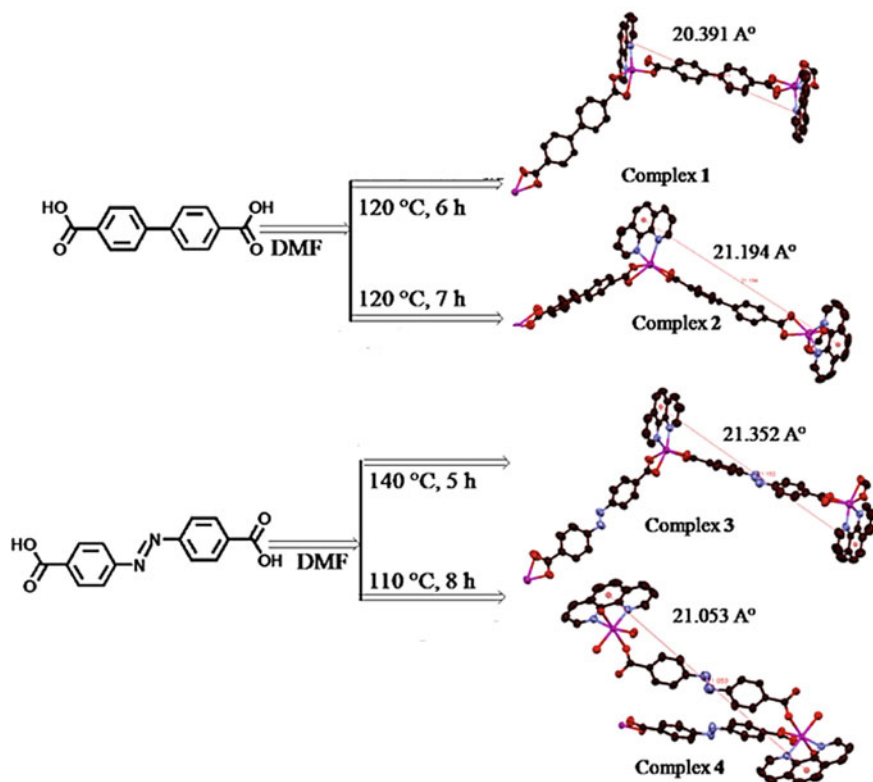
Scheme 6.19 CPs obtained by the reaction of metal [Zn(II), Cd(II)], phen separately with biphenyl-4,4′-dicarboxylic acid and 4,4′-azodibenzoic acid

oxygen L^{2-} and water molecules [482]. It should be noticed that the first and the third CPs are 3D polymers linked by L^{2-} bridge, while the second and the fourth CPs show 2D layered structures linked by L^{2-} bridge, and are additionally collected through H-bonds with formation of 3D supramolecular structures.

Interesting coordination patterns are found in CPs of lanthanides with $[Ln_3L_4(HL)]_n$ (Ln = Ce, Nd and Pr) and $[Ln_2L_3]_n$ (Ln = Er and Tm) blocks based on bpy-6,6′-dicarboxylic acid (H_2L) [483]. Thus, for example, in the first CP (Fig. 6.40) ligands display two different ways of coordination: one ligand is tetradentate for linking one metal ion using two oxygen atoms and two pyridyl nitrogen atoms in chelating regime, another ligand except of chelation of this metal is also linked to another metal ion with another oxygen atom from one of carboxylate groups playing the role of pentadentate ligand.

One more advantage of hydro(solvo)thermal synthesis is using of even so insoluble reagents as metal oxides, which are unsuitable for ordinary synthesis in solution, and thermally stable coordination compounds form, as a rule, as a result of hydro(solvo)thermal reaction. As an example, we shall consider 3D heterometallic
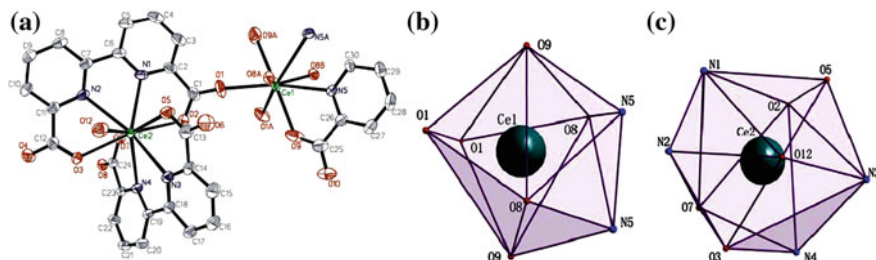
Fig. 6.40 a Numbering scheme and coordination environment around the two crystallographically independent Ce(III) centers in CP. **b** and **c** Highlight of the coordination polyhedra for the two crystallographically independent Ce(III) ions

CP with $[Nd_2Cu_2L_2(L')_4]_n$ block based on bpy-3-carboxylic acid (HL) and oxalate (L'), which is obtained as a result of hydrothermal reaction Nd_2O_3, HL, and oxalic acid in presence of ethanol and water [484]. It is important that in this CP HL shows monodentate character through coordination by carboxylic oxygen, as well as chelating ability with contribution from a bpy fragment. There is interest in other 3d-4f heterometallic CPs based on bpy-5,5-dicarboxylic acid (H_2L) with $[Pr_4(H_2O)_9Cu_{3.5}Cl_{0.5}(L)_{6.5}(OH)_2]_n$ block, built from 2D Pr-O layers and $[CuL_2]^{3-}$ or $[CuLCl]^{2-}$ pillars [485], or CPs with $[Ln_3Co_2L_5(HL)_5(H_2O)_5]_n$ (Ln = Eu, Gd, Tb, Dy, Ho, Tm, Lu) block shaped as 3D sandwich-like framework [486].

Heterocyclic polycarboxylates are widely used in synthesis of CPs containing metal chelate units [1–9]. Thus, hydrothermally synthesized are 2D lanthanide CPs with $[LnL(HL)]_n$ (Ln = Pr, Nd, Sm, Eu and Tb, H_2L = Py-2,3-dicarboxylic acid) block, which are built from sheets consisting of carboxylate-bridging Ln dimers folded along [98] direction and held together by H-bonds between carboxylic groups [487]. Using 1,4-bis(1H-imidazol-1-yl) butane (L') as an ancillary ligand, CPs with $[ZnL(L')]_n$ and $[CdL(L')]_n$ blocks are obtained, first CP of which shows wave-like layered structure, where layers are additionally stacked through π–π interactions to generate 3D supramolecular architecture (Fig. 6.41) [488]. For the second CP 3D three-fold interpenetrating diamondoid architectures are typical.
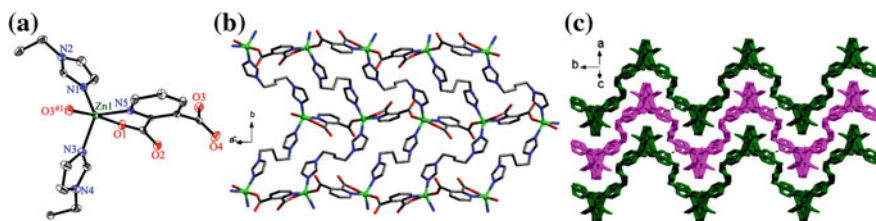
Fig. 6.41 a Coordination environment of the Zn(II) atom in CP. **b** View of the 2D undulating layer of CP. **c** View of the 3D supramolecular architecture connected by face-to-face π–π interactions

In the CP obtained solvothermally from Nd(III) and Py-2,5-dicarboxylic acid, asymmetric block consists of one Nd(III) center, located at the twofold axis, and one L^{2-} ligand [489]. The 3D framework can be considered as built with layers of octacoordinated Nd(III) centers connected through layers of L^{2-} ligands. The CPs with hierarchical micro- and nanostructures with $[CuL]_n$ block based on the same ligand with regulated morphology are obtained through varied synthesis parameters: a reagent concentration, type of a solvent and a surfactant, the reaction temperature [490].

Two CPs with $[Cd_3(OH)_2L_2]_n$ and $[Cd_2L_2(L')]_n$ blocks based on Py-2,4-dicarboxylic acid (H_2L) and 1,2-bis(4-pyridyl)ethene (L′) are obtained under hydrothermal conditions with different pH [491]. The first CP has a 3D framework built from 2D Cd–O(OH) layers and pillared L ligands. The second CP is a 3D MOF with the Cd(II) centers linked with L and L′ ligands. The differences between the structures show that the change in pH has significant effect on the formation and structures of the final polymers. Two types of Cd(II) ions are present in the first CP. The Cd1 atom is six-coordinated in a distorted octahedral geometry with oxygen atoms from two μ_3-OH coordinated groups at the axial positions, three carboxylate oxygen atoms, and one nitrogen atom from three L ligands in the equatorial plane. At the same time, Cd2 atom displaced on a twofold rotation axis, takes a distorted square antiprismatic geometry, and is surrounded by eight oxygen atoms.

We shall also notice 3D CP with $[Co_4L_4(OH_2)_{10}]_n$ block obtained through hydrothermal reaction of Py-2,4-dicarboxylate (L) with metal salts, which is zigzag shaped [492]. It is important that in presence of oxalic acid a protonated polymer $[CoL_2(OH_2)_2]_n$ forms, and excess alkali addition brings to formation of 3D polymer $[Co_3(\mu_3\text{-}OH)_2L_2]_n$.

Py-2,6-dicarboxylic acid (H_2L) was used for synthesis of two structural CPs with $[Ln_2L_3]_n$ (Ln = Pr and Eu) block under hydrothermal conditions. These compounds contain different cycles and form 2D structure, while 3D structures form under action of covalent and H-bonds [493]. Interaction between the same ligand and Pr nitrate under hydrothermal conditions leads to CP with another $[PrL_2]_n$ block, which contains crystals whose adjacent 1D chains are linked by H-bonds with formation of planes integrated into 2D corrugated laminar structures [494]. The same ligand is used in hydrothermal synthesis of CP having 3D hydrotalcite-like structure formed from 2D cation $[\{Ce(H_2O)_5\}_2\{CeL_2(H_2O)_4\}\{CeL_3\}]^{2+}$ layers, supported by α-Keggin $[PW_{12}O_{40}]^{3-}$ anions [495].

Under hydrothermal conditions, two heterometallic CPs with $[KBaL]_n$ and $[KCaErL_2]_n$ blocks are synthesized based on Py-2,4,6-tricarboxylic acid (H_3L), in which both polymers have 3D structure [496].

We shall also notice Ln(III) CPs with $[LnL_3]_n$ (Ln = La, Y, Sm and Nd), $[Gd_2L_3]_n$ and $[CeL]_n$ blocks based on chelidamic acid of 4-hydroxypyridine-2,6-dicarboxylic acid (L) produced by hydrothermal method. The first four isostructural CPs have 2D framework, the fifth polymer contains two different Gd (III) ions linked through a carboxylic group with formation of 2D framework, and the last CP has 2D network of (4^4) topology [497]. Two heterometallic CPs with

$[AgNdL_2]_n$ and $[K_{0.25}NdL_2]_n$ blocks are synthesized with the same ligand [498]. The crystalline structure of the first CP is characterized by the fact that chelate units consisting of one Nd(III) ion and three tridentate chelating L ligands are bound through Ag ions forming 1D chain linked additionally by H-bonds in 3D networks. As regards the second polymer, discrete, independent molecules consisting of Nd (III) ion, K ions, and L ligands are bound through H-bonds with formation of 1D chain, which then is connected through complicated H-bonds resulting to 3D network. Under hydrothermal conditions from $Co(OH)_2$ and chelidamic acid in the molar ratio 1:1 the Co(II) CP with $[Co_{1.5}L]_n$ block is obtained, which crystallizes into 1D stair-like structure [499].

There is interest in CP with $[Ca_2L(L')]_n$ block based on pyrazine-2-carboxylate (L) and benzene-1,3,5-tricarboxylate (L') synthesized by hydro(solvo)thermal method forming a double layered network, in which inorganic zigzag chains of coordination Ca polyhedron are bound with organic ligands [500]. CPs with $[M_2L_4]_n$ block are obtained through interaction between 2,3-pyrazinedicarboxylic acid (H_2L) and Y and Sm nitrates under hydrothermal conditions in presence of ammonia for pH regulation. The obtained CPs are isostructural and show a 3D network structure based on $[M_2L_4(H_2O)_2]$ building units [501].

Different synthetic strategies are used in hydro(solvo)thermal synthesis of 3d-4f heterometallic 3D networks based on Co(II) and Gd(III) cations, and also imidazole-4,5-dicarboxylic acid (H_3L) and oxalate (L'), which serve as the main and auxiliary ligands, respectively [502]. Thus, $[Gd(L')CoL]_n$ is obtained using one-pot synthesis, and $[GdCo(HL)(L')_{1.5}]_n$ is synthesized using precursor of Co(II) complex (Scheme 6.20). Both CPs are crystallized in monoclinic system and are characterized by presence of intricate covalent 3D network. A considerable aspect is the fact that in these centrosymmetric structures Co(L/LH) blocks are arranged along networks forming alternative chiral chains Λ and Δ. Despite the fact that H_3L ligand can link simultaneously 3d- and 4f-cations, there is efficient to include an ancillary ligand, such as oxalate-anions to obtain $[Ln_2Zn_4L_4(L')]_3$ (Ln = La, Nd, Sm, Eu) and $[Ln_4Zn_4L_4(L')]_3$ (Ln = Eu, Gd, Dy, Ho, Er, Yb and Lu) [503]. Using another approach based on Co(II) precursor $[CoL]_n$, where L is Py-dicarboxylic acid, it is possible to generate extended networks, i.e. when a precursor of Co(II) complex is mixed with Gd(III) and La(III) under hydrothermal conditions, 2D network $[LnCoL_2(HL)]_n$, where Ln = Gd, La can be obtained [504]. Obviously, both synthetic methods are efficient for production of 3d-4f heterometallic networks.

We shall also notice CPs with $[Zn_2(\mu_2\text{-}HL)_2(phen)_2]_n$, $[M(\mu_2\text{-}HL)(bpy)]_n$ (M = Ni and Mn) and $[M(\mu_2\text{-}H_2L)_2]_n$ (M = Mn and Co) blocks, carrying 2-p-methoxyphenyl-1H-imidazole-4,5-dicarboxylic acid (H_3L), which have been synthesized hydrothermally (Scheme 6.21) [505]. The first CP is distinguished by an infinite corrugated structure, the second and third CPs show straight chains, and the last two CPs demonstrate isomorphic 2D structures containing similar inorganic motifs with an individual rhombus as SBU.

There is also interest in CPs with $[Sr(HL)]_n$ and $[Cd_2(HL)_2]_n$ blocks, which are obtained through solvothermal reactions with 1-(4-carboxybenzyl)-1H-imidazole-4,5-dicarboxylic acid (H_3L) serving as a dianionic tricarboxylate spacer [506]. While the
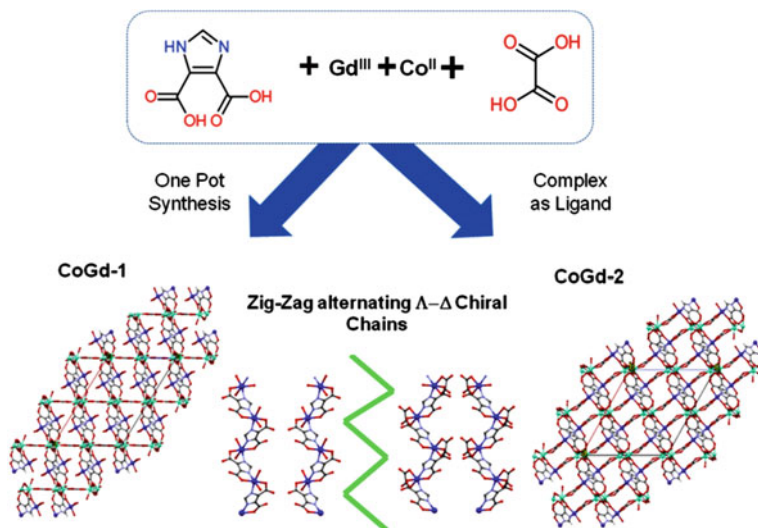
Scheme 6.20 Synthesis of 3d-4f heterometallic 3D networks, based on Co(II)/Gd(III) cations, oxalate and imidazole-4,5-dicarboxylic acid, by a one-pot synthesis and using a Co(II) complex precursor
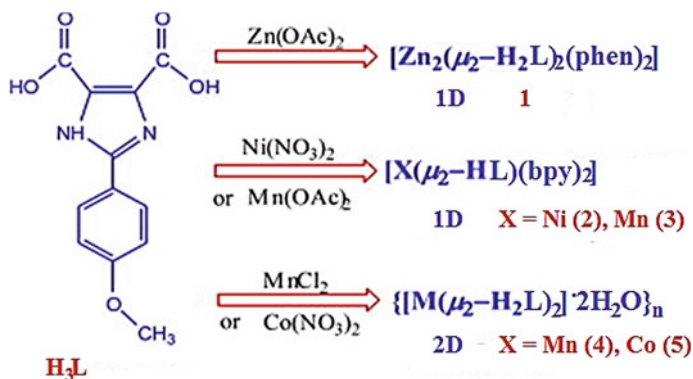
Scheme 6.21 The syntheses of CPs based on 2-*p*-methoxyphenyl-1H-imidazole-4,5-dicarboxylic acid

first CP forms a 3D structure, the second CP is a 1D polymer, which then is assembled in three dimensions through supramolecular interactions (H-bonding). We shall also notice that the first CP consists of Sr(II) ions in distorted dodecahedral coordination geometry, and the second CP includes Cd(II) ions in distorted pentagonal bipyramidal geometry. It is important that the first polymer has a topology based 5,6-connected 3D net architecture (Fig. 6.42).
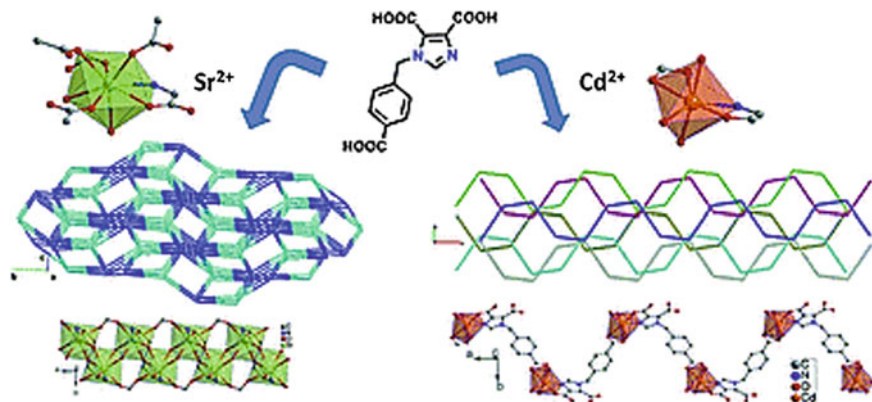
Fig. 6.42 CPs based on 1-(4-carboxybenzyl)-1H-imidazole-4,5-dicarboxylic acid and Sr(II) or Cd (II) ions

Three different MOFs with $[Zn(HL)]_n$, $[Zn_3L_2(H_2O)_3]_n$ and $[Zn(HL)(H_2O)]_n$ blocks are hydrothermally synthesized based on 2-(pyridine-3-yl)-1H-imidazole-4,5-dicarboxylic acid (H_3L) [507]. The H_3L ligands, which are double deprotonated in the first and the third CP, are coordinated into μ_3-mode for generation of 3D or 2D MOFs with respect to two coordination regimes, at that the third CP is a chiral compound. In the second CP ligand is a three deprotonated.

CPs with $[PbL_2]_n$ and $[MnL]_n$ blocks based on imidazo[4,5-f]phen (L) are synthesized using hydrothermal method [508]. In the structure of the first polymer a Pb(II) center is six-coordinated and has octahedral geometry. Moreover, each molecule is additionally linked through π–π interactions in 1D chain. In the second CP Mn(II) ion is six-coordinated with formation of distorted octahedral configuration, and the polymer shows 1D supramolecular chain formed due to H-bonds.

Hydrothermal method was used to synthesize CPs with $[PbL(L')]_n$ and $[PbL_2(L'')]_n$ blocks based on 2-(3-pyridine)imidazo[4,5-f]phen (L), glutaric acid (H_2L'), and hexane dicarboxylic acid (H_2L'') [509]. The first CP has 1D chain structure, in which L ligands are linked to one side of the 1D chain. The second CP shows also 1D chain structure, in which some coupled L ligands are linked from both sides by 1D chain. In these polymers π–π stacking and H-bonding interactions expand 1D chain to 3D supramolecular framework, respectively. It is important that structural differences between complexes point to the value of the length of the fatty aliphatic acid upon creation of molecular architectures.

A porous Co_8 cluster is obtained, which is enveloped with twelve HQ ligands forming large sphere-like $[Co_8(\mu_4-O)Q_{12}]^{2+}$ cation with diameter about 2 nm (Fig. 6.43) [510]. Twelve ligands of the cation form six pairs of intracluster face-to-face π–π-interactions and each cation contacts with four neighbors through six-fold aryl (embrace face-to-edge) π–π interactions with formation of diamondoid supramolecular network. As a result of loose stacking of large cations, most of a crystal (25.7%) determines the diamondoid channel of the network consisting of big
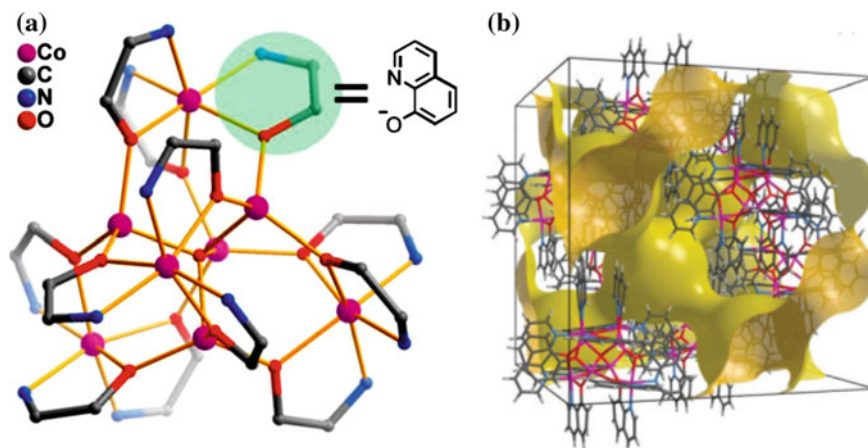
Fig. 6.43 Coordination structure (**a**) and the 3D intersecting diamondoid channel (**b**) of CP

tetrahedral cavities (d = 10 $\overset{\circ}{A}$) and small apertures (d = 4.3 $\overset{\circ}{A}$), which are occupied with disordered anions and guest molecules.

Hydro(solvo)thermal method proves to be very efficient for production of chiral CPs, which are of great interest not only due to intriguing variety of architectures and topologies, but because of their potential applications in many areas [249, 250, 511–516]. It is rather important that chiral CPs can be developed controllably by targeted choice of ligands or metal centers [91, 141, 517–520]. Among the developed by now methods of designing chiral materials, it is worth noticing incorporation of chiral ligands, chiral templates, or chiral ancillary agents, and also spontaneous resolution without chiral auxiliary [252, 521–523]. In this view the most rational method of design of chiral CPs is integration of a chiral center into the structure, such as a chiral ligand; however, this process is not always convenient because of difficulty of a chiral ligand synthesis [524–530]. Besides, more attention is attracted to use of achiral ligands for building of different chiral frameworks, especially by different conformed rotations of a ligand skeleton [531–534] or self-assembling of achiral building units [535, 536]. Principally important strategy for structuring chiral materials is development of left-hand and right-hand helical structures, which requires efficient transfer of stereochemical information between neighboring chiral helixes [537]. Considerable contribution to transfer of chirality between helixes is made by supramolecular interactions including M–L bonds and non-covalent interactions, such as H-bonds and π–π stacking interactions [538–543]. Therefore, it is promising to use associated functionalities providing supramolecular interactions and performing efficient chiral transfer over whole supramolecular assembling. Spontaneous resolution without chiral auxiliary can bring to racemic mixture of enantiomer crystals [58]. At the same time, enantioselective synthesis is straight and efficient method of synthesis enantiopure chiral-open MOF using enantiopure building units as precursors of reagents. Therefore,

many chiral-open frameworks with high thermal stability are obtained using enantioselective synthesis and are successfully used in enantioselective catalysis and separation.

In order to integrate inherent chirality of a ligand and chirality induced by conformation rotations of asymmetric skeleton of the ligand during its coordination, CPs with $[CoL(Py)_2]_n$, $[NiL(Py)_2]_n$, $[CuL(Py)]_n$, $[Zn_2L_2(Py)_2]_n$ and $[Cd_2L_2(Py)_2]_n$ blocks are obtained through the reaction between (1R,3S)-1,2,2-trimethyl-3-{[5-(2-hydroxy)phenyl-1,3,4-oxadiazol-2-yl]}cyclopentanecarboxylic acid (H_2L) and transition metal ions [544]. Among them, the first two CPs had only right-hand helical chains with homochiral helical discrimination due to formation of interhelical non-classic H-bonds C–H···O, and other polymers contained simultaneously alternating right- and left-handed helical chains, interaction between which was due to π–π interactions (CP with Cu atoms) and interchain bonds M–O–M (CPs with Zn and Cd atoms) (Scheme 6.22). In these compounds chirality is stipulated by inherent chirality of a ligand and conformation twisting of the main asymmetric chain of a ligand. Therefore, the effect of metal ion nature on structure of a chiral CP is obvious.

Using solvothermal method with Cd(II) salt and enantiopure chiral ligand based on D-isosorbide (L), a homochiral luminescent porous CP with $[CdL(H_2O)]_n$ block
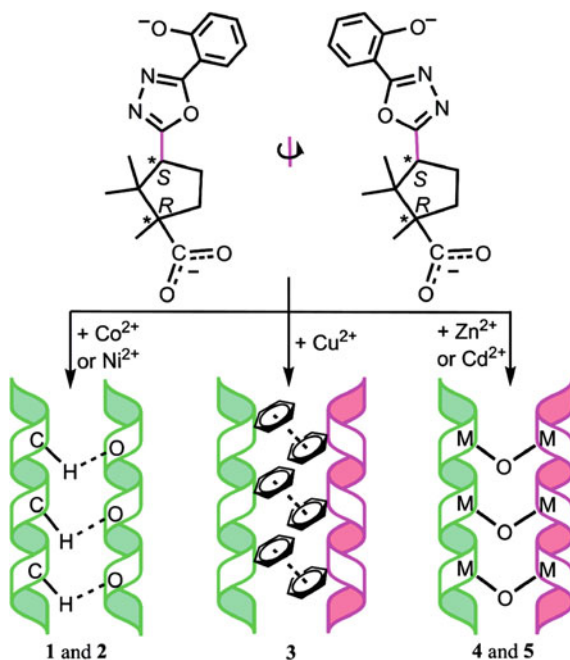
Scheme 6.22 Conformational twists of the asymmetric skeleton of (1R,3S)-1,2,2-trimethyl-3-{[5-(2-hydroxy) phenyl-1,3,4-oxadiazol-2-yl]}cyclopentanecarboxylic acid and different interhelical interactions in the prepared CPs

has been synthesized, which is 2D porous material and forms 1D channel along a axis with the size $\sim 6.2 \times 4.4$ Å^2 [545].

A chiral CP with [AgSCN(phen)]$_n$ block obtained using solvothermal reaction between AgSCN and phen shows unusual asymmetric 1D network formed from a zigzag [Ag-S-Ag]$_n$ chain with thiocyanate ions and phen ligands hanging along opposite sides of the chain respectively (Fig. 6.44a) [546]. It is important that asymmetry of the chain is clear in b direction (Fig. 6.44b), and in one unit cell there are two [AgSCN(phen)]$_n$ chains stacked in opposite direction (Fig. 6.44c). It is interesting to notice that the scheme of the unit cell along b axis is very similar to Chinese "Tai Ji" pattering, which means two opposite principles of nature (Fig. 6.44d).

Also it is worth noticing homochiral CPs with [ML(H$_2$L')]$_n$ block, where M = Zn or Co, based on D-(+) camphoric acid (L) and 4,4'-methylenebis(3,5-dimethylpyrazole) (H$_2$L') obtained through interaction between ligands and transition metal ions under hydrothermal conditions [547].

Of interest is chiral infrequent azolate-based octanuclear metallamacrocyclic 3D [Co$_2$L$_2$(H$_2$O)$_2$]$_n$ complex based on 5'-(pyridin-2-yl)-2H,4'H-3,3'-bi(1,2,4-triazole) (H$_2$L) (Fig. 6.45) [548]. It is important that asymmetric polymer unit consists of one-half Co1 and Co3 ions and one independent Co2 ion, two L^{2-} anions, two aqua-ligands, and four and half lattice water molecules, at that each Co(II) ion is six-coordinated and takes slightly distorted octahedral geometry.

We shall notice promising application of crystal engineering principles in targeted self-assembling of M-Pp in materials with complex topologies, first of all, with emphasis on rational build of robust nanoporous solids and systems with supramolecular chirality [214]. To achieve these purposes, Pp platform is purposively functionalized with different groups of molecular recognition tending to participate in robust supramolecular synthons.

Solvothermal synthesis is successful approach to obtaining of a broad series of 2D and 3D Pp MOFs [190, 193, 209, 549–555]. For this purpose, most often spacers are used based on Pp with carboxylic acid and Py-linked functional groups, in particular, *meso*-tetra(4-carboxyphenyl)-Pp and *meso*-tetra(4-pyridyl)-Pp [77, 188, 201, 220, 222, 246]. It is important to emphasize that during building MOFs based on Pp spacer macrocycles can be metallized in situ with the same metal ions, which present in SBUs [182–184, 186], that is attractive approach for development of high density metallic sites in 3D nanospace, and can be especially enticing for catalysis, if metal centers inside Pp rings, and in SBUs are catalytically active [185, 186].

As an example, we shall notice solvothermal reaction of Fe(III) chloride with the tetrakis(4-carboxyphenyl)-Pp in the presence of different bases, which results in the formation of four Fe-Pp MOFs representing three different topologies and inorganic SBU (Scheme 6.23) [556]. In particular, depending on the synthesis conditions, isolated Fe(III) octahedra, diiron(II) paddlewheel dimers or extended [Fe(III)(OH)O$_4$]$_n$ chains can be obtained controllably.

We shall notice two rare In-based porous MMPF-7 and MMPF-8, which are built under solvothermal conditions via self-assembling of In(III) and two custom-designed Pp-tetracarboxylate ligands 5,10,15,20-tetrakis(4-carboxyphenyl)-Pp and
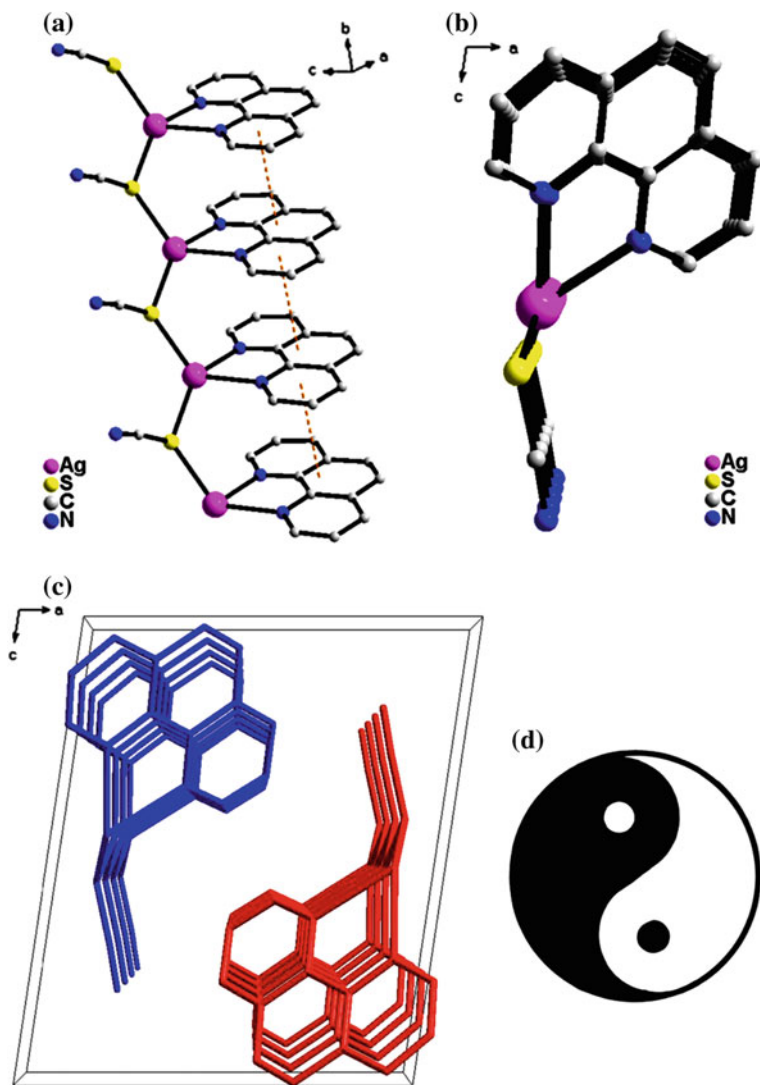
Fig. 6.44 **a** Diagram of the asymmetric chain in CP exhibiting strong π–π interactions among the phen rings (orange dash lines). **b** Perspective view of the chain along the *b* direction. **c** The unit cell packing structure of CP along the *b* direction. **d** The patterning of «Tai Ji»

5,10,15,20-tetrakis(4-carboxybiphenyl)-Pp, respectively [557]. In particular, asymmetric unit of MMPF-7 (Fig. 6.46a) contains one ligand and two In(III) cations, one of which is in the ring of Pp ligand. At the same time, another In(III) ion is eight-coordinate via chelation in a bidentate manner with four carboxylate groups from four different ligands. Each In-Pp is linked with four In(III) ions to form an
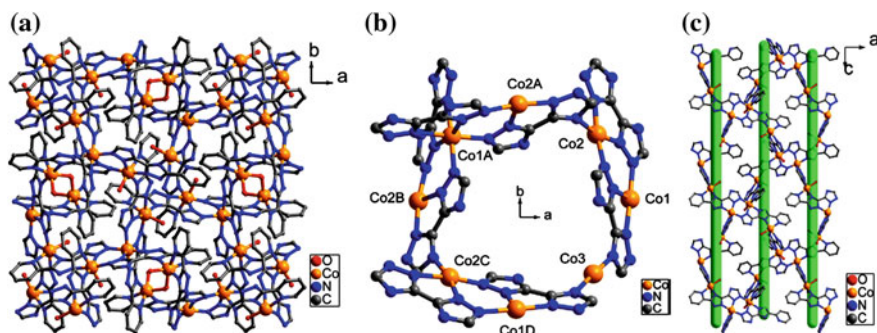
Fig. 6.45 View of **a** the 3D structure along the *c* axis, **b** the octanuclear metallamacrocycle, **c** the unidirectional helixes in CP
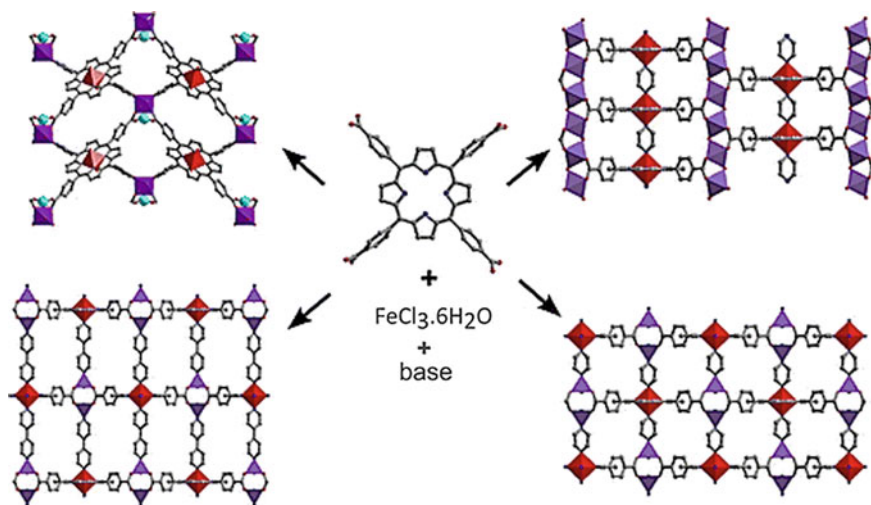
Scheme 6.23 The CPs obtained by the solvothermal reaction of Fe(III) chloride with tetrakis (4-carboxyphenyl)-Pp in the presence of different bases

overall 3D structure for MMPF-7 (Fig. 6.46b, c). Due to the strong π–π interactions between the Pp macrocycles, three-fold interpenetration is observed in the MMPF-7 structure (Fig. 6.46d). Topologically MMPF-7 and MMPF-8 can be described as 4,4-connected **pts** networks, in which each In(III) ion, acting as a 4-connected node, is bridged by In(III)-metallated Pp ligands serving as 4-connected spacers through the carboxylate groups.

Reactions between tetra(4-carboxyphenyl)-Pp and cerium nitrate or between tetra(3-carboxyphenyl)-Pp and thulium oxalate in presence of DMF, water, and acid medium, under solvothermal conditions have given crystalline CPs with 2:3 and 1:1 stoichiometry, respectively [558]. The hybrid Ce-Pp compound is one-framework
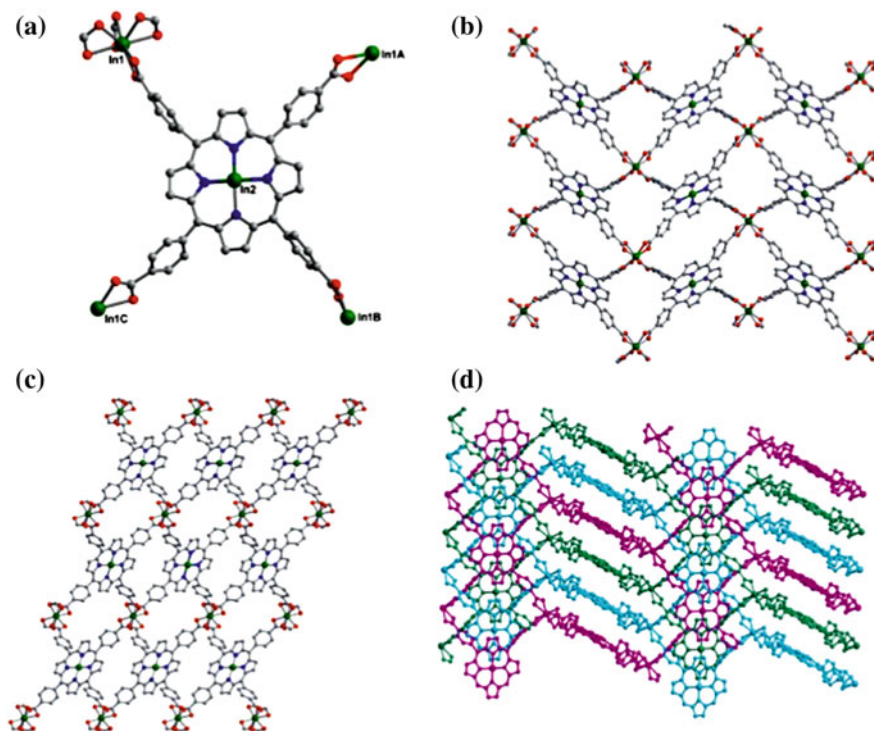
Fig. 6.46 a The asymmetric unit in MMPF-7; **b** the non-interpenetrating structure from the *a* direction; **c** the non-interpenetrating structure from the *b* direction; **d** the three-fold interpenetrating structure of MMPF-7

CP with open 3D architecture sustained by continual coordination of synthon overall volume of a crystal. Each of bridging Ce ion is coordinated simultaneously by several Pp fragments, while each tetradentate Pp is associated through their four carboxylate groups with different Ce bridges. The thulium-Pp compound consists of 2D (not 3D) coordination networks with corrugated surfaces, where each metal ion is associated with four different Pp, while each Pp unit is coordinated through its carboxyphenyl arms with four neighboring thulium centers. Stacking of these 2D massifs along the third dimension is stabilized by Pp-Pp π–π dispersion forces and H-bonds, but not through coordination. Therefore, lanthanide ions are excellent coordination reagents for tessellation of polydentate subjects of carboxy-Pp into 2D and 3D polymer architectures.

We shall notice solvothermally synthesized CPs with M(L-Et$_4$)] block, where M = Zn, Cu, Ni, and [M(L-Me$_4$)] block, in which M = Zn, Cu, Co, based on *meso*-tetra(4-carboxyphenyl)-Pp (L) [559]. First three CPs had ordinary structure with plane macrocycle and metal ions coordinated to four nitrogen pyrrol atoms. At the same time, the fourth CP is characterized as a polymer with 2D coordination, at that one Zn ion is coordinated with four nitrogen atoms and two oxygen atoms. In the

last two CPs Pp macrocycle is not flat, and metal ions are coordinated to four nitrogen atoms.

Among other Pp ligands for CP synthesis, there is interest in octatopic Pp ligand tetrakis{3,5-bis[(4-carboxy)phenyl]phenyl}-Pp, which forms «pillar-free» highly porous M-Pp framework $\{[Zn_2(H_2O)_2]_2 \cdot [(ZnL)(H_2O)_2]\}_n$ called UNLPF-1 (University of Nebraska-Lincoln porous framework) in the solvothermal reaction of L with Zn nitrate in DMF and acetic acid at 80 °C during 72 h [551]. UNLPF-1 has widespread type of SBU, in particular, square paddlewheel $[Zn_2(COO)_4(H_2O)_2]$, which connects four L ligands, and each L ligand links eight in situ generated SBU (four above and four below Pp plane), in order to obtain 3D non-interpenetrating structure (Fig. 6.47). It is important that two adjacent Pp macrocycles along with four paddlewheel SBUs form a cavity of great sizes 14.5×23.7 Å^2. Besides, the same ligand is linked to in situ generated a distorted Co trigonal prism SBU, producing strong, (6, 8, 8)-connected MMPF-2 with **msq** topology [182].

The reaction between Mn(II) and Co(II) with 5,10,15,20-tetrapyridyl-Pp (L) gives polymers of two different metals MMPF-Mn with $([MnL]\cdot H_2O)_n$ block and MMPF-Co with $[CoL]_n$ block under hydrothermal conditions [560]. We shall
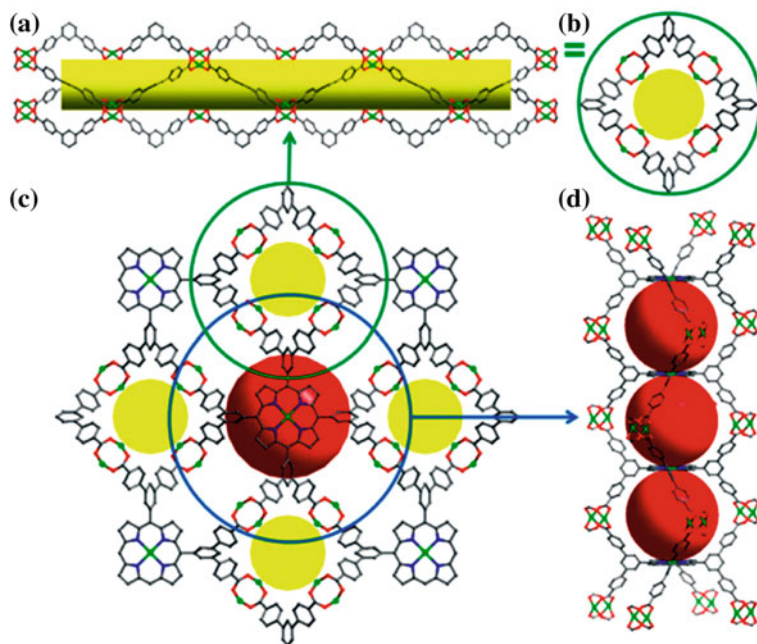
Fig. 6.47 Side view (**a**) and top view (**b**) of a single square-shaped tubular supramolecular building block; **c** 3D network connectivity along the [001] direction between paddlewheels and V-shaped terphenyl arms connecting with the Pp spacer; **d** side view of the 1D eclipsed packing of Pp (cages are represented by red spheres)
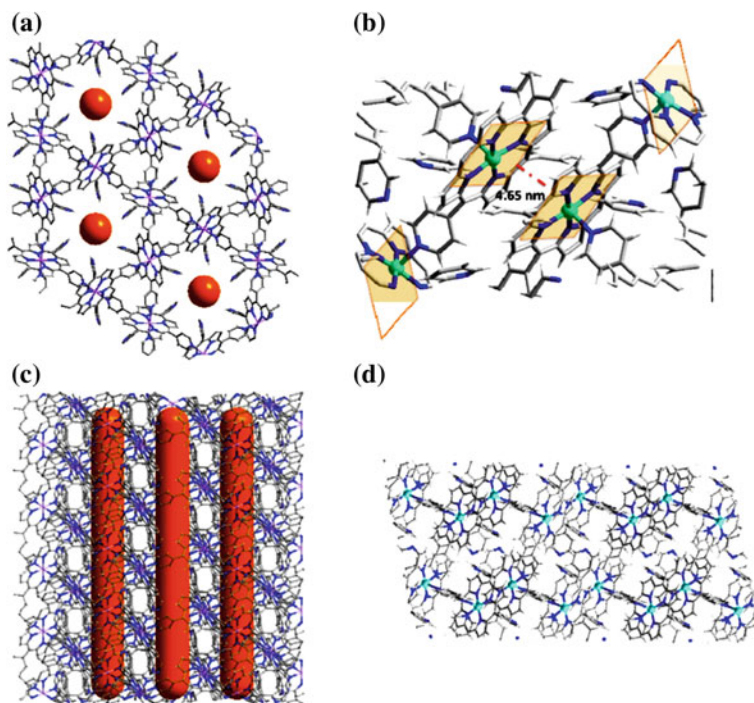
Fig. 6.48 Perspective view of framework structure of MMPF-Mn (**a**, **c**) and MMPF-Co (**b**, **d**)

notice that MMPF-Mn reflects 3D network with NbO topology, big and open hexagonal channels, and MMPF-Co is a simple 1D zigzag chain architecture (Fig. 6.48).

During hydrothermal synthesis of Cd-Pp CPs based on *meso*-tetra-(pyridyl)-Pp the Pp molecule shows three types of coordination regimes, in which each Pp molecule is linked to one, two, four, and five Cd centers [561]. It is important that Cd(II) site shows equally various coordination modes and exists in five different coordination environments. Besides, Pp molecules are linked through Cd(II) cations or $[Cd_3(SC_2H_2OH)_2]^{4+}$ clusters into 2D molecular structures and 3D networks, which are of special interest, since they take interesting and rare framework topologies (of **cds** and **hms** types).

Another attractive ligand 5,10,15,20-tetrakis(4,4-dipyridylamino-phenylene)-Pp can be coordinated with 4–7 metal centers using its multiple peripheral Py and a Pp core bringing to rich structural variety: H-bonding 1D chains bound by $[(H_2O)_2Cl_2]^{2-}$ fragments, 3D structure formed by π–π stacking interactions between interpenetrating 2D networks, 2D structure with big cavities consisting of 50- and 70-members metallomacrocycles (Fig. 6.49), complex 2D structure linked with zigzag chains, and stair-like 2D structure containing binuclear $[Cd_2(CO_2)_4]$ subunits. It is important that
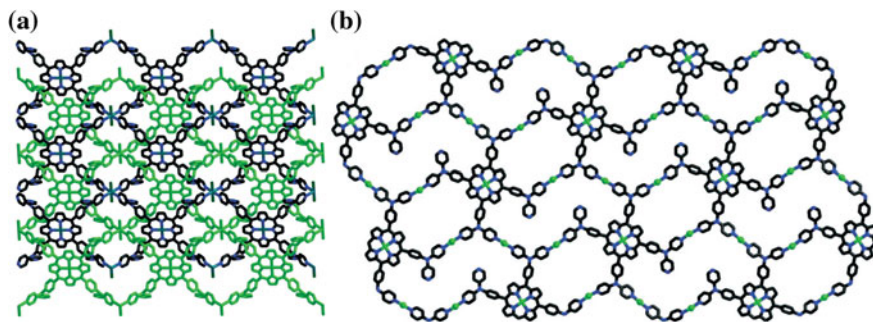
Fig. 6.49 **a** The interpenetrated 2D coordination networks constructed by Pp and MnCl$_2$. **b** The 2D network composed of 50- and 70-membered metallomacrocycles, constructed from Pp and Cu (OAc)$_2$ [562]

4,4′-dipyridylaminophenylene fragments can rotate around Pp framework, bringing to good conformation flexibility of a Pp ligand [562].

Coordination of Mn(II) and Zn(II) acetates with 5,15-bis(4-carboxyphenyl)-10,20-dipyridyl-Pp (H$_4$L) gives two CPs with [Mn(HL)]$_n$ and [Zn(H$_2$L)]$_n$ blocks, respectively [563]. First CP has 2D coordination networks, which are then bound by H-bonds with formation of a 3D network structure. In the second polymer 1D coordination zigzag chains are obtained, and are then linked by H-bonds into a 2D structure (Scheme 6.24). It is important that carboxyl residuals in the CPs are noncoordinated and the Py moieties are either coordinated or noncoordinated, at that noncoordinated carboxyl and Py fragments take part in intermolecular H-bonds, which are favorable for formation of H-bonding networks.

There is a great practical interest in using of a solvothermal approach for production of uniform thin films based on Zr-Pp MOF (MOF-525) grown on conducting glass substrates [564]. In particular, the fabricated MOF-525 thin film is electrochemically addressable in aqueous solution and can be used as an amperometric nitrite sensor.
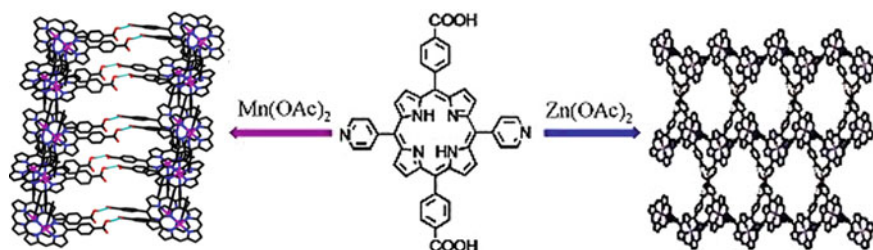
Scheme 6.24 CPs obtained by the interaction of Mn(II) and Zn(II) acetates with 5,15-bis (4-carboxyphenyl)-10,20-dipyridyl-Pp

We shall notice the strategy of kinetically tuned dimensional augmentation for the production of highly crystalline and robust Fe-MOFs with preliminary formed inorganic building units $[Fe_2M(\mu_3\text{-}O)(CH_3COO)_6]$, where M = Fe(II, III), Co(II), Ni(II), Mn(II), Zn(II) [565]. By rationalization of the MOF growth from thermodynamic, as well as from kinetic point of view, large single crystals of 34 Fe-MOFs with different ligands and cluster linking regimes are obtained. Among them, PCN-250(Fe$_2$Co) has shown stability in water and aqueous solutions with a wide range of pH. It is important that this strategy provides more opportunities for MOF production with new structures and attractive properties.

Certain interest is in the microcrystalline structure containing up to 10 different types of bivalent metals, namely, Mg, Ca, Sr, Ba, Mn, Fe, Co, Ni, Zn, and Cd, based on MOF-74 with $[Zn_2L]_n$ block (L = dioxidoterephthalate) [218, 566–571], which has high CO_2 adsorption capacity under practical atmospheric pressure conditions. The one-pot reaction makes it possible to obtain MOF-74 with 2 (Mg and Co), 4 (Mg, Co, Ni, and Zn), 6 (Mg, Sr, Mn, Co, Ni, and Zn), 8 (Mg, Ca, Sr, Mn, Fe, Co, Ni, and Zn), and 10 (Mg, Ca, Sr, Ba, Mn, Fe, Co, Ni, Zn, and Cd) different types of bivalent metals. It occurs that all metal ions used in MOF synthesis are integrated in the same MOF-74 structure, and metal ions are heterogeneously distributed within each of crystalline particles. It should be noted that this approach is also used for incorporation of other metal ions (for example, Ca, Sr, Ba, and Cd), of which the original structure of the MOF cannot be made in the form of monometallic MOF.

Presently combinations of different methods are very popular, and hydro(solvo) thermal method is not and exclusion [572]. In particular, hydro(solvo)thermal hybrid methods are often applied for synthesis of CPs and functional materials, including nanomaterials. A considerable body of studies has been performed for hybridization of the hydrothermal method with microwaves (microwave-hydrothermal treatment), electrochemistry (hydrothermal-electrochemical synthesis), ultrasound (hydrothermal-sonochemical synthesis), mechanochemistry (mechanochemical-hydrothermal synthesis), optical radiation (hydrothermal-photochemical synthesis) and hot pressing (hydrothermal hot pressing). It should be noticed that hydrothermal method, microwave-hydrothermal method and microwave-solvothermal method, in particular, are low temperature methods for preparation of nanophase materials of different sizes and shapes. These methods are energy-saving and environmentally friendly, since the reactions proceed under because reactions take place in a closed system under the insulation. It is important that nanophase materials can be produced either in periodical or continuous process using the abovementioned methods. Contrary to ordinary heating hydro(solvo)thermal method, which requires a lot of time (as a rule, from half to several days) and high electrical power (more than thousand watts), microwave-assisted heating is a greener approach to synthesis of materials for shorter time (from several minutes to several hours), and lower energy consuming (hundreds watts), as a result of direct and uniform heating of a matter. As an example we can consider UV-absorber $(Ti_5O_5F_{12})\cdot L_2$ obtained using microwave-heating-assisted hydrothermal synthesis [573], whose 3D network is built from

∞($Ti_5O_5F_{12}$) infinite inorganic layers separated by guanidinium (L) cations. Under UV irradiation at 254 nm during 40 h white microcrystalline powder transformed into light-purple-gray due to reduction of Ti(IV) to Ti(III), which is confirmed by magnetic measurements.

6.7.4 Urothermal Synthesis

Recently urothermal synthesis has opened a new approach to creation of porous framework materials with promising applications [574–581]. It is based on using of different derivatives of urea as solvents. One of very useful features of urothermal synthesis is reversible coordination of urea derivatives to metal sites, which allows them to competitively link with metal sites of a framework, and in many cases they can be easily removed after crystallization for generation both porosity and open metal sites. Competition for coordination to metal sites among derivatives of urea and other solvents, such as DMF or DEF, is an interesting aspect of this process of synthesis, and can also be used to provide additional structural control.

As an example of production of the CPs containing metal chelate units, we shall notice urothermal synthesis of CP with {[Cu(en)L](e-urea)(H_2O)}$_n$ block based on 1,4-naphtalenedicarboxylic acid (L) and in situ obtained en using 2-imidazolidinone e-urea derivative as a solvent, which shows unprecedented (3,4)-connected **tfi** network. The 2-imidazolidinone plays many roles in self-assembling of this CP [582].

6.7.5 Ionothermal Synthesis

Using room temperature ionic liquids [583, 584] or deep eutectic solvents (DESs) [585] in CP production is called ionothermal synthesis [585–597]. Usually in MOFs synthesis ILs serve as solvents, reagents, structure-directing agents, charge-compensating templates in anion networks or functional inclusions. ILs attract attention as a solvent for chemical synthesis due to their unique properties, such as, actually, zero vapor pressure, excellent solvating properties, easy secondary using, and high thermal stability [598, 599]. They received much attention as promising media for design and production of known and unprecedented new MOFs. As compared with water or traditional molecular organic liquid different and easily tunable properties of the solvent for the ionic liquid supplement considerable attention to eco-friendly and safe solvents [600, 601]. We shall also notice using of chiral ILs, but they are not observed in a final structure [589, 602, 603]. Unfortunately, high cost of ILs limits their usage in large scale synthesis of MOFs.

DES is a mixture of two or more compounds, which have a melting temperature lower than any of its components. DESs show unusual properties of solvents, which

are very similar to those of ionic liquids [588], and therefore they are used for MOF synthesis [599].

Most works concerned with ionothermal MOF synthesis is focused on ILs obtained from 1-alkyl-3-methylimidazolium. They have advantages before other types of ILs, such as simplicity of preparing pure phases from easily available components, low costs, and relative inertness to atmospheric humidity [598]. Thus, 3D MOF {[EMIM][In_3(\mu_3-OH)_2L_2\cdot 2H_2O]}_n based on 1,2,4,5-benzenetetracarboxylate (L) is synthesized using ionic liquid bromide 1-ethyl-3-methylimidazolium ([EMIM]Br) as a solvent [604]. In this polymer 7-coordinated pentagonal bipyramidal In(1) and octahedral In(2) atoms are linked by μ_3-OH groups with formation of infinite $[In_3(\mu_3-OH)_2]_n$ inorganic chain along a axis, which are additionally extended by L ligands for creation of 3D anion microporous framework. The [EMIM]$^+$ cations occupy 1D channels acting as a template and charge-compensating species.

6.7.6   Microfluidic Synthesis

Development of continuous, fast and viable processes of MOF synthesis should meet commercial and industrial demands [605], and microfluidic MOF synthesis can be considered as promising for this purpose (Fig. 6.50). Thus, for example, well-defined and stable liquid-liquid interphase obtained by co-flowing of two different solutions in a microfluidic system under laminar flow conditions is used to produce CP nanofibers [606]. At this approach nanofibers of three different CPs including Cu(II) and aspartic amino acid (L), Ag(I), and cysteine amino acid (L'), and also Zn(II) and ditopic 4,4'-bipy ligand are synthesized on the interphase between two solutions, one of which contains the ligand, and another one contains a metal source (Fig. 6.51). Bundles of Cu(II) fibers with diameter less than 200 nm were obtained. For Ag(I)-L', as well as for Zn(II)-4,4'-bipy nanofibers smaller diameters are observed, from 10 to 50 and from 10 to 75 nm, respectively.
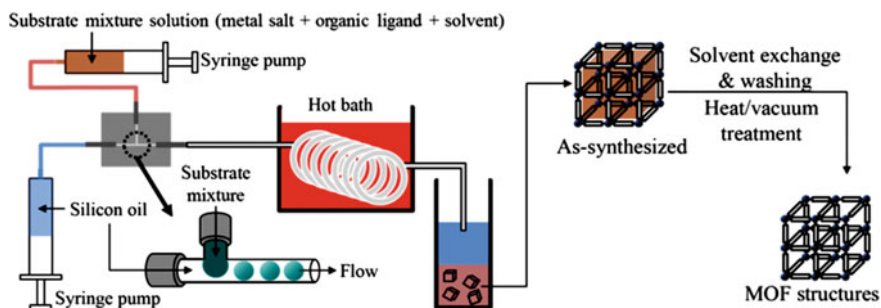
Fig. 6.50 Microfluidic synthesis of MOF structures
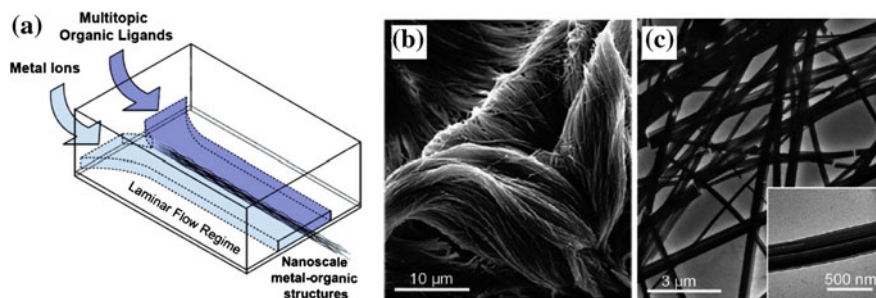
Fig. 6.51 **a** Schematic representation of the microfluidic system used to fabricate CP nanofibers under laminar flow conditions; **b** SEM and **c** TEM micrographs of the Cu(II)-asparagic aminoacid nanofibers obtained. Inset: high-magnification image of a single nanofiber

6.7.7 Synthesis in Supercritical CO_2

Eco-efficient method based on using only supercritical CO_2 as a solvent without the addition of any other additive or co-solvent is applied for synthesis of 1D Cu(II) MOFs [607]. For example, neutral $Cu(acac)_2$ chelates and two linear spacers, the bidentate 4,4′-bipy and trimethylene-4,4′-bipy were subjected to interaction under compressed CO_2 at 60 °C and 20 MPa during 4 or 24 h, respectively (Fig. 6.52). The reaction yield of the CPs synthesized through the supercritical route was close to 100%, since both the reagents were almost completely depleted in the performed

Fig. 6.52 The preparation of Cu(II) 1D MOFs using an eco-efficient method based exclusively on supercritical CO_2 as a solvent

experiments. It should be noted that success reached in synthesis of different 1D MOFs is due to high solubility of reagents in supercritical CO_2.

6.7.8 Surfactant-Thermal Method

Another approach to ensure a high degree of control over size and shape of MOF crystals and over their textural properties is use of surfactants (for example, amphiphiles and block-copolymers) [608, 609]. It is important that the surfactants play different roles in control over morphology of MOF crystals. In particular, under special conditions, surfactants are self-assembling to form micelles, which can act as nanoreactors [571, 587, 602]. Besides, in this case MOFs grow on external surface of a micelle, not inside, so that a surfactant works as a molecular template, not a nanoreactor bringing to formation of meso- and/or macro-pores, which together with intrinsic microporosity of MOF brings to particles with hierarchical porosity [610–612].

As compared with organic solvents, surfactants are more thermally stable and more environmentally. At the same time, surfactants with low or no pressure vapor make reactions in the surfactant medium possible at far higher temperatures. In addition, surfactants have more multifunctional properties than ILs, such as cation, anion, neutral, zwitter-ionic, acid, base, etc. Which is more important, their low cost and commercial abundance of surfactants make them ideal reaction medium for production of functional materials. Presently the surfactant medium is used for preparation of nanomaterials, and it should be noted that use of surfactants as reaction medium for the growth of crystalline materials is unprecedented. Janus characteristics of surfactants, which contain hydrophobic and hydrophilic groups, can increase efficiently solubility of metal ions and organic ligands, making them ideal medium for MOF growth.

We shall consider the study of length-controlled synthesis of 1D M-Pp CP using «bottom-up» strategy under action of anion surfactant [613]. For example, using this method the 1D structure of nanorods and nanowires are obtained. The strategy of growth of crystalline materials is developed: growth of crystalline chalcogenide materials using surfactant-thermal method [608, 614, 615]. Chiral Ni(II) mononuclear chelate $[NiL(H_2O)_3]$ and 3D CP $[NiL(H_2O)]_n$ based on thiazolidine 2,4-dicarboxylic acid (H_2L) are synthesized by the reaction between Ni acetate and H_2L in aqueous solution at 25 and 80 °C, respectively [616]. From the same procedure with polyvinylpyrrolidone (PVp) used as a surfactant another respective micron size Ni(II) CP $[NiL(H_2O)_2]_n$ is obtained at 25 and at 80 °C (Fig. 6.53).

Very important is the fact that surfactants can be capping agents or inhibitors, thus providing steric stabilization, which provides formation of nanoparticles and has a different effect on various faces of a crystal causing growth anisotropy of MOF crystals [589, 603]. In this case surfactants slow down crystal growth rate, providing spatial stabilization of MOF nanoparticles [462, 572, 573, 589, 617] and relative value of different faces of a crystal, which brings to anisotropic growth
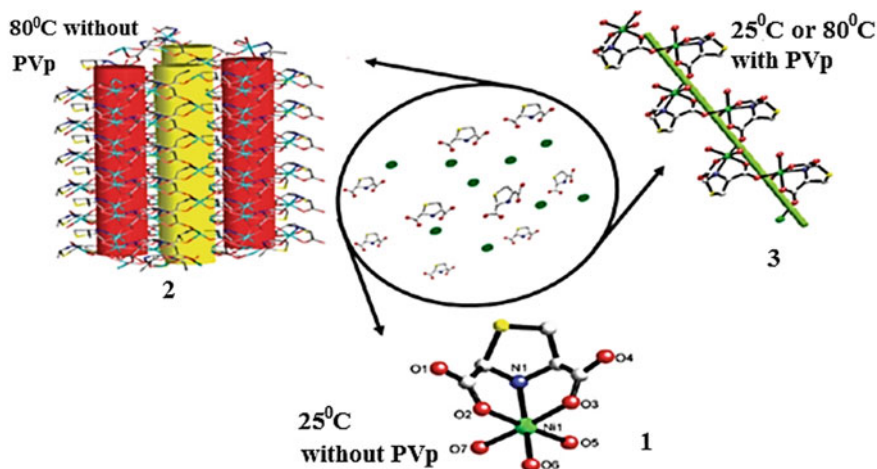
Fig. 6.53 Schematic representation of the generation of discrete **1**, 3D framework **2**, and 1D left helical chain **3** triggered by temperature or polyvinylpyrrolidone

[117, 180, 603, 618–620]. Capping agents, such as trisodium citrate, are used for limitation of growth of nanoparticles and stabilization of their aggregation [496]. Their effect is, as a rule, not long, though using of trisodium citrate with lee and miesel method can bring to particles, which are stable for a month.

We shall notice a typical example of crystal engineering using stabilizing agents [621]. Thus, presence of poly (vinylsulfonic acid sodium salt) in synthetic mixture provides big plates of $[Cu_2L_2(L')]_n$, where L = pyrazine-2,3-dicarboxylate и L′ = pyrazine. Sulfonic units in a polymer stabilize a metal cation due to electrostatic interactions. This is stipulated by steric hindrance in the nucleation sites, thus slowing down kinetics, but inducing at the same time anisotropic growth in parallel to *ac* plane. Really, the higher is polymer/Cu(II) ratio, the bigger sheets are obtained (up to 70 μm).

6.7.9   In Situ Spacer Synthesis

The approach called «in situ spacer synthesis», in which organic spacers are generated in reaction medium in situ from initial materials, attracts more interest in the recent years. To prepare CP, a great variety of in situ reactions of organic transformation have been applied [622]. Synthesis of a spacer in situ has many advantages as compared with ordinary synthetic routes. In particular, this one-pot approach excludes a necessity of synthesis of spacers, thus simplifying long synthesis and multiple stages of purification. Slow release of in situ generated spacers in presence of metal ions can bring to growth of the best crystalline products or even large single

crystals. Moreover, this approach gives suitable alternative ways to MOFs with in situ synthesized spacers, which are unavailable or not easy to obtain by ordinary methods of synthesis [623]. It should be noted that discovery of some in situ synthesized spacers is serendipitous [624]. It is important that in situ hydro(solvo) thermal reactions usually produce very stable materials for potential applications [625–629].

As an example, we shall consider solvothermal reaction of Pb acetate with flexible 1,3-bis(4-pyridyl-3-carboxyl)-propane (H_2L) under different conditions of synthesis through in situ ligand transformation reaction, which give three genuine coordination polymorphs $[PbL^{2-}]_n$, $[Pb_3L_3^{2-}]_n$ and $[(Pb_2L^{2-})\cdot 2H_2O]_n$ (Fig. 6.54) [630]. In these compounds L^{2-} ligand shows different coordination conformations and regimes adjusted to different synthesis conditions, including temperature of reaction, cooling rate and dopants, and designs various architectures linking different building units. Two first polymorphs show 3D framework with 1D channels built from binuclear ring-like $[Pb_2(L^{2-})_2]$ and binuclear semiring-like $[Pb_2L^{2-}]$ blocks, respectively. The last polymorph also has 3D architecture, however it is built from binuclear ring-like $[Pb_2(L^{2-})_2]$ blocks interconnected with L^{2-} ligand.

We shall also notice CPs with $[Cu(II)_2(\mu_3-L)_2(\mu_1-Cl)_2]_n$, $[Cu(I)Cu(II)(\mu_2-L)_2(\mu_2-Cl)(H_2O)]_n$ and $[Cu(I)_2Cu(II)(\mu_2-L)_2(\mu_3-I)_2(H_2O)]_n$ blocks based on chelating ligand of 2-pyrazinecarboxylate (HL), which forms in situ by hydrolysis of the initial N,N'-(5,7-dihydro-1,3,5,7-tetraoxobenzo[1,2-c:4,5-c']dipyrrole-2,6(1H,3H)-diyl)bis-(9CI)-3-pyrazinecarboxamide upon its reaction with Cu(II) chloride, iodide, and perchlorate, respectively [631]. The first CP has 2D double-layer structure, which can be considered as a binodal (3,3)-connected network, the second polymer is (4,4) net, and the third CP has a 3D open framework built by linking of 1D sawtooth chains of Cu(II) iodide clusters with $[Cu(II)(\mu_2-L)]$ units. It is interesting that all compounds cannot be synthesized directly using HL and the respective Cu ions as initial reagents under the same conditions of reaction. Therefore, the structural diversity of this system is adjusted in situ by reactions of hydrolysis.
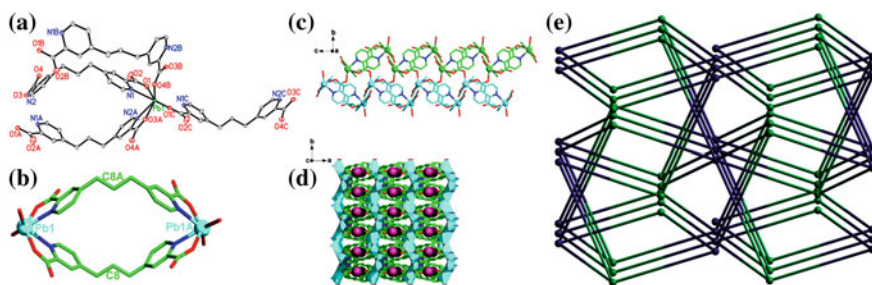
Fig. 6.54 a View of the coordination environments of the Pb1 center in CP. **b** View of one dinuclear $[Pb_2L_2^{-2}]$ ring-like unit of CP. **c** View of a section of the 1D double chain extending along the c axis. **d** View of a 3D porous structure in CP along the c axis. **e** Topological view showing the equivalent 3D framework of CP. The purple pillars represent the 1D channel in CP. Atom color codes: Pb, cyan; O, red; N, blue; and C, green

During hydrothermal preparation of Zn(II) CPs with $[ZnL(L')]_n$ and $[Zn_6L_3(L'')_4]_n$ blocks based on 4'-(4-pyridyl)-tpy (L), fumaric acid (H_2L'), and maleic acid (H_2L'') the in situ ligand reactions take place, in which maleic acid is converted into fumaric acid and malic acid, respectively [632]. In particular, maleic acid transforms in fumaric acid using isomerization reaction, at that the key factor having effect on the in situ reaction is temperature. In situ cis-trans-isomeric transformation of substituted ethylene took place at 140 °C, since fumaric acid is far more stable than maleic acid at high temperature. At the same time, in situ cis-trans-isomerization can take place with several metal salts, such as Cu(I), Cd(II), and Zn(II) ions pointing to the fact that a metal ion is not one of the main factors of the in situ cis-trans-isomerization of maleic acid. At the same time, hydroxylation of ethylene group of maleic acid took place in formation of the second CP. If Zn(II) salts react directly with malate and L ligands, Zn(II) CP can be produced only with L ligands without malate anions, which points to preference of in situ ligand synthesis for CP formation with mixed ligands. We shall notice that the first CP is 1D infinite chain structure, which propagates into supramolecular layer through intermolecular π–π stacking interactions. At the same time, the second polymer shows 3D network structure, in which bidentate bridging L ligands link layers based of tetranuclear Zn(II) subunits with formation of (4, 10)-connected network.

6.8   Alternative Synthesis Routes

In hydro(solvo)thermal processes considerable volumes of a solvent are necessary to produce great quantities of CP for commercial using, which is environmentally unfavorable, and makes products costly. It is also necessary to accelerate crystallization process and generate uniform crystals with diminished size; therefore it is important to develop easily available, non-expensive, fast, and commercially viable synthetic routes. Concerning many efforts were taken for development of alternative methods of CP synthesis, such as electrochemical [36], sonochemical [633], microwave [634], and mechanochemical methods [635–642]. These methods provide possibilities for MOF synthesis in reduced time and with high quality, which is favorable for commercial application of MOFs. In this view detailed studies were performed for optimization of MOF synthesis conditions to obtain high yields of solid products for industrial applications [619, 620]. Besides, using fast reactions, development of continuous synthesis is possible, which is advantageous for large scale production. Reducing the reaction time and decrease in temperature are also very favorable for the more energy-efficient processes and less demanding synthesis equipment. It is important to notice that alternative routes can lead to compounds with different particle sizes and size distributions and morphologies, which have immediate effect on properties of a final material. For example, different particle sizes in porous materials can control diffusion of guest molecules, which is straightly important for catalytic reactions, adsorption, and molecule separation. It is worth noticing that larger single crystals in the range of 100 μm are necessary for

regular analysis of a structure and establishing of structure-property correlations. Obviously, different methods can bring to new compounds, which cannot be obtained in other ways. All this together makes compulsory very detailed studies of the produced materials using additional methods of characteristics, since even small changes in synthesis procedures can lead to compounds with completely different properties [617, 618].

6.8.1   Microwave-Assisted Synthesis

Introduction of energy using microwave radiation is well-established method in synthetic chemistry of MOFs [643]. Microwave-assisted synthesis is based on interaction between electromagnetic waves and mobile electrical charges, which can be polar molecules of solvent/ions in a solution or electrons/ions in solid. Due to direct interaction of irradiation with solution/reagents, microwave-assisted heating is very efficient method of heating. At that, there are possible high heating rates and uniform heating throughout a sample. Substantial attention should be paid to choice of respective solvents and selective energy input, since initial materials can strongly interact with microwave irradiation. Microwave ovens suitable for CP synthesis provide temperature and pressure regulation during reaction, and, respectively, provide more precise control over conditions of the reaction. It is important to emphasize that microwave-assisted MOF syntheses are mainly focused on the following moments: acceleration of crystallization, formation of nanometer materials, improvement of purity of a final product, and selective synthesis of polymorphs. This is stipulated by direct heating of solvents and increase in crystal nucleation rate. To optimize the reaction conditions, systematic studies of changes in the composition and process parameters (solvent, irradiation time, temperature of reaction, power level, the molar ratio of reagents, reagent concentration, etc.) were carried out (Fig. 6.55) [84, 568, 634, 644–647]. It should be noted that microwave irradiation makes it possible to accelerate synthesis of fine crystals as compared
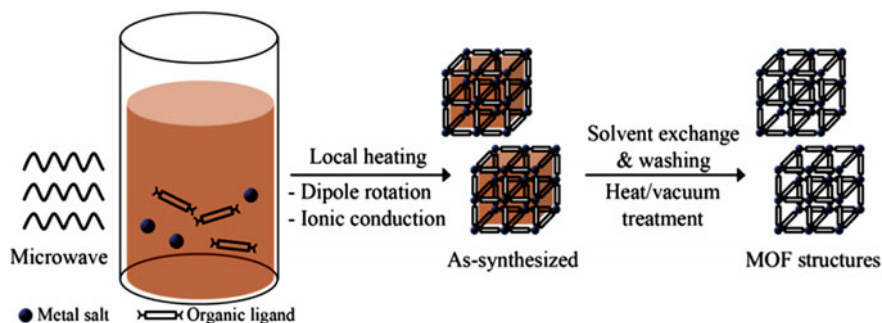
Fig. 6.55   Microwave-assisted solvothermal synthesis of MOF structures

with conventional heating. On the whole, advantages of this method are high efficiency, phase selectivity, particle size diminishing, and morphology control [324, 648, 649].

As an example, we shall consider microwave-assisted synthesis of Co-MOF-74 under different conditions, for example, temperature of synthesis, power level of microwave irradiation, and time of synthesis (Table 6.1) [568]. Optimized Co-MOF-74 is synthesized at 180 °C at 180 W power in a microwave oven during 1 h, which resulted in the highest textural properties (1314 m^2 g^{-1} of BET surface area) with high product yield (about 76% per ligand). Co-MOF-74 (ca. 50 μm long and 8 μm wide) obtained by microwave heating was smaller in size than the solvothermally prepared Co-MOF-74 (ca. 300 μm long and 70 μm wide).

It is important to notice that microwave reaction is invaluable technique for high-rate synthesis, and allows control over size and shape of resulting particles. For example, this MOF synthesis can be finished from 30 s to 2 min, and the yield changes from ∼30% to more than 90% [634]. Another example is production of rare earth based CP submicrospheres from Py-2,5-dicarboxylic acid and $M(NO_3)_3$ using the method of light microwave heating during 5 min with DMF as a solvent [650]. Submicrospheres have diameters 100–400 nm, and the microspheres' surface is smooth. Straw-sheaf-like Tb-based CP architectures are successfully synthesized using a simple and ecological microwave heating in great scales during 15 min without any template or surfactant using 1,2,4,5-benzenetetracarboxylic acid as organic building unit [651]. The measured specific surface area of Tb-based CP was 152.51 m^2 g^{-1}. Individual straw-sheaf has length in the range 70–90 μm, and average diameter in the range 5–8 μm.

Table 6.1 Textural properties of Co-MOF-74 synthesized via microwave-assisted solvothermal method at different conditions

Conditions			S_{BET} (m^2 g^{-1})	V_{pore} (cm^3 g^{-1})	Product yield (%)
Temperature (°C)	Power (W)	Time (min)			
100	180	60	1318	0.49	7
120	180	60	1319	0.51	45
	120	60	1402	0.71	58
	150	60	1411	0.69	63
130	180	30	1193	0.49	69
	180	40	1155	0.47	75
	180	60	1314	0.51	76
	180	70	1273	0.51	74
	210	40	1270	0.65	72
	210	60	1321	0.50	74

6.8.2   Electrochemical Synthesis

Electrochemical MOF synthesis was first reported in 2005. Its main purpose was exclusion of anions, such as nitrate, perchlorate, chloride during synthesis, which are reasonable for large scale production. Therefore, in order to exclude metal salts usage, metal ions are continuously integrated via anode dissolution into the reaction mixture, which contains dissolved spacer molecules and conducting salt [652]. Other advantage of electrochemical route is a possibility to launch a continuous process and a possibility to obtain higher content of solids as compared with batch reactions (Fig. 6.56) [324].

Cathode deposition of metals can be avoided by using protonic solvents, however, in this case H_2 forms. It is suggested to use for these purposes such compounds as acrylonitrile, acryl and maleic esters, which are mostly reduced.

Electrochemical MOF synthesis gives some advantages as compared with conventional synthesis, which in principle could provide better control over crystal growth, such as modulation of a metal cation concentration in solution by regulating current intensity or a possibility of control over oxidation state of a metal. Therefore, it is used for thin film growth on electrodes being metal sources.

Undoubtedly, electrochemical MOF synthesis provides alternative method of synthesis, which does not require additional external source of heat, however, is too expensive to be used at industrial scale. It is important that this approach works through formation of the reagent ions in a solution, thus it is unnecessary to use bases. It is worth noticing that electrochemical methods suits well for formation of MOF membranes due to intrinsic coating reached on scaffolds due to a MOF product deposition.

We shall also notice a distinguished example of MOF morphology controlled by electrochemical synthesis in pure ionic liquid [188].
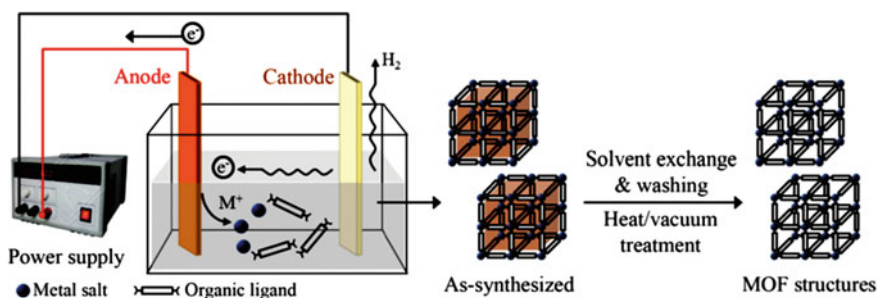
Fig. 6.56 Electrochemical synthesis of MOF structures

6.8.3 Mechanochemical Synthesis

In mechanochemical synthesis the mechanical break of intramolecular bonds followed by chemical transformation occurs (Fig. 6.57) [325, 653, 654]. Mechanochemical synthesis is a promising alternative method for systematic and large scaled CP production. Its advantages include the following: lowering of contamination, low cost, simplicity of the process, easiness of processing, efficient reaction rate, selectivity, and solution of a problem of low solubility of reagents [655]. In particular, reactions can be performed at room temperature under solvent-free conditions, which is especially beneficial when organic solvents can be avoided [656]. Short time of the reaction, as a rule, in the range from 10 to 60 min can lead to quantitative yields and products containing fine particles. Besides, in some cases metal salts can be substituted by metal oxides as initial material, which results in water formation only as a side product. These features are especially important in industry. Nevertheless, presently, application and universality of these mechanochemical methods for CP synthesis are limited and not studied in detail.

Mechanosynthesis or milling is currently used as fast, scaled, and potentially non-toxic way of MOF synthesis. MOFs can also be obtained using mechanochemistry, i.e. grinding of two or more solids using a mechanical ball mill and thus avoiding use of solvents [653, 657]. This is very aggressive technique, which makes it possible to obtain products from micro- to nanocrystals at room temperature for shorter time.

Recently mechanochemical syntheses have been used efficiently for fast MOF synthesis using liquid- or ionic liquid-assisted grinding (LAG), where a small amount of a solvent is added to solid reaction mixture [658]. It has been shown that varying an added solvent during LAG, it is possible to obtain 1D, 2D, and 3D CPs from the same reaction mixture. Besides, addition of small amounts of solvents in LAG can bring to acceleration of mechanochemical reactions because of increase in mobility of reagents at molecular level [653]. Liquid can also work as a structure-directed agent. Extension of LAG method has become very efficient for the selective building of pillar-layered MOFs [653, 654]. However, mechanochemical synthesis is confined to only certain types of MOFs, and it is difficult to obtain a large number of products.
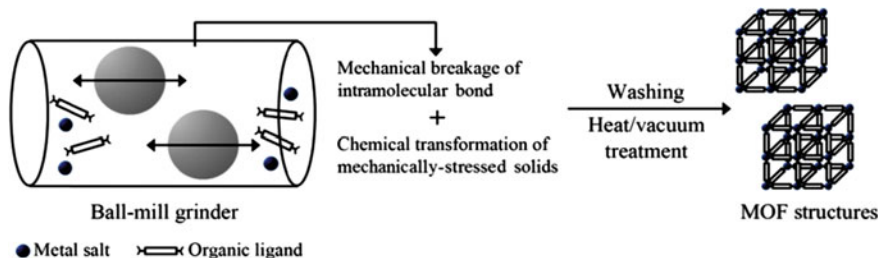
Fig. 6.57 Mechanochemical synthesis of MOF structures

In this view, a substantial interest is in array-based approach in reaction of 12 different metal salts, including metal acetylacetonates and 5 bridging ligands in 60 potential reactions, which revealed main tendencies in reactivity of free-solvent mechanochemical conditions. From the 60 combinations of 38 possible to produce microcrystalline products to be characterized with XRPD, among which non-porous polymers with 1D connection containing $[Cu(acac)_2(4,4'\text{-bipy})]$ and $[Cu(F_6acac)]$ $(4,4'\text{-bipy})]$ blocks should be noted [635].

Using of twin screw and single screw extruders has been shown for continuous synthesis of different CPs, including Ni(salen)-based [659]. Quantitative conversions proceed are preformed to obtain products at the kg h^{-1} rates, which after activation show surface areas and volume of the pores equivalent to materials obtained by conventional solvent-based method.

We shall notice detailed study of mechanochemical synthesis of coordination pillar-layer frameworks (CPLs), in particular, CPL-1 [656]. In the case of CPL-1 two-stage reaction was observed (from the initial reagents to final product), at that moisture had a significant effect at both stages of the reaction. After washing of the final product, it has shown the same ability to adsorption as a product obtained from the process in a solution. Besides, systematic production of other CPLs (CPL-2, 3, 4, 5 and 15) using mechanomecamical method under high moisture conditions is shown, even if some ligands are almost insoluble in water.

There is interest in mechanochemical CPL production from neutral 2D layers consisting of Cu(II) and pyrazine-2,3-dicarboxylic acid (L), which are further connected by pillars through different dipyridyl bridging ligands (L′) for formation of 3D structures $[Cu_2L_2(L')]_n$ with 1D microporous channels and, that is more important, with the same connection of components (Scheme 6.25) [660].

High proton conductivity material has been obtained using economical and ecologically pure mechanochemistry [661]. The reaction is a new synthetic strategy with respect to materials related to technology of fuel cells.

6.8.4 Sonochemical Synthesis

Sonochemistry is a part of studies, in which molecules are subjected to reaction by application of powerful ultrasonic radiation (20 kHz–10 MHz). Ultrasound causes chemical or physical changes caused by cavitation phenomena associated with formation, growth and instant implosive collapse of bubbles in liquid, which can generate local hot spots with the temperature about 5000 °C, pressure about 500 atm, and lifetime several microseconds [232, 233]. These extreme conditions can control chemical reactions, but they can also advance formation of fine crystals (Fig. 6.58) [324] and nanometer particles, mainly, by instant formation of multiple crystallization nuclei. Recently many types of nanomaterials were obtained using this method [662–667]. This is a consequence of instant formation of crystallites in local cavity of a solvent of hot spots, which have very short lifetime (∼ms) and size (of the order of tens microns) [668].
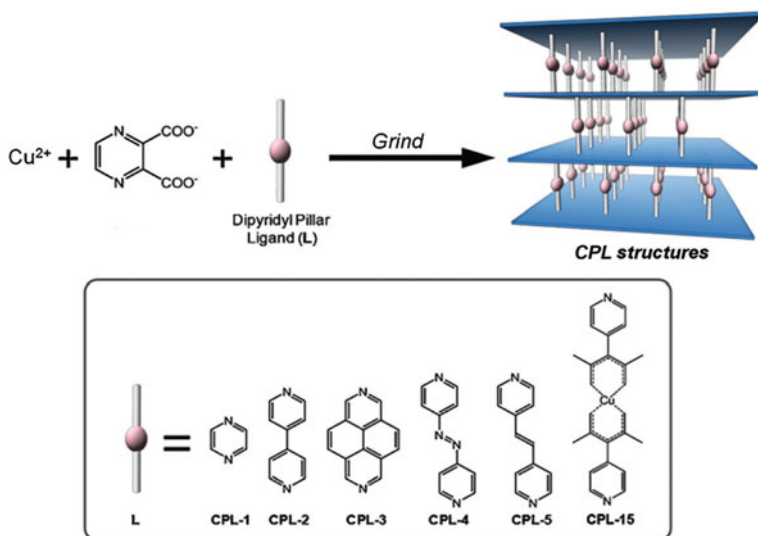
Scheme 6.25 The scheme of mechanochemical preparation of CPs by the interaction of Cu(II) with pyrazine-2,3-dicarboxylic acid and different dipyridyl bridging ligands
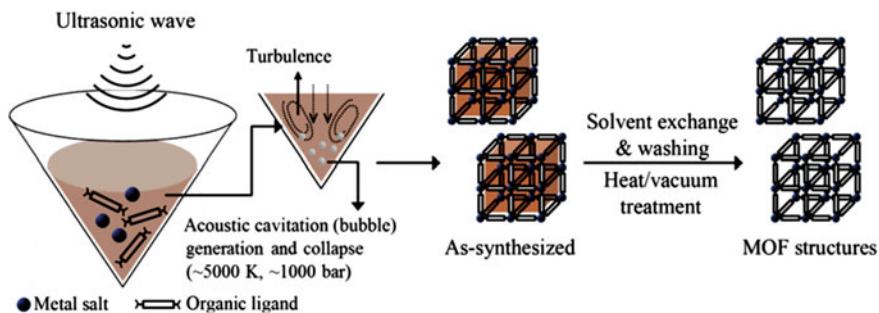
Fig. 6.58 Sonochemical synthesis of MOF structures

It is important that using ultrasound of high intensity provides easy, ecological, and universal synthetic tool for production of nanostructured materials, which are often unavailable for conventional methods [669].

Sonochemical methods through uniform and accelerated nucleation also provide decrease in crystallization time and far less sizes of particles, than those provided by conventional solvothermal synthesis. For this purpose, a solution of mixture of substrates for this MOF structure is input in a horn-type Pyrex reactor equipped with an ultrasonic bar with regulated output power without external cooling. As an example, we shall consider sonochemical synthesis of nanometer MOF with $[Pb_2(N_3)(NO_3)Q_2]$ block [670].

Sonochemically are also obtained nanostructures of 2D CPs with $[Pb_2L_2I_2]_n$ and $[Pb_2L_2Br_2]_n$ blocks based on Py-2-carboxylic acid (HL) [671] and CP with $[Pb(\mu_7\text{-}L)]_n$ block based on maleic acid (H_2L) [672], and also CPs with $[Pb_2L_4]_n$ (HL = 2-pyrazinecarboxylic acid) and $[Pb(L')_2]_n$ (HL′ = 2-quinolinecarboxylic acid) blocks [673].

It should also be noted sonochemically produced nanostructured 1D double-stranded Pb(II) CP with $[Pb(\mu\text{-}HL)(\mu\text{-}Br)(H_2O)]_n$ block (H_2L = 2,3-pyrazinedicarboxylic acid) [674]. Coordination number is six and each Pb atom is coordinated with two oxygen atoms and two nitrogen atoms of L^- ligands, one bromide atom and one oxygen atom of molecule H_2O. There is an interest in sonochemical synthesis of nano-sized Pb(II) CP with 1H-1,2,4-triazole-3-carboxylate ligand [675].

High quality Mg-MOF-74 crystals (1.640 m^2 g^{-1} BET surface area) with particle size about 0.6 μm are successfully synthesized during 1 h by sonochemical method after addition of triethylamine as a deprotonating agent. It is interesting that mesopores are formed, probably, due to competitive linking of triethylamine to Mg (II) ions [567].

6.9   Post-synthetic Approaches

Analysis of the available experimental data shows that the preparation of the CPs containing metal chelate units largely limited by synthetic approaches used for synthesis of most CPs. However, with the development of chemistry of the CPs containing metal chelate units the synthesis of CPs with excellent stability and a desired functionality is becoming increasingly popular for the purpose of importance in practical applications. One of important work directions in CPs studies is development of methods of framework production, which are unavailable with traditional hydro(solvo)thermal methods, but which will be stable or metastable if they really can be produced. It should be noted that there are cases when desired functionalities cannot be realized before or during MOF synthesis. For example, if chelating functional groups impede MOF synthesis, then targeted structures may be not formed immediately from these ligands. Moreover, it is also possible that ligands are too big or cannot sustain the synthesis conditions. It is very difficult to obtain MOFs with these chelating functionalities. Therefore, there is an urgent necessity in development of a method of MOF functionalization after they have been synthesized.

In the recent years, post-synthetic approaches have become powerful tools for synthesis of the CPs containing metal chelate units, which cannot be reached with de novo synthesis due to limited linker solubility, thermal stability, chemical stability, functional group compatibility, and undesired intervention between metal ions and linker of functional fragments during MOF assembling. Removal or substitution of solvents and guest molecules, action of chemically active vapors and external stimuli, such as heat, light or mechanochemical force induce such structural transformations, and they often manifest themselves in different physical

properties, such as color, magnetism, luminescence, chirality, porosity, etc. because of a change in coordination number and geometry, dimensionality, interpenetration, etc. More radical transformations associated with exchange of metal ions, pillar ligands, and insertions of additional ligands between layers were also represented.

On the other hand, post-synthetic approaches are useful tools for MOF synthesis with renewed functionalities. It is important that many desirable but usually unavailable MOFs are direct structural analogues of materials, which, in contrast to this, are easily obtained using regular synthesis methods. CPs have solid state reactivity and structural transformation under different experimental conditions [171]. These approaches provide possibilities for integration of functionalities into CPs, preserving their structural integrity. Achievements in post-synthetic approaches add additional dimension to synthetic variability and broaden sphere of chelating functionalities which can be integrated in CPs.

It would be ideal to have a building set of stable MOFs with different pore sizes, which can be then functioned especially for some necessity in post-synthetic treatment. This will provide systematic change in cavities and design of a range of isostructural MOF networks with different chemical functions and, consequently, different chemical and physical properties. Programming of architectures in a cavity of a porous material can bring to specially developed and deliberated interactions of a given modified MOF with guest molecules [676]. Successful chemical PSM approach can have considerable consequences for MOF chemistry with viable ways to solid state versions of diversely-oriented synthesis. Study and understanding of PSM can finally result in development of combinatory MOFs databases.

Post-synthetic approaches include post-synthetic modification (PSM), post-synthetic deprotection (PSD) and post-synthetic exchange (PSE).

6.9.1 Post-synthetic Modification

Post-synthetic modification (PSM) is a single-crystal to single-crystal (SC-SC) transformation and is the process including transformation of side groups on surface or in pores of MOFs in order to change physical or chemical properties. This can be reached with chemical reaction, adsorption, ligand or metal exchange, light, and pressure stimuli. Post-synthetic MOF modification opens new dimension of structural possibilities, which cannot be reached by conventional synthesis.

PSM provides one more way of changing MOF's functionality, thus solving the problems which arise when using ligands with given functionalities. There are metal centers and initial ligands with functional groups, which can modify a reaction under normal conditions of MOF synthesis, in order to form MOFs with specified crystal structures and pore sizes. Then the functional groups on ligands can take part in the reaction with post-synthetic reagents to obtain final desired functionalities [677].

PSM MOFs can be realized using multiple interactions, among which covalent and coordination bonds are crucial. Post-synthetic methods, which modify MOFs

with chemical reagents with the lattice structure unchanged, make it possible to integrate functional groups in MOFs (Fig. 6.59) [678].

PSM often gives access to CPs, inaccessible by direct synthesis. Direct synthesis not always allows correct topology; therefore stricter control is achieved using tagged ligands with reliable functionality and simple ways of modification in view. For PSM, in order to be successful, a product should preserve crystallinity with a framework remaining a whole. There should not be solving and recrystallization with modified by direct synthesis MOF with a modified ligand. Some reactions on crystals proceed with change in color in MOF, pointing out that modification takes place. PSM is a useful method, since is makes it possible to avoid a script of functional groups linking with metal ions and carboxylic groups during initial structuring of a framework [679]. For most applications a metal component is necessary only in SBU.

There are several advantages of PSM strategy as compared with using of different ligands in one-stage synthesis. First, ligands with different functionalities can bring to different crystal structures during synthesis. At the same time, with RSM, as long as a desired structure is achieved, the crystalline structure becomes identical to post-synthetic modification, and a possibility of producing different structures is excluded. Secondly, even if the synthesis conditions have been previously studied, as a ligand changes to the similar with additional functional groups, it is highly possible that the conditions should be repeatedly optimized. With PSM efforts on optimization of the synthesis conditions can be preserved. The last, but not the least important is that PSM gives a possibility to change one MOF to different others, which have different functionalities or even several functionalities integrated in one MOF.

We shall notice covalent PSM changing functionality of side groups integrated in framework through covalent mechanisms. New MOFs with functional groups bound covalently with pore surface are in demand due to their reliability, designing capacity, and easiness of synthesis. For majority of PSM it is typical to provide
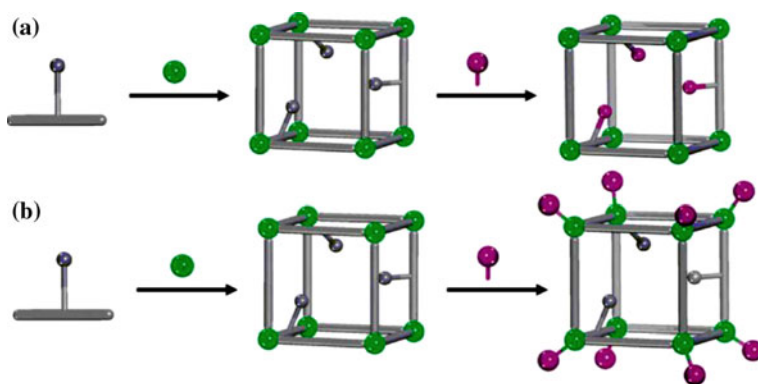
Fig. 6.59 The post-synthetic methods **a** covalent PSM, **b** dative PSM

further change in functional group previously incorporated in substrate structures. In other words, when MOFs are designed, reactive, but still non-coordinated functional groups are, as a rule, parts of ligands. There are two reasons for this: first, it is difficult to change ligands without reactive functional groups under such chemical conditions that MOFs can survive; secondly, if functional groups are already at site, which means that modification positions are determined, it is less probable that a modified structure will be disturbed.

Chelating groups can be introduced more easily by post—than by presynthetic functionalization in MOFs since they may compete in the coordination to inorganic nodes. There are various examples in the literature that show how to produce chelating groups by PSM. It is important that potential chelating fragments can be introduced in MOFs by covalent post-synthetic modification, so that they do not cause interference to the synthesis, but are still available for further coordination modification.

The term «post-synthetic modification» (PSM) was for the first time suggested for description of IRMOF-3 reaction with acetic anhydride [680]. IRMOF-3, amino-derivative of IRMOF-1 (IRMOF-3 spacer = 2-amino-1,4-benzenedicarboxylate), studied exhaustively due to its simple synthesis, porous crystal network and different possible reactions with amino-tag groups [681]. In particular, universality of 2-amino-1,4-benzenedicarboxylate as a building block has been showed: it can be smoothly subjected to PSM in three different prototypic MOF topologies: IRMOF-1, DMOF-1 (D = dabco), and UMCM-1 (UMCM = University of Michigan Crystalline Material) [682]. The important features of PSM on IRMOF-3 include (1) facile introduction of a wide range of functional groups using simple reagents (e.g., anhydrides and isocyanates), (2) the introduction of multiple (as many as four different) substituents into the MOF lattice, and (3) control over reaction conditions to preserve the crystallinity and microporosity of the resultant MOFs.

As a typical example we note imine condensation of IRMOF-3 wetted in toluene solution and excess of salicylaldehyde during 7 days, which has given a PSM-product with $\sim 13\%$ conversion of aminogroups (Scheme 6.26) [682]. Then V(O) acac$_2$ was loaded in the framework for coordination with the salicylidene groups, and the second step was almost quantitative. In this case post-synthetic derivatization of a porous material gives functionalized material, which links a metal complex VO(acac)$_2$ contrary to non-functionalized precursor, which is inactive for complex linking.

A vapor phase PSM (VP-PSM) realized using salicylaldehyde has also brought to imine-functionalized IRMOF-3. Addition with a vapor-phase VO(acac)$_2$ carried out for linking of metal sites in MIXMOF-5 pores (10% of aminogroups incorporated in MOF-5) with quantitative conversion and UiO-66-NH$_2$ (29% conversion) into salicylimino-functionalized material (UiO = Oslo University). An advantage of VP-PSM over PSM in solution is higher conversion and shorter reaction times. A drawback of this PSM method is pores exposing to side products (acids and water), which are highlighted upon degradation of IRMOF framework with anhydrides in VP-PSM [683].
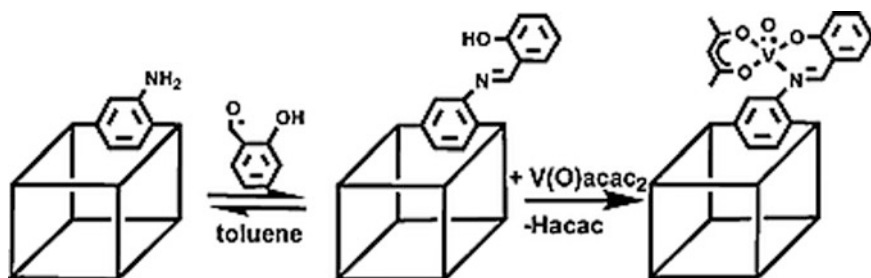
Scheme 6.26 Scheme illustrating for the functionalization of IRMOF-3 with salicylaldehyde and subsequent binding of a vanadyl complex [682]
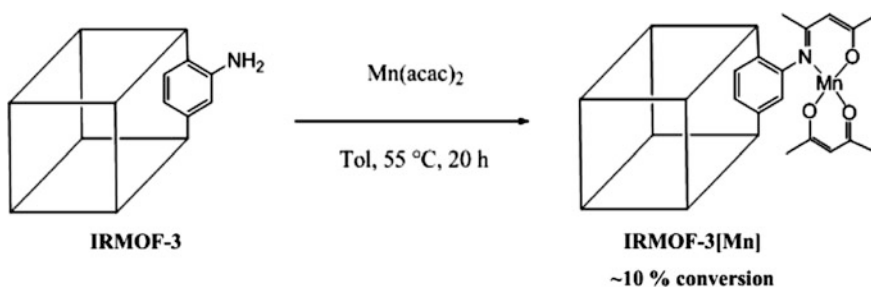
Scheme 6.27 Post-functionalization route of IRMOF-3 for a Mn(II) complex [684]

It should be noted simple one-step example of conversion from amino into imino functional group. IRMOF-3 and Mn(acac)$_2$ are subjected to interaction in one stage in order to tag MOF by iminogroups and to simultaneously coordinate Mn center to it (Scheme 6.27) [684]. The original MOF framework structure was maintained with high phase purity even after the post-synthetic reaction. Different coordination of Mn in the product and in the initial material and ∼10% complexation of aminogroups are shown.

In another example, the crystals of Zn(II) MOF (**A**) based on 2-amino-1, 4-benzenedicarboxylate (Fig. 6.60) were reacted with 2-pyridinecarboxaldehyde to form the covalently bound iminopyridine chelate derivative (**B**), which was reacted with PdCl$_2$(CH$_3$CN)$_2$ to give the metal-complexed MOF (**C**) [685]. The metalation was achieved by adding 1,5 equivs of PdCl$_2$(CH$_3$CN)$_2$ to **B** in anhydrous CH$_2$Cl$_2$, whereupon the yellow crystalline material became dark-purple within several minutes. Remarkably, these reactions and their respective products were achieved without loss of structural order or framework connectivity. This isoreticular metalation is a significant first step in harnessing the intrinsic advantages of molecular coordination chemistry for functionalization of extended solids.
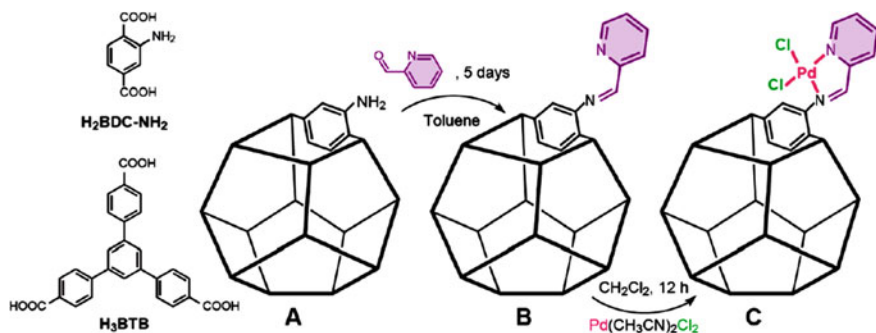
Fig. 6.60 Isoreticular covalent functionalization followed by metalation
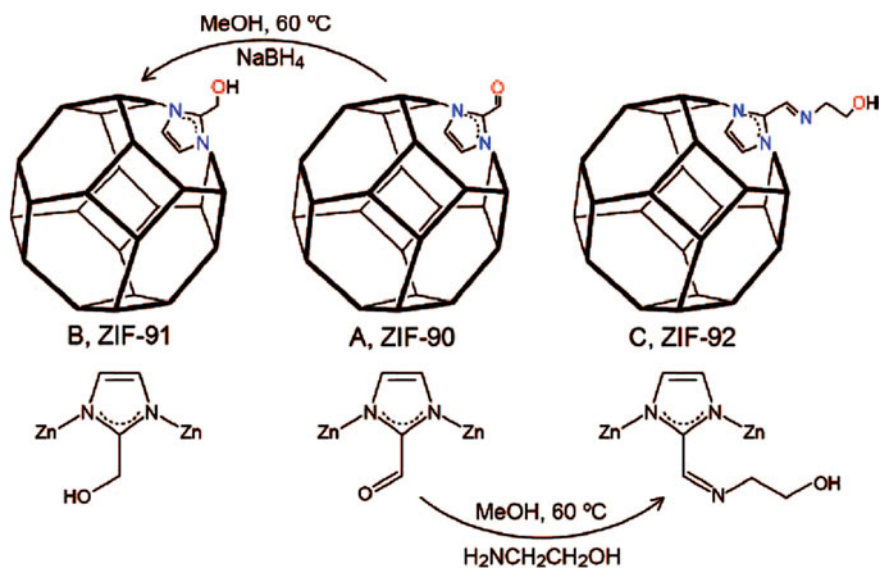
Fig. 6.61 Transformation of ZIF-90 (**a**) by reduction with NaBH$_4$, and reaction with ethanolamine to give ZIF-91 (**b**) and ZIF-92 (**c**)

In conversion of roles aldehyde can be a part of MOF, as in the case of ZIF-90 (isostructural to ZIF-8, but with a tag aldehyde group) [686]. Specifically, reduction of aldehyde to alcohol functionality was successfully achieved by reacting ZIF-90 with NaBH$_4$ in methanol at 60 °C for 24 h to give ZIF-91 с примерно 80% конверсией (Fig. 6.61a). The chemical versatility of the aldehyde group was highlighted by performing another organic transformation on ZIF-90. Reaction of ZIF-90 with ethanolamine in methanol at 60 °C gave ZIF-92 (Fig. 6.61b). Quantitative conversion to the imine was completed within three hours.

Tandem PSM is useful, since it can be realized in one-pot synthesis. PSM MIL-101(Fe)–NH$_2$ with Py-2-carboxaldehyde and NiCl$_2$ in the one-pot reaction has given $\sim 30\%$ conversion of aminogroups into pyridine iminogroups (Scheme 6.28) [99]. Nickel centers are integrated as catalytic sites into pores coordinating with a nitrogen atom of iminogroup and a pyridine nitrogen atom. Ni complex is formed, first of all, to stop any competition with aldehyde reagent for aminogroups.

Heterometallic complex [Yb$_2$L$_6$Cd$_2$][Cd(H$_2$O)$_6$]$_n$ (Yb-Cd) (H$_2$L = oxidiacetic acid) is synthesized under hydrothermal conditions [687]. In Yb–Cd each L is chelated to one Yb(III) center and links up to two Cd(II) ions in anti-anti configuration. Yb and Cd atoms are arranged alternately and linked through O–C–O bridges with formation of cubic octahedral cage as a SBU. Therefore, topologic networks NaCl with high symmetry in cubic spatial group Fd-3c are built. [Cd(H$_2$O)$_6$]$^{2+}$ fragments lying in porosity of anionic MOF are thermodynamically stable species needed to compensate two negative charges [Yb$_2$L$_6$Cd$_2$]$^{2-}$ in Yb–Cd. It is interesting to notice that when Yb–Cd was used as a precursor, and appeared in Mn and Zn perchlorate aqueous solution, the SC-SC transformation process driven by [Cd(H$_2$O)$_6$]$^{2+}$ cations generated heterotrimetallic CP [Yb$_2$L$_6$Cd$_2$][Mn(H$_2$O)$_6$]$_n$ (Yb–Cd–Mn) or [Yb$_2$L$_6$Cd$_2$][Zn(H$_2$O)$_6$]$_n$ (Yb–Cd–Zn). Yb–Cd–Mn and Yb–Cd–Zn are the interesting examples, representing 4d-4f-3d polymers based on polycarboxylic acids (Scheme 6.29).

About almost quantitative transformation of dihydroxylated spacers to carboxylic acid by tagged spacers with cyclic anhydride reacting agent dihydrofuran-2,5-dione is carried out (Scheme 6.30i). Then the second PSM with CuCl$_2$ aqueous solution is performed to demonstrate chelating ability of MOF showing decrease in Cu(II) concentration from 75 to 50 ppm after 4-h exposition (Scheme 6.30ii). This was accompanied by a change in color of the material from light yellow to blue-green [688].

Determination of additional set of examples is observation that traditional batch hydro(solvo)thermal methods of synthesis, as a rule, exclude direct incorporation of
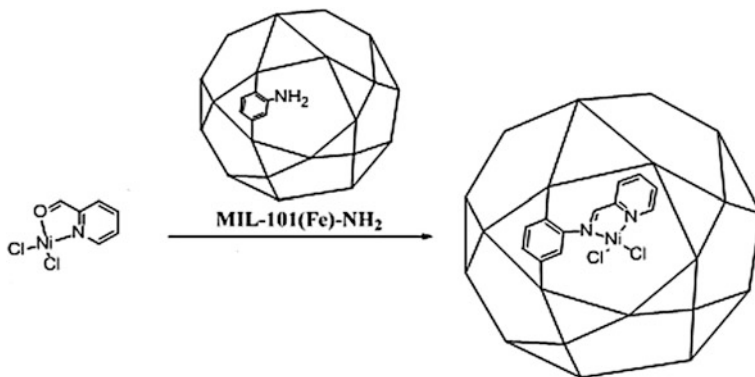
Scheme 6.28 A representation of 30% Ni-functionalized MOF PSM product from MIL-101(Fe)–NH$_2$, reacting with pyridinecarboxaldehyde and NiCl$_2$ in methanol [99]
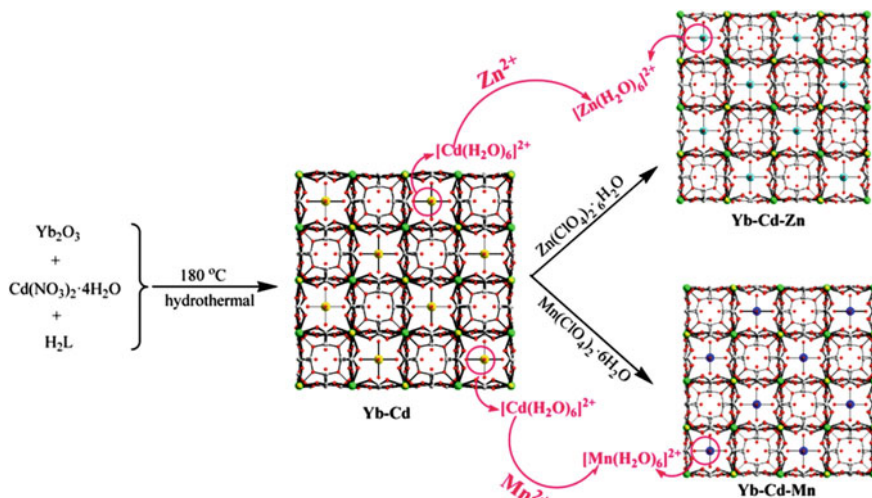
Scheme 6.29 Synthesis of Yb–Cd, Yb–Cd–Mn, and Yb–Cd–Zn
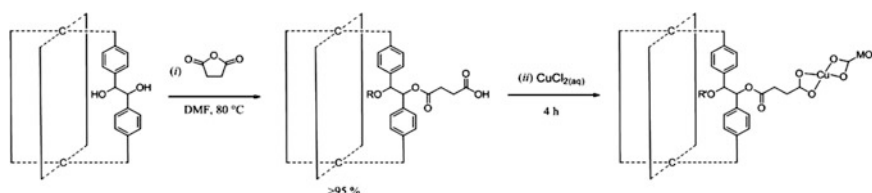
Scheme 6.30 Representation of a tandem PSM of [Zn$_2$(TCPB)(DPG)] by (i) ring opening of cyclic anhydride and (ii) chelation of Cu(II) reagent. C = aromatic backbone, R = carboxylic acid moiety, R′ = chelated Cu(II) moiety

free-base Pp as a spacer in MOF, since spacers spontaneously recruit metal ions present as building blocks and nodes [190, 291]. A promising particular solution of the abovementioned problem is post-synthetic treatment afterwards renamed and generalized in PSM [678, 689, 690], i.e. chemical substitution (atom, ion or functional group, addition, substitution or transformation) of a framework without a change in parent topology. Really, a task with participation of metal-free Pp or salen-based spacers was first met by assembling of metallized spacer in variants of compounds, and then by substitution of non-structural (i.e. spacer-localized) metal ions with a pair of protons. The second stage of PSM accepts new metal ions.

It should be noted that covalent modification of bridging ligands is studied in detail [114, 691, 692]. One of the most widely applied PSM approaches is modification of organic spacers using chemical reactions with preservation of a lattice structure. In particular, azide-functionalized MOFs are used for click reactions [693, 694].

A special interest there is for MOF, where metal centers are subjected to modification. Also a possibility is demonstrated of PSM via coordination of additional metal ions with centers in bridging ligands [695] and addition or removal of metal ions in metal centers [696].

Of particular note is the linker installation method, in which a stable Zr-MOF with inherent missing linker sites, namely, PCN-700, with coordinatively unsaturated Zr_6 clusters was employed and linkers bearing different functional groups were post-synthetically installed (Fig. 6.62) [697]. First, the bpy-5,5′-dicarboxylate and terphenyl-4,4″-dicarboxylate were sequentially installed by treating PCN-700 crystals with solutions of bpy-5,5′-dicarboxylate and terphenyl-4,4″-dicarboxylate in DMF at 75 °C. The modified MOF bears open bpy sites that readily react with CuI in acetonitrile to form the metalated framework. According to the crystal structure, the Cu^+ center is chelated by a bpy group and further coordinated with an N from acetonitrile and an I^- ion as a counter-ion. The Cu^+ center is arranged around the 1D channel along the c-axis, whereas the terphenyl-4,4″-dicarboxylate controls the accessibility of the Cu^+ center by partially blocking the channels. Therefore, the size selectivity of the whole material can be tuned by changing the size of substituents on the terphenyl-4,4″-dicarboxylate linker. In particular, the terphenyl-4,4″-dicarboxylate linker was functionalized by methyl groups, phenyl groups, and hexyl groups, which is expected to result in different selectivity toward the substrates.

Dative PSM on SBUs of MOFs has become the main approach to tune the functionality of MOF pores. As an example, we note dative PSM on SBUs using Zn(II)
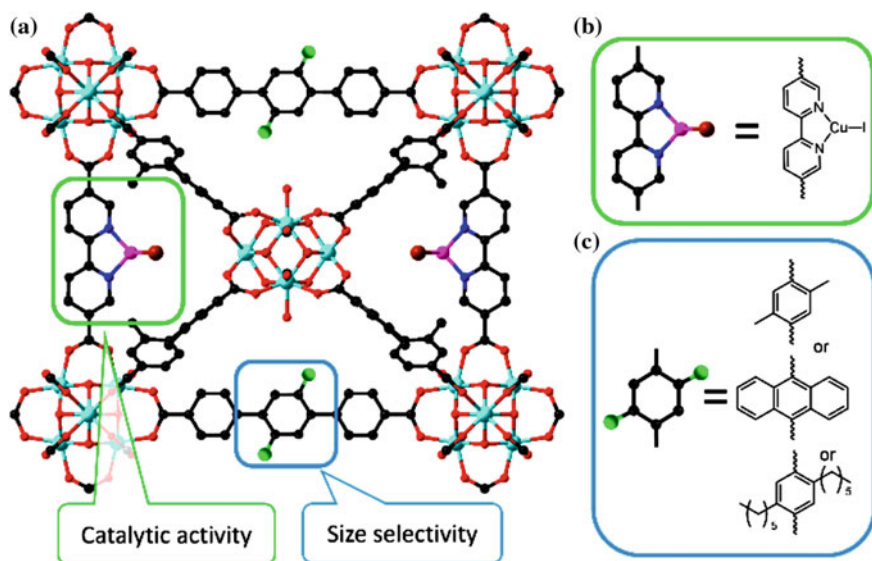
Fig. 6.62 a Size-selective catalytic system for aerobic alcohol oxidation reaction built in PCN-700 through linker installation. **b**, **c** Structure of catalytic center and size-selective moiety. Coordinated CH_3CN on the Cu is removed for clarity
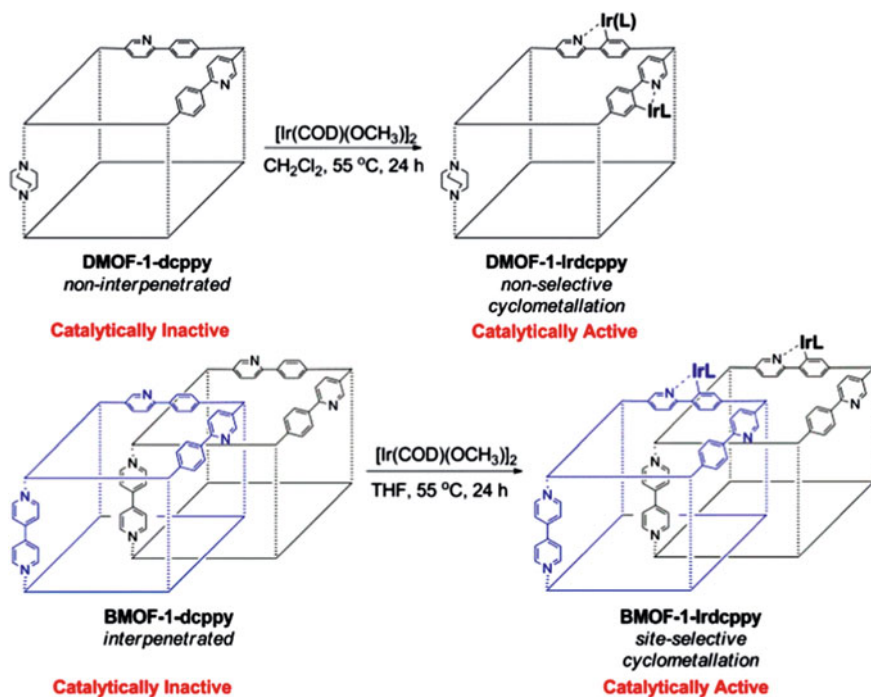
Fig. 6.63 Post-synthetic modification of DMOF-1-dcppy and BMOF-1-dcppy to obtain DMOF-1-Irdcppy and BMOF-1-Irdcppy

paddlewheel derivatives of MOF [549]. Unsaturated metal sited were used in an alternative method, in which MOF with $[Cu_3L_2]$ block (L = 1,3,5-benzenetricarboxylate) was modified with en followed desolvation under vacuum to prepare free coordinating fragments [698]. An interesting example is MOF containing pyridyl donors, which was converted to the active heterogeneous catalyst by post-synthetic treatment with [Ir(COD) (OCH$_3$)]$_2$ (Fig. 6.63) [699]. The cyclometalation of DMOF-1-dcppy (DMOF = dabco MOF, dcppy = 5,4′-phenylpyridinedicarboxylic) and BMOF-1-dcppy (BMOF = 4,4′-bipyridine MOF) with [Ir(COD)(OCH$_3$)]$_2$ produced MOFs with metal-containing units appended to ∼20 and ∼32% of ligand struts within the frameworks.

6.9.2   Post-synthetic Deprotection

PSD is useful for synthesis of functional MOFs, such as those which have groups with a trend to metal complexes formation in direct synthesis. The process includes elimination of complexity in MOF and in production of big cavities. PSD is sometimes also called protection, complexation, and deprotection [700].

By now PSD just begins to draw attention as a post-synthetic method of functionalization. The concept of this method is that a protective functional group is incorporated as an organic spacer, and then the protective group is removed by the post-synthetic method.
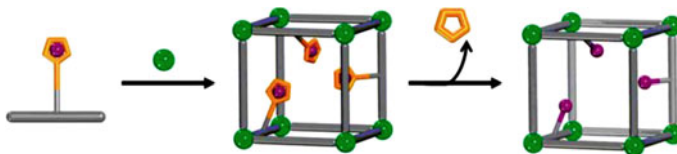
A polluting substance usually found in important amino-substituted MOF UiO-66-NH$_2$ appears as a result of partial formylation during synthesis in DMF [701]. Soft conditions are presently developed for post-synthetic deformylation and for almost complete formylation, offering a new post-synthetic method of deprotection for multifunctional MOFs synthesis.

Catechol (CAT) moieties were successfully incorporated into a MOF by using post-synthetic photochemical deprotection (Scheme 6.31) [702]. UMCM-1-CAT maintained its structural and thermal stabilities under the photochemical conditions. Moreover, UMCM-1-CAT exhibited significant increases in porosity, which is consistent with the liberation of the bulky nitrobenzyl substituents. The metalation tests with UMCM-1-CAT confirmed the presence of the catechol unit, as evidenced by binding of Fe(III) to the MOF.

It should be noted that post-synthetic MOF modification is realized by new way of single-site catalysts [703].

Protection-deprotection methods open new possibilities for «unlock» of protected functionalities for production of highly active and/or coordinating fragments on MOFs. This can facilitate immobilizing of metal-organic catalysts in MOF cavities [704].

6.9.3   Post-synthetic Exchange

Post-synthetic exchange (PSE) also known as a building block replacement [695] includes replacement of basic structural components of preliminary assembled
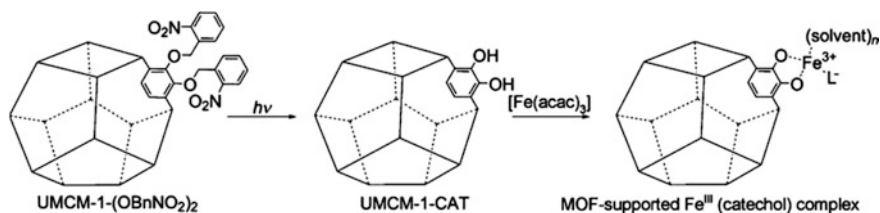
Scheme 6.31 Light-driven deprotection of functionalized frameworks

MOFs. PSE methods include (I) solvent-assisted linker exchange (SALE), (II) non-bridge ligand replacement, and (III) transmetalation. These one-stage or tandem PSE processes suppose exchange of key structural MOF components, which, in turn, should provide evolution of initial MOF structures for MOFs design consisting of absolutely new components, supposedly, using SC-SC-transformations.

SALE is one of most widely used PSE approaches for adjustment of MOF functionality. SALE realization, as a rule, involves holding of MOFs crystals in a solution of a spacer substitution candidate in a thorough chosen solvent [705]. It is worth noticing that SALE goes through exchange of ligands in undamaged MOFs, but not by solution and re-crystallization. Therefore, topology of a parent MOF is reproduced in a daughter structure. SALE was demonstrated for a range of MOFs [144, 187, 705–708], including such, seemingly, inert compounds as ZIFs and, which is more surprising, into UiO-66 [144, 709, 710], the material, which is characterized by unusually strong M–L bonds.

Thus, modification of UiO-66 is executed with catechine using SALE in DMF/H_2O solution during 2 days at 85 °C. After metalation Cr-metallized MOFs were synthesized (Fig. 6.64) [711]. Importantly, insulated metal-monocatecholato fragment is achieved in very strong MOF by two principally different strategies: PSD and PSE. As compared with PSD, PSE is easier and more efficient approach to functioning for MOFs access, which cannot be synthesized directly under solvothermal conditions. Metalation of catechine functionality remained in MOFs has brought to unprecedented Fe-monocatechelato and Cr-monocatechelato types.

PSE was also employed as a strategy to introduce dimercapto functionality into UiO-66 [712]. In particular, PSE was performed by incubating solid UiO-66 in an aqueous solution of 2,3-dithiocatechine-1,4-benzenedicarboxylic acid (tcat-H_2bdc) for 24 h at 85 °C. The linker-exchanged thiocatechol material, UiO-66-TCAT, was isolated as a yellow microcrystalline powder using centrifugation. Immobilized thiocatechol ligands on the UiO-66-TCAT provide an excellent platform to achieve accessible and unsaturated mono(thiocatecholato) metal centers (Scheme 6.32). The metalation of 40% thiocatechol-functionalized UiO-66-TCAT using Pd(OAc)$_2$ in
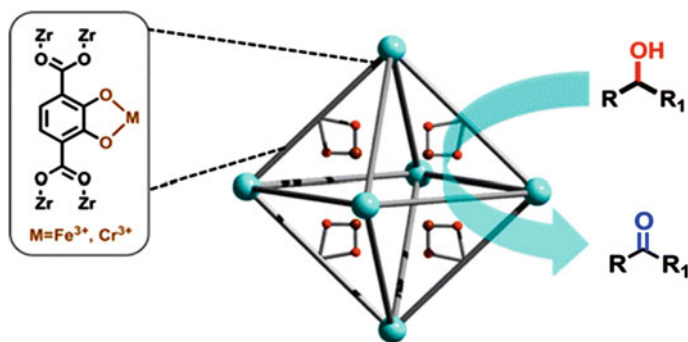
Fig. 6.64 Schematic view of catechol-functionalized UiO-66 after metalation for catalytic oxidation of alcohols to ketones [711]
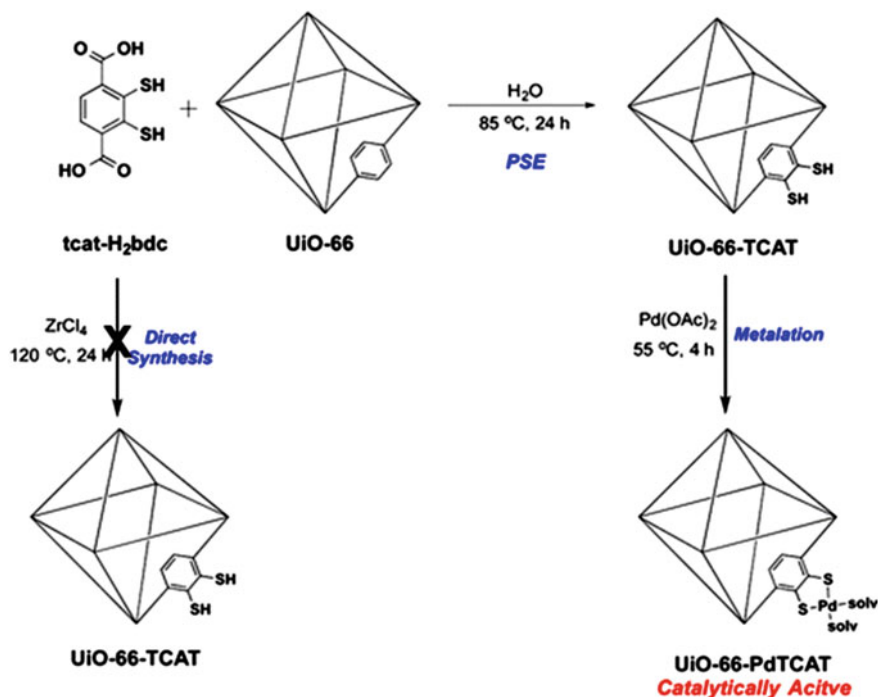
Scheme 6.32 Schematic view of the synthesis of UiO-66-TCAT and UiO-66-PdTCAT [712]

CH_2Cl_2 afforded dark-brown solids. The crystallinity of UiO-66-PdTCAT was maintained upon metalation. It is important to notice that Pd-metalated MOFs are efficient, heterogeneous, and recycled catalysts for regioselective functionalization of sp^2 C–H bond. This material is a rare example of chelating-assisted C–H functionalization performed by a MOF catalyst.

Consecutive process of post-synthetic exchange of ligands was used for production of a range of mono-, di-, and trifunctionalized mesoporous MOFs [713]. Using this process, orthogonal functional groups are established, and after that post-synthetically modified with a dye and quencher molecules, illustrating the level of structural and functional complexity that can be achieved within this system. It is important that the degree of completion and the relative ease of ligand exchange can depend on the lability of the M–L bond within the MOF.

SC-SC transformation as a result of replacement of bridge spacer is possible in extended 2D and 3D MOFs by integration of pillared-paddlewheel MOF structures into a solution containing dipyridyl spacers. In particular, substitution of bridge ligand was observed in two cases of extended 2D (PPF-18) and 3D (PPF-20) Pp MOFs (Scheme 6.33) [187]. Due to porous origin of these MOFs, dipyridyl spacers can enter MOFs interiors and replace existing pillaring dipyridyl units. No side motion of layers during this transformation was observed making the template effect from parent to daughter structure. Despite the fact that these MOFs are
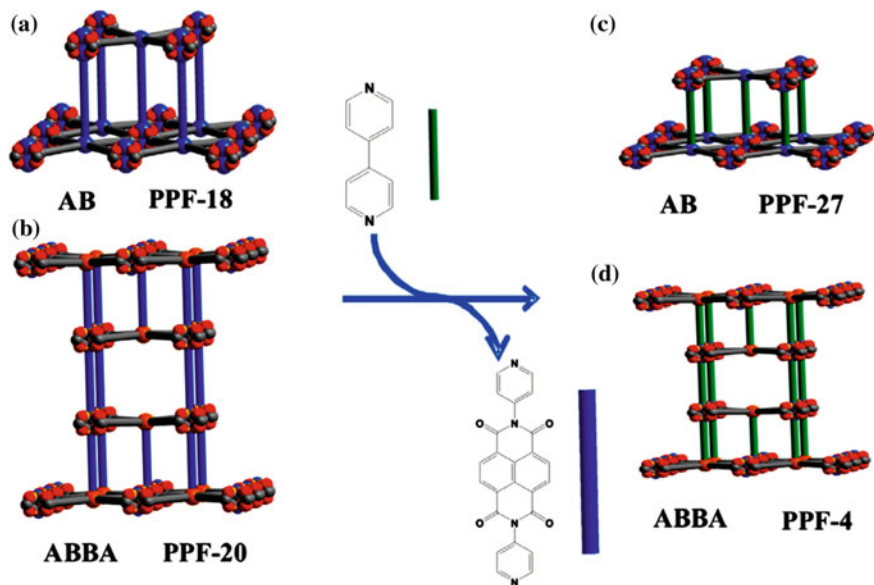
Scheme 6.33 Schematic illustration of the introduction of 4,4′-bipy to the crystals of PPF-18 (**a**) and PPF-20 (**b**) for the transformation of PPF-27 (**c**) and PPF-4 (**d**), respectively

insoluble, this spacer transformation can also be used in staged synthesis independently on whether the frameworks are homogeneous or not (as is seen in PPF-27). As long as daughter frameworks preserve their original topology, the replacement reaction in MOFs along with other staged synthesis methods provides a new way for manipulation with complicated Pp MOFs architecture, which is purposed for specific functions. An extended Pp MOFs family is developed, which includes directly variety of M-Pp through M-Pp and M-bipyridyl Pp as building blocks, which have large available channels and active metal sites [550].

Irreversible SC-SC transformations of 3D Pb(II) CP with a 1H-1,2,4-triazole-3-carboxylic acid (HL) ligand, $[PbL(\mu_2-Br)(H_2O)]_n$, $[PbL(\mu_{1,1}-NCS)(H_2O)]_n$ and $[PbL(\mu_2-Cl)(H_2O)]_n$, into 3D supramolecular compound $[PbL(\mu_2-I)]_n$ through solid state anion-substitution processes in mechanochemical reactions were carried out [714]. These solid state structural transformations are examples of the mechanochemical reactions for conversion of CPs that take place by manual or mechanical grinding with no solvent. In the crystal lattices, bridged bromide, thiocyanate and chloride ions of CPs replace with iodide ion to generate $[PbL(\mu_2-I)]_n$. The morphology and size of the final product obtained using solid state anion-replacements are the same as that observed in initial compounds.

We shall notice the «activation» strategy covering exchange of a solvent with liquid CO_2 followed by supercritical drying [60, 715–718], which has proved its efficiency in prevention of collapse of different MOFs with high initial content of a solvent.

A simple substitution of a solvent is basic for PSM chemistry. As a typical example, we note a solvent replacement in MOF with $[CdL_2(ClO_4)_2]_n$ block, where L = (S)-2,2′-diethoxy-1,1′-binaphthyl-6,6′-bis(4-VP), in which ethanol was reversibly exchanged with benzene in chiral 1D hexagonal channel. It is assumed that this MOF has a good potential for heterogeneous asymmetric catalysis, since the structure can be supported after replacement of a solution [719, 720].

Post-synthetic transmetalation has become a prominent way of synthesis of new crystalline materials based CPs and is especially powerful for orientation of metastable phases, which are unavailable for conventional high temperature synthetic methods [679, 696, 721–723]. Through integration of cations in certain coordination, post-synthetic transmetalation provides rational design of physical properties and chemical reactivity, which otherwise can be physically and chemically inactive. Clear structure-function understanding is required for design of these materials, though their high structural complication undermines at the atomic level structural characterization. Thus, relative occupation of cation on two crystallographically different metal sites in Fe(II)-, Cu(II)-, and Zn(II)-exchanged versions of microporous MnMnL MOF (L = 1,3,5-benzenetristetrazolate), was established. It is important that using dispersion differences between Mn, Fe, Cu, and Zn, degree and localization of cation exchange are determined. Besides, the replacement degree for Mn(II) depends on the identity of the substituting metal [724].

Different amounts of Co and Ni were substituted in Mg-MOF-74 using one-pot solvothermal reaction [725]. Based on elemental analysis, Co and Ni were more efficiently incorporated into MOF-74 framework from solution than Mg was. Besides, temperature of the reaction has stronger effect on the final composition of metal in these mixed metallic (MM) MOF-74 structures than a solvent composition of the reaction.

Fast room-temperature cation exchange is also observed during soaking of CP with $[Pb_2Cl_2(HL)_2(H_2O)_2]_n$ block based on pyrazine-2,3-dicarboxylic acid (H_2L) in Cu(II) aqueous solutions (Scheme 6.34) [368].

Of interest is Zn-MOF $[Zn_3(OH)_2L_2]$ synthesized from dicarboxylate ligands with diimine groups (1,4-bis(4-$CO_2HC_6H_4$)-2,3-dimethyl-1,4-diazabutadiene), which was used to prepare an ethylene oligomerization catalyst with active Ni(II) centers by post-synthetic treatment using nickel dichloride as a nickel source [726].

Series of metallosalen-based MOFs is prepared using post-synthetic modification of Mn^{III}SO-MOF, Mn^{III}(salen)-based MOF [232, 727]. Treatment of Mn^{III}SO-MOF with H_2O_2 brings to removal of Mn^{3+} ions from salen pillar, which then can be remetalated with different metal precursors with formation of isostructural MSO-MOF materials (Scheme 6.35). Presence of new metallosalen pillars in MSO-MOF is entirely confirmed. It is important that remetalated Mn^{II}SO-MOF material reflects similar catalytic activity and porosity to initial MOF.

Exchange of metal cations within a MOF has also been demonstrated for M-Pp MOF. Thus, easy route of M-Pp-based nanoreactor with post-synthetic metal-ion exchange with active metal cations and catalytically inactive MMPF, which consists of nanoscopic multifaced cages is developed [185]. Local coordination of the
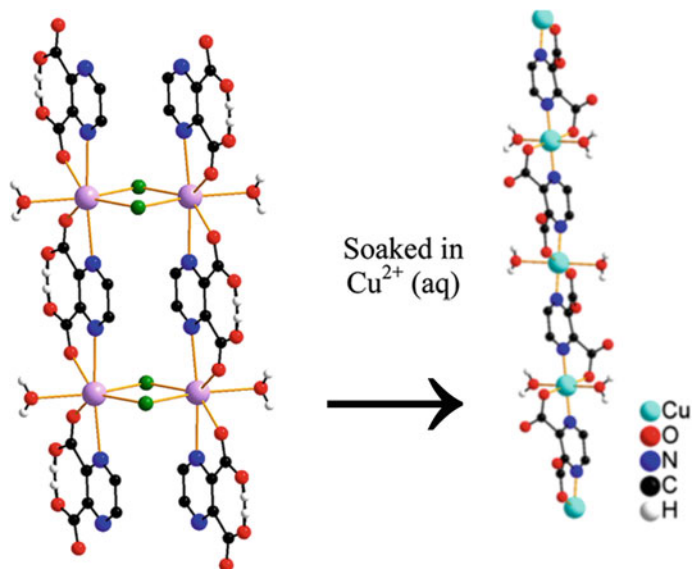
Scheme 6.34 Cation exchange by simple soaking of Pb(II) MOF into an aqueous solution of Cu(II) cation at room temperature
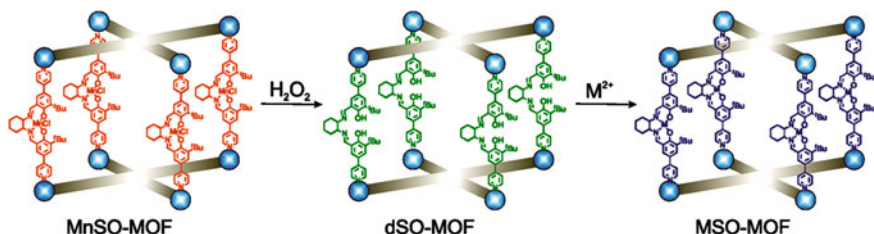
Scheme 6.35 Demetalation of Mn(III)SO-MOF and its subsequent remetalation [232]

active metal center in Pp macrocycle after the metal-ion exchange was crystallographically identified.

It should be noted cationic PCN-223(Fe) formed by synthetic treatment of PCN-223, Pp Zr-MOF with **shp-a** network which is excellent recycled heterogeneous catalyst for hetero-Diels-Alder reaction [728].

Two isostructural Zr-Pp and Hf-Pp MOF (FJI-H6 and FJI-H7) are rationally synthesized and built from 2.5 nm cubic cages [729]. It is worth noticing that in FJI-H6 and FJI-H7 two nitrogen atoms of the Pp ring are not deprotonated, therefore metal ion of another type is integrated in the framework. Submergence of FJI-H6 or FJI-H7 single crystals in 0.5 M solution $Cu(NO_3)_2$ in DMF at the temperature 85 °C during 72 h brings to metalated FJI-H6(Cu) or FJI-H7(Cu). As was expected, both in FJI-H6 and FJI-H7 Cu(II) ions were inbuilt in Pp rings, and Cu(II)

ions in plane-square N_4 coordination with two axial sites were exposed, which is typical of bivalent metal ions in Pp MOFs.

Of interest are isostructural Pp MOFs, in particular, UNLPF-10b, -11, and -12, which consist of In^{III}-, $Sn^{IV}Cl_2$-, and Sn^{IV}-Pp building blocks, respectively [730]. Metalation with high valence metal cations (In^{III} and Sn^{IV}) considerably changes electronic structure of Pp macrocycle and provides high oxidization photoexcited state, which can be subjected to efficient reduction extinguishing processes to facilitate organic reactions. In particular, UNLPF-12 shows extraordinary photo-stability and efficient photocatalytic activities with respect to aerobic hydroxylation of arylboronic acids, amine combination and Mannich reaction.

It should be noted Pp-based MOF MMPF-5, in which each small cubicoctahedral cavity consists of faces of six Cd(II)-metalated tetrakis(3,5-dicarboxyphenyl)porphine units interlinked by eight triangular $Cd(CO_2)_3$ fragments (Fig. 6.65a) [185]. In MMPF-5 crystal structure a Cd(II) cation within Pp ligand ring is far from Pp plane (Fig. 6.65b), which points to weak linking of Cd(II) cations in Pp macrocycle and on a possibility to replace big Cd(II) by a smaller cation of a bivalent metal. Submerging of the MMPF-5 crystals into DMSO solution of $Co(NO_3)_2$ at 85 °C for two days gives Co(II)-exchanged MMPF-5(Co). Complete substitution from Cd(II) to Co(II) is confirmed exclusively within Pp macrocycles, however, Cd(II) cations in the framework have remained untouched, possibly, due to their strong chelating with six carboxylic oxygen atoms. Therefore, small cubicoctahedral cavity in MMPF-5(Co) is distinguished by faces of six Co(II) metalated Pp fragments, which are linked through triangular $Cd(CO_2)_3$ fragments (Fig. 6.65c, d). It is important that MMPF-5 preserves its single crystalline character after the metal ion exchanges with Co(II).

Post-synthetic incorporation of Zn into free-base of Al(III) MOF with formation of light-harvesting MOFs proceeds by similar way [190]. Reaction of MOF with anhydrous zinc acetate in DMF at 100 °C afforded a highly crystalline purple material, consistent with 90% occupancy of the Pp center sites by Zn(II). Visible
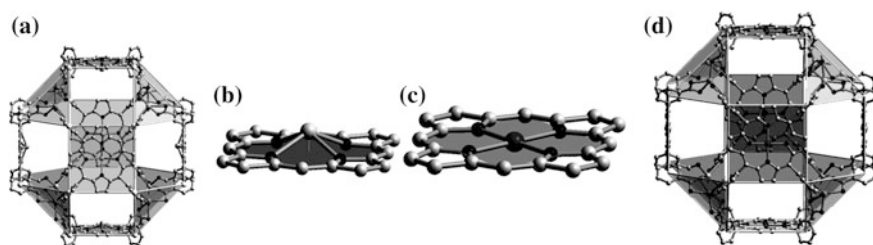
Fig. 6.65 a Representation of the crystal structure of the small cubicuboctahedron in MMPF-5 formed by 6 square Cd-Pp moieties and 8 triangular $Cd(CO_2)_3$ moieties. **b** The M-Pp macrocycle in MMPF-5, showing that the Cd(II) cation lies far out of the Pp plane. **c** The M-Pp macrocycle in MMPF-5(Co), showing that Co(II) cation is located within the plane of the Pp. **d** The small cubicuboctahedron in MMPF-5(Co) formed by 6 square Co-Pp moieties and 8 triangular Cd $(CO_2)_3$ moieties

light catalytic activity of this Zn-Pp based material is shown on sacrificial segregation of hydrogen from water.

Of interest is post-synthetic metalation of reliable chiral and porous BINAP-based Zr-MOFs UiO topologies with $Rh(nbd)_2BF_4$ and $[Rh(nbd)Cl]_2/AgSbF_6$ to give highly active enantioselective one-site solid catalysts for reaction of asymmetric cyclization of 1,6-enynes [731].

Extremely flexible and strong Cd-MOF anion accessible with tetra-acid linker, in particular, 3,3′,5,5′-tetrakis(p-carboxyphenyl)-2,2′,6,6′-tetramethoxy-1,1′-biphenyl, shows abundant post-synthetic metal exchange of metal sites with the metal ion set, which differs significantly by their charges, ion radius, and chemical origin [732]. In particular, there are as many as 16 isostructural new MOFs with transition, lanthanide, and basic groups of metal ions. Post-synthetic metal exchange provides unique transformation of anion framework structure Cd-MOF into cation framework, when bivalent cadmium metal ions are exchanging trivalent Ln(III) ions.

Taking into account universality and practical usefulness of PSM and PSE for access to other difficult-to-synthesize MOFs as bulk materials, their application to MOFs in thin film can also be useful. Among the most universal and useful approaches to synthesis of MOF films is LbL coordination, which is called liquid phase epitaxy [115, 733–743]. LbL approach successfully and repetitively inputs solutions of each building block of a framework in contact with functionalized substrates, and then a MOF film grows. It is important that composition of additional layer not necessarily coincides with previous layers [733, 744–748]. Reliability of LbL-assembled pillared-paddlewheel MOF films in direction of transformation into new or modified MOFs through SALE and post-synthetic metalation is demonstrated [749]. In particular, it is shown that LbL synthesis provides MOFs, which are unavailable through other de novo strategies (Scheme 6.36). MOF contains 5,10,15,20-(4-carboxyphenyl)-Pp units, such as tetratopic spacers, which coordinate pairs of Zn(II) ions in paddlewheel mode, and 4,4′-bipy spacer, which work as Zn(II)-ligating spacers or pillars between Pp defined layers. A dabco was used as a spacer for exchange or replacement of 4,4′-bipy pillars MOF. Besides, after 12 h reaction in excess magnesium bromide diethyl etherate, the free-base Pp containing films grown of quartz slides were transformed into M-Pp form.

It should be noted strain-promoted alkyne-azide cycloaddition which gives almost complete transformation in PSM MOFs context [749]. After optimization of the reaction conditions, conversion yields about 100% in surface-fixed Zn(II) MOF thin films grown on modified Au substrates can be reached.

Nevertheless, there are some drawbacks of post-synthetic approaches. For example, it is difficult to solve spatial distribution of functional groups post-synthetically included in MOF. As a result, most MOF structures are hypothetical. In some cases a degree of post-synthetic incorporation of functional groups in MOFs is very limited. Moreover, further studies should investigate chemical principles of their specific phenomena, including SALE and transmetalation in order to better direct synthesis of MOFs with required chelating functionality.
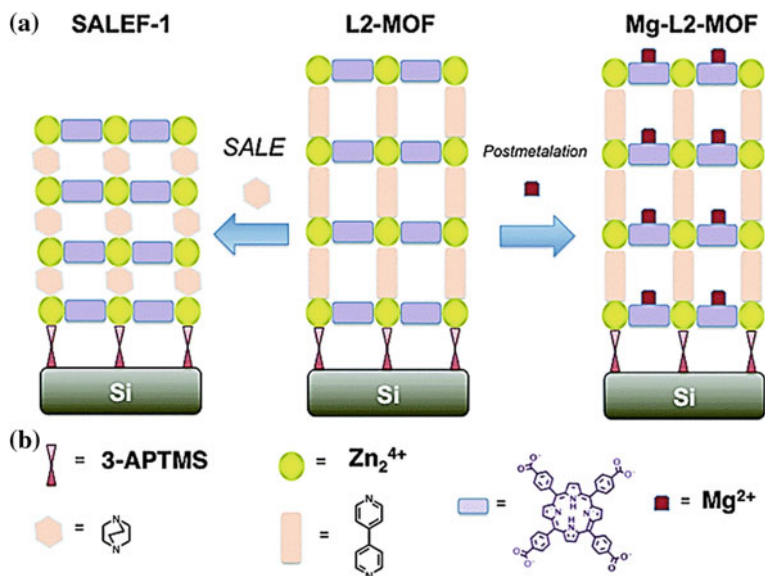
Scheme 6.36 SALE and post-synthetic metalation of MOF films

References

1. K.D. Karlin, D.T.D. Lili, C.L. Cahill, *Coordination Polymers of the Lanthanide Elements* (Wiley, Weinheim, 2008)
2. S.R. Batten, D.R. Turner, M.S. Neville, *Coordination Polymers: Design, Analysis and Application* (RSC, Cambridge, 2009)
3. K. Naka, Metal organic framework (MOF), in *Encyclopedia of Polymeric Nanomaterials*, eds. S. Kobayashi, K. Müllen (Springer, Heidelberg, NY, Dordrecht, London, 2015)
4. R.J. Kuppler, D.J. Timmons, Q.-R. Fang, J.-R. Li, T.A. Makal, M.D. Young, D. Yuan, D. Zhao, W. Zhuang, H.-C. Zhou, Coord. Chem. Rev. **253**, 3042 (2009)
5. M.C. Hong, L. Chen (eds.), *Design and Construction of Coordination Polymers* (Wiley, Weinheim, 2009)
6. J. Jiang (ed.), *Metal-Organic Frameworks: Materials Modeling towards Engineering Applications* (CRC, Boca Raton, 2015)
7. R. Zhai, F. Jiao, H. Lin, F. Hao, J. Li, H. Yan, N. Li, H. Wang, Z. Jin, Y. Zhang, X. Qian, Se Pu. **32**, 107 (2014)
8. L.R. MacGillivray (ed.), *Metal-Organic Frameworks: Design and Application* (Wiley, Weinheim, 2010)
9. L.R. MacGillivray, C.M. Lukehart (eds.), *Metal-Organic Framework Materials* (Wiley, Weinheim, 2014)
10. H. He, D. Collins, F. Dai, X. Zhao, G. Zhang, H. Ma, D. Sun, Cryst. Growth Des. **10**, 895 (2009)
11. J.R. Long, O.M. Yaghi, Chem. Soc. Rev. **38**, 1213 (2009)
12. S. Dalai, J. Phys. Sci. **15**, 223 (2011)
13. H.-C. Zhou, J.R. Long, O.M. Yaghi, Chem. Rev. **112**, 673 (2012)
14. W. Lu, Z. Wei, Z.-Y. Gu, T.-F. Liu, J. Park, J. Park, J. Tian, M. Zhang, Q. Zhang, T. Gentle III, M. Bosch, H.-C. Zhou, Chem. Soc. Rev. **43**, 5561 (2014)

15. S.T. Meek, J.A. Greathouse, M.D. Allendorf, Adv. Mater. **23**, 249 (2011)
16. S. Kitagawa, R. Kitaura, S. Noro, Angew. Chem. Int. Ed. **43**, 2334 (2004)
17. K.M. Fromm, J.L. Sague, L. Mirolo, Macromol. Symp. **291–292**, 75 (2010)
18. A.Y. Robin, K.M. Fromm, Coord. Chem. Rev. **250**, 2127 (2006)
19. O.L. Ortiz, L.D. Ramírez, *Coordination Polymers and Metal Organic Frameworks: Properties, Types, and Applications* (Nova Science Publishers, NY, 2012)
20. J.C. Bailar, Jr., in *Preparative Inorganic Reactions*, ed. by W.L. Jolly, vol. 1 (Interscience, NY, 1964), p. 1
21. Y. Zhao, K. Li, J. Li, Z. Naturforsch. **65b**, 976 (2010)
22. R.I. Walton, Chem. Soc. Rev. **31**, 230 (2002)
23. W. Xuan, C. Zhu, Y. Liu, Y. Cui, Chem. Soc. Rev. **41**, 1677 (2012)
24. O.M. Yaghi, G. Li, H. Li, Nature **378**, 703 (1995)
25. O.M. Yaghi, H. Li, J. Am. Chem. Soc. **117**, 10401 (1995)
26. A.D. Burrows, C.G. Frost, M.F. Mahon, C. Richardson, Angew. Chem. Int. Ed. **47**, 8482 (2008)
27. A.K. Cheetham, C.N.R. Rao, R.K. Feller, Chem. Commun. 4780 (2006)
28. H. Furukawa, K.E. Cordova, M. O'Keeffe, O.M. Yaghi, Science **341**, 1230444 (2013)
29. G. Férey, Chem. Soc. Rev. **37**, 191 (2008)
30. K.M. Fromm, Coord. Chem. Rev. **252**, 856 (2008)
31. W.-Y. Gao, M. Chrzanowski, S. Ma, Chem. Soc. Rev. **43**, 5841 (2014)
32. J.R. Holst, A.I. Cooper, Adv. Mater. **22**, 5212 (2010)
33. C. Janiak, J.K. Vieth, New J. Chem. **34**, 2366 (2010)
34. J.-R. Li, J. Sculley, H.-C. Zhou, Chem. Rev. **112**, 869 (2012)
35. S. Ma, L. Meng, Pure Appl. Chem. **83**, 167 (2011)
36. U. Mueller, M. Schubert, F. Teich, H. Puetter, K. Schierle-Arndt, J. Pastre, J. Mat. Chem. **16**, 626 (2006)
37. L.J. Murray, M. Dinca, J.R. Long, Chem. Soc. Rev. **38**, 1294 (2009)
38. H. Wu, Q. Gong, D.H. Olson, J. Li, Chem. Rev. **112**, 836 (2012)
39. J.-P. Zhang, X.-C. Huang, X.-M. Chen, Chem. Soc. Rev. **38**, 2385 (2009)
40. Q.-L. Zhu, Q. Xu, Chem. Soc. Rev. **43**, 5468 (2014)
41. S.R. Batten, N.R. Champness, X.-M. Chen, J. Garcia-Martinez, S. Kitagawa, L. Öhrström, M. O'Keeffe, M.P. Suhh, J. Reedijk, CrystEngComm **14**, 3001 (2012)
42. A.U. Czaja, N. Trukhan, U. Müller, Chem. Soc. Rev. **38**, 1284 (2009)
43. J.J. Perry, J.A. Perman, M.J. Zaworotko, Chem. Soc. Rev. **38**, 1400 (2009)
44. M. O'Keeffe, O.M. Yaghi, Chem. Rev. **112**, 675 (2012)
45. K. Koh, A.G. Wong-Foy, A.J. Matzger, Angew. Chem. Int. Ed. **47**, 677 (2008)
46. S.-L. Wu, J.-P. Zou, M.-H. Chen, H.-B. Yang, M.-J. Li, X.-B. Luo, F. Luo, M.-F. Wu, G.-C. Guo, Polyhedron **48**, 58 (2012)
47. R. Haldar, N. Sikdar, T. Kumar, Maji. Mater. Today **18**, 97 (2015)
48. A. Umemura, S. Diring, S. Furukawa, H. Uehara, T. Tsuruoka, S. Kitagawa, J. Am. Chem. Soc. **133**, 15506 (2011)
49. L.-L. Wen, Z.-D. Lu, X.-M. Ren, C.-Y. Duan, Q.-J. Meng, S. Gao, Cryst. Growth Des. **9**, 227 (2009)
50. L.-L. Wen, F. Wang, X.-K. Leng, C.-G. Wang, L.-Y. Wang, J.-M. Gong, D.-F. Li, Cryst. Growth Des. **10**, 2835 (2010)
51. D.A. Fowler, A.V. Mossine, C.M. Beavers, S.J. Teat, S.J. Dalgarno, J.L. Atwood, J. Am. Chem. Soc. **133**, 11069 (2011)
52. S.A. Sapchenko, D.N. Dybtsev, D.G. Samsonenko, V.P. Fedin, New J. Chem. **34**, 2445 (2010)
53. S. Zhang, L. Zhen, B. Xu, R. Inglis, K. Li, W. Chen, Y. Zhang, K.F. Konidaris, S.P. Perlepes, E.K. Brechin, Y. Li, Dalton Trans. **39**, 3563 (2010)
54. X.-M. Zhang, J. Lv, F. Ji, H.-S. Wu, H. Jiao, P.R. Schleyer, J. Am. Chem. Soc. **133**, 4788 (2011)

55. K.E. Knope, D.T. Lill, C.E. Rowland, P.M. Cantos, A. Bettencourt-Dias, C.L. Cahill, Inorg. Chem. **51**, 201 (2012)
56. M. O'Keeffe, Chem. Soc. Rev. **38**, 1215 (2009)
57. G. Férey, Dalton Trans. 4400 (2009)
58. M.J. Prakash, M.S. Lah, Chem. Commun. 3326 (2009)
59. D. Sun, G.-G. Luo, N. Zhang, Q.J. Xu, Y.-C. Jin, Z.-H. Wei, C.-F. Yang, L.-R. Lin, R.-B. Huang, L.-S. Zheng, Inorg. Chem. Commun. **13**, 306 (2010)
60. O.K. Farha, J.T. Hupp, Acc. Chem. Res. **43**, 1166 (2010)
61. Y.H. Hu, L. Zhang, Adv. Mater. **22**, E117 (2010)
62. A.M. Spokoyny, M. Alexander, D. Kim, A. Sumrein, C.A. Mirkin, Chem. Soc. Rev. **38**, 218 (2009)
63. R. Peng, M. Li, D. Li, Coord. Chem. Rev. **254**, 1 (2010)
64. H.L. Jiang, T. Akita, T. Ishida, M. Haruta, Q. Xu, J. Am. Chem. Soc. **133**, 1304 (2011)
65. W.Q. Kan, J.F. Ma, Y.Y. Liu, J. Yang, CrystEngComm **14**, 2316 (2012)
66. C.B. Aakeröy, N.R. Champness, C. Janiak, CrystEngComm **12**, 22 (2010)
67. S. Ma, H.-C. Zhou, Chem. Commun. **46**, 44 (2010)
68. D. Farrusseng (ed.), *Metal-Organic Frameworks: Applications from Catalysis to Gas Storage* (Wiley, Weinheim, 2011)
69. K. Sumida, D.L. Rogow, J.A. Mason, T.M. McDonald, E.D. Bloch, Z.R. Herm, T.-H. Bae, J.R. Long, Chem. Rev. **112**, 724 (2012)
70. M.P. Suh, H.J. Park, T.K. Prasad, D.-W. Lim, Chem. Rev. **112**, 782 (2012)
71. Y. He, W. Zhou, G. Qian, B. Chen, Chem. Soc. Rev. **43**, 5657 (2014)
72. S. Qiu, M. Xue, G. Zhu, Chem. Soc. Rev. **43**, 6116 (2014)
73. H.-J. Son, S. Jin, S. Patwardhan, S.J. Wezenberg, N.C. Jeong, M. So, C.E. Wilmer, A.A. Sarjeant, G.C. Schatz, R.Q. Snurr, O.K. Farha, G.P. Wiederrecht, J.T. Hupp, J. Am. Chem. Soc. **135**, 862 (2013)
74. S. Jin, H.-J. Son, O.K. Farha, G.P. Wiederrecht, J.T. Hupp, J. Am. Chem. Soc. **135**, 955 (2013)
75. P. Horcajada, R. Gref, T. Baati, P.K. Allan, G. Maurin, P. Couvreur, G. Férey, R.E. Morris, C. Serre, Chem. Rev. **112**, 1232 (2012)
76. D.M. D'Alessandro, B. Smit, J.R. Long, Angew. Chem. Int. Ed. **49**, 6058 (2010)
77. W. Morris, B. Volosskiy, S. Demir, F. Gándara, P.L. McGrier, H. Furukawa, D. Cascio, J.F. Stoddart, O.M. Yaghi, Inorg. Chem. **51**, 6443 (2012)
78. B. Chen, S. Xiang, G. Qian, Acc. Chem. Res. **43**, 1115 (2010)
79. J.-R. Li, Y. Ma, M.C. McCarthy, J. Sculley, J. Yu, H.-K. Jeong, P.B. Balbuena, H.-C. Zhou, Coord. Chem. Rev. **255**, 1791 (2011)
80. Y.-S. Bae, R.Q. Snurr, Angew. Chem. Int. Ed. **50**, 11586 (2011)
81. J. Liu, P.K. Thallapally, B.P. McGrail, D.R. Brown, J. Liu, Chem. Soc. Rev. **41**, 2308 (2012)
82. C. He, D. Liu, W. Lin, Chem. Rev. **115**, 11079 (2015)
83. K. Lu, C. He, W. Lin, J. Am. Chem. Soc. **137**, 7600 (2015)
84. P. Horcajada, T. Chalati, C. Serre, B. Gillet, C. Sebrie, T. Baati, J.F. Eubank, D. Heurtaux, P. Clayette, C. Kreuz, J.-S. Chang, Y.K. Hwang, V. Marsaud, P.-N. Bories, L. Cynober, S. Gil, G. Férey, P. Couvreur, R. Gref, Nat. Mater. **9**, 172 (2010)
85. J.D. Rocca, D. Liu, W. Lin, Acc. Chem. Res. **44**, 957 (2011)
86. P. Horcajada, C. Serre, G. Maurin, N.A. Ramsahye, F. Balas, M. Vallet-Regí, M. Sebban, F. Taulelle, G. Férey, J. Am. Chem. Soc. **130**, 6774 (2008)
87. Z. Hu, B.J. Deibert, J. Li, Chem. Soc. Rev. **43**, 5815 (2014)
88. L.E. Kreno, K. Leong, O.K. Farha, M. Allendorf, R.P. Van Duyne, J.T. Hupp, Chem. Rev. **112**, 1105 (2012)
89. Y. Cui, Y. Yue, G. Qian, B. Chen, Chem. Rev. **112**, 1126 (2012)
90. J. Heine, K. Muller-Buschbaum, Chem. Soc. Rev. **42**, 9232 (2013)
91. M. Yoon, R. Srirambalaji, K. Kim, Chem. Rev. **112**, 1196 (2012)
92. J. Liu, L. Chen, H. Cui, J. Zhang, L. Zhang, C.-Y. Su, Chem. Soc. Rev. **43**, 6011 (2014)

93. A. Corma, H. Garcia, F.X. Llabres i Xamena. Chem. Rev. **110**, 4606 (2010)
94. V. Lykourinou, Y. Chen, X.-S. Wang, L. Meng, T. Hoang, L.-J. Ming, R.L. Musselman, S. Ma, J. Am. Chem. Soc. **133**, 10382 (2011)
95. P. Phuengphai, S. Youngme, P. Gamez, J. Reedijk, Dalton Trans. **39**, 7936 (2010)
96. T. Zhang, W. Lin, Chem. Soc. Rev. **43**, 5982 (2014)
97. A.H. Chughtai, N. Ahmad, H.A. Younus, A. Laypkov, F. Verpoort, Chem. Soc. Rev. **44**, 6804 (2015)
98. K. Kyogoku, C. Yamada, Y. Suzuki, S. Nishiyama, K. Fukumoto, H. Yamamoto, S. Indo, M. Sano, T. Miyake, J. Jap. Petrol. Inst. **53**, 308 (2010)
99. J. Canivet, S. Aguado, Y. Schuurman, D. Farrusseng, J. Am. Chem. Soc. **135**, 4195 (2013)
100. A.N. Mlinar, B.K. Keitz, D. Gygi, E.D. Bloch, J.R. Long, A.T. Bell, ACS Catal. **4**, 717 (2014)
101. Y. Zhang, Y. Zhou, Y. Zhao, C. Liu, Catal. Today **263**, 61 (2016)
102. A. Bhunia, S. Dey, J.M. Moreno, U. Diaz, P. Concepcion, K. Van Hecke, C. Janiak, P. Van Der Voort, Chem. Commun. **52**, 1401 (2016)
103. S. Ou, C.-D. Wu, Inorg. Chem. Front. **1**, 721 (2014)
104. P. Ramaswamy, N.E. Wong, G.K.H. Shimizu, Chem. Soc. Rev. **43**, 5913 (2014)
105. J.M. Taylor, R.K. Mah, I.L. Moudrakovski, C.I. Ratcliffe, R. Vaidhyanathan, G.K. Shimizu, J. Am. Chem. Soc. **132**, 14055 (2010)
106. T. Yamada, K. Otsubo, R. Makiura, H. Kitagawa, Chem. Soc. Rev. **42**, 6655 (2013)
107. C.-Y. Sun, X.-L. Wang, X. Zhang, C. Qin, P. Li, Z.-M. Su, D.-X. Zhu, G.-G. Shan, K.-Z. Shao, H. Wu, J. Li, Nat. Commun. **4**, 2717 (2013)
108. Y. Cui, F. Zhu, B. Chen, G. Qian, Chem. Commun. **51**, 7420 (2015)
109. J. Pan, C.-P. Liu, F.-L. Jiang, M.-Y. Wu, L. Chen, J.-J. Qian, K.-Z. Su, X.-Y. Wan, M.-C. Hong, CrystEngComm **17**, 1541 (2015)
110. X.-P. Wang, T.-P. Hu, D. Sun, CrystEngComm **17**, 3393 (2015)
111. X. Zhang, W. Wang, Z. Hu, G. Wang, K. Uvdal, Coord. Chem. Rev. **284**, 206 (2015)
112. C. Wang, T. Zhang, W. Lin, Chem. Rev. **112**, 1084 (2012)
113. W. Zhang, R. Xiong, Chem. Rev. **112**, 1163 (2012)
114. S.M. Cohen, Chem. Rev. **112**, 970 (2012)
115. A. Betard, R.A. Fischer, Chem. Rev. **112**, 1055 (2012)
116. Y. Chen, V. Lykourinou, T. Hoang, L.-J. Ming, S. Ma, Inorg. Chem. **51**, 9156 (2012)
117. Y. Chen, V. Lykourinou, C. Vetromile, T. Hoang, L.-J. Ming, R. Larsenand, S. Ma, J. Am. Chem. Soc. **134**, 13188 (2012)
118. G.R. Desiraju, *Crystal Engineering: The Design of Organic Solids* (Elsevier, Netherlands, 1989)
119. G.R. Desiraju, Angew. Chem. Int. Ed. **46**, 8342 (2007)
120. G.R. Desiraju, J. Am. Chem. Soc. **135**, 9952 (2013)
121. K.R. Seddon, M. Zaworotko, *Crystal Engineering: The Design and Application of Functional Solids* (Kluwer, Dordrecht, Boston, London, 1999)
122. B.F. Hoskins, R. Robson, J. Am. Chem. Soc. **112**, 1546 (1990)
123. B.F. Hoskins, R. Robson, J. Am. Chem. Soc. **111**, 5962 (1989)
124. B. Moulton, M.J. Zaworotko, Chem. Rev. **101**, 1629 (2001)
125. S. Horike, S. Hasegawa, D. Tanaka, M. Higuchi, S. Kitagawa, Chem. Commun. 4436 (2008)
126. F. Dai, H. He, D. Sun, J. Am. Chem. Soc. **130**, 14064 (2008)
127. T. Lee, M.S. Lin, Cryst. Growth Des. **7**, 1803 (2007)
128. J. Pasan, J. Sanchiz, F. Lloret, M. Julve, C. Ruiz-Perez, CrystEngComm **9**, 478 (2007)
129. L.F. Ma, Y.Y. Wang, L.Y. Wang, J.Q. Liu, Y.P. Wu, J.G. Wang, Q.Z. Shi, S.M. Peng, Eur. J. Inorg. Chem. 693 (2008)
130. M. Eddaoudi, J. Kim, D.T. Vodak, A. Sudik, J.B. Wachter, M. O'Keeffe, O.M. Yaghi, Proc. Natl. Acad. Sci. U S A **99**, 4900 (2002)
131. M. Eddaoudi, D.B. Moler, H.L. Li, B.L. Chen, T.M. Reineke, M. O'Keeffe, O.M. Yaghi, Acc. Chem. Res. **34**, 319 (2001)

132. O.M. Yaghi, M. O'Keeffe, N.W. Ockwig, H.K. Chae, M. Eddaoudi, J. Kim, Nature **423**, 705 (2003)
133. G. Férey, J. Solid State Chem. **152**, 37 (2000)
134. Y. Liu, J.F. Eubank, A.J. Cairns, J. Eckert, V.C. Kravtsov, R. Luebke, M. Eddaoudi, Angew. Chem. Int. Ed. **46**, 3278 (2007)
135. Y. Liu, V.C. Kravtsov, R. Larsen, M. Eddaoudi, Chem. Commun. 1488 (2006)
136. M. O'Keeffe, M. Eddaoudi, H. Li, T. Reineke, O.M. Yaghi, J. Solid State Chem. **152**, 3 (2000)
137. M. Eddaoudi, J. Kim, N. Rosi, D. Vodak, J. Wachter, M. O'Keeffe, O.M. Yaghi, Science **295**, 469 (2002)
138. Y. Jeon, J. Heo, C.A. Mirkin, J. Am. Chem. Soc. **129**, 7480 (2007)
139. S. Natarajan, P. Mahata, Chem. Soc. Rev. **38**, 2304 (2009)
140. V. Guillerm, D. Kim, J.F. Eubank, R. Luebke, X. Liu, K. Adil, M.S. Lah, M. Eddaoudi, Chem. Soc. Rev. **43**, 6141 (2014)
141. M.P. Yutkin, D.N. Dybtsev, V.P. Fedin, Russ. Chem. Rev. **80**, 1009 (2011)
142. H.-L. Jiang, T.A. Makal, H.-C. Zhou, Coord. Chem. Rev. **257**, 2232 (2013)
143. D.J. Tranchemontagne, J.L. Mendoza-Cortes, M. O'Keeffe, O.M. Yaghi, Chem. Soc. Rev. **38**, 1257 (2009)
144. N.L. Rosi, M. Eddaoudi, J. Kim, M. O'Keefi, Cryst. Eng. Commun. **68**, 401 (2002)
145. T. Devic, O. David, M. Valls, J. Marrot, F. Couty, G. Férey, J. Am. Chem. Soc. **129**, 12614 (2007)
146. K. Wang, D. Feng, T.-F. Liu, J. Su, S. Yuan, Y.-P. Chen, M. Bosch, X. Zou, H.-C. Zhou, J. Am. Chem. Soc. **136**, 13983 (2014)
147. S.G. Baca, I.G. Filippova, T.D. Keene, O. Botezat, I.L. Malaestean, H. Stoeckli-Evans, V.C. Kravtsov, I. Chumacov, S.-X. Liu, S. Decurtins, Eur. J. Inorg. Chem. 356 (2011)
148. D.-X. Xue, A.J. Cairns, Y. Belmabkhout, Ł. Wojtas, Y. Liu, M.H. Alkordi, M. Eddaoudi, J. Am. Chem. Soc. **135**, 7660 (2013)
149. M. Li, D. Li, M. O'Keeffe, O.M. Yaghi. Chem. Rev. **114**, 1343 (2013)
150. N.W. Ockwig, O. Delgado-Friedrichs, M. O'Keeffe, O.M. Yaghi, Acc. Chem. Res. **38**, 176 (2005)
151. J. Eubank, F. Nouar, R. Luebke, A. Cairns, L. Wojtas, M. Alkordi, T. Bousquet, M. Hight, J. Eckert, J. Embs, P. Georgiev, M. Eddaoudi, Angew. Chem. Int. Ed. **51**, 10099 (2012)
152. M. O'Keeffe, M.A. Peskov, S.J. Ramsden, O.M. Yaghi, Acc. Chem. Res. **41**, 1782 (2008)
153. V. Guillerm, S. Gross, C. Serre, T. Devic, M. Bauer, G. Férey, Chem. Commun. **46**, 767 (2010)
154. V. Guillerm, F. Ragon, M. Dan-Hardi, T. Devic, M. Vishnuvarthan, B. Campo, A. Vimont, G. Clet, Q. Yang, G. Maurin, G. Férey, A. Vittadini, S. Gross, C. Serre, Angew. Chem. Int. Ed. **51**, 9267 (2012)
155. V. Guillerm, Ł.J. Weselinski, Y. Belmabkhout, A.J. Cairns, V. D'Elia, Ł. Wojtas, K. Adil, M. Eddaoudi, Nat. Chem. **6**, 673 (2014)
156. F. Nouar, J.F. Eubank, T. Bousquet, L. Wojtas, M.J. Zaworotko, M. Eddaoudi, J. Am. Chem. Soc. **130**, 1833 (2008)
157. J.H. Cavka, S. Jakobsen, U. Olsbye, N. Guillou, C. Lamberti, S. Bordiga, K.P. Lillerud, J. Am. Chem. Soc. **130**, 13850 (2008)
158. M. Dan-Hardi, C. Serre, T. Frot, L. Rozes, G. Maurin, C. Sanchez, G. Férey, J. Am. Chem. Soc. **131**, 10857 (2009)
159. D.-Y. Du, J.-S. Qin, Z. Sun, L.-K. Yan, M. O'Keeffe, Z.-M. Su, S.-L. Li, X.-H. Wang, X.-L. Wang, Y.-Q. Lan, Sci. Rep. **3**, 2616 (2013)
160. G.S. Papaefstathiou, L.R. MacGillivray, Angew. Chem. Int. Ed. **41**, 2070 (2002)
161. M. Andruh, Chimia (Aarau) **67**, 383 (2013)
162. M. Zhu, C. Yuan, S. Feng, L. Lu, Q. Wang, Cryst. Growth Des. **10**, 1706 (2010)
163. Y.-W. Li, H. Ma, Y.-Q. Chen, K.-H. He, Z.-X. Li, X.-H. Bu, Cryst. Growth Des. **12**, 189 (2012)
164. H. Arora, R. Mukherjee, New J. Chem. **34**, 2357 (2010)

165. X. Meng, L. Liu, H. Zhang, Y. Luo, C. Liu, Dalton Trans. **40**, 12846 (2011)
166. X.-Z. Song, S.-Y. Song, C. Qin, S.-Q. Su, S.-N. Zhao, M. Zhu, Z.-M. Hao, H.-J. Zhang, Cryst. Growth Des. **12**, 253 (2012)
167. T.B. Célić, M. Rangus, K. Lazar, V. Kaućić, N.Z. Logar, Angew. Chem. Int. Ed. **51**, 12490 (2012)
168. T.K. Olszewski, D.E. Jaskolska, Heteroat. Chem. **23**, 605 (2012)
169. J. Olchowka, C. Falaise, C. Volkringer, N. Henry, T. Loiseau, Chem.—Eur. J. **19**, 2012 (2013)
170. S.-Y. Zhang, N. Xu, W. Shi, P. Cheng, D.-Z. Liao, Polyhedron **51**, 283 (2013)
171. T.K. Ronson, C. Giri, N.K. Beyeh, A. Minkkinen, F. Topić, J.J. Holstein, K. Rissanen, J.R. Nitschke, Chem.—Eur. J. **19**, 3374 (2013)
172. G.K. Kole, J.J. Vittal, Chem. Soc. Rev. **42**, 1755 (2013)
173. G. Kumar, R. Gupta, Chem. Soc. Rev. **42**, 9403 (2013)
174. J. Heo, Y. Jeon, C.A. Mirkin, J. Am. Chem. Soc. **129**, 7712 (2007)
175. M. Oh, C.A. Mirkin, Angew. Chem. Int. Ed. **45**, 5492 (2006)
176. M. Dincá, J.R. Long, Angew. Chem. Int. Ed. **47**, 6766 (2008)
177. A.M. Spokoyny, D. Kim, A. Sumrein, C.A. Mirkin, Chem. Soc. Rev. **38**, 1218 (2009)
178. J. Lee, O.K. Farha, J. Roberts, K.A. Scheidt, S.T. Nguyen, J.T. Hupp, Chem. Soc. Rev. **38**, 1450 (2009)
179. X. Liu, Angew. Chem. Int. Ed. **48**, 3018 (2009)
180. D. Feng, Z.-Y. Gu, J.-R. Li, H.-L. Jiang, Z. Wei, H.-C. Zhou, Angew. Chem. Int. Ed. **51**, 10307 (2012)
181. Y. Chen, T. Hoang, S. Ma, Inorg. Chem. **51**, 12600 (2012)
182. X.-S. Wang, M. Chrzanowski, C. Kim, W.-Y. Gao, L. Wojtas, Y.-S. Chen, X.P. Zhang, S. Ma, Chem. Commun. **48**, 7173 (2012)
183. X.-S. Wang, L. Meng, Q. Cheng, C. Kim, L. Wojtas, M. Chrzanowski, Y.-S. Chen, X. P. Zhang, S. Ma, J. Am. Chem. Soc. **133**, 16322 (2011)
184. X.-S. Wang, M. Chrzanowski, W.-Y. Gao, L. Wojtas, Y.-S. Chen, M.J. Zaworotko, S. Ma, Chem. Sci. **3**, 2823 (2012)
185. X.-S. Wang, M. Chrzanowski, L. Wojtas, Y.-S. Chen, S. Ma, Chem. – Eur. J. **19**, 3297 (2013)
186. L. Meng, Q. Cheng, C. Kim, W.-Y. Gao, L. Wojtas, Y.-S. Cheng, M.J. Zaworotko, X. P. Zhang, S. Ma, Angew. Chem. Int. Ed. **51**, 10082 (2012)
187. B.J. Burnett, P.M. Barron, C. Hu, W. Choe, J. Am. Chem. Soc. **133**, 9984 (2011)
188. C.Y. Lee, O.K. Farha, B.J. Hong, A.A. Sarjeant, S.B.T. Nguyen, J.T. Hupp, J. Am. Chem. Soc. **133**, 15858 (2011)
189. X.-L. Yang, M.-H. Xie, C. Zou, Y. He, B. Chen, M. O'Keeffe, C.-D. Wu, J. Am. Chem. Soc. **134**, 10638 (2012)
190. A. Fateeva, P.A. Chater, C.P. Ireland, A.A. Tahir, Y.Z. Khimyak, P.V. Wiper, J.R. Darwent, M.J. Rosseinsky, Angew. Chem. Int. Ed. **51**, 7440 (2012)
191. A.M. Shultz, O.K. Farha, J.T. Hupp, S.T. Nguyen, J. Am. Chem. Soc. **131**, 4204 (2009)
192. E.Y. Choi, P.M. Barron, R.W. Novotny, H.T. Son, C. Hu, W. Choe, Inorg. Chem. **48**, 426 (2009)
193. E.Y. Choi, C.A. Wray, C.H. Hu, W. Choe, CrystEngComm **11**, 553 (2009)
194. P.M. Barron, C.A. Wray, C. Hu, Z. Guo, W. Choe, Inorg. Chem. **49**, 10217 (2010)
195. V.S.P.K. Neti, A.J. Metta-Magaña, L. Echegoyen, J. Coord. Chem. **66**, 3193 (2013)
196. S. Matsunaga, N. Endo, W. Mori, Eur. J. Inorg. Chem. 4550 (2011)
197. D. Feng, H.-L. Jiang, Y.-P. Chen, Z.-Y. Gu, Z. Wei, H.-C. Zhou, Inorg. Chem. **52**, 12661 (2013)
198. J.A. Johnson, X. Zhang, T.C. Reeson, Y.S. Chen, J. Zhang, J. Am. Chem. Soc. **136**, 15881 (2014)
199. L.D. DeVries, W. Choe, J. Chem. Crystallogr. **39**, 229 (2008)
200. B.J. Burnett, W. Choe, CrystEngComm **14**, 6129 (2012)

201. H. Chung, P.M. Barron, R.W. Novotny, H.T. Son, C. Hu, W. Choe, Cryst. Growth Des. **9**, 3327 (2009)
202. J.M. Falkowski, T. Sawano, T. Zhang, G. Tsun, Y. Chen, J.V. Lockard, W. Lin, J. Am. Chem. Soc. **136**, 5213 (2014)
203. Z. Zhang, L. Wojtas, M. Eddaoudi, M.J. Zaworotko, J. Am. Chem. Soc. **135**, 5982 (2013)
204. Z. Zhang, M.J. Zaworotko, Chem. Soc. Rev. **43**, 5444 (2014)
205. Z. Zhang, L. Zhang, L. Wojtas, P. Nugent, M. Eddaoudi, M.J. Zaworotko, J. Am. Chem. Soc. **134**, 924 (2012)
206. Z. Zhang, L. Zhang, L. Wojtas, M. Eddaoudi, M.J. Zaworotko, J. Am. Chem. Soc. **134**, 928 (2012)
207. A. Fidalgo-Marijuan, G. Barandika, B. Bazán, M.-K. Urtiaga, M.I. Arriortua, CrystEngComm **15**, 4181 (2013)
208. L. Xu, J. Wang, Y. Xu, Z. Zhang, P. Lu, M. Fang, S. Li, P. Sun, H.-K. Liu, CrystEngComm **16**, 8656 (2014)
209. J.M. Verduzco, H. Chung, C. Hu, W. Choe, Inorg. Chem. **48**, 9060 (2009)
210. T. Ohmura, A. Usuki, K. Fukumori, T. Ohta, M. Ito, K. Tatsumi, Inorg. Chem. **45**, 7988 (2006)
211. S. George, S. Lipstman, I. Goldberg, Cryst. Growth Des. **6**, 2651 (2006)
212. S. Muniappan, S. Lipstman, S. George, I. Goldberg, Inorg. Chem. **46**, 5544 (2007)
213. R. Makiura, S. Motoyama, Y. Umemura, H. Yamanaka, O. Sakata, H. Kitagawa, Nat. Mater. **9**, 565 (2010)
214. I. Goldberg, CrystEngComm **10**, 637 (2008)
215. P.M. Barron, H.-T. Son, C. Hu, W. Choe, Cryst. Growth Des. **9**, 1960 (2009)
216. B.J. Burnett, P.M. Barron, C. Hu, W. Choe, Eur. J. Inorg. Chem. 4885 (2012)
217. C.N. Kato, M. Ono, T. Hino, T. Ohmura, W. Mori, Catal. Commun. **7**, 673 (2006)
218. H. Deng, S. Grunder, K.E. Cordova, C. Valente, H. Furukawa, M. Hmadeh, F. Gandara, A. C. Whalley, Z. Liu, S. Asahina, H. Kazumori, M. O'Keeffe, O. Terasaki, J.F. Stoddart, O.M. Yaghi, Science **336**, 1018 (2012)
219. J. An, O.K. Farha, J.T. Hupp, E. Pohl, J.I. Yeh, N.L. Rosi, Nat. Commun. **3**, 604 (2012)
220. D. Feng, W.-C. Chung, Z. Wei, Z.-Y. Gu, H.-L. Jiang, Y.-P. Chen, D.J. Darensbourg, H.-C. Zhou, J. Am. Chem. Soc. **135**, 17105 (2013)
221. C. Zou, T. Zhang, M.-H. Xie, L. Yan, G.-Q. Kong, X.-L. Yang, A. Ma, C.-D. Wu, Inorg. Chem. **52**, 3620 (2013)
222. C. Zou, M.-H. Xie, G.-Q. Kong, C.-D. Wu, CrystEngComm **14**, 4850 (2012)
223. M.-H. Xie, X.-L. Yang, Y. He, J. Zhang, B. Chen, C.-D. Wu, Chem.—Eur. J. **19**, 14316 (2013)
224. M.-H. Xie, X.-L. Yang, C.-D. Wu, Chem. Commun. **47**, 5521 (2011)
225. M.-H. Xie, X.-L. Yang, C. Zou, C.-D. Wu, Inorg. Chem. **50**, 5318 (2011)
226. S. Matsunaga, N. Endo, W. Mori, Eur. J. Inorg. Chem. 4885 (2012)
227. K.Y. Lee, Y.S. Lee, S. Kim, H.M. Ha, S.-E. Bae, S. Huh, H.G. Jang, S.J. Lee, CrystEngComm **15**, 9360 (2013)
228. Z. Guo, D. Yan, H. Wang, D. Tesfagaber, X. Li, Y. Chen, W. Huang, B. Chen, Inorg. Chem. **54**, 200 (2015)
229. Z. Zhang, J. Li, Y. Yao, S. Sun, Cryst. Growth Des. **15**, 5028 (2015)
230. F. Song, C. Wang, J.M. Falkowski, L. Ma, W. Lin, J. Am. Chem. Soc. **132**, 15390 (2010)
231. S. Cho, Y. Gadzikwa, M. Afshari, T.S. Nguyen, J.T. Hupp, Eur. J. Inorg. Chem. 4863 (2007)
232. A.M. Shultz, A.A. Sarjeant, O.K. Farha, J.T. Hupp, S.T. Nguyen, J. Am. Chem. Soc. **133**, 13252 (2011)
233. J.M. Falkowski, C. Wang, S. Liu, W. Lin, Angew. Chem. Int. Ed. **50**, 8674 (2011)
234. C. Zhu, G. Yuan, X. Chen, Z. Yang, Y. Cui, J. Am. Chem. Soc. **134**, 8058 (2012)
235. S. Jung, M. Oh, Angew. Chem. Int. Ed. **47**, 2049 (2008)
236. S. Cho, B. Ma, T.S. Nguyen, J.T. Hupp, T.E. Albrecht-Schmitt, Chem. Commun. 2563 (2006)

237. B. Chen, X. Zhao, A. Putkham, K. Hong, E.B. Lobkovsky, E.J. Hurtado, A.J. Fletcher, K.M. Thomas, J. Am. Chem. Soc. **130**, 6411 (2008)
238. S.J. Wezenberg, A.W. Kleij, Angew. Chem. Int. Ed. **47**, 2354 (2008)
239. S. Jung, W. Cho, H.J. Lee, M. Oh, Angew. Chem. Int. Ed. **48**, 1459 (2009)
240. Y. Jeon, G.S. Armatas, J. Heo, M.G. Kanatzidis, C.A. Mirkin, Adv. Mater. **20**, 2105 (2008)
241. G. Yuan, C. Zhu, W. Xuan, Y. Cui, Chem.—Eur. J. **15**, 6428 (2009)
242. A. Bhunia, P.W. Roesky, Y. Lan, G.E. Kostakis, A.K. Powell, Inorg. Chem. **48**, 10483 (2009)
243. G. Li, C. Zhu, X. Xi, Y. Cui, Chem. Commun. 2118 (2009)
244. Z.-Y. Gu, J. Park, A. Raiff, Z. Wei, H.-C. Zhou, ChemCatChem **6**, 67 (2014)
245. Y. Huang, T. Liu, J. Lin, J. Lü, Z. Lin, R. Cao, Inorg. Chem. **50**, 2191 (2011)
246. M.C. Das, S. Xiang, Z. Zhang, B. Chen, Angew. Chem. Int. Ed. **50**, 10510 (2011)
247. A. Bhunia, M.A. Gotthardt, M. Yadav, M.T. Gamer, A. Eichöfer, W. Kleist, P.W. Roesky, Chem.—Eur. J. **19**, 1986 (2013)
248. M.C. Das, Q. Guo, Y. He, J. Kim, C.-G. Zhao, K. Hong, S. Xiang, Z. Zhang, K.M. Thomas, R. Krishna, B. Chen, J. Am. Chem. Soc. **134**, 8703 (2012)
249. A. Ali, G. Hundal, R. Gupta, Cryst. Growth Des. **12**, 1308 (2012)
250. G. Kumar, H. Aggarwal, R. Gupta, Cryst. Growth Des. **13**, 74 (2013)
251. A. Mishra, A. Ali, S. Upreti, R. Gupta, Inorg. Chem. **47**, 154 (2008)
252. A. Mishra, A. Ali, S. Upreti, M.S. Whittingham, R. Gupta, Inorg. Chem. **48**, 5234 (2009)
253. A.P. Singh, R. Gupta, Eur. J. Inorg. Chem. **2010**, 4546 (2010)
254. S. Srivastava, A. Ali, A. Tyagi, R. Gupta, Eur. J. Inorg. Chem. **2014**, 2113 (2014)
255. A.P. Singh, A. Ali, R. Gupta, Dalton Trans. **39**, 8135 (2010)
256. A.P. Singh, G. Kumar, R. Gupta, Dalton Trans. **40**, 12454 (2011)
257. S. Srivastava, M.S. Dagur, R. Gupta, Eur. J. Inorg. Chem. **2014**, 4966 (2014)
258. G. Kumar, R. Gupta, Inorg. Chem. Commun. **23**, 103 (2012)
259. D. Bansal, G. Hundal, R. Gupta, Eur. J. Inorg. Chem. **2015**, 1022 (2015)
260. G. Kumar, R. Gupta, Inorg. Chem. **51**, 5497 (2012)
261. G. Kumar, R. Gupta, Inorg. Chem. **52**, 10773 (2013)
262. J. Xiang, W.-L. Man, J. Guo, S.-M. Yiu, G.-H. Lee, S.-M. Peng, G. Xu, S. Gao, T.-C. Lau, Chem. Commun. **46**, 6102 (2010)
263. L.K. Das, A.M. Kirillov, A. Ghosh, CrystEngComm **16**, 3029 (2014)
264. Y.-L. Hou, S.-X. Li, R.W.-Y. Sun, X.-Y. Liu, S.W. Ng, D. Li, Dalton Trans. **44**, 17360 (2015)
265. M. Andruh, J.P. Costes, C. Diaz, S. Gao, Inorg. Chem. **48**, 3342 (2009)
266. P.W. Roesky, A. Bhunia, Y. Lan, A.K. Powell, S. Kureti, Chem. Commun. **47**, 2035 (2011)
267. X. Yang, D. Lam, C. Chan, J.M. Stanley, R.A. Jones, B.J. Holliday, W.-K. Wong, Dalton Trans. **40**, 9795 (2011)
268. A. Bhunia, Y. Lan, V. Mereacre, M.T. Gamer, A.K. Powell, P.W. Roesky, Inorg. Chem. **50**, 12697 (2011)
269. Y.-L. Hou, R.W.-Y. Sun, X.-P. Zhou, J.-H. Wang, D. Li, Chem. Commun. **50**, 2295 (2014)
270. W.-X. Ni, W. Li, S.-Z. Zhan, J.-Z. Hou, D. Li, Inorg. Chem. **48**, 1433 (2009)
271. Q.-L. Zhang, G.-W. Feng, Y.-Q. Zhang, B.-X. Zhu, RSC Adv. **4**, 11384 (2014)
272. A.D. Burrows, M.F. Mahon, C.L. Renouf, C. Richardson, A.J. Warren, J.E. Warren, Dalton Trans. **41**, 4153 (2012)
273. L. Carlucci, G. Ciani, D.M. Proserpio, M. Visconti, CrystEngComm **13**, 5891 (2011)
274. A.D. Burrows, C. Frost, M.F. Mahon, P.R. Raithby, C. Renouf, C. Richardson, A. Stevenson, Chem. Commun. **46**, 5067 (2010)
275. R.W. Seidel, I.M. Oppel, CrystEngComm **12**, 1051 (2010)
276. D. Deb, M. Bhattacharjee, Inorg. Chim. Acta **372**, 286 (2011)
277. S. Khatua, T. Harada, R. Kuroda, M. Bhattacharjee, Chem. Commun. 3927 (2007)
278. S. Khatua, H. Stoeckli-Evans, T. Harada, R. Kuroda, M. Bhattacharjee, Inorg. Chem. **45**, 9619 (2006)
279. S. Khatua, D.R. Roy, P.K. Chattaraj, M. Bhattacharjee, Chem. Commun. 135 (2007)

280. S. Khatua, D.R. Roy, P. Bultinck, M. Bhattacharjee, P.K. Chattaraj, Phys. Chem. Chem. Phys. **10**, 2461 (2008)
281. D. Deb, S. Giri, P.K. Chattaraj, M. Bhattacharjee, J. Phys. Chem. A **114**, 10871 (2010)
282. C. Mohapatra, V. Chandrasekhar, Cryst. Growth Des. **14**, 406 (2014)
283. S. Srivastava, H. Aggarwal, R. Gupta, Cryst. Growth Des. **15**, 4110 (2015)
284. A. Kobayashi, A. Sugiyama, T. Ohba, Y. Suzuki, H.-C. Chang, M. Kato, Chem. Lett. **43**, 1070 (2014)
285. A. Kobayashi, Y. Suzuki, T. Ohba, T. Ogawa, T. Matsumoto, S.-I. Noro, H.-C. Chang, M. Kato, Inorg. Chem. **54**, 2522 (2015)
286. H.-L. Wang, S.-B. Wu, X.-M. Shi, X.-Z. Li, P.-P. Hao, L.-N. Zhu, J. Inorg. Organomet. Polym. **25**, 730 (2015)
287. H. Sakamoto, R. Kitaura, R. Matsuda, S. Kitagawa, Y. Kubota, M. Takata, Chem. Lett. **39**, 218 (2010)
288. C. Zou, C.-D. Wu, Dalton Trans. **41**, 3879 (2012)
289. S. Galli, G. Tagliabue, N. Masciocchi, W.G. Wang, E. Barea, J.A.R. Navarro, Inorg. Chim. Acta **371**, 79 (2011)
290. E. Barea, G. Tagliabue, W.G. Wang, M.J. Pérez-Mendoza, L. Mendez-Lican, F. J. Lypez-Garzon, S. Galli, N. Masciocchi, J.A.R. Navarro, Chem.—Eur. J. **16**, 931 (2010)
291. S. Kitagawa, R. Matsuda, Coord. Chem. Rev. **251**, 2490 (2007)
292. Y. Kubota, M. Takata, R. Matsuda, R. Kitaura, S. Kitagawa, T.C. Kobayashi, Angew. Chem. Int. Ed. **45**, 4932 (2006)
293. T. Uemura, S. Horike, S. Kitagawa, Chem.—Asian J. **1**, 36 (2006)
294. T. Uemura, R. Kitaura, Y. Ohta, M. Nagaoka, S. Kitagawa, Angew. Chem. Int. Ed. **45**, 4112 (2006)
295. L. Wang, J. Morales, T. Wu, X. Zhao, W.P. Beyermann, X. Bu, P. Feng, Chem. Commun. **48**, 7498 (2012)
296. F. Wang, Z.-S. Liu, H. Yang, Y.-X. Tan, J. Zhang, Angew. Chem. Int. Ed. **50**, 450 (2011)
297. J.-R. Li, A.A. Yakovenko, W. Lu, D.J. Timmons, W. Zhuang, D. Yuan, H.-C. Zhou, J. Am. Chem. Soc. **132**, 17599 (2010)
298. J.-R. Li, H.-C. Zhou, Nat. Chem. **2**, 893 (2010)
299. D. Yuan, D. Zhao, D. Sun, H.-C. Zhou, Angew. Chem. Int. Ed. **49**, 5357 (2010)
300. A.J. Cairns, J.A. Perman, L. Wojtas, V.C. Kravstov, M.H. Alkordi, M. Eddaoudi, M. J. Zaworotko, J. Am. Chem. Soc. **130**, 1560 (2008)
301. D.F. Sava, V.C. Kravstov, J. Eckert, J.F. Eubank, F. Nouar, M. Eddaoudi, J. Am. Chem. Soc. **131**, 10394 (2009)
302. M.H. Alkordi, J.A. Brant, L. Wojtas, V.C. Kravtsov, A.J. Cairns, M. Eddaoudi, J. Am. Chem. Soc. **131**, 17753 (2009)
303. Y. Inokuma, T. Arai, M. Fujita, Nat. Chem. **2**, 780 (2010)
304. R. Chakrabarty, P.S. Mukherjee, P.J. Stang, Chem. Rev. **111**, 6810 (2011)
305. H. Furukawa, N. Ko, Y.B. Go, N. Aratani, S.B. Choi, E. Choi, A.O. Yazaydin, R.Q. Snurr, M. O'Keeffe, J. Kim, O.M. Yaghi, Science **329**, 424 (2010)
306. O.K. Farha, A.O. Yazaydin, I. Eryazici, C.D. Malliakas, B.G. Hauser, M.G. Kanatzidis, S.T. Nguyen, R.Q. Snurr, J.T. Hupp, Nat. Chem. **2**, 944 (2010)
307. Z. Ni, M. O'Keeffe, O.M. Yaghi, Angew. Chem. Int. Ed. **47**, 5136 (2008)
308. J.-R. Li, H.-C. Zhou, Angew. Chem. Int. Ed. **48**, 8465 (2009)
309. H. Furukawa, J. Kim, K.E. Plass, O.M. Yaghi, J. Am. Chem. Soc. **128**, 8398 (2006)
310. J.J. Perry, V.C. Kravtsov, G.J. McManus, M.J. Zaworotko, J. Am. Chem. Soc. **129**, 1076 (2007)
311. R. Luebke, J.F. Eubank, A.J. Cairns, Y. Belmabkhout, L. Wojtas, M. Eddaoudi, Chem. Commun. **48**, 1455 (2012)
312. R. Luebke, Ł.J. Weseliński, Y. Belmabkhout, Z. Chen, Ł. Wojtas, M. Eddaoudi, Cryst. Growth Des. **14**, 414 (2014)
313. U. Stoeck, S. Krause, V. Bon, I. Senkovska, S. Kaskel, Chem. Commun. **48**, 10841 (2012)

314. Y.L. Liu, V. Kravtsov, R.D. Walsh, P. Poddar, H. Srikanth, M. Eddaoudi, Chem. Commun. 2806 (2004)
315. J.F. Eubank, H. Mouttaki, A.J. Cairns, Y. Belmabkhout, L. Wojtas, R. Luebke, M. Alkordi, M. Eddaoudi, J. Am. Chem. Soc. **133**, 14204 (2011)
316. R. Liu, T. Yu, Z. Shi, Z. Wang, Int. J. Nanomedicine **11**, 1187 (2016)
317. W. Cai, C.C. Chu, G. Liu, Y.X. Wáng, Small **11**, 4806 (2015)
318. J.T. Hupp, Nat. Chem. **2**, 432 (2010)
319. M. Zhang, Z.-Y. Gu, M. Bosch, Z. Perry, H.-C. Zhou, Coord. Chem. Rev. **293–294**, 327 (2015)
320. J.F. Eubank, L. Wojtas, M.R. Hight, T. Bousquet, V.C. Kravtsov, M. Eddaoudi, J. Am. Chem. Soc. **133**, 17532 (2011)
321. X. Liu, M. Oh, M.S. Lah, Inorg. Chem. **50**, 5044 (2011)
322. X. Liu, M. Oh, M.S. Lah, Cryst. Growth Des. **11**, 5064 (2011)
323. Z. Chen, K. Adil, Ł.J. Weseliński, Y. Belmabkhout, M. Eddaoudi, J. Mater. Chem. A **3**, 6276 (2015)
324. J.L.C. Rowsell, O.M. Yaghi, Micropor. Mesopor. Mater. **73**, 3 (2004)
325. N. Stock, S. Biswas, Chem. Rev. **112**, 933 (2012)
326. Y.-R. Lee, J. Kim, W.-S. Ahn, Korean J. Chem. Eng. **30**, 1667 (2013)
327. Y. Sun, H.-C. Zhou, Sci. Technol. Adv. Mater. **16**, 054202 (2015)
328. C. Dey, T. Kundu, B.P. Biswal, A. Mallick, R. Banerjee, Acta Cryst. **B70**, 3 (2014)
329. K. Liu, H. You, Y. Zheng, G. Jia, Y. Huang, M. Yang, Y. Song, L. Zhang, H. Zhang, Cryst. Growth Des. **9**, 16 (2009)
330. K. Liu, H. You, G. Jia, Y. Zheng, Y. Huang, Y. Song, M. Yang, L. Zhang, H. Zhang, Cryst. Growth Des. **9**, 790 (2009)
331. W.L. Leong, S.K. Batabyal, S. Kasapis, J.J. Vittal, Chem.—Eur. J. **14**, 8822 (2008)
332. N. Shi, L. Xie, H. Sun, J. Duan, G. Yin, Z. Xu, W. Huang, Chem. Commun. **47**, 5055 (2011)
333. S.K. Batabyal, A.M.P. Peedikakkal, S. Ramakrishna, C.H. Sow, J.J. Vittal, Macromol. Rapid Commun. **30**, 1356 (2009)
334. S. Zhang, S. Yang, J. Lan, S. Yang, J. You, Chem. Commun. 6170 (2008)
335. X. Zhang, Z.-K. Chen, K.P. Loh, J. Am. Chem. Soc. **131**, 7210 (2009)
336. Y.-H. Luo, J. Huang, J. Jin, X. Peng, W. Schmitt, I. Ichinose, Chem. Mater. **18**, 1795 (2006)
337. J. Mao, Q. Shu, Y. Wen, H. Yuan, D. Xiao, M.M.F. Choi, Cryst. Growth Des. **9**, 2546 (2009)
338. Z.-W. Wang, C.-C. Ji, J. Li, Z.-J. Guo, Y.-Z. Li, H.-G. Zheng, Cryst. Growth Des. **9**, 475 (2009)
339. P. Mahata, S. Natarajan, Inorg. Chem. **46**, 1250 (2007)
340. D. Sun, H.-R. Xu, C.-F. Yang, Z.-H. Wei, N. Zhang, R.-B. Huang, L.-S. Zheng, Cryst. Growth Des. **10**, 4642 (2010)
341. P. Mahata, D. Sen, S. Natarajan, Chem. Commun. 1278 (2008)
342. M. Zuhayra, W.U. Kampen, E. Henze, Z. Soti, L. Zsolnai, G. Huttner, F.A. Oberdorfer, J. Am. Chem. Soc. **128**, 424 (2006)
343. F. Luo, Y.-X. Che, J.-M. Zheng, Cryst. Growth Des. **9**, 1066 (2009)
344. D.L. Reger, R.P. Watson, M.D. Smith, Inorg. Chem. **45**, 10077 (2006)
345. K.-L. Zhang, Y. Chang, C.-T. Hou, G.-W. Diao, R. Wu, S.W. Ng, CrystEngComm **12**, 1194 (2010)
346. R. Sarma, D. Kalita, J.B. Baruah, Dalton Trans. 7428 (2009)
347. G.-X. Liu, Y.-Q. Huang, Q. Chu, T.-A. Okamura, Q.-Y. Sun, H. Liang, N. Ueyama, Cryst. Growth Des. **8**, 3233 (2008)
348. S.-T. Wu, L.-S. Long, R.-B. Huang, L.-S. Zheng, Cryst. Growth Des. **7**, 1746 (2007)
349. B. Seoane, S. Castellanos, A. Dikhtiarenko, F. Kapteijn, J. Gascon, Coord. Chem. Rev. **307**, 147 (2016)
350. F. Yu, X.-J. Kong, Y.-Y. Zheng, Y.-P. Ren, L.-S. Long, R.-B. Huang, L.-S. Zheng, Dalton Trans. 9503 (2009)
351. B. Wang, A.P. Côté, H. Furukawa, M. O'Keeffe, O.M. Yaghi, Nature **453**, 207 (2008)

352. F. Luo, S.R. Batten, Y. Che, J.-M. Zheng, Chem.—Eur. J. **13**, 4948 (2007)
353. F. Costantino, A. Ienco, S. Midollini, Cryst. Growth Des. **10**, 7 (2010)
354. Y.Y. Liu, J.F. Ma, J. Yang, Z.M. Su, Inorg. Chem. **46**, 3027 (2007)
355. Y.Y. Liu, Z.H. Wang, J. Yang, B. Liu, Y.Y. Liu, J.F. Ma, CrystEngComm **13**, 3811 (2011)
356. J. Yang, J.F. Ma, Y.Y. Liu, J.C. Ma, S.R. Batten, Cryst. Growth Des. **8**, 4383 (2008)
357. W.H. Zhang, Y.Y. Wang, E.K. Lermontova, G.P. Yang, B. Liu, J.C. Jin, Z. Dong, Q.Z. Shi, Cryst. Growth Des. **10**, 76 (2010)
358. L.F. Ma, L.Y. Wang, J.L. Hu, Y.Y. Wang, G.P. Yang, Cryst. Growth Des. **9**, 5334 (2009)
359. W.Q. Kan, Y.Y. Liu, J. Yang, Y.Y. Liu, J.F. Ma, CrystEngComm **13**, 4256 (2011)
360. W.Q. Kan, J. Yang, Y.Y. Liu, J.F. Ma, Polyhedron **30**, 2113 (2011)
361. M.H. Hu, G.L. Shen, J.X. Zhang, Y.G. Yin, D. Li, Cryst. Growth Des. **9**, 4533 (2009)
362. L.L. Wen, F. Wang, J. Feng, K.L. Lv, C.G. Wang, D.F. Li, Cryst. Growth Des. **9**, 3581 (2009)
363. H.Y. Bai, J.F. Ma, J. Yang, L.P. Zhang, J.C. Ma, Y.Y. Liu, Cryst. Growth Des. **10**, 1946 (2010)
364. M. Mishra, K. Tiwari, A.K. Singh, V.P. Singh, Inorg. Chim. Acta **425**, 36 (2015)
365. G. Yuan, G. Hu, W. Shan, S. Jin, Q. Gu, J. Chen, Dalton Trans. **44**, 17774 (2015)
366. S.R. Halper, L. Do, J.R. Stork, S.M. Cohen, J. Am. Chem. Soc. **128**, 15255 (2006)
367. Y. Yoo, V. Varela-Guerrero, H. Jeong, Langmuir **27**, 2652 (2011)
368. F.Y. Wardana, S.-W. Ng, A.C. Wibowo, Cryst. Growth Des. **15**, 5930 (2015)
369. V. Isaeva, V. Chernyshev, E. Afonina, O. Tkachenko, K. Klementiev, V. Nissenbaum, W. Grünert, L. Kustov, Inorg. Chim. Acta **376**, 367 (2011)
370. X.-H. Han, M.-F. Li, D.-L. Wang, X. Song, B. Jiang, Y.-G. Sun, Inorg. Chem. Commun. **14**, 1323 (2011)
371. E.J. Gao, S.H. Liu, T.D. Sun, L. Lin, R.S. Wang, Y.X. Zhang, M. Su, M. Zhang, Russ. J. Coord. Chem. **37**, 439 (2011)
372. H.L. Jiang, D. Feng, K. Wang, Z.Y. Gu, Z. Wei, Y.P. Chen, H.C. Zhou, J. Am. Chem. Soc. **135**, 13934 (2013)
373. X.-Y. Wang, Z.-M. Wang, S. Gao, Chem. Commun. 281 (2008)
374. B. Machura, J. Palion, A. Świtlicka, J. Mroziński, B. Kalińska, R. Kruszyński, Polyhedron **49**, 216 (2013)
375. B. Tao, X. Jiang, X. Li, Y. Zhu, H. Xia, J. Mol. Struct. **111**, 1003 (2011)
376. Z. Abulizi, L. Wang, S. Touhuti, Y. Zhang, Y. Wang, Yingyong huaxue. Chin. J. Appl. Chem. **29**, 938 (2012)
377. M. Hu, H.-F. Li, J.-Y. Yao, Y. Gao, Z.-L. Liu, H.-Q. Su, Inorg. Chim. Acta **363**, 368 (2010)
378. L. Gou, Z.-X. Han, H.-M. Hu, Q.-R. Wu, X.-L. Yang, Z.-H. Yang, B.-C. Wang, F. Wang, M.-L. Yang, G.-L. Xue, Inorg. Chim. Acta **363**, 2590 (2010)
379. D. Feng, S. Liu, W. Zhang, P. Sun, F. Ma, C. Zhang, Z. Anorg, Allg. Chem. **636**, 1133 (2010)
380. S. Banerjee, P. Rajakannu, R.J. Butcher, R. Murugavel, CrystEngComm **16**, 8429 (2014)
381. B. Zheng, H. Dong, J. Bai, Y. Li, S. Li, M. Scheer, J. Am. Chem. Soc. **130**, 7778 (2008)
382. Y.-B. Dong, Y.-Y. Jiang, J. Li, J.-P. Ma, F.-L. Liu, B. Tang, R.-Q. Huang, S.R. Batten, J. Am. Chem. Soc. **129**, 4520 (2007)
383. R.-Q. Fang, X.-M. Zhang, Inorg. Chem. **45**, 4801 (2006)
384. G.-P. Yang, Y.-Y. Wang, P. Liu, A.-Y. Fu, Y.-N. Zhang, J.-C. Jin, Q.-Z. Shi, Cryst. Growth Des. **10**, 1443 (2010)
385. H. Wang, Y.-Y. Wang, G.-P. Yang, C.-J. Wang, G.-L. Wen, Q.-Z. Shi, S.R. Batten, CrystEngComm **10**, 1583 (2008)
386. S.K. Ghosh, S. Bureekaew, S. Kitagawa, Angew. Chem. Int. Ed. **47**, 3403 (2008)
387. R. Sun, S. Wang, H. Xing, J. Bai, Y. Li, Y. Pan, X. You, Inorg. Chem. **46**, 8451 (2007)
388. D.T. de Lill, C.L. Cahill, Chem. Commun. 4946 (2006)
389. X.S. Wang, S. Ma, P.M. Forster, D. Yuan, J. Eckert, J.J. Lopez, B.J. Murphy, J.B. Praise, H.-C. Zhou, Angew. Chem. Int. Ed. **47**, 7263 (2008)
390. D. Maspoch, D. Ruiz-Molina, J. Vaciana, Chem. Soc. Rev. **36**, 770 (2007)

391. E. Biemmi, S. Christian, N. Stock, T. Bein, Micropor. Mesopor. Mater. **117**, 111 (2009)
392. F. Millange, R.E. Osta, M.E. Medina, R.I. Walton, Cryst. Eng. Commun. **13**, 103 (2011)
393. P.M. Forster, N. Stock, A.K. Cheetham, Angew. Chem. Int. Ed. **44**, 7608 (2005)
394. S. Bauer, N. Stock, Angew. Chem. Int. Ed. **46**, 6857 (2007)
395. X.-L. Wang, F.-F. Sui, H.-Y. Lin, J.-W. Zhang, G.-C. Liu, Cryst. Growth Des. **14**, 3438 (2014)
396. X. Li, M. Fang, P. Cui, B. Zhao, Z. Anorg, Allg. Chem. **639**, 626 (2013)
397. D. Shi, C.S. Liu, X.S. Shi, J.R. Li, J.J. Wang, X.H. Bu, Cryst. Growth Des. **6**, 656 (2006)
398. Y. Ren, H. Jiang, B. Cai, J. Lu, Inorg. Chem. Commun. **24**, 114 (2012)
399. T. Uemura, S. Kitagawa, Top. Curr. Chem. **293**, 155 (2010)
400. S. Horike, S. Shimomura, S. Kitagawa, Nat. Chem. **1**, 695 (2010)
401. J. Zhang, L. Wojtas, R.W. Larsen, M. Eddaoudi, M.J. Zaworotko, J. Am. Chem. Soc. **131**, 17040 (2009)
402. N. Klein, I. Senkovska, K. Gedrich, U. Stoeck, A. Henschel, U. Mueller, S. Kaskel, Angew. Chem. Int. Ed. **48**, 9954 (2009)
403. X. Li, B.-L. Wu, R.-Y. Wang, H.-Y. Zhang, C.-Y. Niu, Y.-Y. Niu, H.-W. Hou, Inorg. Chem. **49**, 2600 (2010)
404. L.-Z. Chen, Y. Huang, R.-G. Xiong, H.-W. Hu, J. Mol. Struct. **963**, 16 (2010)
405. C.-G. Wang, Y.-H. Xing, Z.-P. Li, J. Li, X.-Q. Zeng, M.-F. Ge, S.-Y. Niu, Cryst. Growth Des. **9**, 1525 (2009)
406. C.-L. Chen, A.-M. Beatty, J. Am. Chem. Soc. **130**, 17222 (2008)
407. Y.-G. Sun, X.-M. Yan, F. Ding, E.-J. Gao, W.-Z. Zhang, F. Verpoort, Inorg. Chem. Commun. **11**, 1117 (2008)
408. X.J. Wang, M.X. Jiang, C.H. Zhang, Y.L. Feng, Y.H. He, J. Struct. Chem. **30**, 36 (2011)
409. C.H. Zhang, M.X. Jiang, Y.L. Feng, Y.H. He, Polyhedron **29**, 2250 (2010)
410. H.A. Habib, Inorg. Chim. Acta **362**, 2452 (2009)
411. H.A. Habib, A. Hoffmann, H.A. Höppe, C. Janiak, Dalton Trans. 1742 (2009)
412. H.A. Habib, J. Sanchiz, C. Janiak, Dalton Trans. 1734 (2008)
413. B. Wisser, Y. Lu, C. Janiak, Z. Anorg, Allg. Chem. **633**, 11289 (2007)
414. W.D. Buchanan, E.D. Nagle, K. Ruhlandt-Senge, Main Group Chem. **8**, 263 (2009)
415. G.B. Deacon, P.C. Junk, G.J. Moxey, M. Guino-O, K. Ruhlandt-Senge, Dalton Trans. 4878 (2009)
416. M.F. Zuniga, G.B. Deacon, K. Ruhlandt-Senge, Inorg. Chem. **47**, 4669 (2008)
417. M.A. Guino-O, C.F. Campana, K. Ruhlandt-Senge, Chem. Commun. 1692 (2008)
418. J. Langer, S. Krieck, H. Gorls, G. Kreisel, W. Seidel, M. Westerhausen, New J. Chem. **34**, 1667 (2010)
419. S. Krieck, H. Gorls, M. Westerhausen, J. Organomet. Chem. **694**, 2204 (2009)
420. S. Krieck, H. Gorls, L. Yu, M. Reiher, M. Westerhausen, J. Am. Chem. Soc. **131**, 2977 (2009)
421. F. Gschwind, A. Crochet, W. Maudez, K.M. Fromm, Chimia **64**, 299 (2010)
422. J. Spielmann, D.F.J. Piesik, S. Harder, Chem.—Eur. J. **16**, 8307 (2010)
423. W. Guo, C.-H. Jiang, Y.-M. Guo, Inorg. Chim. Acta **405**, 128 (2013)
424. W. Guo, A. Escuer, M. Tang, C.-H. Jiang, M. Du, Inorg. Chim. Acta **403**, 142 (2013)
425. X. Wang, Y.-M. Guo, Inorg. Chem. Comm. **60**, 115 (2015)
426. X. Wang, W. Guo, Y.-M. Guo, J. Mol. Struct. **1096**, 136 (2015)
427. N.J. Hurley, J.M. Rawson, M. Pilkington, Dalton Trans. **44**, 1866 (2015)
428. H.J. Lee, W. Cho, M. Oh, CrystEngComm **12**, 3959 (2010)
429. Y. Song, M.-L. Feng, Z.-F. Wu, X.-Y. Huang, CrystEngComm **17**, 1348 (2015)
430. M. Sánchez-Sánchez, N. Getachew, K. Díaz, M. Díaz-García, Y. Chebude, I. Díaz, Green Chem. **17**, 1500 (2015)
431. D. Cai, H. Guo, L. Wen, C. Liu, CrystEngComm **15**, 6702 (2013)
432. H.-Q. Xu, K. Wang, M. Ding, D. Feng, H.-L. Jiang, H.-C. Zhou, J. Am. Chem. Soc. **138**, 5316 (2016)
433. Z. Xin, J. Bai, Y. Shen, Y. Pan, Cryst. Growth Des. **10**, 2451 (2010)

434. M. Oh, C.A. Mirkin, Nature **438**, 651 (2005)
435. Y.-M. Jeon, G.S. Armatas, D. Kim, M.G. Kanatzidis, C.A. Mirkin, Small **5**, 46 (2009)
436. D. Sun, D.-F. Wang, X.-G. Han, N. Zhang, R.-B. Huang, L.-S. Zheng, Chem. Commun. **47**, 746 (2011)
437. P. Banerjee, S. Kar, A. Bhaumik, G.H. Lee, S.M. Peng, S. Goswami, Eur. J. Inorg. Chem. **2007**, 835 (2007)
438. I. Imaz, M. Rubio-Martínez, W.J. Saletra, D.B. Amabilino, D. Maspoch, J. Am. Chem. Soc. **131**, 18222 (2009)
439. B. Liu, D.J. Qian, M. Chen, T. Wakayama, C. Nakamura, J. Miyake, Chem. Commun. **30**, 3175 (2006)
440. B. Tao, X. Jiang, H. Xia, H. Cheng, J. Mol. Struct. **1011**, 15 (2012)
441. D. Chandra, M.W. Kasture, A. Bhaumik, Micropor. Mesopor. Mater. **116**, 204 (2008)
442. F.A.A. Paz, J. Klinowski, S.M.F. Vilela, J.P.C. Tome, J.A.S. Cavaleiro, J. Rocha, Chem. Soc. Rev. **41**, 1088 (2012)
443. S.T. Zheng, T. Wu, C.T. Chou, A. Fuhr, P.Y. Feng, X.H. Bu, J. Am. Chem. Soc. **134**, 4517 (2012)
444. C.-P. Li, M. Du, Chem. Commun. **47**, 5958 (2011)
445. S.T. Zheng, J.J. Bu, T. Wu, C.T. Chou, P.Y. Feng, X.H. Bu, Angew. Chem. Int. Ed. **50**, 8858 (2011)
446. Y. Liu, M.J.W. Tan, F. Wei, Y. Tian, T. Wu, C. Kloc, F. Huo, Q. Yan, H.H. Hng, J. Ma, Q. Zhang, CrystEngComm **14**, 75 (2012)
447. Y. Liu, L.-M. Yu, S.C.J. Loo, R.G. Blair, Q. Zhang, J. Solid State Chem. **191**, 283 (2012)
448. Q. Zhang, X. Bu, Z. Lin, T. Wu, P. Feng, Inorg. Chem. **47**, 9724 (2008)
449. Z.B. Han, Y.K. He, M.L. Tong, Y.J. Song, X.M. Song, L.G. Yang, CrystEngComm **10**, 1070 (2008)
450. C. Tan, S. Yang, N.R. Champness, X. Lin, A.J. Blake, W. Lewis, M. Schröder, Chem. Commun. **47**, 4487 (2011)
451. Z.B. Han, J.W. Ji, H.Y. An, W. Zhang, G.-X. Han, G.-X. Zhang, L.-G. Yang, Dalton Trans. 9807 (2009)
452. R. Banerjee, A. Phan, B. Wang, C. Knobler, H. Furukawa, M. O'Keeffe, O.M. Yaghi, Science **319**, 939 (2008)
453. N. Stock, Micropor. Mesopor. Mater. **129**, 287 (2010)
454. L. Yan, C.-B. Li, D.-S. Zhu, L. Xu, J. Inorg. Organomet. Polym. **22**, 395 (2011)
455. D.-C. Zhong, H.-B. Guo, J.-H. Deng, Q. Chen, X.-Z. Luo, CrystEngComm **17**, 3519 (2015)
456. Z. Wei, X. Mu, Y. Chen, Synth. React. Inorg., Metal-Org., Nano-Metal Chem. **46**, 147 (2016)
457. Y. Xu, Y.-X. Che, J.-M. Zheng, Z. Anorg, Allg. Chem. **638**, 698 (2012)
458. Z. Chen, S. Xiang, H.D. Arman, P. Li, D. Zhao, B. Chen, Eur. J. Inorg. Chem. 2227 (2011)
459. J. Zhao, P. Su, Y. Zhao, M. Li, Y. Yang, Q. Yang, C. Li, J. Mater. Chem. **22**, 8470 (2012)
460. A.J. Calahorro, D. Fairen-Jiménez, A. Salinas-Castillo, M.E. López-Viseras, A. Rodríguez-Diéguez, Polyhedron **52**, 315 (2013)
461. Z. Shen, S. He, P. Yao, X. Lao, B. Yang, Y. Dai, X. Sun, T. Chen, RSC Adv. **4**, 12844 (2014)
462. Z.-F. Shi, J. Jin, L. Li, Y.-H. Xing, S.-Y. Niu, Wuli Huaxue Xuebao **25**, 2011 (2009)
463. L. Fan, H. Chen, D. Xiao, E.Z. Wang, Z. Anorg, Allg. Chem. **639**, 558 (2013)
464. B.-Y. Zhu, X.-L. Zhang, F. Guo, X.-H. Liu, Inorg. Chim. Acta **391**, 58 (2012)
465. Z.-F. Li, X.-B. Luo, Y.-C. Gao, H.-J. Lu, G. Li, Inorg. Chim. Acta **384**, 352 (2012)
466. Y. Lou, J. Wang, Y. Tao, J. Chen, A. Mishima, M. Ohba, Dalton Trans. **43**, 8508 (2014)
467. A.-T. Pu, J. Yang, W.-Q. Kan, Y. Yang, J.-F. Ma, Polyhedron **50**, 556 (2013)
468. X. Zhang, L. Fan, Z. Sun, W. Zhang, D. Li, P. Wei, B. Li, J. Dou, J. Coord. Chem. **65**, 3205 (2012)
469. Z.X. Du, L.Y. Wang, H.W. Hou, Z. Anorg, Allg. Chem. **635**, 1659 (2009)
470. X.-H. Chang, L.-F. Ma, G. Hui, L.-Y. Wang, Cryst. Growth Des. **12**, 3638 (2012)
471. M. Kariem, M. Yawer, H.N. Sheikh, J. Solid State Chem. **231**, 239 (2015)

472. H.-W. Kuai, X.-C. Cheng, X.-H. Zhu, Polyhedron **50**, 390 (2013)
473. H.-W. Kuai, C. Hou, W.-Y. Sun, Polyhedron **52**, 1268 (2013)
474. L. Yang, L. Liu, C. Lian, M. Liu, Z. Xu, L.-C. Wang, X. Guo, Y. Long, Dyes Pigm. **122**, 246 (2015)
475. R.F. D'Vries, M. Iglesias, N. Snejko, E. Gutiérrez-Puebla, M. Angeles, Monge. Inorg. Chem. **51**, 11349 (2012)
476. X. Wang, Z. Guo, G. Liu, S. Yang, Y. Qu, H. Lin, J. Zhang, J. Coord. Chem. **65**, 2634 (2012)
477. Y.E. Du, L. Aib, Z.B. Han, Russ. J. Coord. Chem. **37**, 176 (2011)
478. L. Wu, Y. Sun, X. Liu, D. Gao, Y. Xu, G. Zhang, Chem. Res. Chin. Univ. **28**, 775 (2012)
479. X. Shi, G. Zhu, X. Wang, G. Li, Q. Fang, G. Wu, G. Tian, M. Xue, X. Zhao, R. Wang, S. Qiu, Cryst. Growth Des. **5**, 207 (2005)
480. P.K. Yadav, N. Kumari, P. Pachfule, R. Banerjee, L. Mishra, Cryst. Growth Des. **12**, 5311 (2012)
481. T.-T. Cao, Y. Ma, C. Yang, D.-Z. Liao, S.-P. Yan, Z. Anorg, Allg. Chem. **636**, 2704 (2010)
482. Z. Zhang, J. Li, R. Liu, W. Zhou, F. Zhang, J. Coord. Chem. **66**, 926 (2013)
483. C. Wang, Z. Wang, F. Gu, G. Guo, J. Mol. Struct. **979**, 92 (2010)
484. Y.-Z. Tang, H.-R. Wen, Z. Cao, X.-W. Wang, S. Huang, C.-L. Yu, Inorg. Chem. Commun. **13**, 924 (2010)
485. A. Cheng, H. Shi, A. Zhao, A. Geng, A. Chen, T. Ma, H. Niu, Russ. J. Coord. Chem. **37**, 302 (2011)
486. M. Fang, P.-F. Shi, B. Zhao, D.-X. Jiang, P. Cheng, W. Shi, Dalton Trans. **41**, 6820 (2012)
487. A.L. Ramirez, K.E. Knope, T.T. Kelley, N.E. Greig, J.D. Einkauf, D.T. de Lill, Inorg. Chim. Acta **392**, 46 (2012)
488. Y.-Y. Liu, B. Liu, J. Yang, J.-F. Ma, Polyhedron **56**, 96 (2013)
489. R. Decadt, K. Van Hecke, D. Depla, K. Leus, D. Weinberger, I. Van Driessche, P. Van Der Voort, R. Van Deun, Inorg. Chem. **51**, 11623 (2012)
490. K. Wang, Z. Geng, M. Zheng, L. Ma, X. Ma, Z. Wang, Cryst. Growth Des. **12**, 5606 (2012)
491. F.-J. Meng, H.-Q. Jia, N.-H. Hu, J.-W. Xu, Inorg. Chem. Commun. **21**, 186 (2012)
492. S.M. Humphrey, G.F. Weldon, P.T. Wood, J. Nanosci. Nanotechnol. **10**, 34 (2010)
493. L. Yang, S. Song, H. Zhang, W. Zhang, L. Wu, Z. Bu, T. Ren, Synth. Metals **162**, 261 (2012)
494. S. Song, C. Shao, H. Zhang, W. Zhang, L. Yang, T. Ren, Z. Bu, Synth. React. Inorg., Metal-Org., Nano-Metal Chem. **43**, 169 (2013)
495. B. Meng, W. You, X. Sun, F. Zhang, M. Liu, Inorg. Chem. Commun. **14**, 35 (2011)
496. W. Zhang, T. Lv, D. Wei, R. Xu, G. Xiong, Y. Wang, E. Gao, Y. Sun, Inorg. Chem. Commun. **14**, 1245 (2011)
497. J.-P. Zou, S.-L. Luo, M.-J. Li, X.-H. Tang, Q.-J. Xing, Q. Peng, G.-C. Guo, Polyhedron **29**, 2674 (2010)
498. J.-P. Zou, M.-H. Chen, S.-L. Luo, X.-H. Tang, Z.-Q. Xiong, Q. Peng, Inorg. Chim. Acta **373**, 243 (2011)
499. X.-Q. Zhao, Y.-C. Li, J. Coord. Chem. **66**, 937 (2013)
500. R.K. Vakiti, B.D. Garabato, N.P. Schieber, M.J. Rucks, Y. Cao, C. Webb, J.B. Maddox, A. Celestian, W.-P. Pan, B. Yan, Cryst. Growth Des. **12**, 3937 (2012)
501. K. Yang, J.-H. Luo, Z.-H. Liu, Inorg. Chim. Acta **391**, 206 (2012)
502. C. Cruz, E. Spodine, A. Vega, D. Venegas-Yazigi, V. Paredes-García, Cryst. Growth Des. **16**, 2173 (2016)
503. Z.G. Gu, H.C. Fang, P.Y. Yin, L. Tong, Y. Ying, S.J. Hu, W.S. Li, Y.P. Cai, Cryst. Growth Des. **11**, 2220 (2011)
504. J.C. Yao, J.B. Guo, J.G. Wang, Y.F. Wang, L. Zhang, C.P. Fan, Inorg. Chem. Commun. **13**, 1178 (2010)
505. X. Cao, Y. Liu, L. Wang, G. Li, Inorg. Chim. Acta **392**, 16 (2012)
506. B. Roy, S. Mukherjee, P.S. Mukherjee, CrystEngComm **15**, 9596 (2013)

507. L. Yang, L. Zeng, W. Gu, J. Tian, S. Liao, M. Zhang, X. Wei, L. Xin, X. Liu, Inorg. Chem. Commun. **29**, 76 (2013)
508. K. Cheng, X.L. Zhang, Russ. J. Coord. Chem. **39**, 458 (2013)
509. X.-L. Wang, Q. Gao, Y.-Q. Chen, G.-C. Liu, A.-X. Tian, Z.-H. Kang, Z. Anorg, Allg. Chem. **637**, 142 (2011)
510. X.N. Cheng, W. Xue, J.B. Lin, X.M. Chen, Chem. Commun. **46**, 246 (2010)
511. E. Anger, M. Rudolph, C. Shen, N. Vanthuyne, L. Toupet, C. Roussel, J. Autschbach, J. Crassous, R. Réau, J. Am. Chem. Soc. **133**, 3800 (2011)
512. G. Li, X. Xi, W. Xuan, T. Dong, Y. Cui, CrystEngComm **12**, 2424 (2010)
513. K. Suh, M.P. Yutkin, D.N. Dybtsev, V.P. Fedin, K. Kim, Chem. Commun. **48**, 513 (2012)
514. T. Kawamoto, N. Suzuki, T. Ono, D. Gong, T. Konno, Chem. Commun. **49**, 668 (2013)
515. X. Wu, S. Ji, Y. Li, B. Li, X. Zhu, K. Hanabusa, Y. Yang, J. Am. Chem. Soc. **131**, 5986 (2009)
516. V. Amendola, M. Boiocchi, V. Brega, L. Fabbrizzi, L. Mosca, Inorg. Chem. **49**, 997 (2010)
517. A.J. McConnell, C.S. Wood, P.P. Neelakandan, J.R. Nitschke, Chem. Rev. **115**, 7729 (2015)
518. Z.L. Luo, S.G. Zhang, Chem. Soc. Rev. **41**, 4736 (2012)
519. F. Vidal, R.R. Gowda, E.Y.X. Chen, J. Am. Chem. Soc. **137**, 9469 (2015)
520. S.C. Xu, Y. Magoon, R.R. Reinig, B.M. Schmidt, A. Ellern, A.D. Sadow, Organometallics **34**, 3508 (2015)
521. X.-L. Tong, T.-L. Hu, J.-P. Zhao, Y.-K. Wang, H. Zhang, X.-H. Bu, Chem. Commun. **46**, 8543 (2010)
522. H. Tan, Y. Li, W. Chen, A. Yan, D. Liu, E. Wang, Cryst. Growth Des. **12**, 1111 (2012)
523. T.-H. Zhou, J. Zhang, H.-X. Zhang, R. Feng, J.-G. Mao, Chem. Commun. **47**, 8862 (2011)
524. L.L. Yan, C.H. Tan, G.L. Zhang, L.P. Zhou, J.C. Bunzli, Q.F. Sun, J. Am. Chem. Soc. **137**, 8550 (2015)
525. B.M. Trost, M. Rao, Angew. Chem. Int. Ed. **54**, 5026 (2015)
526. W.R. Xu, G.J. Xia, H.F. Chow, X.P. Cao, D. Kuck, Chem.—Eur. J. **21**, 12011 (2015)
527. J.P. Byrne, J.A. Kitchen, J.E. O'Brien, R.D. Peacock, T. Gunnlaugsson, Inorg. Chem. **54**, 1426 (2015)
528. T. Kaczorowski, I. Justyniak, T. Lipiñska, J. Lipkowski, J. Lewiñski, J. Am. Chem. Soc. **131**, 5393 (2009)
529. J. Lewiñski, T. Kaczorowski, I. Justyniak, D. Prochowicz, Chem. Commun. **47**, 950 (2011)
530. J. He, G. Zhang, D. Xiao, H. Chen, S. Yan, X. Wang, J. Yanga, E. Wang, CrystEngComm **14**, 3609 (2012)
531. S.-Q. Bai, S. Leelasubcharoen, X. Chen, L.L. Koh, J.-L. Zuo, T.S. Andy Hor, Cryst. Growth Des. **10**, 1715 (2010)
532. X.-H. Zhou, X.-D. Du, G.-N. Li, J.-L. Zuo, X.-Z. You, Cryst. Growth Des. **9**, 4487 (2009)
533. T.J. Burchell, R.J. Puddephatt, Inorg. Chem. **45**, 650 (2006)
534. J.-L. Liu, X. Bao, J.-D. Leng, Z.-J. Lin, M.-L. Tong, Cryst. Growth Des. **11**, 2398 (2011)
535. W. Zhang, Z.-Q. Wang, O. Sato, R.-G. Xiong, Cryst. Growth Des. **9**, 2050 (2009)
536. Y. Gong, T. Wu, J. Lin, B. Wang, CrystEngComm **14**, 5649 (2012)
537. S.-L. Cai, S.-R. Zheng, Z.-Z. Wen, J. Fan, W.-G. Zhang, Cryst. Growth Des. **12**, 2355 (2012)
538. Y. Wei, K. Wu, J. He, W. Zheng, X. Xiao, CrystEngComm **13**, 52 (2011)
539. J. Crassous, Chem. Soc. Rev. **38**, 830 (2009)
540. R.-Q. Zou, R.-Q. Zhong, M. Du, D.S. Pandey, Q. Xu, Cryst. Growth Des. **8**, 452 (2008)
541. A.R. Stefankiewicz, A.D. Cian, J. Harrowfield, CrystEngComm **13**, 7207 (2011)
542. C. He, Y. Zhao, D. Guo, Z. Lin, C. Duan, Eur. J. Inorg. Chem. 3451 (2007)
543. Z. Chen, S. Qin, D. Liu, Y. Shen, F. Liang, Cryst. Growth Des. **13**, 3389 (2013)
544. B. Joarder, A.K. Chaudhari, S.K. Ghosh, Inorg. Chem. **51**, 4644 (2012)
545. L. Song, C. Jiang, C. Ling, Y.-R. Yao, Q.-H. Wang, D. Chen, J. Inorg. Organomet. Polym. **26**, 320 (2016)
546. W. Chen, S.-Q. Su, S.-Q. Song, X.-Z. Song, H.-J. Zhang, Gaodeng xuexiao huaxun xuebao, Chem. J. Chin. Univ. **33**, 215 (2012)

547. Z. Xu, H. Li, A. Li, W. Menga, H. Hou, Y. Fan, Inorg. Chem. Commun. **36**, 126 (2013)
548. A.A. Sinelshchikova, S.E. Nefedov, Y.Y. Enakieva, Y.G. Gorbunova, A.Y. Tsivadze, K.M. Kadish, P. Chen, A. Bessmertnykh-Lemeune, C. Stern, R. Guilard, Inorg. Chem. **52**, 999 (2013)
549. O.K. Farha, A.M. Shultz, A.A. Sarjeant, S.T. Nguyen, J.T. Hupp, J. Am. Chem. Soc. **133**, 5652 (2011)
550. J.A. Johnson, Q. Lin, L.-C. Wu, N. Obaidi, Z.L. Olson, T.C. Reeson, Y.-S. Chen, J. Zhang, Chem. Commun. **49**, 2828 (2013)
551. N.C. Smythe, D.P. Butler, C.E. Moore, W.R. McGowan, A.L. Rheingold, L.G. Beauvais, Dalton Trans. **41**, 7855 (2012)
552. J. Park, D. Feng, S. Yuan, H.-C. Zhou, Angew. Chem. Int. Ed. **54**, 430 (2015)
553. Z. Guo, B. Chen, Dalton Trans. **44**, 14574 (2015)
554. M.H. Alkordi, Y. Liu, R.W. Larsen, J.F. Eubank, M. Eddaoudi, J. Am. Chem. Soc. **130**, 12639 (2008)
555. A. Fateeva, J. Clarisse, G. Pilet, J.-M. Grenèche, F. Nouar, B.K. Abeykoon, F. Guegan, C. Goutaudier, D. Luneau, J.E. Warren, M.J. Rosseinsky, T. Devic, Cryst. Growth Des. **15**, 1819 (2015)
556. W.-Y. Gao, Z. Zhang, L. Cash, L. Wojtas, Y.-S. Chen, S. Ma, CrystEngComm **15**, 9320 (2013)
557. S. Lipstman, I. Goldberg, J. Mol. Struct. **890**, 101 (2008)
558. W. Chen, S. Fukuzumi, Eur. J. Inorg. Chem. 5494 (2009)
559. W. Zhang, P. Jiang, Y. Wang, J. Zhang, P. Zhang, Inorg. Chem. Commun. **61**, 100 (2015)
560. N. Zheng, J. Zhang, X. Bu, P. Feng, Cryst. Growth Des. **7**, 2576 (2007)
561. Q. Zha, C. Ding, X. Rui, Y. Xie, Cryst. Growth Des. **13**, 4583 (2013)
562. X. Rui, Q.-Z. Zha, T.-T. Wei, Y.-S. Xie, Inorg. Chem. Commun. **48**, 111 (2014)
563. C.-W. Kung, T.-H. Chang, L.-Y. Chou, J.T. Hupp, O.K. Farha, K.-C. Ho, Electrochem. Commun. **58**, 51 (2015)
564. D. Feng, K. Wang, Z. Wei, Y.-P. Chen, C.M. Simon, R.K. Arvapally, R.L. Martin, M. Bosch, T.-F. Liu, S. Fordham, D. Yuan, M.A. Omary, M. Haranczyk, B. Smit, H.-C. Zhou, Nat. Commun. **5**, 5723 (2014)
565. J.L.C. Rowsell, O.M. Yaghi, J. Am. Chem. Soc. **128**, 1304 (2006)
566. T.M. McDonald, W.R. Lee, J.A. Mason, B.M. Wiers, C.S. Hong, J.R. Long, J. Am. Chem. Soc. **134**, 7056 (2012)
567. D.A. Yang, H.Y. Cho, J. Kim, S.T. Yang, W.S. Ahn, Energy Environ. Sci. **5**, 6465 (2012)
568. H.Y. Cho, D.A. Yang, J. Kim, S.Y. Jeong, W.S. Ahn, Catal. Today **185**, 35 (2012)
569. D. Britt, H. Furukawa, B. Wang, T.G. Glover, O.M. Yaghi, PNAS **106**, 20637 (2009)
570. S.R. Caskey, A.G. Wong-Foy, A.J. Matzger, J. Am. Chem. Soc. **130**, 10870 (2008)
571. L.J. Wang, H. Deng, H. Furukawa, F. Gándara, K.E. Cordova, D. Peri, O.M. Yaghi, Inorg. Chem. **53**, 5881 (2014)
572. B.I. Kharisov, O.V. Kharissova, U.O. Méndez, Microwave hydrothermal and solvothermal processing of materials and compounds, in *The Development and Application of Microwave Heating*, ed. by W. Cao (InTech, Rijeka, Croatia, 2012)
573. J. Lhoste, X. Rocquefelte, K. Adil, R. Dessapt, S. Jobic, M. Leblanc, V. Maisonneuve, M. Bujoli-Doeuff, Inorg. Chem. **20**, 5671 (2011)
574. J. Zhang, J.T. Bu, S. Chen, T. Wu, S. Zheng, Y. Chen, R.A. Nieto, P. Feng, X. Bu, Angew. Chem. Int. Ed. **49**, 8876 (2010)
575. E. Yang, H.-Y. Li, Z.-S. Liu, Q.-D. Ling, Inorg. Chem. Comm. **30**, 152 (2013)
576. H. Liu, X. Meng, L. Zhang. A. Jia, Austral. J. Chem. **68**, 1299 (2015)
577. Z.-S. Liu, E. Yang, Y. Kang, J. Zhang, Inorg. Chem. Comm. **14**, 355 (2011)
578. Z.-Q. Jiang, G.-Y. Jiang, D.-C. Hou, F. Wang, Z. Zhao, J. Zhang, CrystEngComm **15**, 315 (2013)
579. M. Zhu, W. Fu, G. Zou, J. Coord. Chem. **65**, 4108 (2012)
580. S.-Y. Chen, E. Yang, Z.-S. Liu, X.-L. Ye, Chin. J. Struct. Chem. **31**, 535 (2012)

581. X. Li, Q. Liu, Y. Dong, Synth. React. Inorg., Metal-Org., Nano-Metal Chem. **46**, 1202 (2016)
582. H. Yang, T. Li, Y. Kang, F. Wang, Inorg. Chem. Commun. **14**, 1695 (2011)
583. Z. Lin, D.S. Wragg, R.E. Morris, Chem. Commun. 2021 (2006)
584. R.E. Morris, Chem. Commun. 2990 (2009)
585. P.C. Jhang, Y.C. Yang, Y.C. Lai, W.R. Liu, S.L. Wang, Angew. Chem. Int. Ed. **48**, 742 (2009)
586. E.R. Parnham, R.E. Morris, Acc. Chem. Res. **40**, 1005 (2007)
587. F. Himeur, I. Stein, D.S. Wragg, A.M.Z. Slawin, P. Lightfoot, R.E. Morris, Solid State Sci. **12**, 418 (2010)
588. Z. Lin, A.M.Z. Slawin, R.E. Morris, J. Am. Chem. Soc. **129**, 4880 (2007)
589. J. Zhang, S. Chen, X. Bu, Angew. Chem. Int. Ed. **47**, 5434 (2008)
590. H. Fu, C. Qin, Y. Lu, Z.-M. Zhang, Y.-G. Li, Z.-M. Su, W.-L. Li, E.-B. Wang, Angew. Chem. Int. Ed. **51**, 7985 (2012)
591. E. Ahmed, M. Ruck, Angew. Chem. Int. Ed. **51**, 308 (2012)
592. Y. Zhao, J. Zhang, B. Han, J. Song, J. Li, Q. Wang, Angew. Chem. Int. Ed. **50**, 636 (2011)
593. Z.J. Lin, D.S. Wragg, J.E. Warren, R.E. Morris, J. Am. Chem. Soc. **129**, 10334 (2007)
594. Q. Zhang, I. Chung, J.I. Jang, J.B. Ketterson, M.G. Kanatzidis, J. Am. Chem. Soc. **131**, 9896 (2009)
595. K. Biswas, Q. Zhang, I. Chung, J.-H. Song, J. Androulakis, A. Freeman, M. Kanatzidis, J. Am. Chem. Soc. **132**, 14760 (2010)
596. J.R. Li, Z.L. Xie, X.W. He, L.H. Li, X.Y. Huang, Angew. Chem. Int. Ed. **50**, 11395 (2011)
597. W.X. Chen, H.R. Xu, G.L. Zhuang, L.S. Long, R.B. Huang, L.S. Zheng, Chem. Commun. **47**, 11933 (2011)
598. S.H. Kim, S.T. Yang, J. Kim, W.S. Ahn, Bull. Korean Chem. Soc. **32**, 2783 (2011)
599. J. Zhang, T. Wu, S. Chen, P. Feng, X. Bu, Angew. Chem. Int. Ed. **48**, 3486 (2009)
600. P. Kuhn, M. Antonietti, A. Thomas, Angew. Chem. Int. Ed. **47**, 3450 (2008)
601. J.-L. Xie, Z.-G. Han, W.-B. Pei, Y. Zou, X.-M. Ren, Inorg. Chem. Commun. **14**, 1266 (2011)
602. L. Xu, E.Y. Choi, Y.U. Kwon, Inorg. Chem. **46**, 10670 (2007)
603. S.M. Chen, J. Zhang, X.H. Bu, Inorg. Chem. **47**, 5567 (2008)
604. W.-J. Ji, Q.-G. Zhai, S.-N. Li, Y.-C. Jiang, M.-C. Hu, Inorg. Chem. Commun. **28**, 16 (2013)
605. P.M. Schoenecker, G.A. Belancik, B.E. Grabicka, K.S. Walton, AIChE J. **59**, 1255 (2013)
606. J. Puigmarti-Luis, M. Rubio-Martinez, U. Hartfelder, I. Imaz, D. Maspoch, P.S. Dittrich, J. Am. Chem. Soc. **133**, 4216 (2011)
607. A. López-Periago, O. Vallcorba, C. Frontera, C. Domingo, J.A. Ayllón, Dalton Trans. **44**, 7548 (2015)
608. J. Gao, M. He, Z.Y. Lee, W. Cao, W.-W. Xiong, Y. Li, R. Ganguly, T. Wuc, Q. Zhang, Dalton Trans. **42**, 11367 (2013)
609. S.K. Nune, P.K. Thallapally, B.P. McGrail, H.V.R. Annapureddy, L.X. Dang, D. Mei, N. Karri, K.J. Alvine, M.J. Olszta, B.W. Arey, A. Dohnalkova, A.C.S. Appl, Mater. Interfaces **7**, 21712 (2015)
610. A.J.J. Koekkoek, V. Degirmenci, E.J.M. Hensen, J. Mater. Chem. **21**, 9279 (2011)
611. A. Carné-Sánchez, I. Imaz, M. Cano-Sarabia, D. Maspoch, Nat. Chem. **5**, 203 (2013)
612. H. Furukawa, U. Müller, O.M. Yaghi, Angew. Chem. Int. Ed. **54**, 3417 (2015)
613. Y. Sun, B. Yoo, New J. Chem. **39**, 4218 (2015)
614. G. Lu, S.Z. Li, Z. Guo, O.K. Farha, B.G. Hauser, X.Y. Qi, Y. Wang, X. Wang, S.Y. Han, X.G. Liu, J.S. DuChene, H. Zhang, Q.C. Zhang, X.D. Chen, J. Ma, S.C.J. Loo, W.D. Wei, Y.H. Yang, J.T. Hupp, F.W. Huo, Nat. Chem. **4**, 310 (2012)
615. W.-W. Xiong, E.U. Athresh, Y.T. Ng, J. Ding, T. Wu, Q. Zhang, J. Am. Chem. Soc. **135**, 1256 (2013)
616. Y.-Y. Yin, J.-G. Ma, Z. Niu, X.-C. Cao, W. Shi, P. Cheng, Inorg. Chem. **51**, 4784 (2012)
617. J. Hafizovic, M. Bjørgen, U. Olsbye, P.D.C. Dietzel, S. Bordiga, C. Prestipino, C. Lamberti, K.P. Lillerud, J. Am. Chem. Soc. **129**, 3612 (2007)

618. S.S. Kaye, A. Dailly, O.M. Yaghi, J.R. Long, J. Am. Chem. Soc. **129**, 14176 (2007)
619. J. Kim, S.H. Kim, S.T. Yang, W.S. Ahn, Micropor. Mesopor. Mater. **161**, 48 (2012)
620. H.Y. Cho, J. Kim, S.N. Kim, W.S. Ahn, Micropor. Mesopor. Mater. **169**, 180 (2013)
621. T. Uemura, Y. Hoshino, S. Kitagawa, K. Yoshida, S. Isoda, Chem. Mater. **18**, 992 (2006)
622. X.-M. Zhang, Coord. Chem. Rev. **249**, 1201 (2005)
623. X.M. Chen, M.L. Tong, Acc. Chem. Res. **40**, 162 (2007)
624. H. Zhao, Z.R. Qu, H.Y. Ye, R.G. Xiong, Chem. Soc. Rev. **37**, 84 (2008)
625. W. Kaneko, M. Ohba, S. Kitagawa, J. Am. Chem. Soc. **129**, 13706 (2007)
626. F. Luo, Y.X. Che, J.M. Zheng, J. Mol. Struct. **827**, 206 (2007)
627. X.D. Zhu, J. Lu, X.J. Li, S.Y. Gao, G.L. Li, F.X. Xiao, R. Cao, Cryst. Growth Des. **8**, 1897 (2008)
628. L. Hou, Y.Y. Lin, X.M. Chen, Inorg. Chem. **47**, 1346 (2008)
629. L. Pan, D.H. Olson, L.R. Ciemnolonski, R. Heddy, J. Li, Angew. Chem. Int. Ed. **45**, 616 (2006)
630. D. Deng, L. Liu, B.-M. Ji, G. Yin, C. Du, Cryst. Growth Des. **12**, 5338 (2012)
631. Z.-Z. Wen, X.-L. Wen, S.-L. Cai, S.-R. Zheng, J. Fan, W.-G. Zhang, CrystEngComm **15**, 5359 (2013)
632. J. Song, B.-C. Wang, H.-M. Hu, L. Gou, Q.-R. Wu, X.-L. Yang, Y.-Q. Shangguan, F.-X. Dong, G.-L. Xue, Inorg. Chim. Acta **366**, 134 (2011)
633. W.J. Son, J. Kim, J. Kim, W.S. Ahn, Chem. Commun. 6336 (2008)
634. Z. Ni, R.I. Masel, J. Am. Chem. Soc. **128**, 12394 (2006)
635. A. Pichon, S.L. James, CrystEngComm **10**, 1839 (2008)
636. A. Pichon, A. Lazuen-Garay, S.L. James, CrystEngComm **8**, 211 (2006)
637. D. Braga, S.L. Giaffreda, K. Rubini, F. Grepioni, M.R. Chierotti, R. Gobetto, CrystEngComm **9**, 39 (2007)
638. D. Braga, S.L. Giaffreda, F. Grepioni, A. Pettersen, L. Maini, M. Curzi, M. Polito, Dalton Trans. 1249 (2006)
639. D. Braga, M. Curzi, A. Johansson, M. Polito, K. Rubini, F. Grepioni, Angew. Chem. Int. Ed. **45**, 142 (2006)
640. K. Fujii, A.L. Garay, J. Hill, E. Sbircea, Z.G. Pan, M.C. Xu, D.C. Apperley, S.L. James, K. D.M. Harris, Chem. Commun. **46**, 7572 (2010)
641. W.B. Yuan, T. Friščić, D. Apperley, S.L. James, Angew. Chem. Int. Ed. **49**, 3916 (2010)
642. T. Friščić, L. Fábián, CrystEngComm **11**, 743 (2009)
643. J. Klinowski, F.A.A. Paz, J. Rocha, Dalton Trans. **40**, 321 (2011)
644. K.M.L. Taylor-Pashow, J.D. Rocca, Z. Xie, S. Tran, W. Lin, J. Am. Chem. Soc. **131**, 14261 (2009)
645. A. Centrone, Y. Yang, S. Speakman, L. Bromberg, G.C. Rutledge, T.A. Hatton, J. Am. Chem. Soc. **132**, 15687 (2010)
646. S.H. Jhung, J.H. Lee, J.W. Yoon, C. Serre, G. Férey, J.S. Chang, Adv. Mater. **19**, 121 (2007)
647. J.S. Choi, W.J. Son, J. Kim, W.S. Ahn, Micropor. Mesopor. Mater. **116**, 727 (2008)
648. S.H. Jhung, J.-H. Lee, P.M. Forster, G. Férey, A.K. Cheetham, J.-S. Chang, Chem.—Eur. J. **12**, 7899 (2006)
649. H.-K. Liu, T.-H. Tsao, Y.-T. Zhang, C.-H. Lin, Cryst. Eng. Comm. **11**, 1462 (2009)
650. S. Zhong, H. Jing, Y. Li, S. Yin, C. Zeng, L. Wang, Inorg. Chem. **53**, 8278 (2014)
651. M. Shi, C. Zeng, L. Wang, Z. Nie, Y. Zhao, S. Zhong, New J. Chem. **39**, 2973 (2015)
652. M. Joaristi, J. Juan-Alcaniz, P. Serra-Crespo, F. Kapteijn, J. Gascon, Cryst. Growth Des. **12**, 3489 (2012)
653. T. Friscic, J. Mater. Chem. **20**, 7599 (2010)
654. T. Friščić, D.G. Reid, I. Halasz, R.S. Stein, R.E. Dinnebier, M.J. Duer, Angew. Chem. Int. Ed. **49**, 712 (2010)
655. C.R. Hickenboth, J.S. Moore, S.R. White, N.R. Sottos, J. Baudry, S.R. Wilson, Nature **446**, 423 (2007)
656. A. Lazuen-Garay, A. Pichon, S.L. James, Chem. Soc. Rev. **36**, 846 (2007)
657. H. Sakamoto, R. Matsuda, S. Kitagawa, Dalton Trans. **41**, 3956 (2012)

658. V. Strukil, L. Fabian, D.G. Reid, M.J. Duer, G.J. Jackson, M. Eckert-Maksic, T. Friscic, Chem. Commun. **46**, 9191 (2010)
659. D. Crawford, J. Casaban, R. Haydon, N. Giri, T. McNally, S.L. James, Chem. Sci. **6**, 1645 (2015)
660. J. Yoshida, S. Nishikiori, R. Kuroda, Chem.—Eur. J. **14**, 10570 (2008)
661. D. Matoga, M. Oszajca, M. Molenda, Chem. Commun. **51**, 7637 (2015)
662. M.A. Alavi, A. Morsali, Ultrason. Sonochem. **15**, 833 (2008)
663. M.A. Alavi, A. Morsali, Ultrason. Sonochem. **17**, 441 (2010)
664. A. Askarinejad, A. Morsali, Ultrason. Sonochem. **16**, 124 (2009)
665. A. Askarinejad, A. Morsali, Chem. Eng. J. **150**, 569 (2009)
666. H. Sadeghzadeh, A. Morsali, CrystEngComm **12**, 370 (2010)
667. N. Soltanzadeh, A. Morsali, J. Coord. Chem. **62**, 2869 (2009)
668. J.H. Bang, K.S. Suslick, Adv. Mater. **22**, 1039 (2010)
669. V. Safarifard, A. Morsali, Coord. Chem. Rev. **292**, 1 (2015)
670. M.J.S. Fard, F. Rastaghi, N. Ghanbari, J. Mol. Struct. **1032**, 133 (2013)
671. H. Sadeghzadeh, A. Morsali, V.T. Yilmaz, O. Buyukgungor, Ultrason. Sonochem. **17**, 592 (2010)
672. L. Aboutorabi, A. Morsali, Inorg. Chim. Acta **363**, 2506 (2010)
673. A. Morsali, A. Panjehpour, Inorg. Chim. Acta **391**, 210 (2012)
674. M.J.S. Fard, A. Morsali, J. Inorg. Organomet. Polym. **20**, 727 (2010)
675. V. Safarifard, A. Morsali, Ultrason. Sonochem. **19**, 300 (2012)
676. Y.-F. Song, L. Cronin, Angew. Chem. Int. Ed. **47**, 4635 (2008)
677. Z. Zhang, W.-Y. Gao, L. Wojtas, S. Ma, M. Eddaoudi, M.J. Zaworotko, Angew. Chem. Int. Ed. **51**, 9330 (2012)
678. Z. Wang, S.M. Cohen, Chem. Soc. Rev. **38**, 1315 (2009)
679. J.D. Evans, C.J. Sumby, C.J. Doonan, Chem. Soc. Rev. **43**, 5933 (2014)
680. Z. Wang, K.K. Tanabe, S.M. Cohen, Inorg. Chem. **48**, 296 (2008)
681. M.J. Ingleson, J. Perez Barrio, J.-B. Guilbaud, Y.Z. Khimyak, M.J. Rosseinsky, Chem. Commun. 2680 (2008)
682. M. Servalli, M. Ranocchiari, J.A. Van Bokhoven, Chem. Commun. **48**, 1904 (2012)
683. S. Bhattacharjee, D.-A. Yang, W.-S. Ahn, Chem. Commun. **47**, 3637 (2011)
684. C.J. Doonan, W. Morris, H. Furukawa, O.M. Yaghi, J. Am. Chem. Soc. **131**, 9492 (2009)
685. W. Morris, C.J. Doonan, H. Furukawa, R. Banerjee, O.M. Yaghi, J. Am. Chem. Soc. **130**, 12626 (2008)
686. Y. Wang, X.-G. Wang, B. Yuan, C.-Y. Shao, Y.-Y. Chen, B.-B. Zhou, M.-S. Li, X.-M. An, P. Cheng, X.-J. Zhao, Inorg. Chem. **54**, 4456 (2015)
687. T. Gadzikwa, O.K. Farha, K.L. Mulfort, J.T. Hupp, S.T. Nguyen, Chem. Commun. 3720 (2009)
688. K.K. Tanabe, Z. Wang, S.M. Cohen, J. Am. Chem. Soc. **130**, 8508 (2008)
689. K.K. Tanabe, S.M. Cohen, Chem. Soc. Rev. **40**, 498 (2011)
690. S. Bernt, V. Guillerm, V. Serreb, N. Stock, Chem. Commun. **47**, 2838 (2011)
691. M. Meilikhov, K. Yusenko, R.A. Fischer, J. Am. Chem. Soc. **131**, 9644 (2009)
692. B. Gui, X. Meng, H. Xu, C. Wang, Chin. J. Chem. **34**, 186 (2016)
693. B. Li, B. Gui, G. Hu, D. Yuan, C. Wang, Inorg. Chem. **54**, 5139 (2015)
694. P. Deria, J.E. Mondloch, O. Karagiaridi, W. Bury, J.T. Hupp, O.K. Farha, Chem. Soc. Rev. **43**, 5896 (2014)
695. H. Wang, W. Meng, J. Wu, J. Ding, H. Hou, Y. Fan, Coord. Chem. Rev. **307**, 130 (2016)
696. S. Yuan, Y.-P. Chen, J.-S. Qin, W. Lu, L. Zou, Q. Zhang, X. Wang, X. Sun, H.-C. Zhou, J. Am. Chem. Soc. **138**, 8912 (2016)
697. C. Montoro, E. Garcıa, S. Calero, M.A. Perez-Fernandez, A.L. Lopez, L. Barea, J.A. Navarro, J. Mater. Chem. **22**, 10155 (2012)
698. P.V. Dau, S.M. Cohen, Chem. Commun. **49**, 6128 (2013)
699. T. Yamada, H. Kitagawa, J. Am. Chem. Soc. **131**, 6312 (2009)
700. K.M. Zwoliński, P. Nowak, M.J. Chmielewski, Chem. Commun. **51**, 10030 (2015)
701. K.K. Tanabe, C.A. Allen, S.M. Cohen, Angew. Chem. Int. Ed. **49**, 9730 (2010)

702. J. Canivet, D. Farrusseng, ChemCatChem **3**, 823 (2011)
703. A.S. Gupta, R.K. Deshpande, L. Liu, G.I.N. Waterhouse, S.G. Telfer, CrystEngComm **14**, 5701 (2012)
704. W. Bury, D. Fairen-Jimenez, M.B. Lalonde, R.Q. Snurr, O.K. Farha, J.T. Hupp, Chem. Mater. **25**, 739 (2013)
705. A.F. Gross, E. Sherman, S.L. Mahoney, J.J. Vajo, J. Phys. Chem. A **117**, 3771 (2013)
706. T. Li, M.T. Kozlowski, E.A. Doud, M.N. Blakely, N.L. Rosi, J. Am. Chem. Soc. **135**, 11688 (2013)
707. S. Takaishi, E.J. DeMarco, M.J. Pellin, O.K. Farha, J.T. Hupp, Chem. Sci. **4**, 1509 (2013)
708. D.H. Hong, M.P. Suh, Chem.—Eur. J. **20**, 426 (2014)
709. M. Kim, J.F. Cahill, Y. Su, K.A. Prather, S.M. Cohen, Chem. Sci. **3**, 126 (2012)
710. H. Fei, J. Shin, Y.S. Meng, M. Adelhardt, J. Sutter, K. Meyer, S.M. Cohen, J. Am. Chem. Soc. **136**, 4965 (2014)
711. H. Fei, S.M. Cohen, J. Am. Chem. Soc. **137**, 2191 (2015)
712. C. Liu, T.-Y. Luo, E.S. Feura, C. Zhang, N.L. Rosi, J. Am. Chem. Soc. **137**, 10506 (2015)
713. V. Safarifard, A. Morsali, Inorg. Chim. Acta **405**, 203 (2013)
714. A.P. Nelson, O.K. Farha, K.L. Mulfort, J.T. Hupp, J. Am. Chem. Soc. **131**, 458 (2009)
715. Y.-S. Bae, D. Dubbeldam, A.P. Nelson, K.S. Walton, J.T. Hupp, R.Q. Snurr, Chem. Mater. **21**, 4768 (2009)
716. Z. Xiang, D. Cao, X. Shao, W. Wang, J. Zhang, W. Wu, Chem. Eng. Sci. **65**, 3140 (2010)
717. M.R. Lohe, M. Rose, S. Kaskel, Chem. Commun. 6056 (2009)
718. C.-D. Wu, W. Lin, Angew. Chem. Int. Ed. **44**, 1958 (2005)
719. C.-D. Wu, W. Lin, Inorg. Chem. **44**, 1178 (2005)
720. J.B. Rivest, P.K. Jain, Chem. Soc. Rev. **42**, 89 (2013)
721. Y. Kim, S. Das, S. Bhattacharya, S. Hong, M.G. Kim, M. Yoon, S. Natarajan, K. Kim, Chem.—Eur. J. **18**, 16642 (2012)
722. D. Denysenko, T. Werner, M. Grzywa, A. Puls, V. Hagen, G. Eickerling, J. Jelic, K. Reuter, D. Volkmer, Chem. Commun. **48**, 1236 (2012)
723. C.K. Brozek, A.F. Cozzolino, S.J. Teat, Y.-S. Chen, M. Dincă, Chem. Mater. **25**, 2998 (2013)
724. Y. Jiao, C.R. Morelock, N.C. Burtch, W.P. Mounfield III, J.T. Hungerford, K.S. Walton, Ind. Eng. Chem. Res. **54**, 12408 (2015)
725. S. Liu, Y. Zhang, Q. Huo, S. He, Y. Han, J. Spectroscopy **2015**, Article ID 310162 (2015)
726. A.M. Shultz, O.K. Farha, D. Adhikari, A.A. Sarjeant, J.T. Hupp, S.T. Nguyen, Inorg. Chem. **50**, 3174 (2011)
727. D. Feng, Z.-Y. Gu, Y.-P. Chen, J. Park, Z. Wei, Y. Sun, M. Bosch, S. Yuan, H.-C. Zhou, J. Am. Chem. Soc. **136**, 17714 (2014)
728. J. Zheng, M. Wu, F. Jiang, W. Su, M. Hong, Chem. Sci. **6**, 3466 (2015)
729. J.A. Johnson, J. Luo, X. Zhang, Y.-S. Chen, M.D. Morton, E. Echeverría, F.E. Torres, J. Zhang, ACS Catal. **5**, 5283 (2015)
730. T. Sawano, N.C. Thacker, Z. Lin, A.R. McIsaac, W. Lin, J. Am. Chem. Soc. **137**, 12241 (2015)
731. S. Seth, G. Savitha, J.N. Moorthy, J. Mater. Chem. A **3**, 22915 (2015)
732. M.C. So, S. Jin, H.-J. Son, G.P. Wiederrecht, O.K. Farha, J.T. Hupp, J. Am. Chem. Soc. **135**, 15698 (2013)
733. E. Biemmi, C. Scherb, T. Bein, J. Am. Chem. Soc. **129**, 8054 (2007)
734. L.E. Kreno, J.T. Hupp, R.P. Van Duyne, Anal. Chem. **82**, 8042 (2010)
735. G. Lu, O.K. Farha, L.E. Kreno, P.M. Schoenecker, K.S. Walton, R.P. Van Duyne, J.T. Hupp, Adv. Mater. **23**, 4449 (2011)
736. O. Shekhah, W. Hui, M. Paradinas, C. Ocal, B. Schüpbach, A. Terfort, D. Zacher, R.A. Fischer, C. Wüll, Nat. Mater. **8**, 481 (2009)
737. O. Shekhah, H. Wang, S. Kowarik, F. Schreiber, M. Paulus, M. Tolan, C. Sternemann, F. Evers, D. Zacher, R.A. Fischer, C. Wüll, J. Am. Chem. Soc. **129**, 15118 (2007)

738. V. Stavila, J. Volponi, A.M. Katzenmeyer, M.C. Dixon, M.D. Allendorf, Chem. Sci. **3**, 1531 (2012)
739. A.A. Talin, A. Centrone, A.C. Ford, M.E. Foster, V. Stavila, P. Haney, R.A. Kinney, V. Szalai, F. El Gabaly, H.P. Yoon, M.D. Allendorf, Science **343**, 66 (2014)
740. M. Tu, S. Wannapaiboon, R. Fischer, Inorg. Chem. Front. **1**, 442 (2014)
741. D. Zacher, R. Schmid, C. Wüll, R.A. Fischer, Angew. Chem. Int. Ed. **50**, 176 (2011)
742. P. Szilágyi, R. Westerwaal, R. van de Krol, H. Geerlings, B. Dam, J. Mater. Chem. C **1**, 8146 (2013)
743. D. Zacher, K. Yusenko, A. Bétard, S. Henke, M. Molon, T. Ladnorg, O. Shekhah, B. Schüpbach, T. de los Arcos, M. Krasnopolski, M. Meilikhov, J. Winter, A. Terfort, C. Wöll, R.A. Fischer, Chem.—Eur. J. **17**, 1448 (2011)
744. M. Tu, R.A. Fischer, J. Mater. Chem. A **2**, 2018 (2014)
745. Q.-G. Wang, Y.-S. Xie, F.-H. Zeng, S.-W. Ng, W.-H. Zhu, Inure. Chem. Commun. **13**, 929 (2010)
746. J. Ferrando-Soria, E. Pardo, R. Ruiz-García, J. Cano, F. Lloret, M. Julve, Y. Journaux, J. Pasán, C. Ruiz-Pérez, Chem.—Eur. J. **17**, 2176 (2011)
747. O. Shekhah, K. Hirai, H. Wang, H. Uehara, M. Kondo, S. Diring, D. Zacher, R. Fischer, O. Sakata, S. Kitagawa, Dalton Trans. **40**, 4954 (2011)
748. M.C. So, M.H. Beyzavi, R. Sawhney, O. Shekhah, M. Eddaoudi, S.S. Al-Juaid, J.T. Hupp, O.K. Farha, Chem. Commun. **51**, 85 (2015)
749. Z. Wang, J. Liu, H.K. Arslan, S. Grosjean, T. Hagendorn, H. Gliemann, S. Bräse, C. Wüll, Langmuir **29**, 15958 (2013)

Chapter 7
Supramolecular Chemistry of Polymer Metal Chelates

Abstract In this chapter the basic concepts and synthetic strategies leading to the different types of metallosupramolecular polymers containing metal chelate units including linear, branched, cross-linked as well as heterometallic polymers are summarized and discussed. Included are metallosupramolecular polyelectrolytes, polymer gels, self-assembled metallosupramolecular monolayers, and supramolecular metal chelate dendrimers. Special attention is paid to such new synthetic approaches to the supramolecular polymers as hierarchical and orthogonal self-assembling based on combination of metal–ligand coordination with hydrogen-bonding and host-guest interactions. The stimuli-responsive, self-healing and shape-memory metallo-supramolecular polymers containing metal chelate units are considered.

Within relatively short time interval, with respect to historical scale, supramolecular chemistry has turned into very rapidly developed and interdisciplinary science, which includes chemical, physical, and biological aspects of studying more complicated than molecules chemical systems assembled into integral whole through inter-molecular (non-covalent) interactions [1–8]. Today it is absolutely clear that supramolecular systems have a special niche, a level in hierarchy of matter, in which such principles of organizing and functioning matter as molecular recognition, selective bonding, receptor-substrate interaction, trans-membrane transfer, and supramolecular catalysis are realized. Nature has maximally used these principles for creation of biological objects. Likely to self-assembling most complicated spatial structures in living systems, objects of supramolecular chemistry, supramolecular assemblies, are built spontaneously from complementary, i.e. having geometrical and chemical similarity, fragments. In nanometer world, which is ascribed to 1 to 100-nm scaling elements, supramolecular systems, usually having 1 to 10-nm scale, are the smallest elements of this world. Therefore, it is possible to state that supramolecular chemistry eliminates a gap between molecular world and nanotechnologies, and also provides designing new classes of materials and devices for future nanotechnologies [9]. One of the fundamental problems of contemporary chemistry is oriented structuring such systems, development of highly ordered supramolecular assemblies made

of molecular building blocks, having a given structure and properties. Supramolecular formations are characterized by spatial disposition of their components, their architecture, «suprastructure», and also types of intermolecular interactions, which keep components together.

Two main principles, molecular recognition and supramolecular function, lie in the center of understanding supramolecular chemistry concept [10]. While bonding does not necessary means recognition, molecular recognition is, as a rule, considered as a patterned process with participation of structurally well-defined set of intermolecular interactions, i.e. purported bonding [1]. Based on chemical recognition (which is chemical informatics) self-organizing, programmed self-assembling supramolecular systems are performed. Molecular recognition is a process, in which some molecules («host» or receptor) choose and bound molecules («guest» or substrate) due to intermolecular forces into structurally-organized system. In supramolecular chemistry non-covalent interactions are realized between molecular structural blocks, which form supramolecular fragments using molecular recognition and self-assembling. In these systems each additional block contains exact information on creation via self-assembling (each step of self-organization process) regular final structure inside all possible structures [11]. General structure of purported assembly is controlled using symmetry features of some building blocks. Finally, assemblies can have special properties or supramolecular functions, which can only be found in assembly, but which are not contributing to molecules [12].

Idea of self-assembling is determinative for supramolecular chemistry. This term is referred to spontaneous assembling two or more components under equilibrium conditions bringing to creation of stable, structurally clearly defined discrete oligomer supramolecules or extended supramolecular assemblies, which is realized due to non-covalent interactions [1, 13]. As a rule, non-covalent interactions are weaker than covalent, therefore supramolecular assemblies are less stable thermodynamically, more labile kinetically, and more flexible dynamically than molecules. Even under weak external influence on a supramolecular system it can reversibly change its structure due to change in geometry of mutual positions of atoms comprising the supramolecular system and, respectively, can change characteristics of the whole system.

A special feature of supramolecular systems is their capacity to form different architectures without change in chemical composition of a system. In other words, polymorphism of supramolecular systems should be regarded. Because a structure of a supramolecular system changes under external influence there is a possibility of control over structure of produced supramolecular assemblies and their properties.

Self-organizing is ordered association under given conditions of individual structural components into supramolecular structures [1], which are characterized by definite spatial disposition of components (architecture) and intermolecular interactions keeping them together. Supramolecular structures have definite conformation, thermodynamic, kinetic, and dynamic properties. Self-organization is selective and spontaneous formation of one or more ordered structures in a complex mixture, which in the opposite case could have formed greater variety of structures [14].

Together terms «self-assembly» and «self-organization» involve processes, which give an opportunity for programmed molecular components or tectons (from Greek «tekton»—a builder) to assemble spontaneously, exactly in a definite way forming assemblies, whose organization proceeds in one, two or three dimensions and, probably, though not necessary, in time [15, 16]. Molecules, which form assemblies with typical architectural and functional features, are accepted as tectons [17, 18]. In fact, supramolecular tectons are supramolecular building blocks capable of self-assembling into ordered assemblies. It should be especially noted that supramolecular assemblies should be related, together with other complicated systems, to higher level of tectons, «nanoarchitectonics» for designing and preparation of dynamic functional materials [19, 20]. In the nanoarchitectonics concept these materials are projected through controlled harmonized interactions, which provide development of unexpected functions.

An idea of supramolecular synthons is introduced [21] for designation of structural elements distinguished on the basis of analysis of intermolecular contacts with account for some additional geometric characteristics. The term «supramolecular synthon» is well studied and accepted tool in crystal engineering for designing of desired supramolecular structures [21–23]. Advantage of the terms «supramolecular tectonics» and «supramolecular synthon» is in more comprehensive information on structure as compared with traditional terms («complex», «associate», etc.). Supramolecular synthon plays the same key role in supramolecular polymerization as a synthon plays in covalent synthesis. Supramolecular synthons are spatial positions of intermolecular non-covalent interactions, which are often met in supramolecular assemblies. Numerous examples of supramolecular structures, in which supramolecular synthons were used, point to strength of supramolecular synthons [24–31].

Supramolecular chemistry operates with various intermolecular interactions (supramolecular synthons), which differ in their character, energy and directionality. They include ion-ionic (100–350 kJ mol^{-1}), ion-dipole (50–200 kJ mol^{-1}), dipole-dipole (5–50 kJ mol^{-1}), cation-π-system (50–80 kJ mol^{-1}), π-π-stacking (0–50 kJ mol^{-1}), metallophilic (<10 kJ mol^{-1}), Van der Waals (<5 kJ mol^{-1}) interactions, coordination (40–400 kJ mol^{-1}) and hydrogen (4–120 kJ mol^{-1}) bonds [32]. Therefore there are a great number of possibilities for building supramolecular assemblies using only one type of non-covalent interaction or combination of two or more types, which can additively contribute to common energy and/or integrate a great number of factors for structural control.

7.1 Supramolecular Polymers

Supramolecular chemistry can be divided into two broad, partly superimposed areas, in which supramolecules and supramolecular polymers, respectively, are considered. Supramolecules are represented by well-defined, discrete, oligomolecular formations created due to intermolecular association of several components (receptor and

substrate) according to some «program» operating by principles of molecular recognition. Supramolecular polymers are polymolecular assemblies generated due to spontaneous self-assembling a great number of components in specific phase characterized by more or less definite organization at microscopic level and having macroscopic properties depending on a character of a phase (film, layer, membrane, vesicle, mesomorphic phase, crystal, etc.) [33–40]. In order to overcome a gap between these two abovementioned species, a new class of organized assemblies, suprasupermolecules is proposed [41, 42]. Therefore, «supramolecular chemistry» is a wide term, which relates to chemistry of all types of supramolecular assemblies, including well-defined supramolecules, extended, more or less organized polymolecular assemblies, and their respective combinations.

Supramolecular polymers can be divided in three categories depending on their formation mechanism: isodesmic, cooperative, and ring-chain polymerization processes. Without going in details of these well studied mechanisms of supramolecular polymerization and their thermodynamic aspects [34, 43–45], we shall notice only that isodesmic process can be compared with step-growth polymerization, and all stages of self-assembling are characterized by the same constant values of association, independently on aggregate sizes [43–45]. Cooperative mechanism (or nucleation-growth) includes two states of the process, in which formation of thermodynamically adverse types consisting of limited number of monomer units (nucleation) is followed by more favorable stage of elongation, which is characterized by higher values of association constants (Fig. 7.1a). The result of cooperative polymerization is formation of self-assembled assemblies with high degree of internal order as compared with isodesmic analogues, which bring to random-coil supramolecular polymers without internal ordering.

To separate these two self-assembling mechanisms, it is necessary to choose thoroughly experimental and calculative methods of studying [46–48]. Ideally, there should be a possibility of monitoring of complete transformation from monomer types to completely aggregated types during temperature- or concentration-dependent studies. This happens in the case when α_{agg} parameter (a fraction of aggregated types) can be determined exactly. It changes from 0 (all monomer units are in molecular solved state) to 1 (all monomer units are in aggregated state). The dependence α_{agg} on concentration or temperature will be a curve, which has a shape determined by self-assembling mechanism (Fig. 7.1b).

Ring-chain supramolecular polymerization is typical of ditopic monomer units, in which there is equilibrium between linear and cyclic analogues [43].

Supramolecular polymers are dynamic in nature; therefore, their components are linked via reversible bonds and are subjected to spontaneous and continuous processes of assembling/dissembling under certain conditions [49]. Due to dynamic and reversible character of non-covalent interactions, supramolecular polymers have ability to adapt to environment and have wide spectrum of intriguing properties, such as a tendency to degradation, shape memory, and self-healing, which makes them unique candidates for supramolecular materials [50–65].
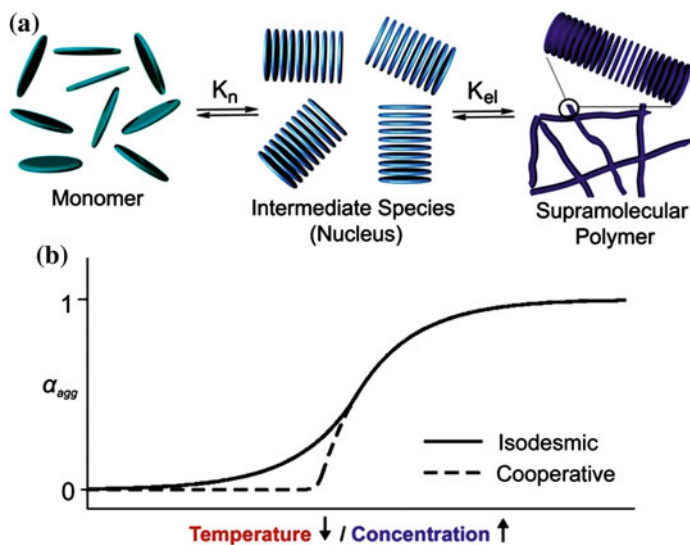
Fig. 7.1 **a** Schematic representation of the supramolecular cooperative growth following the nucleation-elongation pathway. **b** Plot of α_{agg} against increasing temperature and decreasing concentration, respectively, giving rise to characteristic curves corresponding to an isodesmic or cooperative growth [46]

There are different approaches to synthesis of supramolecular polymers, including using hydrogen bonds (H-bonds) [43, 66–74], metal–ligand (M–L) [35, 43, 50, 72, 76–87], ionic [88–90], π-π [38, 43, 70, 72, 91, 92], and Van der Waals interactions [43, 70, 72, 92].

The main difference between covalently bound polymers and supramolecular polymers is dependence of average DP on interaction strength of terminal groups, and, respectively, solvent, temperature and concentration. To estimate DP of reversible supramolecular polymers, (7.1) is used [43, 70, 75, 93–95]:

$$DP \sim \left(K_a[M]\right)^{1/2}, \tag{7.1}$$

where K_a is general association constant, M is concentration of monomer.

Graphical dependence DP on K for different concentrations is presented in Fig. 7.2. To obtain polymers with high DP, high association constant between repeated units is needed. By analogy with covalent polymers, chain length of supramolecular polymers can be changed by addition of monofunctional chain stoppers. The main advantage of supramolecular polymers as compared with their classical analogues is a possibility to produce tailor-made materials using knowledge on association constants.
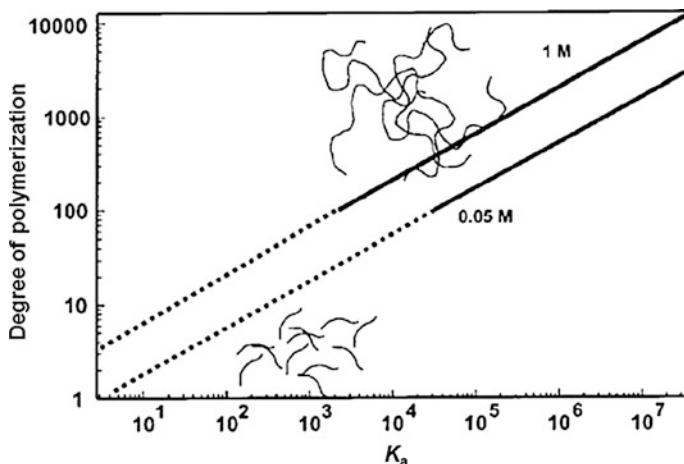
Fig. 7.2 Theoretical relationship between the association constant K_a and DP, using a simple isodesmic association function, or «multistage open association» model [70]

7.2 Metallosupramolecular Polymerization

Metallosupramolecular polymerization is a process of spontaneous self-assembling polytopic organic ligands and metal ions with formation of metallosupramolecular polymers (MSPs) (Fig. 7.3) [96]. Taking into account orientation of this book, hereafter only those MSPs will be considered which include metal chelate units as a basic supramolecular motif. Concept of metallosupramolecular polymerization requires that a chelating monomer would be a telechelic system capable of continuous elongation of a chain in presence of a metal ion via well-known consecutive polycondensation mechanism.

The MSP is a special class of supramolecular polymers obtained from polytopic monomers containing two or more chelating groups (ligands) at each end, where a bond between monomers is provided by M–L coordination [70, 75, 93, 97, 98]. MSP can be considered as a subset of metal-containing polymers, in which M–L interaction is dynamic by its character and, therefore, acts as supramolecular motif. These organic/inorganic hybrid systems potentially offer attractive combination of functionality of metal ions, mechanical properties and workability of polymers, as well as characteristics of self-assembling and dynamic character of supramolecular chemistry.

Self-assembling discrete structures using as a main driving force M–L coordination, is already known for more than two decades, and during this time MSP chemistry is steadily developed [75, 87, 99–113]. It is especially noted that M–L bond of donor centers of organic molecule with a metal ion is one of the strongest types of intermolecular interactions in supramolecular polymers [12, 50, 75, 96, 114–119].
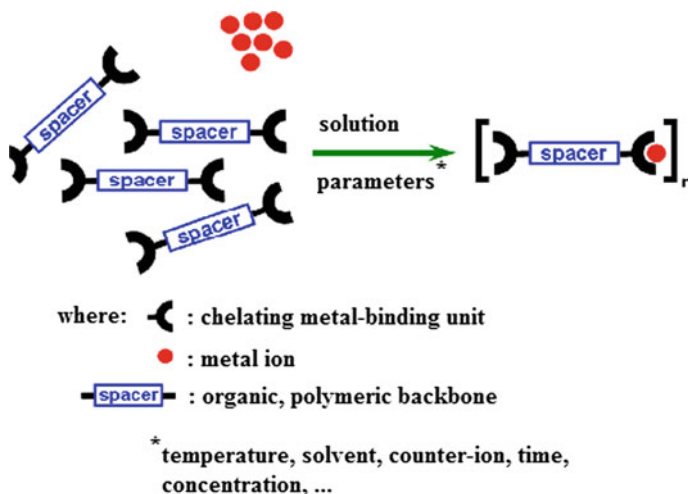
Fig. 7.3 Schematic representation of the metallosupramolecular polymerization process [96]

In MSP metal ions function as bridges for linking organic ligands, thus forming a polymer chain. An advantage of the concept of metallosupramolecular polymerization is a possibility to choose respective M–L combination so as to take control over bond strength (thermodynamic characteristic) and exchange rate (kinetic characteristic). The process of metallosupramolecular polymerization is mainly controlled by strength of M–L bond between a metal and chelating block of a polytopic ligand. Nature of this interaction is predominantly donation of lone-pair of ligand (Lewis base) to a metal ion (Lewis acid) in combination with electrostatic interaction between a positively charged metal ion and negatively polarized/charged donor atom of ligand [120]. When developing MSP, a special attention should be paid to some important factors, which can be used to influence a polymer not only during, but also after building metallosupramolecular assemblies. A possibility of changing a polymer structure of MSP after its preparation has a significant advantage as compared with covalent polymers.

The most important features of coordination-driven self-assembling is narrow directionality of M–L bonds [110], diversity of supramolecular assemblies, stipulated by variety of building blocks (polydentate ligands and different metals), combination of strong and weak bonds, a possibility of control over a reaction mechanism, i.e. its proceeding under conditions of thermodynamic or kinetic control [75, 95]. The principle of molecular recognition in coordination-driven self-assembling is based on the stoichiometric model [121, 122]. The most varied factors, for example, metal cation properties (electronic configuration and size, which define coordination geometry of a metal chelate node), softness or hardness of cations and ligands, chelate effect, etc. should be taken into account in the coordination-driven self-assembling. Contemporary coordination chemistry suggests a vast variety of supramolecular motifs based on metal chelates with different

geometry, appropriate electronic and magnetic properties, which can be included in MSP [123]. If a ligand contains several chelating groups, divergently positioned in a molecule, it can participate in binding of several metal ions in one MSP. Bonds of metal ions with polymers can change almost continuously from strong, actually covalent bonds, which bring to irreversible or «static» binding of a metal, to weak and unstable non-covalent M–L interactions, which provide reversible, «dynamic» or «metallosupramolecular» binding. Since binding energy between a metal and a ligand is relatively high, the obtained structures can be linked with relatively small number of these bonds. This is a main difference of methodology based on M–L interaction from other types of discrete self-assembling, for example, such as self-assembling through H-bonds. Other advantages of M–L interactions, in particular, are in large database of available ligands in line with applied metal ions, containing almost half of the periodical system, which means that there is a broad range of easily available M–L chelates [76]. For intermolecular interactions detailed study of thermodynamics and kinetics of chelation is necessary for choice of appropriate M–L combination for respective application. Thermodynamic properties determined by binding constants, give a possibility to predict whether a complex will be stable or unstable, while kinetic properties are expressed by conditions of inertness or lability, and can be expressed, in particular, in terms of half-life period of respective M–L bond [75, 84, 124–126].

Properties of MSP will depend on such factors as DP, architecture (for example, linear or branched) and dynamics/life-time of assembly, which can be driven with the binding force, stoichiometry, and kinetics of supramolecular motif. To obtain polymers with high molecular weight, the necessary condition is high binding constant and high concentration of initial components [92]. Excess of metal ions should bring to larger assemblies than in the case when there is excess of a monomer, if there is some cooperation, i.e. binding a second ligand is more advantageous, than of the first [76, 127].

Ideal combination is a system, which provides a complex of high thermodynamic stability in connection with high kinetic lability [128]. Thermodynamic stability of M–L interactions will determine size (or DP) of assembly, while their kinetic lability should bring to «dynamic» polymers responsive to environmental factors. This combination provides building MSP, which has advantages of reversible supramolecular systems, i.e. external stimulus can be applied to them, which allows switching from monomer to polymer state or switching between different self-assembling architectures, such as macrocycles and polymers. Some of these systems can be multiply included, oppositely to classic covalent polymers, which are formed irreversibly [43, 50, 77, 129, 130].

It should be noted that metal ions provide geometry and CNs, which are absent or hardly available in covalent chemistry. By choosing chelating ligands, metal ions, counter-ions, and boundary conditions of self-assembling (M:L ratio, concentration, solvent, ionic strength, pH, etc.), it is easy to obtain vast MSP database with resources of kinetic, thermodynamic, and functional properties [73, 131]. Since for most applications, high PD are preferable, and in many cases increase in

concentration is impossible due to practical limitations or low solubility, control over binding force is most important. Increase in K_a can be reached by combination of several interacting binding sites, the simplest of which is using chelating ligands and polyvalent metal ions. Character of M–L interaction has a strong effect on properties of obtained MSP, and the binding constant is the main parameter, which should be taken into account. If M–L interaction is very weak, polymer assemblies are not formed, and if it is too strong, a polymer may be deposited. Intermediate binding constants imply easy exchange with ligands, i.e. soluble MSP are, as a rule, dynamically equilibrium systems. However, dynamic character is a serious problem for establishment of characteristics, because structure and properties of MSP depend on external conditions.

Architecture of synthesized MSP depends on localization of metal chelates [132]. In «main chain» MSP polymer matrix is self-assembled from non-covalently bound low molecular weight monomers through M–L bonds [96, 122]. Other polymer MSP architectures, which are formed, include side chain [34, 95, 133–139], branched [130], cross-linked [140–142], macrocyclic [143–151], helical [152, 153], dendritic [154] or star-like MSP [155, 156].

The aim of MSP synthesis is design of new materials, which can show specific and multifunctional properties. On one hand, presence of metal ions makes it possible to obtain coordination supramolecules with special optical, electric, magnetic and catalytic properties [11, 35, 81, 85, 130, 157–167]. On the other hand, properties of projected materials can be driven not only by thorough choice of metal ions, but also by main polymer chain. At the same time, including metal chelate nodes in supramolecular polymer system makes it possible to obtain hybrid supramolecular materials with synergetic combination of typical features of M–L chelates (special electrochemical, optical, magnetic properties) and properties of polymer (workability, mechanical properties, solubility, etc.) [168–172].

It should be noted that recently coordination-driven self-assembling becomes a powerful tool of synthesis of polymer supramolecules of nanoscale size. Moreover, dynamic character of M–L bonds provides switching capacity of a system imitating behavior of natural supramolecular structures [173, 174]. Building blocks of MSPs should be thoroughly chosen to design new materials with tunable and defined properties, which suggest a convenient platform for development of intelligent materials. Presently M–L coordination is often used as fascinating reversible non-covalent interaction, which simplifies building stimulus-responsive, memory shape, and self-healing MSP [53, 159, 175, 176]. During recent decades associated with flourishing studies on synthesis and properties of MSP solutions [81, 130, 157, 159–161], considerable efforts are taken in building molecular devices using these supramolecular assemblies. These devices include self-assembled nanostructures of MSP, as well as co-assembled objects with other modulus, which are hierarchic assemblies of self-assembled coordination supramolecules.

7.3   Linear Metallosupramolecular Polymers

The simplest way to access linear MSPs is coordination of bis-ligand functionalized ditopic monomers (sometimes called macromonomers if a spacer is oligomer or polymer) to metal ions in the ratio 1:1 bringing to MSP with multiple M–L complexes in a main chain (Fig. 7.4). These polymers usually show dynamic behavior to a greater extent than covalent polymers, because reversibility of M–L coordination provides polymerization/depolymerization and ring-chain equilibrium.

To build dynamic constitutional metallosupramolecular systems, it is possible to apply principles of dynamic constitutional chemistry advancing self-evolution of supramolecular systems to choice of discrete systems made of mixtures of objects, reversibly and continuously changing at nano- and macroscopic scales [177]. This makes it possible to obtain single or double levels of dynamic supramolecular databases using M–L and reversible ligand exchanges. The process of metal ion coordination can put ligands in immediate closeness to each other. This closeness potentially simplifies reversible supramolecular non-covalent interactions bringing to restructuring coordinating ligands within the limits of confined interactional space determined by coordination geometry around metal centers. This made it possible, for example, to automate the process of parallel coordination-driven polymerization of tpy-bis-functionalized PEO using different metal salts [178].

From the beginning MSP studies, the keenest attention of researchers was attracted to chelating polytopic monomers, in particular, polypyridyl ligands, including bpy, phen, and tpy fragments [84, 179–182].

Thus, in one of the first examples variety of constitutionally clearly defined kinetically labile MSP is obtained using phen-based bidentate ligands (Scheme 7.1) [183–186]. Ligand exchange went instantly in coordinating solvents, such as acetonitrile, while in the non-coordinated solvent 1,1,2,2-tetrachloroethane no signs of ligand exchange were observed even during several hours.

Coordination of 5,5′-bound bis-phen ligands with Cu(II), Ni(II), Ag(I), and Zn (II) ions in stoichiometric ratio 1:1 brings to formation of MSP with high molecular weights, more than 100,000 [187]. It is important that properties of MSP are characterized by reversibility depending on external factors, such as electrochemical action or addition of competitive complexing ligands.
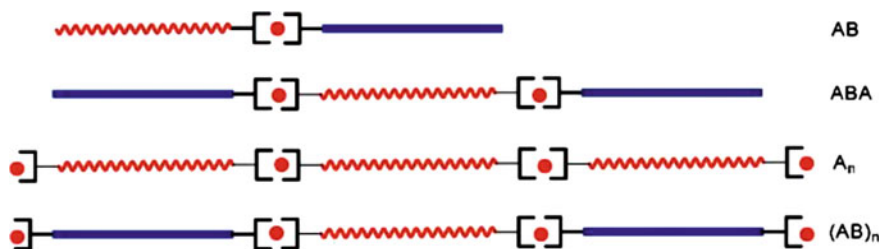
Fig. 7.4 Various accessible architectures of linear MSPs
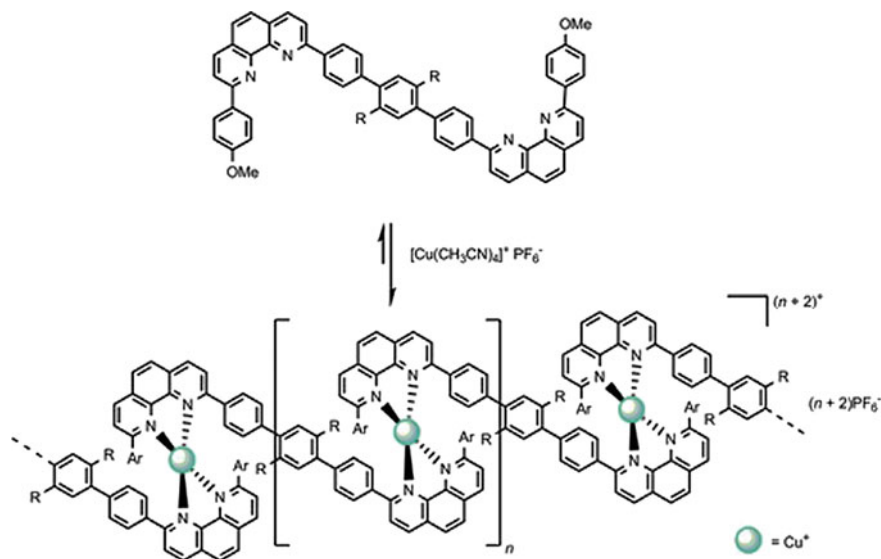
Scheme 7.1 Reversible MSP formed from bifunctional phen-based ligand monomers and Cu(I) ions

MSPs obtained by 1:1 chelation of metal ions with organic ditopic bis-phen ligands have shown unique electro- and photochemical properties based on M–L interactions. Thus, we shall notice green Cu-based MSP, for which there is typical excellent electrochromic color change from green to colorless at electrochemical reduction from Cu(II) to Cu(I) [188].

In the case of Ni(II)-based MSP with bis-phen ligands having different spacers and/or substituents, ionic conductivity of polymer films increases considerably with increase in relative moisture, and a polymer without hydrophobic spacer has shown conductivity 0.75×10^{-3} S cm^{-1} at 98% of relative moisture, which is by about 500 times higher than ionic conductivity of a polymer with a spacer [189].

Fe(II)-, Ru(II)-, and Cu(II)-based MSP films showed reversible electrochromic behavior, which was used in fabrication of devices of electrochromic display (Fig. 7.5). It is interesting that a polymer containing both Fe(II) and Ru(II) ions exhibited multicolor electrochromic properties, and for Eu(III)-based polymer vapoluminascence is typical. Besides, reversible switching emission is reached in the polymer with Fe(II) and Eu(III) ions integrated alternately [99].

A series of functional MSPs based on polyhedral oligomer silsesquioxane and phen ligand was obtained using two-staged approach [190, 191]. At the first stage phen-based ligand is used for synthesis of amino-functionalized complex of a transition metal using Sn(II) chloride, and at the second stage this metal complex is subjected to interaction with octakis(3-chloropropyl) octasilsesquioxane, bringing to MSP carrying a structure of polyhedral oligomer silsesquioxane. The obtained
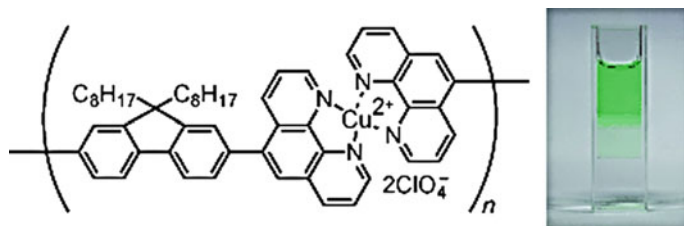
Fig. 7.5 Cu(II)-based MSP obtained by the 1:1 chelation of metal ions and bis(phen)s with reversible electrochromic behavior [99]

MSP has shown electro- and chemo-responsive properties and is a good candidate for smart stimulus-responsive materials.

Polytopic ligands with tpy and structurally related fragments have a considerable place in MSP design. Using similar ligands is interesting for building a vast variety of different architectures including both linear MSPs, and AB block-copolymers, graft-copolymers, and metal supramolecular micelles. In particular, rigid linear building blocks with tpy fragments bring to rod-like MSP, and building blocks with flexible spacer blocks or rigid spacer units, which give well-defined angle between chelating fragments, bring to cyclic structures [125, 192–194]. It has been shown, for example, upon synthesis of MSP such as [bis(tpy-4′-yl)-FeCl$_2$-di(ethylene glycol)]$_n$, [bis(tpy-4′-yl)-Ru(BF$_4$)$_2$-di(ethylene glycol)]$_n$, [bis(tpy-4′-yl)-FeCl$_2$-PEG$_{180}$]$_n$ and [bis(tpy-4′-yl)-Ru(BF$_4$)$_2$-PEG$_{180}$]$_n$ [195].

A rich variety of new ditopic bis-tpy [160] obtained by symmetric and non-symmetric introduction of functional groups in pyridine rings, and also by tuning spacers for linking of two tpy-fragments is described. These bis-tpy are convenient ligands for development of new MSP with different functions, and for studying structure-property relationship. In particular, it occurs that such structural factors of bis-tpy-based MSP as functional group nature in peripheral ring of ligands and spacers between two chelating tpy fragments have a significant effect on charge transfer and electrochemical properties of different types of Co(II) bis-tpy MSP.

Linear MSPs are usually formed between molecules of ditopic ligand (bis-ligand), which have two chelating heads and metal ions, as is shown in Fig. 7.6a [132]. Chelating heads of these ditopic molecules of a ligand often contain di- or tpy-, and sometimes carbonyl groups. Figure 7.6b–d shows some examples of linear MSPs [81, 130, 157, 160, 196, 197]. DP of linear MSPs has a strong dependence on concentration and ratio of components of a mixture [127, 197]. Long chains can only be formed for 1:1 M–L ratio at high concentrations, and deviation from 1:1 mixing brings to such a chain ends formation that the chain growth is stopped. Concentrated 1:1 mixed system of bis-ligands and metal ions can be very viscous and elastic, while diluted system is water-like with small ring oligomers present [197].
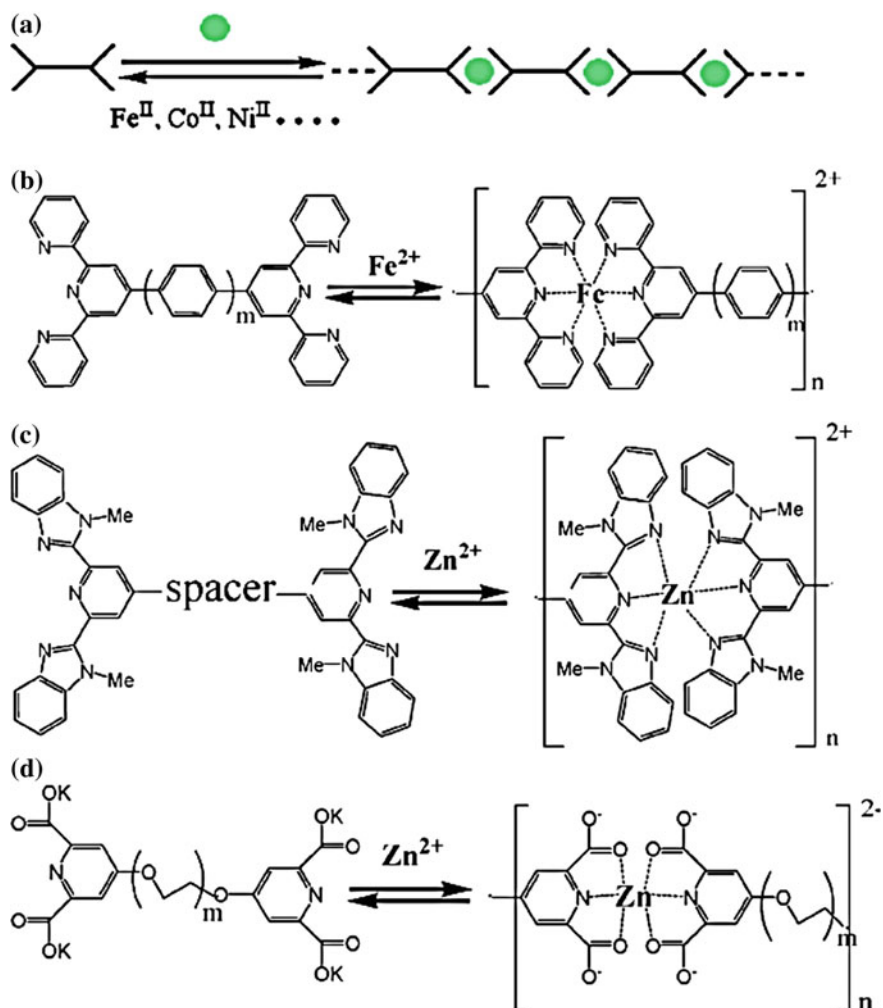
Fig. 7.6 a Schematic representation of formation of linear MSP and **b–d** are appropriate examples [132]

We shall notice the concept of thiol-*para*-fluorine click chemistry used for fast and efficient formation of Ru(II) bis-tpy MSP. Oppositely to widespread methods of MSP assembling, demanding high temperatures and longtime of reaction, using penta-fluorine-phenyl-substituted homoleptic Ru(II) bis-tpy complex as a monomer, thiol-functionalized organic spacer blocks can be easily integrated at low temperatures and for very short reaction time [198].

Soluble MSP based on Ru(II)tpy$_2$ chelate is obtained through two different ways of synthesis: (1) coordination of telechelic tpy ligand with activated Ru(II) species,

(2) Pd-catalyzed polycondensation of Ru(II) bis-tpy chelate carrying functionality of a halogen with diboronic acid (Scheme 7.2) [96]. Comparison of the final products of the reaction has shown that the 1st method has brought to more macromolecular species as compared to the 2nd method, which has given only oligomer structures.

Random Zn(II)-based and alternating Ru(II)-based MSPs containing bis-tpy ligands with different central donor (fluorene or Cz) and acceptor (benzothiadiazole) fragments are synthesized (Scheme 7.3) [199]. It occurs that due to strong donor-acceptor interactions with participation of Zn(II) and Ru(II) ions absorption spectra of obtained MSPs cover a wide range 260–750 nm with a gap width 1.57–1.77 eV.
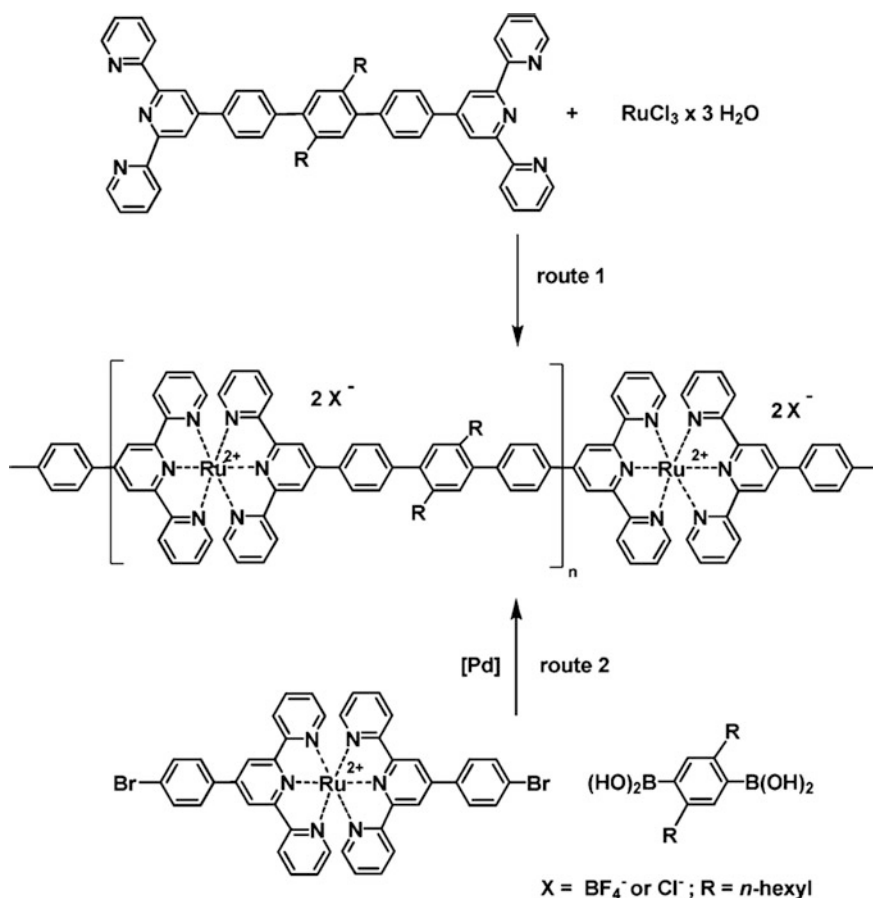
Scheme 7.2 Two different routes of synthesis of Ru(II) chain-extended polymers [96]
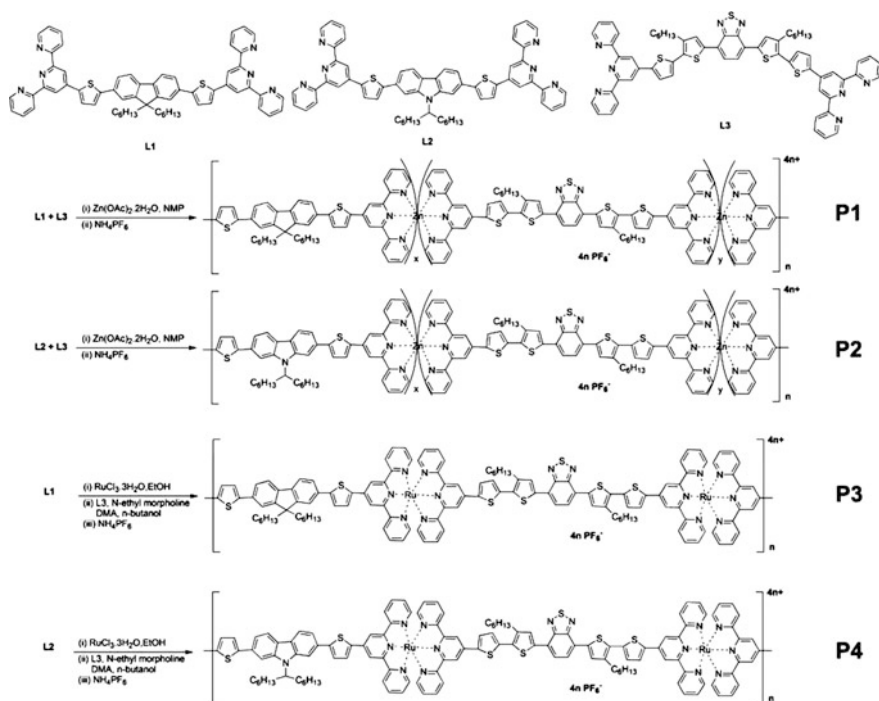
Scheme 7.3 Two random Zn(II)-based and two alternating Ru(II)-based metallo-copolymers containing bis-tpy ligands with various central donor (i.e., fluorene or Cz) and acceptor (i.e., benzothiadiazole) moieties [199]

Similar results were obtained in the studies of Zn(II)-based MSP produced by 1:1 complexation of $Zn(ClO_4)_2$ and bis-tpy ligands with electron-donor (alkoxy) and electron-acceptor (cyano) groups in 6-position of peripheral pyridine fragment [200]. In particular, Zn(II)-based MSPs have shown relatively high quantum yields ($\Phi_{PL} = 0.68–0.76$) in solution at room temperature, and different luminescent colors: blue, light blue, and green in film state due to considerable Stokes shift caused by the effect of a ligand substituents.

Thermodynamics of chelation between tpy ligands and Zn(II) ions is studied in detail [201]. The results of the studies provide conclusions that Zn(II) ions offer interesting balance between reversibility of chelation process and stability of projected structures due to high affinity constants. Besides, telechelic tpy ligands are obtained carrying organic fluorophore spacer.
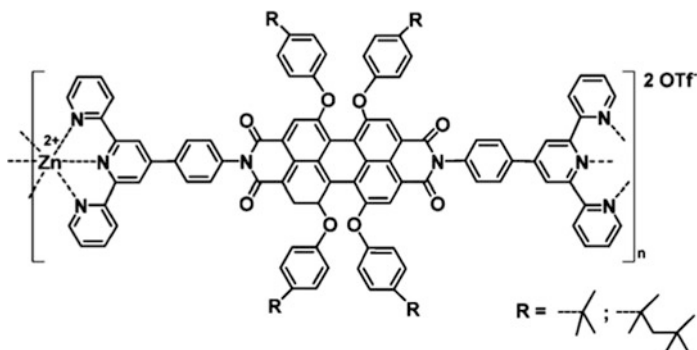
For Zn(II) MSP based on bis-tpy ligands considerable effect of a metal ion on EL properties of synthesized MSP is typical [158, 202]. Zn(II) MSP has shown very good luminescent properties (very strong red-light-emitting) with high potential for integration in layered polyelectrolyte devices. Also incorporation of Zn(II) ions in MSP through polycondensation of bis-tpy ligands carrying different π-conjugated architectures of a spacer is studied (Scheme 7.4) [203]. The obtained chain-extended Zn(II) MSP has shown emission from violet to yellow.

Two routes of incorporation of bis-tpy ligands carrying chromophores or π-conjugated spacer into polymer structures via Zn(II) suprapolymerization have been developed (Scheme 7.5) [204, 205]. For these polymers blue emission of photoluminescence (about 420 nm) with quantum yield from 11 to 23% (in DMF) is typical, and in this case formation of excimers is suppressed by integration of Cz side groups. Besides, obtained MSP have shown green emission of EL (about 550 nm).

A vast variety of labile tpy MSP is obtained [193, 206–208]. In particular, by studying MSP formation based on bis-tpy PEG (M_n = 8000) with different transition metal ions the effect of metal ions such as Cd(II), Cu(II), Co(II), Ni(II), Fe(II) on DP and resulting molecular weights is considered.

We shall also notice [209] MSP production by chelation of dimethyl-substituted bis-tpy ditopic ligand with Ru(II), Fe(II), Co(II) ions in respective solvent. In this case stoichiometry 1:1 of chelation of a ligand with a metal ion in MSP is confirmed, affinity constants (log K) are very high (>9) showing that spatial hindering of the ligand methyl groups has no effect on formation of MSP.

Formation of metal-bis-tpy MSP is influenced by two main factors of chelation. The first is the formation of a mono-tpy-chelate by coordination of one tpy ligand to one metal ion. At the second step the bis-tpy-chelate is formed by addition of another ligand in the system. Possible exchange in the solution between ligand, metal ion, mono-chelate and bis-chelate comprehensively described for tpy MSP [73, 76].

Extremely interesting is production of thin filmed databases of Zn(II) bis-tpy MSP produced by jet-printing for studying structure-property relationship and their possible using for organic photoelectric or PLED applications [210]. During using
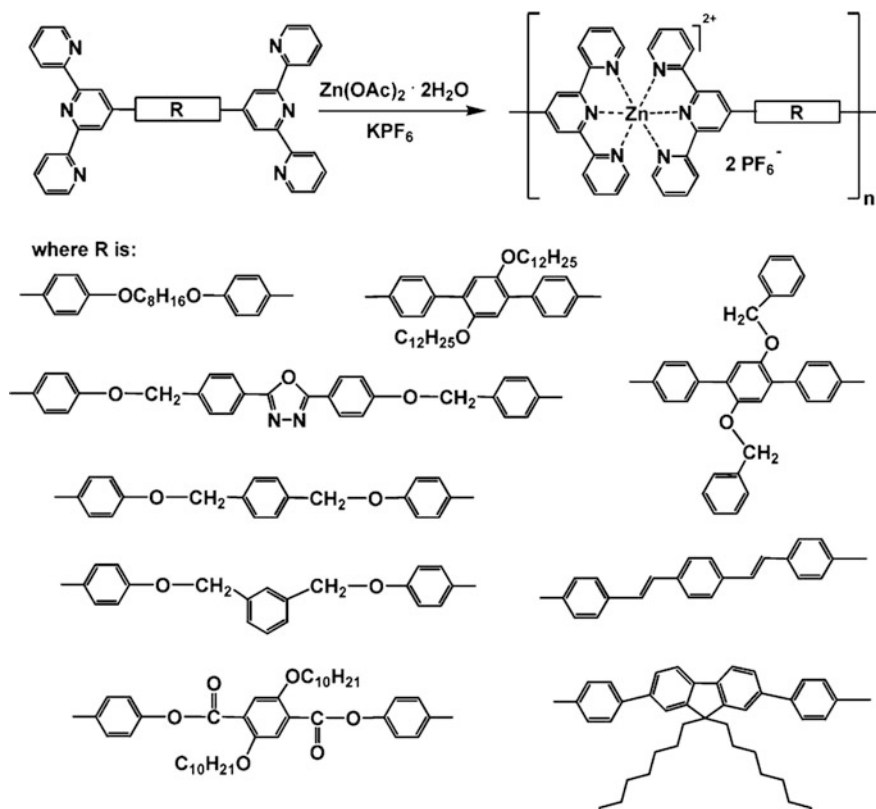
Scheme 7.4 Schematic representation of synthesis of Zn(II) MSP based on bis-tpy ligands [203]

combinatorial approach different important parameters including system of solvents, dot spacing and a substrate temperature, as well as properties of UV-vis absorption and emission were subjected to efficient and reproducible screening in materials. As a result, homogeneous films of thickness 150–200 nm were obtained during printing at 40–50 °C and from the mixture of DMF and acetophenone solvents in the ratio 90/10.

Promising is using labile metal chelates for building chiral forms, since they offer dynamic transformation of chiral molecular form as response to external stimuli (Fig. 7.7) [211].

MSPs are obtained by coordination polycondensation reaction of tpy-functionalized polyhedral silsesquioxane with Co(II) and Cu(II) ions [212]. It occurs that optical and electrochemical properties of MSPs depend on substituent in peripheral pyridine, and MSPs themselves have electrochromism during the oxidation process.

MSPs based on tpy ligands have recently shown their potential to optoelectronic applications based on (i) their excellent properties of charge transfer or
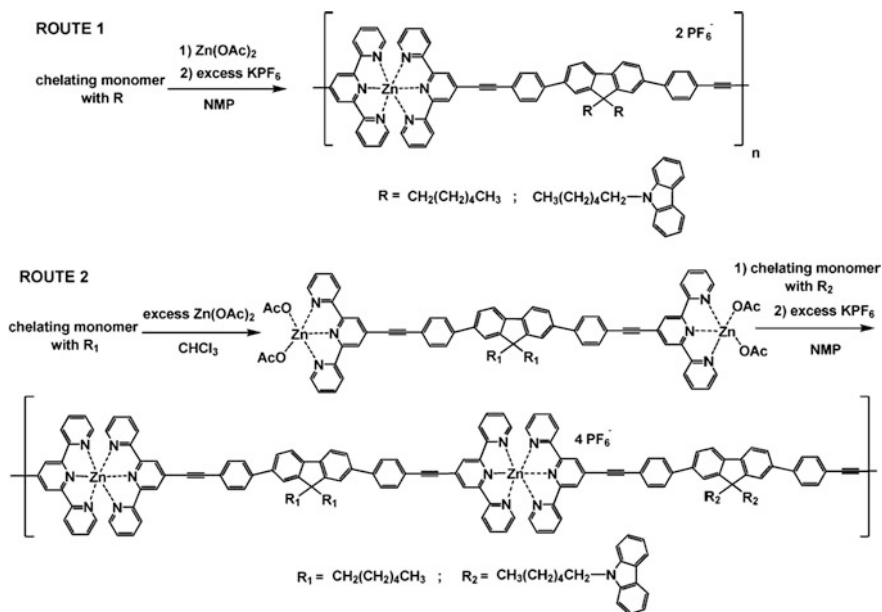
Scheme 7.5 Scheme of synthesis of Zn(II) homopolymers (route 1) and Zn(II)-*alt*-copolymers (route 2) [204]
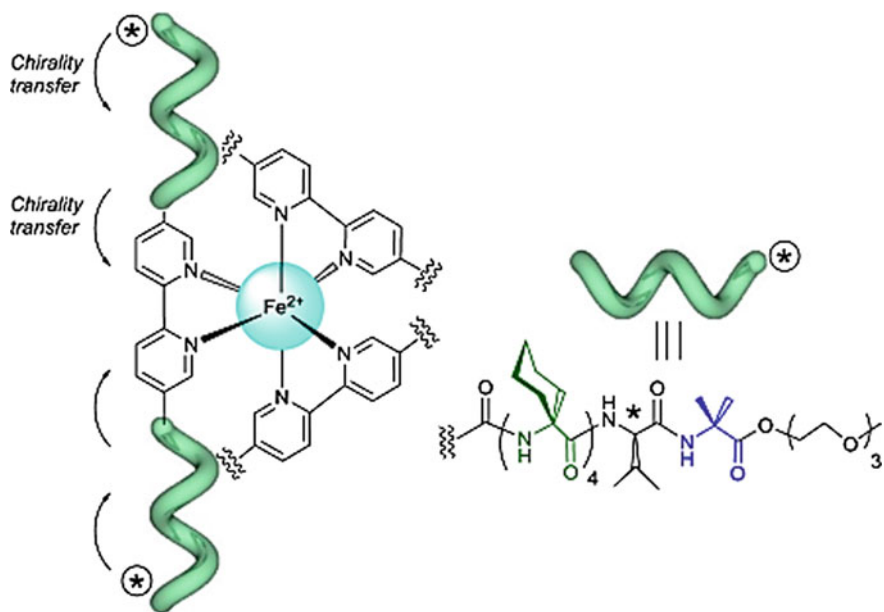
Fig. 7.7 Chirality induction in an octahedral tris-bipyridyl Fe(II) complex induced by (S)-valine via a helical tetrapeptides [211]

(ii) intriguing luminescent properties of the system, depending on their architecture, and the general properties of the luminescence correlate with the polymer structure [213].

Importantly, the architecture of the polymers and types of metal coordinated to tpy-containing MSP, can lead to unique photophysical properties [11, 13, 214]. As a result, quenching or increase in polymer fluorescence can change making it possible to apply MSPs as luminescent sensors for metal ions and in photo elements [13, 75, 215–217]. For example, tpy-containing Ru homo- and copolymers are used for production of polymer solar elements and solar elements sensitized by a dye [217]. These MSPs are obtained on the basis of poly (*p*-phenylene vinylenes) functionalized with terminal tpy residuals, and can quench fluorescence, thus showing that polymers can transfer energy to tpy-containing Ru chelates.

R¹ = R² = H
R¹ = R² = CN
R¹ = CN; R² = H
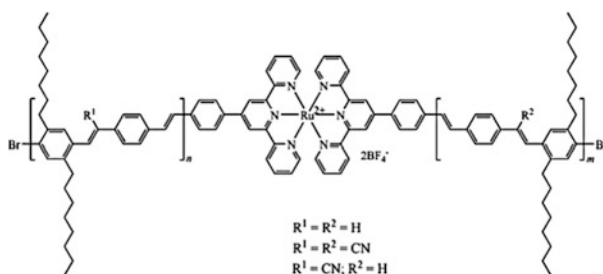
Considerable efforts were taken in recent years for development of new metallosupramolecular architectures of dyes, since they are of keen interest as modeling systems for natural light-harvesting and photosynthetic complexes, and for potential applications in solar energy transformation, photonics, and molecular electronics. Various metallosupramolecular assemblies of dyes are recently built using M–L coordination [218].

Another way to obtain these macromolecular assemblies is integration of fluorescent dye anion (sulforhodamine, SRB) in Fe(II)-based MSP via counter-ion exchange (Fig. 7.8) [219]. Solid state device made using the obtained polymer shows electrochromic properties based on electrochemical redox of Fe(II) ions at voltage ±2.8 V, which displays due to appearance and disappearance of MLCT absorption in MSP.

The Zn and Cd MSPs are produced based on 1,4-diketo-pyrrolo[3,4-*c*] pyrrol derivatives of ditopic tpy-ligands [220]. It occurs that MSPs modified by a phenyl block have shown maximum absorption at about 504 and 506 nm in films, while MSP, in which a thiophene fragment is incorporated, exhibited strong and wide visible absorption at 300–800 nm with a maximum at 601 and 598 nm and shoulder peaks at about 665 and 671 nm, respectively.

The Zn MSP, carrying dibenzo-24-crown-8 arms, is obtained by coordination of Zn(II) ions with conjugated bis-tpy ligand, which shows depending on concentration emissions from blue to white and yellow (Fig. 7.9) [221].
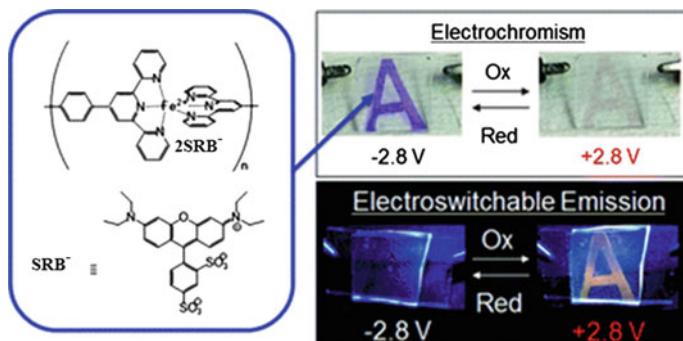
Fig. 7.8 The electrochemically reversible photoluminescence of sulforhodamine B (SRB) anions is demonstrated based on the redox of Fe ions in a MSP [219]

Fig. 7.9 Zn MSP, carrying dibenzo-24-crown-8 arms, which shows depending on acid-base concentration emissions [221]

Tridentate 2,6-bis(1′-methyl-benzimidazolyl)-4-hydroxypyridine (BIP) is a universal ligand for building stimulus-responsive MSP (Scheme 7.6) [196, 222–224].

An interesting class of soluble Eu(III) MSPs is developed [225] on the basis of tridentate ditopic pybox ligand, which shows high metal emission quantum yields up to 73%, and also unique dynamic behavior in solution (Fig. 7.10).

Chelating ligands containing 2,6-bis(1,2,3-triazole-4-yl) pyridine (btp) fragment is one of widespread motifs in chemistry during last decade [226]. This class of ligands formed in one-pot click reaction is studied for different purposes, for example, for generation of supramolecular self-assembling d- and f-metals, and formation of dendritic and polymer networks, etc. For example, Eu(III) and Tb(III)-directed assembly of btp ligands is studied in CH$_3$CN using monitoring of their different photophysical properties. As a result, stoichiometry and stability constants of different chiral supramolecular assemblies in solution have been found [227].
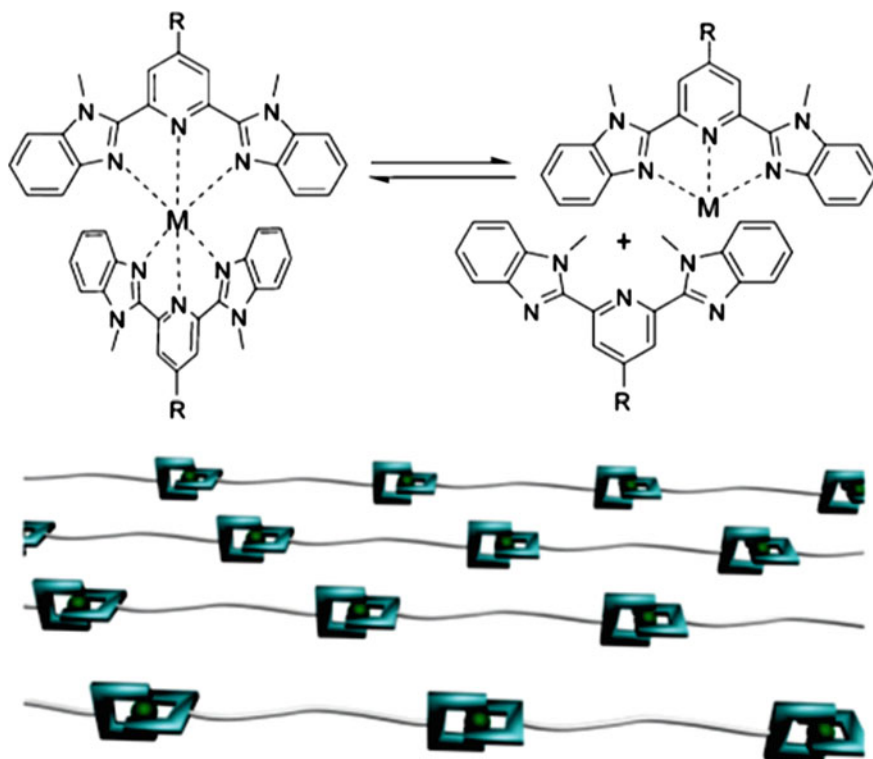
Scheme 7.6 Reversible dimer formation from two BIP molecules driven by M–L coordination and cartoon representation of the formation of MSP based on this dimer formation
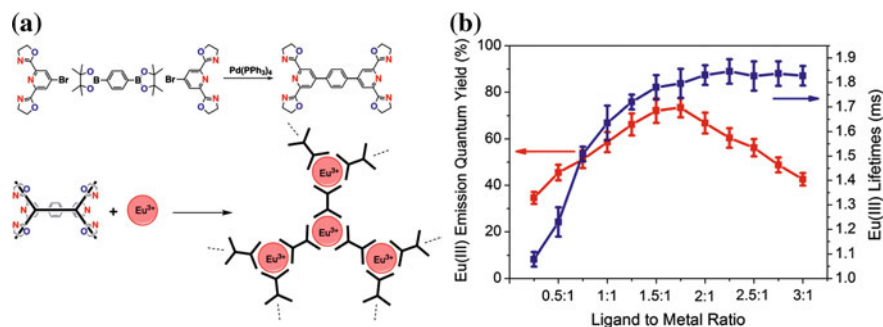
Fig. 7.10 a Ligand synthesis and schematic representation of the preparation of soluble dynamic Eu(III) MSPs with pybox-related ditopic ligands. **b** Relative Eu(III) emission quantum yields (left axes) and Eu(III) emission lifetimes (right axes) for different ligand to metal ratios in chloroform/acetonitrile [225]

Ditopic btp ligands containing π-conjugated spacer and solubilizing groups involved in the click reaction are used for synthesis of Ru(II) MSPs, which have intensive absorption of visible light by MLCT. As it turned out, MSPs obtained have high molecular weight and medium hardness. Studies of polymers in solid state have confirmed formation of MSPs, whose macromolecules have rod-like conformation (Fig. 7.11). Besides, polymers form films by coating solutions drop-casting [228].

Another widespread ligand for MSP production is 2,6-bis(1′-methylbenzimidazolyl) pyridine (Mebip). In particular, MSP synthesis based on poly (*p*-phenylene ethynylene) and poly (*p*-xylene) macromonomers with Mebip terminal groups and different metal salts is developed [229, 230]. It is interesting that oppositely to other MSPs, where character of a metal salt and counter-ion plays important role, only insignificant differences in obtained MSP properties were observed depending on a metal ion, for example, Fe(II), Zn(II), La(III), and counter-ion (ClO_4^-, OTf^-, NTf_2^-). Instead of it, properties of the studied MSPs are determined, first of all, by the character of telechelic oligomer.

Another type of tpy back-to-back ligand 1,4-bis(1,2′:6′,1″-bis-pyrazolylpyridin-4′-yl) benzene was developed [231], which was used for production of linear Fe(II) supramolecular oligomer/polymer (Scheme 7.7). Synthesized MSP has shown reversible spin transition above room temperature with wide hysteresis loop (about 10 K).

Neutral linear dynamic MSPs based on acyl hydrazone bound with Co(II), Ni (II), Zn(II) and Cd(II) ions are obtained using metallosupramolecular polymerization [232]. Choice of monomer ligand, as was established, takes place in a mixture of subcomponents (carboxyaldehydes and bisacyl hydrazides) controlled by hexacoordination to a certain metal ion. It is important that MSPs change their constitution by exchanging and reshuffling their components with other MSPs through exchange of ligands at coordination site of a metal in solution and in neat phase (Fig. 7.12). As a result, these MSPs are subjected to considerable changes of their mechanical and optical properties.
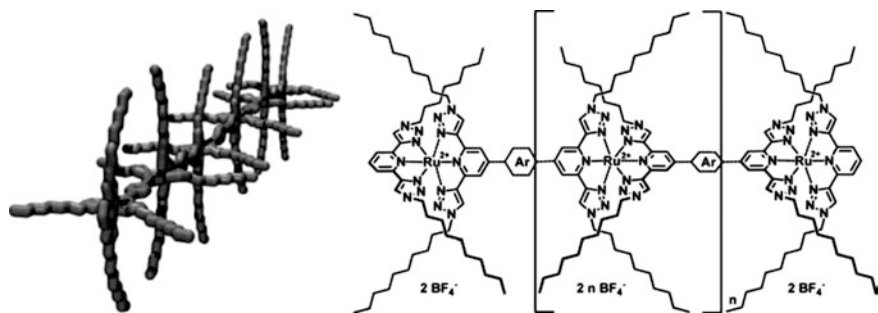
Fig. 7.11 Rod-like conformation in the solid state and structure of Ru MSP based on ditopic btp ligands featuring a π-conjugated spacer and clicked-on solubilizing groups
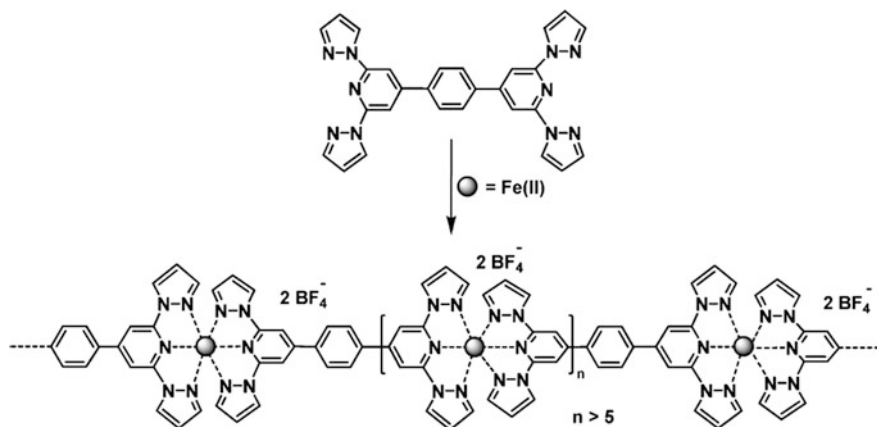
Scheme 7.7 Schematic representation of Fe(II) MSP based on 1,4-bis(1,2′:6′,1″-bis-pyrazolylpyridin-4′-yl) benzene
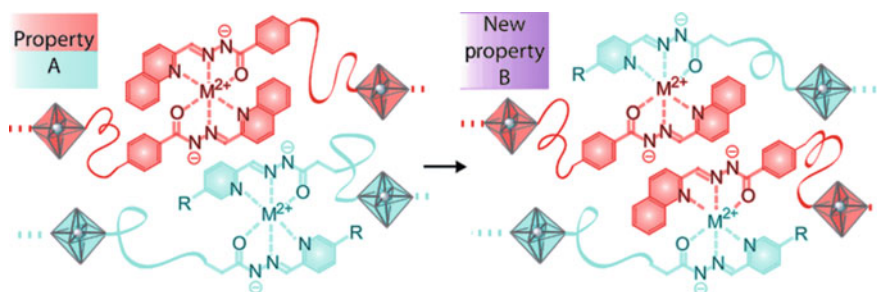
Fig. 7.12 Scheme of the transformation of properties that result from constitutional M–L exchange reactions in dynamic MSPs

Interesting concept for MSP synthesis is application of ionophore ligands, which, as is known, are bound with high affinity to alkali metal ions. Thus, tris (spirotetrahydrofuranyl) ionophores with rigid spacers are constructed from 1,3-butadiyne units, which are selectively linked with Li(I) in 2:1 complex with formation of rigid rod-like MSP, which, however, is limited soluble [233].

Also MSP should be noticed, containing (triethanolamine) Cu(II) fragments linked by pyromellate units, which can be used as a catalyst precursor for peroxidation of cyclohexane into cyclohexanol and cyclohexanene with hydrogen peroxide at room temperature [234, 235].
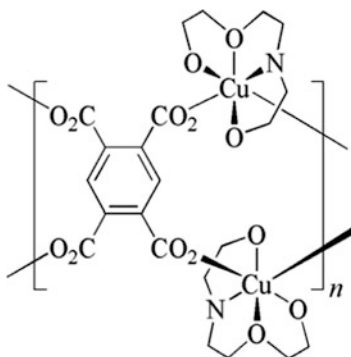
If oligomers or polymers with chelating fragments at a chain ends are used in the process of metallosupramolecular polymerization, various linear metallosupramolecular block-copolymers can be obtained [236]. This brings to systems, which combine typical features of block-copolymers (for example, microphase separation between immiscible constituent blocks), and supramolecular polymers (for example, reversibility and retuning supramolecular bonds strength). In this case M–L coordination can be used for bridging between different blocks of homopolymers or for linking together different block-copolymers.

In this way, for example, di- and tri-block-copolymers (A-[M]-B [237–239], A-[M]-B-[M]-A [240, 241] or A-[M]-B-*b*-C [239, 241] were obtained, where [M] is an M–L center. If A, B, and C blocks are immiscible, then these block-MSPs can behave as amphiphilic block-copolymers with self-assembling character. The only ligand used presently for block-MSP synthesis is tpy [236]. It is important that asymmetrically directed supramolecular interactions should be involved for formation of these complex macromolecular architectures [242]. In other words, the synthesis of block-MSPs requires the formation of heteroleptic complexes, and the formation of homoleptic complexes should not occur. For such selective complexation two-staged procedure of chelation is necessary. Really, first a mono-chelate should is formed, which then is developed into desired bis-chelate under certain conditions [243]. Most extensive studies on the subject were performed for block-MSP Ru, since high stability of bis-tpy-Ru(II) chelates makes it possible to preserve integrity of resulting block-copolymers in different media, such as organic solvents or water, even at extreme pH and salt concentrations [244].

Efficient way of block-MSP synthesis is growth of two polymer blocks from heteroleptic Ru chelate, which acts as double initiator, since chelation will take place between small molecules [243]. The most well-studied system in this aspect is PS-[Ru]-PEO block-copolymer and, in particular, PS$_{20}$-[Ru]-PEO$_{70}$ composition, in which PEO obtained by NMRP method, and commercially available PS are used, and numbers bottom mean average DP of PEO and PS blocks, respectively [245].

It should be noted that formation of homo- and block-MSPs depends considerably on reaction conditions, such as stoichiometry of reagents, a solvent and a salt type, time, temperature, and concentration.

The amphiphilic block-MSPs allow for purposeful formation of micellar aggregates in water [245–248]. Thus, slow and regular water addition, using a syringe pump, to the PS_{20}-[Ru]-PEO_{70} initial solution of copolymer in DMF brings to strictly defined micellar solution almost without further aggregation of micelles. At that, these micelles have shown single-mode size distribution with average molecular weight 318,000, which corresponds to aggregation number 53 of copolymer chains in a micelle [249].

Interesting observations were made when studying PS_{20}-[Ru]-PEO_{70} copolymer in melt. In particular, when hexafluorophosphate (PF_6^-) was used as a counter-ion, the observed morphology was spherical, not expected laminar, taking into account the copolymer composition [249]. Due to aggregation of tpy-Ru(II) chelates and counter-ions spherical aggregates are formed with radius about 1.5 nm surrounded by a polymer shell with external radius about 2.4 nm. When bulk tetraphenylborate (BPh_4^-) was used as a counter-ion, highly ordered laminated melt was obtained with 11.9 nm periods after annealing at 55 °C for 40 h [250]. These studies of nanometer organization of PS_{20}-[Ru]-PEO_{70} in both selective solvents and in volume have shown considerable effect of bis-tpy Ru chelates on microphase separation between PS and PEO blocks. Similar conclusions were made for investigation in melt of viscous-elastic properties of linear supramolecular assemblies obtained by addition of various amounts of Ni ions to linear entangled PEO building blocks with terminal modified tpy group [251]. In particular, it occurs that elasticity of these supramolecular assemblies is mainly determined by dynamic of entanglement of building blocks, while supramolecular interactions impede or suppress their relaxations. At that, by regulation of a number of metal ions, it is possible to control relaxation time and level of low-frequency plateau of these supramolecular assemblies. It is important that additions of metal ions more than 1:2 metal ion/tpy stoichiometric ratios makes it possible to induce secondary supramolecular interactions, which can bound linear supramolecular assemblies and, thus, bring to gelation of a system.

Since the method of production of block-MSPs depends on combination of two macroligands through simple two-staged synthesis, it is quite easy to create database of block-copolymers. For example, thus obtained 4×4 database of PS-[Ru]-PEO block-copolymers and morphology of produced thin films were studied [252]. We shall also notice another 13-member database, which was used for studying behavior of micelle formation of block-MSPs in water [253]. Apart from formation of copolymer databases, one more advantage of block-MSPs is in reversibility of bis-tpy chelates. Really, oxidation of Ru(II) ions to Ru(III) should be accompanied by transformation of initial bis-chelates into mono-chelates. This reversibility can be used predominantly for formation of definite nanoporous structures, which was shown in production of nanoporous thin films of PS_{375}-[Ru]-PEO_{225} copolymer [254].

Apart from PS-[Ru]-PEO metallosupramolecular copolymers, we shall notice amphiphilic poly (ethylene-*co*-butylene)-[Ru]-PEO copolymer, for which quasi-equilibrium state is found between micelles and clusters presumably, due to softness of micellar core. Addition of a great excess of water-soluble competitive ligand brought to decomposition of bis-tpy chelates and appearance of water-dispersed poly (ethylene-*co*-butylene) nanoparticles decorated by charged metal complexes on their surface [237, 238]. Rod-like micelles were obtained [255] from poly (Fc-silane)-[Ru]-PEO copolymer in water and the micelles had a constant diameter, but were rather polydisperse in length. Also synthesis of amphiphilic PS-[Ru]-poly (NIPAM) using RAFT polymerization with tpy-functionalized agent of chain transfer is described [256].

It should be noted amphiphilic diblock-MSPs containing heteroleptic bis-tpy chelates Co(II) and Ni(II) in a block junction of PS and PEO (Fig. 7.13) [257].

Straightforward approach to synthesis of AB_nA block-copolymers through tpy-Ru(II) chelation is described (Scheme 7.8) [258]. The applied approach of combinatorial optimization made it possible to carry out systematic screening of optimal conditions for one-pot polymerization reaction of bis-tpy-hexadecane with $RuCl_3$ under reduction conditions. The established laws were applied for purposeful synthesis of $Ru(II)AB_nA$ supramolecular triblock-copolymer using mono-tpy-PEG as chain stopper during reaction of metallosupramolecular polymerization of bis-tpy-hexadecane.

Individually optimized synthetic approaches were used to study of the formation of AB_nA supramolecular triblock-copolymers based on Ni(II), Fe(II), and Co(II) chelates [240]. For Ni(II) AB_nA supramolecular triblock-copolymers end capper treatment was varied to regulate length of the medium block B. It is important that synthesized triblock-MSPs are self-assembled in aqueous solution due to their amphiphility.

Metallosupramolecular PS-*b*-polyisoprene-[Ni]-PS triblock-copolymer is prepared efficiently using two-stage procedure (Fig. 7.14) [259]. It should be noted that metal chelates are located predominantly in adjacent spherical area and form a core-shell structure, and the obtained multiphase material has different elastomer properties with considerable strength and creep.

Also we should mention triblock-copolymer ABC obtained by chelation of tpy-functionalized PS-*b*-P2VP with tpy-functionalized PEO [241], which is used
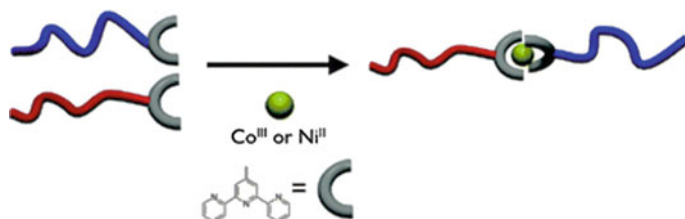
Fig. 7.13 Synthetic scheme towards the formation of PS_{240}-[Co]-PEO_{230} and PS_{240}-[Ni]-PEO_{230} metallosupramolecular block-copolymers [257]
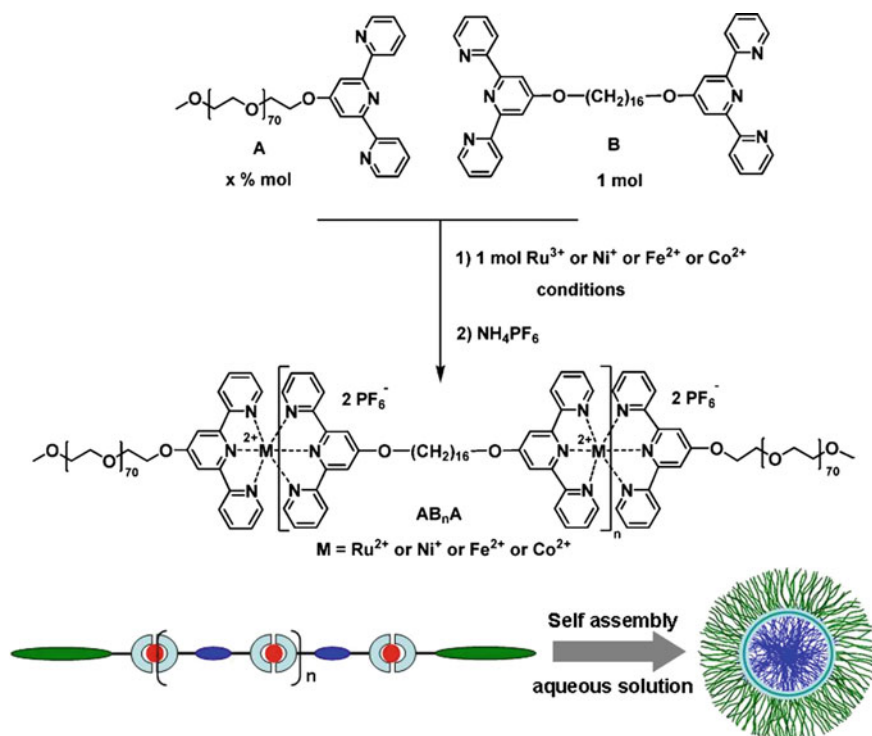
Scheme 7.8 Synthesis of supramolecular M(II)-AB$_n$A triblock-copolymer and schematic representation of micelle formation [258]
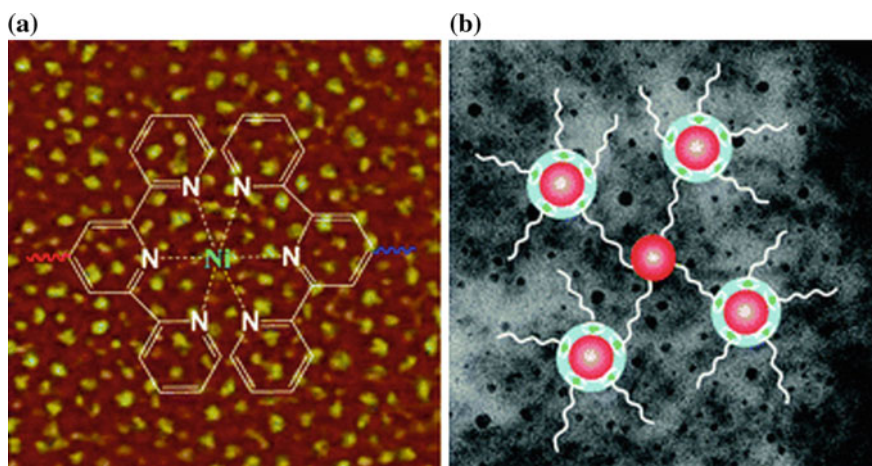
Fig. 7.14 AFM phase image (**a**) and TEM image without staining (**b**) of metallosupramolecular triblock-copolymer

for preparation of core/shell-crown micelles consisting of PS core, P2VP shell, and PEO crown, where P2VP is poly-2-vinylpyridine.

It should be noted that linear MSPs provide control over dynamic helicity at supramolecular level [260]. Strong M–L interactions between individual molecular components in controlled helical nodes, beginning from columnar aggregates to spiral polymers and cholesteric liquid crystals bring to stereo induction from molecular level to the level of supramolecular helical architectures.

7.4   Branched Metallosupramolecular Polymers

Telechelic ligand molecule with three chelating ends can be used to obtain branched MSP (Fig. 7.15a) [140]. Branched MSPs can also be formed in the mixed system of ditopic ligands and f-block of metal ions [77, 129, 261, 262], where f-block metal ions can link three chelating ends, which act as cross-linkers (Fig. 7.15b).

Two constitutional isomers of branched MSPs are self-assembled from tpy-ligands in ternary system [263]. Restrictions of possible outcomes for self-assembling finally provide optimal conditions for isolation of molecular bowtie or its isomer butterfly motif. It is noteworthy that these structural isomers have very different drifts in diversification of ionic mobility corresponding to different sizes and forms at high charge states.

Interesting chelating ligand for branched MSP fabrication is hexathiobenzene carrying six peripheral tpy units (Fig. 7.16), which can excite coupled aggregation-induced emission (AIE) reflected by a core in solid state [264]. Phosphorescence of hexathiobenzene core is involved during chelation of Mg(II) in THF, because M–L coordination impedes intramolecular rotation and the chromophore core motion, thus helping to radiation deactivation of the luminescent excited state. When [Mg(tpy)$_2$]$^{2+}$ units of a polymer structure are excited, the phosphorescence core sensibilization has efficiency >90%. It is important that a polymer light-harvesting
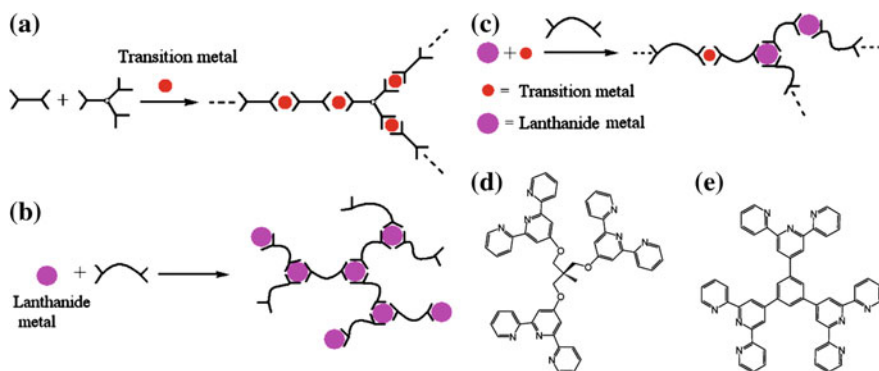
Fig. 7.15 **a–c** Illustration of branched MSP and **d** and **e** examples of branched ligands [140]
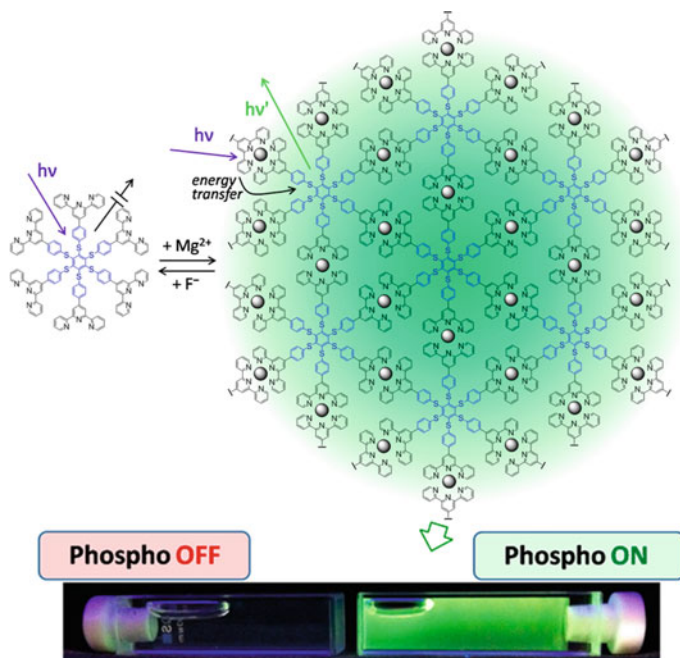
Fig. 7.16 Simplistic 2D representation of the self-assembled structure and aggregation induced phosphorescence of the hexathiobenzene core is turned on upon Mg(II) chelation [264]

antenna can be decomposed with a fluoride ion addition, thus switching off emission and offering a new tool for the fluoride ion probing. In other words, this unique system can be a sensor of cation or anion.

Among branched MSPs, a special place take star-like MSPs [236, 265], obtained using widespread bpy ligand, which forms complexes with a vast variety of metal ions and is ideal candidate for production of multi-armed star-like MSPs, because bpy functionalized in 4- and/or 4′-position can be quite easily synthesized. To produce star-like MSPs, two approaches are made based either on homoleptic chelates, in which metal ion is coordinated with similar chelating ligands, or on heteroleptic chelates, in which different polymer ligands are coordinated around a metal center. An example of the first approach is production of six-armed star-like block-copolymers with $[Fe\{bpy(CH_2Cl)_2\}_3](PF_6)_2$ used as hexafunctional initiator for oxazoline polymerization [266]. The first block was formed from hydrophilic 2-ethyl-2-oxazoline, and the second block is formed from hydrophobic 2-phenyl-2-oxazoline or 2-undecyl-2-oxazoline. Studying morphology of films of six-armed star-like copolymer has shown [267] that 2-ethyl-2-oxazoline block forms cylindrical micro domains in poly (2-undecyl-2-oxazoline) matrix. In another example $[Ru\{bpy(CH_2OH)_2\}_3](PF_6)_2$ is applied as a hexafunctional initiator for production of six-armed star-like copolymer using ROMP and ATRP combination [268]. We shall also notice use of $[Fe(II)\{5,5''\text{-bis(bromomethyl)-tpy}\}_2](PF_6)_2$

complex as a metal supramolecular initiator for living polymerization of 2-ethyl-2-oxazoline bringing to clearly defined hydrophilic polymers with central supramolecular building block and star-like architectures [269]. It is important to emphasize that using metallosupramolecular initiators for living polymerization provides precise control over molecular weight, and also integration of additional (chelating) fragments at the ends of polymer chain [155].

Using approach based on homoleptic complex, also hetero-armed star-like copolymers can be obtained; however, this needs orthogonal synthesis of asymmetric macroligands from a double initiator. The 4-chloromethyl-4′-hydroxymethyl-bpy is used as such a double initiator for consequent polymerization of ε-caprolactone using ROMP and St with ATRP [270]. At the final stage bpy-PS-poly (ε-caprolactone) macroligand is coordinated with Fe(II).

We shall also notice production of hetero-armed star-like copolymers based on heteroleptic complexes. In particular, macroligands carrying one or two PS chains are first ATRP synthesized using 4-(chloromethyl)-bpy and 4,4′-bis-(chloromethyl)-bpy as initiator, respectively [271]. Then bis-bpy Ru complexes are obtained with these macroligands, and at the final stage the second type of a macroligand carrying one or two PMMA chains also produced using ATRP, is linked to bis-complexes giving hetero-armed star-like copolymers with 3 and 6 arms. It should be emphasized that an important factor of adjustment for control over hetero-armed star-like copolymer assembling is polarity of a solvent, which has an effect on conformation of polymer chains.

Six-armed star-like copolymers are obtained via two-staged synthesis: formation of Ru bis-bpy chelate with microligand carrying two PCL chains obtained by ROMP followed by chelation with bpy, carrying either two PS chains (grown using ATRP) or two PEG chains obtained by grafting PEG to 4,4′-bis-(chloromethyl)-bpy using Williamson reaction (Scheme 7.9) [272].

Apart from bpy ligand other chelating ligands were used for synthesis of hetero-armed star-like copolymers. For example, ligands from the family of
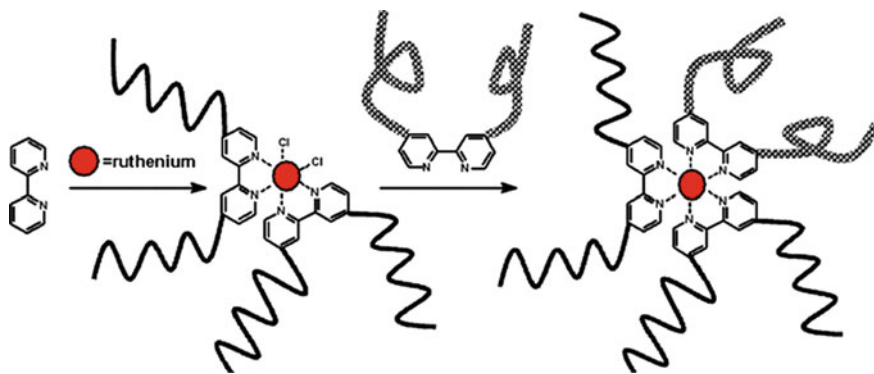
Scheme 7.9 Synthesis of polymeric Ru(II) bis(bpy) dichloride complexes and Ru(II) tris(bpy)-centered heteroarm stars [272]
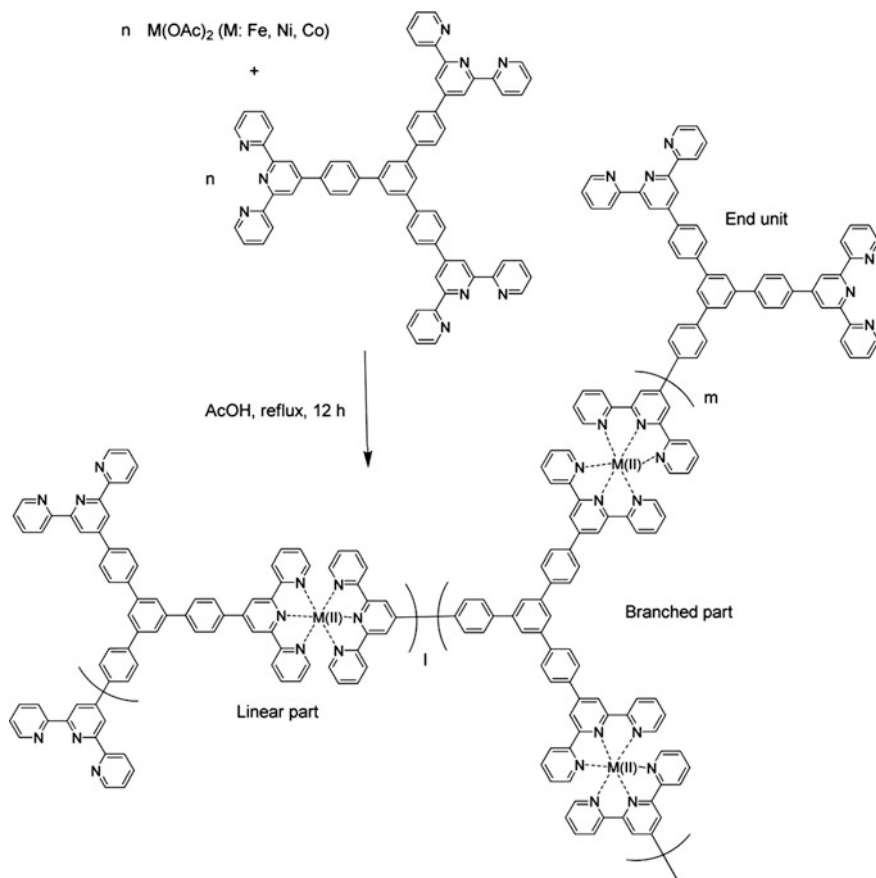
Scheme 7.10 Production of Fe(II)-, Co(II)- and Ni(II)-based MSPs including linear and branched parts [274]

β-diketones in combination with bpy are chosen for building heteroleptic complex with lanthanide ion [273]. First macroligands are obtained by D,L-lactide polymerization using ROMP with dbm functionalized by a hydroxyl group as initiator, and then three macroligands are chelated to Eu(III) to obtain three-armed star. At the final stage, bpy carrying two PCL chains are coordinated to this tris-complex to obtain penta-armed star-like block-copolymer.

There is an interesting application of tris-chelating ligand for production Fe(II)-, Co(II)- and Ni(II)-based MSPs including linear and branched parts in their structure (Scheme 7.10) [274].

It should be especially noted that each part of metallosupramolecular block-copolymers makes its contribution to properties of resulting materials [108]. Besides, self-assembling these copolymers is used in thereafter for development of more advanced architectures, in particular, smart, and stimulus-responsive nanostructures.

7.5   Cross-Linked Metallosupramolecular Polymers

Reversible M–L coordination interactions between monomer units are actively used in synthesis of MSP networks [77, 78, 129, 130, 261, 262, 275, 276]. Multiple MSP networks are synthesized with different mechanical, chemical, and stimulus-responsible properties, which can be easily controlled by fine tuning molecular architecture, and also thermodynamic and kinetic stability choosing respective M–L pairs [75, 76, 277]. It should be emphasized that rational design of MSP networks needs a clear idea on correlation between supramolecular building blocks and properties of resulting material [40, 129, 262, 275, 276].

Thus, self-assembling is done in solution between Eu(III) and rigid ditopic tridentate tpy ligand, which brings to formation of MSP networks (Fig. 7.17) [278]. Depending on M–L ratio used for initial self-assembling process, morphology of these materials can be changed from 1D micron fibers to 3D coordination network. It should be noted that tpy-based ditopic ligand can be efficient sensor for Eu(II) emission, hence, emission lifetimes and energy of a ligand in triplet state of MSP depends considerably on M–L ratio. Therefore, the obtained micron-sized fibers can be efficient optic wave-guide for Eu(II) radiation.

Similar dependence of surface morphology on M–L ratio is established in the series of Fe(II)-based MSPs with 3D structures obtained by staged chelation of Fe(II) salt with different ratios of linear bis-tpy (L1) ligand and branched tris-tpy (L2) ligand (Fig. 7.18) [279]. All 3D polymers had blue color due to MLCT absorption,
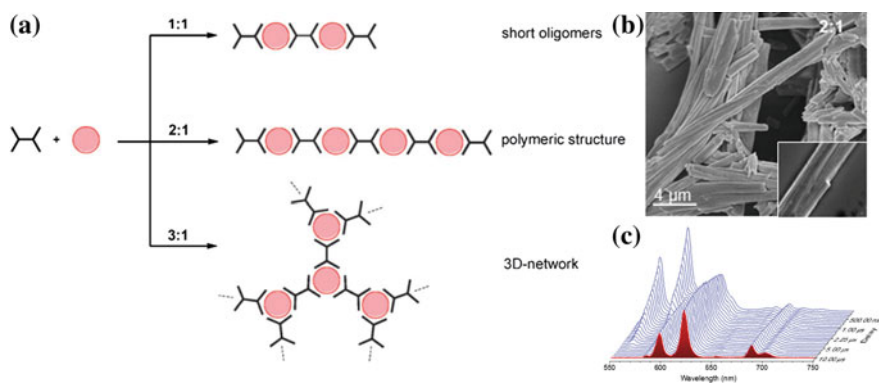
Fig. 7.17   a Proposed mechanism for the self-assembly process in solution at different M:L ratios. **b** SEM images of the samples in the solid state: M:L ratio 1:1 (a), 2:1 (b), 3:1 (c). **c** Time-gated emission maps for the $^5D_1-^7F_J$ (J = 0–3) and $^5D_0-^7F_J$ (J = 0–4) transition recorded between 100 ns and 10 ms (500 ns gate, 2 nm band width) [278]
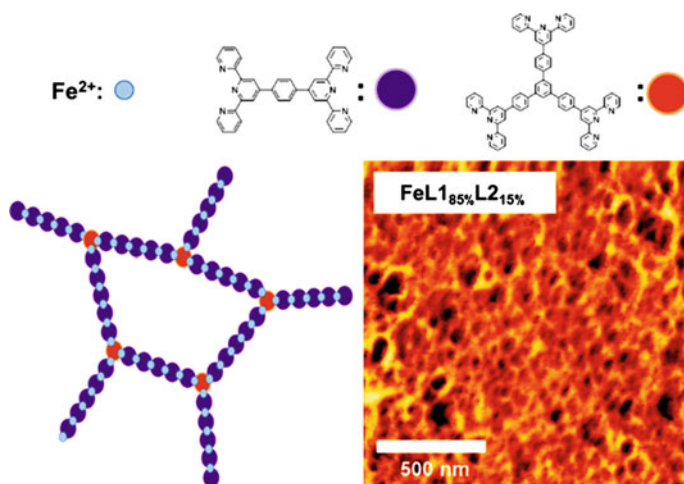
Fig. 7.18 Synthesis and AFM image of the 3D Fe(II)-based MSP with different content of L1 and L2 [279]

and showed excellent electrochromic properties. In particular, the most highly porous 3D structured film has shown the best electrochromic efficiency: as compared with 1D linear polymer, switching times for dying ($0.31 \rightarrow 0.19$ s) and for bleaching ($0.58 \rightarrow 0.36$ s) are improved by 37.9 and 38.7%, respectively. Besides, the transmission coefficient has increased by 21.8% ($41.6 \rightarrow 50.7\%$), and efficiency of dying has increased by 45.3% ($263.8 \rightarrow 383.4$ cm^2 C^{-1}).

It should also be noted that MSP networks can form via M–L coordination with participation of preliminary formed polymer chelating ligands. In particular, coordinated self-assembling Zn(II) ions and polytopic polyiminofluorene-tpy ligands is used for production of electrochromic films with nanometer thickness (Fig. 7.19). The films can be switched between yellow, red, and blue, and show switching times 500 ms, high contrast and high stability [133].

Another example is chelation of ZnCl$_2$ and Fe(ClO$_4$)$_2$ with conjugated copolymer based on poly(phenylene-*alt*-fluorene) main chain and Mebip ligand linked to the main chain with flexible spacer groups (Fig. 7.20) [280]. Multiple successive adsorptions of metal salts and polymer bring to coordinated supramolecular assembling cross-linked MSP on a substrate, and thickness is controlled by a number of applied stages of adsorption. Since fluorescence of the polymer main chain is not completely quenched by M–L interaction, the films have bluish luminescence.

For CPL, it is typical to form micellar structures in diluted solutions, which decompose at addition of transition metal ions with formation of cross-linked MSP (Fig. 7.21). It has been shown, for example, in the cases of tpy end-capped by poly (2-dimethylamino) ethyl methacrylate-*b*-poly (NIPAM) diblock-copolymers [281], PS-*b*-poly (*tert*-butyl acrylate) with tpy-end-capped [282], tpy-terminal hydroxy-telechelic materials Pluronics P105 and P123 [283].
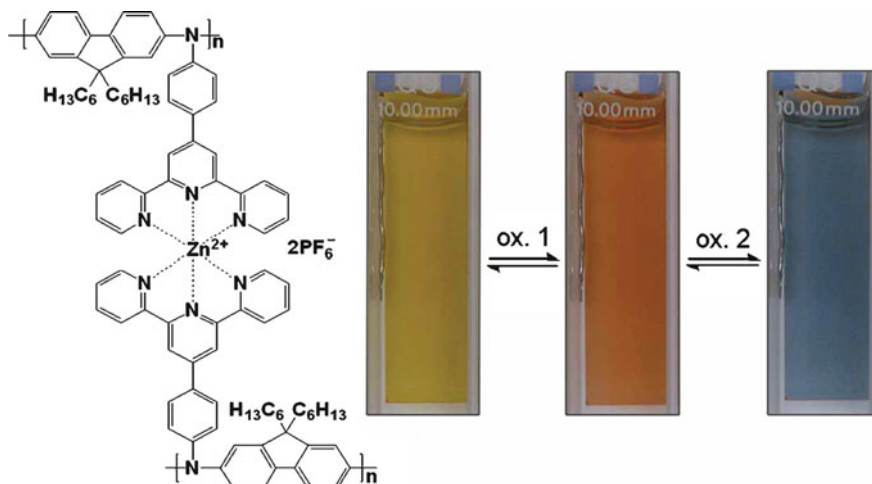
Fig. 7.19 Production of electrochromic films based on Zn(II) ions and polytopic polyiminofluorene-tpy ligands [133]
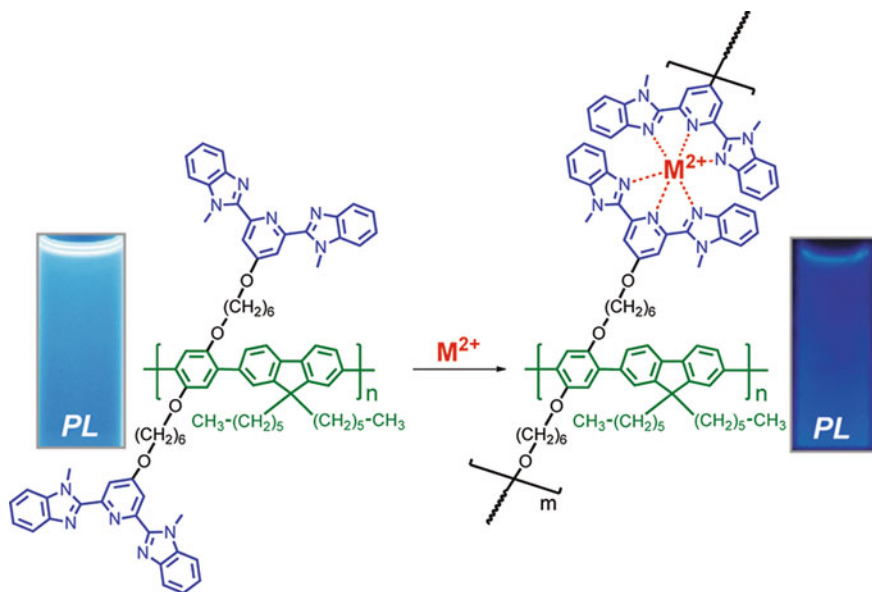
Fig. 7.20 Metal ion coordination of chelating polymer involving cross-linking side chains [280]

The process of formation of metallosupramolecular network based on 3:1 M–L complexes between ditopic oligomers and metal ions proceeds by formation of 1:1 and 1:2 complexes (Fig. 7.22) [284].

Metallo-Assembly | Free chains | Miccelar structures
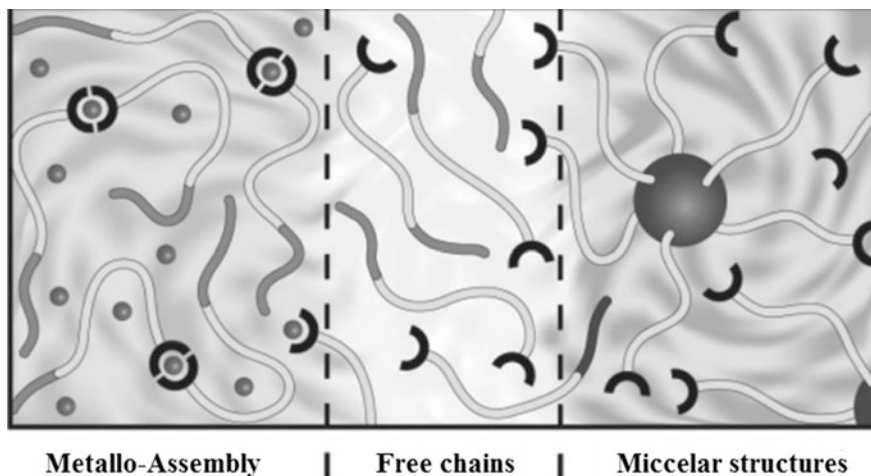
Fig. 7.21 Self-assembly behavior of poly (NIPAM)-*b*-poly [(2-dimethylamino) ethyl methacrylate-tpy] double-hydrophilic diblock-copolymers in aqueous solution in response to heat and transition metal ions [281]

Fig. 7.22 A schematic representation of metallosupramolecular polymers [284]
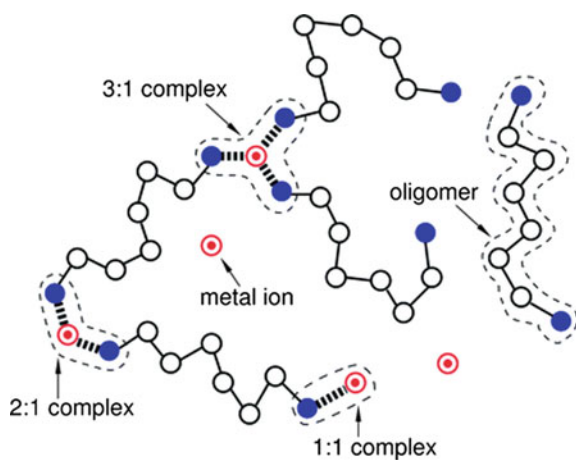
Monte-Carlo modeling has shown that this process is mostly influenced by concentration of chelating ligand and M–L ratio. At a constant concentration of ligand in the ligand-enriched area 3:1 M–L complexes predominate. Their fraction decreases as a metal content increases, bringing to 2:1 complexes with maximum about M–L ratio 1, and fraction of 1:1 complexes has maximum at M–L ratio 2. It follows from analysis of molecular-weight distribution and decreased average size of metallosupramolecular networks that a network formation takes place in restricted

range of M–L ratios. For example, at low concentration the reversible network begins to form in the range of M–L ratios about 0.75, where there is a considerable fraction of 2:1 as well as 3:1 M–L complexes, and as ligand concentration increases, network formation broadens to wider range of M–L ratios. At ligand concentration slightly over the beginning of a network formation it grows via integration of sol molecules into dangling fragments of the network. At higher concentrations this mechanism of network growth becomes inactive, and fraction of dangling fragments begins to decrease simultaneously with sol fraction. In the M–L range close to stoichiometric composition, the total number of oligomers in sol and dangling fragments are almost constant depending on oligomer concentration and becomes unity at the beginning of network formation.

7.6   Heterometallic Supramolecular Polymers

Strategy of coordination-driven self-assembling is successfully used for structuring such interesting assemblies as heterometallic supramolecular polymers (hetero-MSPs). It is principally important that integration of two different metals gives resulting hetero-MSP properties of individual metals as well as new properties stipulated by synergetic effect of one metal on another. To obtain such systems, different synthetic approaches are developed. In particular, the simplest of them includes stepwise chelation of two different metals, at that first monomer bis-complex of one metal with ditopic ligand is formed, and then metallosupramolecular polymerization with another metal takes place. An example of this approach can be stepwise chelation of Eu(III) and Fe(II) ions with asymmetric ligand based on dicarboxylate-substituted tpy and non-substituted tpy [285]. It should be noted that hetero-MSP has shown unique, reversible «ON-OFF» switching Eu(III) luminescence by electrochemical redox of Fe ions in solid state.

In another interesting example, independent coordination of Fe(II) and Rh(I) ions with one heteroditopic ligand containing two metal-coordinating centers at two ends has brought to formation of linear supramolecular polymers (Scheme 7.11) [286]. In this case different metals are specifically bound by different ligand fragments and take a certain kind of coordination geometry. The obtained hetero-MSP is interesting representatives of self-supported heterogeneous chiral catalysts, which have high activity, enantioselectivity, and for more than 10 times repeated use in heterogeneous asymmetric hydrogenation of different derivatives of functionalized olefins. These hetero-MSPs can be obtained by stepwise or one-pot synthesis, in which rigid tpy unit and soft MonoPhos fragment Feringa is coordinated selectively with Fe(II) and Rh(I) independently. It should be noted that Fe ions play a role of «glue» for self-support function way to link discrete fragments of a catalyst together, while Rh part is used as a catalytic center and as a spacer. It would be very
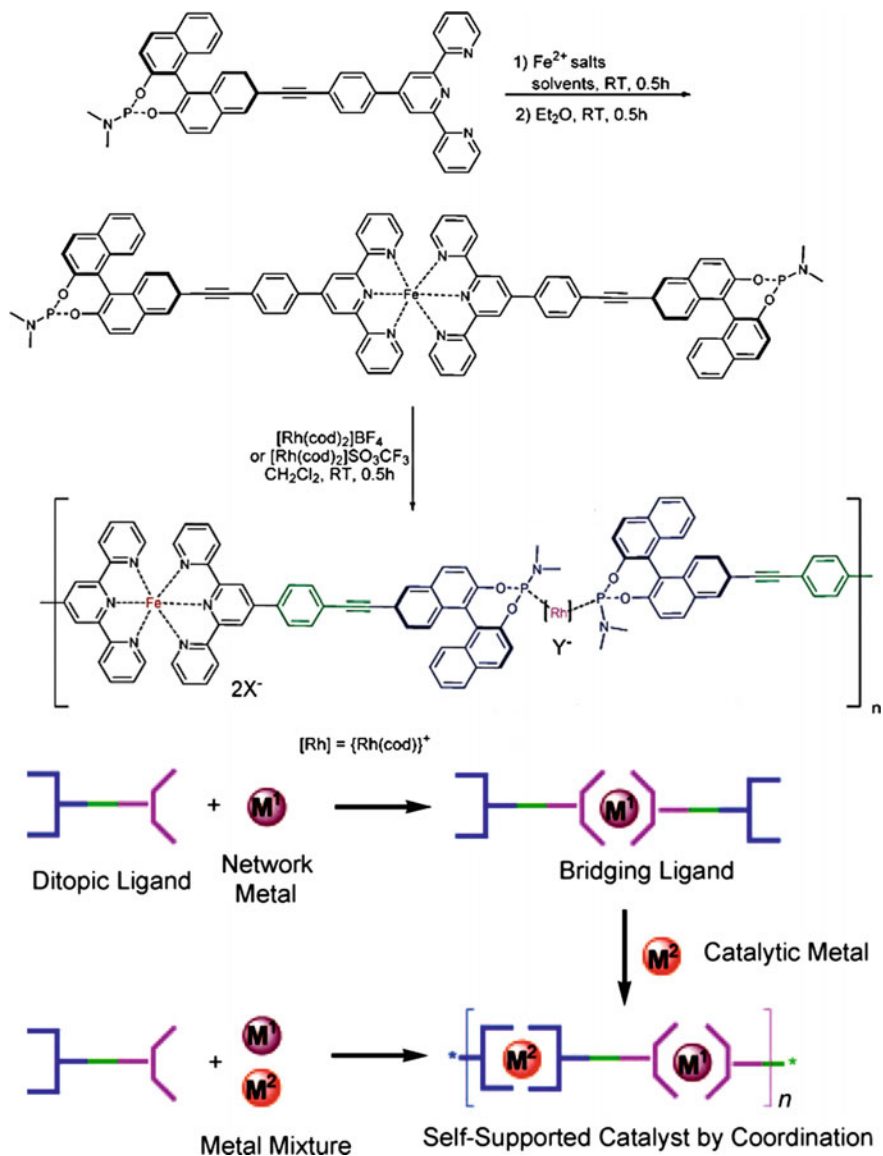
Scheme 7.11 Synthesis of a class of self-supported catalysts through orthogonal coordination of two different metal ions with a single ditopic ligand [286]

difficult to realize the abovementioned functions if only one type of metal ion was applied for self-assembling. In this case the self-sorting comes into effect, i.e. self-assembling some supramolecular assemblies from multicomponent mixtures,
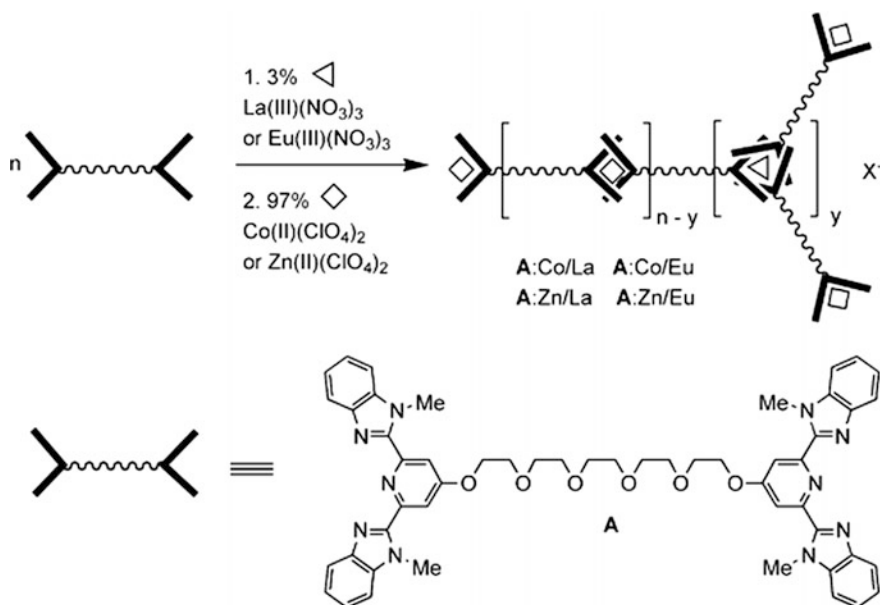
Scheme 7.12 Representative scheme of the formation of MSP by assembling the 2,6-bis (benzimidazolyl)-pyridine ligand, transition metal ions and lanthanides in the appropriate ratio [76]

which is one of important principles in contemporary supramolecular chemistry [287–291]. Strategy of self-sorting is most attractive since it provides approach to very complicated supramolecular architectures. Moreover, metal-driven selection between final MSP types can be quantitatively reached in solution or in crystal state using coupled coordination/packing of interactional algorithms inside dynamic metallosupramolecular databases [292].

Consistent chelation of transition metal ions and lanthanides makes it possible to obtain hetero-MSPs containing linear and branched blocks (Scheme 7.12), which has significantly broaden a range of supramolecular materials with new dynamic properties [76].

Also approaches have been developed when the first metal is used for production of linear MSP, and the second metal is used for cross-linking metallosupramolecular chains (Scheme 7.13). It is interesting that under action of different competitive ligands metallosupramolecular network can be reversibly assembled and disassembled and thus shows dynamic properties [293].

The hetero-MSP formed by a consistent chelation of two different organic building blocks is a kinetic intermediate to final stable hexanuclear metallomacrocycle carrying 4Ru(II) and 2Fe(II) ions obtained through thermodynamic disassembling/repeated assembling route [294].
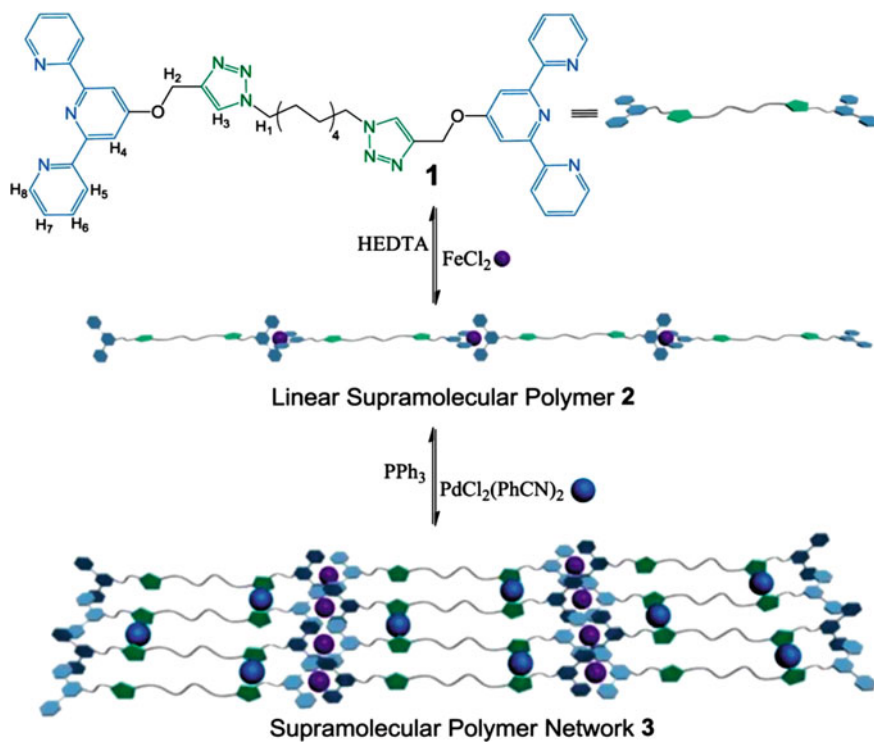
Scheme 7.13 A representation of the self-assembly of the metallosupramolecular network, where (HEDTA) is (2-hydroxyethyl) ethylenediaminetriacetic acid [293]

7.7 Metallosupramolecular Polyelectrolytes

Metallosupramolecular polymerization with neutral polytopic ligands brings to charged MSPs, which are called metallosupramolecular polyelectrolytes (MEPE). In MEPE synthesis bis-tpy are most often used as ditopic ligands, which provide formation of extended rod-like MEPE (Fig. 7.23) [156, 295]. DP of MEPEs in solution depends on concentration of components and on initial M–L ratio and is determined by dynamic equilibrium of association and dissociation. For M:L = 1 chain length grows exponentially with concentration, which means uncontrolled chain length growth. However, if there is excess of one component, growth stops as long as one component is consumed even if total concentration is additionally increased. This means that molecular weight of MEPEs can be controlled by M–L ratio [76]. In the case of Fe(II), Co(II), and Ni(II) a chain is short for M:L less than 1, it is longer for M:L = 1, it is medium for M:L over 1, because the binding constant K_1 associated with initial chelation of metal ion and tpy is lower than K_2, which reflects association of following tpy ligand thus elongating the chain [76]. Using chain monotopic stopper 4′-(phenyl)-tpy, it is possible to predictably control
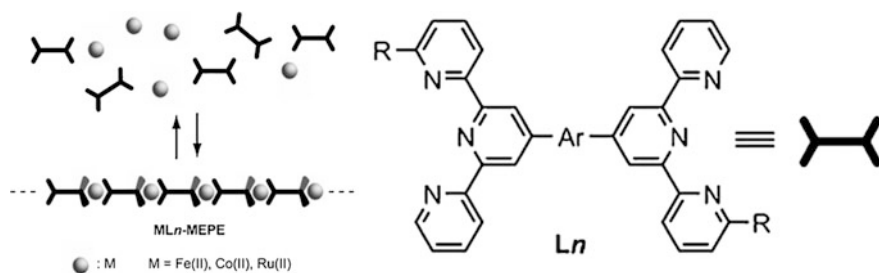
Fig. 7.23 Organic-metallic hybrid polymers (ML$_n$-MEPE) formed by chelation of bis(tpy)s (L$_n$) with metal ions such as Fe(II), Co(II), and Ru(II) ions [295]

average molecular weight, chain length, and viscosity of MEPEs (Fig. 7.24) [296]. The resulting linear bis-tpy-based MEPEs have attracted great attention since they are self-assembling in (aqueous) solution with metal ions such as Fe(II), Co(II), Ni (II), Cu(II), and Zn(II) with several hundred nanometers in length [297].

MEPEs' structure depends on ligand construction and preferable coordination geometry of a metal ion, and also on a solvent character and pH. Choice of a
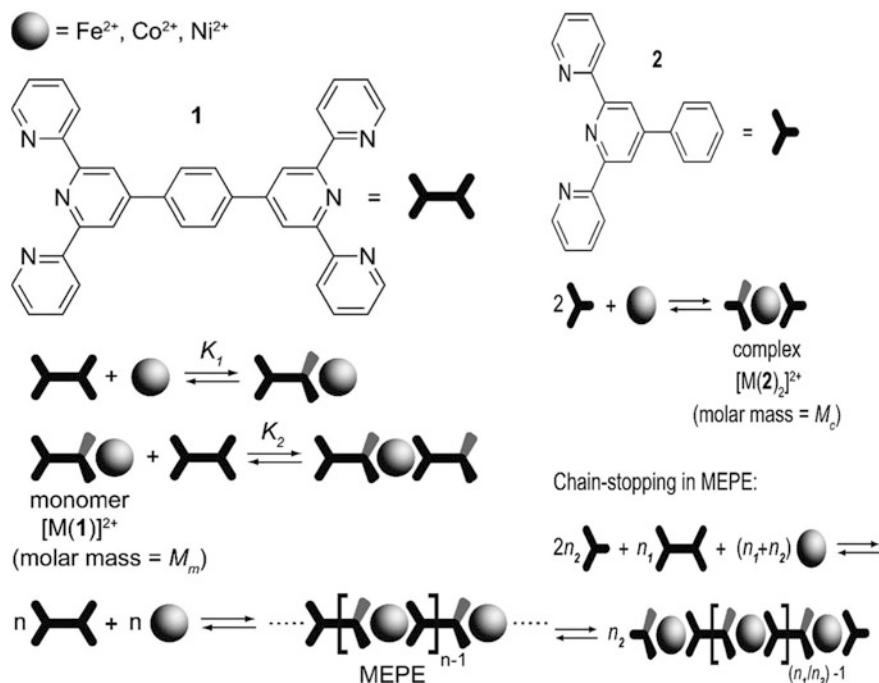
Fig. 7.24 Synthesis of MEPEs with predictably control average molecular weight, chain length, and viscosity using chain forming ligand and chain stopping ligand [296]

counter-ion not only determines solubility of MEPEs in different solvents, but controls microenvironment of metal ions and, thus, has effect on architecture of polyelectrolytes. Modularity of MEPEs self-assembling makes it possible to introduce different metal ions, chelating ligands, and counter-ions, thus generating abundance of materials with wide range of properties [298]. With different metal ions integrated into a polymer chain several interesting functions become available, including magnetic, electrorheological, photophysical, electrochemical, and electrochromic [179]. In this sense important is a fact that attractive optical, electrochemical, and electrochromic properties of MEPEs can be easily studied for their high solubility in different solvents including water. Moreover, conclusions can be made about structure-property correlation of projected structures. Positive charge of a metal ion can be used for integration of MEPEs in different architectures of materials, including liquid crystals, nanostructures and thin films [76, 299].

In most cases, metal-driven self-assembling MEPEs is easily indicated by naked eye due to strong coloring solution at chelation of metal ions. For example, Fe-MEPE shows strong absorption band in visible range about 590 nm relating to MLCT transition, which is responsible for deep blue color. Ligand shows a strong band about 290 nm associated with π-π* transition. Moreover, small bands are generated at 240–340 nm depending on a certain ligand [87, 300–302]. Furthermore, MEPE formation is accompanied by increase in viscosity of solution, which provides additional indication of MEPEs formation. Since viscosity depends on a chain length, increasing viscosity is associated with growing chains. For example, for Fe-MEPE viscosity reaches maximum at M:L = 1 [303].

Studying MEPEs based on bis-tpy Ru(II) chelates with a spacer varying from oligomers to polymers has shown that a spacer length is an important factor for formation of linear or cyclic types and, therefore, it can have an effect on DP [96, 192, 304, 305]. To suppress polyelectrolyte effect of Ru(II)-MEPEs, it was necessary to add different concentrations of salts for viscosity experiments. It is important that lamellar polymer chains should form.

In the recent years MEPEs have gained wide development as a new area for electrochromic applications [75, 76, 81, 132, 157, 160, 175, 306]. As applied potential is increased, metal centers are oxidized to higher valent state, and MLCT decreases. Optically this brings to decrease in visible optical density caused by switching MEPEs from colored to transparent state [295]. Therefore, choice of metal ions and ligands plays a significant role in electrochromic characteristics in MEPE system and has an effect on efficiency of electrochemical and optical properties [307]. In particular, MEPEs easily form thin films of high optical quality using different methods including LbL deposition or coating with linear and continuous film growth [308]. Moreover, MEPE thin films immobilized on transparent conducting electrodes show desired electrochromic properties with high switching rate and low switching (commutation) potential, since, change of redox state is, as a rule, associated with change in optical properties [308]. Metal chelates show redox transitions based on a metal ion and ligand totally up to five redox stages [309]. In other words, MEPE connect universal and usually reversible electrochemistry of MSP with advantage of recycling polymer materials [310, 311]. These highly

efficient electrochromic properties are demonstrated for example for Fe-MEPE, Co-MEPE, and Ru-MEPE based films, for which loss of absorption about 20% is detected after 4000 redox cycles [157, 312, 313]. The compounds show response times from 0.65 s for OMe-substituted Fe-MEPE to 1 s for respective Ru-MEPE, to 3 min for Co-complexes, respectively. Electron-acceptor functional groups, such as bromine, bring to prolonged response times. Electrochromic memory time, which is a period, during which a thin film remains colorless after removal of applied potential, is elongated by MEPE functionalization. Non-substituted MEPEs return in colored state after about 30 s, while functionalized MEPEs require up to 15 min to reduction [81, 313]. These films can be used for stimulus-responsive layers [314] and for electronic displays and devices such as electronic papers or electrochromic windows (smart-windows) [307, 308, 313–315].

It should be noted that during annealing Fe-MEPE based films at temperatures above 100 °C blue color transits to green, and previously reversible electrochromic properties are lost, even after cooling to room temperature [316]. Study of solid Fe-MEPE in situ during annealing has shown that thermo-induced transition is not accompanied by redox process on Fe(II) center, but is related to structural changes in Fe(II) coordination sphere. In particular, in low-temperature state Fe(II) ion is in quasi-octahedral coordination surrounded by six nitrogen atoms of pyridine rings. In this case length of axial Fe–N bond is 1.94 Å, while lengths of equatorial bonds are up to 1.98 Å. At the same time in high temperature state FeN_6-node shows distortion with axial Fe–N bonds elongated to 2.01 Å (Fig. 7.25).

Substantial interest has heterometallic MEPEs including Fe(II) and Co(II) ions, which combine properties of individual MEPEs and, therefore, show their different states: red-violet, blue, and transparent [317].

Very promising direction is also synthesis of cross-linked MEPEs based on bis-tpy Fe(II) chelates [140]. It occurs that molecular weight of networks reaches high values and depends on cross-linking degree, for example, it is shown that from
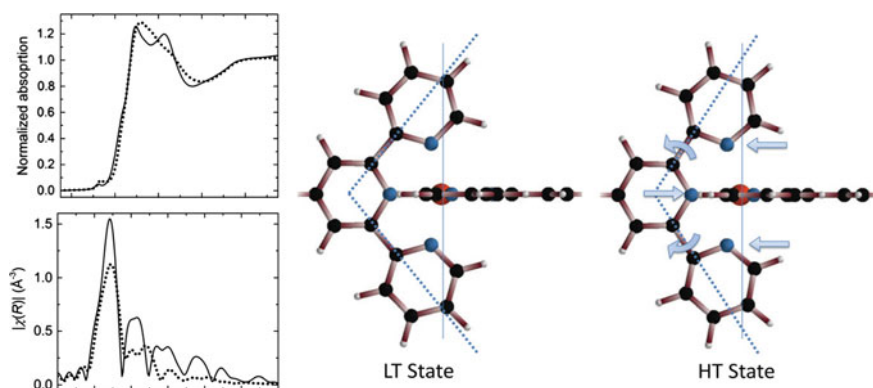
Fig. 7.25 XANES (top) and EXAFS (bottom) spectra of LT (solid line) and HT (dotted line) states of solid Fe-MEPE [316]
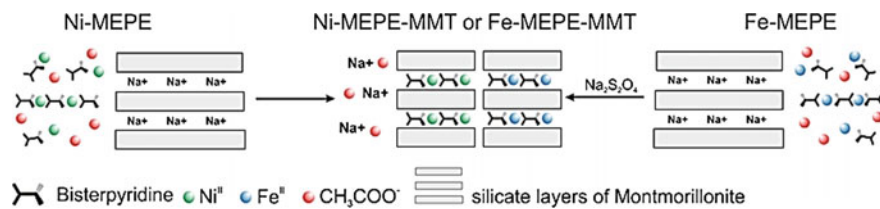
Fig. 7.26 Nanocomposites consisting of montmorillonite glue and Ni(II) or Fe(II) MEPE [321]

1.5 to 9% of cross-linking degree the networks are soluble in aqueous and acetic acid solutions. For higher cross-linking degrees (more than 9%) solutions are heterogeneous with colored deposits precipitated from solution.

We shall notice production of composition materials by incorporation of MEPEs host materials [318, 319]. While most high molecular weight polymers cannot migrate into pores, components of MEPEs can diffuse and collect in a host.

Innovation concept [320] is developed for design of electrorheological liquids based on disperse phase of rigid rod-like MEPE intercalated into mesoporous SBA-15 silica. At electric field applied to this composite dispersed in silicon oil, rheological measurements shows considerable change in elasticity modulus, which points to solidification of fluid medium. Apart from strong electrorheological effect and low current density, five times smaller amount of MEPE is required than in comparable electrorheological liquids based on host-guest systems.

Using water intercalation, nanocomposites are obtained consisting of montmorillonite glue ($Na_{0.6}(Al_{1.64}Mg_{0.36})Si_4O_{10}(OH)_2 \cdot nH_2O$) and MEPE with Fe(II) and Ni(II) ions (Fig. 7.26) [321]. For both nanocomposites substantial electrorheological effect is established, which depends on intercalated MEPE.

It is shown [322] that for diluted solutions, where small MEPE aggregates prevail, nanometer crystals can be grown on interphase boundary. MEPEs form linear rods, which are arranged into sheets, at that, four sheets intersect a unit cell, while adjacent sheets are rotated by 90° with respect to each other.

7.8   Orthogonal Self-assembling

Oppositely to majority of biological systems, synthetic supramolecular chemistry uses, as a rule, only one type of non-covalent interaction. Therefore, there is an important task of stabilization of clearly defined MSP architectures solved with a combination of several non-covalent interactions [169, 323–330]. Using a combination of a set of non-covalent interactions provides additional possibilities for development of very complicated and multifunctional MSPs. For example, dynamic supramolecular polymers with linear or cross-linked topology are reported [331]. Use of supramolecular interactions to direct of spontaneous assembling molecules is of paramount importance due to their very specific character, controlled affinity,

and reversibility. These specific and rather controlled interactions can be manipulated independently and simultaneously, thus providing orthogonal self-assembling of components with several (more than one) motifs of interaction, which do not influence each other [134, 332, 333]. In other words, use of orthogonal self-assembling guarantees that any change in a system caused by one interaction has no effect on another interaction [334]. The greatest advantage of orthogonal combination of different non-covalent bonds in supramolecular structures is its bringing to materials production with some properties, which are responsive under action of different stimuli. It is important that introduction of different supramolecular functional groups (multifunctionalization) into one synthetic fragment can improve substantially possibilities for applications of these materials, and orthogonal self-assembling provides total control over the self-assembling stage, and, therefore, over material properties.

If only one type of supramolecular recognition is present in the main chain of a polymer, usually statistic mixtures are obtained upon action of two or more functional reagents (Scheme 7.14, top) [169]. In this case, control over reaction of self-

Scheme 7.14 Statistical (top) and defined (bottom) multifunctionalization of a polymer by self-assembly [169]
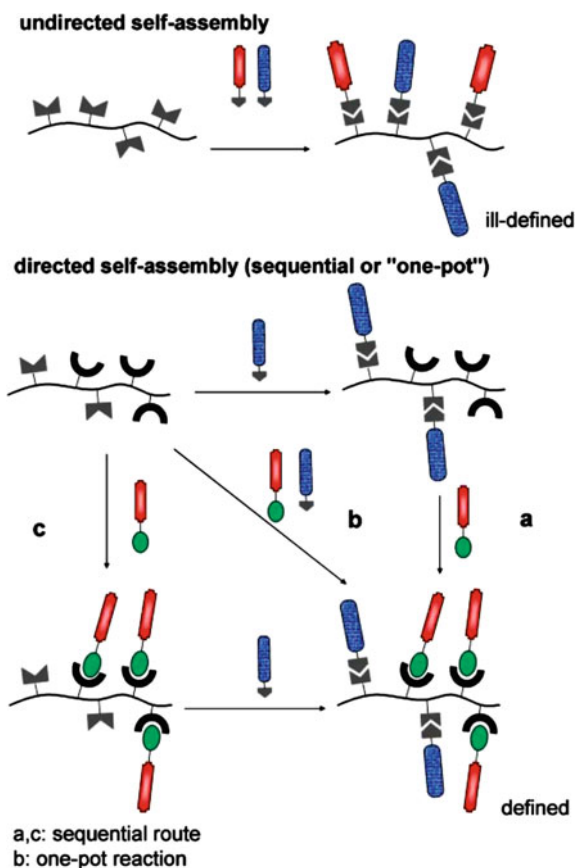
assembling is limited, and a product is weakly defined. A combination of different (orthogonal) supramolecular linking units, however, makes it possible to control the self-assembling stage (Scheme 7.14, bottom). This well-defined multifunctionalization of polymers can be reached if there is high selectivity of orthogonal recognizing elements to their complementary counterparts. For multiply repeated self-assembling two different synthetic ways are possible. Functionality may be introduced via consistent supramolecular self-assembling, and then another one. However, more promising is one-pot approach to a given mulifunctionalized product, because it reduces one stage of reaction. This strategy of controlled multifunctionalization provides fine tuning polymer architectures, and their properties, which shows ways to new specially developed functional materials.

7.8.1 Combination of M–L Coordination with H-Bonding Interactions

Among different non-covalent linking interactions in building supramolecular polymers, M–L coordination and formation of H-bonds are two basic and most studied classes of interactions [11, 169, 335–338]. Therefore, it is not accidentally that particularly these types of supramolecular interactions are widely used in orthogonal self-assembling. In this respect among the most well-known supramolecular motifs there are ureidopyrimidinone as an H-bonding block and tpy as a metal-chelating fragment [169, 261, 339]. In particular, successful dimerization of H-bonding block is shown, as well as metal-tpy chelation with addition of $FeCl_2$ or $Zn(OAc)_2$ in solution. These two linking points at different ends of a spacer provide orthogonal self-assembling in linear polymers through two synthetic routes (Scheme 7.15). It should be noted that using a covalent polymer poly (ε-caprolactone) as a spacer between two linking sites increases solubility of obtained telechelic polymer in non-polar solvents [170]. It is important that MSP shows film-forming properties and transparence at thin thickness of film, which differ considerably from those of opaque and fragile films of original polymers. Besides, MSPs have different physical properties as compared with its initial polymers, just with a few non-covalent linking sites being integrated. Moreover, reversibility of polymer chelation can be controlled by addition of competitive ligand HEEDTA (hydroxyethyl ethylenediaminetriacetic acid) or metal ions opening a way for building new «switching» functional polymers (Scheme 7.16) [340, 341]. These self-assembled polymers can be adjusted using different external stimuli through addressing either quaternary H-bonding block or a tpy-metal supramolecular motif. In particular, formation of H-bonding fragment can be adjusted by temperature or a solvent, while a metal chelate fragment can be modulated using competitive ligands, and electrochemistry.

There is an interesting approach in which tpy fragment is replaced by chiral Feringa MonoPhos ligand for bifunctional monomer synthesis, which can form
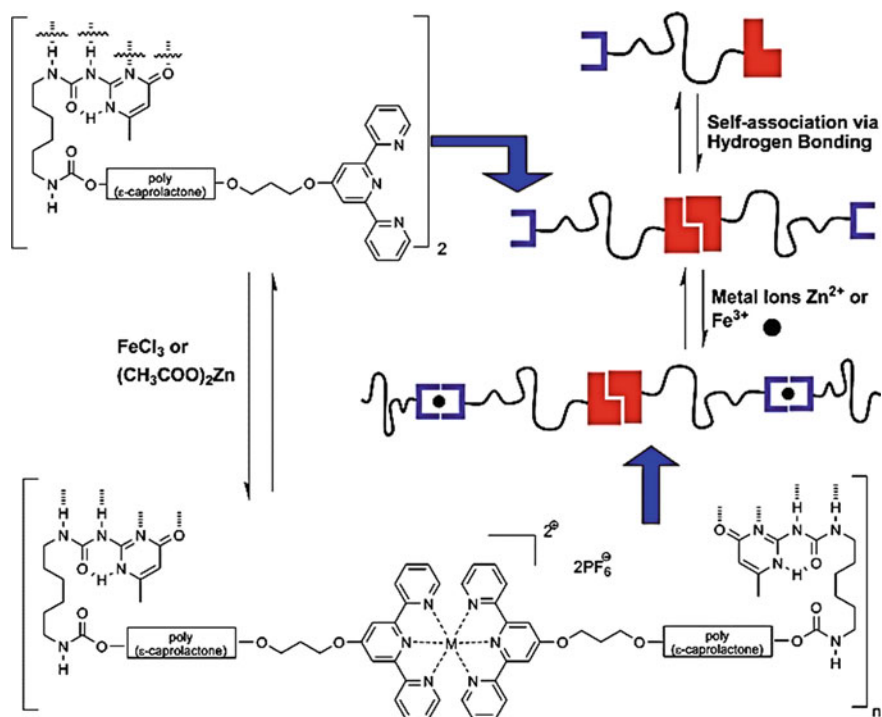
Scheme 7.15 Schematic representation of a supramolecular polymer containing alternating tpy metal chelates and quadruple H-bonds in the main chain [319]

linear self-assembled polymer with alternant orthogonal P–Rh coordination and ureidopyrimidinone dimerization in the main chain by addition of $[Rh(COD)_2]BF_4$ [171]. The obtained MSP is insoluble in non-polar solvents such as toluene, and is highly efficient and enantioselective heterogeneous catalyst of hydrogenation reaction, and can be repeatedly used during many cycles.

We shall notice that supramolecular polymers based on H-bonds are, as a rule, confined to organic solvents, such as chloroform, and are weak in competitive polar solvents such as DMSO. At the same time, switchable MSP obtained on the basis of a small heteroditopic monomer with two orthogonal linking interactions is stable in a strongly polar solvent [324, 337]. This monomer has guanidiniocarbonyl pyrrol carboxylate zwitter-ion motif at one end and tpy block at the other end (Fig. 7.27). High association constants $K > 10^8 \ M^{-1}$ of both tpy-block and of a zwitter-ion motif in DMSO are important preliminary condition of linear supramolecular polymer fiber formation with a considerable DP in polar solvents. This supramolecular system provides production of large aggregates in polar solvent and can be adjusted reversibly between polymers and low molecular weight molecules reacting at external stimuli in two different directions, which can be included in design of functional materials.
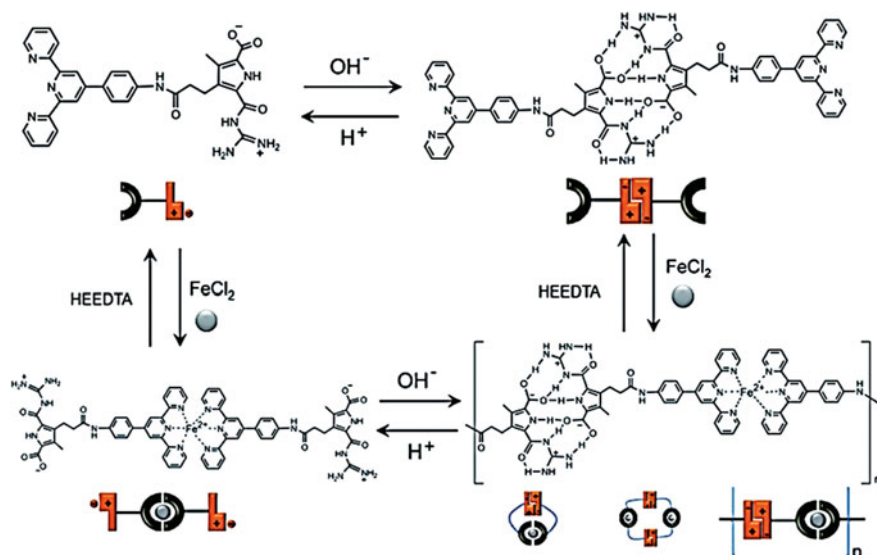
Scheme 7.16 Schematic molecular structure of initial ligand, and the dynamic polymerization of the metal–ligand complex

cyclic oligomers

globular aggregates

linear polymers
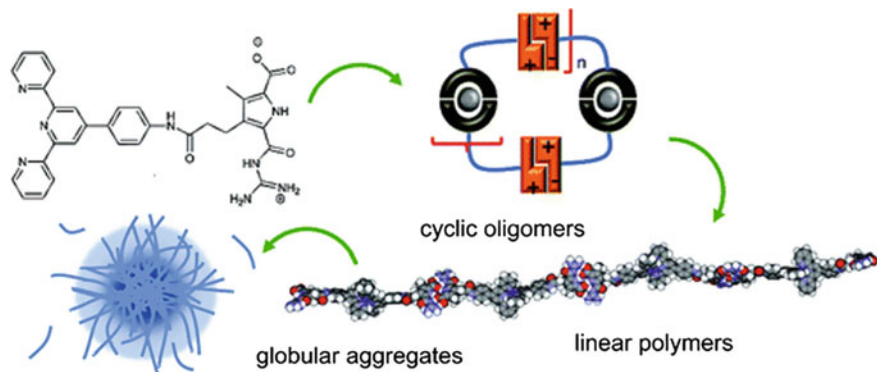
Fig. 7.27 Scheme of the self-assembly of monomer in solution

Very easy and universal approach to these materials is based on traditional polymers carrying different fragments of recognition in a side chain. For example, ROMP is used for synthesis of one type of statistic copolymers based on norbornene carrying Pd-pincer complexes (M–L coordination) and diaminopyridine fragments (H-interactions) as groups of a side chain (Fig. 7.28a) [333]. A copolymer can be functionalized stepwise or by the one-pot method by adding Py and *N*-butyl thymine showing good selectivity and independence from each other within the limits of recognition motif and the main polymer chain. It is important that thermal properties

Fig. 7.28 Schematic representation of cross-linking via a palladated pincer (**a**) and H-bonding units (**b**) with bifunctional complementary recognition units [333]

such as T_g and T_d can be modified by such functionalization, which provides easy way of control over functionalization of a copolymer and makes it possible to design functional materials based on a statistic copolymer. There is another way of functionalization using H-bonding fragment for cross-linking by adding telechelics containing two complementary H-bonding groups (Fig. 7.28b). Besides, for this purpose perylene molecule can be used to incorporate fluorescent dye into a supramolecular polymer. In both cases a supramolecular fragment not taking part in cross-linking was functionalized with mono-functionalized recognition blocks [342].

We shall also notice MSPs built from ABC triblock-copolymers based on covalent bond with orthogonal combination of Pd-pincer-pyridine coordination and H-interaction of heterocomplementary Hamilton receptor–cyanuric acid (Fig. 7.29)

Fig. 7.29 Cartoon representation of the formation of ABC triblock-MSP [342]

[323, 342]. In this synthesis initiator *N,N*′-bis[6-(alkanoylamino) pyridin-2-yl] isophthalamide (often called Hamilton receptor or Wedge) and Py-based chain-terminator are used to obtain heterotelechelic poly (norbornene imide) polymer containing two terminal supramolecular motifs. It should be noted that M–L coordination has no effect on H-bonding fragment in telechelic polymers. Targeted triblock-MSPs are then obtained in one-pot reaction by a simple mixing of three components in solution: two telechelic polymers and one heterochelic polymer.

7.8.2 Combination of M–L Coordination with Host-Guest Interaction

Presently MSPs built using orthogonal self-assembling based on M–L and host-guest interactions attract more and more attention due to their interesting propert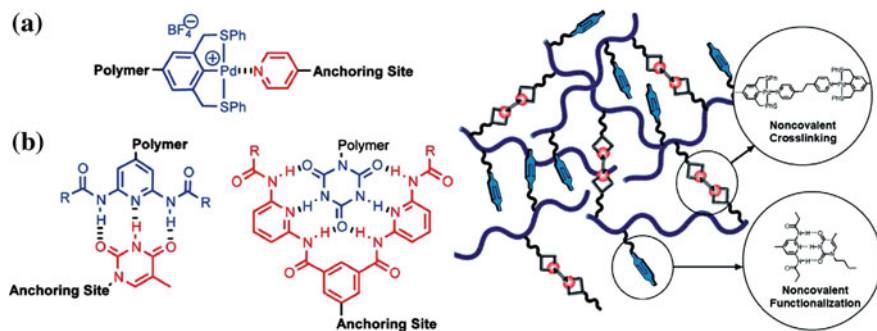ies and potential applications [343]. M–L interactions provide MSP with different coordination geometries, strong, but tunable coordination binding capacities, and also magnetic, redox, photophysical, and electrochromic properties, while host-guest interactions give good selectivity and convenient enviro-responsiveness to these polymers. Therefore, MSP built by orthogonal M–L and host-guest interactions have wide applications in soft matter, fluorescence, probing, hetero-catalysis, electronics, gas storage, etc.

β-CD is one of the most well-known types of a host, which is widely used in MSP building [52]. Thus, through double non-covalent interactions in the main chain consisting of low molecular weight monomers polypseudorotaxane is obtained (Fig. 7.30) [325]. In this case one rod-like host monomer contains two azobenzene groups at two ends bound to viologen units as hydrophilic elec-tropositive barriers, which can be encapsulated in β-CD through hydrophobic host-guest interactions. Another monomer is 4,4′-bipy grafted with β-CD, which can be coordinated with Pd(II)-en nitrate, strong and quantitative bidentate acceptor
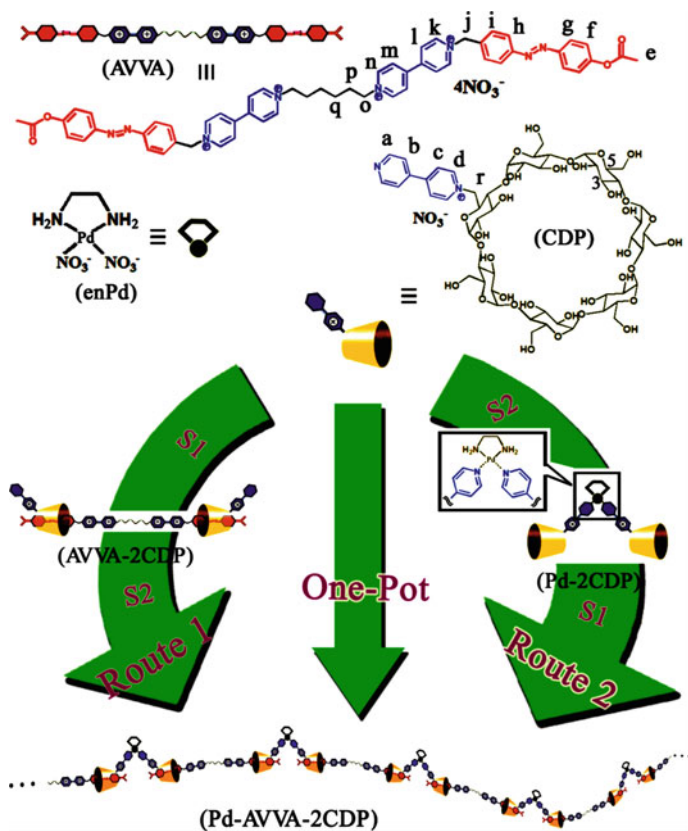
Fig. 7.30 Schematic representation of the construction processes for the functional polypseudorotaxane, based on heteroditopic ligand containing two azobenzene groups on two ends linked with viologen units of 4,4′-bipy grafted with β-CD (AVVA is guest compound containing two azobenzene groups in the two ends linked by viologen units)

for Py derivatives in water. Functional polypseudorotaxane can be obtained by mixing in water three components by spontaneous and orthogonal self-assembling using coordination Pd–N interaction and host-guest azobenzene-β-CD interaction. The desired MSP can also be obtained stepwise through preliminary formation of intermediate complexes based on M–L or host-guest interactions and the second type of interaction involved afterwards. Besides, in this system behavior of assembling/disassembling can be realized with photo isomerization induced by azobenzene in the main chain. Taking into account low cytotoxicity of β-CD in aqueous phase, these sensitive MSP can be of great potential for such applications as biomaterials for drug delivery, gene delivery, tissue engineering, etc.

We shall also notice synthesis of nanometer bis(polypseudorotaxane) based on endowing bridging bis(β-CD) with multiple coordinated metal centers, in which β-CD is a host for amino-terminal polypropylene glycol (PPG) being a guest, and

Ni(II) complexes as template fragments [344]. Two PPG chains were threaded separately in cavities of metal-bridging bis(β-CD) forming two-chained structures, they also played a stabilizing role in the assembling process (Fig. 7.31). It is important that the self-assembling process goes owing to advantageous entropy contributions, which accompany a considerable positive change in enthalpy. Bis (polypseudorotaxane) (~ 20 nm in length) was also successfully preorganized to elongated bis(molecular tube) (~ 200 nm in length) using intra- and intermolecular addition of ~ 10 discrete bis(polypseudorotaxane) units and the following removal of polymer templates [345]. This bis(molecular tube) can efficiently capture C_{60} in holes formed by adjacent metal-bridging bis(β-CD) units, which can be then used for selective recognition of organic/inorganic/biological substrates.

1D metal-containing molecular wire with given properties for molecular electronics materials is obtained through M–L polymerization of Ru(II)-Pp with isolated bridging ligand [346]. It should be noted that this molecular wire combines advantages of organic isolated molecular wires with properties stipulated by presence of transition metal complexes. Quantitative self-inclusion of bis(β-CD) precursor followed by interaction with *p*-iodopyridine through Sonogashira coupling brings to bis(β-CD) containing Py-coordinating sites at both ends (Fig. 7.32). 1D metal-containing isolated wire is formed in situ using UV-irradiation of bis(β-CD) and carbonyl Ru(II)-Pp. As was expected, this wire not only shows hardness, linearity and structural stability, but also high intramolecular mobility of charge. It is important that this MSP can be subjected to reversible monomer-polymer transitions under special conditions, for example, in presence of CO or under UV irradiation. These workabilities obtained from unique reversible character of M–L bond are impossible for ordinary covalent-bound molecular wires.
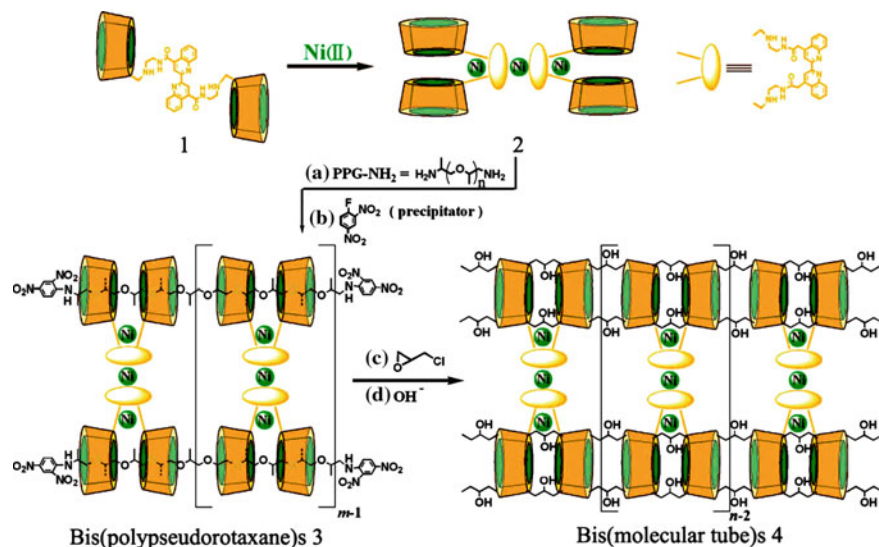

Fig. 7.31 Cartoon representation of the formation of bis(polypseudorotaxanes) by multiple metallo-bridged α-CD
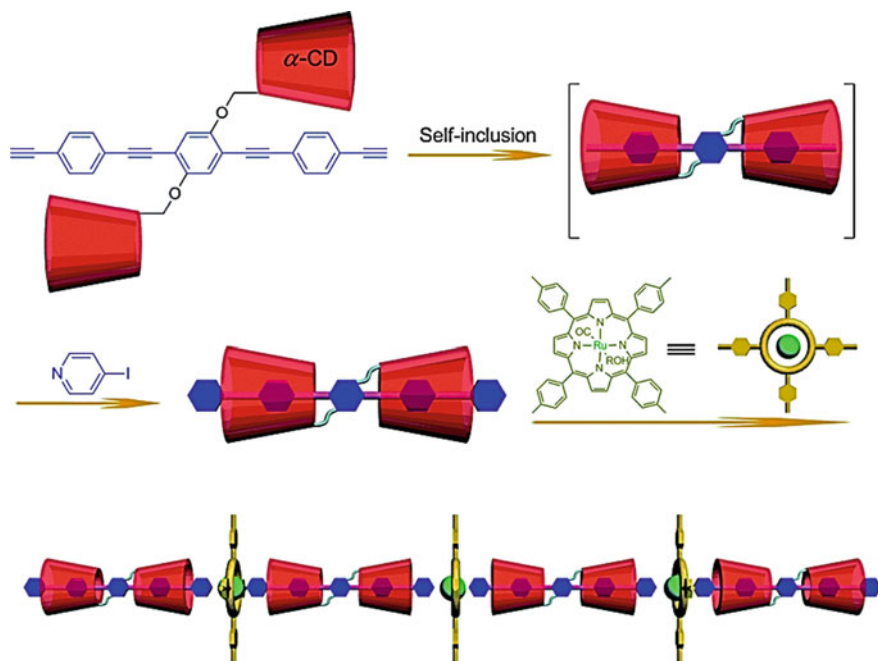
Fig. 7.32 Scheme of the formation of a polymeric insulated molecular wire via orthogonal self-assembly

Another important object in contemporary supramolecular chemistry are cucurbit[n]urils (CB[n], n = 5–8, 10), which are macrocyclic oligomers consisting of six or more glycoluril units. Hydrophobic cavity and polar carbonyl groups surrounding portals belong to structural features of CB[n]. Using carboxylate- and cyano-groups as terminal fragments, and lanthanide metal ions as spacers, which have big ionic radii and higher CNs than transition metal ions, 3D polyrotaxane network is obtained [347]. Besides, using orthogonal approach, double-chained 1D polyrotaxane and zigzag-like 1D polyrotaxane are synthesized from L-like pseudorotaxane and Cd(II) and Co(II) ions, respectively (Fig. 7.33) [348]. It is important that topologically intriguing MSP can be orthogonal assembled from exhaustively developed CB-based host-guest interactions and correctly chosen M–L interactions. CB[8] has an interesting ability of linking two guests simultaneously, which is widely used for building supramolecular assemblies. Combination of this ability with M–L self-assembling will, undoubtedly, advance MSP formation. For example, linear CB[8]-based MSP is obtained in aqueous solution using CB[8]-based host-guest interactions and tpy-Fe coordination as supramolecular motifs [349]. Synthetic route includes production of heteroditopic ligand consisting of naphthalene fragment and tpy-block, which can be bound with Fe(II) ion forming a monomer and two naphthalene residuals at head and tail (Fig. 7.34). The following host-guest CB[8]-naphthalene interaction brings to MSP

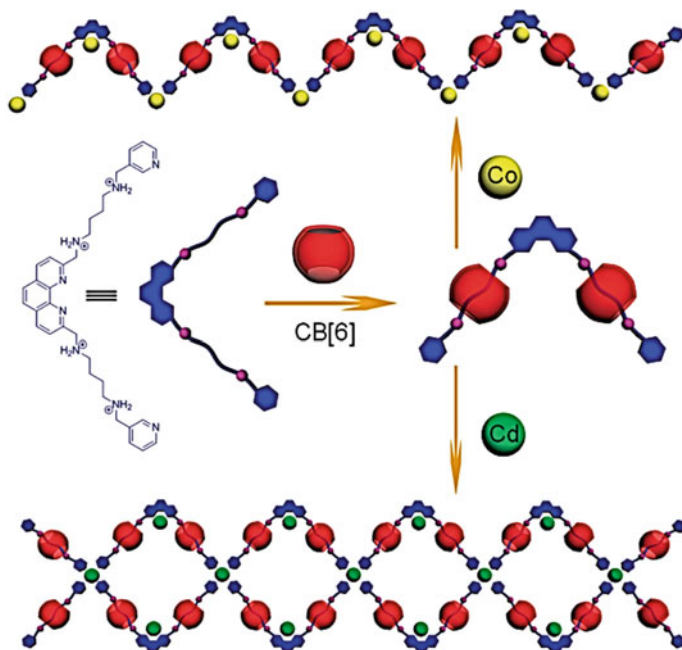**Fig. 7.33** Cartoon representation of the formation of a double-chained 1D polyrotaxane and a zigzag-shaped 1D polyrotaxane
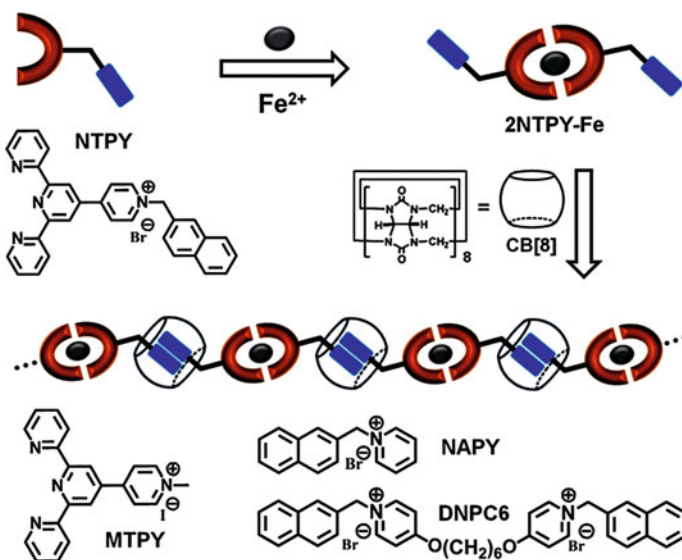

Fig. 7.34 Schematic representation of the orthogonal supramolecular polymerization based on CB[8] and M–L coordination

formation. It is important that introduction of tpy-Fe spacer not only increases solubility of monomers, but suppresses cyclization, thus facilitating efficiency of supramolecular polymerization. Metallosupramolecular polymerization can be controlled by tuning molar ratio of metal-containing monomer and CB[8].

For development of supramolecular chemistry pillar[n]arenes are important, which represent a class of macrocyclic hosts with symmetric pillar architectures and rigid electron-donor cavities [350–353]. Thus, based on amino-modified copillar[5] arene [c2]daisy with tpy stoppers, a solvent-driven muscle-like MSP is prepared [354]. Synthesis included fabrication of double threaded rotaxane dimer in chloroform driven by Van der Waals forces (mainly, dispersion forces) between parts of exo-cavity of long alkyl groups (Fig. 7.35). This monomer can change its length continuously by changing polarity of a solvent similarly to molecular spring based on amino-modified copillar[5]arene [355–357]. The following addition of Fe(II) brings to formation of muscle-like MSP based on individual compression or tension of each sequence of a daisy chain of repeated unit. With daisy units of a chain in broaden geometry at low pH (left) the total length of the polymer l_{ext} is estimated as ~ 15.9 μm. At higher pH (right) compression by ~ 1.2 nm of repeated units decreases length of a polymer 1_{cont} to ~ 9.4 μm, which corresponds to enhancement of nanoscopic motion of more than three orders of magnitude as a result of ~ 3000 artificial molecular machines working coherently in the same polymer chain. Developed MSP can be considered as a new platform for design of artificial molecular machines for imitation of living systems.

One of the promising directions of application of linear supramolecular polymers using pillar[5]arene-based host-guest interactions is design of fluorescent sensors for detection of different metal ions, for example, Cu(II) [358] and Zn(II) [359]. We shall
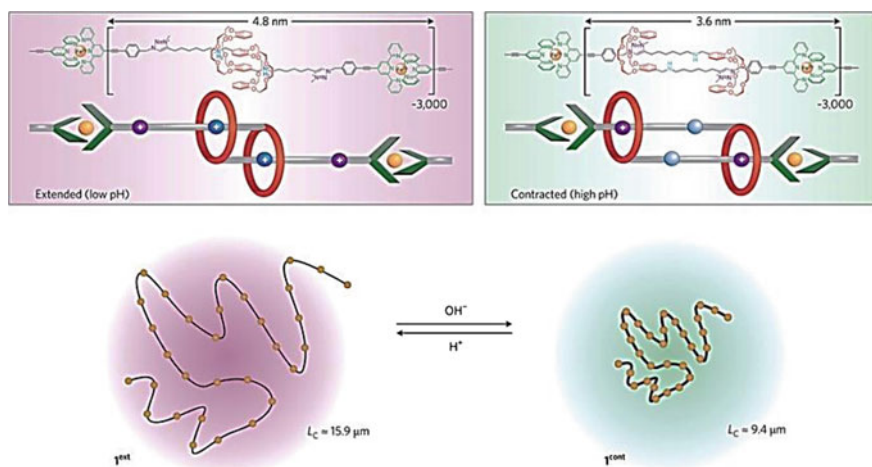

Fig. 7.35 Amplification of muscle-like mechanical actuation within a metallosupramolecular [c2]daisy chain polymer. Dialkylammonium ion (NH_2^+), blue; [24] crown-8, red; neutral amine, light-blue; triazole units, purple; tpy, green [356]

also notice supramolecular polymer networks assembled using combination of orthogonal tpy-Zn(II), carbine-Ag(I) and pillar[10]arene/alkyl chain of recognition motif, which show dynamic properties as response to external stimuli [360].

The most commonly used in supramolecular chemistry are host-guest interactions based on different crown ethers. For example, benzo-21-crown-7 is the smallest benzocrown ether, which can form threaded structures with secondary dialkylammonium salts [361]. Orthogonal self-assembling based on this supramolecular motif and M–L coordination provides efficient way of building highly efficient MSPs [362]. For this, heteroditopic monomer has been developed, which carries secondary ammonium salt fragment and tpy ligand on both sides of a long flexible aliphatic chain. A chelating ligand makes it possible to decrease percent of cyclic oligomers and advances linear expansion, which, finally, brings to relatively low critical concentration of polymerization during supramolecular polymerization. Further on heteroditopic monomer can be complexed with benzo-21-crown-7-based monomer of AA type with formation of [3]pseudorotaxane structure (Fig. 7.36). We shall also notice another heteroditopic monomer which contains benzo-21-crown-7 and tpy blocks on two ends and complementary BB type homoditopic monomer of secondary ammonium salt [363]. Then MSP of the main chain was obtained using one-pot mixing two recognition motifs and metal ions. Since non-covalent interactions used in these systems were the same as the abovementioned ones, the materials have shown analogues dynamic and responsive properties. These two adaptive MSP are attractive objects for further fabrication of intelligent supramolecular materials with given properties.

An MSP is considered obtained through coordination of Zn(II) with a conjugated bis-tpy ligand carrying dibenzo-24-crown-8 arms, which can form stable responsive 1:1 threaded structure with complementary dibenzylammonium salt guest through
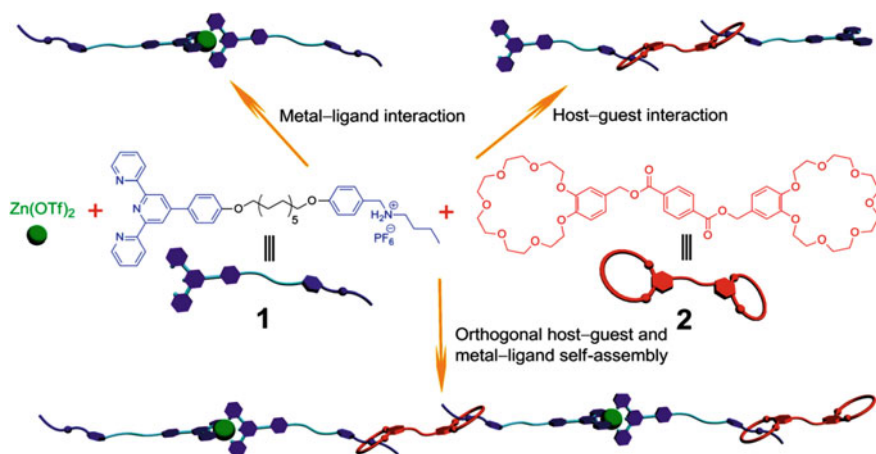

Fig. 7.36 Cartoon representation of the formation of a linear supramolecular polymer and the corresponding intermediates from monomers **1** and **2**

combination of [N$^+$–H···O] and [C–H···O] H-bonds and π-π-stacking [221, 364]. These long chained polymers are characterized by high DP at high concentration. It is interesting that the MSP has shown concentration dependent emissions from turquoise to white and then to yellow color in the range of concentrations 1.25– 125 mM. Following alternative addition of 2.4 equivalent of base (*N-tert*-butyl-*N'*, *N',N'',N'',N''',N'''*-hexamethyl-phosphorimidic triamide) and 2.8 equivalent of CF$_3$COOH has brought to dethreading and rethreading of dibenzylammonium salt in host fragments and, therefore, to reversible fluorescent emission. Recently also excellent responsive MSP networks obtained through orthogonal self-assembling dibenzo-24-crown-8/dibenzylammonium salt and metal-tpy motifs are reported [365, 366]. In this case, successive reversible emissions are realized by acid-base controlled recognition of dibenzo-24-crown-8 residuals in MSP-Zn with dialky-lammonium ion centers.

Elegant combination of special bistable dibenzo-24-crown-8-based [c2]daisy chain rotaxane and M–L-driven supramolecular polymerization was applied to realize linear amplification of muscle-like translation molecular motions by orders of magnitude [367, 368]. These polymer chains were long and quite well soluble, so that micrometric changes in their contour length could be measured at synchro-nizing multiple contractions and expansions. Other binding constants of secondary ammonium and triazolium ions with dibenzo-24-crown-8 motif give a possibility of efficient pH-responsive translation motion at molecular level (Fig. 7.37).
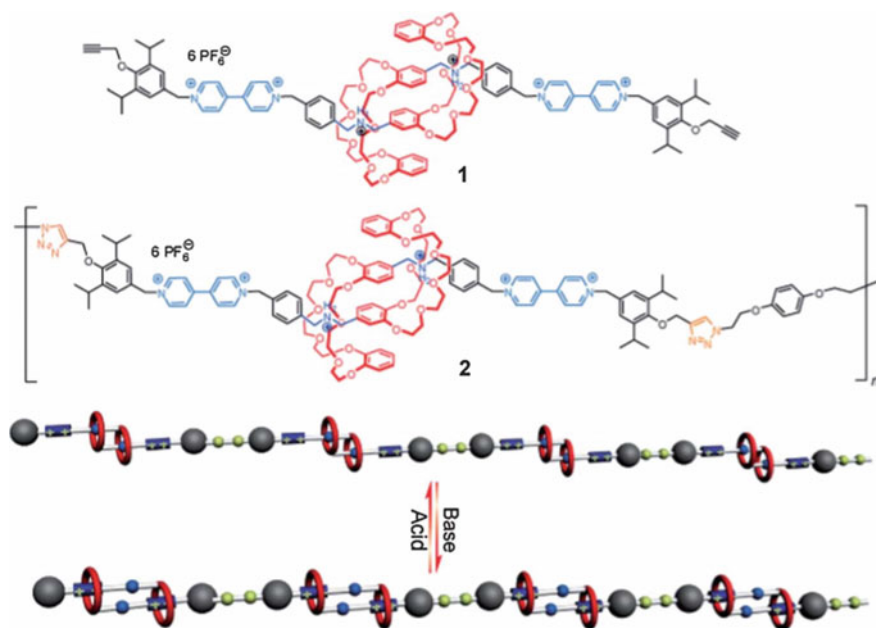

Fig. 7.37 Chemical structure of the difunctional [c2]daisy chain and cartoon representation of the acid-base switching contraction-extension process of the resultant MSP

In particular, M–L driven processes of supramolecular polymerization with Zn (OTf)$_2$ or FeCl$_2$ are confirmed.

We shall also notice fluorescent supramolecular polymer with AIE properties formed by crown ether-based host-guest interactions, which is used as a fluorescent sensor for Pd(II) ions [369].

Recently well-organized supramolecular polymer massifs are successfully built based on «tweezing directed self-assembly» strategy [370]. For this purpose, special heteroditopic monomers were developed and synthesized (Fig. 7.38) [371]. Since two electron-deficient alkynylplatinum(II)-tpy tweezers on molecular unit of a tweezers can specifically encapsulate electron-rich alkynylgold(III) diphenylpyridine, mixing equivalent amounts of heteroditopic monomers gives a dimer complex. Following addition of homotritopic monomer brings to expected A$_2$B$_3$ type supramolecular hyperbranched polymers with potassium cation-responsive character. At the same time, the process of supramolecular polymerization can also be realized using one-pot mixing three monomers, which points to highly specific non-covalent recognition of a tweezers-guest motif. This new supramolecular motif broadens host-guest set of tools and represents universal strategy for MSP fabrication.
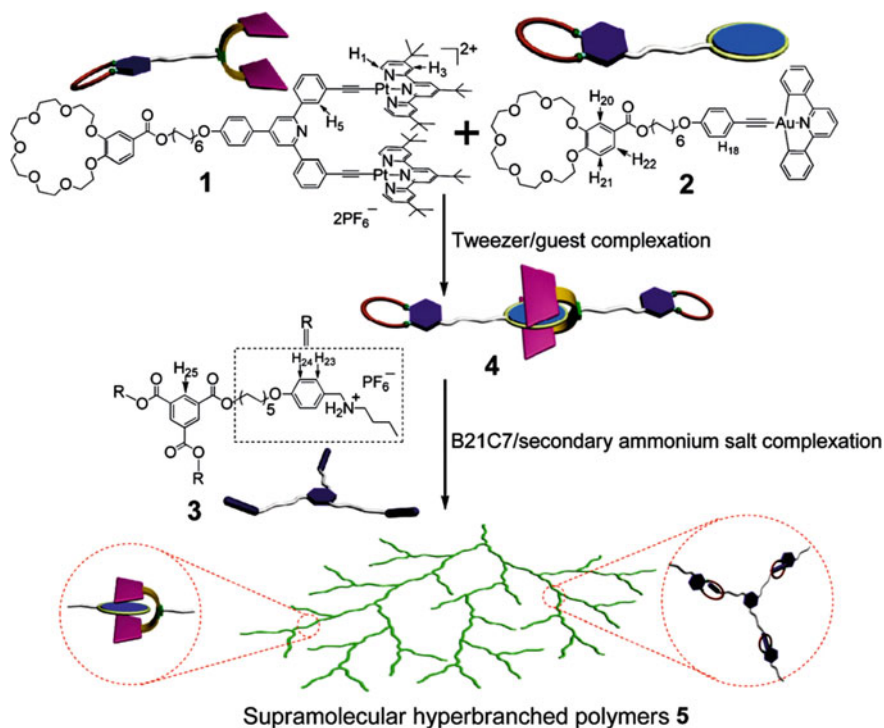

Fig. 7.38 Cartoon representation of the construction of a supramolecular hyperbranched polymer

Substantial attention is given to integration of bioactive types into synthetic supramolecular systems from the point of view of biosensors or «nanoreactors» design. For example, biotin being one of the most known natural non-covalent linking blocks (which forms stable «complexes» with avidin and streptavidin proteins) was linked to tpy fragment. A metal-tpy spacer can be adjusted for regulation of stability and kinetics, and also can be reversibly opened by external stimuli. For these purposes non-polymer and polymer PEG spacers were used [372]. These compounds are the attractive examples of a link between biochemistry and metallosupramolecular chemistry and are convenient building blocks for design of functional (nano)architectures. Another example is functionalization of bpy with biotin and following production of respective Fe(II) complex [373]. This complex is a «redox biotin bridge» for potential applications as a biosensor, since addition of avidin to a complex brings to a change in Fe(II)/Fe(III) redox signal of cyclic voltammetry, thus making it possible to monitor avidin addition. Besides, 3D orientation of biotin fragments provides fixing several avidin units.

Very promising is design of multicomponent supramolecular systems highly complicated due to combination of orthogonal self-assembling and self-sorting approach. For example, driven by orthogonality of M–L coordination and host-guest interactions and directed by several molecular codes during self-sorting, five types of simple components (up to eighteen precursors) were successfully self-assembled into two new tris [2]pseudorotaxanes by one-pot highly selective method (Fig. 7.39) [374].
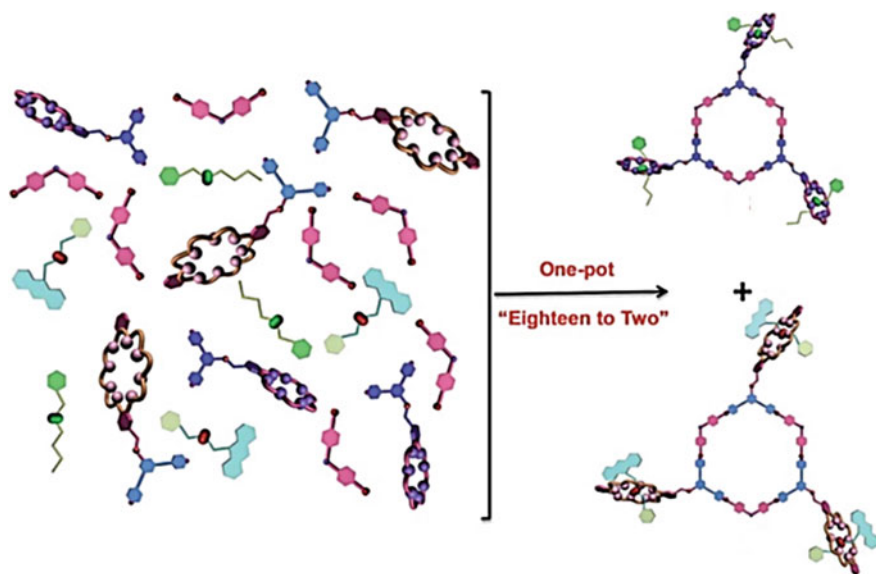

Fig. 7.39 Scheme of combination of orthogonal self-assembling and self-sorting approach

7.9   Hierarchical Self-assembling

Creation of complicated supramolecular architectures has become recently possible due to application of the concept of hierarchical self-assembling, which is determined as multilevel non-covalent self-assembling supramolecules including a range of successive interactions with gradually decreasing strength [133, 345]. It should be noted that hierarchical self-assembling is used at building several systems in nature, such as tobacco mosaic virus and cell cytoskeleton. In this approach supramolecular assemblies are self-organized through coordination of supramolecules between each other or their co-assemblies with other modulus. For example, through electrostatic interaction, M–L-based supramolecules can be integrated in films, liquid crystals, micelles, hydrogels, etc., which have a number of switchabilities and other desirable properties [33]. Besides, hierarchical self-assembling makes it possible to obtain exotic and complicated nanostructures, which are interesting for nanotechnologies and materials science [375, 376].

In recent decades, different strategies have been developed, which bring to hierarchical molecular self-assembling. We shall notice that for greater variety of linear and branched MSP self-assembled from small telechelic ligands and metal ions, it is scarcely possible to form hierarchical structures due to their homopolyelectrolyte character. Nevertheless, MSP based on Zn(II) and ditopic ligand can be organized in spherolites in gels formed by these MSP (Fig. 7.40) [130, 377, 378].
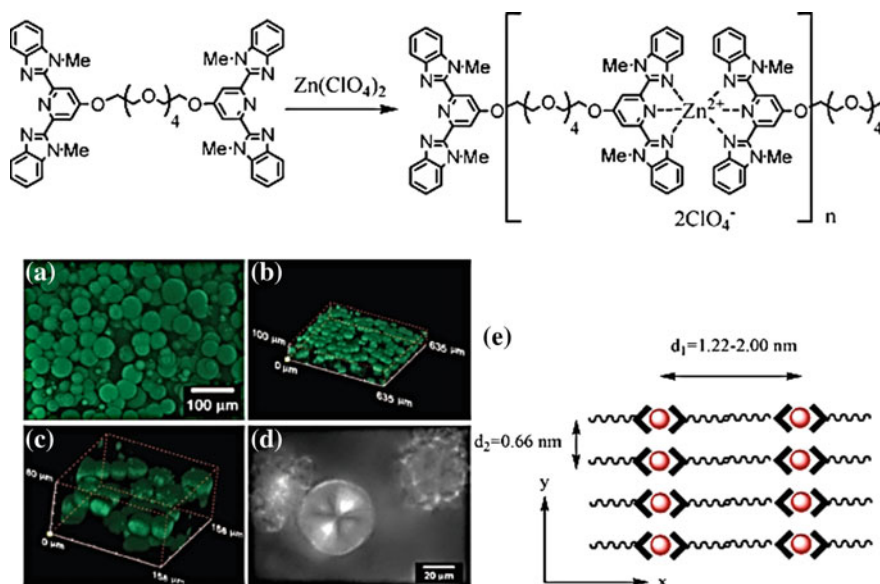
Fig. 7.40 Schematic representation of the formation MSP using ditopic ligand with metal salt, Zn $(ClO_4)_2$, in polar solvents. LSCM images **a** z-projection image, **b** and **c** 3D image of the MSP gel formed in 60/40 (v/v) DMSO/water mixture as shown in (**a**), and **d** polarized images of the MSP gel formed in 70/30 DMSO/water mixture (v/v) showing the coexistence of regular and irregular particles. **e** Illustrates the molecular packing mode in the aggregates

As the results of laser scanning confocal microscopy (LSCM) show, spherolites form through radial lamellar crystallization, and aggregation of these spheres at higher concentrations form a gel skeleton.

Hierarchical self-assembling MSP is easily accessible with block-MSP using if long hydrophobic and hydrophilic polymer blocks coexist in one MSP chain. For example, it is shown that micelles are formed in solution of such block-MSPs as PS_x-[M]-PEO_y [236], poly(ethylene-*co*-butylene)$_{70}$-[M]-PEO_{70} [238], PEO_{70}-[M]-$(CH_2)_{16}$-PEO_{70} [239], PS_{32}-*b*-$P2VP_{13}$-[M]-PEO_{70} [241] and polydimethylsiloxane-[M]-PEO_{70} [379], where [M] indicates position of M–L bond. Addition of HEEDTA to PS_{32}-*b*-$P2VP_{13}$-[M]-PEO_{70} brings to detachment of a PEO block and remains chelating groups on a micelle surface. It is important that PEO block could be restored if detached polymer chains would be mixed with micelles again (Fig. 7.41). This is one of examples of responses on exposure to environmental stimuli of MSP micelles. It is interesting that three-armed star-like block-MSP is self-assembled in vesicles in acetone, while tetra-armed analogue gives micelles again [265].

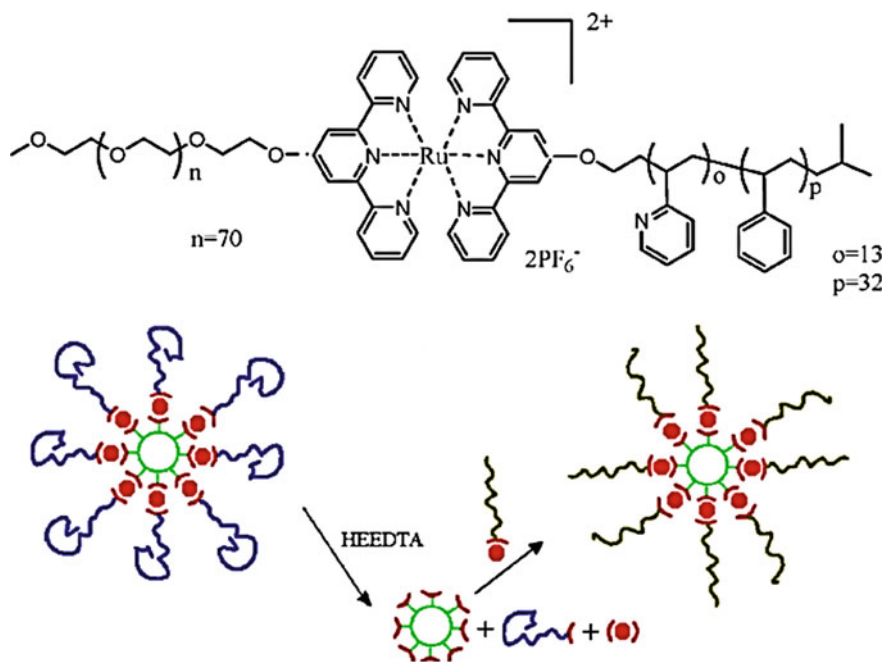**Fig. 7.41** The reversibility of tpy-Ru(II) complexes allow PSM of the micelles. The micellar hydrophobic core (green open circle) is surrounded by tpy (red brackets) Ru (red solid circle) bis-complexes; addition of a strong competing ligand (HEEDTA) allows the release of the coronal chains and the micellar core can be isolated. Reattach the coronal chains to the micellar core can be realized [241]

Multiple studies consider hierarchical self-assembling with MEPE participation, which can interact with such oppositely charged modulus as polymers, colloids or molecules carrying opposite charges [157]. It should be noted that exchange between counter-ions and MEPE brings to respective polyelectrolyte-amphiphilic complexes (PAC) [113, 380]. Whereas MEPEs are easily soluble in aqueous solutions, PACs are neutral and hydrophobic, therefore, soluble in ordinary organic solvents. For example, we shall notice PAC with liquid crystalline properties obtained by self-assembling dihexadecyl phosphate (DHP) with Fe-MEPE and Ni MEPE based on ditopic ligand 6,6′,6″-bis(2-pyridyl)-2,2′:4′,4″:2″,2‴-qua-terpyridine (Fig. 7.42, left) [300, 381–385]. In these PACs MEPE rods are incorporated between interdigitated DHP layers with formation of lamellar structures [300]. It is important that the respective Fe-PACs show unusual temperature-induced spin crossover [383–385].

It is well known that crystalline field of a strong ligand around metal ions forces them to stay in LS state [386, 387]. In particular, Fe(II) ion in Fe(II)-MEPE is diamagnetic, since all electrons are coupled. At low temperature PACs are assembled densely in LB films and in crystalline state, which has no effect on strong crystal field around Fe(II) ions. As temperature increases, energy released during phase transition changes the crystal field abruptly, so that a system becomes HS and paramagnetic (Fig. 7.42, right) [384].

We shall notice interesting shape of multi-comb MSP containing benzene sul-fonate counter-ions with long alkyl tails (Fig. 7.43) [388]. In this case a polymer supramolecule is based on functionalization of side chain of covalent polymer (P4VP) using Zn(II)-2,6-bis-(octylaminomethyl) pyridine M–L coordination, which
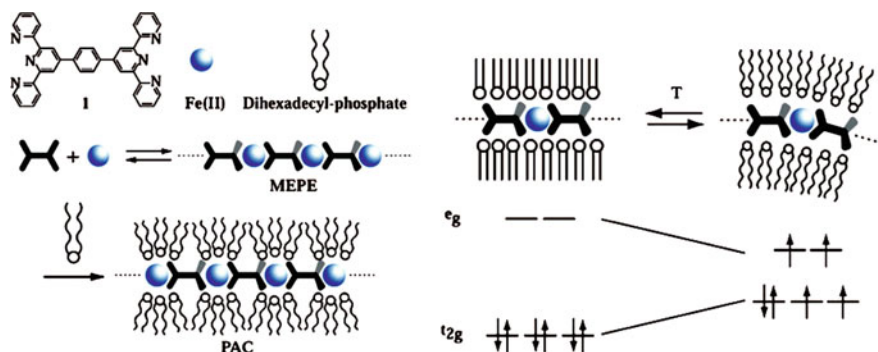
Fig. 7.42 (Left) Self-assembly of ditopic ligand **1** and Fe(OAc)$_2$ results in formation of the linear, rigid-rod-type MEPE. In a consecutive step, MEPE is assembled with DHP, resulting in formation of the corresponding PAC. Spreading PAC at the air-water interface and subsequent transfer of the Langmuir monolayers on a solid support results in a well-defined multilayer, which section is schematically shown in the bottom of the scheme. (Right) Upon heating the multilayer, the alkyl chains of the mesophase melt, resulting in a distortion of the metal ion coordination geometry. The unfavorable coordination of the tpy around the Fe(II) cation results in a lowering of the energy gap between the d-orbital subset, giving rise to a reversible transition from a diamagnetic LS state to a paramagnetic HS state
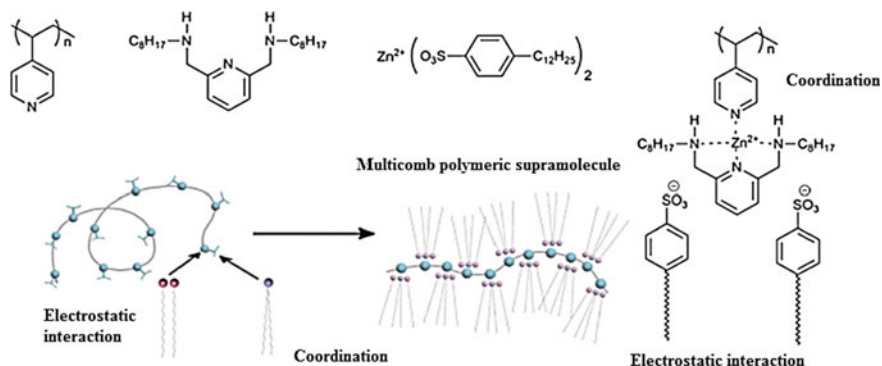
Fig. 7.43 Concept of binding several side chains with respect to one repeating unit of polymer main chain based on coordinated alkylated ligands and alkyl-functionalized counter-ions

then is electrostatically bound with sulfonate counter-ions. It is important that fragments of mutually repulsing overload side chains should reinforce cylindrical organization of the copolymers.

When mixing MSP with oppositely charged diblock-copolymer, neutral micelles can be formed in a solution volume [389]. These micelles belong to the family of the complex of coacervate core micelles (C3Ms) [390] or polyion coacervate (PIC) micelles [391]. It is obvious that MSP acts as homopolyelectrolyte in this micellar system. It should be noted that formation of micelles in supramolecular system includes two synergetic processes: polymerization with M–L coordination and micelle formation. In presence of oppositely charged block-copolymers local concentration of LMC can be increased considerably, so that DP significantly enhanced, in particular, «polymers» come into action.

This long «polymer» corresponds to «chain-matching» criterions to form electrostatic micelles [390]. It is interesting that size of a micellar core can be increased considerably by substitution of a part of diblock polyelectrolyte with homopolyelectrolytes of amphiphilic micellar systems [392]. Thus, the of $Zn-L/P2MVP_{41}$-PEO_{205} core size of micelles is increased with coefficient 10, where P2MVP is poly (2-methylvinylpyridine), and L is 1,11-bis(2,6-dicarboxypyridin-4-yloxy)-3,6,9-trioxaundecane [392]. A number of metal ions in micelles can be controlled, which is very important for such micelles as potential carriers of heavy metal. Like the covalent C3Ms, the micelles formed by M–L coordination are also sensitive to additional salt. For example, for the micellar system $Zn-L/P2MVP_{41}$-PEO_{205} critical concentration of micelle formation depends on salt exponentially [393]. Besides this, micelles show dependence on a character of coordinated metal ion [394]. For example, if transition metals of the first row are used, metal ion excess will have no effect on C3Ms. However, when transition metal ions of the first row are replaced by those from the second or third row, C3Ms can be broken by excess of metal ions. This indicates that metal ions from the first transition row do not extract ligands from a micellar core, while metals from the second and third row do

this, which results in formation of positively charged ends of a coordination chain and C3Ms falling-apart. It is also noticeable that excess of diblock-copolymers brings to formation of worm-like micelles, which remind strings of a spherical micelles, thus showing that there is weak attraction between these micelles [395, 396].

MSP are formed in organic solvents through M–L driven supramolecular self-assembling using 1:1 mixture of (dppp)M(OTf)$_2$ complexes (M = Pd(II) or Pt (II), dppp = bis-(diphenylphosphino)-propane, OTf = triflate) and non-linear bidentate dipyridyl-substituted ligand. In methanol aqueous solutions MSP hollow bubbles form and smaller completely filled nanospheres (Fig. 7.44) [397].

We shall notice universal hierarchical approach to assembling copolymer-metal nanostructures, in which one level of self-assembling guides the next one. For example, at the first stage ultrathin diblock-copolymer films form regular platform of highly anisotropic strip-like domains. At the second stage of assembling, the differential wetting guides diffusing metal atoms to aggregate selectively along the platform making highly-organized metal nanostructures. In this case a metal located on a copolymer matrix provides highly ordered configurations in the case when a system is far from equilibrium. Two different assembling regimes of the metal component of chains can be distinguished, particularly, of separate nanoparticles and of continuous wires; each is characterized by different ordering kinetics and stunningly different current-voltage characteristics [398].

Hydrophilic polymer-linked SCS-pincer Pd(II) complex and Py-functionalized PS form amphiphilic diblock-MSP, which is self-assembled in clearly defined monodisperse non-covalently linked micelles. It is important that hydrophobic domain of a core is easily removed using dialysis at low pH, giving a hollow polymer nanocage with well-defined internal functionality [399].

Spontaneous self-assembling of cationic nanoporous metal-organic coordination cages (nanocages) brings to giant hollow vesicle-like structures in polar solvents. These well-soluble nanocages (macrocations) are separated by hydrophobic areas, and their assembling proceeds not due to hydrophobic interactions, but due to
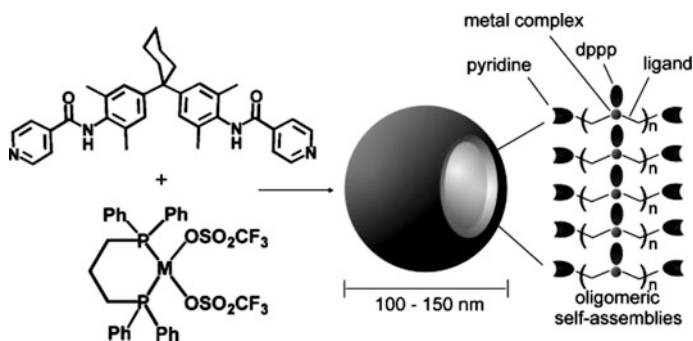

Fig. 7.44 Schematic representation of vesicle formation from self-assembled oligomer coordination compounds [397]

counter-ion driven attractions. As a result, blackberry structure is formed, in which self-assembled nanocages can provide a wide spectrum of functionalities, which cannot be achieved with purely inorganic systems [400].

Higher level of MSP with special functionalities will bring to unexpected surprises in hierarchical self- and/or co-assembling containing MSP. For example, a change in spacer structure of a telechelic ligand of the molecules can cause a considerable effect on function and hierarchical self-assembling properties of MSP and also can have an effect on topological feature of co-assembling with oppositely charged particles. MSP can be fluorescent at incorporation of a fluorescent group into a spacer [158, 401]. Moreover, responsiveness of molecular assemblies containing MSP to stimuli has not being studied thoroughly yet. This will also be very interesting to operate with coordinating force to control hierarchical interaction of molecular assemblies. For example, modified monoligand amphiphil is used to form micelles; these micelles will produce gels initiated by addition of metal ions (Fig. 7.45) [402].

Using a model system of 4-armed PEG hydrogels cross-linked with multiple kinetically distinct dynamic M–L complexes, it is shown that polymer materials with decoupled spatial structure and mechanical characteristics can be developed [403]. This model of hydrogels with kinetically different cross-linkings makes it possible to project time hierarchy of gel networks separately from spatial hierarchy, and thus to show new conceptual frameworks for viscous-elastic materials. In other words, by regulation of relative concentration of two types of M–L cross-linkings, it is possible to control mechanical hierarchy of a material by changing types of cross-linkings, but not by modifying a polymer itself.

The new strategy applied to fine supramolecular nanomaterials is using supracolloidal self-assembling, in which micelles or colloids are used as building blocks [404]. This directed supracolloidal self-assembling is done by dynamic covalent bonds and M–L coordination in water. Conjugation of a ligand precursor to water-soluble block-copolymer through dynamic covalent bonds brings to dehydration and micelle formation of a functionalized polymer. Reversible reaction facilitates penetration of metal ions into core-shell interfaces and, oppositely, M–L coordination advances reaction over interfaces. It should be noted that Cu(II)
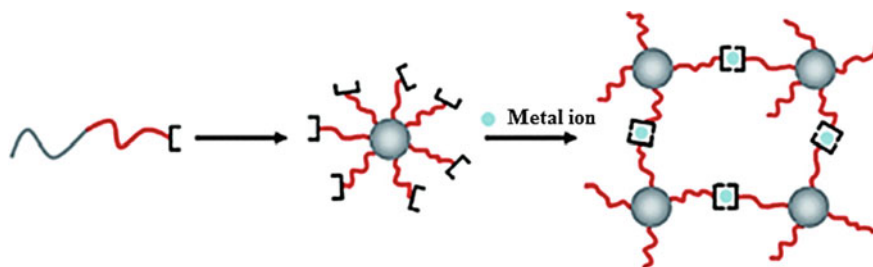

Fig. 7.45 Hierarchical self-assembling PS-*b*-poly (*tert*-butyl acrylate)-copolymer tpy ligand, leading to formation of supramolecular network of micelles [402]

coordination takes place entirely in each isolated micelle. However, Zn(II) coordination induces directed self-assembling, whose nanostructures are developed stepwise from nanorods, nanowires, necklaces, and, finally, to supracolloid networks of increasing scale to several ten microns. Post-reactions of simultaneous dynamic conversion of covalent bond and Zn(II)-coordination over core-shell interfaces provide these supracolloidal networks with vast specific surface for hydrophobic dative metal centers accessible for substrates in water. Therefore, directed supracolloidal self-assembling is a universal platform for creation of metal-hybridized nanomaterials, which are promising as enzyme-inspired water catalysts.

We shall also notice synthesis of supramolecular inorganic/organic hybrid colloids using concurrent and consequent self-assembling [405]. This conception of co-assembling broadens sphere of studying self-assembling block-MSP and provides new routes for design of hybrid colloids. In addition, such self-assembly offers unlimited opportunities for development of inorganic/organic hybrid functional materials.

7.10 Metallosupramolecular Polymer Gels

Gels are formed from a gelator and a liquid-solvent, at that the gelator concentration can be less than 2 wt%. Gels are divided into two categories: organogels and hydrogels, in which gelator molecules immobilize organic solvents and water, respectively.

In the recent years great interest is attracted to metallosupramolecular polymer gels (MSPGs), in which gelators are either MSP or discrete metal chelates self-assembled through other types of non-covalent interactions into supramolecular assemblies [101, 340, 406–415]. Increased attention to MSPGs is caused by their unique properties, ability to change their structure reversibly under action of external physical or chemical forces. It is extremely important that by changing nature and concentration of gelator it is possible to systematically modify and tuning physical properties of a material [166]. The reason for raising interest is in M–L coordination and its variety, which can easily cause or control self-assembling a gel, and therefore, can have an effect on its properties [101, 416–422]. In these special cases presence of metal ions in MSPGs chemical structure generates their fascinating potential applications, which include catalytic activity [423, 424], bioimaging [425, 426], controlled release [427], redox induced gel-sol switching [428], magnetism, color, rheology, adsorption, and photophysical properties [429].

There is extremely diverse range of compounds which can serve as gelators. Low molecular weight gelators are the key area in supramolecular chemistry studies due to spontaneous and controlled self-assembling phenomena [409, 430–453]. Therefore, search for new gelators for MSPGs is important task of contemporary supramolecular chemistry.

Low molecular weight gelators are self-assembled by combination of non-covalent interactions, such as π-π stacking, H-bonds, hydrophobic-hydrophobic interactions and Van der Waals forces, which brings to formation of entangled self-assembled fibrillar networks (SAFINs) [409, 410], which, additionally, form hierarchical 3D networks self-assembled through joint nodes. It is interesting that fine balance and combination of non-covalent interactions can be easily modified with account for these gelators, due to rational choice and design of chelating ligands in metal chelates, which, in turn, can bring to fine tuning gelation and gel morphologies. Molecules of a solvent are then immobilized due to capillary force in such 3D SAFINs, which results in gelation. It is assumed that 1D H-bonding networks advance gelation, while 2D and 3D networks give either weak gels or are not subjected to gelation at all [453]. Probably, anisotropic interactions, such as H-bonding of gelator molecules, which provides one-directional growth, and absence of such interactions in two other directions, prevent side growth thus bringing to 1D fibers advancing SAFIN formation and a resulting gelation [454–458]. Therefore, there is promising design of 1D network forming a supramolecular synthon, which would make it possible to obtain SAFIN and, finally, provides gelation. Gelator molecules generate hierarchical supramolecular structures, which are macroscopically expressed in gelation. Therefore, molecular modification can control nanometer assembling, the process, which finally determines a specific function of a material [457, 458].

Among low molecular weight gelators, the important place has gold chelates [430]. As an example, we shall notice luminescent bis-cyclometalated alkynylgold (III) complexes with long hydrocarbon chains, which can form stable MSPGs in non-polar organic solvents (*n*-hexane and cyclohexane), probably, using strong London dispersion interactions stipulated by long hydrocarbon chains. It is shown that at reasonable choice of coordinating ligands non-covalent interactions such as π-π stacking, and London dispersion forces can be easily corrected for rational MSPGs construction based on the gold(III) system (Fig. 7.46) [431]. Absorption of isobestic point at 408–410 nm supposes complete transformation of supramolecular assemblies into monomer types during sol-gel transition as temperature increases. On the other hand, there is irradiation at 570–620 nm, which is quenched at higher temperatures. This observation is associated with the fact that in gel state hardness of a medium will increase, and this will bring to decrease in molecular vibrations and motions, so that non-radiation deactivation ways will be delayed. At the same time, at higher temperatures non-radiation decay will be increased as a result of emission quenching. It is worth noticing a double functionalized MSP, self-assembled from two cyclometalated Au(III) complexes in acetonitrile [459]. For MSPGs partly aligned nanofibers with diameters and length up to 50 nm and ten micrometers, respectively, are detected (Fig. 7.47), and amino group of guanamine-like fragment of a ligand is involved in H-bonding interactions in the complex self-assembling. A 1D structure of MSPG with alternating H-bonding and π-π stacking interactions between two cations is suggested. It is known that many metal chelates have long living excited triplet states strongly irradiating in visible region, due to which metallogelators are ideal for luminescence-based technologies,
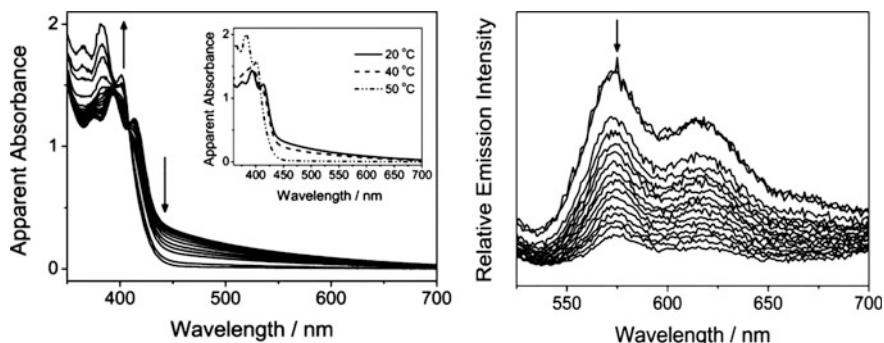
Fig. 7.46 UV-vis absorption spectral traces of the sol-gel phase transition of MSPG in hexane upon an increase in the temperature from 10 to 50 °C. Inset: spectral traces at 20, 40, and 50 °C (left); corrected emission spectra of the hexane gel of MSPG upon an increase in the temperature from 10 to 40 °C (right) [431]
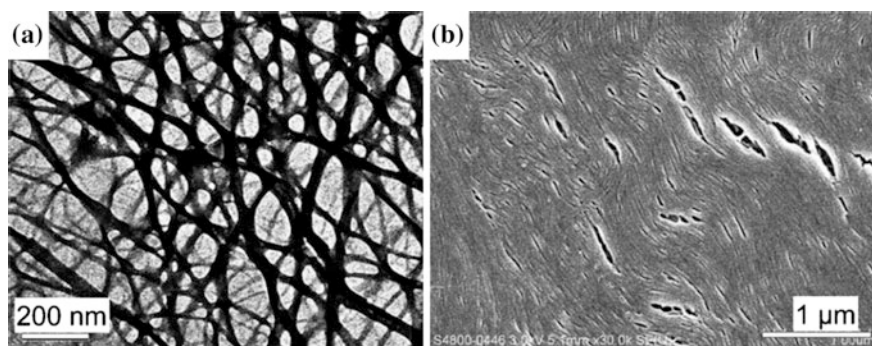

Fig. 7.47 **a** TEM image, **b** SEM image of MSPG. Photographs showing formation of the viscous fluid (supramolecular polymer) of MSP in CH₃CN [459]

photoelectricity and photocatalysis. This principle of design is implemented using trinuclear Au(I) pyrazolate metallocyclic gelator, whose phosphorescence at room temperature can be written in gel phase [418], therefore, these MSPG can be used to obtain safe inks for preparation of rerecording phosphorescent paper.

Among metal chelates of molecular type, the most attention has been attracted to polypyridyl complexes of transition metals. Thus, Cu(I) complex of bis(cholesterol)-functionalized bpy ligand gels PhCN, 1-PrCN and THF-MeCN [428]. It is interesting that greenish-blue gel color formed with Cu(I) chelate in 1-PrCN was absolutely different from reddish-brown sol color (Fig. 7.48). This is, probably, ascribed to distortion of coordination geometry of metal chelate in gel phase induced by molecular packing in gel fibers. Besides, due to presence of redox-active metal center, the sol-gel phase transition can be reversibly induced by addition of oxidants and reducing agents, which also bring to changes in geometry of a metal
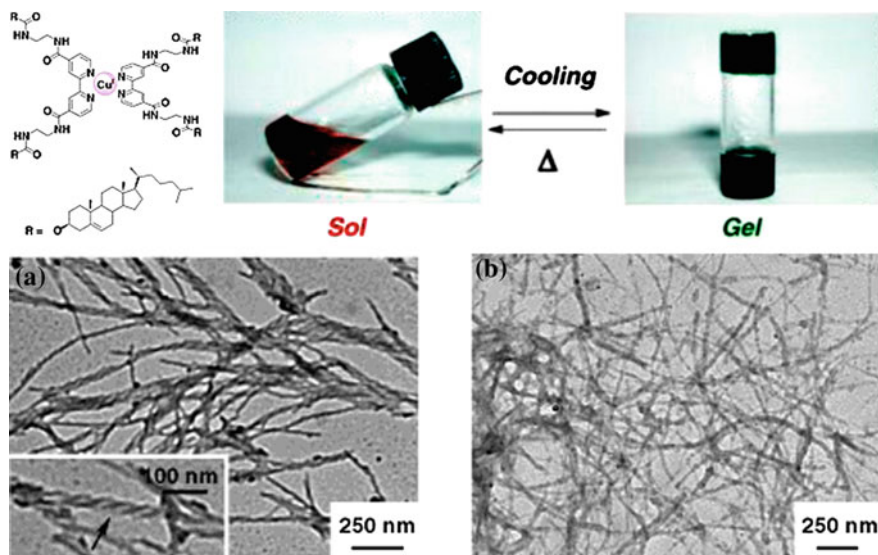
Fig. 7.48 Phase transition and thermochromic behavior of the sol and the gel phases of 1-PrCN gel based on Cu(I) chelate c bpy ligand, and TEM images of 1-PrCN gels prepared from initial ligand and metal chelate [428]

ion coordination as an oxidation degree changes, thus having effect on ability of a complex to π-stacking.

We shall also notice pseudo-planar trinuclear Cu(II) complex with inositol and bpy, which forms hydrogel at pH = 12.4 [460] that gives fiber super-structure. In this case π-π stacking interaction between bpy, presence of axial ligation, and H-bond of hydroxyl promote the formation of hydrophobic cavities, which hold the water molecules to form a hydrogel.

Steroid-phen conjugate is a powerful gelator for MeOH–H$_2$O even at such low gelator-to-solvent ratios as 0.1 wt% in absence of metal ions [461]. In particular, this gel is solved at storage with the formation of transparent solution of low viscosity, which reversibly forms the gel again at heating up to about 70 °C. Drastic differences between a ligand and metal chelate are ascribed to different spatial location of chelating ligands enforced by complexation of a metal.

Metal complexes with tpy ligands are wide range of metal chelate gelators. Chelating ability of tpy ligands provides metal ion capturing, therefore bringing to stable gels with restructured emission properties [462, 463]. Under ultrasonic conditions a range of hydrogels of tpy derivative carrying a carboxyl group is obtained with one equivalent of CeCl$_3$, PtCl$_2$, CuCl$_2$ or EuCl$_3$. We shall also notice chiral BINOL derivative of tpy [464]. Using ultrasound, suspension of Cu(II) chelate of this ligand in CHCl$_3$ gives a gel, which is potentially useful for visual chiral probing. In particular, the gel stayed stable at addition of (R)-phenylglycinol,
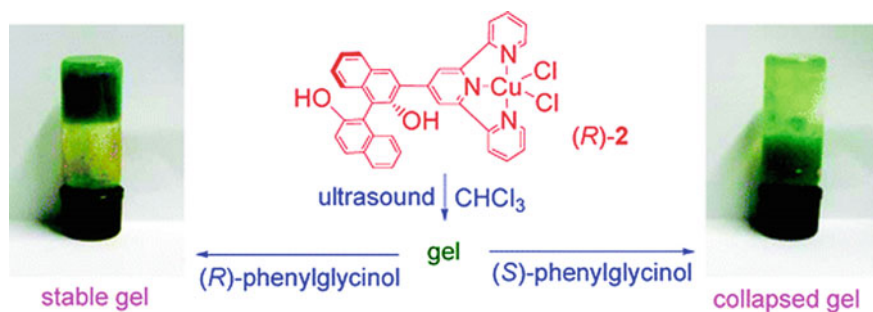
Fig. 7.49 Enantioselective response of the gel of Cu(II) chelate with BINOL derivative tpy in CHCl$_3$ toward (R)-phenylglycinol and (S)-phenylglycinol [464]

while the gel was decomposed under the same conditions at addition of (S)-phenylglycinol (Fig. 7.49).

In the case of ligand based on tpy and benzene-1,3,5-tricarboxamide central core, self-assembling molecules in the helix proceeds through triple H-bonding, and preorganized supramolecular polymers were additionally bound with Eu(III) using coordination between tpy groups and Eu(III) (Fig. 7.50) [83]. In the gel tpy fragments also functionalized as a sensitizing antenna for filling excited state $^5D_0$ Eu (III) and brought to the formation of typical Eu(III)-centered irradiation at 595, 616, 650, and 696 nm.

It is interesting that an iron complex with a tpy ligand carrying long alkyl chains gives stable gel in cyclohexane, while its ruthenium analogue does not form gel [465]. Besides, an initial chelating ligand and its iron complex give liquid crystalline phases in pure melted forms, while again the ruthenium complex does not do so.

We shall also notice metal-pincer complexes, which are efficient gelators. Thus, planar Pt(II) tpy alkynyl complexes blocked by tri(alkoxy)phenyl units carrying long chains of hydrophobic groups are good gelators for dodecane, and Pt···Pt, π-π and hydrophobic interactions take part in gelation [466, 467]. Intermolecular Pt···Pt
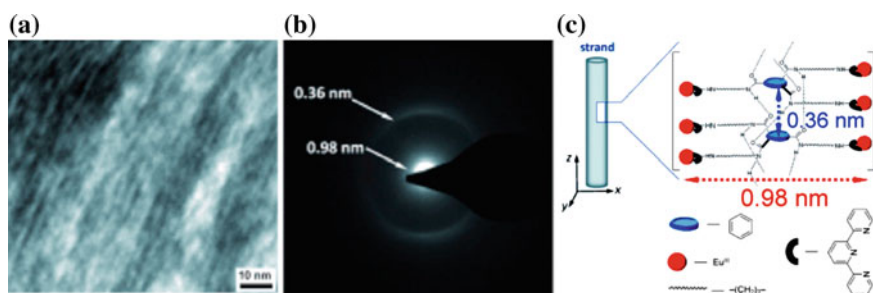

Fig. 7.50 a TEM image and **b** electron diffraction pattern of Eu(III) chelate gel, and c self-assembly of ligand based on tpy and benzene-1,3,5-tricarboxamide central core and Eu(III) into gel fibers

interactions and π-π interaction between Pt(II) tpy alkynyl fragments were also a driving force in the case of Pt(II) complexes of other tridentate N-donor ligands [468–471]. It is important that these Pt(II) alkynyl gels have shown sharp spectroscopic and luminescent changes at the sol-gel transition, in particular, Pt···Pt interaction (about 3.6 Å) provides a change in color and NIR emission [470].

CNC-Pd-pincer bis(imidazolylidene) complex with attached two C$_{16}$ alkyl chains form gels in different protonic and aprotic solvents even at such low concentrations as 0.2 wt% [472]. It is interesting that larger fibers are found in xerogels of protonic solvents (for example, methanol, acetic acid), while dense networks of fine fibers are formed in aprotic solvents (for example, DMF, DMSO, DMA, and THF). In this case, π-π stacking of heteroarene fragments, Van der Waals interactions between alkyl chains, and metal-metal interactions are responsible for aggregation. This Pd-pincer bis(carbene) complex is efficient catalyst for double Michael addition of α-cyanoacetate to methyl vinyl ketone, at that DMSO-based gel has shown higher catalytic activity than that DFM-based. Analogous aromatic-linker-steroidal metallogels have unique ability to visual enantioselective separation of (R)- and (S)-BINAP [473]. In particular, after addition of (S)-BINAP, the gels sustained heating and the following cooling, while gels containing (R)-BINAP decomposed. This response can be caused by blocking intermolecular π-π stacking and metal-metal interactions after substitution of chlorine-containing BINAP ligand. It is interesting that Pt-pincer gelators gel not only a wide range of protonic and aprotic organic solvents, but also different types of Ils, such as imidazolium, pyridinium, piperidinium, pyrazolidinium and ammonium salts [474]. Gel networks formed in Ils contain straight and long cotton-like fibers (10–25 mm in length and about 500 nm in width) (Fig. 7.51). Gelation in these materials is determined by non-covalent interactions, such as π-π interaction of widened planar metal-hybrid (hetero)arene fragments, Van der Waals interactions between alkyl chains and Pd···Pd interactions. Gels are more efficient catalysts for double Michael addition of
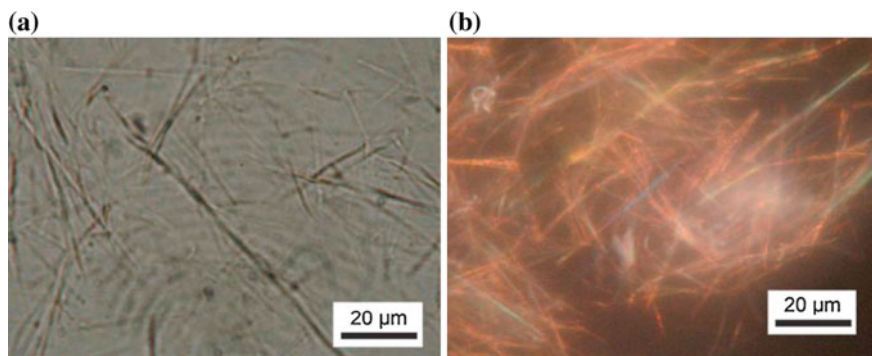

Fig. 7.51 Dark-field optical microscopic images of gels formed by Pd(II) pincer complex (5 mg mL^{-1}) with ionic liquids

α-cyanoacetate to methyl vinyl ketone as compared with respective homogeneous analogues [475].

Among metal chelates of intracomplex type, we shall notice a chiral clothespin-like *trans*-bis(salicylaldiminato) Pd(II) complex, which formed gels with a wide range of solvents without long alkyl chains or H-bond, but only after ultrasonic treatment (Fig. 7.52) [476]. For example, a complex formed by a normal solution in acetone after three second ultrasonic treatment transformed into opaque gel. Other similar complexes either with *syn*-conformation or with longer linking chains formed straightforward solutions, which were not affected by ultrasonic treatment. Ultrasonic irradiation also caused gelation of dipeptidyl Pd(II) complex using H-bonding intermolecular self-assembling [477]. Immediate and precise control over phosphorescent irradiation can be fulfilled using ultrasound-induced gelation of organic liquids with non-emissive solutions of racemic, short-linked dipalladium salicylaldimine complex (n = 5) and optically pure long-linked same chelate (n = 7). In this case increase in emission appears as a result of increase in planarity of chelate nodes in gel fibers. Dimeric homo- and heterometallic chelates first form colloid particles in solution, ultrasonic energy leads to sonocrystals; the following ultrasonic treatment disturbs certain sonocrystal samples to stimulate anisotropic growth of gel fibers (Fig. 7.53) [478]. Irradiation from gels can be controlled by changing the ultrasonic treatment time, a space length, and optical activity of complexes. In other words, structure-dependent homo- and heterochiral aggregations and ultrasonic control of aggregation morphology are key factors for emission enhancement.

We shall also notice integration of chelating HQ and multidentate hydrazinopyridine-IDA motifs in metallogels. Thus, square-planar Pt bis-Q complex functionalized via amide bonds by long chains forms gels with interesting emission behavior [479]. This chelate gels a wide range of solvents at low concentrations with fiber formation of about 50–200 nm in width and several microns in length. The absorption bands are shifted to longer wavelength in the gel (orange) as compared with the sol (yellow) according to π-stacking. A model of packing is
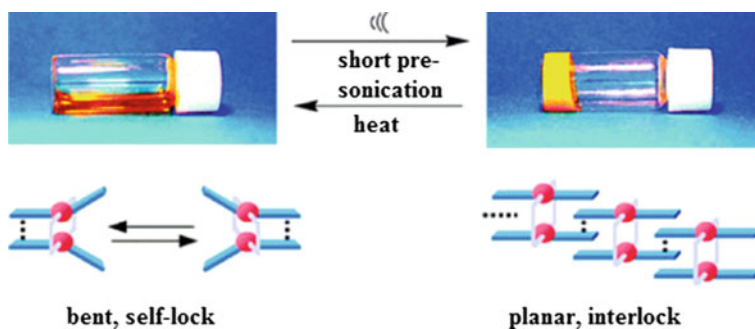

Fig. 7.52 Ultrasound-induced gelation of a chiral clothespin-like *trans*-bis(salicylaldiminato) Pd (II) complex with schematic molecular packing
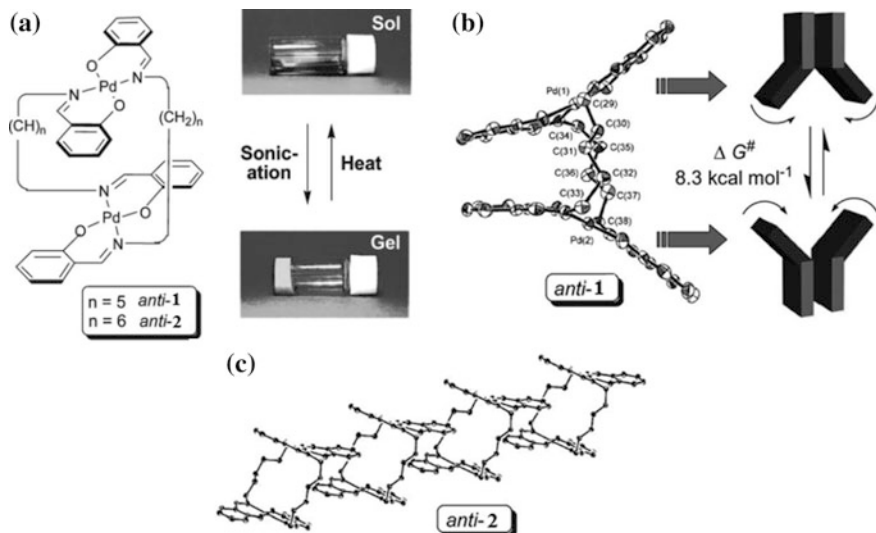
Fig. 7.53 a Molecular structures of anti-1 and anti-2 (left). Photograph showing mechano-responsive behavior of a solution of anti-1 (right). b X-Ray crystal structure of anti-1 (left) and schematic representation of the flipping motion in anti-1 (right). c X-Ray solid-state structure of anti-2
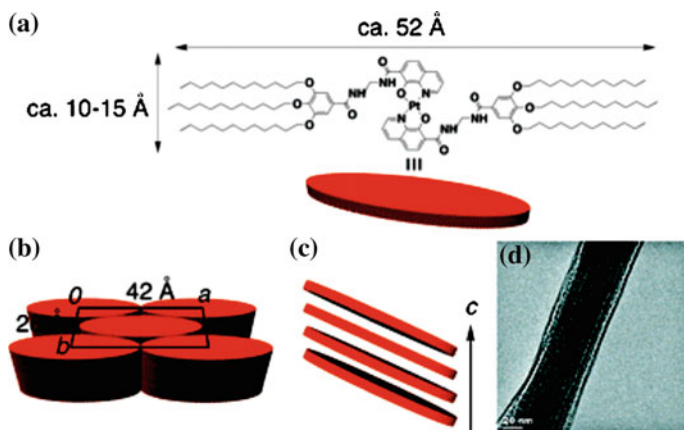
Fig. 7.54 a Molecular scales of Pt bis-Q chelate; b proposed packing model of chelate in the gel tissues; c tilted arrangement of chelate along the c axis; and d HR-TEM image of the chelate and p-xylene gel

proposed based on XRD of the gel phase with intercolumnar spacing 42 Å (Fig. 7.54). Dodecane gel of Eu complex with hydrazinopyridine-IDA nanocoordinated ligand with amide bonds and long chains has shown visible and NIR luminescence [480].

Interesting redox-responsive and enantioselective properties are found in MSPG based on Cu(II) complex of HQ-substituted L-glutamide [481]. In particular, it was shown that MSPG decomposed into sol after reduction and could be reduced after the following oxidation, besides, supramolecular chirality and morphology also changed reversibly with sol-gel transition. It should be noted that MSPG showed enantioselective recognition of chiral aromatic amino acids (Fig. 7.55). Thus, new blue emission band about 393 nm appeared when MSPG encountered with L-aromatic amino acids, while no new blue emission band was observed for respective D-aromatic amino acids. At that, such enantioselectivity was only observed in the gel state and such phenomenon was not observed in solution.

Also planar Cu(II)-β-diketonates functionalized with long chains that gel cyclohexane due to Van der Waals and other non-covalent interactions are interesting as gelators [418, 482]. In particular, there is a considerable decrease in hyperfine coupling at transition from isolated complexes to gel-like state, at that a signal from free complexes is regarded as a shoulder on «aggregated» signal thus showing coexistence of free and aggregated complexes.

Undoubtedly, macrocyclic complexes (M-Pp and M-Pc) are also efficient gelators. One of directions of enhancement of gelating ability of M-Pp is axial coordination of bridging ligands [483, 484]. Thus, for example, Zn-Pp itself does not gel benzene or toluene, however, addition of piperazine as axial ligand actually caused gelation. Triethoxysilyl-functionalized free base Pp could gel some solvents, while its copper analogue gels wider range of solvents at lower concentrations [484, 485]. It is important that in the first case sheet-like structures have formed, while in the second case fiber structures have formed (Fig. 7.56).

In another example, Cu-Pp formed flat ribbons, while free base Pp and Ni-Pp gave helically bent ribbons [486]. It should be noted that it is possible to adjust a helix step by the formation of mixed-Pp ribbons with different Cu/Ni ratios. An interesting observation is made in the case of tri-substituted Zn-Pp, which has three long hydrocarbon chains linked with the Pp core through ester bonds and one group of free acid [487, 488]. Based on combined experimental studies a model of
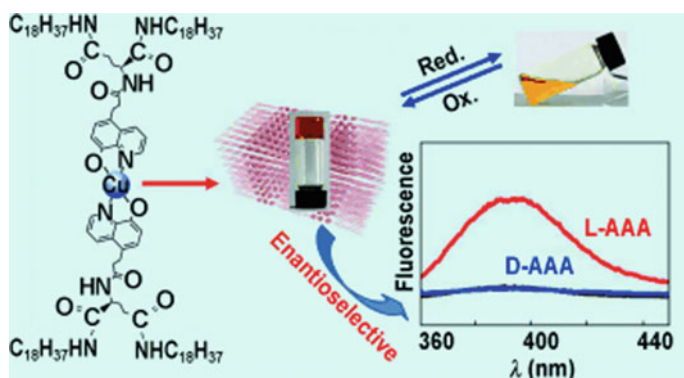

Fig. 7.55 MSPG having enantioselective recognition of chiral aromatic amino acids
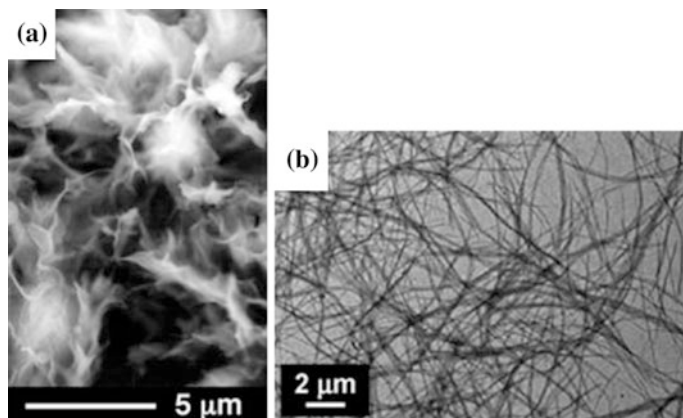
Fig. 7.56 **a** SEM image of the xerogel of self-assembled free base Pp in benzene and **b** TEM image of the xerogel prepared from the anisole gel of Cu-Pp
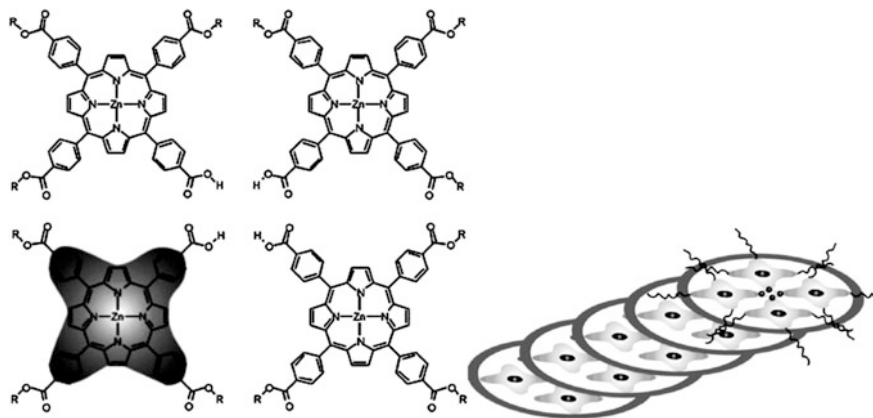
Fig. 7.57 Tetramer association of trimester Zn-Pp and their off-set stacking to produce fibers

packing regime is proposed consisting of planar tetramers with carboxylic acids positioned in centers in the off-set stacking (Fig. 7.57) [488].

Hydrogels are obtained from Fe(III)-tetraphenyl-Pp-functionalized 4-armed PEO films, in which water plays a role of cross-linking agent and swelling agent [489]. It is important that depending on pH, hydrogels present either characteristic of a chemical network or a dynamic transient network, at that intriguing behavior is completely reversible.

Two interesting observations are made during studying some Zn-Pp-cholesterol conjugates [490]. First, only molecules with two or four methylene spacers between Pp and cholesterol groups gave gels, while those with three or five were unable to gel the same solvents. Probably, even spacers give extended molecular conformations

suitable for packing cholesterol groups, while odd spacers give folded conformations. Secondly, addition of C_{60} reinforced the obtained gels; in particular, T_{gel} is abruptly increased (80 °C against 30 °C for initial Zn-Pp) up to Zn-Pp:C_{60} ratio 2:1 corresponding to sandwich-complexes with C_{60}.

We shall also notice M-Pc functionalized by chiral diols, which give fiber assemblies from aqueous solutions [491]. This self-assembling is a result of π-π interaction between Pc rings and H-bonding between diol units. It is important that the rings become closely linked as polarity (water content) of a solvent increases, and fiber aggregates and viscous solutions are observed only for Cu complex, but not for Zn analogue.

The host-guest interactions with participation of LMC are also used for MSPG production. Thus, MSPG is developed, which demonstrates LCST based on back-to-back twin bowls of 3D symmetric tri(spiroborate)-cyclophanes [492]. As compared with standard calix [4] arene (about 12.5–6 Å), cyclophane has wider cavities (about 17–11 Å) on both sides of a symmetry plane, which facilitates its linking with big guest molecules through π-π-stacking and electrostatic interactions. The studies have shown that a host can interactively encapsulate guest molecules [Ir(tpy)$_2$](PF$_6$)$_3$, which brings to MSP formation (Fig. 7.58a). It is interesting that thermal reversibility behavior of gelation is noticed at heating of a host solution (10 mM) and a guest solution (10 mmol) in N,N,N',N',N'',N''-hexamethylphosphor acid triamide (HMPA) above LCST, as a result phase transition takes place with organogel formation (Fig. 7.58b). Upon cooling to environmental temperature, the gel converted to sol during 15 min.
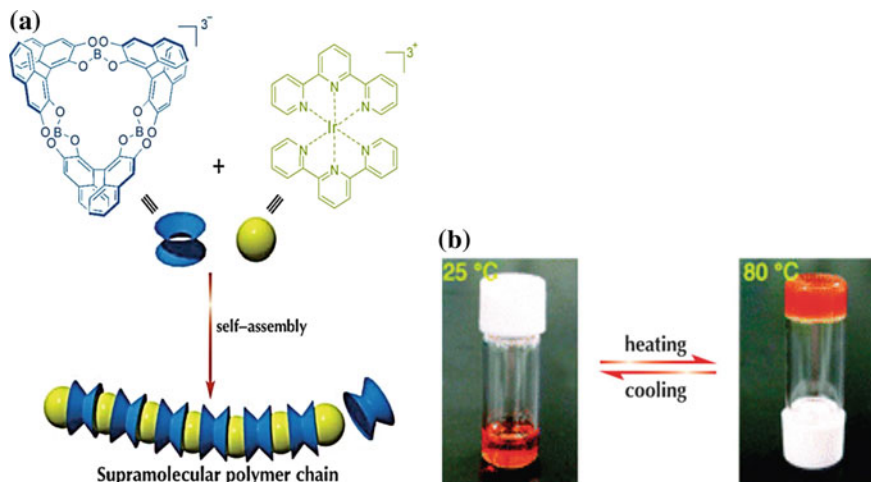

Fig. 7.58 a Cartoon representation of the formation of MSPG by iterative clathration of twin-bowl-shaped cyclophane with guest molecule; **b** illustration of the thermal reversibility of the resultant MSPG

However, the great majority of studies of MSPGs consider using M–L coordination as a main driving force. As a structural feature of MSPGs, these M–L bonds should present either in a polymer chain or as a link between covalent-bound units. Usually a MSPG is a combination of a metal ion and bridging organic ligands, which form multidimensional networks through capturing a solvent as a result of non-covalent interactions. As physical properties of these gels are similar to ordinary macromolecular polymer gels, MSPGs are often entirely reversible and can be assembled and disassembled in presence of additional energy (heat, ultrasound, shaking). Besides, as compared with gels obtained from purely organic gelators, metal ions included in fibrillar networks can give MSPGs with additional functions. Using fine tuning a system by choosing a metal ion and ligand, and directed self-assembling with external stimuli, rational synthesis of practically important systems is possible [248].

Thus, reversible coordination networks are obtained by combination of diphenyl-phosphinite telechelic poly-THF with Rh(I) or Ir(I) ions, which can coordinate four phosphoric ligands [493]. Oppositely to Rh(I)-based gels, in which gelation goes almost instantly, formation of Ir(I) gels needs about 30 min. Two obtained gels show very different mechanical properties, in particular, Ir(I) gels exhibit higher elasticity modulus than Rh(I) gels. This is associated with different linking kinetics of these two metal ions upon transition from the second row of d-block to third, since Ir(I) phosphinite complexes show far lower exchange rates than Rh(I) phosphinite complexes. Sonification has caused gel liquefaction, and when stored, the gel-fraction increased again with the rate determined by kinetics of M–L complexation. It is shown that ultrasonic treatment brings to ligand exchange, leading to decrease in a fraction of metal centers in active cross-linkings, and therefore, to decreased gel-fraction.

Viscous-elastic behavior and responsiveness to sonification of analogues MSPGs from ditopic phosphine-terminal poly-THF oligomers and Pd(II) chloride are studied [494, 495]. In this case collapse of gas bubbles formed during ultrasonic treatment generates shearing forces, which can cause damage in M–L bonds and thus bring to a chain termination and appearance of vacant coordination sites. When tangential stress is removed, MSPGs are reformed.

We shall also notice using bpy-chelating fragments in MSPG synthesis. Thus, polymer linear poly(p-dioxanones) carrying bpy units are cross-linked with Fe(II) ions with the formation of a permanent network, while crystallizing p-dioxanone segments serve as thermal trigger [496]. Another example is hydrogel formation from polyoxazoline containing pendant bpy blocks with many different transition metal ions [497]. Addition of Co(III), Fe(II), Ni(II) or Ru(II) ions has brought to non-covalent cross-linking and swelling bpy-branched polymers, however, stable hydrogels at room temperature are obtained only by treatment with Fe(II) and Ru (II) salts. Inertness and stability constants of bpy-metal complexes and, respectively, MSPG stability are determined by environmental conditions, such as pH, redox state, temperature and a solvent. Thus, thermal stimulus brings to acceleration of ligand exchange causing thermal cleavage of hydrogels, and swelling degree and stability of gels in water depend on bpy group content in a polymer. Bent-shaped

ligand monomers containing dendritic aliphatic side chains of different lengths form a complex with Ag(I) ions through the self-assembling process, which depends on nature of a side chain and counter-ions [498, 499]. In this case responsiveness is a result of a change in a secondary structure of a coordination chain, for example, of a transition from helical to zigzag-shaped chain, when a change in conformation of hydrophilic side groups is initiated by external stimulus or counter-ion size changes.

Extensive studies are concerned with tpy-chelating ligands for MSPG production. Thus, when transition metal ions are added, concentrated aqueous solutions of side chain of a tpy-functionalized poly (2-(dimethylamino) ethyl methacrylate) transform into MSPGs [500]. The PSM of poly(pentafluoride-St) obtained by selective substitution by tpy-functionalized synthones [501] is presented as universal method for MSPG preparation, which were then transformed into gel with addition of Fe(II) ions due to metallosupramolecular linking.

Apart from linear polymers, multiarmed star-like polymers containing tpy fragments have shown their applicability in preparation of metallosupramolecular networks [194] even in combination with ditopic ligands. Thus, four-armed PEG with tpy ends synthesized by post-modification of commercial PEG is used for preparation of MSPGs with addition of Fe(II) ions [502]. The obtained MSPGs have shown chemo-responsiveness, however, they were destroyed by addition of ammonia as a competitive ligand. MSPs based on 8-armed PEG partly substituted by tpy end groups and transition metal ions Ni(II), Fe(II), Co(II), and Zn(II) form nanoparticles under diluted conditions and gels at higher concentrations [503]. In particular, at polymer concentrations higher than 5 wt% cross-linking with addition of transition metals provides hydrogels, at that elastic hydrogels are formed with Ni (II), Fe(II), and Co(II), while Zn(II) gels are relatively viscous. It is important that only Zn(II) gels show thermos-reversed sol-gel transition at the temperature 25 °C independent on a polymer concentration. It is interesting to notice that this observation correlates with the results of study of MSPGs based on PMMA copolymers with tpy units in the side chains [504].

A simple strategy of incorporation of self-assembling behavior of amphiphilic block-copolymers and metal-tpy complexes in hierarchical levels is developed [402]. The first level of self-assembling was reached due to dissolution of tpy terminal-functionalized PS-*b*-poly (*tert*-butyl acrylate) diblock-copolymers in selective solvent for *tert*-butyl acrylate block. As a result, micelles were obtained consisting of PS core and poly (*tert*-butyl acrylate) coronal chains carrying a tpy ligand on their end. The second level is initiated by addition of metal ions [505]. It is important that intra-micellar chelations bring to exclusively flower-like micelles in diluted solutions [282], while micellar MSPG are formed in concentrated solution. At that, by varying conditions (temperature and a co-solvent presence) rod-shaped or spherical micelles with hard or soft cores are obtained [506]. Studies of such amphiphilic copolymer as poly (triethyleneglycol methyl ether methacrylate)-*b*-PS with tpy groups randomly distributed inside a water-soluble block [507] have shown the same results. Micelles of this copolymer form gels after addition of Ni(II) ions at far lower concentration than that of a respective homopolymer, which points to the effect of hydrophobic PS block on critical concentration of gelation.

We shall notice a tripodal tpy ligand, which forms helical 1D supramolecular polymers/gels in solution mediated through H-bonds and π-π interactions. Additional cross-linking these gels into 3D MSPG with a range of metal ions such as Fe(II), Ni(II), Cu(II), Zn(II), and Ru(III) brings to formation of color or colorless gels. Fiber-like morphology of these gels is found, in which metal ions work as «supramolecular glue» linking stands together in large architectures with higher ordering [508].

MSPGs are obtained using a chelating polymer containing a tridentate btp ligand block and transition metal ions and/or lanthanide ions. It is interesting that gelation and gel properties, for example, swelling, can be adjusted using thorough choice of metal ions and their combinations, solvents, concentrations, etc. [509]. Self-assembling direction with participation of polytopic chelating ligands can be regulated by integration of respective substituents in chelating fragments. Thus, interaction of btp trimethyl ether with Eu(III) has shown formation of luminescent 1:3 complex, which has been studied in solution and solid state, while btp tricarboxylic acid forms deep red luminescent hydrogel [510]. It is established that repeated btp unit takes predominantly *anti-anti* conformation and, therefore, extended heteroaromatic polymer strands take helical conformation (Fig. 7.59). Addition of Fe(II), Zn(II), and Eu(II) metal ions has brought to instant gelation as a result of coordination cross-linking of the polymer chains. In other words, in btp ligand based MSPG the bridging metal complexes serve not only as cross-linking points, but provide different functions potentially useful for design of new magnetic or emitting materials [152, 153].

It should be noted poly (*n*-butyl acrylate-*co*-MMA) copolymers carrying Mebip side groups (varied in the range 3.2–7.6%), which form MSPG using the metal salt, Zn trifluoromethanesulfonate [511]. Development of massif of anion sensors based on MSPGs, which can precisely detect CN^-, SCN^-, S^{2-} and I^- in water is interesting. This massif of sensors is based on new design approach called «competitive coordination control AIE mode» for development of anion-responsive MSPG,
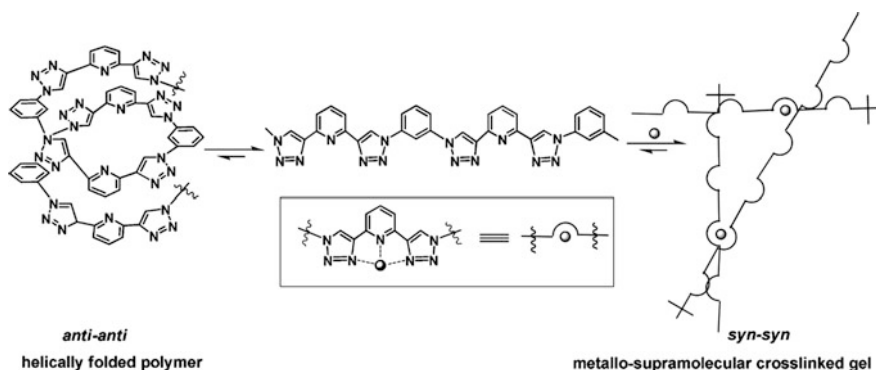

anti-anti
helically folded polymer

syn-syn
metallo-supramolecular crosslinked gel

Fig. 7.59 Schematic representation of metal chain-extended polymers based on BPT chelating units

which need only one synthesized gelator [512]. Rational integration of Ca(II) and Fe(III) into supramolecular gel resulted in production of bimetallic MSPG, which can reversibly «switch on» its fluorescence upon detection of $H_2PO_4^-$ with a certain selectiveness through competitive coordination of Ca(II) and Fe(III) with gelators and $H_2PO_4^-$ [513]. Therefore, bimetallic MSPG can work as $H_2PO_4^-$ test-set and can be used in rerecording safe imaging (display) materials.

We shall notice MSPG formation using P4VP and ditopic metal chelate cross-linkings [78, 514]. Thus, MSPG were obtained during addition of bis-Pd(II)-pincer complex with methyl substituents or more thermodynamically and kinetically stable Pt(II) analogues to P4VP in DMSO. Substitution of *N*-methyl substituent with ethyl has no effect on thermodynamics of N–Pd(II) interaction; however, exchange rate of ligand decreases by about two orders of magnitude. Reversible gel-sol transition can be controlled by tuning pH of a system or using competitive additives, such as dimethylaminopyridine or Cl^--ions, which can displace Py in the main polymer chain [275]. Mixing different cross-linkers, i.e. bifunctional Pd(II) or Pt(II)-pincer complexes with P4VP has given systems with strong to weak gel transition, rather than a distinct gel-sol shift [276]. When concentration of each cross-linker was over the critical percolation threshold, kinetically slow cross-linker, i.e. Pt(II)-containing metallopincers determined properties of a gel. When sufficient amount of competitive cross-linker was added to drop concentration of «active» cross-linking unit below their individual percolation thresholds, but still providing the total number of active cross-linkers being above the percolation threshold, a gel is formed, whose properties are controlled by kinetically rapid cross-linker, Pd(II)-containing metallopincer.

The concept is developed [77, 114, 115, 129, 196, 223, 515–517] of MSPGs building based on chelation of a ditopic ligand monomer with combination of lanthanide(III) ions and transition metal ions. Since ionic radii of lanthanide metals are far bigger than those of transition metals, they can form complexes with three tridentate ligands, which brings to formation of 3:1 M–L complexes, and, therefore, can form strong dynamic coordination networks. In this case, gels are formed by mixing telechelic chelating ligand with combination of lanthanide (cross-linker) and transition (chain extender) metal ions, respectively. Taking into account that lanthanides are weaker binding metal ions, as compared to transition metal ions, metal complexes based on lanthanides can be successfully treated as switching branching points, which can give response with temperature or load changing. Addition of lanthanide ions (<5 mol% per ligand) followed by transition metal ions addition (>95 mol% per ligand) to telechelic chelating monomer solution brings to MSPG production. Bis-tpy linking ligand consisting of two O-Mebip ligands with penta (ethylene glycol) pendant core to each end is used as a telechelic chelating ligand. Under respective conditions transition metal ions such as Co(II) or Zn(II) can bind two O-Mebip ligands and, therefore, act as a chain extender for generation of linear polymers. Lanthanide ions, for example, La(III), Eu(III) can link one or three O-Mebip ligands depending on a counter-ion nature, and, therefore, potentially be the chain growth stopper or a trifunctional cross-linker. MSPG formation can be

easily achieved upon addition of transition metal ions and lanthanide ions to ditopic ligand in appropriate solvent. Since lanthanide complexes are less stable, branching points are open when a gel is heated or if mechanical stress is applied with shaking, forcing gel to liquefy. After cooling or removal of mechanical load, gel immobility is reformed. It is important that Eu(III)-based gels show typical red luminescence of complex Eu(III) ion, which is sensitized by energy transfer from ligand to ion. If Eu (III) complex is open under action of heat or mechanical load, luminescence is changed to blue, which is associated with ligand-centered emission.

Luminescent MSP is developed [518], which is surprisingly subjected to sol-gel transition with rise in temperature. In this approach, a linear conjugated polymer material is synthesized into DMSO through condensation of a linear diamine and dialdehyde subcomponents around Cu(I) templates in presence of bulk trioctylphosphine ancillary ligands. This polymer solution undergoes sol-gel transition with increase in temperature, contrary to behavior of most MSPGs, which do so on cooling. Development of cross-linkings by copper chelation was accompanied by formation of sterically overloaded copper-trioctylphosphine complexes in equilibrium with free phosphine ligands. Since these MSPGs undergo sol-gel transition with temperature, due to formation of active cross-linkings between linear polymer chains, emission intensity and color are easily adjusted depending on temperature. It is interesting that luminescence changed color from orange to green when a sample was heated, and turned back to orange when a sample was left to cool to room temperature.

MSPGs based on catechin-modified four-armed star-like PEG and Fe(III) ions were obtained [519]. Since stoichiometry of pyrocatechin-Fe(III) complexes is determined by protonation degree of pyrocatechin hydroxyls, control over intermolecular cross-linking is possible only via pH. Besides, possible dissolution of cross-linked tris-complex gel using treatment by strong chelating EDTA agent is shown.

Interesting innovated MSPG is developed based on tritopic ligand having a bis-tpy cyclam block and divalent metal ions such as Co(II) and Ni(II) (Scheme 7.17) [520–522]. A ligand metalation in DMF with $Co(ClO_4)_2$ in molar ratio 1:1 brings to red solution, which points to formation of $(tpy)_2Co(II)$ derivative, in which cyclam block remains metal-free. Addition of another equivalent $Co(ClO_4)_2$ to the previous solution brings to formation of a cyclam-Co(II) block and, respectively, to MSPG formation. When ligand metalation is carried out in DMF with addition of two molar equivalents of Co(II), MSPG is formed spontaneously at concentrations below 1.0 wt%. In the gels, respective network includes original fibers (R ≈ 35 Å), bundles of these fibers, and a fraction of limited sized aggregates (rods with the ratio f ≈ 3–5). It is found that distribution of the latter structural components is sensitive to character of metal ions. These MSPG show a range of original constructing features and easy control over developed structures in gels, tuning their thermodynamic parameters.

Achiral benzo-21-crown-7-substituted bis(carbamide) low molecular weight gelator is hierarchically self-assembled in helical fibrils, which then transform into
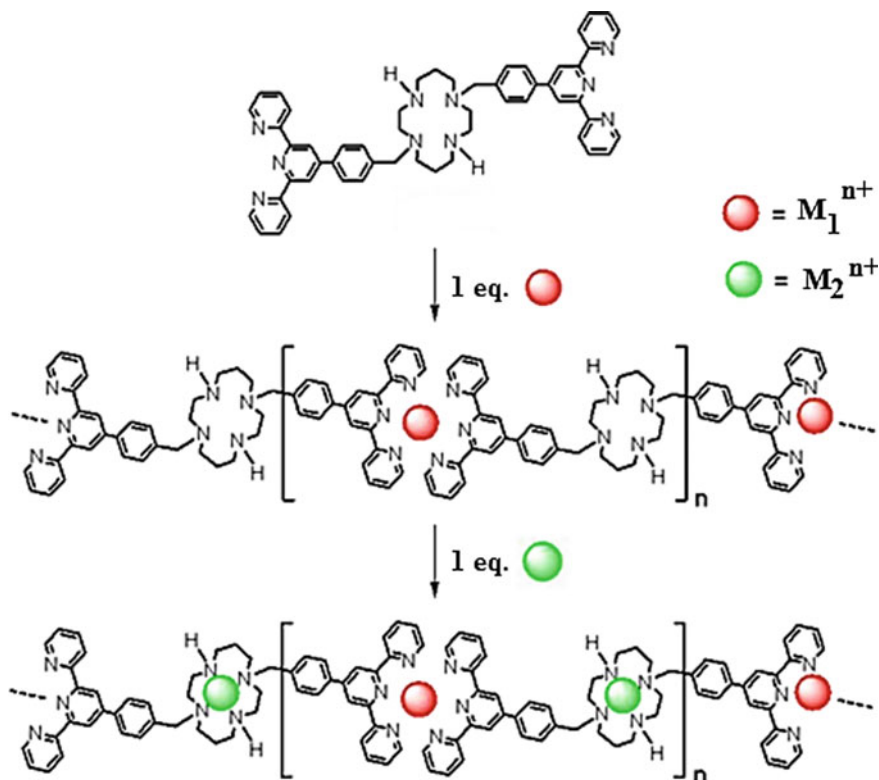
Scheme 7.17 Scheme of the formation of MSP by self-assembly of tritopic ligand, having bis-tpy cyclam unit, and $Co(ClO_4)_2$

bundles and then form stable gel in acetonitrile [523]. K(I) binding to crown ethers causes gel-sol transition, and addition of cryptand, which scavenges K(I) ions, can make this process reversed. Based on this gelator and chemical stimulus, a range of different systems can be developed, which behave how logical gates. Thus, depending on choice of these components OR, AND, XOR, NOT, NOR, XNOR, and INHIBIT elements were realized. In some cases a type of logical element is determined by concentration of input signal, so that even more complicated reaction with gel in direction of two input signals would be achieved.

It is worth noticing using advantage of cationic cobaltocenium as a key building block for switching organogels to hydrogels using highly efficient ion exchange [524]. It is interesting that using unique complexing ability, cobaltocenium fragments provide a robust soft substrate for utilization of antibiotics from water. Besides, a substantial polyelectrolyte nature of MSPG provides to kill bacteria with multiple drug stability.

7.11 Self-assembled Metallosupramolecular Monolayers

Self-assembled monolayers are ordered molecular assemblies spontaneously are formed upon adsorption of adsorbate on a solid surface and organized in more or less large ordered domains [525–529]. SAMs provide a convenient way for formation of surfaces with specific chemical functionalities. The main parameters providing control of molecule positions on surface are stoichiometry of binding, stacking density, binding dynamics, bond strength, order, and reversibility. Covalent immobilization of molecules does not suggest a convenient universality and flexibility for most of these parameters, while supramolecular interactions provide control over these criteria. Really, the self-assembling process of nanometer ordered structures makes it possible to control film composition and thickness with accuracy up to fractions of nanometer. To prepare SAMs, amphiphilic molecules are actively used, which are bound with one functional group to surface, while another functional group is responsible for interaction with other adsorbed molecules. During SAM formation usually a substrate is coated with low-concentrated solution of respective molecules, which through covalent bonds form a self-assembled monolayer, and excess molecules are removed by washing a sample in solvent. Using LbL technique, two or more components are deposited consequently and repeatedly to elongation a monolayer in a controlled way [530–533]. Using M–L interactions in LbL technique provides design and production of new, highly ordered, highly oriented, universal and robust 2D functional multilayered thin films and even 3D nanoarchitectures based on MSP.

Stepwise building multilayered structures using M–L interactions (Fig. 7.60a) has considerable synthetic value, since coordination bonds propose a good balance between hardness and reversibility [534]. Metallosupramolecular structure has an anchor layer consisting of SAM, chemisorbed to surface. Then an anchor ligand follows, which includes chelating fragments. Metal ions play a role of a cross-linking for the following layer of ligands, which has a chelation center of a metal ion. Finally, on the top of this layer alternately deposit the next layer of metal ions and chelating ligands to increase the film thickness. Depending on whether a ligand includes two or three chelating fragments, linear or branched structures can be obtained, respectively. It is important that M–L interactions are subjected to spontaneous and quantitative conjugation between metal sources and ligand molecules, which, in the end, brings to defect-free self-assembled multilayers. The role played by M–L interactions is not confined only to linking of adjusted layers. The resulting M–L supramolecular motifs can give practically important functions to final products, such as redox properties, magnetism, emission, catalytic activity and intermetallic interactions.

To obtain supramolecular SAMs based on M–L interactions the most widely used is the method of solution-based LbL growth. It provides achievement of exactly defined surfaces with different functionalities by pre-functionalization of different substrates (in particular, Au, Si, SiO_2, ITO glass, etc.), for example, with thiol or silicon-organic molecules to start SAM development containing either
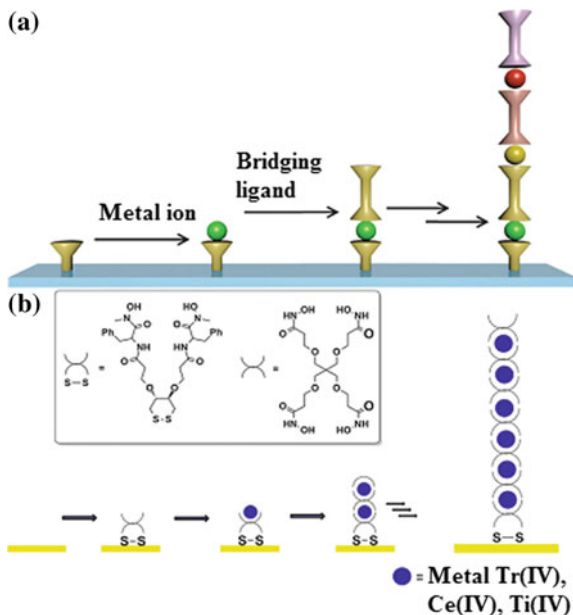
monofunctional OH-, COOH- or N-end groups or chelating fragments. Then surfaces are functionalized with these organic spacers, which provide several available functionalities and long-range 2D order, direct orientation, nucleation, structure, stability, and quality of additionally deposited thin films.

As an example, we shall notice directed self-assembling bishydroxamate-based metal chelate multilayers on Au using LbL approach (Fig. 7.60b) [535]. In this case supramolecular M–L interactions bring to higher thickness, increased roughness, higher electric resistance, and better rigidity of surface. In the same way branched metal chelate multilayer films are obtained on Au surface functionalized with SAM bishydroxamate disulfide molecules by alternate deposition of organic ligand having three bis-hydroxamate arms and a metal ion such as Zr(IV), Ce(IV), and Ti (IV) [536, 537]. However, multilayer assembling is usually very slow process, which, depending on a ligand type, metal ions and used solvent, can take a long time, which is inappropriate for practical commercial applications. In this connection more rapid method is developed [538] for assembling metal chelate M–L-based multilayers on functionalized surfaces called accelerated self-assembling procedure (ASAP). In this method rapid binding organic layers of a ligand proceeds for a few minutes: a small volume of an organic ligand solution is spread on a surface modified by a metal-containing layer and is evaporated under conditions of natural convection, as a result a surface is covered by excess of organic ligand. Further extensive rinsing in pure solvents brings to removal of weakly adsorbed molecules from surface leaving only new metal chelate adsorbed layer.

Non-covalent M–L coordination is developed for assembling supramolecular photocurrent-generating systems [539]. In this case, SAMs are built from molecules

consisting of disulfide alkyl group covalently bound with 12-residual helical peptide and capped with alanine residual containing pyrene chromophore. Consequent deposition of three or more components has brought to pyrene-containing multilayer based on Cu(II)-, Co(II)-, and Fe(III)-chelation (Fig. 7.61a–c). These systems on Au surface have shown high stability and high current generation in presence of methyl viologen and triethanolamine for cathode and anode currents, respectively. It occurs that the highest cathode photocurrent is observed in Cu(II) system, and Fe(III) chelate system has shown the highest anode current.

It is interesting to study behavior of a charge trap in heterometallic chelate SAMs (Fig. 7.61d) [540]. In this case a change in sequence of self-assembling layers of two isostructural bpy-based metal chelates brings to materials with electrochemical properties, which depend on assembling order. Thus, Os chelate layer formed on 8-nm thick Ru chelate layer has shown a sharp peak of catalytic oxidation without a visible reduction wave, while a Ru chelate layer has given a reversible redox wave. And on the contrary, a Ru chelate layer based on thick Os chelate layer has shown a sharp reduction peak and strained oxidation wave, whereas a reversible redox pair of Os chelate layer appeared. This series of phenomena can be explained by electron transfer between the upper layer and the electrode through the bottom layer.
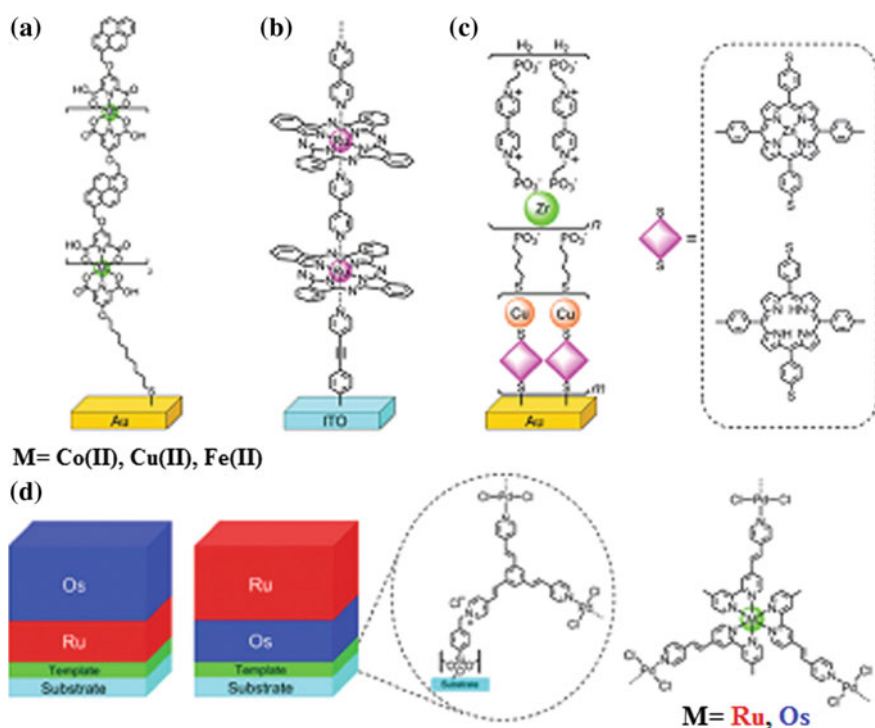

Fig. 7.61 a–c Examples of metal complex multilayers for photocurrent generation. **d** Example of a redox film showing charge trapping

SAMs were obtained by alternating the deposition of $PdCl_2$ and iron bpy complexes 1–4 (Fig. 7.62) from solution on a pyridine-terminated monolayer. This monolayer is covalently bound to the surfaces of ITO, quartz, and silicon substrates through a chlorobenzyl-functionalized coupling layer. SAMs are used for production of highly efficient electrochromic assemblies, which display practical combination of low voltage work and efficient electrochromic switching, and also durable thermal and redox stability (1.12×10^5 cycles) [541]. These molecular assemblies can be integrated into solid-state configuration; at that SAM molecular structure correlates with growth and principle of materials action.

Undoubtedly, most studies of SAM are carried out with tpy ligands. Thus, M–L assembling is performed on Au for preparation of redox-active mono- and polymetallic systems with participation of Co, Cr, and Os chelates with thiol-modified tpy ligand 4′-(5-mercaptopentyl)-tpy and tetrapyridylpyrazine (Fig. 7.63) [542]. It occurs that free ligand, as well as tpy-containing metal chelates are strongly adsorbed on surface of Au electrodes, at that in the case of metal chelates they retain their redox-active responses at potentials very close to non-adsorbed analogues in homogeneous solution.

The similar approach is used for building polymetallic complexes by repeated deposition of Fe(II) and/or Co(II/III) ions with azobenzene-bridging bis-tpy ligand on tpy-terminal SAM on Au [543]. It is interesting that purposed formation of desired number of polymer units, for example, 47-dimensional Co(tpy)$_2$ structures and desired sequence of Co-Fe heterometallic structures in a polymer chain, for example, 10-dimensional Co(tpy)$_2$ plus 5-dimensional Fe(tpy)$_2$ is possible.

We shall notice use of click chemistry for covalent binding acetylene-functionalized Fe(II) bis-tpy chelate on azide-terminal SAM [544]. Using decomplexation of formed supramolecular chelate, ligand-modified monolayer can be obtained, which is then used for additional chelation reactions, leading to reversible functionalization of substrates (Scheme 7.18). It is important that right choice of coordinating ions of transition metals provides tuning binding force and physicochemical properties of formed chelates, and therefore, design of surface properties.
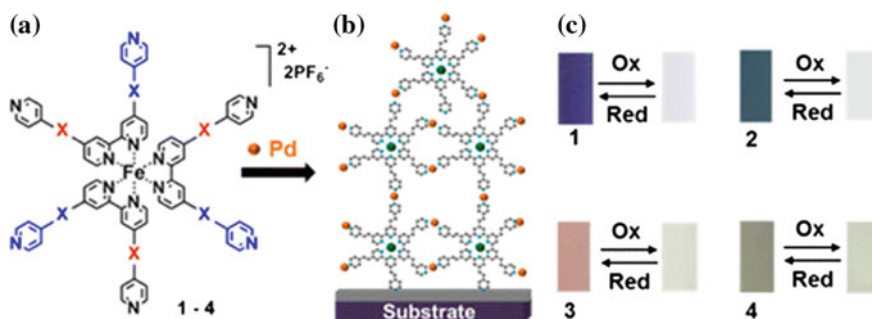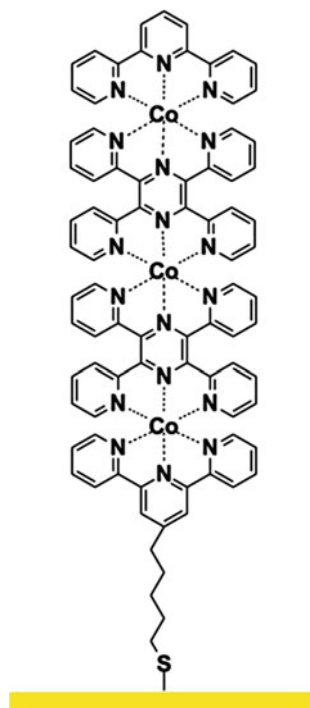

**Fig. 7.62** Molecular structures of polypyridyl complexes **1–4** (**a**) and SAMs (**b**). Electrochromic switching of the SAMs (**c**)

Using chelation of Pt(II) ions with asymmetric ligand containing tpy and pyridyl residues, luminescent MSP is synthesized, which has characteristic dipole moment [545]. A polymer was specifically fixed on Au electrodes to obtain two types of films (films 1 and 2), in which polymer chains are positioned with regard to their dipoles in opposite directions (Fig. 7.64). It occurs that the film 1 has higher conductivity in positive field displacement with an average rectification coefficient 20, while the film 2 has higher conductivity in the negative area displacement with an average rectification coefficient factor 18.

1,3-Butadiyne-cross-linked diruthenium chelate is fixed on Au electrode surface in horizontal position for SAMs formation showing multiple irreversible redox behaviors on the electrode surface (Fig. 7.65) [546]. It is interesting to notice that types of diruthenium with different oxidation degrees, in particular, Ru_2(II, III) states, which are non-stable and cannot be isolated from solution, can be detected in situ using IR spectroscopy.

It should be especially noted that linear and branched bis(tpy) metal chelates based SAMs relate to such interesting class of materials as molecular wires [547, 548]. These systems have a clear and distinctive electronic functionalities, intra-wire redox conductivity and excellent long-range electron transfer capacity [532]. It is important that these systems are built with a wide range of tpy-containing chelating ligands. Wires based on bis(tpy) metal chelates consist of four components: surface-linked tpy ligand (A series), metal ions, bridging tpy
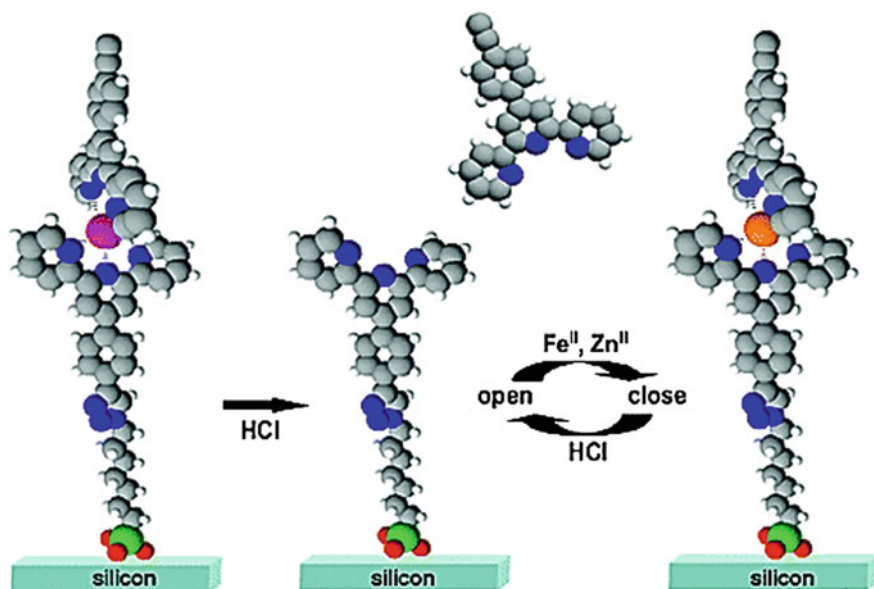
Scheme 7.18 Scheme of reversible functionalization of substrates
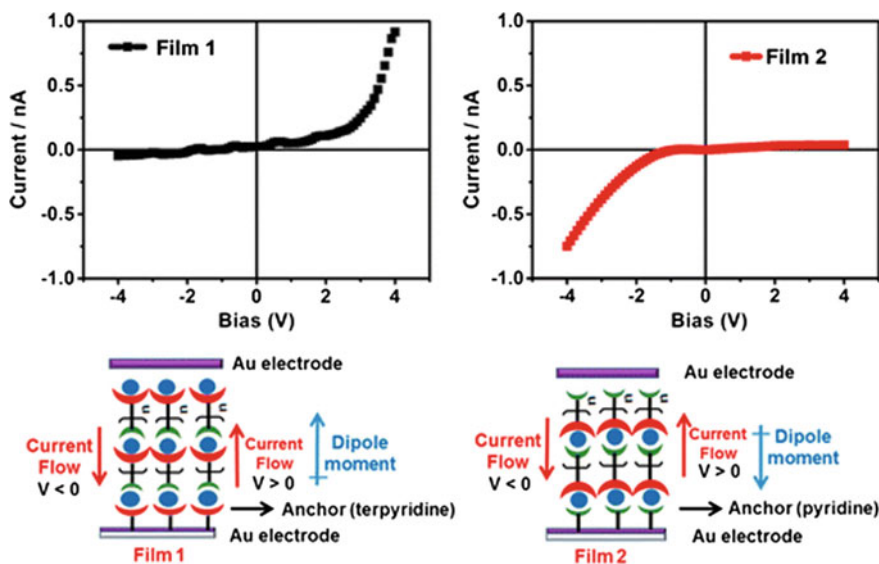

Fig. 7.64 Production of two types of films (films 1 and 2), in which polymer chains are positioned with regard to their dipoles in opposite directions

ligand (series L) and redox-active terminal tpy ligand (series T) (Fig. 7.66). After modification of the electrode surface with, for example, sulfide or hydroxylation
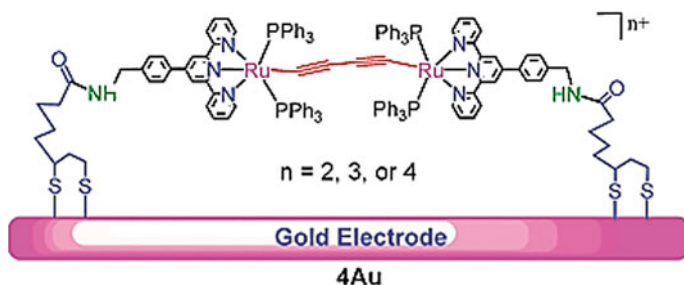
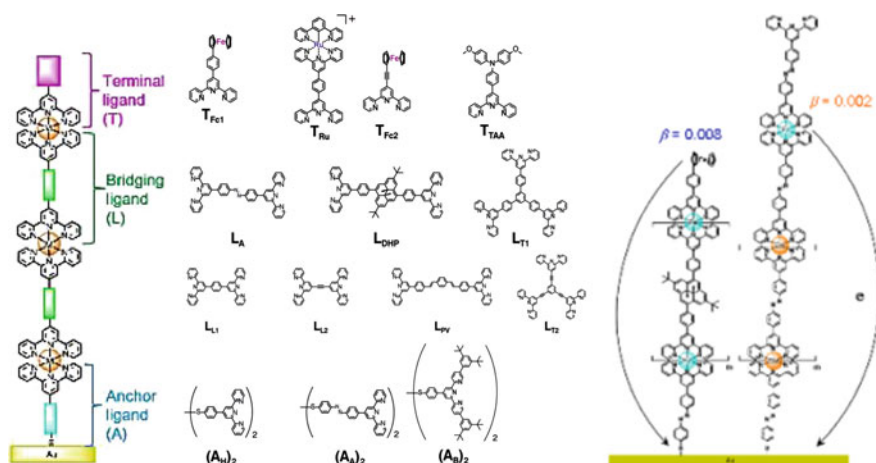**Fig. 7.65** 1,3-Butadiyne-cross-linked diruthenium chelate fixed on Au electrode surface

Fig. 7.66 Long-range electron transport ability of M(tpy)₂ wires

methods, molecular wires are simply produced by consequent submergence of the electrode in metal ion solution and a bridging ligand. The process is ended by decoration a wire end by redox-active functional groups, such as Fc, triarylamine or cyclometalated Ru(II) complexes. Combination of different components can provide different types of molecular wires.

The obtained wires show a lot of interesting function, including behavior of electron transfer and long-range electron transport capacities from redox part of a terminal to electrode through bis(tpy) metal chelates [549, 550]. The rate constant of electron transfer for 1D molecular wire is quantitatively determined as follows:

$$K = k_0 \exp(-\beta^d),$$

where k is the rate constant of electron transfer between the redox part and the electrode, d is a distance between the electrode and redox part, k_0 is the constant of

zero distance, β is a distance attenuation factor. Extraordinary capacities of the long-range electron transport is confirmed by low attenuation coefficient $\boldsymbol{\beta}$ (for example, 0.008 and 0.002 Å^{-1} for Fe and Co chelate-based wires, respectively) [551, 552], which are far lower than for alkyl chains (1 Å^{-1}), DNA chains (0.1–1.4 Å^{-1}) and oligo (phenylene vinylene)-bridging wires (0.01 Å^{-1}). It is important that electron transport capacity can be easily adjusted using respective components of molecular wires, at that bridging ligand and metal ions have a substantial effect on β, while anchor and terminal ligand have no effect on β, but change k_0 (Fig. 7.67) [553].

Unusual nanostructures such as chain-of-beads are obtained from drop-casting of acetone solutions of Fe chelates with 2,6-di[pyrazol-1-yl] pyridine on the surface of HOPG [554]. It is important that beads in each chain are identical in size with diameter in the range 2–6 nm and height up to 10 Å, which correlates with content of small molecular cluster (about 10–50 molecules). It is interesting to notice that the beads can be separated into two types depending on conductivity, which correlates with their positions in chains and can correspond with the molecules containing high-spin and low-spin Fe centers. For some beads switching between two forms was observed during few minutes under a constant bias, which was apparently random [555]. This system is one of a few examples of SAMs, which relate to a wide range of spin-crossovers undergoing a transition between electron spin states under action of temperature, pressure or light [556, 557].

Pd(II)-directed chiral metal chelate multilayers are prepared on surface of the substrates through LbL assembling using hydroquinone anthraquinone-1,4-diyl diether of bidentate ligands as spacer [558]. It is important that molecular chirality of ligands remains in metal chelate multilayers. We shall also notice electrochromic behavior of Fe chelates obtained from tetra-2-pyridyl-1,4-pyrazine and hexacyanoferrate species in polyelectrolyte multilayers on ITO substrate [559]. Modified electrodes have shown excellent electrochromic behavior with intense and persistent dying, and chromatic contrast about 70%.


Fig. 7.67 Dependence of the rate constant of electron transfer versus wire length for bridging ligand, metal ions, anchor and terminal ligand
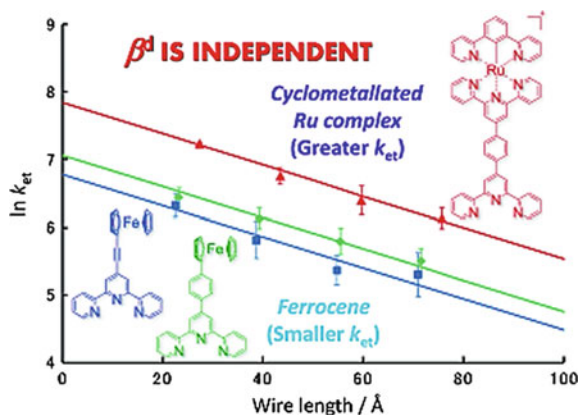
Cavitand-based cages on SAMs are subjected to metal-induced self-assembling, at that, M–L coordination provided direct observation of formation of such assemblies and detection of a single-molecular level [560]. Cavitand functionalized with four alkylthioether groups at the lower rim and four tolylpyridine groups at the upper rim can link with Au surface through thioether groups and form a coordination cage with [Pd(dppp)(CF$_3$SO$_3$)$_2$] via its Py groups [561]. Using complexation of another cavitand, immobilized heterocages can be obtained from solution. It is important that the cages can be reversibly assembled and dissembled on Au surface, and AFM measurements distinguish an individual cavitand and cage molecules 2.5 and 5.8 nm in height, respectively.

M–L interaction is used for studying supramolecular rotors (Scheme 7.19) as potential components of a machine type system, through axial ligation of big π-functional molecules working as rotors, with the surface, which is a stator component [562].

The effect of a number of layers on photocurrent generation with using SAM obtained by coordination of Ru-Pc through 4,4′-bipy bridges (Fig. 7.68) is studied [563–565]. It is found that thicker layers generated lower photocurrents due to internal resistance of molecular wire.
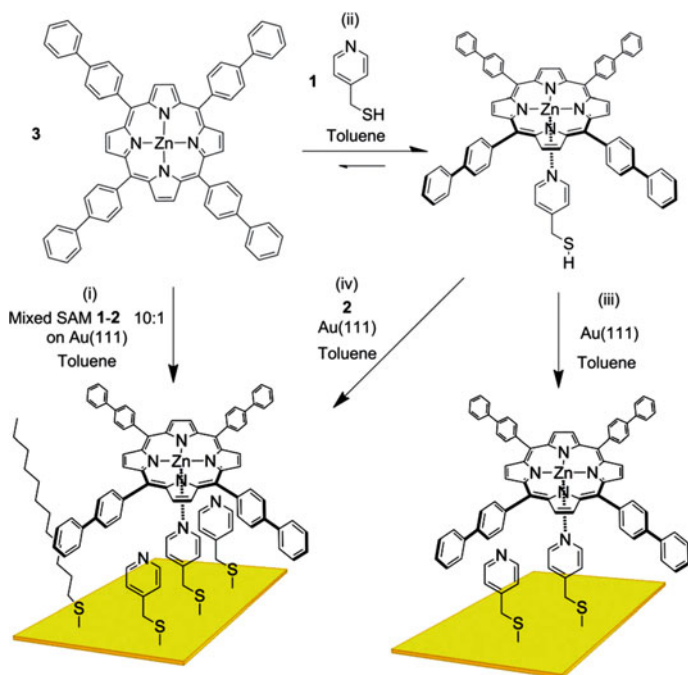
Scheme 7.19 Scheme of supramolecular rotors fabrication through axial ligation of big π-functional molecules working as rotors, with the surface, which is a stator component
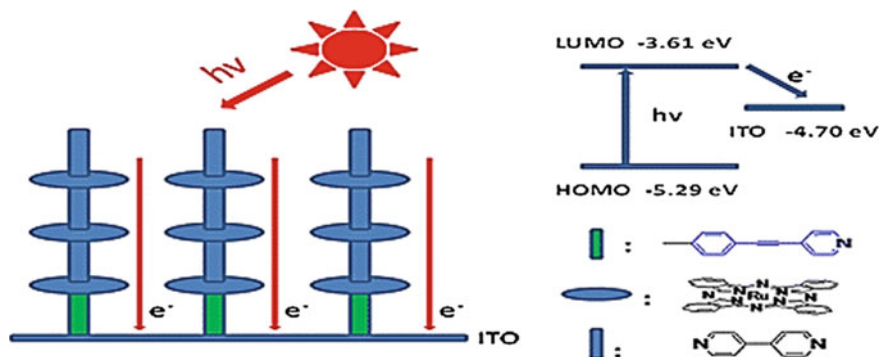
Fig. 7.68 Schematic energy-level diagram for a self-assembled sixbilayer Ru-Pc film on modified ITO electrode

We shall notice multivalent binding of a supramolecular complex on polyvalent host surface by uniting of orthogonal host-guest CD and M-en coordination motifs [566]. In this orthogonal supramolecular system a heterotopic divalent spacer with CD-complexing adamantyl group and chelating en ligand is used. This spacer can link CD in solution and immobilize CD on SAMs (Fig. 7.69). In the similar way vesicles are obtained, which carry host units (CD) by their interaction with guest (adamantyl) functionalized ligands through orthogonal polyvalent host-guest and M–L motifs [567]. Vesicles of amphiphilic CD recognized metal chelates with adamantyl ligands using integration into host caverns on vesicle surfaces. In the case of Cu(II) chelates interaction was predominantly intravesicular, while for Ni(II) chelates interaction was intervesicular, and addition of the guest-metal complex brought to aggregation of vesicles into dense multilayer clusters. Valence of supramolecular recognition on vesicle surface, and balance between intravesicular and intervesicular interactions can be adjusted using M–L coordination of a guest molecule.
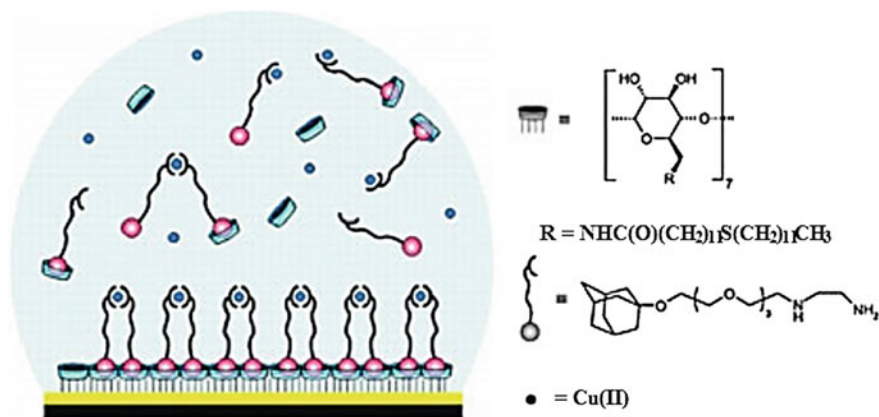

Fig. 7.69 Complexation on CD SAMs by host-guest and M–L coordination

7.12 Supramolecular Metal Chelate Dendrimers

Using dendritic architectures for supramolecular chemistry is focused on unique capability of their branched shell to influence processes of molecular recognition in center, branches and periphery of dendrimers [84, 179, 568–574]. Substantial attention in the recent years has being focused on using of supramolecular dendrimers, since self-assembling of building blocks through non-covalent interactions is a spontaneous process, which brings to the most stable structure and makes it possible to skip most stages of synthesis. Information on a structure programmed in dendritic architecture controls the assembling process and, as a consequence, properties of generated supramolecular structures. Self-assembling provides ideal approach for intensification of branching of small, synthetically available, relatively inexpensive dendritic systems (for example, dendrons) in strongly branched complicated nanometer aggregates. Supramolecular nano-assemblies including dendrimers and such objects as fullerenes, rotaxanes, CB[n], CD, MWCNT, etc. are of great interest [575–581]. Supramolecular dendritic polymers, which perfectly combine advantages of dendritic and supramolecular polymers, are a new class of non-covalently bound strongly branched macromolecules with 3D globular topology [582]. Due to their dynamic/irreversible character, unique topology and exclusive physicochemical properties (for example, low viscosity, high solubility, and a great number of functional terminal groups), supramolecular dendritic polymers have attracted high attention last year's [583]. In particular, reversibility of non-covalent interactions provides ability of supramolecular dendritic polymers to experience dynamic switching of a structure, morphology and function in response to different external stimuli such as pH, temperature, light, stress, and redox agents. Such behavior in future provides flexible and reliable platform for design and development of intelligent supramolecular polymer materials and functional supramolecular devices. Supramolecular dendritic polymers can be classified with respect to their topological structures, which contain the following six classes: supramolecular dendrimers, supramolecular dendronized polymers, supramolecular hyperbranched polymers, supramolecular linear-dendritic block-copolymers, supramolecular dendritic-dendritic block-copolymers, and supra molecular dendritic multi-armed copolymers (Fig. 7.70). These types of supramolecular dendritic polymers differ by morphologies, unique architectures, and specific functions, which provide their high potential for application in different fields. An important fact is that supramolecular dendritic polymers can self-assemble in various supramolecular structures, such as micelles, vesicles, fibers, nanorings, tubes, and many hierarchical structures.

Certainly contemporary supramolecular chemistry of dendrimers includes coordination motifs in studies of synthesis of supramolecular metallodendrimers and, in particular, MCD and their properties [84, 179, 584–589]. The most developed method of directed assembling of supramolecular MCD is using of M–L coordination. Different key strategies are proposed, using which metals are applied in self-assembling of several dendritic building blocks. Most often a metal center
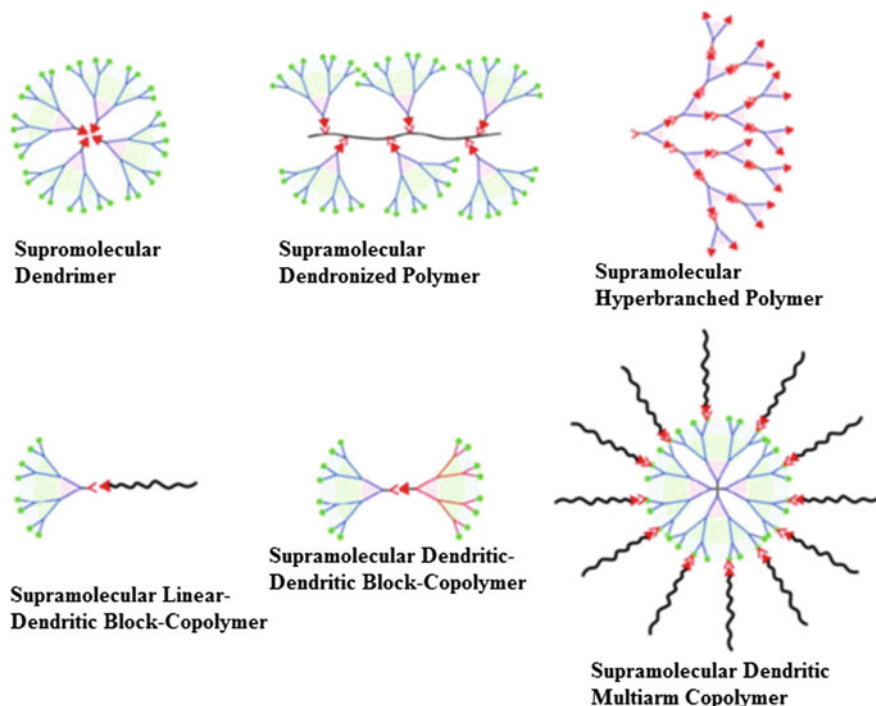
Fig. 7.70 Classes of existing supramolecular dendritic polymers with different topological structures

forms a core of supramolecular MCD with dendrons, which have chelating groups in the focal point coordinated around one central metal ion. Thus, $[Ru(bpy)_3]^{2+}$ core was actively used for this purpose at earlier stage of dendrimer chemistry [590] as a branching point in dendritic architecture, which is subjected to self-assembling with respectively projected ligands for generation of supramolecular MCD in one stage. As an example, supramolecular deca-Ru MCD can be regarded, which includes bpy and 2,3-dipyridyl-pyrazine as a terminal and bridging ligands, respectively (Fig. 7.71) [591–593]. It is interesting that oxidation of six equivalent peripheral Ru(II) centers to Ru(III) generates species containing 26 positive charges. Electrostatic effect of these charges prevents further oxidation of interior Ru(II) centers inside electrochemical window [594, 595]. Similar types of assembling with participation of bridging bis(2,3-pyridyl) pyrazine ligands and additional bpy termini can reach large sizes. For example, the largest dendrimer of this type containing 1090 atoms, 22 from which were metal centers [591], had the assumed size 5 nm and total charge +44 (+2 per a metal center). Apart from 22 metal atoms, this dendrimer consists of 24 terminal ligands and 21 bridging ligands.
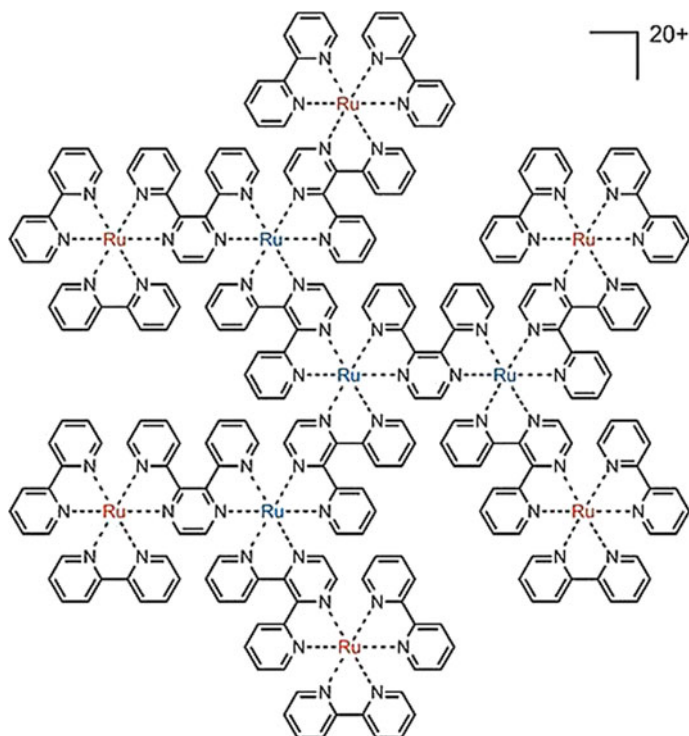
Fig. 7.71 Supramolecular deca-Ru MCD, which includes bpy and 2,3-dipyridyl-pyrazine as a terminal and bridging ligands

It should be noted that multi-tpy chromophores also form 2D networks by M–L complexation, which causes substantial changes in their photophysical properties (Fig. 7.72) [596].

Using interaction of Ru(II) and dendron-functionalized tpy-ligands, dendrimers can be built linked together by tpy-Ru coordination interactions [84, 179]. In order to do this, periphery of spherical dendrimer would be functionalized with several tpy blocks, and the following reaction with Ru(II) focused by a dendron provided location of additional branching layer on dendritic surface using M–L interactions. These structures, as a rule, have several metal ions inside branches holding dendritic structure together. In the same way supramolecular MCD are built, which integrate perylene as a functional core with ⟨tpy-Ru(II)-tpy⟩ termini (Fig. 7.73) [597]. For them, a wide absorption spectrum is typical with enhanced coefficients of molar absorption corresponding to increase in a number of ⟨tpy-Ru(II)-tpy⟩ units.

We shall also notice supramolecular mono-, bis-, and tris-Ru-based MCD, which cover a wide absorption range 250–750 nm with optical band gaps 1.51–1.86 eV [598]. It is important that for these MCD energy levels can be effectively controlled not only by different generations of dendritic thiophene arms, but also by their
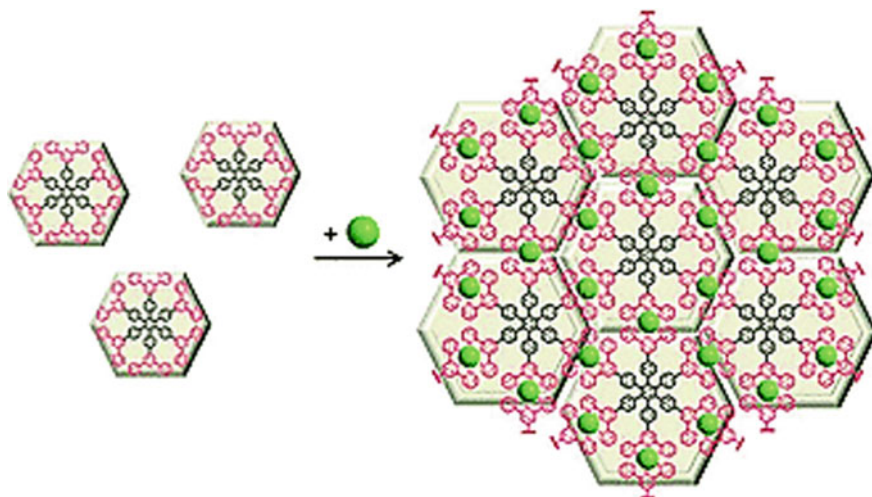
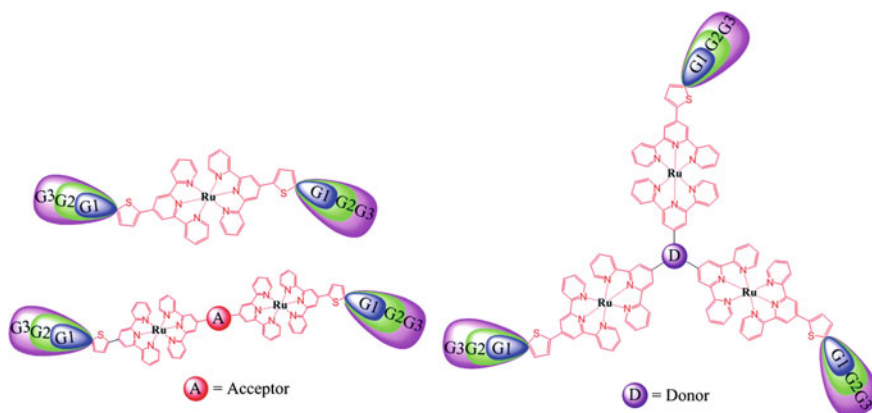**Fig. 7.72** 2D networks formed multi-tpy chromophores by M–L complexation

Fig. 7.73 Supramolecular MCD, which integrate perylene as a functional core with ⟨tpy-Ru(II)-tpy⟩ termini

π-conjugated core ligands carrying different electron-donor (triphenylamine) and acceptor (benzothiadiazole) residuals. Among different generations (G1–G3) dendrimers, G3 has the highest value of efficiency of energy transformation in each series of Ru-based dendrimers. There is an interest in shape-resistant supramolecular MCD, in which ⟨tpy-Ru(II)-tpy⟩ or ⟨tpy-Fe(II)-tpy⟩ connectivities are used as branching fragments or nodes (Fig. 7.74) [599]. A considerable increase in drift time of charge state, photophysical properties (molar extinction coefficients), and electrochemical stability of complexes were observed at increasing of generation of these complexes, which agrees with change in molecular size.
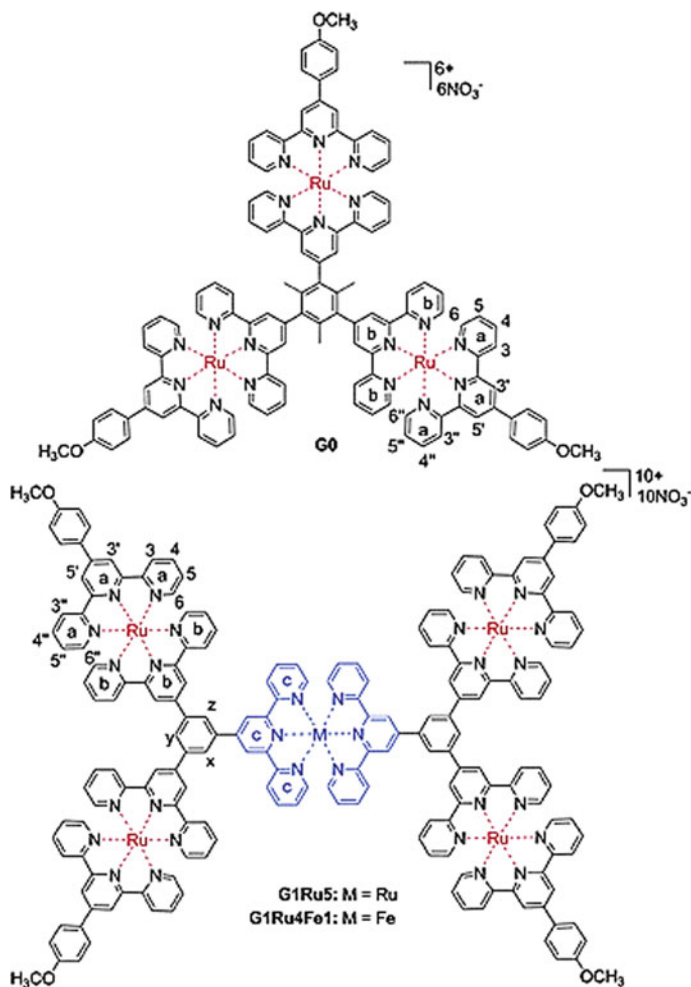
Fig. 7.74 Shape-resistant supramolecular MCD, in which ⟨tpy-Ru(II)-tpy⟩ or ⟨tpy-Fe(II)-tpy⟩ connectivities are used as branching fragments or nodes

Using consistent integration of different metal ions during synthesis with poly-pyridyl ligands, different supramolecular hetero-MCD structures can be obtained [600]. As an example we shall mention a dendritic-like four-nuclear complex [Os{(L_1)Ru(L_2)$_2$}$_3$]$^{8+}$ containing {Os(L_1)$_3$}$^{2+}$ chromophor as a core and three {(L_1)Ru(L_2)$_2$}$^{2+}$ polypyridyl building blocks as peripheral subunits, where L_1 = 2,3-bis(2-pyridyl)pyrazine; L_2 = 1′-((bpy-4-yl)methyl)phenothiazine. This MCD can be considered as integrated system with light-harvesting antenna-reaction center, in which Os subunit is efficient antenna unit in combination with well-known electron-donor subunits (phenothiazine fragments) [601]. In this system light absorbed by peripheral Ru(II) chromophores are transferred to the Os(II) core, however,

luminescence of Os(II) core is efficiently quenched through moderately exergonic reduction electron transfer by peripheral phenothiazine donors, despite presence of intermediate Ru(II) centers.

Coordination-driven self-assembling is a simple and very efficient approach for preparation of cavity-core supramolecular MCD, which have cavities with definite shape and size [602–615]. In general case synthesis based on this strategy is simple, and yield is almost quantitative, therefore a need in the following purification disappears. What is more important is that coordination-driven self-assembling is a powerful tool for building of supramolecular polygons and polyhedra with strictly defined and controlled cavities working as cores. As an example self-assembling of molecular squares can be considered based on simple modulus through interaction between four $(dppp)M(OTf)_2$ (M = Pd, Pt) linear components with 4,4′-bipy bidentate angular units, which are substituted in their 3,3′-positions with Frechet-type dendrons from G0 to G3 (Scheme 7.20) [616]. It is important that in obtained MCD squares there are absent a great number of other polygons or open-chained oligomers. They carry nanometer cavities inside a non-polar dendritic shell. Totally eight amide groups decorate rims of the cavity linking dendrons in a square.

There is interest in dendritic bis(tpy) Fe(II) wires with terminal Fc units synthesized on Au(111) surface by stepwise coordination using three-way tpy ligand, Fc-modified tpy-ligand and Fe(II) ions (Fig. 7.75) [617]. For the obtained systems an unusual phenomenon of electron transfer is found. In particular, current-time profile does not follow exponential decay, which is common for linear molecular wires, and non-exponentiality was more noticeable in the forward direction of
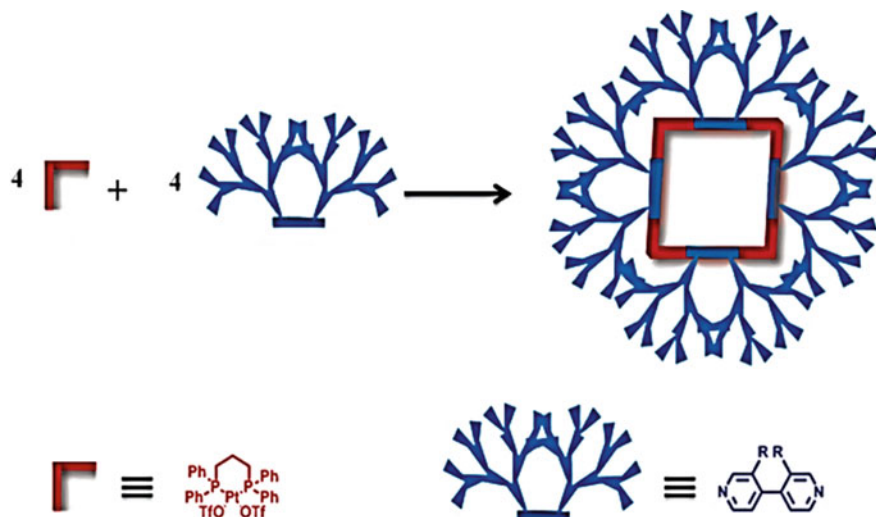
Scheme 7.20 Cartoon representations of the formation of eight-component square MCD from 180° G0–G3 dendritic donors and 90° dendritic acceptor
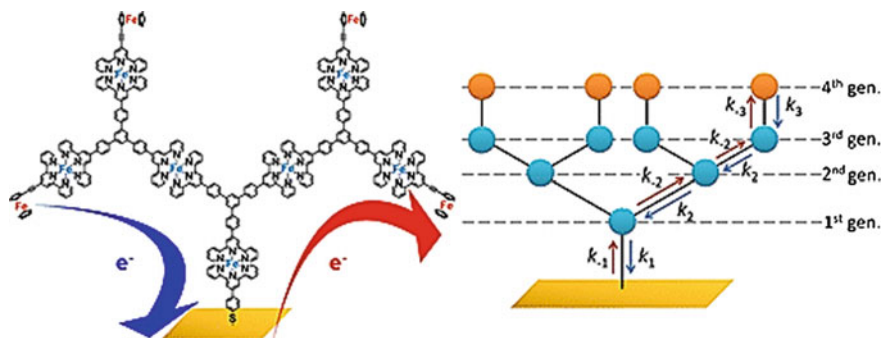
Fig. 7.75 Dendritic bis(tpy) Fe(II) wires with terminal Fc units synthesized on Au(111) surface by stepwise coordination using three-way tpy ligand, Fc-modified tpy-ligand and Fe(II) ions

electron transfer (from terminal Fc to Au electrode, oxidation) than backwards (from Au electrode to terminal Fc, reduction).

We shall also notice examples of using the supramolecular MCD self-assembling concept with participation of orthogonal non-covalent interactions, for example, Hamiltonian receptor-cyanuric acid and Ru(bpy)$_3$ M–L-linking motifs (Scheme 7.21) [618]. It is important that consequent divergent sequence of reactions, as well as one-pot reaction from AB$_2$ building block, which contains a focal bpy fragment and two units of Hamilton receptors, can be applied for synthesis of such supramolecular MCD. It is important that a terminal analogue of derivatives of cyanuric acid can be tailored with a great variety of functional groups.

Another example is supramolecular MCD assembled by two different orthogonal supramolecular interactions: Pd-pincer coordination and cyanuric acid-melamine H-bonded rosette motifs (Scheme 7.22) [619]. The resulting supramolecular MCDs are as big as 28,000, which make them one of the biggest known MCDs.

M-Pp and M-Pc dendrimers are actively used in synthesis of supramolecular MCD. Thus, supramolecular MCD based on multiporphyrin metallodendrimers consisting of focal free Cu-Pp with eight Zn-Pp wings and multipyridyl Cu-Pp with eight pyridyl groups are obtained through multiple axial ligations of pyridyl groups to Zn-Pp [620]. It is important that apparent association constant between two main fragments (2.91×10^6 M^{-1}) is rather high for fiber assembling to form at micromolar concentrations. The fiber assemblies with correct height (about 2 nm) and regular diameter about 6 nm are formed. It should be noted that by formation of supramolecular MCD intramolecular energy transfer changes to intermolecular energy transfer, from Zn-Pp to Cu-Pp with pyridyl groups.

We shall also notice supramolecular MCD consisting of self-assembled derivatives of zinc chlorophyll [621]. In this case, coordination-driven self-assembling of pyridine-pendant zinc chlorophyll derivatives proceeds through intermolecular axial ligation between a nitrogen atom of the pyridine ring and zinc atom in the chlorine ring (Scheme 7.23).
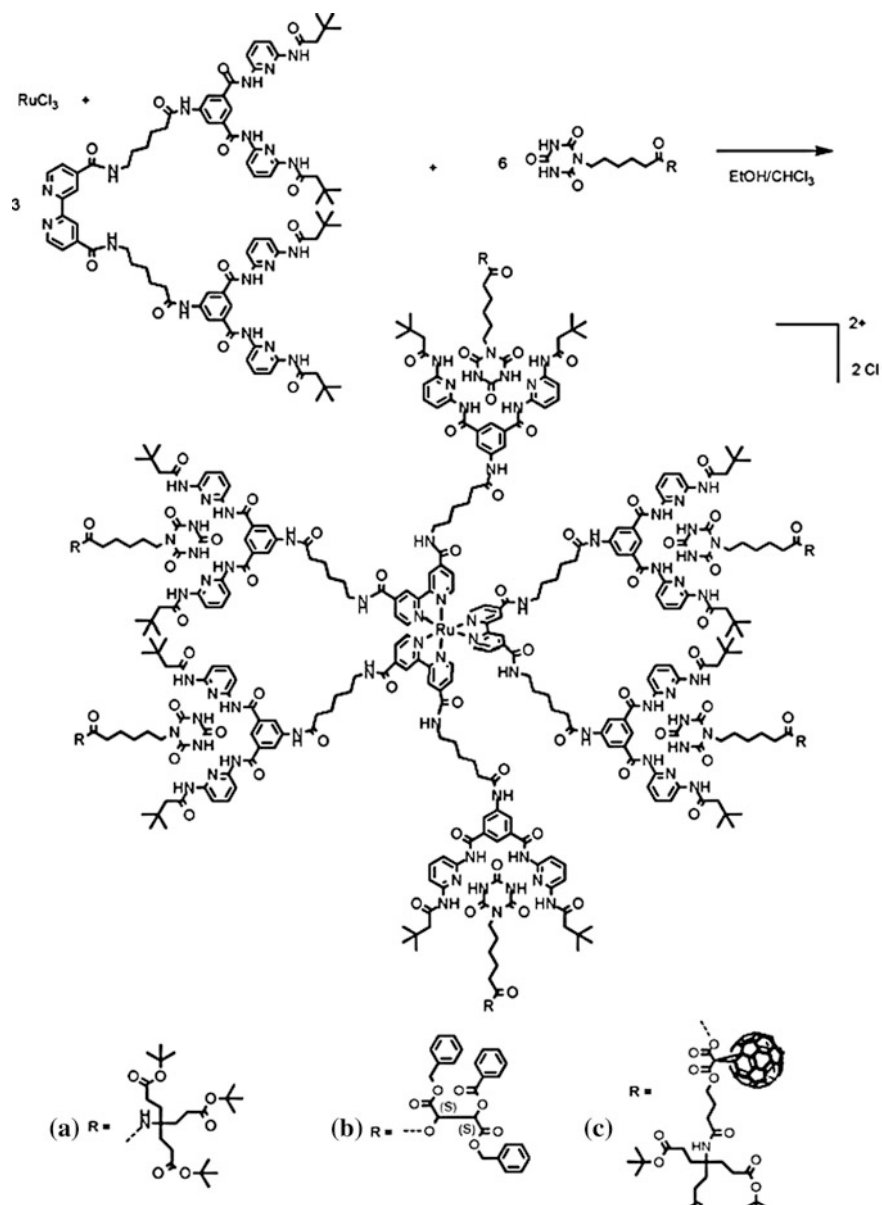
Scheme 7.21 Complete self-assembly of supramolecular structures

The coordination-driven strategy is also used for assembling of fullerene-rich supramolecular MCD [622, 623]. The M-Pp dendrimers form supramolecular complexes with fullerene derivatives through electrostatic interactions, π-π interactions and coordination bonds. For example, fullerene-rich supramolecular dendritic structures
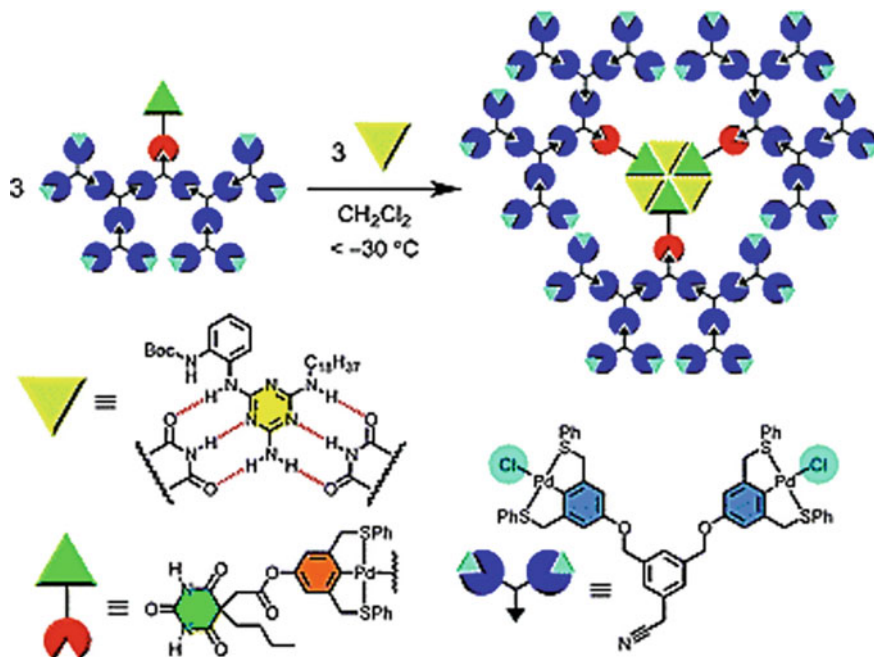
Scheme 7.22 Self-assembled dendrimer featuring orthogonal Pd-pincer coordination and cyanuric acid-melamine H-bonded rosette motifs
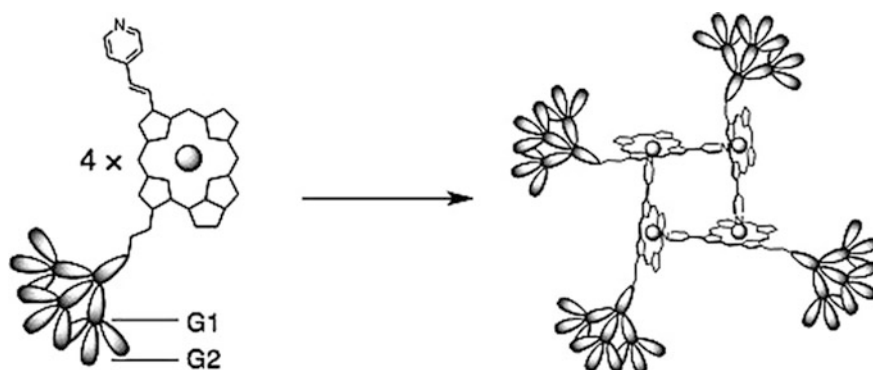
Scheme 7.23 Synthesis of supramolecular MCD by coordination-driven self-assembling pyridine-pendant zinc chlorophyll derivatives

are obtained as a result of apical coordination of C_{60} derivatives carrying pyridyl fragments to dendritic molecules with M-Pp units [624]. It is interesting that clear visualization of the petal-like structure is displayed. Average affinity of binding in assumption 1:1 coordination between separate Zn-Pp blocks and Py is 1.2×10^6 M^{-1}.

This value is more than by 2 orders of magnitude higher than the association constants reported for monodentate coordination between Zn-Pp and Py derivatives, which can be ascribed to simultaneous coordination of two Zn centers by two Py-containing fragments.

In another example, terminal amines of G1–G3 PAMAM dendrimers were modified through grafting of M-Pp derivatives with activated ester [623]. M-Pp dendrimers were then used for formation of supramolecular assemblies with C_{60} using acetonitrile/toluene mixed solvent bringing to clustering of nanometer assemblies (Fig. 7.76).

For efficient delivery of photosensitizers, ionic M-Pp dendrimer is used to form PIC of micelles (Fig. 7.77) [625–630]. We shall notice that M-Pp-including PIC micelles have high stability and high photo cytotoxicity. Moreover, great hydrodynamic volume of micelles brings to quite precisely localized drug delivery to a tumor tissue. In the same way ionic dendrimer Pc with absorption of long-wave light was developed for efficient light delivery at PDT and also formed PIC micelles containing *cis*-dichlorodiammineplatinum (II), anti-cancer drug with PEG-*b*-poly (L-aspartic acid) (molecular weight of a PEG segment is 12,000, DP of a segment of aspartic acid is 68 or 96) [628]. These supramolecular MCD can be efficient nano-devices for anti-cancer drug carriers with sustained release drug and PDT.

We shall also notice supramolecular chiral assemblies obtained by π-π interactions between aromatic rings of M-Pp dendrimers. Thus, dendritic Zn-Pp with two carboxylic groups can form J-aggregates in CHCl₃ through π-π interactions of Pp

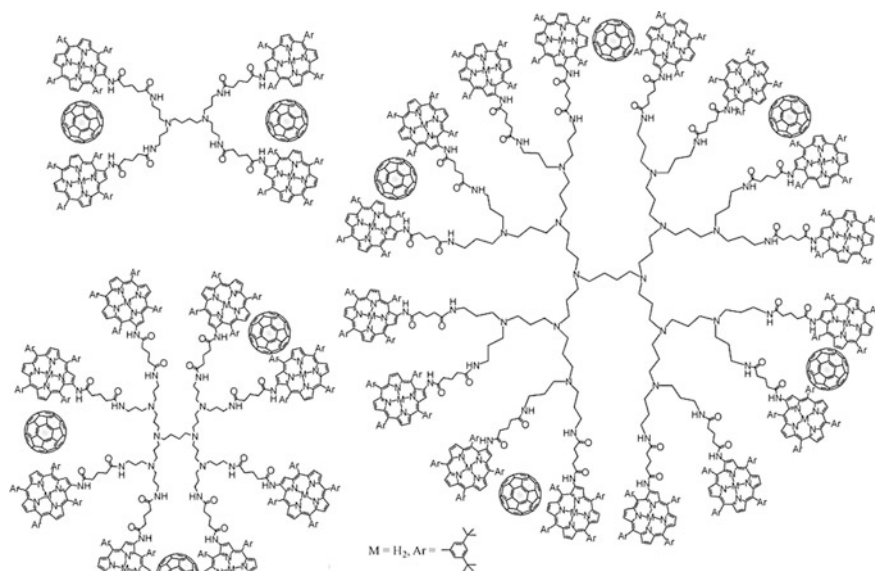**Fig. 7.76** Non-covalent assemblies of C_{60} with G1 to G3 POPAM dendrimers decorated at the surface by multiple Pp macrocycles

Cationic Block Copolymer

Dendrimer Porphyrin

Cationic Block Copolymer

Derdrimer Porphyrin

Electrostatic Interaction
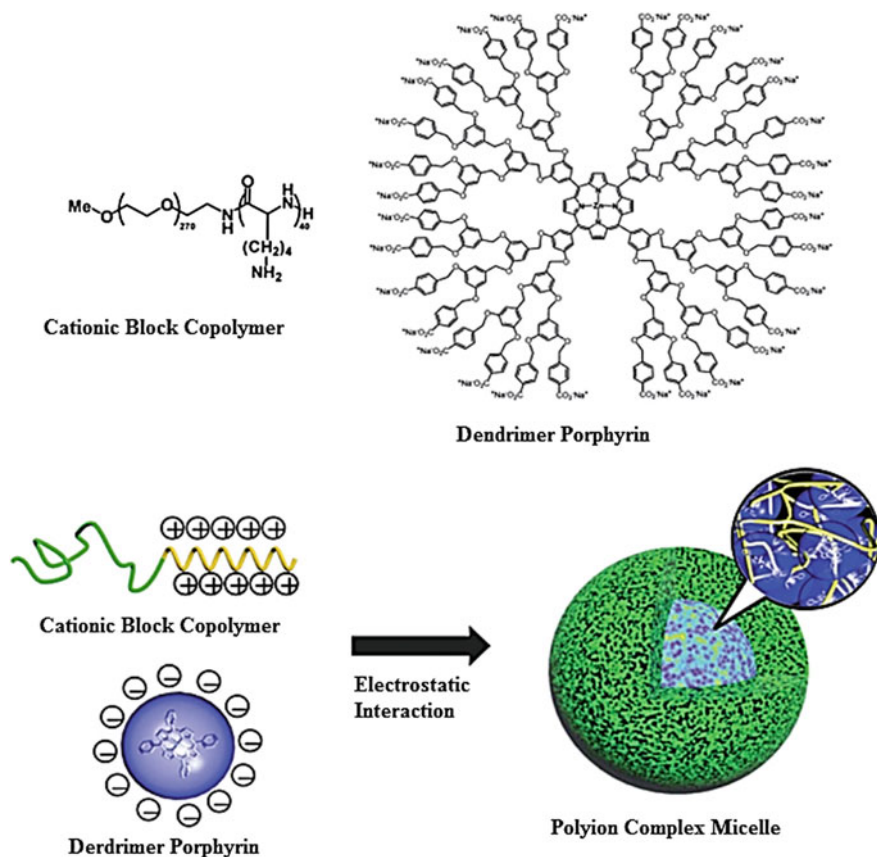
Polyion Complex Micelle

Fig. 7.77 Structures of cationic block copolymer and dendrimer Pp, and formation of its PIC micelle

rings and also aromatic rings of their dendritic substituents (Fig. 7.78) [631]. Besides, H-bonding between carboxylic groups can also be very important driving force for formation of J-aggregates. It is important that centrifugation of J-aggregates solutions would give optically active films, whose chirality can be chosen by spinning direction. Apart from centrifugation mixing of benzene solutions of achiral dendritic Zn-Pp with two carboxylic groups can also produce supramolecular chirality. It is interesting to notice that when direction of mixing is changed from clockwise to anticlockwise, opposite CD signals are detected. For this system nanofibers formed by M-Pp assembling through J-aggregation play very important roles, in particular, some of observed chiroptical activities can also grow from macroscopic chiral alignment of nanofibers [632].

Another direction of the studies of supramolecular MCD is fixing of LMC on preliminary formed supramolecular polymers. In this view very promising is use of such interesting supramolecular polymers as dendrimerosomes [573, 574, 633–636].
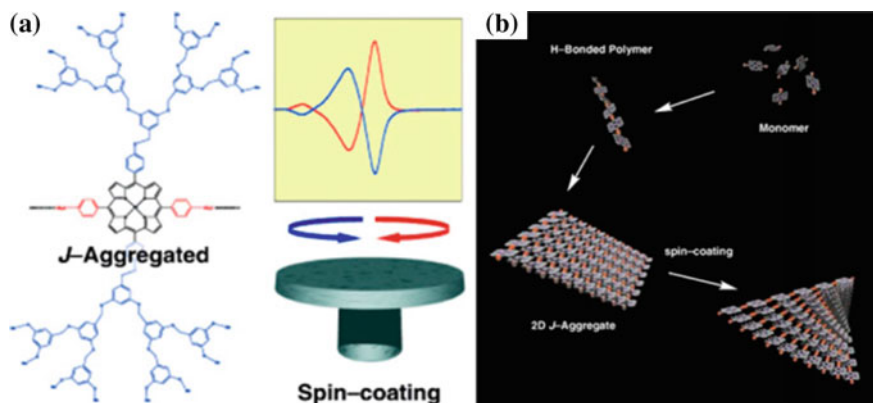
Fig. 7.78 a J aggregation of achiral dendritic Zn-Pp and macroscopic chirality from spinning. **b** Mechanism for the formation of chiral assemblies

These nanostructures are obtained from amphiphilic «Janus dendrimers» one part of which is hydrophilic and another one hydrophobic. A simple injection of amphiphilic Janus dendrimer solution with a definite primary structure into water or a buffer gives uniform submicron onion-like vesicles called dendrimersomes. Size and number of alternating internal closed bilayers is predicted by initial concentration of a Janus dendrimer. The transverse dimension of a dendrimersome shows that this supramolecular structure looks like a double membrane forming a cell wall (Fig. 7.79). A great variety of nanostructures formed spontaneously at placing Janus dendrimers in water has been discovered and studied, at that a family of supramolecular systems is formed, including vesicles, tubes, discs, and other shaped systems. Dendrimerosomes are stable for a long time, they are uniform by size, changing self-organization conditions they can be tailored into a necessary shape and, moreover, they can be quite easily functionalized. Their size, stability, and membrane structures are defined by chemical structure of a Janus dendrimer and the self-assembling method. A simple method of injection for production is available without special equipment, making uniform vesicles, and thus forming promising means for fundamental studies and technological applications in nanomedicine and other areas.

Dendrimerosomes are efficient and universal nanoplatform for fixing LMC, in particular, hydrophilic or amphiphilic MR chelates [637, 638]. Thus, for example, amphiphilic Gd(DOTA)-like complex functionalized by two octadecyl chains, is synthesized and incorporated into bilayer of dendrimerosomes [637]. In other example dendrimerosomes were loaded by clinically proved MRI probe Gadoteroidol (Fig. 7.80) and compared with respective nanoparticles taken from more branched dendrimers [639]. It is important to notice that the lifetime of these systems in blood is comparable with lifetimes of liposomes, which points to a possibility of their using for different biomedical applications.
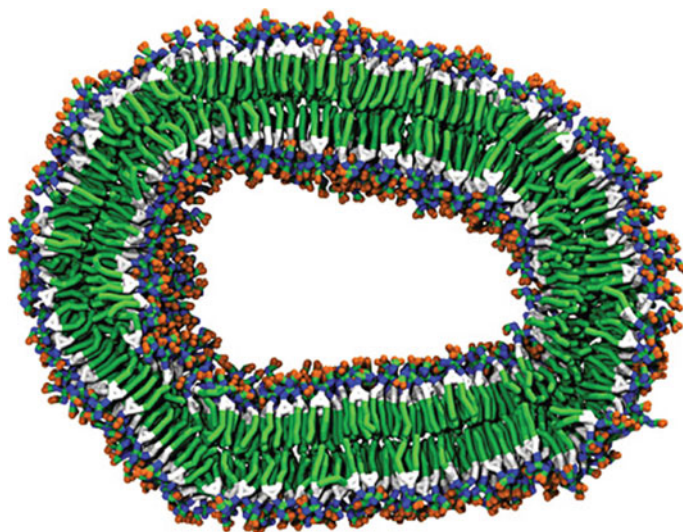
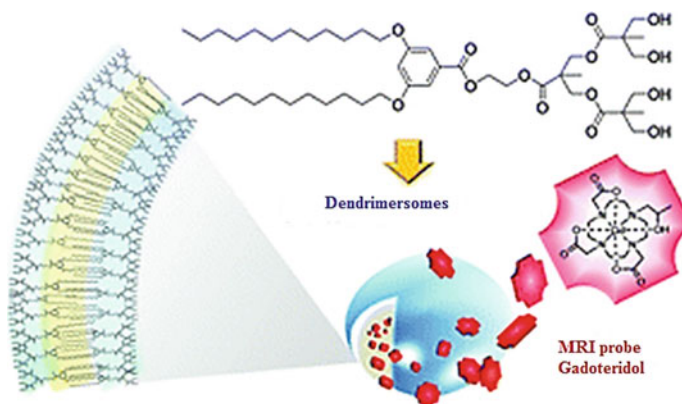**Fig. 7.79** The cross section of dendrimerosomes showing its double layer, similar to the cell membrane

Fig. 7.80 Production of dendrimerosomes loading by clinically proved MRI probe Gadoteroidol

7.13   Stimuli-Responsive Metallosupramolecular Polymers

Stimulus-responsive materials have attracted great interest during recent years, since these materials can show abrupt change in properties as a response to a stimulus application such as light, temperature, mechanical action, pH, ionic force, polarity of a solvent, electric fields, chemical substances, etc. [49, 99, 640–643]. In accordance with a type of a stimulus, to which they respond, these materials are

classified as photo-, chemo-, electro-, or mechano-active substances. Application of a stimulus brings to change in properties of a material, such as fluorescence, mechanical stress, change in color, etc. Such stimulus-responses can be displayed by different materials, from inorganic to organic, from molecular to macroscopic level, and from natural to synthetic materials. A programmed assembling of molecules into supramolecular polymers has a great interest for development of stimulus-responsive «smart» materials. Control over morphology, dynamics, and responsiveness of MSP is of high value for future applications [340, 341]. Due to dynamic and reversible character of non-covalent interactions, MSP can be adapted to environment and have a wide range of intriguing properties, such as degradation, of shape memory and self-healing, which makes them unique candidates for supramolecular materials [644, 645].

Thermo-responsiveness is one of fundamental and most available properties of supramolecular polymer materials, because weak non-covalent interactions are by their character subjected to thermal stimulus. Therefore thermo-responsive supramolecular materials have attracted a wide range of interests. The main advantage of supramolecular polymers is a strong dependence of their melt viscosity on temperature, which makes them easily treated and applied. As an example we can consider Fe(II) and Zn(II) MSP based on PCL of telechelic polymers containing two functional units at their ends: a tpy ligand and ureidopyrimidinone quaternary H-binding motif [170]. Double logarithmic dependence of specific viscosity of Fe (II) MSP solution on concentration has shown two-phase linear dependence pointing to the ring-chain equilibrium. Bulk rheological properties of PCL-Fe(II) MSP are characterized by two abrupt changes in viscosity with temperature. The first change at lower temperature is ascribed to melting of poly (ε-caprolactone) main chain, while the second change is due to weakening of M–L bonds within the supramolecular chain. Oppositely to this, Zn(II)-containing MSP have shown only one change in viscosity at lower temperature. Probably, thermodynamic stability of M–L bonds plays important role in observed rheological behavior of these MSP.

Using ability of tridentate BIP ligand to bind cations of transition metals Zn(II) and Co(II) in the ratio 2:1, and big cations of La(III) and Eu(III) lanthanides in the ratio 3:1 [77], MSP are obtained, in which Zn(II) and Co(II) (95%) are used for linear growth, and La(III) and Eu(III) ions (5%) for cross-linking (Fig. 7.81a) [130]. Gel-like materials based on four combinations of metal cations Co/La, Co/Eu, Zn/La, and Zn/Eu have shown reversible thermo-responsiveness (Fig. 7.81b) and interesting thixotropic behavior (Fig. 7.81c) as a result of gel-sol transition induced by mechanical force (shaking). The mechanism of mechano-responsive behavior involves formation of «loose dangling chain ends» in L:Zn/La system, when it is subjected to mechanical loading [129]. Restoring of the system includes reorganization of «broken ends» and reforming of the initial structure. L:Zn/Eu-containing MSP is, in addition, also chemo-responsive. In particular, adding of formic acid brought to immediate gel-sol transition and quenching of Eu(III) emission, since aromatic BIP ligands, which coordinate Eu(III) cation, are substituted by formate-anions. The process is made reversible by thorough drying of the material followed by repeated swelling in respective organic solvent.
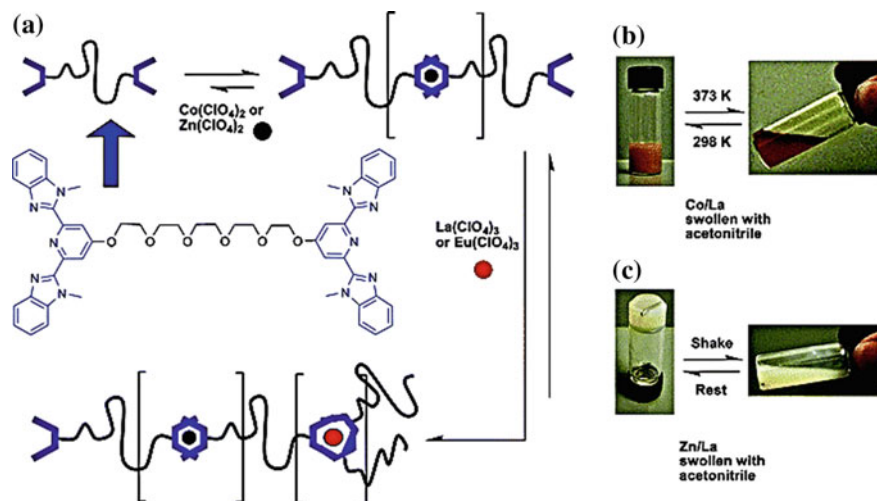
Fig. 7.81 a Schematic representation of the formation of a MSP from bifunctional ligand and lanthanide/transition metal cations. Photographs showing **b** the thermo-responsive nature of the L: Co/La system and **c** the thixotropic nature of the L:Zn/La system

There is also interest in thermo-responsive MSP which use thermally induced interconversion between *cis-* and *trans-*isomers on a cyclam block [646]. In the *cis-* isomer substituents are on one side of the cyclam plane, while in the *trans-*isomer subunits are above and below the cyclam plane. In MSP, formed by bis-tpy-cyclam ligand and Ni(II) ions temperature-initiated *cis-trans* transitions on the cyclam block bring to macroscopic phase sol-gel transition. Initially kinetically preferable *cis-*isomers, which form coil-like aggregates, present in the solution. During heating the *cis-*form transits into the *trans-*form and coils broaden to rod-coils, which brings to aggregates consisting of rigid and flexible segments and to gelation (Fig. 7.82).

Light, as remote stimulus, has a special meaning and is attractive regarding its wide use in molecular devices and smart materials, since it provides a wide range of controlled parameters, such as a wavelength, duration, and intensity. Reversible control over self-assembling of non-covalent building blocks by photo-irradiation is a key process for controlling photo-responsive MSP. Thus, MSP based on rod-like guest compound, containing two azobenzene units, β-CD macrocycle or its derivative, and en Pd(II) nitrate [325] can react to light irradiation due to photoi-somerization of the main chain containing azobenzene fragments.

Supramolecular materials are dynamic non-covalent bond-based materials, therefore any chemical substrate, which can weaken or break non-covalent bonds, will make the materials give a response to it. It is important that integrated chemical agent will change initial chemical environment, and then will have more or less effect on properties of materials. Chemo-responsiveness is an astounding property, which can provide available important applications of MSP.

Fig. 7.82 Schematic representation of coil-rodcoil transition and gelation during heating
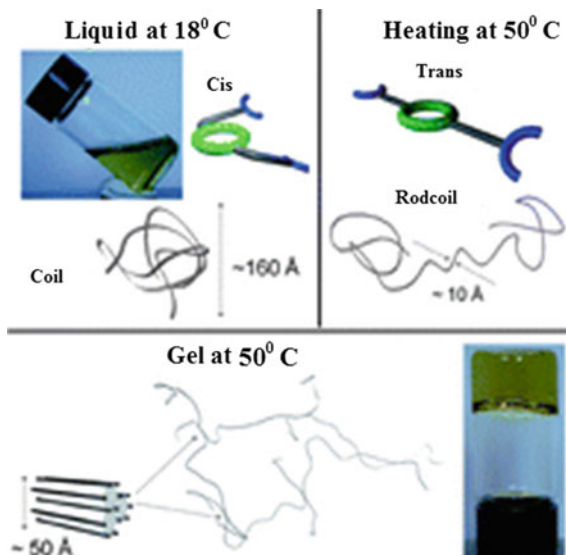
In this view, we shall notice MSP based on polyhedral oligomer silsesquioxane and Co(II) or Cu(II) tpy complexes [212] or amino-phen Sn(II) complex [190], which has shown properties of gelation at high concentrations of metal ions, at that gelation is reversible after addition of competitive metal-chelating agent, such as EDTA. In another interesting example MWCNT functionalized with tpy form MSPs in presence of Co(II) or Ni(II) ions, which can also be de-chelated by EDTA addition, which can be seen by change in color [647]. A pH-induced transformation between mononuclear neutral complexes and MSP in the system consisting of cyclam and bis-tpy fragments is shown (Scheme 7.24) [648]. This ligand at interaction with Cu(II) in molar ratio 1:1 gives green MSP solution, however, in presence of a base, red-pink solution is obtained, which corresponds to square-planar mononuclear Cu(II) complex. It is interesting that both these types become interconvertible with addition of base or acid. Besides, it turned out that addition of second equivalent of a transition metal ion such as Fe(II), Ni(II), Co(II) or Cu(II) to the square-planar mononuclear Cu(II) complex brings to MSP formation consisting of homo- or heterometallic complexes [649]. It is important to notice that addition of acid to homometallic Cu(II) MSP brings to polymer dissociation into binuclear complexes, in which Cu ions are coordinated with tpy fragments.

Using redox reactions for modulation of MSP properties gains substantial attention, since a change in redox conditions can bring to macroscopic changes in their properties. Obviously, MSP are exclusive candidates for creation of electro-responsive supramolecular materials, because metal ions can be subjected to oxidation and reduction with external electrochemical stimulus. Moreover, integration of metal ions also can change aggregation regimes and give approach to a wide
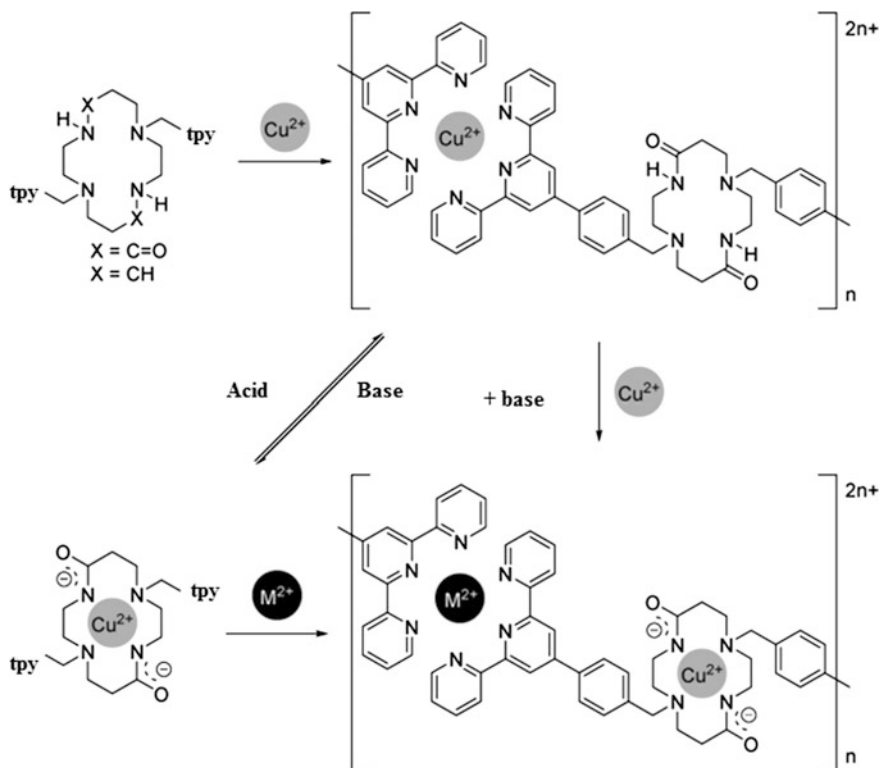
Scheme 7.24 Chelation routes of Cu(II) by ligand in the absence and presence of a base, the subsequent acid-base driven interconversion, and formation of homo- or hetero-MSPs

spectrum of interesting properties. For example, in order to obtain MSP which show a redox-responsive gel-sol transition and electrochromic properties [521, 522], metal ions and polytopic ligand containing two chelating tpy terminal units bound through complexing cyclam macrocycle, are used. It is interesting that these MSP have shown properties of gelation as a function of a solvent composition and of counter-ion nature, and can be controlled by M:L stoichiometry, concentration and temperature. Moreover, the self-assembling process is sensitive to external stimuli, such as electric input (redox-responsiveness) or a counter-ion type (chemoresponsiveness). During electrochemical oxidation of Co(II) to Co(III) gel easily undergoes transformation into solution, at that the gel can be reformed by reduction of Co(III) to Co(II). Incorporation of additional positive charges into polymer chains during oxidation has effect on solubility of the system and destabilizes gel, thus making the gel-sol transition. Variety of colors and reversible gelation of MSP is accumulated by a simple redox stimulus, thus demonstrating advantages of metal ion incorporation into supramolecular systems.

We shall notice redox-responsive MSPs consisting of a ditopic ligand end-capped by a poly-THF macromonomer, self-assembled with Cu ions, in which DP of MSP and, consequently, viscosity of its solutions depends on oxidation degree of copper ion. A combination of methods is used to show that Mebip ligands at the ends of poly-THF link Cu(II) with the ratio 2:1 and Cu(I) with the ratio 2:2 in solution. Therefore, at the fixed 1:1 or 1:2 stoichiometry of a macromonomer to Cu ions, viscosity of their solutions shows dramatic changes due to addition of chemical oxidant (nitroso tetrafluoroborate) or reducing agent (aqueous ascorbic acid) (Fig. 7.83) [650].

An interesting example is MSP containing a tpy-end three-armed PEG, which has shown sol-gel transition during aerobic oxidation [651]. Aerobic oxidation of Co(II) to Co(III) is accompanied by sol-gel transition, at that; the material can be molded in hydrogels of different shapes. Addition of a reducing agent has brought to reversible gel-sol transition and solution under action of air is then re-gelled due to aerobic oxidation of the reducing agent.

While mechanic load on polymer materials is inevitable, mechano-responsive materials act as especially attractive class of intelligent materials. As a rule, mechanical responses of polymer materials are derivatives of chemical and physical structure of polymer chains; therefore, dynamic, reversible non-covalent bonds are attractive candidates for building of mechano-responsive materials via incorporating them into polymer main chains. Thus, it is found [476] that binuclear Pd(II) *anti*-complex is self-assembled into long-chained assemblies in solution forming gel under ultrasonic irradiation. The gel can be easily transformed back into sol upon heating (T_{gel}), at that the sol-gel transition can repeat infinitely without a noticeable degradation of a system. For gelation racemic mixture of *anti*-complex is required as one of two enantiomers ((+)- or (−)-*anti*-complex) or even only *syn*-
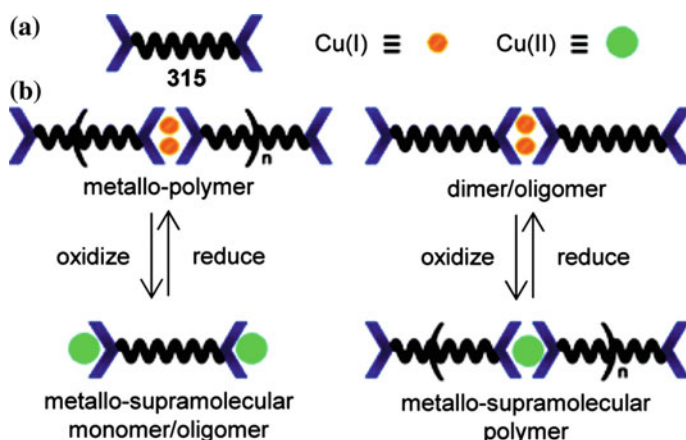

Fig. 7.83 Cartoon representation of **a** ligand and **b** redox regulation DP with Cu:L ratios 1:2 (left) and 1:1 (right)

compex giving a homogeneous solution without any change in properties of a current solution. An assumption is taken that the clothes-PEG-like conformation of *anti*-complex prevents oligomerization because of absence of preliminary organization. However, external stimulus (ultrasound) can have an effect on conformation distribution, which provides formation of a «regular» conformer or insignificant amount of short oligomers with lifetimes, which allow their further extension into the observed aggregates.

There is a great interest in intelligent materials integrated with independent multi-responsiveness, which are reached due to masterly integration between structures of materials and responsiveness of non-covalent interactions. Thus, multi-responsive MSPG [76, 113, 128, 129] are obtained by addition of Zn(II) or Co(II) perchlorate (97 mol% with respect to ligand) to the solution of bis-terdentate bridging ligand, which have shown thermo-, chemo-, and mechano-induced gel-sol behavior phase transition. During heating, and then cooling reversible gel-sol transition was observed. It has been shown that this transition takes place, mostly, due to labile ligand-lanthanide ion interactions, which are different from ligand-transition metal ion interactions. In the same way a gel collapse took place upon addition of 0.85 wt% formic acid to the system due to stronger linking of lanthanide ions to carboxylic acids. One of the most interesting properties of MSPG is mechano-responsivity, which shows thixotropic (shear-thinning) behavior. Free-flowing sol is obtained by shaking of gel, which has reformed opaque gel again after storage. The observations have shown that gelation takes place through flocculation of semi-crystalline colloid particles, whose size can be reduced or even particles disappear under action of mechanical stress. Since nitrate-ion is a coordinating one by nature, branching can increase in presence of non-coordinating perchlorate-ion instead of nitrate-ion, which results in increase in mechano-responsiveness of gels. These gels showed reversible thermo-, chemo-, and mechano-responsive properties. It is obvious that MSPG open possibilities for projecting of multi-responsive organo-inorganic hybrid materials, whose properties can be easily adjusted by changes in combinations of metal ions.

The concept of photo-active mechano-responsive MSP based on using bis-tpy linked ligand, namely, HO-BIP, is developed. An interesting aspect of this concept is that the studied ligands can form 2:1 metal complexes with transition metal ions and 3:1 complexes with lanthanide ions. Therefore, it is possible to create gels by mixing telechelic chelating ligand with combination of lanthanide (cross-linker) and transition (chain extender) metal ions, respectively. These gels show responses to thermo-, chemo- (with formic acid) and mechanical stimuli. Mechano-responsive character of MSP based on Zn/La gel has shown thixotropic (shear-thinning) behavior. It has been found that lanthanide gels have shown very strong luminescent properties based on energy transfer from ligand to metal ion, for example, Eu(III). This photophysical property can be interrupted by heating or mechanical loading, and, consequently, luminescence color changes from red to blue, and emission then respected to the ligand center.

We shall notice a series of stimulus-responsive MSP-based films consisting of Mebip ditopic end-capped poly-THF at different ratios of Zn(II) and Eu(II) [222]. Combination of optical properties of Eu(III) complex with its more labile nature brings to formation of highly stimulus-responsive materials. Films of Eu(III)-containing MSP show expressed optical response to increase in temperature (Fig. 7.84a, b) or under action of chemical substances (Fig. 7.84c, d), such as triethyl phosphate, which was used as imitator for organophosphorus pesticides and nerve gases.

MSP based on btp ligand and Zn(II) and Eu(III) ions have shown different mechanical properties and thermal stability depending on gel composition [652]. For example, photoluminescence properties of the gels can be well adjusted depending on the ratio between Zn(II) and Eu(II) and a solvent used for gelation. Besides, the gels can be converted into sol by heating, which is also accompanied by emission quenching, and its reversibility is detected during cooling. In the similar way these gels have shown mechano-, photo-, and chemo-responsive properties.

Upon linking a tpy motif to linear polymers carrying short hydrophobic segments, primary hydrophobic interactions bring to formation of micellar nanostructures in water [653, 654]. Metallosupramolecular micellar hydrogels, which show thermo-mechanical responsivity, are obtained through hierarchical assembling of hete-rochelate associating polymer. At the first stage the associating polymer is solved in
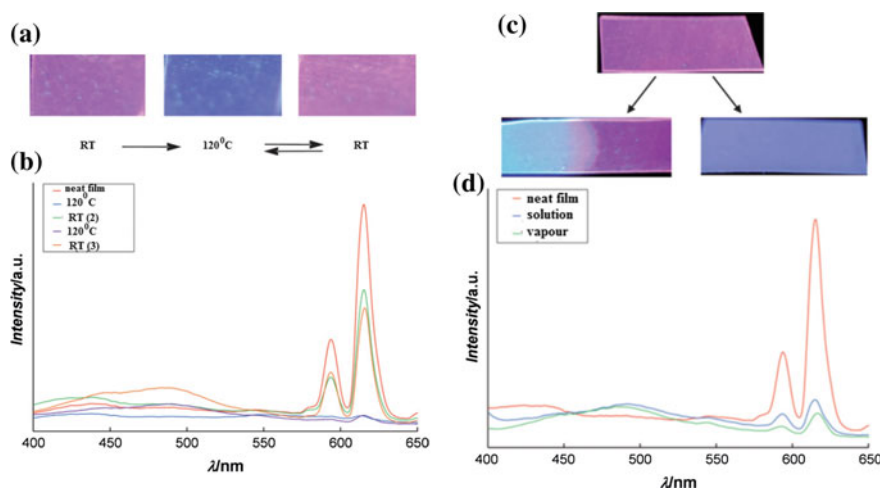

Fig. 7.84 **a** Temperature sensing: sample heated to 120 °C resulting in quenching of the Eu(III) fluorescence and subsequent return upon cooling back to room temperature (Zn(II):Eu(III) 70:30); **b** photoluminescence spectra (excited at 377 nm) of the above films showing the reversible disappearance of the Eu(III) metal-based emission at 590 and 615 nm upon heating and subsequent return with cooling. **c** Picture of a film fluorescing under UV light ($\lambda = 365$ nm) before and after dipping into a 10 mM solution of triethyl phosphate in hexane for 1 min (left) and exposure to triethyl phosphate vapor (24 h., rt) (right); **d** photoluminescence spectra (excited at 377 nm) of the above films. Both films show a decrease in the characteristic Eu(III) emission peaks at 590 and 615 nm

aqueous solution with formation of micellar nanostructures carrying chelating fragments at the end of coronal chains. At the second stage supramolecular assemblies are formed at addition of transition metal ions to micellar solutions, which results in almost instant gelation. These gels have shown reversible gel-sol transitions under mechanic stress and temperature-induced self-healing properties.

Linear MSPs based on Zn(II) and heteroditopic monomer carrying secondary ammonium salt of guest and tpy moiety have shown multistimuli-responsiveness, trigged by heat, pH or competitive ligand, such as cyclen [362]. In particular, specific viscosity of MSP decreases considerably above 50 °C, which points to decomposition of supramolecular polymers at elevated temperature. Besides, addition of 1.5 equivalents of Et$_3$N deprotonates fragments of secondary ammonium salt, which also results in MSP decomposition. Therefore, obviously MSP are highly adaptive materials capable of undergoing reversible transitions under action of different external stimuli.

Multistimulus-responsive behavior of metal-containing system was reported being achieved by using photoisomerization of dithienylethene fragment (Fig. 7.85) [655]. Mixing dithienylethene derivative of dicarboxylic acid with Al(III) has given a transparent solution, from which a metal-containing gel was obtained during heating. The gelation process depends on anion addition: their coordination with Al (III) or formation of H-bonds with ligands disturbs the gelation process. The obtained gels have shown reversible photochromic behavior: yellow solution of the open (O) form transforms into yellow gel of O-form during heating and can be transformed into red gel of the closed (C) form under UV irradiation. The red C-gel transforms into red C-solution during storage at room temperature in dark place and then returns to initial yellow O-solution under action of visible light.

Highly dynamic and adaptive non-covalent interactions forming supramolecular materials can be destructed in presence of competitive reagents (analytes) [656]. A change in physical properties of MSP by pollution, for example, adsorption and emission can be output signals for registration of quantity and quality of analytes, which is a basic principle for supramolecular sensors. It should be noted that some non-covalent interactions such as guest-host interactions [657] are highly specific and this can provide production of and selective sensors for special analyte. Thus, a special amphiphilic receptor TbL$^+$ complex is developed, which is self-assembled in water and forms stable vesicles [658]. The L^{2-} ligand consisted of bis(pyridine) anionic arms and long alkyl chain (Scheme 7.25). Upon addition of different nucleotides there is sigmoidal increase in luminescence intensity, which is ascribed to drift of coordinated water molecules by phosphate groups. Linking of TbL$^+$ complexes to each phosphate block bound by phosphoanhydride bonds goes cooperative, probably, by adaptive change of their molecular orientation in bilayer. Dynamic non-covalent interactions of alkyl chains have brought to adaptive and highly synergetic assembling between highly organized receptors (TbL$^+$ complex) on a membrane surface.
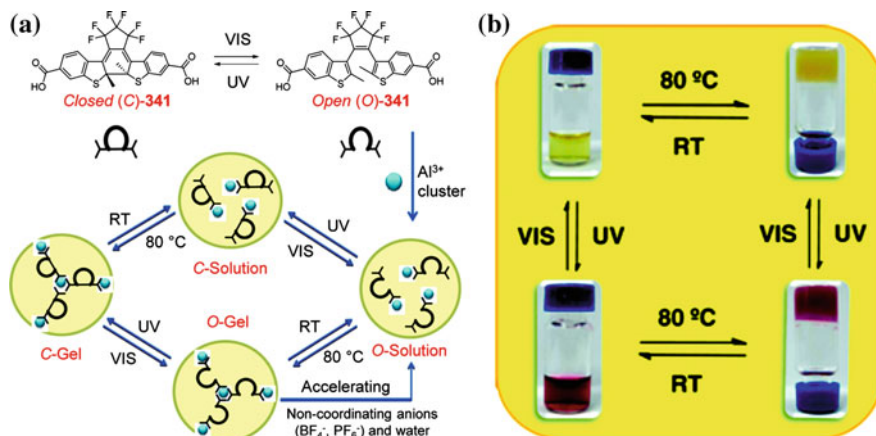
Fig. 7.85 a Reversible photoisomerization between the open- and closed-ring forms of the photochromic dicarboxylic acid ligand, and schematic representation of multiple transformations among gels and solutions in both open and closed forms (denoted as O-gel, O-solution, C-gel, and C-solution) after coordination. **b** Reversible gel-gel and gel-solution transformations of system upon heating/cooling, and UV-vis irradiation, and the multiple responsive behaviors toward color, fluorescence, water, and anions
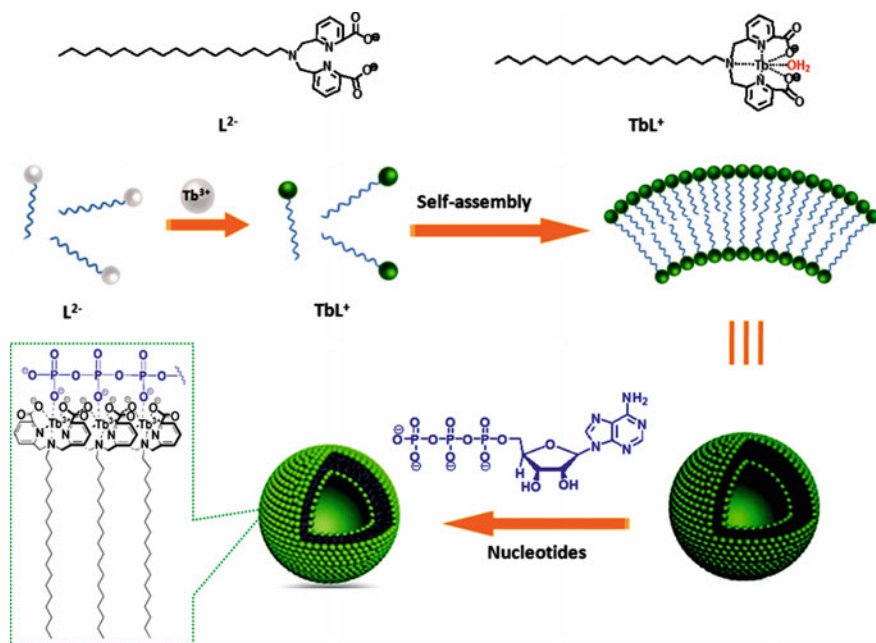
Scheme 7.25 Molecular structures of the ligand L^{2-} and TbL^+ amphiphilic complex and schematic representation for self-assembly of TbL^+ in water for the detection of ATP molecules

7.14 Self-healing and Shape-Memory Metallosupramolecular Polymers

Contemporary materials with inherent ability to repair damage at molecular level can be useful in a wide range of applications. The majority of so far developed healed polymer-based materials require heating a damaged zone above their glass transition temperature, and then pressure application in order to promote a contact, wetting, diffusion and repeated entangling of polymer chains [659–661]. Nevertheless, the healing process is, as a rule, slow and not efficient and hardly applied in practice. More promising in this view is MSP using [662]. Thus, optically healed supramolecular polymers are developed consisting of ditopic Mebip fragment and poly (ethylene-*co*-butylene) motif as a spacer for bridging of metal-binding fragments (Fig. 7.86a) [663, 664]. Under action of UV irradiation M–L motifs are excited, and absorbed energy is transformed into heat, thus bringing materials to depolymerization, dilution, and healing of defects. In this case re-forming of supramolecular polymer comes after a light source removal, which results in healing of a material (Fig. 7.86b). This property of self-healing proceeds through making cuts in 350 to 400-μm thick polymer films, at that, these samples under following irradiation by 320 to 390-nm UV light have shown healing during 30 s (Fig. 7.86c). It is interesting that under light irradiation the cuts were filled, and then appeared.

This work is broaden using MSP consisting of poly (butyl acrylate-*co*-MMA) functionalized by Mebip side chains, which is cross-linked by zinc trifluoromethanesulfonate salt [511]. In particular, this MSP has shown triple shape memory, as a result, it can reversibly gain shape «V», «S» or original rectangular sheet during heating or cooling. Shape reforming and healing is reached upon applying of thermal of light stimulus due to specific M–L interactions, which serve not only as «inert» cross-linkings of a network at low temperature to reform a shape, but also dissociate at high temperature for healing. The healing rate is high and efficiency of healing is close to ∼90% (Fig. 7.87).

There is interest in MSP-based self-healing coatings produced by integration of Fe bis-tpy complexes in polymer network based on methacrylates [665]. We shall also notice supramolecular materials, which can be simultaneously and reversibly self-healed without external stimuli based on metallosupramolecular interactions [666]. In particular, 3D transition supramolecular networks are formed from a macromolecule containing tridentate btp ligand fragments coordinated with transition and/or lanthanide metals. As compared with initial macromolecule, the obtained supramolecular films have improved mechanical properties, such as Young modulus, strength and impact toughness, which can be easily adjusted by the stoichiometric ratio of Zn(II) to Eu(III) and Tb(III). Metallosupramolecular films, as well as gels, show fast and efficient properties of self-healing due to kinetically labile character of M–L interactions. We shall notice thermally-responsive gels, which use thermally induced interconversion between *cis*- and *trans*-isomers on cyclam blocks, displaying self-healing property [667].
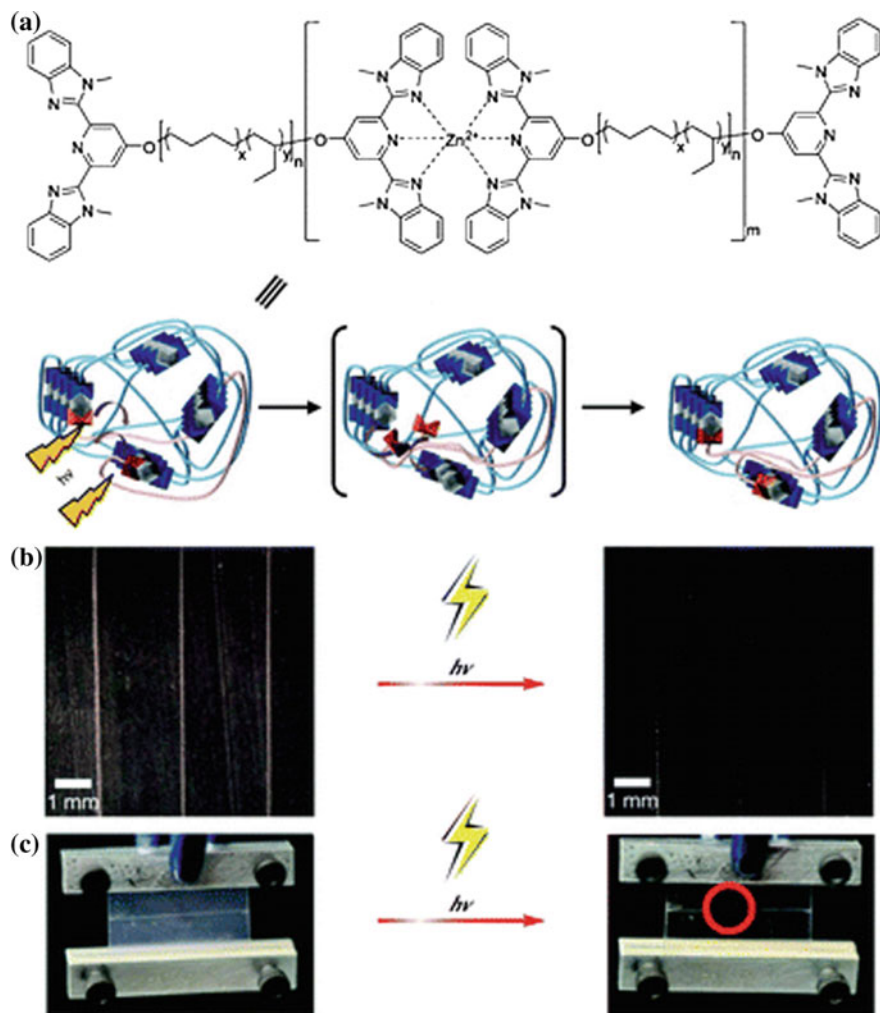
Fig. 7.86 a Chemical structure of the MSP and schematic representation of its self-healing process; **b** optical healing of MSP on exposure to light; **c** optical healing of MSP while under a load

The self-healing process is studied in detail using the MSP example including Fe (II)-tpy complexes and different copolymers [668]. In particular, the best results of self-healing were observed at 100 °C for organogel based on lauryl-methacrylate copolymer, while MMA-based gel does not absolutely show self-healing because of lower T_g and, respectively, lower flexibility of a co-monomer. During heating a degree of cross-linking is constant thus showing that self-healing mechanism is not based on decomplexation of tpy complex. Using thermal-induced self-healing mechanism of MSP based on bis-tpy complexes of Fe(II) sulfate and Cd(II)
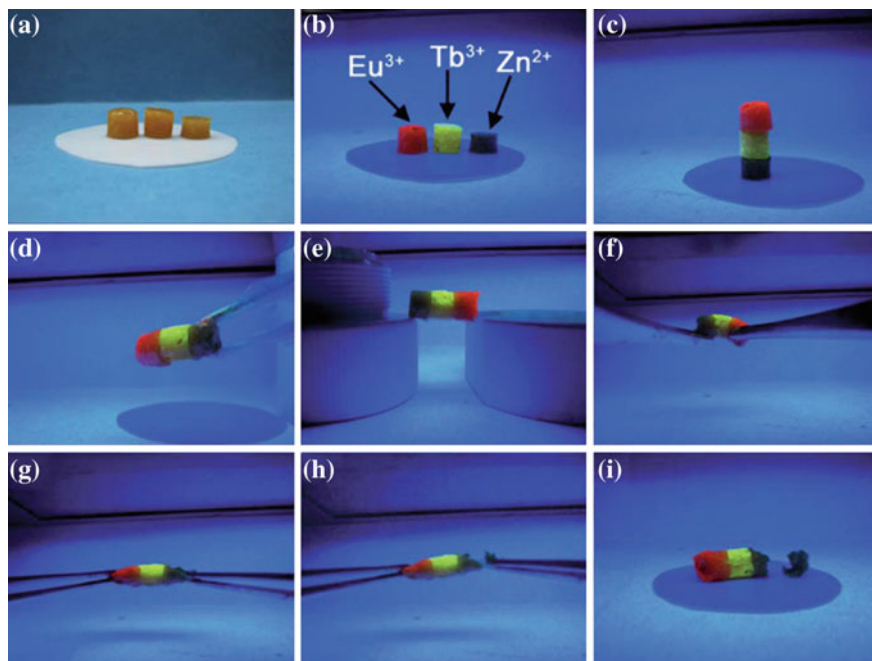
Fig. 7.87 Self-healing the MSPG. **a** Gels containing different metal ions (from left to right are 0:100:0, 0:0:100 and 100:0:0) swollen in toluene; **b** fluorescent image of the three gels under UV light (254 nm); **c** gels were stacked up before self-healing; **d** and **e** the stacked gels were subjected to self-healing under a saturated toluene atmosphere for 1 h; **f–i** the healed gel was then subjected to bending and stretching until fracture

bromide, two possible healing schemes are considered, one of which takes into account decomplexation of cross-linking complexes, and another one is based on dissociation of ionic clusters [669]. It occurs that self-healing mechanisms based on partial decomplexation of cross-linking complexes, are determinative. Apart from nature of a metal, self-healing properties are strongly affected by nature of an anion [670].

We shall also notice using of histidine-metal interactions as reinforcing cross-linkings in self-healing MSP [671]. In particular, a cross-linking of histidine-containing polymers based on butyl methacrylate and lauryl methacrylate with Zn ions brings to MSP networks showing self-healing behavior, which was tunable depending on a certain used Zn salt.

Though polymers with shape memory have been widely developed during the last decade [672], the examples, which use non-covalent interactions in order to fix temporary shape-memory of polymers, are still rare, especially for shape memory of supramolecular polymers [673–676]. The shape memory polymers (SMP) can be deformed to stable temporary shape and reformed to their initial shape using stimuli. These networks are based on presence of two types of pure points to establish their

constant and temporary shapes. Classical strategies for stabilization of temporary shapes are based on cooling below T_g/T_m, where macromolecules are pinned in stressed state. Healing of SMP usually includes heating to temperature above the transition temperature, where a constant shape is remembered. Using of reversible cross-linking groups in SMPs appeared as alternative strategy for stabilization of temporary shapes and providing recyclability to a constant shape.

Ternary (thermo-, photo-, and chemo-) responsive effects with shape memory from photo-cross-linked MSP can be noted as an example [674]. These MSP are obtained by elegant combination of a core of polybutadiene oligomer with capping OMebip ligands and metal ions, in which M–L complexes form a solid phase, which physically cross-links a soft domain of polybutadiene. It is important that any stimulus, which can disturb a solid phase, can be used for fixation of temporary shape and cause its self-healing back into a constant shape, which can be reached by photo-cross-linking of polybutadiene core with tetra-functional thiol through photo-initiated thiol-ene reaction (Fig. 7.88). It has been found that M–L complexes
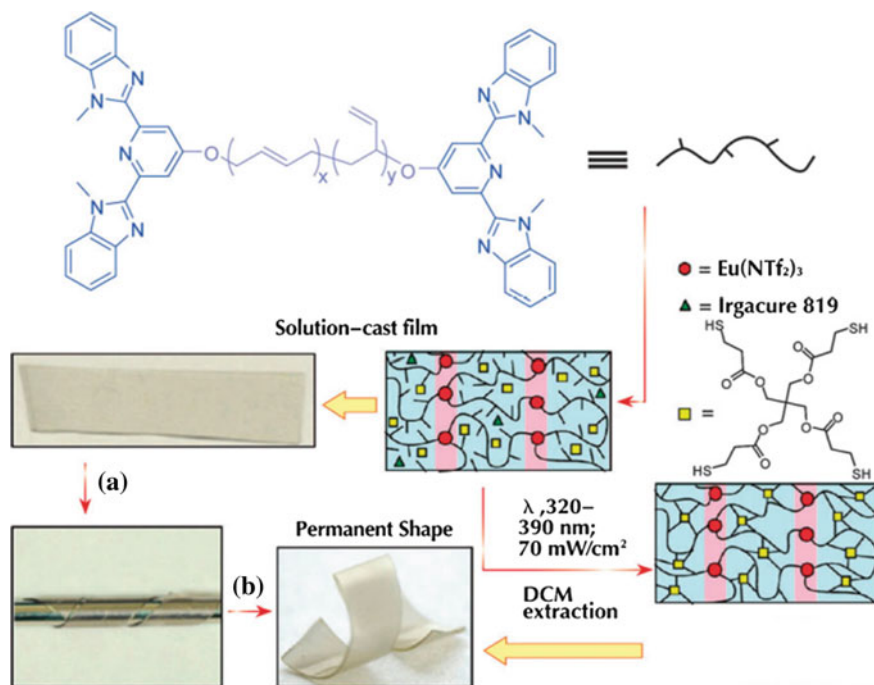

Fig. 7.88 Chelating ligand with terminal groups of polybutadiene macromonomer films, which contain different amounts of tetrathiol cross-linker and photoinitiator (Irgacure 819). Films are solution cast, and the dried films are photo-cross-linked with a targeted 3, 8, and 14 cross-links/chain. The solution-cast uncross-linked films can be fixed into a variety of permanent shapes: **a** a strip of uncross-linked film is wrapped around a cylinder to give a spiral shape, and **b** irradiation with low intensity UV light initiates photo-crosslinking to yield a film with a permanent spiral shape

can absorb light and transfer a part of this energy for heating localization. Therefore, the observed photo-responsive shape memory behavior of MSP film is a result of photothermal transformation process. Besides, chemical substances can also have effect on thermal stability of solid phase of materials through plasticization or decomplexation of M–L chelate. Moreover, a soft phase with different densities of cross-linkings has different shape memory properties with initial restrain of fixation value more than 80% and strain-recovery above 95%.

Such concept of design is used for production of MSPs [677], which react to different stimuli, including influence of heat, UV irradiation, and different solvents. Other SMP are obtained by addition of bistriflimide europium salt [Eu(NTF$_2$)$_3$] to low molecular weight polybutadiene telechelics carrying Mebip ligands bringing to reversible network. In this case a constant SMP shape is obtained by formation of supramolecular elastomer in a necessary shape with the following photo-cross-linking through thiolene reaction between 1,2-vinyl groups of butadiene core and tetrafunctional thiol. Shape memory can be thermally caused with R_f about 90% and fixing ratio (R_f) above 90% (more typically 97%). Good fixations and strain recoveries are reached, and it is shown that a change in metal ion from Eu(III) to Zn(II) (preserving the same counter-ion) has brought to some decrease in fixation immediately after load removal, and a considerable increase in creep of the temporary shape. It is also important that different solvents, including methanol, acetone, and less triethylamine, can be used to cause shape recovery.

Macromolecular linear poly (p-dioxanone) polymers carrying bpy units are cross-linked with Fe(II) ions with formation of a permanent network, while crystallizing segments of p-dioxane serve as a thermal trigger for SMP (Scheme 7.26) [496]. Good shape memory characteristics were observed for these SMP, in particular, the R_f approaches 100%, and the extraction coefficient is beyond 93%.
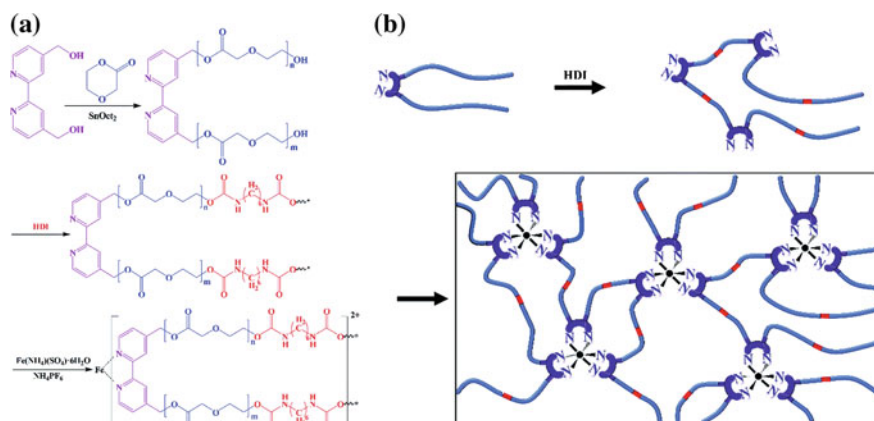
Scheme 7.26 Preparation of metallosupramolecular bpy-poly (p-dioxanone)-Fe. **a** Synthetic route; **b** schematic illustration

The shape memory assisted self-healing (SMASH) polymers include those that combine the shape memory effect with self-healing. Healing of SMASH polymers proceeds in two stages: at the first stage the shape memory effect provides autonomous crack-healing and force applying; at the second stage self-healing of fractured surface takes place. In this view two-component SMASH polymer systems should be noted, in which covalently cross-linked matrices provide the shape memory effect, and healing goes due to diffusion of linear segments of initial polymer ligands at a crack interface [678, 679]. More promising is using of dynamic M–L bond for preparation of SMASH polymers (Fig. 7.89) [511]. Thermal analysis has shown three transitions, which appeared due to Mebip concentration: (a) low T_g of acrylate network (24 °C $\leq T_{g,1} \leq$ 46.8 °C), (b) a glass transition associated with acrylate chains in M–L rich phase divided by domains (68.4 °C $\leq T_{g,2} \leq$ 83.0 °C), (c) a region with high melting point associated with M–L complex decomplexation (95 °C $\leq T_d \leq$ 160 °C). Presence of these two glass transitions and non-covalent network points, ddetermining the permanent shape of SMP, stipulate thermally-induced behavior of the ternary shape memory, and presence of reversible metallosupramolecular bond gives the self-healing capacity. In particular, this was demonstrated by heating of cut and bent samples up to 140 °C, where expected SMASH consequence of shape recovery was observed, crack healing, and self-healing with curable efficiency in the range from 65 to 98%. It is interesting that UV light assisted SMASH has healing efficiencies approaching 100% due to higher temperatures achieved during UV irradiation.
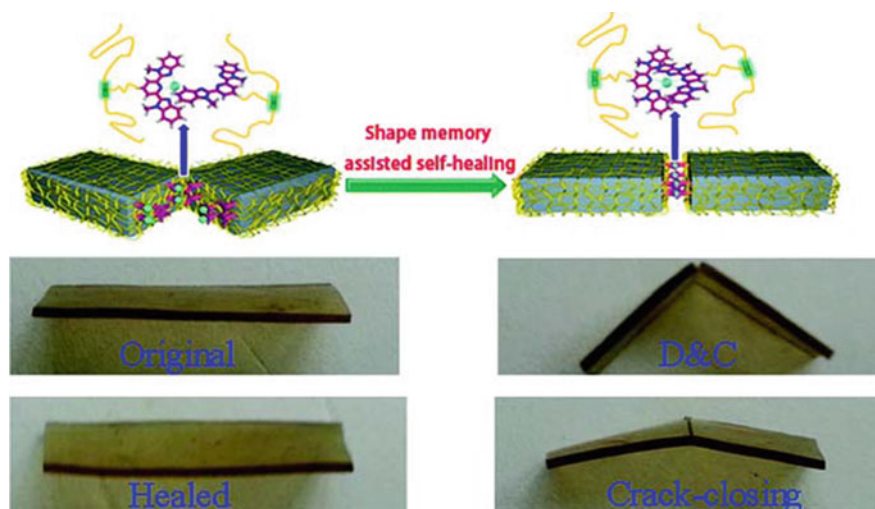

Fig. 7.89 Illustrating the thermal-induced SMASH of supramolecular networks based on poly (*n*-butyl acrylate-*co*-MMA) copolymers bearing Mebip side groups cross-linked by the metal salt zinc trifluoromethanesulfonate. Self-healing experiments conducted as follows: deformation and cracking performed at room temperature; healing performed at 140 °C/25 min

References

1. J.M. Lehn, *Supramolecular Chemistry—Concepts and Perspectives* (Wiley, VCH, Weinheim, 1995)
2. V.G. Machado, P.N.W. Baxter, J.-M. Lehn, J. Braz. Chem. Soc. **12**(4) (2001)
3. J.W. Steed, J.L. Atwood, *Supramolecular Chemistry* (Wiley, Weinheim, 2005)
4. H. Dodziuk, *Introduction to Supramolecular Chemistry* (Kluwer, NY, Boston, Dordrecht, London, Moscow, 2002)
5. J.W. Steed, J.L. Atwood (eds.), *Encyclopedia of Supramolecular Chemistry* (Marcel Dekker, NY, 2004)
6. P.J. Cragg, *Practical Supramolecular Chemistry* (Wiley, Chichester, UK, 2006)
7. K. Ariga, T. Kunitake, *Supramolecular Chemistry—Fundamentals and Applications* (Springer, Heidelberg, 2006)
8. J.W. Steed, D.R. Turner, K.J. Wallace, *Core Concepts in Supramolecular Chemistry and Nanochemistry* (Wiley, Chichester, 2007)
9. R.M. Izatt (ed.), *Macrocyclic and Supramolecular Chemistry: How Izatt-Christensen Award Winners Shaped and Field* (Wiley, Chichester, 2016)
10. G.R. Desiraju, Nature **412**, 397 (2001)
11. A. Wild, A. Winter, F. Schlütter, U.S. Schubert, Chem. Soc. Rev. **40**, 1459 (2011)
12. M. Albrecht, Naturwissenschaften **94**, 951 (2007)
13. W.-S. Tang, X.-X. Lu, K.M.-C. Wong, V.W.-W. Yam, J. Mat. Chem. **15**, 2714 (2005)
14. J.M. Lehn, Proc. Natl. Acad. Sci. U.S.A. **99**, 4769 (2002)
15. O.V. Grineva, Zh Struct, Khim. **47**, 185 (2006)
16. S.Z. Vatsadze, *Comprehensive Problems of Chemistry of Coordination Polymers. Success in the Synthesis of exo-Dentate Tectones* (LAP Lambert Academic Publishing, 2011) (in Russian)
17. M. Simard, D. Su, J.D. Wuest, J. Am. Chem. Soc. **113**, 4696 (1991)
18. E.J. Corey, Pure Appl. Chem. **14**, 19 (1967)
19. K. Ariga, K. Minami, M. Ebara, J. Nakanishi, Polym. J. **48**, 371 (2016)
20. K. Ariga, J. Li, J. Fei, Q. Ji, J.P. Hill, Adv. Mater. **28**, 1251 (2016)
21. G.R. Desiraju, Angew. Chem. Int. Ed. **34**, 2311 (1995)
22. G.R. Desiraju, Angew. Chem. Int. Ed. **46**, 8342 (2007)
23. G.R. Desiraju, J. Mol. Struct. **656**, 5 (2003)
24. C.B. Aakerçy, B.M.T. Scott, M.M. Smith, J.F. Urbina, J. Desper, Inorg. Chem. **48**, 4052 (2009)
25. P.M. Bhatt, Y. Azim, T.S. Thakur, G.R. Desiraju, Cryst. Growth Des. **9**, 951 (2009)
26. R. Banerjee, B.K. Saha, G.R. Desiraju, CrystEngComm **8**, 680 (2006)
27. L.S. Reddy, N.J. Babu, A. Nangia, Chem. Commun. 1369 (2006)
28. C.B. Aakerçy, J. Desper, J.F. Urbina, Chem. Commun. 2820 (2005)
29. D.R. Turner, B. Smith, A.E. Goeta, I.R. Evans, D.A. Tocher, J.A.K. Howard, J.W. Steed, CrystEngComm **6**, 633 (2004)
30. D.K. Kumar, A. Das, P. Dastidar, Cryst. Growth Des. **6**, 216 (2006)
31. S. Kohmoto, Y. Kuroda, Y. Someya, K. Kishikawa, H. Masu, K. Yamaguchi, I. Azumaya, Cryst. Growth Des. **9**, 3437 (2009)
32. H.-J. Schneider, A.K. Yatsimirsky, *Principles and Methods in Supramolecular Chemistry* (Wiley, Chichester, England, 2000)
33. C. Rest, R. Kandanelli, G. Fernández, Chem. Soc. Rev. **44**, 2543 (2015)
34. A. Ciferri, *Supramolecular Polymers*, 2nd edn. (CRC Press, Boca Raton, FL, 2005)
35. U.S. Schubert, C. Eschbaumer, Angew. Chem. Int. Ed. **41**, 2892 (2002)
36. J.M. Lehn, Polym. Int. **51**, 825 (2002)
37. E. Krieg, M.M.C. Bastings, P. Besenius, B. Rybtchinski, Chem. Rev. **116**, 2414 (2016)
38. S. Burattini, B.W. Greenland, D.H. Merino, W. Weng, J. Seppala, H.M. Colquhoun, W. Hayes, M.E. Mackay, I.W. Hamley, S.J. Rowan, J. Am. Chem. Soc. **132**, 12051 (2010)

39. A. Harada (ed.), *Supramolecular Polymer Chemistry* (Wiley-VCH Verlag GmbH & Co. KGaA, Weinheim, 2012)
40. L. Yang, X. Tan, Z. Wang, X. Zhang, Chem. Rev. **115**, 7196 (2015)
41. G.R. Newkome, E.F. He, C.N. Moorefiled, Chem. Rev. **99**, 1689 (1999)
42. G.J. McManus, Z. Wang, M.J. Zaworotko, Cryst. Growth Des. **4**, 11 (2004)
43. T.F.A. De Greef, M.M.J. Smulders, M. Wolffs, A.P.H.J. Schenning, R.P. Sijbesma, E.W. Meijer, Chem. Rev. **109**, 5687 (2009)
44. D. Zhao, J.S. Moore, Org. Biomol. Chem. **1**, 3471 (2003)
45. Z. Chen, A. Lohr, C.R. Saha-Möller, F. Würthner, Chem. Soc. Rev. **38**, 564 (2009)
46. M.M.J. Smulders, M.M.L. Nieuwenhuizen, T.F.A. de Greef, P. van der Schoot, A.P.H. J. Schenning, E.W. Meijer, Chem. Eur. J. **16**, 362 (2010)
47. S.P. Khor, R.J. Varley, S.Z. Shen, Q. Yuan, J. Appl. Polym. Sci. **128**, 3743 (2013)
48. Y. Liu, Z. Wang, X. Zhang, Chem. Soc. Rev. **41**, 5922 (2012)
49. X. Yan, F. Wang, B. Zheng, F. Huang, Chem. Soc. Rev. **41**, 6042 (2012)
50. J.D. Fox, S.J. Rowan, Macromolecules **42**, 6823 (2009)
51. A. Harada, R. Kobayashi, Y. Takashima, A. Hashidzume, H. Yamaguchi, Nat. Chem. **3**, 34 (2011)
52. A. Harada, Y. Takashima, H. Yamaguchi, Chem. Soc. Rev. **38**, 875 (2009)
53. R.J. Wojtecki, M.A. Meador, S.J. Rowan, Nat. Mater. **10**, 14 (2011)
54. T.F.A. de Greef, E.W. Meijer, Nature **453**, 171 (2008)
55. W. Zhang, W. Jin, T. Fukushima, A. Saeki, T. Aida, Science **334**, 340 (2011)
56. E. Krieg, H. Weissman, E. Shirman, E. Shimoni, B. Rybtchinski, Nat. Nanotechnol. **6**, 141 (2011)
57. M.A.C. Stuart, W.T.S. Huck, J. Genzer, M. Müller, C. Ober, M. Stamm, G.B. Sukhorukov, I. Szleifer, V.V. Tsukruk, M. Urban, F. Winnik, S. Zauscher, I. Luzinov, S. Minko, Nat. Mater. **9**, 101 (2010)
58. R.J. Wojtecki, M.A. Meador, S.J. Rowan, Nat. Mater. **10**, 14 (2011)
59. S.K. Yang, A.V. Ambade, M. Weck, Chem. Soc. Rev. **40**, 129 (2011)
60. B. Zheng, F. Wang, S. Dong, F. Huang, Chem. Soc. Rev. **41**, 1621 (2012)
61. T. Aida, E.W. Meijer, S.I. Stupp, Science **335**, 813 (2012)
62. M. Fathalla, C.M. Lawrence, N. Zhang, J.L. Sessler, J. Jayawickramarajah, Chem. Soc. Rev. **38**, 1608 (2009)
63. H.H. Dam, F. Caruso, Adv. Mater. **23**, 3026 (2011)
64. J. Luo, T. Lei, L. Wang, Y. Ma, Y. Cao, J. Wang, J. Pei, J. Am. Chem. Soc. **131**, 2076 (2009)
65. D. Gonzalez-Rodrıgue, A.P.H.J. Schenning, Chem. Mater. **23**, 310 (2011)
66. B.J.B. Folmer, R.P. Sijbesma, R.M. Versteegen, J.A.J. van der Rijt, E.W. Meijer, Adv. Mater. **12**, 874 (2000)
67. L. Sánchez, M.T. Rispens, J.C. Hummelen, Angew. Chem. Int. Ed. **41**, 838 (2002)
68. T. Suzuki, S. Shinkai, K. Sada, Adv. Mater. **18**, 1043 (2006)
69. K.P. Nair, V. Breedveld, M. Weck, Macromolecules **41**, 3429 (2008)
70. L. Brunsveld, B.J.B. Folmer, E.W. Meijer, R.P. Sijbesma, Chem. Rev. **101**, 4071 (2001)
71. E. Kolomiets, E. Buhler, S.J. Candau, J.-M. Lehn, Macromolecules **39**, 1173 (2006)
72. F.J.M. Hoeben, P. Jonkheijm, E.W. Meijer, A.P.H.J. Schenning, Chem. Rev. **105**, 1194 (2005)
73. V.A. Friese, D.G. Kurth, Coord. Chem. Rev. **252**, 199 (2008)
74. D.M.P. Mingos, *Supramolecular Assembly via Hydrogen Bonds* (Springer, Berlin, 2004)
75. R. Dobrawa, F. Würthner, J. Polym. Sci. Part A Polym. Chem. **43**, 4981 (2005)
76. D.G. Kurth, M. Higuchi, Soft Matter **2**, 915 (2006)
77. J.B. Beck, S.J. Rowan, J. Am. Chem. Soc. **125**, 13922 (2003)
78. W.C. Yount, D.M. Loveless, S.L. Craig, J. Am. Chem. Soc. **127**, 14488 (2005)
79. S. Sivakova, D.A. Bohnsack, M.E. Mackay, P. Suwanmala, S.J. Rowan, J. Am. Chem. Soc. **127**, 18202 (2005)
80. J. Adisoejoso, Y. Li, J. Liu, P.N. Liu, N. Lin, J. Am. Chem. Soc. **134**, 18526 (2012)

81. F.S. Han, M. Higuchi, D.G. Kurth, Adv. Mater. **19**, 3928 (2007)
82. F. Peng, G. Li, X. Liu, S. Wu, Z. Tong, J. Am. Chem. Soc. **130**, 16166 (2008)
83. O. Kotova, R. Daly, C.M.G. dos Santos, M. Boese, P.E. Kruger, J.J. Boland, T. Gunnlaugsson, Angew. Chem. Int. Ed. **51**, 7208 (2012)
84. U.S. Schubert, H. Hofmeier, G.R. Newkome, *Modern Terpyridine Chemistry* (Wiley-VCH, Weinheim, 2006)
85. P.R. Andres, U.S. Schubert, Adv. Mater. **16**, 1043 (2004)
86. A.S. Abd-El-Aziz, P.O. Shipman, B.N. Boden, W.S. NcNeil, Prog. Polym. Sci. **35**, 714 (2010)
87. V.A. Friese, D.G. Kurth, Curr. Opin. Colloid Interface Sci. **14**, 81 (2009)
88. Q. Wang, J.L. Mynar, M. Yoshida, E. Lee, M. Lee, K. Okuro, K. Kinbara, T. Aida, Nature **463**, 339 (2010)
89. J.N. Hunt, K.E. Feldman, N.A. Lynd, J. Deek, L.M. Campos, J.M. Spruell, B.M. Hernandez, E.J. Kramer, Adv. Mater. **23**, 2327 (2011)
90. T. Ogoshi, Y. Ichihara, T.A. Yamagishi, Y. Nakamoto, Chem. Commun. **46**, 6087 (2010)
91. J. Fox, J.J. Wie, B.W. Greenland, S. Burattini, W. Hayes, H.M. Colquhoun, M.E. Mackay, S.J. Rowan, J. Am. Chem. Soc. **134**, 5362 (2012)
92. L. Brunsveld, B.J.B. Folmer, E.W. Meijer, MRS Bull. **25**, 49 (2000)
93. A. Cifferi, Macromol. Rapid Commun. **23**, 511 (2002)
94. X. Zhang, C. Wang, Chem. Soc. Rev. **40**, 94 (2011)
95. R. Shunmugam, G.J. Gabriel, K.A. Aamer, G.N. Tew, Macromol. Rapid Commun. **31**, 784 (2010)
96. M. Chiper, R. Hoogenboom, U.S. Schubert, Macromol. Rapid Commun. **30**, 565 (2009)
97. B.M. McKenzie, S.J. Rowan, Metallosupramolecular polymers, networks, and gels, in *Molecular Recognition and Polymers: Control of Polymer Structure and Self-Assembly*, ed. by V. Rotello, S. Thayumanavan (Wiley, Hoboken, 2008)
98. B.M. McKenzie, S.J. Rowan. Metallo-Supramolecular Polymers, in *Encyclopedia of Supramolecular Chemistry*, ed. by J.L. Atwood, J.W. Steed (CRC Press, Boca Raton, 2007)
99. M. Higuchi, J. Mater. Chem. C **2**, 9331 (2014)
100. M. Burnworth, D. Knapton, S.J. Rowan, C. Weder, J. Inorg. Organomet. Polym. **17**, 91 (2007)
101. A.Y.-Y. Tam, V.W.-W. Yam, Chem. Soc. Rev. **42**, 1540 (2013)
102. A.S. Abd-El-Aziz, I. Manners (eds.), *Frontiers in Transition Metal-Containing Polymers* (Wiley, Hoboken, New Jersey, 2006)
103. X.-Y. Hu, T. Xiao, C. Lin, F. Huang, L. Wang, Acc. Chem. Res. **47**, 2041 (2014)
104. Z. Qi, C.A. Schalley, Acc. Chem. Res. **47**, 2222 (2014)
105. K.M.-C. Wong, M.M.-Y. Chan, V.W.-W. Yam, Adv. Mater. **26**, 5558 (2014)
106. J. Zhou, G.R. Whittell, I. Manners, Macromolecules **47**, 3529 (2014)
107. J. Brassinne, C.-A. Fustin, J.-F. Gohy, J. Inorg. Organomet. Polym. **23**, 24 (2013)
108. A.O. Moughton, R.K. O'Reilly, Macromol. Rapid Commun. **31**, 37 (2010)
109. X. Su, I. Aprahamian, Chem. Soc. Rev. **43**, 1963 (2014)
110. G. Lawrance, *Introduction to Coordination Chemistry* (Wiley, Chichester, 2009)
111. L. Cronin, Annu. Rep. Prog. Chem. Sect. A Inorg. Chem. **101**, 348 (2005)
112. O. Costisor, W. Linert, Rev. Inorg. Chem. **23**, 289 (2003)
113. Y. Yan, J.B. Huang, Coord. Chem. Rev. **254**, 1072 (2010)
114. S.J. Rowan, J.B. Beck, Faraday Discuss. **128**, 43 (2005)
115. J.B. Beck, J.M. Ineman, S.J. Rowan, Macromolecules **38**, 5060 (2005)
116. AYu. Tsivadze, Uspehi Khim. **73**, 6 (2004)
117. AYu. Tsivadze, G.V. Ionova, V.K. Mihalko, YuN Kostrubov, Uspehi Khim. **76**, 237 (2007)
118. G.M. Mamardashvili, NZh Mamardashvili, O.I. Koifman, Uspehi Khim. **74**, 839 (2005)
119. G.M. Mamardashvili, NZh Mamardashvili, O.I. Koifman, Uspehi Khim. **77**, 60 (2008)
120. A.N. Khlobystov, A.J. Blake, N.R. Champness, D.A. Lemenovskii, A.G. Majouga, N.V. Zyk, M. Schroder, Coord. Chem. Rev. **222**, 155 (2001)
121. S. Leininger, B. Olenyuk, P.J. Stang, Chem. Rev. **100**, 853 (2000)

122. G.F. Swiegers, T.J. Malefeste, Chem. Rev. **100**, 3483 (2000)
123. YuE Alexeev, B.I. Kharisov, T.C. Hernandez Garcia, A.D. Garnovskii, Coord. Chem. Rev. **254**, 794 (2010)
124. U.S. Schubert, O. Hien, C. Eschbaumer, Macromol. Rapid Commun. **21**, 1156 (2000)
125. S. Schmatloch, M.F. Gonzalez, U.S. Schubert, Macromol. Rapid Commun. **23**, 957 (2002)
126. M.A.R. Meier, B.G.G. Lohmeijer, U.S. Schubert, Macromol. Rapid Commun. **24**, 852 (2003)
127. C.-C. Chen, E. Dormidontova, J. Am. Chem. Soc. **126**, 14972 (2004)
128. B.H. Northrop, Y.-R. Zheng, K.-W. Chi, P.J. Stang, Acc. Chem. Res. **42**, 1554 (2009)
129. Y.Q. Zhao, J.B. Beck, S.J. Rowan, A.M. Jamieson, Macromolecules **37**, 3529 (2004)
130. W.G. Weng, J.B. Beck, A.M. Jamieson, S.J. Rowan, J. Am. Chem. Soc. **128**, 11663 (2006)
131. G. Schwarz, I. Haßlauer, D.G. Kurth, Adv. Colloid Interface Sci. **207**, 107 (2014)
132. Y. Yan, J. Huang, Coord. Chem. Rev. **254**, 1072 (2010)
133. A. Maier, A.R. Rabindranath, B. Tieke, Adv. Mater. **21**, 959 (2009)
134. J.M. Pollino, M. Weck, Chem. Soc. Rev. **34**, 193 (2005)
135. K.A. Aamer, G.N. Tew, Macromolecules **40**, 2737 (2007)
136. M.R. Hammond, A.K. Andreopoulou, E. Pefkianakis, J.K. Kallitsis, R. Mezzenga, Chem. Mater. **21**, 2169 (2009)
137. R. Shunmugam, G. Tew, Macromol. Rapid Commun. **29**, 1355 (2008)
138. K. Calzia, G. Tew, Macromolecules **35**, 6090 (2002)
139. R. Shunmugam, G. Tew, Polym. Adv. Technol. **19**, 596 (2008)
140. T.K. Sievers, A. Vergin, H. Möhwald, D.G. Kurth, Langmuir **23**, 12179 (2007)
141. R. Johnson, C. Fraser, Macromolecules **37**, 2718 (2004)
142. R. Pal, M. Higuchi, D. Kurth, Org. Lett. **11**, 3562 (2009)
143. E. Zangrando, M. Casanova, E. Alessio, Chem. Rev. **108**, 4979 (2008)
144. E.C. Constable, K. Harris, C.E. Housecroft, M. Neuburger, Dalton Trans. **40**, 1524 (2011)
145. P. Wang, C. Moorefield, G. Newkome, Angew. Chem. Int. Ed. **44**, 1679 (2005)
146. B. Zhao, H. Li, Q. Shen, Y. Zhang, Y. Yao, C. Lu, Organometallics **25**, 1824 (2006)
147. R.W. Troff, R. Hovorka, T. Weilandt, A. Lutzen, M. Cetina, M. Nieger, D. Lentz, K. Rissanen, C.A. Schalley, Dalton Trans. **41**, 8410 (2012)
148. P.R. Andres, U.S. Schubert, Synthesis 1229 (2004)
149. G. Seeber, B. Kariuki, L. Cronin, Chem. Commun. 2912 (2002)
150. Z. Ni, J. Tao, W. Wernsdorfer, A. Cui, H. Kou, Dalton Trans. 2788 (2009)
151. C. Smith, E. Constable, C. Housecroft, B. Kariuki, Chem. Commun. 2068 (2002)
152. R.M. Meudtner, S. Hecht, Macromol. Rapid Commun. **29**, 347 (2008)
153. R.M. Meudtner, M. Ostermeier, R. Goddard, C. Limberg, S. Hecht, Chem. Eur. J. **13**, 9834 (2007)
154. D. Astruc, E. Boisselier, C. Ornelas, Chem. Rev. **110**, 1857 (2010)
155. R. Hoogenboom, U.S. Schubert, Chem. Soc. Rev. **35**, 622 (2006)
156. S.J. Payne, G.L. Fiore, C.L. Fraser, J.N. Demas, Anal. Chem. **82**, 917 (2010)
157. F.S. Han, M. Higuchi, D.G. Kurth, J. Am. Chem. Soc. **130**, 2073 (2008)
158. R. Dobrawa, M. Lysetska, P. Ballester, M. Grüne, F. Würthner, Macromolecules **38**, 1315 (2005)
159. V. Marin, E. Holder, R. Hoogenboom, U.S. Schubert, Chem. Rev. Soc. **36**, 618 (2007)
160. F.S. Han, M. Higuchi, Y. Akasaka, Y. Otsuka, D.G. Kurth, Thin Solid Films **516**, 2469 (2008)
161. C.-F. Chow, S. Fujii, J.-M. Lehn, Angew. Chem. Int. Ed. **46**, 5007 (2007)
162. H.J. Yoon, J. Kuwabara, J.-H. Kim, C.A. Mirkin, Science **330**, 66 (2010)
163. N. Masciocchi, S. Galli, A. Sironi, E. Cariati, M.A. Galindo, E. Barea, M.A. Romero, J.M. Salas, J.A.R. Navarro, F. Santoyo-Gonzalez, Inorg. Chem. **45**, 7612 (2006)
164. L.N. Dawe, J. Miglioi, L. Turnbow, M.L. Taliaferro, W.W. Shum, J.D. Bagnato, L.N. Zakharov, A.L. Rheingold, A.M. Arif, M. Fourmigue, J.S. Miller, Inorg. Chem. **44**, 7530 (2005)

165. G.-W. Zhou, Y.-Z. Lan, F.K. Zheng, X. Zhang, M.-H. Lin, G.-C. Guo, J.-S. Huang, Chem. Phys. Lett. **426**, 341 (2006)
166. S. Bidault, L. Viau, O. Maury, S. Brasselet, J. Zyss, E. Ishow, K. Nakatani, H.L. Bozec, Adv. Funct. Mater. **16**, 2252 (2006)
167. N. Gunnlaugsson, J.P. Leonard, Chem. Commun. 3114 (2005)
168. H. Li, L. Wu, Soft Matter **10**, 9038 (2014)
169. H. Hofmeier, U.S. Schubert, Chem. Commun. 2423 (2005)
170. H. Hofmeier, R. Hoogenboom, M.E.L. Wouters, U.S. Schubert, J. Am. Chem. Soc. **127**, 2913 (2005)
171. L. Shi, X.W. Wang, C.A. Sandoval, M.X. Li, Q.Y. Qi, Z.T. Li, K.L. Ding, Angew. Chem. Int. Ed. **45**, 4108 (2006)
172. V. Marin, E. Holder, R. Hoogenboom, E. Tekin, U.S. Schubert, Dalton Trans. 1636 (2006)
173. J.-M. Lehn, Chem. Soc. Rev. **36**, 151 (2007)
174. J.-M. Lehn, Rep. Prog. Phys. **67**, 249 (2004)
175. G.R. Whittell, M.D. Hager, U.S. Schubert, I. Manners, Nat. Mater. **10**, 176 (2011)
176. J.-C. Eloi, L. Chabanne, G.R. Whittell, I. Manners, Mater. Today **11**, 28 (2008)
177. J.-M. Lehn, Constitutional dynamic chemistry: bridge from supramolecular chemistry to adaptive chemistry, in *Constitutional Dynamic Chemistry*, ed. by M. Barboiu (Springer, Heidelberg, Dordrecht, London, NY, 2012)
178. S. Schmatloch, A.M.J. van den Berg, M.W.M. Fijten, U.S. Schubert, PMSE Prepr. **90**, 645 (2004)
179. U.S. Schubert, A. Winter, G.R. Newkome, *Terpyridine-based Materials: For Catalytic, Opto-electronic and Life Science Applications* (Wiley-VCH, Weinheim, 2012)
180. S.V. Vinogradova, V.A. Vasnev, M.L. Keshtov, Polym. Sci. Ser. B **49**, 267 (2007)
181. S. Kelch, M. Rehahn, Macromolecules **32**, 5818 (1999)
182. C.D. Eisenbach, U.S. Schubert, Macromolecules **26**, 7372 (1993)
183. B. Lahn, M. Rehahn, Macromol. Symp. **163**, 157 (2001)
184. U. Velten, M. Rehahn, Macromol. Chem. Phys. **199**, 127 (1998)
185. U. Velten, M. Rehahn, M., Chem. Commun. 2639 (1996)
186. U. Velten, B. Lahn, M. Rehahn, Macromol. Chem. Phys. **198**, 2789 (1997)
187. M.D. Hossain, M. Higuchi, Synthesis **45**, 753 (2013)
188. D. Hossain, T. Sato, M. Higuchi, Chem. Asian J. **8**, 76 (2013)
189. R.K. Pandey, D. Hossain, S. Moriyama, M. Higuchi, J. Mater. Chem. A **1**, 9016 (2013)
190. M.H. Demirel, S. Köytepe, A. Gültek, T. Seçkin, J. Polym. Res. **21**, 345 (2014)
191. M. Demirel, S. Köytepe, A. Gültek, T. Seçkin, J. Polym. Res. **21**, 1 (2014)
192. H. Hofmeier, S. Schmatloch, D. Wouters, U.S. Schubert, Macromol. Chem. Phys. **204**, 2197 (2003)
193. S. Schmatloch, A.M.J. van den Berg, A.S. Alexeev, H. Hofmeier, U.S. Schubert, Macro-molecules **36**, 9943 (2003)
194. S. Schmatloch, U.S. Schubert, Macromol. Symp. **199**, 483 (2003)
195. S. Schmatloch, A.M.J. Van den Berg, H. Hofmeier, U.S. Schubert, Des. Monom. Polym. **7**, 191 (2004)
196. P.K. Iyer, J.B. Beck, C. Weder, S.J. Rowan, Chem. Commun. 319 (2005)
197. T. Vermonden, J. van der Gucht, P. de Waard, A.T.M. Marcelis, N.A.M. Besseling, E.J.R. Sudholter, G.J. Fleer, M.A. Cohen, Stuart. Macromolecules **36**, 7035 (2003)
198. A. Wild, A. Winter, M.D. Hager, H. Görls, U.S. Schubert, Macromol. Rapid Commun. **33**, 517 (2012)
199. H. Padhy, M. Ramesh, D. Patra, R. Satapathy, M.K. Pola, H.-C. Chu, C.-W. Chu, K.-H. Wei, H.-C. Lin, Macromol. Rapid Commun. **33**, 528 (2012)
200. T. Sato, R.K. Pandey, M. Higuchi, Dalton Trans. **42**, 16036 (2013)
201. R. Dobrawa, P. Ballester, F. Würthner, Thermodynamics of 2,2′:6′,2″-terpyridine-metal ion complexation, in *Metal-containing and Metallosupramolecular Polymers and Materials,* ed. by U.S. Schubert, G.R. Newkome, I. Manners, ACS Symposium Series, vol. 928 (Washington D.C., 2006)

202. F. Würthner, Chem. Commun. 1564 (2004)
203. S.C. Yu, C.C. Kwok, W.K. Chan, C.M. Che, Adv. Mater. **15**, 1643 (2003)
204. Y.-Y. Chen, Y.-T. Tao, H.C. Lin, Macromolecules **39**, 8559 (2006)
205. Y.-Y. Chen, H.-C. Lin, J. Polym. Sci. Part A Polym. Chem. **45**, 3243 (2007)
206. M. Chiper, M.A.R. Meier, J.M. Kranenburg, U.S. Schubert, Macromol. Chem. Phys. **208**, 679 (2007)
207. U. Mansfeld, A. Winter, M.D. Hager, R. Hoogenboom, W. Günther, U.S. Schubert, Polym. Chem. **4**, 113 (2013)
208. S. Schmatloch, A.M.J. van den Berg, M.W.M. Fijten, U.S. Schubert, Macromol. Rapid Commun. **25**, 321 (2004)
209. J.-H. Li, M. Higuchi, J. Inorg. Organomet. Polym. **20**, 10 (2010)
210. C. Friebe, A. Wild, J. Perelaer, U.S. Schubert, Macromol. Rapid Commun. **33**, 503 (2012)
211. H. Miyake, Symmetry **6**, 880 (2014)
212. S. Köytepe, M.H. Demirel, A. Gültek, T. Seçkin, Polym. Int. **63**, 778 (2014)
213. R. Siebert, A. Winter, M. Schmitt, J. Popp, U.S. Schubert, B. Dietzek, Macromol. Rapid Commun. **33**, 481 (2012)
214. H. Hofmeier, U.S. Schubert, Chem. Soc. Rev. **33**, 373 (2004)
215. V. Balzani, S. Campagna (eds.), *Photochemistry and Photophysics of Coordination Compounds* (Springer, Berlin, 2007)
216. V. Duprez, M. Biancardo, H. Spanggaard, F.C. Krebs, Macromolecules **38**, 10436 (2005)
217. P. Song, S.-G. Sun, P.-W. Zhou, J.-Y. Liu, Y.-Q. Xu, X.-J. Peng, China. J. Chem. Phys. **23**, 558 (2010)
218. C.-C. You, R. Dobrawa, C.R. Saha-Möller, F. Würthner, Metallosupramolecular dye assemblies, in *Supermolecular Dye Chemistry*, ed. by F. Würthner. Top. Curr. Chem. **258**, 39 (2005)
219. T. Suzuki, T. Sato, J. Zhang, M. Kanao, M. Higuchi, H. Maki, J. Mater. Chem. C **4**, 1594 (2016)
220. X. Chen, K. Guo, F. Li, L. Zhou, H. Qiao, RSC Adv. **4**, 58027 (2014)
221. L. He, J. Liang, Y. Cong, X. Chen, W. Bu, Chem. Commun. **50**, 10841 (2014)
222. J.R. Kumpfer, J. Jin, S.J. Rowan, J. Mater. Chem. **20**, 145 (2010)
223. D. Knapton, M. Burnworth, S.J. Rowan, C. Weder, Angew. Chem. Int. Ed. **45**, 5825 (2006)
224. B.M. Mckenzie, R.J. Wojtecki, K.A. Burke, C. Zhang, A. Jakli, P.T. Mather, S.J. Rowan, Chem. Mater. **23**, 3525 (2011)
225. A. Duerrbeck, S. Gorelik, J. Hobley, J. Wu, A. Hor, N. Long, Chem. Commun. **51**, 8656 (2015)
226. J.P. Byrne, J.A. Kitchen, T. Gunnlaugsson, Chem. Soc. Rev. **43**, 5302 (2014)
227. J.P. Byrne, M. Martínez-Calvo, R.D. Peacock, T. Gunnlaugsson, Chem. – Eur. J. **22**, 486 (2016)
228. B. Schulze, C. Friebe, S. Hoeppener, G.M. Pavlov, A. Winter, M.D. Hager, U.S. Schubert, Macromol. Rapid Commun. **33**, 597 (2012)
229. M. Burnworth, D. Knapton, S.J. Rowan, C. Weder, J. Inorg. Organomet. Polym. **17**, 91 (2007)
230. M. Burnworth, S.J. Rowan, C. Weder, Macromolecules **45**, 126 (2012)
231. C. Rajadurai, O. Fuhr, R. Kruk, M. Ghafari, H. Hahn, M. Ruben, Chem. Commun. 2636 (2007)
232. C.-F. Chow, S. Fujii, J.-M. Lehn, Chem. Asian J. **3**, 1324 (2008)
233. L.A. Paquette, J. Tae, J. Am. Chem. Soc. **123**, 4974 (2001)
234. Y.Y. Karabach, A.N. Kirillov, M.F.C. Guedes da Silva, M.N. Kopylovich, A.J.L. Pombeiro, Cryst. Growth Des. **6**, 2200 (2006)
235. Y.Y. Karabach, A.M. Kirillov, M. Haukka, M.N. Kopylovich, A.J.L. Pombeiro, J. Inorg. Biochem. **102**, 1190 (2008)
236. C.A. Fustin, P. Guillet, U.S. Schubert, J.-F. Gohy, Adv. Mater. **19**, 1665 (2007)
237. J.-F. Gohy, B.G.G. Lohmeijer, U.S. Schubert, Macromol. Rapid Commun. **23**, 555 (2002)
238. J.-F. Gohy, B.G.G. Lohmeijer, U.S. Schubert, Chem. Eur. J. **9**, 3472 (2003)

239. M. Chiper, A. Winter, R. Hoogenboom, D.A.M. Egbe, D. Wouters, S. Hoeppener, C.-A. Fustin, J.-F. Gohy, U.S. Schubert, Macromolecules **41**, 8823 (2008)
240. M. Chiper, M.A.R. Meier, D. Wouters, S. Hoeppener, C.-A. Fustin, J.-F. Gohy, U.S. Schubert, Macromolecules **41**, 2771 (2008)
241. J.-F. Gohy, B.G.L. Lohmeijer, S.K. Varshney, B. Decamps, E. Leroy, S. Boileau, U.S. Schubert, Macromolecules **35**, 9748 (2002)
242. R. Hoogenboom, D. Fournier, U.S. Schubert, Chem. Commun. 155 (2008)
243. B.G.G. Lohmeijer, U.S. Schubert, Angew. Chem. Int. Ed. **41**, 3825 (2002)
244. J.F. Gohy, B.G.G. Lohmeijer, S.K. Varshney, U.S. Schubert, Macromolecules **35**, 7427 (2002)
245. C. Ott, D. Wouters, H.M.L. Thijs, U.S. Schubert, J. Inorg. Organomet. Polym. **17**, 241 (2007)
246. J.F. Gohy, B.G.G. Lohmeijer, U.S. Schubert, Macromolecules **35**, 4560 (2002)
247. O. Regev, J.F. Gohy, B.G.G. Lohmeijer, S.K. Varshney, D.H.W. Hubert, P.M. Frederik, U.S. Schubert, Colloid Polym. Sci. **282**, 407 (2004)
248. G. Mayer, V. Vogel, B.G.G. Lohmeijer, J.F. Gohy, G.A. van den Broek, W. Haase, U.S. Schubert, D. Schubert, J. Polym. Sci. Part A Polym. Chem. **42**, 4458 (2004)
249. M. Al-Hussein, B.G.G. Lohmeijer, U.S. Schubert, W.H. De Jeu, Macromolecules **36**, 9281 (2003)
250. M. Al-Hussein, W.H. De Jeu, B.G.G. Lohmeijer, U.S. Schubert, Macromolecules **38**, 2832 (2005)
251. H. Goldansaz, Q. Voleppe, S. Piogé, C.A. Fustin, J.F. Gohy, J. Brassinne, D. Auhl, E. van Ruymbeke, Soft Matter **11**, 762 (2015)
252. B.G.G. Lohmeijer, D. Wouters, Z. Yin, U.S. Schubert, Chem. Commun. 2886 (2004)
253. P. Guillet, C.A. Fustin, B.G.G. Lohmeijer, U.S. Schubert, J.F. Gohy, Macromolecules **39**, 5484 (2006)
254. C.A. Fustin, B.G.G. Lohmeijer, A.S. Duwez, A.M. Jonas, U.S. Schubert, J.F. Gohy, Adv. Mater. **17**, 1162 (2005)
255. J.F. Gohy, B.G.G. Lohmeijer, A. Alexeev, X.S. Wang, I. Manners, M.A. Winnik, U.S. Schubert, Chem. Eur. J. **10**, 4315 (2004)
256. G. Zhou, I.I. Harruna, Macromolecules **38**, 4114 (2005)
257. C. Mugemana, P. Guillet, S. Hoeppener, U.S. Schubert, C.-A. Fustin, Chem. Commun. 1296 (2010)
258. M.A.R. Meier, D. Wouters, C. Ott, P. Guillet, C.-A. Fustin, J.-F. Gohy, U.S. Schubert, Macromolecules **39**, 1569 (2006)
259. H. Li, W. Wei, H. Xiong, Soft Matter **12**, 1411 (2016)
260. D. Pijper, B.L. Feringa, Soft Matter **4**, 1349 (2008)
261. T. Vermonden, W.M. de Vos, A.T.M. Marcelis, E.J.R. Sudholter, Eur. J. Inorg. Chem. **2004**, 2847 (2004)
262. T. Vermonden, M.J. van Steenbergen, N.A.M. Besseling, A.T.M. Marcelis, W.E. Hennink, E.J.R. Sudholter, M.A. Cohen, Stuart. J. Am. Chem. Soc. **126**, 15802 (2004)
263. A. Schultz, X. Li, B. Barkakaty, C.N. Moorefield, C. Wesdemiotis, G.R. Newkome, J. Am. Chem. Soc. **134**, 7672 (2012)
264. A. Fermi, G. Bergamini, M. Roy, M. Gingras, P. Ceroni, J. Am. Chem. Soc. **136**, 6395 (2014)
265. J.-F. Gohy, M. Chiper, P. Guillet, C.-A. Fustin, S. Hoeppener, A. Winter, R. Hoogenboom, U.S. Schubert, Soft Matter **5**, 2954 (2009)
266. J.E. McAlvin, C.L. Fraser, Macromolecules **32**, 1341 (1999)
267. C. Park, J.E. McAlvin, C.L. Fraser, E.L. Thomas, Chem. Mater. **14**, 1225 (2002)
268. R.M. Johnson, C.L. Fraser, Biomacromol **5**, 580 (2004)
269. U.S. Schubert, C. Eschbaumer, O. Nuyken, G. Hochwimmer, J. Inclusion Phenomena and Macrocyclic Chem. **35**, 23 (1999)
270. A.P. Smith, C.L. Fraser, Macromolecules **35**, 594 (2002)
271. C.L. Fraser, A.P. Smith, X. Wu, J. Am. Chem. Soc. **122**, 9026 (2000)

272. A.P. Smith, C.L. Fraser, Macromolecules **36**, 5520 (2003)
273. J.L. Bender, P.S. Corbin, C.L. Fraser, D.H. Metcalf, F.S. Richardson, E.L. Thomas, A.M. Urbas, J. Am. Chem. Soc. **124**, 8526 (2002)
274. R.K. Pandey, D. Hossain, T. Sato, U. Rana, S. Moriyama, M. Higuchi, RSC Adv. **5**, 49224 (2015)
275. D.M. Loveless, S.L. Jeon, S.L. Craig, Macromolecules **38**, 10171 (2005)
276. D.M. Loveless, S.L. Jeon, S.L. Craig, J. Mater. Chem. **17**, 56 (2007)
277. X. Chu, P. Xing, S. Li, M. Ma, J. Hao, A. Hao, RSC Adv. **5**, 1969 (2015)
278. A. Duerrbeck, S. Gorelik, J. Hobley, A.M. Yong, G.S. Subramanian, A. Hor, N. Long, J. Mater. Chem. C **3**, 8992 (2015)
279. C.-W. Hu, T. Sato, J. Zhang, S. Moriyama, M. Higuchi, A.C.S. Appl, Mater. Interfaces **6**, 9118 (2014)
280. I. Welterlich, B. Tieke, Macromolecules **44**, 4194 (2011)
281. J. Brassinne, E. Poggi, C.-A. Fustin, J.-F. Gohy, Macromol. Rapid Commun. **36**, 610 (2015)
282. P. Guillet, C.-A. Fustin, C. Mugemana, C. Ott, U.S. Schubert, J.-F. Gohy, Soft Matter **4**, 2278 (2008)
283. M. Chiper, S. Hoeppener, U. Schubert, C.-A. Fustin, J.-F. Gohy, Macromol. Chem. Phys. **211**, 2323 (2010)
284. S. Wang, C.-C. Chen, E.E. Dormidontova, Soft Matter **4**, 2039 (2008)
285. T. Sato, M. Higuchi, Chem. Commun. **49**, 5256 (2013)
286. L. Yu, Z. Wang, J. Wu, S. Tu, K. Ding, Angew. Chem. Int. Ed. **49**, 3627 (2010)
287. S. Gosh, L. Isaacs, Complex self-sorting systems, in *Dynamic Combinatorial Chemistry*, ed. by B.L. Miller (Wiley-VCH, Weinheim, 2010)
288. K. Osowska, O.Š. Miljanić, Synlett 1643 (2011)
289. M.M. Safont-Sempere, G. Fernández, F. Würthner, Chem. Rev. **111**, 5784 (2011)
290. M.L. Saha, M. Schmittel, Org. Biomol. Chem. **10**, 4651 (2012)
291. Z. He, W. Jiang, C.A. Schalley, Chem. Soc. Rev. **44**, 779 (2015)
292. I. Kocsis, D. Dumitrescu, Y.-M. Legrand, A. van der Lee, I. Grosu, M. Barboiu, Chem. Commun. **50**, 2621 (2014)
293. Y.-K. Tian, L. Chen, Y.-J. Tian, X.-Y. Wang, F. Wang, Polym. Chem. **4**, 453 (2013)
294. Y. Li, Z. Jiang, J. Yuan, D. Liu, T. Wu, C.N. Moorefield, G.R. Newkome, P. Wang, Chem. Commun. **51**, 5766 (2015)
295. M. Higuchi, Polym. J. **41**, 511 (2009)
296. S.M. Munzert, G. Schwarz, D.G. Kurth, RSC Adv. **6**, 15441 (2016)
297. G. Schwarz, T.K. Sievers, Y. Bodenthin, I. Hasslauer, T. Geue, J. Koetz, D.G. Kurth, J. Mater. Chem. **20**, 4142 (2010)
298. D.G. Kurth, M. Schütte, J. Wen, Colloids Surf.: A: Physicochem. Eng. Asp. **198–200**, 633 (2002)
299. M. Schütte, C. Stolle, D.G. Kurth, Supramol. Chem. **15**, 549 (2003)
300. Y. Bodenthin, G. Schwarz, Z. Tomkowicz, T. Geue, W. Haase, U. Pietsch, D.G. Kurth, J. Am. Chem. Soc. **131**, 2934 (2009)
301. C. Kaes, A. Katz, M.W. Hosseini, Chem. Rev. **100**, 3553 (2000)
302. R.J. Mortimer, Annu. Rev. Mater. Res. **41**, 241 (2011)
303. G. Schwarz, Y. Bodenthin, T. Geue, J. Koetz, D.G. Kurth, Macromolecules **43**, 494 (2010)
304. M.A.R. Meier, H. Hofmeier, C.H. Abeln, C. Tziatzios, M. Rasa, D. Schubert, U.S. Schubert, e-polymers **16**, 1 (2006)
305. M. Rasa, B.G.G. Lohmeijer, H. Hofmeier, H.M.L. Thijs, D. Schubert, U.S. Schubert, C. Tziatzios, Macromol. Chem. Phys. **207**, 2029 (2006)
306. W.-H. Chen, T.-H. Chang, C.-W. Hu, K.-M. Ting, Y.-C. Liao, K.-C. Ho, Solar energy mater. Solar Cells **126**, 219 (2014)
307. S. Bernhard, J.I. Goldsmith, K. Takada, H.D. Abruna, Inorg. Chem. **42**, 4389 (2003)
308. M. Schott, H. Lorrmann, M. Beck, D.G. Kurth, Solar energy mater. Solar Cells **126**, 68 (2014)

309. J. England, C.C. Scarborough, T. Weyhermüller, S. Sproules, K. Wieghardt, Eur. J. Inorg. Chem. **2012**, 4605 (2012)
310. P.M. Beaujuge, J.R. Reynolds, Chem. Rev. **110**, 268 (2010)
311. C.M. Amb, L.D. Aubrey, J.R. Reynolds, Chem. Mater. **23**, 397 (2011)
312. M. Higuchi, Y. Otsuka, R. Shomura, D.G. Kurth, Thin Solid Films **516**, 2416 (2008)
313. M. Higuchi, Y. Akasaka, T. Ikeda, A. Hayashi, D.G. Kurth, J. Inorg. Organomet. Polym. **19**, 74 (2009)
314. H. Krass, G. Papastavrou, D.G. Kurth, Chem. Mater. **15**, 196 (2002)
315. D.G. Kurth, J. Pitarch Lopez, W.-F. Dong, Chem. Commun. 2119 (2005)
316. W. Szczerba, M. Schott, H. Riesemeier, A.F. Thünemann, D.G. Kurth, Phys. Chem. Chem. Phys. **16**, 19694 (2014)
317. M. Higuchi, D.G. Kurth, Chem. Rec. **7**, 203 (2007)
318. D. Akcakayiran, D. Mauder, C. Hess, T.K. Sievers, D.G. Kurth, I. Shenderovich, H.-H. Limbach, G.H. Findenegg, J. Phys. Chem. B **112**, 14637 (2008)
319. D. Akcakayiran, D.G. Kurth, S. Rohrs, G. Rupprechter, G.H. Findenegg, Langmuir **21**, 7501 (2005)
320. G. Schwarz, S. Maisch, S. Ullrich, J. Wagenhöfer, D.G. Kurth, A.C.S. Appl, Mater. Interfaces **5**, 4031 (2013)
321. M.F. Geist, C.S. Peyratout, D.G. Kurth, ChemNanoMat **1**, 489 (2015)
322. U. Kolb, K. Büscher, C.A. Helm, A. Lindner, A.F. Thünemann, M. Menzel, M. Higuchi, D.G. Kurth, Proc. Natl. Acad. Sci. **103**, 10202 (2006)
323. A.V. Ambade, S.K. Yang, M. Weck, Angew. Chem. Int. Ed. **48**, 2894 (2009)
324. G. Gröger, W. Meyer-Zaika, C. Böttcher, F. Gröhn, C. Ruthard, C. Schmuck, J. Am. Chem. Soc. **133**, 8961 (2011)
325. L. Zhu, M. Lu, Q. Zhang, D. Qu, H. Tian, Macromolecules **44**, 4092 (2011)
326. S.K. Yang, A.V. Ambade, M. Weck, J. Am. Chem. Soc. **132**, 1637 (2010)
327. S.-L. Li, T. Xiao, Y. Wu, J. Jiang, L. Wang, Chem. Commun. **47**, 6903 (2011)
328. S.-L. Li, T. Xiao, B. Hu, Y. Zhang, F. Zhao, Y. Ji, Y. Yu, C. Lin, L. Wang, Chem. Commun. **47**, 10755 (2011)
329. S.-G. Chen, Y. Yu, X. Zhao, Y. Ma, X.-K. Jiang, Z.-T. Li, J. Am. Chem. Soc. **133**, 11124 (2011)
330. Z. Niu, F. Huang, H.W. Gibson, J. Am. Chem. Soc. **133**, 2836 (2011)
331. F. Wang, J. Zhang, X. Ding, S. Dong, M. Liu, B. Zheng, S. Li, L. Wu, Y. Yu, H.W. Gibson, F. Huang, Angew. Chem. Int. Ed. **49**, 1090 (2010)
332. E. Elacqua, D.S. Lye, M. Weck, Acc. Chem. Res. **47**, 2405 (2014)
333. J.M. Pollino, L.P. Stubbs, M. Weck, J. Am. Chem. Soc. **126**, 563 (2004)
334. M.L. Saha, S. De, S. Pramanik, M. Schmittel, Chem. Soc. Rev. **42**, 6860 (2013)
335. S.-L. Li, T. Xiao, C. Lin, L. Wang, Chem. Soc. Rev. **41**, 5950 (2012)
336. U. Mansfeld, M.D. Hager, R. Hoogenboom, C. Ott, A. Winter, U.S. Schubert, Chem. Commun. 3386 (2009)
337. G. Gröger, V. Stepanenko, F. Würthner, C. Schmuck, Chem. Commun. 698 (2009)
338. J.A.A.W. Elemans, A.E. Rowan, R.J.M. Nolte, J. Mater. Chem. **13**, 2661 (2003)
339. H. Hofmeier, A. El-ghayoury, A.P.H.J. Schenning, U.S. Schubert, Chem. Commun. 318 (2004)
340. S. Rieth, C. Baddeley, J.D. Badjić, Soft Matter **3**, 137 (2007)
341. W. Li, Y. Kim, J. Lia, M. Lee, Soft Matter **10**, 5231 (2014)
342. J.M. Pollino, K.P. Nair, L.P. Stubbs, J. Adams, M. Weck, Tetrahedron **60**, 7205 (2004)
343. P. Wei, X. Yan, F. Huang, Chem. Soc. Rev. **44**, 815 (2015)
344. Y. Liu, Y. Song, H. Wang, H.-Y. Zhang, X.-Q. Li, Macromolecules **37**, 6370 (2004)
345. Y. Liu, Z.-X. Yang, Y. Chen, Y. Song, N. Shao, ACS Nano **2**, 554 (2008)
346. H. Masai, J. Terao, S. Seki, S. Nakashima, M. Kiguchi, K. Okoshi, T. Fujihara, Y. Tsuji, J. Am. Chem. Soc. **136**, 1742 (2014)
347. E. Lee, J. Heo, K. Kim, Angew. Chem. Int. Ed. **39**, 2699 (2000)
348. K.-M. Park, E. Lee, S.-G. Roh, J. Kim, K. Kim, Bull. Korean Chem. Soc. **25**, 1711 (2004)

349. Y. Liu, Z. Huang, X. Tan, Z. Wang, X. Zhang, Chem. Commun. **49**, 5766 (2013)
350. J.-F. Xu, Y.-Z. Chen, L.-Z. Wu, C.-H. Tung, Q.-Z. Yang, Org. Lett. **15**, 6148 (2013)
351. H. Li, D.-X. Chen, Y.-L. Sun, Y.B. Zheng, L.-L. Tan, P.S. Weiss, Y.-W. Yang, J. Am. Chem. Soc. **135**, 1570 (2013)
352. X. Shu, S. Chen, J. Li, Z. Chen, L. Weng, X. Jia, C. Li, Chem. Commun. **48**, 2967 (2012)
353. M. Xue, Y. Yang, X. Chi, Z. Zhang, F. Huang, Acc. Chem. Res. **45**, 1294 (2012)
354. L. Gao, Z. Zhang, B. Zheng, F. Huang, Polym. Chem. **5**, 5734 (2014)
355. Z. Zhang, C. Han, G. Yu, F. Huang, Chem. Sci. **3**, 3026 (2012)
356. C.J. Bruns, J.F. Stoddart, Nat. Nanotechnol. **8**, 9 (2013)
357. C.J. Bruns, J.F. Stoddart, Acc. Chem. Res. **47**, 2186 (2014)
358. P. Wang, H. Xing, D. Xia, X. Ji, Chem. Commun. **51**, 17431 (2015)
359. B. Shi, K. Jie, Y. Zhou, D. Xia, Y. Yao, Chem. Commun. **51**, 4503 (2015)
360. L. Wu, C. Han, X. Wu, L. Wang, Y. Caochen, X. Jing, Dalton Trans. **44**, 20334 (2015)
361. C. Zhang, S. Li, J. Zhang, K. Zhu, N. Li, F. Huang, Org. Lett. **9**, 5553 (2007)
362. Y. Ding, P. Wang, Y.-K. Tian, Y.-J. Tian, F. Wang, Chem. Commun. **49**, 5951 (2013)
363. Y.-K. Tian, F. Wang, Macromol. Rapid Commun. **35**, 337 (2014)
364. S. Dong, Y. Luo, X. Yan, B. Zheng, X. Ding, Y. Yu, Z. Ma, Q. Zhao, F. Huang, Angew. Chem. Int. Ed. **50**, 1905 (2011)
365. J. Yuan, Q. Li, Q. Hu, Q. Wu, C. Li, H. Qiu, M. Zhang, S. Yin, Chem. Commun. **50**, 722 (2014)
366. J. Zhan, M. Zhang, M. Zhou, B. Liu, D. Chen, Y. Liu, Q. Chen, H. Qiu, S. Yin, Macromol. Rapid Commun. **35**, 1424 (2014)
367. G. Du, E. Moulin, N. Jouault, E. Buhler, N. Giuseppone, Angew. Chem. Int. Ed. **51**, 12504 (2012)
368. X. Yan, B. Zheng, F. Huang, Polym. Chem. **4**, 2395 (2013)
369. D. Chen, J. Zhan, M. Zhang, J. Zhang, J. Tao, D. Tang, A. Shen, H. Qiu, S. Yin, Polym. Chem. **6**, 25 (2015)
370. Y.-K. Tian, Y.-G. Shi, Z.-S. Yang, F. Wang, Angew. Chem. Int. Ed. **53**, 6090 (2014)
371. Y.-K. Tian, Z.-S. Yang, X.-Q. Lv, R.-S. Yao, F. Wang, Chem. Commun. **50**, 9477 (2014)
372. H. Hofmeier, J. Pahnke, C.H. Weidl, U.S. Schubert, Biomacromol **5**, 2055 (2004)
373. N. Haddour, C. Gondran, S. Cosnier, Chem. Commun. 324 (2004)
374. W. Wang, Y. Zhang, B. Sun, L.-J. Chen, X.-D. Xu, M. Wang, X. Li, Y. Yu, W. Jiang, H.-B. Yang, Chem. Sci. **5**, 4554 (2014)
375. A. Wang, J. Huang, Y. Yan, Soft Matter **10**, 3362 (2014)
376. Y. Yan, A. de Keizer, M.A.C. Stuart, N.A.M. Besseling, Adv. Polym. Sci. **242**, 91 (2010)
377. W.G. Weng, A.M. Jamieson, S.J. Rowan, Tetrahedron **63**, 7419 (2007)
378. W.G. Weng, Z. Li, A.M. Jamieson, S.J. Rowan, Macromolecules **42**, 236 (2009)
379. S. Landsmann, A. Winter, M. Chiper, C.-A. Fustin, S. Hoeppener, D. Wouters, J.-F. Gohy, U.S. Schubert, Macromol. Chem. Phys. **209**, 1666 (2008)
380. H. Krass, E.A. Plummer, J.M. Haider, P.R. Barker, N.W. Alcock, Z. Pikramenou, M. J. Hannon, D.G. Kurth, Angew. Chem. Int. Ed. **40**, 3862 (2001)
381. P. Lehmann, C. Symietz, G. Brezesinski, H. Krass, D.G. Kurth, Langmuir **21**, 5901 (2005)
382. Y. Bodenthin, U. Pietsch, J. Grenzer, T. Geue, H. Möhwald, D.G. Kurth, J. Phys. Chem. B **109**, 12795 (2005)
383. B. Arezki, G. Schwarz, Y. Bodenthin, D. Lutzenkirchen-Hecht, C. Markert, R. Wagner, R. Frahm, D.G. Kurth, U. Pietsch, ChemPhysChem **12**, 405 (2011)
384. Y. Bodenthin, U. Pietsch, H. Möhwald, D.G. Kurth, J. Am. Chem. Soc. **127**, 3110 (2005)
385. Y. Bodenthin, G. Schwarz, Z. Tomkowicz, M. Lommel, T. Geue, W. Haase, H. Moehwald, U. Pietsch, D.G. Kurth, Coord. Chem. Rev. **253**, 2414 (2009)
386. Y. Bodenthin, D.G. Kurth, G. Schwarz, Chem. Unserer. Zeeit. **42**, 256 (2008)
387. A.B. Gaspar, M. Seredyuk, Coord. Chem. Rev. **268**, 41 (2014)
388. S. Valkama, O. Lehtonen, K. Lappalainen, H. Kosonen, P. Castro, T. Repo, M. Torkkeli, R. Serimaa, G. ten Brinke, M. Leskelä, O. Ikkala, Macromol. Rapid Commun. **24**, 556 (2003)

389. Y. Yan, N.A.M. Besseling, A. de Keizer, A.T.M. Marcelis, M. Drechsler, M.A. Cohen, Stuart. Angew. Chem. Int. Ed. **46**, 1807 (2007)
390. S. Van der Burgh, A. de Keizer, M.A. Cohen, Stuart. Langmuir **20**, 1073 (2004)
391. A. Harada, K. Kataoka, Macromolecules **31**, 288 (1998)
392. Y. Yan, A. de Keizer, M.A. Cohen Stuart, N.A.M. Besseling, Soft Matter **5**, 790 (2009)
393. Y. Yan, A. de Keizer, M.A. Cohen Stuart, M. Drechsler, N.A.M. Besseling, J. Phys. Chem. B **112**, 10908 (2008)
394. Y. Yan, N.A.M. Besseling, A. de Keizer, M.A. Cohen, Stuart. J. Phys. Chem. B **111**, 5811 (2007)
395. Y. Yan, N.A.M. Besseling, A. de Keizer, M.A. Cohen Stuart, M. Drechsler, J. Phys. Chem. B **111**, 11662 (2007)
396. Y. Yan, L. Harnau, N.A.M. Besseling, A. de Keizer, M. Ballauff, S. Rosenfeldt, M.A. Cohen, Stuart. Soft Matter **4**, 2207 (2008)
397. H.T. Baytekin, B. Baytekin, A. Schulz, C.A. Schalley, Small **5**, 194 (2009)
398. W.A. Lopes, H.M. Jaeger, Nature **414**, 735 (2001)
399. A.O. Moughton, R.K. O'Reilly, J. Am. Chem. Soc. **130**, 8714 (2008)
400. D. Li, J. Zhang, K. Landskron, T. Liu, J. Am. Chem. Soc. **130**, 4226 (2008)
401. R. Dobrawa, F. Wurthner, Chem. Commun. 1878 (2002)
402. P. Guillet, C. Mugemana, F.J. Stadler, U.S. Schubert, C.-A. Fustin, C. Bailly, J.-F. Gohy, Soft Matter **5**, 3409 (2009)
403. S.C. Grindy, R. Learsch, D. Mozhdehi, J. Cheng, D.G. Barrett, Z. Guan, P.B. Messersmith, N. Holten-Andersen, Nat. Mater. **14**, 1210 (2015)
404. N. Xu, J. Han, Z. Zhu, B. Song, X. Lu, Y. Cai, Soft Matter **11**, 5546 (2015)
405. Y. Liu, X. Wang, Polym. Chem. **2**, 2741 (2011)
406. J.W. Steed, Chem. Commun. **47**, 1379 (2011)
407. J.H. Jung, J.H. Lee, J.R. Silverman, G. John, Chem. Soc. Rev. **42**, 924 (2013)
408. J. Zhang, C.-Y. Su, Coord. Chem. Rev. **257**, 1373 (2013)
409. N.M. Sangeetha, U. Maitra, Chem. Soc. Rev. **34**, 821 (2005)
410. R.G. Weiss, P. Terech (eds.), *Molecular Gels. Materials with Self-Assembled Fibrillar Networks* (Springer, Dordrecht, 2006)
411. B. Escuder, J.F. Miravet (eds.), *Functional Molecular Gels* (RSC, Cambridge, 2014)
412. F. Fages (ed.), *Low Molecular Weight Gelators* (Springer, Berlin-Heidelberg, 2005)
413. S. Seiffert (ed.), *Supramolecular Polymer Networks and Gels* (Springer, Heidelberg, NY, Dordrecht, London, 2015)
414. M.J. Mayoral, G. Fernández, Chem. Sci. **3**, 1395 (2012)
415. C. Rest, M.J. Mayoral, K. Fucke, J. Schellheimer, V. Stepanenko, G. Fernández, Angew. Chem. Int. Ed. **53**, 700 (2014)
416. N. Lanigan, X. Wang, Chem. Commun. **49**, 8133 (2013)
417. C.A. Strassert, C.-H. Chien, M.D. Galvez Lopez, D. Kourkoulos, D. Hertel, K. Meerholz, L. de Cola, Angew. Chem. Int. Ed. **50**, 946 (2011)
418. A. Kishimura, T. Yamashita, T. Aida, J. Am. Chem. Soc. **127**, 179 (2005)
419. R. Gavara, J. Llorca, J.C. Lima, L. Rodríguez, Chem. Comm. **49**, 72 (2013)
420. E. Aguiló, R. Gavara, J.C. Lima, J. Llorca, L. Rodríguez, J. Mat. Chem. C **1**, 5538 (2013)
421. A.J. Moro, B. Rome, E. Aguiló, J. Arcau, R. Puttreddy, K. Rissanen, J.C. Lima, L. Rodríguez, Org. Biomol. Chem. **13**, 2026 (2015)
422. J.C. Lima, L. Rodríguez, Chem. Soc. Rev. **40**, 5442 (2011)
423. G. Buhler, M.C. Feiters, R.J.M. Nolte, K.H. Dotz, Angew. Chem. Int. Ed. **42**, 2494 (2003)
424. D.D. Díaz, D. Kühbeck, R.J. Koopmans, Chem. Soc. Rev. **40**, 427 (2011)
425. S.R. Bull, M.O. Guler, R.E. Bras, T.J. Meade, S.I. Stupp, Nano Lett. **5**, 1 (2005)
426. M. Mauro, A. Aliprandi, D. Septiadi, N.S. Kehra, L. de Cola, Chem. Soc. Rev. **43**, 4144 (2014)
427. S. Saha, J. Bachl, T. Kundu, D. Díaz, Chem. Commun. **50**, 7032 (2014)
428. S. Kawano, N. Fujita, S. Shinkai, J. Am. Chem. Soc. **126**, 8592 (2004)
429. T. Vermonden, R. Censi, W.E. Hennink, Chem. Rev. **112**, 2853 (2012)

430. J.C. Lima, L. Rodríguez, Inorganics **3**, 1 (2015)
431. V.K.-M. Au, N. Zhu, V.W.-W. Yam, Inorg. Chem. **52**, 558 (2013)
432. M.-O.M. Piepenbrock, G.O. Lloyd, N. Clarke, J.W. Steed, Chem. Rev. **110**, 1960 (2010)
433. P. Dastidar, Chem. Soc. Rev. **37**, 2699 (2008)
434. M. George, R.G. Weiss, Acc. Chem. Res. **39**, 489 (2006)
435. B.G. Bag, G.C. Maity, S.K. Dinda, Org. Lett. **8**, 5457 (2006)
436. A. Pal, B.S. Chhikara, A. Govindaraj, S. Bhattacharya, C.N.R. Rao, J. Mater. Chem. **18**, 2593 (2008)
437. A. Pal, B. Hajra, S. Sen, V.K. Aswal, S. Bhattacharya, J. Mater. Chem. **19**, 4325 (2009)
438. P. Terech, S. Dourdain, U. Maitra, S. Bhat, J. Phys. Chem. B **113**, 4619 (2009)
439. G. Palui, A. Banerjee, J. Phys. Chem. B **112**, 10107 (2008)
440. C. Vijayakumar, V.K. Praveen, A. Ajayaghosh, Adv. Mater. **21**, 2059 (2009)
441. S. Dutta, A. Shome, S. Debnath, P.K. Das, Soft Matter **5**, 1607 (2009)
442. R. Ghosh, A. Chakraborty, D.K. Maiti, V.G. Puranik, Org. Lett. **8**, 1061 (2006)
443. D.D. Daz, J.J. Cid, P. Vzquez, T. Torres, Chem. Eur. J. **14**, 9261 (2008)
444. A. Dawn, N. Fujita, S. Haraguchi, K. Sada, S. Shinkai, Chem. Commun. 2100 (2009)
445. M. Suzuki, K. Hanabusa, Chem. Soc. Rev. **38**, 967 (2009)
446. M.-O.M. Piepenbrock, G.O. Lloyd, N. Clarke, J.W. Steed, Chem. Commun. 2644 (2008)
447. A.R. Hirst, J.E. Miravet, B. Escuder, L. Noirez, V. Castelletto, I.W. Hamley, D.K. Smith, Chem. Eur. J. **15**, 372 (2009)
448. H. Hopf, H. Greiving, H. Bouas-Laurent, J.P. Desvergne, Eur. J. Org. Chem. 1868 (2009)
449. W. Deng, H. Yamaguchi, Y. Takashima, A. Harada, Chem. Asian J. **3**, 687 (2008)
450. N. Sreenivasachary, J.-M. Lehn, Chem. Asian J. **3**, 134 (2008)
451. A. Ajayaghosh, V.K. Praveen, Acc. Chem. Res. **40**, 644 (2007)
452. A. Ajayaghosh, V.K. Praveen, C. Vijayakumar, Chem. Soc. Rev. **37**, 109 (2008)
453. R. Luboradzki, O. Gronwald, M. Ikeda, S. Shinkai, D.N. Reinhoudt, Tetrahedron **56**, 9595 (2000)
454. A. Ballabh, D.R. Trivedi, P. Dastidar, Chem. Mater. **15**, 2136 (2003)
455. D.R. Trivedi, A. Ballabh, P. Dastidar, Chem. Mater. **15**, 3971 (2003)
456. D.R. Trivedi, A. Ballabh, P. Dastidar, B. Ganguly, Chem. Eur. J. **10**, 5311 (2004)
457. A.R. Hirst, B. Escuder, J.F. Miravet, D.K. Smith, Angew. Chem. Int. Ed. **47**, 8002 (2008)
458. T. Nakanishi, *Supramolecular Soft Matter: Applications in Materials and Organic Electronics* (Wiley, Chichester, 2011)
459. J.-J. Zhang, W. Lu, R.W.-Y. Sun, C.-M. Che, Angew. Chem. Int. Ed. **51**, 4882 (2012)
460. S.A. Joshi, N.D. Kulkarni, Chem. Commun. 2341 (2009)
461. M. Dukh, D. Saman, J. Kroulik, I. Cerny, V. Pouzar, V. Kral, P. Drasar, Tetrahedron **59**, 4069 (2003)
462. K. Hanabusa, T. Hirata, D. Inoue, M. Kimura, H. Shirai, Colloid. Surf. A **169**, 307 (2000)
463. L. Sambri, F. Cucinotta, G. De Paoli, S. Stagnic, L. De Cola, New J. Chem. **34**, 2093 (2010)
464. X. Chen, Z. Huang, S.-Y. Chen, K. Li, X.-Q. Yu, L. Pu, J. Am. Chem. Soc. **132**, 7297 (2010)
465. F. Camerel, R. Ziessel, B. Donnio, D. Guillon, New J. Chem. **30**, 135 (2006)
466. A.Y.-Y. Tam, K.M.-C. Wong, G. Wang, V.W.-W. Yam, Chem. Commun. 2028 (2007)
467. A.Y.-Y. Tam, K.M.-C. Wong, V.W.-W. Yam, Chem. Eur. J. **15**, 4775 (2009)
468. A.Y.-Y. Tam, K.M.-C. Wong, V.W.-W. Yam, J. Am. Chem. Soc. **131**, 6253 (2009)
469. W. Lu, Y.-C. Law, J. Han, S.S.-Y. Chui, D.-L. Ma, N. Zhu, C.-M. Che, Chem. Asian J. **3**, 59 (2008)
470. F. Camerel, R. Ziessel, B. Donnio, C. Bourgogne, D. Guillon, M. Schmutz, C. Iacovita, J.-P. Bucher, Angew. Chem. Int. Ed. **46**, 2659 (2007)
471. A.Y.-Y. Tam, K.M.-C. Wong, N. Zhu, G. Wang, V.W.-W. Yam, Langmuir **25**, 8695 (2009)
472. T. Tu, W. Assenmacher, H. Peterlik, R. Weisbarth, M. Nieger, K.H. Dotz, Angew. Chem. Int. Ed. **46**, 6368 (2007)
473. T. Tu, W. Fang, X. Bao, X. Li, K.H. Dotz, Angew. Chem. Int. Ed. **50**, 6601 (2011)

474. T. Tu, X. Bao, W. Assenmacher, H. Peterlik, J. Daniels, K.H. Dotz, Chem. Eur. J. **15**, 1853 (2009)
475. T. Cardolaccia, Y. Li, K.S. Schanze, J. Am. Chem. Soc. **130**, 2535 (2008)
476. T. Naota, H. Koori, J. Am. Chem. Soc. **127**, 9324 (2005)
477. K. Isozaki, H. Takaya, T. Naota, Angew. Chem. Int. Ed. **46**, 2855 (2007)
478. N. Komiya, T. Muraoka, M. Iida, M. Miyanaga, K. Takahashi, T. Naota, J. Am. Chem. Soc. **133**, 16054 (2011)
479. M. Shirakawa, N. Fujita, T. Tani, K. Kaneko, S. Shinkai, Chem. Commun. 4149 (2005)
480. P. Kadjane, M. Starck, F. Camerel, D. Hill, N. Hildebrandt, R. Ziessel, L.J. Charbonniere, Inorg. Chem. **48**, 4601 (2009)
481. W. Miao, L. Zhang, X. Wang, H. Cao, Q. Jin, M. Liu, Chem. Eur. J. 19, 3029 (2013)
482. A. Kishimura, T. Yamashita, K. Yamaguchi, T. Aida, Nat. Mater. **4**, 546 (2005)
483. T. Kishida, N. Fujita, O. Hirata, S. Shinkai, Org. Biomol. Chem. **4**, 1902 (2006)
484. T. Kishida, N. Fujita, K. Sada, S. Shinkai, Langmuir **21**, 9432 (2005)
485. T. Kishida, N. Fujita, K. Sada, S. Shinkai, J. Am. Chem. Soc. **127**, 7298 (2005)
486. M. Takeuchi, S. Tanaka, S. Shinkai, Chem. Commun. 5539 (2005)
487. T. Zhang, Z. Wen, Y. Hui, M. Yang, K. Yang, Q. Zhou, Y. Wang, Polym. Chem. **6**, 4177 (2015)
488. P. Terech, C. Scherer, P. Lindner, R. Ramasseul, Langmuir **19**, 10648 (2003)
489. P. Terech, C. Scherer, B. Deme, R. Ramasseul, Langmuir **19**, 10641 (2003)
490. M. Schappacher, A. Deffieux, J.-F. Le Meins, Polym. Chem. **4**, 458 (2013)
491. T. Ishi-I, R. Iguchi, E. Snip, M. Ikeda, S. Shinkai, Langmuir **17**, 5825 (2001)
492. H. Danjo, K. Hirata, S. Yoshigai, I. Azumaya, K. Yamaguchi, J. Am. Chem. Soc. **131**, 1638 (2009)
493. J.M.J. Paulusse, D.J.M. van Beek, R.P. Sijbesma, J. Am. Chem. Soc. **129**, 2392 (2007)
494. J. Paulusse, J. Huijbers, R. Sijbesma, Chem. Eur. J. **12**, 4928 (2006)
495. J. Paulusse, R. Sijbesma, Angew. Chem. Int. Ed. **43**, 4460 (2004)
496. T. Zhang, Z. Wen, Y. Hui, M. Yang, K. Yang, Q. Zhou, Y. Wang, Polym. Chem. **6**, 4177 (2015)
497. A. Kokil, I. Shiyanovskaya, K. Singer, C. Weder, J. Am. Chem. Soc. **124**, 9978 (2002)
498. H.J. Kim, J.H. Lee, M. Lee, Angew. Chem. Int. Ed. **44**, 5810 (2005)
499. H.J. Kim, W.C. Zin, M. Lee, J. Am. Chem. Soc. **126**, 7009 (2004)
500. J. Brassinne, F.D. Jochum, C.-A. Fustin, J.-F. Gohy, Int. J. Mol. Sci. **16**, 990 (2015)
501. C. Ott, C. Ulbricht, R. Hoogenboom, U.S. Schubert, Macromol. Rapid Commun. **33**, 556 (2012)
502. M. Kimura, Y. Nakagawa, N. Adachi, Y. Tatewaki, T. Fukawa, H. Shirai, Chem. Lett. **38**, 382 (2009)
503. R. Wang, M. Geven, P.J. Dijkstra, P. Martens, M. Karperien, Soft Matter **10**, 7328 (2014)
504. H. Hofmeier, U.S. Schubert, Macromol. Chem. Phys. **204**, 1391 (2003)
505. C. Mugemana, A. Joset, P. Guillet, M.-S. Appavou, N. De Souza, C.-A. Fustin, B. Leyh, J.-F. Gohy, Macromol. Chem. Phys. **214**, 1699 (2013)
506. J. Brassinne, C. Mugemana, P. Guillet, O. Bertrand, D. Auhl, C. Bailly, C.A. Fustin, J.F. Gohy, Soft Matter **8**, 4599 (2012)
507. F.D. Jochum, J. Brassinne, C.-A. Fustin, J.-F. Gohy, Soft Matter **9**, 2314 (2013)
508. O. Kotova, R. Daly, C.M.G. dos Santos, P.E. Kruger, J.J. Boland, T. Gunnlaugsson, Inorg. Chem. **54**, 7735 (2015)
509. J. Yuan, X. Fang, L. Zhang, G. Hong, Y. Lin, Q. Zheng, Y. Xu, Y. Ruan, W. Weng, H. Xia, G. Chen, J. Mater. Chem. **22**, 11515 (2012)
510. E.P. McCarney, J.P. Byrne, B. Twamley, M. Martínez-Calvo, G. Ryan, M.E. Möbius, T. Gunnlaugsson, Chem. Commun. **51**, 14123 (2015)
511. Z. Wang, W. Fan, R. Tong, X. Lu, H. Xia, RSC Adv. **4**, 25486 (2014)
512. Q. Lin, T.-T. Lu, X. Zhu, B. Sun, Q.-P. Yang, T.-B. Wei, Y.-M. Zhang, Chem. Commun. **51**, 1635 (2015)

513. Q. Lin, B. Sun, Q.-P. Yang, Y.-P. Fu, X. Zhu, Y.-M. Zhang, T.-B. Wei, Chem. Commun. **50**, 10669 (2014)
514. W.C. Yount, D.M. Loveless, S.L. Craig, Angew. Chem. Int. Ed. **44**, 2746 (2005)
515. D. Knapton, P.K. Iyer, S.J. Rowan, C. Weder, Macromolecules **39**, 4069 (2006)
516. D. Knapton, S.J. Rowan, C. Weder, Macromolecules **39**, 651 (2006)
517. M. Burnworth, J.D. Mendez, M. Schroeter, S.J. Rowan, C. Weder, Macromolecules **41**, 2157 (2008)
518. X. de Hatten, N. Bell, N. Yufa, G. Christmann, J.R. Nitschke, J. Am. Chem. Soc. **133**, 3158 (2011)
519. N. Holten-Andersen, M. Harrington, H. Birkedal, B. Lee, P. Messersmith, K. Lee, J. Waite, Proc. Natl. Acad. Sci. U.S.A. **108**, 2651 (2011)
520. L. Qu, J. Fan, Y. Ren, K. Xiong, M. Yan, X. Tuo, P. Terech, G. Royal, Mater. Chem. Phys. **153**, 54 (2015)
521. A. Gasnier, G. Royal, P. Terech, Langmuir **25**, 8751 (2009)
522. A. Gasnier, C. Bucher, J.-C. Moutet, G. Royal, E. Saint-Aman, P. Terech, Macromol. Symp. **304**, 87 (2011)
523. Z. Qi, P. Malo de Molina, W. Jiang, Q. Wang, K. Nowosinski, A. Schulz, M. Gradzielski, C.A. Schalley, Chem. Sci. **3**, 2073 (2012)
524. J. Zhang, J. Yan, P. Pageni, Y. Yan, A. Wirth, Y.P. Chen, Y. Qiao, Q. Wang, A.W. Decho, C. Tang, Sci. Rep. **5**, 11914 (2015)
525. J.G. Vos, R.J. Forster, T.E. Keyes, *Interfacial Supramolecular Assemblies* (Wiley, Chichester, 2003)
526. J.A.A.W. Elemans, S. Lei, S. De Feyter, Angew. Chem. Int. Ed. **48**, 7298 (2009)
527. S. Yu. Zaitsev, *Supramolecular Nano-sized Systems at the Interface. Concepts and Perspectives for Bionanotechnologies* (Lenand, Moscow, 2010) (in Russian)
528. N. Miyashita, D.G. Kurth, J. Mater. Chem. **18**, 2636 (2008)
529. M. Deniz Yilmaz, J. Huskens, Soft Matter **8**, 11768 (2012)
530. W. Tong, X. Song, C. Gao, Chem. Soc. Rev. **41**, 6103 (2012)
531. J. Borges, J.F. Mano, Chem. Rev. **114**, 8883 (2014)
532. Y. Li, X. Wang, J. Sun, Chem. Soc. Rev. **41**, 5998 (2012)
533. Y. Xiang, S. Lua, S.P. Jiang, Chem. Soc. Rev. **41**, 7291 (2012)
534. R. Sakamoto, K.-H. Wu, R. Matsuoka, H. Maeda, H. Nishihara, Chem. Soc. Rev. **44**, 7698 (2015)
535. I. Doron-Mor, H. Cohen, S.R. Cohen, R. Popovitz-Biro, A. Shanzer, A. Vaskevich, I. Rubinstein, Langmuir **20**, 10727 (2004)
536. M. Wanunu, A. Vaskevich, S.R. Cohen, H. Cohen, R. AradYellin, A. Shanzer, I. Rubinstein, J. Am. Chem. Soc. **127**, 17877 (2005)
537. M. Wanunu, A. Vaskevich, A. Shanzer, I. Rubinstein, J. Am. Chem. Soc. **128**, 8341 (2006)
538. M. Greenstein, R.B. Ishay, B.M. Maoz, H. Leader, A. Vaskevich, I. Rubinstein, Langmuir **26**, 7277 (2010)
539. E. Soto, J.C. MacDonald, C.G.F. Cooper, W.G. McGimpsey, J. Am. Chem. Soc. **125**, 2838 (2003)
540. G. de Ruiter, M. Lahav, H. Keisar, M.E. van der Boom, Angew. Chem. Int. Ed. **52**, 704 (2013)
541. S. Shankar, M. Lahav, M.E. van der Boom, J. Am. Chem. Soc. **137**, 4050 (2015)
542. M. Maskus, H.D. Abruna, Langmuir **12**, 4455 (1996)
543. K. Kanaizuka, M. Murata, Y. Nishimori, I. Mori, K. Nishio, H. Masuda, H. Nishihara, Chem. Lett. **34**, 534 (2005)
544. C. Haensch, M. Chiper, C. Ulbricht, A. Winter, S. Hoeppener, U.S. Schubert, Langmuir **24**, 12981 (2008)
545. C. Chakraborty, R.K. Pandey, Md Delwar Hossain, Z. Futera, S. Moriyama, M. Higuchi, ACS Appl. Mater. Interfaces. **7**, 19034 (2015)
546. L.-Y. Zhang, H.-X. Zhang, S. Ye, H.-M. Wen, Z.-N. Chen, M. Osawa, K. Uosaki, Y. Sasaki, Chem. Commun. **47**, 923 (2011)

547. L.D.A. Siebbeles, F.C. Grozema (eds.), *Charge and Exciton Transport through Molecular Wires* (Wiley, Chichester, 2011)
548. L. de Cola (ed.), *Molecular Wires: From Design to Properties*, vol. 257 (Springer-Verlag, Berlin, Heldelberg, 2005) (Topp. Curr. Chem.)
549. H. Maeda, R. Sakamoto, H. Nishihara, Polymer **54**, 4383 (2013)
550. H. Maeda, R. Sakamoto, H. Nishihara, J. Phys. Chem. Lett. **6**, 3821 (2015)
551. A. Bajpayee, H. Maeda, S. Katagiri, R. Sakamoto, H. Nishihara, Chem. Lett. **44**, 1211 (2015)
552. Y. Yamanoi, J. Sendo, T. Kobayashi, H. Maeda, Y. Yabusaki, M. Miyachi, R. Sakamoto, H. Nishihara, J. Am. Chem. Soc. **134**, 20433 (2012)
553. S. Katagiri, R. Sakamoto, H. Maeda, Y. Nishimori, T. Kurita, H. Nishihara, Chem. Eur. J. **19**, 5088 (2013)
554. L. Pukenas, F. Benn, E. Lovell, A. Santoro, L.J. Kershaw Cook, M.A. Halcrow, S.D. Evans, J. Mater. Chem. C **3**, 7890 (2015)
555. A. Grohmann, M. Haryono, K. Student, P. Müller, M. Stocker, Eur. J. Inorg. Chem. 662 (2013)
556. P. Gütlich, H.A. Goodwin (eds.), *Spin Crossover in Transition Metal Compounds I–III*, vol. 234 (Springer, Berlin, Heidelberg, NY, 2004) (Top. Curr. Chem.)
557. M.A. Halcrow (ed.), *Spin-Crossover Materials—Properties and Applications* (Wiley, Chichester, 2013)
558. Y. Tang, M. Chen, D.-J. Qian, L. Zhang, M. Liu, Colloids and Surfaces A: Physicochem. Eng. Asp. **457**, 41 (2014)
559. C.A. da Silva, M. Vidotti, P.A. Fiorito, S.I. Córdoba de Torresi, R.M. Torresi, W.A. Alves, Langmuir **28**, 3332 (2012)
560. S.A. Levi, P. Guatteri, F.C.J.M. van Veggel, G.J. Vancso, E. Dalcanale, D.N. Reinhoudt, Angew. Chem. Int. Ed. **40**, 1892 (2001)
561. E. Menozzi, R. Pinalli, E.A. Speets, B.J. Ravoo, E. Dalcanale, D.N. Reinhoudt, Chem. Eur. J. **10**, 2199 (2004)
562. J. Puigmartı-Luis, W.J. Saletra, A. Gonzalez, D.B. Amabilino, L. Perez-Garcıa, Chem. Commun. **50**, 82 (2014)
563. W. Zhao, B. Tong, Y. Pan, J. Shen, J. Zhi, J. Shi, Y. Dong, Langmuir **25**, 11796 (2009)
564. W. Zhao, B. Tong, J. Shi, Y. Pan, J. Shen, J. Zhi, W.K. Chan, Y. Dong, Langmuir **26**, 16084 (2010)
565. Y. Tong, B. Pan, J. Shi, W. Zhao, J. Shen, J. Zhi, Y. Dong, J. Phys. Chem. C **114**, 8040 (2010)
566. B. Tong, H. Yang, W. Xiong, F. Xie, J. Shi, J. Zhi, W.K. Chan, Y. Dong, J. Phys. Chem. B **117**, 5338 (2013)
567. O. Crespo-Biel, C.W. Lim, B.J. Ravoo, D.N. Reinhoudt, J. Huskens, J. Am. Chem. Soc. **128**, 17024 (2006)
568. C.W. Lim, O. Crespo-Biel, M.C.A. Stuart, D.N. Reinhoudt, J. Huskens, B.J. Ravoo, Proc. Natl. Acad. Sci. U.S.A. **104**, 6986 (2007)
569. C.N. Moorefield, S. Perera, G.R. Newkome, Dendrimer chemistry: supramolecular perspectives and applications, in *Dendrimer-Based Drug Delivery Systems: From Theory to Practice*, ed. by Y. Cheng (Wiley, Chichester, 2012)
570. D.K. Smith, F. Diederich, Supramolecular dendrimer chemistry: a journey through the branched architecture, in *Dendrimers II*, *Architecture, Nanostructure and Supramolecular Chemistry*, vol. 210 (Springer, Berlin, Heidelberg, NY, 2000) (Top. Curr. Chem.)
571. D.K. Smith, A.R. Hirst, C.S. Love, J.G. Hardy, S.V. Brignell, B. Huang, Prog. Polym. Sci. **30**, 220 (2005)
572. D.K. Smith, Chem. Commun. 34 (2006)
573. M. Selin, L. Peltonen, J. Hirvonen, L.M. Bimbo, J. Drug Deliv. Sci. Technol. **34**, 10 (2016)
574. B.N.S. Thota, L.H. Urner, R. Haag, Chem. Rev. **116**, 2079 (2016)
575. H.-J. Sun, S. Zhang, V. Percec, Chem. Soc. Rev. **44**, 3900 (2015)
576. U. Hahn, F. Cardinali, J.-F. Nierengarten, New J. Chem. **31**, 1128 (2007)

577. K.C.-F. Leung, K.-N. Lau, Polym. Chem. **1**, 988 (2010)
578. W. Wang, A.E. Kaifer, Adv. Polym. Sci. **222**, 1 (2009)
579. A.-M. Caminade, R. Laurent, A. Ouali, J.-P. Majoral, Inorg. Chim. Acta **409**, 68 (2014)
580. A.-M. Caminade, A. Ouali, R. Laurent, C.-O. Turrin, J.-P. Majoral, Chem. Soc. Rev. **44**, 3890 (2015)
581. A.-M. Caminade, J.-P. Majoral, Chem. Soc. Rev. **39**, 2034 (2010)
582. K. Ladomenou, V. Nikolaou, G. Charalambidis, A.G. Coutsolelos, Coord. Chem. Rev. **306**, 1 (2016)
583. R. Dong, Y. Zhou, X. Zhu, Acc. Chem. Res. **47**, 2006 (2014)
584. B.M. Rosen, C.J. Wilson, D.A. Wilson, M. Peterca, M.R. Imam, V. Percec, Chem. Rev. **109**, 6275 (2009)
585. M.E. Gallina, G. Bergamini, S. Di Motta, J. Sakamoto, F. Negri, P. Ceroni, Photochem. Photobiol. Sci. **13**, 997 (2014)
586. A.S. Abd-El-Aziz, I. Manners, *Frontiers in Transition-Metal Containing Polymers* (Wiley, NY, 2007)
587. S. Campagna, P. Ceroni, F. Puntoriero (eds.), *Designing Dendrimers* (Wiley, Hoboken, 2012)
588. L.H. Gade (ed.), *Dendrimer Catalysis* (Springer, Berlin, Heidelberg, NY, 2006)
589. Y. Cheng (ed.), *Dendrimer-Based Drug Delivery Systems: From Theory to Practice* (Wiley, Chichester, 2012)
590. D.A. Tomalia, J.B. Christensen, U. Boas, *Dendrimers, Dendrons, and Dendritic Polymers: Discovery, Applications, and the Future* (Cambridge University Press, Cambridge, 2012)
591. F. Vögtle, G. Richardt, N. Werner, *Dendrimer Chemistry: Concepts, Syntheses, Properties, Applications* (Wiley, Weinheim, 2009)
592. P. Ceroni, G. Bergamini, V. Balzani, Angew. Chem. Int. Ed. **48**, 8516 (2009)
593. V. Balzani, P. Ceroni, A. Juris, M. Venturi, S. Campagna, F. Puntoriero, S. Serroni, Coord. Chem. Rev. **219–221**, 545 (2001)
594. V. Balzani, G. Bergamini, P. Ceroni, F. Vogtle, Coord. Chem. Rev. **251**, 525 (2007)
595. V. Balzani, G. Bergamini, P. Ceroni, Adv. Inorg. Chem. **63**, 105 (2011)
596. G.R. Newkome, C. Shreiner, Chem. Rev. **110**, 6338 (2010)
597. F. Puntoriero, A. Sartorel, M. Orlandi, G. La Ganga, S. Serroni, M. Bonchio, F. Scandola, S. Campagna, Coord. Chem. Rev. **255**(21), 2594 (2011)
598. H. El-Batal, K. Guo, X. Li, C. Wesdemiotis, C.N. Moorefield, G.R. Newkome, Eur. J. Inorg. Chem. **2013**, 3640 (2013)
599. R. Satapathy, M. Ramesh, H. Padhy, I.-H. Chiang, C.-W. Chu, K.-H. Wei, H.-C. Lin, Polym. Chem. **5**, 5423 (2014)
600. J.-L. Wang, X. Li, C.D. Shreiner, X. Lu, C.N. Moorefield, S.R. Tummalapalli, F.R. Fronczek, C. Wesdemiotis, G.R. Newkome, New J. Chem. **36**, 484 (2012)
601. I. Angurell, O. Rossell, M. Seco, Inorg. Chim. Acta **409**, 2 (2014)
602. F. Puntoriero, F. Nastasi, M. Cavazzini, S. Quici, S. Campagna, Coord. Chem. Rev. **251**, 536 (2007)
603. L. Xu, L.-J. Chen, H.-B. Yang, Chem. Commun. **50**, 5156 (2014)
604. G.-Z. Zhao, Q.-J. Li, L.-J. Chen, H. Tan, C.-H. Wang, D.A. Lehman, D.C. Muddiman, H.-B. Yang, Organometallics **30**, 3637 (2011)
605. L.-J. Chen, Q.-J. Li, J. He, H. Tan, Z. Abliz, H.-B. Yang, J. Org. Chem. **77**, 1148 (2012)
606. S. Chen, L.-J. Chen, H.-B. Yang, H. Tian, W. Zhu, J. Am. Chem. Soc. **134**, 13596 (2012)
607. J.-K. Ou-Yang, L.-J. Chen, L. Xu, C.-H. Wang, H.-B. Yang, Chin. Chem. Lett. **24**, 471 (2013)
608. N.-W. Wu, J. Zhang, D. Ciren, Q. Han, L.-J. Chen, L. Xu, H.-B. Yang, Organometallics **32**, 2536 (2013)
609. J.B. Pollock, T.R. Cook, P.J. Stang, J. Am. Chem. Soc. **134**, 10607 (2012)
610. S. Shanmugaraju, A.K. Bar, K.-W. Chi, P.S. Mukherjee, Organometallics **29**, 2971 (2010)
611. N.-W. Wu, Q.-J. Li, J. Zhang, J. He, J.-K. Ou-Yang, H. Tan, Z. Abliz, H.-B. Yang, Tetrahedron **69**, 5981 (2013)

612. M. He, Q. Han, J. He, Q. Li, Z. Abliz, H. Tan, L. Xu, H. Yang, Chin. J. Chem. **31**, 663 (2013)
613. L.-J. Chen, G.-Z. Zhao, B. Jiang, B. Sun, M. Wang, L. Xu, J. He, Z. Abliz, H. Tan, X. Li, H.-B Yang. J. Am. Chem. Soc. **136**, 5993 (2014)
614. Q. Han, L.-L. Wang, Q.-J. Li, G.-Z. Zhao, J. He, B. Hu, H. Tan, Z. Abliz, Y. Yu, H.-B. Yang, J. Org. Chem. **77**, 3426 (2012)
615. Y.-R. Zheng, K. Ghosh, H.-B. Yang, P.J. Stang, Inorg. Chem. **49**, 4747 (2010)
616. Q.-J. Li, G.-Z. Zhao, L.-J. Chen, H. Tan, C.-H. Wang, D.-X. Wang, D.A. Lehman, D.C. Muddiman, H.-B. Yang, Organometallics **31**, 7241 (2012)
617. H.T. Baytekin, M. Sahre, A. Rang, M. Engeser, A. Schulz, C.A. Schalley, Small **4**, 1823 (2008)
618. R. Sakamoto, S. Katagiri, H. Maeda, Y. Nishimori, S. Miyashita, H. Nishihara, J. Am. Chem. Soc. **137**, 734 (2015)
619. F. Grimm, K. Hartnagel, F. Wessendorf, A. Hirsch, Chem. Commun. **45**, 1331 (2009)
620. C.-H. Wong, S.C. Zimmerman, Chem. Commun. **49**, 1679 (2013)
621. H. Lee, Y.-H. Jeong, J.-H. Kim, I. Kim, E. Lee, W.-D. Jang, J. Am. Chem. Soc. **137**, 12394 (2015)
622. Y. Shinozaki, T. Tsubomura, K. Sugawa, J. Otsuki, Tetrahedron Lett. **57**, 48 (2016)
623. U. Hahn, F. Vögtle, J.-F. Nierengarten, Polymers **4**, 501 (2012)
624. W.-S. Li, K.S. Kim, D.-L. Jiang, H. Tanaka, T. Kawai, J.H. Kwon, D. Kim, T. Aida, J. Am. Chem. Soc. **128**, 10527 (2006)
625. W.-D. Jang, W.-G. Koh, Dendrimer porphyrin (phthalocyanine), in *Encyclopedia of Biomedical Polymers and Polymeric Biomaterials*, ed. by M. Mishra (Taylor & Francis, Boca Raton, 2015)
626. H.-J. Yoon, W.-D. Jang, J. Mater. Chem. **20**, 211 (2010)
627. F. Figueiraa, P.M.R. Pereiraa, S. Silvaa, J.A.S. Cavaleiroa, J.P.C. Tome, Curr. Org. Synthesis **11**, 110 (2014)
628. J. Kim, H.-J. Yoon, S. Kim, K. Wang, T. Ishii, Y.-R. Kim, W.-D. Jang, J. Mater. Chem. **19**, 4627 (2009)
629. W.-D. Jang, Y. Nakagishi, N. Nishiyama, S. Kawauchi, Y. Morimoto, M. Kikuchi, K. Kataoka, J. Control. Rel. **113**, 73 (2006)
630. W.-D. Jang, N. Nishiyama, K. Kataoka, Supramol. Chem. **19**, 309 (2007)
631. T. Yamaguchi, T. Kimura, H. Matsuda, T. Aida, Angew. Chem. Int. Ed. **43**, 6350 (2004)
632. A. Tsuda, M.A. Alam, T. Harada, T. Yamaguchi, N. Ishii, T. Aida, Angew. Chem. Int. Ed. **46**, 8198 (2007)
633. S. Zhang, H.-J. Sun, A.D. Hughes, B. Draghici, J. Lejnieks, P. Leowanawat, A. Bertin, L.O. De Leon, O.V. Kulikov, Y. Chen, D.J. Pochan, P.A. Heiney, V. Percec, ACS Nano **8**, 1554 (2014)
634. S. Zhang, H.-J. Sun, A.D. Hughes, R.-O. Moussodia, A. Bertin, Y. Chen, D.J. Pochan, P.A. Heiney, M.L. Klein, V. Percec, Proc. Natl. Acad. Sci. U.S.A. **111**, 9058 (2014)
635. M. Peterca, V. Percec, P. Leowanawat, A. Bertin, J. Am. Chem. Soc. **133**, 20507 (2011)
636. V. Percec, D.A. Wilson, P. Leowanawat, C.J. Wilson, A.D. Hughes, M.S. Kaucher, D.A. Hammer, D.H. Levine, A.J. Kim, F.S. Bates, K.P. Davis, T.P. Lodge, M.L. Klein, R.H. DeVane, E. Aqad, B.M. Rosen, A.O. Argintaru, M.J. Sienkowska, K. Rissanen, S. Nummelin, J. Ropponen, Science **328**, 1009 (2010)
637. M. Filippi, D. Remotti, M. Botta, E. Terreno, L. Tei, Chem. Commun. **51**, 17455 (2015)
638. M. Filippi, J. Martinelli, G. Mulas, M. Ferraretto, E. Teirlinck, M. Botta, L. Tei, E. Terreno, Chem. Commun. **50**, 3453 (2014)
639. M. Filippi, D. Patrucco, J. Martinelli, M. Botta, P. Castro-Hartmann, L. Tei, E. Terreno, Nanoscale **7**, 12943 (2015)
640. J. Hardy, F. Schacher (eds.), *Functional Metallosupramolecular Materials* (RSC, Cambridge, 2015)
641. M.W. Urban (ed.), *Handbook of Stimuli-Responsive Materials* (Wiley-VCH Verlag GmbH & Co. KGaA, Weinheim, 2011)
642. M.J.M. Muñoz, G. Fernández, Chem. Sci. **3**, 1395 (2012)
643. A.J. McConnell, C.S. Wood, P.P. Neelakandan, J.R. Nitschke, Chem. Rev. **115**, 7729 (2015)

644. R. Yerushalmi, A. Scherz, M.E. van der Boom, H.-B. Kraatz, J. Mater. Chem. **15**, 4480 (2005)
645. X. Ma, H. Tian, Acc. Chem. Res. **47**, 1971 (2014)
646. M. Yan, S.K.P. Velu, M. Marechal, G. Royal, J. Galvez, P. Terech, Soft Matter **9**, 4428 (2013)
647. S. Köytepe, M.H. Demirel, T. Seçkin, J. Inorg. Organomet. Polym. **23**, 1104 (2013)
648. A. Gasnier, J.-M. Barbe, C. Bucher, F. Denat, J.-C. Moutet, E. Saint-Aman, P. Terech, G. Royal, Inorg. Chem. **47**, 1862 (2008)
649. A. Gasnier, J.-M. Barbe, C. Bucher, C. Duboc, J.-C. Moutet, E. Saint-Aman, P. Terech, G. Royal, Inorg. Chem. **49**, 2592 (2010)
650. A.K. Miller, Z. Li, K.A. Streletzky, A.M. Jamieson, S.J. Rowan, Polym. Chem. **3**, 3132 (2012)
651. T.-A. Asoh, H. Yoshitake, Y. Takano, A. Kikuchi, Macromol. Chem. Phys. **214**, 2534 (2013)
652. J. Yuan, H. Zhang, G. Hong, Y. Chen, G. Chen, Y. Xu, W. Weng, J. Mater. Chem. B **1**, 4809 (2013)
653. J. Brassinne, J.-P. Bourgeois, C.-A. Fustin, J.-F. Gohy, Soft Matter **10**, 3086 (2014)
654. J. Brassinne, A.M. Stevens, E. Van Ruymbeke, J.-F. Gohy, C.-A. Fustin, Macromolecules **46**, 9134 (2013)
655. S.-C. Wei, M. Pan, K. Li, S. Wang, J. Zhang, C.-Y. Su, Adv. Mater. **26**, 2072 (2014)
656. K. Liu, Y. Kang, Z. Wang, X. Zhang, Adv. Mater. **25**, 5530 (2013)
657. A. Hennig, H. Bakirci, W.M. Nau, Nat. Meth. **4**, 629 (2007)
658. J. Liu, M.-A. Morikawa, N. Kimizuka, J. Am. Chem. Soc. **133**, 17370 (2011)
659. S.K. Ghosh, *Self-healing Materials: Fundamental, Design Strategies, and Applications* (Wiley-VCH, Weinheim, 2009)
660. D. Habault, H. Zhang, Y. Zhao, Chem. Soc. Rev. **42**, 7244 (2013)
661. B. Sandmann, S. Bode, M.D. Hager, U.S. Schubert, Adv. Polym. Sci. **262**, 239 (2013)
662. S. Bode, D. Sandmann, M.D. Hager, U.S. Schubert, Metal-complex-based self-healing polymers, in *Self-Healing Polymers: From Principles to Applications*, ed. by W.H. Binder (Wiley, Chichester, 2013)
663. M. Burnworth, L. Tang, J.R. Kumpfer, A.J. Duncan, F.L. Beyer, G.L. Fiore, S.J. Rowan, C. Weder, Nature **472**, 334 (2011)
664. G.L. Fiore, S.J. Rowan, C. Weder, Chem. Soc. Rev. **42**, 7278 (2013)
665. S. Bode, L. Zedler, F.H. Schacher, B. Dietzek, M. Schmitt, J. Popp, M.D. Hager, U.S. Schubert, Adv. Mater. **20**, 1634 (2013)
666. B. Yang, H. Zhang, H. Peng, Y. Xu, B. Wu, W. Weng, L. Li, Polym. Chem. **5**, 1945 (2014)
667. P. Terech, M. Yan, M. Marechal, G. Royal, J. Galvez, S.K.P. Velu, Phys. Chem. Chem. Phys. **15**, 7334 (2013)
668. A. El-ghayoury, H. Hofmeier, B. de Ruiter, U.S. Schubert, Macromolecules **36**, 3955 (2003)
669. S. Kupfer, L. Zedler, J. Guthmuller, S. Bode, M.D. Hager, U.S. Schubert, J. Popp, S. Gräfe, B. Dietzek, Phys. Chem. Chem. Phys. **16**, 12422 (2014)
670. S. Bode, M. Enke, R.K. Bose, F.H. Schacher, S.J. Garcia, S. van der Zwaag, M.D. Hager, U.S. Schubert, J. Mater. Chem. A **3**, 22145 (2015)
671. M. Enke, S. Bode, J. Vitz, F.H. Schacher, M.J. Harrington, M.D. Hager, U.S. Schubert, Polymer **69**, 274 (2015)
672. M. Behl, M.Y. Razzaq, A. Lendlein, Adv. Mater. **22**, 3388 (2010)
673. J. Li, J.A. Viveros, M.H. Wrue, M. Anthamatten, Adv. Mater. **19**, 2851 (2007)
674. J. Li, C.L. Lewis, D.L. Chen, M. Anthamatten, Macromolecules **44**, 5336 (2011)
675. K. Sada, M. Takeuchi, N. Fujita, M. Numata, S. Shinkai, Chem. Soc. Rev. **36**, 415 (2007)
676. C.L. Lewis, E.M. Dell, Inc. J. Polym. Sci. Part B: Polym. Phys. **54**, 1340 (2016)
677. J.R. Kumpfer, J.R. Rowan, J. Am. Chem. Soc. **133**, 12866 (2011)
678. X. Luo, P.T. Mather, ACS Macro Lett. **2**, 152 (2013)
679. E.D. Rodriguez, X. Luo, P.T. Mather, A.C.S. Appl, Mater. Interfaces **3**, 152 (2011)

Chapter 8
Thermal Transformations of Polymeric Metal Chelates and Their Precursors in Nanocomposites Formation

Abstract The thermal transformations of polymeric metal chelates and their most typical precursors, resulting in the formation of nanocomposite materials, are considered. The attention is focused on the methodology of thermolysis including thermogravimetric, linear pyrolysis, volumetric, spray, chemical vapor deposition approaches as well as thermolysis under the action high-energy radiation. The metal chelates as «single-source» precursors are readily decomposed both in the pure state and the polymer matrix due to the formation of the polymeric shell by the destruction of the organic fragment. A new approach using metal chelate monomers as precursors (the conjugate thermolysis) is also considered. This method involves a simultaneous polymerization of monomers and the formation of metal-containing nanoparticles during the thermal transformation. Depending on the nature of the polymeric metal chelates and thermolysis conditions, different nanomaterials (for example, carbon, metal oxide, mixed-oxide, non-oxide nanocomposites, etc.) can be formed.

Existing methods of obtaining nanomaterials can be reduced to two fundamentally various ways: «top down» (descending way) or «bottom-up» (ascending way). The first one consists in grinding all sorts of large particles to nano-sized, «bottom-up» method is in the assembly of nanoparticles from individual atoms (or ions with following reduction) to a predetermined size of nanoparticles in the presence of the polymer matrix (or its precursor). The latter method, because of its diversity and potential, is more widely used than «top down» approach. The researcher can predict in advance the characteristics of the prepared nano-sized particles: choose the composition and properties of the starting components, stabilizing agents, to evaluate their role, to predict the conditions of nucleation and growth of nano-sized particles at all stages of design of the targeted nanocomposites. Properties that can be achieved in such materials are strictly dependent on the synergy between organic and inorganic nature of the components and surely defined nanostructure and the extent of their organization.

Among the known «bottom-up» approaches, high-temperature thermolysis of metal-containing samples is a general method allowing to preparing nanomaterials

with low crystalline defects, narrow size distribution, and regulated shapes [1, 2]. Many interesting concepts, for example, size distribution focusing, selective adhesion shape control and branching, have been developed [3–6]. It should be noted that solid-state thermolysis of different metal chelates is a promising way to the preparation of novel nanostructured materials.

Of particular interest are the polymeric metal chelates which thermal decomposition under different conditions is widely studied in order to obtain metal-containing nanocomposites with tunable sizes and morphologies [7–26]. It is important that various nano-sized materials, for example, metals, metal oxides, metal sulfides and metal halides, can be obtained using PMC or their precursors.

In this chapter, we analyze thermolysis as one of the comfortable, well-reproducible and easily controlled methods of nanocomposites formation an example of different types of metal chelates.

8.1 Thermolysis Methods of Polymeric Metal Chelates

The study of thermal transformations can be carried out using methods of external and internal heating as in isothermal and non-isothermal conditions, in closed or open systems. Depending on tasks the various methods are possible to control the degree of conversion, which determine the choice of equipment for the experimental study of the compounds thermolysis. First of all, it is the weight (thermogravimetry) or volumetric (volumetry) methods. In recent years, there is a tendency to design complex (synchronous) devices that simultaneously combine in a single device several ways for the conversion control in conjunction with their automation, using the capabilities of modern computer technology. We briefly analyze the specifics of the main methods used to study the kinetics of thermal decomposition (thermal degradation) of metal-containing compounds. Thermogravimetric analysis (TGA), differential scanning calorimetry (DSC), thermodilatometry and thermomechanical analysis, dielectrical analysis, micro- and nanoscale thermal analysis, including atomic force microscopy (AFM) and scanning thermal microscopy (STM) are the most frequently used methods of thermal analysis of different compounds, including metal-containing.

8.1.1 Thermogravimetric Methods

Their essence is to measure the relative change in the material weight as a function of temperature during its transformation with a programmed heating. Linear temperature dependence on time is usually used, sometimes TGA combined with tensimetry, in which the substance weight and gassing analysis is carried out simultaneously, usually under isothermal conditions in a dynamic vacuum and can be detected both continuously and discretely. To do this, a spring balance uses

during the study of the kinetics of consumption of volatile products of thermolysis. Modern thermobalance allow continuously (automatically) detect the variation of the sample weight (Δm) of time of the temperature. TGA methods are mostly the traditional non-isothermal variants of linear heating method.

At present, the different thermogravimetric variants found widespread use: differential thermogravimetry (DTG), when weight variation m of the time t (i.e. dm/dt) or of temperature (dm/dT) is recorded; differential thermal analysis (DTA), wherein the temperature difference between the reference and the substance is measured as a function of temperature at a programmed heating. It should be noted the development of a new research method called differential scanning calorimetry (DSC) to increase in the accuracy of quantitative determination of the thermal effects [27].

When the programmed heating rate such concepts as the temperature of the decomposition onset, the decomposition stages, the temperature ranges of stability of the intermediate compounds are the kinetic characteristics of the process [27]. To reduce the distortions introduced by the uncontrolled pressure and by the permanently increasing temperature, a new technique of TGA experiment was developed, which became the basis for the quasi-isothermal quasi-isobaric thermogravimetry method [28]. The principle of the method is based on a fine adjustment of heating, allowing keeping the constant weight change rate or constant pressure.

8.1.2 Linear Pyrolysis Method

Linear pyrolysis (LP) is a steady-state one-dimensional propagation of the reaction front of the thermal transformation in a condensed phase when heat is supplied from an external source [29]. LP is carried out in two regimes depending on the relationship between the parameters. In the first kinetic regime, pyrolysis macrokinetics coincides with the true kinetics of decomposition and $E_{eff} \approx E_{tr}$. The second route is internal diffusion regime (by heat), when $E_{eff} \approx E_{tr}/2$. LP method allows to studying the kinetics of fast high-temperature processes in condensed phase, for which to a change in the rate-limiting stage of the chemical transformation often takes place during the transition from one temperature region to another. The principle of operation of the devices based on LP-method is that the sample of the tested substance is constantly pressed upon the surface of the heating plate at constant temperature.

8.1.3 Volumetric Methods

Volumetric methods allow to studying the decomposition of small amount of a substance and to investigating the dependence of the volume of the evolved gas [$V(t)$] by discretely or continuously manner. The main disadvantage of pressure gauge units

is direct contact of gaseous products which can be chemically aggressive with the corroding metallic parts and mercury. Therefore, the using glass membrane type pressure gauges, where there are no metallic parts, is the more pronissing. The ubdoubted advantages of such setups are short response times, which allows to studying the rates of fast processes in a close reactor space by means of a Bourdon membrane-type pressure gauge. It should be noted that gas evolution during the thermal transformation proceeds in a self-generated atmosphere (SGA). Such method was called RAPET (Reaction under Autogenic Pressure at Elevated Temperature) (see, for example [30]).

8.1.4   Thermolysis Induced by High-Energy Radiation

This method is based on sample exposed to high frequency (HF) electric field as alternative source of heating [31–33]. Its essence lies in the fact that polar units of polymer molecules are oriented in accordance with change of polarity of a variable electric field. At the same time, thermal motion as well as other units hinders such orientation. Energy is spent on overcoming the disorientation of the polar units, as a result of which it dissipates and heats the sample. The electric field strength and frequency of oscillations are the main factors determining the intensity of heating. The absence of contact in the entire volume of the test sample is the main advantage of HF heating. Thus, the effect of high-frequency heating (the heating temperature can reach 510 K) with a frequency of 100–300 MHz of polymers containing electrically conductive metal-containing fillers or soot having a particle size of less than 500 μm in an amount of up to 85% of the weight of the material allows the production of a homogeneous composite material. In another example, the heating temperature reaches 495–770 K during heating metal-containing samples in a muffle oven and exposing to a 2450 MHz electromagnetic field with a 700 W power [34]. The prepared products are characterized by a pronounced crystalline structure, high surface area and particle sizes in the nanometer scale.

8.1.5   Spray Pyrolysis

By nature and design, such method is different from the above-mentioned proce-dures and is an efficient alternative method for obtaining metal and their oxide nanoparticles in the form of powders on a large scale, ceramics, nanostructured materials [35, 36]. Of substantial interest are also the ultrasound-, laser-, plasma-pyrolysis as and flame spray pyrolysis [37–39].

The aerosol spray pyrolysis is a promising strategy for increasing both surface area and crystallinity, enabling sequential, easy, and large-scale production of metal oxide spheres [23, 40–45].

Usually, spray pyrolysis proceeds in five main stages [46]. Although some stages of spray pyrolysis [47] continue to be developed (for example, drop formation [48], evaporation and drying [49], spray through a variety of devices - sprays, atomizers, ultrasonic generators, etc.), however so far there is no deep understanding of the effect the change of reaction conditions (concentration, flow rate, evaporation-precipitation stage of thermolysis) on the mechanism and the possibility of control of uniform nanoparticle formation. The most significant influence on the nanocrystal formation has a temperature. Nanocomposites based on metal oxides obtained by spray pyrolysis, described in sufficient detail (see, for example, [50–57]).

Intensively developing are new areas of gas phase synthesis in the condensed phase for the preparation of new ceramic materials. Of great synthetic potential is the flame spray pyrolysis, including aqua and non-aqua sol-gel technique, hydro- and solvothermal methods, pyrolysis of polymeric materials and high-pressure technique.

8.1.6 Chemical Vapor Deposition

Various variants of vapor deposition technology are commonly used for the preparation of metal-polymer nanocomposites [58, 59]. Their essence is combined or sequential deposition of metal and organic components and the metal nanoparticle formation in the growing composite film. Active metal atoms during the collision with the polymer surface may diffuse into the bulk polymeric matrix trapped by the surface defects, collided with each other, leading to aggregation and formation of cluster particles. The volume fraction of metal nano-sized particles in a polymer film can be regulated by the ratio of deposition rates of metallic and polymer components [60]. Methods of chemical vapor deposition of organometallic precursors are widely used for the preparation of semiconductor film materials [61, 62]. Metal chelate in gas-phase processes for obtaining nanocomposite materials have a number of advantages, because due to the presence of components with preformed bonds they may lead to a quality defect-free products with a stoichiometric composition [63], including thin-film materials based on cadmium [64, 65], iron [66, 67], antimony and bismuth sulfides [68], etc.

8.2 Metal Chelates As «Single-Source» Precursors of Nanocomposites

The synthetic strategy for the preparation of nanostructured materials is often based on the thermolysis of «single-source» precursors (SSP) into hot organic solvent. Usually it is also called «TOPO method», where TOPO is tri-n-octylphosphine

oxide, in which chelating precursor dispersed in tri-*n*-octylphosphine (TOP) or TOPO reacts with the metal compound in the hot surfactant/solvent at temperatures up to 350 °C to form metal-containing nanoparticles [69]. Despite the pervasiveness such approaches starting from two or more precursors they have limitations due to the fact that the formation of the nanocrystal often depends on the relative reactivity of these composite components, their stability, etc. Many of these problems, including the use of toxic and volatile compounds at high temperatures can be avoided if the precursors are metal chelates, which combine in one molecule as a metal ion, and composite elements, for example, chalcogenides to produce semiconductor nanoparticles. Typically, metal chelates are easily synthesized, stable with respect to moisture and atmospheric oxygen at room temperature, safe and in many cases lower cost-effective than multicomponent systems [70–72]. Besides, good scalability and controllability of the thermolysis process of metal chelates in the preparation of nanocomposites based on them are also attractive.

Equally important is the fact that the PMC thermolysis analysis is usually carried out by comparison with low molecular weight analogues, which are used as monomeric metal chelates. Therefore, the study of the kinetics of thermal transformations of metal chelates and the structure of the resulting products is important for the understanding of the general laws of PMC thermolysis.

The range used to date metal chelates is quite wide, including a variety of metals and chelating ligands. Among the most interesting examples of molecular metal chelates we note synthesis of magnetic Co_3O_4 nanostructures via a facile thermal treatment method at 700 °C by using *trans*-Na[Co(L)$_2$(NO$_2$)$_4$]·H$_2$O (L is hexamethylenetetramine) as a precursor [73]. The target Co complex provides good conditions for preparation of magnetic octahedral nanostructures in a facile and surfactant-free method. It is found that the Co_3O_4 nanostructures exhibit a ferromagnetic behavior with a saturation magnetization of 8.69 emu g^{-1} and a coercivity of 305.3 Oe at room temperature. In another example the chelating ligand 2,2′-diamino-5,5′-dimethyl-4,4′-bithiazole (L) was also used for obtaining Co_3O_4 nanoparticles [74]. In particular, Co_3O_4 nanostructures were prepared by direct thermolysis of nanoscale and single crystals of an azido Co(II) complex [Co(L)$_2$(N$_3$)$_2$]0.25CH$_3$OH at 450 °C under air. It should be noted that the CdS nanoparticles were obtained using Cd(II) complex [Cd(L)$_2$(NO$_2$)$_2$] based on the same ligand as precursor via thermal decomposition [75]. However, during thermal decomposition of [Cd(L)$_3$](ClO$_3$)$_2$ an oxide-sulfide nanocomposite CdO–CdS was prepared [76].

The study of mechanism of thermolysis of bpy chelates of Zn(II) and Cd(II) [77, 78] as well as Ni(II) [79] and Fe(II) [80] is based on the composition and structure of the prepared products. In particular, thermolysis of tric(bpy)-Fe(II) dichloride proceeds in two stage (Fig. 8.1).

We note corresponding metal oxide nanocomposites/binary oxides obtained by heating of the heterometallic complexes [M$_2$Mn(OAc)$_6$(bpy)$_2$], where M=Cu, Co, Zn [81].

The thermolysis of [M(en)$_2$](NO$_3$)$_2$ (M=Cu, Co, Ni and Zn) chelates proceeds in two stages through evolving en and monoethylene diamine molecules and the
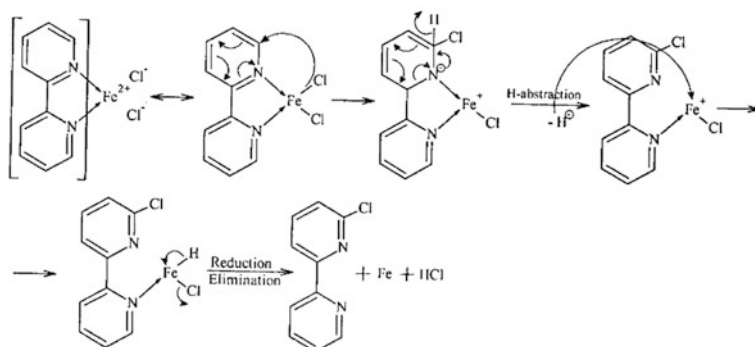
Fig. 8.1 Mechanism of thermal decomposition of tric(bpy)iron(II) dichloride to Fe(0) in an inert atmosphere

formation of high-dispersed metal oxides [82]. The process kinetics corresponds to second- and third-order equations, respectively.

The controlled thermolysis of $[Ni(en)_2(H_2O)_2](NO_3)_2$ chelate leads to the formation of nanocrystalline nickel (18.1 nm) [83]. The kinetics of a solid phase thermolysis of tris (ethylene diamine) nickel (II) sulphate includes two-stage deamination and two-stage decomposition [84].

Melt thermolysis was used to produce different Pd nanostructures based palladium complex with bis-1,2,4-triazole ligand [85]. Interestingly, the binding of the ligand to the metal atom is carried out by means of four N atoms of four 1,2,4-triazole groups without sulfur atoms. This type of coordination leads to the formation of spiro-metallocycle Pd(II) complex (Fig. 8.2). Depending on the temperature and atmosphere in which the complex thermolysis is carried nanoparticles of metallic Pd(0) (800 °C in N_2 medium) or Pd(0)-, Pd–PdO-, PdO- and Pd–PdO-nanostructures can be obtained at temperatures of 300, 500, 700 and 800 °C in air, respectively.

Numerous studies devoted to the investigation of the thermolysis of metal chelates of intracomplex type, in particular metal acetylacetonates. Thus, nanocrystalline α-Al_2O_3 powders were prepared [86] by pyrolysis of $Al(acac)_3$. The optimum calcination temperature of the precursor powder for crystallization of nano α-Al_2O_3 was 1000 °C for 2 h. It was shown that the obtained materials could be modified from segregated nanoparticle to aggregates of nanoparticle with decrease in the volume ratio of alumina to acac from 8:2 to 5:5 in the precursor solutions.

The CdO nanoparticles (45 nm) were obtained by thermolysis of an aza-aromatic base adduct of Cd(II) thenoyltrifluoroacetonate, $[Cd(phen)(TTA)_2]$, at 180 °C with oleic acid as a surfactant [87]. It is important that as a result of this reaction CdO nanoparticles are formed, in comparison with CdS formation from Cd/S-ligand complexes in the majority of the reactions below.

It should be noted using liquid-feed flame spray pyrolysis [88] for synthesis of Mg–Fe-based mixed-metal nanopowders in the $(MgO)_x(Fe_2O_3)_{1-x}$ system from
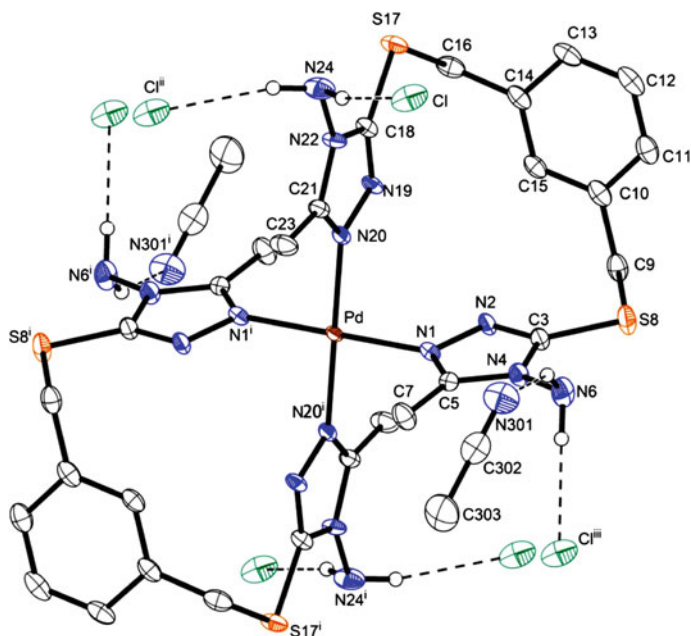
Fig. 8.2 The molecular structure of the metal chelate [PdL$_2$]Cl$_2$·4CH$_3$CN (L = 5,5′-(1,3-phenylenebis(methylene))bis(sulfanediyl)bis(3-methyl-4H-1,2,4-triazol-4-amine)

metal-complex precursors. Iron propionate [Fe(O$_2$CCH$_2$CH$_3$)$_3$] and magnesium acetylacetonate [Mg(acac)$_2$·2H$_2$O] precursors were dissolved in ethanol, aerosolized with oxygen and combusted at 1500 °C and thereafter quenched rapidly. Final powders had a range of compositions (x = 0.30, 0.45, 0.50, 0.65, 0.75, and 0.90 ± 0.02) and particle sizes generally increased as the fraction of MgO increased.

Of interest is a simple method of the preparation of nano-sized Co$_3$O$_4$, which is important p-type semiconductor with catalytic, gas-sensor and electrochemical properties [89–91]. This method based on a solid-phase thermolysis of the metal chelate precursor—bis(salicylaldehydate)$_2$cobalt(II) at 773 K for 5 h in air [92, 93].

The key role of ligands and their dynamics during the nanoparticle synthesis can be clearly illustrated by the preparation of Ge/GeO$_2$ nanoparticles with core-shell structure with a mean diameter close to 5 nm with a narrow size distribution (<15%). It was shown [94] that oleic acid, in addition to the stabilizing function is involved in the mechanism of thermal decomposition of the aminoiminate germanium(II) (ATI)GeZ complex (Z=OMe, NPh$_2$, ATI=N,N′-diisopropyl-aminotroponiminate). Equilibrium is established between the initial metal chelate and formed intermediate (ATI)GeOl (Ol is oleate) even at room temperature during mixing of (ATI)GeOMe with an acid (Scheme 8.1). Substitution of oleic acid by hexadecylamine (HDA) or its mixture with oleic acid does not lead to the nanoparticles formation. In this case it is also important that the original complex
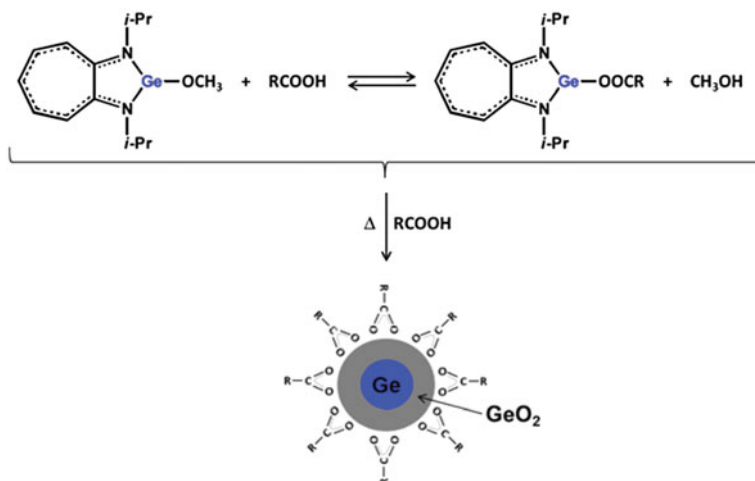
Scheme 8.1 Mechanism of Ge/GeO nanoparticle formation by thermal decomposition of (ATI) GeOMe

(ATI)GeOMe is also in the reaction system. Note that the use of separately obtained (ATI)GeOl complex to produce nanoparticles is unsuccessful. It is assumed that the presence of the original complex (ATI)GeOMe in the system is necessary for the nucleation process, while the oleic acid promotes the decoordination of strong chelating ATI ligand by acidic proton. If in this example thermolysis is carried out at 320 °C, the use of a weaker chelating ligand as amidinate can significantly reduce (up to 160 °C) operating temperatures of the synthesis of germanium nanoparticles [94].
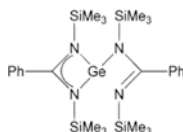
The most detailed study of the thermolysis kinetics and the structure of the resulting products were carried out by the example of chalcogenide and azomethine metal chelates.

8.2.1   Chalcogenide Metal Chelates

Currently, a wide variety of compounds as the metal dithio/diselenocarbamates and imino-bis(diizopropylphosphine)selenides [95–97], and Cd(TePh)$_2$ [98] or Zn

(TePh)$_2$ [99] are used as SSP for the synthesis of CdS, CdSe, ZnSe, CdTe/ZnS and other nanocrystals. A wide selection of solvents and surfactant molecules, varying the synthesis conditions allow largely to control the properties of the final products and to obtain materials with desired characteristics.

Thus, the hexagonal microcrystalline zinc oxide was prepared using Zn(II) cysteine complex [ZnI$_2$(L)]$_n$ (L is 2-amino-3-mercaptopropanoic acid) as precursor by calcination at 600 °C for 2 h [100]. Pure greenish-blue cobalt chromite (CoCr$_2$O$_4$) nanoparticles having narrow particle range of 4.1 ± 1.9 nm and surface area of 78.2 m^2 g^{-1} were prepared by the thermolysis of mixed metal chelates with chelating 2-mercaptopyridine N-oxide sodium salt [101]. Thermolysis led to the formation of nanoparticles with high surface area due to releasing a large amount of gas. It is important that the particle size reduction depends on the temperature and time of thermolysis.

Dimeric cadmium(II) chelate with S-benzyldithiocarbazate (L), [Cd(L)Cl$_2$]$_2$ was used for the bulk synthesis of CdS nanorods [102]. It should be noted that the decomposition of the chelate was carried out by heating at 160 °C in hexamethylene-diamine (HMDA) to form amine capped CdS nanocrystals (rods) with yield ca. 90%.

Of interest is a template-free preparation of CdS microflowers by thermolysis of cadmium thiocyanate complex at 300 °C under open atmosphere [103]. The microflower morphology was self-assembled by intact thin nano-sheets.

It is important to underline that the concentration of the monomer precursor, the reaction temperature, stabilizing agents is important factors that determine the regime (thermodynamic or kinetic) in which the reaction occurs [6]. The high reaction temperatures and low monomer concentration promote the thermodynamic growth regime to the formation of isotropic nanocrystals. In contrast, kinetic nonequilibrium conditions caused by low reaction temperatures and high precursor concentrations lead to anisotropic structures (rods, tetrapods, etc.).

8.2.1.1 Influence of the Ligand Nature

Dialkylthiocarbamates [65, 104–107], thiosemicarbazides [108], xanthates [109, 110], thiourea [111, 112], dialkylchalcogenephosphates, dichalcogeneimidophosphates [113] are the most commonly used chelating ligands of SSP. We note also that one of the most interesting families of chelating ligands for the synthesis of SSP is chalcogenepyridines:
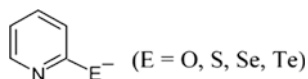
Metal chelates of 2-thio [114] and 2-selenopyridines [115, 116] are well known, while the coordination chemistry of 2-telluriumpyridines begins to develop only [117, 118].

The nitrogen-containing chelating ligands like ppy, bpy, phen have a significant effect on the thermal stability and volatility of the chalcogenide metal complexes [119–121]. This thermal behavior is often confirmed by step weight loss character during TGA. In particular, two stages of thermal decomposition at temperatures of 130 and 320 °C are typical for the pyridine adduct of bis(piperidine dithiocarbamato) cadmium(II) [Cd(pip-dtc)$_2$] [62], the first of which corresponds to a loss of Py ligand (Fig. 8.3a). In contrast, dithiocarbamate Cd(II) complexes, which does not contain donor adducts, decompose single-stage at 331 and 320 °C with weight loss of 64.9 and 70.9% for the piperidine [Cd(pip-dtc)$_2$] and tetrahydroquinoline [Cd(thq-dtc)$_2$] complexes, respectively (Fig. 8.3b) [61]. The non-volatile residues represent 35.1 and 29.1%, that is slightly higher than the estimated values of CdS (33.4 and 27.3%), obtained from these complexes.

A similar thermal behavior is typical for Zn(pip-dtc)$_2$ and Zn(thq-dtc)$_2$ complexes. Their thermograms show a single-stage weight loss corresponding to thermal decomposition of the organic ligand with the endothermic peak on the DSC curves at 341.9 °C ($\Delta H = 214.3$ J g^{-1}) and 294.5 °C ($\Delta H = 188.0$ J g^{-1}) for Zn (pip-dtc)$_2$ and Zn(thq-dtc)$_2$ complexes, respectively [122]. At the same time a two-stage decomposition is observed with a weight loss at 210 (15.6%) and 304 °C (65.5%) in the case of Fe(pip-dtc)$_3$ [123]. According to the proposed mechanism based on the thermal analysis and gas chromatography-mass spectroscopy (GC-MS) the detachment of one of the three dtc ligand (m/z 160) proceeds initially to form a four-coordinated intermediate and then a final removal of organic components (m/z 290) leads to the final FeS (m/z 86) product (Scheme 8.2).

As seen from these examples, in the absence of donor adducts relatively high temperatures are required for decomposition of metal chelates of the considered type to form the desired metal sulfide nanoparticles. An interesting example is the metal chelates, which contain in addition to dithiocarbamate groups and other chelating ligands, in particular, bpy or phen (Fig. 8.4).
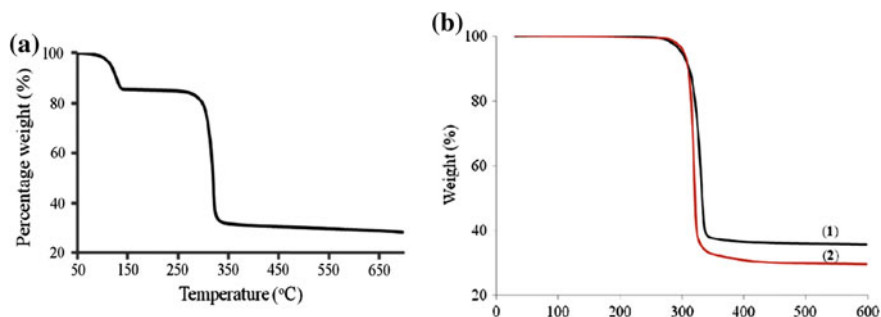
Fig. 8.3 Thermogravimetric curves for complexes of **a** [Cd(pip-dtc)$_2$(Py)] and **b** Cd(pip-dtc)$_2$ (1) and Cd(thq-dtc)$_2$ (2)
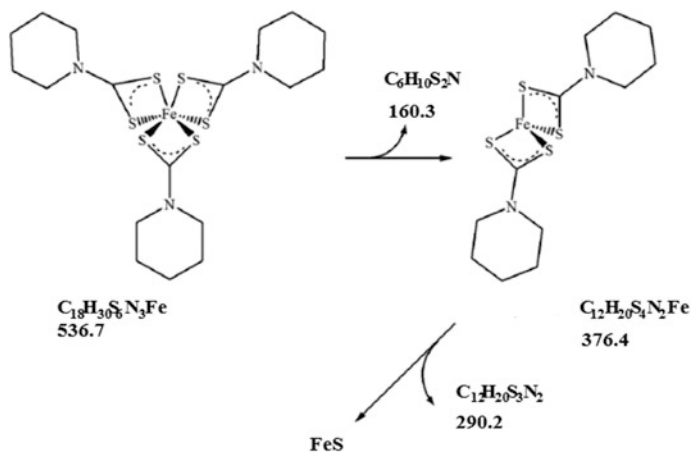
Scheme 8.2 Scheme of the thermal decomposition of Fe(pip-dtc)$_3$
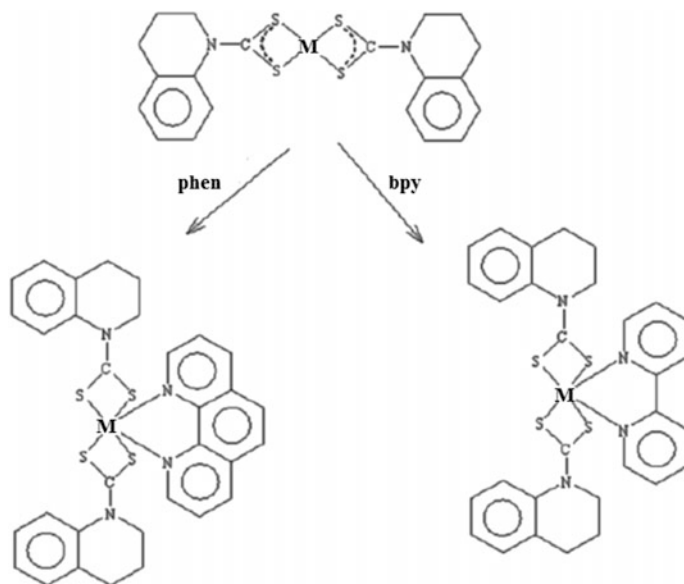
Fig. 8.4 Structure of [Cd(thq-dtc)$_2$] complexes with additional chelating ligands phen or bpy

Additional nitrogen donor atom coordination with metal dithiocarbamate during the formation of adducts causes loosening of partially dual nature of nitrogen-carbon bond and as the result the redistribution of electron density from the carbon to the nitrogen atom in the dtc group:
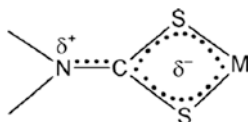
As a rule, M–S bond elongation is observed in such complexes [62, 99], which is explained by an increase in the CN, and the steric influence of donor ligands. Depending on the nature of the substituent on the nitrogen atom in diseleno- and dithiocarbamates symmetrical diselenocarbamate complexes produced selenium clusters during the thermal decomposition, while metal selenides are formed in the case of asymmetric diselenocarbamates [124]. By mass spectrometry with electron ionization (electron ionization mass spectrometry EI–MS) and high resolution pyrolysis GC–MS analysis it shown that slight differences in the alkyl substituents on the nitrogen atom of the diselenocarbamate ligand of $Zn(Se_2CNEt_2)_2$ and $Zn(Se_2CNMe^nHex)_2$ complexes are responsible for the two routes of their decomposition with the formation of Se_n clusters (n = 1–7) from the intermediate diethyldiselenide $EtSe_2Et$ in the first case, and stable five-membered intermediate dihydroselenazole $Zn(Se_2CNMe^nHex)_2$ in the latter case, which completely eliminates from system and the final product thermolysis is metal selenide (Scheme 8.3).

8.2.1.2   Environment Influence

Palladium sulfide Pd_4S nanoparticles of various shapes were obtained from the single-source complex $[PdCl_2(PhS–CH_2CH_2CH_2–NH_2)]$. Thermolysis of 3-phenyl-sulfonylpropylamine complex of palladium chloride (Fig. 8.5) at 195 °C in oleylamine leads to the formation of flower shaped nanoparticles, whereas Pd_4S nano-
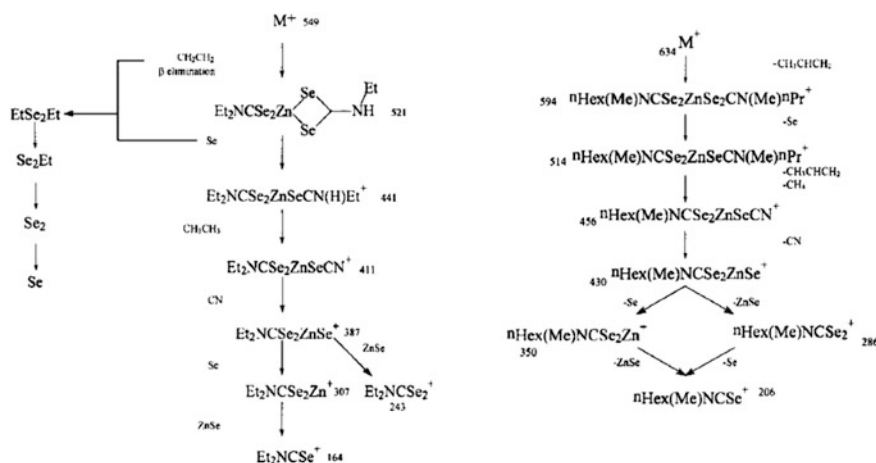
Scheme 8.3 The main routes of decomposition of the complexes $Zn(Se_2CNEt_2)_2$ and $Zn(Se_2CNMe^nHex)_2$ according to data of EI-MS and high resolution pyrolysis GC-MS analysis
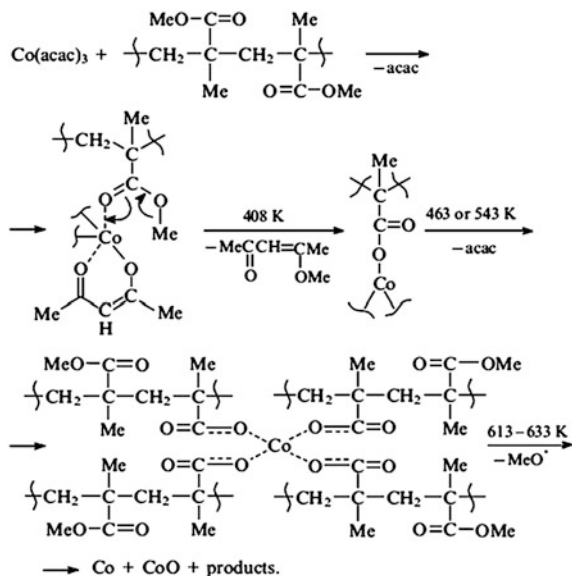
Fig. 8.5 The scheme for obtaining nanoparticles of palladium sulfide from molecular precursor [PdCl$_2$(PhS–CH$_2$CH$_2$CH$_2$–NH$_2$)], where OA is oleic acid, ODE is octadecene, and OAm is oleylamine

spheres are formed in oleic acid and octadecene mixture (1:1) [125]. Perhaps the flower shape of the obtained nanoparticles is determined by the stronger complexing and reducing properties of oleylamine [126, 127].

It is important that the shape of the resulting nanoparticles is not changed by their attachment to the graphene oxide as a carrier and has a significant influence on the catalytic properties of these nanocomposites.

The determining factor in the anisotropic growth of nanocrystals is the surface energy of the crystallographic plane which can be modulated by the selective adsorption of surfactant molecule on the surface [128]. CdS nanoparticles were prepared during the thermal decomposition of Cd(pip-dtc)$_2$ or Cd(thq-dtc)$_2$, and their growth is effectively controlled using capping agents of HDA and TOPO of various concentrations [129]. When thermolysis was performed in HDA medium known by dynamic nature of adsorption on the crystallite surface due to its mobility sufficiently it provides monomeric species access, on the one hand and aggregation preventing of the other. As a result the obtained nanoparticles have the shape of rods, dipodies and tripods (Fig. 8.6).

When TOPO was used as a surfactant the quasi-spherical CdS nanoparticles with an average size of 4.33 ± 0.59 nm was formed. A similar pattern was observed during the preparation of ZnO nanoparticles from Zn(pip-dtc)$_2$ and Zn(thq-dtc)$_2$ complexes in TOPO medium [130]. Interestingly, thermolysis of Cd[E(L)]$_2$ [E = S, Se; L = 2-(4,4-dimethyl-2-oxazolinyl)benzene] in TOPO medium at 280 °C led to cadmium sulfide or selenide nanoparticles with a sufficiently large size up to 200 nm according to the following scheme [131]:

1 E = S, **2** E = Se
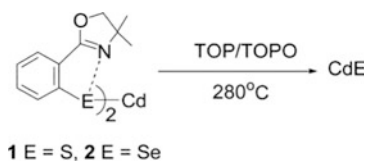
We note that the solution colloidal synthetic methods of chalcogenide nanoparticles preparation in TOP/TOPO medium are widely used [66, 119, 132], despite the high temperature reactions (200–350 °C) and the use of air-sensitive and highly toxic reagents, since they allow to obtain crystalline monodisperse, defect-free particles. Approach [133–135] based on the thermolysis of SSP of metal alkylxanthate type (dithiocarbamates, trithiocarbonates, dithiophosphates) in the medium
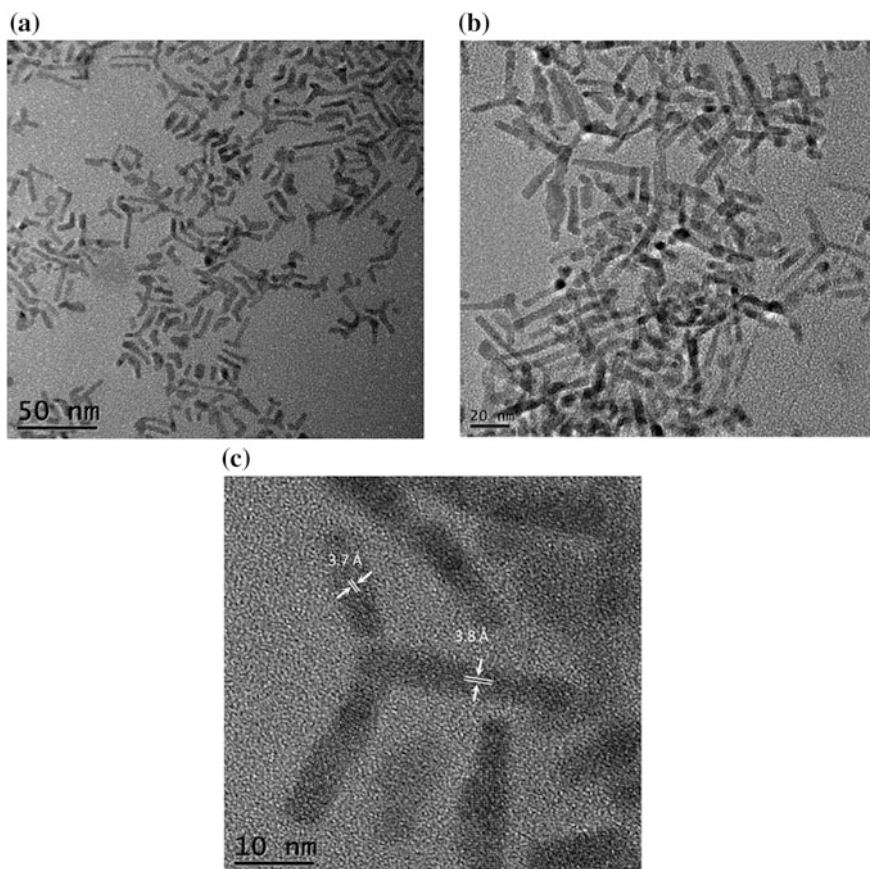
Fig. 8.6 TEM (**a**, **b**) and HRTEM (**c**) CdS nanoparticles images obtained by thermolysis of Cd (pip-dtc)$_2$ at temperatures 140 (**a**) and 180 °C (**b**, **c**) in HDA

of Lewis base performing a function of a thermal decomposition promoter and a stabilizing agent at a time, at moderate temperatures (120–150 °C) can be regarded as sufficient general method of nanoparticle synthesis for a wide range of metal chalcogenides (Cd, Zn, Pb, Hg, Cu, Ni, Mn, etc.), including nano-objects with the core-shell structure. It is expected that the thermal decomposition of cadmium dixanthate can proceeded through the concert mechanism of the shift of three electron pairs under the catalytic effect of the solvent. In this case, the solvent can activate O–C–S$_2$Cd group shifting the charge density from C–S bond to S–C bond according to scheme A (Fig. 8.7). In addition, the Lewis base as protonated intermediate may facilitate proton transfer required for the reaction (scheme B) and, finally, be a stabilizing ligand, reducing at least one of Cd–S bonds in dixantate, thereby promoting the CdS formation (scheme C).

Experimental results [136] indicate that the ligand role in the reaction system is important not only for formed nanocrystals and starting precursor molecules.
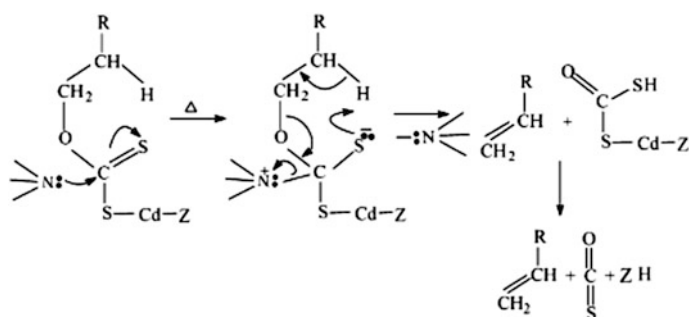
(A) Nucleophilic attack on the (thio) carbonyl center
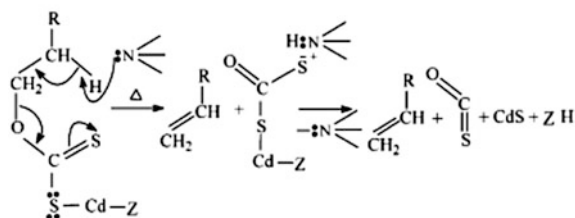
(B) Protonated intermediates
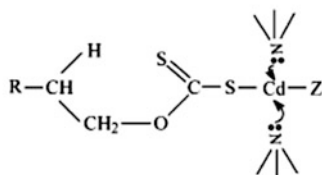
(C) Ligand stabilization of the metal center

Fig. 8.7 Possible ways of decomposition of metal chelate Cd(II) dixantate with a Lewis base Z=R–O–C(=S)–S

Rigidly-bound ligand with the monomer molecule determines primarily nucleation process, while strong ligands on the nanocrystal surface are crucial for the growth stage. Generally, it can be monitored the morphology and form of the obtained nanoparticles, as well as their phase composition. For ZnS thermodynamically stable sphalerite structure with a zig-zag conformation in the direction <111> and kinetically stable wurtzite structure with hindered conformation in the direction <002> is characteristic. The differences in the steric effect and coordinating capacity between HDA and TOP determine the diversity of their binding character. TOP is relatively strong ligand for the monomer precursor, i.e. it forms stable complexes. Therefore, nucleation proceeds slow and complexes have time to adapt advantageously, and steric hindrance between them and the ZnS lattice during growth is minimized. The staggered conformation is preferred in TOP, and the resulting ZnS has sphalerite structure [132, 137]. Due to the high symmetry of the structure spherical shape particles are formed predominantly, despite the monomer high concentration. Because the HDA is a weak ligand for the monomer and strong for zinc sulfide nanocrystals the nucleation occurs rapidly in alkylamine solution, and the resulting nanocrystals are associated with HDA molecules. Due to the absence of steric hindrances the clusters are connected to each other to form a wurtzite structure with the particle shape in the form of elongated rods.

It should be emphasized that SSP rational design, the appropriate choice of the ligands or substituents on metal atoms allows synthesis of nanostructured materials under milder conditions that successfully demonstrated for the nanocrystals based on many transition metals and their oxides, as well as main group elements [138–140].

8.2.1.3   Temperature Influence

It is known that the nanorod aspect ratio decreases with temperature increasing [141], i.e., at high nanoparticle synthesis temperatures, growth thermodynamic regime is preferred, which is reflected in the formation of isotropic particles (spherical or cubic), while at lower temperatures, a nonequilibrium kinetic regime promotes the formation of anisotropic particles [142]. CdS nanoparticles, obtained by [Cd(pip-dtc)$_2$Py] thermolysis at 190 °C had rod form with a length of 64.38 ± 4.62 nm and a width of 5.20 ± 0.98 nm with an aspect ratio of 12.38 (Fig. 8.8) [62]. At 230 °C nanorods had a size of 24.84 ± 4.42 nm in length and 6.58 ± 1.02 nm in width, whereas at 270 °C oval shape nanoparticles with a diameter of 16.8–23.3 nm along with rod shape nanoparticles are formed.

Nanoparticle synthesis temperature plays an important role in the structural-phase transformations. For example, for CdS nanoparticles it is demonstrated that the hexagonal phase is the predominant phase at high synthesis temperatures [143, 144]. During CdS nanoparticle preparation by thermolysis of Cd(pip-dtc)$_2$ in castor oil at 190, 230, 270 and 300 °C hexagonal phase c reflexes (100), (002), (101), (110) (103) and (112) in the diffractograms was formed at all temperatures, while during the Cd (thq-dtc)$_2$ thermolysis at 190 and 230 °C metastable cubic phase was observed, and thermodynamically stable hexagonal phase was observed at 270 and 300 °C [145].
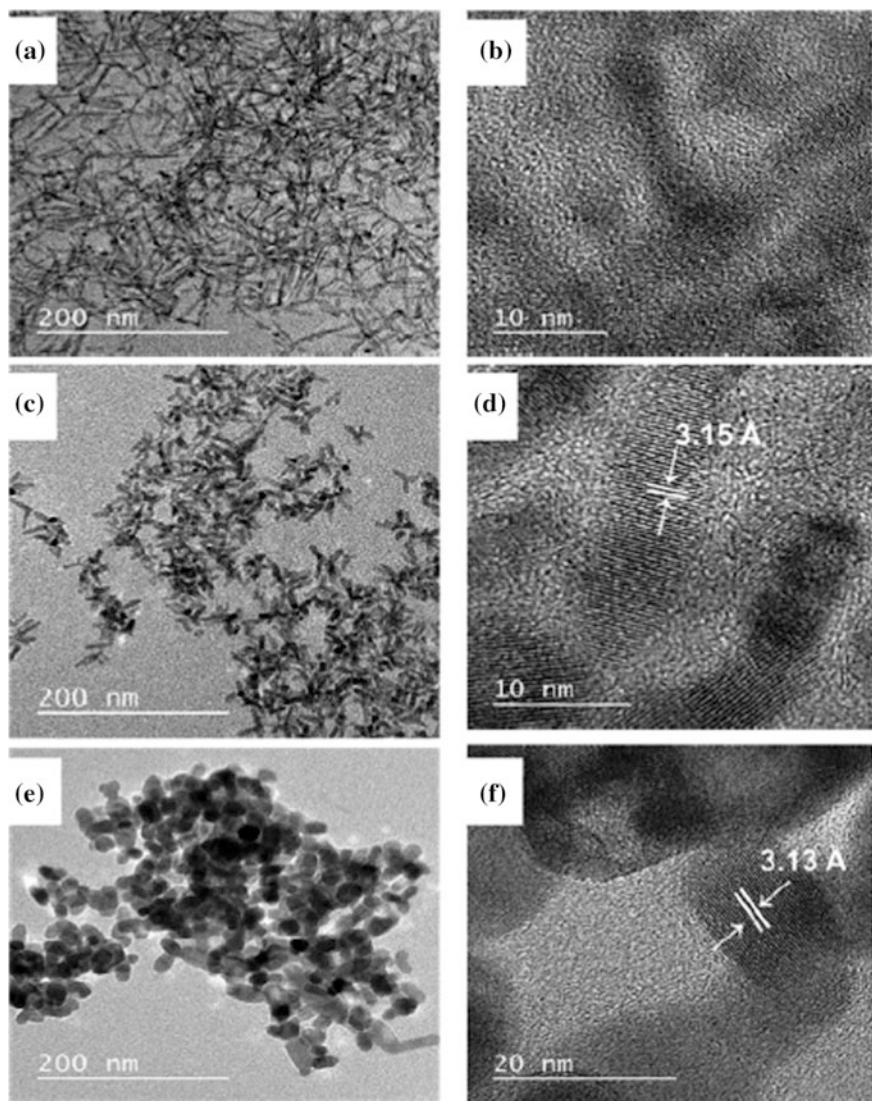
Fig. 8.8 Electron micrographs of CdS nanoparticles obtained by thermolysis of [Cd(pip-dtc)$_2$Py] at temperatures of 190 (**a**, **b**), 230 (**c**, **d**) and 270 °C (**e**, **f**)

In contrast, thermolysis of these complexes in the ricinoleic acid at all temperatures leads to the cubic phase formation. It should be noted that the occurrence of CdS metastable cubic phase also shows the demonstration of the quantum confinement effect, because the cubic phase is characterized only for CdS nanocrystal unlike the hexagonal form which occurs in both nanocrystalline and the bulk material [146]. The wide variation in morphology (Fig. 8.9) and the phase composition of thin films of iron sulfide from dithiocarbamate Fe(III) complexes is observed when the
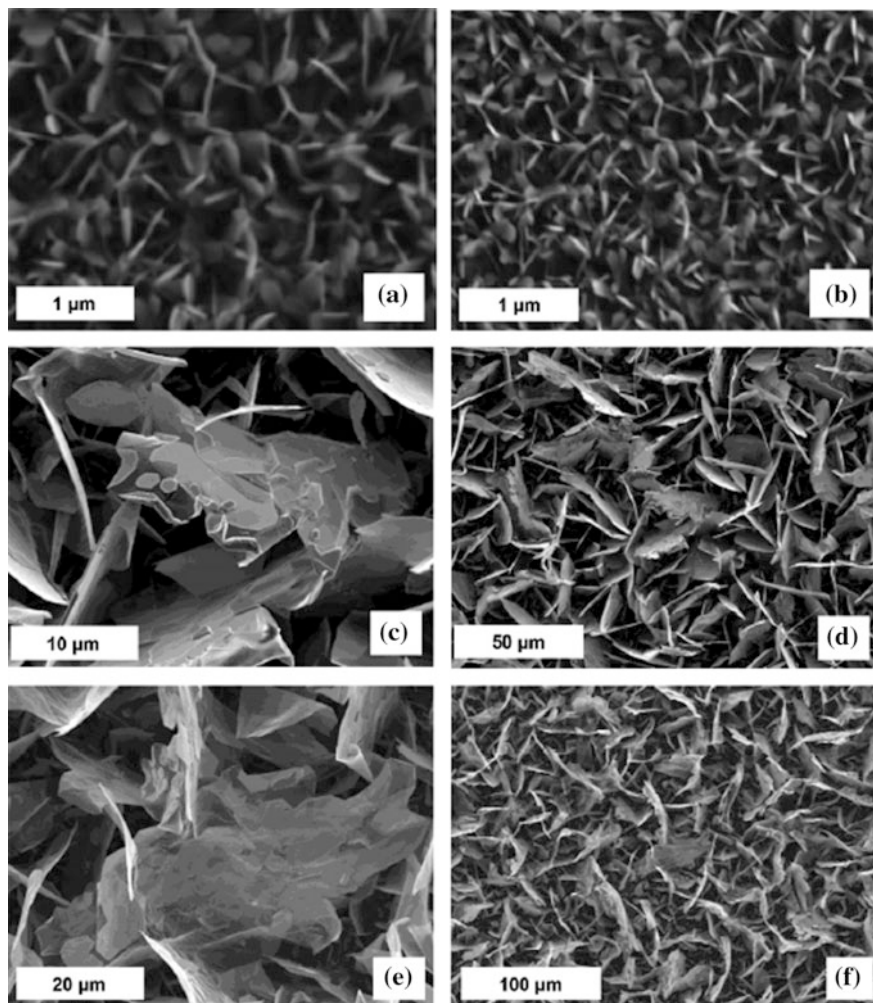
Fig. 8.9 SEM images of the iron sulfide thin films deposited at 350 °C (**a**, **b**), 400 °C (**c**, **d**) and 450 °C (**e**, **f**) using complex Fe(pip-dtc)$_3$

conditions change during Aerosol Assisted Chemical vapor deposition (AACVD), e.g. temperature, the precursor nature, the solvent type (Table 8.1) [114].

Crystal packing defects, particle sizes, etc. can also act as determining factors [147]. For CdS hexagonal wurtzite structure is characterized by particles with a diameter >5 nm, while the nanoparticles with very small size ($\sim$3 nm) have a cubic sfarelite structure.

By varying the reaction conditions, it can be generally activated two mechanism of nanoparticle formation, i.e. with the dominance of the growth process and processes due to nucleation, when it can be temperature-dependent control of

Table 8.1 The morphology and phase composition of the iron sulfide thin films obtained at different reaction conditions

Precursor	Conditions	Morphology	Phase composition
Fe (pip-dtc)$_3$	Toluene, 350–450 °C, 2 h	Leaf, flake, sheet	Hexagonal (Fe$_{0.975}$S), marcasite (FeS$_2$)
	Chloroform, 350–450 °C, 30 min	Fiber	Hexagonal (Fe$_{0.975}$S), smythite (Fe$_3$S$_4$)
	tert-Butyl thiol, 450 °C, 2 h	Flower, spherical-globular	Greigite (Fe$_3$S$_4$)
Fe (thq-dtc)$_3$	Toluene, 350–450 °C, 2 h	Leaf, flake, sheet	Pyrrhotite (Fe$_{0.95}$S$_{1.05}$), hexagonal (Fe$_{0.975}$S)
	Chloroform, 350–450 °C, 30 min	Fiber	Hexagonal (Fe$_{0.975}$S)
	tert-Butyl thiol, 450 °C, 2 h	Spherical and flake	Greigite (Fe$_3$S$_4$)

nanoparticle sizes. Such examples are numerous. CuS nanoparticles were obtained by Cu(II) butylaminodithiocarbamate thermolysis at two different temperatures in a typical TOP and HDA medium [148]. Nanoparticle dimensions were 3–7 nm and 21–38 nm at synthesis temperatures of 120 and 180 °C, respectively, and the product is also characterized by a narrow particle size distribution in the first case. The band gap exceeds that value for the bulk semiconductor and was 4.33 and 3.98 eV for the products obtained at 180 and 120 °C, respectively.

Thus, chalcogenide metal chelates are effective precursors for the preparation of the nanocomposites, stabilized against further aggregation by thermolysis products of complexes ligand shell (Table 8.2).

8.2.2 Controlled Thermolysis of Azomethine Transition Metal Chelates

To date, considerable experimental material on thermolysis of azomethine transition metal chelates has been prepared. Among the most typical examples we note the synthesis of cubic Co$_3$O$_4$ nanoparticles by thermolysis of chelate [Co^{II}{(μ-L)(μ-OAc)Co^{III}(NCS)}$_2$], where H$_2$L is salen type ligand 1,6-bis(2-hydroxyphenyl)-2,5-diazahexa-1,5-diene, as precursor [149]. It is important that thermolysis of the chelate at 600 °C in the presence of citric acid leads to the formation of Co$_3$O$_4$ nanoparticles with the average crystallite size of ∼13 nm. In another example the thermolysis of praseodymium chelate ([PrL(NO$_3$)$_2$]NO$_3$, where L is N,N′-bis(2′-hydroxyacetophenonimine)-*o*-dipropylene triamine) was studied at different temperatures of 300–800 °C [150]. In this case, praseodymium oxide with small grain size, very uniform sphere-like shape and pure cubic phase is the main product of the thermolysis at 600 °C.

Table 8.2 Chalcogenide metal chelates as SSP of the nanostructured materials

SSP	Chelating ligand	Thermolysis conditions	Phase composition, nanoparticle shape and dimensions	References
[Sb{Se–C$_5$H$_3$(Me)N}$_3$]·1.5H$_2$O	(R = H or Me)	200 °C, HDA, CH$_2$Cl$_2$, hot injection; 400–450 °C, argon 375–500 °C (AACVD)	Sb$_2$Se$_3$, rods, width 40–60 nm, length 0.6–1.4 μm; thin film (Sb$_2$Se$_3$, nano-wires, 240–500 nm)	[65]
[Bi{Se–C$_5$H$_3$(Me)N}$_3$]·0.5H$_2$O	(R = H or Me)	235 °C, HDA, CH$_2$Cl$_2$, hot injection; 400–450 °C, argon 375–500 °C (AACVD)	Bi$_2$Se$_3$, flake, width 30 nm, length ~760 nm; thin film (Bi$_3$Se$_4$, boat/half hexagon—petals, sheets, hazy wool-like)	[65]
Cd(pip-dtc)$_2$		350–450 °C (AACVD)	CdS, thin film, 57.37 nm (350 °C), 63.57 nm (400 °C), 72.97 nm (450 °C)	[61]
Cd(thq-dtc)$_2$		350–450 °C (AACVD)	CdS, thin film, 160–220 nm, cubic to spherical	[61]
[Cd(thq-dtc)$_2$(phen)]		Diethylenetriamine, 199 °C, 2 min	CdS nanorods ca. 7 nm, length 50–75 nm	[57]
Metal alkyl xanthates M=Cd, Zn, Pb, Hg, Cu, Ni, Mn	R–O–C(=S)–S⁻K⁺, R = ethyl, decyl, hexadecyl	HDA, decylamine, trioctylamine, 120–140 °C	CdS, ZnS (4.5 nm), spherical. CdS rods (5 nm width, 20 nm length), CdS/ZnS, CuS, NiS, MnS (spherical, rods), PbS and HgS (r.t., decylamine)	[133]
Metal hexadecyldithiocarbamate M=Cd, Zn, Pb, Hg, Cu, Ni, Mn	C$_{16}$H$_{33}$–NH–C(=S)–S⁻K⁺	HDA, 170–200 °C	CdS, ZnS (spherical), ZnS/CdS (70–170 °C)	[133]

(continued)

Table 8.2 (continued)

SSP	Chelating ligand	Thermolysis conditions	Phase composition, nanoparticle shape and dimensions	References
Metal hexadecyltrithiocarbamate M=Cd, Zn, Pb, Hg, Cu, Ni, Mn	$C_{16}H_{33}$—S—C(=S)—S^-K^+	HDA, 180–200 °C	CdS (5 nm)	[133]
[Cd(pip-dtc)$_2$Py]		HDA, TOP, 190 °C; thin films, chloroform, (AACVD, 350, 400, 450 °C)	CdS, rods, 64.38 ± 4.62 nm length, 5.20 ± 0.98 nm width (190 °C), 24.84 ± 4.42 nm length, 6.58 ± 1.02 nm breadth (230 °C), oval, 16.8–23.3 nm; CdS, thin film	[62]
Cd[S(L)]$_2$, L = 2-(4,4-dimethyl-2-oxazolinyl) benzene]		TOP, TOPO, 280 °C	CdS, hexagonal phase, 200 nm	[129]
Cd[Se(L)]$_2$, L = 2-(4,4-dimethyl-2-oxazolinyl) benzene]		TOP, TOPO, 280 °C	CdSe, hexagonal phase, 200 nm	[129]
Cd(pip-dtc)$_2$		TOP, HDA, 180 °C	CdS, rods, bipods, tripods (19.11 ± 7.29 nm length, 3.64 ± 0.78 breadth)	[128]
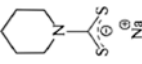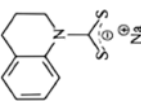
(continued)

Table 8.2 (continued)

SSP	Chelating ligand	Thermolysis conditions	Phase composition, nanoparticle shape and dimensions	References
Cd(thq-dtc)$_2$		TOP, HDA, 180 °C	CdS, rods, bipods (21.61 ± 6.08 nm length, 4.55 ± 1.04 breadth)	[128]
Cd(pip-dtc)$_2$		TOP/TOPO, 240 °C	CdS, spheres, 3.97 ± 0.69 nm, 4.33 ± 0.59 nm	[128]
Cd(thq-dtc)$_2$		Castor oil, ricinoleic acid, 190–300 °C, N$_2$, 30 min–2 h	CdS (castor oil), spherical, short rods and oval, 15.53 ± 3.18 nm (230 °C), 15.6 ± 3.74 nm (270 °C), 17.96 ± 1.95 nm (300 °C); CdS (ricinoleic acid) 21.12 ± 3.57 nm (270 °C), 22.67 ± 3.58 nm (300 °C)	[139]
Cd(thq-dtc)$_2$		Castor oil, ricinoleic acid, 190–300 °C, N$_2$, 30 min–2 h	CdS, oval rod, 13.36 ± 1.82 nm (270 °C), spherical 15.7 ± 1.73 nm (300 °C)	[139]
Cd(II) butyl amine dithiocarbamate	butyl amine dithiocarbamate sodium salt	TOP, HDA, 180–120 °C, 60 min, N$_2$	CuS, spherical, 15.8 nm (180 °C), 6.61 nm (120 °C)	[150]
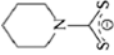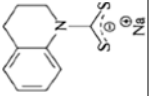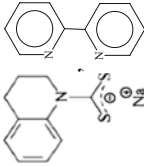
(continued)

Table 8.2 (continued)

SSP	Chelating ligand	Thermolysis conditions	Phase composition, nanoparticle shape and dimensions	References
Zn(Se$_2$CNEt$_2$)$_2$	diethyldiselenocarbamate diethyl ammonium salt	Pyrolysis GC-MS, 280 °C	Se$_n$, n ~ 1 ± 7, ZnSe	[123]
Cd(Se$_2$CNEt$_2$)$_2$	diethyldiselenocarbamate diethyl ammonium salt	Pyrolysis GC-MS, 280 °C	Se$_n$, n ~ 1 ± 7, CdSe	[123]
Zn(Se$_2$CNMe^{n}Hex)$_2$, bis [methyl(n-hexyl)-diselenocarbamato]-zinc	methyl(n-hexyl)-diselenocarbamate	Pyrolysis GC-MS, 280 °C	ZnSe	[123]
Cd(Se$_2$CNMe^{n}Hex)$_2$	methyl(n-hexyl)-diselenocarbamate	Pyrolysis GC-MS, 280 °C	CdSe	[123]
Fe(pip-dtc)$_3$		AACVD, chloroform, toluene, 350–450 °C	Fe$_{0.975}$S, FeS$_2$ (350, 400 °C), FeS, hexagonal-phase (450 °C); sheet-like (350 °C), nano-leaf/flake like (400, 450 °C)	[122]
Fe(thq-dtc)$_3$		AACVD, chloroform, toluene, 350–450 °C	FeS, hexagonal (350, 400 °C), nanosheet-like; Fe$_{0.95}$S$_{1.05}$, hexagonal-pyrrhotite (450 °C)	[122]
[PdCl$_2$(PhS–CH$_2$CH$_2$CH$_2$–NH$_2$)]	3-(phenylsulphanyl) propylamine	Oleylamine, oleic acid: octadecene (1:1), 195 °C	Pd$_4$S, nanoflowers, ~23–38 nm (oleylamine); nanospheres, 15–28 nm (oleic acid: octadecene)	[124]

(continued)

Table 8.2 (continued)

SSP	Chelating ligand	Thermolysis conditions	Phase composition, nanoparticle shape and dimensions	References
Zn(pip-dtc)$_2$		HDA, TOP, TOPO, 180, 270 °C	ZnS, spherical to elongated), 4.74 ± 0.64 nm (180 °C), 6.43 ± 0.60 nm (270 °C)	[121]
Zn(thq-dtc)$_2$		HDA, TOP, TOPO, 180, 270 °C	ZnS, spherical, 5.94 ± 0.25 nm (270 °C)	[121]
Zn(thq-dtc)$_2$(bpy)		Triethylenetetraamine, 299 °C, solvothermal method	ZnS nanosheets, 75–225 width, 90–375 nm length	[6]

Thermolysis of nickel salen chelate at temperature 700 K in the absence of any template or surfactant leads to uniform NiO particles [151].

Also, metal N,O-containing chelates can be used for obtaining doped nanoparticles. For example, the thermolysis of an unusual square pyramid Mn(III) chelate, $[Mn(L)(H_2L)]PF_6$, where L is (5,5′-dimethoxy-2,2′-(propane-1,2-diyl-bis (nitrilomethylidyne))diphenolato), results in Mn-doped ZnO nanoparticles [152].

It should be noted the Ni(II) complexes $[Ni(L)_2](ClO_4)_2$ and $[Ni(L)_2(NO_3)_2]$, where L is the Schiff base 4,5,9,13,14-pentaaza-benzo[b]triphenylene, which were used for obtaining NiO nanoparticles by calcination at 500 °C [153]. Complexes of various Schiff bases and related ligands can also be precursors for nanoparticles of oxides of copper and other metals. Thus, a symmetric tetradentate Schiff base ligand, N,N′-bis(5-bromosalicylaldehyde)-1,3-phenylenediamine (L), and its Cu(II) and Co(II) chelates with general formula $M_2(L)_2$, where M=Co or Cu, were used as precursors for corresponding metal oxide nanoparticles [154]. Preparation of single phases of CuO, CoO, and NiO nanoparticles using Cu(II), Co(II), and Ni(II) chelates $\{[Cu(H_2L)(H_2O)_2(Cl)]Cl$, $[Co(H_2L)(H_2O)_3]Cl_2 \cdot 3H_2O$ and $[Ni(H_2L)(H_2O)_2]$ $Cl_2 \cdot 6H_2O\}$, where H_2L is 2-[(5-*o*-chlorophenylazo-2-hydroxybenzylidene)amino] phenol Schiff base, as precursors by a solid-state thermolysis was carried out [155].

In recent years, special attentions is paid to the synthesis of new bi- and tridentate azomethine ligands with oxygen-, nitrogen-, sulfur-containing chelating fragments and their metal chelates [156–159]. The possibility of a wide variation of heteroligand environment in such chelates (Fig. 8.10), their high thermal and chemical stability, relatively simple synthetic schemes and the availability of the starting reagents allow considering such metal chelates as promising precursor for the preparation of metal-polymer nanocomposites in which the specific polymer (oligomer) shell is formed from ligand degradation products.

Thermolysis (370 and 600 °C) of metal chelates of this type in the condensed phase, apparently, is a multi-step process, the total scheme of which can be represented as follows (Scheme 8.4) [160].

The thermal behavior of azomethine metal chelates is defined as the metal nature, the composition and structure of framing functional ligands and the metal-ligand bond nature, and, in general, stability of the metal chelate.

8.2.2.1   Nickel(II) Chelates

Thermal characteristics of mononuclear nickel chelates **Ni1–Ni4** are shown in Table 8.3 [161]. Of interesting is thermal behavior of nickel chelate **Ni4**: up to 390 °C the weight increase is observed by 3.6%, due, apparently, to the oxidation process, then at 450 °C a dramatic weight drop proceeds up to 31%, than this process slows down, and at 800 °C the weight loss is 43%. The melting peak is recorded on the DSC at 365.2 °C. As can be seen from the obtained data, the thermal stability of nickel azomethine chelates depends on the ligand type. The melting point is maximum for **Ni4**, decomposition beginning temperature increases in the series of chelates **Ni3 < Ni2 < Ni1 < Ni4**, and weight loss at 800 °C is
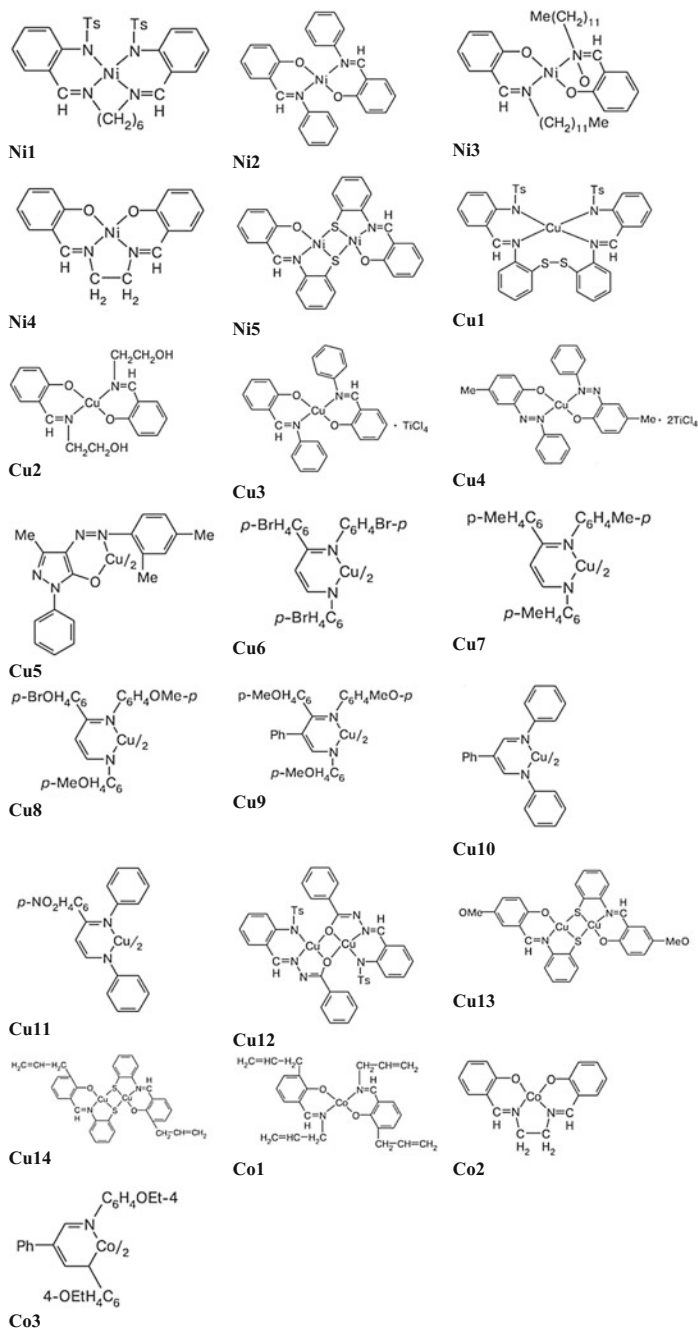
Fig. 8.10 Structures of azomethine metal chelates

Scheme 8.4 Thermolysis of
azomethine metal chelates

$$M - Cu, Co, Ni$$
$$X - O, NTs$$
$$Ts - SO_2C_6H_3Me$$
$$R - C_2H_5, C_6H_5, C_{10}H_7$$
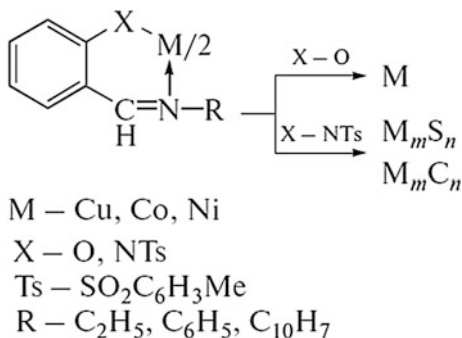
Table 8.3 Thermal properties of azomethine chelates [157–159]

Chelate	Temperature (°C)				Weight loss in full decomposition (%)
	Melting	Decomposition onset	Decomposition at 50%	Decomposition end	
Ni1	—[a]	350	390	750	70.8
Ni2	—[a]	225	435	740	62.5
Ni3	92.8	320	390	550	79.9
Ni4	365.2	380	–	780	35.7
Cu1	225	270	–	760	40.4
Cu2	177	190	292	700	67.8
Cu3	110	325	–	680	45.8
Cu4	140	100	–	700	47.4
Cu5	245	260	422	660	60.2
Cu6	–	285	720	780	53.3
Cu7	–	265	780	790	50.1
Cu8	–	200	–	730	46.0
Cu9	286	200	402	620	68.9
Cu10	318.3	330	375	730	84.6
Cu11	–	210	–	740	37.0
Co1	138.1	323	–	560	48.8
Co2	351.9	355	–	730	35.2
Co3	191	220	–	700	42.7

[a]Prior to the decomposition onset the melting is not observed

minimum for **Ni4** chelate. In other words, metal chelates of tetradentate azomethine ligands **Ni1** and **Ni4** are significantly more stable than metal chelates based on bidentate azomethine ligands, and introduction of allyl fragments in aldehyde and amine moieties leads to significant reduction in the melting point.

8.2.2.2   Copper(II) Chelates

As in the case of nickel chelates, the chelate **Cu1** based on tetradentate azomethine ligand has a higher melting point. Introduction of alcohol fragments in the amine moiety in **Cu2** chelate lowers the melting point, as well as introduction of alkyl substituents. The chelates **Cu3** and **Cu4** are less stable and already begin to melt at 110 and 140 °C, respectively (see Table 8.3). In the case of chelates **Cu6–Cu9** and **Cu11** introduction of Me- and OMe-groups in the phenyl ring lowers the melting point from 222 to 191 °C. For chelates **Cu9** and **Cu10** introduction of alkoxy (OMe) groups in the benzene rings of the amine fragments also causes a decrease in melting point compared with unsubstituted analogues. Except chelates **Cu9** and **Cu10**, copper complexes are more thermostable than nickel complexes: for them weight loss at 500 °C as determined by thermal analysis is not more than 50 wt% (Fig. 8.11) [158, 162].

8.2.2.3   Cobalt(II) Chelates

Cobalt chelate **Co1** is stable substance up to 200 °C, the weight loss occurs in two steps: up to 310 °C (21.8%), then the process slows down and the total weight loss as a result of thermolysis up to 800 °C is 48.8%. Melting peak according to DSC data corresponds to 138.1 °C with heat absorption of 50.67 J g^{-1}, and at 323.2 °C the exothermal process with heat of 258 J g^{-1} is observed. Above 550 °C the chelate decomposes. Of the analyzed cobalt chelates **Co2** is most stable: its melting point is 351.9 °C, and the weight loss during thermolysis up to 800 °C is only 35.2% (see Table 8.3). As in the case of nickel chelates, the introduction of the allyl

Fig. 8.11 TGA data for azomethine copper(II) chelates
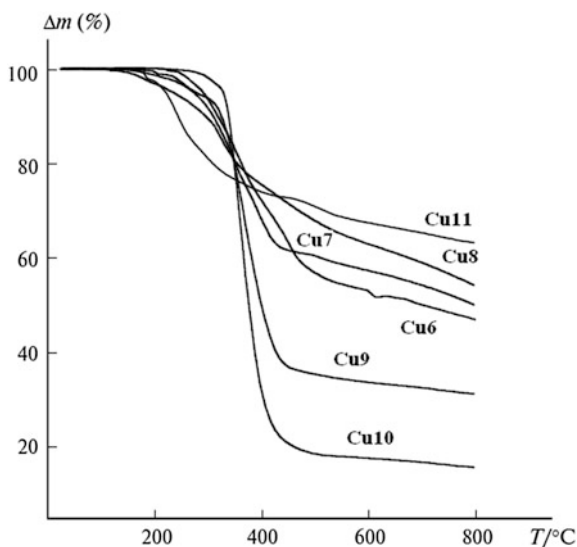
substituents compared with the aryl substituents lowers the melting point. Chelate **Co2** based on salen tetradentate ligand has a significantly higher melting point (>300 °C) as compared with chelates of bidentate ligands.

8.2.2.4 Composition and Structure of Thermolysis Products of Azomethine Metal Chelates

Solid phase products of the thermolysis are matrix-stabilized metal nanoparticles which are homogeneously distributed in size and in the space of a matrix. We note that the chelating ligand nature and consequently formed stabilizing matrix on their basis has a significant influence on the sizes of obtained nanoparticles and the character of their size distribution, as exemplified by the thermolysis products of binuclear copper(II) chelates **Cu12** and **Cu13** (Fig. 8.12) [158]. The size of cobalt nanoparticles in the thermolysis product of **Co2** (T = 600 °C), estimated by the Scherrer equation was ∼15 nm.

For different metal chelates the formation of self-organized nanocomposites based on crystalline cobalt sulfide clusters Co_9S_8 (thermolysis at 593 K) and Co_6S_5 (thermolysis at 873 K), Ni_3S_2 and NiC, nanocrystalline copper with structure core-shell, where a nanocrystalline core of 2–3 nm particles collected in aggregates of 10–20 nm and even larger, and shell is formed from the ligand degradation products [157].
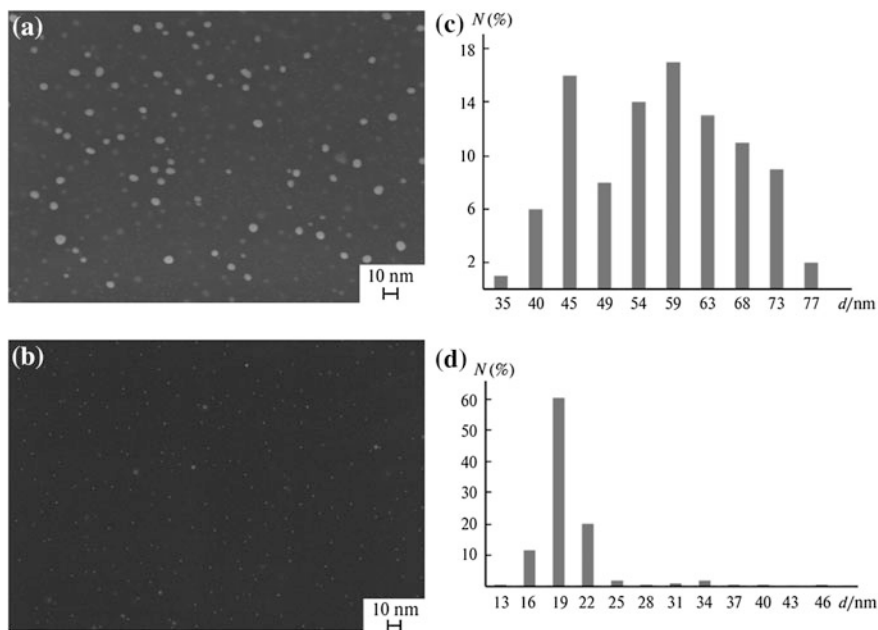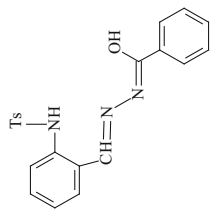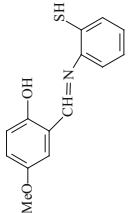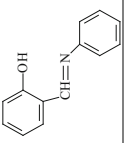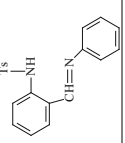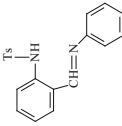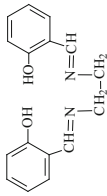
Fig. 8.12 SEM images (**a**, **b**) and hystograms showing the size distribution of nanoparticles (**c**, **d**) for the thermolysis products (600 °C) of Cu chelates Cu12 (**a**, **c**) and Cu13 (**b**, **d**)

Table 8.4 Azomethine metal chelates as SSP of the nanostructured materials

SSP	Chelating ligand	Thermolysis conditions	Phase composition, nanoparticle shape and sizes	References
Bis[(2-N-tosylaminobenzylidene) benzoylhydrazonato]dicopper(II)		Solid phase thermolysis, SGA, 600 °C	Cu, 40–70 nm	[160]
Bis[(2-hydroxy-5-methoxybenzylidene)-2'-mercaptophenyliminato] dicopper(II)		Solid phase thermolysis, SGA, 600 °C	Cu, 20 nm	[160]
Bis[(2-hydroxybenzylidene) phenyliminato]copper(II)		Solid phase thermolysis, SGA, 600 °C	Cu	[159]
Bis[(2-N-tosylaminobenzylidene) phenyliminato]cobalt(II)		Solid phase thermolysis, SGA, 320, 600 °C	Co_9S_8 (320 °C); Co_6S_5 (600 °C)	[159]

(continued)

Table 8.4 (continued)

SSP	Chelating ligand	Thermolysis conditions	Phase composition, nanoparticle shape and sizes	References
Bis[(2-N-tosylaminobenzylidene) phenyliminato]nickel(II)		Solid phase thermolysis, SGA, 600 °C	Ni$_3$S$_2$, NiC	[159]
N,N′-Bis[(2-hydroxybenzylidene)-1,2-diaminoethane]cobalt(II)		Solid phase thermolysis, SGA, 600 °C	Co, ∼ 15 nm	[160]

Thus, transition metal chelates based on Schiff bases are effective precursors for self-assembled nanocomposites stabilized against further aggregation by thermolysis products of chelate ligand shell. Thermolysis optimization of these chelates (Table 8.4), the possibility of the formation of alloys based on complexes with various metals, along with the identification of the thermolysis mechanism and detailed characteristic of the properties of emerging products will promote further research into the development of advanced nanocomposite materials.

8.2.3 Metal Chelate Thermolysis in Polymer Matrix

The incorporation of metal-containing precursors into a polymer matrix is a broad area of current research [8]. In this case there are two possibilities. The ex situ (in a second moment) process involves adding and mixing micro- or nanoparticles of the inorganic precursor to the finished polymer. At the same time, in the in situ method the initial nanoparticles are generated directly in the polymer matrix using, for example, polymeric metal chelates and their subsequent decomposition.

We emphasize the important fact connected with the processes of the thermolysis of the precursors with relatively bulky organic ligands. For example, under inert atmosphere, ruthenium-carbon composites with a ruthenium content of 20–32% (wt.) are formed from the ruthenium chelates $[RuL_3]X_2$, where L is bpy, phen; X is OH^-, Cl^- [163]. This is a result of a multi-stage destruction process of the organic ligand. At a temperature of 873 K intensive complex decomposition is completed with evolution of its fragments (pyridine and dipyridyl molecular ions). Further there is the destruction of the resulting condensed material to evolve light hydrocarbon fragments. The Ru-containing composites obtained at 873–973 K have high specific surface area of 424–477 $m^2 \ g^{-1}$, and ruthenium clusters are practically amorphous to X-rays. Superfine (d $\sim$ 1.5–2.0 nm) and relatively uniform size ruthenium particles in the Ru/C composite are in the form of planar Ru_6 hexagon associates. During thermolysis enveloping layers of turbostratic graphite-like carbon are formed by carbonization of organic ligand. In parallel-oriented turbostratic carbon layers with an interplanar distance of $\sim$ 0.34 nm are tightly pressed to ruthenium particles, preventing them from sintering under the drastic pyrolysis conditions (973 K). Thus, the structure of the resulting composite can be represented as a set of spheres (coils), the center of which is a ruthenium nanoparticle («core»), and the outer shell is lined with layers of turbostratic carbon («shell»).

Gold(I) dodecylthiolate as a precursor for the formation of nano-sized particles in a PS matrix was prepared according to the scheme [164, 165]:

$$HAuCl_4 + 3HSC_{12}H_{25} \rightarrow AuSC_{12}H_{25} + H_{25}C_{12}S-SC_{12}H_{25} + 4HCl$$
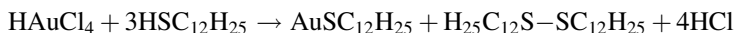
A thin (0.1–0.3 nm) transparent film was obtained by the addition of the precursor (5–10%) to the PS matrix (M_w is 230,000) with intensive sonication and solvation in acetone, and followed casting on a glass surface [165]. This film placed

between sheets of aluminum foil was subjected to short-term (40–105 s) thermolysis at 573 K. Gold nano-sized particles were formed according to the possible scheme:

$$2AuSC_{12}H_{25} \rightarrow 2Au^{\circ} + H_{25}C_{12}S-SC_{12}H_{25}.$$
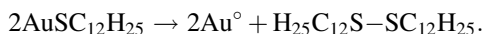
However it is not ruled out the emergence of polynuclear complexes of the type —(–Au^{1}SR–)$_n$– with their further transformation to nanocrystals. As a result, polydisperse gold nanoparticles with a size of 1.8 nm (about 150 gold atoms), homogeneously distributed in the PS matrix were formed. Decomposition of Sb $(SC_{12}H_{25})_3$ in PS at 623 K results in the formation of Sb and Sb_2S_3 nanoclusters (15–30 nm) homogeneously distributed in the amorphous polymeric phase [166]. Thermolysis of metal dithiolates to form sulfide semiconductors in thin films was successfully carried out [167] under the action of laser radiation (or electron beam): the laser beam is defocused in a small beam diameter of 4 mm, which is concentrated a 2 kW power, and pulsing of 10–50 ms. Temperature in thin beam theoretically calculated from the parameters of the polymer and beam, and can be monitored. Thermolysis of thin films of the $Pd(SC_{12}H_{25})$/PS is performed for 5 min at 443 K [168], but in air the formation of metal oxides in the polymeric matrix can occur (to prevent this process TOPO is used as the stabilizing antioxidant, for example, for CdS, ZnS, CdSe with size 2–4 nm, introduced ex situ [169]). Indeed, the thermolysis of the iron(II) mercaptide system $Fe(SC_{12}H_{25})_2$/PS at 473 K for 2 min is accompanied by the formation of completely transparent light-brown film (almost complete light transmittance above 550 nm), in which nanoparticles with an average size of 10 × 50 nm are uniformly distributed [170]. Thermolysis of Pb (II) dithiocarbamate or xanthate in a PS matrix ($M_w \sim$ 280,000) was carried out as a model system of the process of forming the polymer-nanoparticle hybrid layers in photovoltaic devices [171]. Chalcogenide complexes are most appropriate precursors for the preparation of such materials in situ. As noted earlier, they are quite stable compounds, do not decompose under the ordinary temperature conditions, stable in air and to moisture. As a rule, they are soluble in many organic solvents, and can thermally decompose at relatively low temperatures, i.e., thereby preventing undesirable degradation of the polymer matrix. By sufficiently technologically simple scheme consisting of spin coating of the polymer solution and the chelate precursor ($Pb(S_2COBu)_2$, $Pb(S_2COHex)_2$, $Pb(S_2COOct)_2$, $Pb(S_2CNBu_2)_2$, $Pb(S_2CNBu_2)_2$(phen)) on a substrate followed by heating the polymer film PbS nanoparticles in PS matrix were obtained. By varying the synthesis conditions, it is possible to obtain nanoparticles with different morphologies including PbS nanowires, which is of particular interest for photovoltaic applications. Similarly, by thermolysis in situ CdS nanoparticles in PVA matrix were synthesized using metal thiolate [172] or thiourea in aqueous Cd(II) solution [173] as a precursor.

The systems of M(acac)$_n$—polymer matrix are widespread. In this case, M(acac)$_n$ thermolyzes to form nanoparticles and interacts with the matrix, initiating its destruction and depolymerization. In this regard, the thermal decomposition of Co(acac)$_3$—PMMA system is indicative (Scheme 8.5) [174, 175].

Scheme 8.5 Mechanism of the thermal destruction in the system of PMMA-Co(acac)$_3$

Table 8.5 Thermal stability of PMMA and its complexes with Mn(acac)$_3$ [175]

Polymer	The number of monomer units per Mn(acac)$_3$ molecule	T_d, K	T_{max}, K
High-molecular-weight PMMA	See[a]	483	623
	50	403	638
	10	398	673
Low-molecular-weight PMMA	See[a]	493	633
	50	403	638
	10	403	673

[a]Neat polymer

Thermolysis of Mn(acac)$_3$ in PMMA proceeds in a similar manner and the major process proceeds at higher temperatures that for pure PMMA (Table 8.5).

It should be noted that the thermolysis of Rh(acac)$_3$ in the presence of polyols as reducing agents leads to the formation of rhodium nano-sized crystals with various shapes (for example, multipods, cubes, horns, cuboctedra) [176]. More promising approach to the production of such nano-sized particles (size 5 ± 15 nm) consists of one-stage reduction of the rhodium chelate Rh(acac)$_3$ in the presence of butane-1,4-diol and PVp (M$_w$ = 55,000) at temperatures of 240 ± 300 K [177]. This process results in triangular, pentagonal and hexagonal particles, capable to form Langmuir-Blodgett films on the silicon surface.

It is important that thermolysis of analyzed systems is multi-step process and is usually developing in two main mutually influencing directions: immediate decomposition of the precursor and inhibition of various transformations of a polymer chain (depolymerization, migration of double bonds, cross-linking, degradation, etc.). At the same time, formed nanoclusters may have a catalytic effect on carbonization and graphitization processes of polymers, in particular, the deep stages of decomposition of organic polymers, mechanisms which in most cases is not fully clear. It promotes the study of such interactions. Obvious is only trend: an increase of nanoparticle dispersion during thermal transformations contributes to an increase in the polar group content in the polymer [10].

8.3 The Conjugate Thermolysis—Nanoparticle and Polymer Matrix Formation Process

At present, different approaches for stabilizing nano-sized particle are developed [178]. Among them, the method of self-regulated stabilization based on simultaneous polymerization and thermolysis of metal-containing precursors or monomers is more promising.

Thermolysis of metal chelate monomers is poorly studied but intensively rapidly developing field of research, which may be the best embodiment of the idea of nanoparticle stabilization in situ. We consider this process an example of such interesting class of metal chelate monomers as metal carboxylates of unsaturated mono- and dicarboxylic acids [8, 11, 14, 15, 18, 179, 180]. Such compounds include acrylates (MAcr$_n$), methacrylates, maleates (MMal$_n$), itaconates, fumarates of alkali, alkaline earth, transition metals, their polysalts [13, 15]. This number can be added by acetylenecarboxylic acid salts [181–183].

Metal carboxylates are a large group of metal complexes containing a carboxylate functional group with a different type of coordination with a metal atom, including by chelation type [11, 12]. In the most typical cases RCOO$^-$ carboxylate group can be coordinated with the metal as a monodentate (I) anti- and syn-configuration, bidentate cyclic (chelating) (II), bidentate bridging (III), tridentate (IV), and the tetradentate ligand (V). Such a large variety of possible compositions and structures of metal carboxylates in the case of unsaturated analogs may be supplemented by the structural function of the multiple bonds, which, as known, is able to participate in coordination with a metal atom to form π-bond (VI):
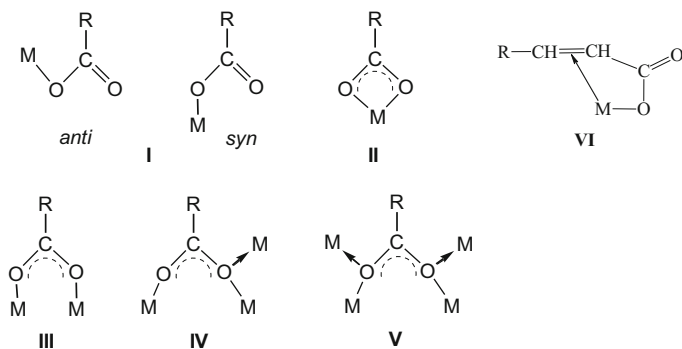
In addition, chelating donor ligands such as, phen, bpy, mono-, di-, and tri-ethanolamine, and others are often contained in the composition of metal carboxylate complex. The formation of four-membered cycles during chelate addition of carboxyl group requires large strain in the valence angles of the metal atom. In the compounds of rare-earth elements such strain does not arise and the possibility of bidentate cyclic coordination increases. Probably, it is promoted by increasing the polarity of the metal-ligand bond, and high coordination numbers of the metal. For example, in the heteronuclear Cu_2La_2– [184, 185] or CoCe– [186] methacrylate complexes the chelate groups are also on lanthanide center along with bridging groups. Moreover, in the carboxylates of this type the tridentate coordination of methacrylate groups is not uncommon, where one of the O atoms of the carboxyl group forms the bonds simultaneously with two metal atoms. In the isomorphic binuclear complexes of trans-2,3-dimethacrylates La or Gd [M(OOC(CH$_3$)C(CH$_3$)CH)$_3$(phen)]$_2$ metal atoms are connected by two bridging bidentate and two tridentate carboxylate groups [187]:
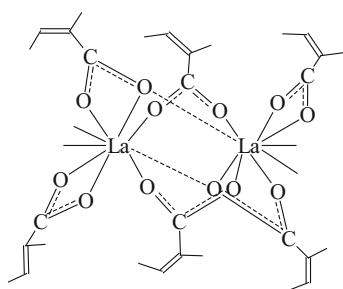
The character of the magnetic behavior of the complexes of Cu(II) (meth)acrylates, [Cu(CH$_2$CHCOO)$_2$Cu(OH)$_2$] [188], and [Cu(CH$_2$C(CH$_3$)COO)$_2$Cu(OH)$_2$] [189] is associated with their possible tetrameric structure:
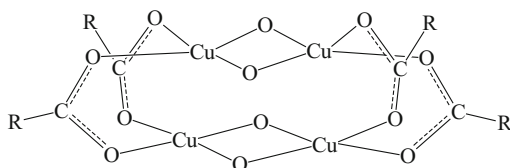
Although synthesis of fine metal and (or) their oxides by thermal decomposition of organic acid salts in the solid phase, in particular, of formates, acetates, oxalates are widely used in practice [13], problems related to the ratio of the kinetic parameters of the solid phase transformation of this type of compounds and the dispersion level of their products, i.e. border of control capabilities of their dispersion, to date are relevant. Studies of thermal decomposition of some metal acrylates in thermal analysis regime in air and in an inert atmosphere [190, 191] give only a qualitative pattern of the transformations taking place during their thermolysis.

8.3.1 Thermolysis Kinetics of Metal Carboxylates

The most complete information on the effect of different factors on the kinetics, and the dispersion of the resulting products can be obtained under isothermal studies of thermolysis of the metal carboxylates in SGA. The thermolysis mechanism of metal carboxylates based on saturated carboxylic acids was most fully studied in a series of works [192–194]. In particular, thermal transformations of Fe(II), Fe(III), Ni(II), Cu(II), Pb(II) formates $M(HCOO)_n$ and the oxalate $Fe_2(C_2O_4)_3 \cdot 5H_2O$ are temperature-separated sequential processes, involving dehydration with subsequent decomposition of the anhydrous carboxylate. Thermolysis proceeds successively in two macrostages to form metal carboxylates with a low metal oxidation state as intermediates bound, apparently with sufficiently low redox potentials of the $E^0[Fe(III)/Fe(II)] = +0.771$ V and $E^0[Cu(II)/Cu(I)] = +0.158$ V pairs. Thermolysis of Co(II) formate can be also conditionally divided into two stages: dehydration and a subsequent thermolysis. The first stage is studied in sufficient detail [195]. Thermolysis of the anhydrous product is accompanied by evolution of gaseous products H_2, CO and CO_2; water vapor, evaporating also during dehydration stage, as well as CH_3OH, CH_3COOH, formic acid thermolysis products [196–198]. The topography of the thermolysis of anhydrous metal formates is characterized by the following features: both the crystals of the starting compounds and solid-state termolysis products have a block structure with preservation of their habitus. The blocks are of sufficient porous and are «fastened» to a crystal by the polymer substance which is expected to be $-[-CH(R)-O-]_s-[-CH(COOH)-O-]_r-$, where $r \ll s$. It is expected that the polymer formation under the SGA conditions is

associated with catalytic thickening (polymerization) of the gaseous decomposition products CO_2, H_2, CO, H_2O, HCOOH under the action of formed catalytically active transition metal clusters.

It should be noted widespread thermolysis of oleate complexes dissolved in 1-octadecene [199–202]. Superparamagnetic iron oxide particles were prepared by thermolysis of iron acetylacetonate (at 538 K) in the presence of phenyl ether, oleylamine and 1,2-hexadecandiol [203] or anhydrous iron oleate (at 573 K) [201, 204].

1D Eu_2O_3 nanorods of 10–20 nm-thick with a 50–100 nm width, and a length ranging from hundreds nanometers to several micrometers are prepared by thermolysis of the complex Eu(L)·$6H_2O$ obtained from an aqueous solution of europium nitrate and 1,3,5-benzenetricarboxylic acid (H_3L) [205–207]. Interestingly, during thermolysis below 873 K (two main stages of weight loss in TGA curves which are corresponded to elimination of water molecules at 383 K and elimination of the organic ligand at 742 K) 1D crystal thread of formed nanomaterial Eu_2O_3 is retained. Generally speaking, Eu_2O_3 was produced as nanoparticles of different shape: rods [208], nanowires [209], hollow spheres [210], and nanotubes [211]. Attention to such structures is due to their properties in the achievement of many physical and chemical parameters [212].

Thermal transformations were studied for a number of unsaturated metal carboxylates, in particular, d-element acrylates of copper(II) $CuAcr_2$ [213], cobalt(II) $CoAcr_2$ [214], nickel(II) $NiAcr_2$ [215, 216], polynuclear oxoacrylate Fe(III) $FeAcr_3$ [217], cocrystallizates $FeAcr_3$ and $CoAcr_2$, $FeAcr_3$ and $NiAcr_2$ with atomic ratio of Fe:Co equal to 1:0.8 (FeCoAcr) and 2:1 (Fe_2CoAcr) [218], Fe:Ni = 2:1 (Fe_2NiAcr), Hf(IV) (meth)acrylate and fumarate derivatives [219, 220], maleates Co(II) (CoMal, Co[OOCCH=CHCOO]·$2H_2O$) [221] and Fe(III) (FeMal, $Fe_3O(OH)$[OOCCH= CHCOOH]$_6$·$3H_2O$) [222], and for acrylamide complex of Co(II) nitrate (CoAAm) [223]. Thermolysis of the studied compounds is accompanied by gassing and weight loss of samples due to dehydration and subsequent thermal conversion of the dehydrated compounds. These processes occur sequentially in different temperature ranges.

8.3.2   Key Temperature-Separation Stages of Thermal Transformations of Metal Carboxylates

In general, the thermolysis study of metal carboxylates based on unsaturated acids in either the thermal analysis (TA), and SGA regimes revealed the general pattern of the nature of their transformation, consisting in a sequence of three main differing in temperature macrostages [14, 179, 180]: dehydration (desolvation) of the initial metal-containing monomer(s) (403–473 K); solid-state homo- or copolymerization of dehydrated metal-containing monomer(s) (473–573 K); decarboxylation of the resulting metallopolymer to a metal-containing phase and oxygen-free

polymer matrix at temperatures >523 K (in the case of copper carboxylates above 453 K), accompanied by intensive gassing.

8.3.2.1 Dehydration

At low thermolysis temperatures T_{therm} (T_{therm} < 473 K) dehydration of monomeric crystallohydrates occurs. According DTA-, TG-, DTG-research acrylates dehydration occurs at T_{therm} = 353–487 K (FeAcr$_3$), 413–453 (CoAcr$_2$), 373–473 K (NiAcr$_2$), maleates at 393–433 K (CoMal) and 373–433 K (FeMal), for Co(II) acrylamide complex at 328–362 K (Fig. 8.13).

A detailed study of the CoAcr$_2$ dehydration conditions under isothermal conditions at T_{therm} = 303–433 K indicates that it is reversible process. This is according to the IR spectroscopic studies. As a result of dehydration absorption bands associated with the modes of crystallization water ν(O–H) 3000–3600 cm^{-1}, ρ_{ω}(O–H) + ν(Co–OH$_2$) 880 cm^{-1} disappear. Intensity of modes due δ(O–H) + ν(C=C) 1655 cm^{-1}, ρ_{ω}(CH$_2$) + δ(Co–OH$_2$) 690 cm^{-1}, δ(CH$_2$) + δ(Co–OH$_2$) 595 cm^{-1} simultaneously decreases. In some cases, there are two areas of evaporation. For example, during the CoAcr$_2$ dehydration in a completely isothermal conditions evaporation at 303–348 K is limited by the evaporation of dehydrated water, P_{H2O}(T_{therm}) = $1.7 \times 10^7 \exp[-9200/RT)]$ кPa, and the evaporation heat
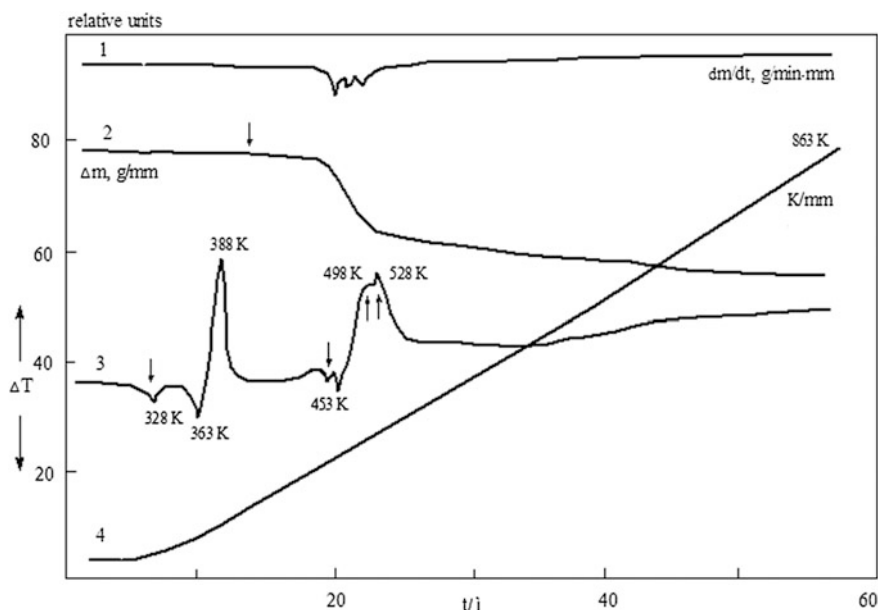
Fig. 8.13 Derivatograms of acrylamide complex Co(II) nitrate: 1—DTGA (dm/dt × 0.8 g min^{-1} mm^{-1}), 2—TGA (Δm × 2.5 × 10^3 g mm^{-1}), 3—DTA (ΔT × 0.88 K min^{-1} mm^{-1}), 4—TA (T × 0.5 K mm^{-1}) (heating rate 10 °C min^{-1}, sample weight is 45.8 × 10^{-3} g)
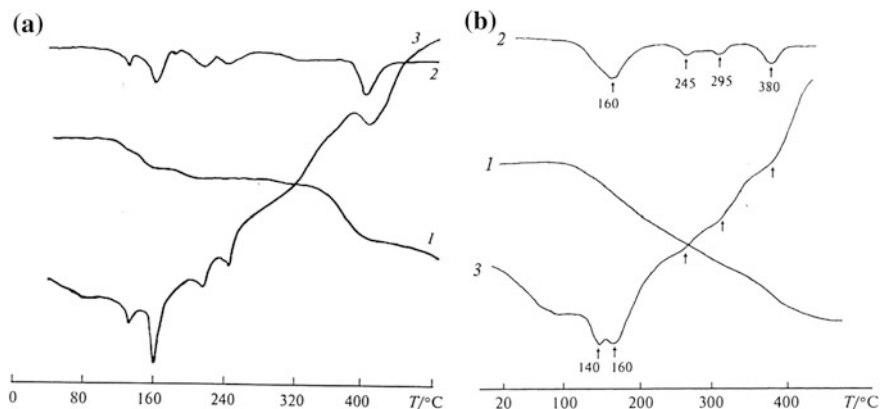
Fig. 8.14 Thermoanalytical curves of the thermolysis of maleinates Co(II) (**a**) and Fe(III) (**b**): 1—TGA, 2—DTGA, 3—DTA

$\Delta H_{st}(H_2O) = 38.5$ kJ mol^{-1} is close to the H$_2$O evaporation heat, $\Delta H_{evap}(H_2O) = 43.9$ kJ mol^{-1} [224]. Evaporation at $T_{therm} > 348$ K is described by dependent $P_{H2O}(T_{therm}) = 2.7 \times 10^4 \exp[-4800/RT)]$ кPa and is limited directly by dehydration, $\Delta H_{evap}(H_2O) = 20.1$ kJ mol^{-1}. A similar dehydration process is observed in the case of thermolysis of Co(II) maleate (Fig. 8.14).

Endoeffects at 400 and 433 K are associated with two-step process of CoMal dehydration and are accompanied by weight loss, equals to 15.2 wt% (calc. 17.23%).

During dehydration in a vacuum the crystals of cobalt and zinc acetylenedicarboxylates (CoADC·2H$_2$O and ZnADC·2H$_2$O) [180] are stable only up to a certain minimum content of the coordinated water, at which there is a sharp release of gaseous products of decomposition and formation of reactive moieties capable of initiating the solid phase metal monomer polymerization. With the help of quantum-chemical calculations (DFT) the dehydration energy of crystallohydrates CoADC·2H$_2$O and ZnADC·2H$_2$O is evaluated which is 150–200 kJ mol^{-1} [13]. Such a large quantity can lead to the mechanochemical activation of the decomposition of crystal and coordination structures CoADC·2H$_2$O and ZnADC·2H$_2$O during their dehydration.

8.3.2.2 Polymerization

The temperature increasing of the dehydrated monomer to $T_{therm} = 473–573$ K leads to a solid state polymerization. The transformation of the investigated monomers in the conditions of TA and SGA showed that in this temperature range a slight gas evolution is observed, along with a minor loss of sample weight ($\ll 10$ wt%). In the case of metal acrylates and maleates main contribution is made by CO$_2$ and vapor CH$_2$=CHCOOH and HOOCCH=CHCOOH, condensed on the walls reactor at room

temperature, respectively. This is confirmed by IR and mass spectroscopy. Typical polymerization temperature ranges T_{polym}, according to the TA, are ~ 543 K ($CoAcr_2$), ~ 563 K ($NiAcr_2$), ~ 510 K ($CuAcr_2$), ~ 518 K ($FeAcr_3$), 488–518 K ($CoMal$), ~ 518 K ($FeMal$). During the polymerization there is a change in the IR absorption spectrum of the dehydrated monomer associated with decreasing band absorption intensity of the valence modes of the C=C bond and stretching absorption frequency of the valence modes of the C=O bond, leading to the emergence of a broadened absorption band in the region 1540–1560 cm^{-1} (Tables 8.6, 8.7 and 8.8). It is characteristic that regularly band (RB) with the $\Psi = 1.27$ (δ_{C-H} 830 cm^{-1}, ν_{C-H} 2930 cm^{-1}) appears during the thermal transformations of $NiAcr_2$ ($T_{exp} = 593$ K), at low degrees of gassing (about warm-up time), which disappears with increasing conversion and is not observed at $T_{exp} = 573$ K. The appearance of the RB indicates the proceeding polymerization process, which precedes the main gassing.

According to the TA analysis results during Fe(III) maleate thermolysis the sample weight loss Δm in DTA-effect region with maxima at 433 and 518 K is, respectively, 31.2 and 8.7 wt%. First endoeffect (sufficiently strong) is associated with a dehydration process (5.2% loss of three moles of water molecules), and, apparently, with partial elimination of three molecules of maleic acid (36.8% calc.). The second weak heat effect accompanied by weight loss of the sample is most likely due to the polymerization of desolvated monomer. Finally Δm in this area is about 40%.

8.3.2.3   Decarboxylation

At $T_{therm} > 523$ K (for $CuAcr_2$ $T_{therm} > 453$ K) thermopolymerized samples are subjected to intense gassing (basic gassing). Kinetics of the process under isothermal conditions and in a SGA studied [225] for $CuAcr_2$ ($<T_{therm}> = 363–513$ K), $CoAcr_2$ (623–663 K), $NiAcr_2$ (573–633 K), $FeAcr_3$ (473–643 K), $FeCoAcr$ (613–633 K), Fe_2CoAcr (613–633 K), Fe_2NiAcr (603–643 K), $CoMal$ (613–643 K), $FeMal$ (573–643 K).

The rate of gas evolution $W = d\eta/dt$ decreases monotonically with increasing conversion $\eta = \Delta\alpha_{\sum, t}/\Delta\alpha_{\sum, f}$, where $\Delta\alpha_{\sum, t} = \alpha_{\sum, t} - \alpha_{\sum, 0}$, $\Delta\alpha_{\sum, f} = \alpha_{\sum, f} - \alpha_{\sum, 0}$, $\alpha_{\sum, f}$, $\alpha_{\sum, t}$ and $\alpha_{\sum, 0}$, respectively, the final, current and initial moles of the separated gaseous products on 1 mol of the initial sample at room temperature. Kinetics of gassing $\eta(\tau)$ in general (up $\eta \leq 0.95$) satisfactorily approximated by the equation for the two parallel reactions:

$$\eta(\tau) = \eta_{1f}[1 - \exp(-k_1\tau)] + (1-\eta_{1f})[1 - \exp(-k_2\tau)] \qquad (8.1)$$

where $\tau = t - t_0$ (t_0—the warm-up sample, $\eta_{1f} = \eta(\tau)|_{k_2t\to 0,\ k_1t\to\infty}$, k_1, k_2—effective rate constants. Parameters k_1, k_2, η_{1f}, $\Delta\alpha_{\sum, f}$ depend on T_{therm}:

Table 8.6 Values of vibration frequencies in the IR spectra of Cu(II) acrylate, its polymer and decomposition products [210]

CuAcr₂			Polyacrylate Cu(II)			CuAcr₂ decomposition product		
ν, cm⁻¹	I_{rel}	Assignment	ν, cm⁻¹	I_{rel}	Assignment	ν, cm⁻¹	I_{rel}	Assignment
3100	0.02	ν_{as} C–H (=CH₂)						
3045	0.10	ν_{as} C–H (=CH–)						
3030 sh	0.02							
2950	0.03	ν_s C–H (=CH₂)	2975	0.06	ν_s C–H(–CH₂–)	2970	0.10	ν_{as} C–H (–CH₂–)
2930	0.06	ν_s C–H (=CH–)	2925	0.10	ν_s C–H(–CH₂–)	2920	0.23	ν_s C–H (–CH₂–)
2900 sh	0.02		2915	0.12		2860	0.175	ν_s C–H (=CH–)
2850	0.03		2850	0.05	ν(=C–H)	2860	0.27	ν(=C–H)
2790	0.02							
2730	0.02							
1945	0.02					1770	0.13	
1645	0.49	ν C–C (C=C)	1640	0.08	ν C–C (C=C)$_{conc}$			
1580	1.00	ν_{as} C–O (COO)	1560	1.00	ν_{as} C–O (COO)	1595	1.00	ν_{as} C–O (COO)
1560 sh	0.44		1550 sh	0.51				
1515	0.33	δC–H (–CHCH₂)	1515	0.32	δC–H (–CHCH₂)	1500	0.57	δC–H (–CHCH₂)
1440	0.82		1415	0.44		1395	1.00	
1370	0.46	ν_s C–O (COO)	1345	0.26	ν_s C–O (COO)	1345	0.62	ν_s C–O (COO)
1275	0.34	ρ_t (CH₂)	1275	0.14	ρ_t (CH₂)	1240	0.24	ρ_t (CH₂)
			1240	0.19				
1065	0.27	ν C–C (=CH–C)	1075	0.19	ν C–C (=CH–C)	1077	0.58	ν C–C (=CH–C)
995	0.41	π(–CHCH₂)	980	0.13	π(CH₂)	980	0.32	π(CH₂)
975	0.46		940	0.19		935	0.47	
915	0.09	π(–CHCH₂)				900	0.41	π(–CHCH₂)
830	0.50	ρ_w(CH₂)	815	0.20	ρ_w(CH₂)	815	0.53	ρ_w(CH₂)
695	0.48	ρ_t(CH₂)	678	0.20	ρ_r(CH₂)	680	0.81	ρ_t(CH₂)

Note $I_{rel} = D_\nu/D_\nu^{max}$ is relative intensity, D_ν is absorption at ν frequency. Vibrations: ν stretching, δ bending, ρ_t twisting, ρ_w wagging, ρ_r rocking, π out-of-plane

Table 8.7 Values of vibration frequencies in the IR spectra of Fe$_2$CoAcr and decomposition products [215]

| Cocrystallizate Fe$_2$CoAcr | | | Fe$_2$CoAcr decomposition products | | | | | | Assignment |
| v/cm^{-1} | I_{rel} | Assignment | Δm = 25.1% | | Δm = 37.3% | | Δm = 42.0% | | |
			v/cm^{-1}	I_{rel}	v/cm^{-1}	I_{rel}	v/cm^{-1}	I_{rel}	
3000–3600 br		ν(OH) (H$_2$O)							
3045		ν$_{as}$(CH)							ν(CH)
2960		ν$_s$(CH)	2930						
1630	0.74	ν(C=C), δ(OH)(H$_2$0)	1640	0.35	1680	0.46	1685	0.38	ν(C=C)
1575	1.00	ν$_{as}$(COO) (Fe cluster)	1555	1.00	1555	1.00	1565	1.00	ν$_{as}$(COO) (Fe cluster)
1540	0.80	ν$_{as}$ (COO) (Co)	1540	0.99	1540	0.99	1550	1.07	ν$_{as}$(COO) (Co)
1525	0.77	ν$_{as}$(COO) (Fe cluster)	1520	0.92	1520	0.98	1520	0.99	ν$_{as}$(COO) (Fe cluster)
1505	0.485	ν$_{as}$(COO) (Co)	1505 sh	0.715	1498	0.89			ν$_{as}$(COO) (Co)
1490 sh	0.39	δ(CH)	1490	0.6					δ(CH)
1435	0.92	ν$_s$(COO) (Fe cluster)	1435	0.85	1440	1.02	1420	1.23	ν$_s$(COO) (Fe cluster), ν(OH$_2$) (–CH$_2$–CHR–)
1420	0.92	ν$_s$(COO) (Co)	1415	0.85	1408	1.07			ν$_s$(COO) (Co), δ(OH$_2$) (H$_2$C–CR–)
1360	0.82	ν$_s$(COO) (Fe cluster)	1400	0.97	1395	1.10	1400	1.20	ν$_s$(COO) (Fe cluster), δ(OH$_2$) (CH$_2$=CR–)
1350	0.71		1315	0.57					ν$_s$(COO) (Co), δ(OH) (–CH$_2$–CHR–)
1270	0.44	ρ$_t$(CH$_2$)	1280sh	0.51	1270 sh	0.665	1265	1.08	ρ$_t$(CH2) (CH$_2$–CH=CH–) trans
			1185	0.35	1160		1150	1.37	ν(C–C) (=CH–CHR–)

(continued)

Table 8.7 (continued)

| Cocrystallizate Fe$_2$CoAcr | | | Fe$_2$CoAcr decomposition products | | | | | | |
| ν/cm⁻¹ | I$_{rel}$ | Assignment | Δm = 25.1% | | Δm = 37.3% | | Δm = 42.0% | | Assignment |
			ν/cm⁻¹	I$_{rel}$	ν/cm⁻¹	I$_{rel}$	ν/cm⁻¹	I$_{rel}$	
1120 br	0.10								
1068	0.32	ν(C–C)							
990	0.38	π(CH) (–CH=CH$_2$)							
965	0.31	(–CH=CH$_2$)							
910	0.07	ρ(OH) (H$_2$0), ν(M–OH$_2$)	855	0.08	860	0.15	875	0.33	δ(CH) (–CH=CHR)
830	0.61	ρ$_w$(CH$_2$)	835	0.09	830	0.10	830	0.20	ρ$_w$(CH) (–CH$_2$–CHR–)
728	0.12		775	0.07	755	0.11	750	1.11	
673	0.50	ρ$_t$(CH$_2$), δ(M–OH$_2$)	645 br	0.03					ρ$_t$(CH) (–CH$_2$–CR=CH–)cis, δ(CH$_2$)
598	0.11	δ(CH$_2$), δ(M–OH$_2$)	592	0.02					ρ$_w$(CH) (–CH=CHR)
545	0.07	δ(CH$_2$), δ(M–OH$_2$)							

Table 8.8 Values of vibration frequencies in the IR spectra of CoAcr₂, its polymer and decomposition products [211]

CoAcr₂·H₂O			Polyacrylate Co(II)			CoAcr₂ dehydration products			CoAcr₂ decomposition products		
ν, cm⁻¹	I_{rel}	Assignment	ν, cm⁻¹	I_{rel}	Assignment	ν, cm⁻¹	I_{rel}	Assignment	ν, cm⁻¹	I_{rel}	Assignment
3000–3600 br	0.24	(3400 cm⁻¹) ν O–H				3000–3600 br	0.02	(3400 cm⁻¹) ν O–H			
3100	0.03	ν_{as} C–H (=CH₂)				3100	0.04	ν_{as} C–H (=CH₂)			
3050	0.03	ν_{as} C–H (=CH–)				3050	0.03	ν_{as}C–H (=CH–)			
3025	0.03	ν_s C–H (=CH₂)									
2985	0.03										
2925	0.03		2930	0.15	ν_s C–H–CH₂–)	2925	0.03	ν_s C–H (=CH₂)	2940	0.26	ν_s (C–H–CH₂–)
2850	0.02	ν_s C–H (=CH–)	2860	0.06	ν_s C–H(=CH–)	2860	0.03	ν_s C–H (=CH–)	2860	0.175	ν_s C–H(–CH–)
1975	0.02	overtone (2 × 960)	1925	0.04	Overtone				2730	0.07	
1655	0.63	ν(C=C), δO–H (H₂O)	1655	0.92’	ν(C=C)_conc	1655	0.50	ν(C=C)	1675 sh	0.16	ν(C=C)
1595	1.00	ν_{as} C–O (COO)	1595	0.92	ν_{as} C–O (COO)	1580	0.90	ν_{as} C–O (COO)	1565	1.00	ν_{as} C–O (COO)
1585	1.00		1575	1.00					1535 sh	0.78	
			1535 sh	0.66							
1450	1.00	δC–H (–CHCH₂)	1450	0.92	δC–H (–CHCH₂)	1455	1.00	δC–H (–CHCH₂)	1435	0.53	δC–H (–CHCH₂)
			1435 sh	0.79					1415	0.63	
1370	0.68	ν_s C–O (COO)	1375	0.68	ν_s C–O (COO)	1365	0.675	ν_s C–O (COO)	1385	0.51	ν_s C–O (COO)

(continued)

Table 8.8 (continued)

CoAcr₂·H₂O			Polyacrylate Co(II)			CoAcr₂ dehydration products			CoAcr₂ decomposition products		
ν, cm⁻¹	I_{rel}	Assignment	ν, cm⁻¹	I_{rel}	Assignment	ν, cm⁻¹	I_{rel}	Assignment	ν, cm⁻¹	I_{rel}	Assignment
1285	0.44	$\rho_t(CH_2)$	1285	0.49	$\rho_t(CH_2)$	1280	0.57	$\rho_t(CH_2)$	1260	0.39	$\rho_t(CH_2)$
1070	0.15	ν C–C (=CH–C)	1060	0.14	ν C–C (=CH–C)$_{conc}$	1070	0.10	ν C–C (=CH–C)	1235	0.375	
995	0.31	π(–CHCH₂)	995	0.21	π(–CHCH₂)	990	0.31	π(–CHCH₂)	1130	0.06	
960	0.28		975	0.17		965	0.28		1080	0.05	ν C–C (=CH–C)
880	0.05	ρOH (H₂O), ν(M–OH₂)							1010	0.14	π(–CHCH₂)
840	0.42	$\rho_w(CH_2)$	835	0.26	$\rho_w(CH_2)$	835	0.43	$\rho_w(CH_2)$	985	0.125	
685	0.24	$\rho_t(CH_2)$, δ(M–OH₂)	685	0.06	$\rho_t(CH_2)$	690	0.195	$\rho_t(CH_2)$			
590	0.06	δ(CH₂), δ(M–OH₂)				590	0.032	δ(CH₂)			

$$\eta_{1f}, \Delta\alpha_{\Sigma,f} = A\exp\left[-E_{a,eff}/(RT_{therm})\right] \tag{8.2}$$

$$k_{eff} = k_{0,eff}\exp\left[-E_{a,eff}/(RT_{term})\right] \tag{8.3}$$

where A, $k_{0,eff}$ is pre-exponential factor, $E_{a,eff}$ is the effective activation energy.

The initial rate of gas evolution $W_{\tau=0} = W_0$ will

$$W_0 = \eta_{1f}k_1 + (1-\eta_{1f})k_2 \tag{8.4}$$

Equations (8.1) and (8.4) describe the kinetics of the gassing $NiAcr_2$, FeCoAcr, Fe_2CoAcr, Fe_2NiAcr and FeMal (Fig. 8.15) [213, 215, 219].

At $k_2 \approx 0$, $\eta_{1f} \rightarrow 1$

$$\eta(\tau) \approx 1 - \exp(-k_1\tau) \tag{8.5}$$

$$W_0 \approx k_1 \tag{8.6}$$

Equations (8.5) and (8.6) describe the kinetics of the gassing during thermal transformations of $CoAcr_2$ and CoMal (Figs. 8.16 and 8.17).

In the case where $\tau \ll 1/k_2$, $k_1 \gg k_2$,

$$\eta(\tau) \approx \eta_{1f}[1-\exp(-k_1\tau)] + (1-\eta_{1f})k_2\tau \tag{8.7}$$

$$W_0 \approx \eta_{1f}k_1 \tag{8.8}$$

The dependence η of the time (t) during $CuAcr_2$ thermolysis satisfactorily described by (8.7) (Fig. 8.18).

The kinetic parameters of gas evolution at thermal transformations of the studied compounds are presented in Table 8.9.
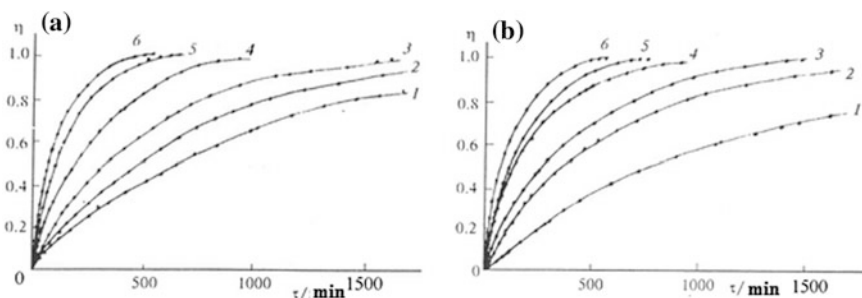
Fig. 8.15 The kinetics of accumulation of gaseous products at thermal transformation of cocrystallizates FeCoAcr (**a**) and Fe_2CoAcr (**b**). Curves are calculation of the (8.1), points are the experimental values: T_{exp} = 613 (1), 623 (2), 633 (3), 643, 653 (5), 663 K (6); m_0/V = 1.80 ($\pm$0.05) $\times 10^{-3}$

Fig. 8.16 Kinetics of the thermal decomposition of CoAcr: **a** dependence $\eta(t)$ at various temperatures: 663 (1), 653 (2), 643 (3), 633 (4) 623 K (5); **b** the dependence $\lg k$ versus $1/T$
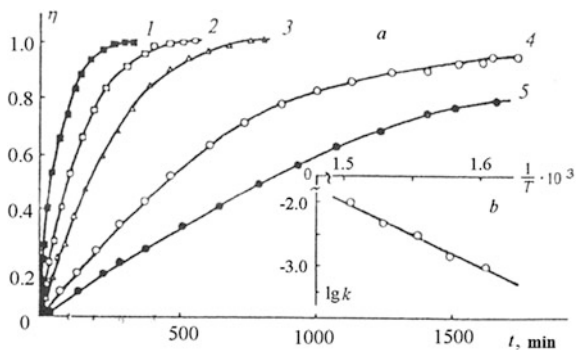
Fig. 8.17 Gas evolution kinetics $\eta(\tau)$ (**a**) and semilogarithmic lines (log $(1 - \eta)$ vs. τ) (**b**) for the thermolysis of Co(II) maleate (CoMal) in SGA at 653 (1), 643 (2), 633 (3), 623 (4), and 613 K (5)
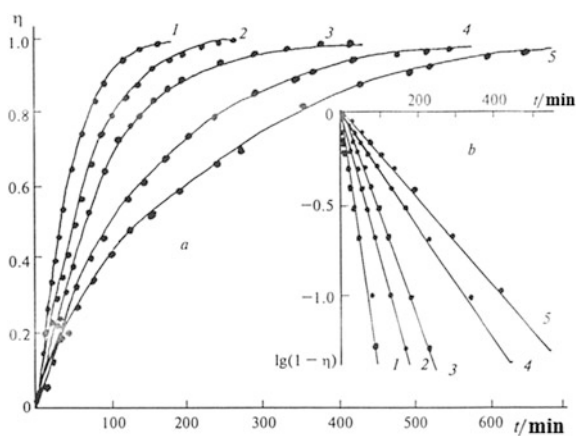
Fig. 8.18 Dependence $\eta(t)$ during the thermolysis of CuAcr$_2$: 1—463, 2—473, 3—483, 4—493, 5—503, 6—513 K; $m_0/v = 2.45$ $(\pm 0.1) \times 10^{-3}$
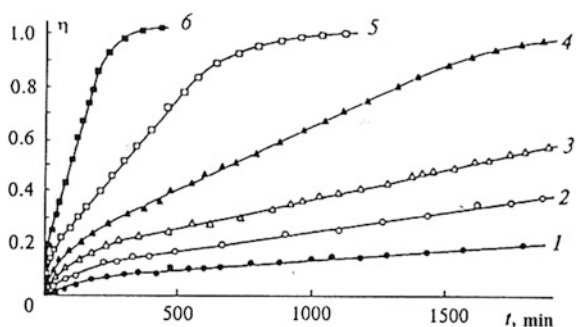
Table 8.9 Kinetic parameters of gassing during thermolysis of metal acrylates and maleates [181, 225]

Sample	$\eta_{1f}, \Delta\alpha_{\sum,f} = A \exp[-E_{a,eff}/(RT_{therm})]$			k	$k_{eff} = k_{0,eff} \exp[-E_{a,eff}/(RT_{therm})]$		$W_0 = k_{0,eff}\exp[-E_{a,eff}/(RT_{therm})]$	
	$\eta_{1f}, \Delta\alpha_{\sum,f}$	A	$E_{a,eff}$ (kJ mol^{-1})		$k_{0,eff}$ (s^{-1})	$E_{a,eff}$ (kJ mol^{-1})	$k_{0,eff}$ (s^{-1})	$E_{a,eff}$ (kJ mol^{-1})
CuAcr$_2$	η_{1f}	1.8×10^4	48.1	k_1	9.5×10^{11}	154.7	9.5×10^{11}	202.7
	$\Delta\alpha_{\sum,f}$	3.6	12.5	k_2	9.2×10^{11}	163.0		
CoAcr$_2$	η_{1f}	1.0	0	k_1	3.0×10^{14}	238.3	3.0×10^{14}	238.3
	$\Delta\alpha_{\sum,f}$	1.55	0	k_2		0		
FeAcr$_3$ (473–573 K) (573–643 K)	η_{1f}	1.0	0	k_1	4.2×10^{21}	246.5	4.2×10^{21}	246.5
	$\Delta\alpha_{\sum,f}$	1.6×10^2	25.5	k_2	0	0	1.3×10^6	127.5
	η_{1f}	1.0	0	k_1	1.3×10^6	127.5		
	$\Delta\alpha_{\sum,f}$	1.7×10^2	26.3	k_2	0			
NiAcr$_2$	η_{1f}	2.6	4.6	k_1	1.7×10^{17}	242.4	4.4×10^{17}	247.0
	$\Delta\alpha_{\sum}, f<593\ K$	1.4×10^{11}	125.4	k_2	7.5×10^8	156.7		
	$\Delta\alpha_{\sum}, f>633\ K$	1.2	10.5					
FeCoAcr	$\eta_{1f} = 0.45\ (663\ K) - 0.65\ (613\ K)$			k_1	2.3×10^{12}	207.0	1.3×10^{12}	207.0
	$\Delta\alpha_{\sum,f}$	5.25×10^2	31.3	k_2	6.0×10^6	138.0		
Fe$_2$CoAcr	$\eta_{1f} = 0.35\ (663\ K) - 0.50\ (613\ K)$			k_1	2.6×10^{12}	205.0	1.1×10^{12}	205.0
	$\Delta\alpha_{\sum,f}$	1.5×10^2	25.1	k_2	6.6×10^5	125.5		
Fe$_2$NiAcr	η_{1f}	4.4×10^7	75.0	k_1	6.1×10^6	129.5	2.7×10^{14}	205.0
	$\Delta\alpha_{\sum,f}$	6.5×10^2	25.5	k_2	0.6×10^2	79.4		
CoMal	η_{1f}	1.0	0	k_1	1.1×10^6	125.4	1.1×10^6	125.4
	$\Delta\alpha_{\sum,f}$	1.3×10^2	23.4	k_2	0			
FeMal	η_{1f}	0.59×10^2	23.4	k_1	3.3×10^7	133.8	1.9×10^9	157.2
	$\Delta\alpha_{\sum,f} = 4.78\ (573\ K) - 7.40\ (643\ K)$			k_2	1.0×10^7	110.8		

It should be noted that two gassing areas are observed at heating thermopolymerized $FeAcr_3$ (Fig. 8.19) [225]: low temperature ($\langle T_{therm} \rangle$ = 473–573 K) and high temperature ($\langle T_{therm} \rangle$ = 603–643 K). Their gassing rate is well approximated by the (8.5–8.6), but with different values of k and $\Delta \alpha_{\sum, f}$ (see Table 8.9). It is possible that the difference in kinetic parameters of $FeAcr_3$ thermolysis in low- and high-temperature areas, or in the case of FeCoAcr, Fe_2CoAcr, Fe_2NiAcr difference in η_{1f} value level at a constant other kinetic parameters ($\Delta \alpha_{\sum,f}$, k_1, k_2), is due to the presence of two parallel processes of gassing.

Using the values W_0, studied metal acrylates can be arranged in series to reduce the reactivity of a gassing: Cu $\geq$ Fe > Co > Ni. At that the values of effective activation energies of the initial rate of gas evolution in a SGA of $CuAcr_2$ ($E_{a,eff}$ = 202.7 kJ mol^{-1}), $NiAcr_2$ ($E_{a,eff}$ = 246.6 kJ mol^{-1}) shown in Table 8.9 are close to the calculated values of $E_{a,eff}$ for thermolysis in TA regime [190]: 211.1 and 244.1 kJ mol^{-1}. At the same time, $E_{a,eff}$ = 238.3 kJ mol^{-1} of initial rate of $CoAcr_2$ thermolysis in SGA is above the corresponding value of $E_{a,eff}$ = 206.1 kJ mol^{-1} for thermal transformation in a TA conditions. Attention is drawn to the difference in gassing rate constants of cobalt acrylate and maleate thermolysis. The values of the activation parameters of FeMal are close to the values of the activation parameters of gassing rate constants of $FeAcr_3$, FeCoAcr, Fe_2CoAcr, and Fe_2NiAcr in this T_{therm} region.
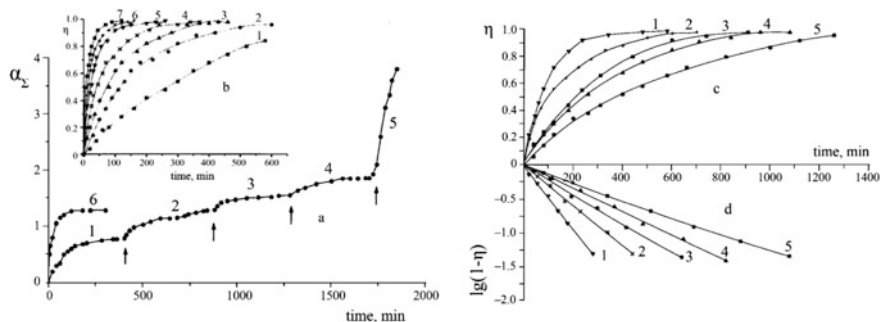
Fig. 8.19 **a** The kinetics of gas evolution from $FeAcr_3$ at T_{exp}(^{0}C): 1, 215; 2, 250; 3, 275; 4, 300; 5, 350; 6, 240. The moment of T_{exp} increasing is shown by pointer. **b** Dependence $\eta(T)$ on T_{exp}(^{0}C): 1, 200; 2, 205; 3, 210; 4, 215; 5, 220; 6, 230, 7, 240 (m_o/V = 6.7 × 10^{-3} g cm^3 where m_o is start mass of sample). **c** The dependence $\eta(t)$ on T_{exp} = 300–370 °C: 1, 370; 2, 360; 3, 350; 4, 340; 5, 330 °C. **d** The semilogarithmic anamorphous of the dependence $\eta(t)$

8.3.3 The Composition of the Gaseous and Solid Thermolysis Products of Metal-Containing Monomers

8.3.3.1 The Gaseous and Condensed Products

The major gaseous product of the conversion of the investigated acrylates and maleates metals, their cocrystallizates is CO_2. This is confirmed by IR spectroscopy and mass spectrometry (MS) observations. CO (IR, MS), H_2 (MS), and condensed at T_{room} H_2O vapor (IR, MS) and ligands CH_2=CHCOOH (IR, MS), HOCOCH= CHCOOH (IR, MS), which are the products pyrolysis of the corresponding complexes, are evolved in a much smaller amount. The evolution of the main quantity of condensed product vapor is observed in the early stages of the gas evolution (during the warm-up sample $\alpha_{\sum,0}$) and is associated with dehydration and solid state polymerization processes, which are the previous main gassing. This is evidenced by a comparison of the amount of the evolved gaseous products and sample weight loss. Besides these gaseous products CH_4 (IR, MS) was detected in the case $CoAcr_2$ (trace) and $NiAcr_2$ (co-measurable with the amount of CO_2) (Table 8.10). C_2H_4 (IR, MS) is formed in the transformation products of $CuAcr_2$ in measurable quantities.

In the IR spectra of gaseous products that condense at 88 K (Fig. 8.20) there is a system of characteristic absorption bands in the regions 3600–3700, 2320–2340, 625–670 cm^{-1} associated with CO_2 oscillations. Absorptions at frequencies 2990, 2930, 1750sh, 1725, 1630, 1370, 1350 cm^{-1} related to oscillations ν(C–H), ν(C=O),

Table 8.10 The composition of the gaseous and condensable thermolysis products of metal-containing monomers [213, 214, 218, 221, 222]

Sample	Products (% об.)						
	Condensable at 88 K				Non-condensable at 88 K		
	CO_2	C_2H_4	Vapor CH_2=CHC(O)OH (HOC(O)CH=CHC(O)OH)	Vapor H_2O	H_2	CO	CH_4
$CoAcr_2$	>90	–	+	+	56.8	34.0	9.2
$CuAcr_2$	>90	5–6	+	+	19.4	77.6	3
$NiAcr_2$	79		+	+	0.5	∼0.5	18.5 (from α^{Σ})
$FeAcr_3$	90–93	–	+	2.3	(2.7 from α^{Σ})	–	–
CoMal	90	–	+	+	2–2.5 from α^{Σ}	2–2.5 from α^{Σ}	–
FeMal	90	–	+	+	Trace	≤10 from α^{Σ} CO_2	

Fig. 8.20 The IR absorption spectra of the gaseous products (1) and the product condensed on the walls of the reaction vessel (2) during the thermal transformations of CoAcr$_2$
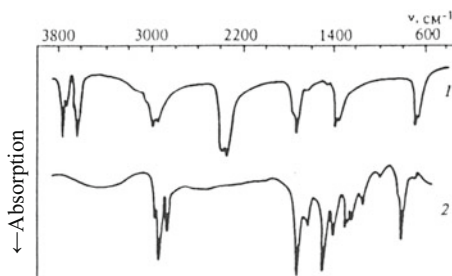
Fig. 8.21 The IR absorption spectra of the gaseous products of thermal transformations of CuAcr$_2$, non-condensing at 88 K
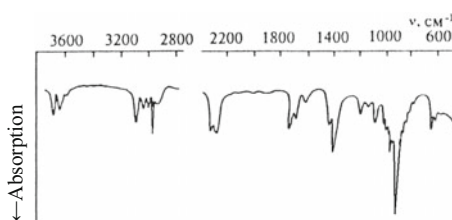
ν(C=C), δ(C–H) are likely to be due to the presence of vapor CH$_2$=CHCOOH. In the case of CuAcr$_2$ in similar IR spectra there also are absorption bands characteristic C$_2$H$_4$ (ν(CH) 3106, 3020, 3000, 2970 cm^{-1}; ν(C=C) 1625 cm^{-1}; δ_{as}(CH$_2$) 1445 cm^{-1}; δ_s(CH$_2$) 1380 cm^{-1}; ρ_w(CH$_2$) 950 cm^{-1}. In the IR spectra of the gaseous products which are not condensable at 88 K, there are absorption bands in the region 2140 and 2100 cm^{-1} associated with CO oscillations (Fig. 8.21) [213].

The level of total gassing at the transformation end ($\alpha_{\sum, f}$) is different for each of the studied acrylates and maleates, and increases with T_{therm} (see Table 8.9). At a constant value of T_{therm}, $\alpha_{\sum, f}$ increases with increasing content of Acr-ligands in the acrylate monomers. With increasing T_{therm} sample weight loss at the end of gas evolution also increases, but does not reach the values that can be expected from the decomposition of metal carboxylates to the metal or its oxide.

8.3.3.2 The Composition of the Solid-Phase Products

During the transformation of investigated metal-containing monomers with increasing $\alpha_{\sum, t}$ changes in the IR absorption spectra of solid thermolysis products are observed. They lie in the evolution of the relative intensity of the absorption bands I_{rel} and shift the absorption frequencies. Despite the inherent individuality of each of the studied compounds in the changes in the IR absorption spectrum, there are general patterns associated primarily with the mode system of C=C and COO bonds:

(i)   At low gassing degrees, including FeAcr$_3$ thermolysis at low temperatures, I$_{rel}$
      of modes $\nu(>C=C<)$, $\rho(CH_2)$, $\nu(=C-C)$, $\pi(-CH=CH_2)$ falls and IR absorption
      spectrum becomes closest to the IR absorption spectrum of polyacrylate [226]
      and polymaleates [227, 228] of corresponding metal. This is evidenced by a
      comparison I$_{rel}$ in the IR spectra of the thermolysis products and individual
      polyacrylate and polymaleate.

(ii) Increasing the gassing degree leads to a drop I$_{rel}$ of stretching $\nu(C(O)-O)$ and
      bending $\delta(C-O)$ modes up to their complete disappearance. This indicates
      decomposition of carboxylate groups.

iii) (iii) Simultaneously with the fall I$_{rel}$ of the C(O)O-mode, a shift of the
      absorption bands of the stretching $\nu(C-H)$ modes in the high-frequency
      region is observed that indicates the reinforcement of C–H bond. This is
      typical of =CH-fragments.

(iv) Absorption in the region 1630–1655 cm^{-1} related to $\nu(C=C-)$ modes, shifted
      in high-frequency region 1685–1720 cm^{-1} with decreasing I$_{rel}$. This may be
      due to the appearance of stretching modes in the conjugated C=C-fragments
      of products.

In general, quantitative monitoring of evolution in the transformation of the IR
absorption spectra of the solid thermolysis products of the studied carboxylates
suggest the decarboxylation of metal-containing fragments and the appearance of
conjugated C=C bonds.

Electron microscopic study of the final thermolysis products of CoAcr$_2$, FeAcr$_3$,
CoMal, Fe$_2$NiAcr, FeCoAcr, Fe$_2$CoAcr showed that they are characterized by a
morphologically close pattern: there are electron-dense particles dispersed in the
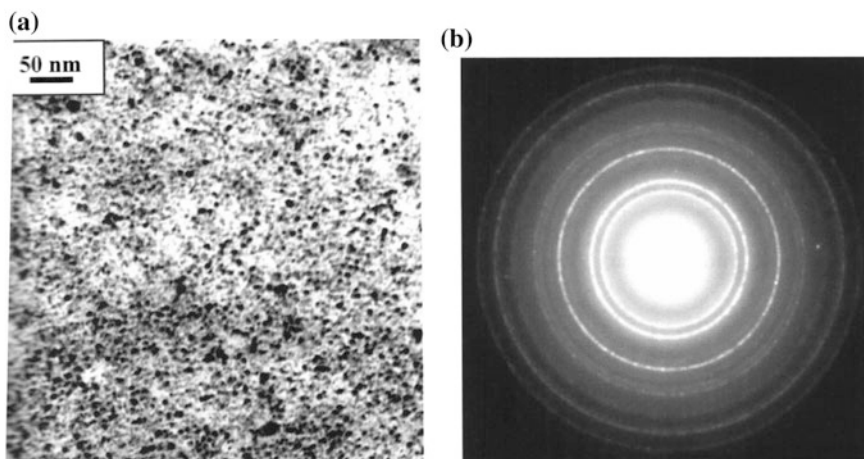
Fig. 8.22 TEM microstructure (**a**) and electron diffraction (**b**) of the thermolysis product of
CoAcr$_2$ at 643 K
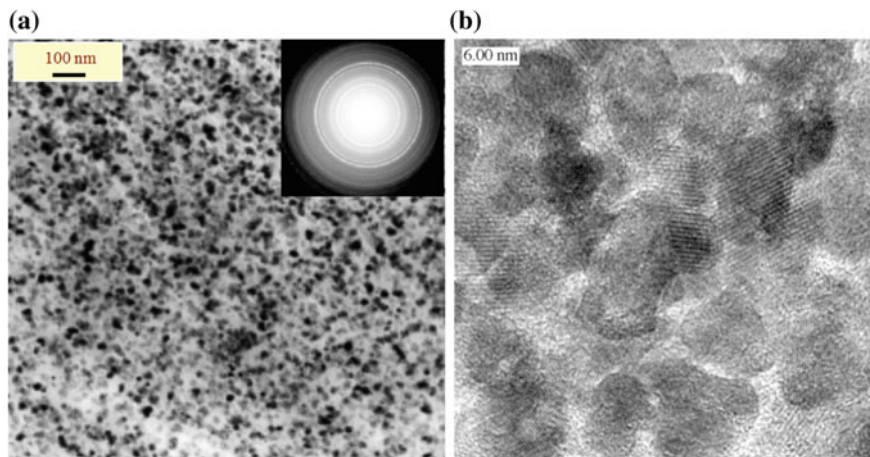
Fig. 8.23 Thermolysis product microstructure of Fe_2CoAcr at 643 K according to the TEM (**a**) and HRTEM (**b**)

Table 8.11 The average size of the spherical clusters in decarboxylated matrix

Sample	$CoAcr_2$	$FeAcr_3$	FeCoAcr	Fe_2CoAcr	Fe_2NiAcr	CoMal
$d_{EM,\,av}$, nm	7	7–9	5–6	5–6	6–8	3–4

electron-less dense matrix. The particles are close to spherical in shape, have a narrow size distribution and are present both individually and in the form of aggregates of 3–10 particles (Figs. 8.22 and 8.23). The average particle diameter ($d_{EM,\,av}$) is shown in Table 8.11.

Nanoscale particles are sufficiently uniformly in the matrix with a mean particle centers distance from each other of 8–10 nm. In the case of CoMal, along with nano-sized spherical particles relatively large aggregates in the form of a cubic crystal habitus with dimensions of 10–20 nm are simultaneously observed. Assuming that the volume of the starting acrylate consumed to form a metal-containing particle MO_x (size d_{MOx} and specific density ρ_{MOx}) has as initial particle $MAcr_n$ itself, spherical symmetry and a diameter d_{Acr}, the final product is a decarboxylated matrix $-(-CH_2-CH=CH-CH_2-)_n-$ with immobilized MO_x molecules in it and has an average density of $\overline{\rho}_{prod} \approx 0.5(\rho_{MOx} + \rho_{Acr})$, where ρ_{Acr} is the density of the starting monomer ($\rho_{Acr} = 1.5$ g cm^{-3}), we get the average distance d_{prod} between the centers of nano-sized particles:

$$d_{prod} = d_{MOx}\xi^{1/3}$$

($\xi = \rho_{MOx}(1 + n\mu_2/\mu_1)/\overline{\rho}_{prod}$, $\mu_1 = \mu_{MOx}$ is molecular weight of MO_x, $\mu_2 = \mu_{CH2CH}$, n is the number of Acr groups in the starting monomer per one atom M).
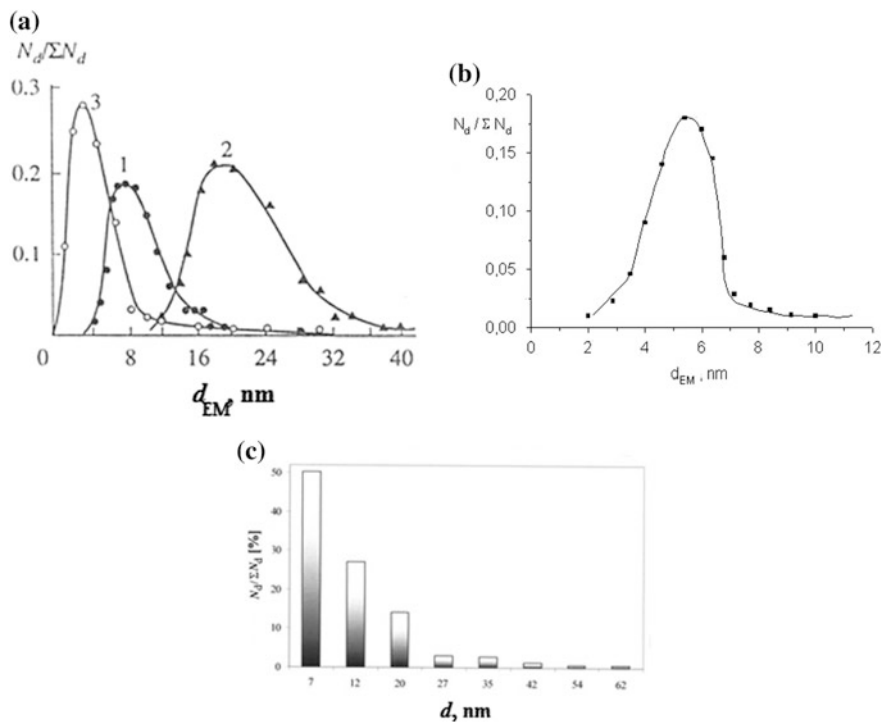
Fig. 8.24 The size distribution of metal-containing particles. Products of thermal transformation of metal carboxylates **a**: 1—FeAcr$_3$, 2—Fe(HCOO)$_2$·2H$_2$O, 3—CoMal, **b** cocrystallizate Fe$_2$CoAcr and **c** CoAcr$_2$

For $\rho_{MOx} = 5.2$ g cm^3 (specific density of Fe$_3$O$_4$ or Fe$_2$CoO$_4$), $\overline{\rho}_{prod} = 3.35$ g cm^3, $\mu_{MOx} = 78$, $\mu_{CH2CH} = 27$, n = 3 we have $d_{prod} \cong 1.5\ \overline{d}_{MOx}$. Thus for $\overline{d}_{MOx} = 5.0–9.0$ nm we have $\overline{d}_{prod} = 7.5–13.5$ nm, which is close to the observed distance between the particles in the decarboxylated matrix.

It should be noted that the average size of the particles formed during thermolysis of unsaturated metal carboxylates is lower than that observed for the products of thermal transformations of saturated metal carboxylates (Fig. 8.24) [229].

Thus, during the process of thermal transformations of metal carboxylates the material consisting of nanoscale metal particles stabilized in the matrix with a narrow size distribution is formed. The phase composition, morphology and structure of the formed nanocomposites are discussed in more detail below.

8.3.4 Kinetic Schemes and Thermal Transformation Reactions of Metal-Containing Monomers

Thermal transformations of metal-containing monomers are associated with the following three successive macrostages:

(i)   Dehydration of monomer crystallohydrates (T_{therm} < 423 K) with the simultaneous restructuring of the ligand environment, accompanied by the evolution of the carboxylate ligands (acrylic acid and maleic acid, respectively);

(ii) Solid state polymerization of rebuilt dehydrated monomer ($T_{therm} \approx 453$–493 K);

(iii) Decarboxylation of the resulting (co)polymer at high temperatures (T_{therm} > 473 K). The main gassing and sample weight loss during thermolysis is connected with the latter process.

Metal carboxylate thermal stability can be measured by the relative strength of the interatomic M–O and C–O bonds in its crystallochemical structure. The M–O and C–O bond lengths within the coordination polyhedron can vary significantly, which indicates their energy disparities. According to IR spectroscopy of dehydrated monomers (see Tables 8.5, 8.6 and 8.7), during dehydration the basic structure unit of metal-containing monomers is generally conserved. But in this case a denticity of certain portion of unsaturated ligands may change and like anhydrous carboxylates of unsaturated acids they are started simultaneously perform the role of a ligand, and a missing solvate function in the crystal structure. Increasing ligand denticity leads to distortion of the metal oxygen environment with a corresponding change in the M–O and C–O distances in the structure, and hence a change in their strength. In particular, the energy disparity of the M–$OOCCH=CH_2$ in $FeAcr_3$ indicates [230] dependence of the $CH_2=CHCOO$–ion fragmentation on the voltage of the accelerating field in the MS studies on fragmentation of $[Fe_3O(CH_2=CHCOO)_6]^+$ ion. The mass spectrum at U = 400 V (Fig. 8.25) of the ions with m/z = 539, 468, 397 corresponds to the evolution of one, two or three Acr-groups, and an ion with m/z = 341 corresponds to the evolution of $FeAcr_3$ molecules from the $[Fe_3O(CH_2=CHCOO)_6]^+$ molecular ion.

8.3.4.1 The Total Kinetic Scheme and the Decomposition Pathways of the Metal-Containing Monomers

With increasing the level of the thermal vibrations of the lattice of the dehydrated monomer (with increasing temperature) the break of the weakest M–O bonds is very likely to form a mono- or biradicals of the ligands: $CH_2=CHCOO^{.}$ in the case of acrylates and $^{.}OOCCH=CHCOO^{.}$ if maleates. Interaction of these radicals with the metal-containing maleate or acrylate moieties leads to the corresponding acids and the radical $R^{.}$ with H-depleted acrylate (maleate) group:
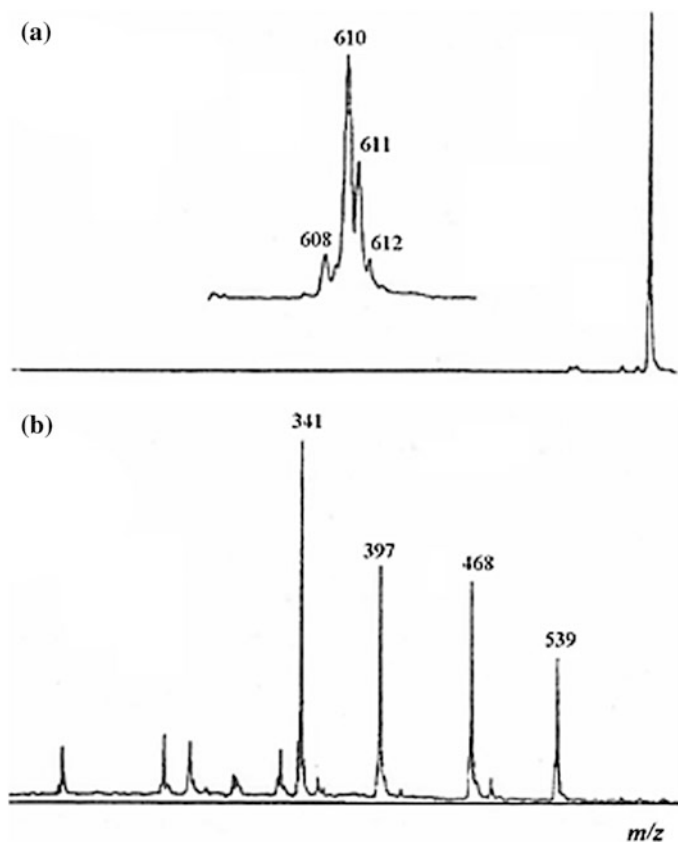
Fig. 8.25 Mass-spectra of positive ions extracted from the aqueous alcoholic solution of FeAcr$_3$ at $U = 200$ V (**a**) and 400 V (**b**)

$$CH_2{=}CHCOO^{\cdot} + RH \rightarrow CH_2{=}CHCOOH + R^I, \qquad (8.9)$$

$$^{\cdot}OOCCH{=}CHCOO^{\cdot} + RH \rightarrow HOOCCH{=}CHCOOH + R^I \qquad (8.10)$$
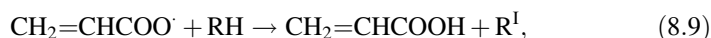
where RH = $(CH_2CHCOO)M_{1/n}^{n+}$, $R^I = (^{\cdot}CHCHCOO)M_{1/n}^{n+}$ (in the case of acrylate); RH = $(CHCOO)_2M_{2/n}^{n+}$, $R^I = (^{\cdot}CCOO)_2M_{1/n}^{n+}$ (in the case of maleate).

The resulting R^I radical involved in the growth and chain termination reaction to form a polymer of network or linear structure:

$$R^I + s(CH_2{=}CHCOO)M_{1/n}^{n+} \rightarrow R^I{-}\left[{-}CH_2{-}CHCOOM_{1/n}{-}\right]_s{-}R^I \qquad (8.11)$$

$$R^I + s(OOCCH{=}CHCOO)M_{2/n}^{n+} \rightarrow R^I{-}\left[{-}M_{1/n}OOCCH{-}CHCOOM_{1/n}{-}\right]_s{-}R^I \qquad (8.12)$$
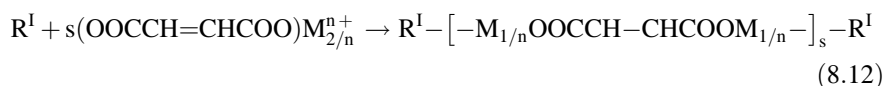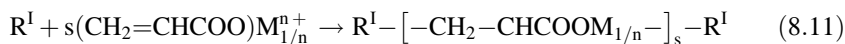
With increasing temperature, the metal-containing groups of the formed polymer undergo decarboxylation to form metal and (or) its oxide:

$$R^I - \left[-CH_2 - CHCOOM_{1/n}-\right]_s - R^I \rightarrow CH_2$$
$$= CH - CH = CH - \left[-CH_2 - CH = CH - CH_2 -\right]_{s/2} - CH = CH - CH = CH_2 \quad (8.13)$$
$$+ 2(s+1)CO_2 + (s+2)M$$

$$R^I - \left[-M_{1/n}OOCCH - CHCOOM_{1/n}-\right]_s - R^I \rightarrow CH \equiv C - \left[-CH - CH-\right]_s - C$$
$$\equiv CH + 2(s+2)CO_2 + (s+2)M. \quad (8.14)$$
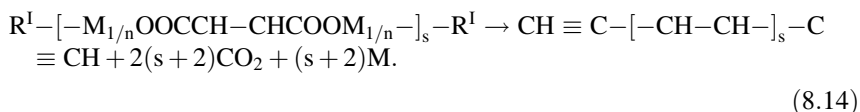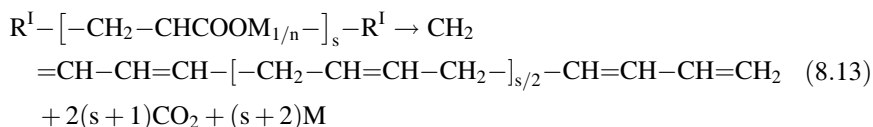
Additional thermopolymerization with participation of multiple bonds in decarboxylated products probably contributes to a cross-linked network structure, as indicated by the absence of reaction product solubility in organic solvents.

Thus, in general form solid product composition change during thermal transformation of metal acrylates and maleates can be expressed as fraction C–H–O-fragments.

$$MO_z(CH_2CHCOO)_{p-x}(CHCHCOO)_{q-y}(CH_2CH)_x(CHCH)_H, \text{ (for acrylates)} \quad (8.15)$$

$$MO_z(=CHCOO)_{2p-x}(=CCOO)_{2q-y}(=CH-)_x(\equiv C-)_H, \text{ (for maleates)} \quad (8.16)$$
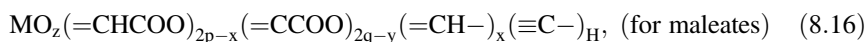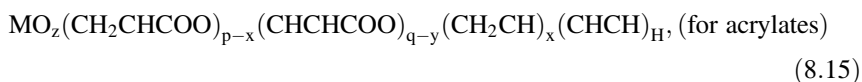
where $x = y = z = 0$ ($z \neq 0$ in the case of $FeAcr_3$ and FeMal), p and q are accordingly the number of intrachain and terminal H-depleted groups (p + q = 1). The most likely way of forming metal oxides is the oxidation reaction.

$$M + \lambda_1 CO_2 = MO_z + (\lambda_1 - z)CO_2 + zCO \quad (8.17)$$

$$M + \lambda_2 H_2O = MO_z + (\lambda_2 - z)H_2O + zH_2 \quad (8.18)$$
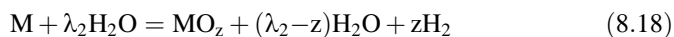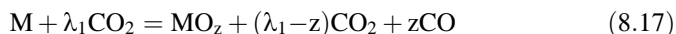
By solving the equations of mass balance using quantitative data on gassing, the sample weight loss, low temperature fractionation and mass spectral analysis of the CO_2, H_2 and CO gaseous products composition and yields of thermolysis product of the analyzed complexes were calculated [213, 214, 217, 221]. Consider this in more detail on the example of $CoAcr_2$.

8.3.4.2 Transformation Pathways of Cobalt Acrylate

As mentioned above, as a result of dehydration (desolvation) the denticity of the portion of Acr-ligands changes, which results in disparity of M–O bonds. As a consequence the break of weak M−O bond occurs to form a radical $CH_2=CHCOO^\cdot$

$$Co(CH_2=CHCOO)_2 \rightarrow CH_2=CHCOO^{\cdot} + [Co(CH_2=CHCOO)]$$
$$\rightarrow Co + 2CH_2=CHCOO^{\cdot} \qquad (8.19)$$
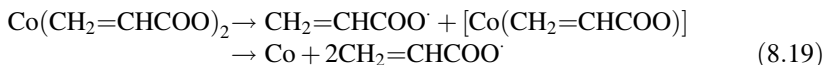
The resulting radical $CH_2=CHCOO^{\cdot}$ can later be spent on the following channels:

$$CH_2=CHCOO^{\cdot} \rightarrow CO_2 + CH_2=CH^{\cdot} - 218.2 \text{ kJ mol}^{-1} \qquad (8.20)$$

$$CH_2=CHCOO^{\cdot} + RH \rightarrow CH_2=CHCOOH + R^{\cdot} + (0-20.9 \text{ kJ mol}^{-1})^{\#} \qquad (8.21)$$
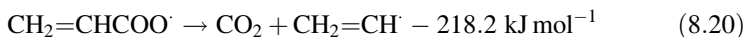
($^{\#}$Believed that E(CH2CHCOO–H) (g)) = 461.5 kJ mol^{-1}.)

$$R^{\cdot} = \overset{\cdot}{C}H=CH \quad CH_2=CH$$
$$\qquad\quad | \qquad\qquad |$$
$$\qquad O=CO-Co-OC=O$$

where
and further

$$CH_2=CH^{\cdot} + RH \rightarrow CH_2 = CH_2 + R^{\cdot} + \sim 0 \text{ kJ mol}^{-1}) \qquad (8.22)$$

$$CH_2=CHCOOH \rightarrow C_2H_4 + CO_2 - (0 \pm 4.18 \text{ kJ mol}^{-1})^{*}[185] \qquad (8.23)$$
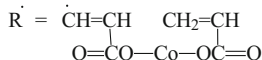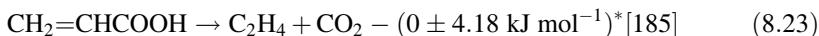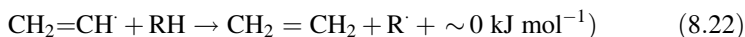
(*Estimates of the thermal effects were carried out for the gas-phase reaction. At that the following data and assumptions are used: E(CH2CHCOO–H) (g)) $\approx$ E (MeC(O)O–H = 461.5 kJ mol^{-1}, ΔH°_f(CH2CHCOOH) (l)) = −384.6 kJ mol^{-1}, ΔHev(CH2CHCOOH) (l)) = 545.6 kJ mol^{-1}. Then ΔH°_f(CH2CHCOOH) (g)) = 96.2 kJ mol^{-1}, ΔH°_f(CH2CH (g)) $\approx$ 271.7 kJ mol^{-1}, ΔH°_f(C2H4 (g)) = 52.3 kJ mol^{-1}, ΔH°_f(CO2 (g)) = −393 kJ mol^{-1}).)

$$CH_2=CHCOOH \rightarrow \text{output from the reaction zone(evaporation)} \qquad (8.24)$$
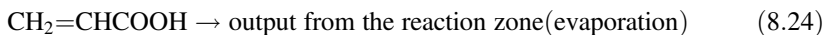
Since C_2H_4 in the gaseous decomposition products of CoAcr$_2$ (see Table 8.9) is not detected, it can be assumed that in the investigated temperature decomposition range of CoAcr$_2$ disappearance of the radical $CH_2=CHCOO^{\cdot}$ occurs mainly on the reactions (8.21) and (8.24). The radical formed by the reaction (8.21) can participate in a polymerization of a monomeric carboxylate, and AA [(8.26) and (8.27)], followed by decarboxylation of COOH and $Co(CO_2)_2$ fragments of polymer product. It is also likely that these processes are preceded by intramolecular opening of the double bond in R.

$$\overset{\cdot}{C}H=CH \quad CH_2=CH \qquad\longrightarrow\qquad CH_2=C-CH_2-\overset{\cdot}{C}H$$
$$\quad | \qquad\qquad | \qquad\qquad\qquad\qquad | \qquad\qquad |$$
$$O=CO-Co-OC=O \qquad\qquad O=CO-Co-OC=O \qquad (8.25)$$
$$R^1$$

$$2R^1 + CH_2=CH \quad CH_2=CH \longrightarrow R^1-(CH_2-CH-CH_2-CH)_n R^1$$
$$\qquad\quad | \qquad\qquad | \qquad\qquad\qquad\qquad | \qquad\qquad |$$
$$\qquad O=CO-Co-OC=O \qquad\qquad O=CO-Co-OC=O \qquad (8.26)$$

It is assumed that it is possible both linear and network structure of the formed polymer:

$$
\begin{array}{c}
\text{R}^1\!\!\left(\!\text{CH}_2\!-\!\text{CH}\!-\!\text{CH}_2\!-\!\text{CH}\!\right)_{\!n}\!\!\text{R}^1 \\
\text{O}=\!\text{C}\diagdown_{\text{O}} \quad \text{O}\diagup^{\text{C}=\text{O}} \\
\text{Co} \qquad \text{Co} \\
=\!\text{C}\diagup^{\text{O}} \quad \text{O}\diagdown_{\text{C}=\text{O}} \\
\text{R}^1\!\!\left(\!\text{CH}_2\!-\!\text{CH}\!-\!\text{CH}_2\!-\!\text{CH}\!\right)_{\!n}\!\!\text{R}^1
\end{array}
\qquad (8.27)
$$

$$
2\text{R}^1 + 2s\,\text{CH}_2\!\!=\!\!\text{CHCOOH} \longrightarrow \text{R}^1\!\!\left(\!\text{CH}_2\!-\!\underset{\text{COOH}}{\text{CH}}\!-\!\text{CH}_2\!-\!\underset{\text{COOH}}{\text{CH}}\!\right)_{\!s}\!\!\text{R}^1
$$

$$
\underset{\text{O}=\text{CO}-\text{Co}-\text{OC}=\text{O}}{\text{R}^1\!\!\left(\!\text{CH}_2\!-\!\text{CH}\!-\!\text{CH}_2\!-\!\text{CH}\!\right)_{\!n}\!\!\text{R}^1} \longrightarrow (n+2)\text{Co} + (2n+2)\text{CO}_2 + \text{R}^2\!\!\left(\!\text{CH}_2\!-\!\text{CH}\!\!=\!\!\text{CH}\!-\!\text{CH}_2\!\right)_{\!n}\!\!\text{R}^2 \qquad (8.28)
$$

$$
\text{R}^1\!\!\left(\!\text{CH}_2\!-\!\underset{\text{COOH}}{\text{CH}}\!-\!\text{CH}_2\!-\!\underset{\text{COOH}}{\text{CH}}\!\right)_{\!s}\!\!\text{R}^1 \longrightarrow (2s+2)\text{CO}_2 + \text{R}^2\!\!\left(\!\text{CH}_2\!-\!\text{CH}_2\!-\!\text{CH}_2\!-\!\text{CH}_2\!\right)_{\!s}\!\!\text{R}^2 \qquad (8.29)
$$

where

$$
\text{R}^2 = \text{CH}_2\!\!=\!\!\text{CH}\!-\!\text{CH}\!\!=\!\!\text{CH}.
$$

After transformation, the polymeric product (PPr) may have the following composition:

$$
(\text{CoC}_6\text{H}_6\text{O}_4)_{p-x}(\text{C}_4\text{H}_6)_x((\text{CoC}_6\text{H}_4\text{O}_4)_{q-y}(\text{C}_4\text{H}_4)_y(\text{C}_6\text{H}_8\text{O}_4)_{1-z}(\text{C}_4\text{H}_8)_z
$$

However, with regard to CoAcr_2 decomposition that occurs at 623–653 K, it is difficult to expect that $\left(\!\text{CH}_2\!-\!\underset{\text{COOH}}{\text{CH}}\!\right)$ groups may be present in the PPr, as the latter is eliminated quantity of CO_2 already at 473–488 K [231].

In the non-condensable at 88 K gaseous decomposition products, as already noted, the main components are H_2 and CO, whose appearance is most likely due to the oxidation processes of the resulting metal by H_2O and CO_2 vapor:

$$
\text{Co} + \lambda_1\text{CO}_2 \rightarrow \text{CoO}_r + (\lambda_1 - r)\,\text{CO}_2 + r\text{CO} \qquad (8.30)
$$

$$
\text{Co} + \lambda_1\text{H}_2\text{O} \rightarrow \text{CoO}_r + (\lambda_1 - r)\text{H}_2\text{O} + r\text{H}_2 \qquad (8.31)
$$

Based on the gassing and sample weight loss data as a result of CoAcr_2 transformations the following system of equations is compiled relating the values α_i of degradation products:

$$6\alpha_{C_6H_8O_4} + 4\alpha_{C_4H_8} + 6\alpha_{CoC_6H_6O_4} + 4\alpha_{C_4H_6} + 6\alpha_{CoC_6H_4O_4} + 4\alpha_{C_4H_4}$$
$$= 6 - \alpha_{CO_2} - \alpha_{CO} - 3\alpha_{C_3H_4O_2}$$
$$4\alpha_{C_6H_8O_4} + 4\alpha_{C_4H_8} + 3\alpha_{CoC_6H_6O_4} + 3\alpha_{C_4H_6} + 2\alpha_{CoC_6H_4O_4} + 2\alpha_{C_4H_4}$$
$$= 4 - \alpha_{H_2} - \alpha_{H_2O} - 2\alpha_{C_3H_4O_2}$$
$$4\alpha_{C_6H_8O_4} + 4\alpha_{CoC_6H_6O_4} + 4\alpha_{CoC_6H_4O_4} = 5 - 2\alpha_{CO_2} - \alpha_{CO} - 2\alpha_{C_3H_4O_2} - \alpha_{H_2O} - r\alpha_{CoO_r}$$
$$\alpha_{CoO_r} + \alpha_{CoC_6H_6O_4} + \alpha_{CoC_6H_4O_4} = 1$$
$$\alpha_{H_2} + \alpha_{CO} = p = r\alpha_{CoO_r}, \quad \alpha_{H_2}/\alpha_{CO} = \beta$$
$$\alpha_{H_2} + \alpha_{H_2O} = 1, \quad \alpha_{CO} + 1.64\alpha_{C_3H_4O_2} = \alpha$$

$$(8.32)$$

Here $\alpha_{CO_2}, \alpha_{H_2} + \alpha_{CO} = p$, $\alpha = 1/44(\Delta m/n_o - 18 + 16p) - \alpha_{CO_2}$ is the experimentally determined values (Δm is sample weight loss; n_0 is number of moles of (8.18) in the sample before the experiment).

Assuming that $\alpha_{C_6H_8O_4} = 0$, $\beta = 2$ (according to mass spectrometric determination) the transformation products yield was calculated and various variants for the PPr were analyzed. Experimental data satisfies the polymer composition $(CoC_6H_6O_4)_{p-x}$ $(C_4H_6)_x(C_4H_4)_y$.

At higher temperatures (Fig. 8.26) values $\alpha_{CO_2}, \alpha_{H_2O}$ are somewhat reduced and $\alpha_{CO}, \alpha_{H_2}, \alpha_{C_3H_4O_2}$ and α_{CoO_r} increase, and $\alpha_{C_3H_4O_2}$ increases strongly enough:

$$\alpha_{C_3H_4O_2} = 2.5 \cdot 10^8 \exp[-100/(RT)].$$

The ratio of $[O]:[Co] = r$ does not depend on T_{therm} and is equal 0.43 ± 0.03, which corresponds to a mixture of a metal and its oxide $(Co + \lambda CoO)$, where λ is $0.75, 0.20, 0.16$ for CoO, Co_2O_3, and Co_3O_4, respectively.

Fig. 8.26 Product yield at the decomposition end of CoAcr$_2$: 1—α_{CO_2}; 2—α_{CoO_r}; 3—$\alpha_{CH_2CHCOOH}$; 4—α_{H_2O}; 5—α_{H_2}; 6—α_{CO}
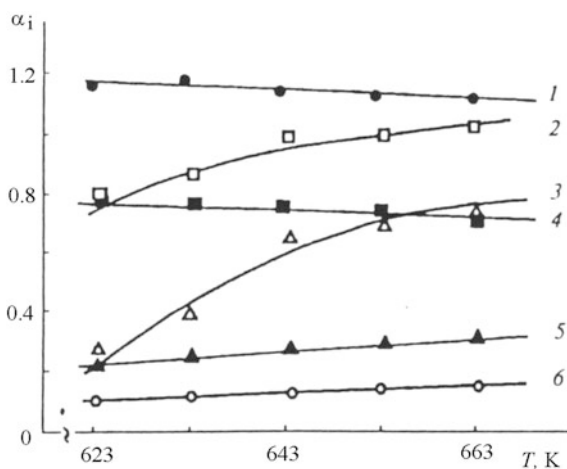
The main CO_2 source during $CoAcr_2$ decomposition apparently are decarboxylation processes, while additional reactions associated with the appearance of C_2H_4 and CO_2 [reactions (8.20) and (8.23)] occur in the $CuAcr_2$ decomposition.

Absence of PAA fragments in PPr indicates that the resulting AA out of the reaction zone is faster than the time to start polymerization. The presence in PPr composition of C_4H_4 fragments that arise by decarboxylation of $CoC_6H_6O_4$ fragments apparently, as in the case of other tested carboxylates indicates a low thermal stability of the metal carboxylate units. Ratio of $CoC_6H_6O_4$, C_4H_6 and C_4H_4 fragments in PPr depends on T_{therm} (Table 8.12).

It is noteworthy that with increasing T_{therm}:

– The total yield of PPr ($\alpha_{\Pi\Pi} = \alpha_{CoC_6H_6O_4} + \alpha_{C_4H_6} + \alpha_{C_4H_4}$) falls $\alpha_{PPr} = 1.9 \cdot 10^{-3}$ exp[34/(RT)];
– The yield $\alpha_{CoC_6H_6O_4}$, $\alpha_{C_4H_6}$ decreases and $\alpha_{C_4H_4}$ increases;
– The ratio $\omega = p/y$ decreases and $\alpha_{C_4H_6}/\alpha_{CoC_6H_6O_4} = \gamma$ increases

$$\omega = 4.7 \times 10^{-16} \exp[192/(RT)]$$
$$\gamma = 7.1 \times 10^{19} \exp[-238/(RT)]$$

Given that the $CoC_6H_4O_4$ fragments (after C_4H_4 decarboxylation) short polymer chains, ω fall may indicate a reduction in the length of the Co-polyacrylate chains in PPr with increasing T_{therm}. While $CoC_6H_4O_4$ fragments decarboxylate at $T_{therm} < 623$ K $CoC_6H_6O_4$ fragments at 623 K is still quite stable (their proportion is $\sim 30\%$), but even at 663 K, they are practically absent in PPr (<4%). Match the effective activation energy of the rate constants of gassing and the activation parameter of the temperature dependence $\gamma(T)$ ($E_a = 238.3$ kJ mol^{-1}) indicates that the decarboxylation reaction of polyacrylate fragments ($CoC_6H_4O_4$) is the rate-limiting stage in gassing process.

Table 8.12 The composition of PPr $(CoC_6H_6O_4)_{p-x}(C_4H_6)_x(C_4H_4)_y$ at various T_{therm}

PPr composition	623 K	633 K	643 K	653 K	663 K
$\alpha_{CoC_6H_6O_4} = p - x$	0.22 (0.26)	0.16 (0.20)	0.03 (0.04)	0.02 (0.03)	0.01 (0.02)
$\alpha_{C_4H_6} = x$	0.51 (0.59)	0.45 (0.56)	0.31 (0.46)	0.28 (0.46)	0.26 (0.41)
$\alpha_{C_4H_4} = y$	0.13 (0.15)	0.19 (0.24)	0.33 (0.49)	0.31 (0.51)	0.36 (0.57)
$\alpha_{CoC_6H_6O_4} + \alpha_{C_4H_6} = p$	0.73 (0.85)	0.61 (0.76)	0.34 (0.50)	0.30 (0.49)	0.27 (0.43)
$\alpha_{CoC_6H_6O_4} + \alpha_{C_4H_6} + \alpha_{C_4H_4}$	0.86	0.80	0.67	0.61	0.63
$\alpha_{C_4H_6}/\alpha_{CoC_6H_6O_4} = \gamma$	2.32	2.81	10.3	14.0	26.0

Note In parenthesis is given the proportion of fragment in the overall composition of the PPr

As part of the proposed transformation scheme appearance of $(C_2H_2)_2$ (or C_4H_4) fragments is possible only through polymer radicals R^3 recombination, formed from R^1 radical to form PPr and subsequent decarboxylation.

$$
\begin{array}{c}
\text{CH}_2{=}\overset{|}{\text{C}}{-}\text{CH}_2{-}\overset{|}{\text{CH}}\!\!\left(\text{CH}_2{-}\overset{|}{\text{CH}}{-}\text{CH}_2{-}\overset{|}{\text{CH}}\right)_{\!n}\!\!\text{CH}_2{-}\overset{|}{\text{CH}}{-}\text{CH}_2{-}\overset{\bullet}{\overset{|}{\text{CH}}} \longrightarrow \\
\text{O}{=}\text{CO}{-}\text{Co}{-}\text{OC}{=}\text{O}\quad \text{O}{=}\text{CO}{-}\text{Co}{-}\text{OC}{=}\text{O}\quad \text{O}{=}\text{CO}{-}\text{Co}{-}\text{OC}{=}\text{O} \\
R3
\end{array}
$$

$$
\longrightarrow\;
\begin{array}{c}
\text{CH}_2{=}\overset{|}{\text{C}}{-}\text{CH}_2{-}\overset{|}{\text{CH}}\!\!\left(\text{CH}_2{-}\overset{|}{\text{CH}}{-}\text{CH}_2{-}\overset{|}{\text{CH}}\right)_{\!2n}\!\!\!\!{-}\overset{|}{\text{CH}}{-}\text{CH}_2{-}\overset{|}{\text{C}}{=}\text{CH}_2 \longrightarrow \\
\text{O}{=}\text{CO}{-}\text{Co}{-}\text{OC}{=}\text{O}\quad \text{O}{=}\text{CO}{-}\text{Co}{-}\text{OC}{=}\text{O}\;\,\text{O}{=}\text{CO}{-}\text{Co}{-}\text{OC}{=}\text{O}
\end{array}
\quad (8.33)
$$

$$
\xrightarrow[-2\text{CO}_2]{}\quad
\begin{array}{c}
\text{CH}_2{=}\text{CH}{-}\text{CH}{=}\text{CH}\!\!\left(\text{CH}_2{-}\overset{|}{\text{CH}}{-}\text{CH}_2{-}\overset{|}{\text{CH}}\right)_{\!2n}\!\!\!\!{-}\text{CH}{=}\text{CH}{-}\text{CH}{=}\text{CH} \\
\text{O}{=}\text{CO}{-}\text{Co}{-}\text{OC}{=}\text{O}
\end{array}
$$
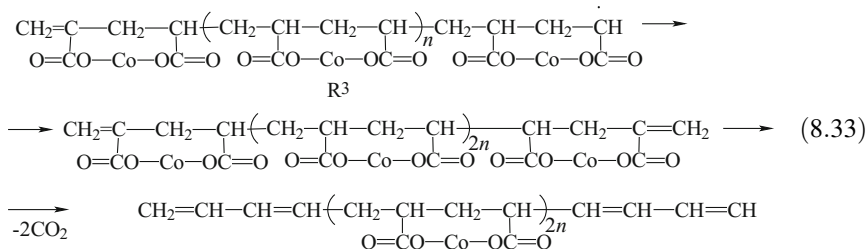
Assuming that the formed radicals R^3 are highly reactive, it can make the assumption that during the $CoAcr_2$ transformation the kinetic equilibrium concentration of growing radicals are installed in the reaction zone, and the number of recombining radicals R^3 at the transformation end is close to the number of formed AA. As a result, the value of ω is the ratio of the growth rate of the polymer radical (W_P) to the PPr formation rate (R^3 recombination rate). Therefore, $W_P \approx W_{PPr} \approx k_{PPr}\omega[R^3]^2 \approx k_{PPr}\omega\alpha^2_{CH_2CHCOOH} = 0.26 \times 10^2 \exp[-8/(RT)] \cdot k_{PPr}$, where k_{PPr} is rate constant of radical R^3 recombination. AA yield is equal to the ratio of the AA formation rate and $CoAcr_2$ spending rate:

$$
\alpha_{CH_2CHCOOH} = \frac{W_{CH_2CHCOOH}}{W_o + W_{CH_2CHCOOH} + W_p} \approx \frac{W_o}{W_o + W_p}, \qquad (8.34)
$$

where W_0 is the rate of radical $CH_2{=}CHCOO^{\cdot}$ formation.

Assuming $W_P \gg W_0$, we get

$\alpha_{CH_2CHCOOH} - \frac{W_o}{W_p}$ и $W_o \approx \alpha_{CH_2CHCOOH}$ $W_p \approx 6.5 \times 10^9$ $\exp[-109/(RT)] \cdot k_{PPr} = 6.5 \times 10^9 \exp[-(E_a + 109)/(RT) \cdot k^0_{PPr}$.

The effective activation energy of radical $CH_2{=}CHCOO^{\cdot}$ formation $E_a \geq 109.0$ kJ mol^{-1}. Thus, by increasing T_{therm} the proportion of monomer molecules $CoAcr_2$, directly exposed to thermal decomposition increases with the part of them which is involved in the polymerization process. Composition of PPr and its evolution at higher temperatures indicate that the terminal metal carboxylate groups are considerably more subjected to decarboxylation than $CoC_6H_6O_4$ fragments.

Similar product yields depending at the gassing end at different T_{therm} and during the transformation is observed in the case and other carboxylates (Figs. 8.27 and 8.28) [221, 222].

Analysis of experimental data and calculation results show the following:

(i) Polymerization and accordingly $CH_2{=}CHCOOH$ and $HOOCCH{=}CHCOOH$ formation proceed significantly at lower temperatures than the characteristic

Fig. 8.27 The dependence of the product yield at the transformation end of CoMal from at $T_{therm}(m_0/V).10^3 = 2.04$ g cm^{-3}: 1—$\alpha\sum f$, 2—$\alpha CO_2 f$, 3—$\alpha H_2 f$, αCOf, 4—α (= CHCOO)$_2 f$, 5—10α (=CHCOOH)$_2 f \approx 10\alpha$ ($\equiv$C–)$_2 f$, 6—α(=CH–)$_2 f$, 7—$\alpha COOf$, 8—$\alpha H_2 Of$, 9—($\Delta m/\pi O$) . 10^{-2}
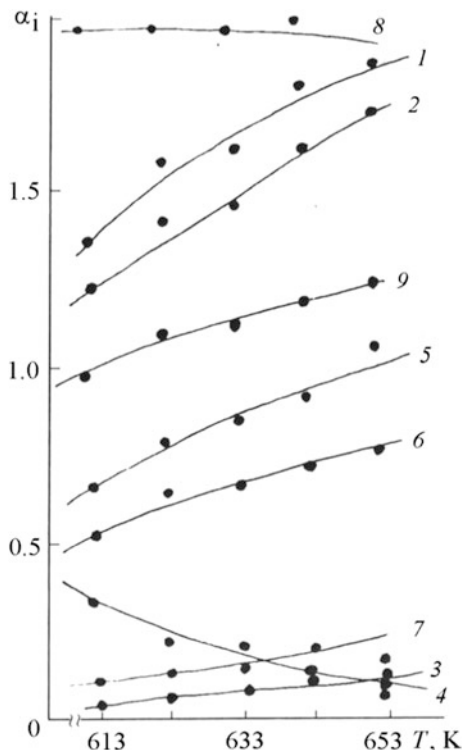
of main gassing. In the latter case, most of the condensable at T_{room} products appears in the early stages of transformation (warm-up period in the sample).

(ii) The formation of radicals (CH$_2$=CHCOO$^{.}$, $^{.}$OCOCH=CHCOO$^{.}$) resulting in polymerization initiation depends on the thermal stability of the M–O bond in desolvated monomer. For example, studies of thermolysis of cocrystallizates FeCoAcr and Fe$_2$CoAcr showed that the main role in initiating the copolymerization process play radicals CH$_2$=CHCOO$^{.}$, formed from Fe-containing cluster monomer, which is less thermally stable than the Co-containing monomer. In this system at high T_{therm} the elimination of two CH$_2$=CHCOO-radicals per dehydrated [Fe$_3$O(CH$_2$=CHCOO)$_6$](OH) molecule is possible.

(iii) Decarboxylation is key reaction in the gassing process. Thus metal carboxylate H-depleted end groups are significantly more susceptible to decarboxylation than the corresponding intrachain ones. This is consistent with the concept of increased energy saturation of the end groups of long-chain polymers [232]. Thus, during CuAcr$_2$, CoAcr$_2$, CoMal thermolysis decomposition of end metal carboxylate groups already takes place during the warm-up tested sample and the decarboxylation degree of intrachain metal carboxylate groups at the gassing end depends on the temperature and only at high T_{therm} elimination of CO$_2$ is achieved almost completely. The pattern is
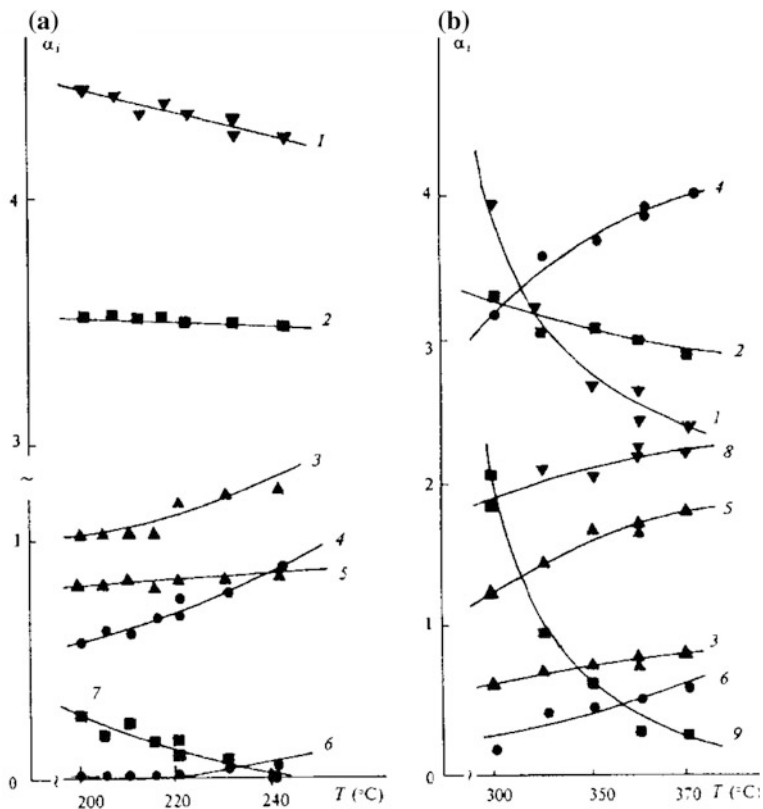
Fig. 8.28 The yield of the products of FeAcr decomposition at 200–240 °C (**a**) and 330–370 °C (**b**): $\alpha CH_2=CH + \alpha CH_2CH$ (*1*); αH_2O (*2*); $2z(a)$, $z(b)$ (*3*); αCO_2 (*4*); $\alpha CH_2=CHCOOH = \alpha CHCHCOO + \alpha CHCH$ (*5*); αH_2 (*6*); αCH_2CH (*8*); αCH_2CHCOO (*9*)

very significant for FeAcr$_3$ thermolysis. The decomposition of the terminal carboxylate groups is a major contributor to gassing at low temperatures (see Fig. 8.28a) on the background of the thermal stability of the respective intrachain groups that decompose at high temperatures (see Fig. 8.28b).

(iv) In the copolymers based on FeCoAcr and Fe$_2$CoAcr, unlike enhanced thermal stability of CoAcr$_2$ compared to FeAcr$_3$ intrachain and terminal Co-containing carboxylate fragments are thermally less stable than the corresponding Fe-containing ones to elimination of CH$_2$=CHCOO-radical.

(v) The ratio γ equals to amount of metal carboxylate groups in the polymer chain, including decarboxylated groups, to the number of terminal groups at the gassing end [$\gamma = (\alpha_{CH2CHCOO} + \alpha_{CH2CH})/(\alpha_{CHCHCOO} + \alpha_{CHCH})$ for acrylates, and $\gamma = (\alpha_{(=CHCOO)2} + \alpha_{(=CH-)2})/(\alpha_{(=CCOO)2} + \alpha_{(=C-)2})$ for maleates] reduced with increasing T_{therm}. Thus, the γ value level is in the range 5.75 (473 K) ÷ 5.0 (513 K), and 2.64 (603 K) ÷ 1.4 (643) for FeAcr$_3$,

respectively, in the high temperature and low temperature areas; 12.9 (613 K) ÷ 9.2 (653 K) for CoMal. In the case of Fe–Co-cocrystallizates under the same T_{therm} = 613–663 K the γ value level is slightly higher values than FeAcr$_3$ and CoAcr$_2$, and γ = 7.7 ÷ 5.0 (FeCoAcr); 5.5 ÷ 3.8 (Fe$_2$CoAcr). Value 2γ can characterize the effective length of the formed polymer chain, and its variation with increasing T_{therm} indicates a change in ratio of elimination rate and reaction zone of thermoinitiated radical (CH$_2$=CHC(O)O˙, ˙OC(O)CH=CHC(O)O˙) and radical polymerization rate. Most strongly it manifests itself at the thermal transformation of CuAcr$_2$ and CoAcr$_2$, for which γ decrease is also observed with the growth of T_{therm}. However for CoAcr$_2$ at T_{therm} > 643 K, and for CuAcr$_2$ over the studied T_{therm} range value of γ < 1. This is probably due to the high concentration of the radicals initiating polymerization in the transformation zone, in particular, with the competition of polymerization initiation process and radical recombination with subsequent decarboxylation of recombination products.

(vi) The composition of the metal-containing phase in solid transformation products of metal carboxylates at the gassing end depends on T_{therm}. With increasing temperature, the proportion of metal oxide phase increases, which is associated with an increase in the oxidation rate of the reactions (8.17) and (8.18), and is accompanied by an increase in the yield of CO and H$_2$. In the case of CuAcr$_2$ a Cu formed at low temperatures, but at T_{therm} > 503 K copper oxides (z ≤ 0.05) appear. After CoAcr$_2$ thermolysis value z is equal to 0.43 ± 0.03, which corresponds to the composition 0.25Co + 0.75 CoO (Fig. 8.29). The proportion of the oxide phase in CoMal at the thermolysis end is less than 15.0 mol% of the total metal content in the starting compound. During FeAcr$_3$ thermolysis metal-containing products are a mixture of Fe + FeO$_z$: at T_{therm} over the entire range in the high-temperature region (see Fig. 8.28) 0 < z < 1. Assuming FeO$_z$≡Fe$_3$O$_4$ α_{Fe3O4} value is close to the values of the Fe atom content in the Fe$_3$O$_4$ (Fig. 8.30) determined by measuring the specific magnetization of solid phase products. The z value in MO$_z$ in thermolysis products of FeCoAcr and Fe$_2$CoAcr (where M = Fe$_{1-a}$Co$_a$) also increases with T_{therm}. At the same time the ferrite yield $\alpha_{CoFe2O4}$ < 1, which is below the maximum expected for FeCoAcr and Fe$_2$CoAcr (Fig. 8.31). At that CoFe$_2$O$_4$ formation occurs only in the final stages of the thermal transformation during the decarboxylation of Fe-containing carboxylate groups, as evidenced by the dynamics of change in the magnetic characteristics of solid-state products: strong increase of χ_σ, σ_s, H_C due to the appearance CoFe$_2$O$_4$ phase at the thermolysis.

Thus, thermolysis of unsaturated metal carboxylates and the study of the properties of the products points to the first example of combining nanoparticle synthesis with simultaneous their stabilization by the resulting decarboxylated matrix of controlled thickness («one-pot» process).
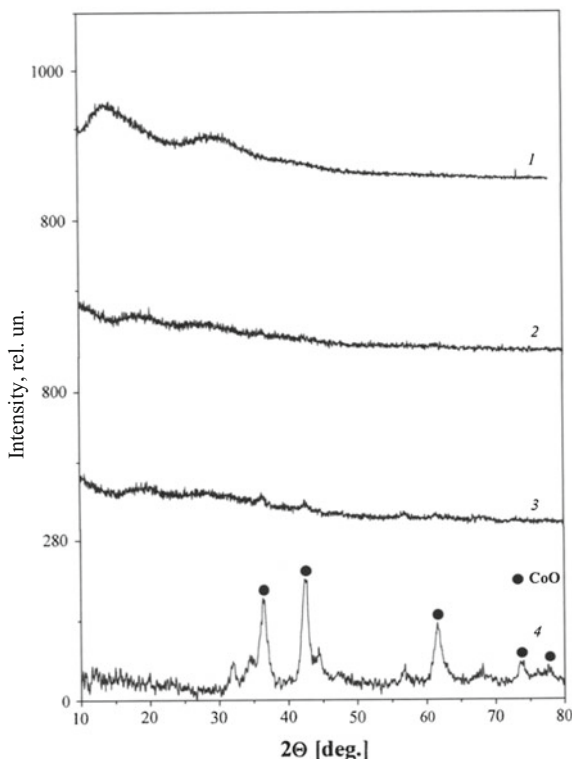
8.4 Thermolysis of Polymeric Metal Chelates

Recently polymeric metal chelates have become widely used as templates for a variety
of nanomaterials [16, 233]. Unlike other templates they produce monodisperse
nanoparticles of high quality, while maintaining the porosity and morphology of the
template precursor. Especially PMC widely used for the preparation of metal, metal
oxide and carbon nanomaterials.

Thermolytic transformations of polymeric metal chelates are very diverse [234–
243]. In particular, thermolysis of polymeric copper chelates based on polyacry-
lamidoxime fibers [244] proceeds through the three temperatures separated stages:
at 398–603 K (14.3% mass loss), 603–715 K (10.8%), and 715–965 K (68.6%).
The main weight loss occurs at the final transformation stage, which is somewhat
lower than in the case of the original polymer. Apparently, the copper ions have a
catalytic effect on the polymer degradation, which rate increases with increasing
copper ion content.

In the case of matrices having «active» to the complexing groups by reacting
MX$_n$ [9] (M=Cu(II), Ni(II), Co(II), Zn(II), Mn(II), VO(II), UO(II), Zr(IV), Ti(IV))
with the amino, hydroxyamino- and hydroxyl-groups, corresponding complexes are

Fig. 8.30 X-ray diffraction patterns of FeAcr$_3$ (1) and the thermolysis products at 663 K and different depths conversion: Δm = 27.4% (2) 33.3% (3) 55.5% (4)
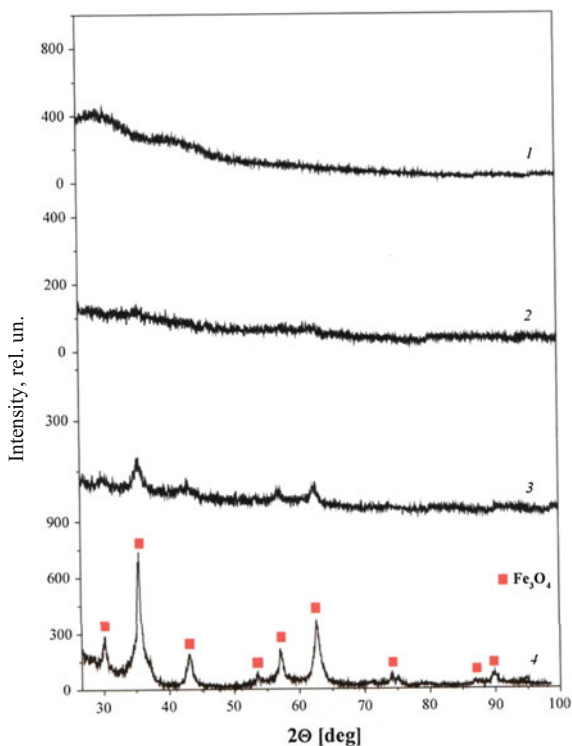
formed. The thermal stability of metal chelates falls in the number of Ni > Zn > Mn > Co > Cu > Ti > UO > Zr > VO, and the original polymers have the highest thermal stability. This is also the case for a number of diaminoalkane copolymers with Schiff base of 5,5′-methylene-bis(3-bromsalicylaldehyde) [245, 246].

Thermal behavior (473–1073 K) of polymeric Cu(II) and Co(II) chelates with poly (N-phenylmaleimide-*co*-AA) was studied by varying the comonomer ratio and different methods of metal binding [247]. Increasing N-phenylmaleimide units in copolymer chain increases the macrocomplex T_g and thermal stability, however, this increase is not as significant as one might expect (optimally from 623 to 646 K, and for some of the copolymer compositions even decreasing to 488 K).

Of interest is kinetic regularities of thermolysis of polymeric Co(II), Ni(II) and Cu(II) chelates based on oligo-2-[(4-bromophenylimino)methyl]phenol (OBPIMP) [248]. Thermodynamic and kinetic parameters of the decomposition of such systems, calculated by Coats-Redfern equation presented in Table 8.13. The values of the apparent activation energy of thermal decomposition of oligomer metal complexes vary among OBPIMP–Cu > OBPIMP–Ni > OBPIMP–Co.

As a typical example, we note the strategy of using MOF thermolysis for the preparation of metal and metal oxides nano-sized particles, such as Cu/CuO, Co/Co$_3$O$_4$, ZnO, Mn$_2$O$_3$, MgO and CdS/CdO [233]. According to this strategy, during

Fig. 8.31 X-ray diffraction patterns of Fe_2CoAcr (1) and the thermolysis products at 643 K and different depths conversion: $\Delta m = 25.1\%$ (2) 37.3% (3) 42.0% (4)
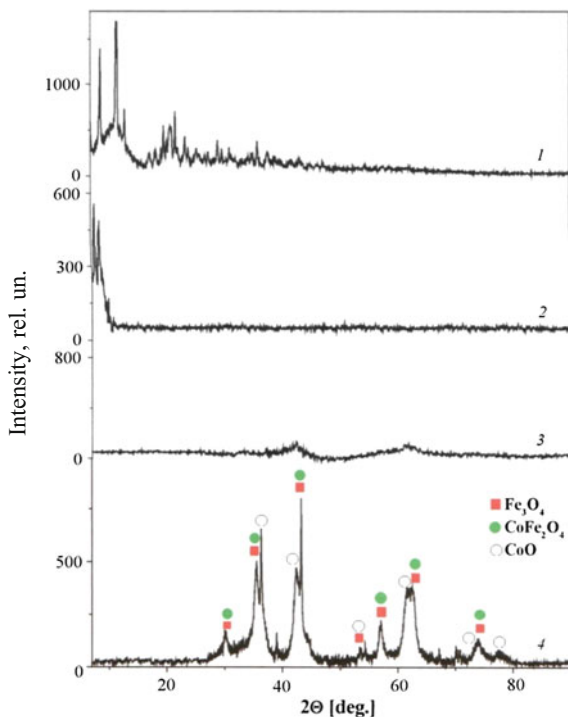
thermolysis in N_2 metals with a reduction potential of -0.27 V or higher contained in MOFs always form pure metal nano-sized particles, whereas metals with a reduction potential lower than -0.27 V form metal oxide nano-sized particles (Fig. 8.32). It is important that there is a relationship between the size of the formed nanoparticle and the distance between the SBU inside the MOF precursors. Besides, the crystallinity of the carbon matrix was also influenced by the thermolysis conditions (N_2 and air).

8.4.1   Synthesis of Carbon Materials

Interest in various forms and allotropic modifications of carbon is very wide from use as adsorbents [249], carriers for catalysts [250] and drug delivery [251] to the electrode materials [252]. The highly porous carbon materials may be prepared by various methods, including physical and chemical activation of the carbon, polymer aerogels carbonization and templating methods using zeolites and mesoporous silica [253–256]. Often, however, obtained mesoporous carbon materials are characterized

Table 8.13 Thermodynamic and kinetic parameters of thermal decomposition of OBPIMP-chelates

Compound	Stage[a]	n	E_a (kJ mol^{-1})	ln A (c^{-1})	ΔS^* (kJ mol^{-1})	ΔH^* (kJ mol^{-1})	ΔG^* (kJ mol^{-1})
OBPIMP	I (180–308 °C)	0.9	96.31	19.53	−87.52	91.76	139.6
OBPIMP–Co	I (202–317 °C)	0.2	39.84	5.81	−201.6	35.31	145.0
	II (353–724 °C)	0.9	31.34	0.693	−248.4	23.75	250.3
OBPIMP–Cu	I (229–353 °C)	0.5	100.2	18.16	−99.75	95.29	155.2
	II (353–724 °C)	1.0	65.36	6.33	−201.3	57.96	235.5
OBPIMP–Ni	I (257–383 °C)	0.8	62.04	6.48	−197.3	56.76	181.9
	II (383–626 °C)	0.4	48.81	6.82	−195.7	42.65	187.5

[a] I and II are the temperature regions of initial and 50% weight loss
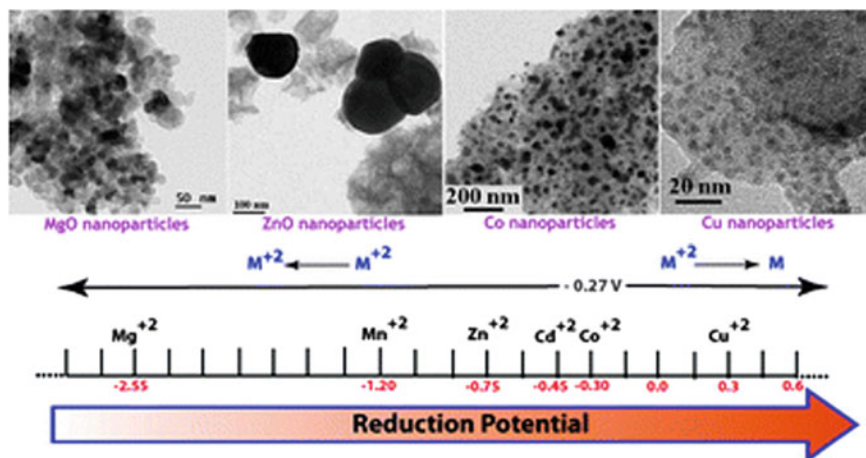
Fig. 8.32 Relation between the formed nanoparticle size and reduction potential

by a broad polydispersity to micron-sized particle and their fuzzy shape. Such materials have certain restrictions on the use, for example, in biomedical applications.

The direct thermal transformation of PMC, in particular MOFs or CPs, is an effective method for producing carbon materials, the hallmarks of which, as was first shown in [257] are ultra-developed specific surface area, ultra-high volume and controlled pore structure. This method was used for the preparation of porous carbons with special morphologies (for example, cube and polyhedron etc.) [258–260], and their pore structures may be easily varied depending on the as-formed metal or metal oxide nano-sized particles. However, using thermolysis of MOFs and CPs for the preparation of nanocomposites is restrained by their high cost [258, 261].

Carbon materials can be prepared by a «direct carbonization» of PMC without additional introduction of other carbon precursors [262–264], or in the presence of a carbon precursor such as furfuryl alcohol [257, 265, 266], a phenolic resin, carbon tetrachloride or ethylene diamine [267]. Zn- or Al-based MOFs are used most widely as a template MOFs. The synthetic protocol using additional carbon precursor includes its impregnation and subsequent polymerization within the MOFs micropores. During thermal carbonization porous carbon network formation and MOFs decomposition takes place simultaneously, i.e. MOFs is also the sacrificial template and secondary carbon precursor. The carbonization product is thoroughly washed with acid solution to remove metal nanoparticles, or a metal is evaporated and thus removed from the reaction system during the processes that are conducted at higher temperatures (up 1000 °C).

As an example, we consider MOF-5, which has 3D interconnected channel system with 18 Å cavities [268]. During the carbonization process at a temperature
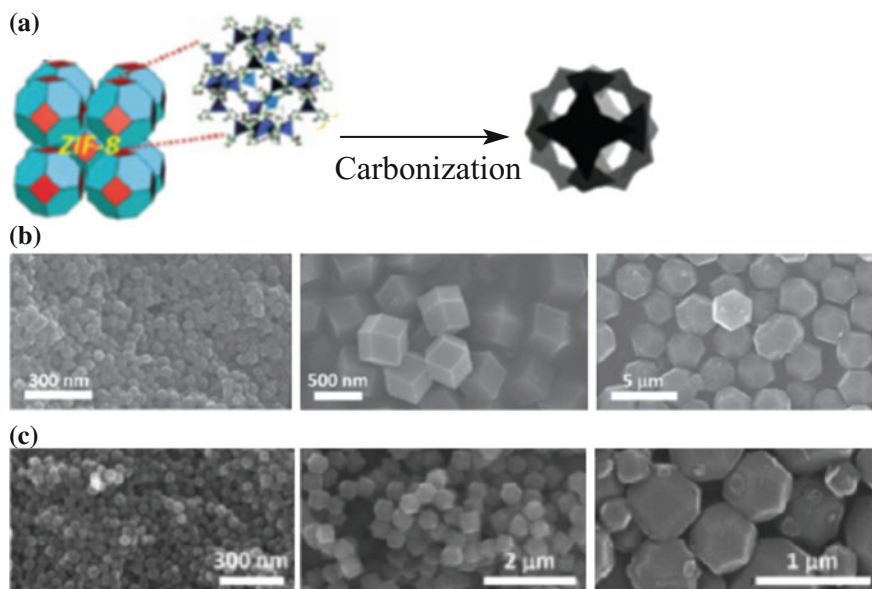
Fig. 8.33 **a** Synthesis scheme of nanoporous carbon by the direct carbonization of ZIF-8 precursor; **b** SEM micrographs of ZIF-8 crystals of various sizes; **c** SEM micrograph of nanoporous carbon of various sizes, obtained by the direct carbonization of ZIF-8

of 1000 °C under an argon stream MOF-5 is decomposed to form nanoporous carbon with a specific surface area and pore volume 2872 m^2 g^{-1} and 2.06 cm^3 g^{-1} [257]. Imidazole-based MOF ZIF-8 is zeolite-like pore structure [269]. Its crystals with different particle sizes directly carbonized at 800 °C in a one-pot process to form a nanoporous carbon [270, 271], which retains the morphology of the initial precursor (Fig. 8.33), and the adsorption-desorption N$_2$ isotherms of the obtained material are isotherms character typical for microporous materials (Table 8.14) [264].

Interestingly, for the ZIF-8 carbonization products obtained at the temperature range 600–1000 °C unlike nanoporous carbon-based Al-PCP [262] and MOF-5 [272] the formation of meso- and macropores are not observed (Table 8.15) [263], which, apparently, due to the structural features of the original templates.

3D framework structure of aluminum naphthalenedicarboxylate (Al-PCP) contains two types of square shaped pores, in particular, large and small channels with dimensions 7.7 × 7.7 Å^2 and 3.0 × 3.0 Å^2, respectively (Fig. 8.34) [273]. Apparently, such a structure of the coordination template in direct carbonization conditions at 800 °C promotes the formation of nanoporous carbon with extremely high surface area (5500 m^2 g^{-1}) (Fig. 8.35). But during carbonization over 900 °C specific surface area decreases up to 200 m^2 g^{-1} due to the structure collapse caused by the product graphitization. In such cases additional sources of carbon

Table 8.14 The surface area and pore volume for the initial ZIF-8 template and produced nanoporous carbon [264]

Sample	Average particle size (nm)	Surface area (m^2 g^{-1})	Pore volume (cc g^{-1})
Small-size ZIF-8	50	1530	1.3
Middle-size ZIF-8	300	1570	0.9
Large-size ZIF-8	2000	1960	1.2
Small-size carbon	50	1160	1.2
Middle-size carbon	300	1390	0.8
Large-size carbon	2000	1610	1.1

Table 8.15 Surface are and pore size of carbon materials obtained by direct carbonization of ZIF-8 [263]

Sample[a]	Surface area (m^2 g^{-1})		Total pore volume (cm^3 g^{-1})	Micropore volume (cm^3 g^{-1})		Pore diameter (Å)
	BET method	Langmuir method		t-Plot method	NL-DFT method	
Z-600	24	28	0.05	–	–	–
Z-700	520	580	0.27	0.19	0.19	10.6
Z-800	720	810	0.37	0.26	0.26	10.6
Z-900	1075	1215	0.57	0.38	0.39	10.2, 11.7
Z-1000	1110	1250	0.62	0.39	0.40	11.7, 12.7

[a]The numbers at Z denote the carbonization temperature NL-DFT is the nonlocal density functional theory

require to preserve the porous structure in the system, such as the use of a typical carbon precursor, for example, furfuryl alcohol [274].

As can be seen, the carbonization temperature of MOFs templates complex influences the characteristics of the resulting carbon material. As noted above, MOF-5 is characterized by mesoporous structure. Curves character of adsorption-desorption isotherms indicates the presence of macropores along with a low content of micropores (Fig. 8.36) [199].

Nanoporous carbon obtained at 530 °C (3040 m^2 g^{-1}) has the largest surface area, and with a further increase in temperature from 650 to 800 °C specific surface area decreased from 1521 to 1141 m^2 g^{-1}. But if the carbonization temperature exceeds 900–1000 °C an increase the specific surface area from 1647 to 2524 m^2 g^{-1} is again observed, which may be due to evaporation of Zn vapor at temperatures above 800 °C.

Al-DTPA microfibers were used as cost-effective precursors (Fig. 8.37) to prepare nitrogen-doped carbon microfibers (NCF) [275]. In particular, thermal transformation and acid-leaching of Al-DTPA leads to the well-defined NCFs. It is important to underline that the microfiber morphology of Al-DTPA persists in the
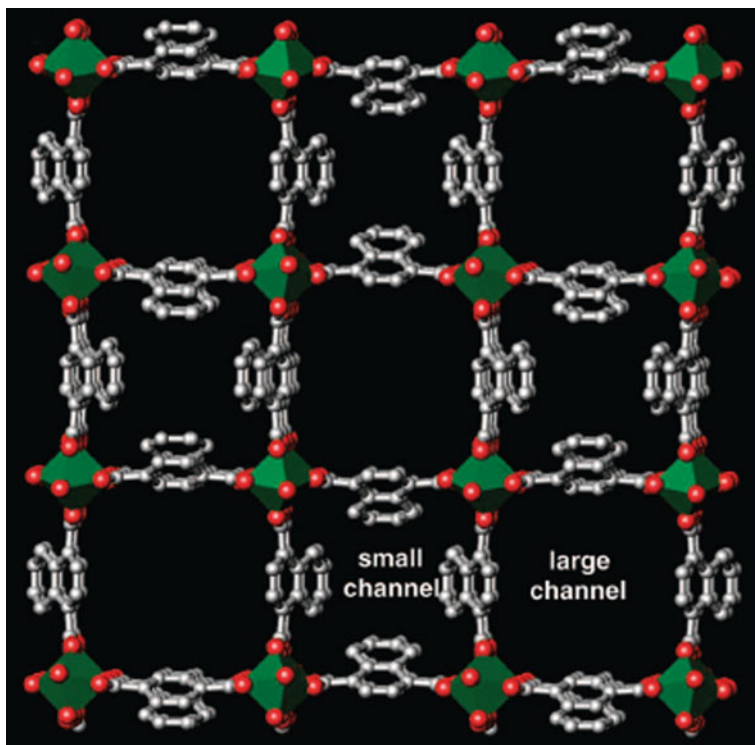
Fig. 8.34 Crystal structure of coordination polymer Al-PCP
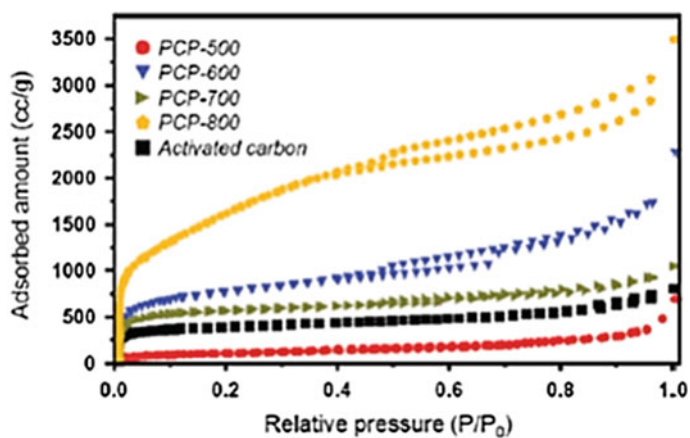
Fig. 8.35 The adsorption-desorption N_2 isotherms for carbonization products of coordination polymer Al-PCP at different temperatures
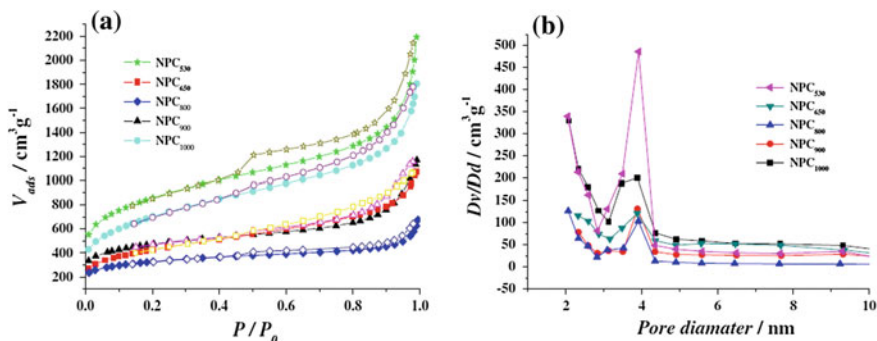
Fig. 8.36 The nitrogen adsorption-desorption isotherms (**a**) and pore size distribution (**b**) of carbonation products for MOF-5 obtained at various temperatures

Table 8.16 Textual data of NCFs obtained at 750, 900 and 1000 °C

Samples	S_{BET} (cm^2 g^{-1})	S_{meso} (cm^3 g^{-1})	S_{micro} (cm^3 g^{-1})	V_{total} (cm^3 g^{-1})	V_{micro}^T (cm^3 g^{-1})
750	604	84	520	0.39	0.28
900	933	108	825	0.58	0.43
1000	1072	67	1005	0.65	0.55

Fig. 8.37 Schematic illustration of the formation process of the nanoporous N-doped carbon microfibres and solid acids microfibers
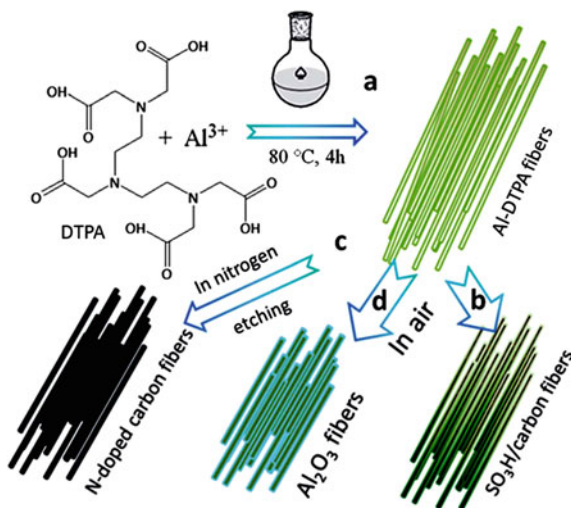
resulting carbon materials (Fig. 8.38b–e). The typical NCFs prepared at 900 °C (NCF-900) have the diameters of ∼500 nm and lengths of about 50 mm (Fig. 8.38b–d). It should be noted that some graphitization regions are observed in

Fig. 8.38 **a** SEM images of Al-DTPA microfibers; **b**, **c** SEM images of NCF-900; **d**, **e** TEM images of NCF-900. Inset is the corresponding selected area electron diffraction pattern of NCF-900; **f** SEM images of γ-Al$_2$O$_3$ obtained by heating Al-DTPA at 800 °C in air
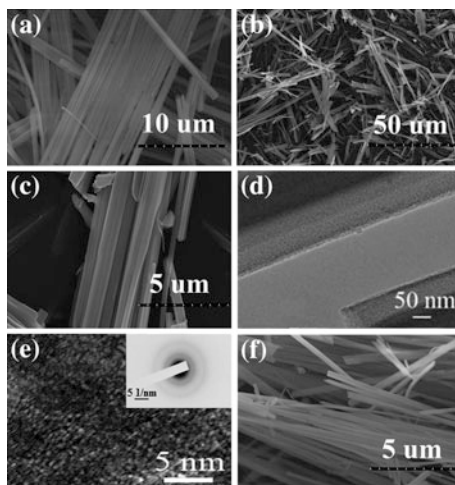
the high-resolution TEM image of NCF-900 (Fig. 8.38e). Increasing thermolysis temperature leads to a slight increase in the graphitization degree of carbon microfibers (Fig. 8.38e inset). Moreover, considerable interconnected pores are homogeneously distributed in the whole microfibers (Fig. 8.38d). The pore size distribution curves exhibited the mesopores with sizes of 2–30 nm. The total BET surface area of NCF-750, -900, and -1000 are equal to 604, 933 and 1072 m^2 g^{-1}, respectively (Table 8.16). Thus, the NCFs with nanoporous structure, uniform fiber morphology, and appropriate degree of graphitization were successfully obtained by thermolysis of Al-DTPA.

It should be noted that Al-DTPA microfibers can be also used as the precursors of γ-Al$_2$O$_3$ microfibers. After thermolysis of Al-DTPA in air at 800 °C, the well-defined microfiber morphology in γ-Al$_2$O$_3$ was observed in SEM images (Fig. 8.38f). As compared to Al-DTPA microfibers, there is decreasing the diameter (350 nm) and length (50 mm) (Fig. 8.38a). The prepared γ-Al$_2$O$_3$ has a smaller BET surface area (50 m^2 g^{-1}) and pore size distribution in the range of 2–15 nm.

It should be noted high contents of doped nitrogen atoms in the resulted NCFs. The N peaks at 398.3, 400.3, 401.2, and 403.6 eV in the deconvoluted N 1s XPS spectra (Fig. 8.39) corresponds to pyridinic, pyrrolic, graphitic and oxidized type of nitrogen atoms, respectively (Fig. 8.39 inset). Dominant nitrogen types in NCF-900 are the pyridinic- and graphitic-like nitrogen atoms.

Thus, various types of porous carbon materials may be prepared in a simple manner, based on the MOF structures as template molecules and a carbon source. Due to the high thermal stability, the nanoporous structure and the possibility to penetrate into the pores of small molecules with their subsequent participation in different «ship-in-bottle» reactions, MOFs can be considered as rigid templates similar to the mesoporous silica gel and zeolites [276–278]. Given the wide variety of MOFs of different compositions and morphology the carbon materials can be produced with controlled pore texture and surface area. Moreover, the synthetic

Fig. 8.39 The XPS survey spectra and the deconvoluted N 1s XPS spectra (inset) of NCF-750 (a), NCF-900 (b) and NCF-1000 (c)
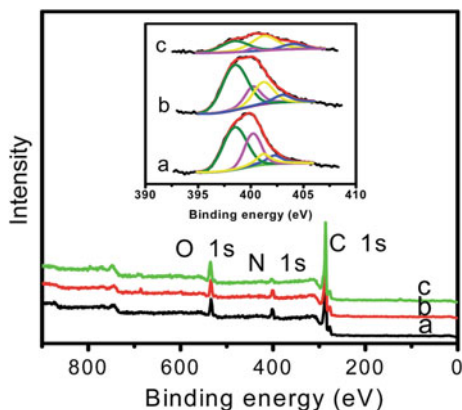
strategy based on MOFs allows to produce various carbon materials with catalytic [279], magnetic [280], energy storage and improved mechanical properties [281], including carbon nitrides [282].

Advantages of MOFs templates can be realized very efficiently in the production of various composite carbon materials, for example, type M/MO@C (Fig. 8.40). The general approach of the synthesis is based on the fact that the 1st stage of polymerization is carried out in MOFs carbon precursor (Fig. 8.40a), then a M@C nanocomposite is formed by thermolysis (Fig. 8.40b), and finally post-thermal treatment is carried out to convert the metal to metal oxide nanoparticles (Fig. 8.40c). The porosity of the carbon matrix and M/MO nanoparticle sizes are controlled in stages. According the similar scheme Cu@C, Cu_2O@C or CuO@C nanocomposites from MOF HKUST-1 [283] with maintaining the octahedral morphology of the starting MOF and Zn@C, ZnO@C based on MOF-5 [284] were obtained. In the resulting material the functional nanoparticles are interconnected by nanoporous carbon matrix, the diffusion properties of which are very attractive for use of such materials as electrode materials or in heterogeneous catalysis.

It should be noted the obtaining a porous cobalt oxide-carbon hybrid by carbonizing in an inert atmosphere and subsequently air-calcining nanocrystals of ZIF-67 [285]. It is important that the synthesized carbon composite material can act as an efficient electrochemical water oxidation catalyst.
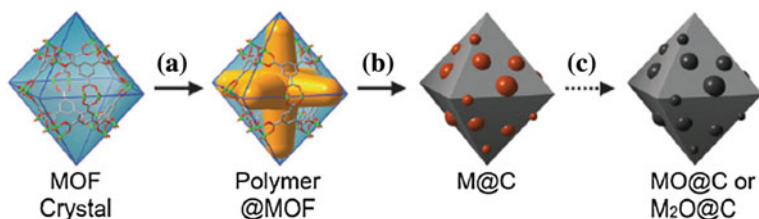
Fig. 8.40 Scheme of the transformation of MOFs in M/MO@C composite

8.4.2 The Preparation of Metal Oxide Materials

Methods for producing metal oxide nanocomposites from PMC are well developed and described in the literature (see recent review [16]). The basis of these methods is generally a single-stage solid-phase thermolysis of the precursor source, and, in general, quite comfortable, well-reproducible and easily scalable process. The methodology was used in the synthesis of nanoparticles of various metal oxides, for example, PbO [286–288], ZnO [151, 289, 290], Fe_2O_3 [291–294], Co_3O_4 [295–298], CdO [16], CuO/Cu_2O [299, 300], Tl_2O_3 [301] etc. We consider some of the most common examples.

Thus, $[Pb_2(2,9\text{-dimethyl-phen})_2(\mu\text{-}N_3)_2(\mu\text{-}ClO_4)_2]_n$ [302] and [Cd(2,9-dimethyl-phen)(TTA)_2]_n [303] were used for PbO and CdO nanoparticles preparation, respectively. Thermal decomposition of the 3D CP $[Pb(phen)(1\text{-}N_3)(1\text{-}NO_3)]_n$ containing an azide-anion ligand gave PbO nanoparticles [304].

ZnO nanomaterials with desired morphologies have been obtained by thermal decomposition of appropriate CPs and MOF precursors [16, 53, 289, 290, 305, 306]. For example, calcination of infinite rectangular-tubular helices $[ZnCl_2L]$ and $[ZnBr_2L]$ (L is bis(3-pyridyl)cyclotetramethylenesilane) at 500 °C gives uniform hexagonal tubular spire crystals of $1.2 \times 1.2 \times 4.0 \ \mu m^3$ dimensions and spheres, respectively [307]. SEM images of the products of $[MX_2L]$ thermolysis at 500 °C

Fig. 8.41 SEM images of thermal decomposition residue of $[ZnCl_2L]$ (**a**) and $[ZnBr_2L]$ (**b**) calcined at 500 °C for 2 h
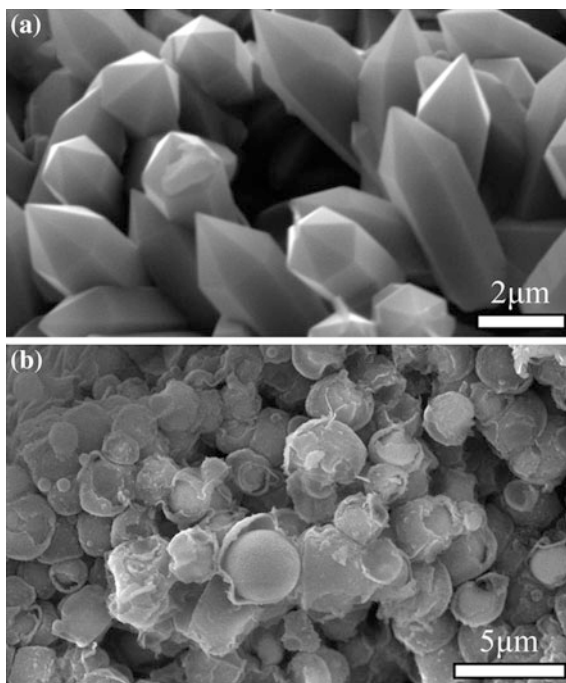
(Fig. 8.41) show that the compounds ultimately change to zinc(II) oxide crystals. For [ZnCl$_2$L], calcination at 500 °C leads to the growth of each ZnO single crystal.

The Zn(II) oxide and Cd(II) oxide nanoparticles were prepared by thermolysis of Zn(II) and Cd(II) CPs, [Zn(L)$_2$(N$_3$)$_2$]$_n$, [Zn(L)$_2$(SCN)$_2$]$_n$, [Cd(L)$_2$(N$_3$)$_2$]$_n$ and [Cd(L)$_2$(SCN)$_2$]$_n$, where L is 2-aminomethylpyridine [308]. SEM images exhibit the average size of prepared ZnO and CdO nanoparticles of 60–70 nm. We also note the preparation of ZnO nano-sized particles using Zn-isophthalate [309] and CdO nanowires from Cd-terephthalate complexes [310].

The calcinations of nanoparticles of a 3D Cd(II) compound, [Cd(L)$_2$(H$_2$O)$_2$] (L$^-$ is 1H-1,2,4-triazole-3-carboxylate), at 650 °C under air yielded CdO nanoparticles [311].

A series of lead-containing polymeric complexes have been applied for PbO nanoparticle formation. PbO nanoparticles serve as catalyst [312] for multicomponent organic synthesis reactions, for instance Paal-Knorr reaction and oxidative coupling of methane, due to the significant catalytic property with operational simplicity, high reactivity, environmental friendliness, reduction of reaction times, and reusability of PbO nanoparticles [313]. In this respect, a CP of lead(II) nitrate complexes with bridging trans-1,2-bis(4-pyridyl) ethene (L) ligand, [Pb(μ-NO$_3$)$_2$(L) (MeOH)]$_n$, was used [314] to prepare PbO nanoparticles using two different methods. Nano-structured PbI$_2$ and PbO were synthesized from Pb(II) metal-organic polymer, [Pb(μ-L)(μ-I)$_2$]$_n$, where L is pyrazine, by calcination with argon and air, respectively [315]. Different N-heterocyclic ligands with carboxyl or carboxamide groups have also been used. Thus, after calcination of nanobelts of a lead(II) CP, [Pb(L)$_2$]$_n$, HL = 3-pyridinecarboxylic acid, at 400 °C, pure phase nano-sized lead(II) oxide was produced [316].

The nanostructure of 1D copper CP, [Cu(HL)NO$_3$]$_n$ (H$_2$L is [2-[1-(2-hydroxypropylimino)ethyl] phenol]), was used as precursor to obtain single phase CuO nano-sized particles by thermolysis [317]. According to the SEM images the diameters of the prepared products were equal to 40 nm (Fig. 8.42).

Calcinations of the nano-sized copper(II) polymeric compound, [Cu(L)(H$_2$O)$_2$]$_n$ [L = 2,6-pyridinedicarboxylate], at 500 °C under air yielded CuO nanoparticles [318]. Oriented growth of single crystalline Cu(111) flake was reached by the thermolysis of a 1D chain-like hybrid CP [(CuBr)$_2$(bpy)]$_n$ (Fig. 8.43) [319].

After calcining, the cerium-based CPs micro/nanostructures such as nanoparticles, nanorods, and microflowers based on three isomers of benzenedicarboxylic acid at high temperature, ceria with retained morphologies were achieved [320].

Thermolysis of the porous CPs with nanorod morphology based on a catechol-substituted Pp [meso-tetrakis(3,4-dihydroxyphenyl)-Pp] led to carboniferous materials containing metal oxide nanoparticles with large surface areas (up to 800 m^2 g^{-1}) [321].

A porous indium(III) MOF, [In$_2$(OH)$_2$(L)]$_n$·2nH$_2$O (MIL-60, L = 1,2,4,5-benzenetetracarboxylate), was used for obtaining In$_2$O$_3$ nanoparticles by thermolysis of MIL-60 at 450 °C under air [322].

The advantages of these PMC precursors are simplicity of processing and long-range ordering that allow the synthesis of metal oxides with various morphologies.
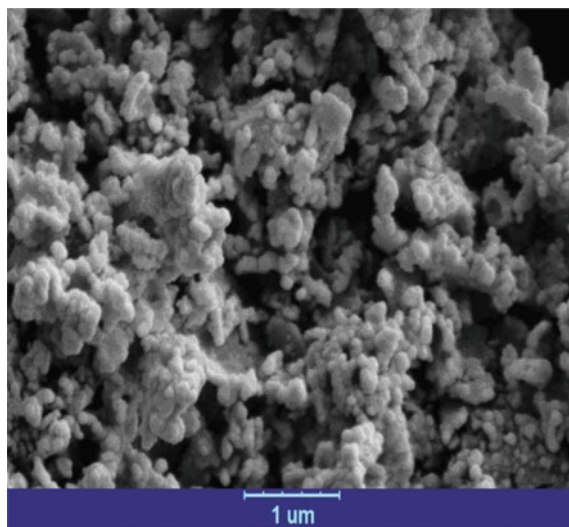
Fig. 8.42 SEM images of CuO nanoparticles prepared by direct calcination of Cu(II) CP
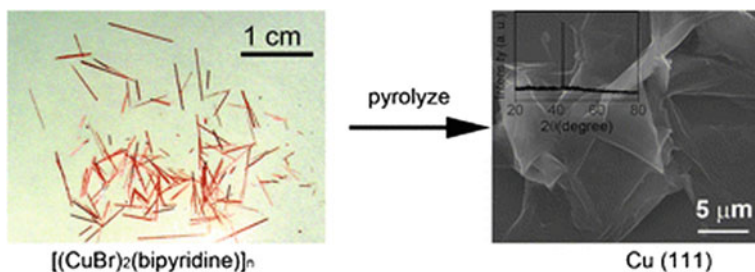
Fig. 8.43 The preparation of Cu(111) flake by pyrolysis of [Cu(Br$_2$)(bpy)] under N$_2$ at 750 °C

Phase composition and properties of the resulting metal oxide nanocomposites depend on the crystal structure and morphology of the starting PMC precursor, its particle size, and the synthesis conditions (the influence of the temperature, environment, the nature of the surfactant and etc.).

8.4.2.1 Influence of the Original Morphology and Particle Size of Polymeric Metal Chelates

Size and morphology of the produced nanomaterials are highly dependent on the type and morphology of the PMC precursor [16, 323–325]. Thus, hollow and non-hollow In$_2$O$_3$ particles with different morphologies may be selectively obtained

from the PMC according to their chemical composition and porosity. Hexagonal rod microparticles of the CPP-1 based on 1,4-benzenedicarboxylate and indium(III) ions during the calcination at 550 °C also form hexagonal polycrystalline particles (consisting of ~ 20 nm crystallites) of In_2O_3 in the form of rods whose size is about 35% less than the original precursor [326]. A similar character of morphology transformation during thermolysis is shown in another example of a coordination polymer (CPP-2) composed of In(III) and 2,6-bis[(4-carboxyanilino) carbonyl] pyridine with the particles in the form of hexagons (Fig. 8.44). As indicated, depending on the precursor decomposition mechanism the hollow and non-hollow particles of In_2O_3 can be obtained, on the basis of the CPs with hollow and non-hollow structure of the particles, respectively.

The nanorod morphology is characteristic of the thermolysis products of CP with $[Zn(4,4'-bipy)Cl_2]_n$ block [327], while during the decomposition of MOF with $[Zn(ox)(4,4'-bipy)]_n$ block (where ox is oxalate) ZnO nanostructure formed in a radially spaced nanoneedles (Fig. 8.45), i.e. different framework structure of the initial CPs influences the final morphology of the formed ZnO nanostructures. Intermediates in forming ZnO nanorods are rod-shaped nanoparticles while intermediates of needle-like ZnO nanostructures are spherically agglomerated nanoparticles.

Porous γ-Fe_2O_3 nanoparticles were prepared via a solid-state transformation process of a mesoporous iron(III) carboxylate crystal, MIL-100(Fe) [328]. The N_2 adsorption-desorption analysis also demonstrates the mesoporous character of the derived γ-Fe_2O_3 material, with type IV N_2 isotherm at 77 K. This material has a relatively large specific surface area 123.5 m^2 g^{-1}, which is presumed to be benefited from the two-step calcination of the template MIL-100(Fe). On the other hand, the pore size distribution reveals that most of the pores are focused on 10 nm, indicating the mesopores are effective formed for the γ-Fe_2O_3.

Of interest is using MOF thermolysis to develop the porous iron oxides [257, 295, 329–333]. As an example, we note the fabrication of spindle-like mesoporous α-Fe_2O_3 using MOF MIL-88(Fe) as template [294]. The prepared spindle-like mesoporous α-Fe_2O_3 was composed of clustered Fe_2O_3 nanoparticles with size of <20 nm. In another example a facile synthesis of porous Fe_2O_3 nanocubes by simultaneous oxidative decomposition of Prussian blue nanocubes was demonstrated [334, 335]. The derived porous Fe_2O_3 nanocubes are composed of very fine Fe_2O_3 nanoparticles with size of several nanometers. It is important that MOFs show distinct advantages due to their well-ordered crystalline structure, high porosity, large surface area, and tunable pore size, in comparison with other templates.

It should be noted that during the MOF pyrolysis it can also be prepared metal oxide nanostructure consisting of the same primary particles, but with a different secondary and tertiary architecture thus modulating the macroscopic structure of the initial CP. For example, two types of Co_3O_4 nanomaterials with plate-like and rod-like morphology of the nanoparticles, based on the Co-containing plate-shaped $[Co_3(L)_3(DMF)_4]_n$, p-MOF) and rod-shaped $([Co(L)(DMSO)]_n$, r-MOF) coordination polymers, consisting of the same composite units (Co^{2+} and 1,4-benzenedicarboxylate (L)) (Fig. 8.46), were prepared through pseudomorphic transformation
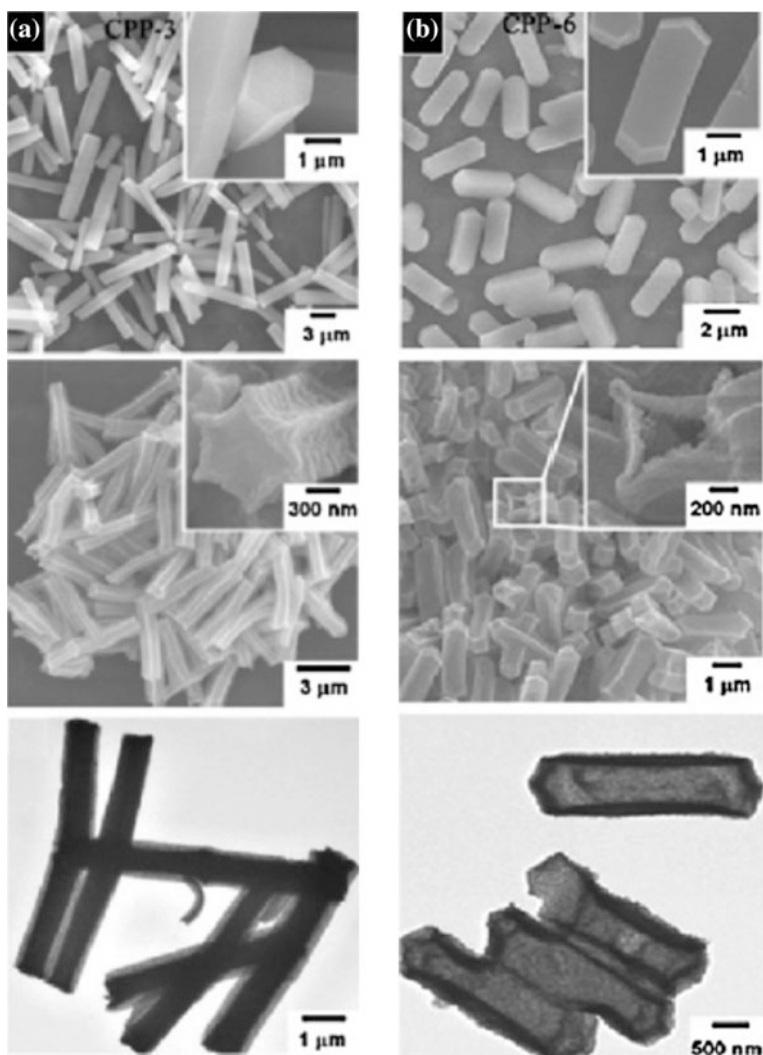
Fig. 8.44 a SEM images of (a-top) hexagonal rod-shaped precursor CPP-1, **b** (b-top) elongated hexagon-shaped precursor CPP-2. SEM (middle) and TEM (bottom) images of (**a**) non-hollow hexagonal rod-shaped In_2O_3, (**b**) hollow elongated hexagon-shaped In_2O_3

[335]. ZnO nano-sized materials were prepared by thermolysis of the host and the apohost framework of $[Zn_2(L)_2(dabco)]·4DMF·0.5H_2O$ with the same L ligand [336]. However, ZnO microrods composed of ZnO nanoparticles were prepared by the thermolysis of fully desolvated framework of this compound. It was concluded that the role of guest DMF in obtaining ZnO nano-sized particles from the solvated
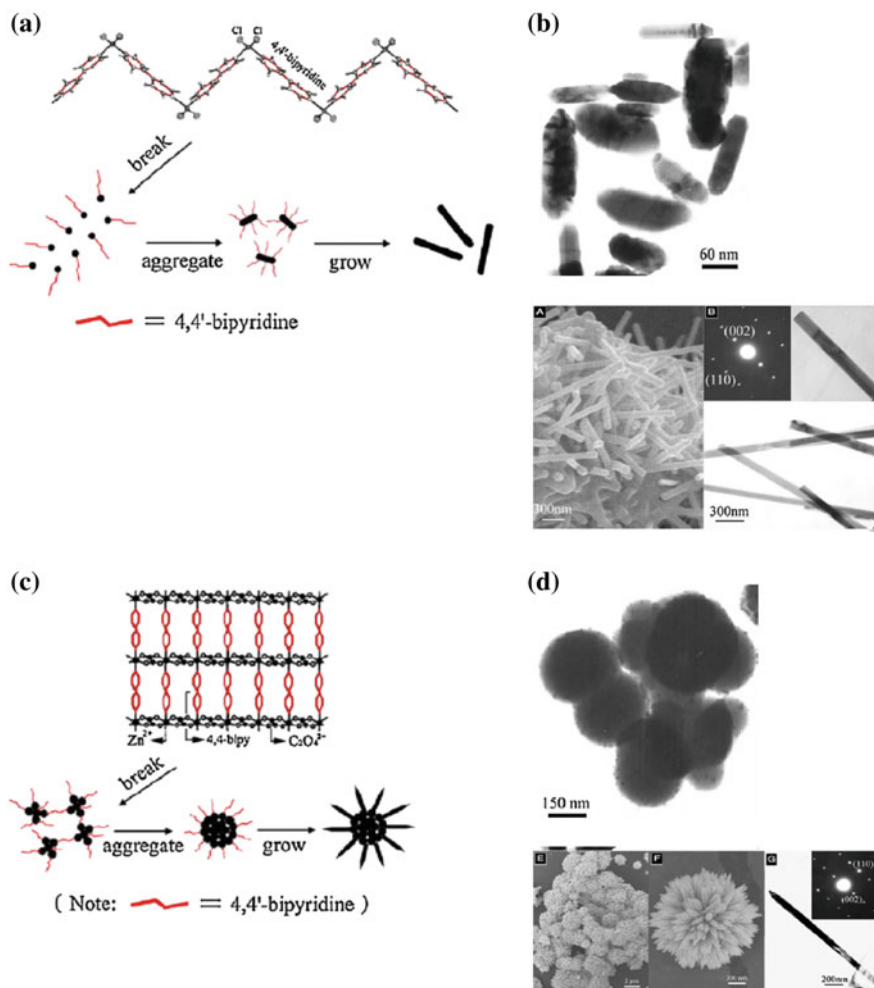
Fig. 8.45 Scheme of formation of ZnO nanorods and nanoneedles during thermolysis of [Zn(4,4′-bipy)Cl₂]ₙ (**a**) and [Zn(ox)(4,4′-bipy)]ₙ (**c**) and TEM (top) and SEM (bottom) micrographs of intermediate (top) and final decomposition products (bottom) of CPs [Zn(4,4′-bipy)Cl₂]ₙ (**b**) and [Zn(ox)(4,4′-bipy)]ₙ (**d**)

complex is similar to the role of polymer stabilizers in the formation of nano-sized particles.

Thermolysis of nano plates of two Cd(II)-based MOFs, $[Cd_2(L)_2(L')_2]_n \cdot (DMF)_x$ (TMU-8) and $[Cd(L)(4,4'-bipy)]_n \cdot (DMF)_y$ (TMU-9) where H_2L is V-shaped flexible dicarboxylate ligand 4,4′-oxybis(benzoic acid) and the L′ is N-donor ligand 1,4-bis (4-pyridyl)-2,3-diaza-1,3-butadiene, leads to CdO nano-sized particles (Fig. 8.47) [337]. SEM images of the products exhibit the formation of aggregation of CdO nano-sized particle in the range of 60–160 nm. Particle sizes of CdO prepared by
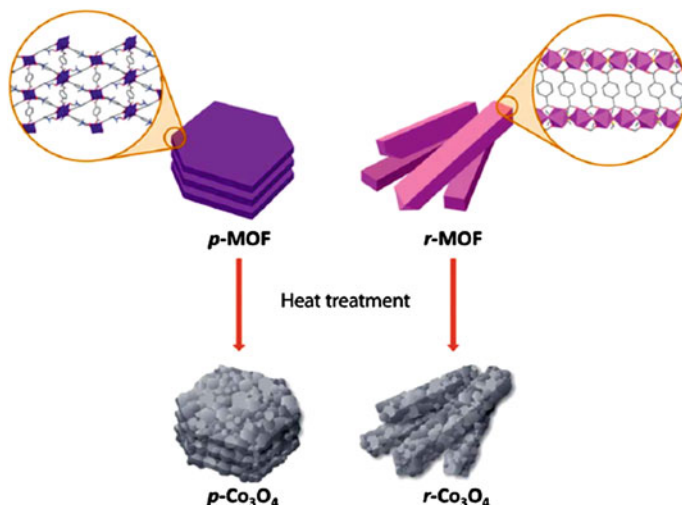
Fig. 8.46 Scheme of pseudomorphic conversion of Co-based MOFs
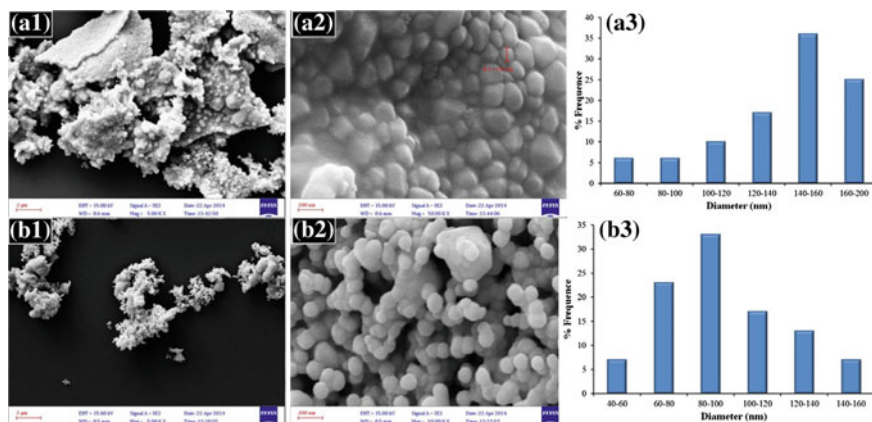
Fig. 8.47 FE-SEM images and the corresponding particle size distribution histogram of CdO nanoparticles prepared by thermolysis of **a** TMU-8 and **b** TMU-9 at 550 °C

thermolysis of TMU-9 are smaller than those prepared from calcination of TMU-8 that is associated with the influence of the structures of these two MOFs on the final morphologies of CdO particles [16].

The 1D CP, [Zn(4,4′-bpy)(H$_2$O)$_4$](L).4H$_2$O (H$_2$L is acetylenedicarboxylic acid), and 3D MOF, Zn(L)$_2$.(L′)$_2$ (L′ is triethylamine) were applied as precursors for the synthesis of ZnO nanocrystals via direct thermal decomposition [338]. Interestingly, changing the precursor from 1D CP to 3D MOF changes the morphology from nanorods to nanoparticles. In particular, the SEM images (Fig. 8.48) exhibited
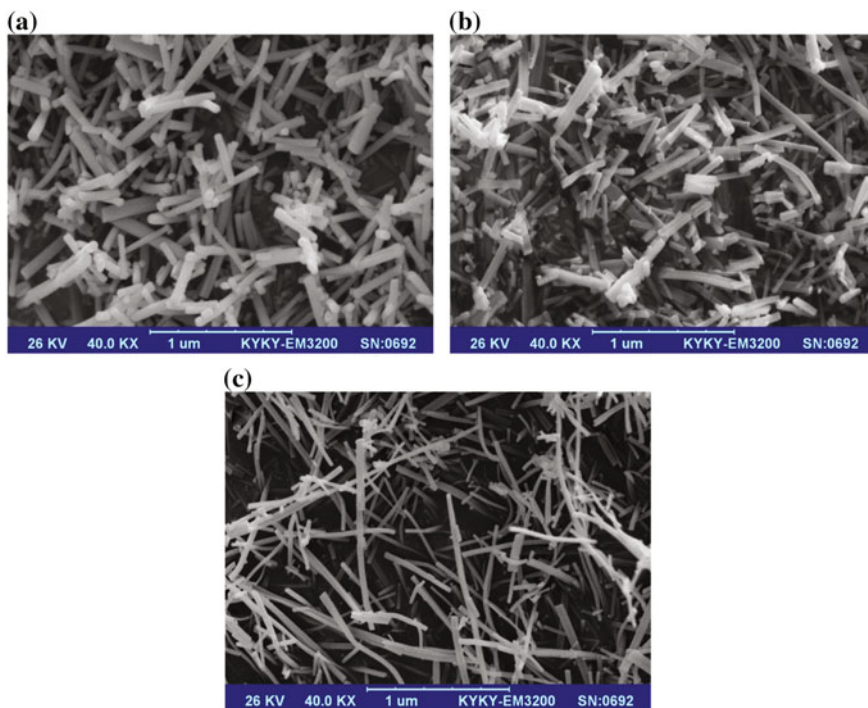
Fig. 8.48 The SEM images of ZnO nanorods obtained by annealing CP at **a** 400 **b** 500 and **c** 600 °C
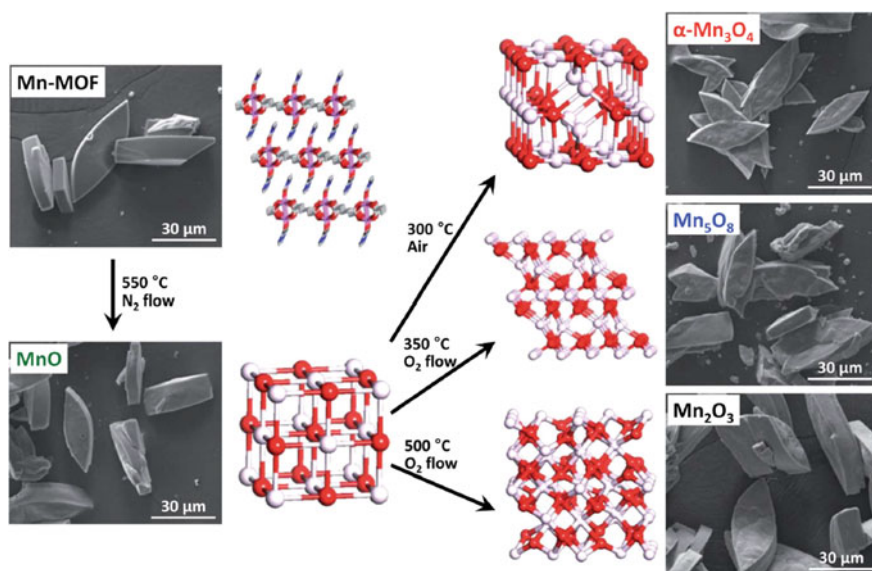
Fig. 8.49 SEM micrographs and diagram of structural transformations of ([Mn$_2$(L)(DMA)$_2$]$_n$ in manganese oxides during thermolysis

nanorods with 30–60 nm in diameter and a few micrometers in length. Inspection of the images reveals that calcination of the first CP at 600 °C resulted in the formation of more uniform rods with longer length (Fig. 8.49c). Moreover, the results show that thermolysis temperature can influence the length of ZnO nanorods obtained from the first CP.

The thermolysis of the Zn(II) CPs $(NH_4)_n[Zn(HL)Cl_2]_n$, $[Zn(L)(H_2O)_2]_n$, $[Zn(HL)_2]_n \cdot 4nH_2O$ (H_2L = iminodiacetic acid) was used for the preparation of zinc oxide [339]. In particular, the product based on first polymer has the shape of a regular hexagonal pyramid with the mean diameter and length of ZnO crystal of 2.6 and 4.6 mm respectively, and the aspect (length/width) ratio of 1.8:1. The regular granular crystallites of ZnO having diameters of 25–202 nm were prepared from second and third polymers. Thus, the structure of the initial CPs has a substantial effect on the shape and size of formed ZnO nanomaterials [340, 341].

Thermolysis of the bulk powder and nano-sized Ni(II) MOF with cubic building blocks and 1D open channels, i.e. $\{[Na_{16}(Ni_8L_{12})(H_2O)_{20}(H_2O)_4](CH_3CN)(H_2O)_{18.5}\}\infty$ (H_3L = 4,5-imidazoledicarboxylic acid), at 700 °C under air yielded NiO nanoparticles, which size and morphology depends on the particle size of the initial compound [342].

The crystalline and nano-structures of two Pb(II) CPs, $[Pb_2(L)_4(MeOH)]_n$ (L = 2-pyrazinecarboxylic acid) and $[Pb(L')_2]_n$ (L' = 2-quinolinecarboxylic acid), were thermalized to prepare PbO nanoparticles with various morphology and size [343].

It should be noted that N,S-containing ligands were used not only to prepare metal sulfide nanoparticles, as expected, but also metal oxides, more thermodynamically stable in air. Thus, a ZnO nanostructure was prepared by thermolysis of nanoparticles of a Zn(II) CP, $[Zn(L)(CH_3COO)_2]_n$ (L = 2,2′-diamino-5,5′-dimethyl-4,4′-bithiazole), at 500 °C under air [344].

Saving macroscopic MOFs structure during their thermal transformation may serve as a promising strategy in the design of nanomaterials with predetermined properties and morphology.

8.4.2.2 Influence of Temperature

Temperature is an important parameter controlling the phase composition and morphology of the resulting nanostructures. Thus, controlled thermolysis of $[Mn_2(L)(DMA)_2]_n$ (L is *meso*-butane-1,2,3,4-tetracarboxylate, DMA is N,N-dimethylacetamide) [345] and $Mn_2(L')$ (L' is 2,5-dihydroxyterephthalate) [346] by varying the temperature and the atmosphere leads to the formation of a series of nanoporous manganese oxides with different degrees of oxidation: MnO, Mn_3O_4, Mn_5O_8, and Mn_2O and preserving the original morphology of the starting precursor (Fig. 8.49). Besides, varying the thermolysis temperature (300–7000 °C) of $Mn_2(L')$ [346] leads to reduction of lattice defects, increasing the crystallinity degree of the thermolysis products. At the same time, the crystal surface becomes uneven and a plurality of voids appears with temperature increasing. The prepared MnO_x are characterized by type IV adsorption isotherms, indicating their mesoporous structure. It should be noted that in this way rare low-valence oxides MnO and

metastable phases of Mn_5O_8 with nanoporous architecture can be obtained, i.e. MOF thermal transformation can significantly enrich the composition, structure and functional properties of the resulting nanoporous metal oxide materials [347].

Similar patterns are characteristic of thermal transformations of MIL-100(Fe) [348]. The average size of nanorods Fe_2O_3, obtained at temperatures of 350, 550 and 750 °C is 50, 150 and 200 nm, respectively. Character of adsorption-desorption isotherms in this case is consistent with the general trend of the formation of the mesoporous structure of metal oxide nanocomposites obtained by MOF thermolysis. As a rule, surface area, pore volume, and pore size decreases with increasing thermolysis temperature, which also is in agreement with the fact that the thermally controlled crystal growth reduces the porosity with increasing process temperature.

The thermal decomposition of Prussian blue $Fe_4[Fe(CN)_6]_3$ [291] at 350 and 450 °C leads to β- and cubic spinel γ-Fe_2O_3 hematite polymorphic modifications, respectively. At the same time, calcining $Fe_4[Fe(CN)_6]_3$ at 250 °C results in the formation of spongy Fe_2O_3 with developed specific surface area 200–400 m^2 g^{-1} depending on the particle size of the starting precursor. Structural changes during MOFs calcination process reflected in the evolution of nanoparticle morphology from spherical form to nanorods when changing the reaction temperature, for example, that is characteristic of ZnO nanoparticles produced by thermolysis of MOF based on Zn(4-[(1H-imidazol-4-yl)methylamino]benzoate) [349]. In this case MOF was used as precursor as well as sacrificial template to synthesize hexagonal ZnO nanomaterials by calcination in air.

Thermolysis temperatures of two silver(I) CPs, $[Ag(HQ)(Q)]_n$ and $\{[Ag(HQ)_2]NO_3\}_n$, has effect on the formation of silver nanomaterials [350]. In particular, increasing temperature leads to increase of agglomeration of silver nanoparticles.

Calcination of sinusoidal CP $[Ag(L)](ClO_4)$, where L is a diethylbis(4-pyridyl) silane, at 400 °C gives circle morphology with evolving burned organics. At the same time, at 600 °C, network circles involving of a silver(0)/silver chloride (chlorargyrite)/silicon(IV) oxide composite with a micro-sized convexo-concave surface are formed [351]. However, thermolysis of $[Ag(L)](BF_4)$ crystals at 600 °C gives silver(0) nanocomposites without silicon(IV) oxide.

It should be noted the zinc(II) oxide nanoparticles prepared by thermolysis of $[Zn(L)_2(H_2O)_4]_n$, $[Zn(L')_2(H_2O)_2]_n$ and $[Zn(H_2O)_6]\cdot(L'')_2$, where L is nicotinic acid N-oxide, L′ is picolinic acid N-oxide and L″ is isonicotinic acid N-oxide, at two temperatures (200 and 600 °C) using two methods (with surfactant and without surfactant) [352]. Analysis of the SEM images of the prepared ZnO nanoparticles exhibits that small and spherical ZnO nanoparticles were prepared by thermolysis of compounds at 200 °C using surfactant (oleic acid).

Also, spongy CuO (average diameter from 10 to 20 μm) was synthesized [353] by thermolysis of $Cu_3(L)_2$ (L = benzene-1,3,5-tricarboxylate). The product consisted of nanosheets with average edge length of 80–200 nm and thickness of about 30 nm.

8.4.2.3 Influence of Surfactants

It should be noted using surfactants in the synthesis of nanomaterials to change the morphology and particle size. For example, polymeric Zn(II) chelates were used for the preparation of nano-sized materials in the presence of surfactants [354–358].

Iron(III) oxide nanoparticles were prepared by thermolysis of a Fe(II) 1D CP, $[Fe(L)_2](SCN)_2.MeOH$, where L is 4′-(4-pyridyl)-tpy, in oleic acid (surfactant) [359]. Pure phase ZnO nanoparticles with various morphologies and sizes were synthesized by thermolysis of zinc(II) CPs, $[Zn(L)(OAc)]ClO_4$, $[Zn(L)I_2]$, and $[Zn(L)_2](ClO_4)_2(H_2O)_{2.9}$ based on the same ligand L [360].

Of interest is the synthesis of PbO nanoparticles (~ 30 nm) by thermolysis of a Pb(II) complex, $\{[Pb_2(L)_2(NO_3)_4].MeOH\}_n$, where L is N,N′,N″-tris(pyrid-3-ylmethyl)-1,3,5-benzenetricarboxamide, at 180 °C with oleic acid as a surfactant [361].

$[Co(L)(H_2O)]_n$ polymer, where H_2L is phthalic acid, was used for the preparation of Co_3O_4 in the presence of oleic acid and triphenylphosphine [92]. The organic surfactants (oleic acid and triphenylphosphine) allow to preparing nanomaterials with narrow size distributions, size control and crystallinity of individual nanocrystals. The TEM image (Fig. 8.50a, b) shows that the particles with particle size about 20–30 nm are not fully spherical, however, each nanoparticle is separated from its neighbors by the organic surfactant shell. The comparison of the nanoparticles obtained in the presence of oleic acid and triphenylphosphine (Fig. 8.50b) and in the presence of oleic acid without triphenylphosphine (Fig. 8.50c) indicates that the nanoparticles prepared in first case are smaller without any agglomeration.

The thermolysis of Pb(II) 2D CPs, $[Pb_2(\mu_2\text{-}L)_2(NO_3)_4]_n$, where L is 1,6-bis (2-pyridyl)-2,5-diaza-1,5-hexadiene, in oleic acid as a surfactant led to PbO particles about 60 nm [362]. We note also PbO nanoparticles (~ 25 nm) obtained by thermolysis of plate-shaped nanostructures of a 1D lead(II) CP involving the $Pb_2(\mu\text{-}I)_2$ fragment, $[Pb(L)I_2]_n$ (L = neocuproine or 2,9-dimethyl-phen), with oleic acid as a surfactant [363].

The ZnO nanoparticles were synthesized by thermolysis of nano-compound [Zn (5,5′-di-*tert*-butyl-bpy)Cl$_2$]$_n$ and similar compound, $[Zn(5,5′\text{-dimethyl-bpy})Cl_2]_n$, using two methods (with and without surfactant) [364]. The average size of ZnO nanoparticles is equal to 78 and 50 nm for these compounds, respectively. The ZnO nano-sized particles were also prepared by thermolysis of 1D CP, $\{[Zn(\mu\text{-}L)(L)_2(H_2O)_2](ClO_4)_2\cdot L\}_n$, where L is 1,4-bis(3-pyridyl)-2,3-diaza-1,3-butadiene, at 400 °C under air atmosphere as well as in oleic acid at 200 °C [365]. The diameter of the prepared product is equal to 40 nm (Fig. 8.51).

Fig. 8.50 a SEM, **b** TEM images of Co_3O_4 nanoparticles obtained in the presence of OA and TPP and **c** TEM image of Co_3O_4 nanoparticles obtained in the presence of OA without TPP
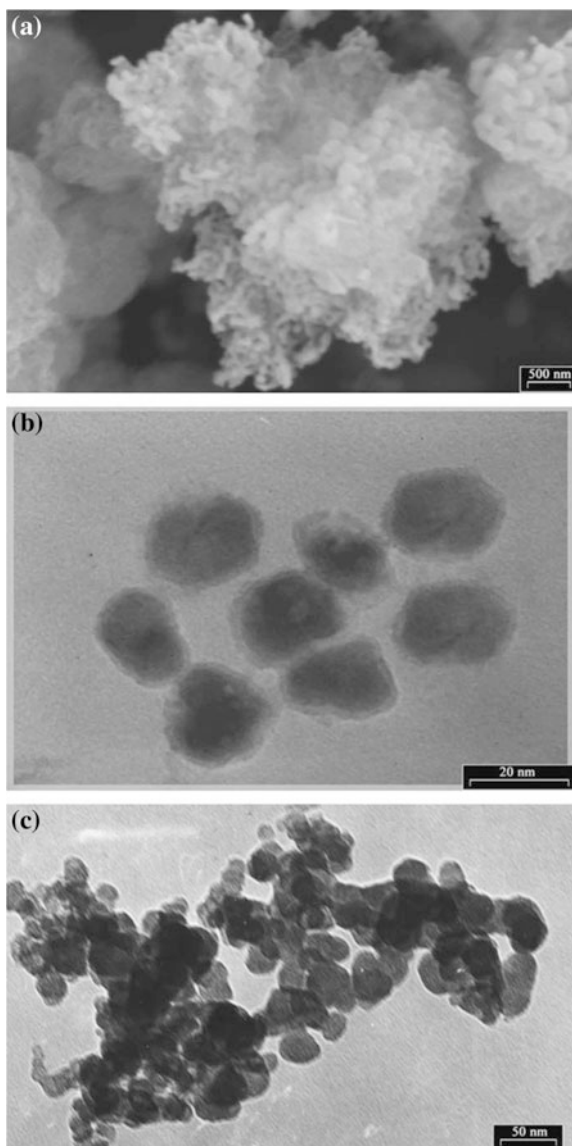
8.4.3 Polymer Derived Non-oxide Nanocomposites

At present, using different targeted silicon-based preceramic polymers [366], such as polysiloxane, polycarbosilane and polysilazane as precursors for polymer-derived ceramics (PDCs) [367, 368] has become widespread [369–374].

Fig. 8.51 SEM images of ZnO nanoparticles prepared by direct calcination of {[Zn (μ-L)(L)$_2$(H$_2$O)$_2$](ClO$_4$)$_2$·L}$_n$
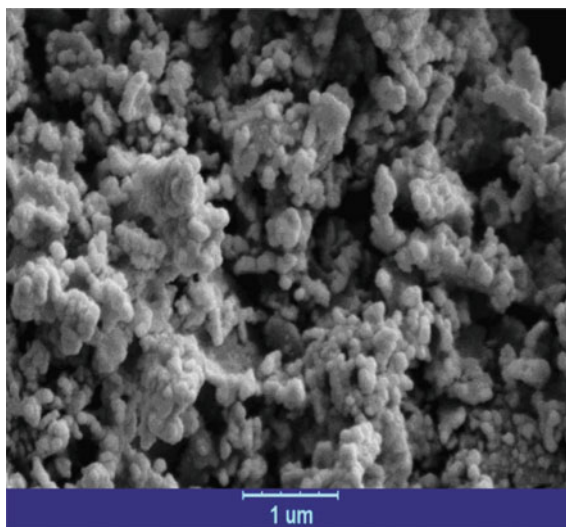
Controlled thermolysis of silicon-based preceramic polymers allows to preparing nano-sized ceramics, which structure is determined by the spatial organization of precursors, ways of their processing and thermolysis parameters. In particular, silicon-based preceramic polymers are subjected to different transformations depending on the temperature (Fig. 8.52) [368]. These transformations include polymerization, shaping, cross-linking, pyrolysis and annealing.

It should be noted that the preparation of PDCs is a relatively new technology possessing a number of advantages over the classical production [375]. Using metal chelates for modification of the polymer allows to producing new ceramic materials with high purity and homogenous distribution of the elements at relatively lower temperatures (1000 °C).

As an example, we consider the chemical modification of commercially available polysilazane (HTT1800) by an aminopyridinato Ni(II) chelate based on (4-methylpyridin-2-yl) trimethylsilanylamine for the production of nanoporous silicon
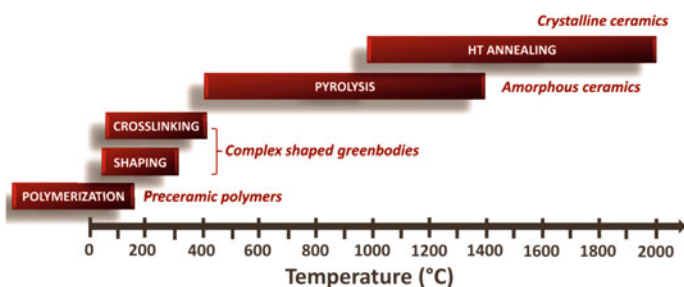
Fig. 8.52 Polymer-to-ceramic transformation of preceramic polymers

oxycarbo-nitride ceramics contained Ni nano-sized particles [376]. It is important that amido complexes involve the same elements (Si, C and N atoms), which are in the precursor polymer, thus avoiding the inclusion of other elements into the ceramic nanomaterials. The Ni-polysilazane precursors are superparamagnetic indicating formation of nickel nano-sized particles ($\sim$2–3 nm). The thermolysis of polysilazane precursors modified by aminopyridinato nickel chelate at 700 °C leads to nanoporous ceramic composites with a BET surface area of 215 m^2 g^{-1}, a micropore surface area of 205 m^2 g^{-1}, and a micropore volume of 0.113 cm^3 g^{-1}.

Analogous microporous nanomaterials with specific surface area $\approx$400 m^2 g^{-1} including nickel nano-sized particles were prepared by using various and controlled Si:Ni ratios in THF [377]. The amido nickel complex catalyzed the cross-linking of HTT1800 by hydrosilylation at room temperature. The formation of nickel nano-sized particles and micropores occurs by thermolysis at 600 °C according to an agreed mechanism.

Of interest is Ni-containing SiC ceramics prepared via the self-assembly of allylhydridopolycarbosilane-*b*-PE [378]. It is important that the added aminopyridinato nickel chelate also catalyzed the cross-linking the allylhydridopolycarbosilane block.

During modification of the HTT1800 by the aminopyridinato copper complexes the metal transfer from the chelate to the polymer occurs (Fig. 8.53) [379]. The ^{1}H and ^{13}C NMR studies of the reaction confirm the transfer of the metal to the nitrogen donor atoms of the polymer (Fig. 8.54). The thermolysis at 1000 °C of a metal modified polymer cross-linked with use of dicumylperoxide results in copper-containing SiCN (Cu@SiCN). It is important that the size of the Cu particles in Cu@SiCN depends on the content of copper chelate (Fig. 8.55).

Unusual behavior was observed for palladium aminopyridinates which produce intermetallic nano-sized particles. In particular, an aminopyridinato palladium chelate allows to simultaneous modification of the polyorganosilazane and its cross-linking [380]. It is important that the ceramic yield was even higher than that for the pure polyorganosilazane. Besides, the amount of the added palladium chelate increases their population density but does not affect the particle size (Fig. 8.56).

Of interest is the modification of HTT1800 by aminopyridinato metal chelates (M=Fe, Co, Pt, Cu, Ag, Au) along with the addition of the sacrificial filler (PE), which allows to generating both porosity (Fig. 8.57) and MWCNT (Figs. 8.57c and 8.58) [381]. It should be noted that cobalt and iron are more effective in the production of MWCNT than the other metals.

8.4.4 Mixed-Oxide Nanocomposites

Heterometallic chelates are of interest for preparation of functional oxide materials (e.g., metal-oxide ceramics). The main advantages of using heterometallic chelates
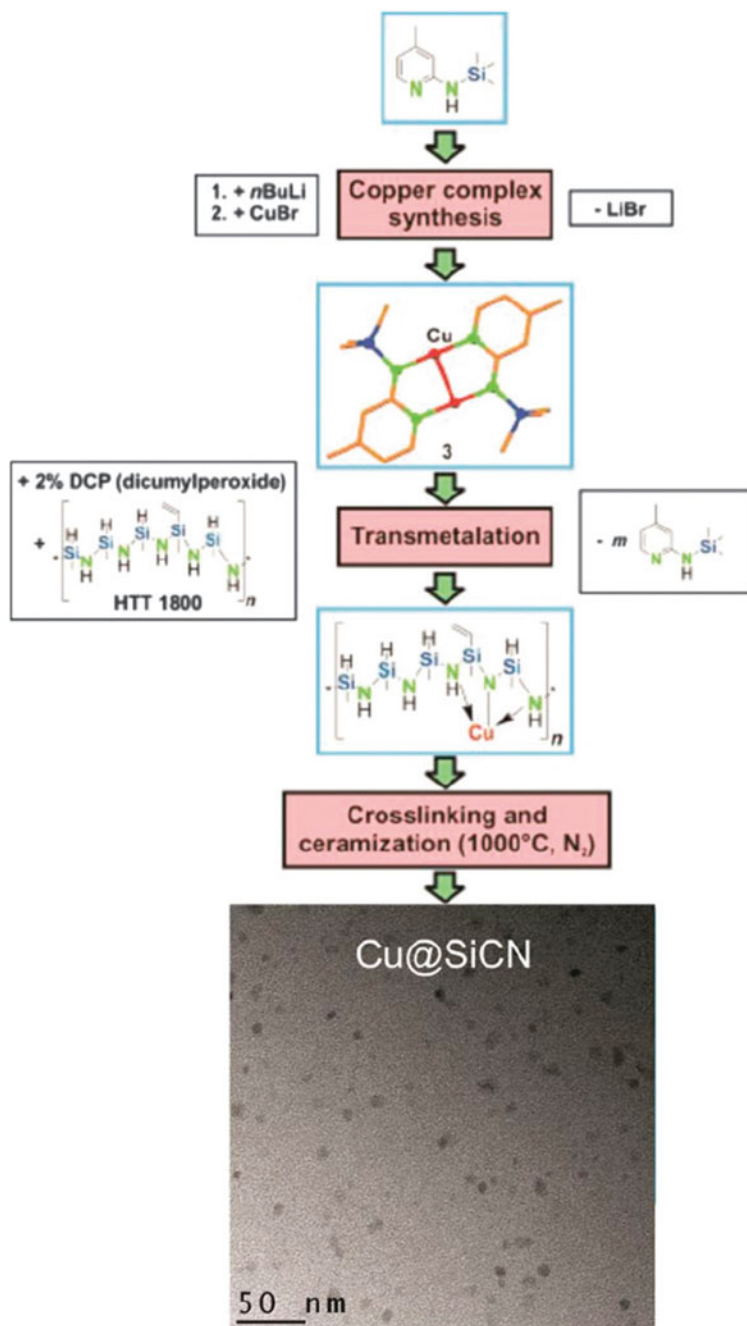
Fig. 8.53 Modification of HTT1800 with an aminopyridinato copper complex leading to Cu-containing SiCN ceramics by pyrolysis to 1000 °C under nitrogen
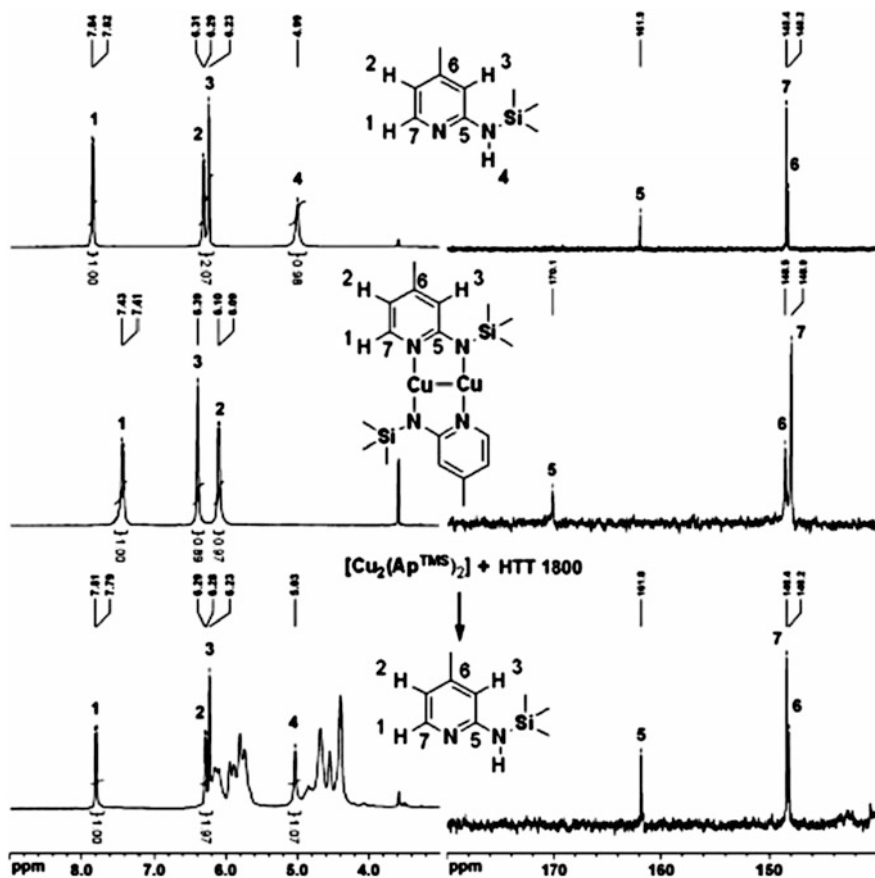
Fig. 8.54 ^{1}H (left) and ^{13}C NMR spectra (right) of ApTMSH (top), [Cu$_2$Ap$_2$TMS] (middle), and after its reaction with HTT1800 (bottom)

as precursors of nanomaterials are low temperature of thermolysis, the exact ratio of metal ions, the formed nanoparticle size control, etc. [42, 382–388].

As a typical example, we consider using mixed lanthanide CPs for the production of rare earth oxides [389]. In particular, well-defined cylindrical or spherical micro-morphologies can be prepared by varying solvents (water or THF) which were discovered in the resulting oxides after thermal treatment. Such bimetallic CPs were synthesized by the interaction of chlorides or nitrates of Ce, Nd, Gd with 2,5-dihydroxy-1,4-benzoquinone and used as precursors for mixed oxide ceramics. Thermolysis at 850 °C of the CPs leads to mixed Nd$_x$Gd$_{(1-x)}$ and Nd$_x$Ce$_{(1-x)}$ oxides as solid solutions, in which x varies between 0 and 1. It should be noted that using well-characterized CPs as precursors allows to controlling over the atom sequences in the chains, the number of coordination bonds and the dimensionality of the precursor structure.
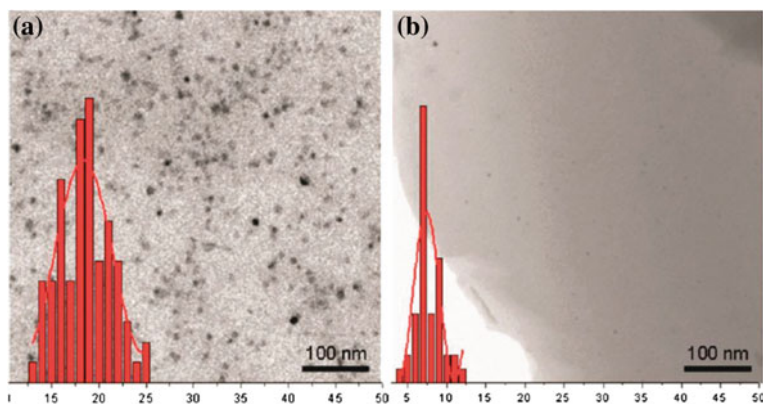
Fig. 8.55 TEM micrographs of Cu@SiCN: **a** Si/Cu = 10 **b** Si/Cu = 100 including particle size distribution statistics
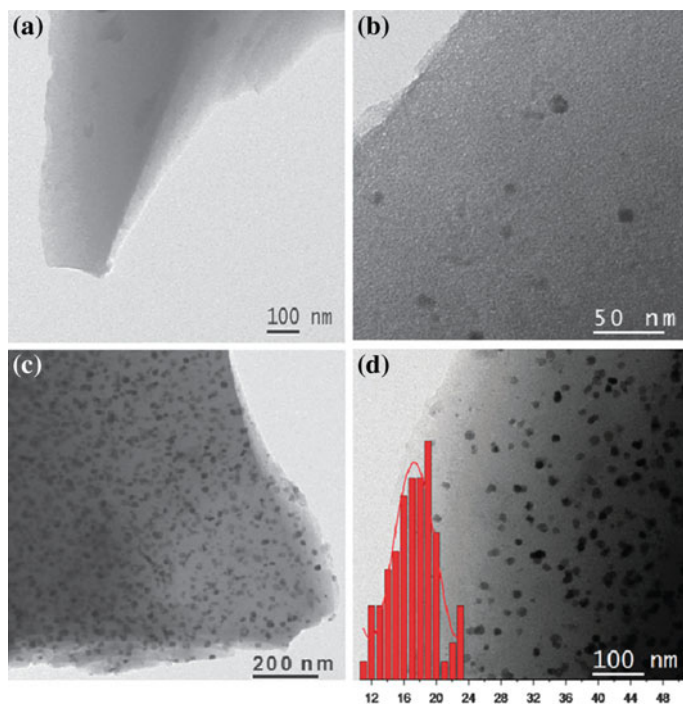
Fig. 8.56 TEM micrographs of ceramic materials. **a** SiCN ceramic without palladium loading does not show any particles; **b** lower loading of palladium (0.2 wt%, Si/Pd ratio 1000) decreases the density of particles keeping their size in the same regime; **c** Pd_2Si particles uniformly distributed over the ceramic support Si/Pd = 20 (8 wt% Pd); **d** particle size distribution for the sample shown in (**c**)
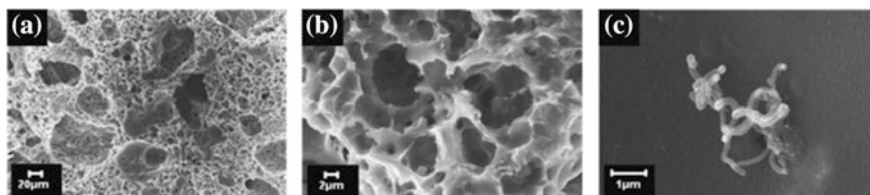
Fig. 8.57 **a**–**c** SEM micrographs of an Au@SiCN ceramic (1000 °C/N$_2$; Au:Si = 1:50)

The thermolysis of CPs [BaCu(L)$_2$]$_n$, [BaCu(L)$_2$(H$_2$O)]$_n$ and [Ba$_3$Cu$_3$(L)$_6$ (H$_2$O)$_{11}$]$_n$·2n(H$_2$O), where H$_2$L is 1,1-cyclopropanedicarboxylic, 1,1-cyclobutanedi-carboxylic and butylmalonic acid, respectively, occurs above 170 °C and leads to the formation of BaCuO$_2$ [390]. It is important that the thermolysis conditions have effect on the phase compositions of nanomaterials and the formation of BaCuO$_2$ proceeds under milder conditions from latter CP than those from the first two CPs.

It should be noted isostructural polymeric complexes [Ln(L)(acac)$_2$(H$_2$O)]$_n$ (Ln = Eu, Gd, Tb, Dy, Ho, Er; L = (η^5-C$_5$H$_4$)Mn(CO)$_3$), thermolysis of which in air and under Ar atmosphere affords LnMnO$_3$ phases [391]. For the Dy and Ho chelates adiabatic calorimetric data permit to calculate standard thermodynamic functions.

Of interest are 3D-porous CPs [(H$_2$O)$_3$(μ-H$_2$O)$_2$CuBa(μ_3-L)(L)]$_n$ and [(μ-H$_2$O) CuBa(μ_3-L)(μ_4-L)]$_n$, where HL is dimethylmalonic acid [392]. Complete solid-phase thermolysis of the CPs leads to a mixture of BaCuO$_2$, BaCO$_3$, and CuO. It is important that a crystalline phase of pure cubic BaCuO$_2$ can be obtained using special conditions. The thermal dehydration of Ba–Co and Ba–Zn heterometallic 3D CPs [BaM(H$_2$O)$_5$(L)$_2$]$_n$ based on the same ligand occurs in one step [393]. Crystalline BaCoO$_{3-x}$ and BaZnO$_2$ are products of solid state thermolysis of the **CPs** under the following conditions: air flow rate 60 ml min^{-1}, heating rate 10 °C min^{-1} up to t = 800 °C (**1**) or 750 °C (**2**), followed by storage for 12 h at the same temperatures (Fig. 8.59).

Of interest is using in situ polymerizable complex method for the preparation of a polymeric precursor of the phase La$_2$Mo$_2$O$_9$ [394]. SEM reveals a different morphology of powder nanoparticles after thermolysis at selected temperatures and powder X-ray diffraction patterns were prepared for phase identification (Fig. 8.60).

Mixed-metal oxalates were used for preparation of bimetallic or mixed-oxide nanostructures. Thus, thermolysis of 2D polymetallic oxalate-bridged polymeric networks [395] of the formula [M^{II}(H$_2$O)$_2$]$_3$[M^{III}(ox)$_3$]$_2$(18-crown-6)$_2$ (M^{III} = Cr, Fe; M^{II} = Mn, Fe, Co, Ni; 18-crown-6) leads to pure phases of mixed oxides with spinel-like structures as (Mn,Co,Fe)$_3$O$_4$.

Mesoporous nickel ferrite (NiFe$_2$O$_4$) spheres were prepared by an aerosol spray pyrolysis method using Pluronic F127 as a structure-directing agent, and metal nitrates were used as inorganic precursors for the oxide [396]. Self-assembly of organic and inorganic species followed by metal nitrate decomposition and inorganic polymerization were accomplished in the ethanol aerosol droplets in N$_2$
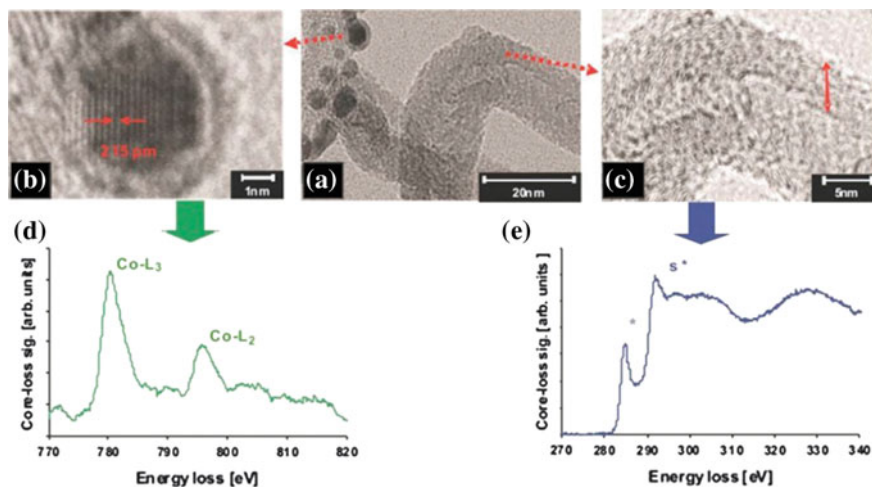
Fig. 8.58 a–c TEM micrographs of a Co@SiCN ceramic (Co:Si ratio = 1:50) **d** core-loss EELS of the metal particle **e** core-loss EELS of the carbon nanotube
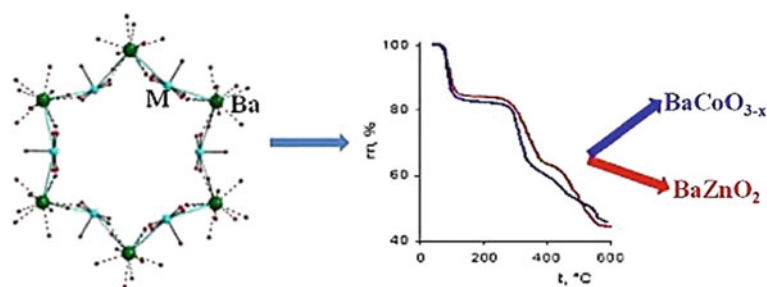
Fig. 8.59 Preparation of crystalline $BaCoO_{3-x}$ and $BaZnO_2$ as a result of solid state thermolysis of the CPs

atmosphere at 400 °C. It is important that the solvent evaporation at 50 °C in the chamber induced the self-assembly between the structure-directing agent and the metal ions. It should be noted that mesoporous crystalline nickel ferrite spheres were obtained after the spheres were calcined at 300 °C in air to remove the structure-directing agent and increase crystallinity. Mesoporous $NiFe_2O_4$ spheres of high specific surface area (278 m^2 g^{-1}) with a highly crystalline framework were prepared by adjusting the amount of structure-directing agent and the calcining condition.

Of interest is the preparation of Ni–Fe bimetallic oxide nanotubes with a hollow and porous structure by MOF thermolysis [397]. It is important that the Ni/Fe molar ratios in the binary metal oxide can be regulated. In particular, $Ni_{0.62}Fe_{2.38}O_4$
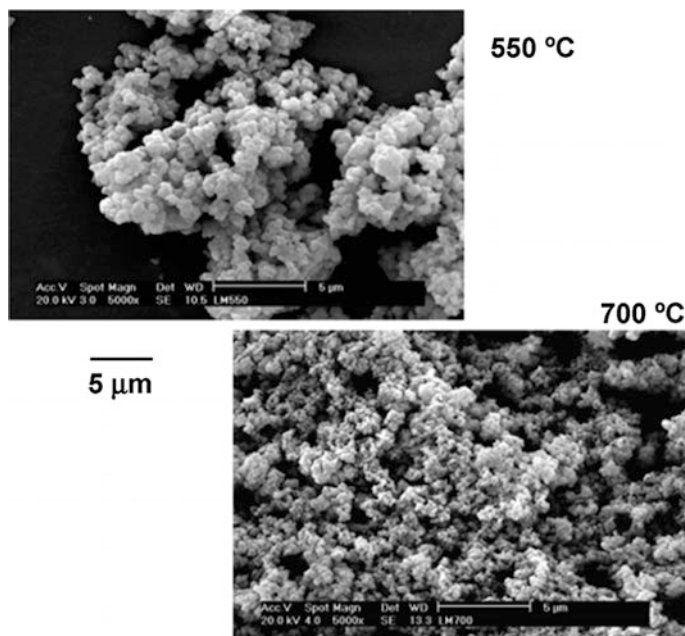
Fig. 8.60 SEM of the phase $La_2Mo_2O_9$ prepared at different temperatures

nanotubes with a tube shell of around 10 nm have a specific surface area of 134.3 m^2 g^{-1} and are composed of nano-sized primary particles.

Of course, the range of nanostructures produced in the course of thermal transformations of PMC is quite wide, and is not limited to the examples discussed here. Huge selection of precursor organometallic structures and coordination polymers with a wide arsenal of synthetic methods for their preparation, ease of many recipes, scalability and acceptable ratio price/quality provide a methodological platform to build on the basis of PMC promising new materials including metal nanostructures [398–400], nanoalloys [401, 402], metal chalcogenides [403–405], metal carbides [406], etc.

References

1. T. Zhang, J. Ge, Y. Hu, Y. Yin, Nano Lett., ASAP Article
2. A.P. Reverberi, N.T. Kuznetsov, V.P. Meshalkin, M. Salerno, B. Fabiano, Theor. Found. Chem. Eng. **50**, 59 (2016)
3. W.L. Leong, J.J. Vittal, Chem. Rev. **111**, 688 (2010)
4. H. Liu, J. Owen, A.P. Alivisatos, J. Am. Chem. Soc. **129**, 305 (2007)
5. L.H. Qu, W.W. Yu, X.P. Peng, Nano Lett. **4**, 465 (2004)
6. Z.A. Peng, X.G. Peng, J. Am. Chem. Soc. **124**, 3343 (2002)
7. C.R. Bullen, P. Mulvaney, Nano Lett. **4**, 2303 (2004)

8. A.D. Pomogailo, G.I. Dzhardimalieva, *Nanostructured Materials Preparation via Conden-sation Ways* (Springer, Dordrecht, 2014)

9. D. Wohrle, A.D. Pomogailo, *Metal Complexes and Metals in Macromolecules* (Wiley-VCH, Weinheim, 2003)

10. A.D. Pomogailo, A.S. Rozenberg, I.E. Uflyand, *Metal Nanoparticles in Polymers* (Khimiya, Moscow, 2000)

11. A.D. Pomogailo, G.I. Dzhardimalieva, V.N. Kestelman, *Macromolecular metal carboxy-lates and their nanocomposites* (Springer, Heidelberg, 2010)

12. G.I. Dzhardimalieva, A.D. Pomogailo, Russ. Chem. Rev. **77**, 259 (2008)

13. A.D. Pomogailo, A.S. Rozenberg, G.I. Dzhardimalieva, Russ. Chem. Rev. **80**, 257 (2011)

14. A.D. Pomogailo, V.V. Savostyanov, *Synthesis and Polymerization of Metal-Containing Monomers* (CRC Press, Boca Raton, London, NY, 1994)

15. A.D. Pomogailo, G.I. Dzhardimalieva, *Monomeric and Polymeric Metal Carboxylates* (Fizmatlit, Moscow, 2009)

16. M.Y. Masoomi, A. Morsali, Coord. Chem. Rev. **256**, 2921 (2012)

17. B.I. Kharisov, O.V. Kharissova, U.O. Méndez, J. Coord. Chem. **66**, 3791 (2013)

18. A.D. Pomogailo, G.I. Dzhardimalieva, *Metallopolymeric Hybride Nanocomposites* (Nauka, Moscow, 2015)

19. *Nanocrystals: synthesis, properties and application*, eds. by C.N.R. Rap, P.J. Thomas, G.U. Kulkarni (Springer, Berlin, Heidelberg, 2007)

20. O. Carp, Materials Obtained by Solid-State Thermal Decomposition of Coordination Compounds and Metal-Organic Coordination Polymers, in *Reactions and Mechanisms in Thermal Analysis of Advanced Materials*, eds. by A. Tiwari, B. Raj (Scrivener Publishing LLC, Salem, Massachusetts, 2015)

21. Y. Song, X. Li, L. Sun, L. Wang, RSC Adv. **5**, 7267 (2015)

22. J.-K. Sun, Q. Xu, Energy Environ. Sci. **7**, 2071 (2014)

23. M. Ramazani, A. Morsali, Ultrason. Sonochem. **18**, 1160 (2011)

24. M.A. Malik, P. O'Brien, *Organometallic and Metallo-Organic Precursors for Nanoparticles. Precursor Chemistry of Advanced Materials* (Springer, Berlin, Heidelberg, 2005)

25. M. Ramanathana, S.B. Darling, Polym. Int. **62**, 1123 (2013)

26. B.I. Kharisov, H.V. Rasika Dias, O.V. Kharissova, V.M. Jiménez-Pérez, B.O. Pérez, B.M. Flores, RSC Adv. **2**, 9325 (2012)

27. V.A. Logvinenko, F. Paulik, I. Paulik, *Kvaziravnovesnaya Termogravimetriya v Sovremennoi Neorganicheskoi Khimii (Quasi-equilibrium Thermpgravimetry in Modern Inorganic Chemistry)* (Nauka, Novosibirsk, 1989)

28. J. Paulik, F. Paulik, Therm. Acta. **100**, 23 (1986)

29. A.S. Shteinberg, *Fast Reactions in Energetic Materials: High-Temperature Decomposition of Rocket Propellants and Explosives* (Fizmatlit, Moscow, 2006)

30. S.V. Pol, V.S. Pol, A. Gedanken, Chem. - Eur. J. **10**, 4467 (2004)

31. J.Q. Sun, X.P. Shen, L.J. Guo, K.M. Chen, Q. Liu, Phys. E. Low Dimens. Syst. Nanostr. **41**, 1527 (2009)

32. J.Q. Sun, X.P. Shen, K.M. Chen, Q. Liu, W. Liu, Solid State. Comm. **147**, 501 (2008)

33. M. Bowtell, Adhes. Age. **40**, 62 (1997)

34. G.P. Shveikin, I.V. Nikolaenko, Theor. Found. Chem. Eng. **43**, 553 (2009)

35. Y.C. Kang, S.B. Park, I.W. Lenggoro, K. Okuyama, J. Mater. Res. **14**, 2611 (1999)

36. I.W. Lenggoro, T. Hata, F. Iskandar, J. Mater. Res. **15**, 733 (2000)

37. H.K. Kammler, L. Mädler, S.E. Pratsinis, Chem. Eng. Technol. **24**, 583 (2001)

38. E.K. Athanassiou, R.N. Grass, W.J. Stark, Nanotechnol. **17**, 1668 (2006)

39. M.T. Swihart, Curr. Opin. Colloid. Interf. Sci. **8**, 127 (2003)

40. C. Boissiere, D. Grosso, A. Chaumonnot, L. Nicole, C. Sanchez, Adv. Mater. **23**, 599 (2011)

41. C.-K. Tsung, J. Fan, N. Zheng, Q. Shi, A.J. Forman, J. Wang, G.D. Stucky, Angew. Chem. Int. Ed. **47**, 8682 (2008)

42. T.A. Ostomel, Q. Shi, C.-K. Tsung, H. Liang, G.D. Stucky, Small **2**, 1261 (2006)

43. L. Li, C.-K. Tsung, Z. Yang, G.D. Stucky, L.D. Sun, J.F. Wang, C.H. Yan, Adv. Mater. **20**, 903 (2008)
44. Y. Lu, H. Fan, A. Stump, T.L. Ward, T. Rieker, C.J. Brinker, Nature. **398**, 223 (1999)
45. A.K.P. Mann, S.E. Skrabalak, Chem. Mater. **23**, 1017 (2011)
46. J.B. Pang, J.N. Stuecker, Y.B. Jiang, A.J. Bhakta, E.D. Branson, P. Li, J. Cesarano, D. Sutton, P. Calvert, C.J. Brinker, Small. **4**, 982 (2008)
47. D.S. Jung, S.B. Park, Y.C. Kang, Korean J. Chem. Eng. **27**, 1621 (2010)
48. J.-C. Lin, J.W. Gentry, J. Aerosol Sci. **31**, 797 (2000)
49. N. Reuge, B. Caussat, Comput. Chem. Eng. **31**, 1088 (2007)
50. I.W. Lenggoro, Y. Itoh, K. Okuyama, T.O. Kim, J. Mater. Res. **19**, 3534 (2004)
51. W.-N. Wang, A. Purwanto, K. Okuyama, in *Handbook of Atomization and Sprays*, ed. by N. Ashgriz (Springer Science Business Media, LLC, 2011)
52. Y.C. Kang, Y.S. Chung, S.B. Park, J. Am. Ceram. Soc. **82**, 2056 (1999)
53. K. Okuyama, I.W. Lenggoro, Chem. Eng. Sci. **58**, 537 (2003)
54. W.-N. Wang, I.W. Lenggoro, Y. Terashi, T.O. Kim, K. Okuyama, Mat. Sci. Eng. B. **123**, 194 (2005)
55. Y.C. Kang, S.B. Park, Mater. Res. Bull. **35**, 1143 (2000)
56. W.-N. Wang, I.W. Lenggoro, Y. Terashi, Y.C. Wang, K. Okuyama, J. Mater. Res. **20**, 2873 (2005)
57. I.W. Lenggoro, Y. Itoh, N. Iida, K. Okuyama, Mater. Res. Bull. **38**, 1819 (2003)
58. H. Biederman, *in Plasma Polymer Films* (Imperial College Press, London, 2004)
59. A. Biswas, Z. Marton, J. Kanzow, J. Kruse, V. Zaporojtchenko, F. Faupel, T. Strunskus, Nano Lett. **3**, 1 (2003)
60. H. Takele, H. Greve, C. Pochstein, V. Zaporojtchenko, F. Faupel, Nanotechnology. **17**, 3499 (2006)
61. D. Barreca, A. Gasparotto, C. Maragno, E. Tondello, C. Sada, Chem. Vap. Deposition. **10**, 229 (2004)
62. K. Ramasamy, M.A. Malik, P. O'Brien, J. Raftery, Dalton Trans. **39**, 1460 (2010)
63. D. Barreca, A. Gasparotto, C. Maragno, R. Seraglia, E. Tondello, A. Venzo, V. Krishnan, H. Bertagnolli, Appl. Organometal. Chem. **19**, 129 (2005)
64. S. Mlowe, L.D. Nyamen, P.T. Ndifon, M.A. Malik, J. Raftery, P. O'Brien, N. Revaprasadu, Inorg. Chim. Acta. **434**, 181 (2015)
65. S. Mlowe, D.J. Lewis, M.A. Malik, J. Raftery, E.B. Mubofu, P. O'Brien, N. Revaprasadu, New J. Chem. **38**, 6073 (2014)
66. R. Morrish, R. Silverstein, C.A. Wolden, J. Am. Chem. Soc. **134**, 17854 (2012)
67. V.G. Bessergenev, R.J.F. Pereira, A.M.B. do Rego. Surf. Coat. Technol. **201**, 9141 (2007)
68. R.K. Sharma, G. Kedarnath, V.K. Jain, A. Wadawale, M. Nalliath, C.G.S. Pillai, B. Vishwanadh, Dalton Trans. **39**, 8779 (2010)
69. C.B. Murray, D.J. Norris, M.G. Bawendi, J. Am. Chem. Soc. **115**, 8706 (1993)
70. N.L. Pickett, P. O'Brien, Chem. Rec. **1**, 467 (2001)
71. M.A. Malik, N. Revaprasadu, P. O'Brien, Chem. Mater. **13**, 913 (2001)
72. J. Rodriguez Castro, K.C. Molloy, Y. Liu, C.S. Lai, Z. Dong, T.J. White, E.R.T. Tiekink, J. Mater. Chem. **18**, 5399 (2008)
73. H. Liang, J.M. Raitano, L. Zhang, S.-W. Chan, Chem. Commun. 7569 (2009)
74. A. Hosseinian, S. Jabbari, H.R. Rahimipour, A.R. Mahjoub, J. Mol. Struct. **1028**, 215 (2012)
75. A. Hosseinian, A.R. Mahjoub, J. Mol. Struct. **985**, 270 (2011)
76. A. Hosseinian, A.R. Mahjoub, M. Movahedi, Int. J. Nano Dim. **1**, 65 (2010)
77. D. Czakis-Sulikowska, J. Radwannska-Doczekalska, M. Markiewicz, M. Pietrzak, J. Them. Anal. Calor. **93**, 789 (2008)
78. D. Kumar, I.P.S. Kapoor, G. Singh, N. Geol, U.P. Singh, J. Therm. Anal. Calor. **107**, 325 (2011)
79. N. Parveen, R. Nazir, M. Mazhar, J. Therm. Anal. Calor. **111**, 93 (2013)
80. R. Nazir, M. Mazhar, T. Wakeel, M.J. Akhtar, M. Siddique, M. Nadeem, N.A. Khan, M.R. Shah, J. Therm. Anal. Calor. **110**, 707 (2012)

81. V.G. Makhankova, O.V. Khavryuchenko, V.V. Lisnyak, V.N. Kokozay, V.V. Dyakonenko, O.V. Shishkin, B.W. Skelton, J. Jezierska, J. Solid State Chem. **183**, 2695 (2010)

82. G. Singh, D.K. Pandey, Propellant. Explor. Pyrotech. **28**, 231 (2003)

83. P.R. Ponminiessary, A. Vasudevan, M. Sebastian, U.A. Chennampilly, K.M.Y. Karukapadath, J. Therm. Anal. Calor. **100**, 733 (2010)

84. K.S. Pejitha, S. Mathew, J. Therm. Anal. Calor. **93**, 213 (2008)

85. S. Bahemmat, M. Ghassemzadeh, M. Afsharpour, K. Harms, Polyhedron **89**, 196 (2015)

86. J. Chandradass, K.H. Kim, Mater. Manuf. Processes. **24**, 541 (2009)

87. Y. Hanifehpour, B. Mirtamizdoust, S.W. Joo, Z. Anorg, Allg. Chem. **638**, 357 (2012)

88. S. Kumar, J.A. Azurdia, R.M. Laine, J. Ceram. Proc. Res. **11**, 517 (2010)

89. X. Wang, X.Y. Chen, L.S. Gao, H.G. Zheng, Z. Zhang, Y.T. Qian, J. Phys. Chem. B **108**, 16401 (2004)

90. J.Z.L. Zhang, H.R. Geng, L.S. Zheng, D. Du, J. Alloys Compd. **392**, 317 (2005)

91. A. Khansari, M. Salavati-Niasari, A.K. Babaheydari, J. Clust. Sci. **23**, 557 (2012)

92. F. Mohandes, F. Davar, M. Salavati-Niasari, J. Magn. Magn. Mater. **322**, 872 (2010)

93. A. Khansari, M. Enhessari, M. Salavati-Niasari, J. Clust. Sci. **24**, 289 (2013)

94. D. Matioszek, W.-S. Ojo, A. Cornejo, N. Katir, M. El Ezzi, M. Le Troedec, H. Martinez, H. Gornitzka, A. Castel, C. Nayral, F. Delpech, Dalton Trans. **44**, 7242 (2015)

95. T. Trindade, P. O'Brien, Adv. Mater. **8**, 161 (1996)

96. M. Lazell, P. O'Brien, J. Chem. Soc. Chem. Commun. 2041 (1999)

97. D.J. Crouch, P. O'Brien, M.A. Malik, P.J. Skabara, S.P. Wright, J. Chem. Soc. Chem. Commun. 1454 (2003)

98. S. Taniguchi, M. Green, J. Mater. Chem. C **3**, 8425 (2015)

99. Y.W. Jun, C.S. Choi, J. Cheon, J. Chem. Soc. Chem. Commun. 101 (2001)

100. M. Ranjbar, N. Shahsavan, M. Yousefi, Am. Chem. Sci. J. **2**, 111 (2012)

101. M. Edrissi, A.R. Keshavarz, Nano-Micro Lett. **4**, 83 (2012)

102. P. Bera, C.H. Kim, S.I. Seok, Solid State Sci. **12**, 532 (2010)

103. R. Amutha, S. Akilandeswari, A.N. Kannappan, M. Muruganandham, M. Sillanpää, Adv. Sci. Lett. **3**, 398 (2010)

104. A.L. Abdelhady, M. Afzaal, M.A. Malik, P. O'Brien, J. Mater. Chem. **21**, 18768 (2011)

105. N. Srinivasan, S. Thirumaran, S. Ciattini, J. Mol. Struct. **1026**, 102 (2012)

106. N. Srinivasan, S. Thirumaran, S. Ciattini, Spectrochim. Acta. Part A: Mol. Biomol. Spectr. **102**, 263 (2013)

107. W. Qingqing, X. Gang, H. Gaorong, J. Solid State Chem. **178**, 2680 (2005)

108. S.N. Mlondo, N. Revaprasadu, P. Christian, P. O'Brien, Polyhedron **28**, 2097 (2009)

109. Y. Li, X. Li, C. Yang, Y. Li, J. Mater. Chem. **13**, 2641 (2003)

110. P.S. Nair, T. Radhakrishnan, N. Revaprasadu, G.A. Kolawole, P. O'Brien, J. Mater. Chem. **12**, 2722 (2002)

111. J.C. Bruce, N. Revaprasadu, K.R. Koch, New J. Chem. **31**, 1647 (2007)

112. N. Moloto, N. Revaprasadu, M.J. Moloto, P. O'Brien, M. Helliwell, Polyhedron **26**, 3947 (2007)

113. G. Kedarnath, V.K. Jain, S. Ghoshal, G.K. Dey, C.A. Ellis, E.R.T. Tiekink, Eur. J. Inorg. Chem. 1566 (2007)

114. E.S. Raper, Coord. Chem. Rev. **165**, 475 (1997)

115. S. Narayan, V.K. Jain, B. Varghese, J. Chem. Soc. Dalton Trans. 2359 (1998)

116. J. Laube, S. Jager, C. Thone, Eur. J. Inorg. Chem. 198 (2001)

117. S. Dey, V.K. Jain, J. Singh, V. Trehan, K.K. Bhasin, B. Varghese, Eur. J. Inorg. Chem. 744 (2003)

118. G. Kedarnath, V.K. Jain, A. Wadawale, G.K. Dey. Dalton Trans. 8378 (2009)

119. M. Chunggaze, M.A. Malik, P. O'Brien, Adv. Mater. Opt. Electron. **7**, 311 (1997)

120. P. O'Brien, in *Inorganic materials*, eds. by D.W. Bruce, D. O'Hare (Wiley, NY, 1992)

121. N. Srinivasan, S. Thirumarana, S. Ciattini, J. Mol. Struct. **936**, 234 (2009)

122. L.D. Nyamen, A.A. Nejo, V.S.R. Pullabhotla, P.T. Ndifon, M.A. Malik, J. Akhtar, P. O'Brien, N. Revaprasadu, Polyhedron **67**, 129 (2014)

123. S. Mlowe, D.J. Lewis, M.A. Malik, J. Raftery, E.B. Mubofu, P. O'Brien, N. Revaprasadu, Dalton Trans. **45**, 2647 (2016)
124. M. Chunggaze, M.A. Malik, P. O'Brien, J. Mater. Chem. **9**, 2433 (1999)
125. V.V. Singh, U. Kumar, S.N. Tripathi, A.K. Singh, Dalton Trans. **43**, 12555 (2014)
126. Z. Xu, C. Shen, Y. Hou, H. Gao, S. Sun, Chem. Mater. **21**, 1778 (2009)
127. W. Bu, Z. Chen, F. Chen, J. Shi, J. Phys. Chem. C. **113**, 12176 (2009)
128. L. Manna, E.C. Scher, A.P. Alivisatos, J. Am. Chem. Soc. **122**, 12700 (2000)
129. L.D. Nyamen, V.S.R. Pullabhotla, A.A. Nejo, P. Ndifon, N. Revaprasadu, New J. Chem. **35**, 1133 (2011)
130. J.M. Rawson, R.E.P. Winpenny, Coord. Chem. Rev. **139**, 313 (1995)
131. K. Kandasamy, H.B. Singh, S.K. Kulshreshtha, J. Chem. Sci. **121**, 293 (2009)
132. X.G. Peng, L. Manna, W.D. Yang, J. Wickham, E.C. Scher, A. Kadavanich, A.P. Alivisatos, Nature. **404**, 59 (2000)
133. N. Pradhan, S. Efrima, J. Am. Chem. Soc. **125**, 2050 (2003)
134. N. Pradhan, B. Katz, S. Efrima, J. Phys. Chem. B. **107**, 13843 (2003)
135. Y. Li, X. Li, C. Yang, Y. Li, J. Phys. Chem. B. **108**, 16002 (2004)
136. W.W. Yu, Y.A. Wang, X.G. Peng, Chem. Mater. **15**, 4300 (2003)
137. X.G. Peng, Adv. Mater. **15**, 459 (2003)
138. C. Amiens, B. Chaudret, D. Ciuculescu-Pradines, V. Colliere, K. Fajerwerg, P. Fau, M. Kahn, A. Maisonnat, K. Soulantica, K. Philippot, New J. Chem. **37**, 3374 (2013)
139. G.A. Seisenbaeva, V.G. Kessler, Nanoscale. **6**, 6229 (2014)
140. M.A. Malik, M. Afzaal, P. O'Brien, Chem. Rev. **110**, 4417 (2010)
141. M. Nell, J. Marohn, G. Mclendon, J. Phys. Chem. B. **94**, 4359 (1990)
142. L. Spanhel, M. Haase, H. Weller, A. Henglein, J. Am. Chem. Soc. **109**, 5649 (1987)
143. M. Kim, H. Kim, S. Lee, S. Sohn, Mol. Cryst. Liq. Cryst. **564**, 162 (2012)
144. J. Xiao, B. Wen, R. Melnik, Y. Kawazoe, X. Zhanga, Phys. Chem. **16**, 14899 (2014)
145. G.B. Shombe, E.B. Mubofu, S. Mlowe, N. Revaprasadu, Mater. Sci. Semicond. Proces. **43**, 230 (2016)
146. R. Banerjee, R. Jayakrishnan, P. Ayyub, J. Phys. Condens. Matter. **12**, 10647 (2000)
147. C. Ricolleau, L. Audinet, M. Gandais, T. Gacoin, Eur. Phys. **9**, 565 (1999)
148. N.L. Botha, P.A. Ajibade, Mater. Sci. Semicond. Proces. **43**, 149 (2016)
149. M. Ghiasi, A. Malekzadeh, H. Mardani, Mater. Sci. Semicond. Proc. **42**, 311 (2016)
150. S. Zinatloo-Ajabshir, M. Salavati-Niasari, M. Hamadanian. J. Mater. Sci. Mater. Electron. **27**, 998 (2016)
151. Z.R. Ranjbar, A. Morsali, Ultrason. Sonochem. **18**, 644 (2011)
152. M.H. Habibi, E. Askari, Synth. React. Inorg., Met.-Org., Nano-Met. Chem. **43**, 406 (2013)
153. L.A. Saghatforoush, R. Mehdizadeh, F. Chalabian, Transition Met. Chem. **35**, 903 (2010)
154. A.D. Khalaji, D. Das, J. Therm. Anal. Calorim. **114**, 671 (2013)
155. M.S. Refat, M.Y. El-Sayed, A.M. Adam, J. Mol. Struct. **1038**, 62 (2013)
156. A.S. Burlov, V.N. Ikorskii, S.A. Nikolaevskii, YuV Koschienko, V.G. Vlasenko, Ya.V. Zubavichus, A.I. Uraev, I.S. Vasilchenko, D.A. Garnovskii, G.S. Borodkin, A.D. Garnovskii, Russ. J. Inorg. Chem. **53**, 1566 (2008)
157. A.D. Garnovskii, I.S. Vasilchenko, D.A. Garnovskii, A.S. Burlov, A.I. Uraev, Ros. Khim. Zh. (Mendeleev Chem. J.) **53**, 100 (2009)
158. S.A. Nikolaevskii, A.S. Burlov, A.S. Bogomyakov, V.G. Vlasenko, A.D. Garnovskii, A.G. Starikov, Ya.V. Zubavichus, I.S. Vasilchenko, S.I. Levchenkov, A.I. Uraev, Russ. J. General Chem. **82**, 1770 (2008)
159. A.S. Burlov, V.G. Vlasenko, Ya.V. Zubavichus, S.I. Levchenkov, YuV Koschienko, A.S. Bogomyakov, S.A. Nikolaevskii, D.A. Garnovskii, A.I. Uraev, T.V. Lifintseva, E.V. Korshunova, Russ. J. Coord. Chem. **39**, 219 (2013)
160. A.D. Pomogailo, A.S. Burlov, N.D. Golubeva, L.A. Petrova, S.A. Mashchenko, S.I. Pomogailo, G.I. Dzhardimalieva, A.D. Garnovskii, Inorg. Mater. **47**, 876 (2011)

161. A.D. Pomogailo, G.I. Dzhardimalieva, S.I. Pomogailo, N.D. Golubeva, G.V. Shilov, E.A. Dzhavadyan, A.S. Burlov, S.A. Mashchenko, D.A. Garnovskii, Izv. Akad. Nauk. Ser. Khim. **139** (2016)

162. B.A. Komarov, A.T. Kapasharov, E.A. Dzhavadyan, V.A. Lesnichaya, G.I. Dzhardimalieva, A.S. Burlov, A.I. Uraev, S.A. Mashchenko, D.A. Garnovskii, A.D. Pomogailo, Russ. Chem. Bull. **64**, 936 (2015)

163. N.B. Shitova, P.G. Tsyrulnikov, D.A. Shlyapin, P.S. Barbashova, D.I. Kochubei, V.I. Zaikovskii, J. Struct. Chem. **50**, 268 (2009)

164. G. Carotenuto, B. Martorana, P.B. Perlo, L. Nicolais, J. Mater. Chem. **13**, 2927 (2003)

165. A.S. Susha, M. Ringler, A. Ohlinger, M. Paderi, N. LiPira, G. Carotenuto, A.L. Rogach, J. Feldman, Chem. Mater. **20**, 6169 (2008)

166. F. Capezzuto, G. Carotenuto, F. Antolini, E. Burresi, M. Palomba, P. Perlo Exp, Polym. Lett. **3**, 219 (2009)

167. F. Antolini, A. Ghezelbash, C. Esposito, E. Trave, L. Tapfer, B.A. Korgel, Mater. Lett. **60**, 1095 (2006)

168. G. Carotenuto, L. Nicolais, P. Perlo, Polym. Eng. Sci. 1016 (2006)

169. A. Petrella, M. Tamborra, M.L. Curri, M. Striccolli, P.D. Cozzoli, A. Adostano, J. Phys. Chem. B **109**, 1554 (2005)

170. G. Carotenuto, G. Pepe, D. Davino, B. Martorana, P. Perlo, D. Acierno, L. Nicolais, Microw. Opt. Technol. Lett. **48**, 2505 (2006)

171. E.A. Lewis, P.D. McNaughter, Z. Yin, Y. Chen, J.R. Brent, S.A. Saah, J. Raftery, J.A.M. Awudza, M.A. Malik, P. O'Brien, S.J. Haigh, Chem. Mater. **27**, 2127 (2015)

172. T. Di Luccio, A.M. Laera, L. Tapfer, S. Kempter, R. Kraus, B. Nickel, J. Phys. Chem. B. **110**, 12603 (2006)

173. D. Saikia, P.K. Saikia, P.K. Gogoi, M.R. Das, P. Sengupta, M.V. Shelke, Mater. Chem. Phys. **131**, 223 (2011)

174. I.C. McNeill, J.J. Liggat, Polym. Degrad. Stabil. **29**, 93 (1990)

175. I.C. McNeill, J.J. Liggat, Polym. Degrad. Stabil. **37**, 25 (1992)

176. S.M. Humphrey, M.E. Grass, S.E. Habas, L. Niesz, G.A. Somorjai, T.D. Tilley, Nano Lett. **7**, 785 (2007)

177. Y. Zhang, M.E. Grass, S.E. Habas, F. Tao, T. Zhang, P. Yang, G.A. Somorjai, J. Phys. Chem. C. **111**, 12243 (2007)

178. A.D. Pomogailo, Ros. Khim. Zh. (Mendeleev Chem. J.) **46**, 64 (2002)

179. Y.Y. Wang, Q. Shi, Q.Z. Shi, Y.C. Gao, X. Hou, Polyhedron **19**, 891 (2000)

180. Y.Y. Wang, Q. Shi, Q.Z. Shi, Acta Chim. Sinica. **58**, 675 (2000)

181. V.A. Shershnev, G.I. Dzhardimalieva, D.P. Kiryuhin, V.A. Zhorin, A.D. Pomogailo, Izv. Akad. Nauk. Ser. Khim. 1649 (2013)

182. N.N. Volkova, G.I. Dzhardimalieva, B. E. Krisyuk, N.V. Chukanov, V.A. Shershnev, G.V. Shilov, Izv. Akad. Nauk. Ser. Khim. (2016)

183. V.A. Shershnev, G.V. Shilov, G.I. Dzhardimalieva, A.D. Pomogailo, M. Izydorzak, M. Leonowicz, Macromol. Symp. **317–318**, 180 (2012)

184. B. Wu, W.-M. Lu, X.-M. Zheng, Chin. J. Chem. **20**, 846 (2002)

185. B. Wu, W. Lu, X. Zheng, Transit. Met. Chem. **28**, 323 (2003)

186. B. Wu, W. Lu, X. Zheng, J. Coord. Chem. **56**, 65 (2003)

187. Y. Lu, W. Lu, B. Wu, L. Wang, J. Coord. Chem. **53**, 15 (2001)

188. P.A. Vasiljev, Zh. Neorg. Khim. **30**, 1688 (1994)

189. P.A. Vasiljev, A.L. Ivanov, O.N. Rubacheva, A.N. Glebov, Zh. Neorg. Khim. **41**, 1747 (1996)

190. A. Gronowski, Z. Wojtczak, J. Therm. Anal. **26**, 233 (1983)

191. Z. Wojtczak, A. Gronowski, J. Therm. Anal. **36**, 2357 (1990)

192. A.S. Rozenberg, E.I. Aleksandrova, Izv. Akad. Nauk. Ser. Khim. 72 (1996)

193. A.S. Rozenberg, N.V. Chukanov, Izv. Akad. Nauk. Ser. Khim. 350 (1996)

194. A.S. Rozenberg, V.P. Syepanov, Izv. Akad. Nauk. Ser. Khim. 1406 (1996)

195. S.V. Davidovich, F.F. Vecher, T.F. Gusev, Thermochim. Acta. **89**, 383 (1985)

196. I.V. Fedorova, V.A. Shurov, A.A. Fedorov, M.S. Gaisinovich, Zh Prikl, Khim. **65**, 736 (1992)
197. I.V. Arkhangel'skii, L.N. Komissarova, A. Gorski, A. Kras'nicka, J. Therm. Anal. **32**, 1234 (1987)
198. A. Gorski, A. Kras'nicka, J. Therm. Anal. **32**, 1345 (1987)
199. E. Tirosh, G. Shemer, G. Markovich, Chem. Mater. **18**, 465 (2006)
200. N. Bao, L. Shen, Y. Wang, P. Padhan, A. Gupta, J. Am. Chem. Soc. **129**, 12374 (2007)
201. J.H. Park, N.M. Hwang, T. Hyeon, Nat. Mater. **3**, 891 (2004)
202. S. Sun, H. Zeng, D.B. Robinson, S. Raoux, P.M. Rice, S.X. Wang, G. Li, J. Am. Chem. Soc. **126**, 273 (2004)
203. S. Sun, H. Zeng, J. Am. Chem. Soc. **124**, 8204 (2002)
204. M.M. Lin, D.K. Kim, J. Nanopart. Res. **14**, 688 (2012)
205. K. Liu, H. You, G. Jia, Y. Zheng, Y. Song, M. Yang, Y. Huang, H. Zhang, Crystal. Growth Des. **9**, 3519 (2009)
206. B.L. Chen, Y. Yang, F. Zapata, G.N. Lin, G.D. Qian, E.B. Lobkovsky, Adv. Mater. **19**, 1693 (2007)
207. J.R. William, M.L. Kathryn, H.Y. An, W.L. Lin, W.B. Lin, J. Am. Chem. Soc. **128**, 9024 (2006)
208. V.G. Pol, O. Palchik, A. Gedanken, I. Felner, J. Phys. Chem. B. **106**, 9737 (2002)
209. K.-L. Wong, G.-L. Law, M.B. Murphy, P.A. Tanner, W.-T. Wong, P.K. Lam, L.M. Hon-Wah, Inorg. Chem. **47**, 5190 (2008)
210. L. Zhang, J. Luo, M. Wu, H. Jiu, Q.W. Chen, Mater. Lett. **61**, 4452 (2007)
211. H. Yang, D. Zhang, L. Shi, J. Fang, Acta Mater. **56**, 955 (2008)
212. J. Goldberg, R. Fan, P.D. Yang, Acc. Chem. Res. **39**, 239 (2006)
213. E.I. Aleksandrova, G.I. Dzhardimalieva, A.S. Rozenberg, A.D. Pomogailo, Izv. Akad. Nauk. Ser. Khim. **303** (1993)
214. E.I. Aleksandrova, G.I. Dzhardimalieva, A.S. Rozenberg, A.D. Pomogailo, Izv. Akad. Nauk. Ser. Khim. **308** (1993)
215. A.S. Rozenberg, G.I. Dzhardimalieva, A.D. Pomogailo, Polym. Adv. Technol. **9**, 527 (1998)
216. A.S. Rozenberg, G.I. Dzhardimalieva, N.V. Chukanov, A.D. Pomogailo, Coll. J. **67**, 57 (2005)
217. A.S. Rozenberg, E.I. Aleksandrova, G.I. Dzhardimalieva, А.Н. Титков, A.D. Pomogailo, Izv. Akad. Nauk. Ser. Khim. 1743 (1993)
218. A.S. Rozenberg, E.I. Aleksandrova, G.I. Dzhardimalieva, N.V. Kiryakov, P.E. Chizhov, V.I. Petinov, A.D. Pomogailo, Izv. Akad. Nauk. Ser. Khim. 885 (1995)
219. A.D. Pomogailo, A.S. Rozenberg, G.I. Dzhardimalieva, A.M. Bochkin, S.I. Pomogailo, N.D/ Golubeva, V.M. Grischenko, Neorg. Mater. **42**, 164 (2006)
220. A.D. Pomogailo, G.I. Dzhardimalieva, A.S. Rozenberg, V.N. Kestelman, J. Thermoplastic Composite Mater. **20**, 151 (2007)
221. A.S. Rozenberg, E.I. Aleksandrova, N.P. Ivleva, G.I. Dzhardimalieva, A.V. Raevskii, O.I. Kolesova, I.E. Uflyand, A.D. Pomogailo, Izv. Akad. Nauk. Ser. Khim. 265 (1998)
222. A.T. Shuvaev, A.S. Rozenberg, G.I. Dzhardimalieva, N.P. Ivleva, V.G. Vlasenko, T.I. Nedoseikina, T.A. Lubeznova, I.E. Uflyand, A.D. Pomogailo, Izv. Akad. Nauk. Ser. Khim. 1505 (1998)
223. A.S. Rozenberg, A.V. Raevskii, E.I. Aleksandrova, O.I. Kolesova, G.I. Dzhardimalieva, A.D. Pomogailo, Izv. Akad. Nauk. Ser. Khim. 862 (2001)
224. R.A. Lidin, L.L. Andreeva, V.A.Molochko, *Spravochnik po Neorganicheskoi Khimii. Konstanty Neorganicheskikh Veshestv* (The Handbook on Inorganic Chemistry. The Constants of Inorganic Substancies). (Khimiya, Moscow, 1987)
225. A.D. Pomogailo, G.I. Dzhardimalieva, A.S. Rozenberg, D.N. Muraviev, J. Nanoparticle Res. **5**, 497 (2003)
226. G.I. Dzhardimalieva, A.D. Pomogailo, S.P. Davtyan, V.I. Ponomarev, Izv. Akad. Nauk. Ser. Khim 1531 (1988)
227. G.I. Dzhardimalieva, A.D. Pomogailo, Macromol. Symp. **131**, 19 (1998)

228. N.P. Porollo, Z.A. Aliev, G.I. Dzhardimalieva, I.N. Ivleva, I.E. Uflyand, A.D. Pomogailo, N.S. Ovanesyan, Russ. Chem. Bull. **46**, 362 (1997)
229. A.S. Rozenberg, G.I. Dzhardimalieva, A.D. Pomogailo, Dokl. Akad. Nauk **356**, 66 (1997)
230. Y.M. Shulga, O.S. Roschupkina, G.I. Dzhardimalieva, I.V. Chernushevich, A.F. Dodonov, Y.V. Baldokhin, P.Y. Kolotirkin, A.S. Rozenberg, A.D. Pomogailo, Izv. Akad. Nauk. Ser. Khim. 1739 (1993)
231. C. McNeiel, S.M. Sadeghi, Polym. Degrad. Stabilit. **26**, 233 (1990)
232. N.V. Chukanov, I.V. Kumpanenko, V.V. Losev, N.G. Entelis, Dokl. Akad. Nauk. **261**, 135 (1981)
233. R. Das, P. Pachfule, R. Banerjee, P. Poddar, Nanoscale. **4**, 591 (2012)
234. R. Coskun, M. Yigitoglu, M. Sacak, J. Appl. Polym. Sci. **75**, 766 (2000)
235. D. Bilba, L. Bejan, L. Tofan, Croat. Chem. Acta. **71**, 155 (1998)
236. B.W. Zhang, K. Fischer, D. Bieniek, A. Kettrup, React. Polym. **24**, 49 (1994)
237. R.X. Liu, B.W. Zhang, H.X. Tang, J. Appl. Polym. Sci. **70**, 7 (1998)
238. N. Kabay, H. Egawa, Sep. Sci. Technol. **29**, 135 (1994)
239. R. Lei, X. Jie, X. Jun, Z. Ruijun, J. Appl. Polym. Sci. **53**, 325 (1994)
240. E.H. Rifi, M.J.F. Leroy, J.P. Brunette, C. Schloesserbecker, Solvent Extr. Ion Exch. **12**, 1103 (1994)
241. H. Kubota, Y. Shigehisa, J. Appl. Polym. Sci. **56**, 147 (1995)
242. N. Pekel, N. Sahiner, O. Güven, J. Appl. Polym. Sci. **81**, 2324 (2001)
243. I.H. Park, J.M. Suh, Angew. Makromol. Chem. **239**, 121 (1996)
244. G. Moroi, D. Bilba, N. Bilba, C. Ciobanu, Polym. Degrad. Stabil. **91**, 535 (2006)
245. M.N. Patel, V.J. Patel, Indian J. Chem. A. **28**, 428 (1989)
246. M.N. Patel, D.H. Sutaria, G.J. Patel, Synth. React. Inorg. Metal-Org. Chem. **24**, 401 (1994)
247. O.G. Marambio, G. del C. Pizzaro, M. Jeria-Orell, M. Huerta, C. Olea-Azar, W.D. Habicher, J. Polym. Sci.: Part A: Polym. Chem. **43**, 4933 (2005)
248. I. Kaya, A. Solguntekin, J. Appl. Polym. Sci. **113**, 1994 (2009)
249. H. Suda, K. Haraya, Chem. Commun. 93 (1997)
250. F. Rodeiquez-Reinoso, Carbon **36**, 159 (1998)
251. Y. Fang, D. Gu, Y. Zou, Z. Wu, F. Li, R. Che, Y. Deng, B. Tu, D. Zhao, Angew. Chem. Int. Ed. **49**, 7987 (2010)
252. J. Maruyama, K. Sumino, M. Kawaguchi, I. Abe, Carbon **42**, 3115 (2004)
253. Y. Tao, M. Endo, M. Inagaki, K. Kaneko, J. Mater. Chem. **21**, 313 (2011)
254. J. Lee, J. Kim, T. Hyeon, Adv. Mater. **18**, 2073 (2006)
255. Y. Xia, Z. Yang, R. Mokaya, Nanoscale. **2**, 639 (2010)
256. T.-Y. Ma, L. Liu, Z.-Y. Yuan, Chem. Soc. Rev. **42**, 3977 (2013)
257. B. Liu, H. Shioyama, T. Akita, Q. Xu, J. Am. Chem. Soc. **130**, 5390 (2008)
258. Q. Tian, Z. Zhang, L. Yang, S. Hirano, Carbon **93**, 887 (2015)
259. C.P. Li, J. Chen, C.S. Liu, M. Du, Chem. Commun. **51**, 2768 (2015)
260. R. Matsuoka, R. Toyoda, R. Sakamoto, M. Tsuchiya, K. Hoshiko, T. Nagayama, Y. Nonoguchi, K. Sugimoto, E. Nishibori, T. Kawai, H. Nishihara, Chem. Sci. **6**, 2853 (2015)
261. W. Xia, A. Mahmood, R. Zou, Q. Xu, Energy Environ. Sci. **8**, 1837 (2015)
262. M. Hu, J. Reboul, S. Furukawa, N.L. Torad, Q. Ji, P. Srinivasu, K. Ariga, S. Kitagawa, Y. Yamauchi, J. Am. Chem. Soc. **134**, 2864 (2012)
263. W. Chaikittisilp, M. Hu, H. Wang, H.-S. Huang, T. Fujita, K.C.-W. Wu, L.-C. Chen, Y. Yamauchi, K. Ariga, Chem. Commun. **48**, 7259 (2012)
264. N.L. Torad, M. Hu, Y. Kamachi, K. Takai, M. Imura, M. Naito, Y. Yamauchi, Chem. Commun. **49**, 2521 (2013)
265. L. Radhakrishnan, J. Reboul, S. Furukawa, P. Srinivasu, S. Kitagawa, Y. Yamauchi, Chem. Mater. **23**, 1225 (2011)
266. H.-L. Jiang, B. Liu, Y.-Q. Lan, K. Kuratani, T. Akita, H. Shioyama, F. Zong, Q. Xu, J. Am. Chem. Soc. **133**, 11854 (2011)
267. J. Hu, H. Wang, Q. Gao, H. Guo, Carbon **48**, 3599 (2010)
268. H. Li, M. Eddaoudi, M. O'Keeffe, O.M. Yaghi, Nature **402**, 276 (1999)

269. X.C. Huang, Y.Y. Lin, J.P. Zhang, X.M. Chen, Angew. Chem. Int. Ed. **45**, 1557 (2006)
270. N.L. Torad, Y. Li, S. Ishihara, K. Ariga, Y. Kamachi, H.-Y. Lian, H. Hamoudi, Y. Sakka, W. Chaikittisilp, K.C.-W. Wu, Y. Yamauchi, Chem. Lett. **43**, 717 (2014)
271. R.R. Salunkhe, Y. Kamachi, N.L. Torad, S.M. Hwang, Z. Sun, S.X. Dou, J.H. Kim, Y. Yamauchi, J. Mater. Chem. A **2**, 19848 (2014)
272. S.J. Yang, T. Kim, J.H. Im, Y.S. Kim, K. Lee, H. Jung, C.R. Park, Chem. Mater. **24**, 464 (2012)
273. A. Comotti, S. Bracco, P. Sozzani, S. Horike, R. Matsuda, J. Chen, M. Takata, Y. Kubota, S. Kitagawa, J. Am. Chem. Soc. **130**, 13664 (2008)
274. B. Liu, H. Shioyama, H.L. Jiang, X.B. Zhang, Q. Xu, Carbon **48**, 456 (2010)
275. Z. Han, Y. Yu, Y. Zhang, B. Dong, A. Kong, Y. Shan, J. Mater. Chem. A **3**, 23716 (2015)
276. J.P. Paraknowitsch, J. Zhang, D. Su, A. Thomas, M. Antonietti, Adv. Mater. **22**, 87 (2010)
277. Y. Wang, J. Zhang, X. Wang, M. Antonietti, H. Li, Angew. Chem. Int. Ed. **49**, 3356 (2010)
278. A. Thomas, A. Fischer, F. Goettmann, M. Antonietti, J.O. Müller, R. Schloegl, J.M. Carlssonc, J. Mater. Chem. **18**, 4893 (2008)
279. W. Chaikittisilp, N.L. Torad, C. Li, M. Imura, N. Suzuki, S. Ishihara, K. Ariga, Y. Yamauchi, Chem. Eur. J. **20**, 4217 (2014)
280. N.L. Torad, M. Hu, S. Ishihara, H. Sukegawa, A.A. Belik, M. Imura, K. Ariga, Y. Sakka, Y. Yamauchi, Small. **10**, 2096 (2014)
281. X. Jin, V.V. Balasubramanian, S.T. Selvan, D.P. Sawant, M.A. Chari, G.O. Lu, A. Vinu, Angew. Chem. Int. Ed. **48**, 7884 (2009)
282. M. Hu, J. Reboul, S. Furukawa, L. Radhakrishnan, Y. Zhang, P. Srinivasu, H. Iwai, H. Wang, Y. Nemoto, N. Suzuki, S. Kitagawa, Y. Yamauchi, Chem. Commun. **47**, 8124 (2011)
283. W. Bak, H.S. Kim, H. Chun, W.C. Yoo, Chem. Commun. **51**, 7238 (2015)
284. L. Zhang, Y.H. Hu, J. Phys. Chem. C. **114**, 2566 (2010)
285. M. Zhang, Y.-L. Huang, J.-W. Wang, T.-B. Lu, J. Mater. Chem. A. **4**, 1819 (2016)
286. L. Aboutorabi, A. Morsali, Inorg. Chim. Acta. **363**, 2506 (2010)
287. H. Sadeghzadeh, A. Morsali, J. Coord. Chem. **63**, 713 (2010)
288. B. Mirtamizdoust, D.C. Bienko, Y. Hanifehpour, E.R.T. Tiekink, V.T. Yilmaz, P. Talemi, S.W. Joo, J. Inorg. Organomet. Polym. **26**, 819 (2016)
289. S. Aghabeygi, F. Bigdeli, A. Morsali, J. Inorg. Organomet. Polym Mater. **22**, 526 (2012)
290. H.-Y. Shi, B. Deng, S.-L. Zhong, L. Wang, A.-W. Xu, J. Mater. Chem. **21**, 12309 (2011)
291. R. Zboril, L. Machala, M. Mashlan, V. Sharma, Cryst. Growth Des. **4**, 1317 (2004)
292. M. Hu, J.-S. Jiang, Y. Zeng, Chem. Commun. **46**, 1133 (2010)
293. W. Cho, S. Park, M. Oh, Chem. Commun. **47**, 4138 (2011)
294. X. Xu, R. Cao, S. Jeong, J. Cho, Nano Lett. **12**, 4988 (2012)
295. F. Zhang, L. Hao, L. Zhang, X. Zhang, Int. J. Electrochem. Sci. **6**, 2943 (2011)
296. B. Liu, X. Zhang, H. Shioyama, T. Mukai, T. Sakai, Q. Xu, J. Power Sour. **195**, 857 (2010)
297. C. Li, X. Yin, L. Chen, Q. Li, T. Wang, Chem. Eur. J. **16**, 5215 (2010)
298. F. Zhang, D.-D. Qi, X.-G. Zhang, Int. J. Electrochem. Sci. **11**, 189 (2016)
299. L. Hu, Y. Huang, F. Zhang, Q. Chen, Nanoscale **5**, 4186 (2013)
300. S. Zhang, H. Liu, C. Sun, P. Liu, L. Li, Z. Yang, X. Feng, F. Huo, X. Lu, J. Mater. Chem. A. **3**, 5294 (2015)
301. M. Moeinian, K. Akhbari, J. Inorg. Organomet. Polym. **26**, 1 (2016)
302. B. Mirtamizdoust, B. Shaabani, A. Khandar, H.-K. Fun, S. Huang, M. Shadman, P. Hojati-Talemi, Z. Anorg, Allg. Chem. **638**, 844 (2012)
303. Y. Hanifehpour, B. Mirtamizdoust, S.W. Joo, J. Inorg. Organomet. Polym. **22**, 816 (2012)
304. Y. Hanifehpour, B. Mirtamizdoust, A.R. Farzam, S.W. Joo, J. Inorg. Organomet. Polym. **22**, 957 (2012)
305. F. Bigdeli, A. Morsali, Mater. Lett. **64**, 4 (2010)
306. K. Bijanzad, A. Tadjarodi, O. Akhavan, Chin. J. Catal. **36**, 742 (2015)
307. H. Kim, M. Park, H. Lee, O.S. Jung, Dalton Trans. **44**, 8198 (2015)
308. F. Marandi, L. Hashemi, A. Morsali, H. Krautscheid, J. Inorg. Organomet. Polym. **26**, 962 (2016)

309. G.M. Duffy, S.C. Pillai, D.E. McCormack, Smart Mater. Struct. **16**, 1379 (2007)
310. F. Zhang, F.-L. Bei, J.-M. Cao, X. Wang, J. Solid State Chem. **181**, 143 (2008)
311. V. Safarifard, A. Morsali, Ultrason. Sonochem. **19**, 1227 (2012)
312. S.K. Pasha, V.S.V. Satyanarayana, A. Sivakumar, K. Chidambaram, L.J. Kennedy, Chin. Chem. Lett. **22**, 891 (2011)
313. A.V. Borhadea, B.K. Uphadeb, D.R. Tope, J. Chem. Sci. **125**, 583 (2013)
314. L. Hashemi, A. Aslani, A. Morsali, J. Inorg. Organomet. Polym. **22**, 867 (2012)
315. A. Aslani, A. Morsali, Inorg. Chim. Acta **362**, 5012 (2009)
316. H. Sadeghzadeh, A. Morsali, Ultrason. Sonochem. **18**, 80 (2011)
317. S. Saeednia, P. Iranmanesh, H.A. Rudbari, L. Saeednia, J. Macromol. Sci. Part A: Pure Appl. Chem. **53**, 227 (2016)
318. R. Gupta, S. Sanotra, H. Nawaz Sheikh, B. Lal Kalsotra, V. Kumar Gupta, Rajnikant, J. Coord. Chem. **65**, 3917 (2012)
319. Z.-F. Liu, A.-X. Zhu, C.-K. Lam, G.-W. Xie, C.-L. Liang, X.-M. Chen, Z.-P. Qiao, Cryst. Eng. Comm. **11**, 1303 (2009)
320. L. Wang, H. Zou, Y. Li, X. Li, S. Zhong, Mater. Manufact. Proc. (2016)
321. S. Jin, J.P. Hill, Q. Ji, L. Kumar Shrestha, K. Ariga, J. Mater. Chem. A. **4**, 5737 (2016)
322. M.S. Yazdan Parast, A. Morsali, Inorg. Chem. Commun. **14**, 450 (2011)
323. L. Hashemi, A. Morsali, J. Inorg. Organomet. Polym. **22**, 272 (2012)
324. M.A. Alavi, A. Morsali, S.W. Joo, B.K. Min, Ultrason. Sonochem. **22**, 349 (2015)
325. A. Mehrani, A. Morsali, Y. Hanifehpour, S.W. Joo, Ultrason. Sonochem. **21**, 1430 (2014)
326. W. Cho, Y.H. Lee, H.J. Lee, M. Oh, Chem. Commun. 4756 (2009)
327. Z. Li, Y. Xiong, Y. Xie, Nanotechnology **16**, 2303 (2005)
328. S. Hei, Y. Jin, F. Zhang, J. Chem. **2014**, Article ID 546956 (2014)
329. F. Meng, Z. Fang, Z. Li, W. Xu, M. Wang, Y. Liu, J. Zhang, W. Wang, D. Zhao, X. Guo, J. Mater. Chem. A. **1**, 7235 (2013)
330. N. Nasihat Sheno, A. Morsali, S. Woo Joo, Mater. Lett. **117**, 31 (2014)
331. W. Cho, Y.H. Lee, H.J. Lee, M. Oh, Adv. Mater. **23**, 1720 (2011)
332. M. Hu, A.A. Belik, M. Imura, K. Mibu, Y. Tsujimoto, Y. Yamauchi, Chem. Mater. **24**, 2698 (2012)
333. L. Zhang, H.B. Wu, S. Madhavi, H.H. Hng, X.W. Lou, J. Am. Chem. Soc. **134**, 17388 (2012)
334. L. Zhang, H.B. Wu, R. Xu, X.W. Lou, CrystEngComm, **15**, 9332 (2013)
335. K.J. Lee, T.-H. Kim, T.K. Kim, J.H. Lee, H.-K. Song, H.R. Moon, J. Mater. Chem. A **2**, 14393 (2014)
336. K. Akhbari, A. Morsali, J. Coord. Chem. **64**, 3521 (2011)
337. M.Y. Masoomi, A. Morsali, Ultrason. Sonochem. **28**, 240 (2016)
338. A. Abbasi, M. Gharib, M. Najafi, J. Sci. I. R. Iran. **27**, 217 (2016)
339. L.-B. Ni, R.-H. Zhang, Q.-X. Liu, W.-S. Xia, H. Wang, Z.-H. Zhou, J. Solid State Chem. **182**, 2698 (2009)
340. J. Rautio, P. Per, J. Honkamo, H. Jantunen, Microchem. J. **91**, 272 (2009)
341. K.S. Cho, J.I. Hong, C.I. Chung, Polym. Eng. Sci. **44**, 1702 (2004)
342. A. Tahmasian, A. Morsali, Inorg. Chim. Acta. **387**, 327 (2012)
343. A. Morsali, A. Panjehpour, Inorg. Chim. Acta. **391**, 210 (2012)
344. A. Hosseinian, S. Jabbari, A. Reza Mahjoub, M. Movahedi, J. Coord. Chem. **65**, 2623 (2012)
345. J.H. Lee, Y.J. Sa, T.K. Kim, H.R. Moon, S.H. Joo, J. Mater. Chem. A **2**, 10435 (2014)
346. H. Jiang, C. Wang, H. Wang, M. Zhang, Mater. Lett. **168**, 17 (2016)
347. T.K. Kim, K.J. Lee, J.Y. Cheon, J.H. Lee, S.H. Joo, H.R. Moon, J. Am. Chem. Soc. **135**, 8940 (2013)
348. Z.-M. Liu, S.-H. Wu, S.-Y. Jia, F.-X. Qin, S.-M. Zhou, H.-T. Ren, P. Na, Y. Liu, Mater. Lett. **132**, 8 (2014)
349. J. Xu, Q. Liu, W.-Y. Sun, Solid State Sci. **12**, 1575 (2010)
350. K. Akhbari, N.B. Bahman, A. Morsali, P. Retailleau, J. Iran. Chem. Soc. **13**, 165 (2016)

351. S.Y. Moon, M.W. Park, T.H. Noh, O.-S. Jung, J. Mol. Struct. **1054–1055**, 326 (2013)
352. F. Marandi, L. Hashemi, A. Morsali, H. Krautscheid, Ultrason. Sonochem. **32**, 86 (2016)
353. L. Chen, C. Zhao, S. Wei, S. Wang, Y. Gu, Mater. Lett. **65**, 446 (2011)
354. Z. Rashidi, A. Morsali, J. Mol. Struct. **936**, 206 (2009)
355. L. Hashemi, A. Morsali, J. Inorg. Organomet. Polym. **20**, 856 (2010)
356. L. Hashemi, A. Morsali, P. Retailleau, Inorg. Chim. Acta **367**, 207 (2011)
357. F. Shahangi Shirazi, K. Akhbari, Inorg. Chim. Acta **436**, 1 (2015)
358. M. Moeinian, K. Akhbari, J. Solid State Chem. **225**, 459 (2015)
359. A. Mehrani, A. Morsali, J. Inorg. Organomet. Polym. **21**, 476 (2011)
360. A. Mehrani, A. Morsali, P. Ebrahimpour, J. Coord. Chem. **66**, 856 (2013)
361. G.H. Shahverdizadeh, F. Hakimi, B. Mirtamizdoust, A. Soudi, P. Hojati-Talemi, J. Inorg. Organomet. Polym. **22**, 903 (2012)
362. L. Hashemi, A. Morsali, J. Coord. Chem. **64**, 4088 (2011)
363. B. Mirtamizdoust, B. Shaabani, A. Khandar, H. Pourradi, Y. Abbasityula, H. Goudarziafshar, D. Viterbo, G. Croce, P. Hojati-Talemi, J. Inorg. Organomet. Polym. **22**, 1293 (2012)
364. M. Hossienifard, L. Hashemi, V. Amani, K. Kalateh, A. Morsali, J. Inorg. Organomet. Polym. **21**, 527 (2011)
365. Z.R. Ranjbar, A. Morsali, P. Retailleau, Inorg. Chim. Acta **376**, 486 (2011)
366. G. Mera, E. Ionescu, Silicon-Containing Preceramic Polymers, in *Encyclopedia of Polymer Science and Technology* (John Wiley & Sons, Inc., Hoboken, NJ, USA, 2013)
367. P. Colombo, G. Mera, R. Riedel, G.D. Sorarù, J. Am. Ceram. Soc. **93**, 1805 (2010)
368. E. Ionescu, R. Riedel, Polymer Processing of Ceramics, in *Ceramics and Composites Processing Methods*, eds. by N. Bansal, A. Boccaccini (Wiley, Hoboken, NJ, USA, 2012)
369. C. Vakifahmetoglu, D. Zeydanli, P. Colombo, Mater. Sci. Eng. R Rep. **106**, 1 (2016)
370. G. Mera, M. Gallei, S. Bernard, E. Ionescu, Nanomaterials. **5**, 468 (2015)
371. R. Riedel, G. Mera, R. Hauser, A. Klonczynski, J. Ceram. Soc. Jpn. **114**, 425 (2006)
372. G. Mera, R. Riedel, Organosilicon-Based Polymers as Precursors for Ceramics, in *Polymer Derived Ceramics: From Nanostructure to Applications*, eds. by P. Colombo, R. Riedel, G.D. Soraru, H.-J. Kleebe (DEStech Publications Inc., Lancaster, PA, USA, 2010)
373. E. Ionescu, H.-J. Kleebe, R. Riedel, Chem. Soc. Rev. **41**, 5032 (2012)
374. E. Ionescu, C. Gervais, F. Babonneau, Polymer-to-Ceramic Transformation, in *Polymer Derived Ceramics: From Nanostructure to Applications*, eds. by P. Colombo, R. Riedel, G.D. Soraru, H.-J. Kleebe (DEStech Publications Inc., Lancaster, PA, USA, 2010)
375. M. Zaheer, T. Schmalz, G. Motz, R. Kempe, Chem. Soc. Rev. **41**, 5102 (2012)
376. M.S. Bazarjani, H.-J. Kleebe, M.M. Müller, C. Fasel, M.B. Yazdi, A. Gurlo, R. Riedel, Chem. Mater. **23**, 4112 (2011)
377. M. Zaheer, C.D. Keenan, J. Hermannsdorfer, E. Roessler, G. Motz, J. Senker, R. Kempe, Chem. Mater. **24**, 3952 (2012)
378. M. Zaheer, J. Hermannsdorfer, W.P. Kretschmer, G. Motz, R. Kempe, ChemCatChem **6**, 91 (2014)
379. G. Glatz, T. Schmalz, T. Kraus, F. Haarmann, G. Motz, R. Kempe, Chem. – Eur. J. **16**, 4231 (2010)
380. M. Zaheer, G. Motz, R. Kempe, J. Mater. Chem. **21**, 18825 (2011)
381. T. Schmalz, T. Kraus, M. Guenthner, C. Liebscher, U. Glatzel, R. Kempe, G. Motz, Carbon **49**, 3065 (2011)
382. D. Ghoshal, T.K. Maji, T. Mallah, T.-H. Lu, G. Mostafa, N.R. Chaudhuri, Inorg. Chim. Acta. **358**, 1027 (2005)
383. M. Sakamoto, K. Manseki, H. Okawa, Coord. Chem. Rev. **219–221**, 379 (2001)
384. E. Coronado, J.R. Galán-Mascaro, C. Martı-Gastaldo, Inorg. Chem. **46**, 8108 (2007)
385. Z.-G. Gu, S.C. Sevov, J. Mater. Chem. **19**, 8442 (2009)
386. B.-H. Ye, M.-L. Tong, X.-M. Chen, Coord. Chem. Rev. **249**, 545 (2005)
387. I.G. Fomina, ZhV Dobrokhotova, G.G. Aleksandrov, M.L. Kovba, V.I. Zhilov, A.S. Bogomyakov, V.M. Novotortsev, I.L. Eremenko, Russ. Chem. Bull. **59**, 699 (2010)

388. E.V. Orlova, A.E. Goldberg, M.A. Kiskin, P.S. Koroteev, A.L. Emelina, M.A. Bykov, G.G. Aleksandrov, ZhV Dobrokhotova, V.M. Novotortsev, I.L. Eremenko, Izv. Akad. Nauk. Ser. Khim. **60**, 2195 (2011)

389. T. Demars, M. Boltoeva, N. Vigier, J. Maynadié, J. Ravaux, C. Genre, D. Meyer, Eur. J. Inorg. Chem. **2012**, 3875 (2012)

390. Z.V. Dobrokhotova, N.V. Gogoleva, E.N. Zorina-Tikhonova, M.A. Kiskin, V.V. Chernyshev, A.L. Emelina, M.A. Bukov, A.S. Goloveshkin, I.S. Bushmarinov, A.A. Sidorov, A.S. Bogomyakov, M.L. Kovba, V.M. Novotortsev, I.L. Eremenko, Eur. J. Inorg. Chem. **2015**, 3116 (2015)

391. A.V. Gavrikov, P.S. Koroteev, Z.V. Dobrokhotova, A.B. Ilyukhin, N.N. Efimov, D.I. Kirdyankin, M.A. Bykov, M.A. Ryumin, V.M. Novotortsev, Polyhedron. **102**, 48 (2015)

392. N. Zauzolkova, Z. Dobrokhotova, A. Lermontov, E. Zorina, A. Emelina, M. Bukov, V. Chernyshev, A. Sidorov, M. Kiskin, A. Bogomyakov, A. Lytvynenko, S. Kolotilov, Y. Velikodnyi, M. Kovba, V. Novotortsev, I. Eremenko, J. Solid State Chem. **197**, 379 (2013)

393. M.A. Ryumin, Z.V. Dobrokhotova, A.L. Emelina, M.A. Bukov, N.V. Gogoleva, K.S. Gavrichev, E.N. Zorina-Tikhonova, L.I. Demina, M.A. Kiskin, A.A. Sidorov, I.L. Eremenko, V.M. Novotortsev, Polyhedron **87**, 28 (2015)

394. R.A. Rocha, E.N.S. Muccillo, Chem. Mater. **15**, 4268 (2003)

395. E. Coronado, C. Martí-Gastaldo, J.R. Galán-Mascarós, M. Cavallini, J. Am. Chem. Soc. **132**, 5456 (2010)

396. D. Hong, Y. Yamada, M. Sheehan, S. Shikano, C.-H. Kuo, M. Tian, C.-K. Tsung, S. Fukuzumi, ACS Sustainable Chem. Eng. **2**, 2588 (2014)

397. Y. Xia, B. Wang, G. Wang, X. Liu, H. Wang, ChemElectroChem **3**, 299 (2016)

398. L. Chen, Y. Shen, J. Bai, C. Wang, J. Solid State Chem. **182**, 2298 (2009)

399. K. Akhbari, A. Morsali, Cryst. Eng. Comm. **12**, 3394 (2010)

400. R. Bashiri, K. Akhbari, A. Morsali, Inorg. Chim. Acta. **362**, 1035 (2009)

401. M. Yamada, R. Ohkawa, M. Miyake, I.E.E.J. Trans, Electron. Inf. Syst. **127**, 1342 (2007)

402. B. Folch, J. Larionova, Y. Guari, L. Datas, C. Guerin, J. Mater. Chem. **16**, 4435 (2006)

403. Y.W. Koh, C.S. Lai, A.Y. Du, E.R.T. Tiekink, K.P. Loh, Chem. Mater. **15**, 4544 (2003)

404. M. Nagarathinam, K. Saravanan, W.L. Leong, P. Balaya, J.J. Vittal, Cryst. Growth Des. **9**, 4461 (2009)

405. J.X. Yang, S.M. Wang, X.L. Zhao, Y.P. Tian, S.Y. Zhang, B.K. Jin, X.P. Hao, X.Y. Xu, X. T. Tao, M.H. Jiang, J. Cryst. Growth. **310**, 4358 (2008)

406. Y. Meng, G.-H. Wang, S. Bernt, N. Stock, A.-H. Lu, Chem. Commun. **47**, 10479 (2011)

Conclusions and Future Prospects

As the contents of this book show, currently new branch of science, chemistry of polymeric metal chelates, is mainly formed at the junction of polymer chemistry and chemistry of coordination compounds. It operates its own objects and is based on its design principles and methodological approaches. The attractive and reliable chemical synthetic pathways of polymeric metal chelates are developed, which are analogs of almost all known low molecular weight compounds.

The development of the chemistry of polymeric metal chelates will certainly contribute useful outputs of synthesized compounds in adjacent areas and in particular least in catalysis, in the creation of composite and biologically active materials.

We can confidently assert that the current stage of development of polymeric metal chelates has reached its peak in the accumulation of experimental facts and their theoretical interpretation and generalization; all major groups of researchers are involved in this area of science.

How we see development of the chemistry of polymeric metal chelates?

Firstly, it is the search for more "precision" of the directed synthesis of both macroligands and chelating sites with controlled flexibility of the (co)polymer chain, allowing design of the unstressed metallocycles. In this regard, structural homogeneity of polymeric metal chelates, the lack of functional groups capable of forming coordination centers that structure are important. This applies especially to the preparation of stereoregular, alternating and optically active (co)polymers. It is important to develop polymeric metal chelates, chelating centers which include non-traditional heteroatoms, as well as including new types of inorganic and natural polymers in terms of chelating polymers. The optimization of the synthesis methods of polymeric metal chelates will continue by reducing the number of synthetic steps (for example, by combining the synthesis of chelating polymer and macroligand on the basis, etc.).

At this level, the greatest attention should be clearer identification of the specificity of macromolecular chelating ligands, their chain nature, and the transformations which they undergo during chelation. This is due to the fact that during PMC synthesis a complex reorganization of the ligand processes which caused by rotation of all parts of the original and the reacted chain. Its conformation and

various equilibriums (ionic, tautomeric, etc.) in solution depend on the nature of the solvent, pH, temperature; conversion of functional groups, etc. These factors, coupled with the structure of the functional unit, the nature of the connecting bridge between the chelating moiety and the polymer chain, its stiffness has a decisive effect on the characteristics of the resulting metal chelates, change of bond lengths and, to a greater extent, the distortion of bond angles.

Of particular interest is the identification of changes in the PMC during phase transitions of macroligands, "tuning" of the local chelating moiety and the associated energy costs.

It is obvious that a successful study of chelation processes in such systems is possible only when comparative analysis of chelate effects, stability constants and metal center buildings, their structural organization and topochemistry. Probably, in the near future we should expect significant progress in these areas of research. The same applies to non-traditional methods of the preparation of PMC including electro-, photo-, mechano-chemical and radiation methods of initiating polymerization of the corresponding chelating ligands followed by post-polymerization modifications involving metal compounds.

The direct synthesis techniques of the PMC, in particular, polymerization, copolymerization, graft polymerization and polycondensation of the metallomonomers of chelate type, are waiting for their further development. Among most important problems, solution of which would give a possibility of revealing general principles of MCM chemistry, we shall note the development of new methods of MCM production; determination of activation ways of multiple bonds in MCM, detailed analysis of the effect of metal nature on different stages of polymerization, searching for new methods of initiating homopolymerization processes; studying of reactivity of multiple MCM bonds in other reactions (hydration, isomerization, oxidation, ozonolysis, hydroformylation, etc.); investigation of special features of MCM copolymerization with each other and with traditional monomers; establishment of kinetic rules of polycondensation processes with MCM participation; studying of changes of a metal ion during polymerization and polycondensation.

We believe that in the near future chemistry of poly- and heteronuclear PMC, particularly in terms of identifying the role of the polymer chain in the implementation of metal-metal interactions, will receive a special development. Perhaps, these approaches will be promising in the creation of organic and molecular ferromagnets, for example, organometallic polymers with particular structural organization. Among other problems that decision would have a significant social impact, we isolate the complex task of concentration and selective separation (in hydrometallurgy, analytical chemistry, affinity chromatography, the separation of enantiomers, and others). In recent years, macromolecular ligands and chelates have been successfully used for this purpose.

It should be noted that the metal chelate dendrimers, star and hyperbranced polymers as well as coordination polymers containing metal chelate units and supramolecular metal chelate polymers make and important contribution to developing the chemistry of polymeric metal chelates. Among the most important tasks in this direction are the continued development and optimization of low cost, high-yielding

synthetic routes toward final PMC with minimal impurities or contaminations; the continued introduction of new "green" chemistries and solvent-free or aqueous solution polymerization processes (in the absence of organic solvents) into synthetic methodologies of PMC, which would minimize the cost and environmental impact; control over site-specific functionality (for example, core-shell-periphery); design of shape/morphology changing PMC on application of an external stimulus; further investigation into PMC for targeted biological applications.

The promising way will be further development of nanomaterials preparation by thermolysis of polymeric metal chelates. This is an intensely developed field of chemistry and materials science, which possesses its objects and investigation methods. Information in this field is accumulated continuously collecting the facts, which seemed odd before and completing logical structuring of new ways of production of nanomaterials with high marketing potential. Nevertheless, till now, as a rule, it is impossible to recognize correlations between content, structural features, and properties of the nanomaterials prepared by this method, which in many respects restrains scientifically grounded approach to structuring of these materials and prediction of their promising properties.

Index